UNIVERSITEIT VAN PRETORIA
UNIVERSITY OF PRETORIA
YUNIBESITHI YA PRETORIA

UNIVERSITY OF THE WITWATERSRAND, JOHANNESBURG

FINAL REPORT

STUDY INTO THE CAUSES OF THE JAGERSFONTEIN FINE TAILINGS STORAGE DAM FAILURE ON 11 SEPTEMBER 2022

Prepared by: University of Pretoria and University of the Witwatersrand Departments of Civil Engineering

Prepared for: Department of Water and Sanitation

Project: 1/2/4/295/2023/24

Date: 9 September 2024

Report No: Revision 1

water & sanitation

Department:
Water and Sanitation
REPUBLIC OF SOUTH AFRICA

RECORD OF REVISIONS

Revision Number	Issue Date	Changes Made	Issued by
0	8 July 2024	First issue for comment	SW Jacobsz
1	9 Sept 2024	Addressed comments by A. Havenga	SW Jacobsz

ABSTRACT

This report presents an investigation into the geotechnical causes of the Jagersfontein Fine Tailings Storage Dam failure which occurred at approximately 06h00 on the morning of Sunday 11 September 2022. The dam is registered with the Department of Water and Sanitation as the "Jagersfontein Fine Tailings Storage Facility Dam", a Category III dam with a safety risk. It is owned by Jagersfontein Developments (Pty) Ltd who focuses on reprocessing legacy tailings dumps from previous mining operations. The De Beers mining company operated the Jagersfontein mine until it ceased operations in 1971. The mine and associated tailings dam remained dormant until 2010 when reprocessing of legacy tailings dumps, without any further underground activities, commenced. Jagersfontein Developments (Pty) Ltd developed two new tailings deposition compartments adjacent to an old tailings dam built by the De Beers Group during their tenure of the Jagersfontein Mine. Construction of the first compartment began in 2010 immediately to the west of the old dam. Construction of the second compartment began in 2015, located to the south and east of the old dam. The new eastern compartment merged with the old tailings dam between 2017 and 2018. At that point the tailings facility consisted of two main areas, a western and eastern compartment. These two compartments merged between 2020 and 2021 to create a facility that consisted of a single deposition area. It was the southern wall of the eastern compartment, of which construction began in 2015, that failed on 11 September 2022.

The Investigation Panel comprised geotechnical engineers from the Universities of Pretoria and the Witwatersrand appointed by the Directorate: Dam Safety Regulation of the Department of Water and Sanitation. A second and parallel study, documented in a separate report, involved a dam breach study by hydraulic engineers of the University of Pretoria.

The geotechnical study included three site visits: The first involved a site walkover and collection of a limited number of samples. During the second site visit a piezocone (CPTu) investigation was carried out as well as sample collection. The third visit comprised a seismic CPTu investigation, Mostap sampling and further collection of samples for index testing. Due to legal reasons the Investigation Panel was not permitted to discuss the tailings dam failure with personnel of Jagersfontein Developments (Pty) Ltd.

The investigation included a desk study of documentation provided to the Investigation Panel via the Department of Water and Sanitation, as well as a study of aerial and satellite images, some freely available and some purchased. Available data also included several surveys of the dam carried out from time to time.

The design report (Robinson, 2015) for the eastern compartment of which the southern wall failed indicated that the compartment was constructed on land already impacted by legacy fine tailings deposits. This was supported by aerial and satellite images. The design report indicated that the fine tailings had a low shear strength, recommending a 20° effective friction angle and a very low permeability of 1×10^{-12} m/s. In brief, the design for the eastern compartment comprised outer walls constructed from coarse tailings (grits), to contain the fine tailings slurry (slimes) deposited hydraulically in the tailings dam. The outer walls were raised via upstream construction.

The satellite images showed signs of instability along the eastern third of the southern wall of the tailings dam starting in Feb 2019. This eastern third of the tailings dam wall was adjacent to a water

storage dam known as Dam 10. The first signs of instability were seen just after Dam 10 filled up rapidly from rainfall after being empty during the dry first half of the 2018 - 2019 summer. Based on available information, the slope showing signs of instability was constructed at what is believed to be the natural angle of repose of the coarse tailings (grits) (1:1.5 or approximately 33°). This is steeper than the recommended design angle available to the Investigation Panel (1:2 or approximately 27°). It appears that this section of the wall is underlain at least partially by an old tailings dump, referred to as Dump 10, which the Investigation Panel believes represents a foundation of inadequate shear strength.

Satellite imagery showed a large amount of southward movement taking place along the toe of the affected section of the dam wall from February 2019 until the failure in September 2022. Changes in the alignment of the access road directly downstream of the southern wall of the dam show how an initially straight road became curved around the affected part of the wall, eventually deviating 87 m from its original alignment. Satellite images showed substantial increased construction activity along the affected section of the wall, which is interpreted to have been efforts to maintain stability while the dam was kept in use. The affected section of the wall had a footprint width of approximately twice the footprint width of any other part of the dam wall at the time of the failure.

Stability analyses show that the section of the wall that first showed signs of distress was unstable when assuming drained strength parameters. The first slope instability was likely triggered by the rapid filling of Dam 10. Thereafter, near continuous movement seems to have occurred, which the Investigation Panel believe would have resulted in undrained conditions along an interface between the dam wall and its foundation. Such undrained conditions would have reduced the strength to levels insufficient to ensure stability. Satellite images indicate a reduction in the rate of movement at the toe in the months preceding the failure, but some acceleration in the rate of inward widening of the embankment crest along parts of the southern wall during this time. As the dam did not have a decant facility, no beach could form and water and/or fine tailings slurry often extended right up against the inner slopes of the crest. Upstream raising of the dam therefore had to be constructed on poorly consolidated tailings. An eyewitness account indicates that, on the morning of the failure, part of the crest failed to the inside. This was followed by slumping of the crest, overtopping and the uncontrolled release of approximately 5.1 million m^3 of tailings slurry and water. The Investigation Panel believes that the failure at the inside of the crest provided a trigger to remobilise undrained conditions at the base of the dam wall, reducing the shear strength along the zones where movement had been occurring for a long time, resulting in the failure of the Jagersfontein Fine Tailings Storage Dam.

TABLE OF CONTENTS

1. INTRODUCTION 11

2. INVESTIGATION 13

3. THE TAILINGS DAM LOCALITY PLAN 14

4. HISTORY OF THE JAGERSFONTEIN TAILINGS DAM FROM AERIAL AND SATELLITE IMAGERY 15

4.1. AERIAL PHOTOGRAPHY 16
4.2. OVERVIEW OF HIGH-RESOLUTION SATELLITE IMAGERY 17
4.3. ADDITIONAL INFORMATION FROM THE LITERATURE 28
4.4. DISCUSSION OF OBSERVATIONS FROM AERIAL AND SATELLITE IMAGES 29
4.5. OBSERVATIONS REGARDING DAM 10 34

5. DESIGN FOR THE EASTWARD EXTENSION OF THE TAILINGS DAM 36

5.1. GENERAL DESIGN OVERVIEW 36
5.2. STABILITY ASSESSMENT 38
5.3. SLURRY DEPOSITION 40
5.4. DECANTING 40
5.5. COMMENT ON SIGNIFICANT ASPECTS OF THE DESIGN 40

6. SURVEY DATA 42

6.1. VERIFICATION OF SURVEY DATA INTEGRITY 42
6.2. SIDE SLOPE GEOMETRY 44
6.3. FREEBOARD 44
6.4. RATE OF RISE 46
6.5. DEPOSITION 46
6.6. RAISING OF THE OUTER DAM WALLS 47
6.7. EVIDENCE OF OUTER WALL INSTABILITY 48
6.8. LAST STABLE CROSS-SECTION PROFILE AT BREACH LOCATION 49

7. THE FAILURE EVENT 51

7.1. SEQUENCE OF EVENTS 51
7.2. HYPOTHESISED GEOTECHNICAL CAUSES OF THE FAILURE 55
7.2.1. Slippage along the base 55
7.2.2. Shear displacement between sliding and intact parts of the embankment (Erosion Scars 1 & 3) 61
7.2.3. Consideration of drained instability as the cause of the failure 63
7.2.4. Consideration of drained stability of the February 2019 profile 64
7.2.5. Consideration of undrained instability 66
7.2.6. Stabilising the slope 72

8. SUMMARY AND CONCLUSIONS 75

9. RECOMMENDATIONS 79

9.1. THE URGENCY OF POST-FAILURE GEOTECHNICAL INVESTIGATIONS. 79
9.2. THE VALUE OF OPTICAL SATELLITE IMAGERY 79
9.3. MONITORING OF PORE PRESSURES AND EMBANKMENT SETTLEMENT OR MOVEMENT. 80
9.4. DAM 10 ADJACENT TO THE TAILINGS DAM TOE 80
9.5. FURTHER INVESTIGATION 80
9.6. DOCUMENTATION 81
9.7. LESSONS FROM CASE HISTORIES 81

ACKNOWLEDGEMENTS **83**
REFERENCES **84**

LIST OF APPENDICES

Appendix A **Aerial photography**

Appendix B **High resolution satellite images**

Appendix C **Presentation of Planetscope imagery**

Appendix D **Presentation of Sentinel-2 imagery**

Appendix E **Geotechnical parameters**

Appendix F **SCPTu report**

LIST OF FIGURES

Figure 1 Jagersfontein town locality map (Google Maps). 12
Figure 2 Locality plan showing the town of Jagersfontein and some of the extent of the impact form the failure (Google Earth). Image dated 16 September 2022. 12
Figure 3 Jagersfontein Tailings Dam locality plan (Google Earth). Image dated 13 August 2022. 15
Figure 4 comparison between 1973 aerial photograph (left) and the Google Earth image dated 29 May 2010 (right) shows virtually no changes to the De Beers Tailings Dam over 37 years. 17
Figure 5 South-eastern corner of the Jagersfontein Tailings Dam from the 2 May 2019 Google Earth image showing signs of instability. 23
Figure 6 North-south cross-section from the photogrammetry survey dated 6 November 2019through the donut-shaped feature. 24
Figure 7 (a) Cracks visible on the southern wall from the Google Earth satellite image dated 2020/9/24; (b) western crack enlarged; (c) and eastern crack enlarged. 26
Figure 8 Displacement vectors associated with the failure event and the alignment for the critical cross-section studied for stability assessment showing (a) the latest available pre-failure high resolution satellite image and (b) the earliest available post-failure high resolution image. 28
Figure 9 Evolution of upstream water line and road's edge at southern toe at breach location from February 2019 to July 2022 seen in plan. 30
Figure 10 Displacement of southern edge of access road over time. 30
Figure 11 "The Wandering Tree": Movement of a tree or large shrub tracked near the northern end of the Dam 10 embankment from satellite images dated 9 July 2020 to 28 July 2022 (Figures B15 to B22) (total extent of movement was 28 m). 31
Figure 12 Identifiable feature tracked using satellite images from 22 March 2019 to 7 March 2023 (Figures B11 to B24), showing displacement at the toe of the dam wall amounting to 87 m. 32
Figure 13 Displacement with time of the feature tracked in Figure 12 (recorded from 22 March 2019). 32
Figure 14 (a) Comparing toe displacement and cumulative rainfall and (b) actual rainfall (source for rainfall data: Jagersfontein Developments). 33
Figure 15 Jagersfontein rainfall record for February 2019 (source: Jagersfontein Developments). 33
Figure 16 Long-section along the dam 10 embankment (looking west) showing the crest rising towards the tailings dam – Dec 2021 dam safety inspection crest survey (Jacobsz, 2021). 35
Figure 17 Plan for the extension of the JD tailings dam, showing the proposed new wall in red (Robinson, 2015). 37
Figure 18 Anticipated rate of rise from design report (Robinson, 2015) 38
Figure 19 Proposed cross-section of starter wall (Robinson, 2015). 39
Figure 20 Proposed cross-section for raising of the wall (Robinson, 2015). 39
Figure 21 Cross-section profiles from available survey data at critical section. 42
Figure 22 Cross-section profiles at control section before adjustment. 43
Figure 23 Cross-section profiles at control section after adjustment. 43
Figure 24 Cross-section profiles at failure after adjustment. 43

Figure 25 Locations where cross-section profiles were studied (27 April 2022 survey). 44
Figure 26 Sections through the Jagersfontein tailing dam showing the pond and freeboard based on the 27 April 2022 survey. Note: The inset show in yellow the cross-sections being presented. 45
Figure 27 Freeboard over time from survey data taken at the embankment cross-section where the failure occurred. 45
Figure 28 Rate of rise determined from survey data. 46
Figure 29 Annualised deposition record in cubic metres per year calculated from survey data. 46
Figure 30 Cross-sections on the southern wall from surveys illustrating the raising of the outer dam wall over time. 47
Figure 31 Selected cross-sections illustrating deformation mechanism 48
Figure 32 Long-section survey data along the southern and eastern walls of the tailings dam from 2019 to 2022. (Shaded area = area impacted by breach.) 49
Figure 33 Cross-section profiles closest in time to Feb 2019. 50
Figure 34 Features associated with the failure event. Image from 12 September 2022. 52
Figure 35 Enlarged image from the failure area showing areas reached by overtopping fine tailings (Image from 24 September 2022). 52
Figure 36 The north-eastern part of the tailings dam before and after failure (26 July 2022 and 12 Sept 2022 respectively). The white streaks on the northern and eastern slopes visible on the post-failure image suggest that limited overtopping may have occurred at these locations. 54
Figure 37 Images from cell phone footage taking during helicopter inspection on 12 September 2022 showing possible signs of limited overtopping near north-Eastern corner of dam (Source: Mr A Havenga and/or Mr WM Ramokopa). 55
Figure 38 The pre-failure embankment geometry and failure scars shown in yellow, overlying tailings deposits from dump 10, the South Dump and the North Dump (dump toe shown in red). Compiled from the present image (29 May 2010) and early aerial images. 57
Figure 39 Extract from 22 November 2010 satellite image colour enhanced by photosat (Nell, 2024). 57
Figure 40 Contour drawing based on 26 February 2011 satellite imagery identifying various materials identified (Source: Rivet, 2023 (Photosat)). The outline of the “unknown material” corresponds closely with the toes of the tailings dumps outlined in red in Figure 38. 58
Figure 41 The breach floor comprises a layer of consolidated tailings that resisted erosion during the failure. (a) Looking down towards the breach from the eastern side of the breach. (b) Looking south along the western side of the breach. (c) Taken from helicopter on 12 September 2022 showing embankment underlain by consolidated tailings. 60
Figure 42 Granular material that remained in the breach still showing signs of movement on the underlying layer of tailings. (Location indicated in Figure 41 above). 60
Figure 43 Evidence of sliding on the base suggested by block separating from embankment toe (curly bracket). 61
Figure 44 Scar 3 already developed as the outrush of fine tailings from the dam was occurring through the main breach. (Source: https://www.youtube.com/watch?v=_nd_LoNoj8Y). 62

Figure 45 The location of cracks (in red) observed on the 24 Sept 2020 satellite image, superimposed on the failed southern embankment, shows close correlation with erosion scars 1 & 3. 63
Figure 46 Residual friction angle values for clays, tills and shales against plasticity index (I_P), with the I_P range for Jagersfontein indicated (Knappett & Craig, 2012). 64
Figure 47 Cross-section profile for slope stability analysis of February 2019 downstream slope. ... 64
Figure 48 Drained slope stability analysis 1 (FoS = 1.03). 66
Figure 49 Drained slope stability analysis 2 (FoS = 0.92). 66
Figure 50 Drained slope stability analysis 3 (FoS = 0.96). 66
Figure 51 Cross-section used for slope stability analysis to assess the undrained shear strength ratio mobilised during long-term slope deformation. 69
Figure 52 Normal upstream raising of embankment 69
Figure 53 Candidate rear scarp of failure surface before 11 Sept 2022 event (Source: Mr A Havenga and/or Mr WM Ramokopa). 69
Figure 54 Materials zones analysed for final stability analysis 70
Figure 55 Failure surface associated with a yield strength ratio of 0.11 giving a factor of safety of unity matching long-term movement observed on embankment (FoS = 1.00). 70
Figure 56 Hypothetical cross-section associated with the 11 September 2022 failure event. 72
Figure 57 Overall slip surface associated with a YSR of 0.175 giving a factor of safety of one. 72
Figure 58 The effect of placement of material on a slope on the stability of the slope under drained and undrained conditions. 73
Figure 59 Simplified cross-section of the critical section of the Jagersfontein Tailings Dam. 74

List of abbreviations

CDNGI	Chief Directorate: National Geospatial Information
Comp	Compartment (as in Comp 1, Comp 2)
c'	Effective cohesion
CPTu	Cone Penetration Test with pore pressure measurement
c_u	Undrained shear strength
DEM	Digital Elevation Model
DWS	Department of Water and Sanitation
FoS	Factor of safety
InSAR	Interferometric Synthetic Aperture Radar
I_p	Plasticity index
JD	Jagersfontein Developments
MAP	Mean Annual Precipitation
SCPTu	Seismic Cone Penetration Test with pore pressure measurement
SHANSEP	Stress History and Normalized Soil Engineering Properties (modelling undrained shear strength)
vs	versus
YSR	Yield strength ratio
β	slope angle
γ	bulk unit weight
γ_b	bulk unit weight
γ'	buoyant unit weight
σ'_v	Vertical effective stress
ϕ'	Effective friction angle (°)

1. Introduction

On 27 October 2023 the Directorate: Dam Safety Regulation (D: DSR) of the national Department of Water and Sanitation (DWS) of the Republic of South Africa appointed a team of engineers from the University of Pretoria and the University of the Witwatersrand ("the Investigation Panel") under research contract number 1/2/4/295/2023/24 to carry out an independent investigation into the technical causes of the failure of the Jagersfontein Fine Tailings Storage Dam which occurred on Sunday, 11 September 2022. The dam is registered with the Department of Water and Sanitation as the "Jagersfontein Fine Tailings Storage Facility Dam", a Category III dam with a safety risk. The dam is referred to in the remainder of this report as the "tailings dam" or the "Jagersfontein Tailings Dam".

The Jagersfontein operations, of which the tailings dam formed part, belonged to the diamond mining house, the De Beers Group, until 2010 when it was sold to the Superkolong Consortium, a broad-based black economic empowered company (Shacinda, 2010; Marais et al., 2024). De Beers Group acquired the mine in 1931 (Torres Cruz & O'Donovan, 2023). In 2011, Superkolong merged with Reinet Investments to form a joint venture, Jagersfontein Developments (Pty) Ltd ("JD"), the current owner of the operations, including the tailings dam. Reinet Investments sold their shares to Star Gems of Dubai in April 2022 (Marais et al., 2024). JD was reprocessing tailings dumps left behind by earlier mining operations at the time of the tailings dam failure. The recent history of the Jagersfontein Tailings Dam, relevant to the present study into the causes of its failure, is summarised in Section 4 of this report. The history of the Jagersfontein mining and dump reclamation operations is summarised in more detail by others (e.g. Marais et al., 2024).

The town of Jagersfontein is located in the southwestern Free State Province of South Africa, 116 km southwest of Bloemfontein (see locality map, Figure 1). A more detailed locality plan based on a satellite image taken five days after the disaster, is presented in Figure 2. This image shows the town of Jagersfontein, the failed tailings dam and some of the areas impacted by the discharge of tailings. It is estimated that approximately 5.1 million cubic metres of fluid fine tailings and water were released from the tailings dam during the failure (Coetzee, 2024). Figure 2 shows that from the tailings dam, tailings flowed over the R704 provincial road and flooded parts of the townships of Skoti (part of Itumeleng) and Charlesville. Further downstream, the tailings stream again crossed the R704 road and entered the Proses Spruit (NB: the term "spruit" is commonly used to denote a stream or minor river in South Africa) and eventually flowed into the Kalkfontein Dam (not shown in Figure 2), approximately 60 km downstream. The disaster resulted in the loss of three people, destruction of nearly 200 houses, other property damage, and impacted approximately 1600 ha of agricultural and grazing land and some livestock (Marais et al., 2024).

This report, produced by a panel of geotechnical engineers from the Universities of Pretoria and the Witwatersrand, describes an investigation into the technical causes that resulted in the failure. The report is accompanied by a second report which describes a comprehensive dam break study relevant to the disaster, produced by hydraulic engineers from the University of Pretoria (Coetzee, 2024).

FIGURE 1 JAGERSFONTEIN TOWN LOCALITY MAP (GOOGLE MAPS).

FIGURE 2 LOCALITY PLAN SHOWING THE TOWN OF JAGERSFONTEIN AND SOME OF THE EXTENT OF THE IMPACT FORM THE FAILURE (GOOGLE EARTH). IMAGE DATED 16 SEPTEMBER 2022.

The report comprises a description of the investigation, an overview of the recent history of the tailings dam relevant to the failure compiled from aerial and satellite imagery, focussing specifically on the period 2010 to 2022. Furthermore, a brief overview of the design of the wall that failed, an overview of observations based on available survey data, a description of the failure event and associated considerations of stability and conclusions, as well as recommendations emanating from the study are included in this report. A number of additional supporting reports were compiled during the course of the study which are included in the appendices. These are:

APPENDIX A	Aerial photography
APPENDIX B	High-resolution satellite images
APPENDIX C	Presentation of Planetscope imagery
APPENDIX D	Presentation of Sentinel-2 imagery
APPENDIX E	Geotechnical parameters
APPENDIX F	SCPTu investigation

2. Investigation

The investigation into the causes of the failure of the Jagersfontein Tailings Dam commenced with the Investigation Panel being briefed by engineers of the D: DSR of DWS who were on site late on the day of the failure. The engineers shared their experiences and available documentation. The field investigation included three visits to the site, the first being an exploratory site walkover on Thursday 12 October 2023, followed by two more visits (29 January to 2 February 2024 and 4 to 9 March 2024) during which a piezocone (SCPTu) investigation was carried out and soil and tailings samples collected for laboratory testing. The piezocone investigation included the recovery of Mostap samples during the March visit, as well as shear wave velocity testing. Due to wet conditions along the toe of the dam and inside the dam basin, all sampling, with the exception of the Mostap samples, was done by hand and was therefore limited to what could be recovered at or just below the surface. The piezocone investigation assisted with the characterisation of the pore pressure regime in the dam wall near the location of the failure (albeit 18 months after the failure event), as well as the identification of material types which were necessary for compiling a cross-section profile for slope stability analysis.

A study of satellite images that are freely available for research purposes (GoogleEarth, Sentinel-2 and PlanetScope) provided a considerable amount of insight into activities and events leading up to the failure and played a crucial role in piecing together the recent history of the tailings dam in this study. Free satellite images were supplemented by purchasing additional high-resolution satellite imagery from various suppliers. In addition to the satellite images, old aerial photographs dating as far back as 1944 provided further valuable insight into conditions on site prior to the construction of the enlarged Jagersfontein Tailings Dam which eventually failed. Valuable information was also obtained

by studying survey data from photogrammetry commissioned from time to time between 2010 and the time of the failure (2022), in addition to a post-failure LIDAR survey.

The Investigation Panel needs to point out that, for legal reasons, the Panel was prevented from interviewing employees of JD and/or JD's Consultants, and could therefore not discuss aspects of the study with them.

3. The tailings dam locality plan

Figure 3 presents a locality plan identifying various features referred to in this report. Central to the figure is the Jagersfontein Tailings Dam which is partially surrounded by different parts of the town of Jagersfontein. The portion labelled "Jagersfontein" in Figure 3 is the main hub of the town and is located to the north of the dam. Itumeleng is located to the east and Charleville to the southeast. The open pit diamond mine is visible to the northwest and the old tailings dump from previous mining operations to the west. The processing plant is located immediately to the west of the tailings dam. A water dam, known as Dam 10, receiving runoff from a catchment to the west of the tailings dam, is located immediately to the south of the tailings dam. Labelled as the "De Beers Dam" is the tailings dam as it existed when De Beers closed the mine in 1973 (details in Section 4). In 2010, when reprocessing of the old tailings dumps commenced, new tailings deposition space was required and this was provided by constructing a new compartment immediately to the west against the De Beers Dam. This western compartment is referred to as Compartment 1 in this report. In 2015 work commenced on the construction of a new compartment against the southern and eastern sides of the De Beers Dam which eventually covered the De Beers Dam. In this report, the union of the De Beers Dam and the expansions built after 2010 to its east and south are referred to as Compartment 2 (Figure 3). It is the southern wall of Compartment 2 that failed on 11 September 2022.

FIGURE 3 JAGERSFONTEIN TAILINGS DAM LOCALITY PLAN (GOOGLE EARTH). IMAGE DATED 13 AUGUST 2022.

4. History of the Jagersfontein Tailings Dam from aerial and satellite imagery

Mining in Jagersfontein began during the 1870s, shortly after the discovery of the first diamond in 1869 (Philip, 2014). From 1910 to 1913 there was a gradual transition from open pit to underground mining and in 1931 the mine was acquired by De Beers Consolidated Mines (Philip, 2014). De Beers closed the mine in August 1971 due to depletion of the ore body (Philip, 2014). The mine remained closed until 28 September 2010 when De Beers Group sold the mine to the Superkolong Consortium (Shacinda, 2010; Marais et al., 2024). Henceforth, activities focused exclusively on the reprocessing of the mine waste stockpiles that were already on the ground surface, with no further underground extraction of ore.

The discussion below refers to a series of aerial photographs dating from 1944 to 1973, whereafter an overview of a series of relatively high-resolution satellite images, dating from 2010 to 2023, is presented. In addition, reference is made to lower resolution PlanetScope satellite imagery available at a higher temporal interval than the other images utilised. The aerial, high resolution satellite images and PlanetScope satellite images are presented in Appendix A, B and C respectively. Not all available PlanetScope images are included in Appendix C, but links to video sequences containing all the images are given in Appendix C. It is recommended that, when reading the report, these appendices be displayed in presentation mode on a screen as it is insightful to be able to alternate rapidly between images to identify various features referred to, especially movement.

4.1. Aerial photography

Figure A1 (Appendix A) presents aerial photography from the South African Chief Directorate: National Geospacial Informaton (CDNGI), dated 31 December 1944, showing the De Beers Tailings Dam to the southeast of the opencast pit. The earth dam storing water, referred to as Dam 10, is located to the south of the De Beers Tailings Dam. A raised area, referred to as Dump 10, was located between the tailings dam and Dam 10. The photo appears to have been taken relatively early in the life of the De Beers tailings dam as a section of wall still had to be constructed between the Dump 10 and the tailings dam. Two features resembling two gently sloping dumps are located to the east of the De Beers tailings dam. The dumps are respectively referred to as the North Dump and South Dump in the discussions that follow. The South Dump appears to pre-date the North Dump as the former was well covered by vegetation, which appears to be mature trees and shrubs, in the 1944 image (Figure A1). The North Dump appeared largely devoid of vegetation. Examining the development of the De Beers Dam following Figure A2 to A5, it appears that these two dumps initially formed the eastern containment of the tailings dam. As the tailings dam gained height, a containment embankment was constructed between the crests of the two dumps as visible in Figure A5, which shows the layout of the dam in 1973. The origin of the two dumps is not known to the Investigation Panel, but they appear to have comprised of fine tailings/slimes. A similar dump is visible at the southern end of the Dam 10 embankment (Figures A2 to A4) but is not relevant to the current report. These dumps were also identified in a report by Rivet (2023), discussed in Section 7.2, which includes colour enhanced images which assisted with delineation of the extent of various features.

In an image dated 7 August 1955 (Figure A3) it appears that deposition on the tailings dam took place from a single discharge point in the west, with discharge flowing to the east and the southeast. Water appears to have been ponding in the south-eastern corner of the tailings dam. Natural particle sorting after deposition can be expected to have caused coarse materials to settle out nearest to the discharge point, with deposited materials becoming progressively finer towards the southeast, where the pond was present.

Returning to the 1973 configuration of the De Beers Dam, an access ramp leading to the southwestern corner of the dam, not visible in earlier images, can be seen (Figure A5). Also, there appears to be a poolwall in the north-western corner of the dam and water ponding in the south-eastern corner of the dam (Figure A5). Figure 4 compares two images of the Jagersfontein Dam, one captured in 1973, approximately two years after the 1971 mine closure, and another one captured in May 2010, shortly before the reprocessing of the legacy mine waste began. The similarities between the two images confirm that the tailings dam remained inactive between 1973 and 2010.

Raised features along the southern edge of the South Dump (see Figures A1 and A5), which suggest a relatively thick tailings deposit at the toe of the South Dump, are visible at the northern end of the Dam 10 embankment in all the aerial photographs, as well as the 29 May 2010 satellite image. Their extent is indicated by red curves in selected satellite images that follow (see Appendix B). The approximate easterly extent of tailings from the North and South Dumps, as visible on the 2010 satellite image (including a 2010 colour-enhanced image by Rivet (2023), discussed in Section 7.2.1), is indicated in selected satellite images.

A desk study was carried out of available satellite imagery captured from 2010 onwards to shed light on the events leading up the failure of the Jagersfontein tailings dam on 11 September 2022.

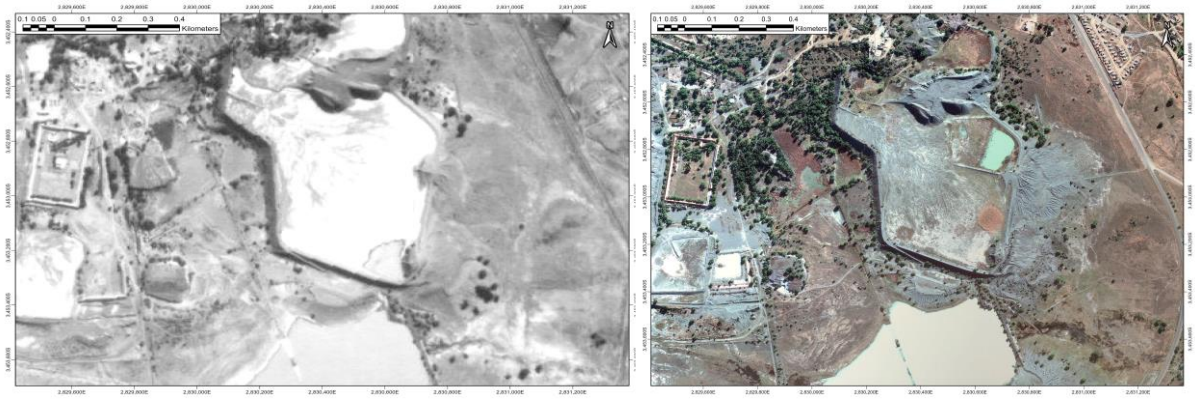

FIGURE 4 COMPARISON BETWEEN 1973 AERIAL PHOTOGRAPH (LEFT) AND THE GOOGLE EARTH IMAGE DATED 29 MAY 2010 (RIGHT) SHOWS VIRTUALLY NO CHANGES TO THE DE BEERS TAILINGS DAM OVER 37 YEARS.

4.2. Overview of high-resolution satellite imagery

The recent history of the Jagersfontein Tailings Dam was first studied using PlanetScope satellite images. Observations from this study are presented in Appendix C. Subsequent to this, a number of high-resolution satellite images were purchased to study the development of the Jagersfontein Tailings Dam dating back to 2010, the time when the operations were sold to the Superkolong Consortium, in greater detail. The images referred to in this section are included in Appendix B. The image acquisition details are summarised in Table 1, which includes information about the Digital Elevation Models used for orthorectification. The following description of events is based on the Investigation Panel's interpretation of the satellite images listed in Table 1 .

TABLE 1 ACQUISITION AND ORTHORECTIFICATION DETAILS OF SATELLITE IMAGES USED IN THE STUDY

Figure No.	Acquisition details				Image details			Orthorectification	
	Date (yyyy-mm-dd)	Time (UTC hh:mm:ss)	Satellite	Source	View angle (°)	Azimuth (°)	Nominal Spatial Resolution (cm)	DEM used	DEM date
B1	2010-05-29	08:22:27	GeoEye1	Google Earth Pro	20.1	Unknown	50	Google Earth	Unknown
B2	2010-11-22 [2011-02-26]	08:48:26	WorldView 2	ESRI World Imagery Wayback	15.5	43.9	50	ESRI	Unknown
B3	2012-10-04	08:30:55	Pléiades 1	GAF	18.9	180.0	50	Copernicus 30m DEM	2011 to 2014
B4	2012-11-25	08:29:44	Pléiades 1	GAF	15.2	180.0	50	Copernicus 30m DEM	2011 to 2014
B5	2014-09-25	08:34:00	Pléiades 1	GAF	6.1	179.9	50	Copernicus 30m DEM	2011 to 2014
B6	2015-08-13		Aerial	CDNGI	Unknown	Unknown	50	CDNGI	Unknown
B7	2016-03-10	08:24:28	WorldView 2	ESRI World Imagery Wayback	12.8	20.1	50	ESRI	Unknown
B8	2017-07-30		Aerial	CDNGI	Unknown	Unknown	25	CDNGI	Unknown
B9	2017-08-13	08:44:22	GeoEye1	Google Earth Pro	29.3	Unknown	50	Google Earth	Unknown
B10	2019-02-04	08:30:16	Pléiades 1	Google Earth Pro	15.3	180.0	50	Google Earth	Unknown
B11	2019-03-22	09:17:11	TripleSat	CGG	7.4	260.4	80	Survey	2019-06-04
B12	2019-05-02	08:43:23	WorldView 2	Google Earth Pro	21.9	52.1	50	Google Earth	Unknown
B13	2019-09-14	08:47:44	SuperView	CGG	0.4	49.6	50	Survey	2019-06-04
B14	2020-01-16	08:54:01	SuperView	CGG	10.4	280.4	50	Survey	2019-06-04
B15	2020-07-09	07:59:10	Jilin1	CGG	5.4	207.4	75	Survey	2020-09-10
B16	2020-08-28	08:37:26	Pléiades 1	Google Earth Pro	22.6	180.0	50	Google Earth	Unknown
B17	2020-09-24	08:23:31	WorldView 2	Google Earth Pro	23.2	8.7	50	Google Earth	Unknown
B18	2021-01-24	08:25:01	WorldView 2	Google Earth Pro	2.4	331.9	50	Google Earth	Unknown
B19	2021-02-17	08:29:08	SuperView	CGG	3.6	284.4	50	Survey	2020-09-10
B20	2022-01-12	07:42:39	Jilin1	CGG	10.7	249.9	50	Survey	2022-04-28
B21	2022-05-24	08:31:10	Pléiades Neo	GAF	12.8	180.0	30	Survey	2022-04-28
B22	2022-07-28	08:30:55	Pléiades Neo	GAF	7.1	179.6	30	Copernicus 30m DEM	2011 to 2014
B23	2022-09-12	06:03:36	SkySat	Planet Labs Inc.	18.1 / 14.4	341 / 111	65	SkySat Stereopair	2022-09-12

Figure No.	Acquisition details				Image details			Orthorectification	
	Date (yyyy-mm-dd)	Time (UTC hh:mm:ss)	Satellite	Source	View angle (°)	Azimuth (°)	Nominal Spatial Resolution (cm)	DEM used	DEM date
B24	2022-09-24	08:28:08	WorldView 2	ESRI World Imagery Wayback	5.8	251.6	50	Unknown	Unknown
B25	2023-03-07	08:07:03	Jilin1	CGG	3.0	216.4	50	Post-failure LIDAR	2022-11-12

Figures B1 and B2 show two images respectively dated 29 May 2010 and 22 November 2010. All the features mentioned in the discussion of the aerial photography (Section 4.1) are still visible in the May 2010 satellite image. The apex of the roughly conical North Dump had been flattened, but the apex of the South Dump, which also had a roughly conical shape, can still be identified. From the two 2010 images it can be seen that the earthworks for the expansion of the De Beers Tailings Dam (now the Jagersfontein Tailings Dam) towards the west commenced in 2010. The November 2010 image shows an access road constructed south of the De Beers Tailings Dam, crossing Dump 10.

The following available image was captured on 4 April 2012 (Figure B3). The figure shows that the starter walls for the western compartment (Compartment 1) of the enlarged dam had been completed. Compartment 1 appears divided into two sub-compartments; a smaller sub-compartment to the north and a larger sub-compartment to the south. For each sub-compartment, deposition from a discharge point on the western wall had commenced. The deposited tailings were already covering nearly the entire footprint of the newly created compartment. The access road crossing Dump 10 is clearly visible. The 25 November 2012 image (Figure B4) is similar, showing evidence of the deposition of more material.

The following available image was captured 22 months later on 25 September 2014 (Figure B5). The western compartment (Compartment 1) was by now entirely submerged under tailings, with only the tops of the trees in the northern part of the compartment remaining uncovered. The walls of Compartment 1 had been significantly widened, with evidence of a large volume of material having been placed along the southern wall. Remining of the North and South Dumps and the southern wall of the De Beers Dam was underway. A conveyor belt had been established from near the northern end of the Dam 10 embankment to the plant along the southern wall of the tailings dam under construction, crossing over Dump 10, presumably to facilitate the reworking of the North and South Dumps. Comparing to the 2012 images (Figures B3 and B4), it appears that at least some of the Dump 10 material to the south of the conveyor had been removed. However, it is evident when comparing Figure B4 and B5 that not all of the material forming Dump 10 was removed prior to construction of the conveyor.

By August 2015 (Figure B6), all tailings were still being deposited in Compartment 1. Activity in the area that would become the eastern expansion of the dam was underway as JD appeared to rework the North and the South Dumps. It can be seen on the image that much of these dumps seems to have been excavated. The extent of the excavation of material along the southern wall of the De Beers Dam was similar to that visible in September 2014 (Figure B5), showing a 'gulley' between the De Beers Dam and what would become the footprint of the new southern wall of Compartment 2. The approximate extent of the southern edge of the South Dump is indicated in Figure B6. At least some of the material forming this part of the South Dump can be seen to have been left in place. The extent of Dump 10 is also indicated.

As indicated in Figure 3, the combined regions comprising the original De Beers Dam and its eastern and southern expansion are referred to as Compartment 2 in discussions below.

By March 2016 (Figure B7) starter walls of the newly constructed eastern expansion of Compartment 2 were in place. Freshly deposited tailings are apparent in two areas of Compartment 2: the north-

eastern corner and the south-eastern corner of the De Beers Dam. It appears that the tailings being deposited in Compartment 2 were deposited from a single deposition point on the west wall of Compartment 1 and then travelled to Compartment 2 by flowing first through a gap in the wall that separated Compartment 1 and the De Beers Dam and then through a second gap on the eastern wall of the De Beers Dam. Figure B7 also shows that a new southern wall for Compartment 2 had been built. The area between this new southern wall and the old De Beers dam appears to have been at least partly infilled with placed (not hydraulically deposited) tailings. Ponded water is present in this area. The toe of the new southern wall crossed the footprint of Dump 10 from east to west. The material comprising the southern extremities of the former South Dump still appear to be in place and their extent is indicated.

Figure B7 also shows a plume of white discharge entering Dam 10, which appears to emanate from the south-eastern corner of Compartment 1, opposite the cross-wall separating Compartments 1 and 2. Similar discharge appears to have been occurring since commissioning of Compartment 1 and can be identified in most images from October 2012 (Figure B3) onwards. The design report for the eastward extension of the dam (Robinson, 2015), discussed in more detail in Section 5, also refers to this seepage, stating "Seepage permanently accumulates in a small shallow basin formed within the remnant mining waste, at a higher elevation than the downstream water dam level. The water is re-cycled from the sump to the process plant. It is uncertain as to whether there is some unique geo-hydrological feature, inadvertently created by past buried activities/infrastructure connecting the slimes dam basin and walls to the sump, or whether this will continue to be the status quo with the west extension."

By July 2017 (Figure B8) the conveyor belt along the southern wall of the dam had been removed. An access ramp giving access to the crest of the southern wall of Compartment 2 had been constructed over the footprint of Dump 10. A considerable amount of deposition had taken place in the new eastern compartment (Compartment 2), also filling the area between the new southern wall of the dam and the old De Beers Dam to the same level with fluid tailings. Tailings still entered the Compartment 2 via two trenches connected to the gap in the wall that separated Compartment 1 and Compartment 2. One trench ran predominantly towards the east while the other trench ran predominantly towards the south (Figure B8). The walls of Compartment 2 had been raised considerably since March 2016 (Figure B7). It appears that a rectangular pond was located immediately to the south of the south-eastern corner of Compartment 2. It also appears that an effluent trench, possibly containing water, was located along the southern part of the eastern wall. A number of haul trucks are visible on the southern wall of Compartment 2 and recently placed heaps of, presumably, coarse tailings are evident along the inside crest edge of the northern and eastern walls of Compartment 2.

An image captured two weeks later in August 2017 (Figure B9) shows similar details as above, but with coarse tailings deposited along the northern wall, north-eastern corner and southern wall of Compartment 2. Dam 10 appeared dry at the time.

A GoogleEarth image from February 2019 (Figure B10) shows the dam to have been raised significantly in the time since the July/August 2017 images (Figures B9 and B10), with the footprint of the walls of Compartment 2 having been widened considerably both to the inside and outside of the dam. This is

particularly noticeable for the eastern wall and south-eastern corner. The access ramp on the southern dam wall had been covered up. Similar changes, but of a lesser extent, are visible along the walls of Compartment 1. The tailings in Compartment 2 had by now entirely covered the De Beers Dam. Deposition in Compartment 2 was still occurring via a gap in the northern part of the wall between Compartments 1 and 2. Figure B10 shows that the road that runs parallel to the southern wall of the dam had an essentially straight alignment. Dam 10 was virtually empty.

Figure B10 (February 2019) indicates the alignment of the south edge of the access road along the southern wall of the dam. To keep track of the evolution of the southern edge of the road, all subsequent figures in Appendix B show this alignment, as well as a second line parallel to the February 2019 alignment and tangent to the southern edge of the road.

Figure B11 presents an image dated 22 March 2019. The image is somewhat obscured by thin cloud cover. Dam 10 had filled with water since the previous image, taken about six weeks earlier. A slight curve towards the south is visible in the alignment of the access road along the southern wall of the tailings dam where the road passes to the north of Dam 10. An arc-shaped feature is visible on the southern wall crest of Compartment 2 that was not identified on the GoogleEarth image of 4 February 2019. An examination of PlanetScope Imagery (Appendix C) available around the same time shows no evidence of such a feature until 7 February 2019 when a dark patch appeared where the arch shape feature formed (Appendix C, Figure 1 (top)). It is presumed that this feature might have been the results of fresh coarse tailings being dumped as part of wall building operations. However, in the two months that followed, this feature seemed to evolve into what resembles a rear scarp of a slip surface (see Appendix C, Figures 3 to 6a).

The alignment of the southern access road along the downstream toe of the dam was perfectly straight at the beginning of February 2019. Dam 10 filled with water from nearly completely empty during the ten days after 7 February 2019. First signs of possible movement of the wall towards the south is evident in PlanetScope images from 16 to 18 February 2019. Over the following months substantial activity was evident along the southern wall of Compartment 2 and it is evident that further movement and signs of slip failures and slope instability were occurring along the said section of wall. Of particular significance are the dates of 26 to 28 February 2019, 7 to 10 March 2019 and 13 to 17 March 2019 (see PlanetScope images in Appendix C). From 7 March 2019 until the end of March 2019 a large amount of movement was evident, clearly causing the alignment of the access road along the downstream southern wall of the dam to deviate significantly towards the south.

PlanetScope imagery shows that during the course of April 2019, a buttress appears to have been constructed at mid-height (not at the toe) along the slope of the southern wall of Compartment 2, advancing from west towards the east. When the buttress approached the south-eastern corner of Compartment 2 on 28 April 2019, significant movement was evident along the southern wall east of Dam 10 in PlanetScope images. Continued movement was evident until the end of May 2019. A considerable amount of wall building activity was evident at the same time on the southern wall, raising its crest.

Examining a GoogleEarth image dated 2 May 2019 (Figure B12) reveals signs of slope instability at the south-eastern corner of the dam. An enlargement of the relevant part of the dam wall is presented

in Figure 5. Measured at the crest, the length of wall affected by apparent instability amounted to approximately 100 m, widening to more than 150 m at the toe. The toe at the south-eastern corner was displaced outwards, bounded to the east and west by what appears to be steps or cracks, giving rise to apparent elevation differences between the affected area and the adjacent part of the slopes not affected by the movement. Signs of bulging were evident at the toe of the wall in this area. In addition, a linear feature identified on the 4 February 2019 image appears to have undergone substantial non-uniform displacement by 2 May 2019 as indicated in Figure 5.

It is noted that no construction activity could be observed on images following Feb 2019 when signs of instability appeared that indicate an effort to stabilise or arrest movement at the southern toe of the tailings dam. Instead, material continued to be placed on the crest and mid-slope on the southern slope of the dam embankment. The placement of weight to stabilise a slope is considered in Section 7.2.6.

The next high resolution satellite image is dated 14 September 2019 (Figure B13). It shows the footprint of the southern wall of Compartment 2 having expanded significant towards Dam 10 as indicated by the southward shift of the southern access road. It shows a similar expansion in the south-eastern corner of the tailings dam. No other expansion of the footprint of the dam is evident between May and September 2019, except for some material having been placed along a portion of the northern toe of Compartment 2. The expansion in the south does not appear to be due to material placement, but due to movement of the toe and material downstream of it, except perhaps in the south-eastern-most corner.

FIGURE 5 SOUTH-EASTERN CORNER OF THE JAGERSFONTEIN TAILINGS DAM FROM THE 2 MAY 2019 GOOGLE EARTH IMAGE SHOWING SIGNS OF INSTABILITY.

By September 2019 the alignment of the access road along the toe of the southern wall of Compartment 2 had become visibly more curved compared to six months prior (compare Figure B11 and B13). It is also evident that material between the access road and Dam 10 had begun to encroach

into Dam 10. Dam 10 had emptied significantly compared to six months prior (compare Figure B11 and B13), most probably as this was the end of the dry season. Movement of material along the southern toe of the tailings dam into Dam 10 had taken place since the previous image, partly burying a dark feature (probably vegetation – see 4 February 2019 image (B10)) visible in the north-eastern corner of Dam 10.

The next high-resolution satellite image is dated 16 January 2020 (Figure B14). Some footprint expansion is evident along the north-eastern toe of Compartment 2, in the southwestern corner of Compartment 1, with some construction activity evident in the south-eastern corner of Compartment 2 to the east of the Dam 10 dam embankment. Additional movement of the access road along the southern toe of the dam is not evident since the September 2019 image (Figure B13).

An unusual feature visible in Figure B14 is a donut-shaped embankment constructed inside the pool against the upstream face of the southern wall of Compartment 2. Examination of the PlanetScope images available for this period revealed that construction of the feature commenced around 18 September 2019 and that the ring was completed by 20 October 2019. The feature remained visible in images up to July 2020 by which time it was covered by tailings as deposition continued.

Without being allowed access to JD employees, the Investigation Panel can only speculate as to the reason for this feature, but it is consistent with measures that may have been taken in an attempt to isolate piping or a sinkhole that may have appeared in the affected area. A photogrammetry survey dated 6 November 2019 indicates that the depth of the depression, closed off by the circular embankment, amounted to approximately 6.4 m below the surrounding tailings surface (see cross-section presented in Figure 6).

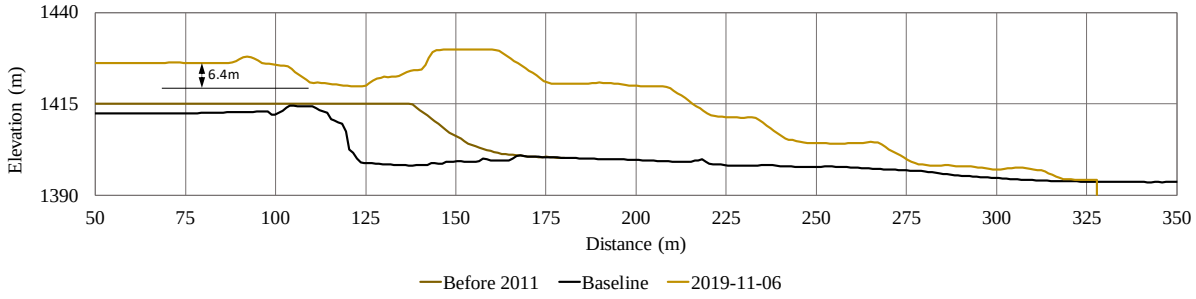

FIGURE 6 NORTH-SOUTH CROSS-SECTION FROM THE PHOTOGRAMMETRY SURVEY DATED 6 NOVEMBER 2019 THROUGH THE DONUT-SHAPED FEATURE.

Figure B15 presents an image dated 9 July 2020. Comparing this image to that of 16 January 2020 (Figure B14) demonstrates a large amount of movement along the toe of the southern wall of Compartment 2 towards Dam 10 (the south) (17.5 m scaled). The water level in Dam 10 rose substantially during this time, but despite this, the shoreline of Dam 10 moved substantially to the south, indicating large ground movements into the dam basin of Dam 10. The alignment of the southern wall access road bulged towards the south by many metres compared to its original alignment. Signs of material bulging at the toe of the tailings dam are also visible to the east of the Dam 10 embankment. The remnant of the donut-shaped embankment that was first identified in Figure B14 is still visible in Figure B15.

A large volume of material seems to have been placed on the southern wall of Compartment 2 since the January 2020 image (Figure B14) as the downstream toe of the tailings dam wall moved to the south, while the upstream water line remained approximately stationary. The berms on the southern wall were widened significantly. No significant signs of footprint expansion were evident elsewhere on the tailings dam since January 2020.

Examining PlanetScope Images indicate considerable movement of the tailings dam southern wall into Dam 10 over the course of February to May 2020 as more weight was placed on the slopes by widening of the berms and raising of the tailings dam wall crest. Movements then appeared to stabilise for some time.

Similiary, PlanetScope images show a continued and gradual migration of the toe of the southern wall of Compartment 2 towards Dam 10 from Aug 2020 (Figure B16) to the end of Feb 2021 (Figure B19). The berms continued to be widened and the dam crest raised along the Compartment 2 southern wall during this time. To the east of the Dam 10 embankment, movement is evident in the corner between the Dam 10 embankment and tailings dam toe.

Two high resolution GoogleEarth images, taken approximately a month apart, respectively dated 20 August 2020 (Figure B16) and 24 September 2020 (Figure B17), are available within the above-mentioned period. Again, when comparing against the previous GoogleEarth image of May 2019 (Figure B12), substantial movement of the toe of the southern wall of Compartment 2 into Dam 10 is evident, resulting in increasing curvature in the alignment of the southern access road. Examination of the southern wall of Compartment 2 in the September 2020 (Figure B17) image reveals two features resembling cracks. These features are indicated in Figure B17 by red lines. Enlargements of the cracks are presented in Figure 7.

The eastern feature seems to be accompanied with a step across the middle berm and upper slope of the tailings dam, suggesting subsidence of the wall to the west of the feature. What appears to be the same feature can also be seen in the GoogleEarth image of 2 May 2019 (Figure B12). It seems that the feature formed the eastern boundary of the previously discussed instability that affected the south-eastern corner of the tailings dam (as discussed previously).

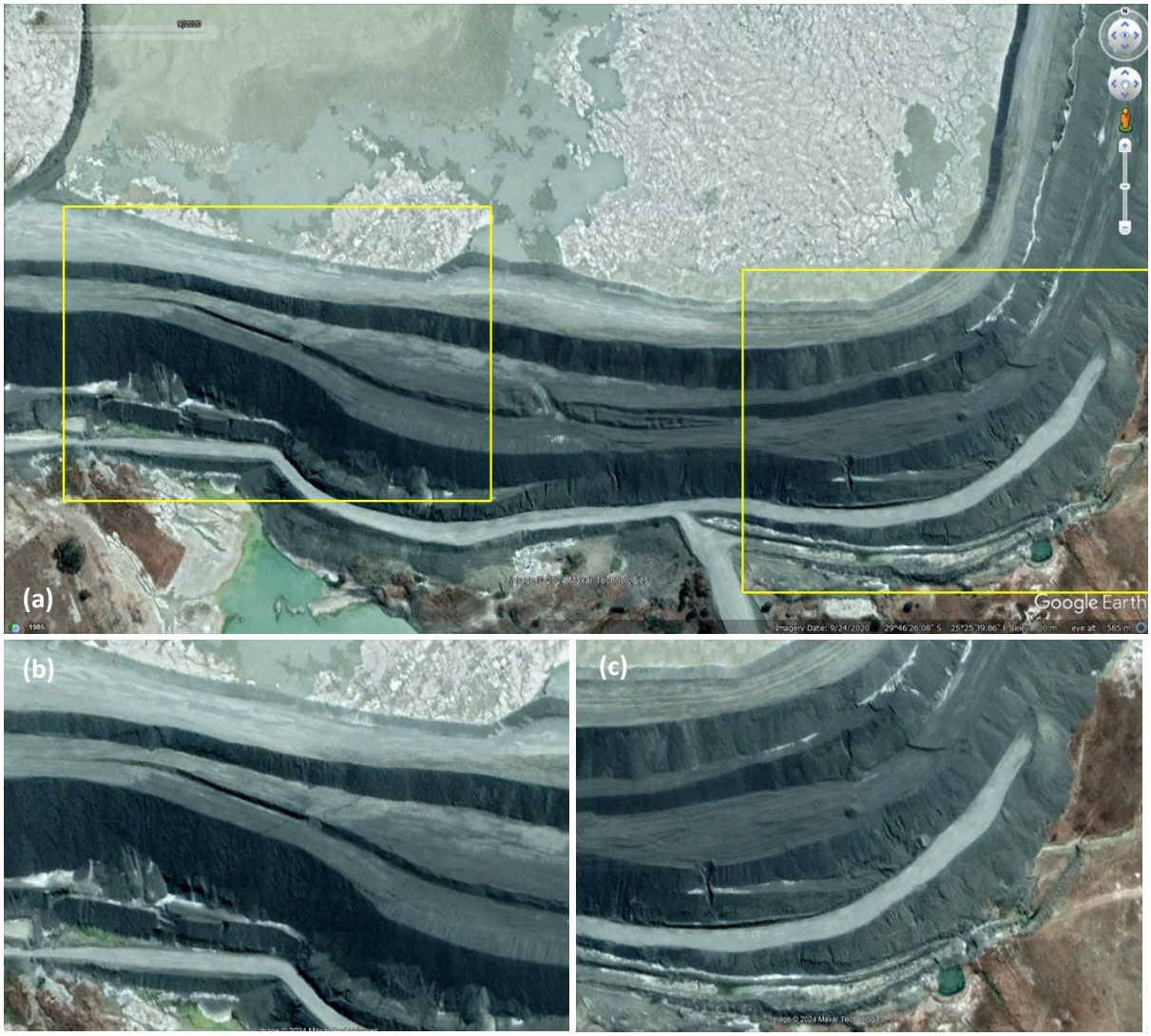

FIGURE 7 (A) CRACKS VISIBLE ON THE SOUTHERN WALL FROM THE GOOGLE EARTH SATELLITE IMAGE DATED 2020/9/24; (B) WESTERN CRACK ENLARGED; (C) AND EASTERN CRACK ENLARGED.

The western feature seemed to be less severe but is also indicative of movement within the dam wall. Figure B17 was captured by the WorldView2 satellite which has a resolution of approximately 50 cm. Accordingly, it is estimate that the cracks must have had a thickness of at least half a pixel (i.e. 25 cm) to be clearly detectable.

Comparison of the satellite image from September 2020 (Figure B17) to the images captured in January and February 2021 (Figures B18 and B19) shows a large amount of movement towards the south as evident from the alignment of the access road along the southern wall of Compartment 2 (14 m scaled). Further movement is also evident in the corner between the Dam 10 embankment and tailings dam toe to the east of the Dam 10 embankment. Figures B18 and B19 also show that the division wall between Compartments 1 and 2 was beginning to be submerged by tailings slurry.

Fast forward approximately one year, Figure B20 shows a high-resolution image dated 12 January 2022. In this image the partition wall between the two compartments had been

completely submerged by tailings slurry and the entire Compartment 2 covered by tailings slurry and water. Compartment 1 is also largely covered by water and/or tailings, with some patches of vegetation growth still visible. The inside or upstream side of Compartment 2's southern wall crest had been straightened compared to a year prior, which would have involved placement of a large volume of coarse tailings (grit) on soft tailings along the edge of the pond. A large amount of movement to the south is again evident along the toe of the southern wall of Compartment 2 into the Dam 10 basin (10m scaled since February 2021) and to the east of Dam 10, while similar movement is not evident elsewhere on the tailings dam.

Figure B23 presents a satellite image captured on the morning of 12 September 2022, the day after the failure. The image shows essentially three major failure scars, i.e. the largest scar where the tailings dam breached opposite the Dam 10 embankment (Scar 2), as well as an eastern (Scar 3) and western scar (Scar 1) consistent with the locations where cracks were observed in the September 2020 Google Earth image (indicated in red). It is noted that Scar 1 exits the dam at the location where long-term seepage was mentioned to have been occurring by Robinson (2015) since shortly after commissioning of Compartment 1 (discussed in the overview of the March 2016 image). Comparing the post-failure to the last pre-failure images indicates that the part of the embankment bounded by the main failure and the western scar (Scar 1) displaced largely intact by approximately 19 m (scaled from image) to the south-southwest (at, on average, approximately 22° west of south). Similar movement, but of a lesser extent, is evident for the part of the wall between the main failure and the eastern scar (Scar 3). The failure resulted in the uncontrolled discharge of virtually all tailings slurry and water in Compartment 2 that were deposited after 2010, i.e., tailings that were not part of the De Beers dam. Additionally, the tailings slurry in Compartment 1 lying above the crest of the partition wall between Compartments 1 and 2 were also discharged. The partition wall between the compartments remained largely intact. The discharge of tailing resulted in the old De Beers Dam becoming exposed. Figures B24 to B25 show additional post-failure high-resolution satellite images captured in September 2022 and March 2023 respectively.

Figure 9a shows the last pre-failure satellite image from 28 July 2022 and highlights points that are also identifiable in a post-failure satellite image from 7 March 2023 which is shown in Figure 8b. Tracking these points enabled the estimation of the displacement vectors shown in Figure 8b. The reason for not using an earlier post-failure image of September 2022 (Figures B23 and B24) is that their resolution was not as good as that of the March 2023 image. This reduced resolution made identification of features difficult. Additionally, there was uncertainty regarding the digital elevation model used for the orthorectification of the image from 24 September 2022. Vector lengths are indicated in some cases. These lengths are approximate due to inaccuracies associated with scaling and orthorectification of the images. Additionally, since the post-failure image (Figure 8b) was captured on March 2023, and not immediately after the failure, the vectors may overestimate the real displacement if post-failure movement took place before March 2023. Indeed, a somewhat smaller movement of approximately 14 m is suggested by pre- and post-survey data (see Section 6.7).

Also shown in Figure 8 is the alignment (in plan) of the cross-section profile that was studied in the stability assessment that follows in Section 7.2. The cross-section was chosen to be parallel to the predominant direction of the displacement vectors and to pass approximately through the centre of the block that displaced towards the south-southwest during the failure.

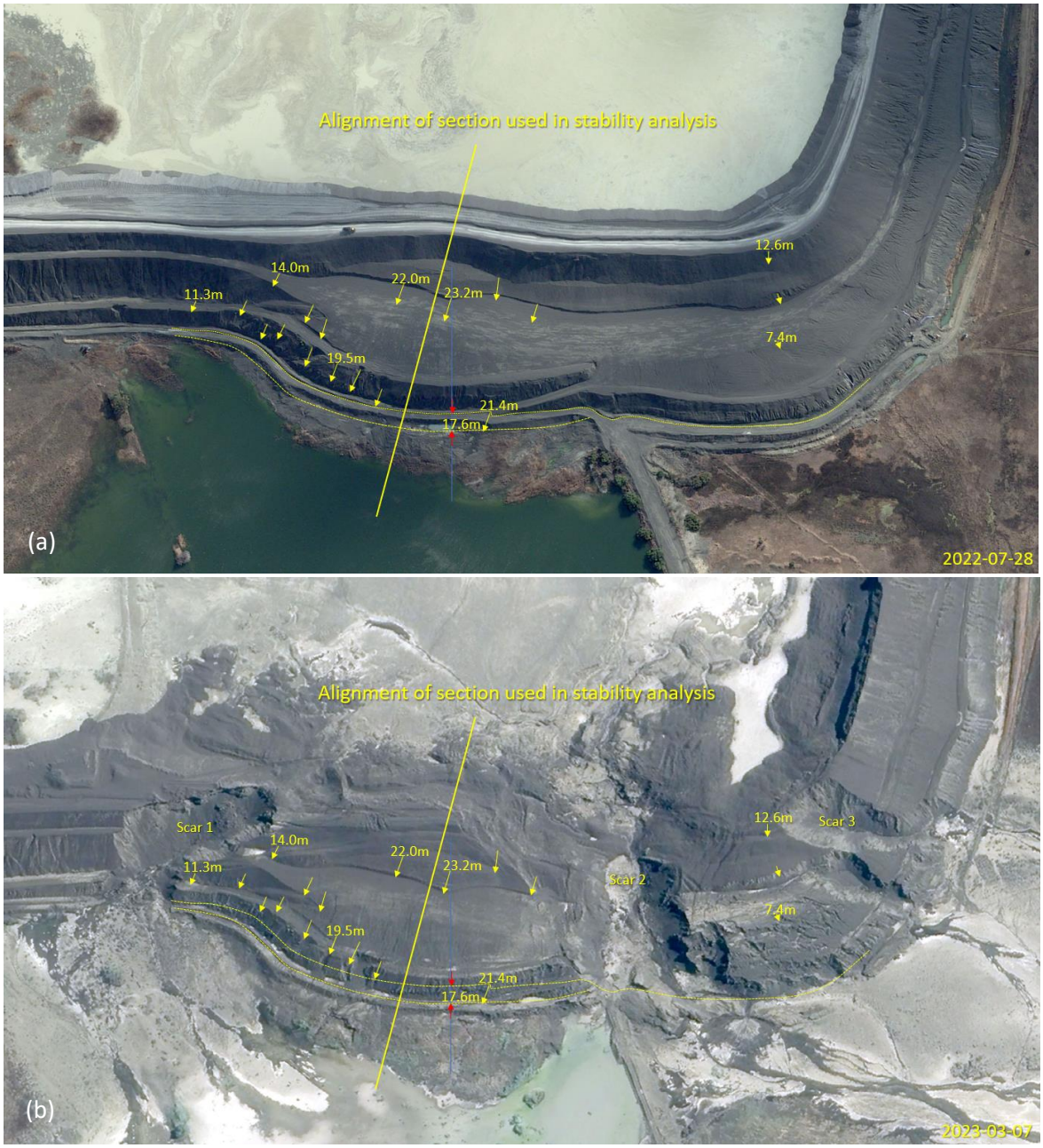

FIGURE 8 **DISPLACEMENT VECTORS ASSOCIATED WITH THE FAILURE EVENT AND THE ALIGNMENT FOR THE CRITICAL CROSS-SECTION STUDIED FOR STABILITY ASSESSMENT SHOWING (A) THE LATEST AVAILABLE PRE-FAILURE HIGH RESOLUTION SATELLITE IMAGE AND (B) THE EARLIEST AVAILABLE POST-FAILURE HIGH RESOLUTION IMAGE.**

4.3. Additional information from the literature

Rivet & Nishiyama (2023) used a range of ortho-rectified satellite images (Keyhole, Landsat, Sentinel-2 and WorldView) to investigate displacements of the Jagersfontein Dam post failure. They identified a horizontal southward movement of 6 m of features such as the access road along the toe of the southern wall of Compartment 2 from 24 September 2020 to 24 January 2021. A maximum horizontal error of 2 m is quoted. An additional 2 m movement is reported for the period from 24 January 2021 to 9 February 2021 and a further 35 m between 9 February 2021 (pre failure) and 28 September 2022 (post failure). In addition, Perdikou & Lees (2023) presented the results of a an InSAR study which identified some movement along the crest of the tailings dam over a number of years preceding the

failure in the vicinity where the dam failed (magnitude not mentioned). In agreement with the analysis presented herein, these studies identified the large displacements that the southern wall Compartment 2 underwent during the months and years before its failure. Additionally, Torres-Cruz & O'Donovan (2023) used satellite imagery to investigate the construction sequence of the Jagersfontein Dam and the immediate consequences of failure. Collectively, these studies highlight the advantages of modern space-based technologies for tailings dam surveillance.

4.4. Discussion of observations from aerial and satellite images

The study of old aerial photos and satellite images confirmed that the De Beers Tailings Dam has been dormant between 1973 and 2010. In 2010 work on the expansion of the dam commenced. The operation of the dam involved raising containment walls to provide a reservoir into which tailings slurry were pumped via, as far as could be determined, a single discharge point in the western wall of Compartment 1. The dam was not equipped with any return water facility and the only means for water to leave the dam was by means of evaporation and seepage through the walls or infiltration into the native ground. Evidence of large-scale seepage emerging from the dam was not evident from information available to the Investigation Panel, with the exception of seepage from the south-eastern corner of Compartment 1, visible in satellite images from the end of 2012 (Figure B3 onward) and reported in the design report for Compartment 2 (Robinson, 2015). The dam was operated with a large pool or pond, usually extending right up against the inside slopes of the containment walls constructed from coarse tailings. Therefore, no well-developed beach was allowed to form against the upstream slopes of the outer walls as is normally the case with tailings dams.

From the record of satellite images studied it appears that the raising of the containment walls and deposition of tailings slurry within proceeded without identifiable incidents until February 2019. During the course of February 2019, a large amount of southward movement is evident along the southern wall of Compartment 2, particularly just north of the Dam 10 basin. As the water level in Dam 10 varied over time, the movement is best illustrated by changes in the alignment of the southern access road, along the toe of the tailings dam, rather than observing the Dam 10 water line. The access road was a straight road at the beginning of February 2019. The southern road's edge of the access road had displaced southward by approximately 18 m by 22 March 2019 (based on scaling from the satellite image dated 22 March 2019 and taking the 4 February 2019 image as baseline). Satellite images show how, from March 2019, displacement of the access road continued to take place until the failure of the tailings dam on 11 September 2022.

The alignment of the southern edge of the southern access road, as well as the alignment of the upstream water line as the tailings dam was raised, traced from satellite images between February 2019 and July 2022 (Figures B10 to B22), are presented in Figure 9. Over this time, the toe of the tailings dam was displaced by more than 80 m to the south opposite the Dam 10 wall and basin, while minimal movement was evident along the section of the wall to the west of the old De Beers Dam, the separation dividing Compartments 1 and 2 of the tailings dam. The increasing spacing between successive waterlines indicates an acceleration in the northward widening of the crest, which is the crest that failed to the inside of the dam on the morning of 11 September 2022 (Chapter 7). The two most recent pre-failure images are from May and July 2022 (Figures B21 and B22) and suggest large

amounts of water and slurry slurry in the dam. The most recent of these pre-failure images (Figure B22) was captured just over six weeks before the failure on 28 July 2022.

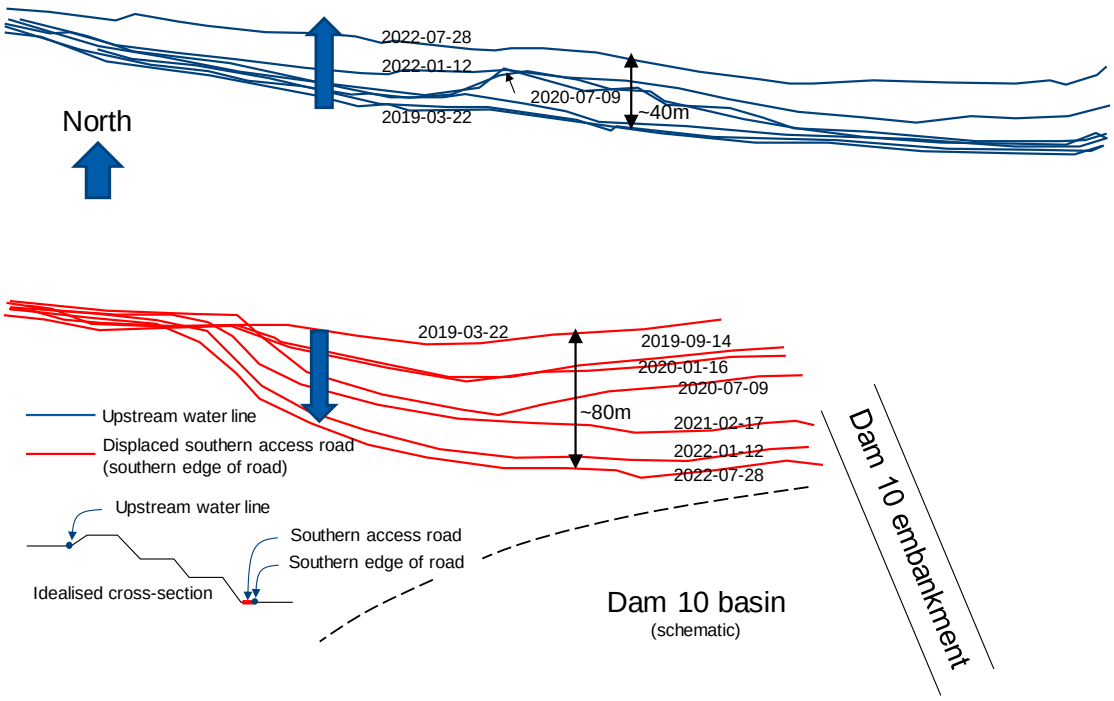

FIGURE 9 EVOLUTION OF UPSTREAM WATER LINE AND ROAD'S EDGE AT SOUTHERN TOE AT BREACH LOCATION FROM FEBRUARY 2019 TO JULY 2022 SEEN IN PLAN.

Figure 10 presents the development over time of the distance between the original alignment of the southern edge of the southern access road and a line parallel to the original alignment and tangent to the southern edge of the access road. Very large displacement occurred during February and March 2019 and displacement then continued at a very high rate of, on average, 79 mm per day over the remainder of 2019 until early 2021. The rate of movement then appeared to have slowed down to an average of 27 mm per day until failure. The displacement of 35 m observed by Rivet & Nishiyama (2023) between the dates of 09 February 2021 (pre-failure) and 28 September2022 (post-failure) is indicated in Figure 10 and is in close agreement with the observations presented as determined by the Investigation Panel.

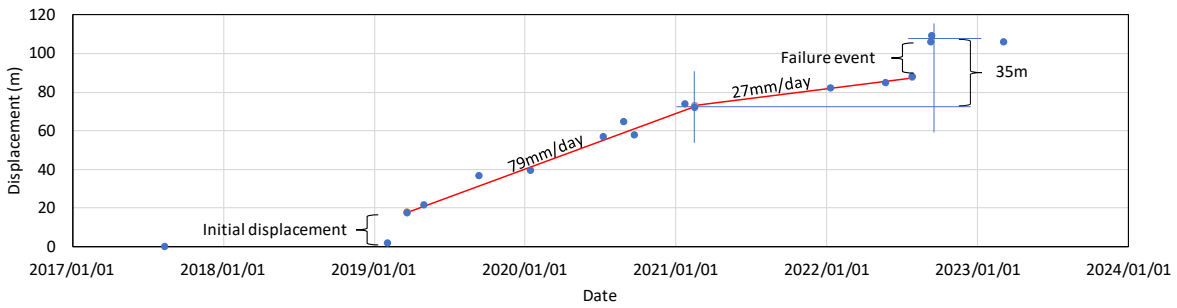

FIGURE 10 DISPLACEMENT OF SOUTHERN EDGE OF ACCESS ROAD OVER TIME.

In addition to changes in the alignment of the southern access road, it is interesting to observe trees or shrubs in the south-eastern corner between the Dam 10 embankment and the tailings dam. Between 9 July 2020 and 28 July 2022 (Figures B15 to B22), a tree or large shrub, tracked in Figure 11, was displaced from the toe of the Dam 10 embankment by approximately 28 m towards the southeast. This occurred due to substantial ground movement. The fact that the tree remained green suggests that it was moved with at least some of its roots intact, suggesting deep-seated movement. Given this magnitude of movement, it is believed that the Dam 10 embankment must have required substantial maintenance to maintain its ability to hold water and structural integrity.

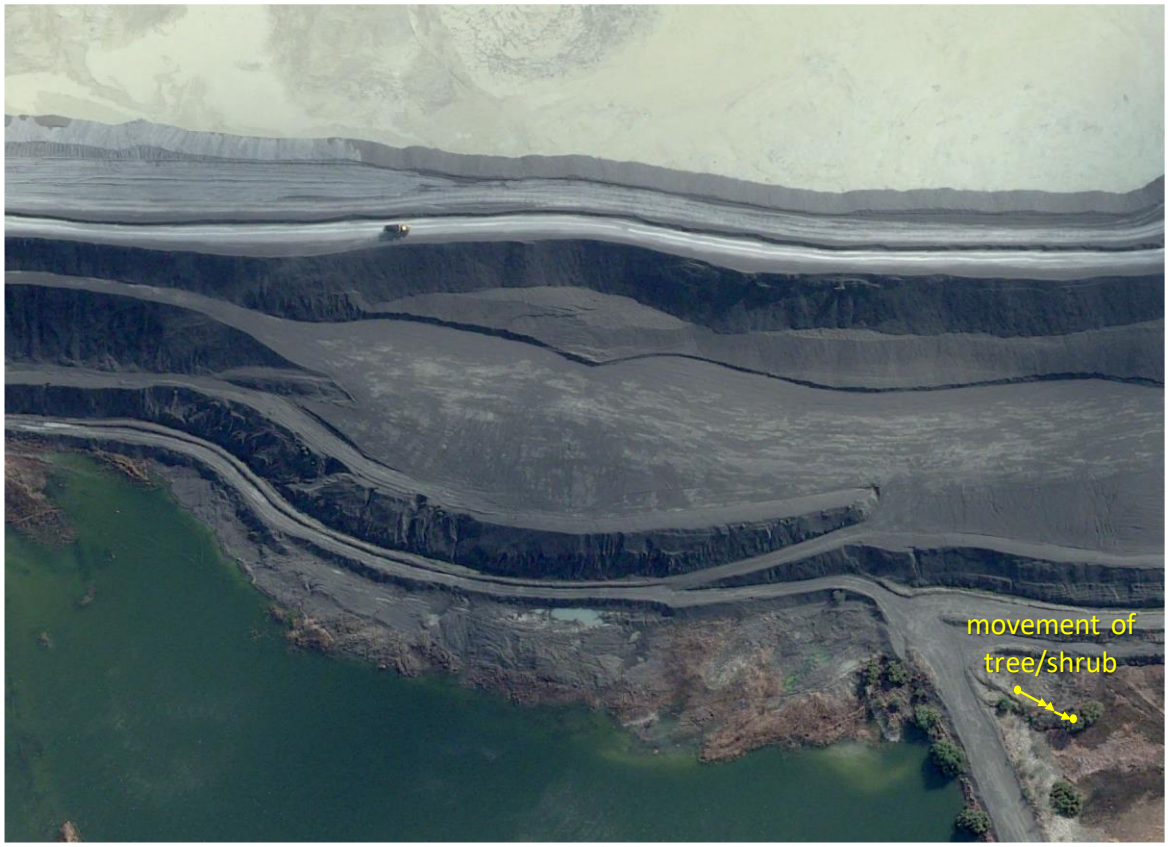

FIGURE 11 "THE WANDERING TREE": MOVEMENT OF A TREE OR LARGE SHRUB TRACKED NEAR THE NORTHERN END OF THE DAM 10 EMBANKMENT FROM SATELLITE IMAGES DATED 9 JULY 2020 TO 28 JULY 2022 (FIGURES B15 TO B22) (TOTAL EXTENT OF MOVEMENT WAS 28 M).

In addition, Figure 12 presents the displacement of a feature (probably a rock or shrub), originally located to the south of the access road along the toe of the tailings dam, tracked on satellite images from 22 March 2019 to 7 March 2023 (Figures B11 to B24). The displacement is plotted against time in Figure 13. The movement is in close agreement with the displacement of the access road.

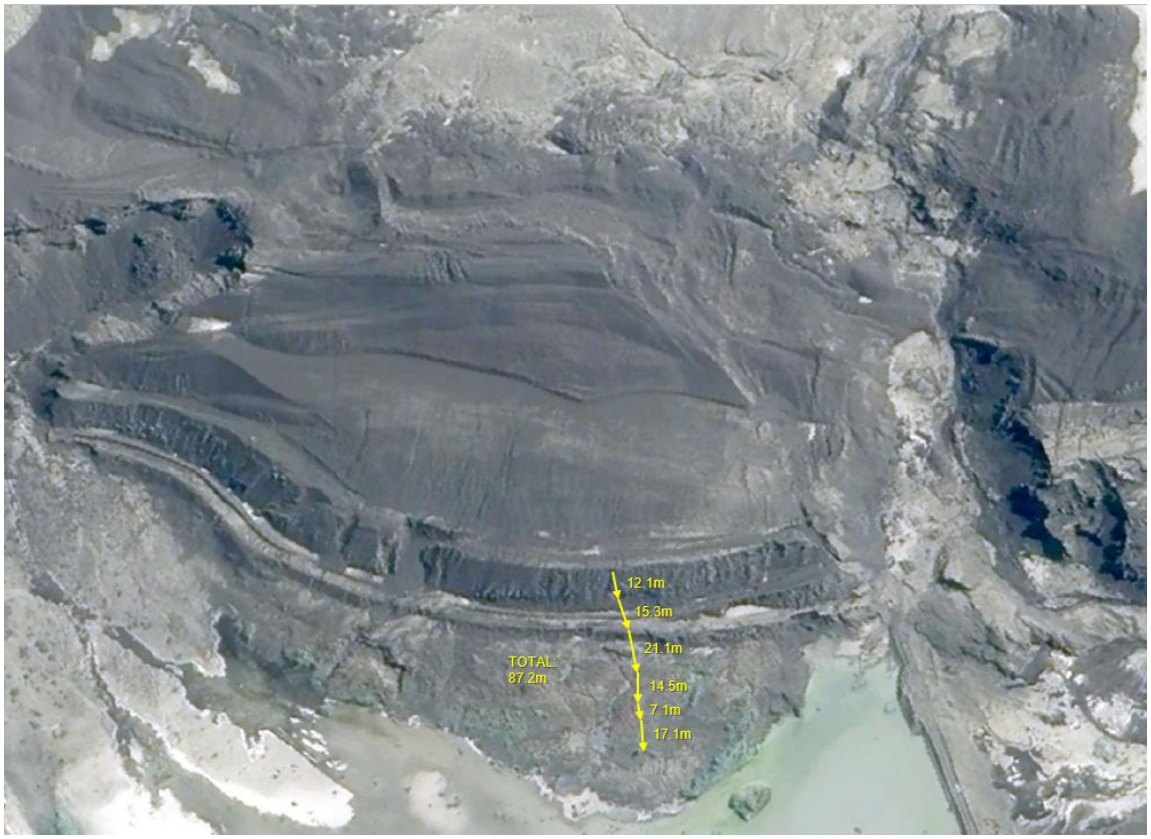

FIGURE 12 IDENTIFIABLE FEATURE TRACKED USING SATELLITE IMAGES FROM 22 MARCH 2019 TO 7 MARCH 2023 (FIGURES B11 TO B24), SHOWING DISPLACEMENT AT THE TOE OF THE DAM WALL AMOUNTING TO 87 M.

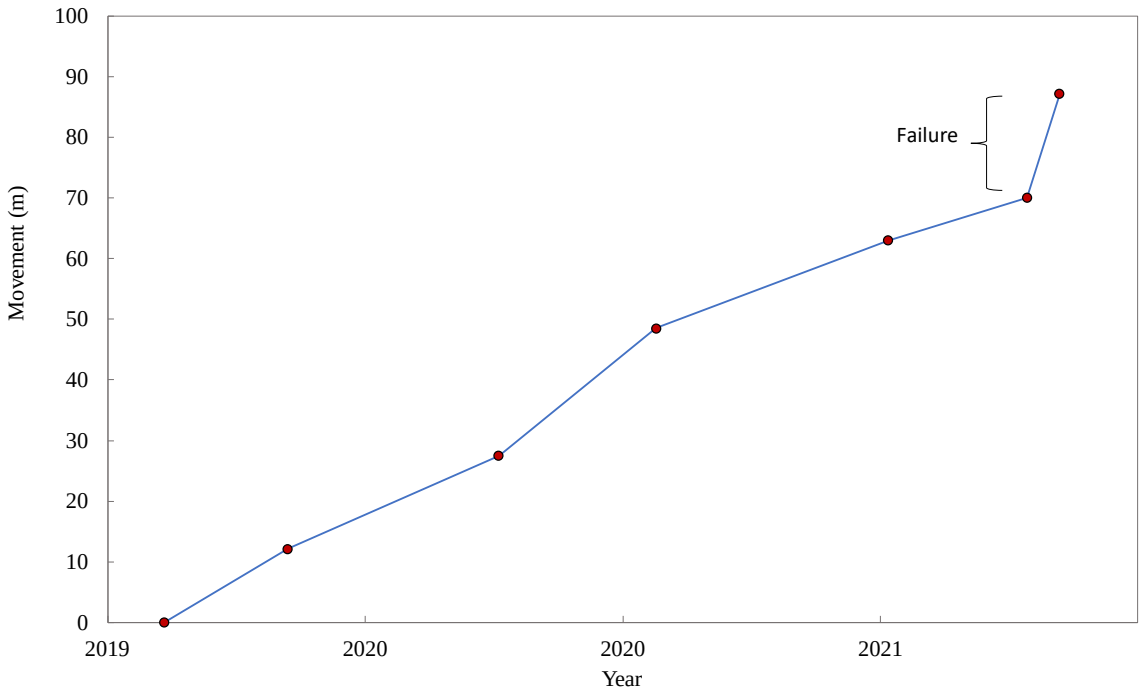

FIGURE 13 DISPLACEMENT WITH TIME OF THE FEATURE TRACKED IN FIGURE 12 (RECORDED FROM 22 MARCH 2019).

The displacement presented in Figure 10 is compared to the cumulative rainfall occurring from 2017 until the end of 2023 in Figure 14(a) and against the actual rainfall over this period in Figure 14(b). The Mean Annual Precipitation (MAP) of the Jagersfontein area of 407 mm is indicated, as well as the annual rainfall figures for each of the years presented. The years 2020 to 2022 were significantly wetter than the average, and resulted in Dam 10 at the toe of the tailings dam, holding water, starting from Feb 2019 until the time of the failure based on the available satellite imagery. The last rainfall event preceding the failure amounted to 30 mm occurring on 23 June 2022.

Figure 15 presents the rainfall record for February 2019, the month in which the first signs of instability were observed. PlanetScope images show Dam 10 to be empty at the beginning of February 2019. Dam 10 then received water from the rainfall in the first half of February 2019 and was never empty again until failure of the tailings dam. Water in Dam 10 would have contributed to an elevated water table at the toe of the tailings dam which would have reduced pore water suction and which is not beneficial to slope stability. A correlation between the observed movement at the toe of the dam wall and rainfall is not obvious.

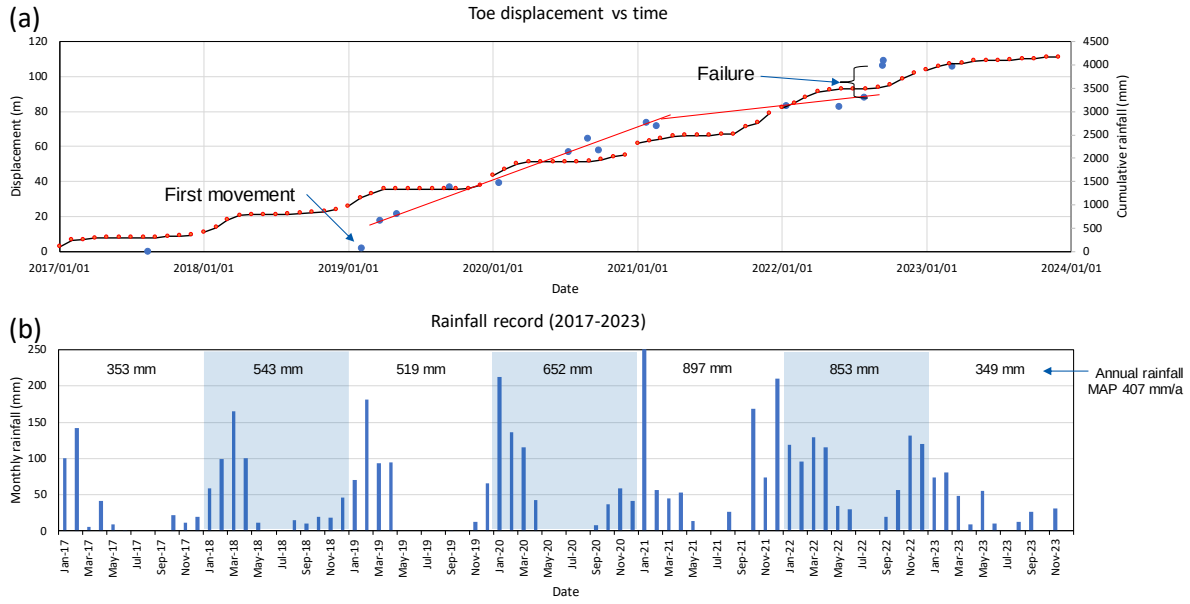

FIGURE 14 (A) COMPARING TOE DISPLACEMENT AND CUMULATIVE RAINFALL AND (B) ACTUAL RAINFALL (SOURCE FOR RAINFALL DATA: JAGERSFONTEIN DEVELOPMENTS).

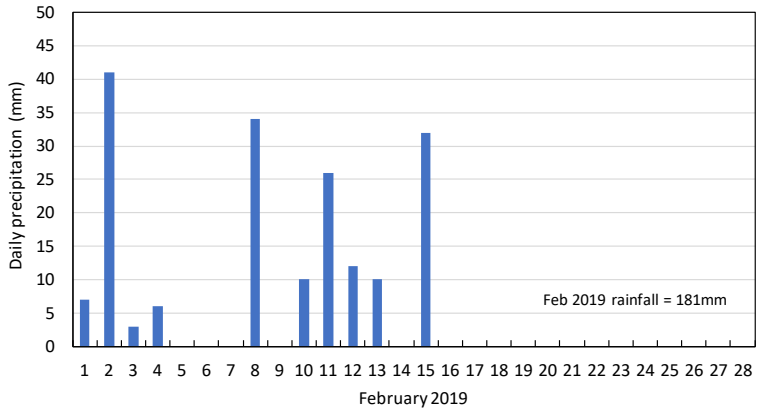

FIGURE 15 JAGERSFONTEIN RAINFALL RECORD FOR FEBRUARY 2019 (SOURCE: JAGERSFONTEIN DEVELOPMENTS).

Since the first signs of instability in February 2019 construction activity seemed to be much more prolific along the southern wall of Compartment 2 than anywhere else on the tailings dam. The tailings dam embankment or outer wall in this area was also significantly wider than elsewhere. This may partly reflect the fact that the tailings dam wall was at its highest in this location, but more significantly, a consequence of work which appeared to have been carried out to attempt to stabilise the dam wall where movement was taking place on a near-continuous basis.

4.5. Observations regarding Dam 10

An earth dam immediately to the south of the old De Beers Dam is evident in the first aerial photo available of the area, dating from 1944. This dam, locally known as Dam 10, is a clean water dam and does not normally receive water from the JD's operations, except perhaps when there was seepage occurring from the tailings dam as evident in the March 2016 satellite image (Figure B7) and others.

A safety inspection of Dam 10 was carried out in December 2021 (Jacobsz, 2021), nine months before the failure of the tailings dam. The dam safety inspection report includes a long-section survey of the Dam 10 embankment and showed the crest elevation of the Dam 10 wall to rise gradually, by approximately 3 m, from the mean crest level over a distance of approximately 150 m towards the tailings dam (see Figure 16). This is unusual because dam wall crests are normally constructed level. One possible explanation for this could be the construction of an access ramp by JD, linking up with the access roads along the southern wall of the tailings dam. However, given the large amount of displacement of the southern wall of the tailings dam towards the south, it seems plausible that the Dam 10 embankment acted like a prop, providing a buttressing action against the southward moving tailings dam wall. The upward heaving along the northern part of the Dam 10 embankment might have been as resulted of the large southward displacement of the toe of the tailings dam. As movement occurred both to the west and east of the Dam 10 embankment, forcing the Dam 10 embankment to thrust against the moving wall, it is perhaps not a coincidence that the main breach developed immediately adjacent to the Dam 10 embankment.

The presence of Dam 10 immediately to the south of the tailings dam provided a source of water which would have kept at least some of the material, which had been subjected to near-continuous displacement for three-and-a-half years leading up to the failure, saturated. The presence of water means that pore water suction could not develop and saturated conditions means that undrained conditions were possible at the tailings dam toe.

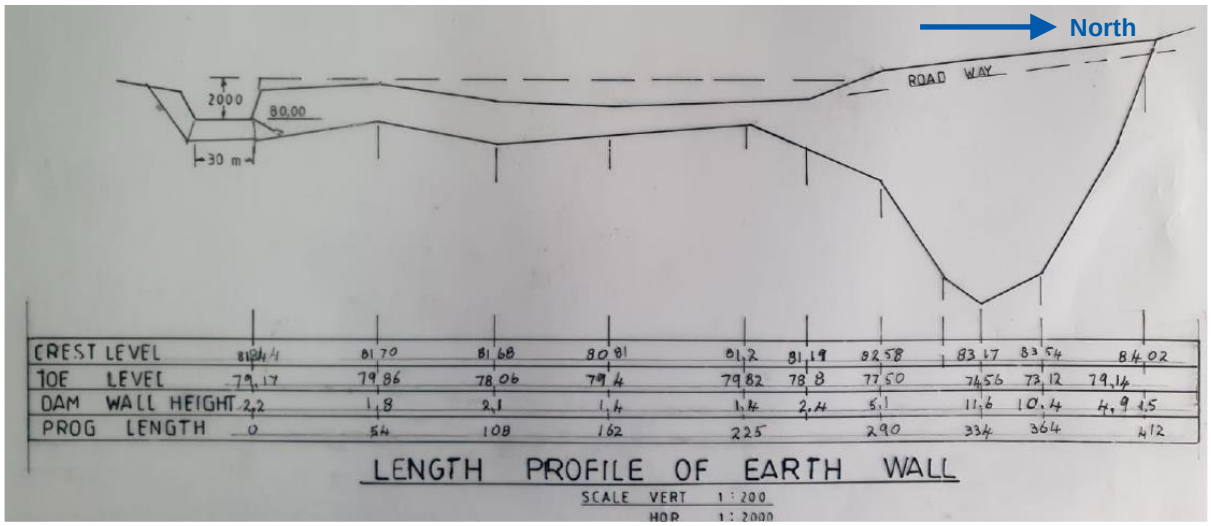

FIGURE 16 LONG-SECTION ALONG THE DAM 10 EMBANKMENT (LOOKING WEST) SHOWING THE CREST RISING TOWARDS THE TAILINGS DAM – DEC 2021 DAM SAFETY INSPECTION CREST SURVEY (JACOBSZ, 2021).

5. Design for the eastward extension of the tailings dam

The design for the eastward extension of the Jagersfontein Tailings Dam, i.e. the construction of Compartment 2 (refer to Figure 3), is presented by Robinson (2015). Elements of the design are repeated here and later referred to when evaluating the pre-failure geometry of the JD tailings dam (Section 6).

5.1. General design overview

The design report indicates that the JD tailings dump remining process produced coarse tailings, termed "grits" and fine tailings termed "slimes" in a ratio 55:45 (grits : slimes). Typical particle size distributions provided in the design report are presented in Appendix E (Figures 6). The grits were disposed of dry (mechanically) and the latter wet (hydraulically). Robinson's report refers to the "existing second-generation disposal facility between the De Beers Dam and the plant", which is referred to as Compartment 1 in this report on the failure investigation. The coarse grits were used for the construction of containment walls that hold the fine tailings (slimes). At the time of drafting the design report, the tailing level in Compartment 1 was beginning to approach the elevation of the De Beers Dam and new storage capacity was therefore required. The design of the eastward extension of the facility is applicable to the section of the tailings dam wall that failed on 11 September 2022. A conceptual design for the extension of the tailings dam is presented by Robinson (2014) and a conceptual design for a final tailings dam by Robinson (2016).

The layout of the extended tailings dam is presented in Figure 17, showing the proposed new wall for Compartment 2 in red. This corresponds relatively closely to what was eventually constructed. The design allowed for the removal (for reprocessing) of the coarse walls of the of the De Beers Dam and coarse dumps (presumably the North- and South Dumps identify in Figure A1) which would provide additional capacity. The plan was to develop the extended tailings dam on land already impacted by previous deposition which would serve to minimise the impact on ground water and further surface contamination. The report recognised that the very fine Kimberlite clay had insufficient strength to allow a self-supporting tailings dam and therefore advocated the construction of impoundment walls using the coarse grits to contain the slimes, similar to Compartment 1 which existed at the time. The design advocated for the use of dry fine tailings from the De Beers Dam (shown in orange in Figure 17) in combination with grits, the latter to provide strength for the construction of the new walls. It is presumed that the use of fine tailings was considered to make up the shortfall in terms of the availability of grits.

The report explicitly states: "The extended footprint remains on top of old tailings and is hence an impacted area already – or could even be considered to be part of the tailings footprint" [underlining added herein for emphasis for selected quotes]. Two important objectives stated in the design report with the design of the dam were "1. Remain within the bounds of the already impacted tailings area, and 2. Ensure drainage around the toe of the wall."

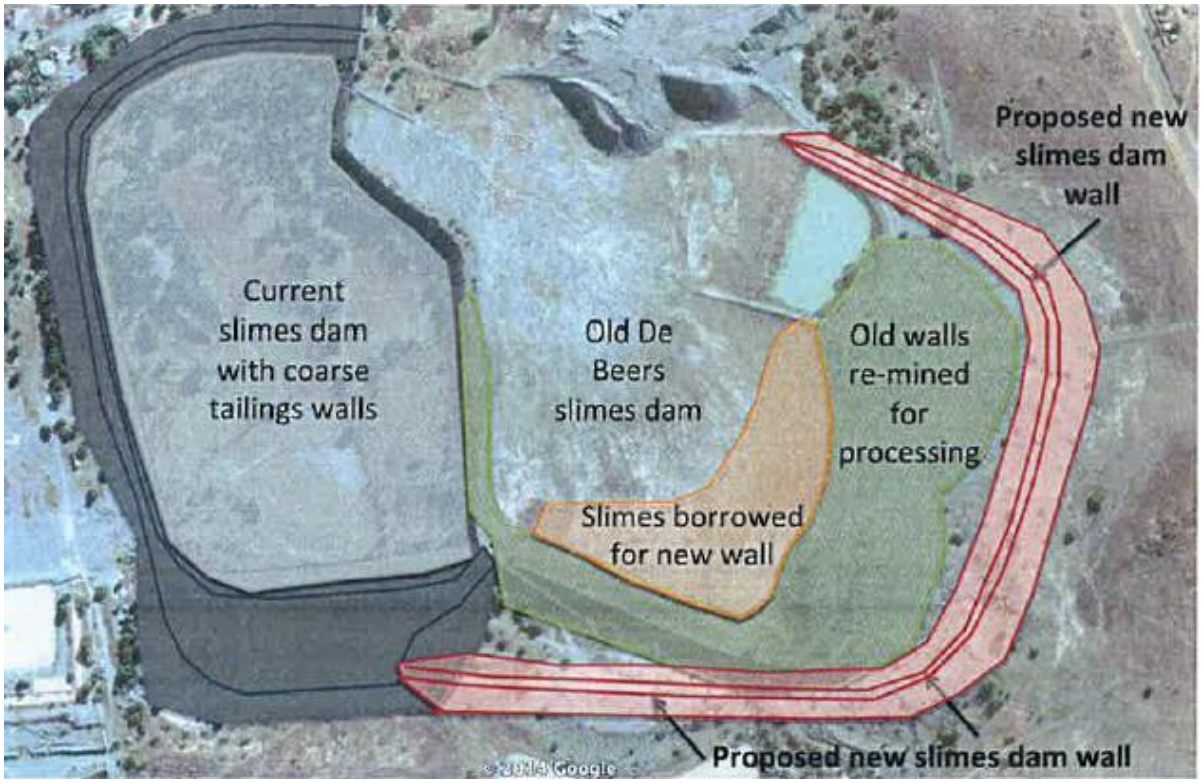

FIGURE 17 PLAN FOR THE EXTENSION OF THE JD TAILINGS DAM, SHOWING THE PROPOSED NEW WALL IN RED (ROBINSON, 2015).

Ground conditions along the southern wall of the proposed tailings dam extension are described as follows: "The ground along this flank is basically level, having been built up with waste from past operations….", and "To the east the ground slopes gently away from the proposed dam and has been historically covered by tailings, some deliberately and the rest from decades of erosion off the old dumps that have now been removed." From this information it is apparent that it was intended to construct the walls for the extended tailings dam on the remaining tailings (i.e. tailings not removed deliberately or by erosion) and not to remove this material. The rational for this was that the tailings would provide a low-permeability "lining" underneath the newly extended tailings dam, limiting the impact on ground water.

The crest elevation for the starter walls to be constructed from grits was set at the elevation of the De Beers Dam (1411 m above sea level) and coincided with the elevation of the crest of Compartment 1 at the time.

After the started walls, raising of the dam was planned to take place by means of upstream construction as follows: "…the grits wall to be extended upstream partially over the slimes to raise the wall in 2 to 4 m lifts."

The final proposed crest elevation of the dam was 1460 m, or a height of 65 m. However, it was stated that the "ability to achieve this height will need to be assessed by investigation….". The crest elevation at the time of the failure (estimated from the April 2022 survey) was approximately 1437 m in the vicinity of the failure (approximately 43 m above the downstream toe).

The anticipated rate of rise of the tailings dam at the design stage is presented in Figure 18 versus slimes elevation. A very high initial rate was anticipated until ground had been broken and the De Beers Dam covered, but then the predicted rate of rise stabilised at about 3 m per year (based on the

figure). However, 4 m per year was mentioned in the report as the designed rate of rise. It was stated that at 4 m per year, upstream walls can be raised around the perimeter by dumping along the inside crest and dozing material into the basin. Heavier grits were expected to "displace fines, compressing and pushing them into the basin". The slimes were expected to gain strength through compression until they could support the overlying grits. A 15 to 20 m wide crest was recommended.

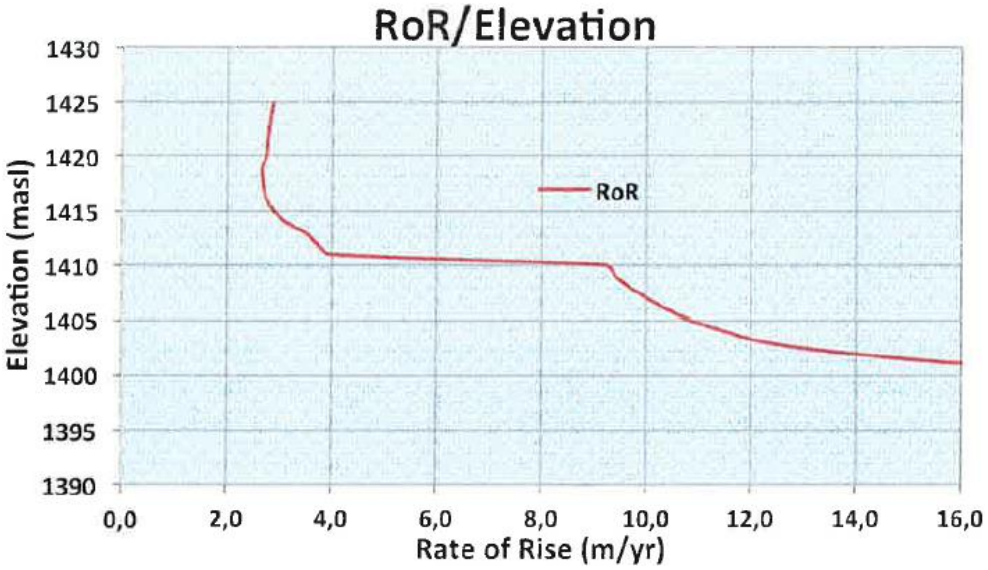

FIGURE 18 ANTICIPATED RATE OF RISE FROM DESIGN REPORT (ROBINSON, 2015)

5.2. Stability assessment

The design report reports that samples of the fines and grits were taken for laboratory testing and the following material properties were recommended in the report (see Table 2). The permeability of the fines was mentioned to be of the order of 1 x 10^{-12} m/s, i.e. virtually impermeable. The grits were reported to be expected to be three orders of magnitude more permeable (i.e. 1 x 10^{-9} m/s, which is still practically impervious).

TABLE 2 ASSIGNED MATERIAL PARAMETERS (ROBINSON, 2015)

Material	Density (kN/m^3)	Friction angle °	Cohesion kPa	Permeability m/s*
Foundation	20	32	5	
Grits	17	30	0	1 x 10^{-9}
Compacted fines	13	20	20	1 x 10^{-12}
Consolidated slimes	13	20	20	1 x 10^{-12}
Slurry	12	15	10	

* Column added by Investigation Panel.

The comment is made "Borrowing fines dry from the existing dam and replacing them in compacted layers, material is expected to exhibit reasonable shear strength." Also, the statement is made that "The underlying foundation materials are either waste rock on in situ residual soils with typical strength parameters". However, much of the new walls were built on slimes, as acknowledged earlier in this report, to keep the potential impacts unchanged as construction was going to take place on

already impacted areas. No mention is made about the strength parameters of these materials which do not have the usual strength parameters as suggested by the triaxial results on the slimes (friction angle of 20° recommended by Robinson, 2015).

The design report goes on to state "The base of an embankment is generally critical to the stability, which is also a function of the level of the phreatic surface" and therefore recommended the construction of a 3 m thick blanket drain comprising of grits. In addition, a 5 m wide layer of grits was specified along the upstream slope of the embankment (outer walls) as illustrated in the recommended cross-section, Figure 19. The design report then states that "The remainder of the wall, which essentially just adds load without having to significantly contribute to shear strength, can be formed with compacted dry fines."

A downstream slope of 1:2 (27°) was recommended, which Robinson considered insufficient and it was therefore recommended to add a "buttress (of grits) along the toe of the slope below 1403 masl, creating a bench that effectively flattens the overall slope angle, enhancing stability." The proposed starter wall cross-section design is presented in Figure 19. Seepage was expected to flow form the slurry into the upstream grits zone and along the blanket drain, idealised by a "conservative" phreatic surface as shown. An idealised cross-section profile for the raising of the tailings dam is presented in Figure 20.

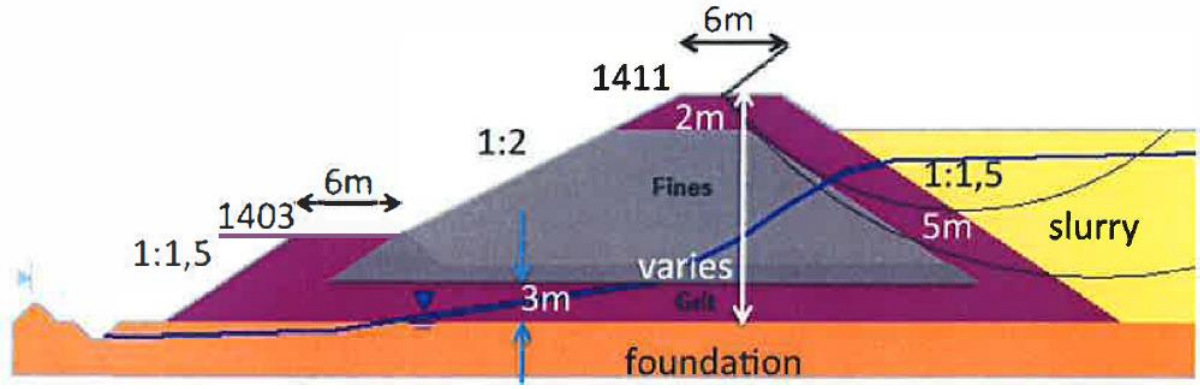

FIGURE 19 PROPOSED CROSS-SECTION OF STARTER WALL (ROBINSON, 2015).

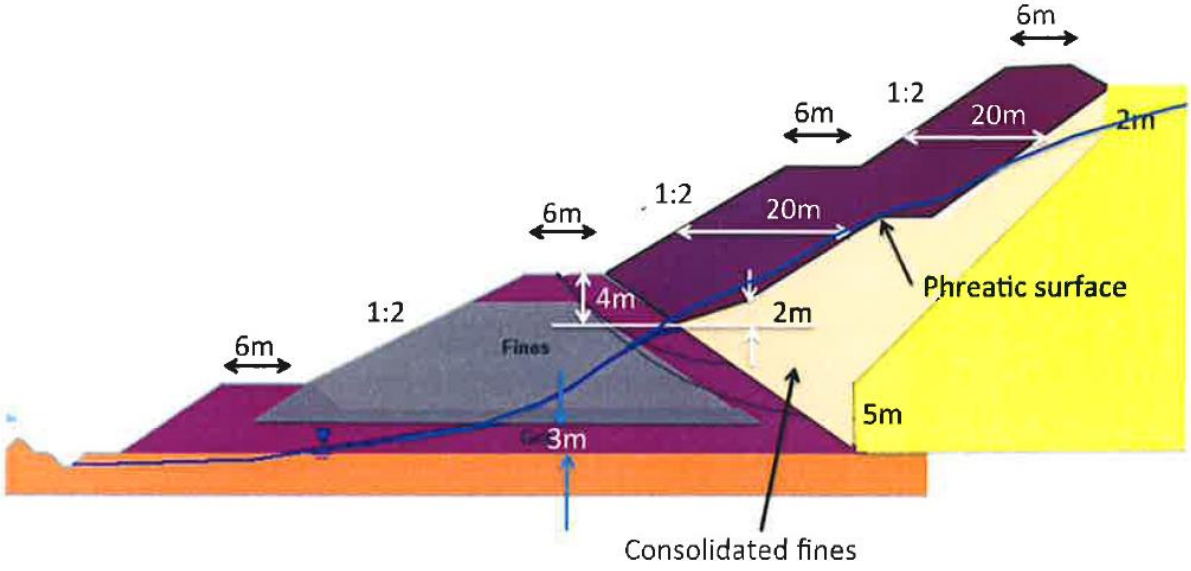

FIGURE 20 PROPOSED CROSS-SECTION FOR RAISING OF THE WALL (ROBINSON, 2015).

The design report describes on a series of slope stability analyses carried out and mentioned satisfactory factors of safety, including "…upstream failure of the embankment into the basin. It should be noted that no significant slope failures have occurred into the basin of the existing dam confirming the reliability of the angle of repose (of) grits slope around the basin."

5.3. Slurry deposition

The design report mentioned the practice of using a single open-ended deposition point to deposit fine tailing on Compartment 1 up to the time of writing his report and stated that "The Mine has successfully deployed this system since re-processing commenced, providing motivation for its continued use going forward". However, he recommended that a discharge point would be required in the north-eastern corner of the extended dam to fill the extension and that a 1600 m long pipeline would be required for this purpose. He further recommended that this delivery system will have to be extended around "most of the perimeter of the ring dyke dam to be raised upstream" and that "…deposition points are spaced to enable control of the basin filling to ensure beaching away from the walls and maintenance of the basin low point centrally".

5.4. Decanting

The design report mentions that Compartment 1 was designed with a penstock tower in the south-eastern corner. The penstock tower was originally constructed, but no pond developed as drainage occurred through the grit embankments (outer walls), leaving the penstock inoperable and it was subsequently abandoned. The design report recommended that provision be allowed for the installation of a floating pumped decant system. Robinson states "If it proves necessary to have a floating decant system, i.e. if a supernatant pond develops, then it will be necessary to control the pond centrally in the basin once the upstream ring-dyke dam development commences."

5.5. Comment on significant aspects of the design

The design report states that "The underlying foundation materials are either waste rock or in-situ residual soils with typical strength parameters." However, the Investigation Panel was not able to find evidence of a geotechnical investigation having been carried out to confirm such parameters. Surprisingly, the DWS was not able to provide a copy of the Water Use License (WUL) application for the extension and/or construction of the tailings dam, nor the necessary supporting documentation. No documentation was available to the Investigation Panel in terms of geotechnical conditions relevant to the tailings dam other than the information presented here and a report on the geology of the area by Colliston (2021), describing the geology around the tailings dam in some detail. Selected information from Colliston (2021) is summarised in Appendix E where geotechnical properties determined from the field investigation by the Investigation Panel are presented.

On a number of instances, the design report refers to the fact that the intention was to build Compartment 2 on a previously impacted area covered by tailings, which the Investigation Panel believes included fine tailings. The friction angle of 20° recommended for this material is very low. The design report does not quantify the impact of such a low strength layer of material on the stability of the proposed embankment.

The Investigation Panel is not in agreement with the high cohesion values assigned to all materials, excluding the grits. Such values may provide an overly-optimistic indication of slope stability. Also, the Investigation Panel considers the recommended downstream slope of 1:2 (27°) very steep for a material with a friction angle of 20°, keeping in mind that "cohesion" is not a reliable soil property. Due to its low shear strength the Investigation Panel is not supportive of the use of dry fine tailings from the De Beers Dam as fill in the expanded dam, especially not to form part of the downstream slope of newly constructed outer walls.

The Investigation Panel agrees that the coarse tailings (grits) used for the construction of the outer walls of the dam is a competent material, suitable for the construction of such containment walls. This is demonstrated by the satisfactory performance of the outer walls of the tailings dam along the perimeter of the dam other than the section that failed.

The design did not consider undrained shear strength of any materials in the stability assessment.

The Investigation Panel note that the design did not make mention of filter compatibility criteria between the fine and coarse tailings. Such criteria ensure compatibility between materials forming interfaces through which flow occurs. Filter criteria need to be complied with to prevent piping and ensure sufficient permeability of drainage structures. If the materials are not compatible in terms of both piping and permeability criteria, piping and/or stability problems may result due to poor drainage. Significant surface erosion observed especially on the western slopes of the tailings dam (see Appendix E) prompted the Investigation Panel to assess the potential dispersiveness of a sample of the coarse tailings from the south-western corner of the tailings dam. The material classified as highly dispersive according to the criteria presented in Appendix E, which means that the material is prone to piping (refer to Section 7.2.2 and Appendix E). The Investigation Panel believes that piping played a significant role in the failure of the tailings dam as discussed in Section 7.2.2.

The expected permeability for the grits, at three orders of magnitude higher than that reported for the fines (i.e. 1×10^{-9} m/s for the grits vs 1×10^{-12} m/s for the fines), is still very low (being equal to the upperbound permeability typically quoted for clays) and is too low for use in drains.

The design report recommended the provision of additional tailings discharge points and a pumping decant system on the tailings dam in the case that a pool forms. The purpose of these measures is to assist with pool control, keeping the pool centrally located and away from the outer walls to allow for the formation of a beach. A beach, if present, would have been subjected to drying, desiccation and the associate strength gain which might have enabled the beach to provide a stable foundation for the raising of the dam wall crest, constructed partially overlying the beach. With the pool normally extending right up against the outer walls of the dam, opportunity for such strength gain was not provided, jeopardizing the stability of newly constructed raised sections of the dam wall crest. This aspect, which the Investigation Panel considers significant in the case of the JD tailings dam failure, is considered further in Section 7.2.5 where the dam failure is discussed.

No as-built drawings could be sourced to confirm the extent to which the design proposed in the design report was actually implemented. Furthermore, slumping of the side slopes of the main breach (Scar 2) into the breach prevented assessment during the site visits of whether the drainage system had been installed or not.

6. Survey data

Photogrammetry surveys of the Jagersfontein Tailings Dam were carried out from time to time since 2010 and, in addition to a post-failure LIDAR survey, provide information on changes in the geometry of the dam embankment over time. A summary of digital elevation models available for the purposes of the study of the tailing dam failure is presented in Table 3. Cross-sections drawn along the alignment identified in Figure 8 are presented in Figure 21 for all survey records available. The cross-section profiles show how the toe of the dam advanced over time to the south (right), while the crest generally advanced slowly towards the north (left) as the dam was raised. The geometry of the old De Beers Dam is presented by the profile labelled "Before 2011", shown in brown. Part of the southern wall of the old De Beers Dam was reprocessed and thus removed before construction of the enlarged tailings dam. The profile labelled "Baseline", shown in black, represents the geometry underlying the raised dam wall and compiled from several sets of survey data. The newly constructed southern wall is presented by the 2017 cross-section. Survey data showing the cross-section profile in February 2019, the time when the first signs of instability were identified, is not available. However, the Investigation Panel reconstructed the February 2019 geometry by examining the December 2017 and June 2019 surveys, in combination with available satellite images (refer to Section 7.2.4).

TABLE 3 DIGITAL ELEVATION MODELS AVAILABLE FOR THE STUDY.

Date	Source	Method	Data presentation
2011 to 2014	Copernicus 30m DEM	Regional stereoscopic photogrammetry	TIF DEM
2017/12/13	Mine survey	Breaklines	Triangles (dwg)
2019/06/04	Mine survey	Photogrammetry	Triangles (dwg)
2019/11/06	Mine survey	Photogrammetry	Triangles (dwg)
2020/09/10	Mine survey	Photogrammetry (2019-11-06) + crest breaklines	Triangles (dwg)
2021/07/15	Mine survey	Photogrammetry	Triangles (dwg)
2022/04/27	Mine survey	Photogrammetry	Triangles (dwg)
2022/09/12	Wits University	High resolution satellite photogrammetry	TIFF DEM
2022/11/25	Post Failure Investigation	LiDAR	Point cloud (xyz)

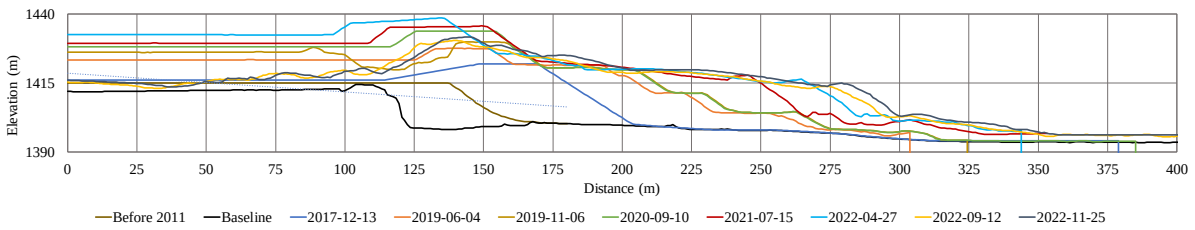

FIGURE 21 CROSS-SECTION PROFILES FROM AVAILABLE SURVEY DATA AT CRITICAL SECTION.

6.1. Verification of survey data integrity

The integrity of the survey data was verified by plotting cross-section profiles at a second section towards the west of the failure zone where it is apparent from the satellite imagery that significant movement had not occurred. The cross-section profiles are presented in Figure 22. It can be seen that some of the profiles do not line up well at the toe of the dam. Significantly, the

12 September 2022 survey (yellow profile), taken the day after the failure, also does not line up well at the toe. Adjustment of the surveys dated 4 June 2019, 6 November 2019, 10 September 2020 and 12 September 2022 by 4 m towards the south resulted in profiles matching well. The profiles after adjustment are shown in Figure 23, showing improved alignment. The 4 m correction to the south was applied at the cross-sections taken where the dam failed for data from the abovementioned dates, the result of which is presented in Figure 24. No adjustment was made to the elevation data.

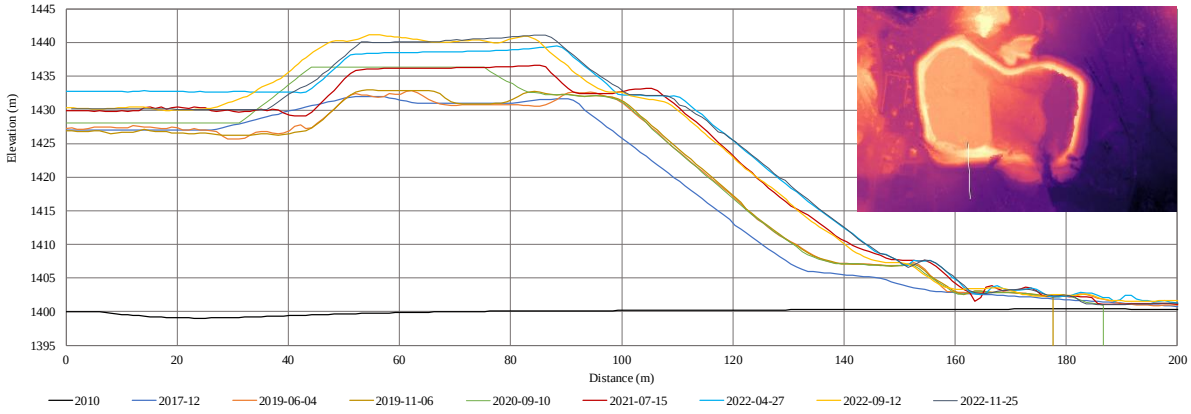

FIGURE 22 CROSS-SECTION PROFILES AT CONTROL SECTION BEFORE ADJUSTMENT.

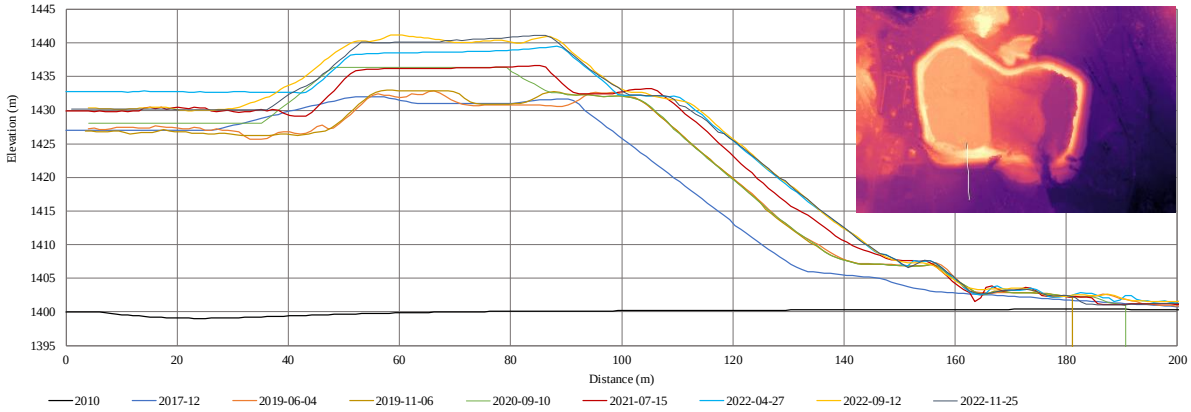

FIGURE 23 CROSS-SECTION PROFILES AT CONTROL SECTION AFTER ADJUSTMENT.

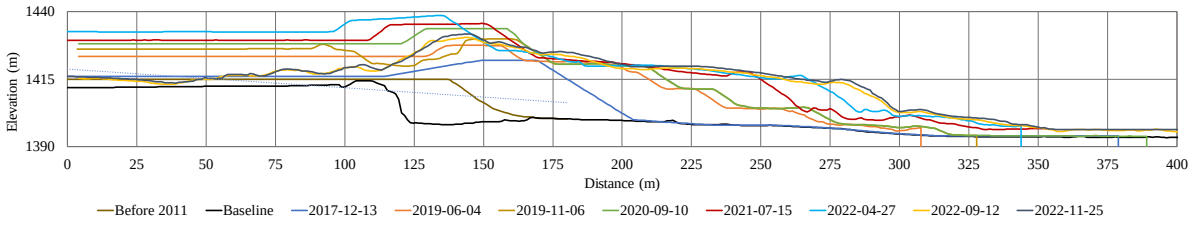

FIGURE 24 CROSS-SECTION PROFILES AT FAILURE AFTER ADJUSTMENT.

6.2. Side slope geometry

The side slope geometry of the outer walls of the tailings dam was investigated based on the 27 April 2022 survey to assess slope angles and hence the angle of repose of the material comprising the walls. Cross-section profiles were studied at the locations shows in Figure 25. The average slope angle measured was approximately 34°, but the side slopes were as steep as nearly 40° at location 3, opposite the plant, and 36° on the eastern slopes at location 8. An effective friction angle of 33° was assumed to be a cautious estimate of the shear strength of the coarse tailings based on the measured angles of repose. This value was used for slope stability assessments presented in Section 7.2, informed by limited triaxial testing of the coarse tailings (see Appendix E).

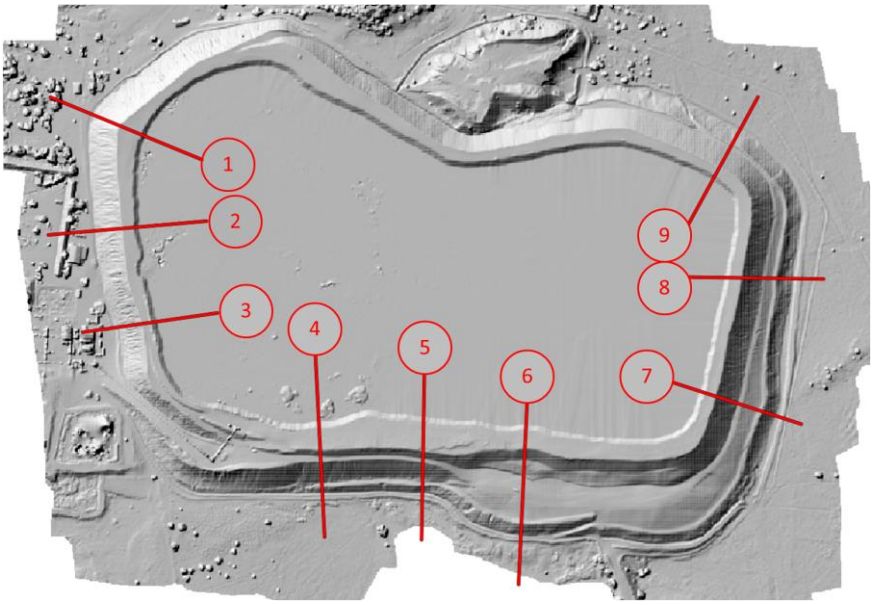

FIGURE 25 LOCATIONS WHERE CROSS-SECTION PROFILES WERE STUDIED (27 APRIL 2022 SURVEY).

6.3. Freeboard

Figure 26 presents two north-south and one east-west cross-section through the tailings dam at the locations shown to illustrate the pond and freeboard at the time of the 27 April 2022 survey. The relevant cross-section is indicated by the yellow line in the plan view in each figure. The mean pond elevation was at 1432.5 m. The pond was essentially level across both compartments based on the survey. The dividing wall between the two compartments had by now been submerged by the pool. The freeboard varied from 3 m in the southwestern part of the dam to more than 6 m along the northern wall.

The survey pre-dates the failure by approximately 4.5 months. The freeboard was subsequently also estimated from the 28 July 2022 satellite image by scaling the slope length from the ortho rectified image and multiplying by multiplying by the tangent of the upstream slope of the wall which was estimated to be 33°. This calculation yielded a free board of approximately 7 m. The variation in freeboard at the failure zone determined from survey data is presented in Figure 27.

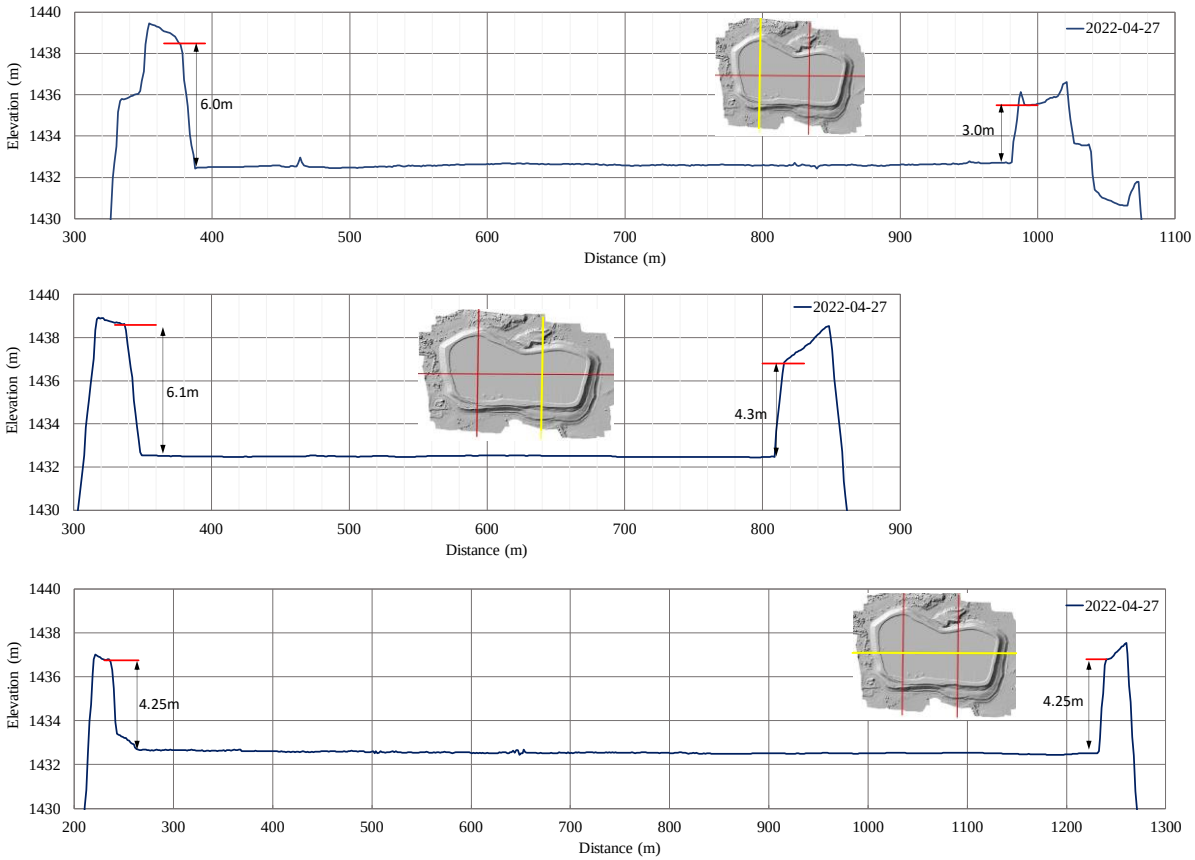

FIGURE 26 SECTIONS THROUGH THE JAGERSFONTEIN TAILING DAM SHOWING THE POND AND FREEBOARD BASED ON THE 27 APRIL 2022 SURVEY. NOTE: THE INSET SHOW IN YELLOW THE CROSS-SECTIONS BEING PRESENTED.

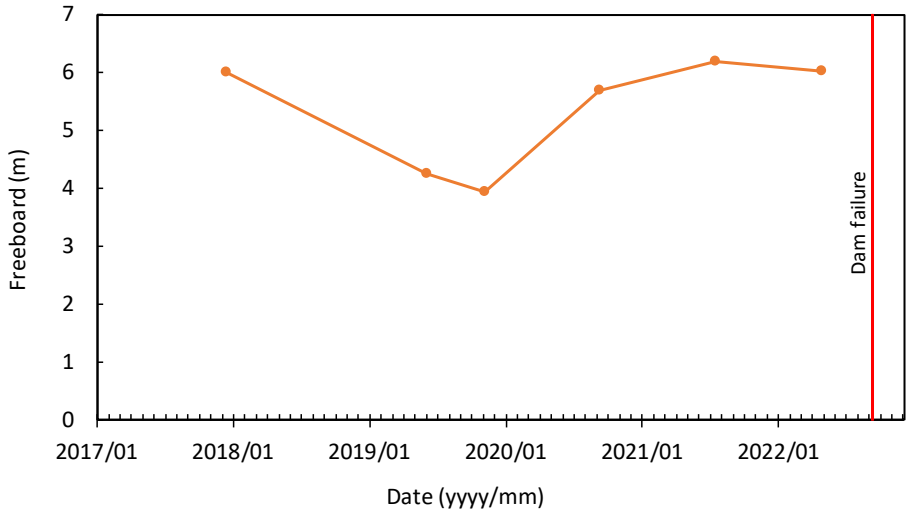

FIGURE 27 FREEBOARD OVER TIME FROM SURVEY DATA TAKEN AT THE EMBANKMENT CROSS-SECTION WHERE THE FAILURE OCCURRED.

6.4. Rate of rise

The annualised rates of rise in the crest and pond levels, measured on the critical cross-section (Figure 8), determined from the available survey data, were found to amount to an average of 3.8 m per year for both the pond and embankment crest since 2018. Figure 28 presents the embankment crest and pool elevations plotted against time, as well as the annualised crest and pool rates of rise recorded between surveys. Rates of rise on a number of occasions exceeded the rate of rise of 4 m per year quoted in the design report (Robinson, 2015) (see Section 5).

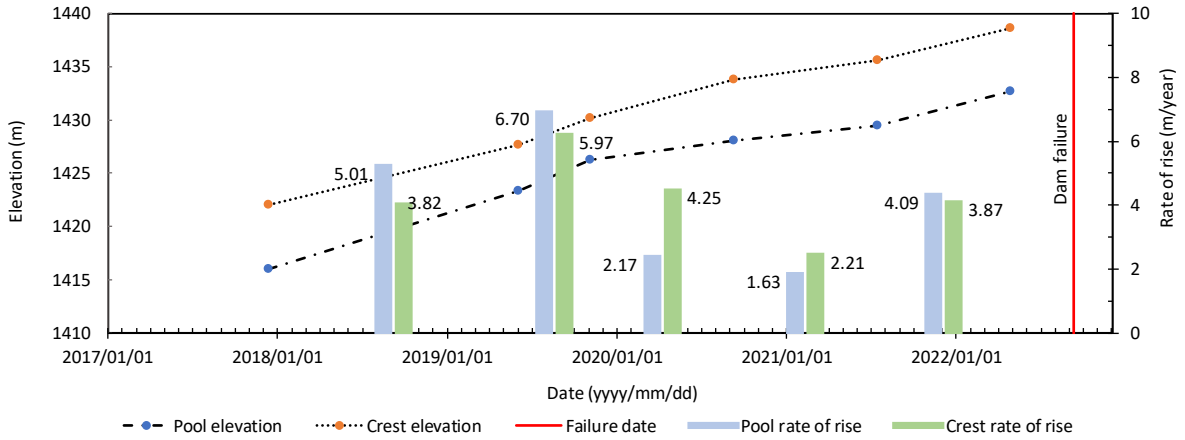

FIGURE 28 RATE OF RISE DETERMINED FROM SURVEY DATA.

6.5. Deposition

The deposition record on the tailings dam, measured in cubic metres per year as measured from the survey data is, presented in Figure 29. The deposition volume was calculated by measuring the surface area of the pond and multiplying the average area between surveys by the difference in pool elevation and annualising the result.

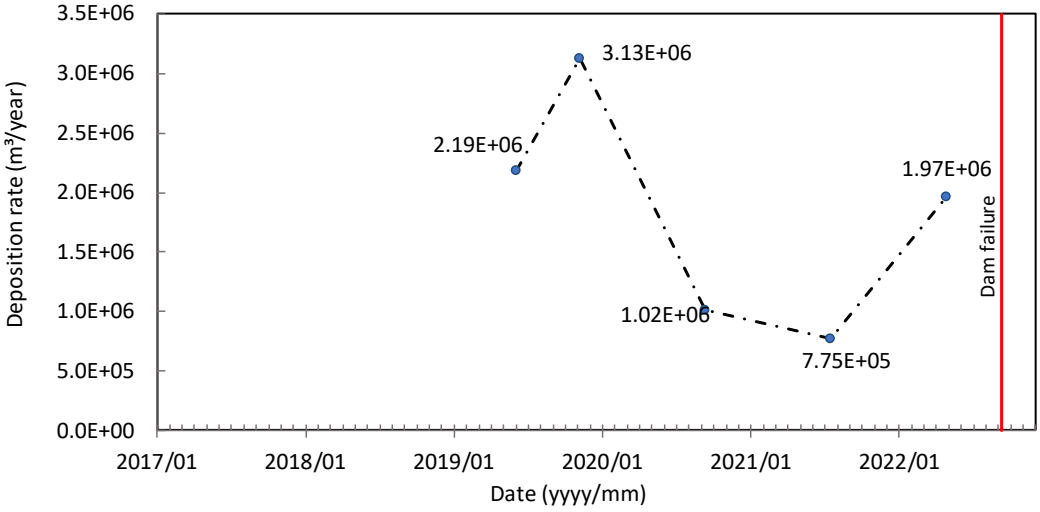

FIGURE 29 ANNUALISED DEPOSITION RECORD IN CUBIC METRES PER YEAR CALCULATED FROM SURVEY DATA.

6.6. Raising of the outer dam walls

The tailing dam was operated as a containment dam with no return water facility. The outer walls were raised over time using coarse tailings comprising silty sand with fine gravel from Kimberlite (referred to as grits in the design report by Robinson (2015) – Section 5). The CPTu investigation showed the consistency to increase from loose or medium dense near the surface, becoming dense or very dense with depth. The material was so dense in places that the CPTu refused and/or the anchors providing reaction to the rig down pulled out. Side slope angles were measured on site at approximately 33°, lower than the friction angle of approximately 38° for the coarse tailings measured during limited triaxial testing (refer to Appendix E for the geotechnical properties).

Tailings slurry was pumped into the pond created by the grit containment walls. The slurry from the plant was discharged via single discharge point located on the western wall of the dam. The Investigation Panel is not aware of any other discharge points on the dam. The dam was not equipped with any return water facility. Substantial freeboard was provided to ensure sufficient capacity for deposition and rainfall.

The satellite images in Appendix B show that the surface of the compartments on the dam was generally kept submerged under tailings, maintaining tailings ponding right up against the outer walls. There was no beach present, except near the southwestern corner of the dam (Compartment 1) where some vegetation growth is evident. Figure 30 shows the development of the dam wall crest over time determined from survey data. As the dam was raised in the upstream direction, each successive lift rested partially on tailings that had been hydraulically deposited. Given that the water pond often rested right against the containment wall, it is likely that this resulted on lifts being built on unconsolidated tailings. It is not clear whether this led to instability problems along the inside slope of the raised wall prior to the failure. Stability problems along the inside slope is an aspect that the investigation panel would have wished to discuss with JD employees, had communication been allowed.

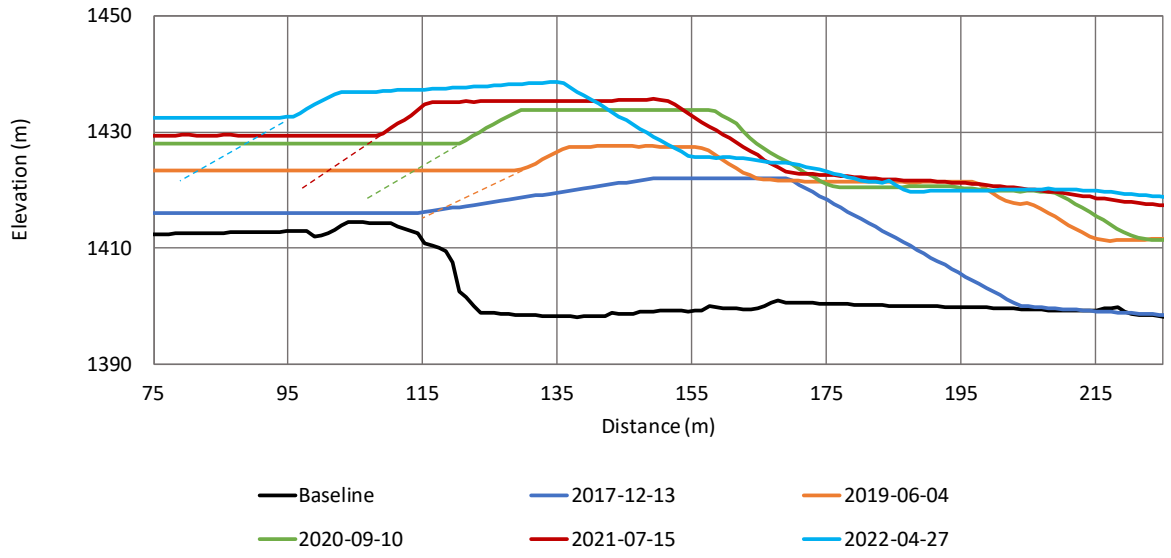

FIGURE 30 CROSS-SECTIONS ON THE SOUTHERN WALL FROM SURVEYS ILLUSTRATING THE RAISING OF THE OUTER DAM WALL OVER TIME.

6.7. Evidence of outer wall instability

Figure 31 presents selected cross-section profiles taken along the alignment of the section selected for stability assessment previously identified. The foundation on which the enlarged tailings dam was constructed, as well as the 2021 and 2022 surveyed cross-section profiles are shown. Comparing the 2021 and 2022 profiles reveals a southward displacement of the access road and berm breakpoint indicated in Figure 31 by 19 m in the time between the two surveys. The slope along the baseline is highlighted by a red dashed line that was subjected to two parallel offsets to intersect first the access road surface and then the berm breakpoint. It is evident that the road and berm breakpoint displaced parallel to the baseline slope. It appears that movement was consistent with sliding along the foundation profile (labelled "Baseline" in Figure 31). The period between the two surveys was approximately nine months. A displacement of 19 m over this time implies a rate of movement of approximately 66 mm per day. The slope on which sliding occurred measures on average 2.7° (1:21.4).

While the toe of the dam displaced towards the south, the crest of the dam embankment seems to have moved north. Given the very large movements, large volumes of material must have been placed to compensate for the movement of material towards the south. Of particular interest is the reason for material apparently being lost from the downstream slope of the crest between the 15 July 2021 and 27 April 2022 surveys (blue shaded area in Figure 31). Typical raising of an embankment would not be accompanied by material being removed downstream of the crest. Rather, material would normally be added to raise the crest, leaving the slope downstream of the crest in place. It appears plausible that the rear scarp of the failure surface might have exited in this area impacting the shaded material in the figure.

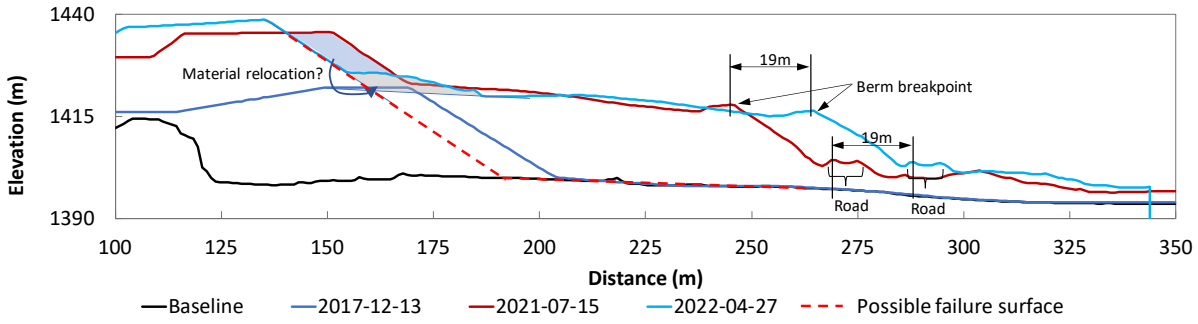

FIGURE 31 SELECTED CROSS-SECTIONS ILLUSTRATING DEFORMATION MECHANISM.

Figure 32 presents long-section profiles extracted from survey data available for the period 2019 to 2022 along the section of crest indicated. The area affected by the breach is shaded in blue in the figure. The 2020 and 2021 profiles are generally smooth except along the portion that would eventually fail. This could be a manifestation of the pre-failure instability issues encountered along this length of wall which could have prompted the large amount of construction activity seen along this stretch of the embankment in the high-resolution satellite images.

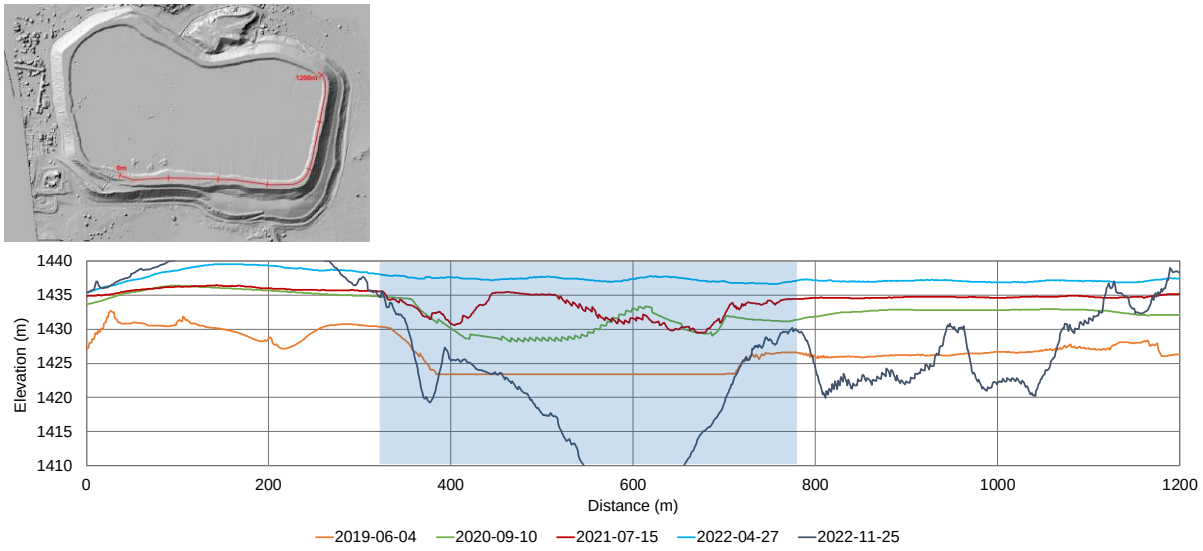

FIGURE 32 LONG-SECTION SURVEY DATA ALONG THE SOUTHERN AND EASTERN WALLS OF THE TAILINGS DAM FROM 2019 TO 2022. (SHADED AREA = AREA IMPACTED BY BREACH.)

6.8. Last stable cross-section profile at breach location

The discussion of the satellite image record (Chapter 4) mentioned that the first visual signs of slope instability appeared in February 2019. No survey was available around this date. The last survey preceding February 2019 is from December 2017, 14 months prior, while the first survey after is from June 2019, i.e. 4 months after. The critical cross-section profiles from these surveys (i.e. profiles taken along the alignment indicated in Figure 8) are presented in Figure 33. The profile from December 2017 (blue curve) shows a steep uniform outer slope measuring 33°. Examining the satellite images reveals that the downstream toe of the slope remained unchanged in the images from July 2017 to February 2019 (Figures B8 to B10). The downstream embankment toe inferred from the December 2017 survey is therefore concluded to be applicable to February 2019 when the first signs of instability appear in the satellite images. The uniform slope from the December 2017 survey is also in agreement with the satellite image from February 2019 which does not show any berms or step-ins on the lower part of the slope (Figure B10). A step-in can be identified near the crest on the February 2019 image, which agrees with the crest geometry of the June 2019 survey. It therefore appears that the cross-section profile shown by the red dotted line is a good approximation of the geometry that first exhibited instability problems in February 2019. The stability of this cross-section profile is considered in Section 7.2.4.

It is significant to note that the entire downstream buttress representing the difference between the 13 December 2017 and 4 June 2019 surveys, shaded light brown in Figure 33, was built from February to early June 2019. The intense activity in the area can be seen in the satellite images and was presumably an effort to stabilise the slope. However, as shown by subsequent surveys and satellite images, these efforts were not successful to arrest movement.

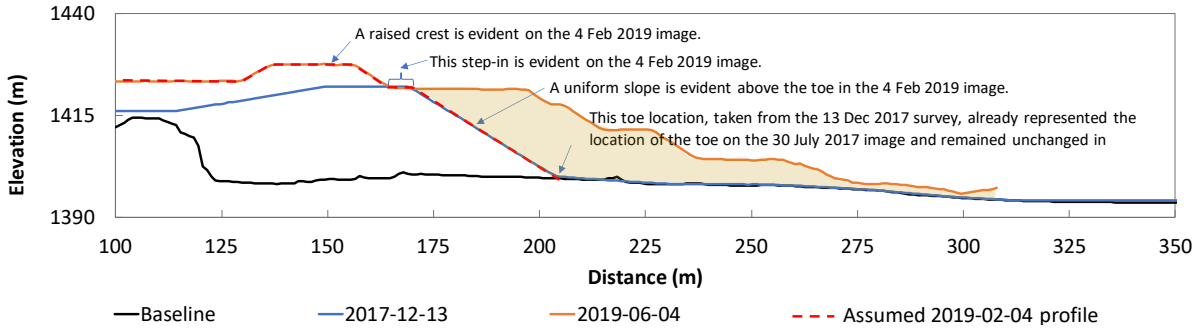

FIGURE 33 CROSS-SECTION PROFILES CLOSEST IN TIME TO FEB 2019.

7. The failure event

7.1. Sequence of events

Figure 34 indicates a number of features associated with the failure of the Jagersfontein Tailings Dam referred to in this discussion.

The failure occurred shortly after 06h00 on Sunday 11 September 2022. In his affidavit (Havenga, 2023), Mr Alwyn Havenga of the DWS, D: DSR reported that the Mine Manager, Mr Johan Combrink, was summoned to the dam shortly after 06h00. The southern wall of the dam in the vicinity of the main breach failed to the inside of the dam shortly after Mr Combrink's arrival. This was followed by what was described in the affidavit as "slumping of the crest" in this vicinity, resulting in the dam wall being overtopped in this area. This is the location where the main breach formed, referred to as Scar 2 in Figure 34 and Figure B23.

The main breach developed just to the east of where the Dam 10 embankment abuts the southern wall of the tailings dam. Comparing satellite images captured on 28 July 2022 and 12 September 2022, captured before and after failure of the dam respectively, shows the blocks labelled A and B to have displaced, largely intact, by distances of between 11 m and more than 20 m towards the south-southwest and south respectively (see Figure 8). Block A moved more than Block B. Erosion scars labelled 1 and 3 in Figure 34 and Figure B23 formed the western and eastern boundaries of the part of the dam wall that failed. The companion dam breach analysis by the Investigation Panel (Coetzee, 2024) suggests that erosion Scar 1 developed first, discharging the tailings responsible for the westerly and southerly impacted area between the dam and Charlesville (see Figure 2). The dam breach analysis indicates that, had the breach occurred only at label 2, insufficient energy would have been available to impact the southwestern extremities of the impacted area to the extent it had been affected. However, discharge form erosion Scar 1 appears to have stopped early in the sequence of events. This aspect is discussed later (see Section 7.2.2).

Figure 35 presents an image of the failed southern embankment, captured on 26 September 2022. This image is of higher resolution than the image from 12 September 2022 (Figure B23), the first post-failure satellite image, and is therefore used for this discussion. The discharge from the tailings dam is clearly distinguishable because of its off-white to light grey colour. Looking at the main breach area (Scar 2), parts adjacent to the breach reached by tailings during the early stages of the overtopping event are indicated by white material deposited on the downstream berms of the embankment (labelled J in Figure 35). Although tailings discharged down the slopes in these areas, it did not result in much damage as the duration of overtopping at these locations must have been limited, probably due to rapid development of the breach at Scar 2, causing most tailings slurry to be released there.

It is interesting to note in Figure 35 that some signs of overtopping are also evident at Scar 1 (see labels K and L). Tailings did not seem to progress further than the first berm at K, but some tailings did reach the lower berm (below L). The exact location where overtopping occurred at L has probably been eroded away in erosion Scar 1. The 12 September 2022 survey indicates that the crest of Block A is approximately 8 m lower than the elevation of the crest of the intact embankment to the west (the free board is estimated to have been about 7 m at the time of the failure).

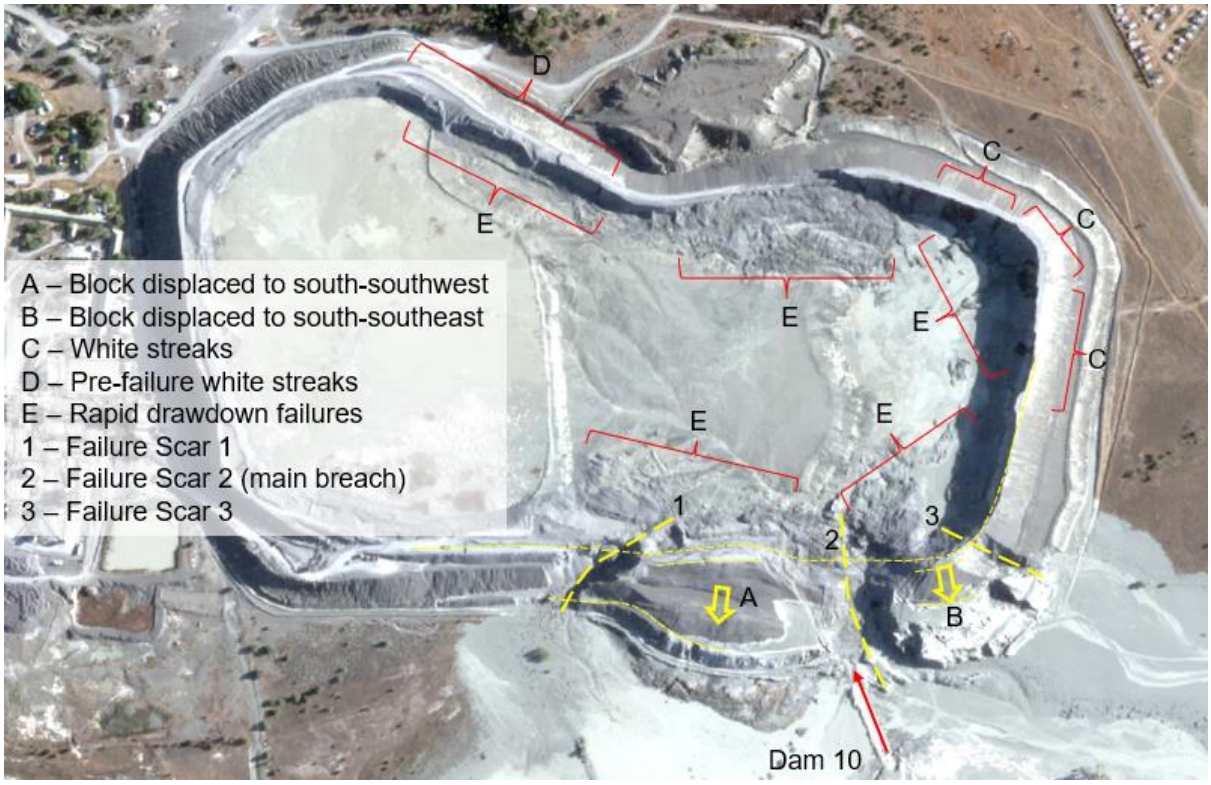

FIGURE 34 FEATURES ASSOCIATED WITH THE FAILURE EVENT. IMAGE FROM 12 SEPTEMBER 2022.

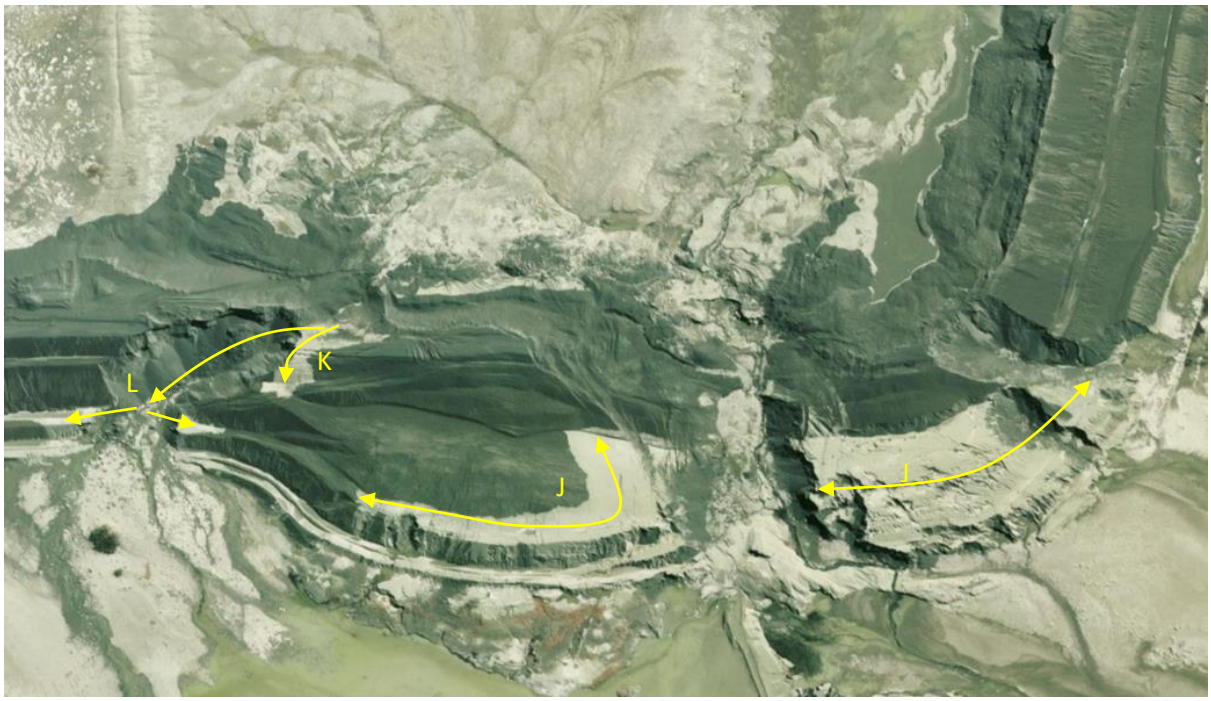

FIGURE 35 ENLARGED IMAGE FROM THE FAILURE AREA SHOWING AREAS REACHED BY OVERTOPPING FINE TAILINGS (IMAGE FROM 24 SEPTEMBER 2022).

The prominent colour difference between the fluid fine tailings and the coarse tailings suggests that limited overtopping also may have occurred along the northern and eastern walls of the tailings dam.

Figure 36 presents part of the northern and eastern walls of the dam before and after the failure (images dated 28 July 2022 and 12 September 2022, see also Figures B22 and B23). White streaks can be seen on the northern wall and on the eastern wall (labels C in Figure 34). These streaks are also visible in helicopter video footage captured the day after the failure (Figure 37). Similar signs are visible long the western part of the northern wall on the 12 September 2022 image (label D in Figure 34), but these are also visible on the 27 July 2022 image (Figure B22) which implies that they (i.e. the streaks along the western part of the northern wall) are probably not related to the failure.

A possible explanation for limited overtopping of the parts of the dam wall crest mentioned above could be the formation of a wave due to the inward failure of the southern embankment which would have rapidly deposited a large volume material into the dam basin, displacing a large volume of tailings slurry. A wave thus formed could have travelled across the pond, causing a surge, possibly reaching and occasionally overtopping the crest at locations close to the north-eastern corner. (Refer to the Dam Breach analysis by Coetzee (2024) for such a simulation). It is of interest to test this hypothesis against eye witness accounts.

The rapid discharge of tailings from the tailings dam after the breach had developed was followed by extensive rapid draw-down failures around the northern, eastern and southern walls of the eastern compartment (labelled E in Figure 34).

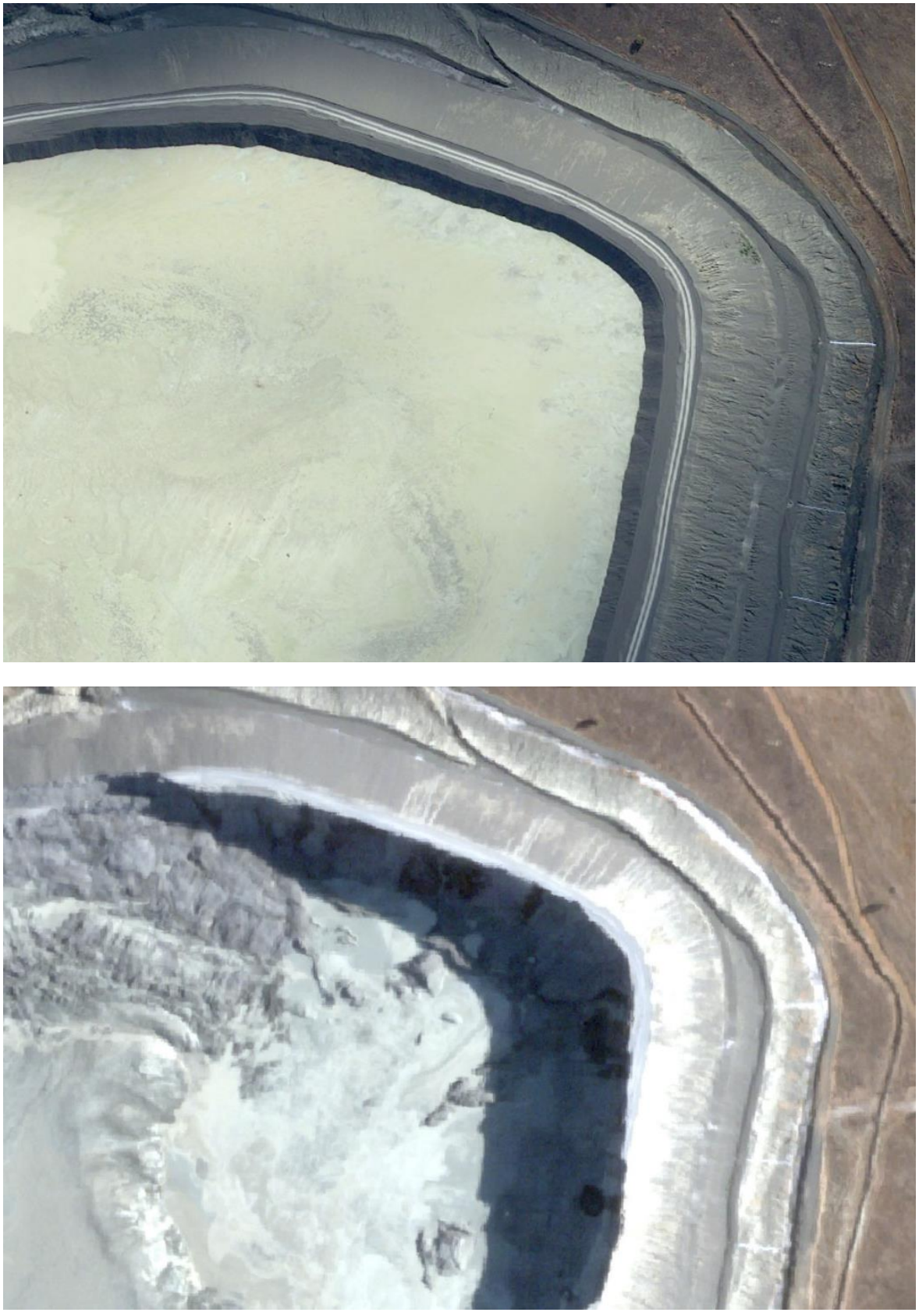

FIGURE 36 THE NORTH-EASTERN PART OF THE TAILINGS DAM BEFORE AND AFTER FAILURE (26 JULY 2022 AND 12 SEPT 2022 RESPECTIVELY). THE WHITE STREAKS ON THE NORTHERN AND EASTERN SLOPES VISIBLE ON THE POST-FAILURE IMAGE SUGGEST THAT LIMITED OVERTOPPING MAY HAVE OCCURRED AT THESE LOCATIONS.

FIGURE 37 IMAGES FROM CELL PHONE FOOTAGE TAKING DURING HELICOPTER INSPECTION ON 12 SEPTEMBER 2022 SHOWING POSSIBLE SIGNS OF LIMITED OVERTOPPING NEAR NORTH-EASTERN CORNER OF DAM (SOURCE: MR A HAVENGA AND/OR MR WM RAMOKOPA).

7.2. Hypothesised geotechnical causes of the failure

7.2.1. Slippage along the base

The large displacement undergone by Blocks A and B (Figure 34), the fact that they remained largely intact, the history of movement since February 2019 (Figure 10), the movement of the tree or large shrub close to the toe of the southern wall (Figure 11), the movement of the rock or shrub-like feature (Figure 12) and the analysis of the cross-sections from the available survey data are all consistent with a mechanism involving deep-seated slippage of the southern embankment on a weak layer or interface underneath the dam embankment. As discussed in Section 6.7, the cross-sections from survey data are consistent with movement having occurred on an interface between the embankment and the profile labelled "Baseline" in Figure 31. Old tailings dumps, remnants from early mining operations, predating the first available aerial photograph from 1944 (Figure A1), were mentioned in Section 4.1. From the satellite imagery discussed in Section 4.2 (Figures B5 to B7) it is apparent that the North- and South dumps were reclaimed or removed by JD during 2014 and 2015 before constructing Compartment 2. Although it appears that some material was removed from Dump 10, it appears that much of the material from this dump remained in place. It was also mentioned in Section 5 that the design intended for the extension of the tailings dam, Compartment 2, to be constructed on previously impacted land.

The approximate extent of Dump 10 and tailings from the North and South dumps are indicated on the 29 May 2010 satellite image in Figure 38 using red curves. A colour-enhanced satellite image from 12 November 2010 by Photosat (Nell, 2024), shows the extent of the dump material more clearly (see Figure 39) and assisted with the delineation of its extent. (Considering how the material appears to fan out from a central discharge point resembles material deposited from a pipe, but this is speculation.) The upstream pre-failure water line and the pre-failure toe, as determined from the 28 July 2022 satellite image (Figure B22), are indicated by yellow curves in Figure 38. The 2014 alignment of the access road along the southern toe of the dam is also indicated in yellow. Two "heaps" of presumably tailings and identified as "raised features" in selected images in Appendix B, located to the east and west of the northern end of the Dam 10 embankment, are labelled M. These heaps are also identifiable in the 1944 aerial photograph (see Figure A1). Figure 38 also shows the locations of failure Scars 1, 2 and 3. There is a strong correlation between the extent of the parts of the embankment that failed (the part between Scars 1 and 3), the extent of Dump 10 and tailings presumably left behind after reprocessing the South Dump and the heaps or raised features labelled M.

The exact spatial extent and depth to which material was removed from the South Dump before the construction of Compartment 2 are not known, but based on satellite images from September 2014 and August 2015 (Figures B5 and B6), some material was left behind, especially near the south-eastern corner of the tailings dam. Deposits of what are presumed tailings forming Dump 10 and the North and the South Dumps were also identified in 2011 satellite imagery in a Photosat report by Rivet (2023), shown in brown in Figure 40, where it was labelled as "unknown material". The design report by Robinson (2015) mentions "The extended footprint remains on top of old tailings…" which seems to be confirmed by the observations presented here.

When inspecting the breach area during the Investigation Panel's site visits, it was evident that the remaining parts of the embankment adjacent to the main breach seem to be underlain by fine tailings forming a "floor" underlying the displaced parts of the embankment, evident in Figure 41(a), (b) and (c). Seepage was visible, occurring from the interface between overlying coarse tailings and the fine tailings, indicating that the latter formed an impervious base underneath the overlying coarser embankment material. An effort was made during the February 2024 site visit to manually dig into the coarse embankment material overlying the tailings using a spade to confirm whether the tailings did in fact extend underneath the coarse material. From this limited investigation, this did appear to be the case. This layer of fine tailings was sufficiently resistant at the time of the failure to have remained in place throughout the failure event and it must have been heavily over-consolidated and hence stiff consistency at the time due to the thickness of overburden that had covered it before (up to >30m in places).

Since the failure, the breach floor had been subjected to seepage from within the dam and rainfall and the tailings in the breach floor had softened significantly. During the second visit to site a number of hand vane shear tests were carried out in this material (29 January 2024). Much of the fine tailings was very soft, unable to support the weight of a person. It was possible to push the vane by hand to 1.45 m and very low undrained shear strength values were measured. However, these low strengths are not considered representative of conditions at the time of the failure due to the fact that the overburden under which it occurred had been removed and drainage allowed softening to occur in the nearly 18 months after failure. Nonetheless, the fine tailings material is considered to have had a

low shear strength as suggested by the friction angle of 23° measured for the fine tailings as reported by Robinson (2015). Additional reports of shear strength measurements on the various materials are presented in the geotechnical report contained in Appendix E. The vane shear test results are also contained Appendix E.

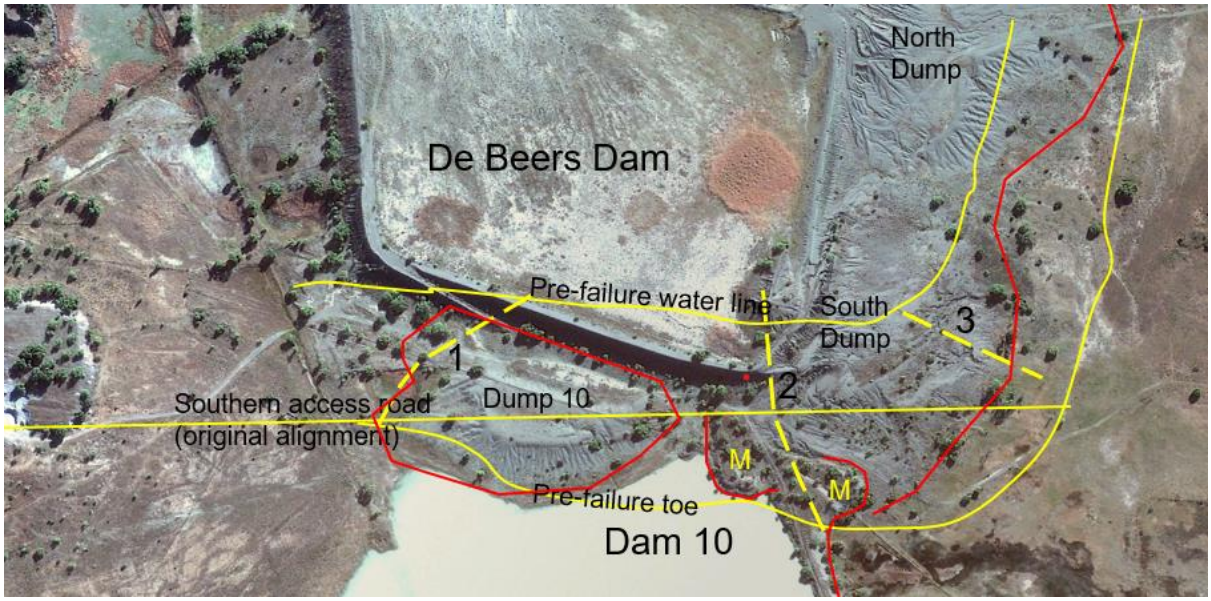

FIGURE 38 THE PRE-FAILURE EMBANKMENT GEOMETRY AND FAILURE SCARS SHOWN IN YELLOW, OVERLYING TAILINGS DEPOSITS FROM DUMP 10, THE SOUTH DUMP AND THE NORTH DUMP (DUMP TOE SHOWN IN RED). COMPILED FROM THE PRESENT IMAGE (29 MAY 2010) AND EARLY AERIAL IMAGES.

FIGURE 39 EXTRACT FROM 22 NOVEMBER 2010 SATELLITE IMAGE COLOUR ENHANCED BY PHOTOSAT (NELL, 2024).

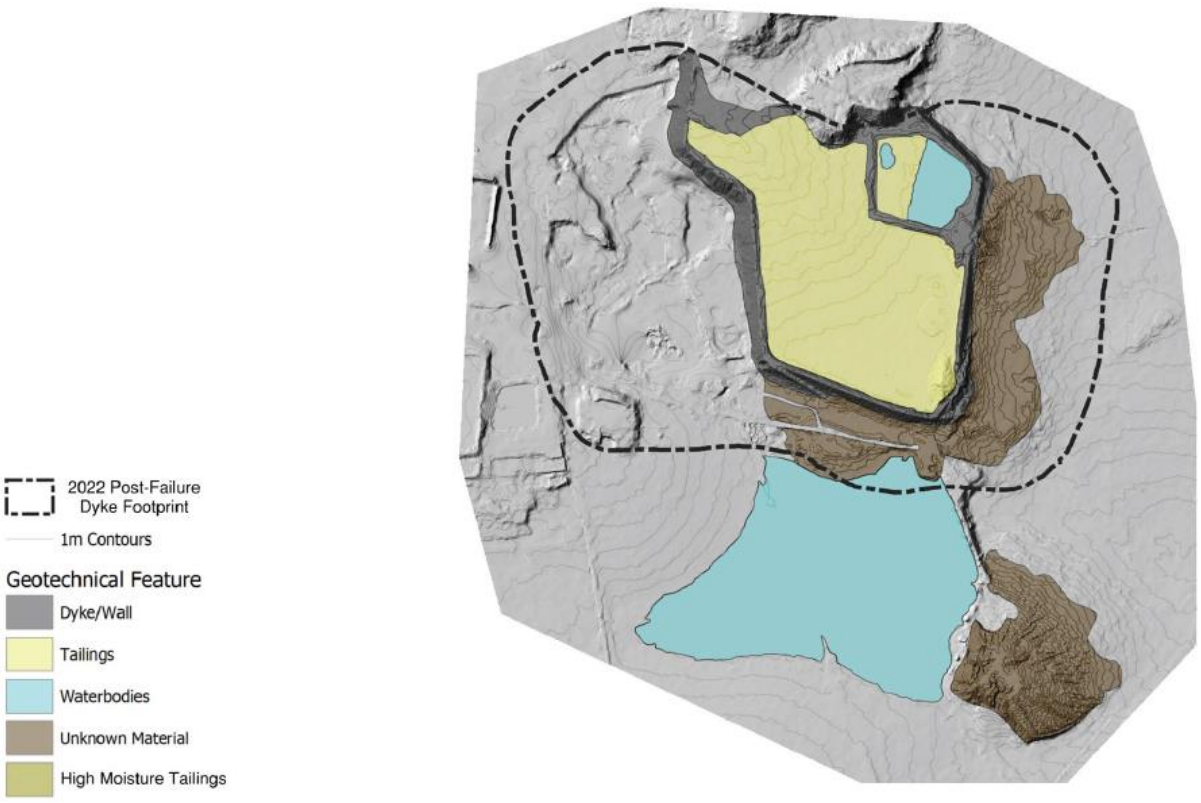

FIGURE 40 CONTOUR DRAWING BASED ON 26 FEBRUARY 2011 SATELLITE IMAGERY IDENTIFYING VARIOUS MATERIALS IDENTIFIED (SOURCE: RIVET, 2023 (PHOTOSAT)). THE OUTLINE OF THE "UNKNOWN MATERIAL" CORRESPONDS CLOSELY WITH THE TOES OF THE TAILINGS DUMPS OUTLINED IN RED IN FIGURE 38.

Figure 42 presents a photo showing a heap of apparently coarse granular material than remained in the breach floor. It is underlain by the fine tailings forming the breach floor. Its location is indicated in Figure 41. The visible cracks may suggest movement on the underlying material.

Figure 43 presents a portion of the 12 September 2022 satellite image captured shortly after the failure indicating a block of material separating from the toe of the embankment. This is a further suggestion of sliding on an underlying interface.

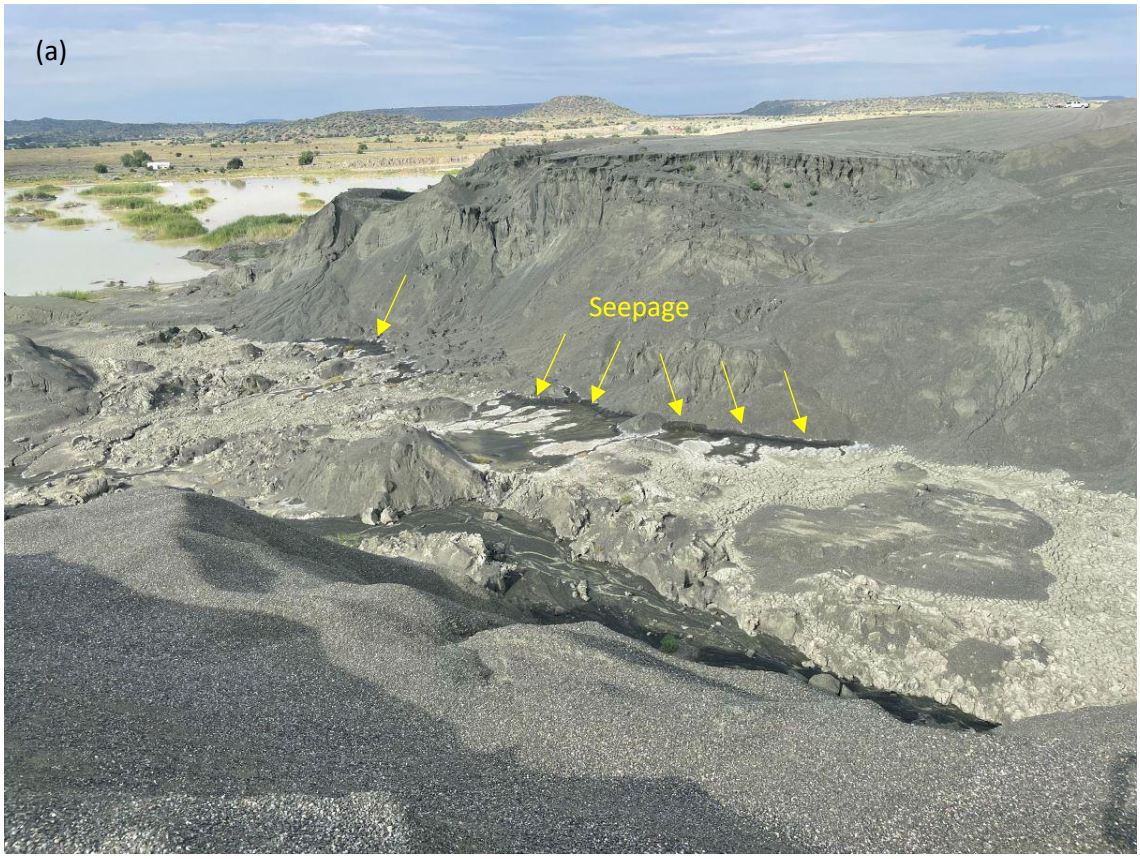
(a)
Seepage

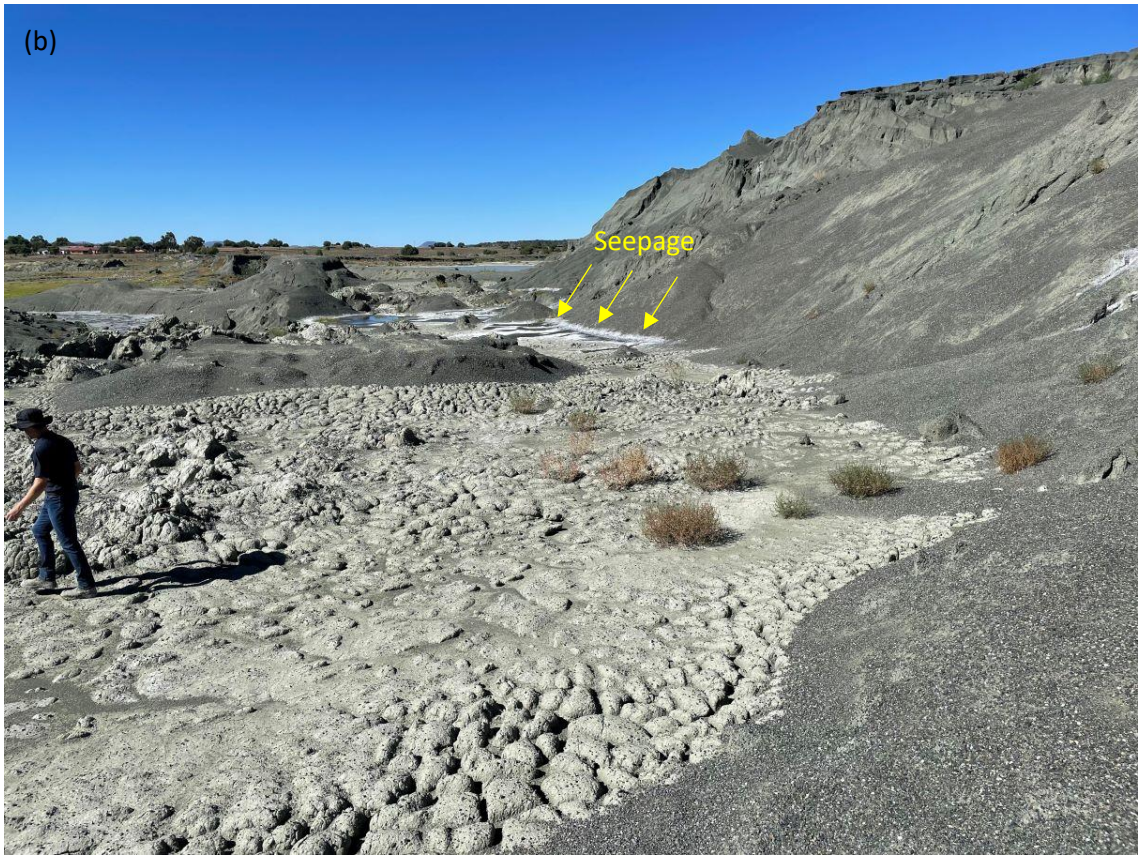
(b)
Seepage

FIGURE 41 THE BREACH FLOOR COMPRISES A LAYER OF CONSOLIDATED TAILINGS THAT RESISTED EROSION DURING THE FAILURE. (A) LOOKING DOWN TOWARDS THE BREACH FROM THE EASTERN SIDE OF THE BREACH. (B) LOOKING SOUTH ALONG THE WESTERN SIDE OF THE BREACH. (C) TAKEN FROM HELICOPTER ON 12 SEPTEMBER 2022 SHOWING EMBANKMENT UNDERLAIN BY CONSOLIDATED TAILINGS.

FIGURE 42 GRANULAR MATERIAL THAT REMAINED IN THE BREACH STILL SHOWING SIGNS OF MOVEMENT ON THE UNDERLYING LAYER OF TAILINGS. (LOCATION INDICATED IN FIGURE 41 ABOVE).

FIGURE 43 EVIDENCE OF SLIDING ON THE BASE SUGGESTED BY BLOCK SEPARATING FROM EMBANKMENT TOE (CURLY BRACKET).

7.2.2. Shear displacement between sliding and intact parts of the embankment (Erosion Scars 1 & 3)

During their site visits the Investigation Panel noted that Scars 1 and 3 in Figure 34 did not breach through the dam embankment into the pond. This was an unexpected finding for the panel because the post-failure satellite images (e.g. Figures B23 and B24) strongly suggest that tailings were released not only from the large Scar 2 but also from Scars 1 and 3. Cell phone video footage taken as the failure was occurring (https://www.youtube.com/watch?v=XNcbLhwcI8A), shows that Scar 3 had already developed while the outrush of tailings slurry was occurring from the main breach (see Figure 44). It therefore appears that at least Scar 3 developed relatively early after commencement of the failure and that the amount of fluid it released was small compared to the discharge from the main breach. Comparison of the post-failure satellite images from 12 and 24 September 2022 (Figures B23 and B24) suggests that seepage continued to occur from Scars 1 and 3 after the failure, more so from Scar 3 than Scar 1.

In light of the foregoing observations, Scars 1 and 3 in Figure 34 are believed to be the result of piping (internal seepage) along the shear interfaces which formed where blocks A and B displaced relative to the adjacent stationary parts of the embankment. The dispersive nature of the tailings would have contributed to the material's tendency to pipe (see Appendix E). The locations of the cracks visible in the 24 September 2020 satellite image (Figure B17), superimposed on the post-failure image dated 12 September 2022 (Figure B23), are presented in Figure 45. The locations of the Scars 1 and 3 correspond closely with these cracks, with the western crack occurring along the southern edge of Scar 1 and the eastern crack passing through Scar 3.

The Investigation Panel believe that shearing along the location of scars 1 and 3 created preferential seepage paths. Seepage resulting in piping and erosion likely formed these scars. Tests on a coarse

tailings sample collected from the southwestern corner of the dam where significant surface erosion of the side slopes is evident, indicated the sample to be highly dispersive (see Appendix E). Dispersiveness would have exacerbated the material's tendency to pipe. However, due to the largely cohesionless nature of the material comprising the walls, internal pipes could not be sustained and collapsed, possibly resulting in piping self-healing. Alternatively, or in addition to this mechanism, the progression of piping was stopped by the subsiding fluid level in the dam as the outrush of tailings progressed. However, the massive outrush of tailings still in progress as Scar 3 appeared fully developed in Figure 44 suggest that self-healing of the piping mechanism is a plausible explanation as there still appears to have been a large volume of material in the dam at this time.

FIGURE 44 SCAR 3 ALREADY DEVELOPED AS THE OUTRUSH OF FINE TAILINGS FROM THE DAM WAS OCCURRING THROUGH THE MAIN BREACH. (SOURCE: HTTPS://WWW.YOUTUBE.COM/WATCH?V=_ND_LONOJ8Y).

FIGURE 45 THE LOCATION OF CRACKS (IN RED) OBSERVED ON THE 24 SEPT 2020 SATELLITE IMAGE, SUPERIMPOSED ON THE FAILED SOUTHERN EMBANKMENT, SHOWS CLOSE CORRELATION WITH EROSION SCARS 1 & 3.

7.2.3. Consideration of drained instability as the cause of the failure

Substantial evidence suggests that Blocks A and B (Figure 34) slid on an underlying weak layer or interface. The interface between the coarse tailings forming the dam embankment with the fine tailings from Dump 10 and tailings left behind after reclaiming the South Dump appears a likely candidate. The satellite image record indicates that, in the case of Block A, a southward movement approaching 90 m had taken place since February 2019 up to the time of the failure. The magnitude of movement would have been more than adequate for the mobilisation of low residual frictional strengths along the shearing interface. It was reported in Section 6.7 that it appears that the slippage was occurring along the baseline surface indicated in Figure 31 along a slope of approximately 2.7° (1:21.4). Figure 46 presents residual friction angle values for clays, tills and shales, plotted against plasticity index (I_P) (Knappett & Craig, 2012). The range of I_P values measured during the investigation at Jagersfontein was narrow, falling between 8% and 15%, for which Figure 46 indicates residual friction angle values between about 16° and 31°.

The drained factor of safety (FoS) against slip parallel to a uniform infinite dry slope can be expressed as $FoS = \frac{tan\phi'}{tan\beta}$, where ϕ' is the effective friction angle and β the slope angle. Even when considering a very low residual friction angle value of 10° and the 2.7° slope angle mentioned above, the calculation yields a factor of safety of 3.7, indicating stability. In the presence of a water table with flow occurring parallel to an infinite slope, the expression for the drained factor of safety reduces to $FoS = \frac{\gamma'}{\gamma}\frac{tan\phi'}{tan\beta}$, with γ' the buoyant unit weight and γ the saturated unit weight. Taking the ratio $\frac{\gamma'}{\gamma}$ to be approximately 0.5, a drained factor of safety of 1.9 is calculated for saturated conditions and the parameters above. This still indicates stability despite being a very conservative idealisation of the Jagersfontein situation. Drained instability therefore does not appear to explain the movement over time along the flat 2.7° slope. It is therefore believed that slippage has been occurring under

undrained conditions which must first have developed during the instability experienced in February 2019 (discussed below) and which appear to have been sustained as movement never appeared to have completely stopped before the failure event.

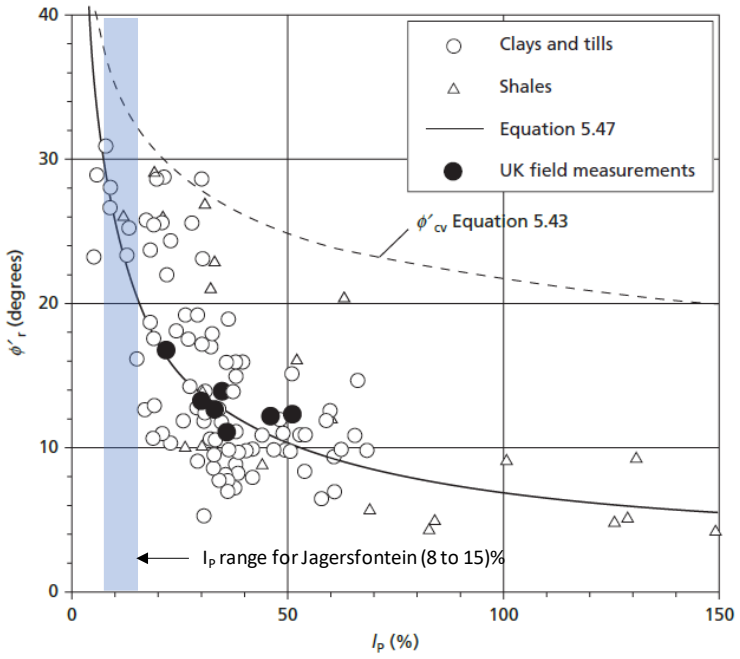

FIGURE 46 RESIDUAL FRICTION ANGLE VALUES FOR CLAYS, TILLS AND SHALES AGAINST PLASTICITY INDEX (I_P), WITH THE I_P RANGE FOR JAGERSFONTEIN INDICATED (KNAPPETT & CRAIG, 2012).

7.2.4. Consideration of drained stability of the February 2019 profile

The assumed February 2019 profile along the alignment shown in Figure 8, was presented in Figure 33. The downstream slope was at the angle of repose of the coarse tailings, i.e. approximately 33°, significantly steeper than the 1:2 (27°) slope angle recommended by Robinson (2015) (Figure 20). The base of the embankment is believed to be underlain by fine tailings from Dump 10. The piezocone investigation did identify layers of clay-like material that may correspond to material from Dump 10 (Appendix F). An idealised cross-section profile used for the stability analysis of the downstream slope, as estimated from survey data and the CPTu soundings, is shown in Figure 47.

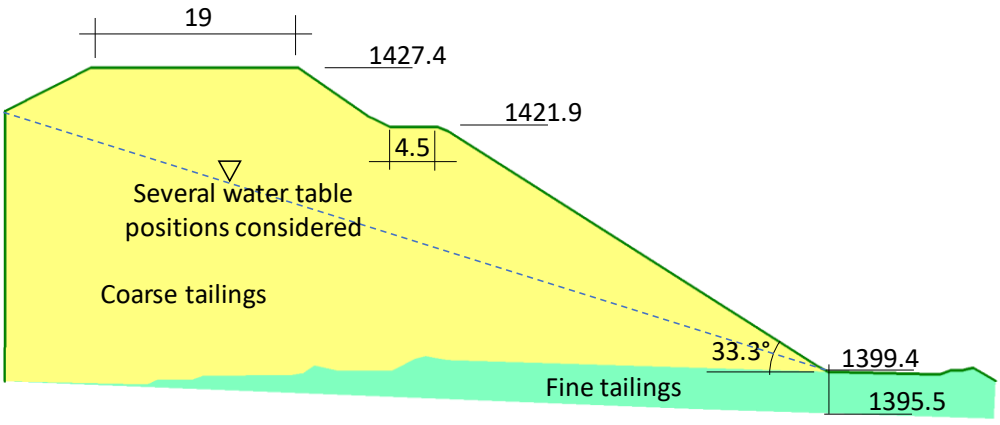

FIGURE 47 CROSS-SECTION PROFILE FOR SLOPE STABILITY ANALYSIS OF FEBRUARY 2019 DOWNSTREAM SLOPE.

The Investigation Panel assumed that the fine tailings underlying the coarse tailings have similar properties to the fine tailings in the De Beers Dam. A set of triaxial tests was therefore carried out on fine tailings collected from the De Beers Dam, giving a friction angle of 26.5°. This can be compared to the friction angle of 23.2° referred to in the design report for the Dam (Robinson, 2015). A set of direct simple shear (DSS) tests was also carried out on the fine tailings which showed a friction angle of only 22.5°. A set of triaxial tests was also carried out on the coarse-grained tailings and produced a friction angle of 38°. More details of the geotechnical laboratory investigation carried out for this study are presented in Appendix E.

Table 4 presents the material properties selected for the fine and coarse tailings for the slope stability analysis of the February 2019 geometry. Zero cohesion was assumed. Note that the friction angle value selected for the fine tailings is possibly not conservative when considering the simple shear result and the value by Robinson (2015) and the DSS test results.

TABLE 4 SOIL PARAMETERS FOR DRAINED SLOPE STABILITY ANALYSIS.

Material	Effective friction angle (ϕ')	Bulk unit weight (γ_b)
Coarse tailings	33°	19 kN/m^3
Fine tailings	26.5°	18 kN/m^3

Several water table positions were considered: The first is presented in Figure 48, extending from the pool edge inside the dam down to the interface between the fine and coarse tailings, remaining at this interface below the downstream slope of the dam. A water table at the top of the fine tailings is considered realistic given the way that seepage was emerging above the fine tailings as reported in Section 7.2.1 and given the presence of Dam 10 immediately adjacent to the downstream slope of the tailings dam. (The occurrence of instability during or shortly after the rapid filling of Dam 10 during significant rainfall in the first two weeks of February 2019 may not be a coincidence.)

The slope stability analysis was carried out using the Morgenstern-Price limit equilibrium method. The most critical slip surface for this analysis is relatively shallow and is shown in Figure 48. The associated factor of safety was 1.03, indicating marginal stability. Figure 49 presents the situation with a water table extending from the edge of the pool in the tailings dam to the toe of the dam, giving a factor of safety of only 0.92, indicating instability. Figure 50 presents the factor of safety of 0.96 for a failure surface extending to the dam crest which is believe to be representative of the situation illustrated in the March 2019 satellite photo where signs of severe instability, reaching the dam crest, were evident (Figure B11). Although the position of the water table is not known, the water table in Figure 50 is considered realistic. (A steady-state seepage analysis assuming an upstream water level at the pool edge predicts a substantially higher water table and hence a considerably lower drained factor of safety.) The low factors of safety and the large associated failure surface are consistent with the instability experienced in 2019 and indicates an unstable slope when analysed based on drained conditions.

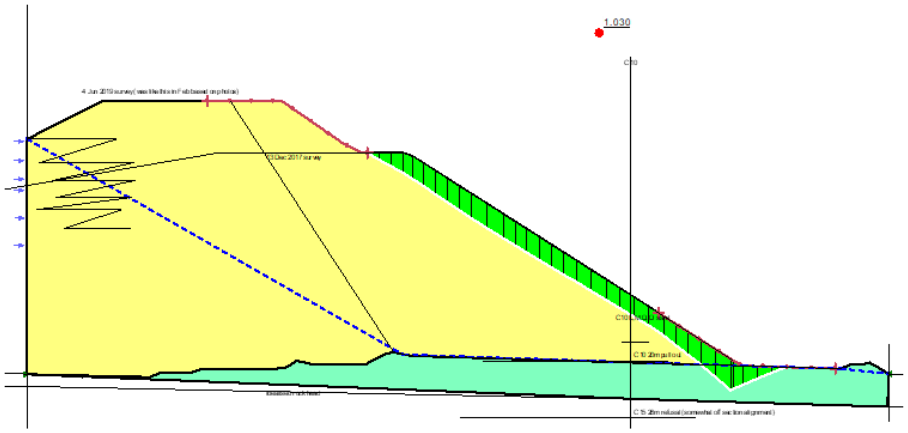

FIGURE 48 DRAINED SLOPE STABILITY ANALYSIS 1 (FOS = 1.03).

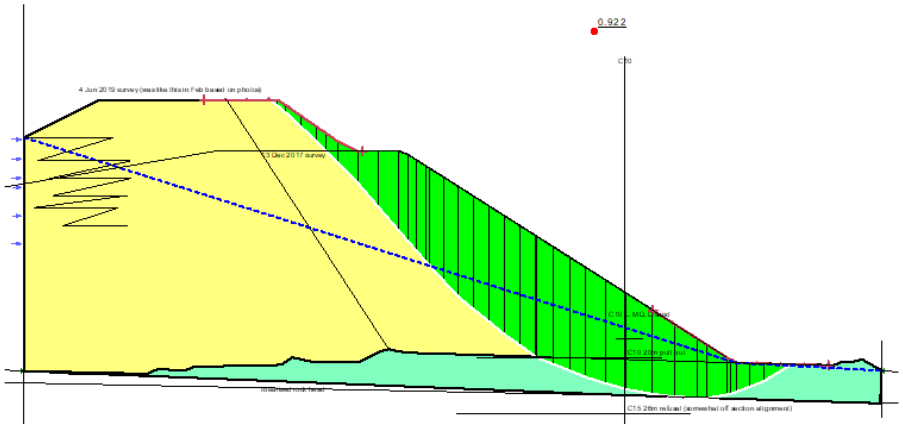

FIGURE 49 DRAINED SLOPE STABILITY ANALYSIS 2 (FOS = 0.92).

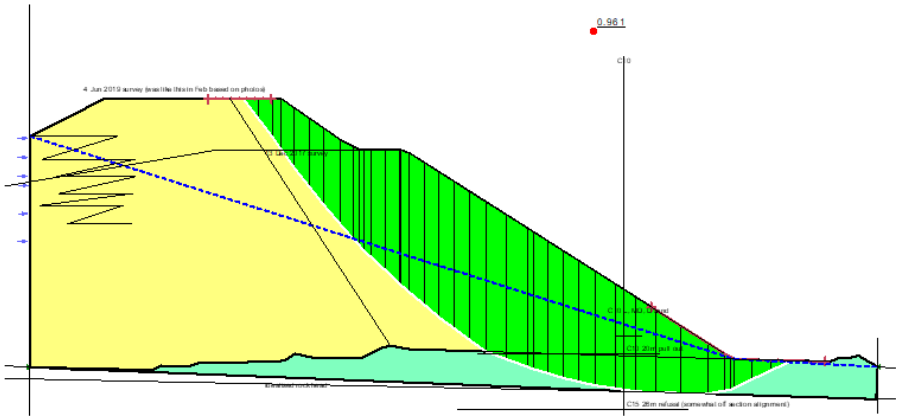

FIGURE 50 DRAINED SLOPE STABILITY ANALYSIS 3 (FOS = 0.96).

7.2.5. Consideration of undrained instability

A cross-section through the part of the dam that failed on 11 September 2022 is included in Figure 51 and is based on the last available survey before the failure, dated 27 April 2022. The geometry of the Baseline survey, December 2017 survey and the July 2021 survey are also included. The purpose of presenting theses cross-sections is to consider possible failure surfaces consistent with the movement observed for the purpose of back calculating a mobilised undrained shear strength ratio (c_u/σ'_v).

As mentioned in Section 6.7, the movement that occurred from February 2019 to the time of failure was consistent with that of sliding along the Baseline profile (Figure 30). As mentioned above, there is evidence that the southern toe of the dam experienced southward movement of up to 90 m over the course of the 3.5 years preceding the failure. It is hypothesised that these movements would have resulted in undrained conditions being mobilised and sustained along the failure plane, i.e. the generation of positive pore pressures (assuming that the interface was sufficiently contractive and impervious), resulting in a substantially reduced shear strength. It is hypothesised that the continued movement of many tens of millimetres per day, in combination with the low permeability of the fine tailings, would have sustained the undrained conditions and low mobilised shear strength.

It was attempted to determine factors of safety for two different scenarios, i.e.:

1) The situation where progressive movement continuously took place along an interface.

2) The failure event of 11 September 2022.

7.2.5.1. Long-term movement prior to failure

It has been shown that the cross-section profile of the southern wall of the tailings dam was unstable when analysed based on drained conditions and first experienced stability problems in February 2019 as determined from available satellite images. This was followed by remedial action attempting to stabilise the slope, but movement of the slope continued to occur, apparently along an interface underlying the buttress presumably constructed to stabilise the embankment.

Figure 51 shows two unusual features. The first is the large movement of approximately 19 m between July 2021 and April 2022 evident at the downstream toe, which was discussed previously, and the second is the observation that the downstream slope of the crest seemed to have moved in an upstream (northward) direction. Normal raising of an upstream dam is illustrated conceptually in Figure 52, showing material being placed on the crest, raising the dam embankment towards the inside in an upstream direction while the downstream face of the slope remains static. Why would the downstream slope near the crest have migrated in an upstream direction between the 15 July 2021 and 27 April 2022 surveys? (Retrogressive movement of the downstream cress slope is actually evident since the 10 September 2020 survey. See Figure 30.) It is hypothesised that this was the area where the rear scarp of the failure surface exited as slippage continued to occur over a long time, causing material to be removed from the downstream crests slope due to instability.

An examination of the satellite images, best seen on PlanetScope images from February - June 2019 (Figure 3 to 6a in Appendix C), shows that large volumes of material were regularly placed at mid-slope, which was presumably done in an attempt to stabilise the slope after February 2019 and to compensate for the loss material due to the long-term slippage, removing material in a southerly direction. (Note that more effective slope stabilisation generally involves placing material (weight) at the toe, not at mid-slope. Also, it is important that such material be placed on a competent drained foundation. The Investigation Panel have not observed evidence of weight specifically being placed at the toe from the satellite images after the construction of the buttress between February and June 2019.)

Satellite images show that, as the embankment crest slowly advanced towards the north as the dam embankment was raised, the downstream toe continued migrating southwards, and at a greater rate. The interface on which movement was taking place must have been underneath this buttress. The observations suggest that the rear scarp associated with the continued movement must have exited near the toe of the downstream crest slope. Two possible locations where the rear scarp might have exited are shown on an excerpt of the post-failure helicopter video footage shown in Figure 53. A candidate failure surface associated with the abovementioned mechanism is shown in Figure 51.

The cross-section was subdivided into material types as indicated in Figure 54. The geometry of the old De Beers Dam, as excavated prior to extension of the tailings dam, was taken from survey data, as was the baseline underneath the embankment. The trapezium-shaped zone, labelled 13 December 2017, stems from a survey from that date and represents the newly constructed southern wall of the dam when Compartment 2 was constructed. It was assumed that material in the area between the old De Beers Dam and this zone contained saturated fine tailings as the satellite image dated 30 July 2017 (Figure B8) indicates that at least some of this area was backfilled with tailings slurry. The phreatic surface used in the stability analysis was determined from the recent piezocone investigation and the assumption that the water table extended from the dam basin through the embankment as shown. Some CPTu positions are indicated on Figure 54 based on the positions where they were carried out on the post-failure geometry. (It should be kept in mind that the pre-failure geometry moved approximately up to 20 m during, and possibly also after the failure, before the piezocone investigation was carried out.) The material below the assumed water table in the upstream part of the raised embankment was taken as fine tailings deposited hydraulically in the dam, overlain by coarse tailings placed as the dam was raised.

Approximate bounds were set for the slip surface entry and exit zones to match the failure surface hypothesised in Figure 51. The Morgenstern-Price limit equilibrium method was used and slip surface optimisation was applied. For the purposes of the stability back-analysis, all fine tailings zones located below the water table were assumed to act undrained, with the same yield strength ratio. A drained shear strength associated with a friction angle of 33° and bulk unit weight of 19 kN/m^3 were assigned to the coarse tailings. The SHANSEP equation (constant value c_u/σ'_v; Ladd & Foott, 1974) was used to model undrained shear strength.

A yield strength ratio of 0.11 resulted in a factor of safety of unity for the failure surface shown in Figure 55. This yield strength ratio magnitude is well below the lower bound for value of 0.23 quoted by Olson & Stark (2003), back calculated from failure case histories, and below the values by Olson & Matson (2008) for triaxial shear. It is also below the range for simple shear (lower limit of 0.13) quoted by Olson & Matson (2008). Due to the ongoing long-term nature of the movement experienced, it is more appropriate to compare the back-calculated undrained shear strength ratio to the range of liquefied strength ratios back-calculated from failure case studies (0.02 - 0.12 quoted by Olson & Stark (2002)) where it falls near the upper bound. The value falls right in the middle of the range (0.01 – 0.22 quoted by Olson & Mattson, 2008) for triaxial shear. An effective friction angle of between 6° and 7° is required to produce a factor of safety of 1 for a similar failure surface under drained instability, again illustrating that drained instability is unlikely to have been the mechanism of the long-term deformation. It appears that the long-term instability was due to sliding along an underlying interface where undrained conditions were maintained by the ongoing movement and the low

permeability of the material along the failure surface. Instability first initiated due to drained instability as explained in Section 7.2.4.

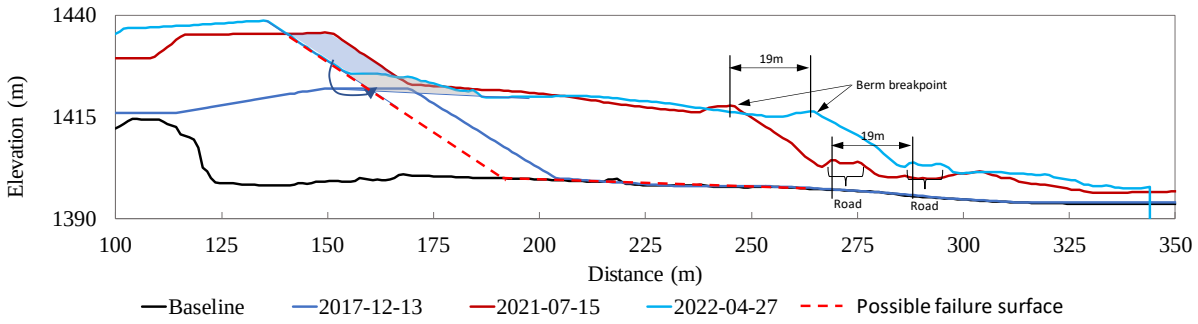

FIGURE 51 CROSS-SECTION USED FOR SLOPE STABILITY ANALYSIS TO ASSESS THE UNDRAINED SHEAR STRENGTH RATIO MOBILISED DURING LONG-TERM SLOPE DEFORMATION.

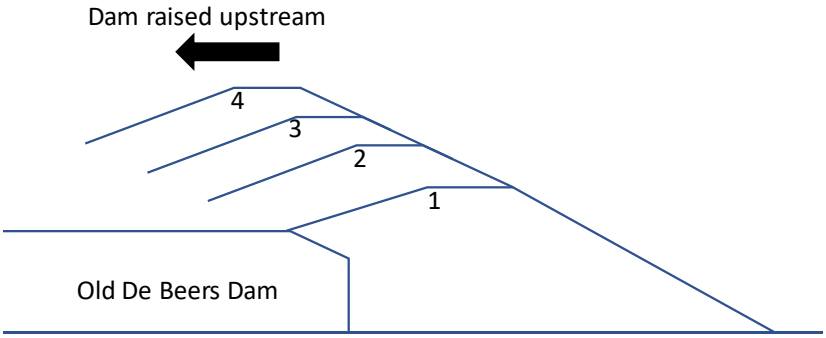

FIGURE 52 NORMAL UPSTREAM RAISING OF EMBANKMENT

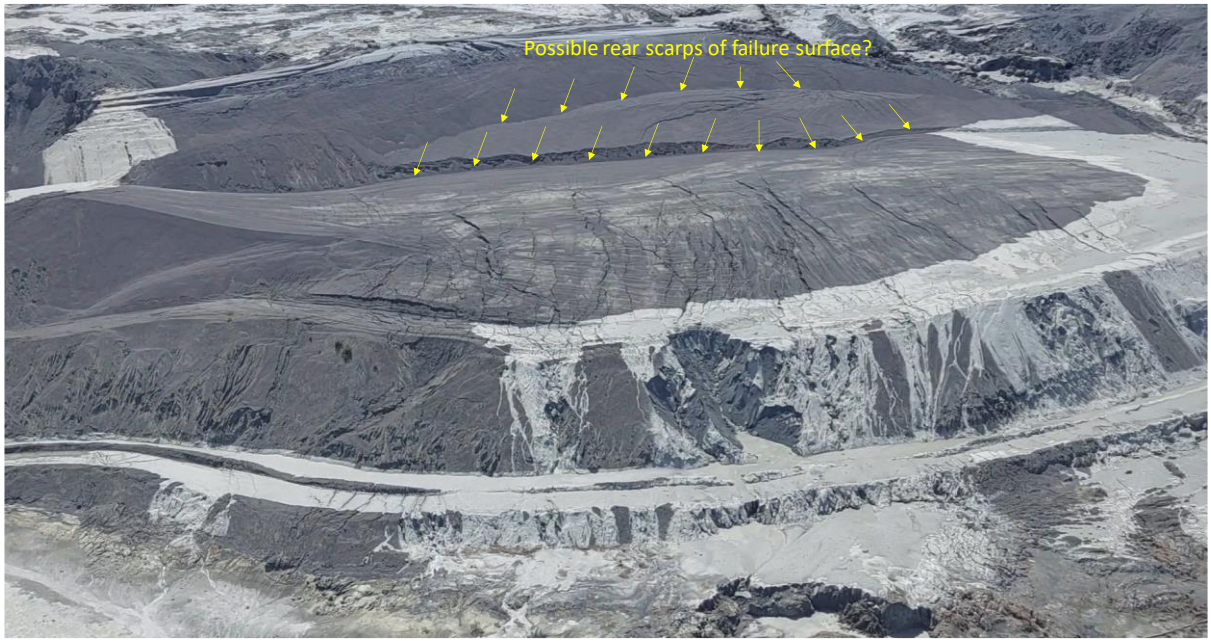

FIGURE 53 CANDIDATE REAR SCARP OF FAILURE SURFACE BEFORE 11 SEPT 2022 EVENT (SOURCE: MR A HAVENGA AND/OR MR WM RAMOKOPA).

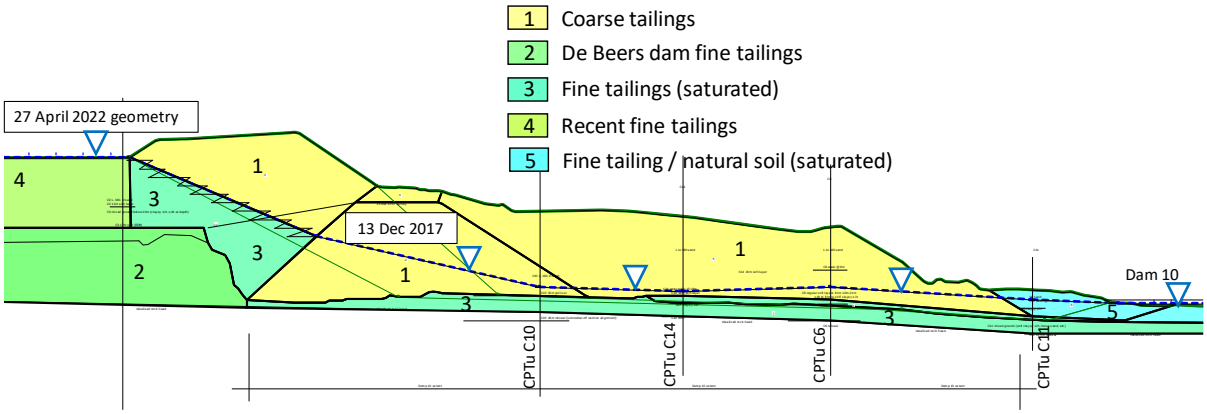

FIGURE 54 MATERIALS ZONES ANALYSED FOR FINAL STABILITY ANALYSIS

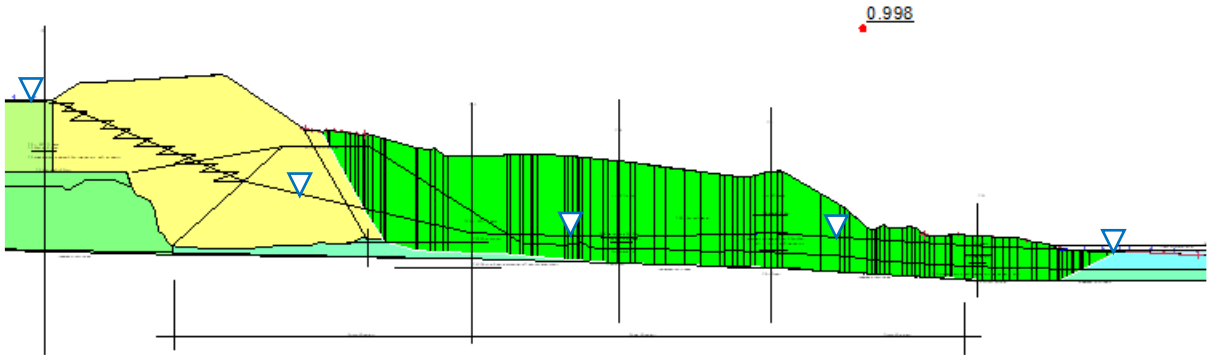

FIGURE 55 FAILURE SURFACE ASSOCIATED WITH A YIELD STRENGTH RATIO OF 0.11 GIVING A FACTOR OF SAFETY OF UNITY MATCHING LONG-TERM MOVEMENT OBSERVED ON EMBANKMENT (FOS = 1.00).

7.2.5.2. The 11 Sept 2022 failure event

It was reported in Section 7.1 that on the early morning of 11 September 2022, the wall of the tailings dam failed to the inside at the location of the main breach. This was followed by what was described as "slumping of the crest", followed by overtopping of the slumped part (Havenga, 2023). Comparison of the post-failure survey carried out on 12 September 2022 to the survey from 27 April 2022 indicates movement of approximately 15 m to the south in the alignment of the access road at the toe. Scaling from the satellite images suggests even larger movements as discussed in Section 4.2. It is not known how much of this movement took place before the failure, but the rate of movement seems to have slowed down during the months before the failure (see Figure 10). Movement could not be identified on the dam by visually comparing the 24 May 2022 and 28 July 2022 satellite images (Figures B21 and B22).

It was mentioned in Section 4.2 that the upstream toe of the southern wall of the dam advanced significantly towards the inside of the dam between 12 January 2022 and 24 May 2022 (approximately 14 m scaled from satellite images opposite Scar 2). PlanetScope images indicate significant activity associated with further widening of the wall towards the inside, right up to the week before the failure. The accelerated wall building activity was probably necessitated by deposition which did seem to have increased in the year before the failure (Figure 29). It is hypothesised that the failure to the inside of

the dam on the morning of 11 September 2022 occurred due to the relatively rapid placement of coarse tailings over unconsolidated fine tailings in the pond during wall building, thereby rapidly adding weight to the underlying weak material, consequently overloading this weak material. The dam was often operated without a beach in 2022, especially in Compartment 2 (see satellite images from 2022, Figures B20 to B22), with tailings slurry and water ponding right up against the outer walls, contrary to the recommendations in the design report (Robinson, 2015).

Signs of movement were not clearly evident on the southern wall of the tailings dam in the months preceding the failure, but the continued raising and filling of the dam would have increased the shear stresses mobilised in the foundation. It appears that the dynamic impact associated with the slip to the inside was the proverbial straw that broke the camel's back. It is hypothesised that this event provided the trigger for the sliding along the interface associated with the failure event where slippage had been occurring for more than three years (see Figure 8 and Figure 34). This slippage led to the failure of the dam. The slippage is believed to have resulted in the slumping observed at the crest, reported by Havenga (2023).

Figure 56 presents the April 2022 cross-section profile and the post-failure profile from 12 September 2022 survey along the critical alignment (Figure 8). It shows a relatively small hypothetical failure surface at the crest to the inside of the dam, the proposed trigger, and a hypothetical failure surface associated with the subsequent slumping of the crest and sliding displacement of the embankment during the main failure.

The cross-section at the failure was subdivided into material types as indicated in Figure 54. Approximate bounds were set for the slip surface entry and exit zones to match what occurred during the actual failure. Again, the Morgenstern-Price method was used and slip surface optimisation was applied. For the purposes of the stability back-analysis, all fine tailing zones located below the water table were again assumed to act undrained, with the same yield strength ratio. An undrained strength ratio of 0.175 resulted in a factor of safety of unity for the large overall failure surface shown in Figure 57. This strength ratio falls between the ranges for the yield strength ratio (0.23 to 0.31) and liquefied strength ratio (0.02 to 0.12) back calculated from failure case studies quoted by Olson & Stark (2002 and 2003) and is at the lower bound of yield strength ratios quoted by Olson & Matson (2008) for triaxial shear, but in the mid-range for values determined from simple shear for fine sands and silty sands. The observation that movement seems to have reduced in the months preceding the failure (see Figure 10) may have resulted in mixed drainage conditions along the slip interface, resulting in the single back-calculated strength ratio falling between the normal bounds for peak and liquefied values quoted above.

A drained friction angle of 9° is required to produce a factor of safety of unity (1) for a similar failure surface under drained conditions, again illustrating that undrained instability was the likely mechanism.

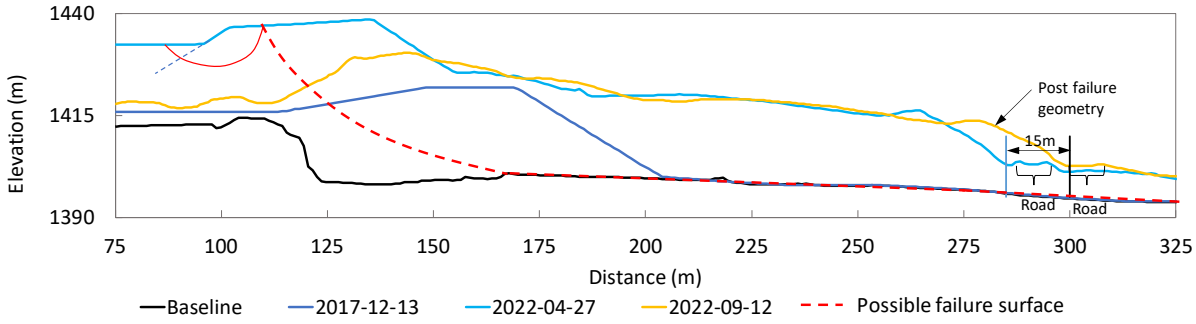

FIGURE 56 HYPOTHETICAL CROSS-SECTION ASSOCIATED WITH THE 11 SEPTEMBER 2022 FAILURE EVENT.

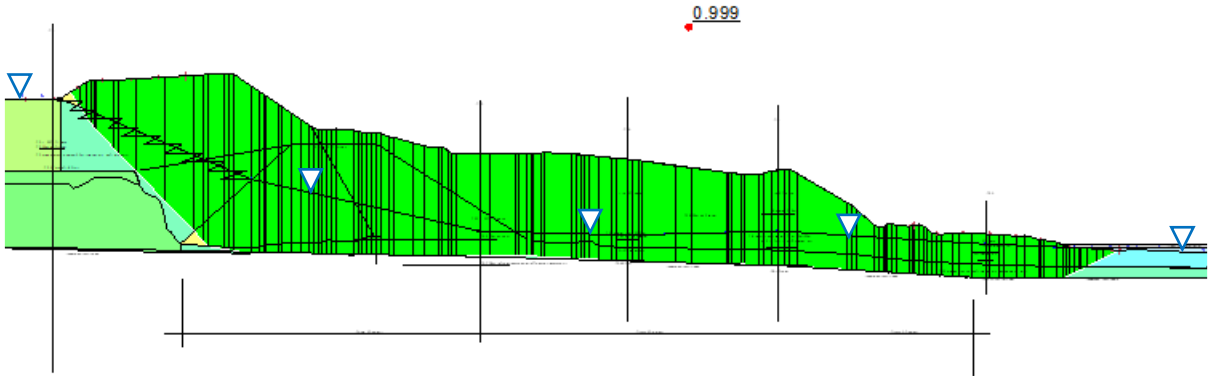

FIGURE 57 OVERALL SLIP SURFACE ASSOCIATED WITH A YIELD STRENGTH RATIO OF 0.175 GIVING A FACTOR OF SAFETY OF ONE.

The critical failure surface can be seen to extend through the zone of saturated fine tailings underneath the embankment crest. This zone was subsequently modelled as drained with the same properties as that of the coarse tailings, which reduced the required yield strength ratio for a factor of safety of one to 0.16, not very different from the 0.175 first calculated.

7.2.6. Stabilising the slope

The record of satellite images show that large volumes of material were placed along the section of the dam wall that eventually failed, resulting in this section of wall being considerably wider than elsewhere along the dam's perimeter. The additional material placed presumably reflected attempts to stabilise the slope against the movement that was occurring.

In terms of slope stability, the placement of material on a slope can have a stabilising or destabilising effect, depending on the geometry of the problem and dependent on whether conditions are drained or undrained. Refer to Figure 58. Placing weight on a slope has two effects:

1. Increasing the component of the weight parallel to an underlying slip surface.
2. Increasing the stress in the slope.

Figure 58 illustrates a curved failure surface in a slope. Weight placed to the right of the centre of rotation will add to the stabilising moment and will always increase the resistance against slope failure whether conditions are drained or undrained. (An important aspect requiring consideration is the rate at which load is placed. Care must be taken that load placement is not so rapid that it results in undrained instability. The discussion here assumes sufficiently slow placement of weight as to not causing undrained instability.)

The influence of weight placed to the left of the centre of rotation is more complex and a distinction needs to be drawn between drained and undrained conditions. Under undrained conditions, weight placed here will add to the destabilising moment without affecting soil strength. The effect on slope stability will therefore always be negative. In the case of drained conditions, the added weight will affect both the component of the weight driving failure, but also the soil strength. If the slope of the failure surface under the area where weight is placed is flatter than the friction angle of the soil, the increase in soil strength will exceed the additional component of weight driving failure ("B" in Figure 58). If the underlying failure surface is steeper than the friction angle of the soil ("C" in Figure 58), the increase in the component of weight driving failure will exceed the increase in strength and the effect on slope stability will be negative.

In the case of a planar failure surface, the effect of weight added to the slope will always be negative under undrained conditions. In the case of drained conditions, the effect of weight will be negative if the failure surface is steeper than the soil friction angle and positive if the failure surface is flatter than the soil friction angle.

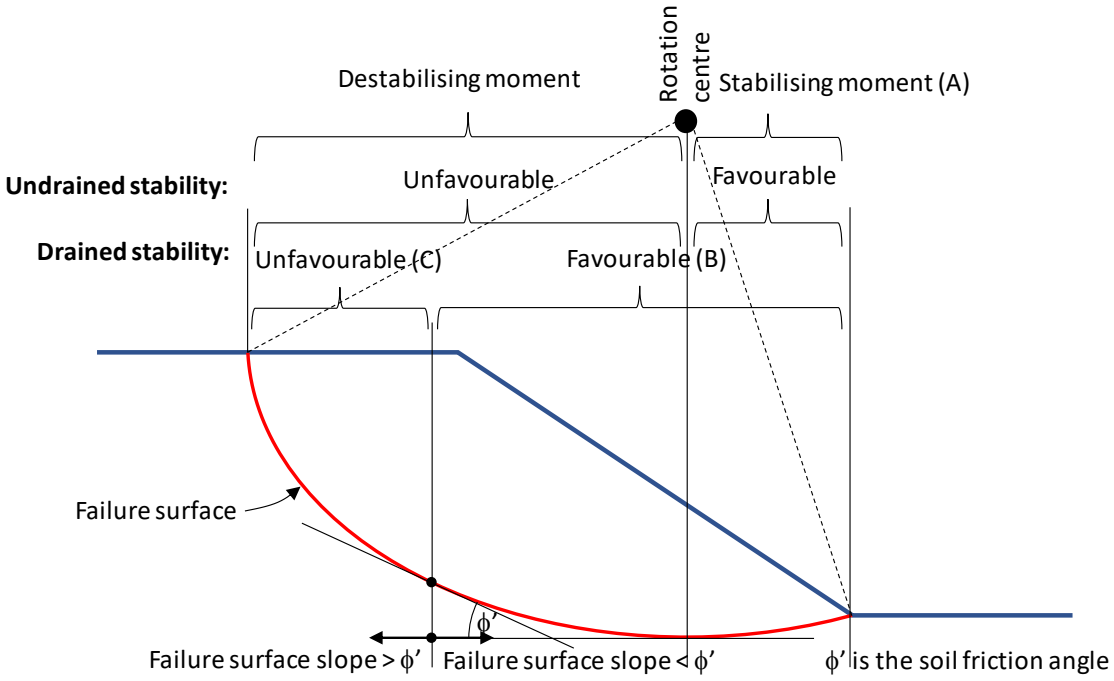

FIGURE 58 THE EFFECT OF PLACEMENT OF MATERIAL ON A SLOPE ON THE STABILITY OF THE SLOPE UNDER DRAINED AND UNDRAINED CONDITIONS.

Figure 59 presents a simplified idealised cross-section of the Jagersfontein Tailings Dam at the section that failed. It shows the coarse tailings embankment overlying a zone of fine tailings in which undrained conditions have been mobilised. Undrained conditions are sustained by constant movement along this interface. Placement of weight, irrespective of the location (1, 2 or 3), will not stabilise the slope because of the undrained conditions on the interface where movement is taking place. In fact, it will add to the component of the weight parallel to the slope driving movement, although the component will be small due to the flat slope on which slip is occurring. In addition, the added weight may serve to sustain the undrained conditions if placed rapidly. In order to stabilise the slope, movement must first be arrested to stop the generation of undrained conditions. Only then may weight be placed on the slope to increase the effective stress and hence drained strength of the fine tailings layer, taking care not to cause further undrained conditions by excessively rapid placement. Any structure to stabilise the slope, such as construction of a buttress at the toe, must be founded on a sound foundation below the interface on which movement occurs.

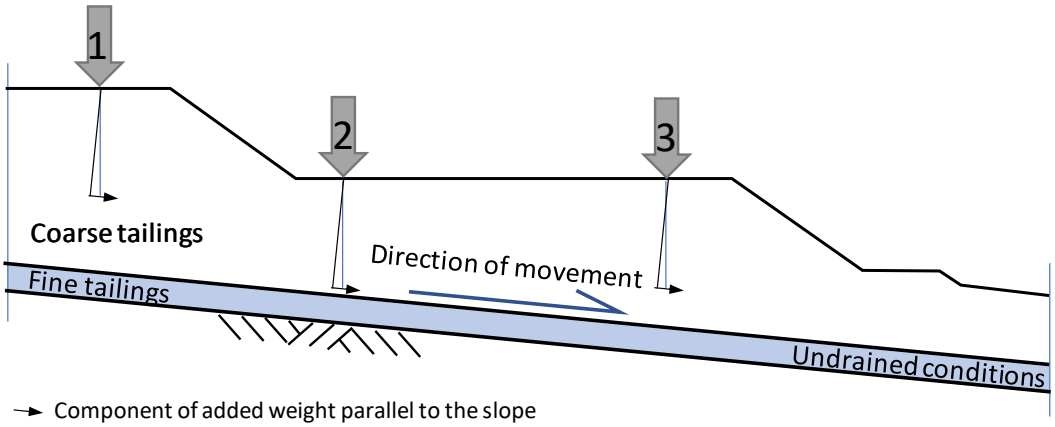

FIGURE 59 SIMPLIFIED CROSS-SECTION OF THE CRITICAL SECTION OF THE JAGERSFONTEIN TAILINGS DAM.

8. Summary and Conclusions

The Investigation Panel were not allowed to interview employees of JD or discuss with them aspects of the tailings dam failure and events leading up to it. Accordingly, we resorted to alternative sources referenced in this report to describe the likely events leading up to the failure. Some details may be subject to refinement had communication with JD been possible.

It is unclear when construction on the old De Beers Tailings Dam commenced, but it is believed to have been between 1931, when the Jagersfontein Diamond Mine was acquired by De Beers Group, and 1944, the date of the first available aerial image of the dam. The dam was required to accommodate increased production, generating greater volumes of waste than what could be accommodated by a complex of waste dumps (Marais et al., 2024), later to be remined. In 1971 mining operations were halted and little changed on the tailings dam until 2010 when the remining of the old dumps commenced. Much of the ground around the old De Beers Dam has historically been covered by tailings, some deliberately and some by decades of erosion from the old dumps (Robinson, 2015).

In 2010, the old De Beers Dam was expanded by construction of a new tailings disposal compartment (Compartment 1) to the west and immediately adjacent to the De Beers Dam. The facility comprised the construction of containment walls from coarse tailings (grits) to store fine tailings (slimes) deposited hydraulically within. The coarse tailings are competent material for the construction of the containment walls. Compartment 1 began to reach its capacity by 2014. Additional deposition space was provided by the construction of a new compartment (Compartment 2) immediately to the east and south of the De Beers Dam, commencing in 2015. The walls forming this compartment comprised a northern, eastern and southern wall, with the old De Beers Dam forming its western boundary. The area on which Compartment 2 was developed had previously been impacted by tailings. Some of the tailings were removed or partially removed by reprocessing operations, but some of it, notably Dump 10 (to the south of the De Beers Dam) and some of the material from the South Dump (to the southeast of the De Beers Dam) remained. The fine tailings at Jagersfontein have a low shear strength with an effective friction angle of 20° recommended in the design report for Compartment 2 (Robinson, 2015). The material also has a very low permeability (Robinson, 2015). Parts of the southern wall of Compartment 2 were constructed at least partially overlying this low-strength material.

Satellite images show that slimes deposition in Compartment 2 commenced in 2016. Deposition on the tailings dam took place via a single discharge point on the western wall of Compartment 1. Tailings slurry from Compartment 1 flowed into Compartment 2 via a gap in the wall separating the two compartments located almost directly east of the discharge point in Compartment 1. Compartment 2 filled up and by February 2019 the De Beers Dam had been completely submerged.

The first signs of instability along the part of the southern wall of Compartment 2 adjacent to Dam 10 can be identified in satellite images from February 2019 at the time just after Dam 10 had filled up rapidly with water following rainfall. A series of slope failures appear to have occurred in February and March of 2019 on the downstream slope of Compartment 2 opposite Dam 10 and were immediately followed by considerable construction activity, presumably to restore the stability of the wall. However, the additional weight on the downstream slope did not stabilise the dam wall due to

undrained conditions mobilised on the underlying interface where slip was occurring and most probably only served to add somewhat to the problem. (The component of weight parallel to the underlying slip surface would have amounted to a small percentage of the total weight placed due to the flat slope angle along which movement occurred (i.e. about 2.7°.)

From February 2019 a portion of the access road along the southern wall of the tailings dam, adjacent to Dam 10, began to be displaced to the south because of movement of the ground underneath. The originally straight road began to curve in the area affected by the slope instability. Scaled from satellite images, this movement continued at an average rate of 79 mm per day over the course of two years until early 2021 and then slowed down to an average rate of 26 mm per day until the failure took place on 11 September 2022. The total southerly displacement of the road's edge from early February 2019 until the date of the last available pre-failure satellite image (28 July 2022) amounted to approximately 87 m. Additional examples of movement include the movement of a tracked feature (rock or a shrub), located between the road and Dam 10 (which also amounted to 87 m), a tree adjacent to the northern end of the Dam 10 embankment that moved 28 m over two years, and the observation that the Dam 10 crest sloped upwards by 3 m towards the tailings dam from its "normal" crest elevation (dam crests are typically constructed level). The affected wall section saw much more construction activity than any other section, presumably as JD attempted to compensate for movement in the area between February 2019 and September 2022 when the wall eventually failed. This wall section was also much wider than any other. This section of the tailings dam wall also saw unusual activity such as the construction of the donut-shaped feature seen in satellite images from late 2019 into 2020, which must have been a response to a problem, probably sinkhole formation or piping, likely indicative of a potential stability problem.

The February 2019 geometry of the tailings dam wall was constructed from two sets of survey data, informed by satellite images. Slope stability analyses based on this cross-section profile and the Investigation Panel's finding that the wall was constructed over low-strength slimes, indicate instability when assuming drained strength parameters. Practically all slopes on the tailings dam, including the February 2019 slope that showed signs of instability, were constructed at the angle of repose of the coarse tailings (~33°). The design by Robinson (2015) recommended a downstream slope of 1:2 (27°). Due to the lack of availability of as-built drawings, the Investigation Panel were not able to confirm whether other aspects of the design, such as the drainage system, were constructed or not. A multi-point delivery system and decant facility, required for pool management, recommended in the design report, were not constructed. As a consequence, the pool normally extended right against the outer walls and no beach was present. As such, drying and desiccation and the associated strength gain of the beach, i.e. the foundation on which the dam wall crest was raised by upstream construction, could not occur. It is the Investigation Panel's view that this played a major role in the slope failure to the inside (i.e. upstream) of the dam which was reported to have occurred on the morning of the failure, and which preceded the failure of the southern wall of the tailings dam.

The evidence suggests that, since February 2019, the movement of the southern wall of the tailings dam occurred along the interface between the weak fine tailings and the overlying embankment constructed from coarse tailings (grits) (see Section 7). The CPTu soundings performed by the Investigation Panel indicate the presence of clay-like soils at depth, occurring below the water table as identified from the CPTu pore pressure measurements, in several of the locations probed. In addition, shear wave velocity measurements indicate somewhat reduced shear wave velocities in the

clayey soils at depth. Although it is difficult to point to a single interface on which movement mobilised, the observations presented corroborate the existence of such a zone or plane. It is believed that the continued movement, in combination with the low permeability of the material, maintained undrained conditions on the interface. This allowed movement to take place along the flat interface slope in question (2.7°) over a long time.

Satellite images suggest that, in the months preceding the failure, there were both a deceleration of movement and an increase in construction activity to widen and raise the crest in the area of the failure. The Investigation Panel believe that the raising of the crest over poorly consolidated fine tailings resulted in the slope failure to the inside (i.e. upstream) of the tailings dam on the morning of 11 September 2022 and that this event triggered the failure. The low undrained shear strength available along the interface where movement had been occurring for a long time was insufficient to maintain equilibrium so that a large amount of horizontal displacement occurred (up to approximately 20 m), which was accompanied by slumping of the crest by approximately 8 m. The freeboard at the time was estimated at approximately 7 m. This resulted in overtopping of the tailings dam where the main breach occurred and shear interfaces developing at failure Scars 1 and 3, leading to piping. The piping eventually self-healed or became inactive due to the lowering of the fluid level in the dam as the outrush of water and tailings slurry progressed. As a result of the embankment failure, the mobilisable contents of the tailings dam, amounting to approximately 5.1 million m^3 of fine tailings slurry and water, was discharged into the Proses Spruit.

In summary, the Investigation Panel considers the following the most likely sequence of events:

1. Drained slope instability occurred along the downstream slope of the southern wall of Compartment 2 adjacent to Dam 10 in February 2019 soon after Dam 10 filled up following rainfall.

2. Movement mobilised along an interface below and downstream of the tailings dam wall toe. The interface probably developed between the coarse tailings comprising the outer walls and legacy fine tailings of very low shear strength covering significant parts of the dam wall footprint.

3. Due to the low permeability along the interface, undrained conditions were maintained in the interface by the movement taking place.

4. JD placed material on the affected section of wall underlain by the plane on which movement was taking place. Due to the undrained conditions on the interface this action did not stabilise the wall.

5. Movement continued to take place and more material was added by JD to compensate for this movement.

6. Movement reduced in the months preceding failure, possibly allowing some drainage to occur on the interface.

7. All-the-while the tailings dam outer walls were regularly raised upstream by tipping and dozing coarse tailings onto the unconsolidated water-logged beach.

8. The inner slope of the tailings dam crest failed to the inside of the dam on 11 September 2022.

9. This event provided the trigger to remobilised undrained conditions on the previously mobilised interface.

10. Equilibrium could not be maintained any longer, a large amount of slip occurred on the mobilised interface and the dam failed.

9. Recommendations

9.1. The urgency of post-failure geotechnical investigations.

Jefferies and Been (2016) stated that the "Number 1" task for any site investigation is the assessment of the phreatic conditions. It is thus essential that any CPTu investigation aimed at determining the pore pressure regime in a tailings dam that failed be carried out as soon as possible after the failure, before the pore pressure regime changes significantly. As an example, it is known that a CPTu probe was established on the Merriespruit Tailings Dam in less than three weeks after the failure (Rust, 2024).

It is understood that DWS issued a directive to JD the day after the failure to commission an investigation into the causes of the failure, but that this directive was subsequently withdrawn due to concerns about potential conflict of interest. In the opinion of the Investigation Panel, this withdrawal is regrettable because the pore pressure regime as measured by the CPTu investigation that was carried out nearly 17 months after the failure would have changed very significantly from that present shortly after the event. In addition, drainage and consolidation of the materials, playing a role in the failure, would have taken place, changing conditions significantly from that shortly after failure.

It is the Investigation Panel's opinion that a geotechnical investigation into similar failures should be commissioned as soon as possible after the failure event and that concerns regarding potential conflict of interest be addressed through suitable peer review processes. It is further recommended that the Emergency Preparedness Plan (EPP) for major tailings dams contain contact details of suitable geotechnical consultants and adequately equipped and experienced contractors who can be approached at short notice to assist with such investigations.

9.2. The value of optical satellite imagery

Engineers make extensive use of freely available satellite imagery, the most common source of which is arguably GoogleEarth. This study demonstrated the value of using freely available optical satellite imagery together with commercial satellite imagery to identify developments over the life of the Jagersfontein Tailings Dam. The movements identified from satellite imagery in the case of the Jagersfontein Tailings Dam are best visualised by displaying the images in rapid succession, by creating an animation on a screen. Due to the time required to display images for viewing on GoogleEarth or similar platforms (also dependent on the internet connection speed), movements may be missed. It is therefore recommended that an effort be made obtain an adequate number of images to create such image sequences which may be useful to identify movement and other phenomena.

In addition to Google Earth, high temporal and spectral resolution imagery is available freely from the United States National Aeronautics and Space Administration (NASA) and the European Space Agency (ESA) via Sentinel-Hub. While this data is not the high spatial resolution satellite imagery engineers are accustomed to from Google Earth, which usually has a spatial resolution of less than 1 m per pixel, Sentinel-Hub does provide imagery at a high temporal resolution (approximately five days or better), allowing near-real-time sights of the ground surface. This data is multispectral, providing Near Infrared and Shortwave Infrared wavelength data which can be used to assess soil, or tailings moisture and

water conditions. While not a replacement for in-situ site data, this free imagery can be used alongside existing monitoring methods and to fill data gaps.

9.3. Monitoring of pore pressures and embankment settlement or movement

It is standard practice to monitor the pore pressure regime in the walls of tailings dams using suitable piezometers because the pore pressure regime plays a crucial role in slope stability. Suitable piezometers may be standpipe piezometers read manually at suitably regular time intervals using a dip meter, or electronic pore pressure transducers, preferably connected to an automated data acquisition system. In the experience of the Investigation Panel, vibrating wire piezometers connected to a suitable data acquisition system, are robust and have a rapid response time and their use is preferred over traditional standpipe piezometers. Standpipe piezometers are likely to be unsuitable in the case of the Jagersfontein Tailings Dam due to the low permeability of the tailings, which will result in unacceptable slow response time. Complementing the pore pressure monitoring system, a Trigger Action Response Plan (TARP) should be set up and maintained by the Engineer of Record to direct the required actions to be taken, depending on the pore pressures observed.

It is also recommended that a system for settlement or deformation monitoring be employed to monitor for any movement in the walls of tailings dams. The simplest system is probably a number of settlement plinths monitored using precise levelling on a monthly basis. These can be installed in parts of the tailings dam walls not impacted by the regular raising of the walls. Suitable locations include accessible berms or steps in the slopes.

Arrangements must be in place to ensure that monitored pore pressures and settlements are reviewed at suitably regular intervals by the Engineer of Record. The Investigation Panel is not aware of any pore pressure or deformation monitoring system or associated TARPs in the case of the Jagersfontein Tailings Dam.

9.4. Dam 10 adjacent to the tailings dam toe

The southern wall of the tailings dam was constructed near (immediately adjacent to) Dam 10. Being a water reservoir, Dam 10 likely raised the ground water level in the vicinity, saturating materials, including part of the foundation of the southern wall of the tailings dam, dissipating pore water suctions and thereby impacting soil and/or tailings strengths negatively. The proximity between embankments of any type and dams, or allowing dams to be constructed, causing saturation of embankment foundations, should be carefully considered at the design stage. It may be significant that the first signs of instability of the Jagersfontein Tailings Dam wall occurred when Dam 10 filled up after being empty for some time. We believe that the presence of Dam 10 had a negative impact on the stability of the tailings dam wall that failed (i.e., the south-eastern wall).

9.5. Further investigation

Due to time and budget constraints the extent of the present study was limited to the scope described in this report. Further investigation may be conducted to carry out additional sampling and laboratory

testing, but the Investigation Panel believes that it is unlikely for such studies to reveal a significantly different failure mechanism from what was found by this investigation.

9.6. Documentation

DWS could not provide a copy of the Water Use License (WUL) application, nor associated supporting documentation for the Jagersfontein Tailings Dam. The WUL application and Record of Decision (RoD) likely contained critical information documenting grounds for the granting of the WUL. Of special significance would have been a review of the design report and the report on the geotechnical investigations for the enlargement of the tailings dam. The geotechnical report is a crucial document and could not be produced. It is recommended that steps be taken to ensure that, in the future, this type of documentation is readily made available to any team or panel investigating dam failures.

9.7. Lessons from case histories

The Jagersfontein Tailings Dam failure was the consequence of a number of mistakes which find precedents in the literature, some of which are mentioned below:

In the case of the Mount Polley tailings dam failure on 4 August 2014, Morgenstern et al. (2015) mentioned “The type and extent of the pre-failure site investigations were not sufficient to detect this stratum [n]or identify its critical nature”. It appears that the ground investigation for the Jagersfontein Tailings Dam, if conducted at all, was also insufficient to detect a weak foundation.

The design for the Mount Polley Dam recommended an outer slope of 1:2. However, due to operational constraints, the slope was built to a temporary, interim slope of 1:1.4. Similarly, the downstream slope of the Jagersfontein Tailings Dam that failed was also constructed steeper than the design, i.e. 1:1.5 instead of 1:2.

A large volume of water stored on the Mount Polley tailings dam contributed significantly to the severity and consequences of its failure (Morgenstern et al., 2015). Similar observations were made by Wagener (1997) concerning the 1994 Merriespruit tailings dam failure. The large volume of water and tailings slurry on the Jagersfontein tailings dam also contributed to the severity of its failure. Decant and return water facilities, as recommended in the design report (Robinson, 2015), would have enabled less fluid to be stored, resulting in less severe consequences. Wagener (1997) recommended that legislation be implemented to make it compulsory to provide water retention facilities downslope of tailings dams. To the knowledge of the Investigation Panel no such legislation has been implemented in South Africa to date.

In the case of the Edenville Dam failure which occurred in Michigan in the USA on 19 May 2020, France et al. (2022) made the following statement: “With respect to the human judgements, decisions, actions, and inactions during the project history leading up to the May 2020 event, the dam failures were foreseeable and preventable”. In the opinion of the Investigation Panel this statement is equally valid for the Jagersfontein Tailings Dam failure. Given ample warning signs of instability, the first of which dates to 3.5 years prior to the failure, human decisions, actions and inactions contributed in an important way to this failure which was certainly also foreseeable and preventable.

Prof SW Jacobsz Pr Eng
For University of Pretoria

Dr Luis Torres-Cruz CEng
For University of the Witwatersrand

Acknowledgements

The Investigation Panel would like to express our gratitude to:

The Department of Water and Sanitation Directorate: Dam Safety Regulation for their assistance in providing data and arranging access to facilitate the study.

Jagersfontein Developments for their assistance in providing plant and assistance to create access to various parts of the tailings dam to allow the field investigation to proceed.

Prof Gerhard Heymann for his valuable insights and discussions.

Messrs Christopher O'Donovan, Alvino Bezuidenhout, Philippus Schoeman and Vian Venter for technical assistance.

References

Chief Directorate: National Geospatial Information (CDNGI). – Source of historic aerial images

Coetzee, G.L. 2024. A Numerical Replication and Analysis of the Jagersfontein Fine Tailings Storage Facility's Dam Breach. University of Pretoria.

Colliston, W.P. 2021. Geological investigation of the area around the principal slimes dam (TSF) at Jagersfontein Development (Pty) Ltd. Report No. R2021827/JAGGL.1. Report compiled for MR S. Staats, GHT Consulting Scientists.

French, R. H., Stern, R., Taylor, C. E., Wright, S. G., & Wolff, T. F. 2022. Edenville and Sanford Dam Failures, Michigan: Investigation Report. Association of State Dam Safety Officials (ASDSO).

Havenga, A. 2023. Combined affidavit/certificate pursuant to Sections 212(4) and 234(1) of the Criminal Procedures Act, Act 51 of 1977. Signed in Pretoria on 19 July 2023.

Jacobsz, S.W. (Snr). 2021. Dam safety inspection – Dam 10 Jagersfontein. Report compiled for Jagersfontein Developments Pty Ltd.

Jefferies, M. and Been, K. 2016. Soil liquefaction – A critical state approach. CRC Press.

Ladd, C. C., and R. Foott. 1974. "New design procedure for stability of soft clays." ASCE Journal of Geotechnical Eng. Div. 100 (7), pp 763–786. https://doi.org/10.1061/AJGEB6.0000066.

Marais, L., Kemp, D., Van der Watt, P., Matebesi, S., Cloete, J., Harri, J., Ang Li Ern, M. and Owen, J.R. 2024. The catastrophic failure of the Jagersfontein Tailings Dam: An industrial disaster 150 years in the making. International Journal of Disaster Risk Reduction 109. https://doi.org/10.1016/j.ijdrr.2024.104585.

Morgenstern, N. R., Vick, S. G., & Van Zyl, D. 2015. Report on Mount Polley Tailings Storage Facility Breach. Independent Expert Engineering Investigation and Review Panel. British Columbia Ministry of Energy and Mines. Retrieved from https://www.mountpolleyreviewpanel.ca/final-report.

Nell, V. 2024. Photosat. Personal communication via email (May 2024).

Olson, S.M. and Stark, T.D. 2002. Liquefied strength ratio from liquefaction flow failure case histories. Canadian Geotechnical Journal 39, pp 629–647. DOI: 10.1139/T02-001.

Olson, S.M. and Stark, T.D. 2003. Yield Strength Ratio and Liquefaction Analysis of Slopes and Embankments. ASCE Journal of Geotechnical and Geoenvironmental Engineering 129 (8), pp 727-737.

Olson, S.M. and Mattson, M.M. 2008. Mode of shear effects on yield and liquefied strength ratios. Canadian Geotechnical Journal 45, pp 574–587.

Perdikou, S. and Lees, A. 2023. Could regular satellite InSAR monitoring have helped prevent the Jagersfontein Tailings Dam failure? Proceedings of 76th Canadian Geotechnical Society Annual Conference – GeoSaskatoon (2023). Canadian Geotechnical Society.

Philip, L. 2014. The historic built environment and a sense of place: Jagersfontein: a mining town in the Free State, South Africa. Unpublished Master's Dissertation, University of Cape Town, Cape Town.

Rivet, S. 2023. Historical topographic surveys of Jagersfontein Tailings Dam produced from archive satellite images. Photosat. Vancouver.

Rivet, S. and Nishiyama, M. 2023. Historical topographic surveys of Jagersfontein Tailings Dam produced from archive satellite images. Photosat. Vancouver.

Robinson, B. 2014. Concept design for extension of the Jagersfontein Tailings Dam. Beric Robinson Tailings Consultant. BRT-06-2014. Jagersfontein Developments.

Robinson, B. 2015. Design for the extension of the Jagersfontein De Beers Tailings Dam. Beric Robinson Tailings Consultant. BRT-03-2015. Jagersfontein Developments.

Robinson, B. 2016. Concept design for a final Jagersfontein Tailings Dam. Beric Robinson Tailings Consultant. BRT-06-2016. Jagersfontein Developments.

Rust, E. 2024. Personal communication.

Shacinda, S. 2010. De Beers sells old S.Africa mine to black investors. Reuters (Online), 28 September 2010. https://www.reuters.com/article/idUSLDE68R2C7/.

Torres Cruz, L.A. & O'Donovan, C. 2023. Public remotely sensed data raise concerns about history of failed Jagersfontein dam. Scientific Reports 13:4953 | https://doi.org/10.1038/s41598-023-31633-5.

Wagener, F. von M. 1997. The Merriespruit slimes dam failure: Overview and lessons learnt. Journal of the South African Institution of Civil Engineering 39(3), pp 11-15.

UNIVERSITEIT VAN PRETORIA
UNIVERSITY OF PRETORIA
YUNIBESITHI YA PRETORIA

UNIVERSITY OF THE WITWATERSRAND, JOHANNESBURG

ADDENDUM 1 TO REPORT

STUDY INTO THE CAUSES OF THE JAGERSFONTEIN FINE TAILINGS STORAGE DAM FAILURE ON 11 SEPTEMBER 2022

Prepared by: University of Pretoria and University of the Witwatersrand Departments of Civil Engineering

Prepared for: Department of Water and Sanitation

Project: 1/2/4/295/2023/24

Date: 9 December 2024

Report No: Revision 0

water & sanitation

Department:
Water and Sanitation
REPUBLIC OF SOUTH AFRICA

RECORD OF REVISIONS

Revision Number	Issue Date	Changes Made	Issued by
0	9 Dec 2024	First draft for comment	SW Jacobsz

EVIDENCE OF INSTABILITY ALONG INTERNAL DAM WALL CREST BEFORE THE 11 SEPTEMBER 2022 FAILURE

It was stated in the report on the Jagersfontein tailings dam failure investigation that it appears that a slope failure along the inside crest edge, which occurred on the morning of the failure (11 September 2022), was the likely trigger, initiating the failure of the dam wall. Due to the surface area of the dam being covered by fine tailings and water in the absence of a return water facility, upstream raising of the walls of the dam involved the placement of material on the saturated unconsolidated material along the inside dam wall crest edge. Such material could likely form a weak foundation for the raising of the wall.

During the discussion of the report into the dam failure with the State Prosecutor on 19 September 2024, the question was asked whether evidence exists of prior failures of this nature at the Jagersfontein tailings dam. The Investigation Panel examined available satellite images and found evidence of such an event from Planet Scope images around the date of 25 March 2022, approximately six months before the failure. The location coincides with the position where the main failure scar (referred to as Scar 2 in the report on the failure investigation) developed. Figure 1 (a) shows the tailings dam on 16 March 2022, showing the inside edge of the dam wall crest to be straight in the vicinity where the wall failed in September 2022. By 25 March 2022 the inside toe exhibits a deviation in alignment, labelled “A” in Figure 1 (b), that could have been due to a local loss of stability. By 28 March 2022 (Figure 1 (c)) the affected area seems to have been repaired with material showing up in the darker colour (labelled “B” in Figure 1(c)). The darker colour could be indicative of the higher moisture content of newly placed material before it had dried out.

New information concerning the “donut”-shaped embankment visible on satellite images from late 2019 to early 2020 (Figures B14 – B17 in the failure study report) was brought to the attention of the Investigation Panel, suggesting that this embankment was constructed as part of efforts to recover plant that presumably fell or slipped off the wall crest into the pond. The fact that such an event had occurred also points to the possibility of poor stability along the inside crest edge of the dam, possibly a consequence of raising the dam wall over weak unconsolidated material.

In conclusion: Evidence does suggest that pre-failure instability along the inside crest edge of the Jagersfontein Tailings Dam wall may have occurred.


(a)
planet.
2022.03.16


(b)
planet.
2022.03.25
A
A

FIGURE 1 **PLANETSCOPE IMAGES FROM MARCH 2022 SHOWING SIGNED OF INSTABILITY ALONG INTERNAL CREST EDGE OF DAM WALL.**

Prof SW Jacobsz Pr Eng

ADDENDUM 2 TO REPORT

STUDY INTO THE CAUSES OF THE JAGERSFONTEIN FINE TAILINGS STORAGE DAM FAILURE ON 11 SEPTEMBER 2022

Prepared by: University of Pretoria and University of the Witwatersrand Departments of Civil Engineering

Prepared for: Department of Water and Sanitation

Project: 1/2/4/295/2023/24

Date: 8 May 2025

Report No: Revision 0

water & sanitation

Department:
Water and Sanitation
REPUBLIC OF SOUTH AFRICA

RECORD OF REVISIONS

Revision Number	Issue Date	Changes Made	Issued by
0	8 May 2025	First draft for comment	SW Jacobsz

TABLE OF CONTENTS

Contents

1. INTRODUCTION **4**
2. REASONS FOR THE EXISTENCE OF THE "DONUT SHAPED EMBANKMENT" **4**
3. SIGNS OF STRUCTURAL DISTRESS ALONG THE TOE OF THE SOUTHERN WALL OF THE DAM **5**
4. SIGNS OF DISTRESS ALONG THE DAM 10 EMBANKMENT **9**
5. ANECDOTAL INFORMATION SHARED ON 26/3/2025 ..... **11**
6. ASSESSMENT OF FILTER COMPATIBILITY BETWEEN FINE AND COARSE TAILINGS **12**
7. CONCLUSIONS **13**

ADDITIONAL EVIDENCE RECEIVED FROM INVESTIGATING OFFICER DURING APRIL 2025

1. Introduction

Additional information and photographs concerning the Jagersfontein tailings dam failure were received in April 2025 from the Investiging Officer on which the Investigation Panel was requested to comment. In addition, we were requested to assess filter compatibiltiy between the coarse and fine tailings on the Jagersfontein Tailings Dam site. This addendum to our original report presents the information thus requested.

2. Reasons for the existence of the "donut shaped embankment"

Our report refers to a "donut shaped" embankment (see p 24), which can be identified on satellite images from late September 2019 until July 2020. The reason for this structure was not clear, but according to the information provided to us in April 2025 the circular embankment was constructed as part of an effort to recover a bulldozer which ended up in the dam due to what was reported to be a suicide attempt by the operator. Accordingly, it is not believed that this structure played a role in the stability of the tailings dam wall.

FIGURE 1 VIEW TOWARDS THE INSIDE OF THE "DONUT-SHAPED EMBANKMENT" SEEN FROM THE SOUTHERN DAM WALL CREST. (DATED 12 DECEMBER 2019.)

3. Signs of structural distress along the toe of the southern wall of the dam

A number of photos received in April 2025 show evidence of wet conditions along the toe of the southern wall of the dam prior to the failure. In some cases, the photographs suggest the presence of ground slumping and horizontal cracks consistent with structural distress. Movement typically occurs perpendicular to transverse cracks and such cracks are evident in a number of photos shown below.

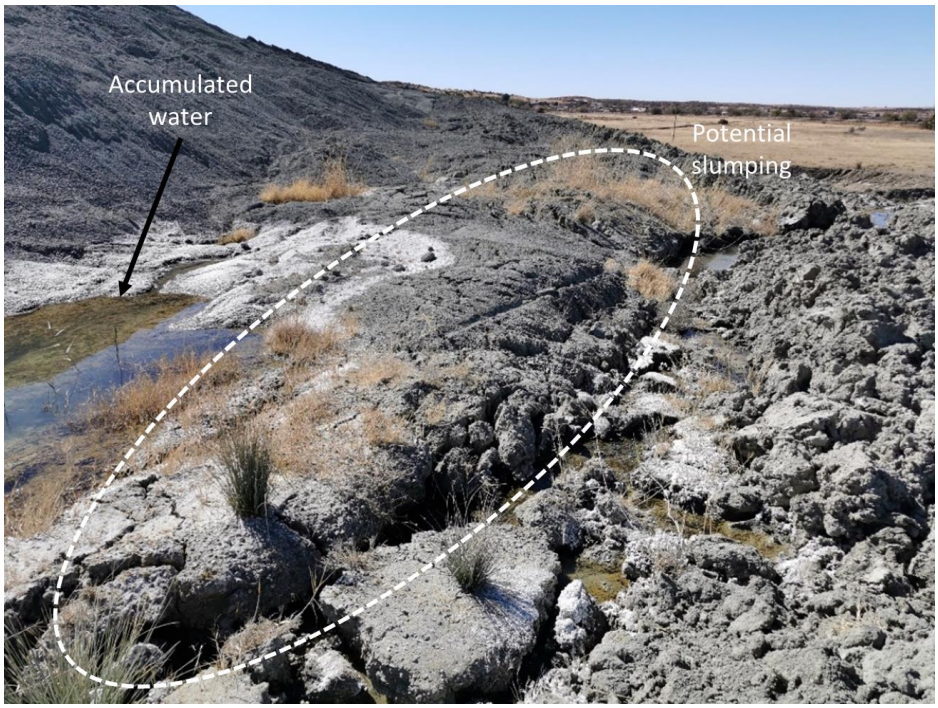

FIGURE 2 **WET CONDITIONS AND SLUMPING ALONG THE TOE OF THE DAM WALL TO THE EAST OF DAM 10. COMPARE TO SIGNS OF BULGING IN SATELLITE IMAGES B12 AND LATER. (DATED 14 AUGUST 2019.)**

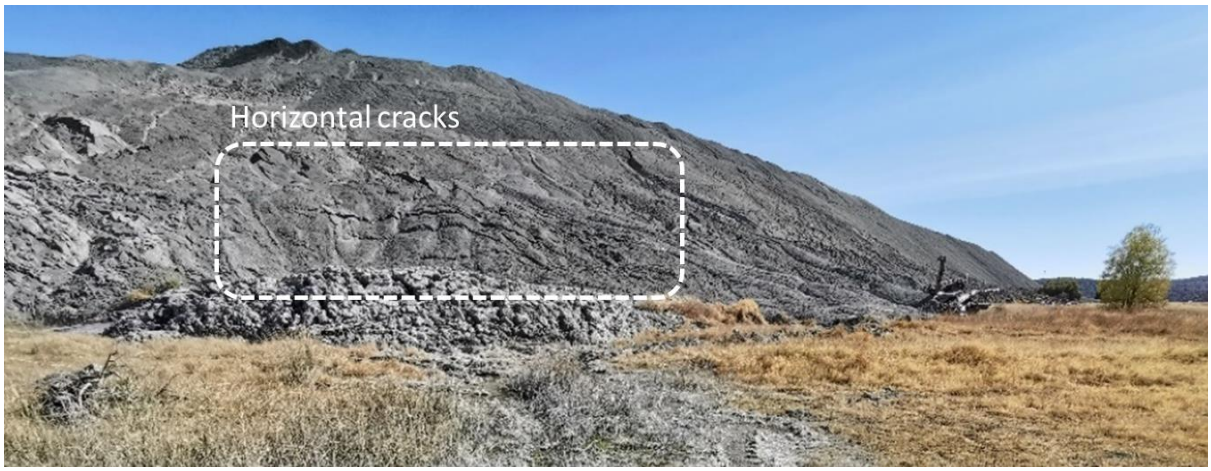

FIGURE 3 **WET CONDITIONS ALONG THE SOUTH-EASTERN TOE OF THE DAM WALL. NOTE HORIZONTAL CRACKS VISIBLE ALONG EMBANKMENT SLOPE, POSSIBLY INDICATIVE OF MOVEMENT. (DATED 28 AUGUST 2019.)**

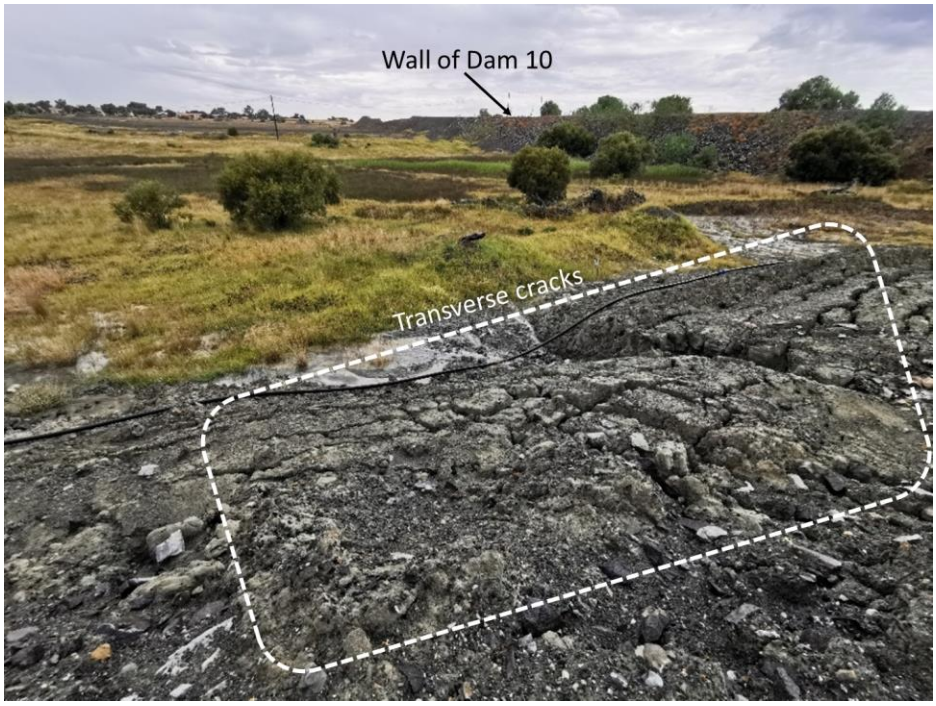

FIGURE 4 TRANSVERSE CRACKS ON SOUTHERN WALL INDICATIVE OF MOVEMENT PERPENDICULAR TO CRACK DIRECTION. (DATED 21 APRIL 2020.)

FIGURE 5 ALTERNATIVE VIEW OF LOCATION SHOWN IN FIGURE 4, WITH CRACKS VISIBLE TO THE LEFT AND ACCUMULATED WATER VISIBLE NEAR THE CENTRE. (DATED 21 APRIL 2020.)

Turbid seepage water can be seen emerging from the toe of the tailings dam opposite Dam 10 in Figure 6. Turbid seepage water could be a sign of piping (i.e. internal erosion). The likelihood of piping in the context of filter compatibility between the coarse (grits) and fine tailings (slimes) is assessed in Section 6.

FIGURE 6 TURBID SEEPAGE WATER EMERGING FROM THE TOE OF THE TAILINGS DAM OPPOSITE DAM 10. (DATED 28 MARCH 2022.)

FIGURE 7 CIRCLED AREA HIGHLIGHTING TRANSVERSE CRACKS ON THE SOUTH-EASTERN WALL WHICH MAY BE INDICATIVE OF SUBSIDENCE TOWARDS THE DOWNSTREAM TOE OF THE DAM WALL. THE CIRCLED AREA COINCIDES WITH FAILURE SCAR 3. COMPARE TO SATELLITE IMAGE B23. (DATED 27 JULY 2022.)

FIGURE 8 **SIMILAR VIEW TO FIGURE 6 WITH THE DAM 10 EMBANKMENT VISIBLE ON THE RIGHT, INDICATING CRACKS VISIBLE IN THE BUTTRESS ALONG THE SOUTH-EASTERN CORNER OF THE TAILINGS DAM WALL. (DATED 27 JULY 2022.)**

4. Signs of distress along the Dam 10 embankment

Anecdotal information communicated to the Investigation Panel described an approximately 500 mm high step due to a “crack” that appeared diagonally across the Dam 10 embankment near where it abuts the southern wall of the tailings dam. The feature appears to have formed the western boundary of the soil mass associated with the movement of the “wandering tree” (see p 31 of report). When zooming in on the area, the feature is discernible in satellite images B16 to B18 and its occurrence coincides with the time during which the displacement of the tree referred to above was occurring. Although not clearly evident from the photograph in Figure 9 due to the lighting conditions at the time, the feature was reported to be sufficiently severe that a light delivery vehicle (bakkie) could not cross the cracks.

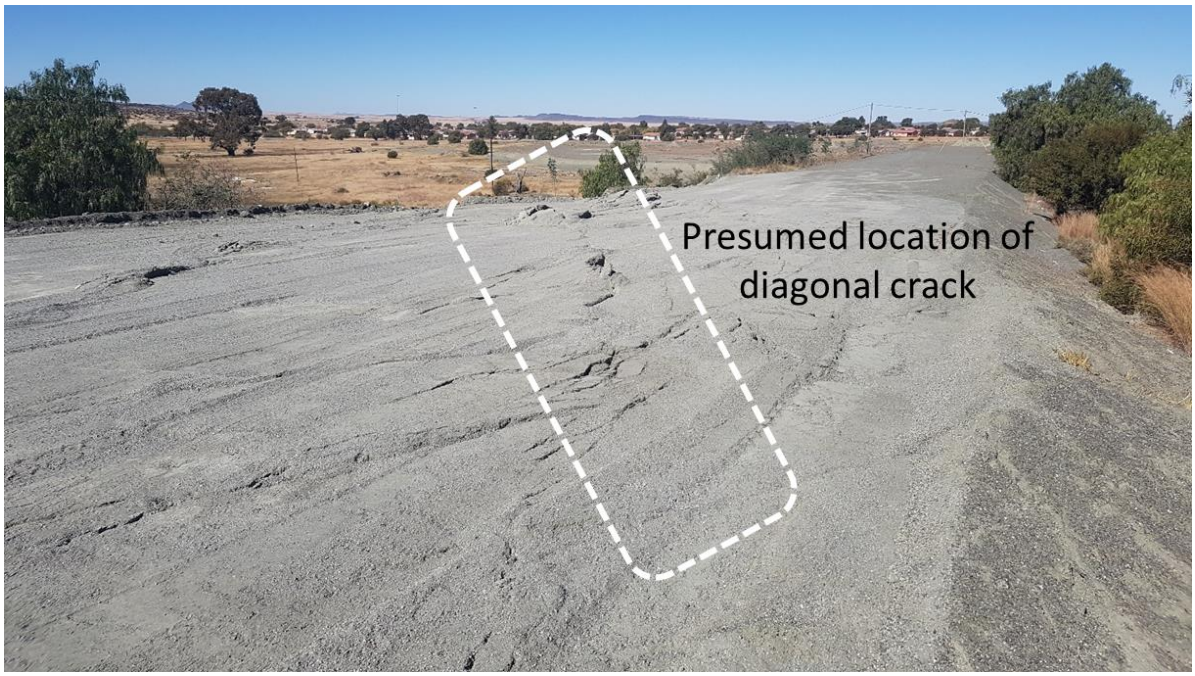

FIGURE 9 VIEW ALONG THE DIRECTION OF CRACKS WHICH APPEARED WHERE THE DAM 10 EMBANKMENT ABUTS THE SOUTHERN WALL OF THE TAILINGS DAM. (DATED 1 JUNE 2020.)

The curvature of the side walls of the seepage water sump, located just off the south-eastern corner of the tailings dam (Figure 10) is indicative of structural distress and could be related to ground movement near the toe of the tailings dam.

FIGURE 10 CURVED WALLS OF THE SUMP LOCATED IMMEDIATELY TO THE SOUTHEAST OF THE TAILINGS DAM. (DATED 30 AUGUST 2022.)

5. Anecdotal information shared on 26/3/2025

The information below represents anecdotal information shared with the investigation panel on 26 March 2025.

- The witness was contacted at 07h00 on 11 September 2022 by the Mine Manager, Mr Johan Combrink, and informed that the tailings dam had failed.
- It was reported that around 02h00 in the morning of 11 September 2022 material tipped along the inside of the dam wall at the south-eastern corner kept disappearing, not accumulating as was normally observed.
- The tailings dam was operated 24 hours a day. Activity on the dam the night preceding the failure was therefore not abnormal.
- Tailings discharge from Failure Scar 1 (see report Figure 34, p 52) stopped early during the failure event as the breach was closed with tailings falling from the adjacent steeply eroded slopes.
- Berrick Robinson Tailings (BRT) carried out a concept design for a tailings dam and the 2011 construction work (i.e. construction of the new Western Compartment) was based on the concept design without engineering involvement from BRT. The intention was to eventually use the opencast pit for deposition space and therefore a large tailings dam was not envisaged at that stage.
- The construction of the buttress (wider section) along the southern wall of the dam was attributed to the need to provide improved access in the area where the dozer had to be recovered. This raises the questions of why the buttress was constructed to such a length and width and why work on it continued for years up to the time of the failure.
- Water was found in the boreholes commissioned by Mr Jan Viljoen drilled in the dam wall which was reported to have raised some concern at Jagersfontein Developments (JD)
- The Department of Water and Sanitation (DWS) issued a directive at the end of 2020 to stop deposition on the dam, pending the submission of a closure plan. The plant was subsequently stopped from 7 January 2021 until June 2021. The closure plan was not accepted by DWS, but DWS lifted the directive. JD had to appoint an engineer to carry out quarterly inspections of the tailings dam and appointed Mr Jan Viljoen to conduct these. The intention was for MVD Kalahari to take over this role from the end of 2021 as Mr Viljoen reached retirement age. Inspections typically comprised driving around the crest and the toe of the dam and issuing a letter report.
- SRK was appointed in 2021 around the time of the DWS directive to produce a continuation plan. They required drilling to assess the integrity of the wall and were tasked to produce a report for upstream raising of the dam. The tailings dam was to be registered as a dam with a safety risk after a December 2021 meeting to discuss the DWS directive. SRK's involvement came to an end at the end of 2021 as they were only tasked to produce a continuation report for the upstream raising of the dam.
- The Dam 10 spillway was blocked by JD by dumping mine waste (pointed out in the 2021 dam safety inspection report, Jacobsz (2021)) to store more water which resulted in ponding to a

higher water level than the original full supply level against the toe of the southern wall of the tailings dam. The water level remained at this high level until the failure occurred.

- Borehole 10, located approximately opposite Failure Scar 1, downstream of the toe of the tailings dam, showed artesian flow in August 2022, with water flowing from the casing which extended approximately 500mm above the surrounding ground level. The water level in Dam 10 was reported to have reached Borehole 10 in July-August 2022.
- A spot where long term sloughing, associated with wet conditions, occurred was reported to have been present for a long time on the lower berm where Failure Scar 1 formed upon failure. This sloughing may have been associated with a penstock outlet from the old De Beers Dam but this has not been confirmed.

6. Assessment of filter compatibility between fine and coarse tailings

We were requested to assess the filter compatibility between the fine (slimes) and coarse tailings (grits) occurring at the Jagersfontein tailings dam site. Compatibility was therefore assessed in terms of the coarse tailings acting as a filter against the fine tailings. Particle size distribution curves for the various materials collected during the field investigation are plotted in Figure 11. The particle size distributions of the fine tailings are shown in light grey to allow them the be distinguished from the coarse tailings.

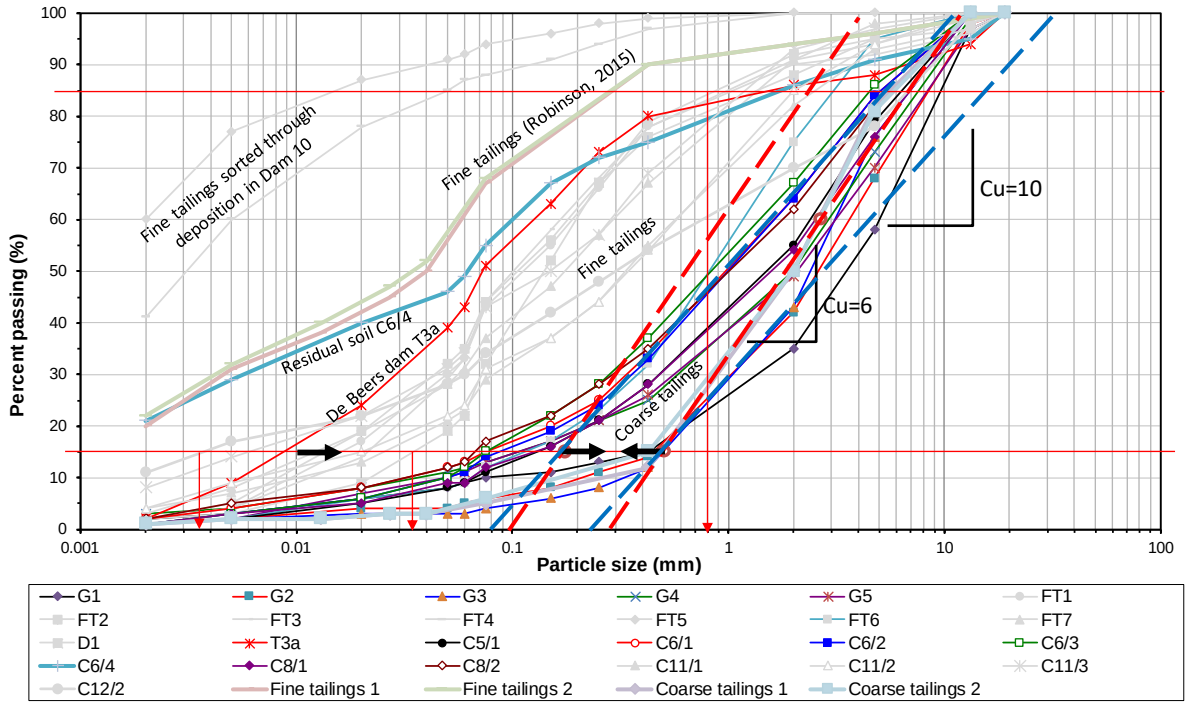

FIGURE 11 PARTICLE SIZE DISTRIBUTIONS OF VARIOUS MATERIALS SAMPLED DURING THE FIELD INVESTIGATION AT THE JAGERSFONTEIN TAILINGS DAM.

The following filter criteria, as presented in most standard soil mechanics texts, were used to assess compatibility:

In order to retain fine particles: $D_{15f} < 5\ D_{85s}$ (where D_{15f} is the 15th percentile particle size of the filter material and D_{85s} is the 85th percentile particle size of the material to be filtered, i.e. the fine tailings). With a minimum D_{85s} value of 0.8 mm (see Figure 11), this implies $D_{15f} < 4$ mm. However, when filtering fine materials a $D_{15f} < 0.5$mm is the standard recommendation.

In order to ensure sufficient permeability of the fine particles: $D_{15f} > 5\ D_{15s}$ (where D_{15s} is the 15th percentile particle size of the material to be filtered, i.e. the fine tailings). With a maximum D_{15s} value of 0.035 mm (see Figure 11), this implies $D_{15f} > 0.175$ mm.

Relatively uniform sand filters are preferred, so that $6 < D_{60f} / D_{10f} < 10$.

Combining the above criteria produces the filter envelopes shown in Figure 11 in red for $D_{60f} / D_{10f} = 6$ and blue for $D_{60f} / D_{10f} = 10$. The figure shows that the coarse material is sufficiently fine to retain the fine materials based on the samples collected during the field investigation (i.e. $D_{15f} < 0.5$ mm is generally satisfied). However, the finer fraction of the coarse tailings is too fine to ensure free drainage (i.e. $D_{15f} > 0.175$ mm is not generally satisfied). This suggests that filters made from unscreened coarse tailings are prone to clogging which may have contributed to higher than expected water levels in the dam wall.

Figure 11 also includes the grading curves for fine materials taken from Robinson (2015). Using the filter criteria above, the coarse tailing was found to be sufficiently fine to also retain this material, while, in this case, being coarse enough to allow free drainage of this material.

The results suggest that piping is unlikely to have been a primary cause of the failure. However, piping may have occurred as a consequence of failure after internal displacement had taken place within the dam wall.

7. Conclusions

The photographic evidence provided in this addendum illustrates that the southern wall of the Jagersfontein tailings dam exhibited potential signs of distress as far back as more than three years prior to the failure. This is evident from the wet conditions along the toe of the dam wall and the cracks visible in some of the images.

Raising of the spillway of Dam 10 increased ponding along the toe of the tailings dam wall, resulting in pore water suction dissipation which could have impacted negatively on slope stability. However, the panel has not conducted analyses to quantify this impact.

A filter compatibility check suggests that piping was not a primary cause of the failure, but that it may have been a consequence of movement in the wall associated with the failure.

Prof SW Jacobsz Pr Eng

APPENDIX A

AERIAL PHOTOGRAPHY

Source: Chief Directorate: National Geospatial Information (CDNGI)

Appendix A: Archival Aerial Imagery

Historical analogue aerial photographs available from the Chief Directorate of National Geospatial Information (CDNGI).

See http://cdngiportal.co.za/CDNGIPortal/ for access to imagery.

Figure A1: CDNGI aerial photograph acquired on 1944/12/31 showing the tailings and waste management system at Jagersfontein mine.

* Scale is approximate as imagery is not georeferenced or orthorectified.

Figure A2: CDNGI aerial photograph of 1948/08/31.

Figure A2: CDNGI aerial photograph of 1948/08/31.

* Scale is approximate as imagery is not georeferenced or orthorectified.

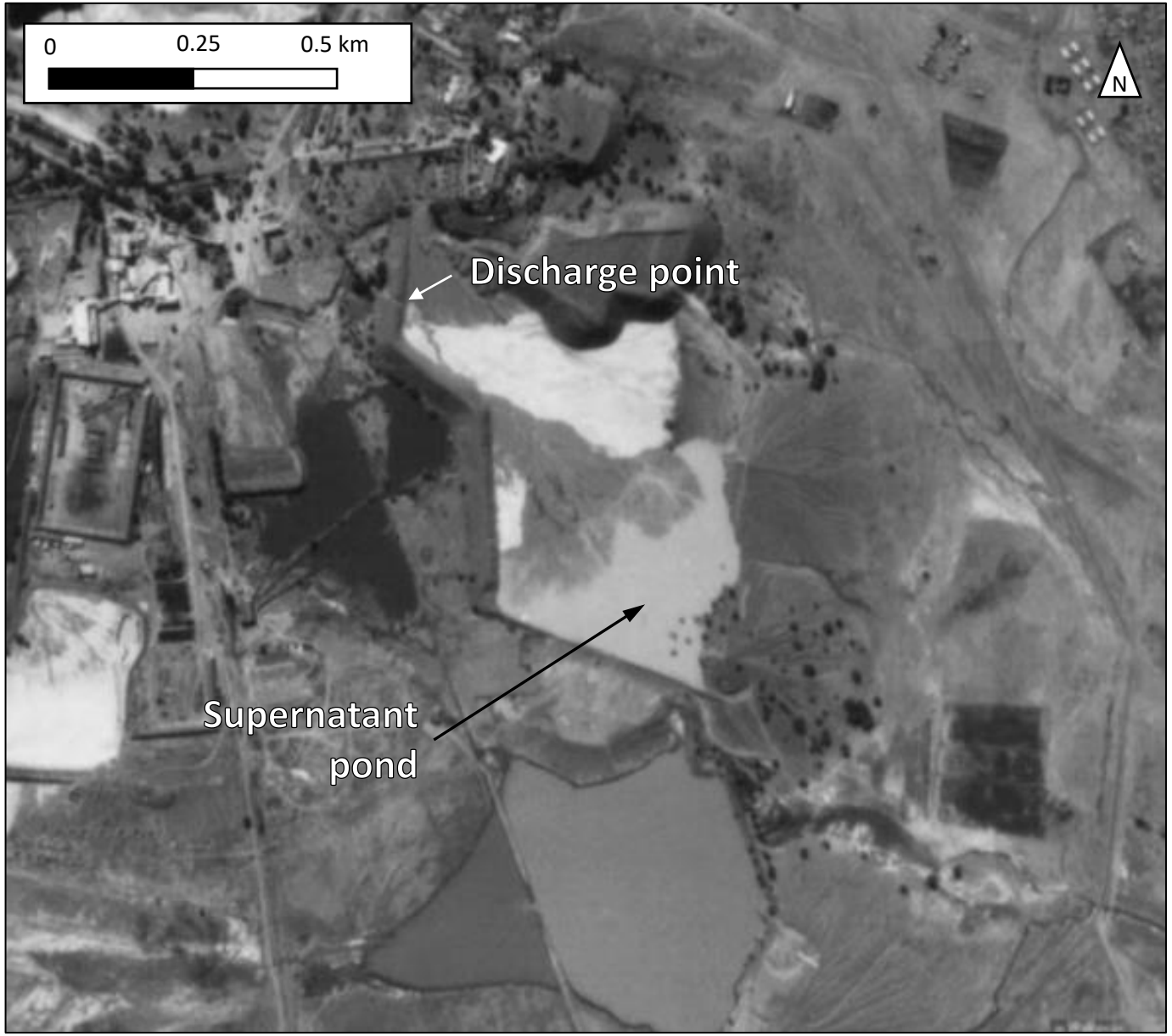

Figure A3: CDNGI aerial photograph of 1955/08/07.

* Scale is approximate as imagery is not georeferenced or orthorectified.

Figure A4: CDNGI aerial photograph of 1962/09/04.

* Scale is approximate as imagery is not georeferenced or orthorectified.

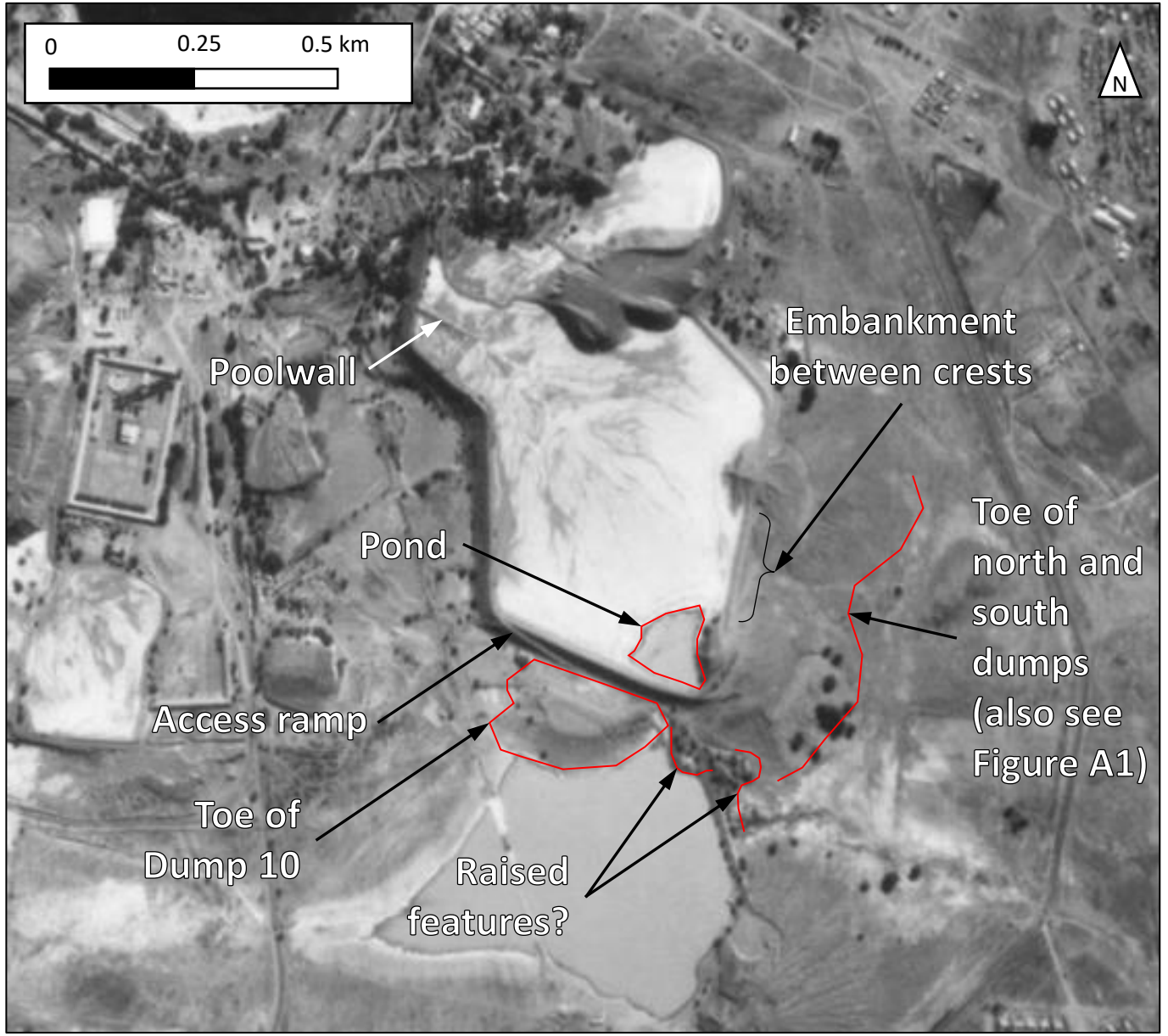

Figure A5: CDNGI aerial photograph of 1973/07/16 showing the general layout of the Jagersfontein tailings dam, dumps and water reservoir after the initial mining operations had completed.

* Scale is approximate as imagery is not georeferenced or orthorectified.

APPENDIX B

HIGH RESOLUTION SATELLITE IMAGES

Appendix B: High Resolution Satellite and Aerial Imagery

A collection of high-resolution satellite and aerial imagery of the Jagersfontein tailings dam and mine site dating back to May 2010 intended to aid in the re-creation of the construction history of the site.

Imagery has been sourced from public domain sources, such as Google Earth Pro and ESRI World Imagery Wayback, as well as commercial satellite imagery resellers. See discussion and further image details in Section 4.2 of the report.

N.B. Changes between consecutive images are best appreciated by viewing the document in full screen mode.

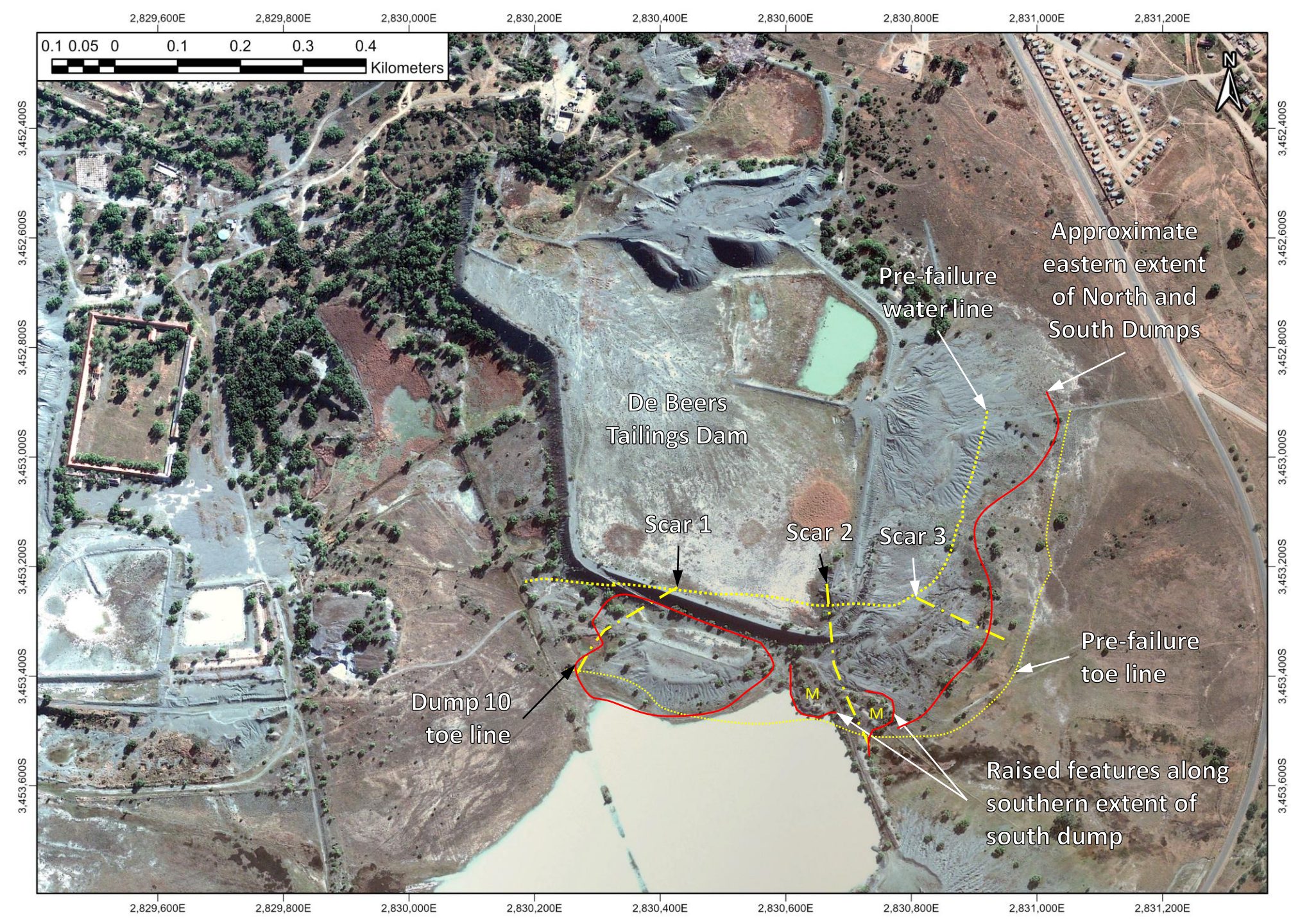

Figure B1: 2010-05-29 GeoEye1 satellite image showing the tailings dam breach locations, the locations of the pre-failure toe and pond water line, and the extent of the historic dumps.

Figure B2: 2010-11-22 WorldView 2 satellite image showing the extent of the historic dumps.

Figure B3: 2012-10-04 Pléiades 1 satellite image showing the extent of the historic dumps.

Figure B4: 2012-11-25 Pléiades 1 satellite image showing discharge points on the west wall and the extent of the historic dumps.

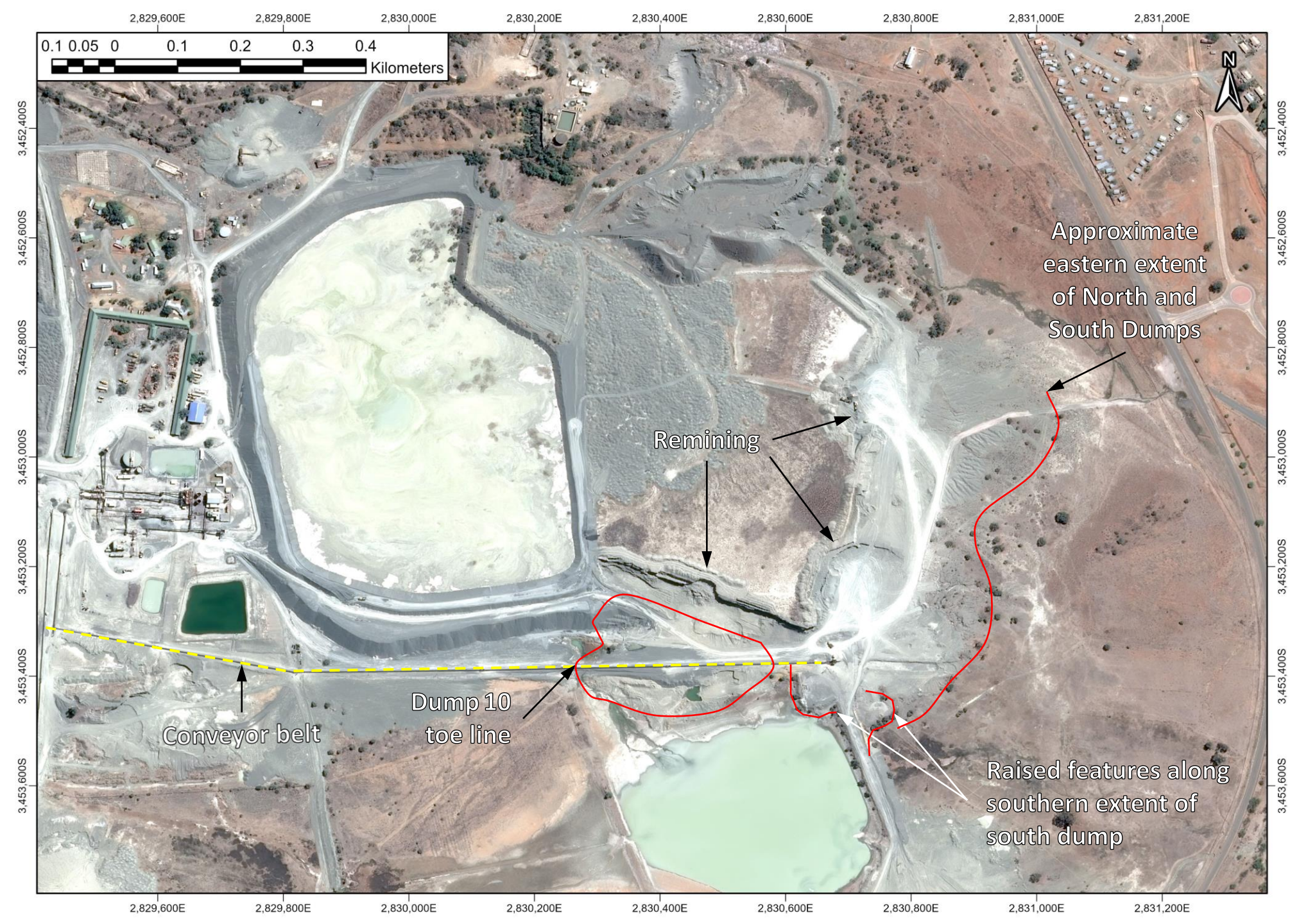

Figure B5: 2014-09-25 Pléiades 1 satellite image showing the extent of the historic dumps.

Figure B6: 2015-08-13 aerial image showing the alignment of a conveyor belt and the extent of the historic dumps.

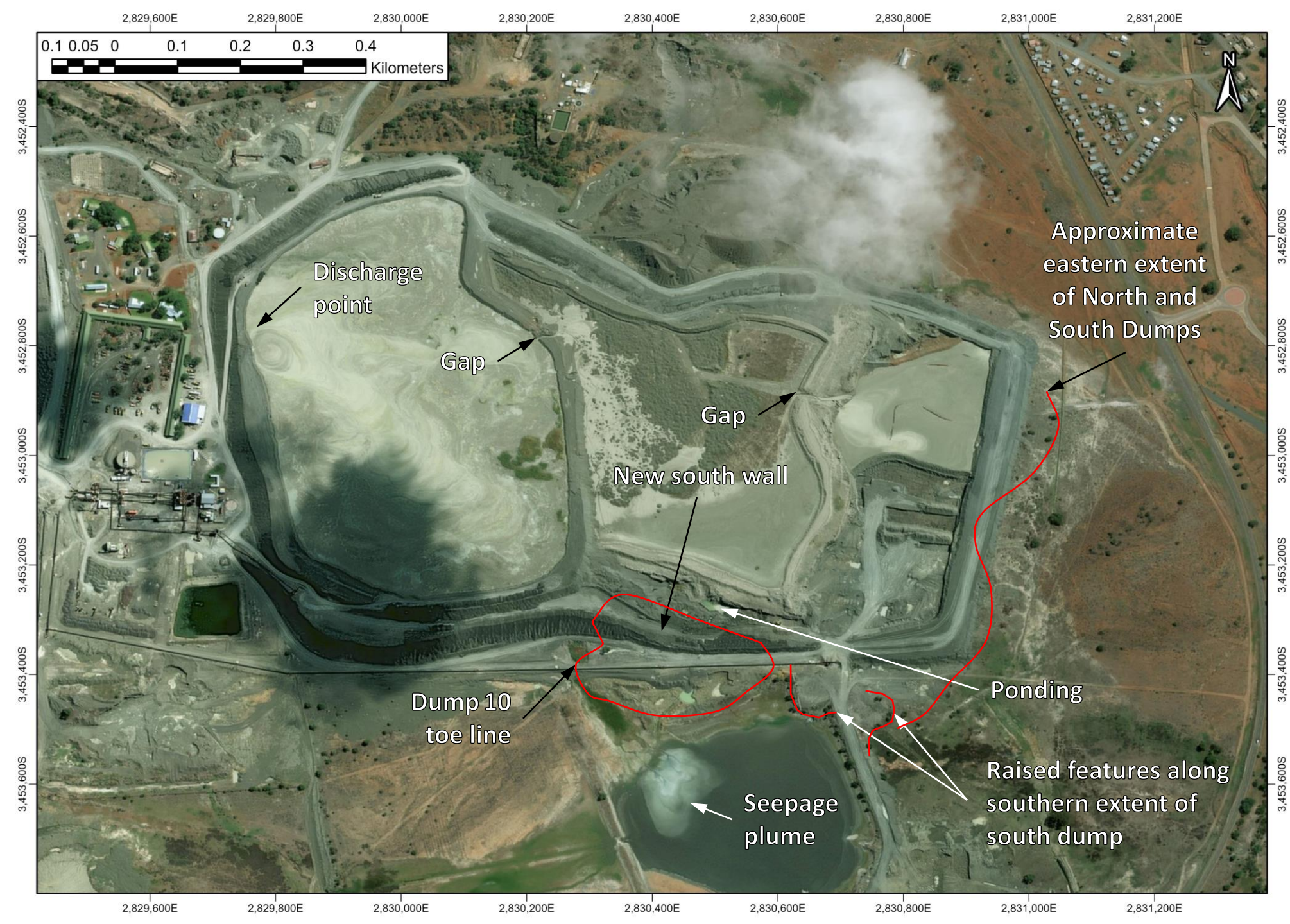

Figure B7: 2016-03-10 WorldView 2 satellite image showing the extent of the historic dumps.

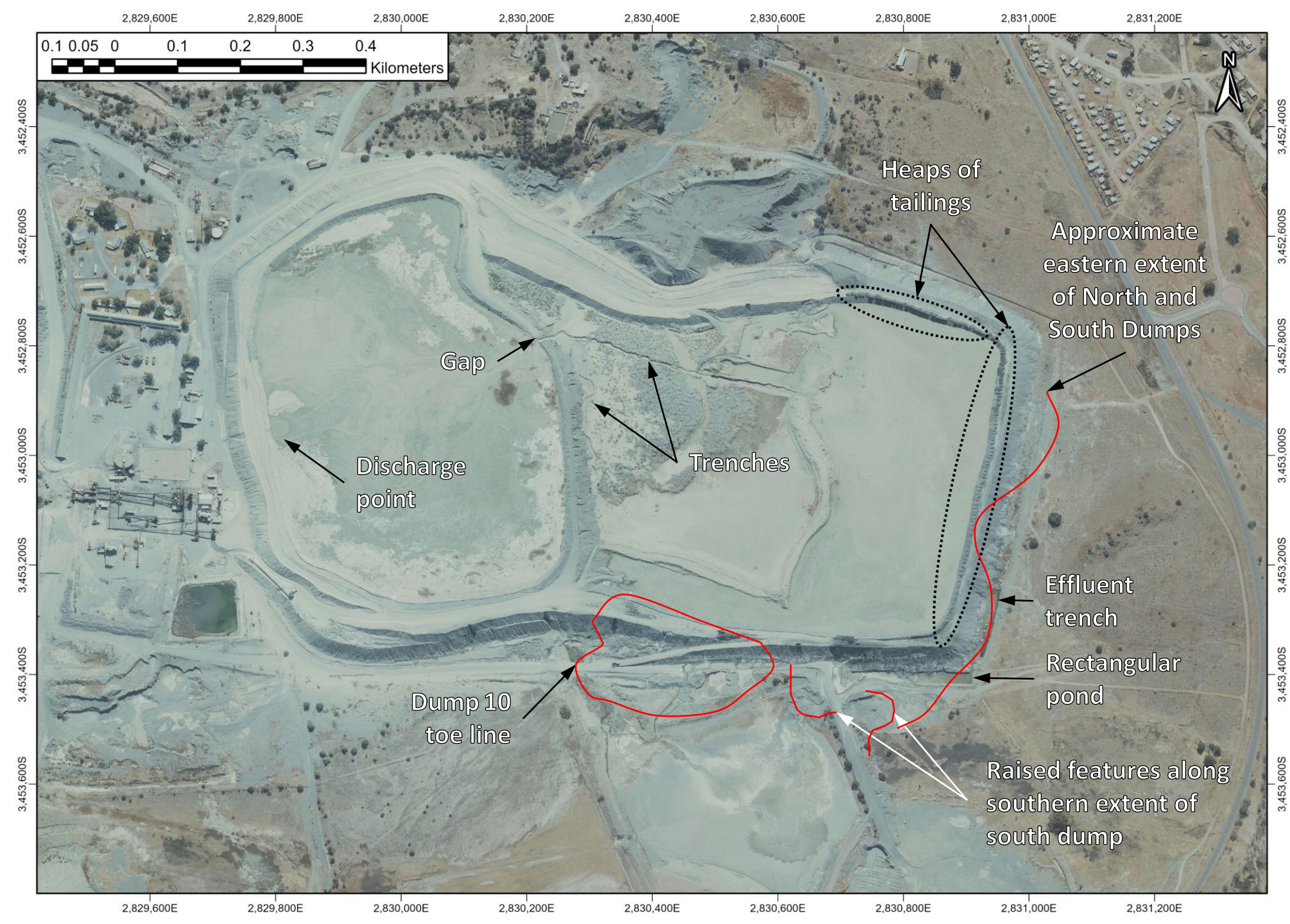

Figure B8: 2017-07-30 aerial image showing the extent of the historic dumps.

Figure B9: 2017-08-13 GeoEye1 satellite image showing the extent of the historic dumps.

Figure B10: 2019-02-04 Pléiades 1 satellite image showing the southern access road alignment.

Figure B11: 2019-03-22 TripleSat satellite image highlighting the separation between the February 2019 (Figure B10) and the current location of the southern edge of the southern access road.

Figure B12: 2019-05-02 WorldView 2 satellite image highlighting the separation between the February 2019 (Figure B10) and the current location of the southern edge of the southern access road.

Figure B13: 2019-09-14 SuperView satellite image highlighting the separation between the February 2019 (Figure B10) and the current location of the southern edge of the southern access road.

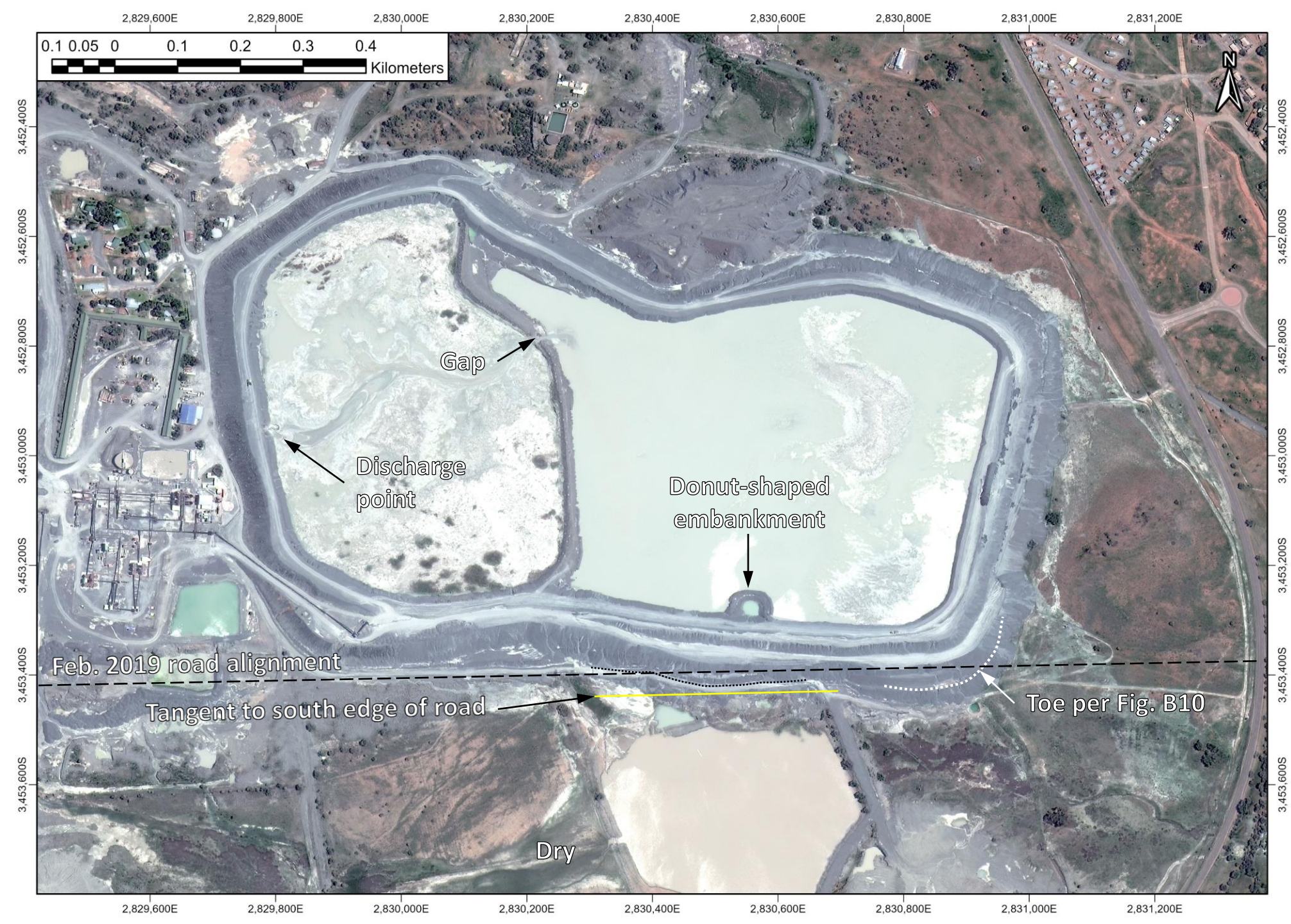

Figure B14: 2020-01-16 SuperView satellite image highlighting the separation between the February 2019 (Figure B10) and the current location of the southern edge of the southern access road. A donut-shaped embankment built against the southern wall is visible.

Figure B15: 2020-07-09 Jilin-1 satellite image highlighting the separation between the February 2019 (Figure B10) and the current location of the southern edge of the southern access road. Remnants of the donut-shaped embankment built against the southern wall are visible.

Figure B16: 2020-08-28 Pléiades 1 satellite image highlighting the separation between the February 2019 (Figure B10) and the current location of the southern edge of the southern access road. Remnants of the donut-shaped embankment built against the southern wall are visible.

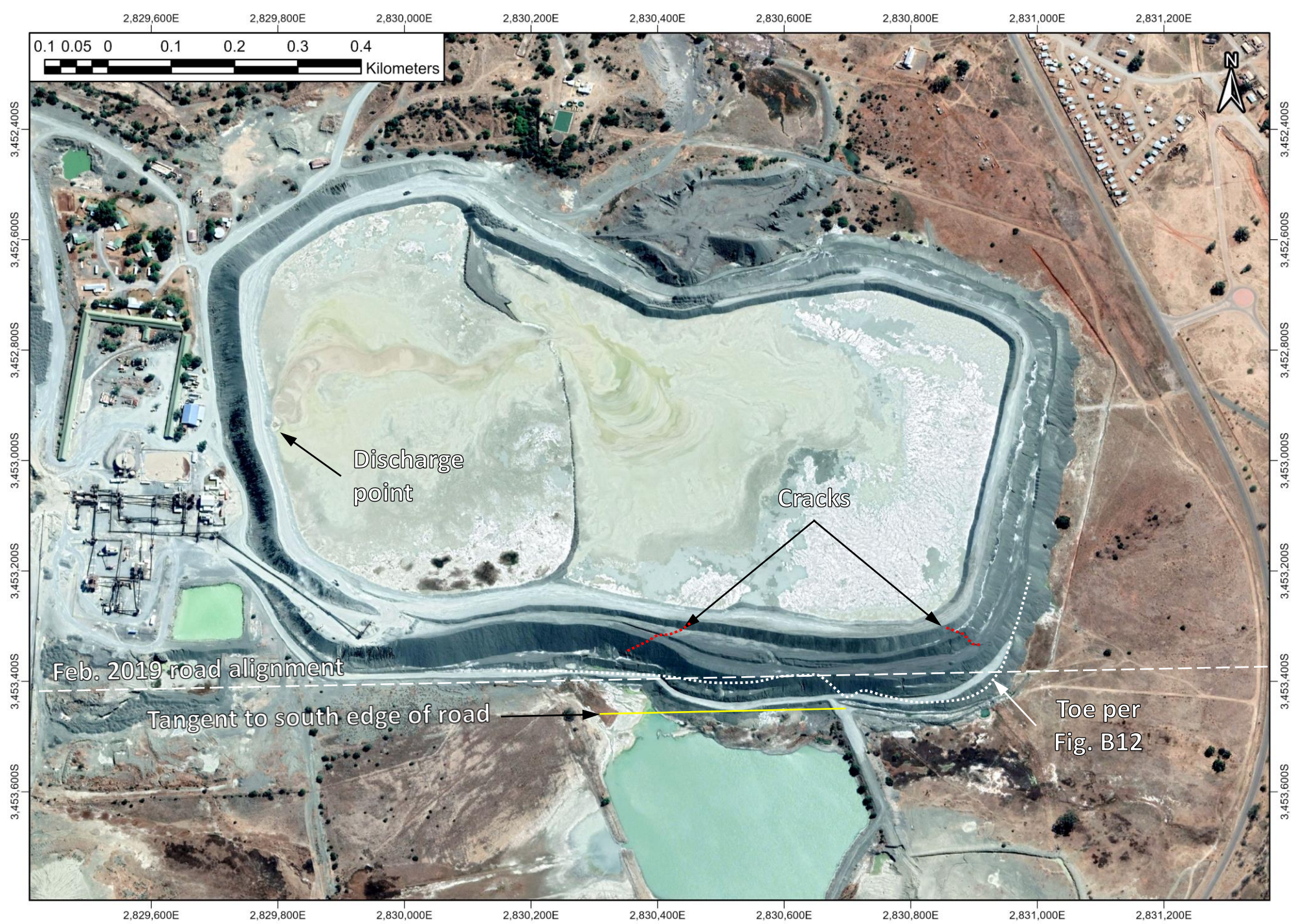

Figure B17: 2020-09-24 WorldView 2 satellite image highlighting the separation between the February 2019 (Figure B10) and the current location of the southern edge of the southern access road. Cracks visible in the southern wall are also indicated. Note: Cracks can be better appreciated by viewing the image in Google Earth Pro.

Figure B18: 2021-01-24 WorldView 2 satellite image highlighting the separation between the February 2019 (Figure B10) and the current location of the southern edge of the southern access road.

Figure B19: 2021-02-17 SuperView satellite image highlighting the separation between the February 2019 (Figure B10) and the current location of the southern edge of the southern access road.

Figure B20: 2022-01-12 Jilin-1 satellite image highlighting the separation between the February 2019 (Figure B10) and the current location of the southern edge of the southern access road.

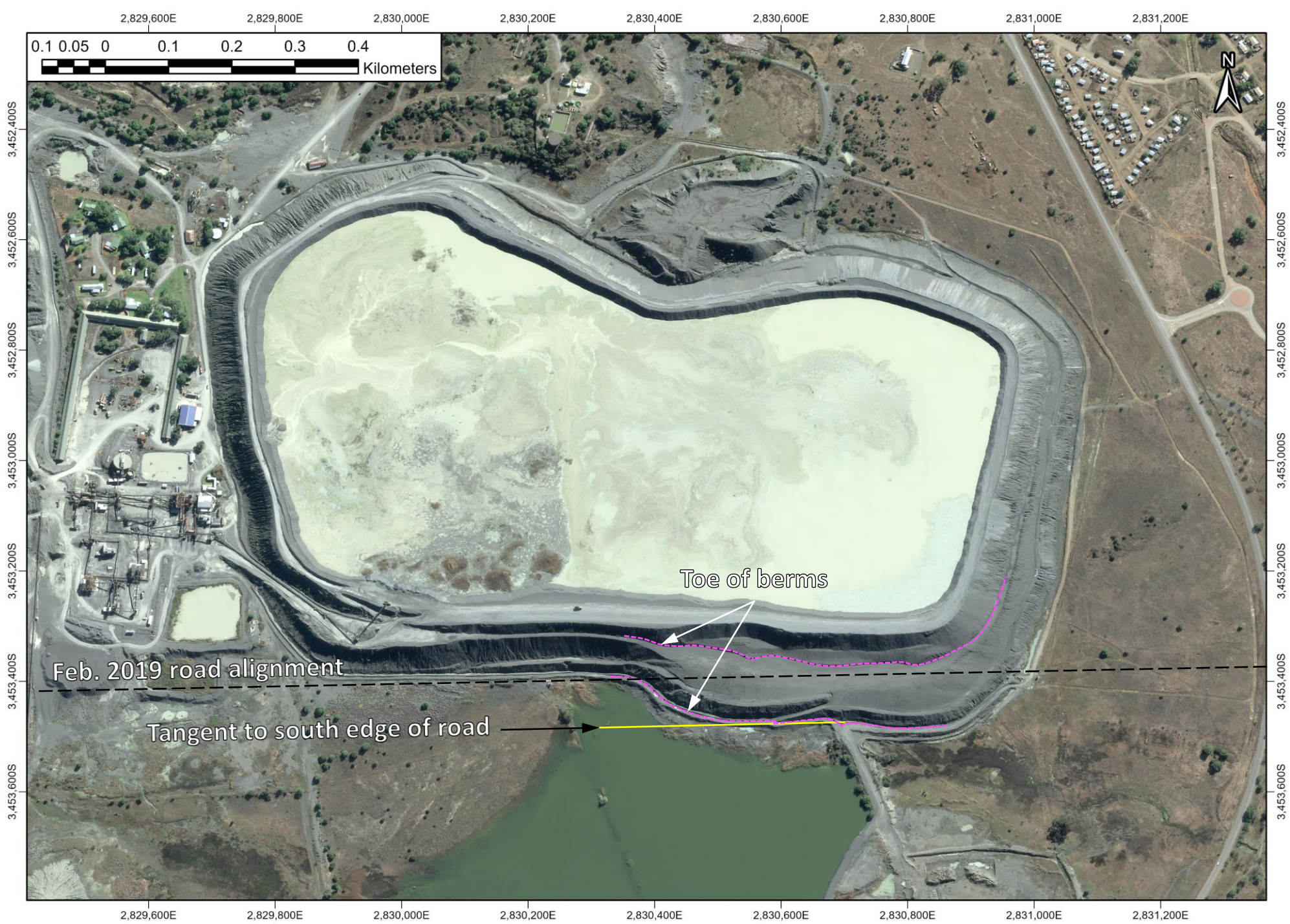

Figure B21: 2022-05-24 Pléiades Neo satellite image highlighting the separation between the February 2019 (Figure B10) and the current location of the southern edge of the southern access road. The pre-failure location of the toe of the upper and lower benches is highlighted.

Figure B22: 2022-07-28 Pléiades Neo satellite image showing: the separation between the February 2019 (Figure B10) and the current location of the southern edge of the southern access road; the location of the toe of the upper and lower benches; and the extent of the historic dumps.

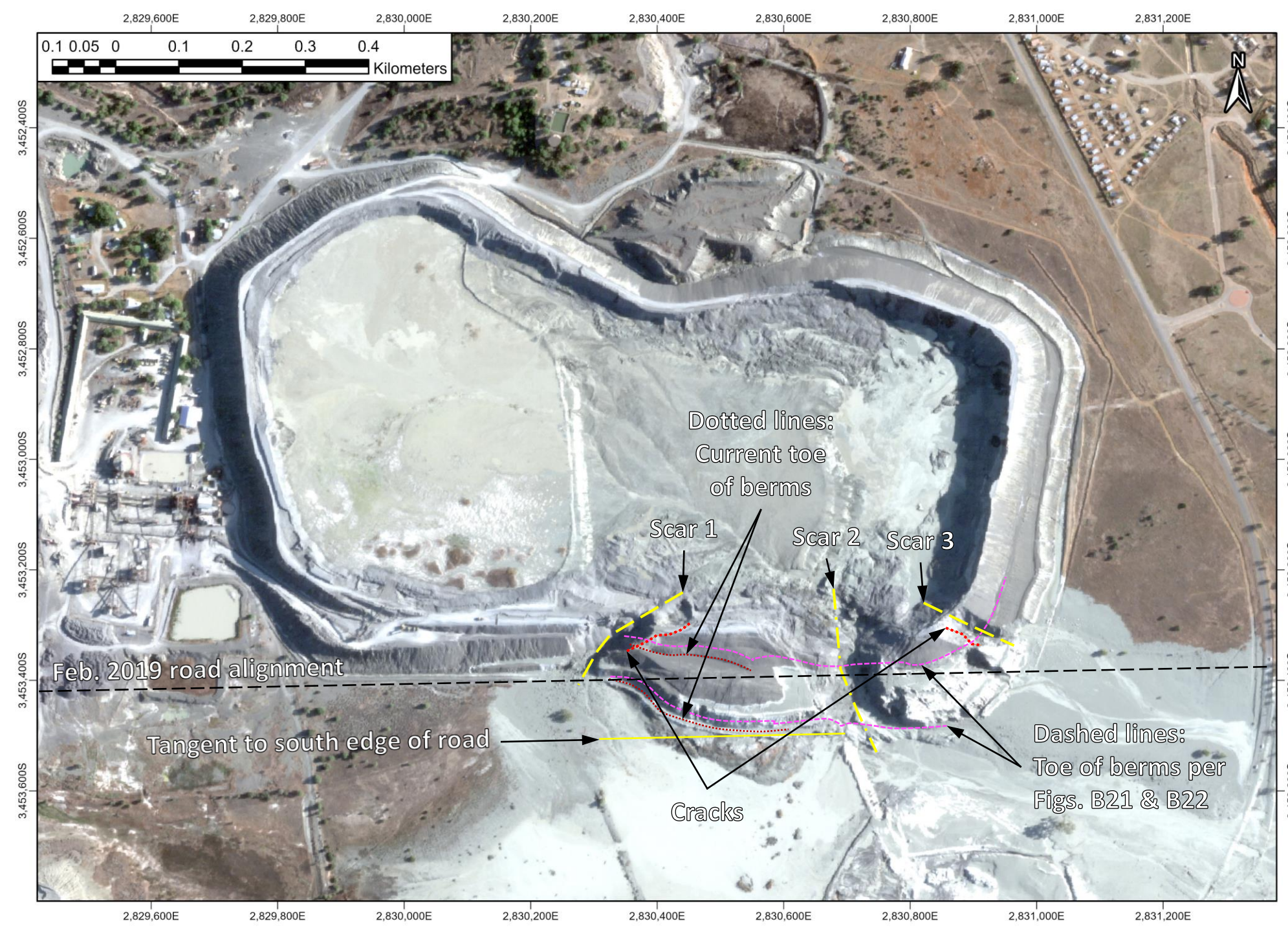

Figure B23: 2022-09-12 SkySat satellite image showing: the separation between the February 2019 (Figure B10) and the current location of the southern edge of the southern access road; the pre-failure location of the toe of the upper and lower berms on the southern wall per Figures B21 & B22; current location of the toe of the berms; the location of the pre-failure cracks per Figure B17; and the three scar locations.

Figure B24: 2022-09-24 WorldView 2 satellite image highlighting the separation between the February 2019 (Figure B10) and the current location of the southern edge of the southern access road.

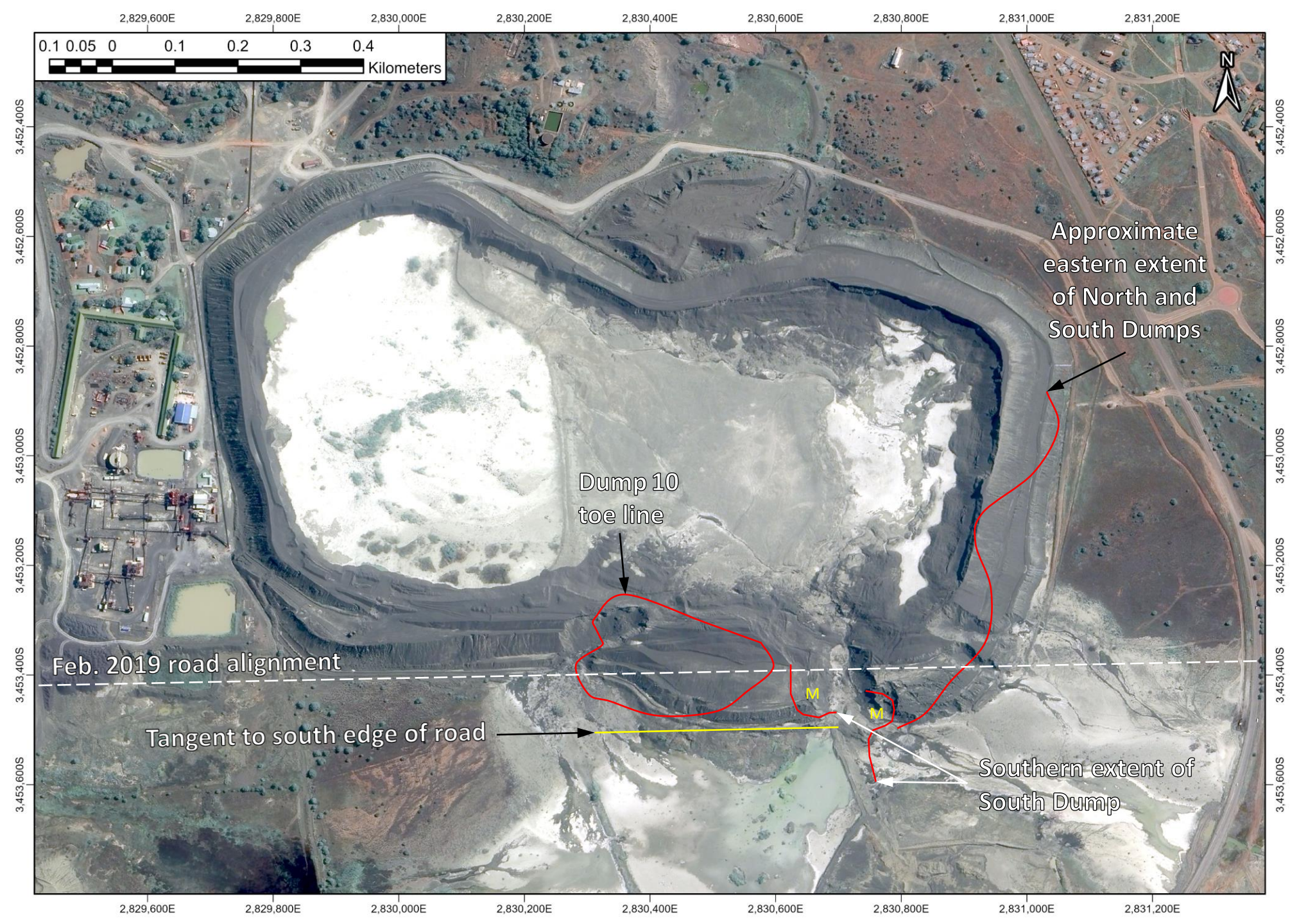

Figure B25: 2023-03-07 Jilin-1 satellite image showing: the separation between the February 2019 (Figure B10) and the current location of the southern edge of the southern access road; and the extent of historic dumps.

APPENDIX C

PRESENTATION OF PLANETSCOPE IMAGERY

1. Overview of significant events from PlanetScope imagery

PlanetScope images contain data in the Visible and Near Infrared parts of the spectrum at a 3-4m per pixel resolution.

The section below highlights several instances of what appears to be signs of slope instability observed on the dam by means of satellite imagery over the last 5 years. The satellite images from which observations are made are presented below, but it is pointed out that comparison of sets of images is best achieved by flicking between images displayed electronically on a screen. For this purpose video sequences of the available PlanetScope images can be found at the links below.

Jan – May 2019

https://www.planet.com/stories/jagersfontein-jan-may-2019-tTzCNy4Ig

Sept 2019 – July 2020

https://www.planet.com/stories/jagersfontein-sept-2019-july-2020-D-xy0r4SR

Jan – April 2020

https://www.planet.com/stories/jagersfontein-jan-april-2020-VxKEze4Sg

August 2020 - Feb 2021

https://www.planet.com/stories/jagersfontein-august-2020-feb-2021-USWGpSIIR

Feb 2021 - July 2021

https://www.planet.com/stories/jagersfontein-feb-2021-july-2021-pAx2pISSg

July 2021 - December 2021

https://www.planet.com/stories/jagersfontein-july-2021-december-2021-CqrQtSSIg

Dec 2021 - May 2022

https://www.planet.com/stories/jagersfontein-dec-2021-may-2022-p9CqpIIIg

April – Sept 2022

https://www.planet.com/stories/jagersfontein-april-sept-2022-cXDyYsVSR

1.1. Feb – March 2019

Figure 1 (a) and (b) respectively present images taken on 2019/02/07 and 2019/02/11. The access road along the southern wall of the tailings dam is straight and is indicated by a thin yellow dotted line. Dam 10, immediately to the south of the wall of Compartment 2, appeared empty on 2019/02/07. The dam's natural catchment is located towards the west. By 2019/02/11 the dam had received a significant amount of water. However, no water is visible to the west of the embankment bordering the water body, indicating that the influx of water from the dam was not from its natural catchment. In fact, water can be observed to spill from Dam 10 towards the west on 2019/02/16 as shown in Figure 2, suggesting that water in Dam 10 is coming from a source other than its natural catchment.

FIGURE 1 **PLANETSCOPE SATELLITE IMAGES TAKEN ON 2019/02/07 AND 2022/02/11 SHOWING RAPID FILLING OF DAM 10.**

FIGURE 2 **PLANETSCOPE SATELLITE IMAGES TAKEN ON 2019/02/16 SHOWING WATER DISCHARGING FROM DAM 10, UPSTREAM TOWARDS THE WEST, SUGGESTION THAT WATER IN DAM IS DID NOT ORIGINATE FROM NATURAL RUN-OFF.**

The rainfall record for this period will be examined to provide additional insight into causes of the sudden filling of Dam 10.

Figure 3 (a) and (b) present PlanetScope images respectively recorded on 2019/02/23 and 2019/03/08. Signs of slope instability are visible along the southern wall of Compartment 2, with Figure 3(b) showing what appears to be a slip failure towards the south as indicated by label 2.

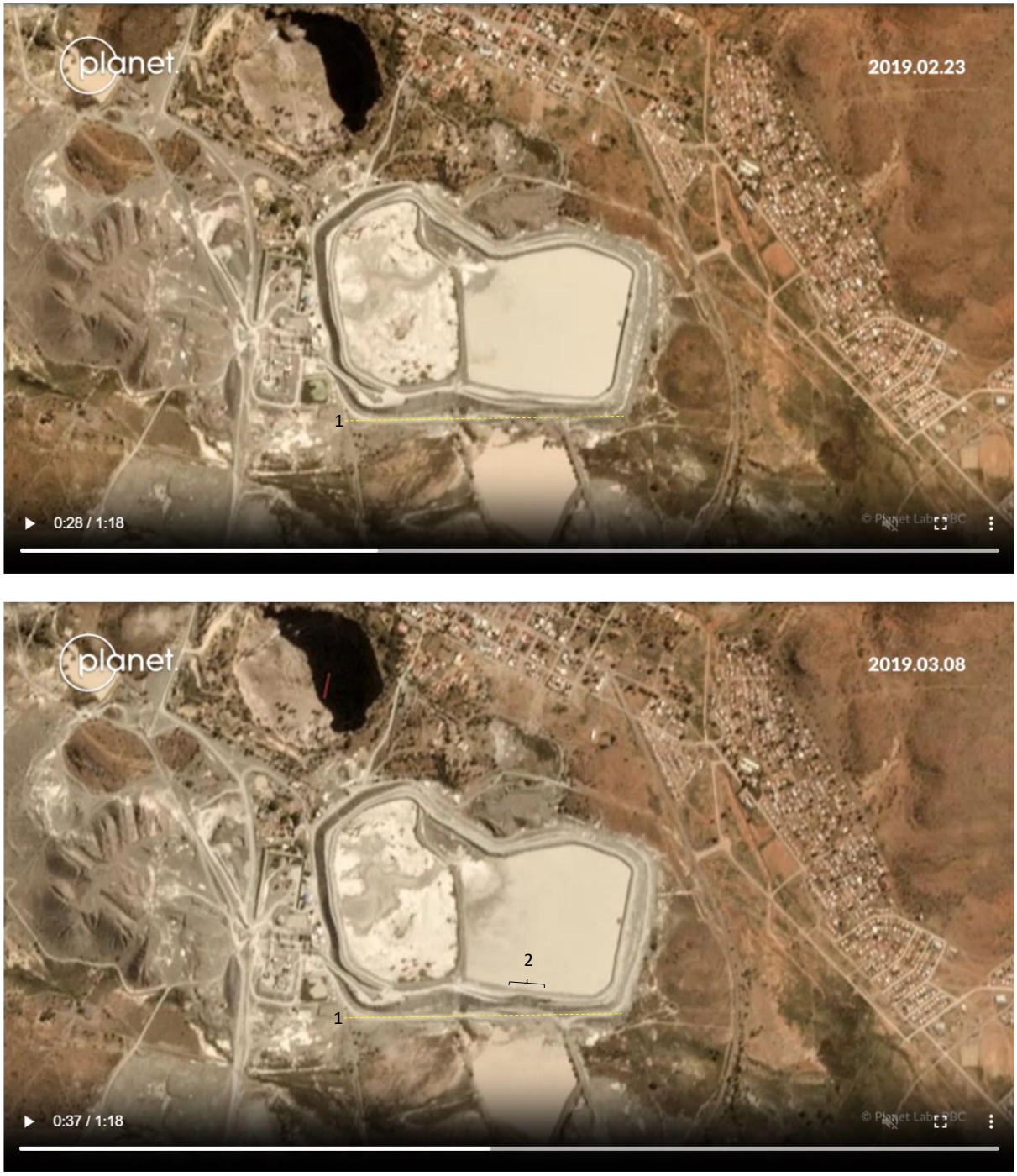

FIGURE 3 PLANETSCOPE SATELLITE IMAGES TAKEN ON 2019/02/23 AND 2022/03/08 SHOWING SIGNS OF SLOPE INSTABILITY ALONG THE SOUTHERN WALL OF COMPARTMENT 2.

Figure 4 (a) and (b) present PlanetScope images respectively recorded on 2019/03/13 and 2019/03/17, demonstrating further signs of slope instability, with a significant slip visible towards the south on 2019/03/17. Closer examination of the toe of the southern wall of compartment 2, where the wall borders Dam 1, reveals an amount of movement that appears to amount to several metres towards the south (Label 3).

The PlanetScope satellite image in Figure 5, taken on 2019/03/20, shows that the access road along the toe of the southern wall of Compartment 2 had been displaced to the south by several metres

where it runs along Dam 10 and that it was no longer a straight road. Additional signs of movement taking place over the remainder of March and April 2019 are evident in PlanetScope imagery (not shown here).

FIGURE 4 **PLANETSCOPE SATELLITE IMAGES TAKEN ON 2019/03/13 AND 2022/03/17 SHOWING FURTHER SIGNS OF SLOPE INSTABILITY ALONG THE SOUTHERN WALL OF COMPARTMENT 2.**

FIGURE 5 PLANETSCOPE SATELLITE IMAGE TAKEN ON 2019/03/20 SHOWING MOVEMENT ALONG THE TOE OF THE SOUTHERN WALL OF COMPARTMENT 2.

Probably in response to the instability described above, JD placed a large amount of additional material on the slopes of the southern wall of Compartment 2 during the course of April 2019. An impression of the amount of material placed and the work done can be gained by comparing images recorded on 2019/03/30 and 2019/05/01, presented in Figure 6. Comparing Figure 5 and Figure 6 (a) also reveals a significant amount of additional movement along the toe of the wall into Dam 10 (opposite label 4). Previously unidentified movement in the southeastern corner of the dam, extending from label 4 outwards to the toe in a south-southeasterly direction, can be identified when comparing Figure 6 (a) and (b).

Signs of instability at the crest of the southeastern corner of the dam are evident by 2019/05/02, possibly due to the movement reported above. This is also visible in a GoogleEarth image, dated the same day, see Figure 7 (b). Signs of bulging are visible at the toe of this zone of instability. A linear feature visible in Figure 7 (a) is identified in Figure 7 (b), demonstrating movement and deformation along the toe of the southern wall against Dam 10.

FIGURE 6 PLANETSCOPE SATELLITE IMAGES TAKEN ON 2019/03/30 AND 2019/05/01 SHOWING THE PLACEMENT OF MATERIAL ON THE SLOPE OF THE SOUTHERN WALL OF COMPARTMENT 2.

FIGURE 7 **GOOGLEEARTH IMAGERY DATED (A) 2019/02/04 AND (B) 2019/05/02, WITH THE LATTER SHOWING SIGNS OF INSTABILITY IN THE SOUTHEASTERN CORNER OF THE DAM.**

Figure 8 presents PlanetScope images recorded on 2019/05/02 and 2019/05/29. It illustrates considerable activity on the slopes of the southern wall of Compartment 2 and material placed along the southern and southeastern toe of the dam. A significant amount of movement to the south is evident along the toe, especially near the southeastern corner of the dam. Take note of the position of the original straight access road along the southern wall of the dam which has by the end of May 2019 undergone a large amount of displacement towards the south.

FIGURE 8 PLANETSCOPE SATELLITE IMAGES TAKEN ON 2019/05/02 AND 2019/05/29 SHOWING ACTIVITY AND MOVEMENT ALONG THE SOUTHERN AND SOUTHEASTERN TOE OF COMPARTMENT 2.

1.2. Sept 2019 – July 2020

On 2019/09/16 a faint dark spot can be identified against the inside-crest of the southern wall of Compartment 2 as shown in Figure 9 (a). (Check water index before and after this time). By 2019/10/20 the dark spot had been encircled by an embankment which appeared to fade until 2019/11/10 when a large amount of deposition seemed to have taken place (10-12 Nov 2019). The deposition made the circular embankment feature stand out prominently. The feature remained visible for several months, eventually fading towards the end of July 2023 as deposition on the dam proceeded and the walls were raised.

FIGURE 9 PLANETSCOPE IMAGING DATED (A) 2019/09/16 AND (B) 2019/11/12 SHOWING A DARK SPOT APPEARING ALONG SOUTHERN EMBANKMENT, SUBSEQUENTLY ENCIRCLED BY EMBANKMENT.

The question is "What was the intention with the circular embankment?" Without further information it could be speculated that it was intended as a measure to isolate a sinkhole / rathole, which might possibly have been drawing water(?) (check water index before and after this time). It will be of interest to discuss this matter with JD.

Figure 10 presents PlanetScope images recorded on (a) 2020/01/16 and (b) 2020/07/23. The original alignment of the originally straight access road along the southern toe of the dam is indicated. It appears that a significant amount of southward movement took place along the southern toe of

Compartment 2 to the east and west of the Dam 10 embankment during the first half of 2020 (locations 1 and 2 indicated in Figure 10 (b)). A large amount of material seems to have been placed on the slopes of the southern wall of Compartment 2, but not against the toe.

A question is raised “Why does movement seem to take place to the east and west where the Dam 10 embankment abuts the southern wall of Compartment 2, and why does less movement appear to have taken place where the embankment meets the tailings dam?” The impression is gained that the Dam 10 embankment may have been acting as a restraint against the toe of the dam, locally limiting movement towards the south. The effect is especially visible in Figure 10 (b).

FIGURE 10 PLANETSCOPE IMAGING DATED (A) 2020/01/16 AND (B) 2020/07/23 SHOWING DISPLACEMENT ALONG THE SOUTHERN AND SOUTHEASTERN WALLS OF COMPARTMENT 2.

Figure 11 presents PlanetScope imaging dated (2020/08/25) and (2021/02/26) from which further bulging towards the south and southeast is apparent. The southern wall also seemed to have expanded towards the north into the dam basin, most probably reflecting the raising of the walls as part of the operation of the dam.

FIGURE 11 PLANETSCOPE IMAGING DATED (A) 2020/08/25 AND (B) 2021/02/26 SHOWING MORE DISPLACEMENT ALONG TOE OF THE SOUTHERN AND SOUTHEASTERN WALLS OF COMPARTMENT 2.

Figure 15 (a) and (b) present PlanetScope images dated 2021/03/01 and 2021/07/29 respectively. Examining the alignment of the southern access road does not suggest visible movement over this five-month period along the toe of the southern wall. However, looking at the location of the inside toe of the wall (red dotted line), it appears that wall raising occurred towards the outside, allowing the crest of the southern wall of Compartment 2 to be straightened.

FIGURE 12 PLANETSCOPE IMAGING DATED (A) 2021/03/01 AND (B) 2021/07/29 SHOWING NO VISIBLE SOUTHWARDS MOVEMENT ALONG SOUTHERN TOE OF COMPARTMENT 2, BUT WALL RAISING EVIDENT (DOTTED RED LINE).

Figure 15Figure 13 (a) and (b) present PlanetScope images dated 2021/08/31 and 2021/09/28 respectively in which a significant amount of additional deformation can be identified along the southern and southeastern toe of Compartment 2. This deformation occurred nearly exactly one year before the failure of the dam. During this time the crest of the dam seemed to have been widened to the inside of the dam associated with raising of the walls. Significant additional movement can also be identified on the southern wall during spring of 2021 and the remainder of the year (images not shown). Clearly defined movement is not evident on the dam during 2022 with the exception of what is discussed below.

FIGURE 13 PLANETSCOPE IMAGING DATED (A) 2021/08/31 AND (B) 2021/09/28 SHOWING SIGNIFICANT ADDITIONAL DEFORMATION ALONG SOUTHERN AND SOUTHEASTERN TOE OF COMPARTMENT 2.

Figure 14(a) and (b) present PlanetScope images dated 2022/07/25 and 2022/09/08, shortly before the failure. Similar images from April to July 2022 show a large amount of turbid water on the dam during the winter of 2022, but the dam seemed to show significant signs of drying during August as indicated by dry patches in the basin identifiable in Figure 14 (b). The red arrow in Figure 14 (a) indicates the location of a patch of vegetation at the end of July. The same location is indicated in Figure 14 (b). It is apparent that the patch of vegetation moved to the east during the six weeks between the two images. It can be noted that the two compartments on the dam had merged into one by this time.

FIGURE 14 PLANETSCOPE IMAGING DATED (A) 2022/07/25 AND (B) 2022/09/08 SHOWING SIGNS OF DRYING.

1.3. Failure event on 11 Sept 2022

Figure 15 (a) and (b) respectively present PlanetScope satellite imagery of the Jagerfontein tailings dam taken shortly before and after the failure event that took place on 11 September 2022. Prominent slope break-lines are highlighted in both images by yellow dotted lines. Comparison of the two images is best achieved by flicking between them when displayed electronically on a screen. Studying the two images reveal that a considerable amount of movement occurred along the southern wall of the tailings dam associated with the failure. Block A, bordered by the blue broken lines numbered 1 and 2 respectively in Figure 15 (b) can be observed to have moved in a generally southerly direction, with block B, located between the blue broken lines numbered 2 and 3, moving in the south-southeasterly direction. The magnitude of movement associated with the failure event was estimated using before and after Google Earth imagery to be of the order of 20 m.

FIGURE 15 **PLANETSCOPE SATELLITE IMAGES TAKEN BEFORE (2022/09/08) AND AFTER (2022/09/12) THE FAILURE EVENT**

APPENDIX D

PRESENTATION OF SENTINEL-2 SATELLITE IMAGERY

Sentinel-2 imagery history

Sentinel-2 is a multispectral satellite earth imaging system managed by the European Space Agency (ESA). The system is currently comprised of two optical satellites in a tandem orbit. Each satellite carries the same imaging system with a 290 km wide field of view, providing a revisit time of five days. The dataset used here is the orthorectified surface reflectance Sentinel-2 product delivered by the ESA (S2 Level 2A). The dataset is intended to provide atmospherically corrected spectral reflectance imagery of the earth which begins coverage of the Jagersfontein site in early 2017. The S2 Level 2A dataset has a maximum spatial resolution of 10 m for the visible and wide near infrared (NIR) spectrum bands (B2, B3, B4 and B8), 20 m for red edge, narrow band NIR and shortwave infrared (SWIR) spectrum bands (B1, B5, B6, B7, B8A, B11 and B12) and 60 m for coastal aerosol, water vapour and cirrus cloud detection spectrum bands (B1 and B10) (ESA, 2015). The water vapor or aerosol detection band (B09) is predominantly used for atmospheric characterisation and is omitted from the S2 Level 2A surface reflectance product. For the purpose of observing changes in the construction of a tailings dam, the higher spatial resolution visible spectrum bands (B2, B3, B4) are of interest. To detect supernatant water and the presence of high soil surface moisture content the NIR (B8) and SWIR bands (B11) are of interest as clear water and moist soil are strong absorbers of solar radiation in these spectrums, respectively. A complete list of all bands is provided in the table below. The bands of interest to this report are underlined in bold.

Table 1 Sentinel-2 Bands

Band No.	Spectrum / Description	Central Wavelength	Native Resolution
		(µm)	(m/pixel)
B1	Aerosols	0.443	60
B2	**Blue**	0.490	10
B3	**Green**	0.560	
B4	**Red**	0.665	
B5	Vegetation red edge	0.705	20
B6	Vegetation red edge	0.740	
B7	Vegetation red edge	0.783	
B8	**NIR - Wide**	0.842	10
B8A	NIR - Narrow	0.865	20
B9	Water vapour	0.945	60
B10	Cirrus (Only in L1A)	1.375	60
B11	**SWIR**	1.610	20
B12	SWIR	2190	

Sentinel-Hub was used to generate a time history of all Sentinel-2 Level 2A images for both the Jagersfontein Tailings Dam and Dam 10, located immediately to the south of the tailings dam. For completeness, cloud obstructed images are included and not filtered from this history, which follows at the end of this appendix. NIR (B8) and SWIR (B11) images are displayed using the same greyscale colour ramp, shown in Figure D1 below. Black pixel values correspond to zero reflectance and pixel values of white correspond to reflectance values of 0.5 and greater.

Figure D1 NIR and SWIR greyscale colour ramp

Additionally, an aggregation of the Sentinel-2 NIR (B8) and SWIR (B11) band data for the eastern compartment of the Jagersfontein dam is given below. The time series was generated using Google Earth Engine (GEE), the script for which may be access here: https://code.earthengine.google.com/6306a24de34b78542b36fbcd3ddffe7a.

In this aggregate product, clouds have been masked out of the dataset using the Sentinel-2 Cloud Probability dataset. Cloud shadows were also estimated by projecting clouds 1 km horizontally according to the solar azimuth angle. Images with a cloud or cloud shadow obstruction of more than 1% of the area of the Area of Interest (AoI) were excluded from the aggregate analysis. The AoI is shown in Figure D2 and time series summaries of NIR band 08 and SWI Band 11 are shown in Figure D3, which follows.

Figure D2 Area of Interest (AoI) over eastern compartment

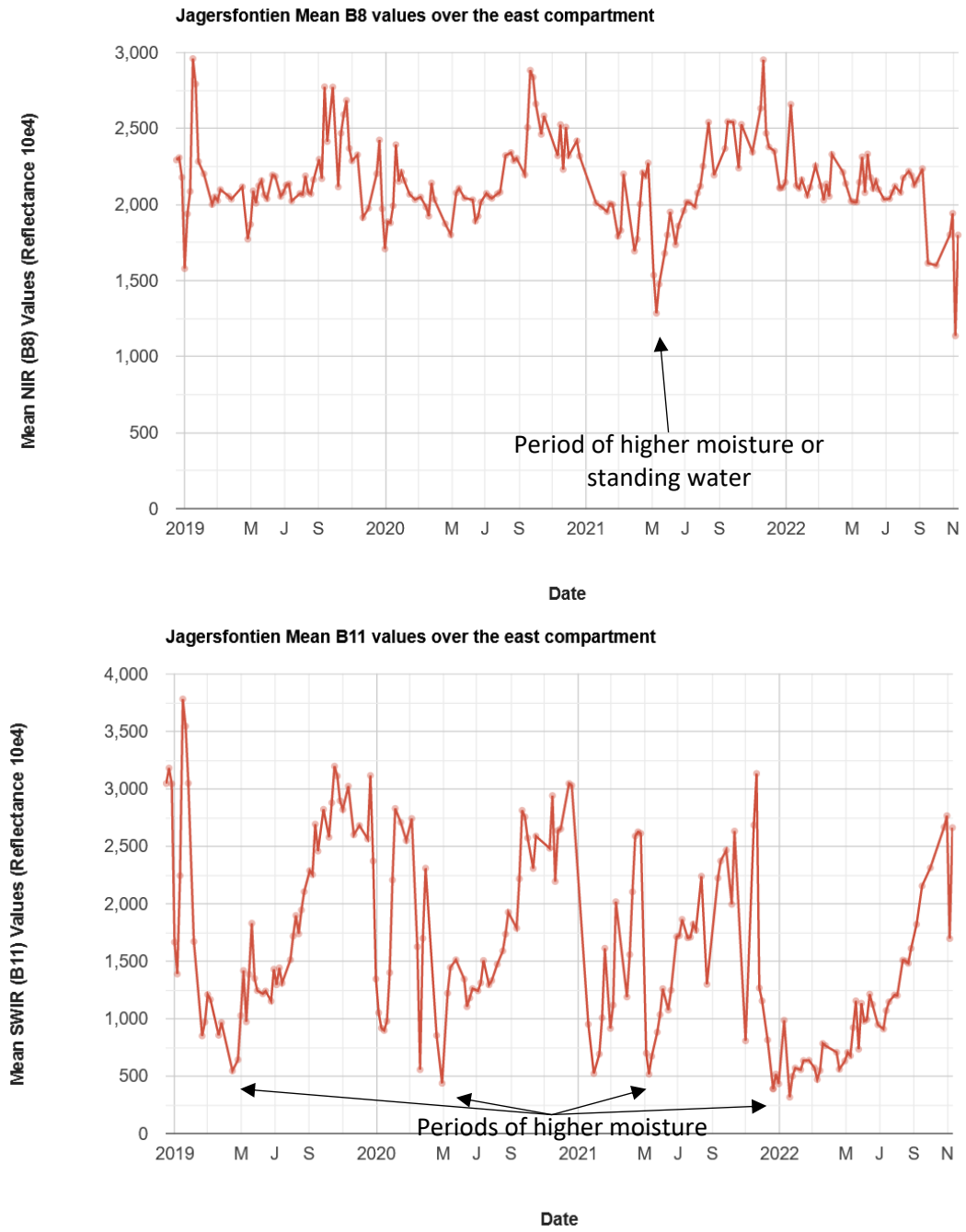

Figure D3 Mean NIR (B8) and SWIR (B11) values for the Jagersfontein Tailings Dam Eastern Compartment with time

In Figure D3, high mean values of NIR and SWIR correspond to dryer conditions over the eastern compartment, while low mean values of NIR and SWIR correspond to wetter conditions. It should be noted that NIR reflectance is sensitive to deeper open water, while SWIR is sensitive to very shallow water bodies as well as soil moisture content. As such, low NIR reflectance is likely to indicate the presence of standing water. However, the turbidity of and suspended solids within a water body will increase the water surface's NIR reflectance, leading to difficulty distinguishing it from other. On the other hand, high SWIR reflectance values indicate dry soil conditions, while low SWIR values are strongly associated with water, both shallow and deep, as well as high soil moisture content. As such, in the context of a tailings dam, low SWIR reflectance values may indicate standing water, or recently

deposited tailings paste or slurry. As such, SWIR reflectance, may be used to assess the deposition patterns of tailings and the location of the decant pond, but cannot necessarily be used to differentiate between standing water and very wet tailings.

References

European Space Agency (ESA). 2015. Sentinel User Handbook and Exploitation Tools (SUHET): Sentinel-2 User Handbook. European Commission. ESA Standard Document 24/07/2015 Issue 1 Rev. 2.

Natural Colour (RGB - Bands 4, 3, 2)

Near Infrared (NIR - Band 8)

Shortwave Infrared (SWIR - Band 11)

Natural Colour (RGB - Bands 4, 3, 2)

Near Infrared (NIR - Band 8)

Shortwave Infrared (SWIR - Band 11)

Natural Colour (RGB - Bands 4, 3, 2)	Near Infrared (NIR - Band 8)	Shortwave Infrared (SWIR - Band 11)
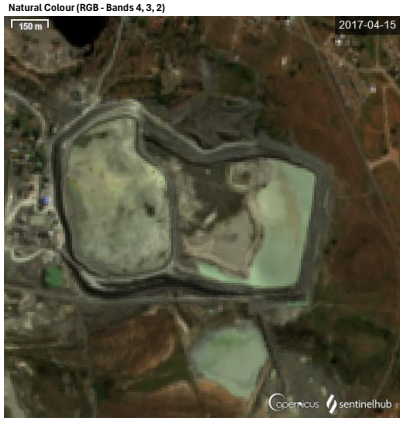		
		
		
		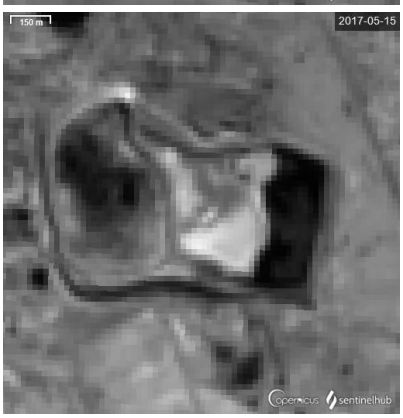
		

Natural Colour (RGB - Bands 4, 3, 2)

Near Infrared (NIR - Band 8)

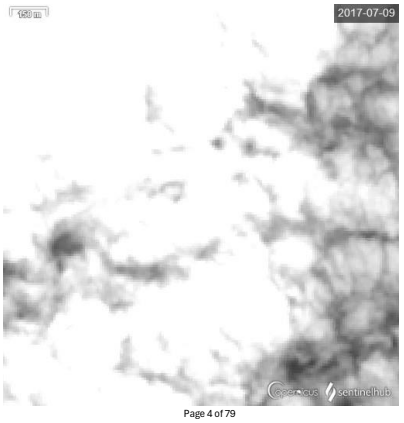

Shortwave Infrared (SWIR - Band 11)

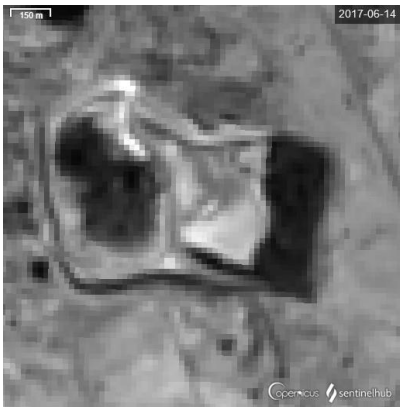

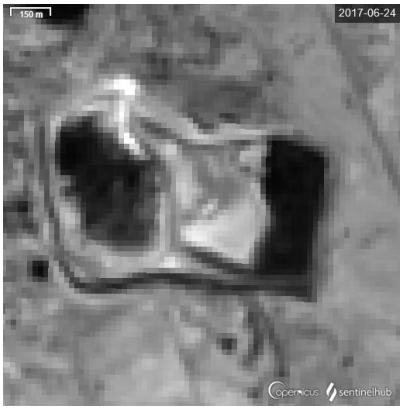

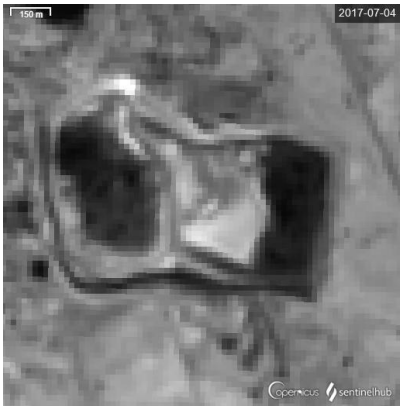

Natural Colour (RGB - Bands 4, 3, 2)

Near Infrared (NIR - Band 8)

Shortwave Infrared (SWIR - Band 11)

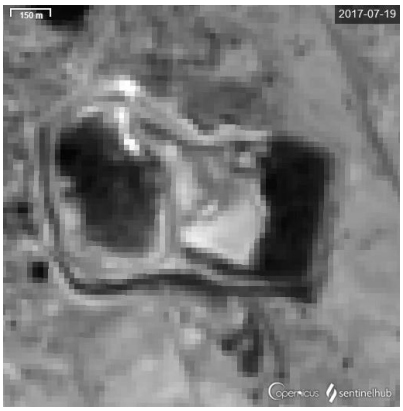

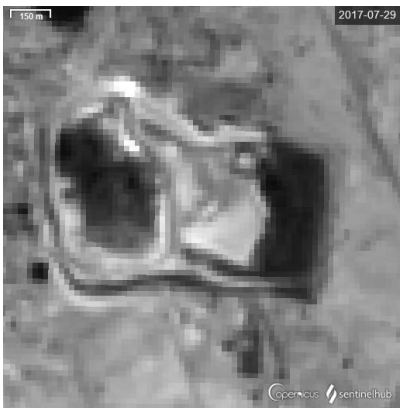

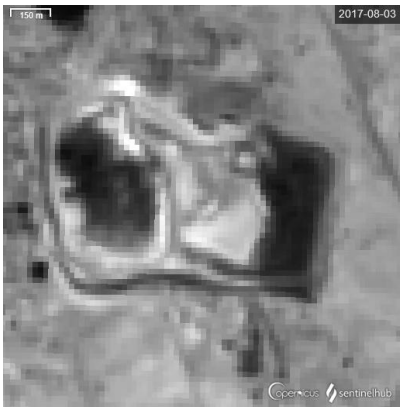

Natural Colour (RGB - Bands 4, 3, 2)

Near Infrared (NIR - Band 8)

Shortwave Infrared (SWIR - Band 11)

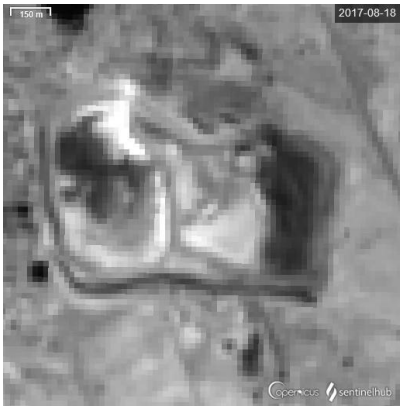

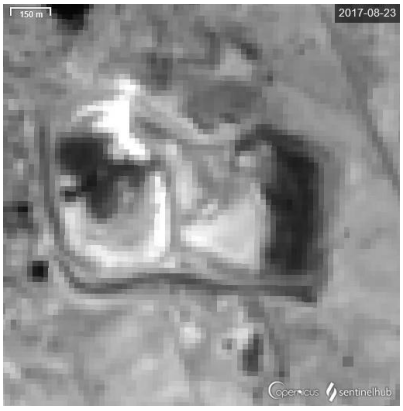

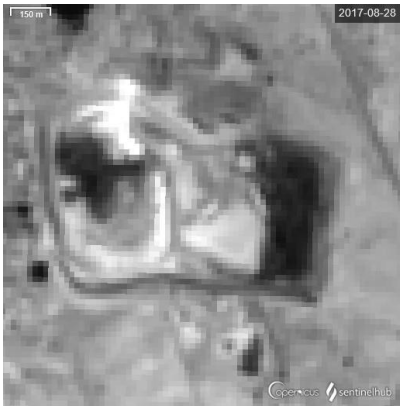

Natural Colour (RGB - Bands 4, 3, 2)	Near Infrared (NIR - Band 8)	Shortwave Infrared (SWIR - Band 11)
		
		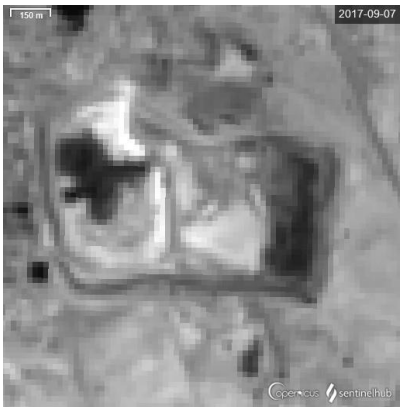
		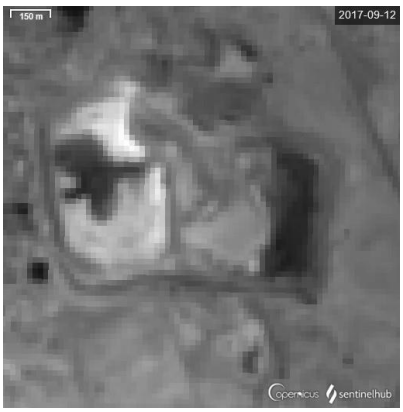
		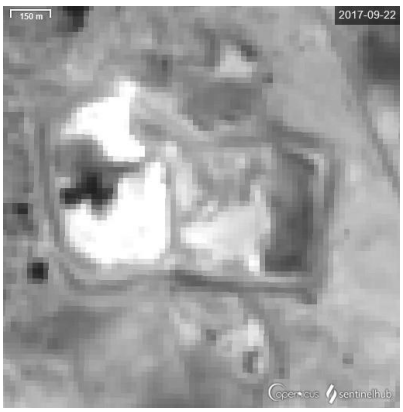
		

Natural Colour (RGB - Bands 4, 3, 2)	Near Infrared (NIR - Band 8)	Shortwave Infrared (SWIR - Band 11)
		
		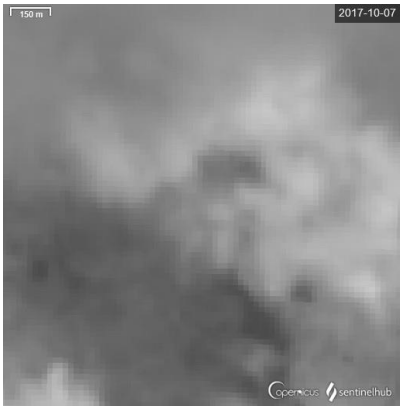
		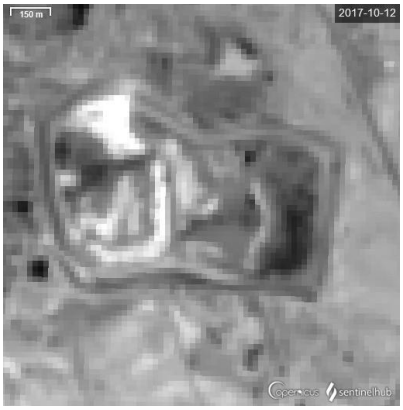
		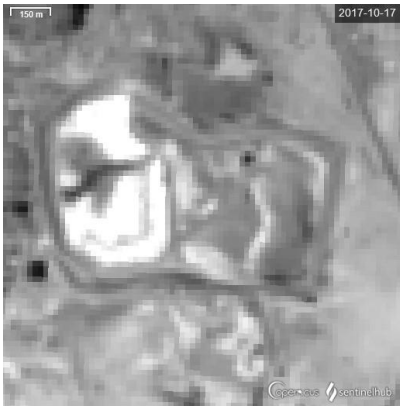
		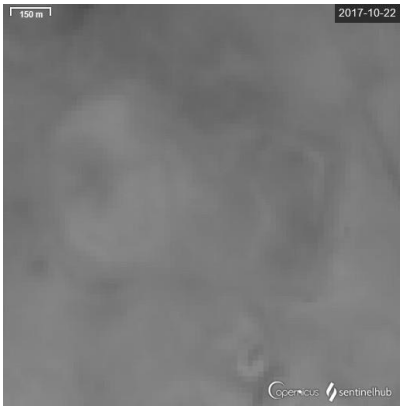

Natural Colour (RGB - Bands 4, 3, 2)

Near Infrared (NIR - Band 8)

Shortwave Infrared (SWIR - Band 11)

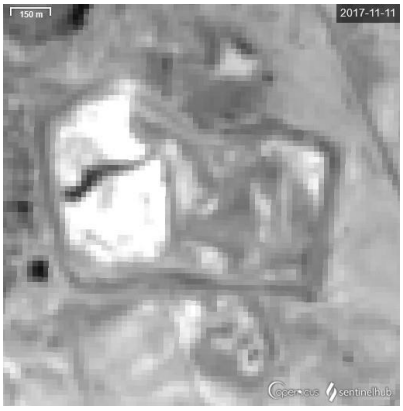

Natural Colour (RGB - Bands 4, 3, 2)

Near Infrared (NIR - Band 8)

Shortwave Infrared (SWIR - Band 11)

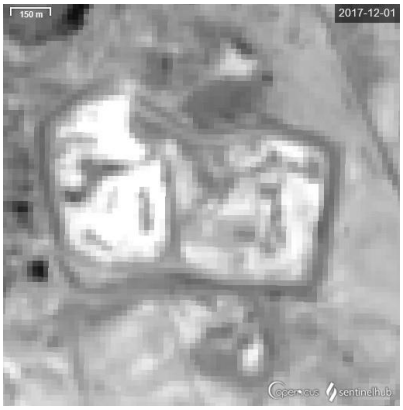

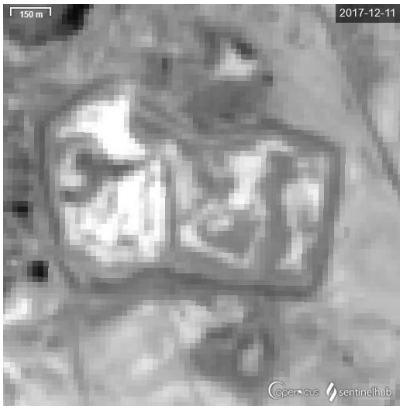

Natural Colour (RGB - Bands 4, 3, 2)

Near Infrared (NIR - Band 8)

Shortwave Infrared (SWIR - Band 11)

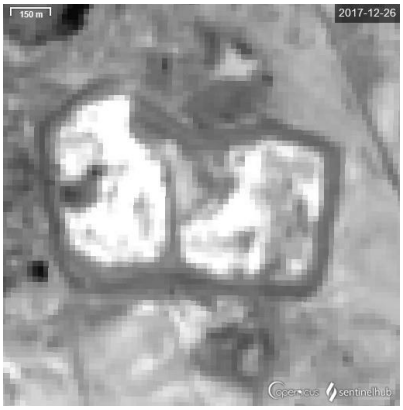

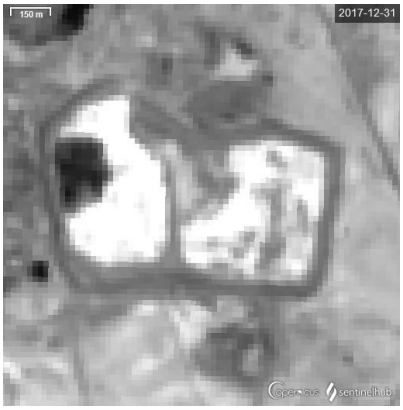

Natural Colour (RGB - Bands 4, 3, 2)	Near Infrared (NIR - Band 8)	Shortwave Infrared (SWIR - Band 11)
		
		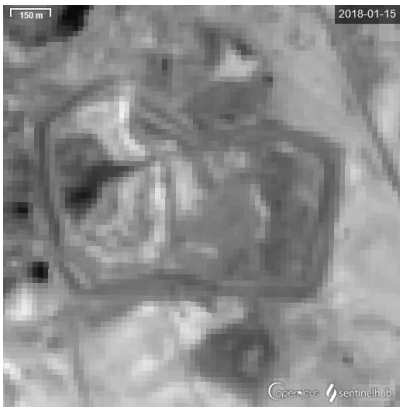
		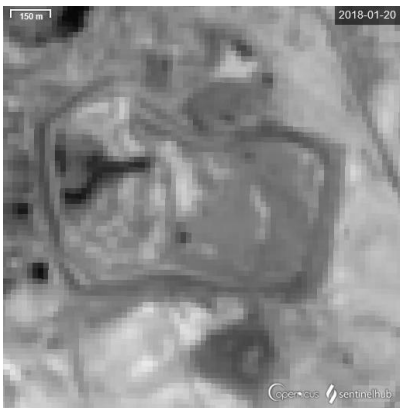
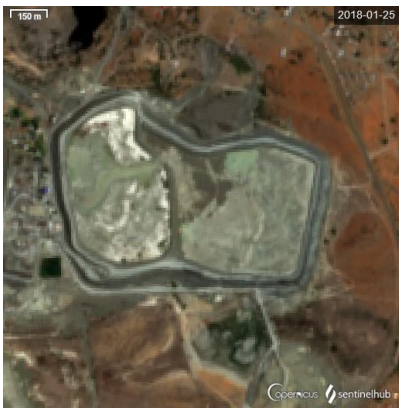		
		

Natural Colour (RGB - Bands 4, 3, 2)

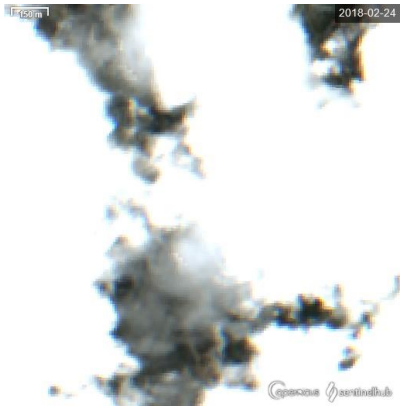

Near Infrared (NIR - Band 8)

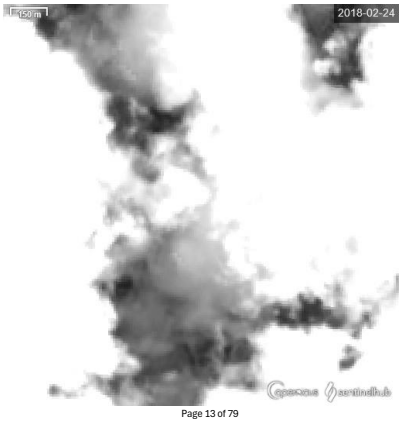

Shortwave Infrared (SWIR - Band 11)

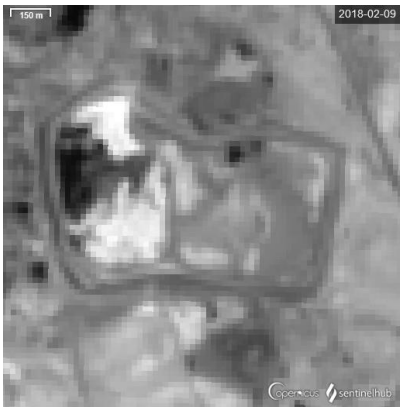

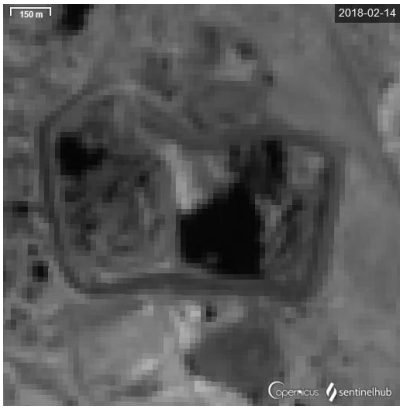

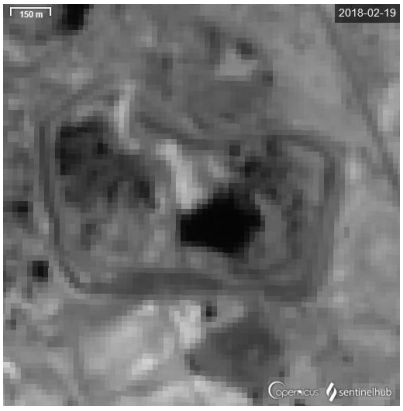

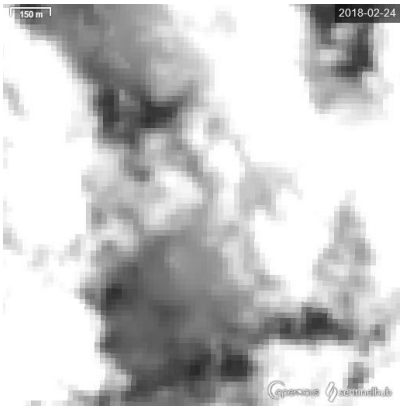

Natural Colour (RGB - Bands 4, 3, 2)

Near Infrared (NIR - Band 8)

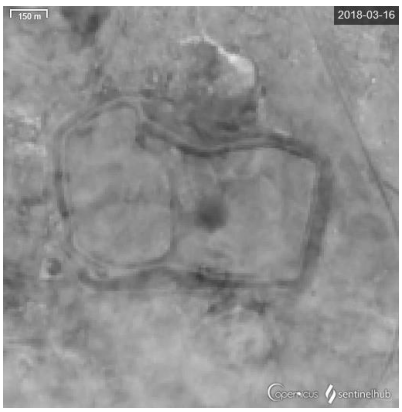

Shortwave Infrared (SWIR - Band 11)

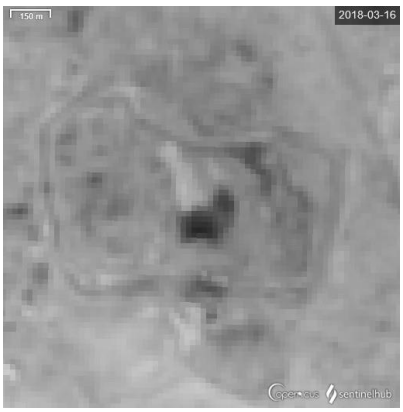

Natural Colour (RGB - Bands 4, 3, 2)

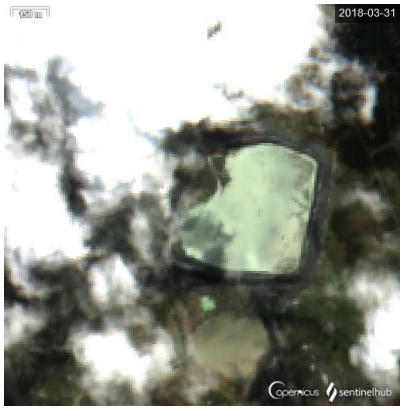

Near Infrared (NIR - Band 8)

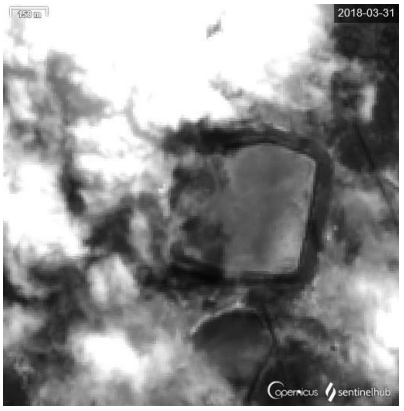

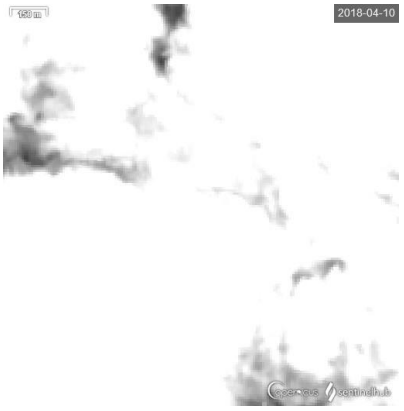

Shortwave Infrared (SWIR - Band 11)

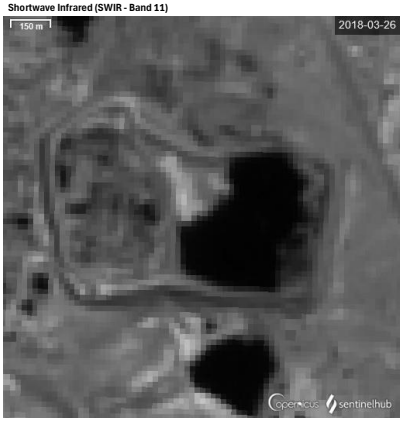

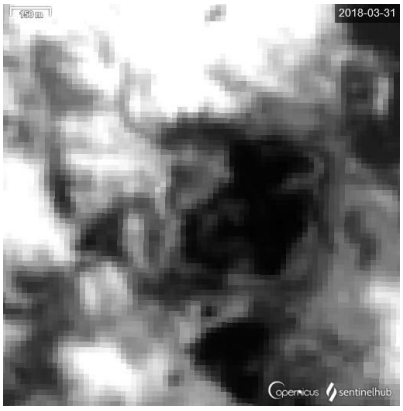

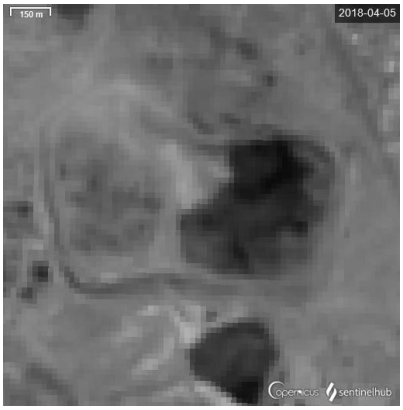

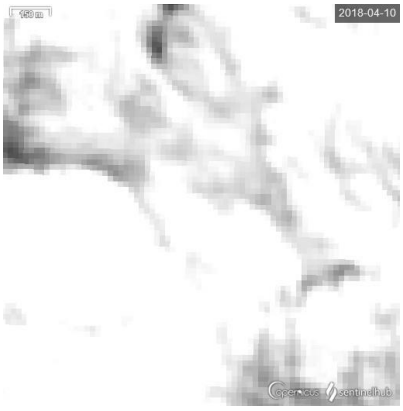

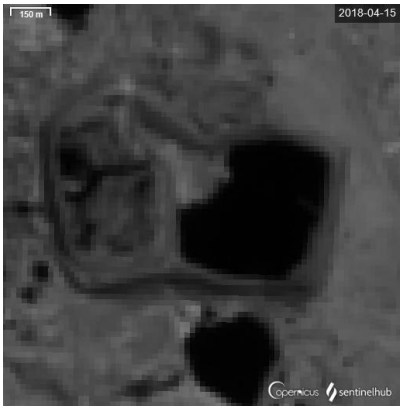

Natural Colour (RGB - Bands 4, 3, 2)

Near Infrared (NIR - Band 8)

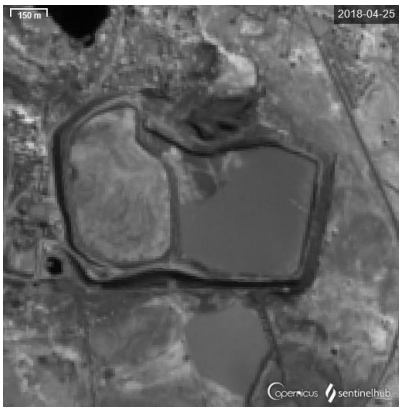

Shortwave Infrared (SWIR - Band 11)

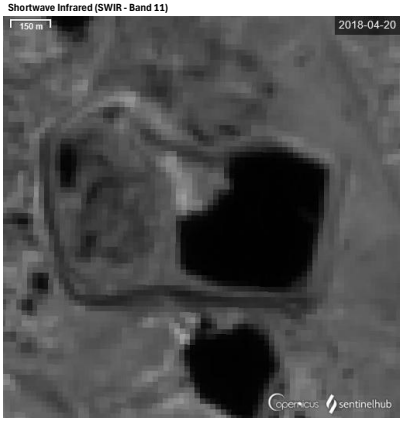

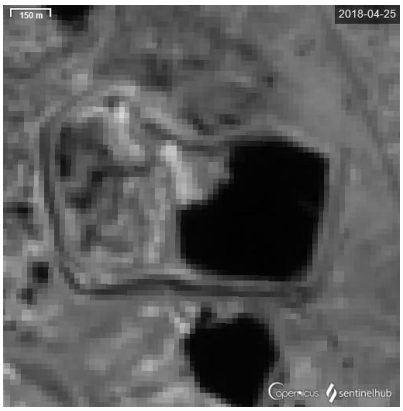

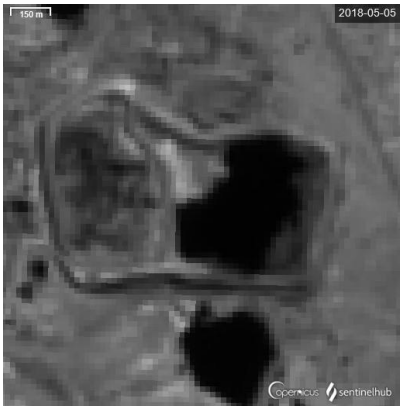

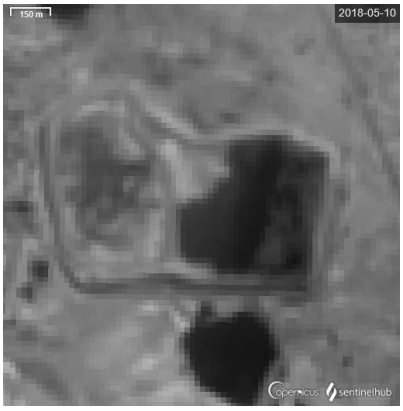

Natural Colour (RGB - Bands 4, 3, 2)

Near Infrared (NIR - Band 8)

Shortwave Infrared (SWIR - Band 11)

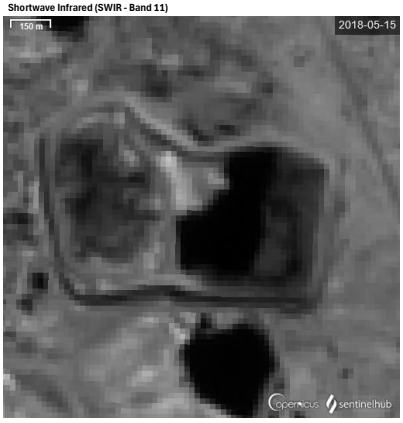

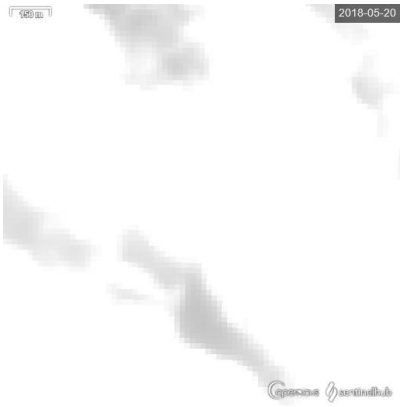

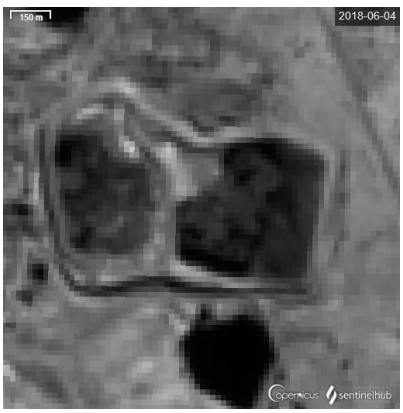

Natural Colour (RGB - Bands 4, 3, 2)	Near Infrared (NIR - Band 8)	Shortwave Infrared (SWIR - Band 11)
		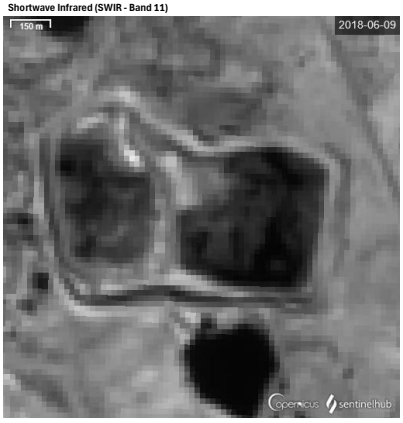
		
		
		
		

Natural Colour (RGB - Bands 4, 3, 2)

Near Infrared (NIR - Band 8)

Shortwave Infrared (SWIR - Band 11)

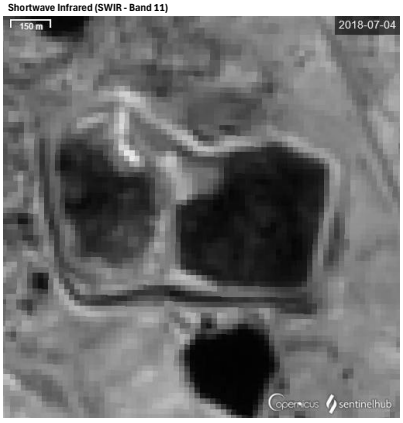

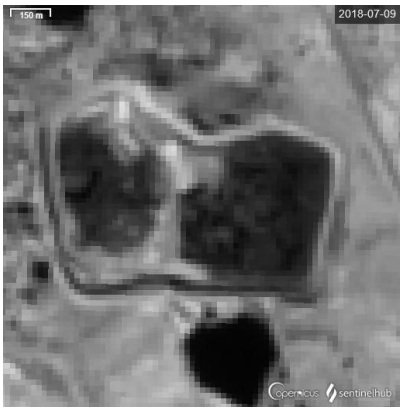

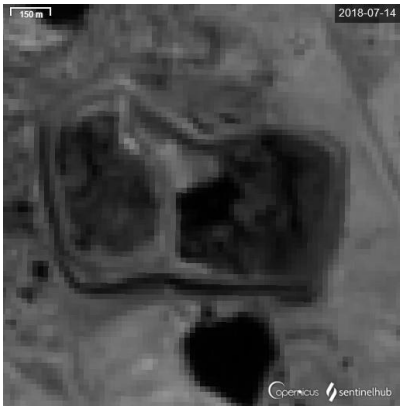

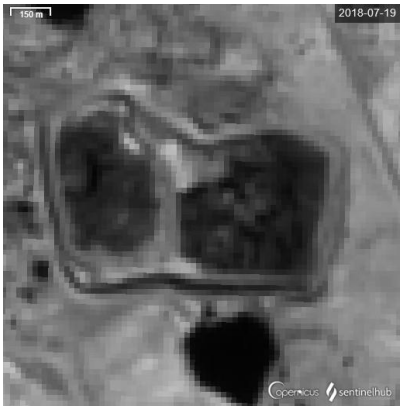

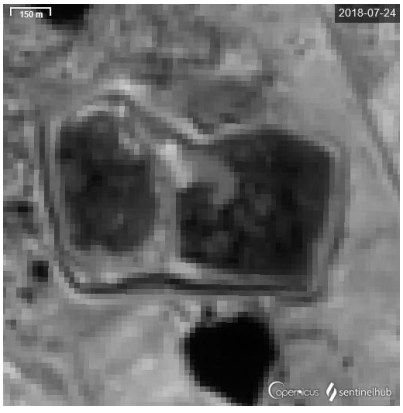

Natural Colour (RGB - Bands 4, 3, 2)	Near Infrared (NIR - Band 8)	Shortwave Infrared (SWIR - Band 11)
		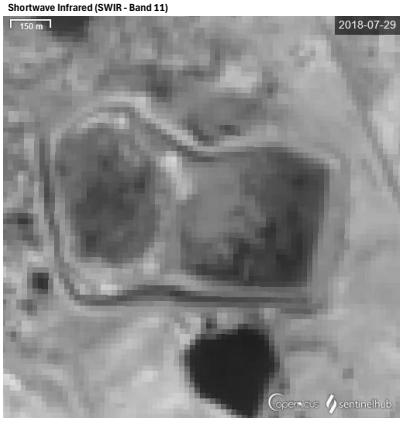
		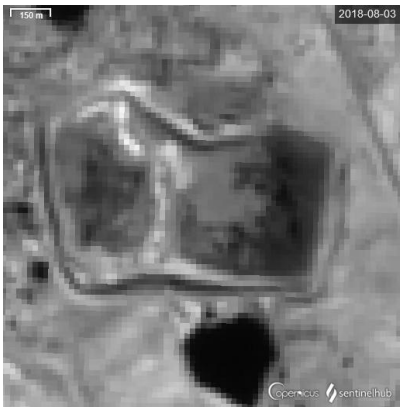
		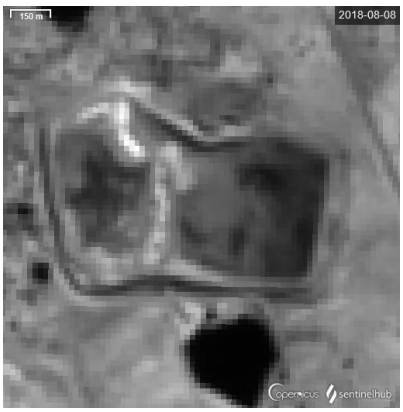
		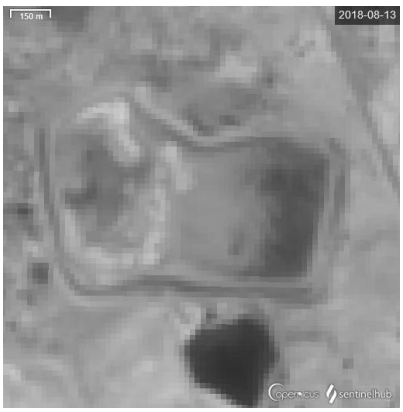
		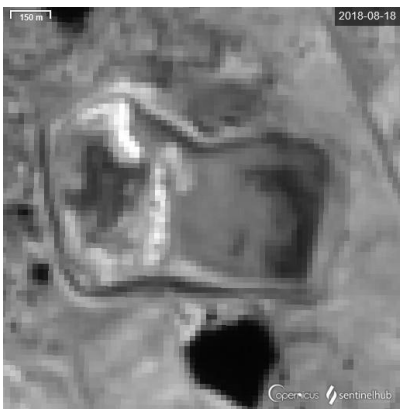

Natural Colour (RGB - Bands 4, 3, 2)

Near Infrared (NIR - Band 8)

Shortwave Infrared (SWIR - Band 11)

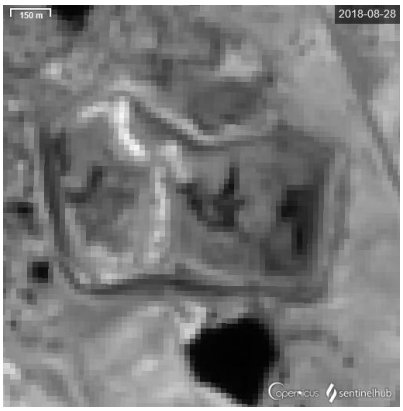

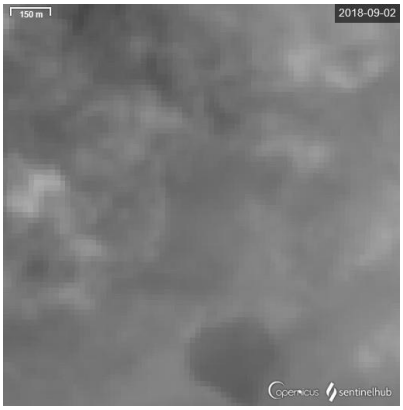

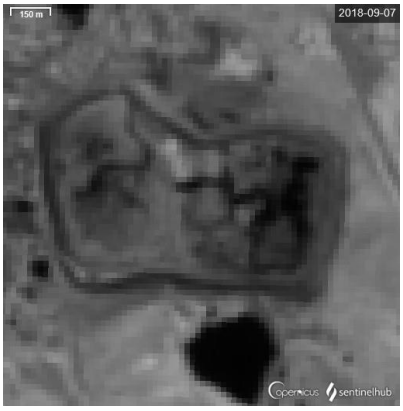

Natural Colour (RGB - Bands 4, 3, 2)	Near Infrared (NIR - Band 8)	Shortwave Infrared (SWIR - Band 11)
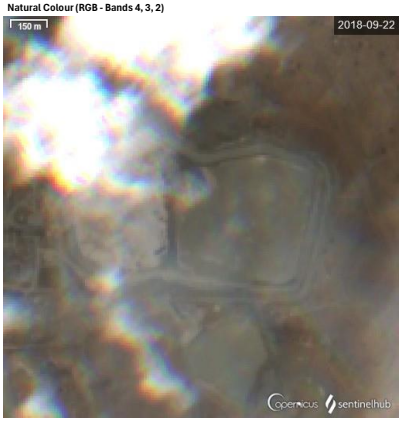	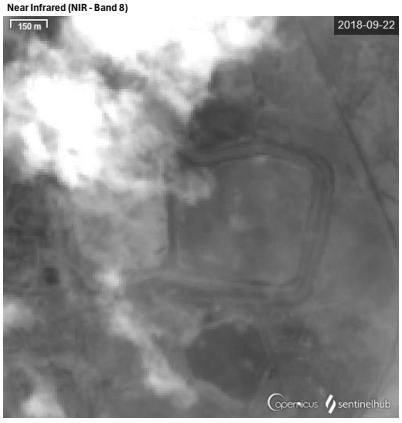	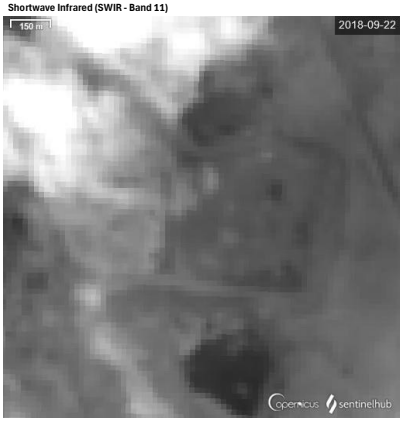
		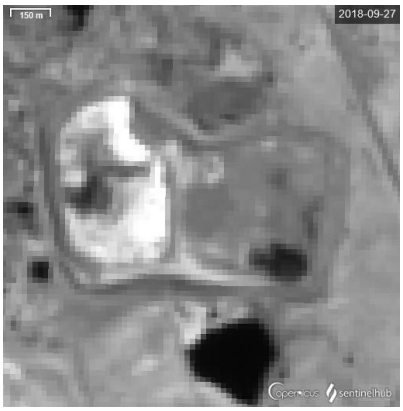
		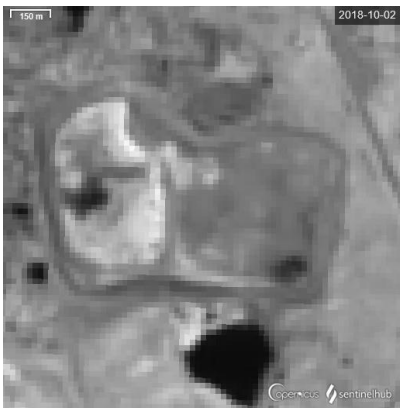
		
		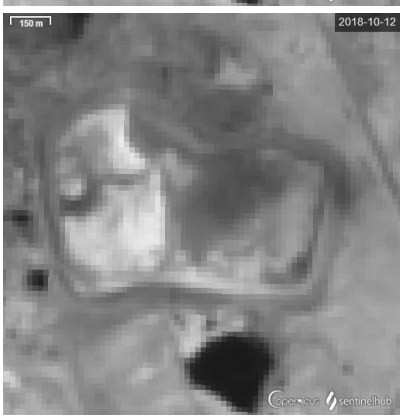

Natural Colour (RGB - Bands 4, 3, 2)

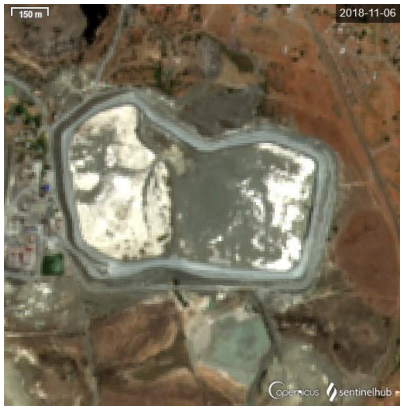

Near Infrared (NIR - Band 8)

Shortwave Infrared (SWIR - Band 11)

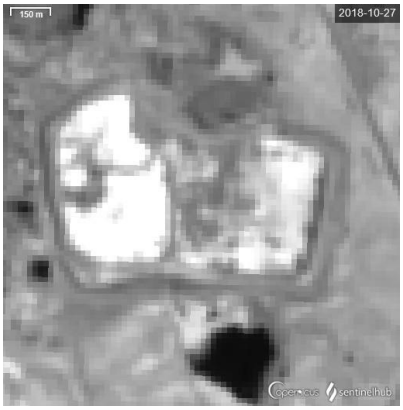

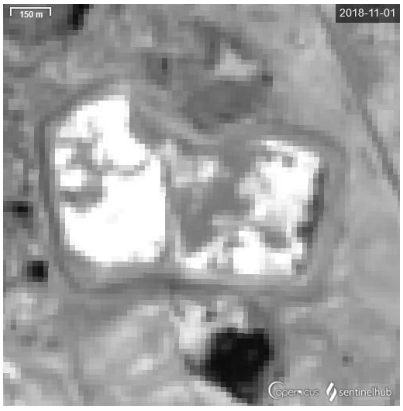

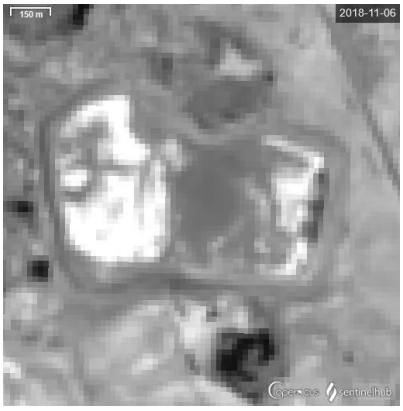

Natural Colour (RGB - Bands 4, 3, 2)

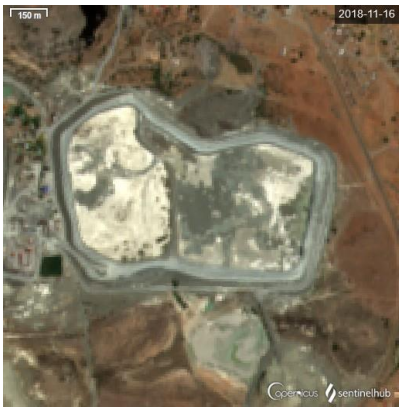

Near Infrared (NIR - Band 8)

Shortwave Infrared (SWIR - Band 11)

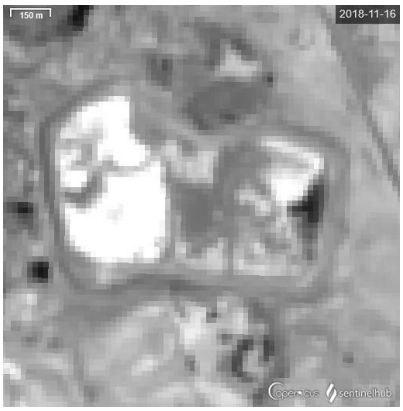

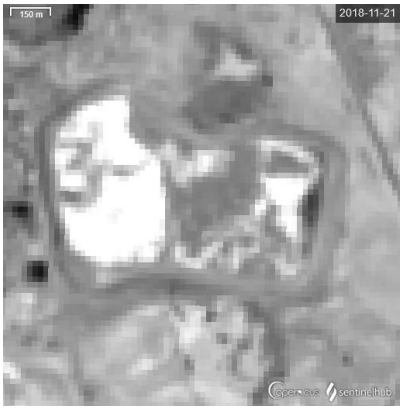

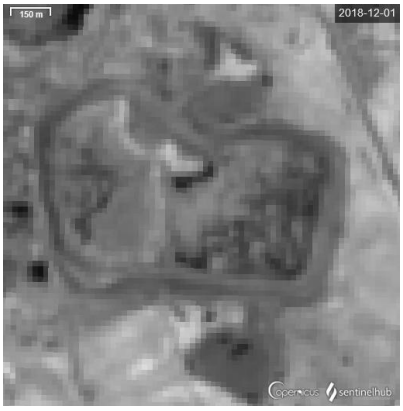

Natural Colour (RGB - Bands 4, 3, 2)	Near Infrared (NIR - Band 8)	Shortwave Infrared (SWIR - Band 11)
		
		
		
		
		

Natural Colour (RGB - Bands 4, 3, 2)	Near Infrared (NIR - Band 8)	Shortwave Infrared (SWIR - Band 11)
		
		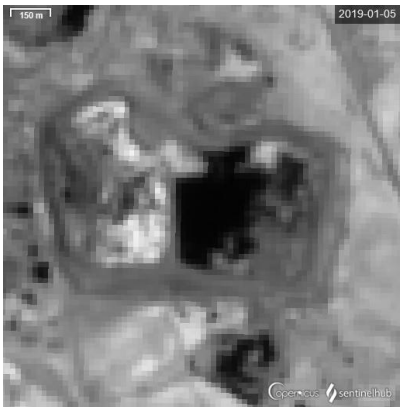
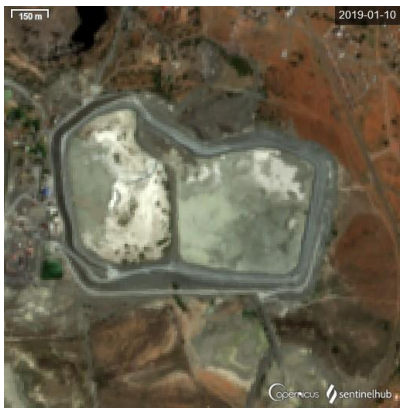		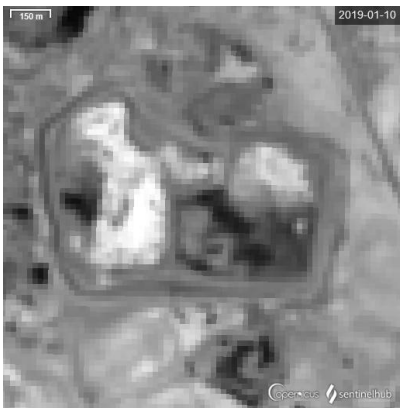
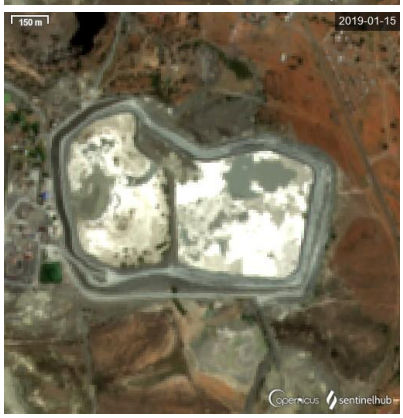		
		

Natural Colour (RGB - Bands 4, 3, 2)

Near Infrared (NIR - Band 8)

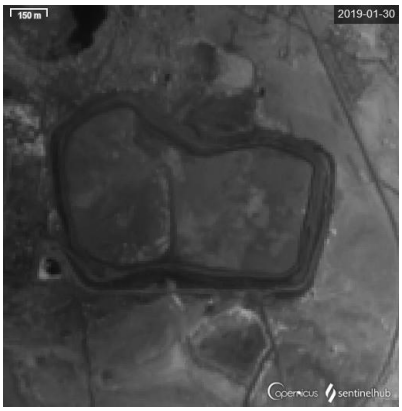

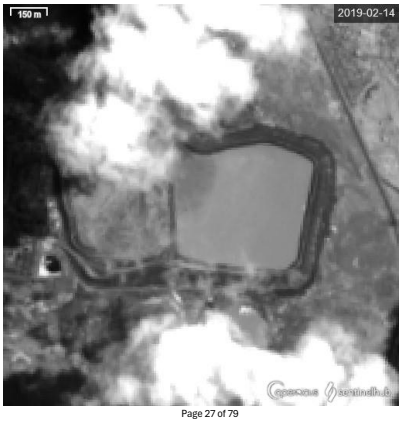

Shortwave Infrared (SWIR - Band 11)

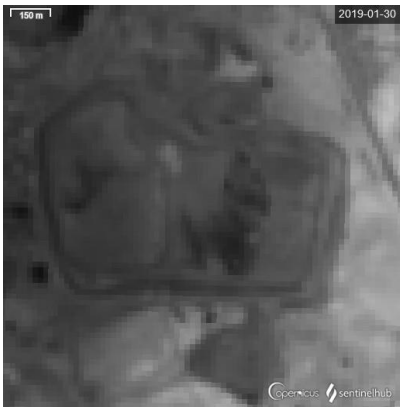

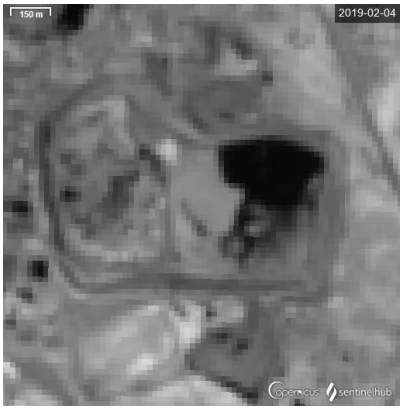

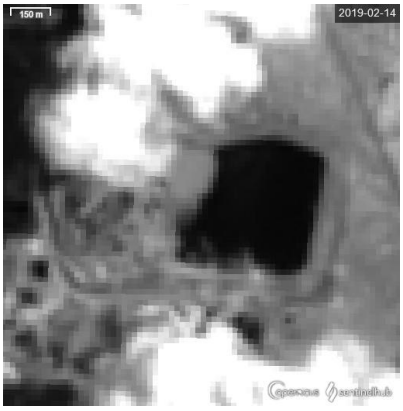

Natural Colour (RGB - Bands 4, 3, 2)

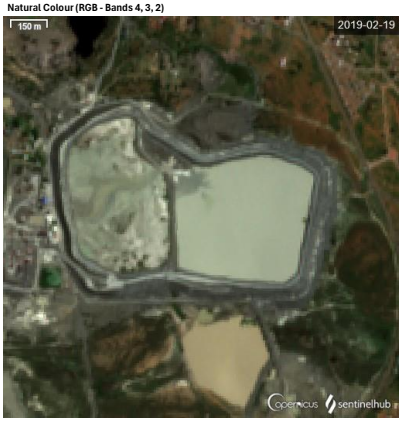

Near Infrared (NIR - Band 8)

Shortwave Infrared (SWIR - Band 11)

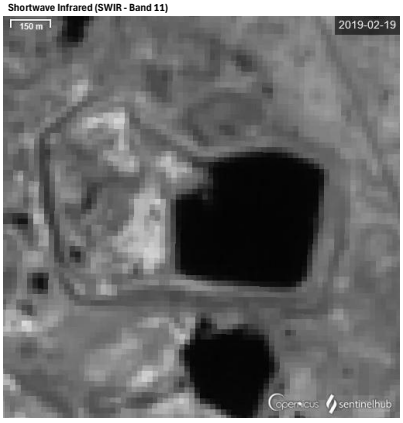

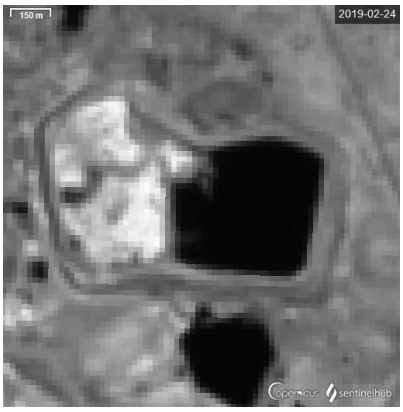

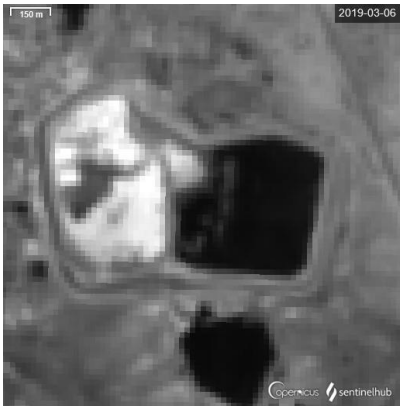

Natural Colour (RGB - Bands 4, 3, 2)

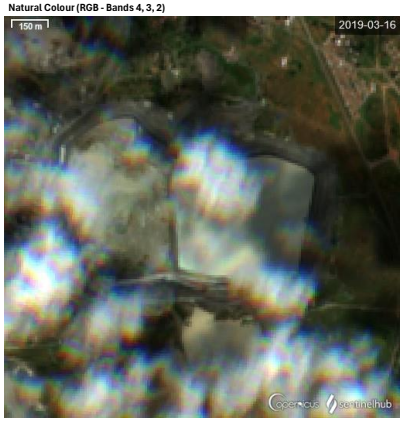

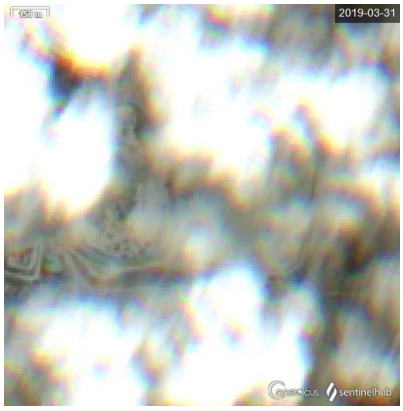

Near Infrared (NIR - Band 8)

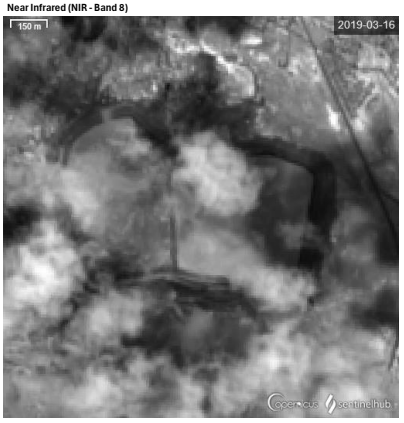

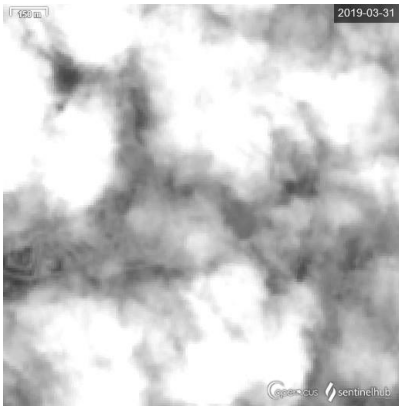

Shortwave Infrared (SWIR - Band 11)

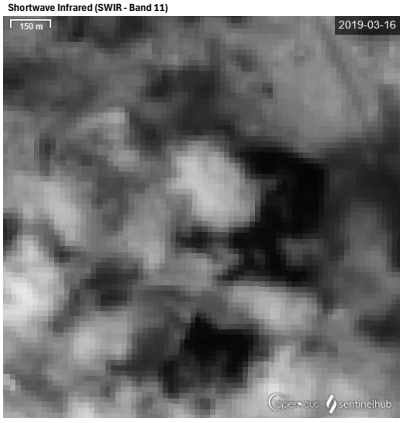

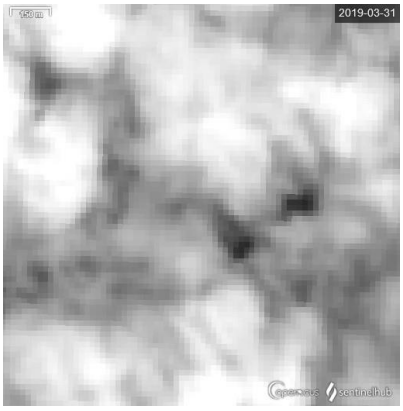

Natural Colour (RGB - Bands 4, 3, 2)	Near Infrared (NIR - Band 8)	Shortwave Infrared (SWIR - Band 11)
	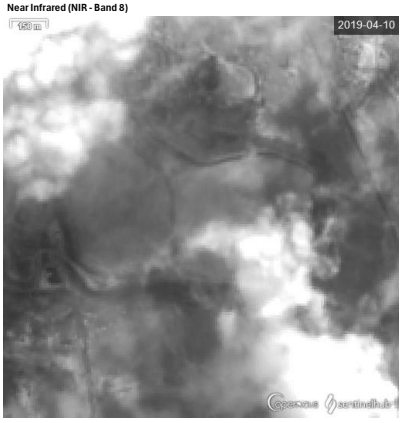	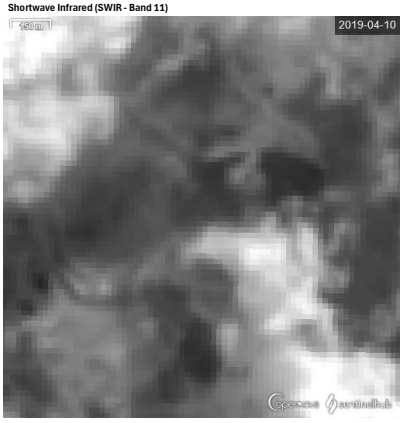
	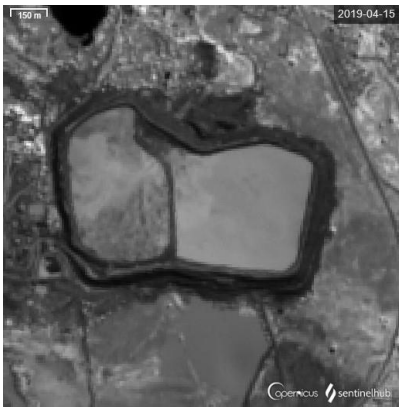	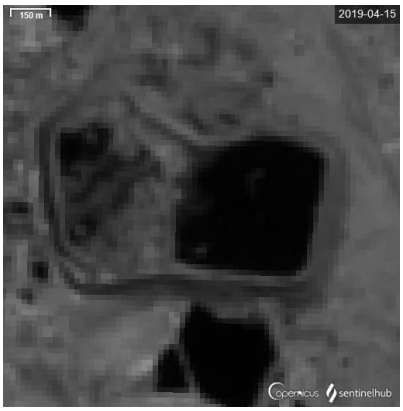
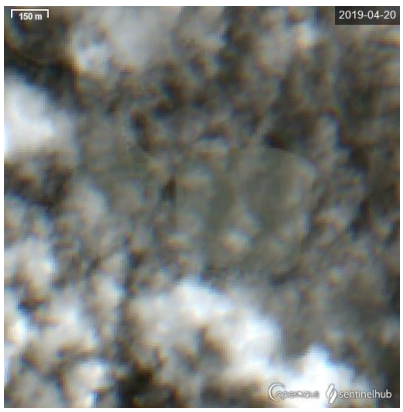	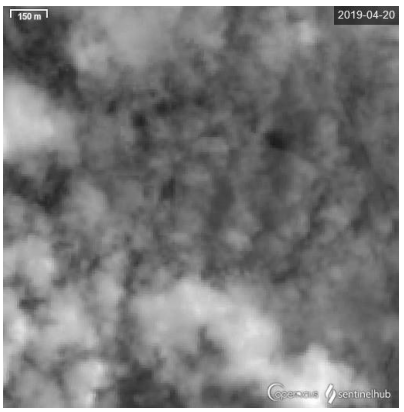	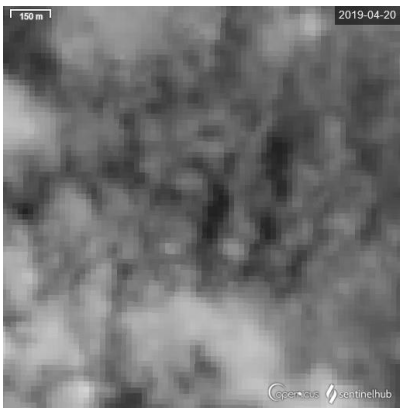
	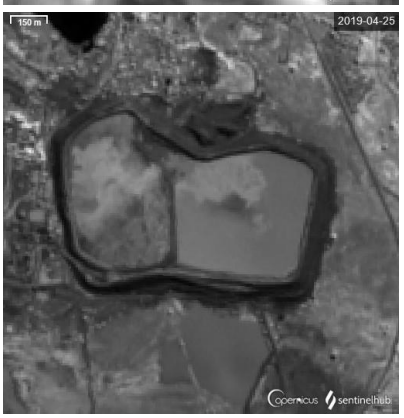	
	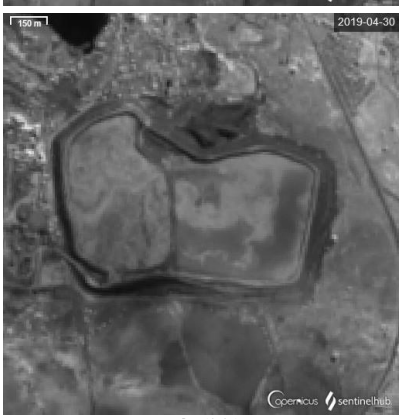	

Natural Colour (RGB - Bands 4, 3, 2)	Near Infrared (NIR - Band 8)	Shortwave Infrared (SWIR - Band 11)
		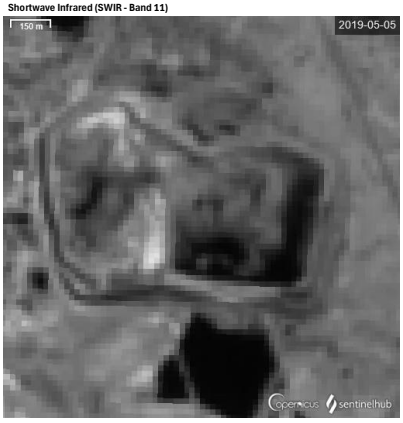
		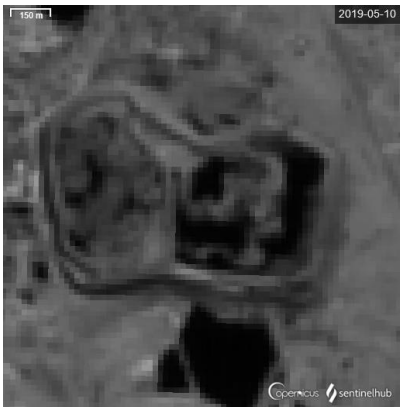
		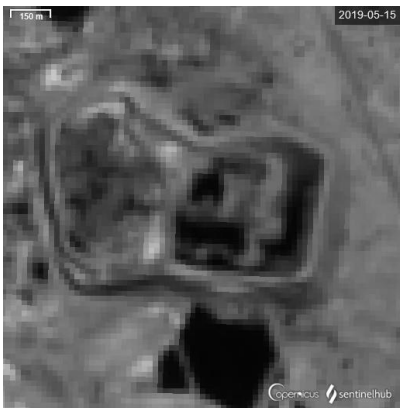
		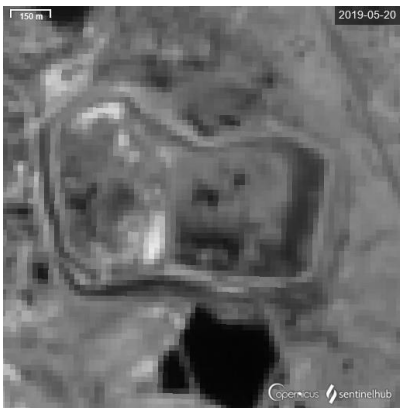
		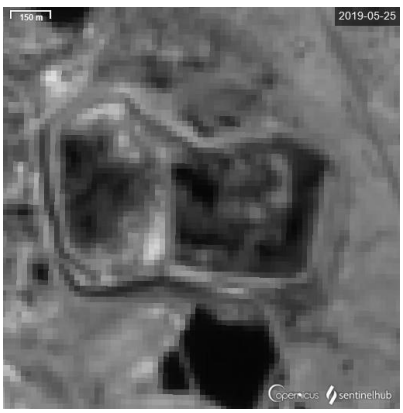

Natural Colour (RGB - Bands 4, 3, 2)

Near Infrared (NIR - Band 8)

Shortwave Infrared (SWIR - Band 11)

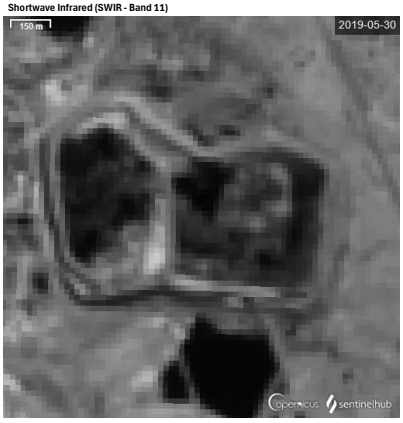

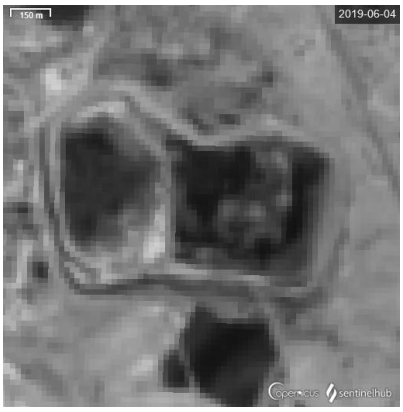

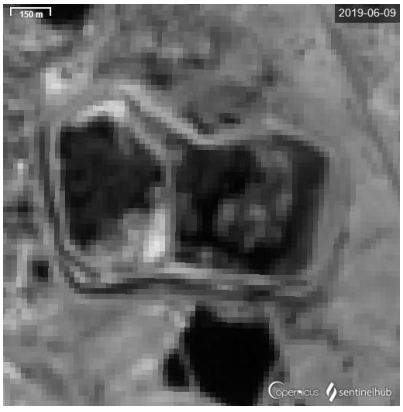

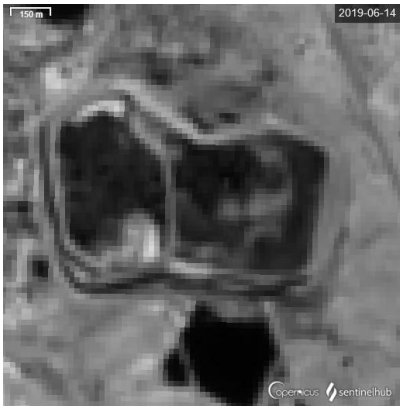

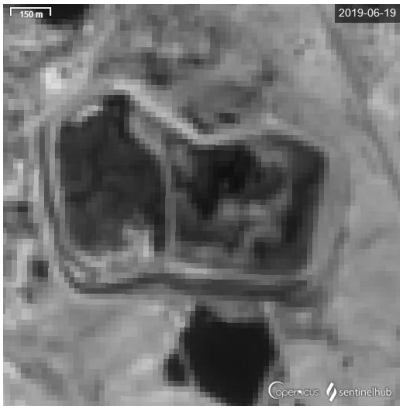

Natural Colour (RGB - Bands 4, 3, 2)

Near Infrared (NIR - Band 8)

Shortwave Infrared (SWIR - Band 11)

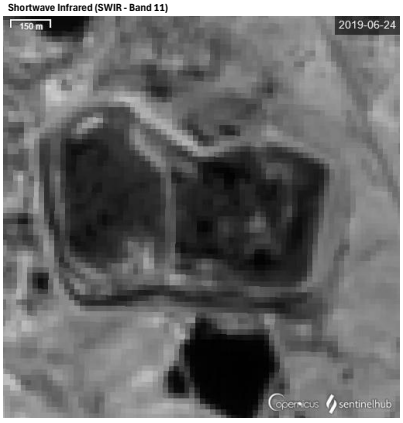

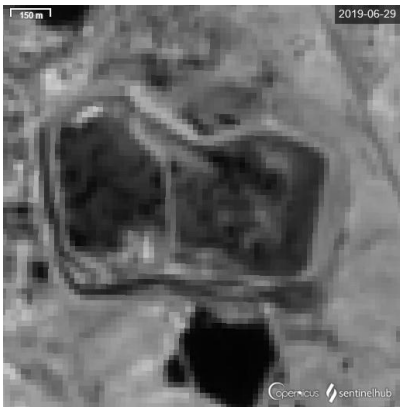

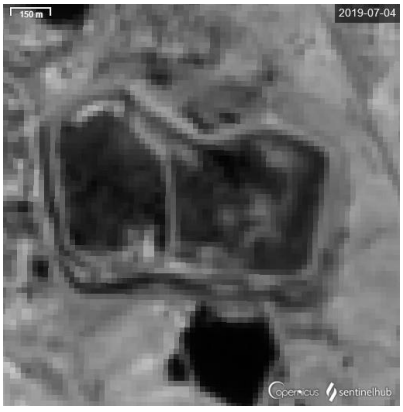

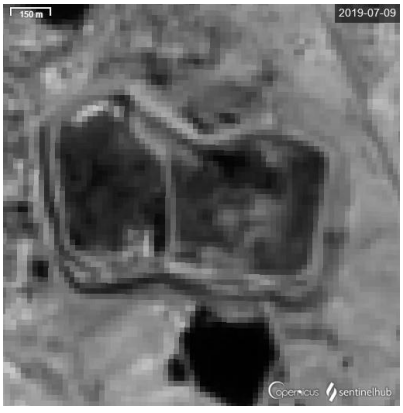

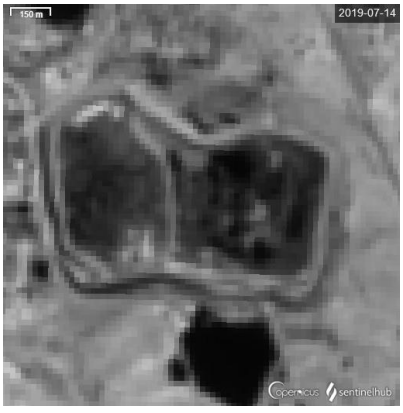

Natural Colour (RGB - Bands 4, 3, 2)	Near Infrared (NIR - Band 8)	Shortwave Infrared (SWIR - Band 11)
		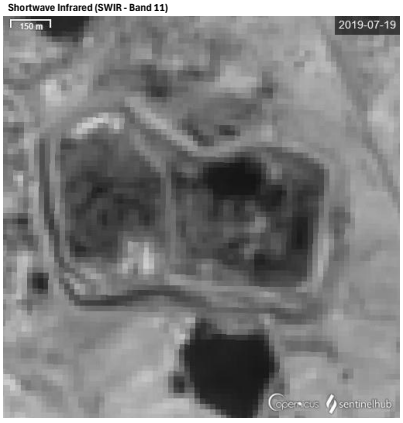
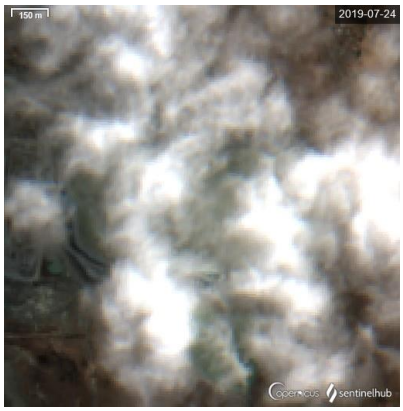	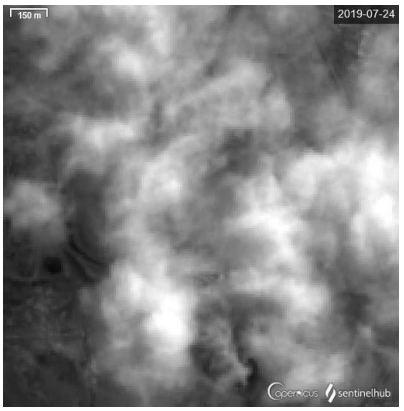	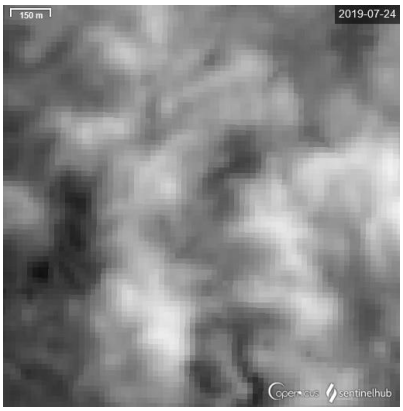
		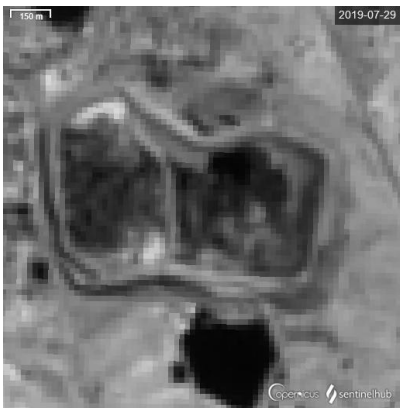
		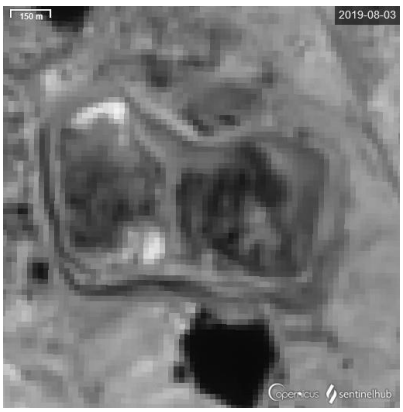
		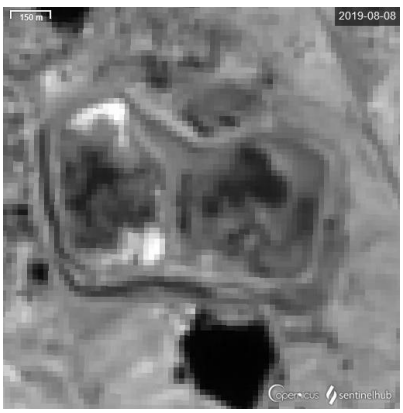

Natural Colour (RGB - Bands 4, 3, 2)	Near Infrared (NIR - Band 8)	Shortwave Infrared (SWIR - Band 11)
		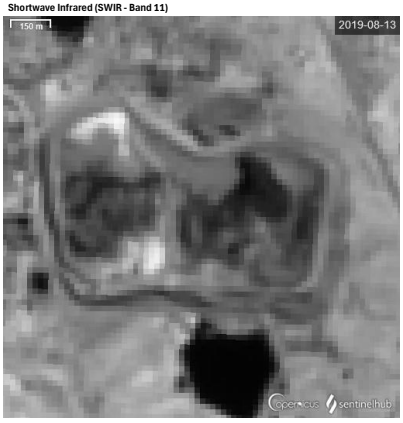
		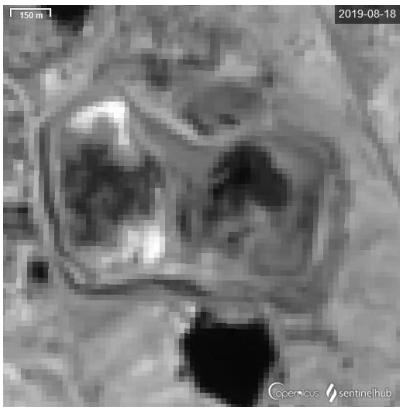
		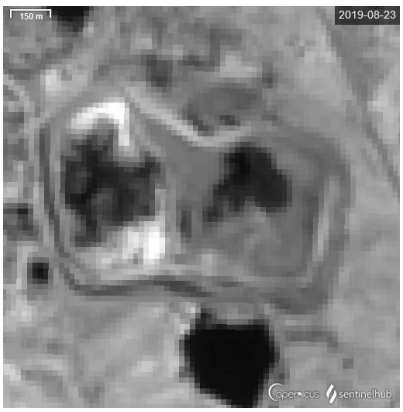
		
		

Natural Colour (RGB - Bands 4, 3, 2)

Near Infrared (NIR - Band 8)

Shortwave Infrared (SWIR - Band 11)

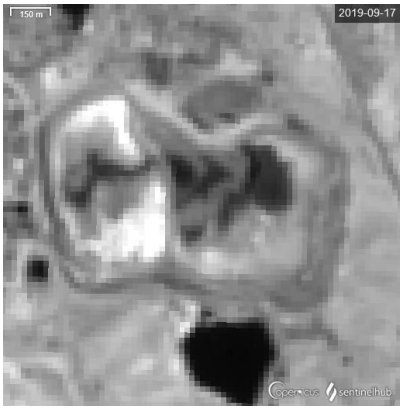

Natural Colour (RGB - Bands 4, 3, 2)	Near Infrared (NIR - Band 8)	Shortwave Infrared (SWIR - Band 11)
		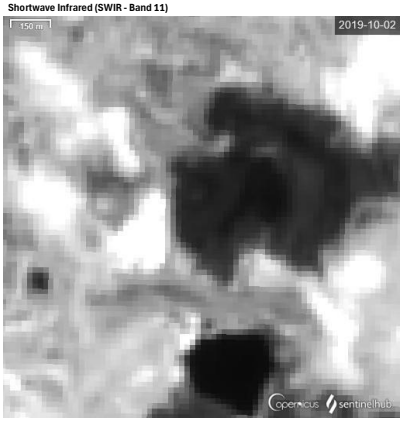
		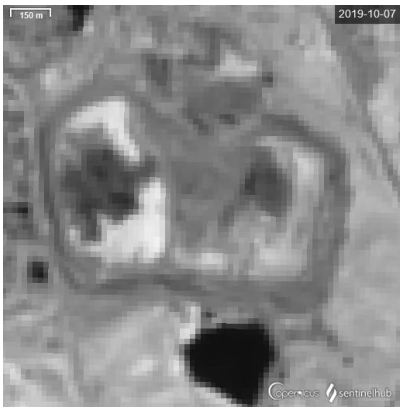
		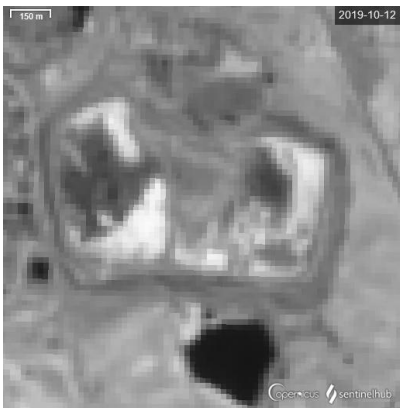
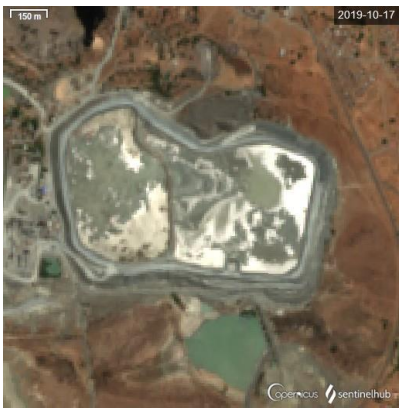		
		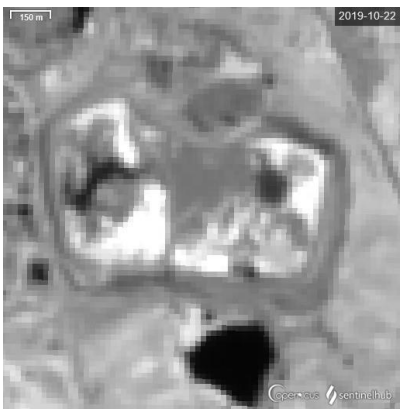

Natural Colour (RGB - Bands 4, 3, 2)

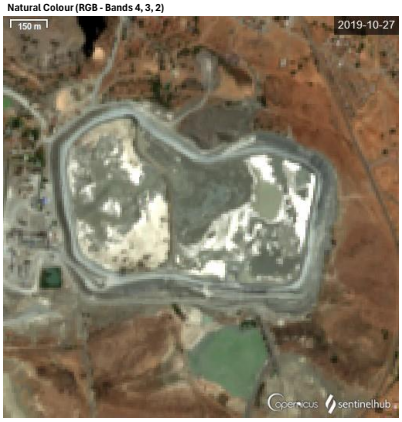

Near Infrared (NIR - Band 8)

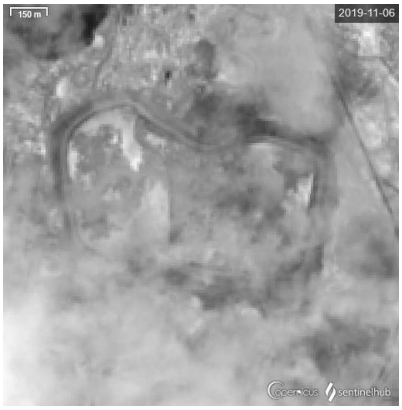

Shortwave Infrared (SWIR - Band 11)

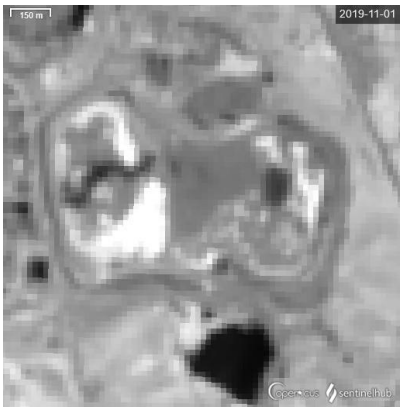

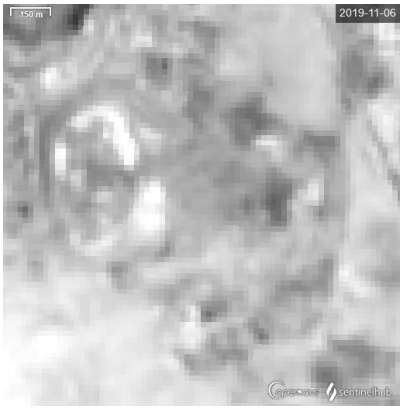

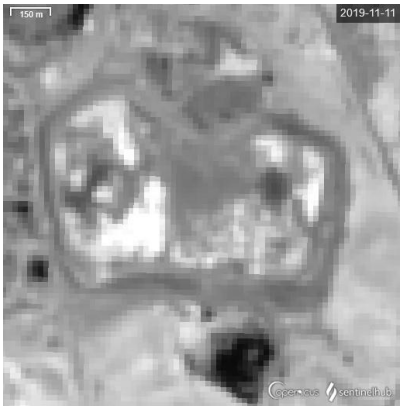

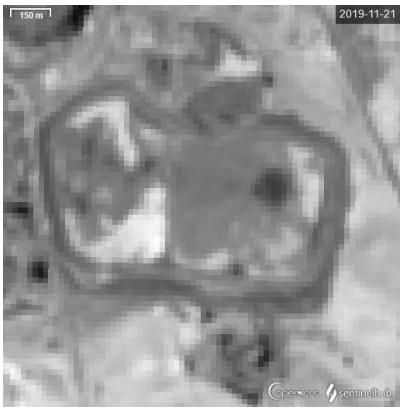

Natural Colour (RGB - Bands 4, 3, 2)

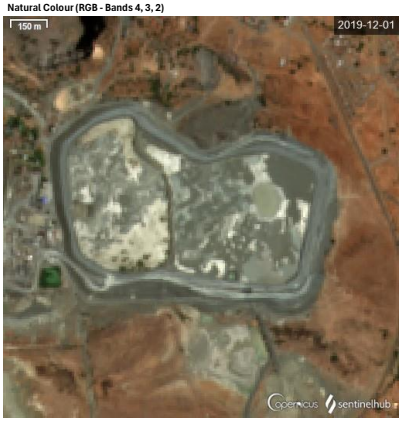

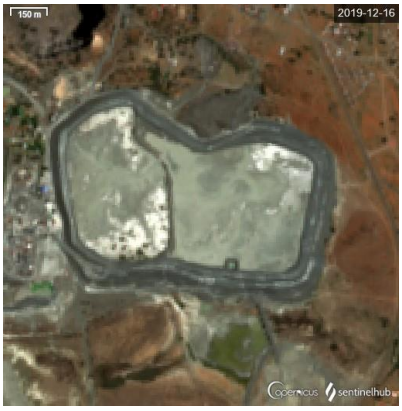

Near Infrared (NIR - Band 8)

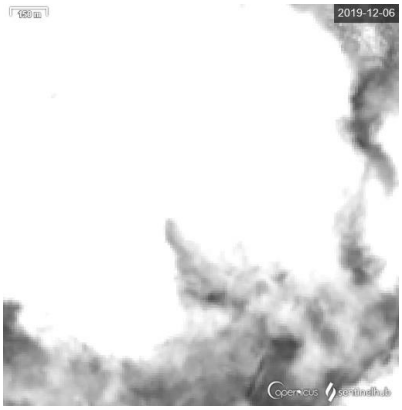

Shortwave Infrared (SWIR - Band 11)

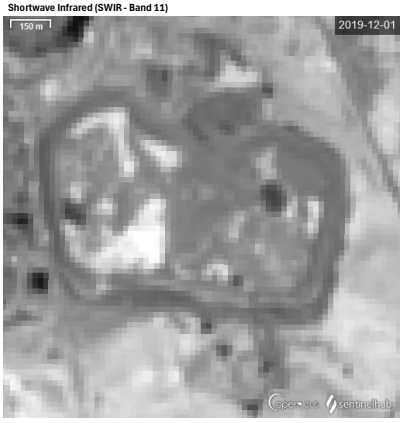

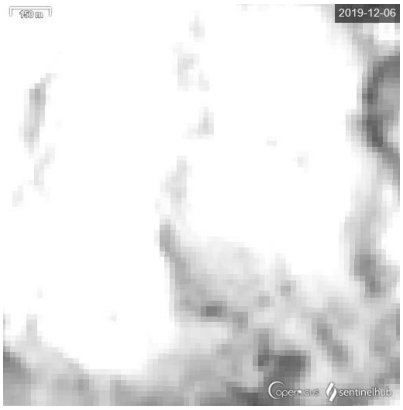

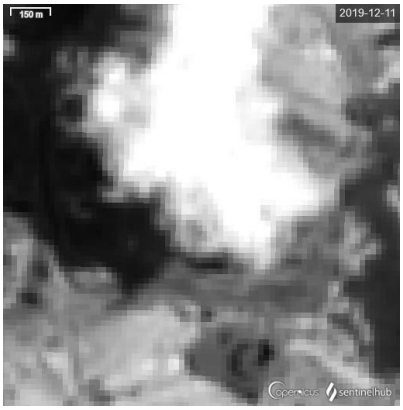

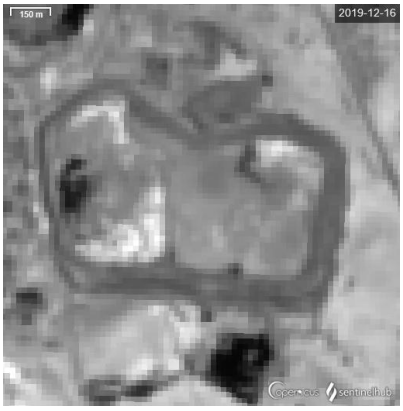

Natural Colour (RGB - Bands 4, 3, 2)	Near Infrared (NIR - Band 8)	Shortwave Infrared (SWIR - Band 11)
		
		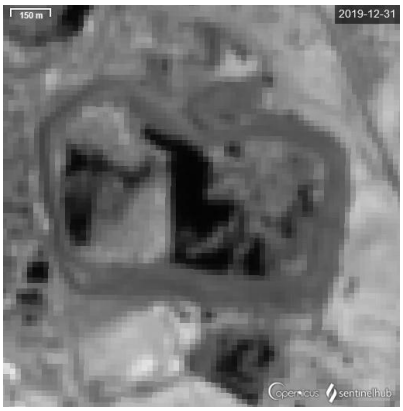
		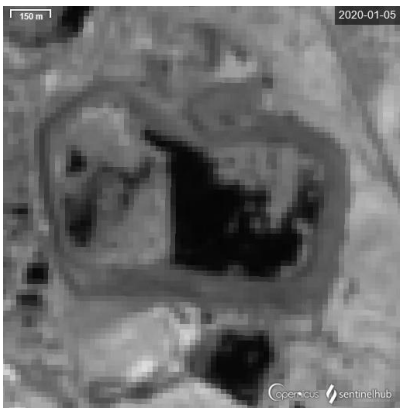
		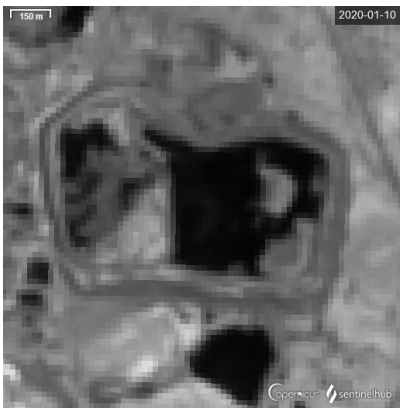
	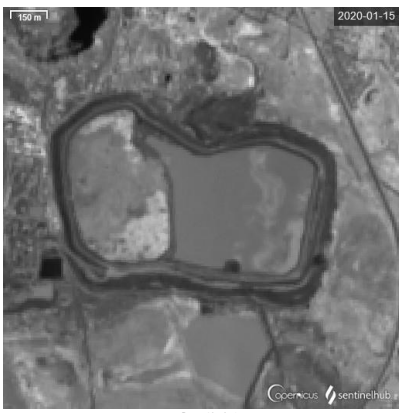	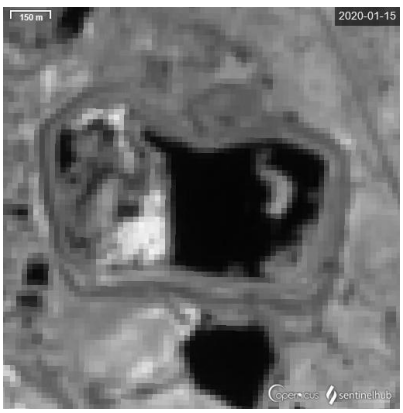

Natural Colour (RGB - Bands 4, 3, 2)

Near Infrared (NIR - Band 8)

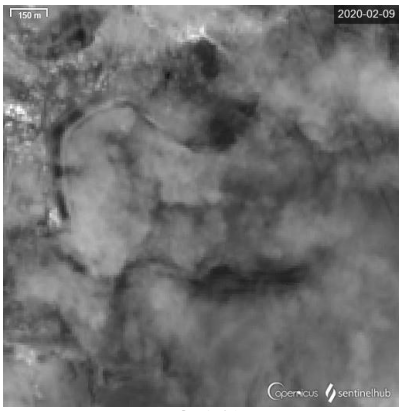

Shortwave Infrared (SWIR - Band 11)

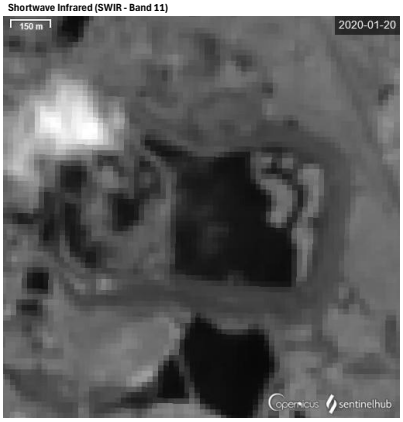

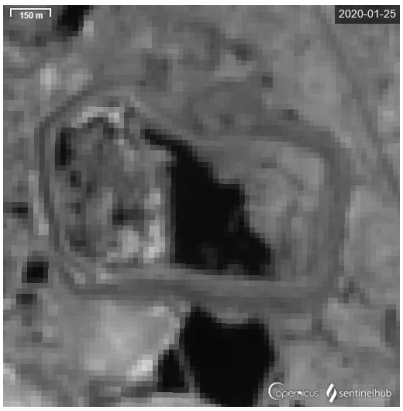

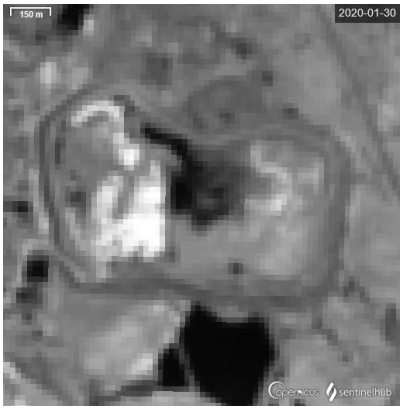

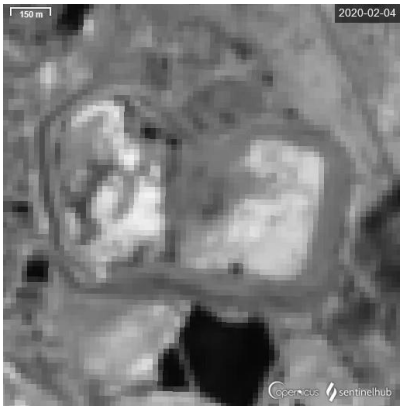

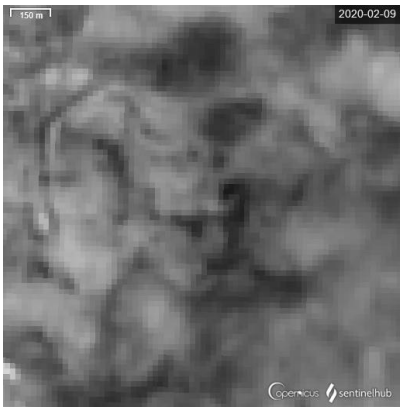

Natural Colour (RGB - Bands 4, 3, 2)

Near Infrared (NIR - Band 8)

Shortwave Infrared (SWIR - Band 11)

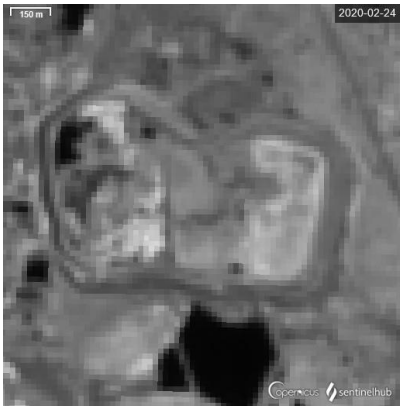

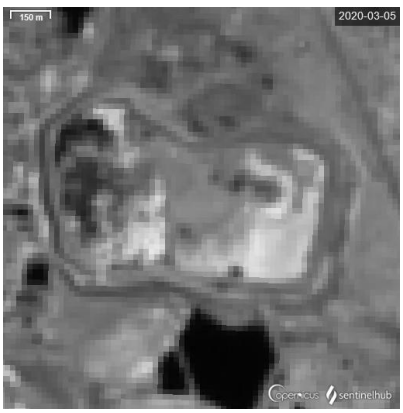

Natural Colour (RGB - Bands 4, 3, 2)

Near Infrared (NIR - Band 8)

Shortwave Infrared (SWIR - Band 11)

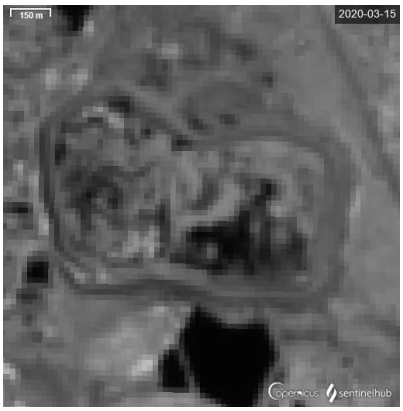

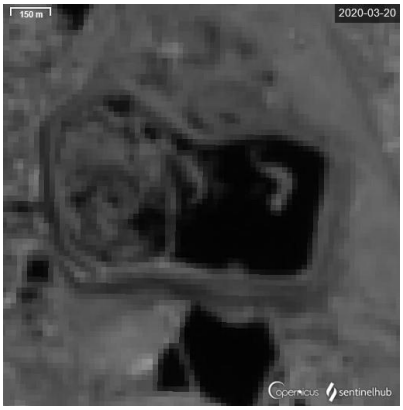

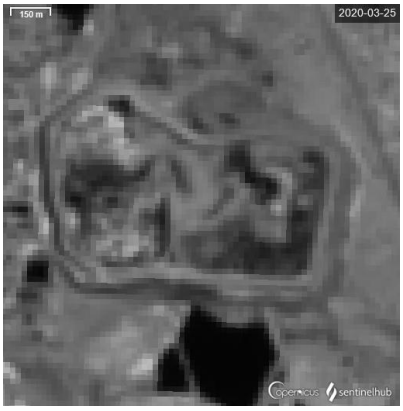

Natural Colour (RGB - Bands 4, 3, 2)

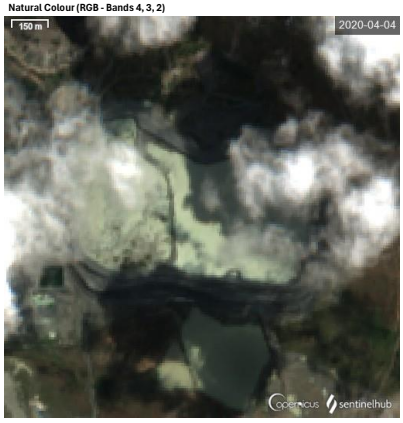

Near Infrared (NIR - Band 8)

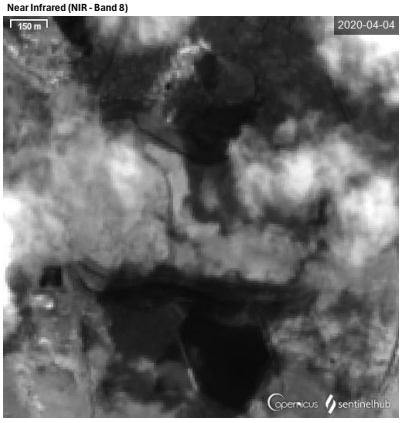

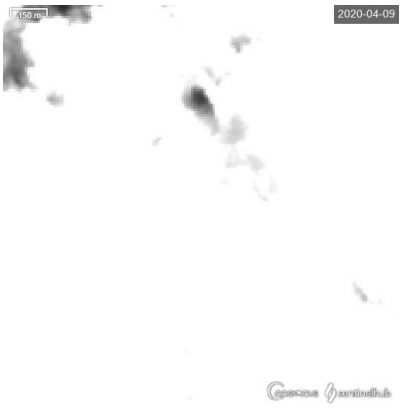

Shortwave Infrared (SWIR - Band 11)

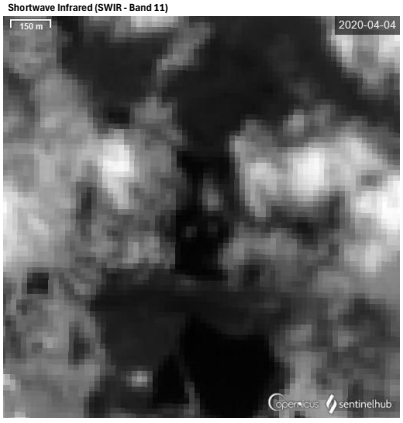

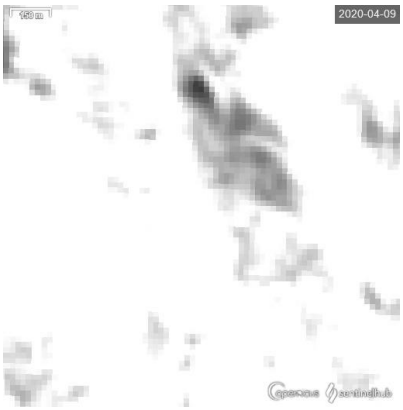

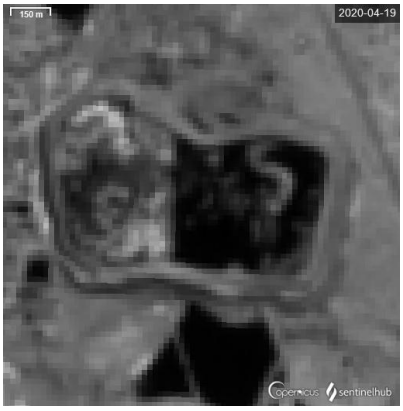

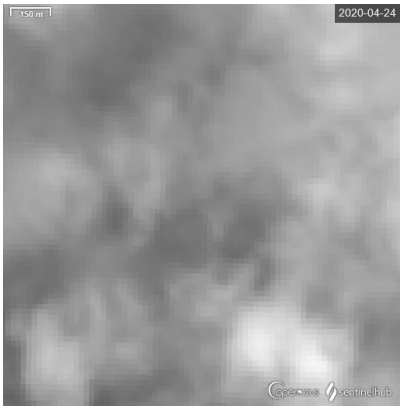

Natural Colour (RGB - Bands 4, 3, 2)

Near Infrared (NIR - Band 8)

Shortwave Infrared (SWIR - Band 11)

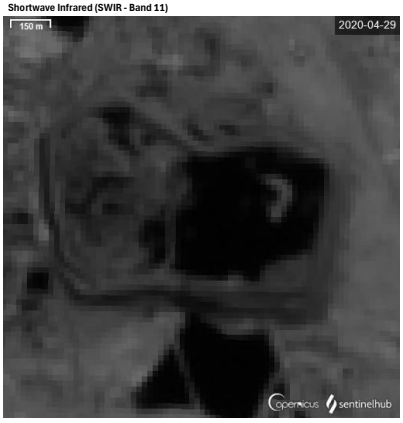

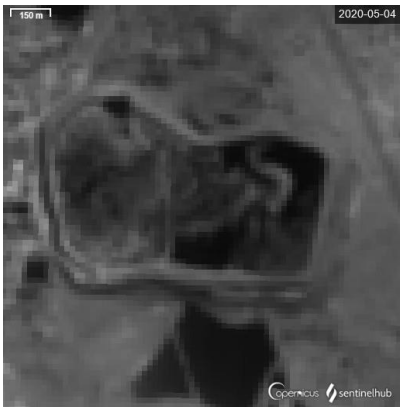

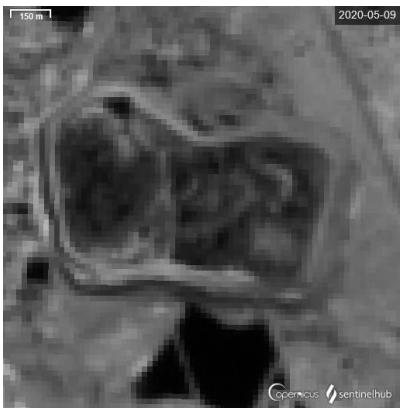

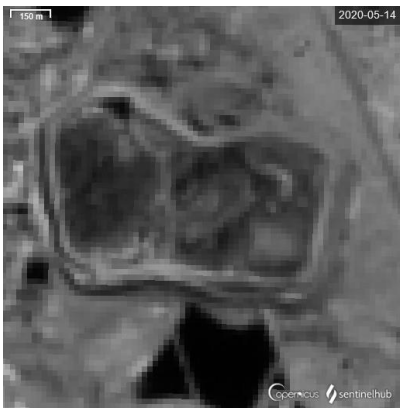

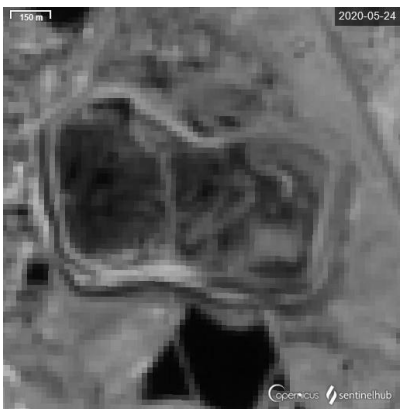

Natural Colour (RGB - Bands 4, 3, 2)	Near Infrared (NIR - Band 8)	Shortwave Infrared (SWIR - Band 11)
		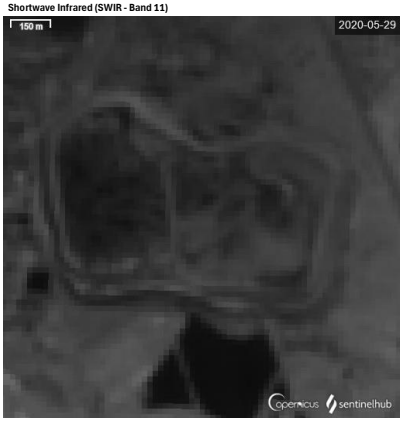
		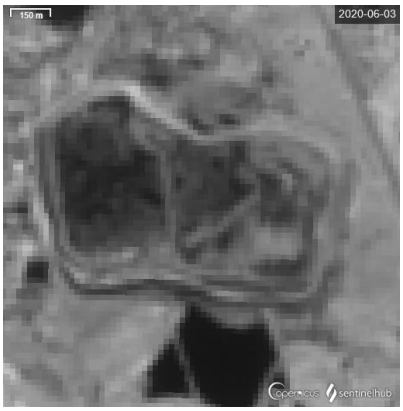
		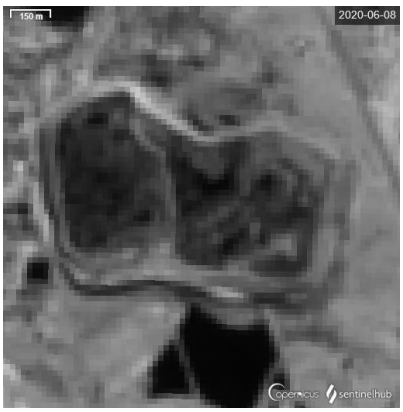
		
		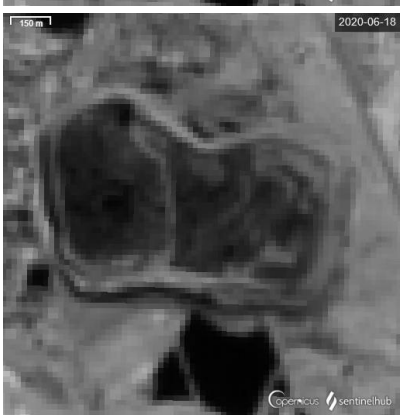

Natural Colour (RGB - Bands 4, 3, 2)

Near Infrared (NIR - Band 8)

Shortwave Infrared (SWIR - Band 11)

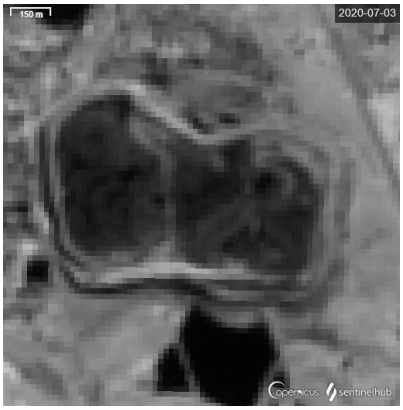

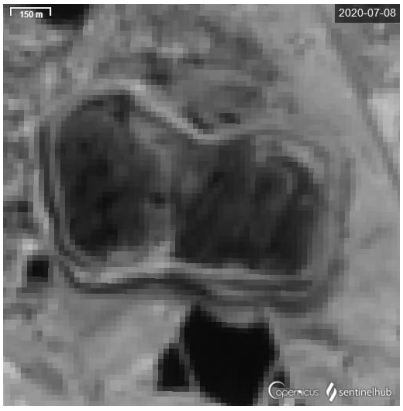

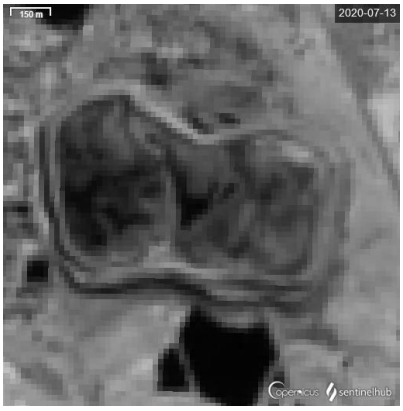

Natural Colour (RGB - Bands 4, 3, 2)	Near Infrared (NIR - Band 8)	Shortwave Infrared (SWIR - Band 11)
		
		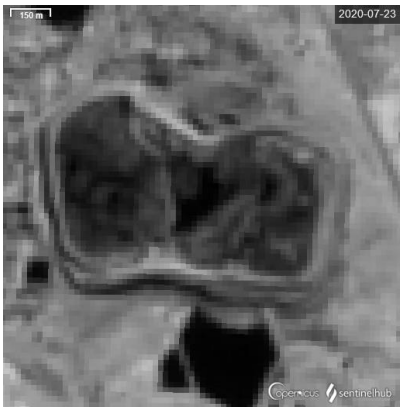
		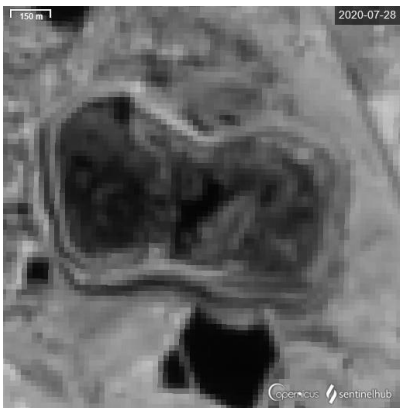
		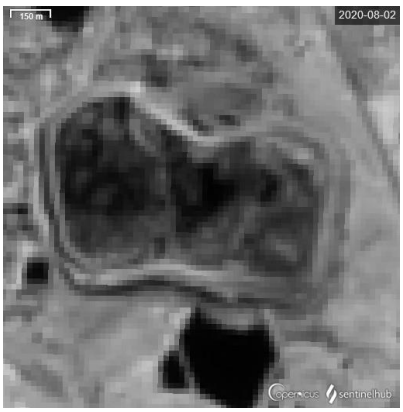
		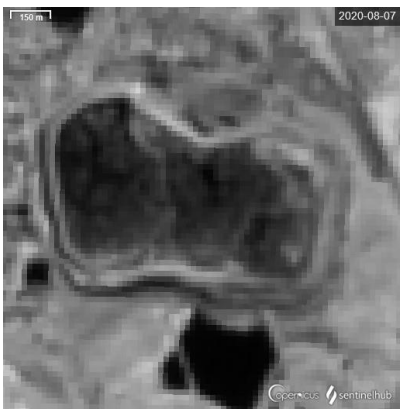

Natural Colour (RGB - Bands 4, 3, 2)

Near Infrared (NIR - Band 8)

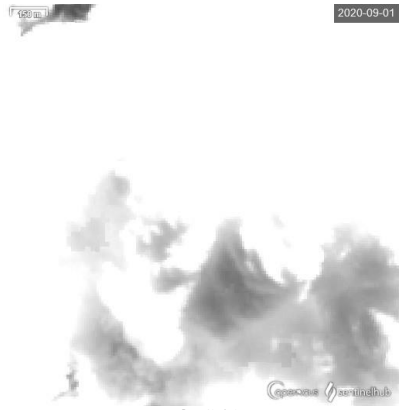

Shortwave Infrared (SWIR - Band 11)

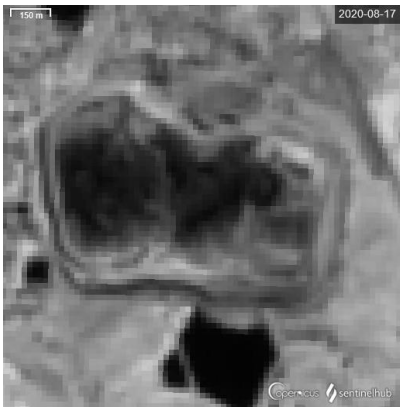

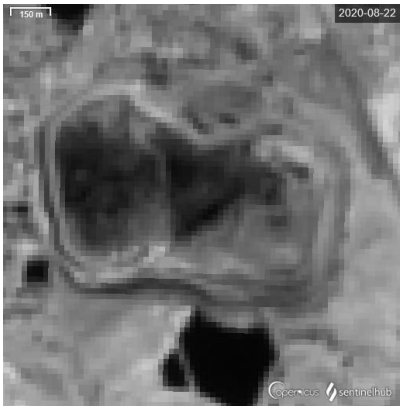

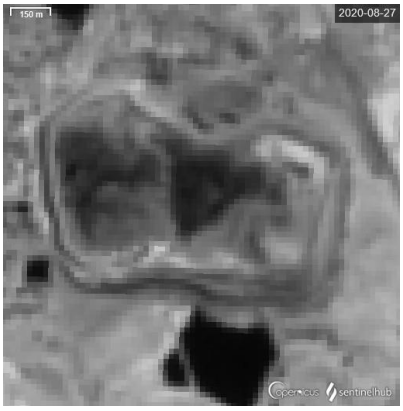

Natural Colour (RGB - Bands 4, 3, 2)	Near Infrared (NIR - Band 8)	Shortwave Infrared (SWIR - Band 11)
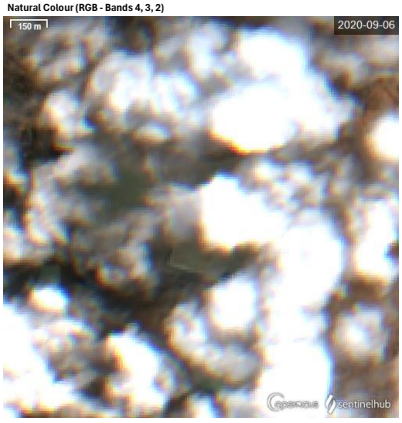	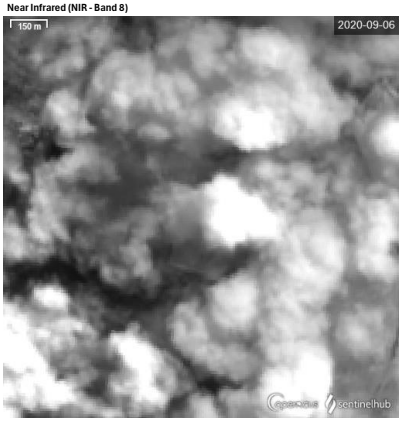	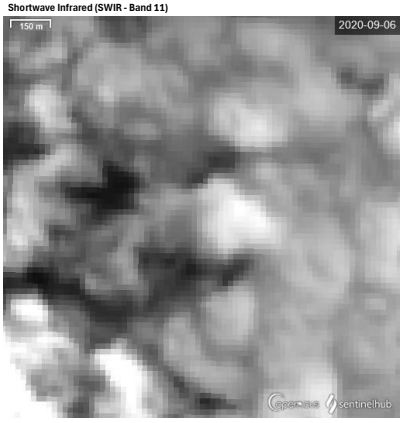
		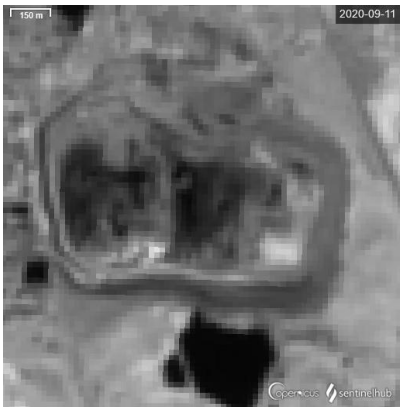
		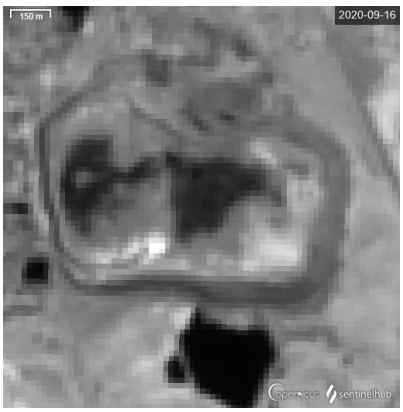
		
		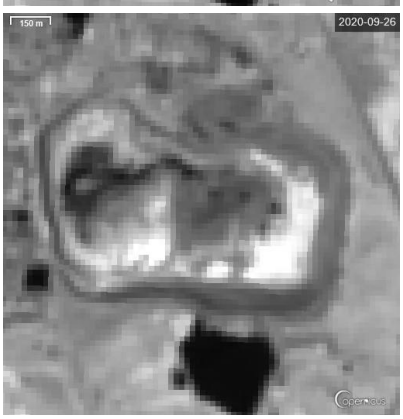

Natural Colour (RGB - Bands 4, 3, 2)

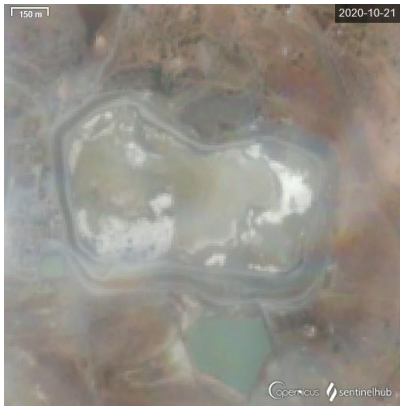

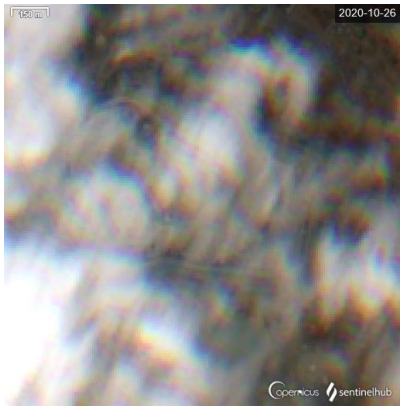

Near Infrared (NIR - Band 8)

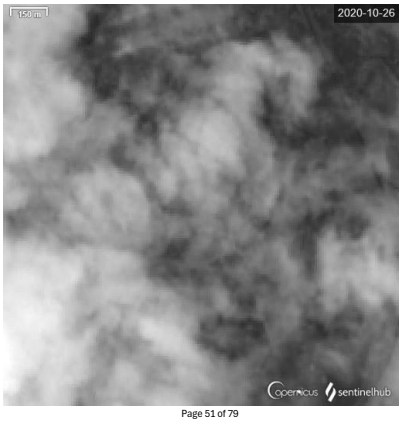

Shortwave Infrared (SWIR - Band 11)

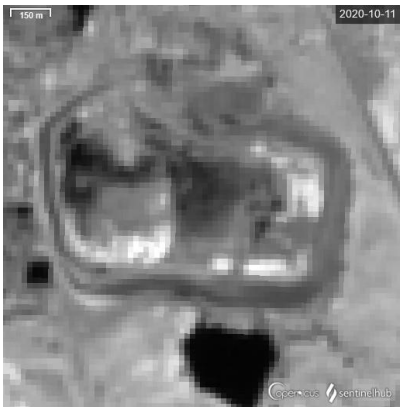

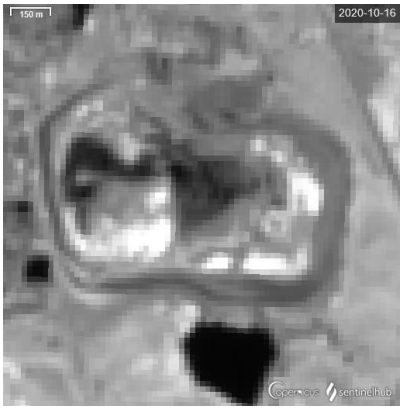

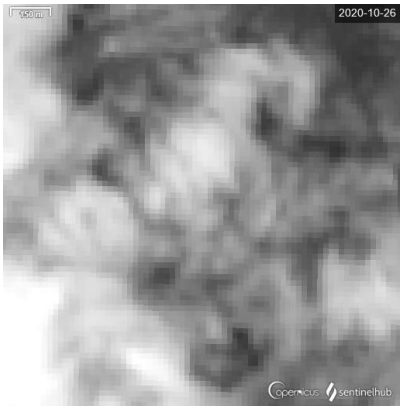

Natural Colour (RGB - Bands 4, 3, 2)

Near Infrared (NIR - Band 8)

Shortwave Infrared (SWIR - Band 11)

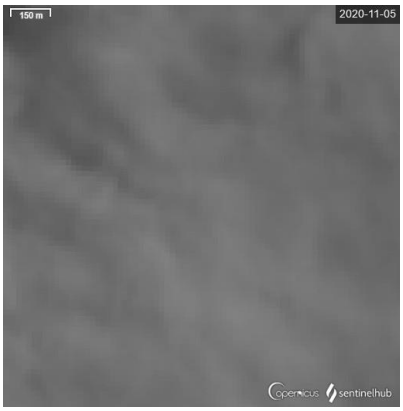

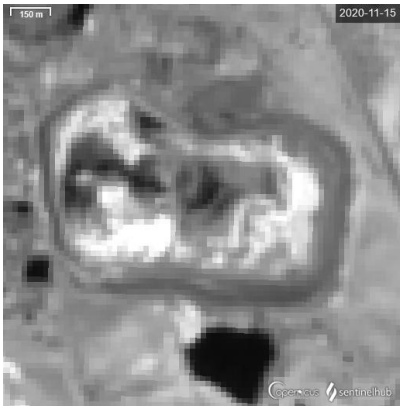

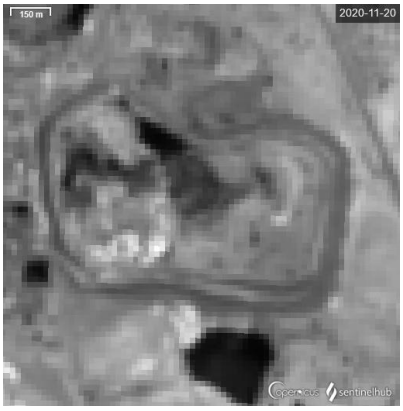

Natural Colour (RGB - Bands 4, 3, 2)	Near Infrared (NIR - Band 8)	Shortwave Infrared (SWIR - Band 11)
		
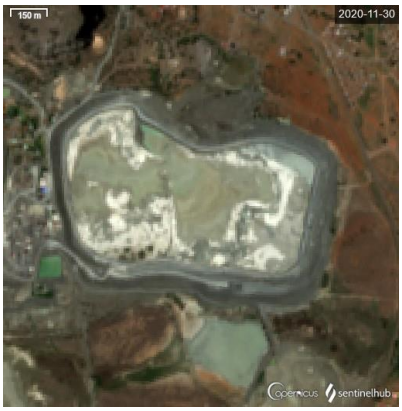		
		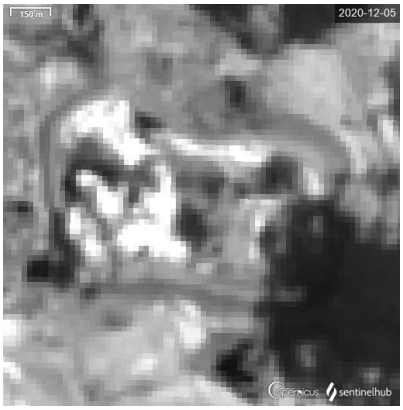
		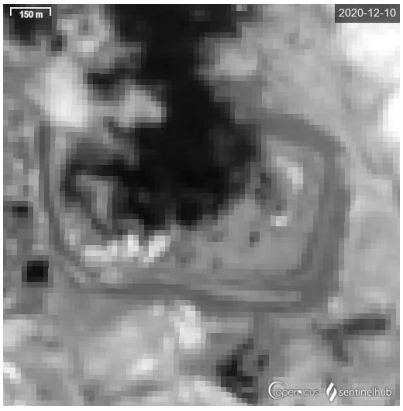
		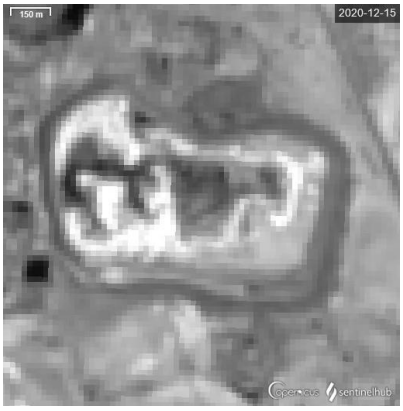

Natural Colour (RGB - Bands 4, 3, 2)

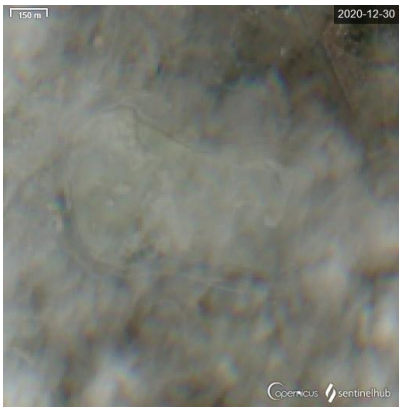

Near Infrared (NIR - Band 8)

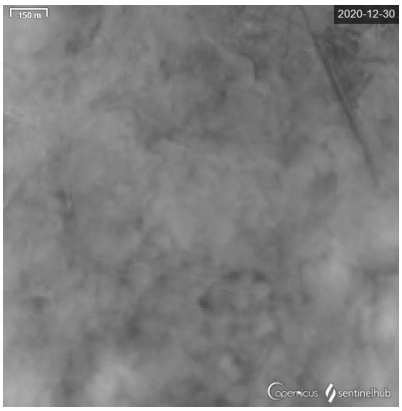

Shortwave Infrared (SWIR - Band 11)

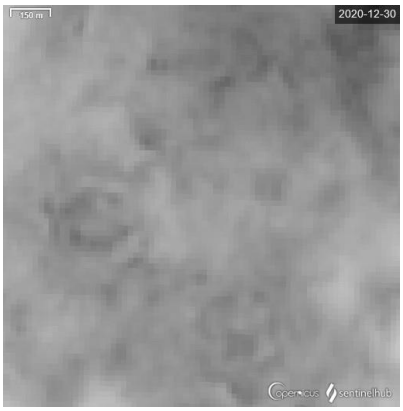

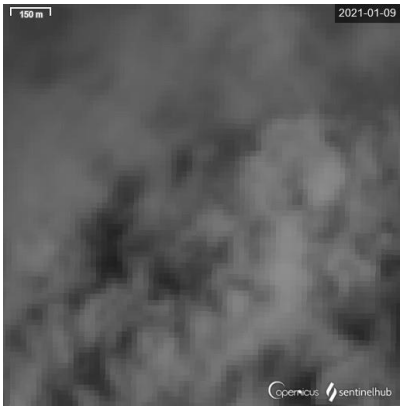

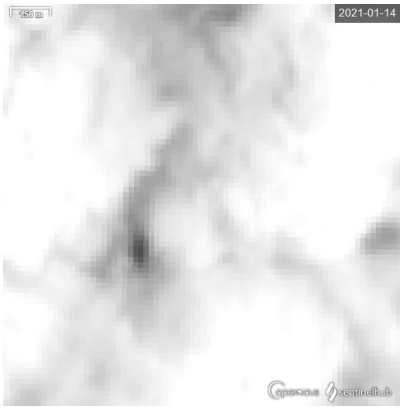

Natural Colour (RGB - Bands 4, 3, 2)

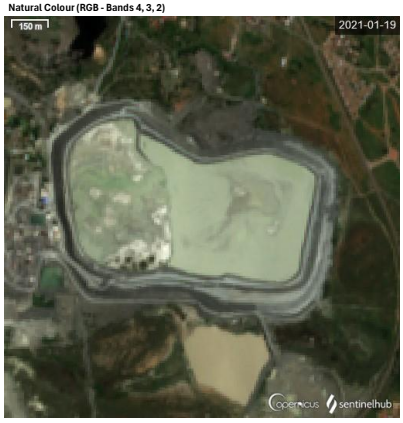

Near Infrared (NIR - Band 8)

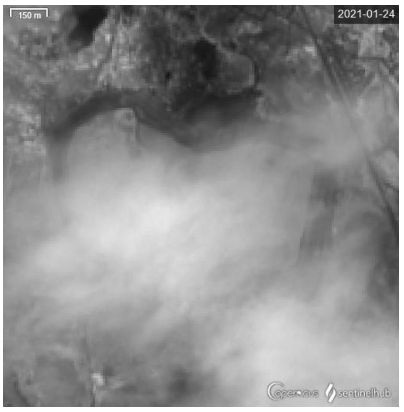

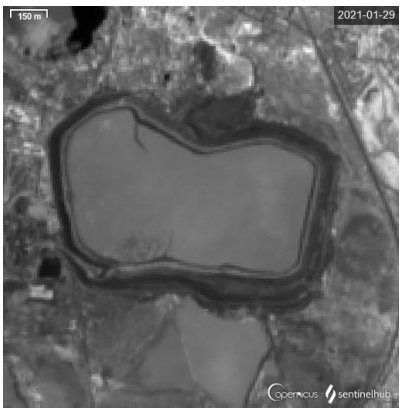

Shortwave Infrared (SWIR - Band 11)

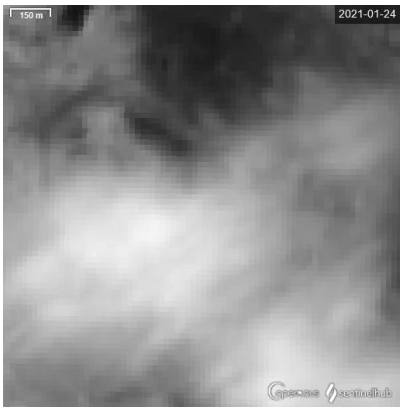

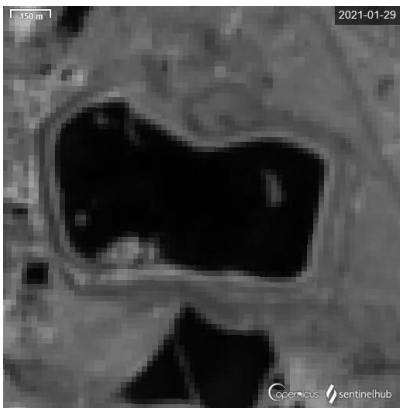

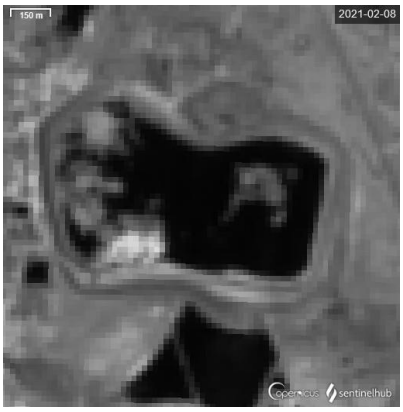

Natural Colour (RGB - Bands 4, 3, 2)

Near Infrared (NIR - Band 8)

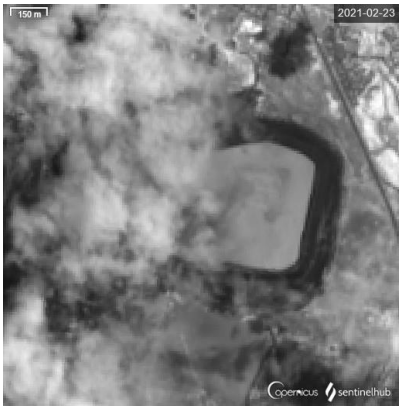

Shortwave Infrared (SWIR - Band 11)

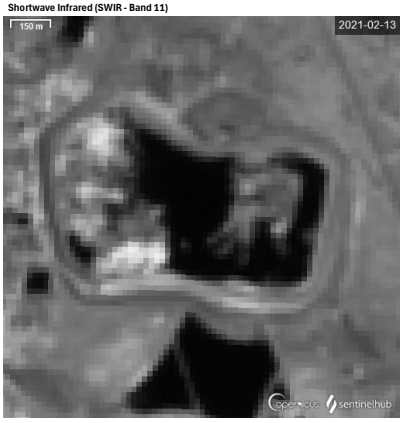

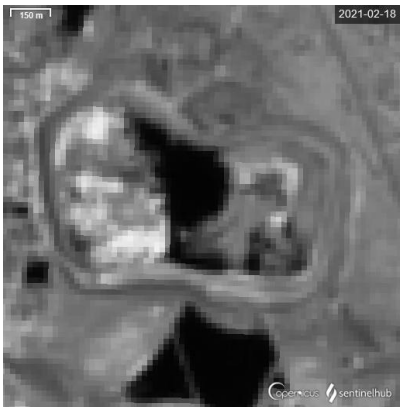

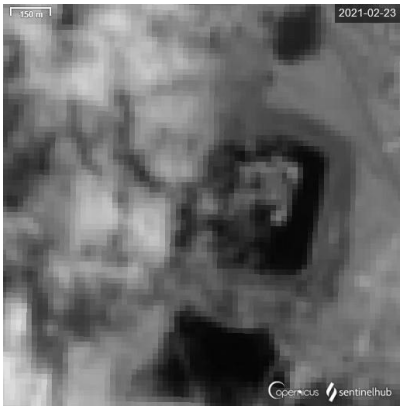

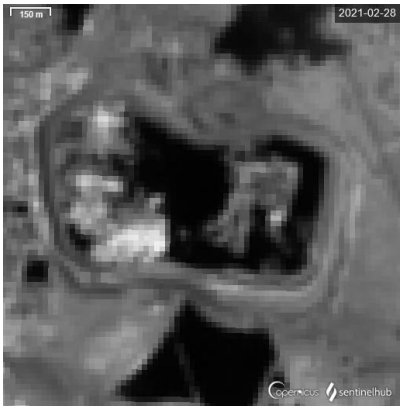

Natural Colour (RGB - Bands 4, 3, 2)

Near Infrared (NIR - Band 8)

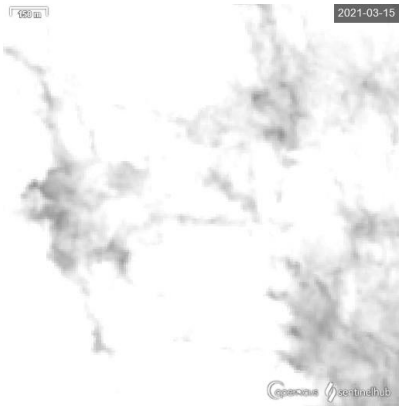

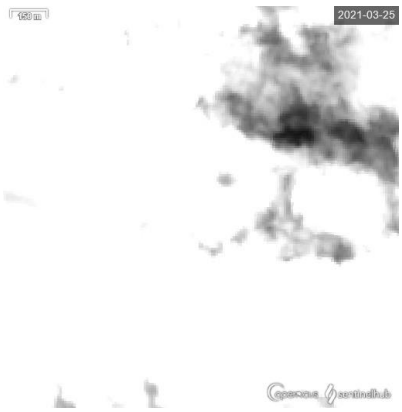

Shortwave Infrared (SWIR - Band 11)

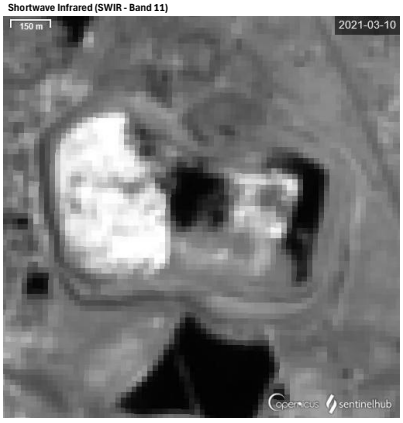

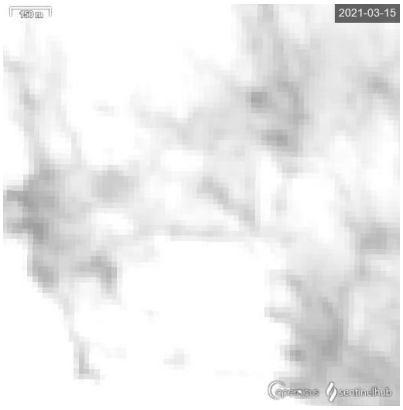

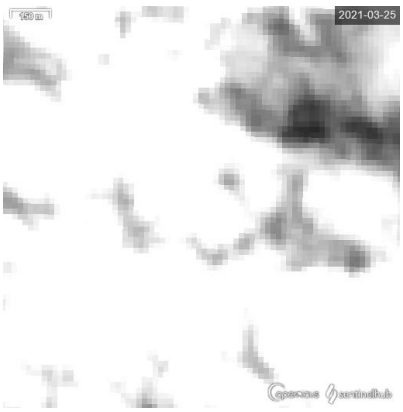

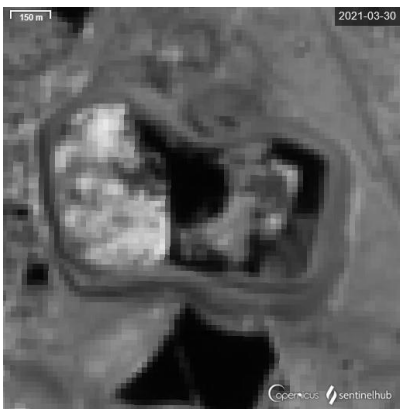

Natural Colour (RGB - Bands 4, 3, 2)

Near Infrared (NIR - Band 8)

Shortwave Infrared (SWIR - Band 11)

Natural Colour (RGB - Bands 4, 3, 2)	Near Infrared (NIR - Band 8)	Shortwave Infrared (SWIR - Band 11)
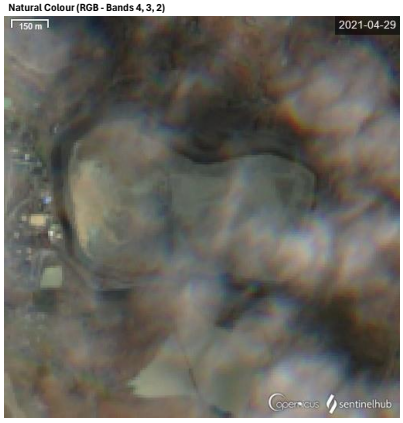	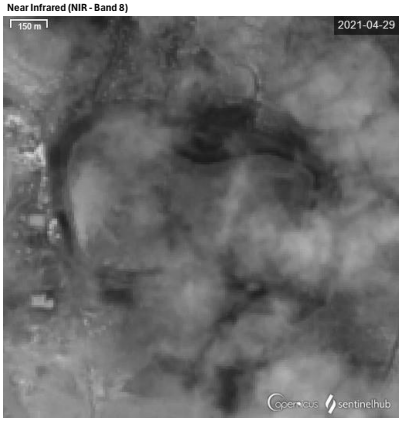	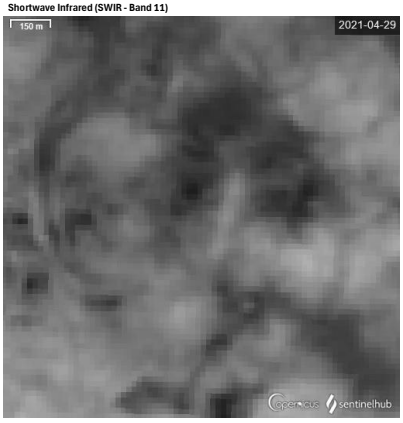
		
		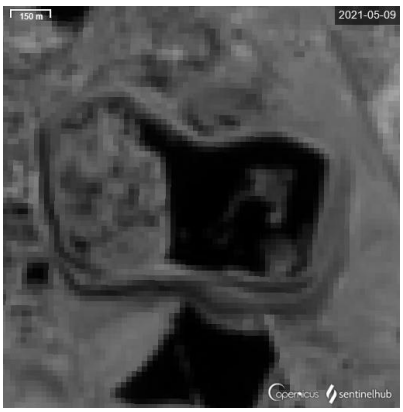
		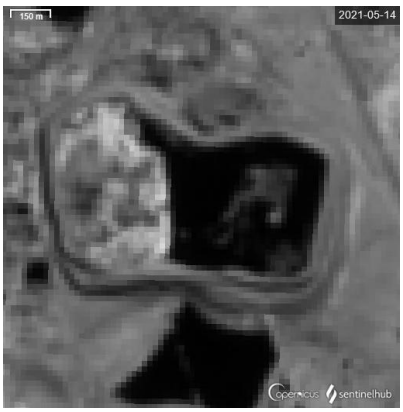
	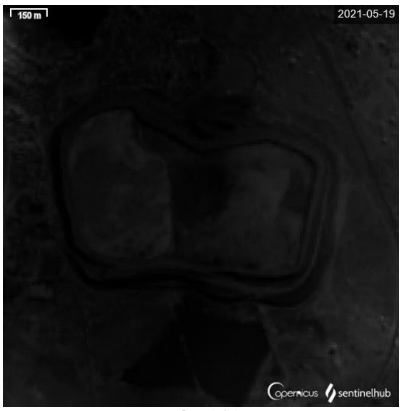	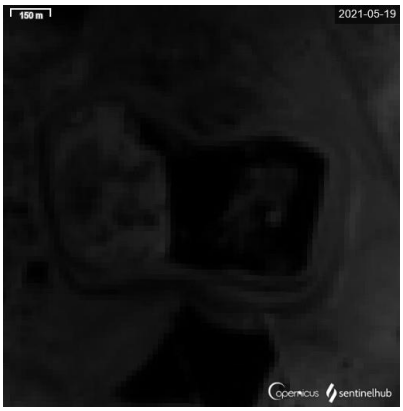

Natural Colour (RGB - Bands 4, 3, 2)

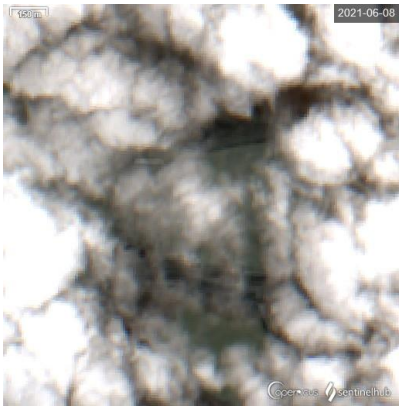

Near Infrared (NIR - Band 8)

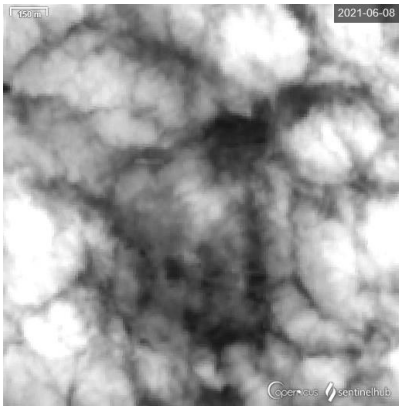

Shortwave Infrared (SWIR - Band 11)

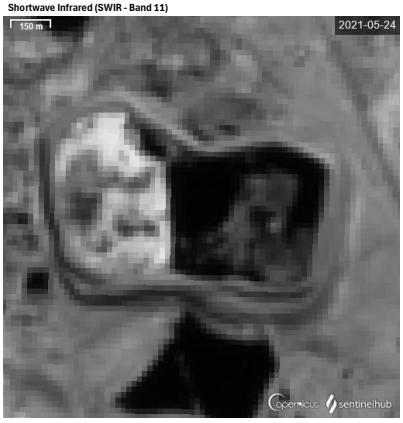

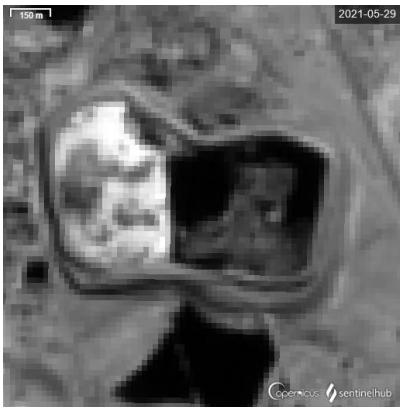

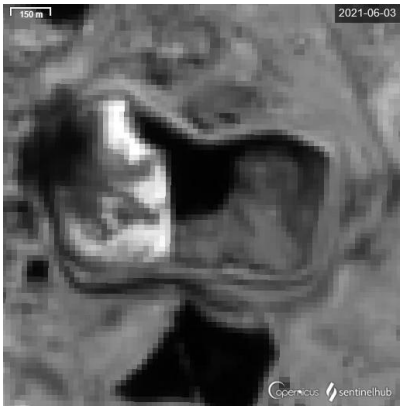

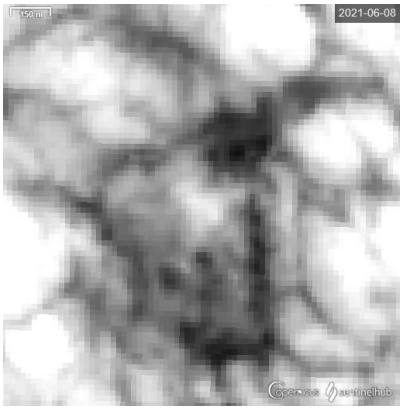

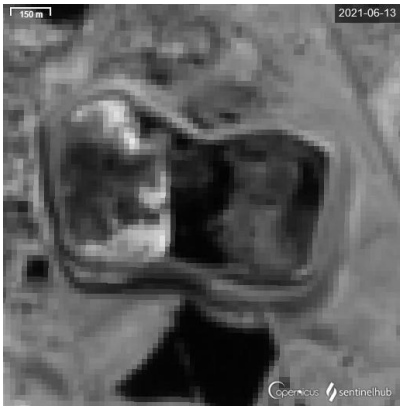

Natural Colour (RGB - Bands 4, 3, 2)	Near Infrared (NIR - Band 8)	Shortwave Infrared (SWIR - Band 11)
		
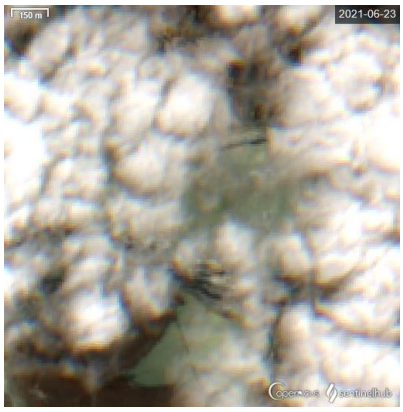	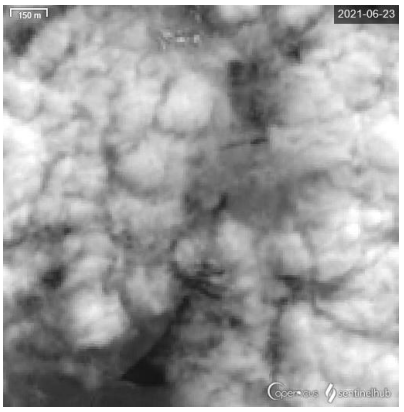	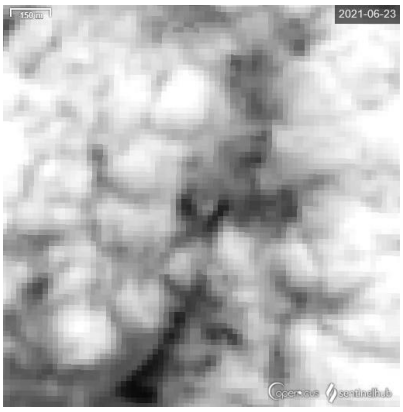
		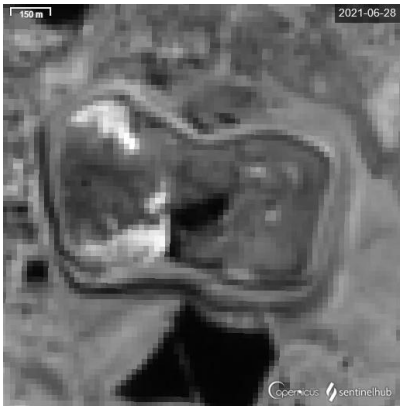
		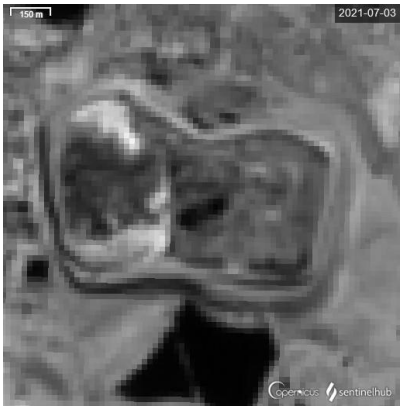
		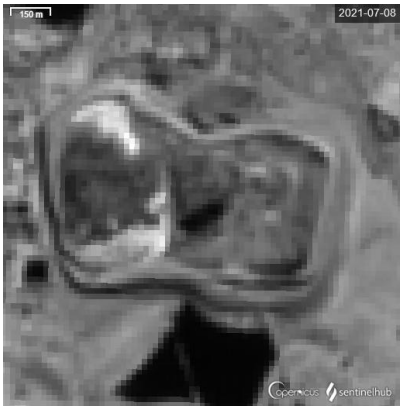

Natural Colour (RGB - Bands 4, 3, 2)

Near Infrared (NIR - Band 8)

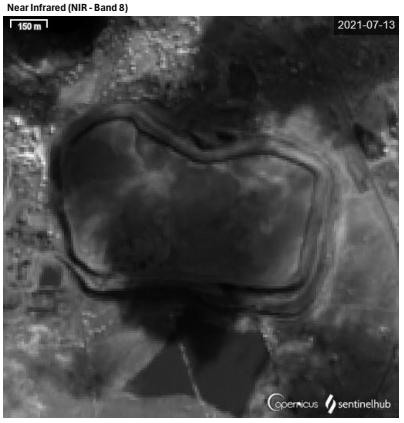

Shortwave Infrared (SWIR - Band 11)

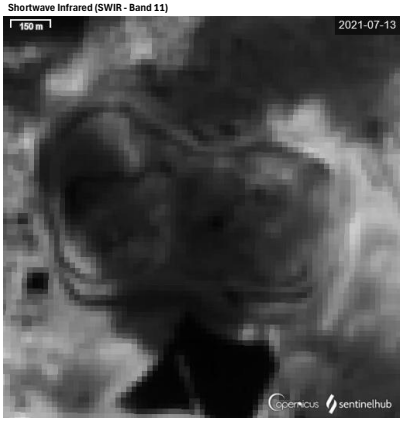

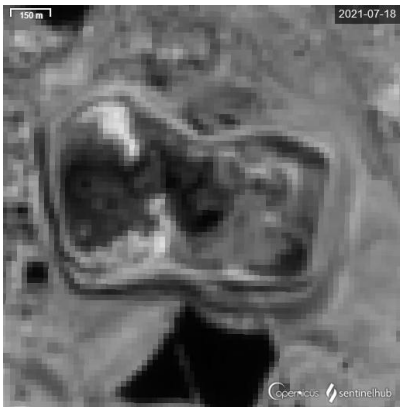

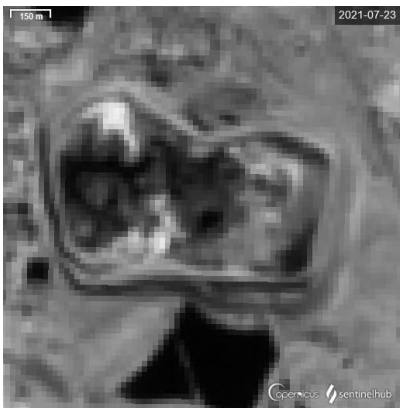

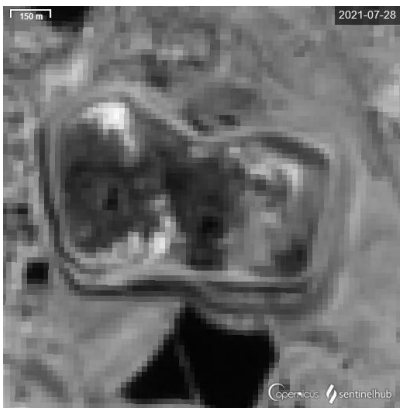

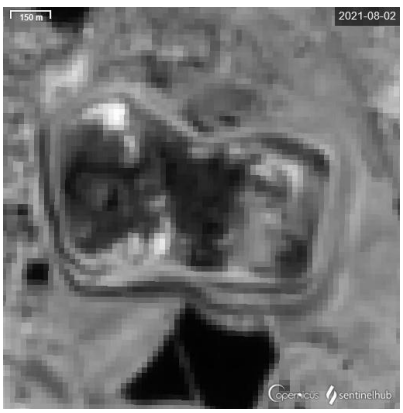

Natural Colour (RGB - Bands 4, 3, 2)

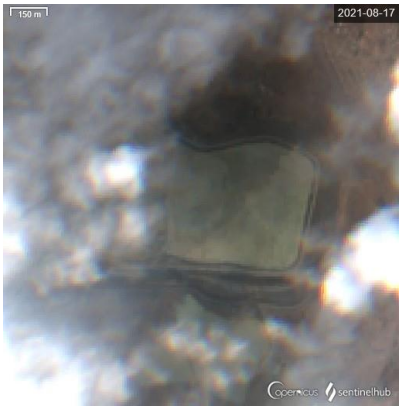

Near Infrared (NIR - Band 8)

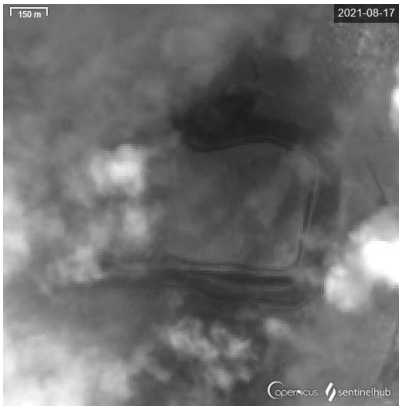

Shortwave Infrared (SWIR - Band 11)

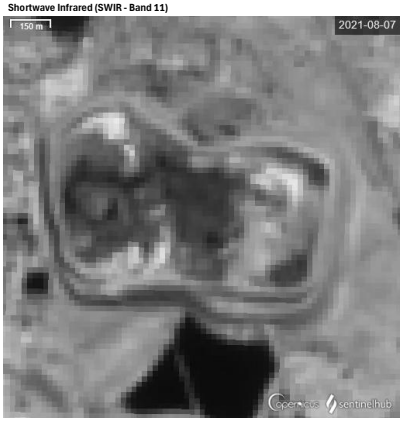

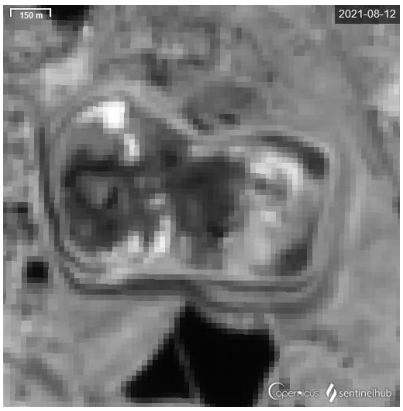

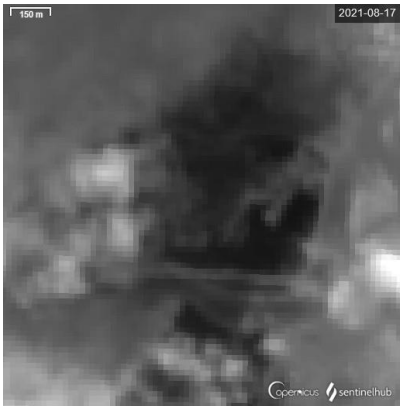

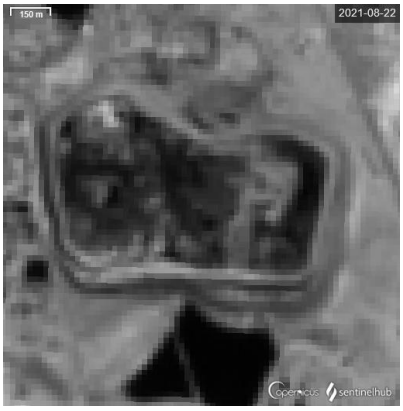

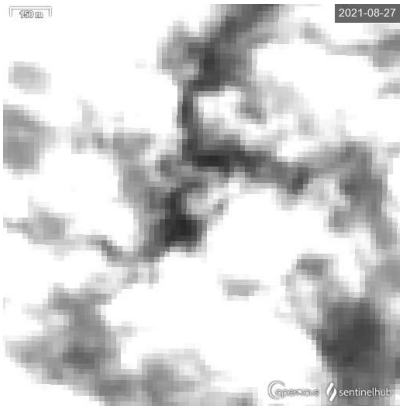

Natural Colour (RGB - Bands 4, 3, 2)

Near Infrared (NIR - Band 8)

Shortwave Infrared (SWIR - Band 11)

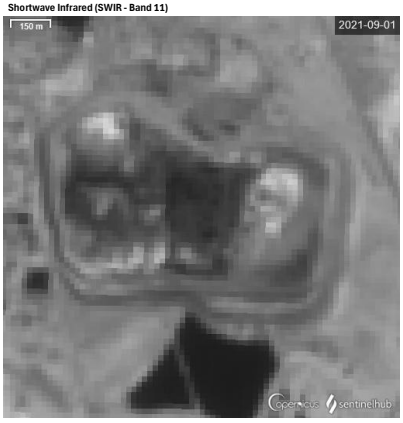

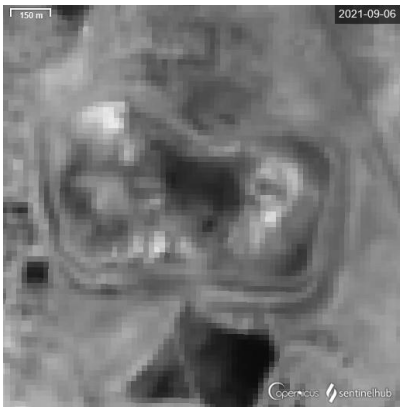

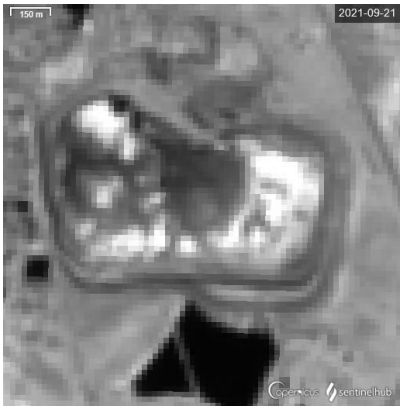

Natural Colour (RGB - Bands 4, 3, 2)

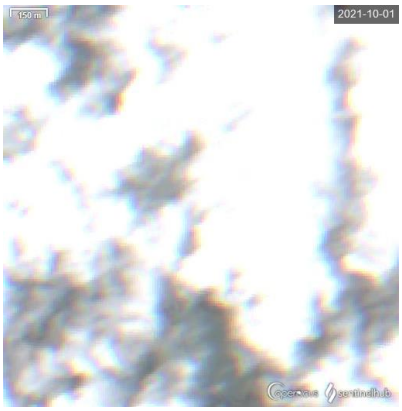

Near Infrared (NIR - Band 8)

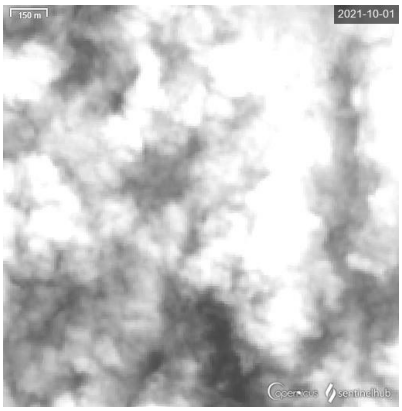

Shortwave Infrared (SWIR - Band 11)

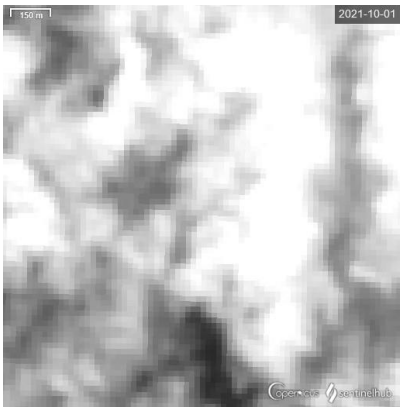

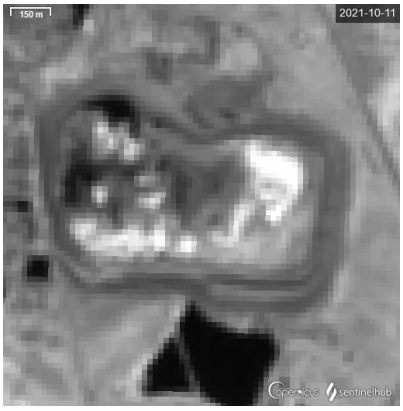

Natural Colour (RGB - Bands 4, 3, 2)

Near Infrared (NIR - Band 8)

Shortwave Infrared (SWIR - Band 11)

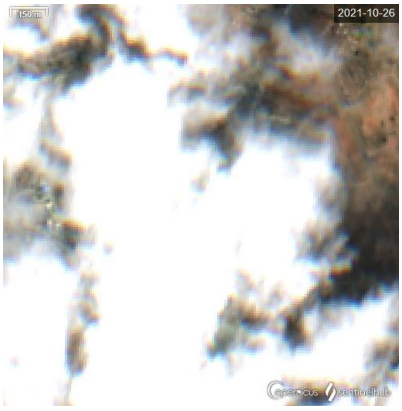

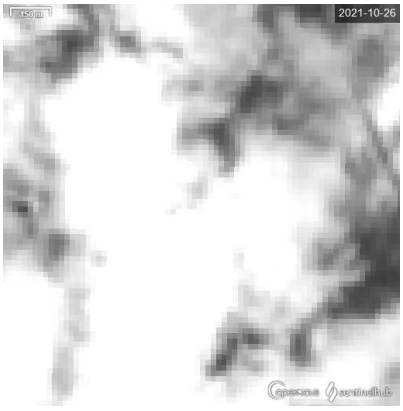

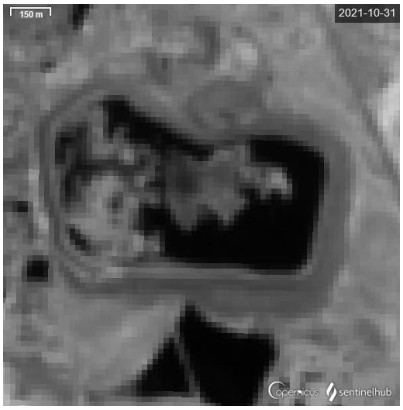

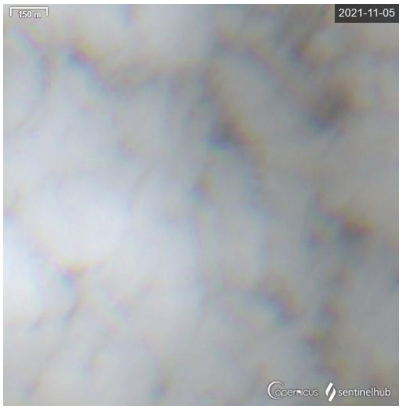

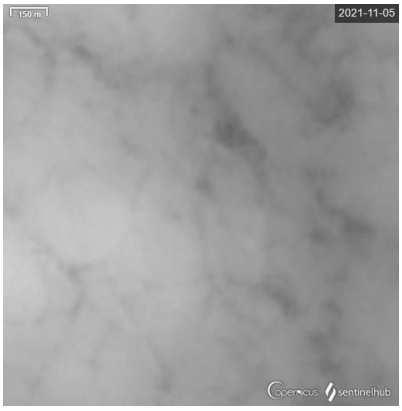

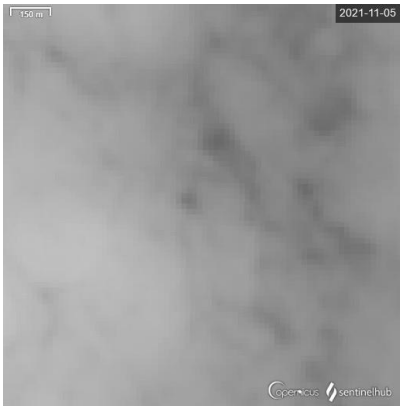

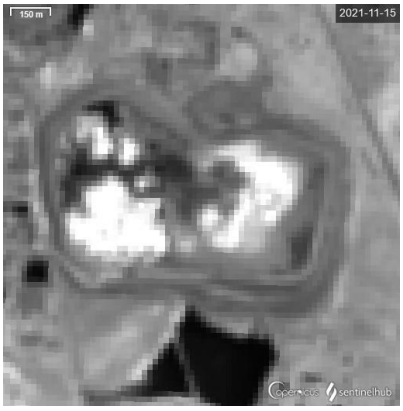

Natural Colour (RGB - Bands 4, 3, 2)

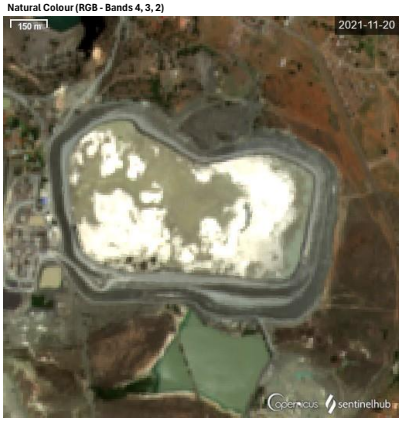

Near Infrared (NIR - Band 8)

Shortwave Infrared (SWIR - Band 11)

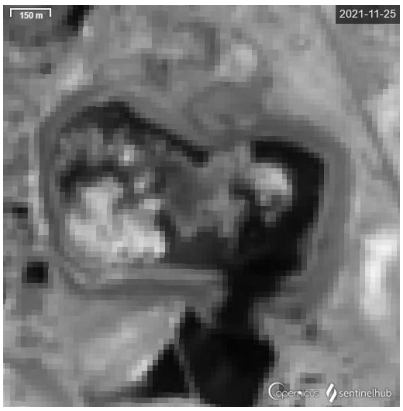

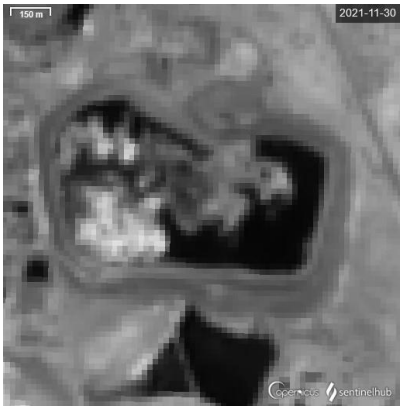

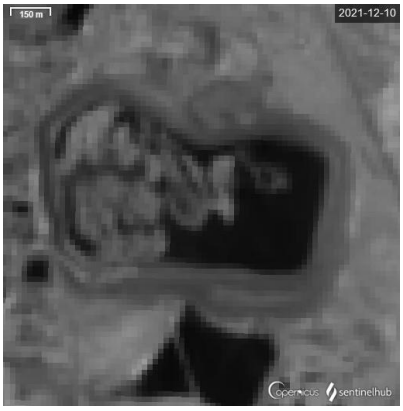

Natural Colour (RGB - Bands 4, 3, 2)

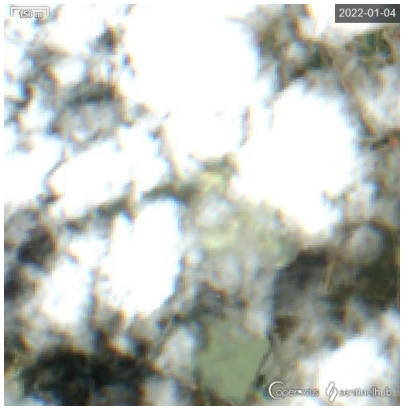

Near Infrared (NIR - Band 8)

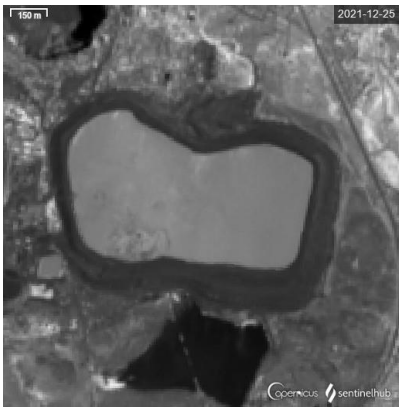

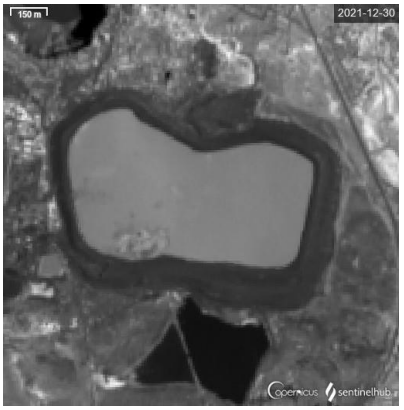

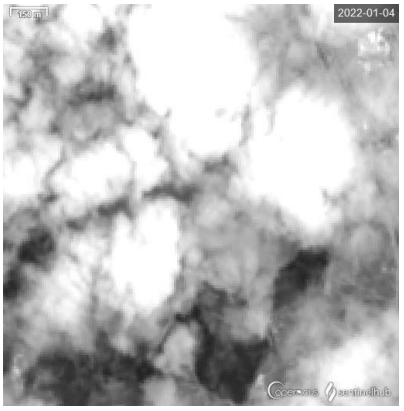

Shortwave Infrared (SWIR - Band 11)

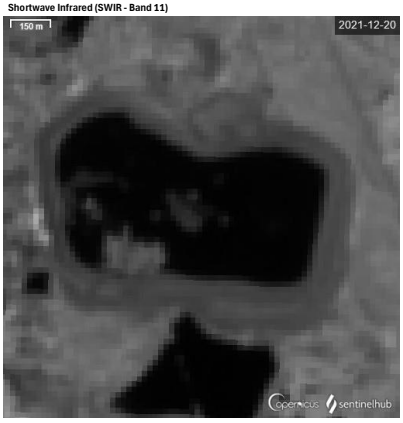

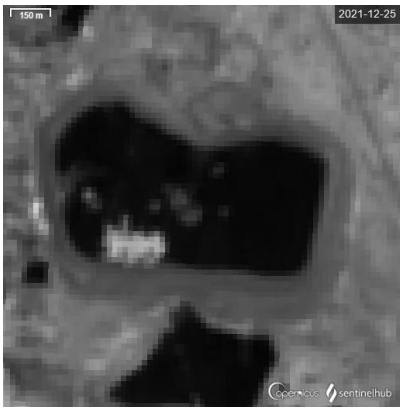

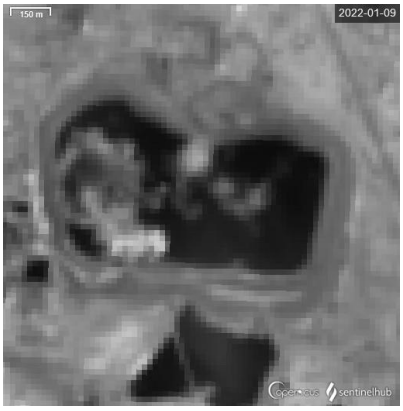

Natural Colour (RGB - Bands 4, 3, 2)

Near Infrared (NIR - Band 8)

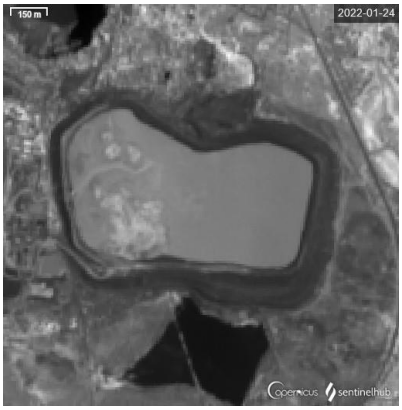

Shortwave Infrared (SWIR - Band 11)

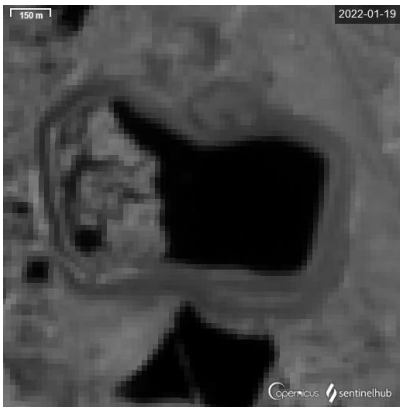

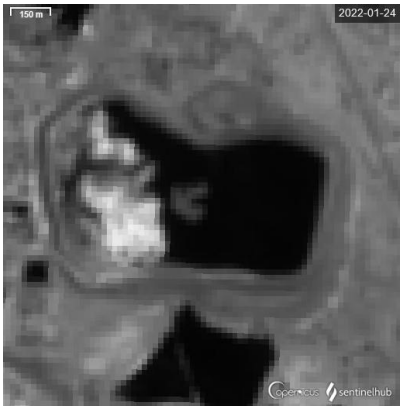

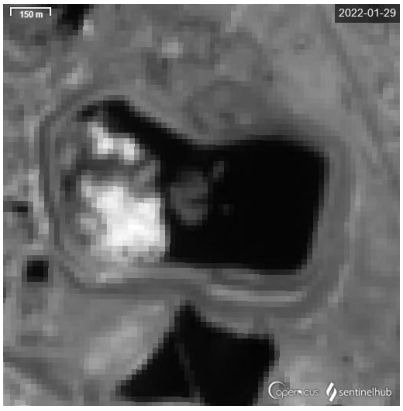

Natural Colour (RGB - Bands 4, 3, 2)

Near Infrared (NIR - Band 8)

Shortwave Infrared (SWIR - Band 11)

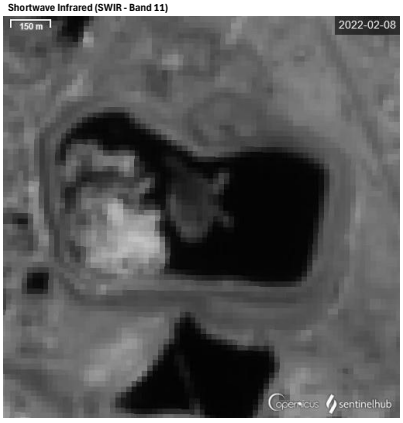

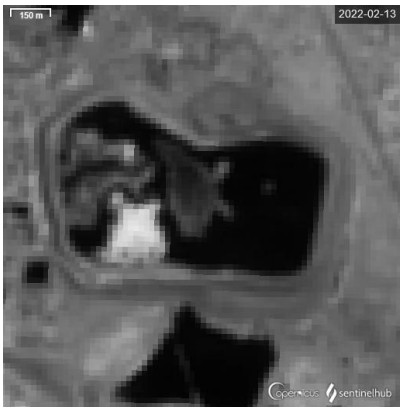

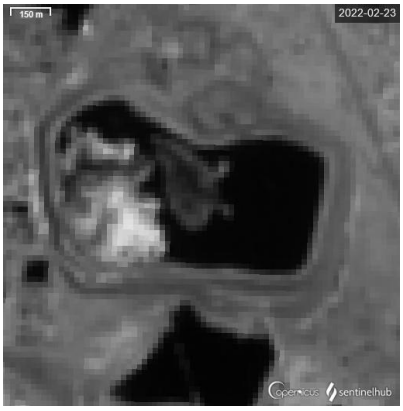

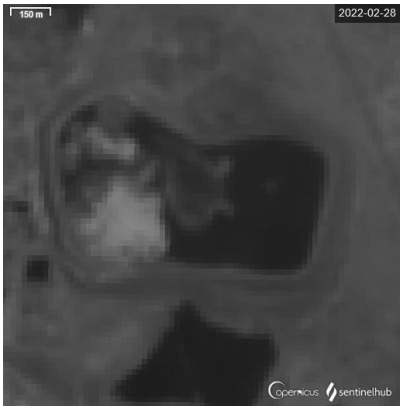

Natural Colour (RGB - Bands 4, 3, 2)

Near Infrared (NIR - Band 8)

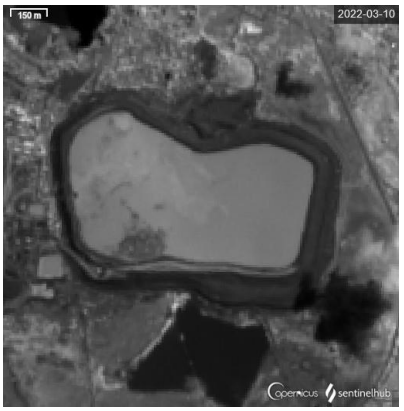

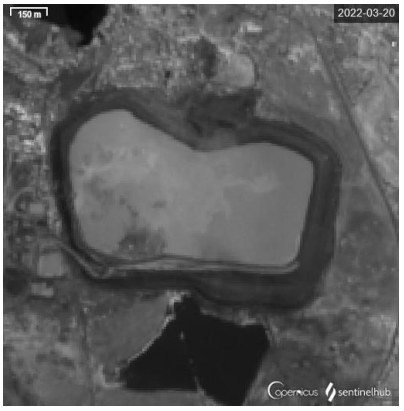

Shortwave Infrared (SWIR - Band 11)

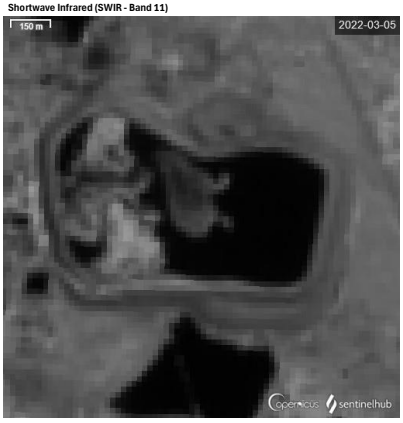

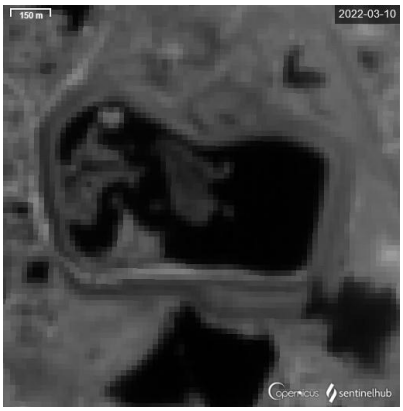

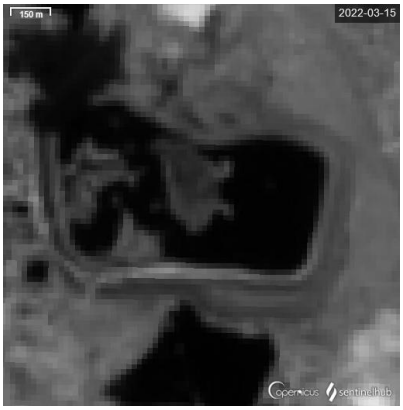

Natural Colour (RGB - Bands 4, 3, 2)

Near Infrared (NIR - Band 8)

Shortwave Infrared (SWIR - Band 11)

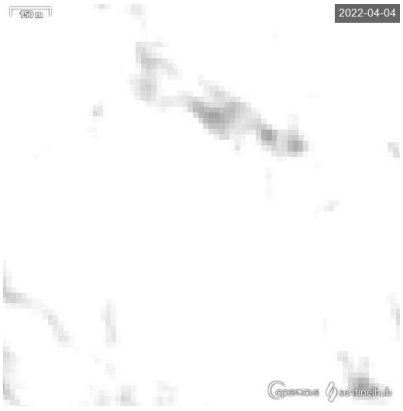

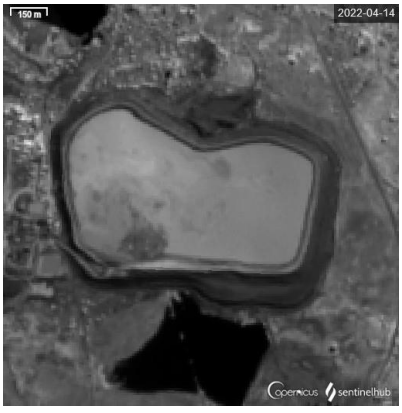

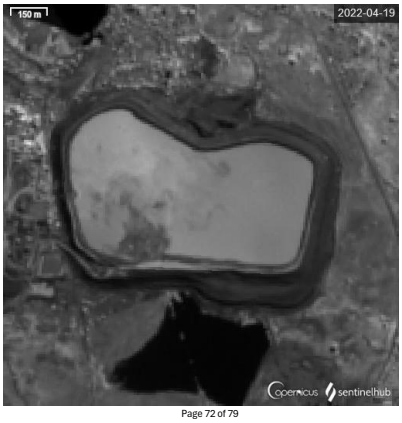

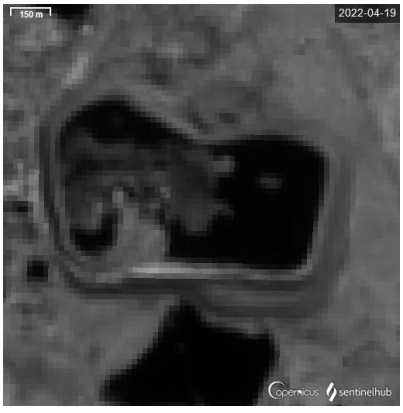

Natural Colour (RGB - Bands 4, 3, 2)

Near Infrared (NIR - Band 8)

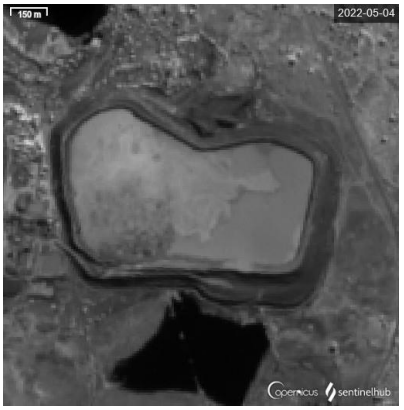

Shortwave Infrared (SWIR - Band 11)

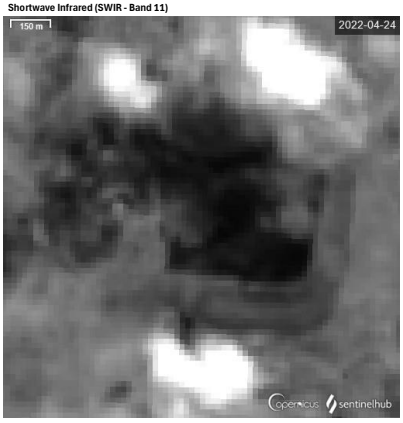

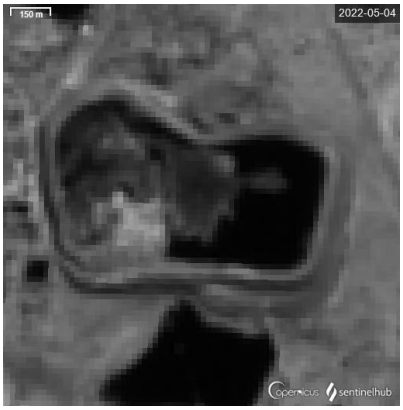

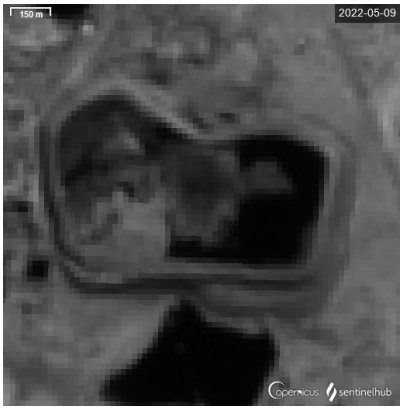

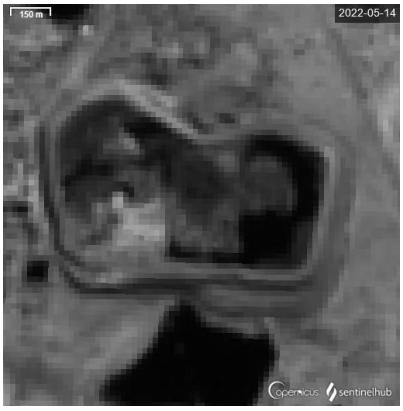

Natural Colour (RGB - Bands 4, 3, 2)

Near Infrared (NIR - Band 8)

Shortwave Infrared (SWIR - Band 11)

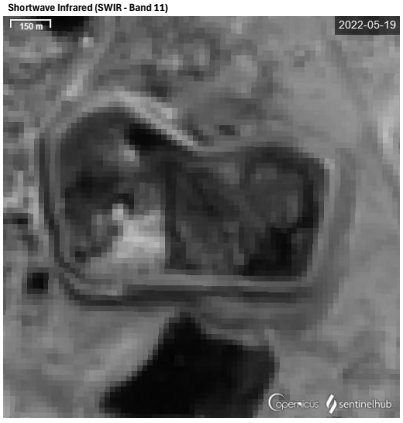

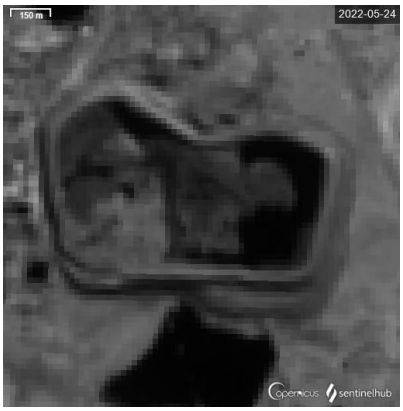

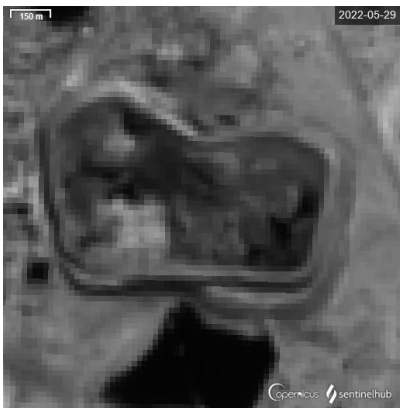

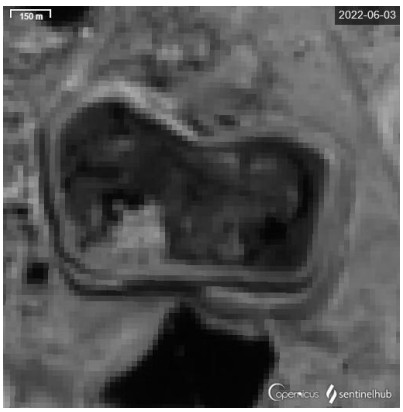

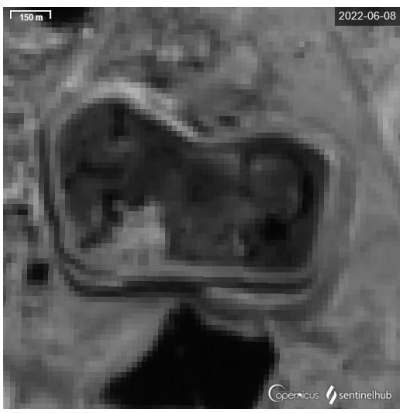

Natural Colour (RGB - Bands 4, 3, 2)

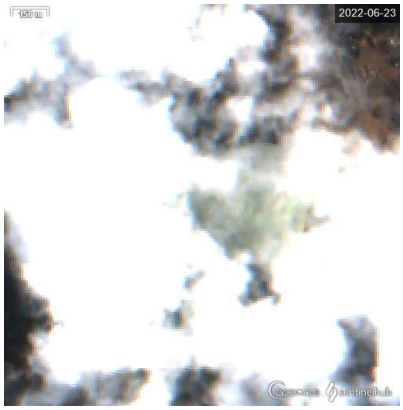

Near Infrared (NIR - Band 8)

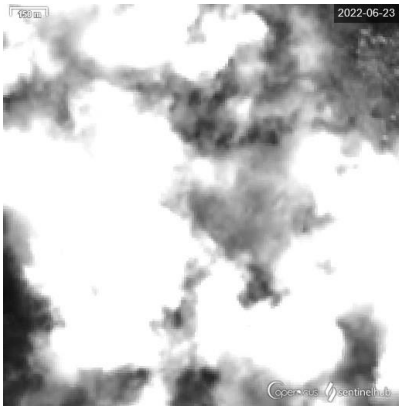

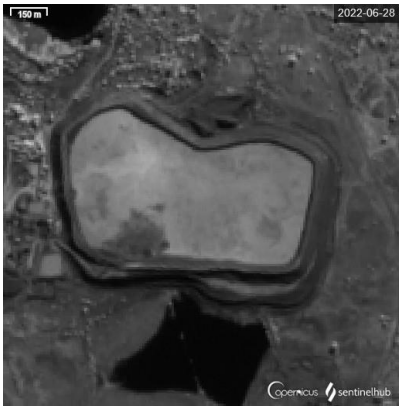

Shortwave Infrared (SWIR - Band 11)

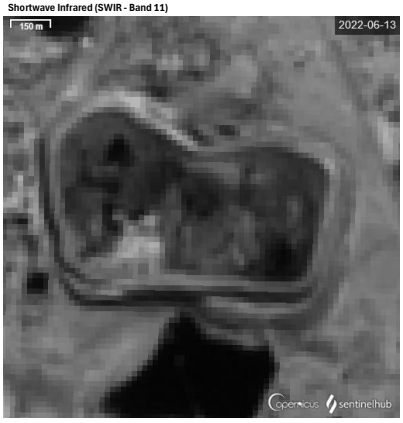

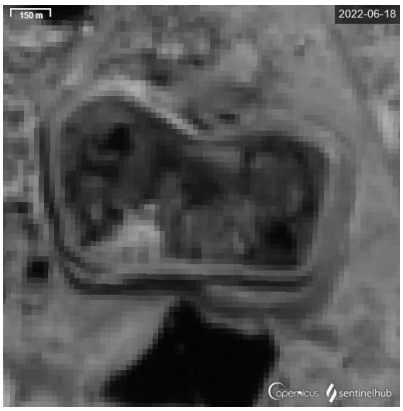

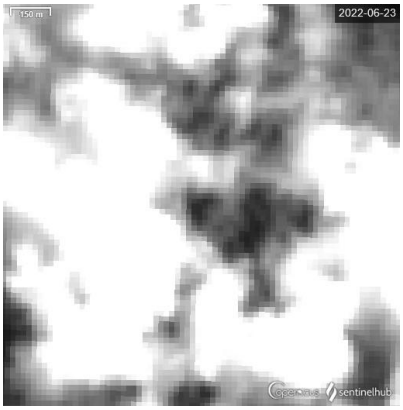

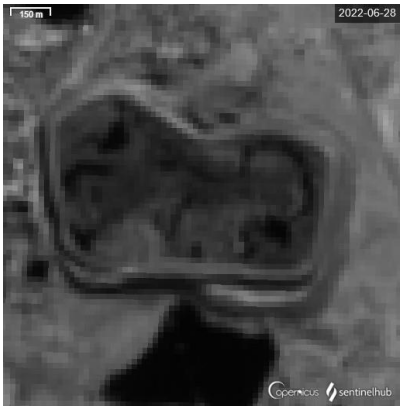

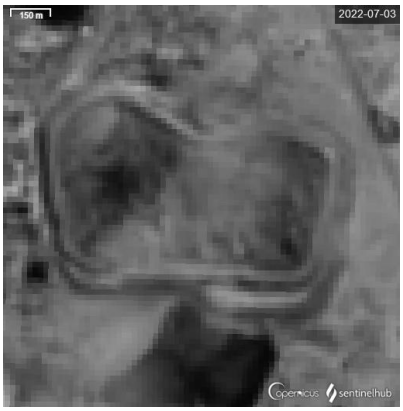

Natural Colour (RGB - Bands 4, 3, 2)	Near Infrared (NIR - Band 8)	Shortwave Infrared (SWIR - Band 11)
		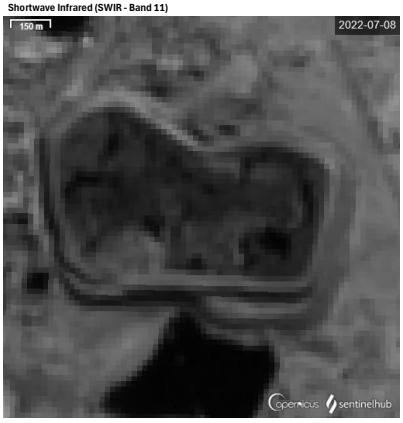
		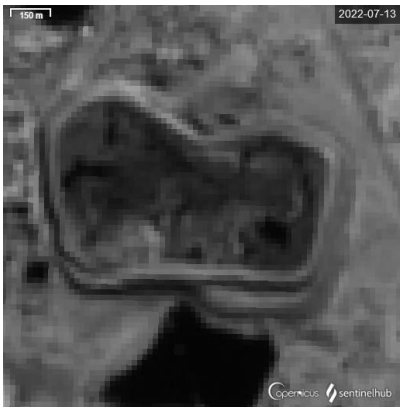
		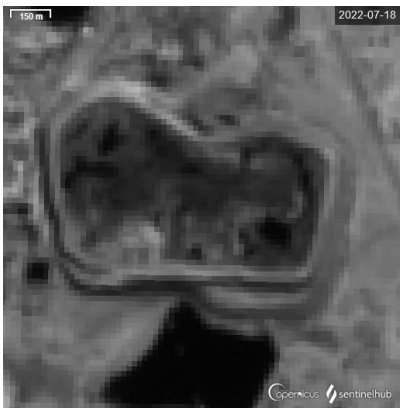
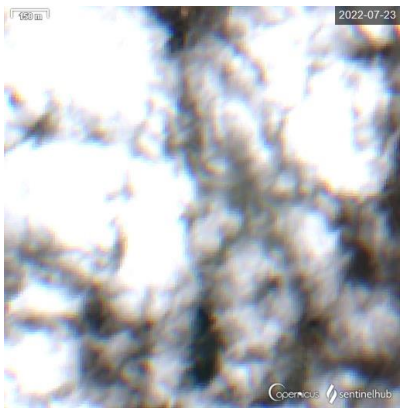	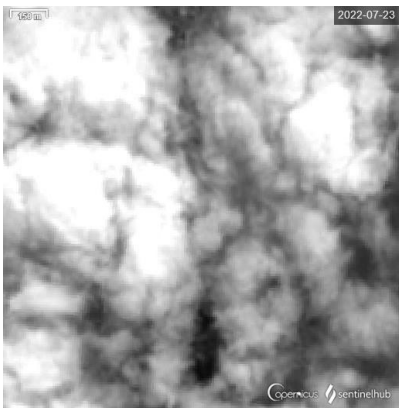	
	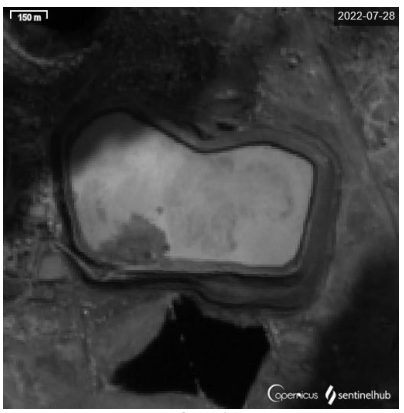	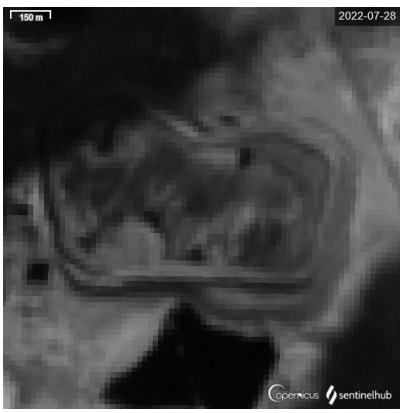

Natural Colour (RGB - Bands 4, 3, 2)

Near Infrared (NIR - Band 8)

Shortwave Infrared (SWIR - Band 11)

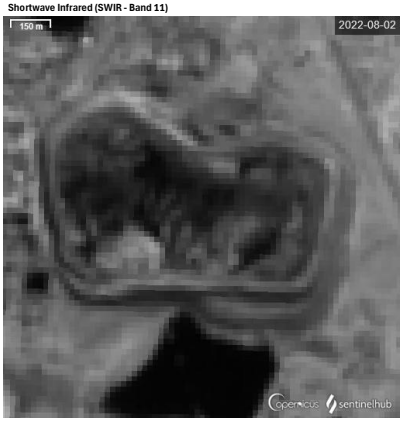

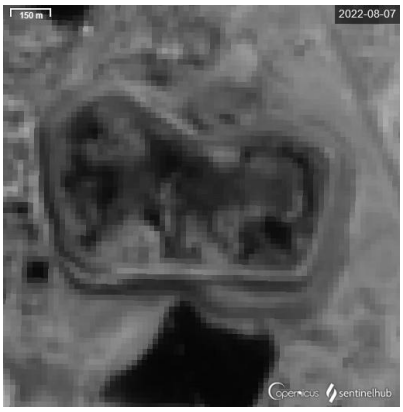

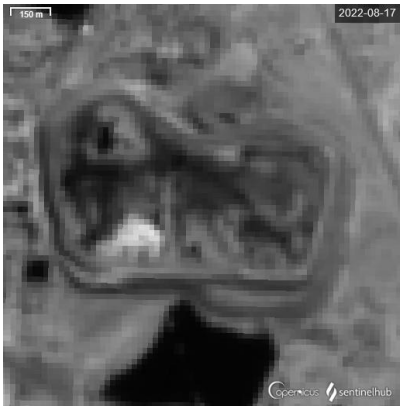

Natural Colour (RGB - Bands 4, 3, 2)

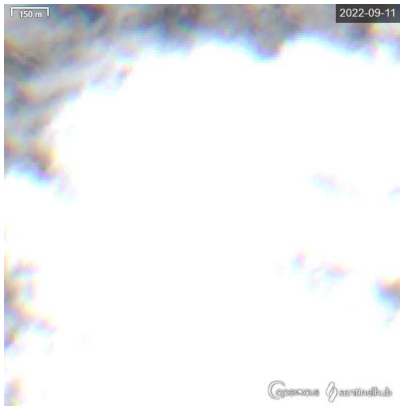

Near Infrared (NIR - Band 8)

Shortwave Infrared (SWIR - Band 11)

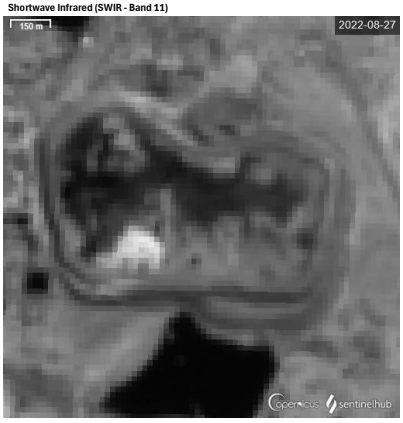

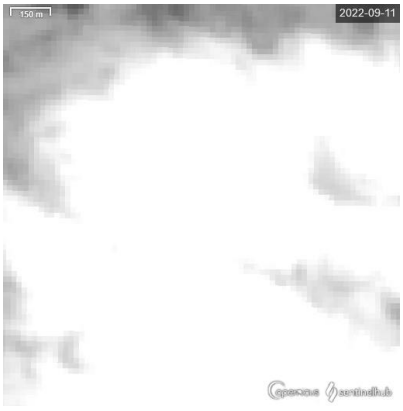

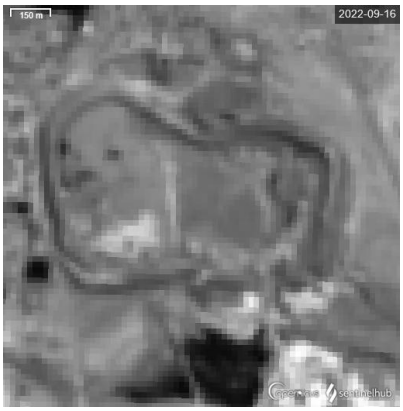

Natural Colour (RGB - Bands 4, 3, 2)

Near Infrared (NIR - Band 8)

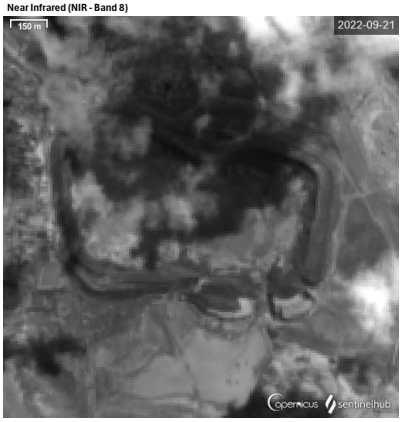

Shortwave Infrared (SWIR - Band 11)

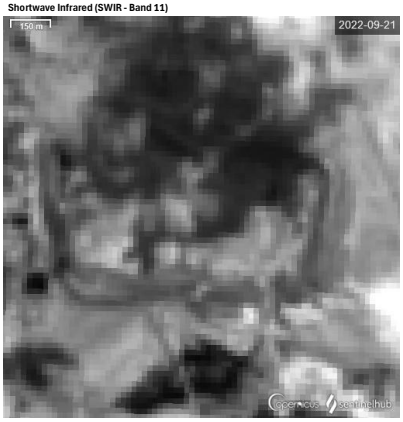

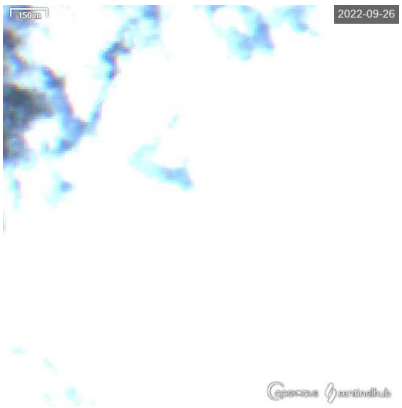

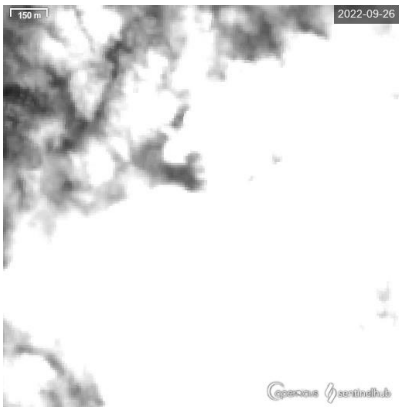

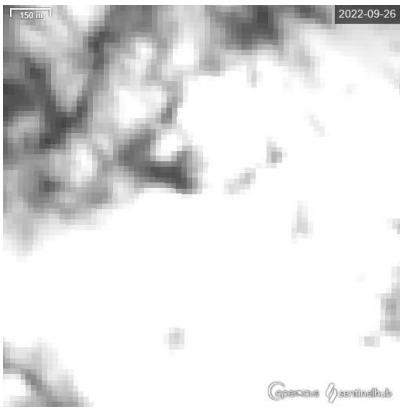

APPENDIX E

GEOTECHNICAL PARAMETERS

TABLE OF CONTENTS

1. INTRODUCTION 3

2. GEOLOGY 3

2.1. REGIONAL GEOLOGY 3

2.2. LOCAL GEOLOGY BELOW THE JAGERSFONTEIN TAILINGS DAM 4

3. MATERIAL PROPERTIES 6

3.1. SAMPLES TESTED 6

3.2. GRADING AND ATTERBERG LIMITS 9

3.3. MINERALOGY 19

3.4. SCANNING ELECTRON MICROSCOPY 20

3.5. SHEAR STRENGTH 22

3.5.1. Triaxial and Direct Simple Shear tests 22

3.5.2. Vane shear test results 40

3.6. DISPERSIVENESS 42

REFERENCES 42

LIST OF FIGURES

Figure 1 Water logged conditions along the southern toe prevented access beyond the access road. 3

Figure 2 Excerpt from geological map of the Jagersfontein tailings dam area by Colliston (2021). . 4

Figure 3 Section 2, extending from northwest to southeast across the tailings dam basin (modified from Colliston, 2021). 5

Figure 4 Section EH, extending approximately north-south under the western wall of the tailings dam (from Colliston, 2021). 5

Figure 5 Sampling locations 8

Figure 6 Particle size distribution (a) focussing on coarse tailings; (b) focussing on fine tailings. 9

Figure 7 Summary of mineralogy determined from XRD analysis. 19

Figure 8 Fine tailings magnified 1000 times showing agglomerations of particles. 20

Figure 9 Platy minerals visible at 50 000 times magnification. 21

Figure 10 Second image of platy minerals visible at 50 000 times magnification. 21

Figure 11 P-Q Stress paths from CU triaxial tests on fine tailings suggesting an effective friction angle of 26°. 22

Figure 12 Shear stress – normal stress stress paths for undrained direct simple shear tests on fine tailings suggestion an effective friction angle of 22.5°. 23

Figure 13 P-Q Stress paths from CU triaxial tests on coarse tailings suggesting an effective friction angle of 38.7° 23

Figure 14 Locations of vane shear test results in breach floor. 41

Figure 15 results of vane shear test carried out in the floor of the breach on 29 Jan 2024. 41

Figure 16 Significant slope erosion suggestion potential for dispersiveness. 42

1. Introduction

In addition to the seismic piezocone investigation described in Appendix F, which included the collection of Mostap samples, a limited materials investigation was carried out on samples collected during the various site visits, and submitting these for laboratory testing to determine the relevant geotechnical properties. Due to water logged conditions around the area affected by the failure, access with plant was very difficult and generally not possible, although efforts were made: A bulldozer got stuck on the inside slope of the dam and a TLB near the downstream toe in the area affected by the failure.

FIGURE 1 WATER LOGGED CONDITIONS ALONG THE SOUTHERN TOE PREVENTED ACCESS BEYOND THE ACCESS ROAD.

2. Geology

2.1. Regional geology

The regional geology of the Jagersfontein area was described by Colliston (2021), summarised below:

The geological history of the Jagersfontein region is primarily composed of Triassic-age Adelaide Subgroup sediments from the Beaufort Group (Karoo Supergroup), which were intruded by dolerite sills and dykes around 180 million years ago. During the Cretaceous period, 80 to 60 million years ago, clusters of kimberlite pipes and dykes intruded the area, leading to the founding of Jagersfontein in

1870. Erosion of the Karoo occurred over 170 million years following uplift. The underlying strata consist of litho-feldspathic sandstone layers, separated by dolerite sills, with significant variability in thickness. The sandstones and siltstones exhibit ripple lamination and contain vertical and inclined fractures, while the superficial deposits include red dune sand, weathered kimberlite tailings and clay, with thicknesses ranging from 0.2 to 3 meters.

2.2. Local geology below the Jagersfontein tailings dam

Colliston (2021) presents the local geology from the Jagerfontein tailings dam area, with an excerpt of his geological map reproduced below in Figure 2. Approximately the northern half of the tailings dam footprint is underlain by a dolerite sheet. Over the southern half of the dam footprint, the dolerite is overlain by fine-grained sandstone, followed by lower siltstone at depth. The sandstone cover increases in thickness towards the southeast to about 10m under the eastern wall. An excerpt along Section 2, indicated on the geological map, is presented in Figure 3 and an excerpt along Section EH in Figure 4.

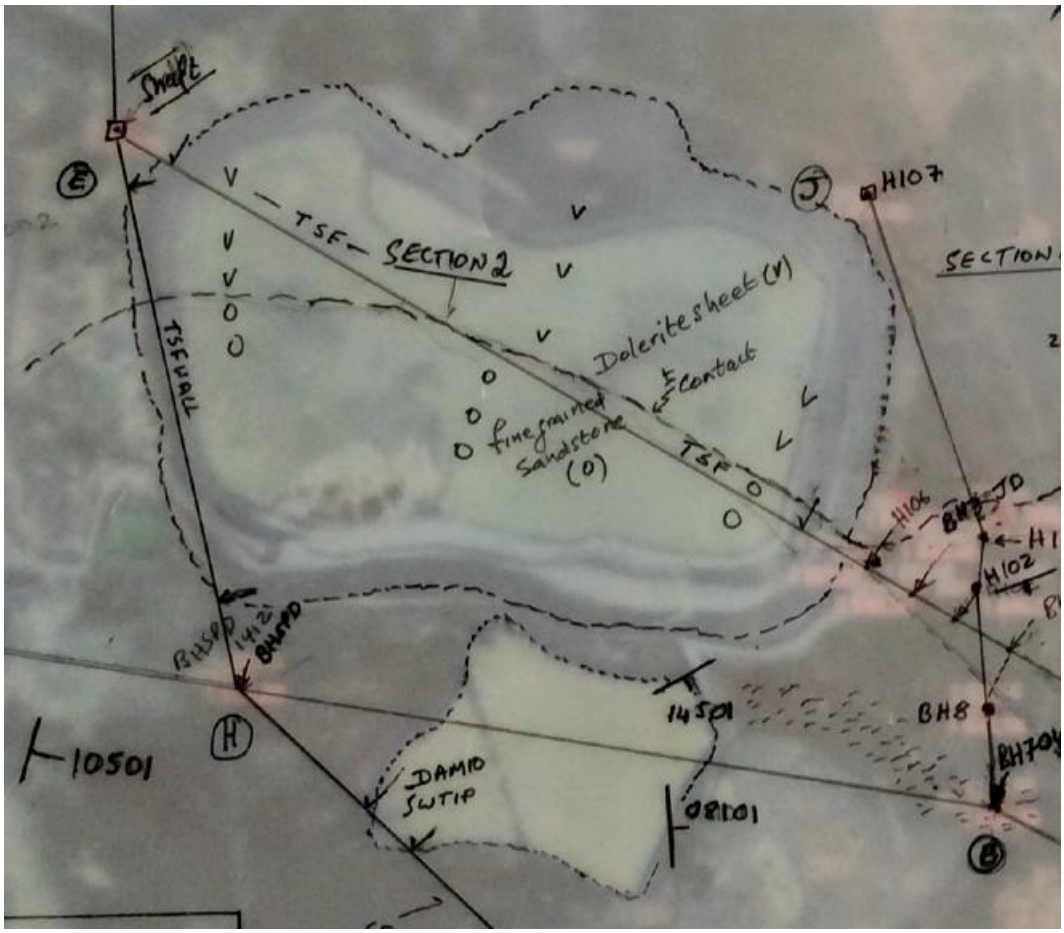

FIGURE 2 EXCERPT FROM GEOLOGICAL MAP OF THE JAGERSFONTEIN TAILINGS DAM AREA BY COLLISTON (2021).

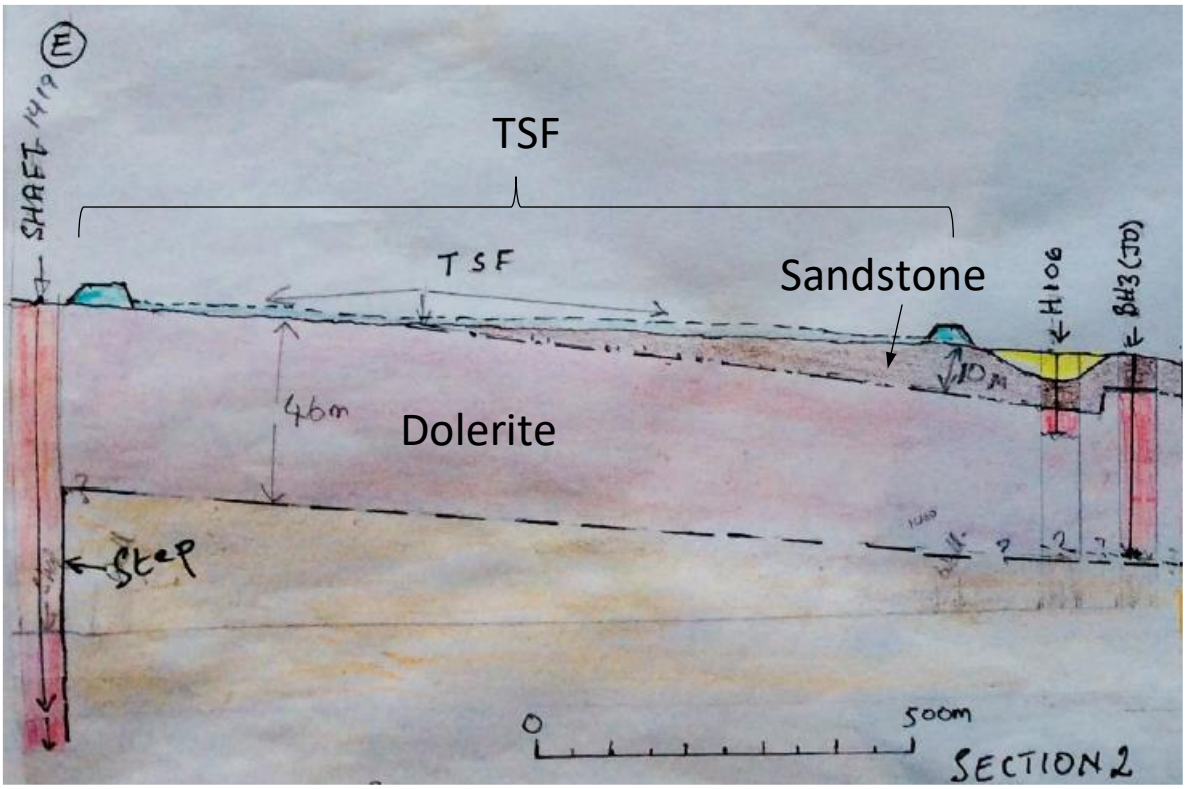

FIGURE 3 **SECTION 2, EXTENDING FROM NORTHWEST TO SOUTHEAST ACROSS THE TAILINGS DAM BASIN (MODIFIED FROM COLLISTON, 2021).**

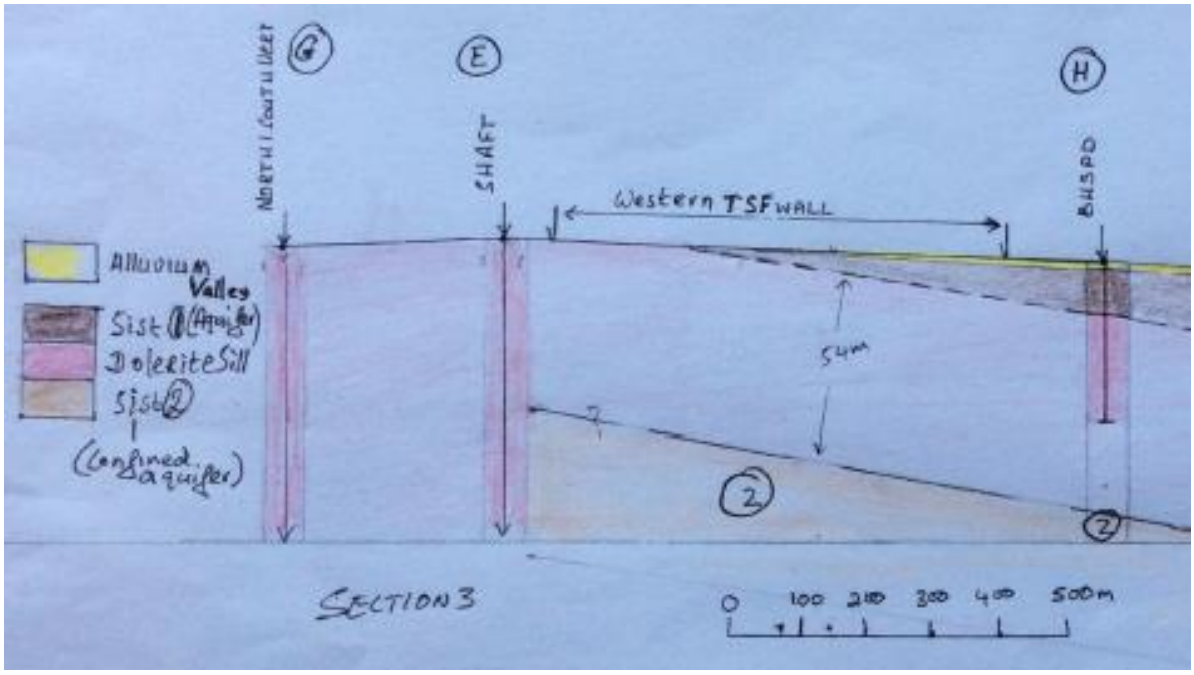

FIGURE 4 **SECTION EH, EXTENDING APPROXIMATELY NORTH-SOUTH UNDER THE WESTERN WALL OF THE TAILINGS DAM (FROM COLLISTON, 2021).**

3. Material properties

3.1. Samples tested

A list of indicator samples collected at the ground surface during the site visits are presented in Table 1. The Mostap samples collected during the piezocone investigation are summarised in Table 2. The sampling locations are indicated in Figure 5. It was intended to collect samples of the fine tailings (slimes) material underlying the dam walls, as well as the coarse tailings (grits) used for the construction of the dam. With the Mostap sampling it was generally intended to sample the fine tailings (slimes) underneath the dam and the residual material underlying the dam where possible, but coarse tailings were also sampled.

TABLE 1 INDICATOR SAMPLES COLLECTED AT SURFACE.

Sample name	Tests carried out	General material description (Fine tailings / coarse tailings)	Classification based on grading
FT1	XRD, FI, SG	Fine tailings (Breach footprint)	SILTY SAND
FT2	XRD, FI, SG	Fine tailings (Breach footprint)	SILTY SAND
FT3	XRD, FI	Fine tailings (Dam toe adjacent to access road)	SILTY SAND
FT4	XRD, FI, SG	Fine tailings (sorted through deposition in Dam 10)	SILTY CLAY
FT5	XRD, FI, SG	Fine tailings (sorted through deposition in Dam 10)	CLAY
FT6	XRD, FI, SG	Coarse tailings (next to Dam 10)	SAND
FT7	XRD, FI, SG	Fine tailings (next to Dam 10)	SILTY SAND
T3a	XRD, FI, SG	Fine tailings (De Beers Dam)	SILTY SAND
T3b	XRD, TRIAX, DSS	Fine tailings (De Beers Dam)	
G1	XRD, FI, SG	Coarse tailings (from inside slope)	SAND
G2	XRD, FI	Coarse tailings (from inside slope)	SAND
G3	XRD, FI, TRIAX	Coarse tailings (from dam wall just west of breach)	SAND
G4	XRD, FI	Coarse tailings (from dam wall just west of breach)	SAND
G5	XRD, FI	Coarse tailings (from dam wall west of breach)	SAND
D1	FI, Dispersiveness	Fine tailings (from south-western corner)	SILTY SAND

Notes:
General material description: FT = fine tailings (slimes); G = gravel (grits), T = De Beers Dam fine tailings, D = cation exchange (dispersiveness).
FI = Foundation indicators (Grading and Atterberg limits); XRD = X-ray diffraction; SG = specific gravity (density of grains); TRIAX = CU triaxial test; DSS = Direct simple shear (undrained).
Sample T3 was split into T3a and T3b which are considered to be identical.

TABLE 2 MOSTAP SAMPLES COLLECTED.

Sample name	Depth (m)	Tests carried out	General material description (Fine tailings / coarse tailings)	Classification based on grading
C5/1	18.20 - 19.10	XRD, FI	Coarse tailings (Gravel)	SAND
C6/1	15.00 – 15.82	XRD, FI	Coarse tailings (Gravel)	SAND
C6/2	17.00 - 17.88	XRD, FI	Coarse tailings (Gravel)	SAND
C6/3	18.50 - 19.32	XRD, FI	Coarse tailings (Gravel)	SAND
C6/4	20.58 - 21.12	XRD, FI	Residual material underlying dam	CLAYEY SAND
C8/1	20.20 - 21.00	XRD, FI	Coarse tailings (Gravel)	SAND
C8/2	21.40 - 22.10	XRD, FI	Coarse tailings (Gravel)	SAND
C11/1	6.60 - 7.50	XRD, FI	Mixed tailings	SILTY SAND
C11/2	9.30 - 10.17	XRD, FI	Mixed tailings	SILTY SAND
C11/3	11.00 - 11.90	XRD, FI	Fine tailings	SILTY SAND
C12/2	6.40 - 7.30	XRD, FI	Mixed tailings	SAND

Notes: Sample names correspond with piezocone test positions shown in Figure 5.
Material samples generally fell in two groups, i.e. coarse grained tailings, also referred to as gravel or grits, and fine grained tailings, also referred to as slimes. Particle size distribution are presented in 3.2

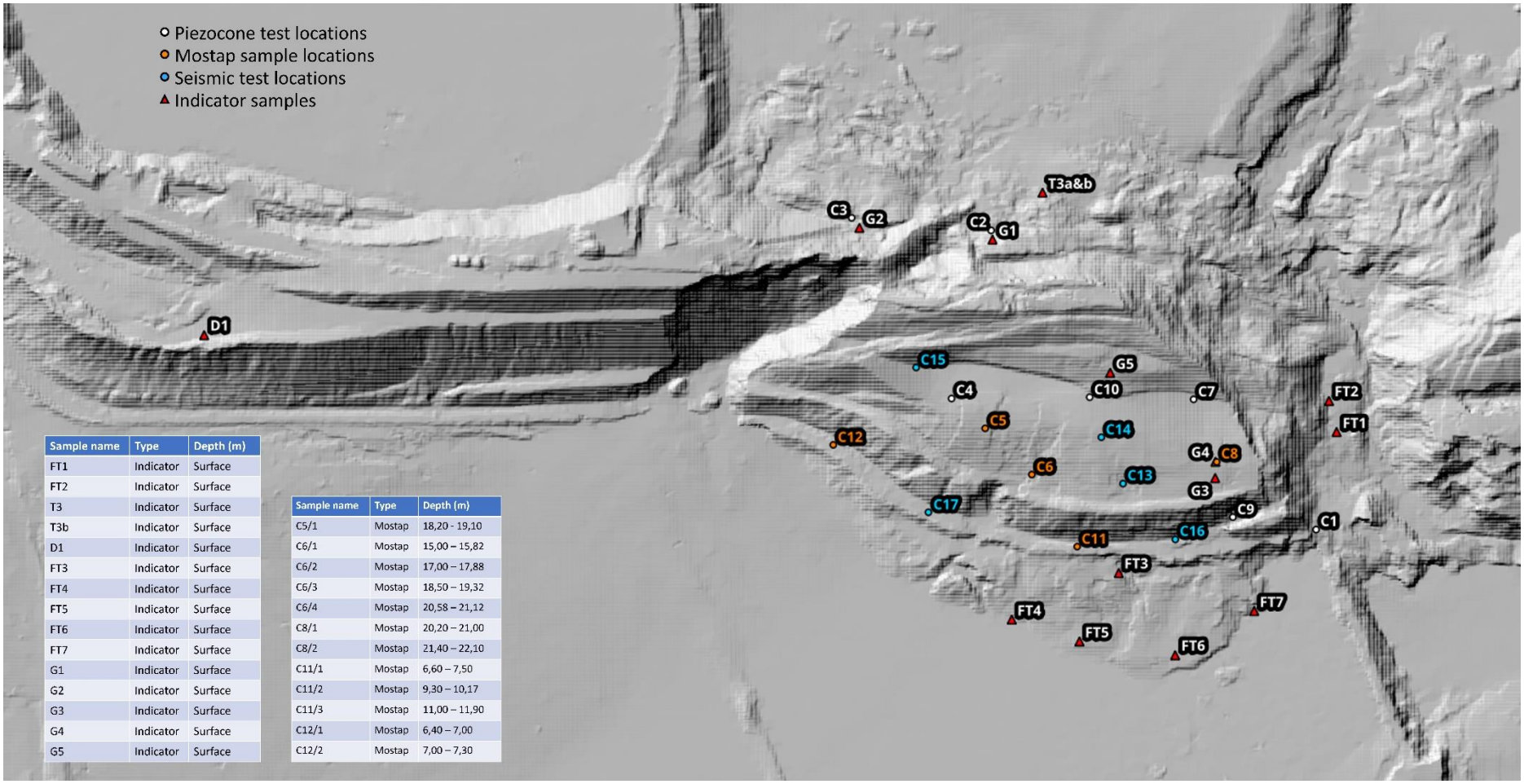

Sample name	Type	Depth (m)
FT1	Indicator	Surface
FT2	Indicator	Surface
T3	Indicator	Surface
T3b	Indicator	Surface
D1	Indicator	Surface
FT3	Indicator	Surface
FT4	Indicator	Surface
FT5	Indicator	Surface
FT6	Indicator	Surface
FT7	Indicator	Surface
G1	Indicator	Surface
G2	Indicator	Surface
G3	Indicator	Surface
G4	Indicator	Surface
G5	Indicator	Surface

Sample name	Type	Depth (m)
C5/1	Mostap	18,20 - 19,10
C6/1	Mostap	15,00 – 15,82
C6/2	Mostap	17,00 – 17,88
C6/3	Mostap	18,50 – 19,32
C6/4	Mostap	20,58 – 21,12
C8/1	Mostap	20,20 – 21,00
C8/2	Mostap	21,40 – 22,10
C11/1	Mostap	6,60 – 7,50
C11/2	Mostap	9,30 – 10,17
C11/3	Mostap	11,00 – 11,90
C12/1	Mostap	6,40 – 7,00
C12/2	Mostap	7,00 – 7,30

FIGURE 5 SAMPLING LOCATIONS

3.2. Grading and Atterberg Limits

Figure 6 presents the particle size distribution of various material collected. Figure 6(a) focuses on coarse tailings, while Figure 6(b) focuses on the fine tailing. The following samples are highlighted: Residual soil sample from Mostap sample C6/4, De Beers tailings T3a, the fine tailings grading from the design report by Robinson (2015), as well as the coarse tailings grading by Robinson (2015). Very fine graded material sampled from immediately adjacent to the Dam 10 water's edge is indicated.

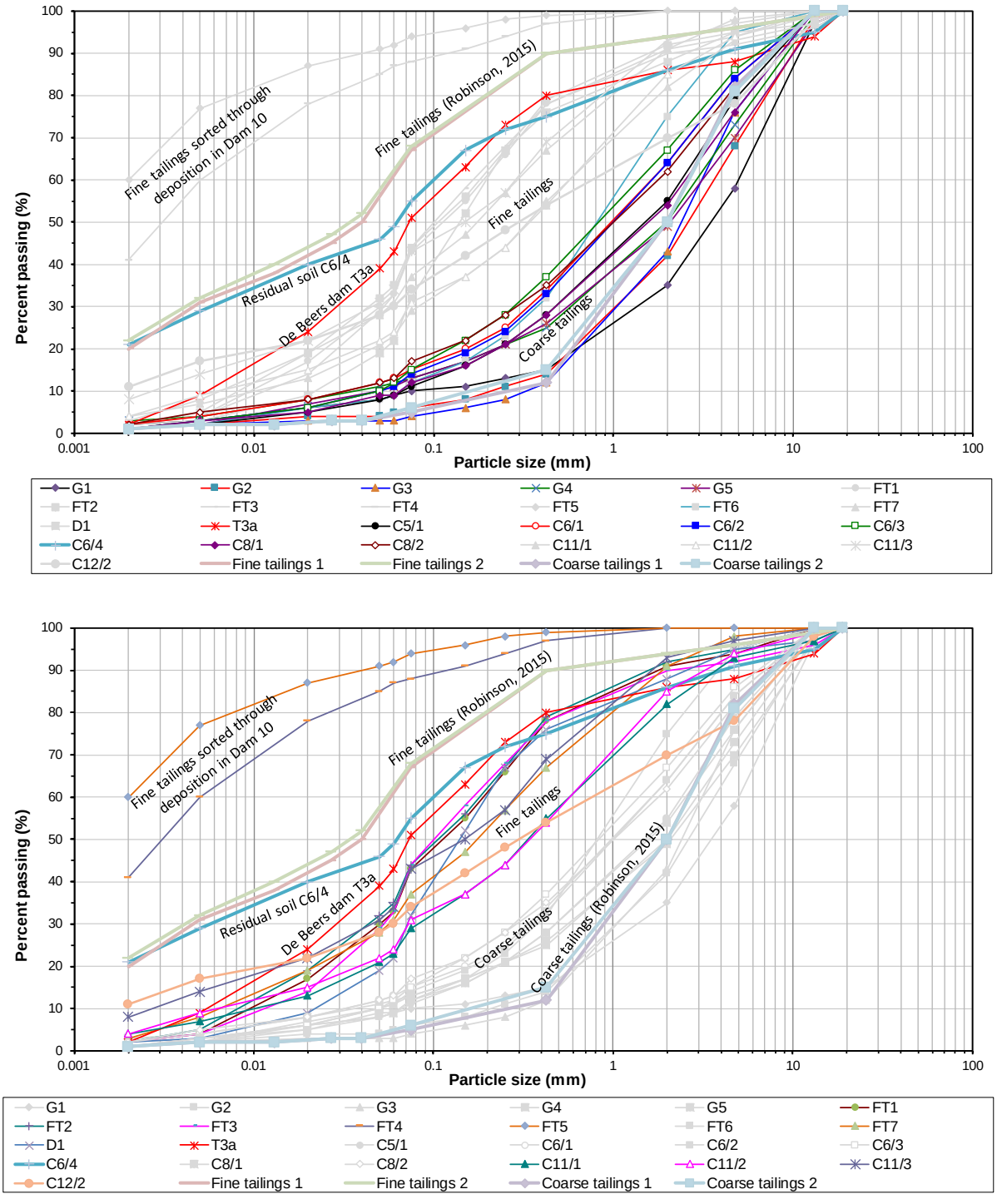

FIGURE 6 PARTICLE SIZE DISTRIBUTION (A) FOCUSSING ON COARSE TAILINGS; (B) FOCUSSING ON FINE TAILINGS.

The grading and Atterberg limits from samples tested are summarised in the tables below:

In terms of particle size distribution, the fine tailings generally classify as silty sands and the coarse tailings as sands. The actual clay percentages determined from the percentage passing 0.002mm are generally below 10%. However, based on the plasticity chart the coarse and fine tailings classify as silts and clay of low to intermediate plasticity. The different between the fine and coarse tailings is small as the coarser fraction (>0.425mm) is screened out for Atterberg limit determination.

Classification Data

Hole no. / Sample Name / Depth / Description		m	1 FT1 Surface	2 FT2 Surface	3 FT3 Surface	4 FT4 Surface	5 FT5 Surface	6 FT6 Surface	7 FT7 Surface	8 T3a Surface	9	10
Specific Gravity:	G_s		2.624	2.598	2.598	2.678	2.673	2.750	2.725	2.592		
Grading:												
		19.0	100	100	100	100	100	100	100	100		
		13.2	100	100	96	100	100	100	100	94		
	No 4	4.75	94	95	92	100	100	95	98	88		
	No 10	2.00	91	92	90	100	100	75	91	86		
	No 40	0.425	78	79	78	97	99	32	67	80		
	No 60	0.250	66	67	68	94	98	23	57	73		
	No 100	0.150	55	56	58	91	96	17	47	63		
	No 200	0.075	43	44	44	88	94	12	37	51		
	No 230	0.060	33	35	33	87	92	9	31	43		
	Hydrometer	0.040	30	32	29	85	91	8	28	39		
		0.020	17	19	14	78	87	6	19	24		
		0.005	4	5	4	60	77	2	8	9		
		0.002	2	2	2	41	60	1	3	2		
Grading Properties												
D_{10}		*mm*	0.009	0.008	0.011			0.065	0.006	0.005		
D_{30}		*mm*	0.040	0.036	0.044			0.378	0.052	0.026		
D_{60}		*mm*	0.189	0.181	0.166	0.005	0.002	1.165	0.293	0.126		
Coefficient of Uniformity	CU		20.0	22.0								
Coefficient of Curvature	CC		0.9	0.9								
Grading Modulus	**GM**		**0.88**	**0.85**	**0.88**	**0.15**	**0.07**	**1.81**	**1.05**	**0.83**		
Gravel	G	%	9	8	10	0	0	25	9	14		
Sand	S	%	58	57	57	13	8	66	60	43		
Silt	M	%	31	33	31	46	32	8	28	41		
Clay	C	%	2	2	2	41	60	1	3	2		
Fines	M+C	%	33	35	33	87	92	9	31	43		
Atterberg Limits												
Liquid Limit	LL	%	34	35	29	74	93	34	36	38		
Plastic Limit	PL	%	23	23	21	46	67	25	25	30		
Linear Shrinkage	LS	%	5.0	5.0	4.0	13.0	12.0	5.0	5.0	4.0		
Plasticity Index	PI	%	11	12	8	28	26	9	11	8		
PI Whole Sample		%	9	9	6	27	26	3	7	6		
Liquidity Index	LI		1.5	1.8	-2.1	-1.5	-2.4	-2.4	0.4	-3.6		
Clay Activity	A		5.50	6.00	4.00	0.68	0.43	9.00	3.67	4.00		
Vd Merwe Swell		%	Low	Low	Low	High	Low	Low	Low	Low		
Brackley Swell												
Natural Moisture Content	w	%	39.5	44.7	4.2	3.7	4.4	3.7	29.6	1.4		
Dry Density	ρ_d	kg/m^3										
Saturation	S	%										
Swell @ p(kPa)	50	%										
	125	%										
	250	%										
Classification **Matrix Description** **British** **AASHTO** **Unified**			**Silty SAND** **CLS** **A-6[2]** **SC**	**Silty SAND** **CIS** **A-6[2]** **SC**	**Silty SAND** **CLS** **A-4[2]** **SC**	**Silty CLAY** **MV** **A-7-5[19]** **MH/OH**	**CLAY** **ME** **A-7-5[18]** **MH/OH**	**SAND** **SW/SP** **A-2-4[0]** **SW/SP**	**Silty SAND** **MIS** **A-6[1]** **SM**	**Silty SAND** **MIS** **A-4[3]** **ML/OL**		

Gradings

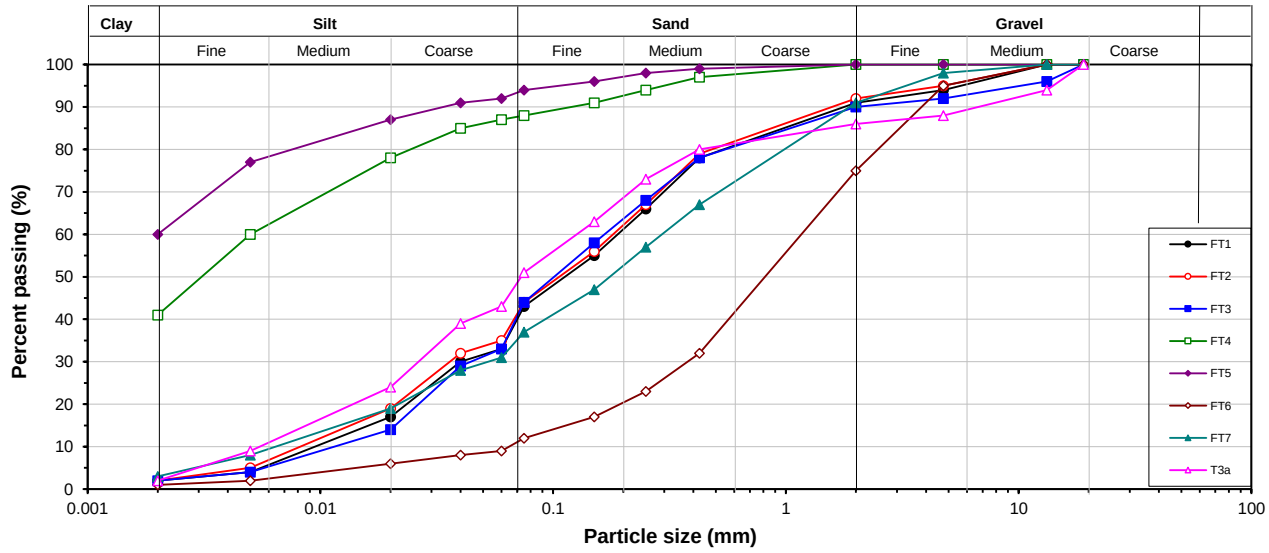

Plasticity Chart

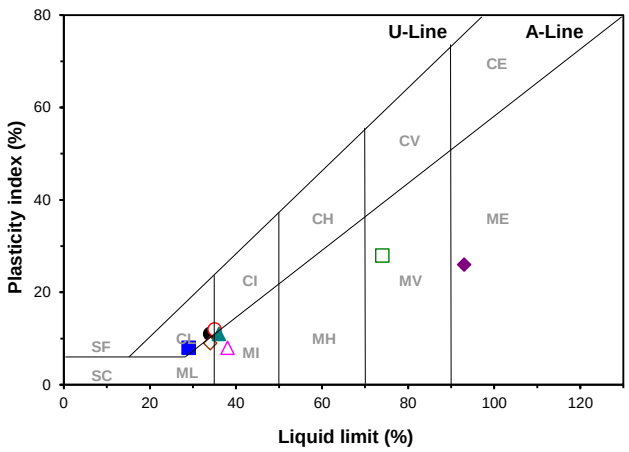

Van der Merwe Heave

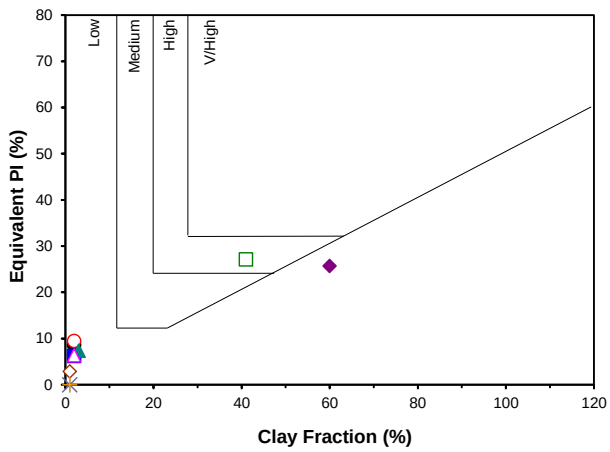

California Bearing Ratio

Unconfined Compressive Strength

Classification Data

Hole no. Sample Name Depth Description		m	1 G1 Surface	2 G2 Surface	3 G3 Surface	4 G4 Surface	5 G5 Surface	6 D1 Surface	7	8	9	10
Specific Gravity:	G_s		2.592	2.592	2.592	2.592	2.592	2.592				
Grading:												
		19.0	100	100	100	100	100	100				
		13.2	97	98	100	99	97	97				
	No 4	4.75	58	68	76	73	70	95				
	No 10	2.00	35	42	43	50	49	88				
	No 40	0.425	15	14	12	25	26	76				
	No 60	0.250	13	11	8	21	21	67				
	No 100	0.150	11	8	6	17	17	52				
	No 200	0.075	10	6	4	13	13	32				
	No 230	0.060	9	5	3	12	11	22				
	Hydrometer	0.050	8	4	3	11	10	19				
		0.020	6	4	3	8	7	9				
		0.005	3	2	2	4	2	3				
		0.002	2	1	1	3	1	2				
Grading Properties												
D_{10}		*mm*	0.075	0.211	0.326	0.037	0.050	0.022				
D_{30}		*mm*	1.358	1.030	1.045	0.579	0.556	0.072				
D_{60}		*mm*	5.006	3.640	3.123	2.913	3.146	0.217				
Coefficient of Uniformity	CU		66.7	17.3	9.6	79.1	62.9	9.9				
Coefficient of Curvature	CC		4.9	1.4	1.1	3.1	2.0	1.1				
Grading Modulus	**GM**		**2.40**	**2.38**	**2.41**	**2.12**	**2.12**	**1.04**				
			70	61	59	56	57					
Gravel	G	%	65	58	57	50	51	12				
Sand	S	%	26	37	40	38	38	66				
Silt	M	%	7	4	2	9	10	20				
Clay	C	%	2	1	1	3	1	2				
Fines	M+C	%	9	5	3	12	11	22				
Atterberg Limits												
Liquid Limit	LL	%	37	33	28	29	29	30				
Plastic Limit	PL	%	27	22	19	19	21	19				
Linear Shrinkage	LS	%	5.0	5.0	4.0	5.0	4.0	5.0				
Plasticity Index	PI	%	10	11	9	10	8	11				
PI Whole Sample		%	2	2	1	3	2	8				
Liquidity Index	LI		-1.3	-1.5	-1.5	-1.5	-1.6	-1.6				
Clay Activity	A		5.00	11.00	9.00	3.33	8.00	5.50				
Vd Merwe Swell		%	Low	Low	Low	Low	Low	Low				
Brackley Swell												
Natural Moisture Content	w	%	14.0	5.2	5.3	4.3	7.9	1.9				
Dry Density	ρ_d	kg/m^3										
Saturation	S	%										
Swell @ p(kPa)	50	%										
	125	%										
	250	%										
Classification **Matrix Description** **British** **AASHTO** **Unified**			**SAND** **GPM** **A-2-4[0]** **SP-SM**	**SAND** **GWC** **A-2-6[0]** **SW-SC**	**SAND** **GW** **A-2-4[0]** **SW**	**SAND** **GPC** **A-2-4[0]** **SC**	**SAND** **GWC** **A-2-4[0]** **SC**	**Silty SAND** **SCL** **A-2-6[0]** **SC**				

Gradings

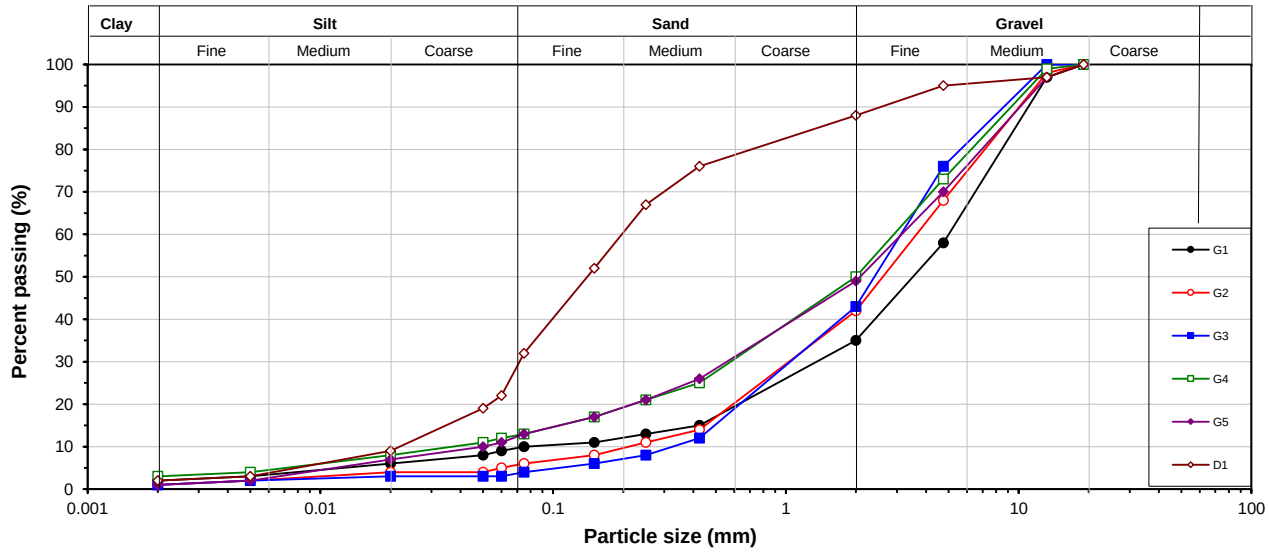

Plasticity Chart

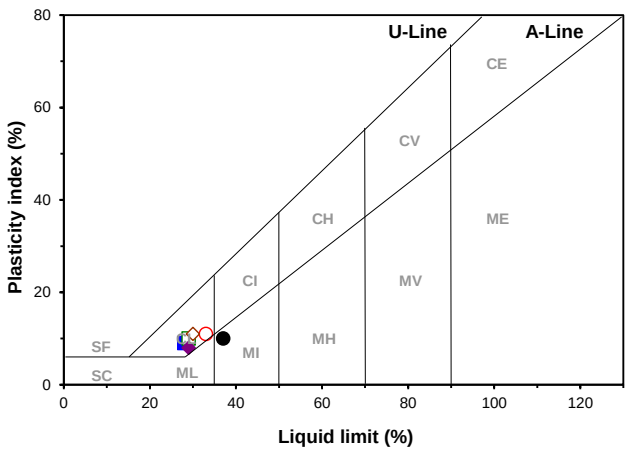

Van der Merwe Heave

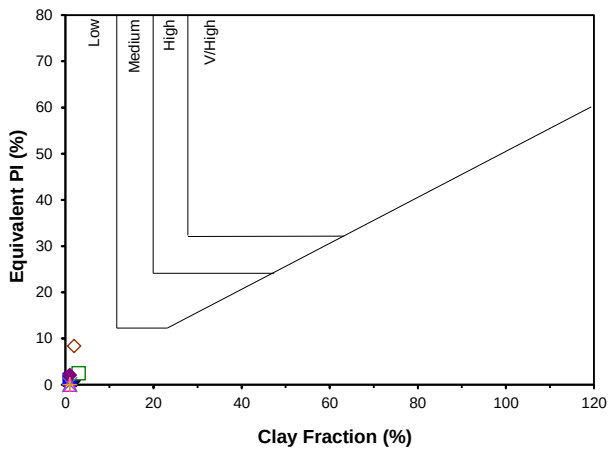

California Bearing Ratio

Unconfined Compressive Strength

Classification Data

Hole no.			1	2	3	4	5	6	7	8	9	10
Sample Name			C5	C6	C6	C6	C6/4	C8	C8	C11	C11	C11
Depth		*m*	C5/1 Surface	C6/1 Surface	C6/2 Surface	C6/3 Surface	C6/4 Surface	C8/1 Surface	C8/2 Surface	C11/1 Surface	C11/2 Surface	C11/3 Surface
Description												
Specific Gravity:	G_s		2.635	2.631	2.624	2.597	-	2.614	2.598	2.579	2.523	2.500
Grading:												
		19.0	100	100	100	100	100	100	100	100	100	100
		13.2	100	100	100	100	95	100	100	97	99	100
	No 4	4.75	79	84	84	86	91	76	82	93	94	97
	No 10	2.00	55	64	64	67	86	54	62	82	85	93
	No 40	0.425	28	34	33	37	75	28	35	55	54	69
	No 60	0.250	21	25	24	28	72	21	28	44	44	57
	No 100	0.150	16	20	19	22	67	16	22	37	37	50
	No 200	0.075	11	15	14	15	55	12	17	29	31	43
	Hydro meter	0.020	5	8	6	6	40	5	8	13	15	22
		0.005	2	4	3	3	29	3	5	7	9	14
		0.002	1	2	1	1	21	1	2	4	4	8
Grading Properties												
D_{10}		*mm*	0.067	0.032	0.050	0.050		0.057	0.032	0.010	0.006	0.003
D_{30}		*mm*	0.477	0.336	0.356	0.281	0.006	0.479	0.291	0.082	0.073	0.045
D_{60}		*mm*	2.395	1.627	1.638	1.393	0.100	2.532	1.783	0.566	0.574	0.285
Coefficient of Uniformity	CU		35.7	51.4	32.8	27.9		44.2	56.4	56.6	91.0	105.2
Coefficient of Curvature	CC		1.4	2.2	1.5	1.1		1.6	1.5	1.2	1.5	2.6
Grading Modulus	**GM**		**2.06**	**1.87**	**1.89**	**1.81**	**0.84**	**2.06**	**1.86**	**1.34**	**1.30**	**0.95**
			50	43	42	39	39					
Gravel	G	%	45	36	36	33	14	46	38	18	15	7
Sand	S	%	46	51	53	55	37	45	49	59	61	59
Silt	M	%	8	11	10	11	28	8	11	19	20	26
Clay	C	%	1	2	1	1	21	1	2	4	4	8
Fines	M+C	%	9	13	11	12	49	9	13	23	24	34
Atterberg Limits												
Liquid Limit	LL	%	32	37	35	32	42	39	35	46	51	55
Plastic Limit	PL	%	22	27	23	23	27	30	29	31	36	40
Linear Shrinkage	LS	%	4.0	5.0	6.0	5.0	7.0	4.0	3.0	7.0	7.0	7.0
Plasticity Index	PI	%	10	10	12	9	15	9	6	15	15	15
PI Whole Sample		%	3	3	4	3	11	3	2	8	8	10
Liquidity Index	LI		-1.9	-2.4	-1.6	-2.2	-1.6	-3.0	-4.3	-1.7	-2.0	-2.2
Clay Activity	A		10.00	5.00	12.00	9.00	0.71	9.00	3.00	3.75	3.75	1.88
Vd Merwe Swell		%	Low	Low	Low	Low	Low	Low	Low	Low	Low	Low
Brackley Swell												
Natural Moisture Content	w	%	2.6	3.3	3.5	3.5	3.1	3.3	3.5	5.9	6.5	6.5
Dry Density	ρ_d	*kg/m* ^{3}										
Saturation	S	%										
Swell @ p(kPa)	50	%										
	125	%										
	250	%										
Classification												
Matrix Description			**SAND**	**SAND**	**SAND**	**SAND**	**Clayey SAND**	**SAND**	**SAND**	**Silty SAND**	**Silty SAND**	**Silty SAND**
British			**GWC**	**SWM**	**SWC**	**SWC**	**MIS**	**GWM**	**SMI**	**SMI**	**SMH**	**MHS**
AASHTO			**A-2-4[0]**	**A-2-4[0]**	**A-2-6[0]**	**A-2-4[0]**	**A-7-6[6]**	**A-2-4[0]**	**A-2-4[0]**	**A-2-7[1]**	**A-2-7[1]**	**A-7-5[4]**
Unified			**SW-SC**	**SM**	**SC**	**SC**	**ML/OL**	**SW-SM**	**SM**	**SM**	**SM**	**SM**

Gradings

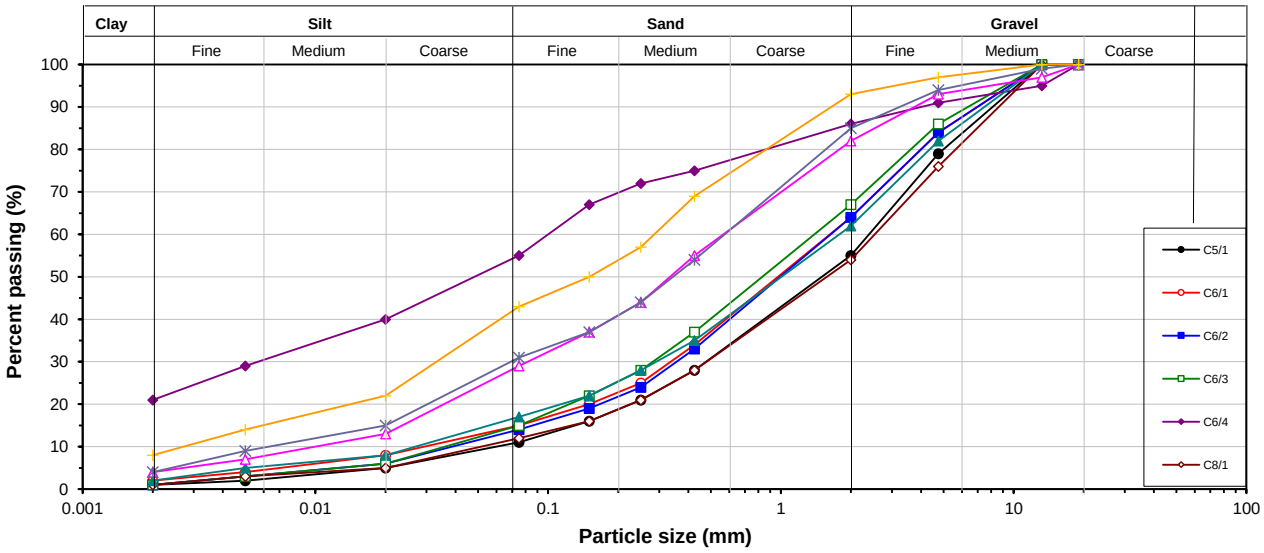

Plasticity Chart

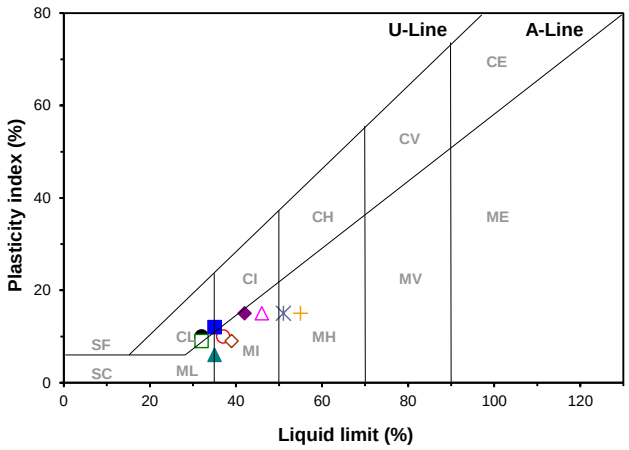

Van der Merwe Heave

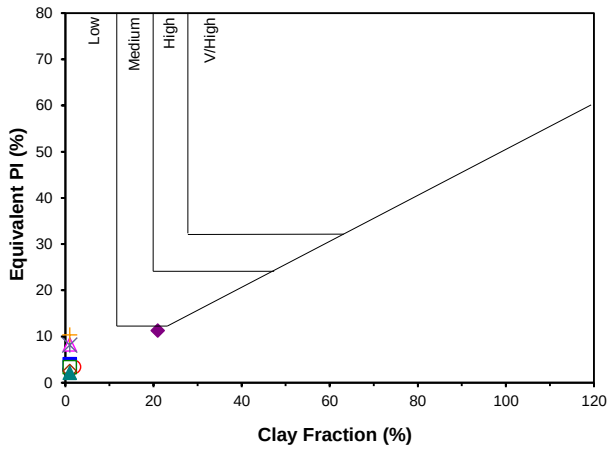

California Bearing Ratio

Unconfined Compressive Strength

Classification Data

Hole no. / Sample Name / Depth / Description			1 C12 C12/2 Surface	2	3	4	5	6	7	8	9	10
		m										
Specific Gravity:	G_s		2.635									
Grading:												
		19.0	100									
		13.2	98									
	No 4	4.75	78									
	No 10	2.00	70									
	No 40	0.425	54									
	No 60	0.250	48									
	No 100	0.150	42									
	No 200	0.075	34									
	Hydro meter	0.020	22									
		0.005	17									
		0.002	11									
Grading Properties												
D_{10}		*mm*	0.011	0.032	0.050	0.050		0.057	0.032	0.010	0.006	0.003
D_{30}		*mm*	0.048	0.336	0.356	0.281	0.006	0.479	0.291	0.082	0.073	0.045
D_{60}		*mm*	0.760	1.627	1.638	1.393	0.100	2.532	1.783	0.566	0.574	0.285
Coefficient of Uniformity	CU		69.3	51.4	32.8	27.9		44.2	56.4	56.6	91.0	105.2
Coefficient of Curvature	CC		0.3	2.2	1.5	1.1		1.6	1.5	1.2	1.5	2.6
Grading Modulus	**GM**		**1.42**									
			35									
Gravel	G	%	30									
Sand	S	%	61									
Silt	M	%	-2									
Clay	C	%	11									
Fines	M+C	%	9									
Atterberg Limits												
Liquid Limit	LL	%	42									
Plastic Limit	PL	%	27									
Linear Shrinkage	LS	%	8.0									
Plasticity Index	PI	%	15									
PI Whole Sample		%	8									
Liquidity Index	LI		-1.6									
Clay Activity	A		1.36									
Vd Merwe Swell		%	Low	Low	Low	Low	Low	Low	Low	Low	Low	Low
Brackley Swell												
Natural Moisture Content	w	%	2.6	3.3	3.5	3.5	3.1	3.3	3.5	5.9	6.5	6.5
Dry Density	ρ_d	kg/m^3										
Saturation	S	%										
Swell @ p(kPa)	50	%										
	125	%										
	250	%										
Classification												
Matrix Description			**SAND**									
British			**SMI**									
AASHTO			**A-2-7[1]**									
Unified			**SM**									

Gradings

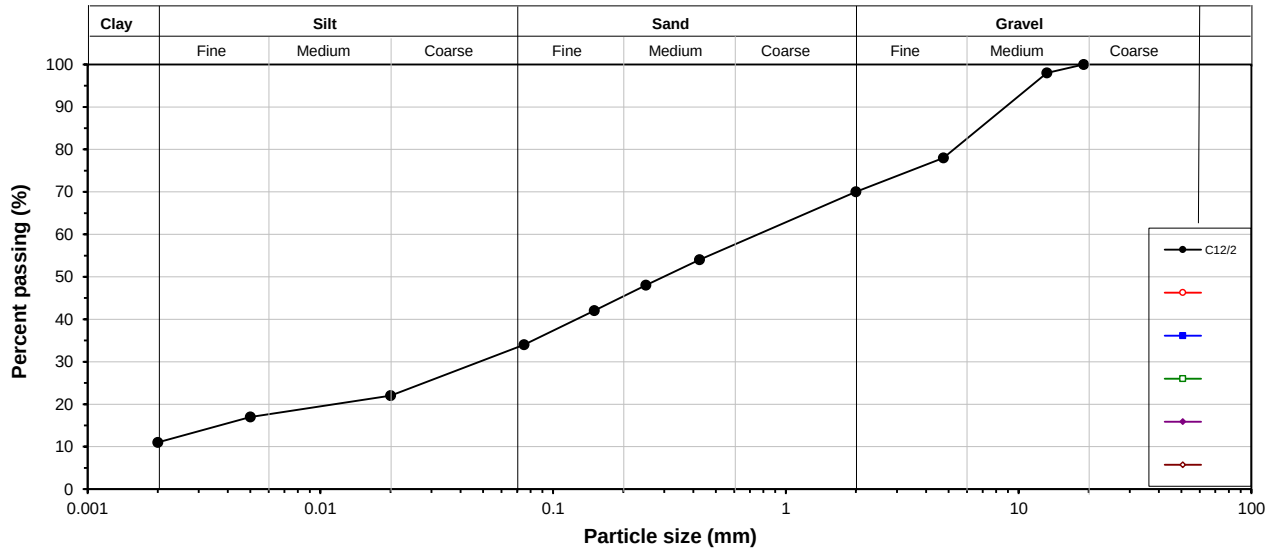

Plasticity Chart

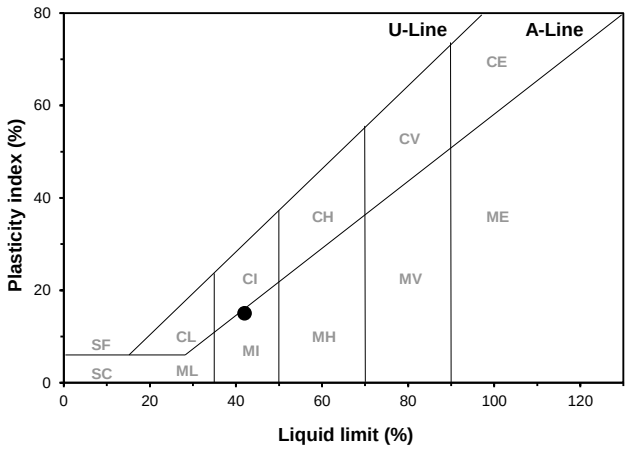

Van der Merwe Heave

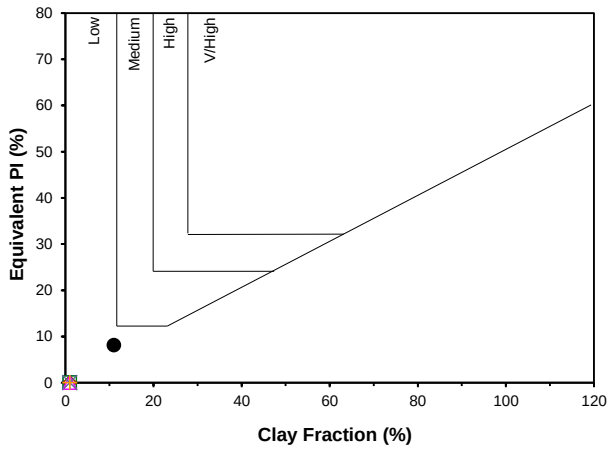

California Bearing Ratio

Unconfined Compressive Strength

3.3. Mineralogy

A semi-quantitative mineralogical determination was carried out using x-ray diffraction on an all Mostap samples and a number of indicator samples at the University of Pretoria. The purpose of the mineralogical assessment was to assess the origin of the materials sampled. It was of interest to know whether material sampled at depth were of residual origin or from tailings. It was also of interest to screen for clay minerals.

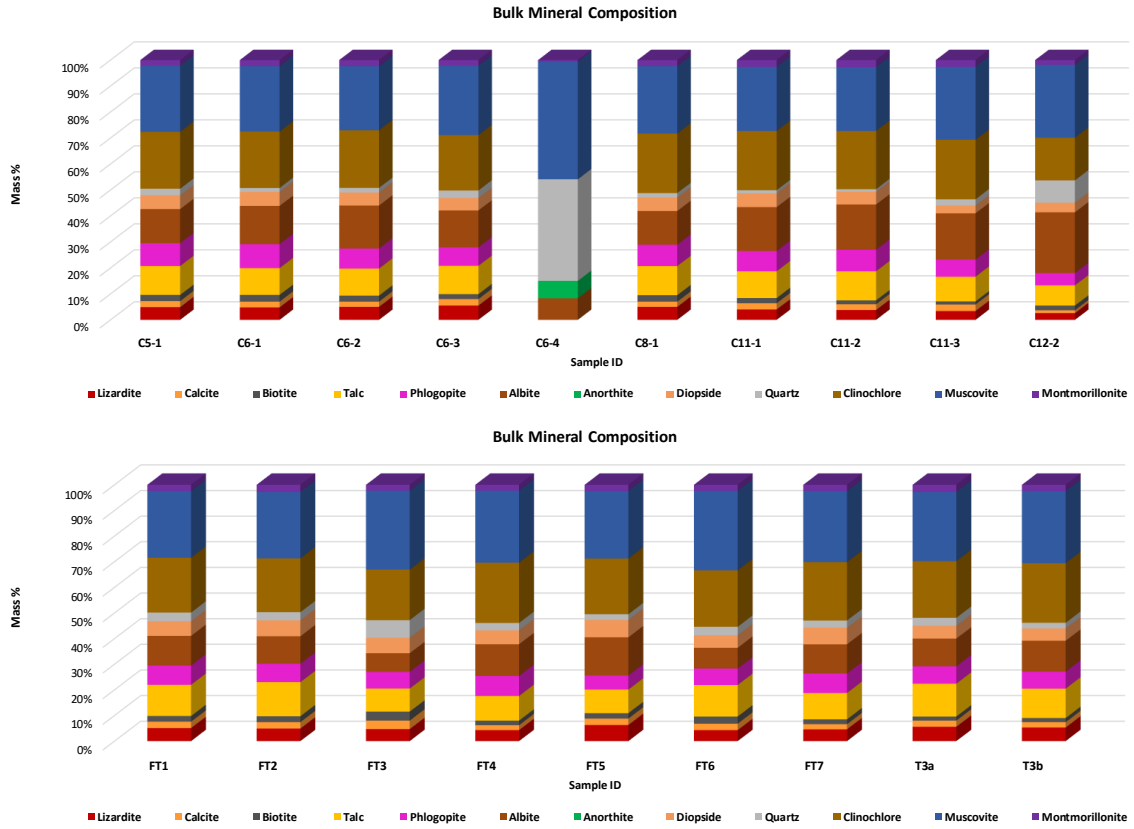

Sample ID	C5-1	C6-1	C6-2	C6-3	C6-4	C8-1	C11-1	C11-2	C11-3	C12-2	FT1	FT2	FT3	FT4	FT5	FT6	FT7	T3a	T3b
Lizardite	4.9	4.8	5	5.5	0	5	4	3.8	3.4	2.6	5.1	4.9	4.7	4.3	6.3	4.3	4.6	5.6	5.3
Calcite	2.3	2.2	2	2.5	0	2	2.4	2.2	2.5	1.1	2.5	2.5	3.3	1.9	2.5	2.5	2	2.4	2.1
Biotite	2.4	2.6	2.3	1.9	0	2.5	2	1.5	1.2	1.8	2.2	2.3	3.5	1.8	2.1	2.8	1.9	1.6	1.6
Talc	11.1	10.3	10.4	10.9	0	11.2	10.3	11.2	9.5	7.8	12.2	13.3	9	9.6	9.2	12.3	10.3	12.8	11.5
Phlogopite	8.8	9.2	7.7	7.1	0	8.2	7.8	8.3	6.6	4.7	7.5	7.2	6.5	7.8	5.5	6.4	7.6	6.8	6.6
Albite	13.1	14.7	16.5	14.2	8.3	13	16.9	17.4	17.8	23.4	11.6	10.7	7.3	12.4	14.9	8.1	11.4	10.8	12.1
Anorthite	0	0	0	0	6.7	0	0	0	0	0	0	0	0	0	0	0	0	0	0
Diopside	5.3	5.4	5	4.8	0	5.2	5.3	4.9	3	3.7	5.7	6.2	6	5.4	6.8	4.9	6.5	5	4.8
Quartz	2.5	1.5	1.8	2.9	39.1	1.7	1.2	1	2.4	8.6	3.4	3.2	6.9	2.9	2.2	3.3	2.8	3.1	2.2
Clinochlore	21.9	21.7	22.1	21.3	0	22.9	22.8	22.4	22.9	16.4	21.4	21	19.7	23.5	21.7	22	22.8	22.1	23.3
Muscovite	25.4	25.1	24.6	26.7	45.2	25.9	24.7	24.6	28.1	28	26	25.9	30.8	28.1	26.3	31	27.7	27	28.1
Montmorillonite	2.2	2.4	2.4	2.2	0.7	2.4	2.6	2.7	2.6	1.9	2.5	2.8	2.3	2.3	2.5	2.4	2.5	2.8	2.5
Total	100	100	100	100	100	100	100	100	100	100	100	100	100	100	100	100	100	100	100

FIGURE 7 SUMMARY OF MINERALOGY DETERMINED FROM XRD ANALYSIS.

The XRD analysis showed the mineralogy of all samples tested to be very similar, with the exception of C6/4, which is believed to represent the residual material underlying the dam wall. The bulk of the minerals are from the mica family and low-grade metamorphic products, which is to be expected given that the tailings originate from Kimberlite. Of the minerals, only Lizardite, talc and montmorrilonite classify as clay minerals. They represent respectively about 5%, 10% and 2.5% of the bulk of the tailings, which together, represents a significant clay component. This is of interest to take note of because clay minerals are subject to reorientation upon large shear displacements, resulting in the mobilisation of potentially low residual friction angle values.

3.4. Scanning electron microscopy

Scanning electron microscope (SEM) images were taken of the fine tailings to identify platy particles associated with the clay content of the material. At a magnification of 1000 times the tailings appear as agglomerations of finer particles (see Figure 8).

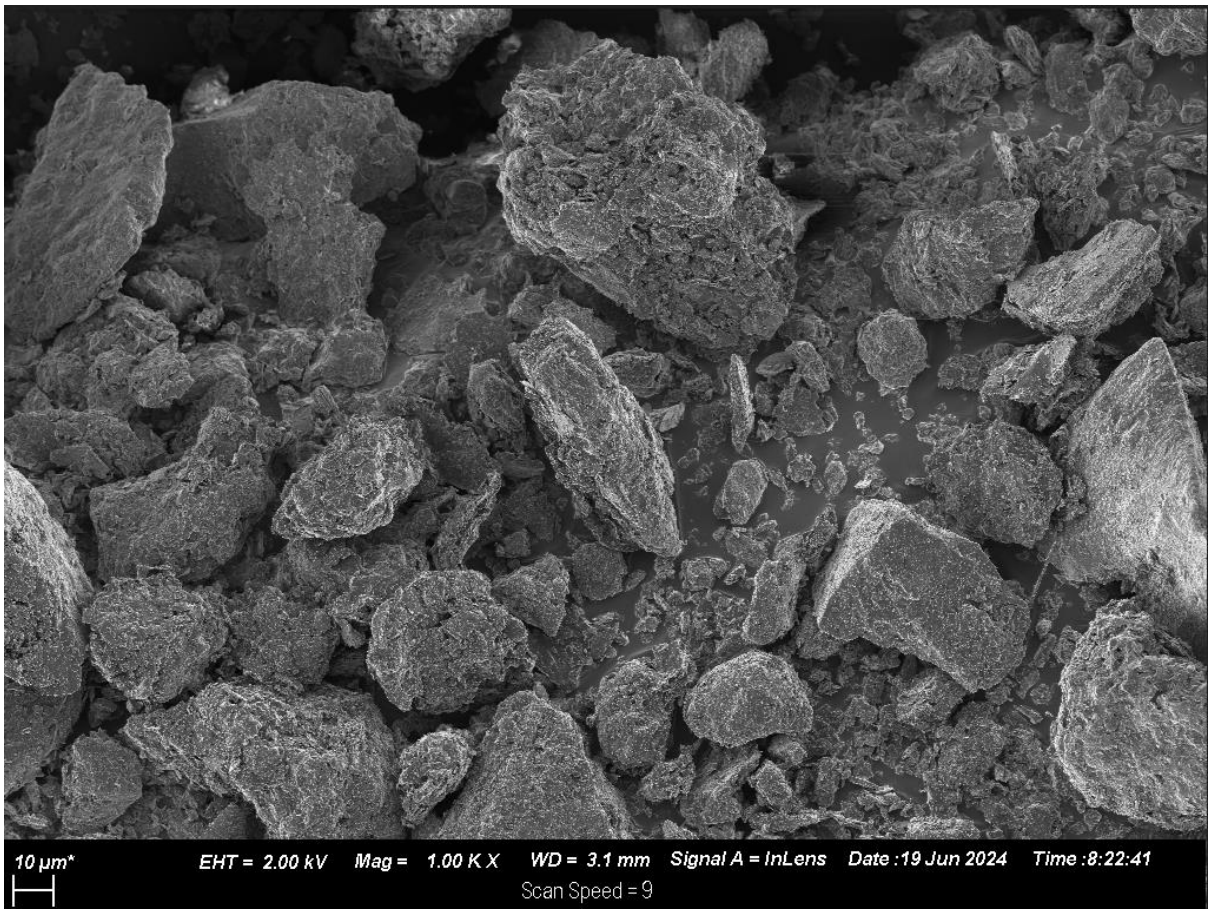

FIGURE 8 FINE TAILINGS MAGNIFIED 1000 TIMES SHOWING AGGLOMERATIONS OF PARTICLES.

At a magnification of 50 000 times platy minerals are clearly visible which may suggest that the material will be prone to developing low residual shear strengths associated with the reorientation of particles, given sufficient shear displacement (see Figure 9 and Figure 10).

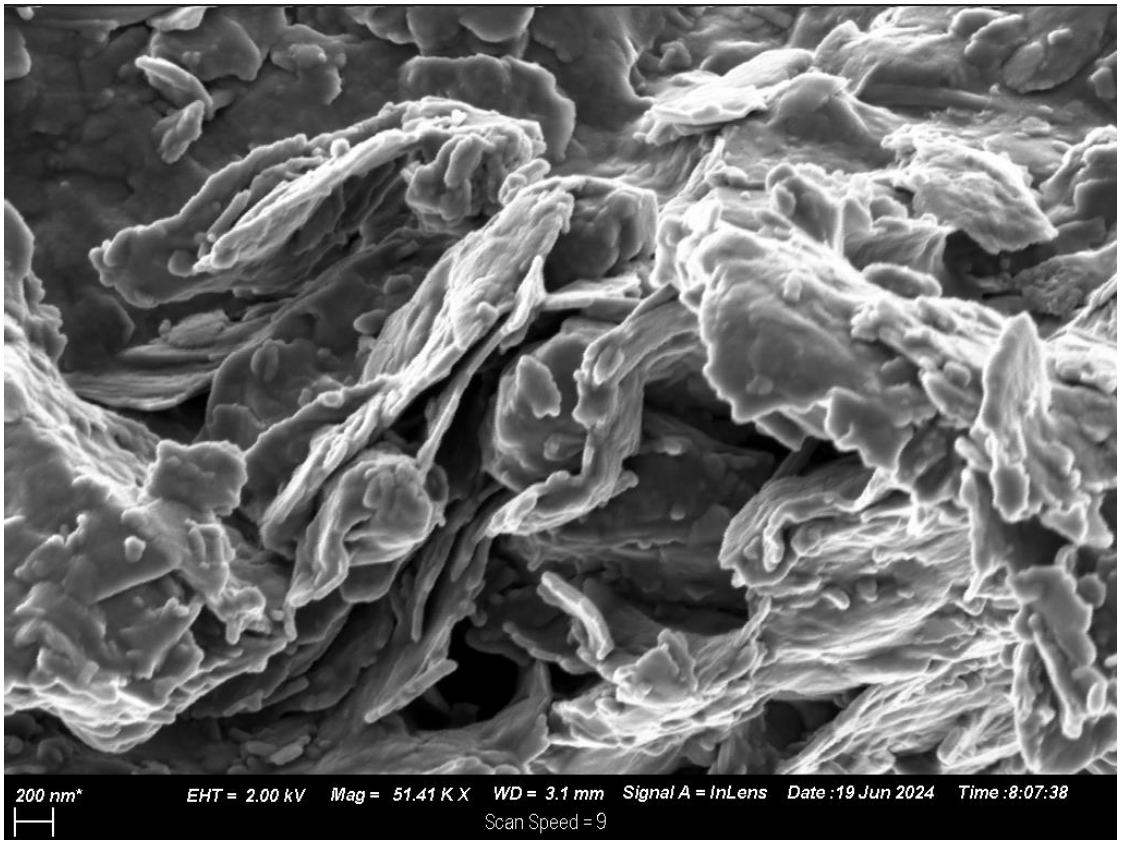

FIGURE 9 PLATY MINERALS VISIBLE AT 50 000 TIMES MAGNIFICATION.

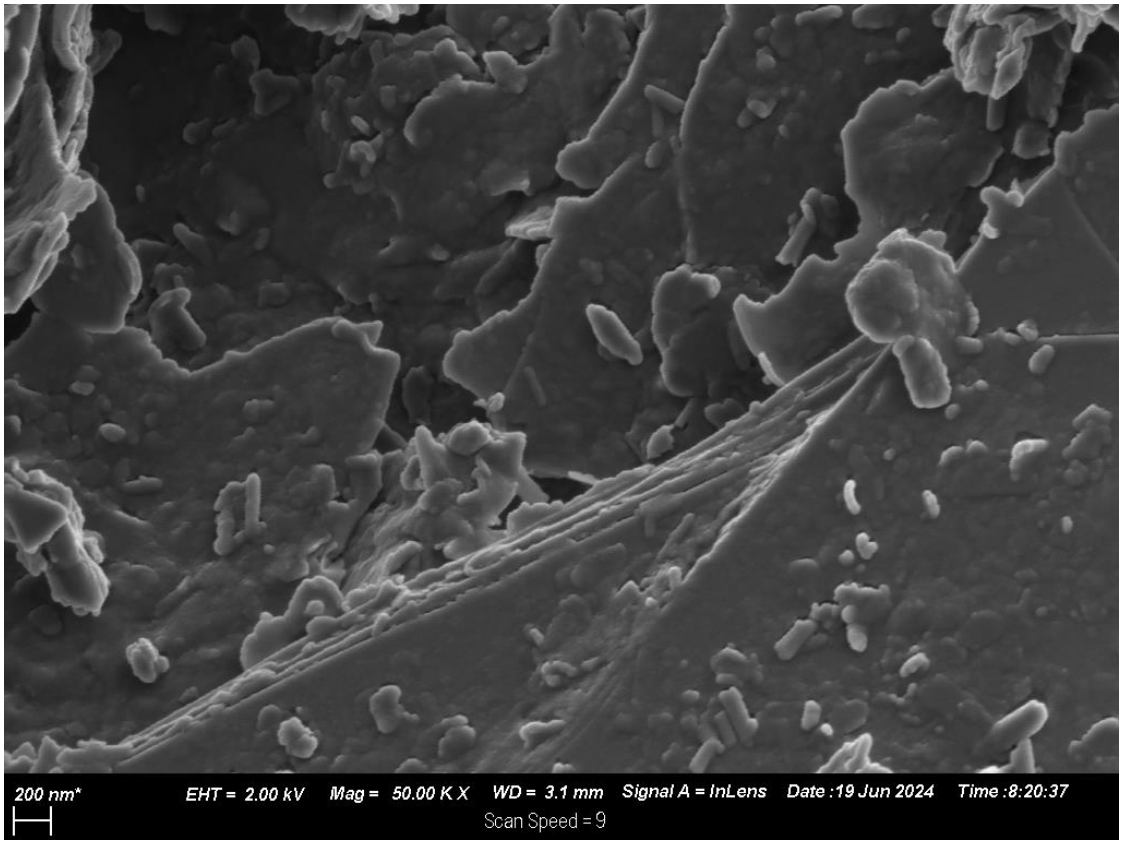

FIGURE 10 SECOND IMAGE OF PLATY MINERALS VISIBLE AT 50 000 TIMES MAGNIFICATION.

3.5. Shear strength

3.5.1. Triaxial and Direct Simple Shear tests

Robinson (2015) recommended friction angle values of 32° and 20° respectively for the coarse and fine tailings (i.e. grits and fines) at Jagersfontein. A limited number of triaxial tests were carried out on reconstituted samples of these materials. Course tailings sample G3 was selected and a sample of fine tailings was taken from the old De Beers Dam (T3a). A set of triaxial tests was carried out on the coarse and file tailings each, and the set of direct simple shear tests was carried out on the fine tailings sample.

The effective friction angles tabulated in Table 3 were measured and indicate that the friction angle values by Robinson (2015) were conservative. However, the high cohesion value of 20kPa was not. Effective stress paths for the three sets of tests are presented below and detailed results are appended.

TABLE 3 EFFECTIVE FRICTION ANGLES MEASURED FOR FINE AND COURSE TAILINGS.

Fine tailings		Course tailings
CU triaxial test a	DSS test	CU triaxial test
26.5°	22.5°	38.7°

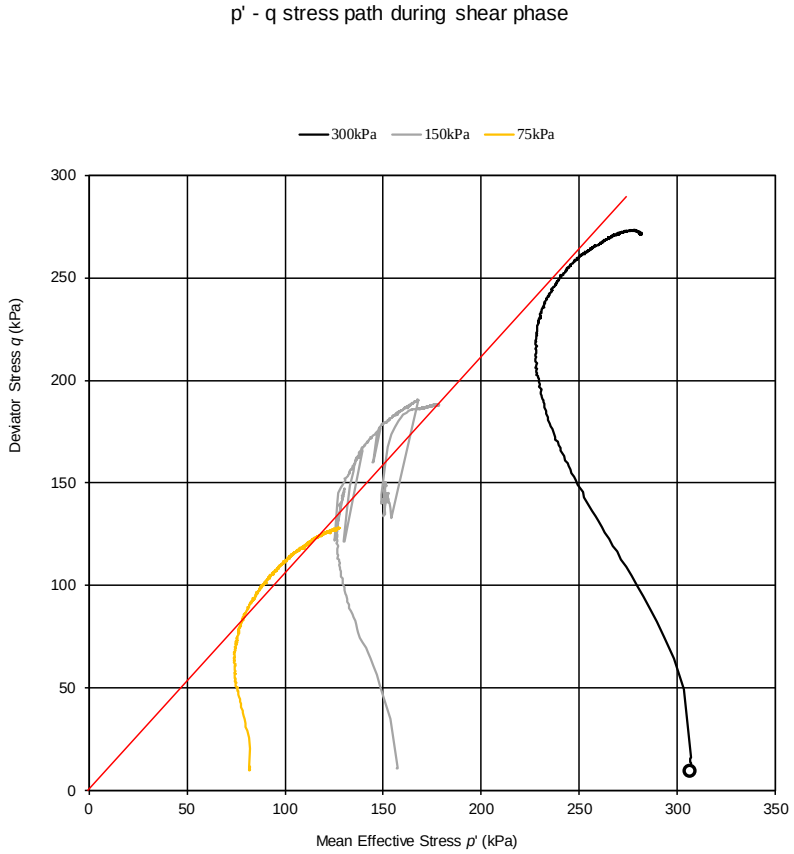

FIGURE 11 P-Q STRESS PATHS FROM CU TRIAXIAL TESTS ON FINE TAILINGS SUGGESTING AN EFFECTIVE FRICTION ANGLE OF 26°.

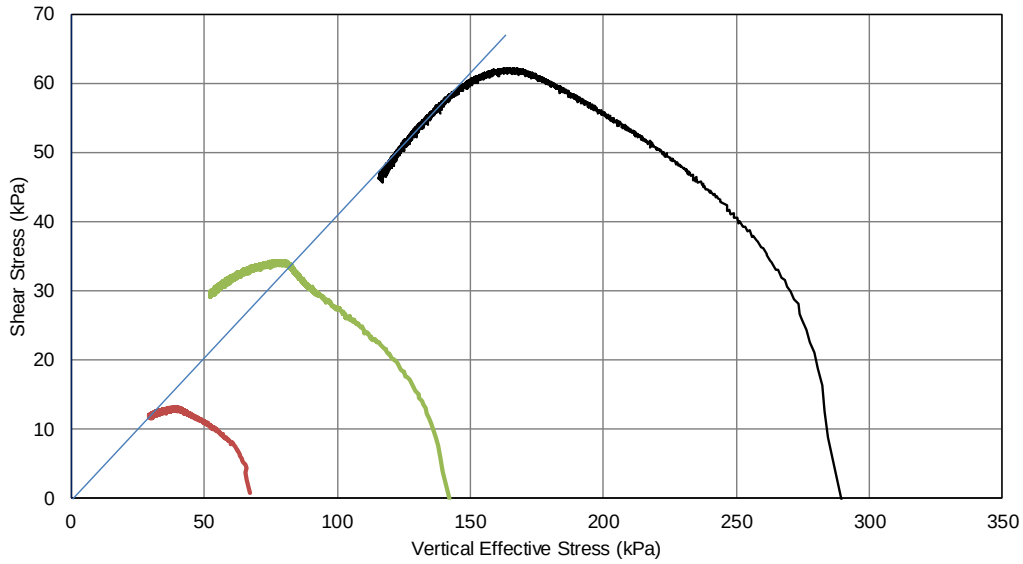

FIGURE 12 SHEAR STRESS – NORMAL STRESS STRESS PATHS FOR UNDRAINED DIRECT SIMPLE SHEAR TESTS ON FINE TAILINGS SUGGESTION AN EFFECTIVE FRICTION ANGLE OF 22.5°.

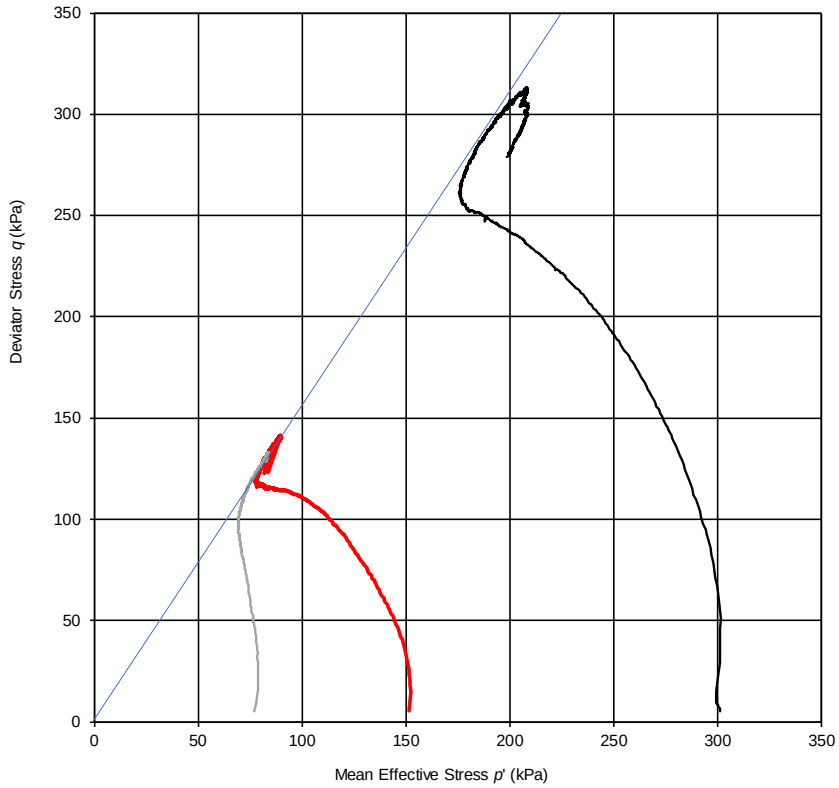

FIGURE 13 P-Q STRESS PATHS FROM CU TRIAXIAL TESTS ON COARSE TAILINGS SUGGESTING AN EFFECTIVE FRICTION ANGLE OF 38.7°.

Monotonic Direct Simple Shear Test Report - Consolidated Undrained

UNIVERSITEIT VAN PRETORIA
UNIVERSITY OF PRETORIA
YUNIBESITHI YA PRETORIA

Client:	UP	**Date:**	08/05/2024
Address:	-	**Project No.:**	24-UP-02
Project:	Jagersfontein	**Sample ID:**	-
Location:	-	**SG:**	2.65

Effective Vertical Stress (kPa)	75.00	Initial Void Ratio (e)	0.91
Diameter (mm)	70.00	Final Void Ratio (e)	0.76
Shearing Height (mm)	23.81	Initial Dry Density (t/m^3)	1.39
Shearing Strain Rate (mm/min)	0.020	Final Dry Density (t/m^3)	1.51

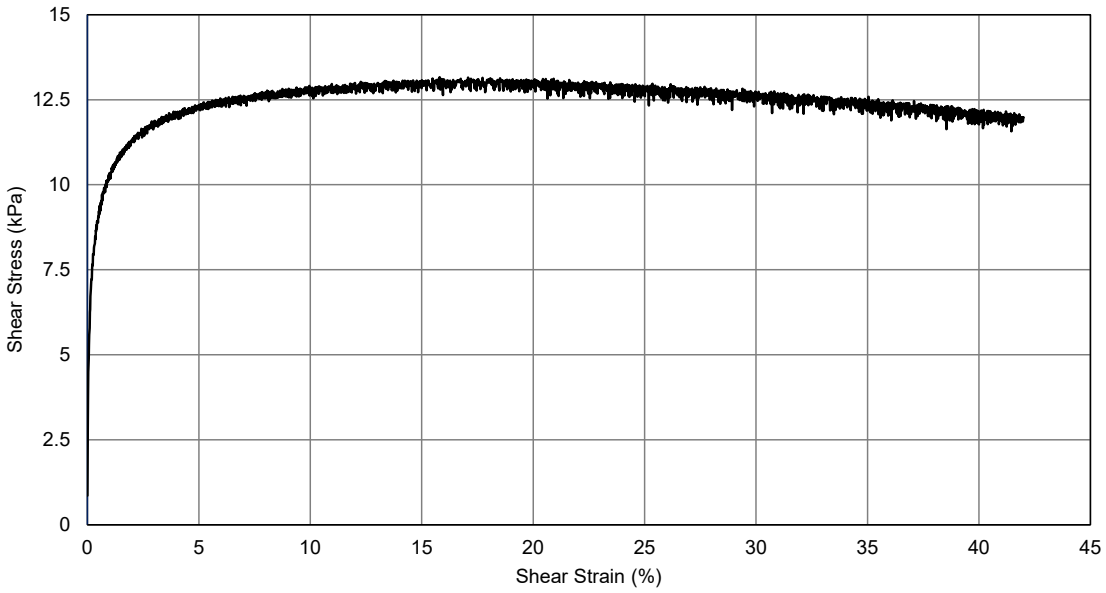

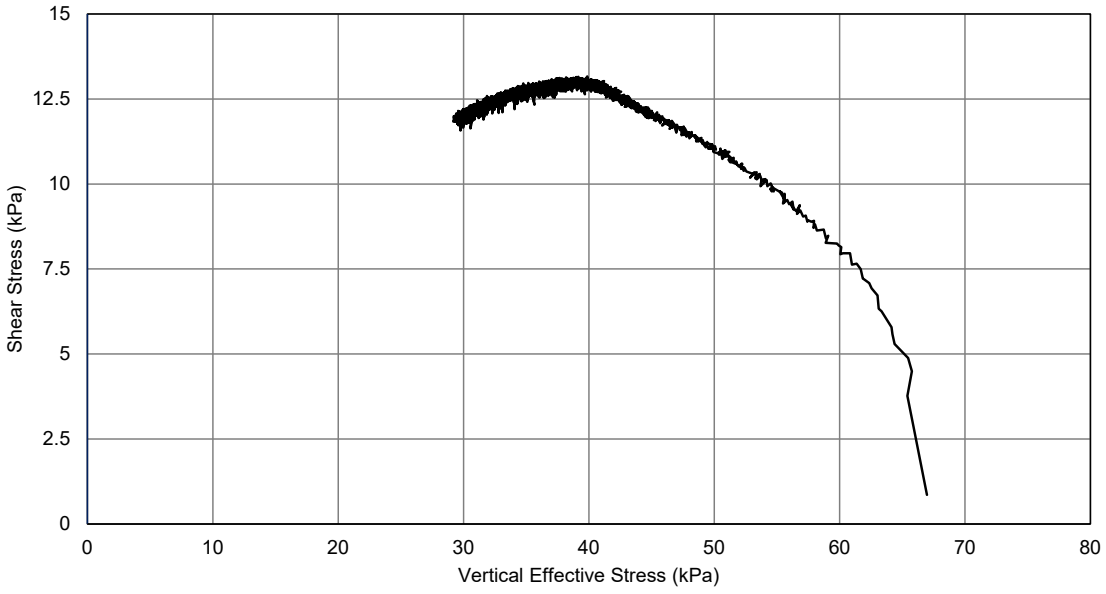

Preparation Notes:	Remolded sample	Tested by:	V.Venter
		Reviewed by:	SW. Jacobsz

THIS DOCUMENT SHALL ONLY BE REPRODUCED IN FULL

Monotonic Direct Simple Shear Test Report - Consolidated Undrained

UNIVERSITEIT VAN PRETORIA
UNIVERSITY OF PRETORIA
YUNIBESITHI YA PRETORIA

Client:	UP	**Date:**	08/05/2024
Address:	-	**Project No.:**	24-UP-02
Project:	Jagersfontein	**Sample ID:**	-
Location:	-	**SG:**	2.65

Effective Vertical Stress (kPa)	150.00	Initial Void Ratio (e)	0.88
Diameter (mm)	70.00	Final Void Ratio (e)	0.71
Shearing Height (mm)	24.02	Initial Dry Density (t/m^3)	1.41
Shearing Strain Rate (mm/min)	0.020	Final Dry Density (t/m^3)	1.55

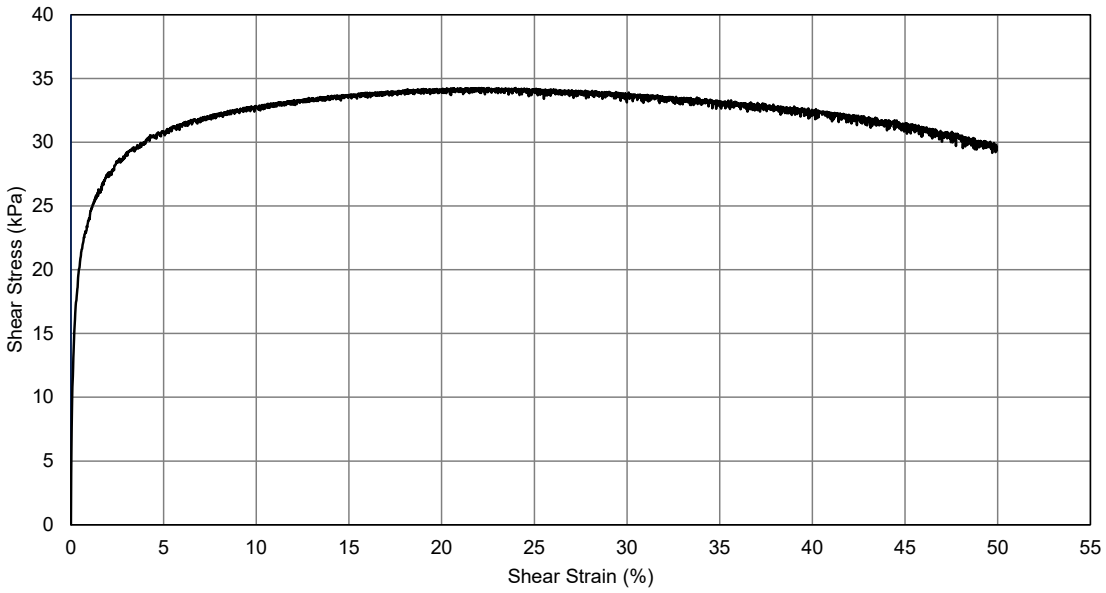

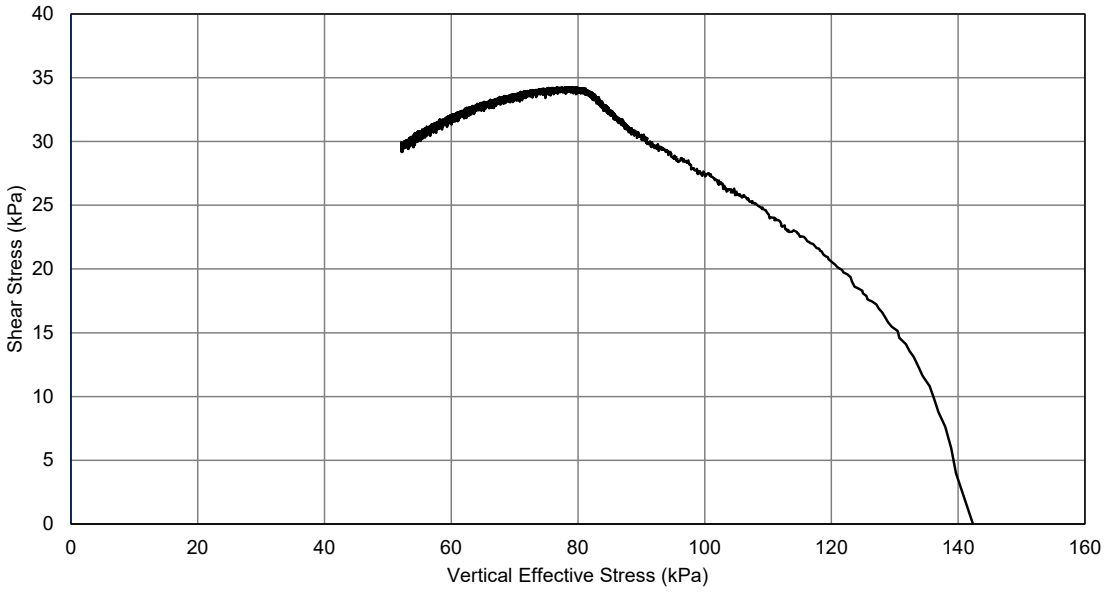

Preparation Notes:	Remolded sample	Tested by:	V.Venter
		Reviewed by:	SW. Jacobsz

THIS DOCUMENT SHALL ONLY BE REPRODUCED IN FULL

Monotonic Direct Simple Shear Test Report - Consolidated Undrained

UNIVERSITEIT VAN PRETORIA
UNIVERSITY OF PRETORIA
YUNIBESITHI YA PRETORIA

Client:	UP	**Date:**	08/05/2024
Address:	-	**Project No.:**	24-UP-02
Project:	Jagersfontein	**Sample ID:**	-
Location:	-	**SG:**	2.65

Effective Vertical Stress (kPa)	150.00	Initial Void Ratio (e)	0.93
Diameter (mm)	70.00	Final Void Ratio (e)	0.59
Shearing Height (mm)	21.22	Initial Dry Density (t/m^3)	1.37
Shearing Strain Rate (mm/min)	0.018	Final Dry Density (t/m^3)	1.67

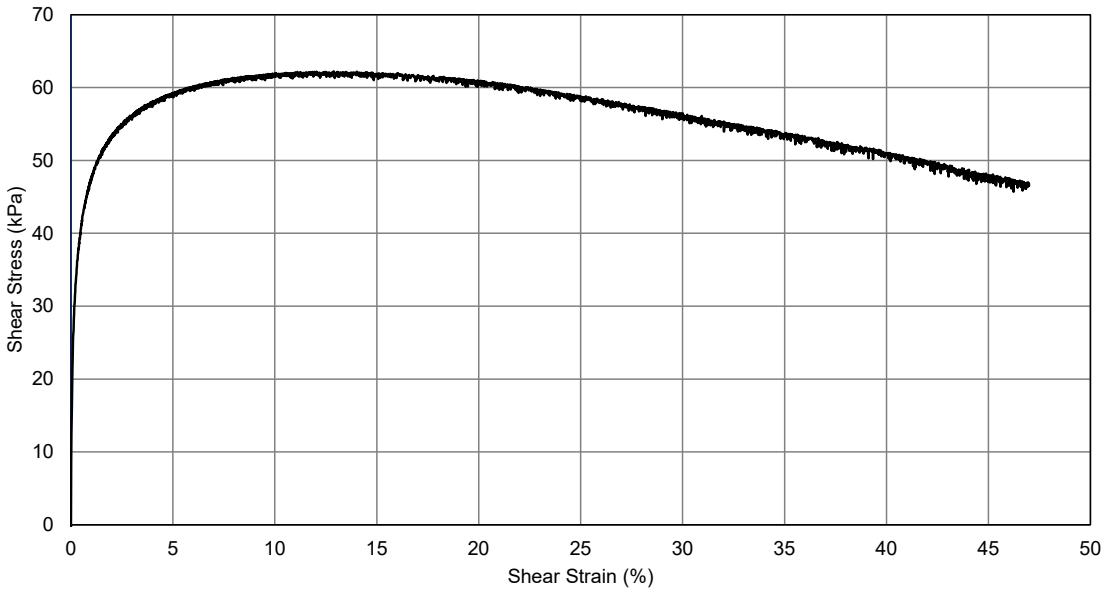

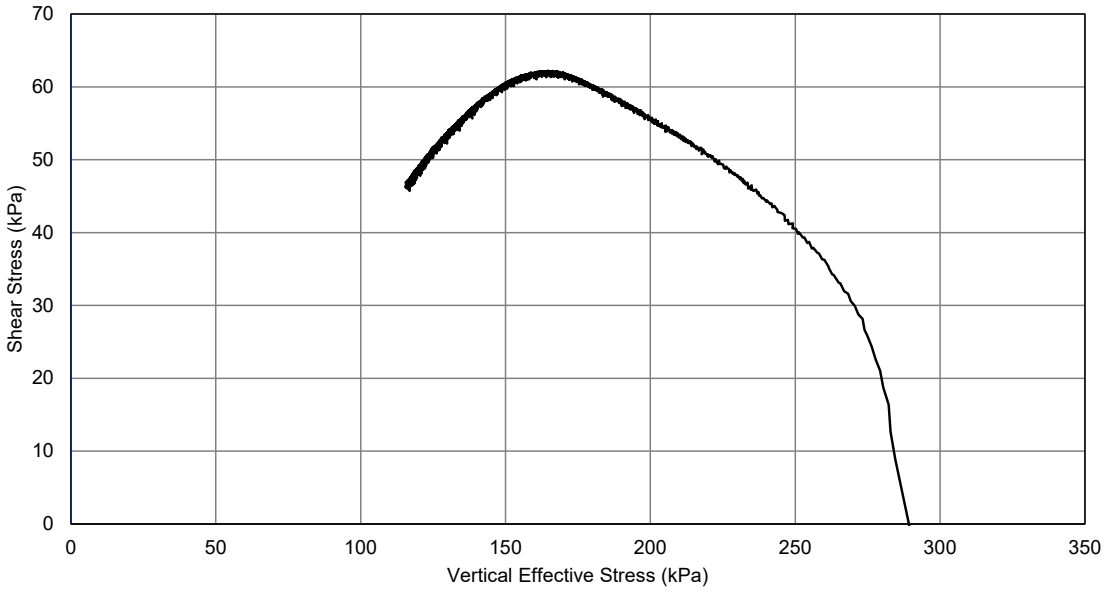

Preparation Notes:	Remolded sample	Tested by:	V.Venter
		Reviewed by:	SW. Jacobsz

THIS DOCUMENT SHALL ONLY BE REPRODUCED IN FULL

Monotonic Direct Simple Shear Test Report - Consolidated Undrained

UNIVERSITEIT VAN PRETORIA
UNIVERSITY OF PRETORIA
YUNIBESITHI YA PRETORIA

Client:	UP	**Date:**	2024/07/05
Address:	-	**Project No.:**	24-UP-02
Project:	Jagersfontein	**Sample ID:**	-
Location:	-	**SG:**	2.65

Effective Vertical Stress (kPa)	150.00	Initial Void Ratio (e)	0.93
Diameter (mm)	70.00	Final Void Ratio (e)	0.59
Shearing Height (mm)	21.22	Initial Dry Density (t/m^3)	1.37
Shearing Strain Rate (mm/min)	0.018	Final Dry Density (t/m^3)	1.67

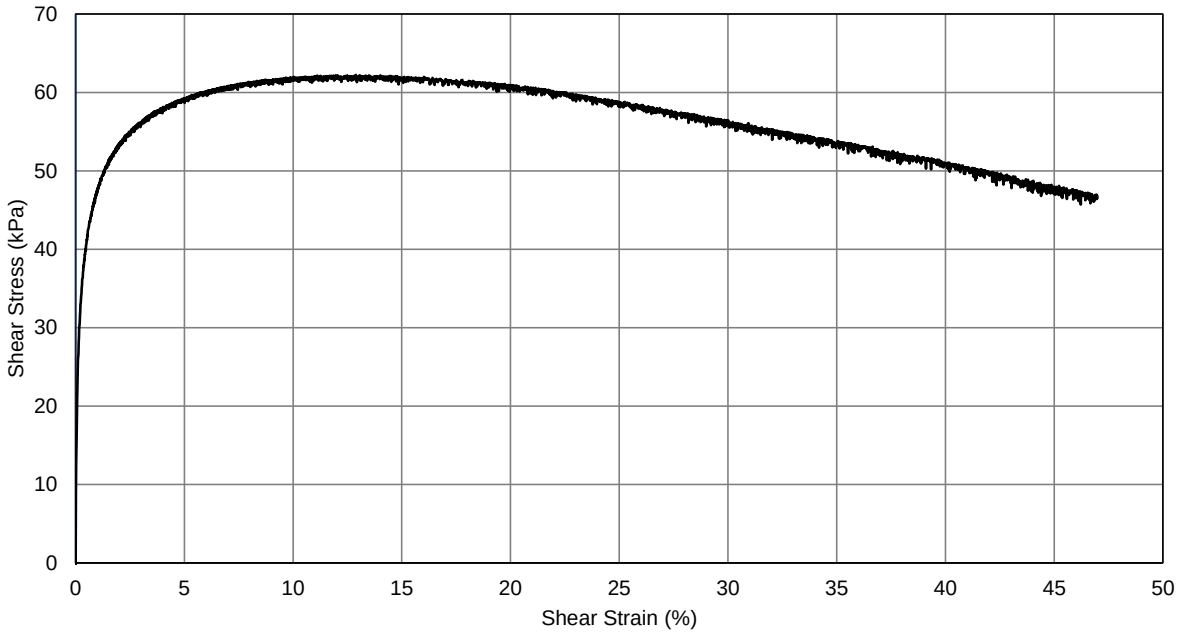

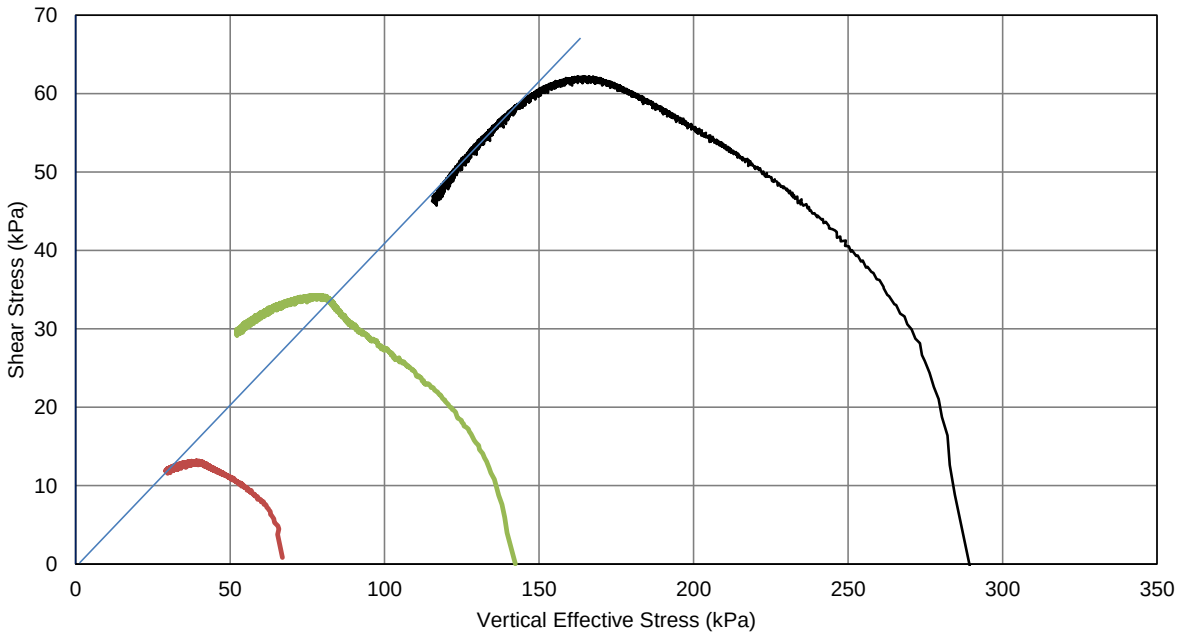

Preparation Notes:	Remolded sample	Tested by:	V.Venter
		Reviewed by:	SW. Jacobsz

THIS DOCUMENT SHALL ONLY BE REPRODUCED IN FULL

Consolidated Undrained Triaxial Report

UNIVERSITEIT VAN PRETORIA
UNIVERSITY OF PRETORIA
YUNIBESITHI YA PRETORIA

Client:	UP		
Address:	-		
Project:	Jagersfontein		
Location:	-		
Date:	2024/07/05		
Project No.:	1		
Sample ID:	Gravel 3		
Test ID:	TX4-CIU-75kPa		
Tested by:	M. Rammala	**Reviewed by:**	V. Venter

Initial Height (mm):	140.2	Final Moisture Content (%):	22.4%	Strain Rate (mm/min):	0.047
Initial Diameter (mm):	70.3	Final Dry Density (t/m^3):	1.66	B Response (%):	99%
Initial Moisture content (%):	6.8%	Final Void Ratio (-):	0.59	Mean Effective Consolidation Stress (kPa):	77
Initial Dry Density (t/m^3):	1.64	Specific Gravity	2.65	Geostatic Stress Ratio K_0 (-):	0.94
Method for Sample Area:	End of Test			Area Correction:	Right Cylindrical
Preparation Notes:	Sample was moist tamped to specific density				

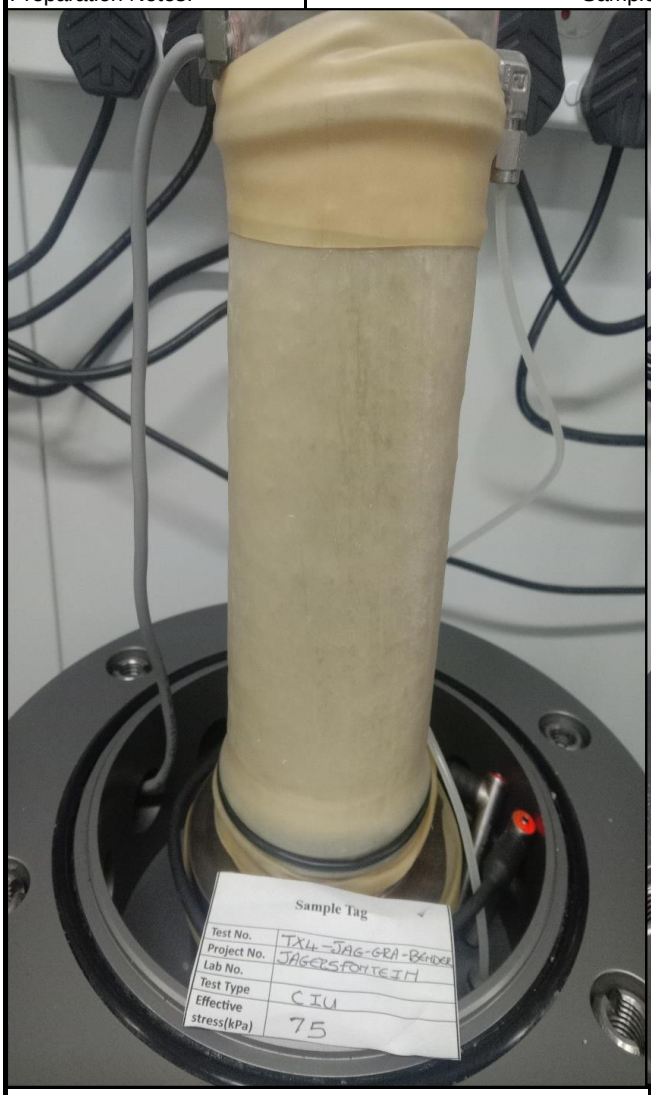

Sample Before Test

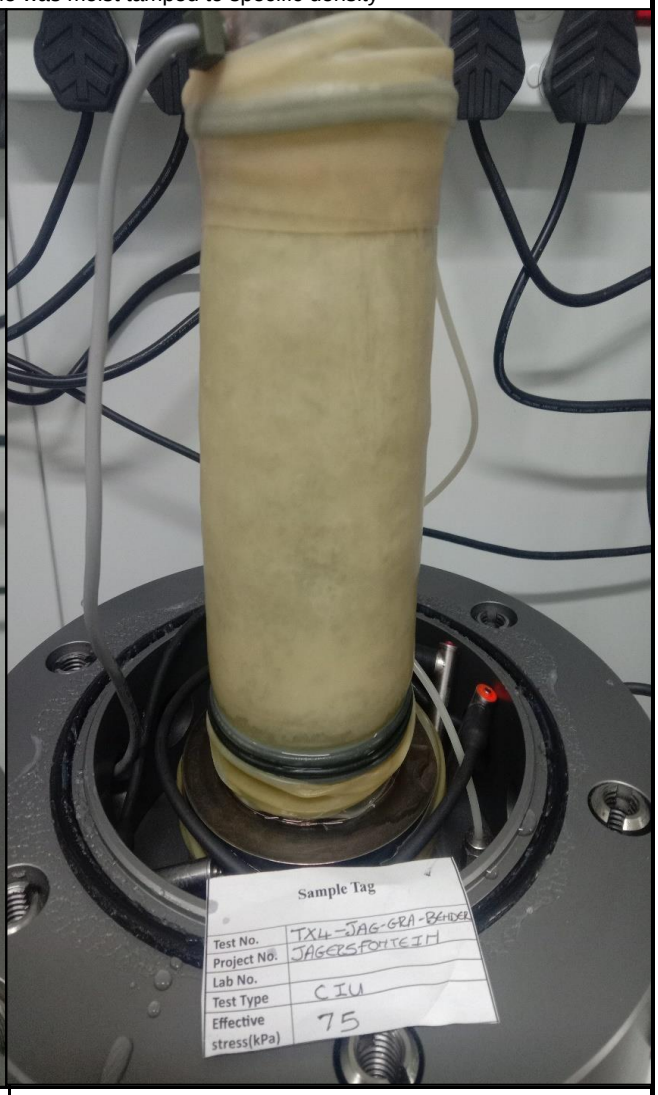

Sample After Test

Consolidated Undrained Triaxial Report

UNIVERSITEIT VAN PRETORIA
UNIVERSITY OF PRETORIA
YUNIBESITHI YA PRETORIA

Client:	UP
Address:	-
Project:	Jagersfontein
Location:	-
Date:	2024/07/05
Project No.:	1
Sample ID:	Gravel 3
Test ID:	TX4-CIU-75kPa
Tested by:	M. Rammala **Reviewed by:** V. Venter

Initial Height (mm):	140.2	Final Moisture Content (%):	22.4%	Strain Rate (mm/min):	0.047
Initial Diameter (mm):	70.3	Final Dry Density (t/m^3):	1.66	B Response (%):	99%
Initial Moisture content (%):	6.8%	Final Void Ratio (-):	0.59	Mean Effective Consolidation Stress (kPa):	77
Initial Dry Density (t/m^3):	1.64	Specific Gravity	2.65	Geostatic Stress Ratio K_0 (-):	0.94
Method for Sample Area:	End of Test		Area Correction:	Right Cylindrical	
Preparation Notes:	Sample was moist tamped to specific density				

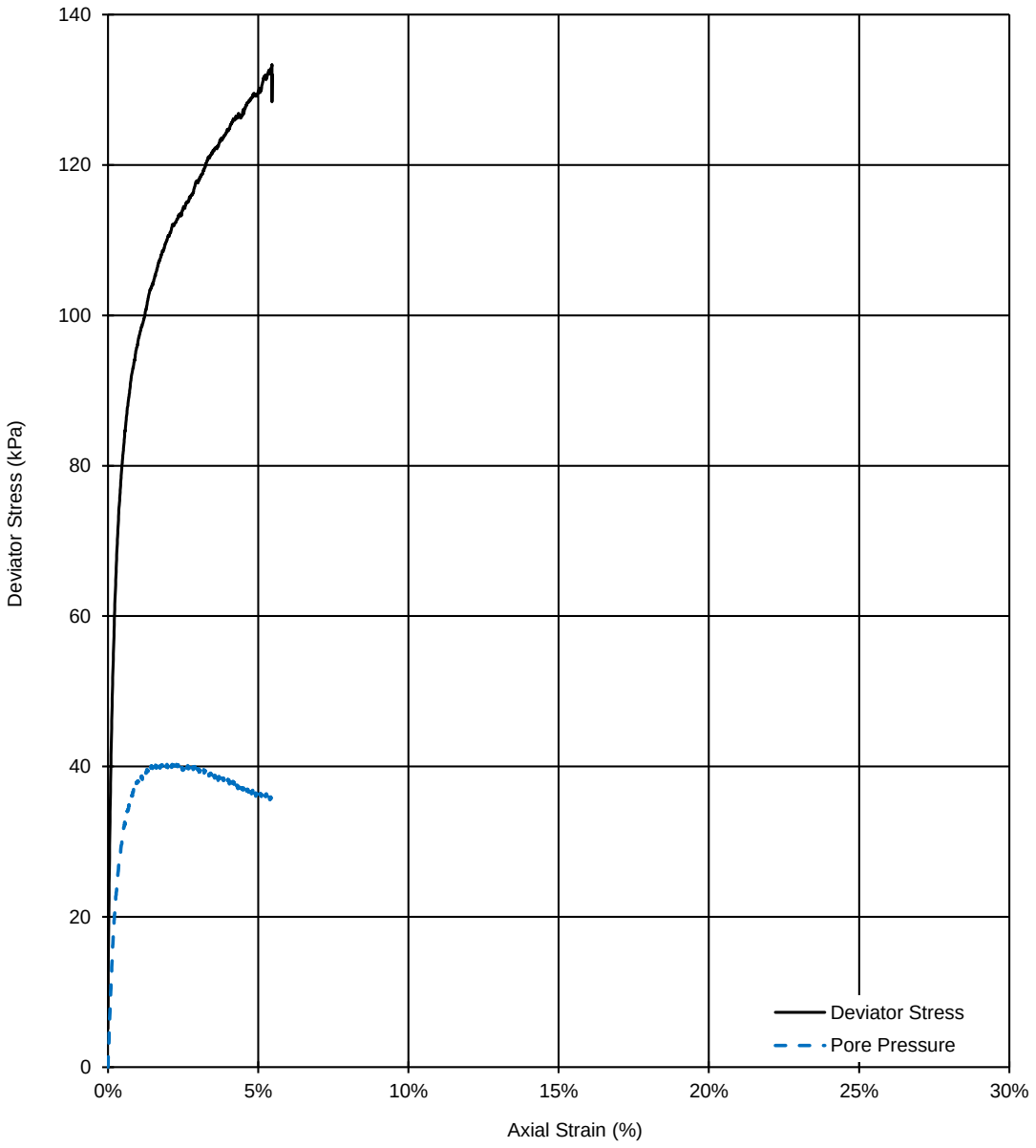

Preparation Notes:	Sample was moist tamped to specific density	Tested by:	M. Rammala
		Reviewed by:	V. Venter

THIS DOCUMENT SHALL ONLY BE REPRODUCED IN FULL

Consolidated Undrained Triaxial Report

UNIVERSITEIT VAN PRETORIA
UNIVERSITY OF PRETORIA
YUNIBESITHI YA PRETORIA

Client:	UP
Address:	-
Project:	Jagersfontein
Location:	-
Date:	2024/07/05
Project No.:	1
Sample ID:	Gravel 3
Test ID:	TX4-CIU-75kPa
Tested by:	M. Rammala **Reviewed by:** V. Venter

Initial Height (mm):	140.2	Final Moisture Content (%):	22.4%	Strain Rate (mm/min):	0.047
Initial Diameter (mm):	70.3	Final Dry Density (t/m^3):	1.66	B Response (%):	99%
Initial Moisture content (%):	6.8%	Final Void Ratio (-):	0.59	Mean Effective Consolidation Stress (kPa):	77
Initial Dry Density (t/m^3):	1.64	Specific Gravity	2.65	Geostatic Stress Ratio K_0 (-):	0.94
Method for Sample Area:	End of Test		Area Correction:	Right Cylindrical	
Preparation Notes:	Sample was moist tamped to specific density				

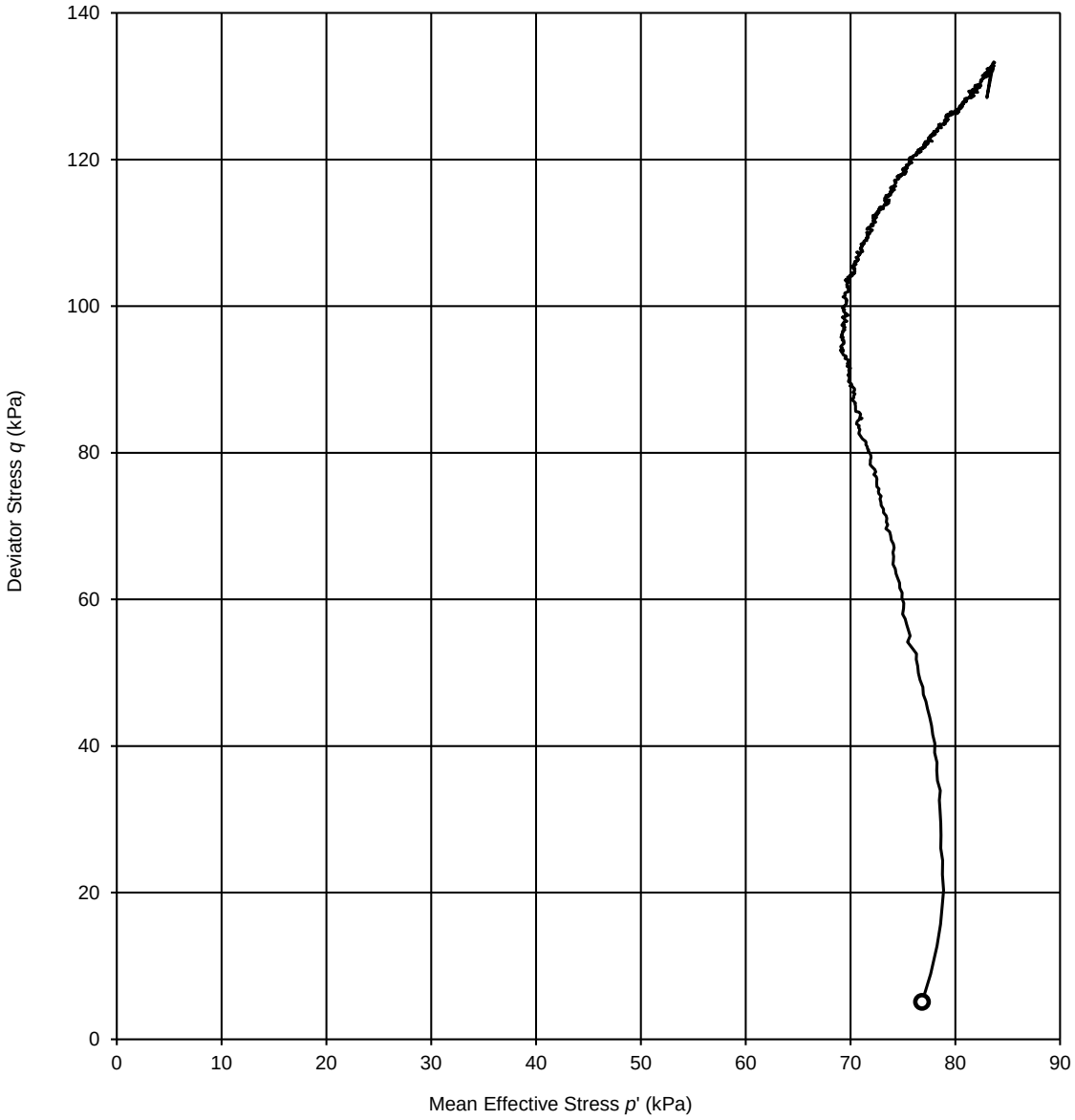

Preparation Notes:	Sample was moist tamped to specific density	Tested by:	M. Rammala
		Reviewed by:	V. Venter

THIS DOCUMENT SHALL ONLY BE REPRODUCED IN FULL

Consolidated Undrained Triaxial Report

UNIVERSITEIT VAN PRETORIA
UNIVERSITY OF PRETORIA
YUNIBESITHI YA PRETORIA

Client:	UP
Address:	-
Project:	Jagersfontein
Location:	-
Date:	2024/07/05
Project No.:	1
Sample ID:	Gravel 3
Test ID:	TX4-CIU-75kPa
Tested by:	M. Rammala **Reviewed by:** V. Venter

Initial Height (mm):	140.2	Final Moisture Content (%):	22.4%	Strain Rate (mm/min):	0.047
Initial Diameter (mm):	70.3	Final Dry Density (t/m^3):	1.66	B Response (%):	99%
Initial Moisture content (%):	6.8%	Final Void Ratio (-):	0.59	Mean Effective Consolidation Stress (kPa):	77
Initial Dry Density (t/m^3):	1.64	Specific Gravity	2.65	Geostatic Stress Ratio K_0 (-):	0.94
Method for Sample Area:	End of Test		Area Correction:	Right Cylindrical	
Preparation Notes:	Sample was moist tamped to specific density				

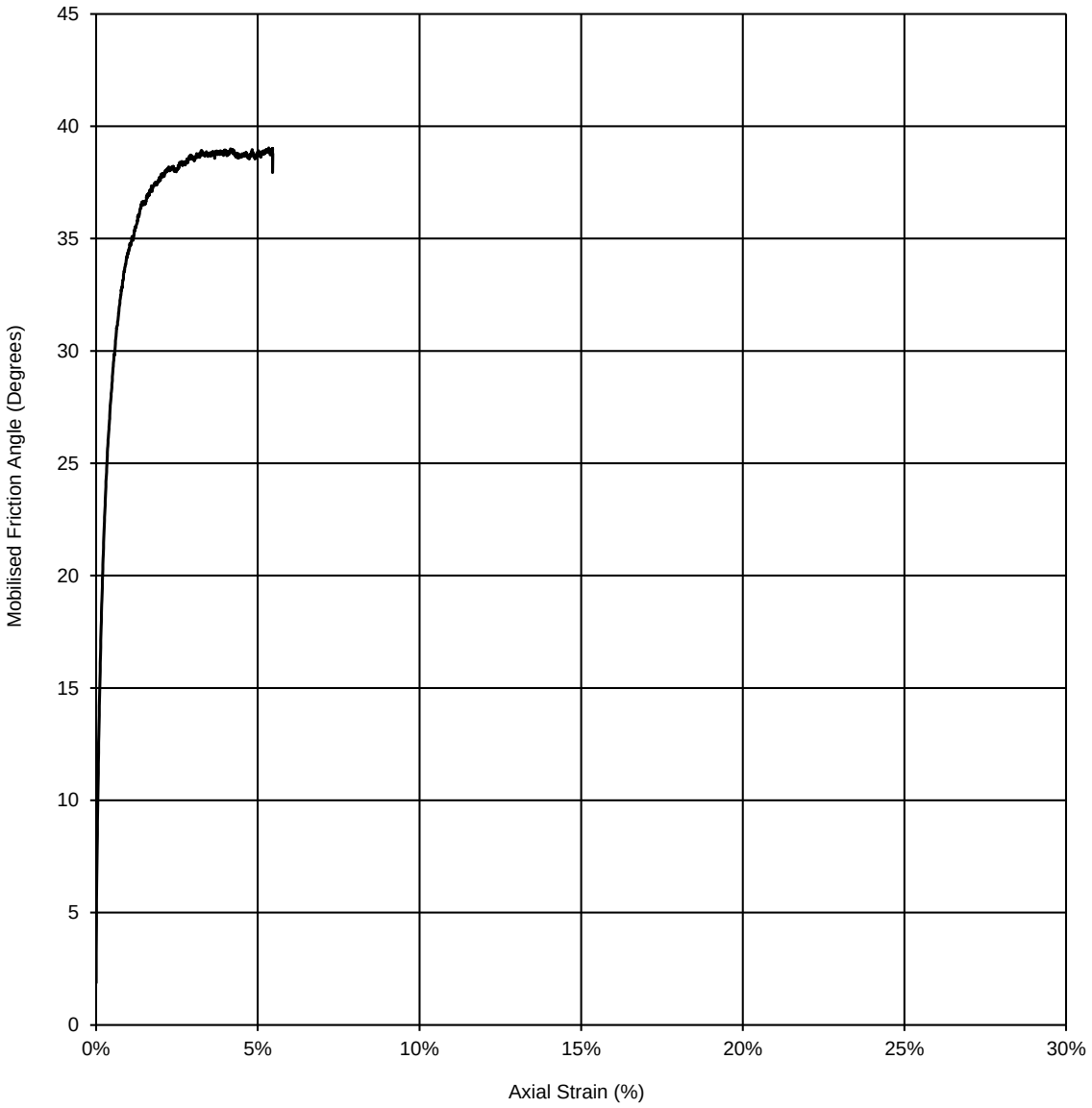

Preparation Notes:	Sample was moist tamped to specific density	Tested by:	M. Rammala
		Reviewed by:	V. Venter

THIS DOCUMENT SHALL ONLY BE REPRODUCED IN FULL

Consolidated Undrained Triaxial Report

UNIVERSITEIT VAN PRETORIA
UNIVERSITY OF PRETORIA
YUNIBESITHI YA PRETORIA

Client:	UP		
Address:	-		
Project:	Jagersfontein		
Location:	-		
Date:	2024/07/05		
Project No.:	1		
Sample ID:	Gravel 3		
Test ID:	TX3-CIU-150kPa		
Tested by:	M. Rammala	**Reviewed by:**	V. Venter

Initial Height (mm):	140.2	Final Moisture Content (%):	20.2%	Strain Rate (mm/min):	0.046
Initial Diameter (mm):	70.6	Final Dry Density (t/m^3):	1.73	B Response (%):	100%
Initial Moisture content (%):	6.6%	Final Void Ratio (-):	0.53	Mean Effective Consolidation Stress (kPa):	152
Initial Dry Density (t/m^3):	1.54	Specific Gravity	2.65	Geostatic Stress Ratio K_0 (-):	0.96
Method for Sample Area:	End of Test			Area Correction:	Right Cylindrical
Preparation Notes:	Sample was moist tamped to specific density				

Sample Before Test

Sample After Test

Consolidated Undrained Triaxial Report

UNIVERSITEIT VAN PRETORIA
UNIVERSITY OF PRETORIA
YUNIBESITHI YA PRETORIA

Client:	UP		
Address:	-		
Project:	Jagersfontein		
Location:	-		
Date:	2024/07/05		
Project No.:	1		
Sample ID:	Gravel 3		
Test ID:	TX3-CIU-150kPa		
Tested by:	M. Rammala	**Reviewed by:**	V. Venter

Initial Height (mm):	140.2	Final Moisture Content (%):	20.2%	Strain Rate (mm/min):	0.046
Initial Diameter (mm):	70.6	Final Dry Density (t/m^3):	1.73	B Response (%):	100%
Initial Moisture content (%):	6.6%	Final Void Ratio (-):	0.53	Mean Effective Consolidation Stress (kPa):	152
Initial Dry Density (t/m^3):	1.54	Specific Gravity	2.65	Geostatic Stress Ratio K_0 (-):	0.96
Method for Sample Area:	End of Test		Area Correction:	Right Cylindrical	
Preparation Notes:	Sample was moist tamped to specific density				

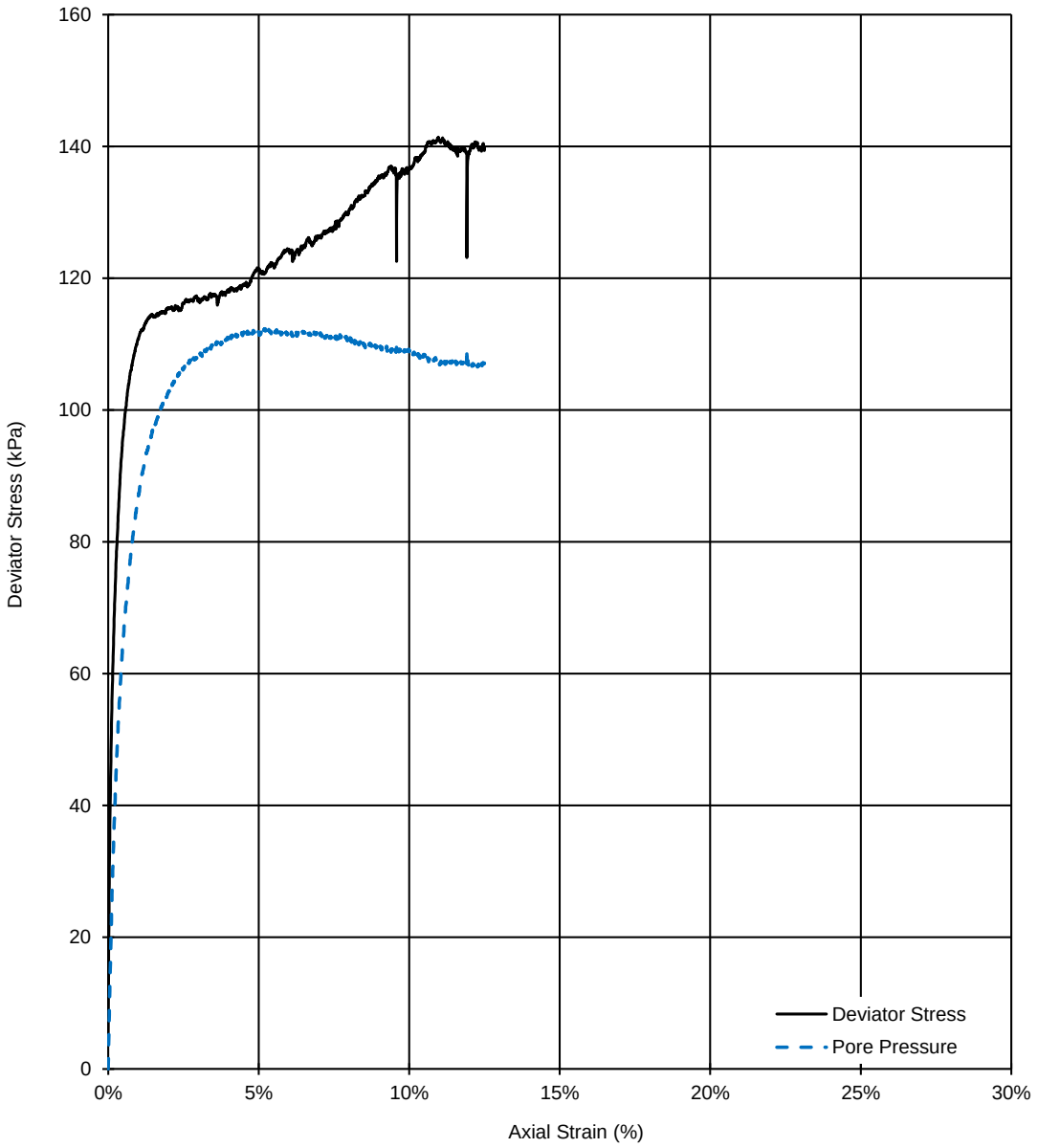

Preparation Notes:	Sample was moist tamped to specific density	Tested by:	M. Rammala
		Reviewed by:	V. Venter

THIS DOCUMENT SHALL ONLY BE REPRODUCED IN FULL

Consolidated Undrained Triaxial Report

UNIVERSITEIT VAN PRETORIA
UNIVERSITY OF PRETORIA
YUNIBESITHI YA PRETORIA

Client:	UP
Address:	-
Project:	Jagersfontein
Location:	-
Date:	2024/07/05
Project No.:	1
Sample ID:	Gravel 3
Test ID:	TX3-CIU-150kPa
Tested by:	M. Rammala
Reviewed by:	V. Venter

Initial Height (mm):	140.2	Final Moisture Content (%):	20.2%	Strain Rate (mm/min):	0.046
Initial Diameter (mm):	70.6	Final Dry Density (t/m^3):	1.73	B Response (%):	100%
Initial Moisture content (%):	6.6%	Final Void Ratio (-):	0.53	Mean Effective Consolidation Stress (kPa):	152
Initial Dry Density (t/m^3):	1.54	Specific Gravity	2.65	Geostatic Stress Ratio K_0 (-):	0.96
Method for Sample Area:	End of Test		Area Correction:	Right Cylindrical	
Preparation Notes:	Sample was moist tamped to specific density				

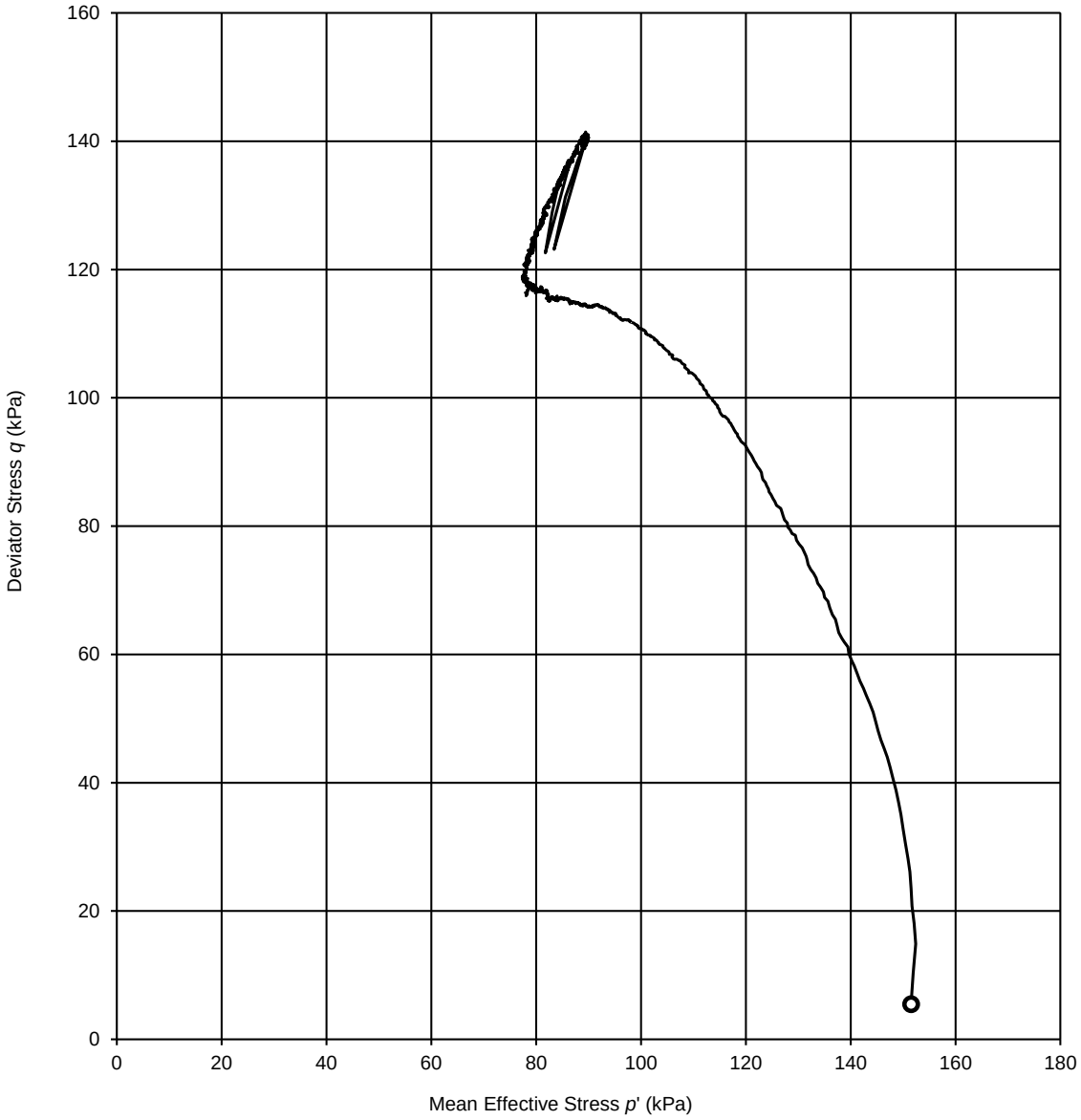

Preparation Notes:	Sample was moist tamped to specific density	Tested by:	M. Rammala
		Reviewed by:	V. Venter

THIS DOCUMENT SHALL ONLY BE REPRODUCED IN FULL

Consolidated Undrained Triaxial Report

UNIVERSITEIT VAN PRETORIA
UNIVERSITY OF PRETORIA
YUNIBESITHI YA PRETORIA

Client:	UP
Address:	-
Project:	Jagersfontein
Location:	-
Date:	2024/07/05
Project No.:	1
Sample ID:	Gravel 3
Test ID:	TX3-CIU-150kPa
Tested by:	M. Rammala **Reviewed by:** V. Venter

Initial Height (mm):	140.2	Final Moisture Content (%):	20.2%	Strain Rate (mm/min):	0.046
Initial Diameter (mm):	70.6	Final Dry Density (t/m^3):	1.73	B Response (%):	100%
Initial Moisture content (%):	6.6%	Final Void Ratio (-):	0.53	Mean Effective Consolidation Stress (kPa):	152
Initial Dry Density (t/m^3):	1.54	Specific Gravity	2.65	Geostatic Stress Ratio K_0 (-):	0.96
Method for Sample Area:	End of Test		Area Correction:	Right Cylindrical	
Preparation Notes:	Sample was moist tamped to specific density				

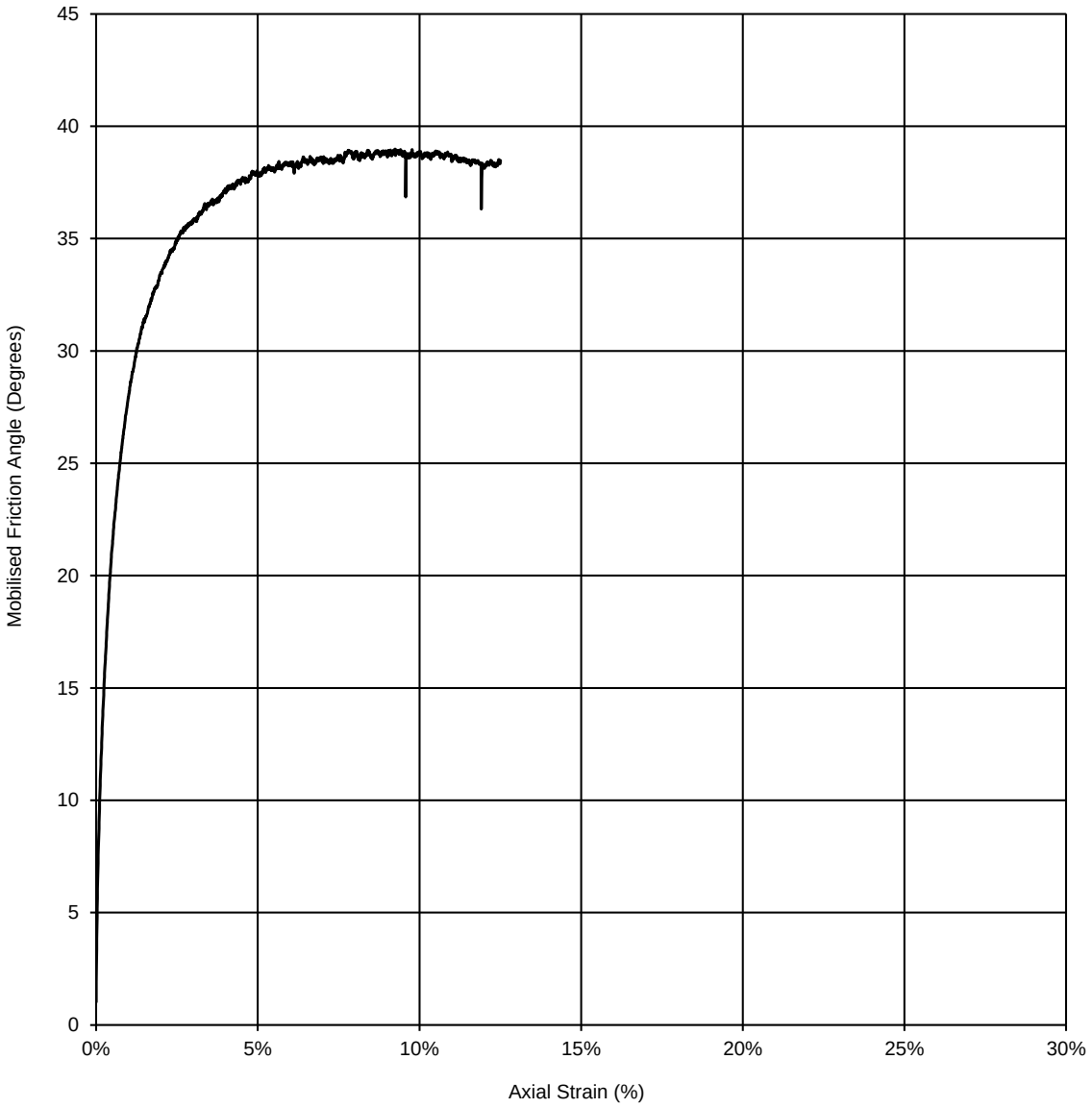

Preparation Notes:	Sample was moist tamped to specific density	Tested by:	M. Rammala
		Reviewed by:	V. Venter

THIS DOCUMENT SHALL ONLY BE REPRODUCED IN FULL

Consolidated Undrained Triaxial Report

UNIVERSITEIT VAN PRETORIA
UNIVERSITY OF PRETORIA
YUNIBESITHI YA PRETORIA

Client:	UP		
Address:	-		
Project:	Jagersfontein		
Location:	-		
Date:	2024/07/05		
Project No.:	1		
Sample ID:	Gravel 3		
Test ID:	TX5-CIU-300kPa		
Tested by:	M. Rammala	**Reviewed by:**	V. Venter

Initial Height (mm):	140.2	Final Moisture Content (%):	19.2%	Strain Rate (mm/min):	0.046
Initial Diameter (mm):	69.6	Final Dry Density (t/m^3):	1.76	B Response (%):	99%
Initial Moisture content (%):	6.4%	Final Void Ratio (-):	0.51	Mean Effective Consolidation Stress (kPa):	301
Initial Dry Density (t/m^3):	1.73	Specific Gravity	2.65	Geostatic Stress Ratio K_0 (-):	0.98
Method for Sample Area:	End of Test			Area Correction:	Parabolic
Preparation Notes:	Sample was moist tamped to specific density				

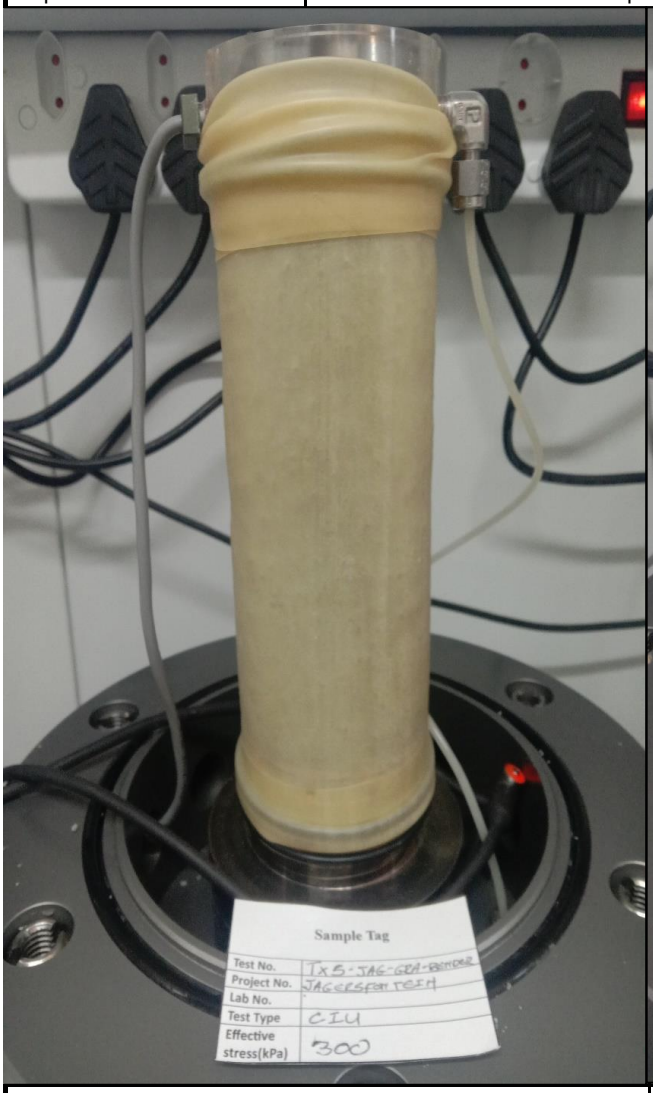

Sample Before Test

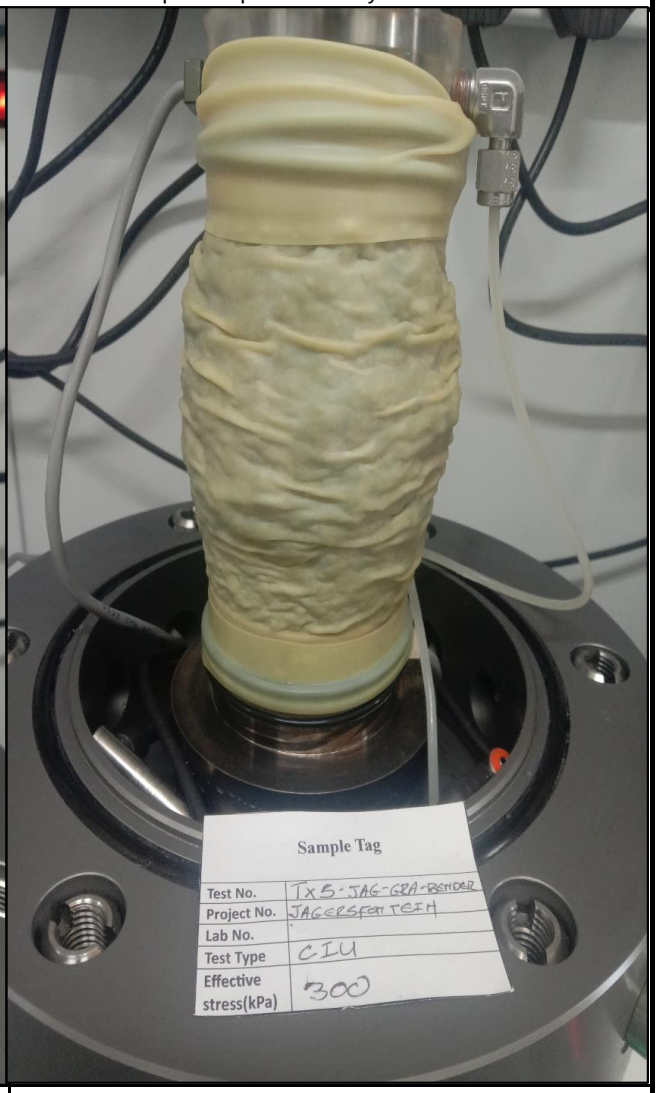

Sample After Test

Consolidated Undrained Triaxial Report

UNIVERSITEIT VAN PRETORIA
UNIVERSITY OF PRETORIA
YUNIBESITHI YA PRETORIA

Client:	UP
Address:	-
Project:	Jagersfontein
Location:	-
Date:	2024/07/05
Project No.:	1
Sample ID:	Gravel 3
Test ID:	TX5-CIU-300kPa
Tested by:	M. Rammala **Reviewed by:** V. Venter

Initial Height (mm):	140.2	Final Moisture Content (%):	19.2%	Strain Rate (mm/min):	0.046
Initial Diameter (mm):	69.6	Final Dry Density (t/m^3):	1.76	B Response (%):	99%
Initial Moisture content (%):	6.4%	Final Void Ratio (-):	0.51	Mean Effective Consolidation Stress (kPa):	301
Initial Dry Density (t/m^3):	1.73	Specific Gravity	2.65	Geostatic Stress Ratio K_0 (-):	0.98
Method for Sample Area:	End of Test		Area Correction:	Parabolic	
Preparation Notes:	Sample was moist tamped to specific density				

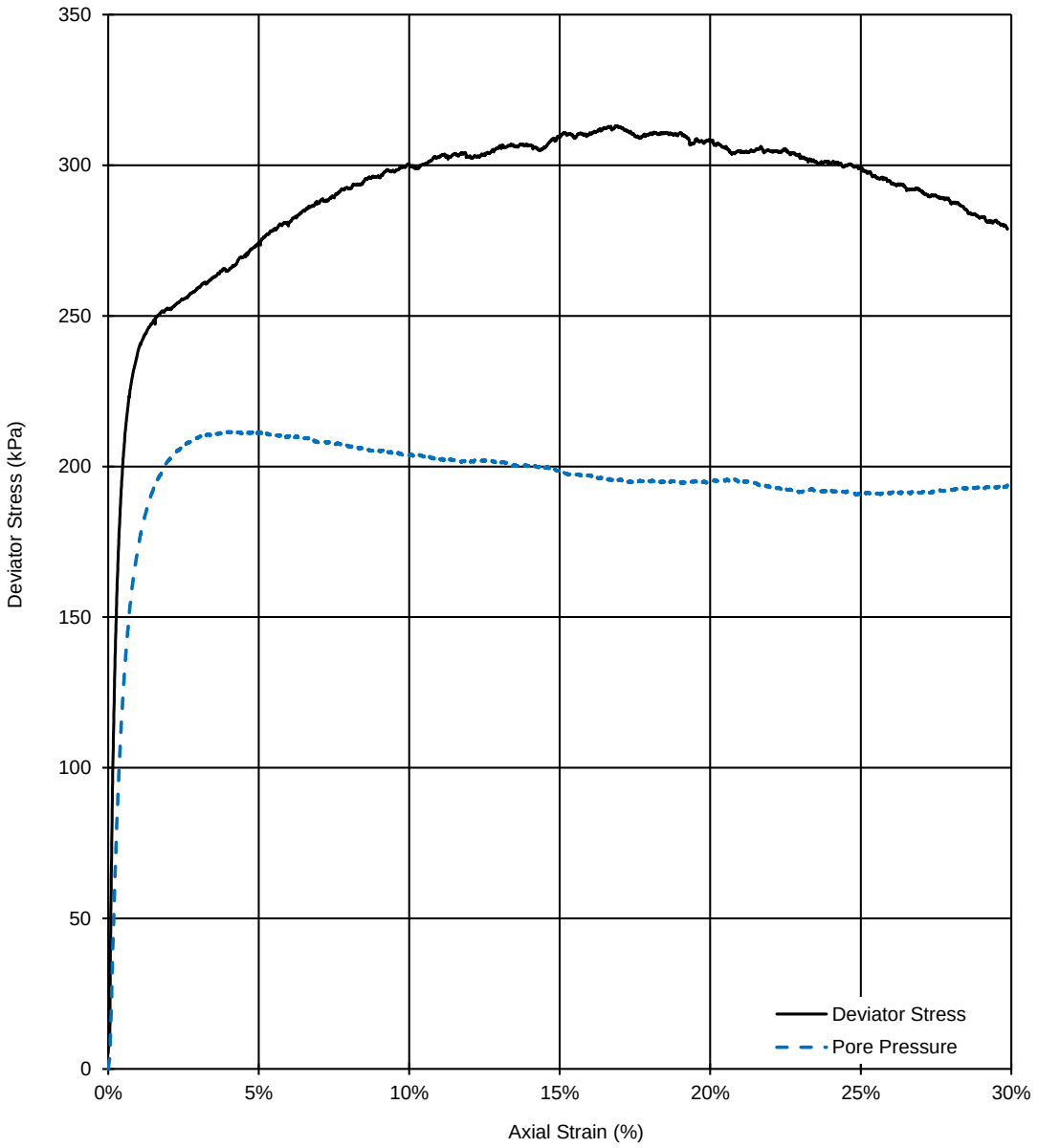

Preparation Notes:	Sample was moist tamped to specific density	Tested by:	M. Rammala
		Reviewed by:	V. Venter

THIS DOCUMENT SHALL ONLY BE REPRODUCED IN FULL

Consolidated Undrained Triaxial Report

UNIVERSITEIT VAN PRETORIA
UNIVERSITY OF PRETORIA
YUNIBESITHI YA PRETORIA

Client:	UP
Address:	-
Project:	Jagersfontein
Location:	-
Date:	2024/07/05
Project No.:	1
Sample ID:	Gravel 3
Test ID:	TX5-CIU-300kPa
Tested by:	M. Rammala **Reviewed by:** V. Venter

Initial Height (mm):	140.2	Final Moisture Content (%):	19.2%	Strain Rate (mm/min):	0.046
Initial Diameter (mm):	69.6	Final Dry Density (t/m^3):	1.76	B Response (%):	99%
Initial Moisture content (%):	6.4%	Final Void Ratio (-):	0.51	Mean Effective Consolidation Stress (kPa):	301
Initial Dry Density (t/m^3):	1.73	Specific Gravity	2.65	Geostatic Stress Ratio K_0 (-):	0.98
Method for Sample Area:	End of Test		Area Correction:	Parabolic	
Preparation Notes:	Sample was moist tamped to specific density				

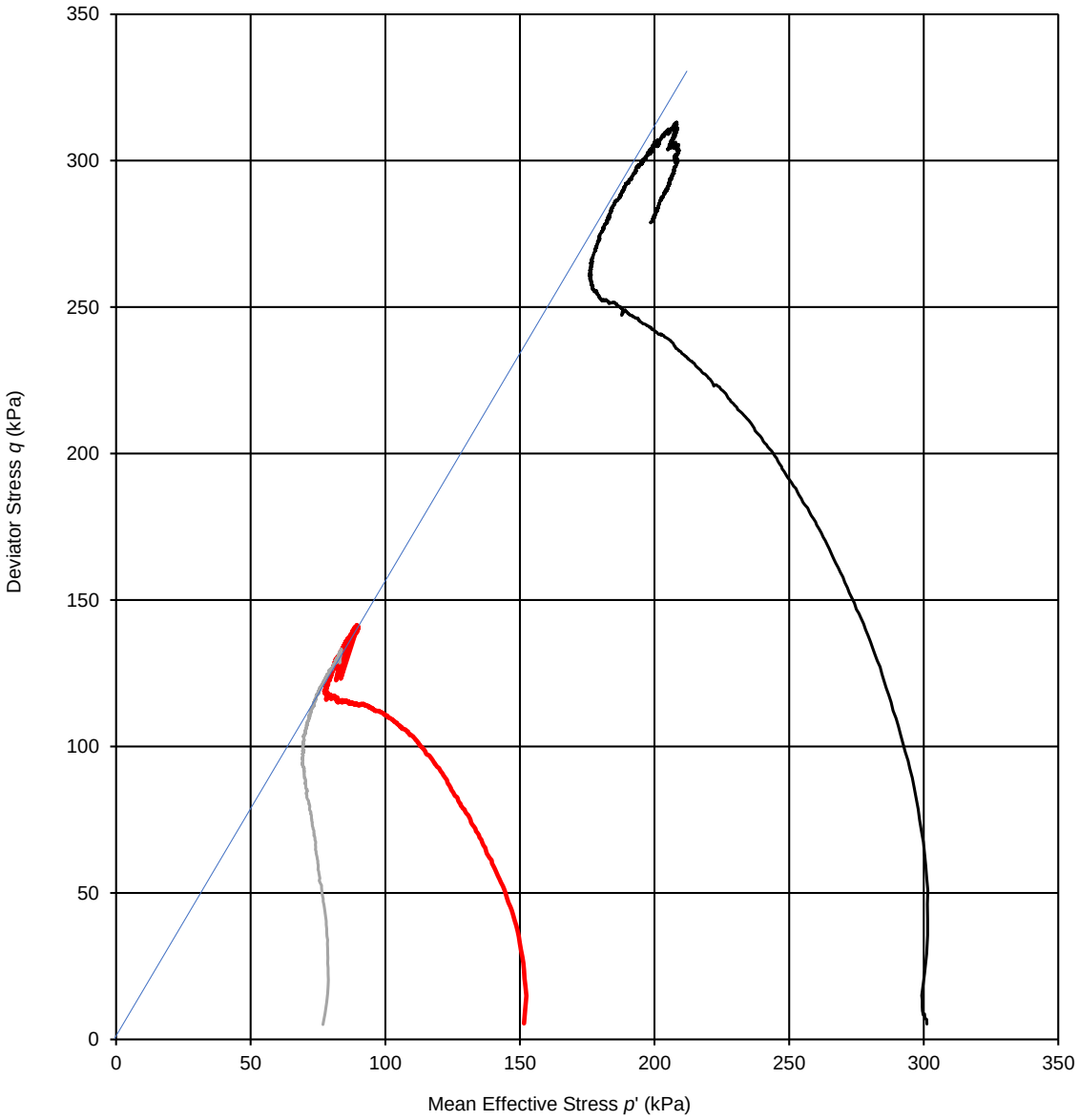

Preparation Notes:	Sample was moist tamped to specific density	Tested by:	M. Rammala
		Reviewed by:	V. Venter

THIS DOCUMENT SHALL ONLY BE REPRODUCED IN FULL

Consolidated Undrained Triaxial Report

UNIVERSITEIT VAN PRETORIA
UNIVERSITY OF PRETORIA
YUNIBESITHI YA PRETORIA

Client:	UP		
Address:	-		
Project:	Jagersfontein		
Location:	-		
Date:	2024/07/05		
Project No.:	1		
Sample ID:	Gravel 3		
Test ID:	TX5-CIU-300kPa		
Tested by:	M. Rammala	**Reviewed by:**	V. Venter

Initial Height (mm):	140.2	Final Moisture Content (%):	19.2%	Strain Rate (mm/min):	0.046
Initial Diameter (mm):	69.6	Final Dry Density (t/m^3):	1.76	B Response (%):	99%
Initial Moisture content (%):	6.4%	Final Void Ratio (-):	0.51	Mean Effective Consolidation Stress (kPa):	301
Initial Dry Density (t/m^3):	1.73	Specific Gravity	2.65	Geostatic Stress Ratio K_0 (-):	0.98
Method for Sample Area:	End of Test		Area Correction:	Parabolic	
Preparation Notes:	Sample was moist tamped to specific density				

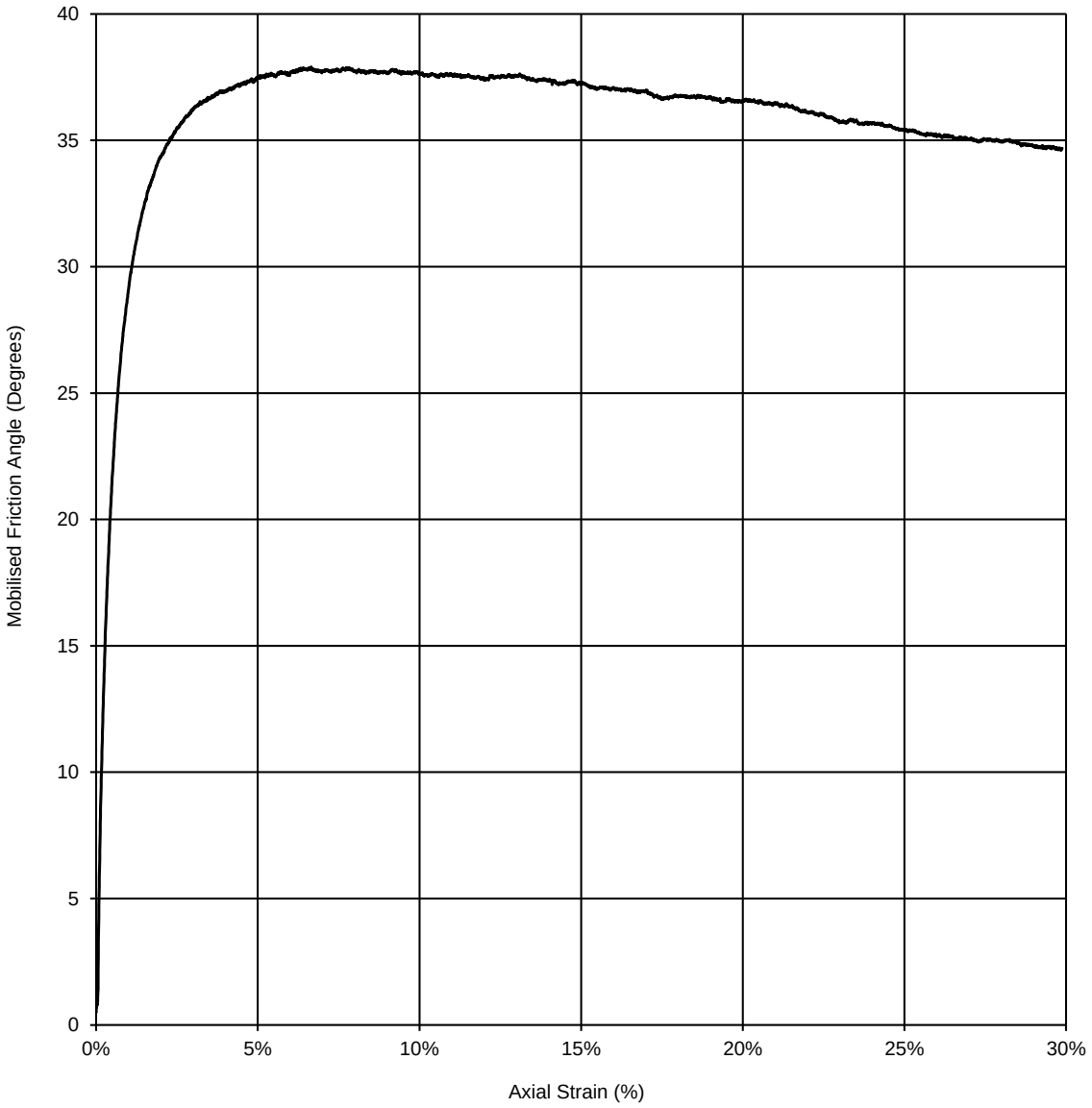

Preparation Notes:	Sample was moist tamped to specific density	Tested by:	M. Rammala
		Reviewed by:	V. Venter

THIS DOCUMENT SHALL ONLY BE REPRODUCED IN FULL

3.5.2. Vane shear test results

A number of hand vane shear tests were carried out in the floor of the breach on 29 January 2024 at locations shown in Figure 14. The handheld apparatus used for the vane shear tests has a built-in dial that yields the shear strength. This value was taken as the result without any further modifications. Table 4 presents the peak shear strength recorded at locations VS1 to VS4. At these four locations, tests were conducted only at a depth of 0.3 m. A number vane shear tests were also performed over a range of depths to a maximum depth of 1.45 m. These tests focused on characterising the peak strength of the tailings that remained in the breached portion of the southern wall.

Figure 15 presents the results of the Vane Shear test at locations VS5 to VS11, all of which included tests at different depths, also in the floor of the breach. While hand-held VSTs are generally assumed to provide measurements of undrained shear strength, in tailings, it is difficult to ascertain whether undrained conditions were indeed achieved (Reid et al., 2023). In addition, the vane shear tests were carried out approximately 18 months after the failure which implies that the overburden stress was removed and, due to the long time after failure, significant drainage and hence softening would have occurred, mostly likely completely changing the undrained shear strength. Given this uncertainty, the results of the VSTs were not considered further.

TABLE 4 PEAK SHEAR STRENGTH AT TEST LOCATIONS VS1 TO VS4.

Test	Shear strength (kPa)
VS1-0.3	68
VS2-0.3	49
VS3-0.3	113
VS4-0.3	33

TABLE 5 IDS AND DEPTHS OF THE HANDHELD VANE SHEAR TESTS.

Test ID	Depth (m)	Test ID	Depth (m)	Test ID	Depth (m)
VS1-0.3	0.3	VS6-1.45	1.45	VS9-0.9	0.9
VS2-0.3	0.3	VS7-0.3	0.3	VS9-1.2	1.2
VS3-0.3	0.3	VS7-0.6	0.6	VS9-1.45	1.45
VS4-0.3	0.3	VS7-0.9	0.9	VS10-0.3	0.3
VS5-0.3	0.3	VS7-1.2	1.2	VS10-0.6	0.6
VS5-0.6	0.6	VS7-1.45	1.45	VS10-0.9	0.9
VS5-0.9	0.9	VS8-0.3	0.3	VS10-1.2	1.2
VS5-1.2	1.2	VS8-0.6	0.6	VS10-1.45	1.45

VS5-1.45	1.45	VS8-0.9	0.9	VS11-0.3	0.3
VS6-0.3	0.3	VS8-1.2	1.2	VS11-0.6	0.6
VS6-0.6	0.6	VS8-1.45	1.45	VS11-0.7	0.7
VS6-0.9	0.9	VS9-0.3	0.3	--	--
VS6-1.2	1.2	VS9-0.6	0.6	--	--

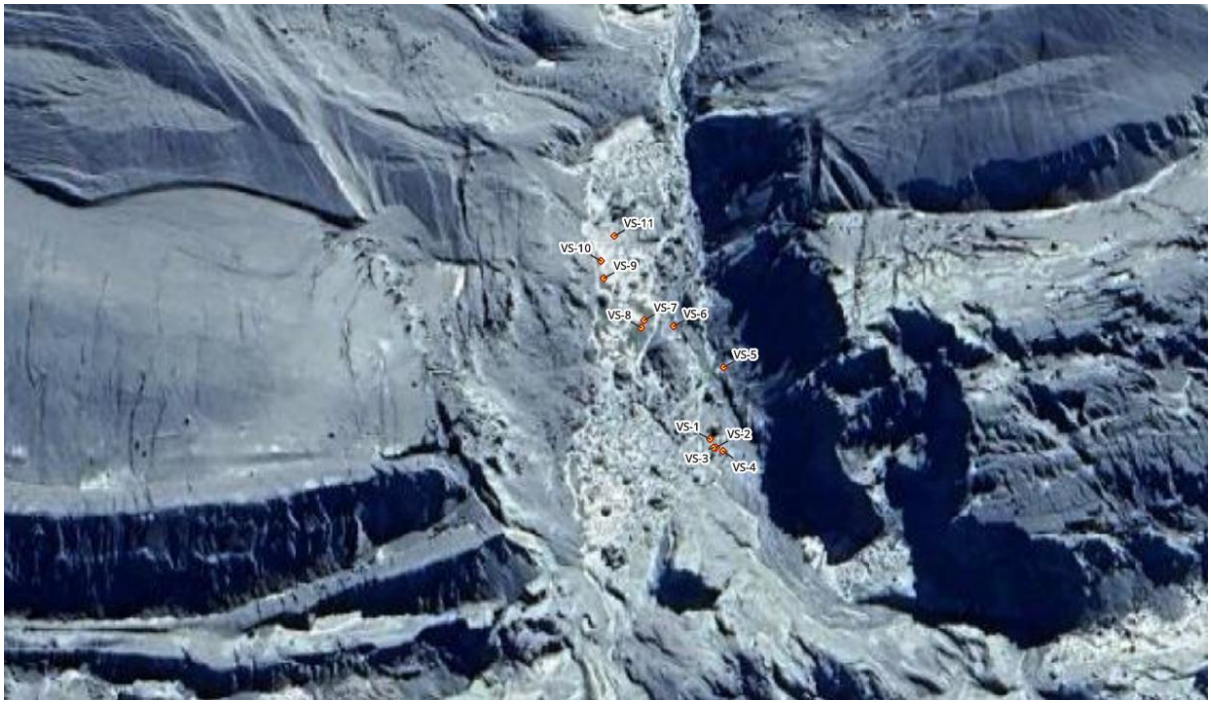

Figure 14 Locations of vane shear test results in breach floor.

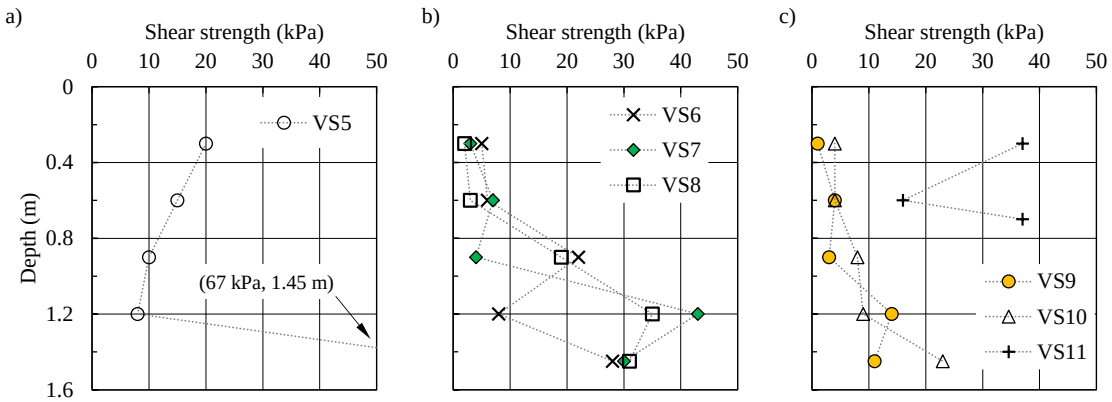

FIGURE 15 RESULTS OF VANE SHEAR TEST CARRIED OUT IN THE FLOOR OF THE BREACH ON 29 JAN 2024.

3.6. Dispersiveness

Signs of quite severe side slope erosion is evident on especially the western and south-western walls of the Jagerfontein tailings dam. A sample was submitted for chemical dispersion tests, the result of which is tabulated below.

FIGURE 16 SIGNIFICANT SLOPE EROSION SUGGESTION POTENTIAL FOR DISPERSIVENESS.

TABLE 6 RESULTS ON CHEMICAL DISPERSION TEST ON SAMPLE S4.

Lab Nommer	Sample Reference	K AmAc *	Na AmAc *	Ca AmAc *	Mg AmAc *	EXCH ACID KCl *	Mg (AmAc) *	Na (AmAc) *	ECEC *	ESP (AmAc) *	EMgP (AmAc) *	Na (Sat-Paste) *	Ca (Sat-Paste) *	Mg (Sat-Paste) *	Ca (Sat-Paste) *	K (Sat-Paste) *	Mg (Sat-Paste) *	Na (Sat-Paste) *	pH (Sat-Paste) *	EC (Sat-Paste) *	SAR (Sat-Paste) *
Lab Number	Monsterverwysing	mg/kg	mg/kg	mg/kg	mg/kg	cmol(+)/kg	cmol(+)/kg	cmol(+)/kg	cmol(+)/kg	%	%	Me/l	Me/l	Me/l	mg/l	mg/l	mg/l	mg/l	-	mS/m	-
G35-102233	Site J, ESP Sample 1	961	1220	4331	374	0.00	3.07	5.30	32.49	16.33	9.44	57.90	2.91	0.85	58.17	172.35	10.68	1331.59	8.01	582.00	42.21

Based on the recommendations of Gerber & Harmse (1987) the material classifies as dispersive, in fact highly dispersive. Its dispersive nature means that the tailings material may be prone to piping.

References

Gerber, F.A. and Harmse, H.J. von M. 1987. Proposed procedure for identification of dispersive soils by chemical testing. The Civil Engineer in South Africa, 29, 397-399.

Reid, D., Rodriguez, C., Fourie, A., Tiwari, B. 2023. Partial drainage effects during vane shear tests, with an emphasis on the measurement of remoulded strengths. Proceedings of Tailings and Mine Waste Conference. Vancouver, Canada.

APPENDIX F

SCPTu INVESTIGATION

TABLE OF CONTENTS

1. INTRODUCTION 1
2. DESCRIPTION OF THE TWO IN SITU TESTING CAMPAIGNS 1
   2.1. CPT SOUNDINGS PERFORMED BY SRK CONSULTING (SOUTH AFRICA) 1
   2.2. CPT SOUNDINGS PERFORMED BY THE INVESTIGATION PANEL 4
3. DATA PROCESSING 6
   3.1. CONE PENETRATION TESTS 6
4. RESULTS AND DISCUSSION 11
   4.1. CONE PENETRATION TESTS PERFORMED BY SRK 11
   4.2. CONE PENETRATION TESTS PERFORMED BY THE INVESTIGATION PANEL 34
5. MOSTAP SAMPLES 70
6. CROSS SECTION PROFILE FROM SCPTU RESULTS FOR STABILITY ANALYSIS 70
7. CONCLUDING REMARKS 71

REFERENCES 72

ATTACHMENT F1 CPTu RESULTS BY OSIMO

ATTACHMENT F2 PORE PRESSURE DISSIPATION DATA

ATTACHMENT F3 SCPTu SHEAR WAVE DATA BY OSIMO

LIST OF FIGURES

Figure 1 Location of the 11 CPT soundings performed by SRK. Source: PMI (2023). 2

Figure 2 Location of the 17 CPT soundings performed by the investigation panel. Note: Sounding codes ending in 's' indicate measurement of V_s. Sounding codes ending in 'm' indicate Mostap sampling. Red lines indicate approximate extent of Dump 10, North Dump and South Dump. 5

Figure 3 The four charts used herein to aid the interpretation of CPT results. a) Q vs f_s/σ'_{v0} (Saye et al. 2017), b) Q vs $U2$ (Schneider et al. 2008, Fourie et al. 2022) c) Q' vs F (Jefferies and Been 2015) and d) Q_{tn} vs F (Robertson 2022). 8

Figure 4 Criterion used to distinguish uncemented from cemented soils. From Robertson (2016). 11

Figure 5 Profiles of CPTu sounding JDFTSF01: (a) cone tip resistance q_t (b) sleeve friction f_s (c) dynamic and interpolated u_0 pore pressures (d) Δ_Q (e) B_q and (f) soil behaviour index $I_{c\text{-}JD}$. 12

Figure 6 Soil behaviour type charts for CPT position JDFTSF01 (a) Q vs f_s/σ'_{vo} (b) Q vs $U2$ (c) Q' vs F and (d) Q_{tn} vs F. 13

Figure 7 Profiles at CPT position JDFTSF02: (a) cone tip resistance q_t (b) sleeve friction f_s (c) dynamic and interpolated u_0 pore pressures (d) Δ_Q (e) B_q and (f) soil behaviour index $I_{c\text{-}JD}$. 14
Figure 8 Soil behaviour type charts for CPT position JDFTSF02 (a) Q vs f_s/σ'_{vo} (b) inset from Q vs f_s/σ'_{vo} (c) Q vs $U2$ (d) Q' vs F and (e) Q_{tn} vs F. 15
Figure 9 Profiles of the CPTu sounding JDFTSF03: (a) cone tip resistance q_t (b) sleeve friction f_s (c) dynamic and interpolated u_0 pore pressures (d) Δ_Q (e) B_q and (f) $I_{c\text{-}JD}$. 16
Figure 10 Soil behaviour type charts for CPT position JDFTSF03 (a) Q vs f_s/σ'_{vo} (b) inset from Q vs f_s/σ'_{vo} (c) Q vs $U2$ (d) Q' vs F and (e) Q_{tn} vs F. 17
Figure 11 Profiles at CPT position JDFTSF04 (a) cone tip resistance q_t (b) sleeve friction f_s (c) dynamic and interpolated u_0 pore pressures (d) Δ_Q (e) B_q and (f) $I_{c\text{-}JD}$. 18
Figure 12 Soil behaviour type charts for CPT position JDFTSF04 (a) Q vs f_s/σ'_v (b) enlarged Q vs f_s/σ'_v space (c) Q vs $U2$ (d) Q' vs F and (e) Q_{tn} vs F. 19
Figure 13 Profiles at CPT position JDFTSF05 (a) cone tip resistance q_t (b) sleeve friction f_s (c) dynamic and interpolated u_0 pore pressures (d) Δ_Q (e) B_q and (f) $I_{c\text{-}JD}$. 20
Figure 14 Soil behaviour type charts for CPT position JDFTSF05 (a) Q vs f_s/σ'_v (b) enlarged Q vs f_s/σ'_v space (c) Q vs $U2$ (d) Q' vs F and (e) Q_{tn} vs F. 21
Figure 15 Profiles at CPT position JDFTSF06 (a) cone tip resistance q_t (b) sleeve friction f_s (c) dynamic and interpolated u_0 pore pressures (d) Δ_Q (e) B_q and (f) $I_{c\text{-}JD}$. 22
Figure 16 Soil behaviour type charts for CPT position JDFTSF06 (a) Q vs f_s/σ'_v (b) enlarged Q vs f_s/σ'_v space (c) Q vs $U2$ (d) Q' vs F and (e) Q_{tn} vs F. 23
Figure 17 Profiles at CPT position JDFTSF07 (a) cone tip resistance q_t (b) sleeve friction f_s (c) dynamic and interpolated u_0 pore pressures (d) Δ_Q (e) B_q and (f) $I_{c\text{-}JD}$. 24
Figure 18 Soil behaviour type charts for CPT position JDFTSF07 (a) Q vs f_s/σ'_v (b) enlarged Q vs f_s/σ'_v space (c) Q vs $U2$ (d) Q' vs F and (e) Q_{tn} vs F. 25
Figure 19 Profiles at CPT position JDFTSF13 (a) cone tip resistance q_t (b) sleeve friction f_s (c) dynamic and interpolated u_0 pore pressures (d) Δ_Q (e) B_q and (f) $I_{c\text{-}JD}$. 26
Figure 20 Soil behaviour type charts for CPT position JDFTSF13 (a) Q vs f_s/σ'_v (b) enlarged Q vs f_s/σ'_v space (c) Q vs $U2$ (d) Q' vs F and (e) Q_{tn} vs F. 27
Figure 21 Profiles at CPT position JDFTSF14 (a) cone tip resistance q_t (b) sleeve friction f_s (c) dynamic and interpolated u_0 pore pressures (d) Δ_Q (e) B_q and (f) $I_{c\text{-}JD}$. 28
Figure 22 Soil behaviour type charts for CPT position JDFTSF14 (a) Q vs f_s/σ'_v (b) Q vs $U2$ (c) Q' vs F and (d) Q_{tn} vs F. 29
Figure 23 Profiles at CPT position JDFTSF15 (a) cone tip resistance q_t (b) sleeve friction f_s (c) dynamic and interpolated u_0 pore pressures (d) Δ_Q (e) B_q and (f) $I_{c\text{-}JD}$. 30
Figure 24 Soil behaviour type charts for CPT position JDFTSF15 (a) Q vs f_s/σ'_v (b) Q vs $U2$ (c) Q' vs F and (d) Q_{tn} vs F. 31
Figure 25 Profiles at CPT position JDFTSF16 (a) cone tip resistance q_t (b) sleeve friction f_s (c) dynamic and interpolated u_0 pore pressures (d) Δ_Q (e) B_q and (f) $I_{c\text{-}JD}$. 32
Figure 26 Soil behaviour type charts for CPT position JDFTSF16 (a) Q vs f_s/σ'_v (b) Q vs $U2$ (c) Q' vs F and (d) Q_{tn} vs F. 33
Figure 27 Profiles of CPT01: (a) cone tip resistance q_t (b) sleeve friction f_s (c) dynamic and interpolated u_0 pore pressures (d) Δ_Q (e) B_q and (f) soil behaviour index $I_{c\text{-}JD}$. 36
Figure 28 Soil behaviour type charts for CPT position C1 (a) Q_t vs f_s/σ'_{vo} (b) inset from Q_t vs f_s/σ'_{vo} (c) Q vs $U2$ (d) Q' vs F and (e) Q_{tn} vs F. 37

Figure 29 Profiles at CPT position C2 (a) cone tip resistance q_t (b) sleeve friction f_s (c) dynamic and interpolated u_0 pore pressures (d) Δ_Q (e) B_q and (f) soil behaviour index $I_{c\text{-}JD}$. 38
Figure 30 Soil behaviour type charts for CPT position C2 (a) Q_t vs f_s/σ'_{vo} (b) inset from Q_t vs f_s/σ'_{vo} (c) Q vs U2 (d) Q' vs F and (e) Q_{tn} vs F. 39
Figure 31 Profiles at CPT position C3 (a) cone tip resistance q_t (b) sleeve friction f_s (c) dynamic and interpolated u_0 pore pressures (d) Δ_Q (e) B_q and (f) soil behaviour index $I_{c\text{-}JD}$. 40
Figure 32 Soil behaviour type charts for CPT position C3 (a) Q_t vs f_s/σ'_{vo} (b) inset from Q_t vs f_s/σ'_{vo} (c) Q vs U2 (d) Q' vs F and (e) Q_{tn} vs F. 41
Figure 33 Profiles at CPT position C4 (a) cone tip resistance q_t (b) sleeve friction f_s (c) dynamic and interpolated u_0 pore pressures (d) Δ_Q (e) B_q and (f) soil behaviour index $I_{c\text{-}JD}$. 42
Figure 34 Soil behaviour type charts for CPT position C4 (a) Q_t vs f_s/σ'_{vo} (b) inset from Q_t vs f_s/σ'_{vo} (c) Q vs U2 (d) Q' vs F and (e) Q_{tn} vs F. 43
Figure 35 Profiles at CPT position C5 (a) cone tip resistance q_t (b) sleeve friction f_s (c) dynamic and interpolated u_0 pore pressures (d) Δ_Q (e) B_q and (f) soil behaviour index $I_{c\text{-}JD}$. 44
Figure 36 Soil behaviour type charts for CPT position C5 (a) Q_t vs f_s/σ'_{vo} (b) inset from Q_t vs f_s/σ'_{vo} (c) Q vs U2 (d) Q' vs F and (e) Q_{tn} vs F. 45
Figure 37 Profiles at CPT position C6 (a) cone tip resistance q_t (b) sleeve friction f_s (c) dynamic and interpolated u_0 pore pressures (d) Δ_Q (e) B_q and (f) soil behaviour index $I_{c\text{-}JD}$. 46
Figure 38 Soil behaviour type charts for CPT position C6 (a) Q_t vs f_s/σ'_{vo} (b) inset from Q_t vs f_s/σ'_{vo} (c) Q vs U2 (d) Q' vs F and (e) Q_{tn} vs F. 47
Figure 39 Profiles at CPT position C7 (a) cone tip resistance q_t (b) sleeve friction f_s (c) dynamic and interpolated u_0 pore pressures (d) Δ_Q (e) B_q and (f) soil behaviour index $I_{c\text{-}JD}$. 48
Figure 40 Soil behaviour type charts for CPT position C7 (a) Q_t vs f_s/σ'_{vo} (b) inset from Q_t vs f_s/σ'_{vo} (c) Q vs U2 (d) Q' vs F and (e) Q_{tn} vs F. 49
Figure 41 Profiles at CPT position C8 (a) cone tip resistance q_t (b) sleeve friction f_s (c) dynamic and interpolated u_0 pore pressures (d) Δ_Q (e) B_q and (f) soil behaviour index $I_{c\text{-}JD}$. 50
Figure 42 Soil behaviour type charts for CPT position C8 (a) Q_t vs f_s/σ'_{vo} (b) inset from Q_t vs f_s/σ'_{vo} (c) Q vs U2 (d) Q' vs F and (e) Q_{tn} vs F. 51
Figure 43 Profiles at CPT position C9 (a) cone tip resistance q_t (b) sleeve friction f_s (c) dynamic and interpolated u_0 pore pressures (d) Δ_Q (e) B_q and (f) soil behaviour index $I_{c\text{-}JD}$. 52
Figure 44 Soil behaviour type charts for CPT position C9 (a) Q_t vs f_s/σ'_{vo} (b) inset from Q_t vs f_s/σ'_{vo} (c) Q vs U2 (d) Q' vs F and (e) Q_{tn} vs F. 53
Figure 45 Profiles at CPT position C10 (a) cone tip resistance q_t (b) sleeve friction f_s (c) dynamic and interpolated u_0 pore pressures (d) Δ_Q (e) B_q and (f) soil behaviour index $I_{c\text{-}JD}$. 54
Figure 46 Soil behaviour type charts for CPT position C10 (a) Q_t vs f_s/σ'_{vo} (b) inset from Q_t vs f_s/σ'_{vo} (c) Q vs U2 (d) Q' vs F and (e) Q_{tn} vs F. 55
Figure 47 Profiles at CPT position C11 (a) cone tip resistance q_t (b) sleeve friction f_s (c) dynamic and interpolated u_0 pore pressures (d) Δ_Q (e) B_q and (f) soil behaviour index $I_{c\text{-}JD}$. 56
Figure 48 Soil behaviour type charts for CPT position C11 (a) Q_t vs f_s/σ'_{vo} (b) inset from Q_t vs f_s/σ'_{vo} (c) Q vs U2 (d) Q' vs F and (e) Q_{tn} vs F. 57
Figure 49 Profiles at CPT position C12 (a) cone tip resistance q_t (b) sleeve friction f_s (c) dynamic and interpolated u_0 pore pressures (d) Δ_Q (e) B_q and (f) soil behaviour index $I_{c\text{-}JD}$. 58
Figure 50 Soil behaviour type charts for CPT position C12 (a) Q_t vs f_s/σ'_{vo} (b) inset from Q_t vs f_s/σ'_{vo} (c) Q vs U2 (d) Q' vs F and (e) Q_{tn} vs F. 59

Figure 51 Profiles at CPT position C13 (a) cone tip resistance q_t (b) sleeve friction f_s (c) dynamic and interpolated u_0 pore pressures (d) Δ_Q (e) B_q and (f) soil behaviour index $I_{c\text{-}JD}$. 60
Figure 52 Soil behaviour type charts for CPT position C13 (a) Q_t vs f_s/σ'_{vo} (b) inset from Q_t vs f_s/σ'_{vo} (c) Q vs U2 (d) Q' vs F (e) Q_{tn} vs F and (f) Q_{tn} vs I_G. 61
Figure 53 Profiles at CPT position C14 (a) cone tip resistance q_t (b) sleeve friction f_s (c) dynamic and interpolated u_0 pore pressures (d) Δ_Q (e) B_q and (f) soil behaviour index $I_{c\text{-}JD}$. 62
Figure 54 Soil behaviour type charts for CPT position C14 (a) Q_t vs f_s/σ'_{vo} (b) inset from Q_t vs f_s/σ'_{vo} (c) Q vs U2 (d) Q' vs F (e) Q_{tn} vs F and (f) Q_{tn} vs I_G. 63
Figure 55 Profiles at CPT position C15 (a) cone tip resistance q_t (b) sleeve friction f_s (c) dynamic and interpolated u_0 pore pressures (d) Δ_Q (e) B_q and (f) soil behaviour index $I_{c\text{-}JD}$. 64
Figure 56 Soil behaviour type charts for CPT position C15 (a) Q_t vs f_s/σ'_{vo} (b) inset from Q_t vs f_s/σ'_{vo} (c) Q vs U2 (d) Q' vs F (e) Q_{tn} vs F and (f) Q_{tn} vs I_G. 65
Figure 57 Profiles at CPT position C16 (a) cone tip resistance q_t (b) sleeve friction f_s (c) dynamic and interpolated u_0 pore pressures (d) Δ_Q (e) B_q and (f) soil behaviour index $I_{c\text{-}JD}$. 66
Figure 58 Soil behaviour type charts for CPT position C16 (a) Q_t vs f_s/σ'_{vo} (b) inset from Q_t vs f_s/σ'_{vo} (c) Q vs U2 (d) Q' vs F (e) Q_{tn} vs F and (f) Q_{tn} vs I_G. 67
Figure 59 Profiles at CPT position C17 (a) cone tip resistance q_t (b) sleeve friction f_s (c) dynamic and interpolated u_0 pore pressures (d) Δ_Q (e) B_q and (f) soil behaviour index $I_{c\text{-}JD}$. 68
Figure 60 Soil behaviour type charts for CPT position C17 (a) Q_t vs f_s/σ'_{vo} (b) inset from Q_t vs f_s/σ'_{vo} (c) Q vs U2 (d) Q' vs F and (e) Q_{tn} vs F. 69
Figure 61 Cross section profile showing material zones for stability analysis. 71

1. Introduction

This chapter describes the in situ geotechnical tests performed at the Jagersfontein dam to investigate the cause of failure. All the tests described herein were performed after the failure. The investigation panel did not have access to any pre-failure in situ testing results.

Two testing campaigns are considered herein:

1) Cone penetration tests (CPTs) performed by the engineering firm SRK Consulting (South Africa), hereafter referred to as SRK. This campaign included a total of 11 soundings with measurements of tip resistance (q_c), sleeve friction (f_s), dynamic pore water pressure (u_2) and ambient pore water pressure (u_0) via pore water pressure dissipation tests (PPDTs).

2) CPTs performed by the investigation panel. This campaign included a total of 17 soundings. In addition to measuring q_c, f_s, u_2 and u_0 via PPDTs, some of the soundings included measurements of shear wave velocity (V_s) and Mostap sampling.

2. Description of the two in situ testing campaigns

2.1. CPT soundings performed by SRK consulting (South Africa)

SRK performed 11 CPT soundings (Table 1), as per ISO 22476-1:2012, at the Jagersfontein dam during the first half of June 2023. The investigation panel was granted access to the raw data of the CPT campaign in digital format and to the factual report prepared by the CPT contractor PMI Construction Services (PMI, 2023). All soundings were located within the footprint of the dam but not on the dam wall section that failed (Figure 1).

Predrilling was not used for any of the soundings, so readings began at ground level. All soundings were performed to refusal with a 200 kN pushing rig and subtraction cones with a projected area of 15 cm^2 and a friction sleeve surface of 225 cm^2. The soundings measured q_c, f_s, u_2, u_0 via PPDTs and biaxial inclination. 18 Mostap samples were also recovered during this campaign (PMI, 2023). However, the investigation panel was not granted access to any information regarding these samples so they will not be mentioned further herein.

Figure 1 shows the location of soundings JDFTSF1 to JDFTSF7 and JDFTSF13 to JDFTSF16. Soundings JDFTSF8 to JDFTSF12 were initially planned but finally not executed due to difficulties in accessing their proposed locations.

As described below, our CPT interpretation approach varied depending on whether the probed soil was saturated or partially saturated. We assumed that layers were saturated only when their u_2 response deviated from zero by more than ±4 kPa (Rust and Rust, 2023). Table 1 indicates layers thicker than ~1 m that were saturated and which included at least one u_0 estimate from a PPDT. Regardless of their thickness, saturated layers without a u_0 estimate could not be analysed as saturated because such analysis requires the calculation of the excess pore water pressure $u_e = u_2 - u_0$. Furthermore, we hypothesised that the u_2 response

in thin layers may be affected by the proximity of partially saturated soils. Accordingly, layers that were thinner than ~1 m were also analysed as being partially saturated.

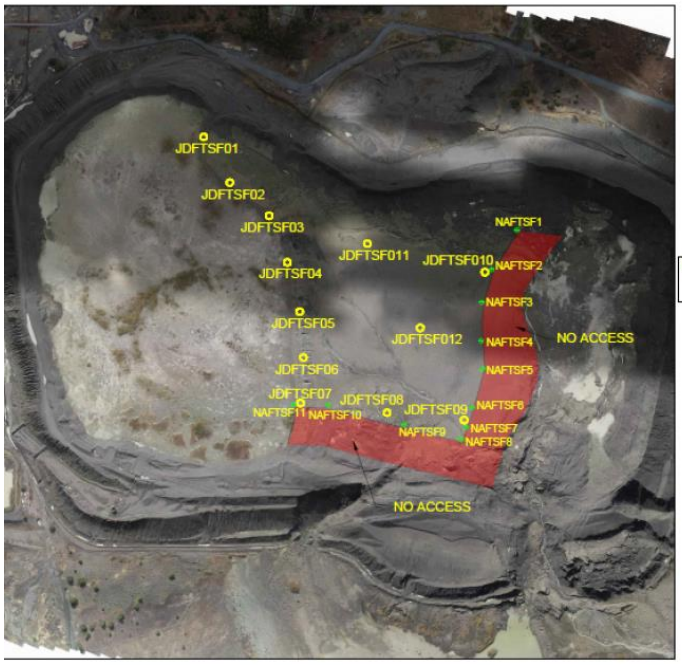

COORDINATE LIST WGS 84 - LO 25		
CPT LOCATIONS		
POINT	Y-COORD	X-COORD
JDFTSF1	-40923.15	3294546.78
JDFTSF2	-40964.93	3294619.83
JDFTSF3	-41027.94	3294673.19
JDFTSF4	-41057.11	3294747.63
JDFTSF5	-41077.07	3294826.79
JDFTSF6	-41082.96	3294900.21
JDFTSF7	-41078.16	3294973.19
JDFTSF8	-41216.97	3294988.74
JDFTSF9	-41340.54	3295000.56
JDFTSF10	-41373.69	3294763.41
JDFTSF11	-41185.28	3294717.95
JDFTSF12	-41270.09	3294852.81
NO ACCESS AREA		
POINT	Y-COORD	X-COORD
NAFTSF1	-41425.31	3294695.74
NAFTSF2	-41384.82	3294759.27
NAFTSF3	-41368.81	3294812.03
NAFTSF4	-41367.62	3294873.70
NAFTSF5	-41369.99	3294918.16
NAFTSF6	-41353.38	3294980.42
NAFTSF7	-41343.30	3295012.44
NAFTSF8	-41335.11	3295032.00
NAFTSF9	-41244.18	3295007.53
NAFTSF10	-41122.60	3294976.86
NAFTSF11	-41067.43	3294976.27

NOTES:
- NO TEST LOCATIONS WITHIN THE HATCHED ZONE.
- NO ACCESS OF ANY TYPE WITHIN HATCHED ZONE.
- POINTS JDFTSF01 TO JDFTST07 ARE LOCATED ALONG THE CREST OF THE DE BEERS TSF. IF ANY POINTS ARE FOUND TO BE CLOSE TO COMPARTMENT 2, THEN PLEASE SHIFT THE POINT IN AN EASTERLY DIRECTION UNTIL ACCESS IS POSSIBLE.
- POINTS JDTSF07 TO JDTSF09 ARE LOCATED 70m AWAY FROM THE SOUTHERN EDGE OF THE EMBANKMENT. IF ANY POINTS ARE FOUND TO BE WITHIN "NO ACCESS" ZONE THEN PLEASE SHIFT THE POINT IN A NORTHERLY DIRECTION UNTIL AT LEAST 10m AWAY FROM THE ZONE.

FIGURE 1 LOCATION OF THE 11 CPT SOUNDINGS PERFORMED BY SRK. SOURCE: PMI (2023).

Table 1. Summary of CPT soundings performed by SRK.

Sounding	Depth (m)	PPDT depths (m)	Saturated layers (m)	Coordinates	
				Northing	Easting
JDFTSF01	11.1	10; 11.1	n/a	S29°46'09"	E25°25'23"
JDFTSF02	11.0	2; 4; 6; 9; 11	n/a	S29°46'09"	E25°25'24"
JDFTSF03	8.3	2; 4; 6; 8; 8.2; 8.3	1.1 to 3.4	S29°46'11"	E25°25'27"
JDFTSF04	10.6	2; 4; 7; 10; 10.6	2 to 6	S29°46'13"	E25°25'28"
JDFTSF05	18.4	2; 4; 6; 8; 10; 12; 15; 18; 18.4	11.5 to 18	S29°46'16"	E25°25'28"
JDFTSF06	10.4	3; 6; 9; 10.3; 10.4	4.1 to 6.9	S29°46'19"	E25°25'29"
JDFTSF07	23.2	2; 4; 6; 7; 9; 11; 13; 15; 17; 19; 23.2	2 to 7; 17 to 22.4	S29°46'20"	E25°25'29"
JDFTSF13	11.2	2; 4; 6; 9; 11.2	2.3 to 5.9	S29°46'21"	E25°25'29"
JDFTSF14	10.2	2; 4; 6; 9; 10.1; 10.2	2.8 to 6	S29°46'19"	E25°25'29"
JDFTSF15	14.0	2; 4; 6; 8; 10; 12; 14	2.8 to 14	S29°46'18"	E25°25'29"
JDFTSF16	18.1	2; 4; 6; 8; 10; 12; 14; 16; 18; 18.1	n/a	S29°46'14"	E25°25'28"
Totals	146.6	--	--	--	--

2.2. CPT soundings performed by the investigation panel

We performed 17 CPT soundings (Table 2) during two visits to the Jagersfontein dam that took place between January and March 2024. We received the raw data of the CPT campaign in digital format as well as data plots prepared by the CPT contractor Osimo. All soundings were located close to the area of the southern wall that failed (Figure 2).

Table 2. Summary of CPT soundings performed by the investigation panel.

Sounding[a]	Depth (m)	PPDT depths[b] (m)	Saturated ranges (m)
CPT01	8.6	1 to 3; 5; 7; 8.6	2 to 8.6
CPT02	11.6	1 to 9; 9.6; 11; 11.6	10 to 11.6
CPT03	17.3	1 to 9; 11 to 13; 15; 17; 17.3	6 to 17.3
CPT04-m	25.1	1 to 15; 17; 19 to 21; 25; 25.1	13.8 to 25
CPT05-m	18.9	2 to 17; 18.9	16 to 19
CPT06-m	21.3	1 to 9; 11; 13; 16; 18; 20	9 to 20
CPT07	7.6	1 to 4; 6; 7; 7.6	4.4 to 7
CPT08-m	25.9	2 to 4; 6 to 20; 25.9	18 to 25.9
CPT09	8.9	1 to 8; 8.9	6.2 to 7.4
CPT10	19.6	2 to 18; 18.6; 19.6	16.4 to 19.6
CPT11-m	12.4	1 to 3; 5; 8; 12.4	2 to 12.3
CPT12-m	7.3	2; 4 to 6; 7.3	2 to 3.4; 5 to 7.3
CPT13-s	24.1	0.3; 0.9; 2 to 8; 8.9 to 12.9; 16; 17; 21; 24.1	11.9 to 24
CPT14-s	23.7	1 to 10; 11.1 to 18.1; 20; 21; 23.7	17.4 to 23.8
CPT15-s	26.3	1 to 5; 6.1 to 9.1; 10.2 to 13.2; 16.3; 18.3; 23.3	12.5 to 26.3
CPT16-s	13.3	0.9; 1.9 to 3.9; 4.6; 4.8 to 6.8; 8.8; 13.3	3.9 to 13.3
CPT17-s	7.1	0.3; 1; 1.9; 2.9; 7.1	1.1 to 7.1

Notes: a) Sounding names ending in "m" and in "s" indicate Mostap sampling and measurement of shear wave velocity, respectively; b) Where a range is reported (e.g. 1 to 4), soundings were made at 1 m intervals inclusive of the initial and final depth of the range.

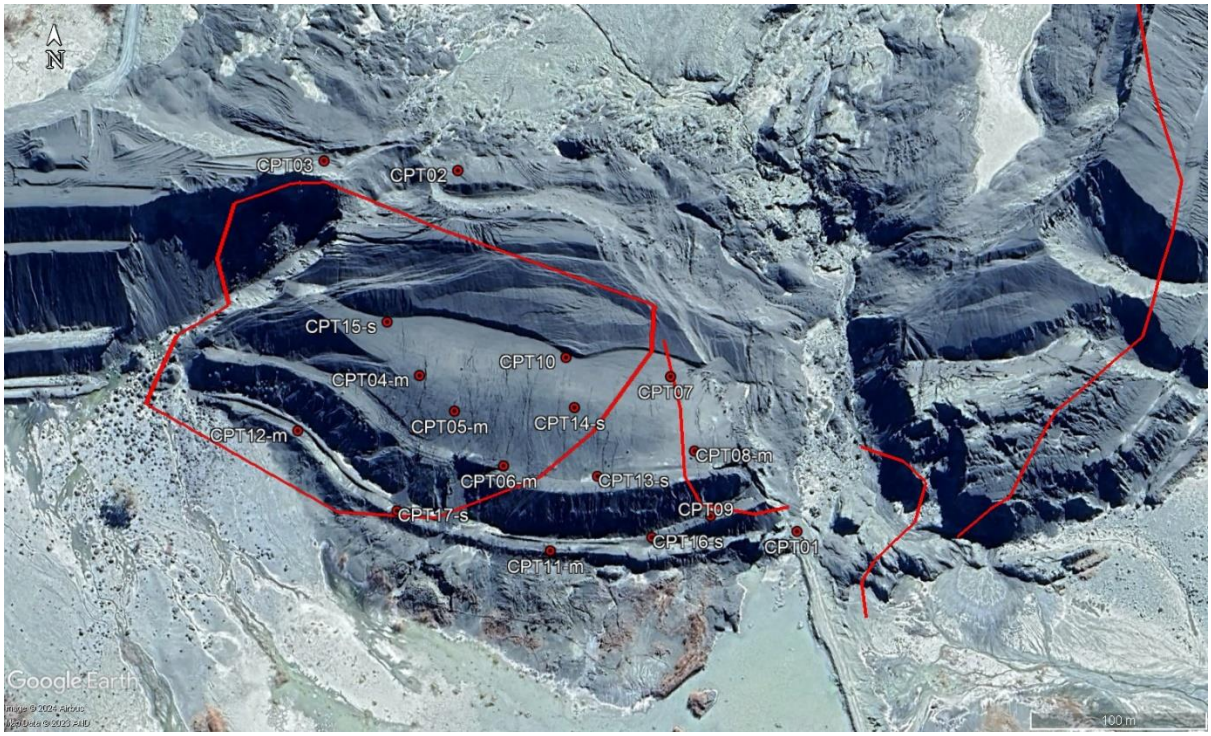

FIGURE 2 **LOCATION OF THE 17 CPT SOUNDINGS PERFORMED BY THE INVESTIGATION PANEL. NOTE: SOUNDING CODES ENDING IN 'S' INDICATE MEASUREMENT OF V_S. SOUNDING CODES ENDING IN 'M' INDICATE MOSTAP SAMPLING. RED LINES INDICATE APPROXIMATE EXTENT OF DUMP 10, NORTH DUMP AND SOUTH DUMP.**

Predrilling was not used for any of the soundings, so readings began at ground level. The soundings were performed with subtraction cones with a projected area of 10 cm^2. The soundings measured q_c, f_s, u_2, and PPDTs. Additionally, five soundings included shear wave velocity (V_s) measurements and Mostap sampling was performed at six sounding locations (Table 2 and Figure 2).

For the same reasons as for the CPT data collected by SRK, we treated saturated layers that were either thinner than ~1 m or which did not have u_0 data as being only partially saturated. Table 2 indicates saturated layers thicker than ~1 m with u_0 estimates.

3. Data processing

3.1. Cone penetration tests

Total cone tip resistance q_t was computed as

$$q_t = q_c + u_2(1 - a)$$	(1)

where a is the unequal area cone factor reported as a = 0.8 by both CPT contractors that worked at Jagersfontein.

We shifted f_s measurements upwards by 110 mm to account for the geometry of the 10 cm^2 cone which results in simultaneous measurements of q_c and f_s being vertically offset (ASTM D5778-20). We deleted sudden spikes and drops in q_c, f_s or u_2 at depths were PPDTs had been performed. These spikes and drops are likely an artefact caused by the pause in cone advancement to perform the PPDT and not actual soil response (Campanella and Robertson 1988, ASTM D5778-20).

The way in which we interpreted the CPT results depended on whether the soil was saturated or not. We assumed that layers were saturated only when their u_2 response deviated from zero by more than ±4 kPa (Rust and Rust, 2023).

Due to time constraints, several PPDTs had to be terminated prior to full dissipation of the excess pore water pressure. We inferred u_0 from these incomplete PPDTs using a semi-empirical extrapolation scheme (Scheremeta 2014). The adopted scheme considers that the porewater pressure u_t measured at any time t after a PPDT has begun is given by

$$u_t = u_0 + \Delta u_t$$	(2)

where u_0 is the sought ambient porewater pressure which remains constant with time and Δu_t is the excess porewater pressure which varies with time. By making an initial guess of u_0 and considering the actual u_t values measured during the PPDT, Δu_t can be computed for any time from Equation 2. Additionally, Δu_t is also computed using the following equations (Scheremata 2014).

$$\Delta u_t = (\Delta u_{vol})_i \left[1 + 50\frac{c_h t}{a^2 (I_R)^{0.75}}\right]^{-1} + (\Delta u_{shear})_i \left[1 + 5000\frac{c_h t}{a^2 (I_R)^{0.75}}\right]^{-1}$$	(3)
$$(\Delta u_{vol})_i = \sigma_v' \left(\frac{12\ sin\ sin\ \phi'}{9 - 3\ sin\ sin\ \phi'}\right)\left(\frac{OCR}{2}\right)^{1-\frac{C_s}{C_c}} ln\ ln\ (I_R)$$	(4)
$$(\Delta u_{shear})_i = \sigma_v' \left[1 - \left(\frac{OCR}{2}\right)^{1-\frac{C_s}{C_c}}\right]$$	(5)

Where $(\Delta u_{vol})_i$ is the initial excess pore water pressure due to the volume reduction induced by the cone, $(\Delta u_{shear})_i$ is the initial excess pore water pressure due to the shearing induced by the cone, c_h is the coefficient of horizontal consolidation, a is the radius of the cone penetrometer, I_R is the rigidity index, σ'_v is the pre-CPT vertical effective stress, φ' is the effective friction angle, OCR is the overconsolidation ratio, C_s is the swelling index, and C_c is the coefficient of compression.

Equations 3 to 5 involve several soil parameters that are seldom known in general and which were not measured at Jagersfontein in particular. Accordingly, as per Scheremeta (2014), we implemented Equation 3 in a Microsoft Excel spreadsheet and used the 'Solver' tool to vary the initial guess of u_0 together with the values of all parameters involved in Equations 3 to 5, except a in order to maximise the agreement between $\Delta u_t = u_t - u_0$ and Δu_t from Equation 3.

This approach involved varying five parameters (C_h, I_R, φ', OCR, and C_s/C_c) which we could not validate against experimental data. Accordingly, as it was implemented herein, our approach to estimate u_0 was essentially a curve fitting exercise. To guard against spurious results, we checked that our extrapolated u_0 values were consistent with non-extrapolated values. We did not find any cases in which the extrapolated u_0 values had an obvious inconsistency with the non-extrapolated values. Notwithstanding, our u_0 profiles distinguish between extrapolated and non-extrapolated values.

We computed the following normalised parameters to process the CPT results.

$$Q = \frac{q_t - \sigma_v}{\sigma'_v}$$	(6)
$$U2 = \frac{u_2 - u_0}{\sigma'_v}$$	(7)
$$Q' = \frac{q_t - u_2}{\sigma'_v}$$	(8)
$$F = \left(\frac{f_s}{q_t - \sigma_v}\right) 100\%$$	(9)
$$Q_{tn} = \left(\frac{q_t - \sigma_v}{p_a}\right)\left(\frac{p_a}{\sigma'_v}\right)^n$$	(10)
$$n = 0.381 I_{c-RW} + 0.05\frac{\sigma'_v}{p_a} - 0.15$$	(11)
$$I_{c-RW} = \sqrt{(3.47 - Q_{tn})^2 + (F)^2}$$	(12)

Where σ_v is the vertical total stress, p_a is the atmospheric pressure, n is a stress level exponent that varies between 0.5 and 1, and $I_{c\text{-}RW}$ is a soil behaviour type index initially proposed by Robertson and Wride (1998) and updated in Robertson (2009). Equations 10 to 12 are interdependent and require iterative calculations to converge to final values.

We used the normalised parameters defined in Equations 6 to 12 to plot CPT results in the four charts shown in Figure 3:

1) The Q vs f_s/σ'_{v0} chart proposed in Saye et al. (2017)
2) The Q vs $U2$ chart initially proposed in Schneider et al. (2008) and later modified in Fourie et al. (2022)
3) The Q' vs F chart proposed in Jefferies and Been (2015)
4) The Q_{tn} vs F chart proposed in Robertson (2022)

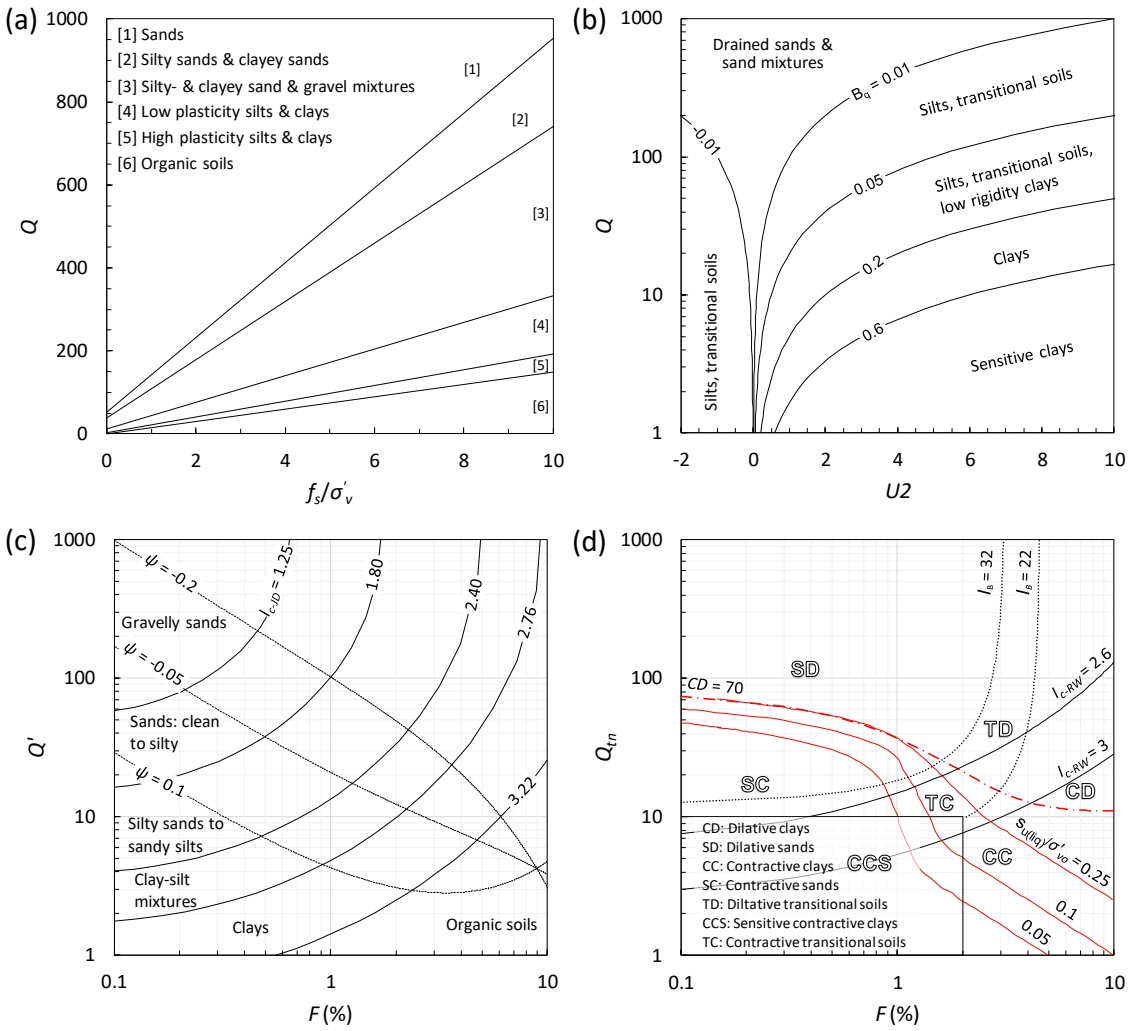

FIGURE 3 THE FOUR CHARTS USED HEREIN TO AID THE INTERPRETATION OF CPT RESULTS. A) Q VS F_S/Σ'_{V0} (SAYE ET AL. 2017), B) Q VS $U2$ (SCHNEIDER ET AL. 2008, FOURIE ET AL. 2022) C) Q' VS F (JEFFERIES AND BEEN 2015) AND D) Q_{TN} VS F (ROBERTSON 2022).

The Q vs f_s/σ'_{v0} chart (Figure 3a) is suitable for use regardless of saturation level. Accordingly, all CPT results were plotted in the Q vs f_s/σ'_{v0} chart. The Q vs $U2$ and Q' vs F charts (Figures 3b and 3c) use u_2 measurements and as such can only be expected to yield meaningful results in saturated soils. Accordingly, only CPT results from saturated depths were plotted in these charts. The Q_{tn} vs F chart (Figure 3d) does not use u_2 measurements, however, it was developed in the context of liquefied strength assessments. Since liquefaction only occurs in saturated or nearly saturated soils, only CPT results from saturated depths were plotted on the Q_{tn} vs F chart.

The four different plots in Figure 3 are divided, at least approximately, into areas of different soil behaviour type by contours of ΔQ (Saye et al. 2017), B_q (Fourie et al. 2022), $I_{c\text{-}JD}$ (Been and Jefferies 1992, Jefferies and Davies 1993) and I_B (Robertson 2016). These four parameters can thus be interpreted as soil behaviour type indices and are defined as

$$\Delta_Q = \frac{(Q+10)}{\left[\left(\frac{f_s}{\sigma'_{v0}}\right)+0.67\right]}$$	(13)
$$B_q = \frac{u_2-u_0}{q_t-\sigma_v} = \frac{U2}{Q}$$	(14)
$$I_{c-JD} = \sqrt{(3-Q')^2+(1.5+1.3F)^2}$$	(15)
$$I_B = \frac{100(Q_{tn}+10)}{(70+Q_{tn}F)}$$	(16)

The contours of the state parameter ψ (Been and Jefferies 1985) on the Q' vs F (Figure 3c) chart were computed as per the following equations (Jefferies and Been 2015).

$$\psi = ln\ ln\left[\frac{\frac{3(Q'-1)}{1+2K_0}+1}{M\left(3+\frac{0.85}{\lambda_{10}}\right)}\right]\left(\frac{1}{13.3\lambda_{10}-11.9}\right)$$	(17)
$$\lambda_{10} = \frac{F}{10}$$	(18)

Equations 17 and 18 are slightly modified version of the Plewes method (Plewes et al. 1992). While the Plewes method does not enable measurements of ψ that are accurate enough for detailed characterisation of tailings (Torres-Cruz 2021), we use it here as a means of informing the "relative susceptibility of soils to liquefaction" (Plewes et al. 1992).

The "CD = 70" contour in the Q_{tn} vs F chart (Figure 3d) represents an empirical boundary between contractive and dilative behaviour which is applicable when soils do not exhibit significant interparticle bonding or cementation (Robertson 2016). The contour is defined as follows (Robertson 2016).

$$CD = (Q_{tn}-11)(1+0.06F)^{17} = 70$$	(19)

Additionally, the contours of the undrained residual strength ratio (S_r/σ'_v) in the Q_{tn} vs F chart (Figure 3d) are partly defined by Equations 20 to 22 which are valid when $I_{c\text{-}RW} < 3$, $20 < Q_{tn,cs} < 80$ and $\sigma'_v \leq 300$ kPa (Robertson 2022).

$\frac{S_r}{\sigma_v^{'}} = 0.0007exp\left(0.084Q_{tn,cs}\right) + \frac{0.3}{Q_{tn,cs}}$	(20)
$Q_{tn,cs} = K_c Q_{tn}$	(21)
$K_c = 15 - \frac{14}{1 + \left(\frac{I_c}{2.95}\right)^{11}}$	(22)

Robertson (2022) further indicates that if $I_{c\text{-}RW} < 3$, $Q_{tn,cs} < 20$ and, presumably, $\sigma'_v \leq 300$ kPa, then $S_r/\sigma'_v = 0.02$ but that $S_r = 1$ kPa should be used as a lower bound when $\sigma'_v < 50$ kPa to avoid underestimations at low σ'_v.

When $I_{c\text{-}RW} < 3$ and $Q_{tn,cs} \geq 80$, Robertson (2022) proposes that the controlling ratio of residual shear strength to vertical effective stress (τ/σ'_v) is given by

$\frac{\tau}{\sigma_v^{'}} = tan\ tan\ \phi_c^{'}$	(23)

where φ'_c is the effective critical state friction angle.

When $I_c \geq 3$, the residual undrained shear strength is approximated by the equation below (Robertson 2022).

$\frac{S_r}{\sigma_v^{'}} = \frac{f_s}{\sigma_v^{'}} = \frac{FQ_{tn}}{100}$	(24)

We used shear wave velocity V_s coupled with Q_{tn} to distinguish between uncemented tailings and tailings with interparticle bonding. The distinction was made assuming that uncemented soils yield $100 < K^*_G < 330$ and cemented soils yield $K^*_G \geq 330$ (Robertson 2016). This criterion is illustrated in Figure 5. K^*_G is given by

$K_G^* = \frac{G_0}{q_t - \sigma_v} Q_{tn}^{0.75}$	(25)
$G_0 = \rho V_s^2$	(26)

where ρ is the total density of the soil which we determined to be 1900 kg/m^3 from moist tamped specimens collected for triaxial testing.

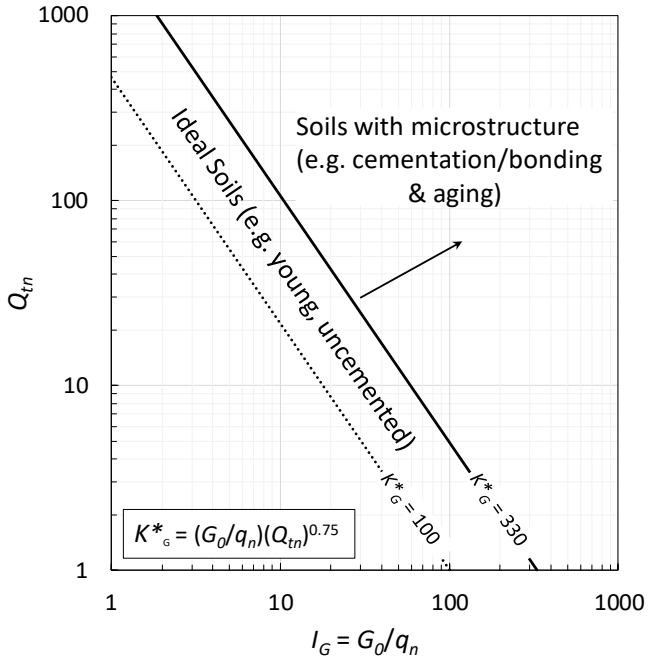

FIGURE 4 CRITERION USED TO DISTINGUISH UNCEMENTED FROM CEMENTED SOILS. FROM ROBERTSON (2016).

4. Results and discussion

4.1. Cone penetration tests performed by SRK

As the CPT soundings performed by SRK were not located close to the area of the failure, these soundings are not of significant relevance to our analysis of the hypothesised failure mechanism. As such, we present the processed results from Figures 6 to 27 for completeness but do not delve any further into these results.

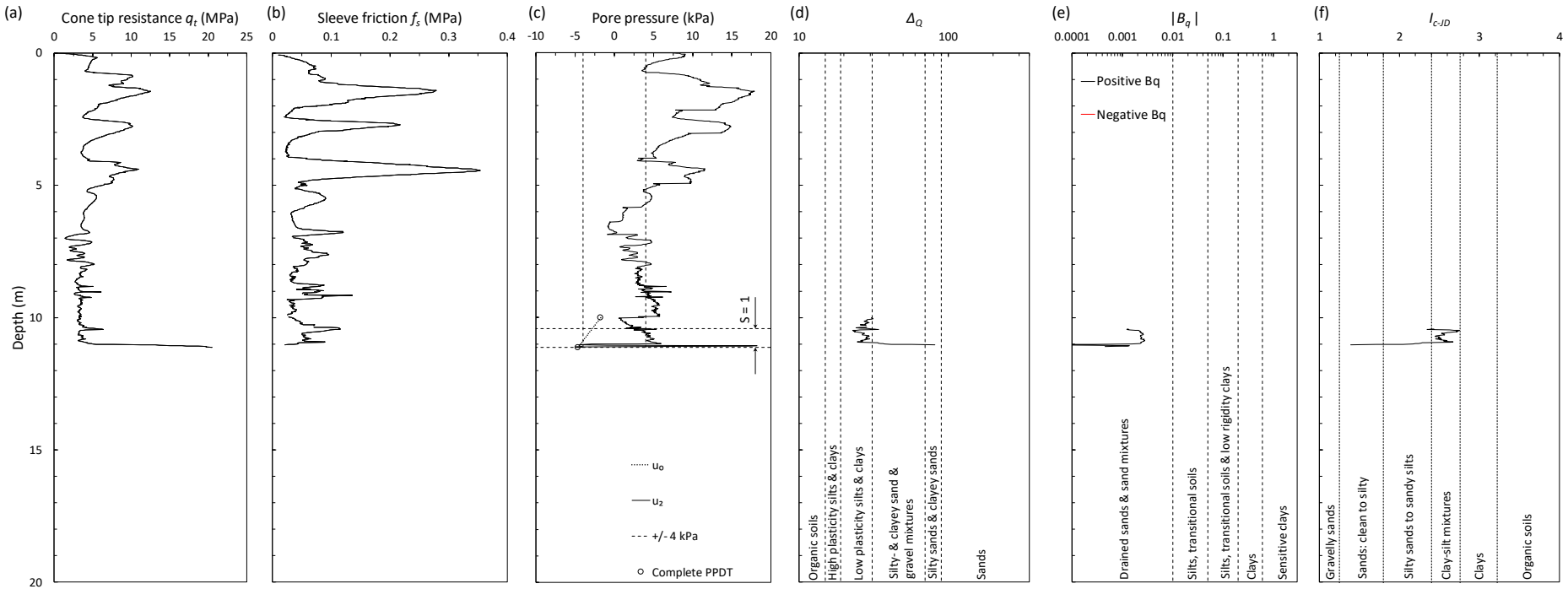

FIGURE 5 PROFILES OF CPTU SOUNDING JDFTSF01: (A) CONE TIP RESISTANCE Q_T (B) SLEEVE FRICTION F_S (C) DYNAMIC AND INTERPOLATED U_0 PORE PRESSURES (D) Δ_Q (E) B_Q AND (F) SOIL BEHAVIOUR INDEX $I_{C\text{-}JD}$.

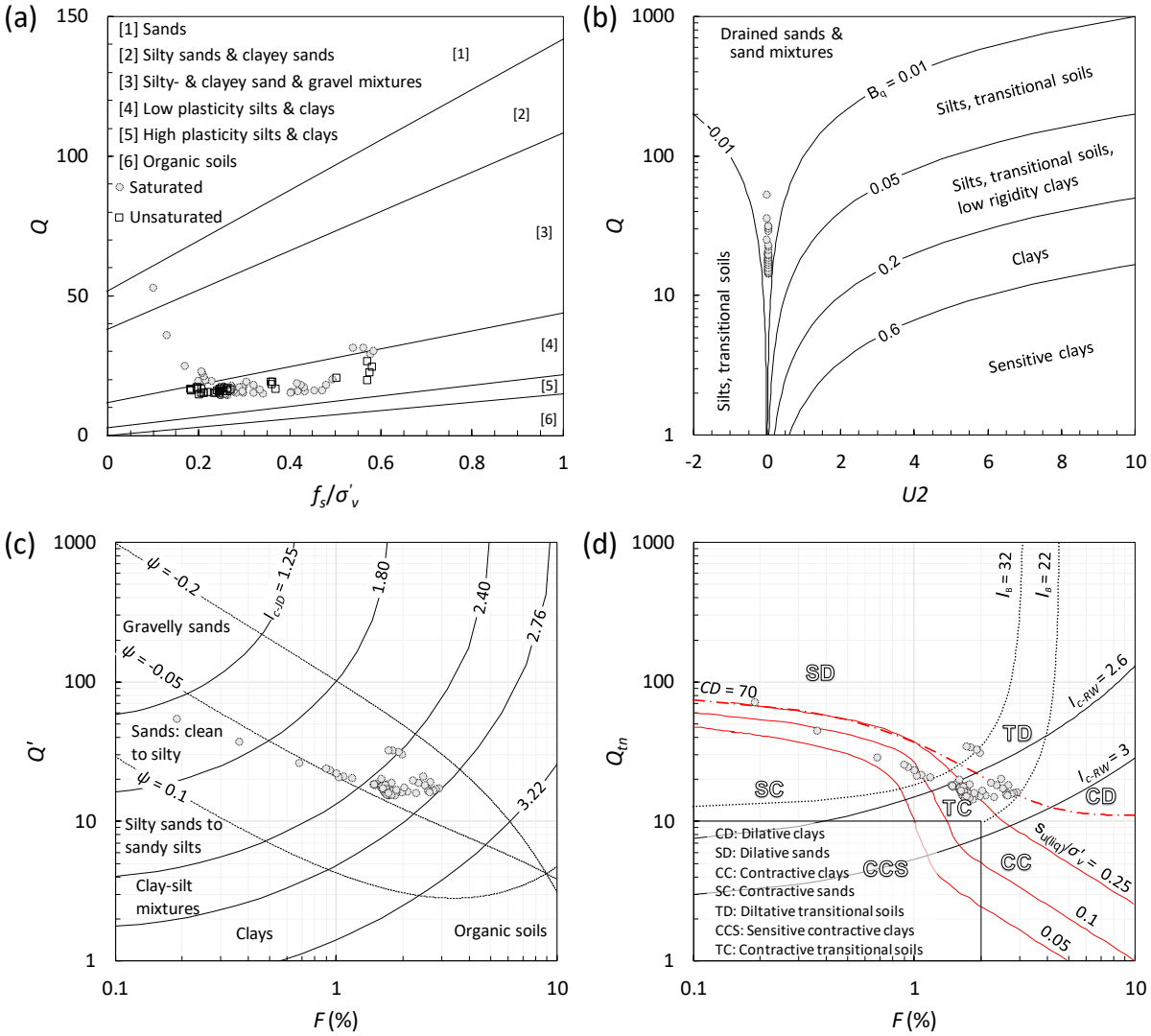

FIGURE 6 SOIL BEHAVIOUR TYPE CHARTS FOR CPT POSITION JDFTSF01 (A) *Q* VS F_S/Σ'_{VO} (B) *Q* VS *U2* (C) Q' VS *F* AND (D) Q_{TN} VS *F*.

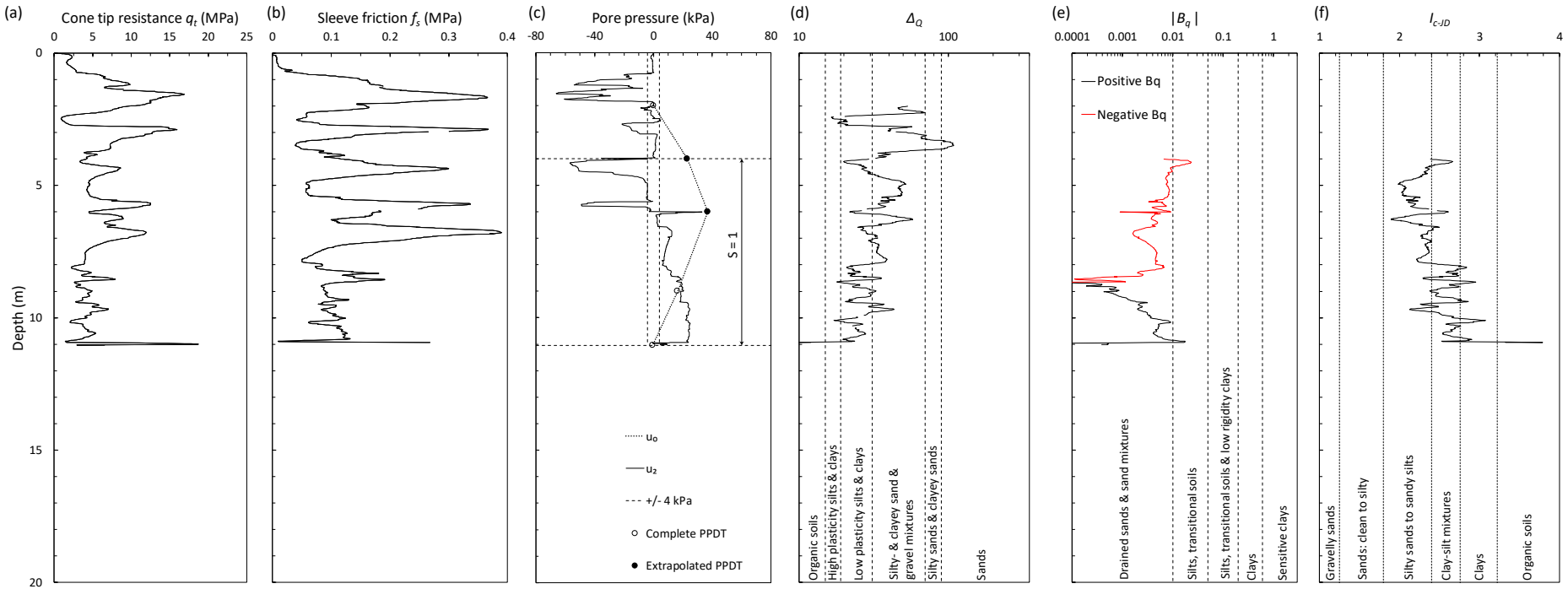

FIGURE 7 PROFILES AT CPT POSITION JDFTSF02: (A) CONE TIP RESISTANCE Q_T (B) SLEEVE FRICTION F_S (C) DYNAMIC AND INTERPOLATED U_0 PORE PRESSURES (D) Δ_Q (E) B_Q AND (F) SOIL BEHAVIOUR INDEX I_{C-JD}.

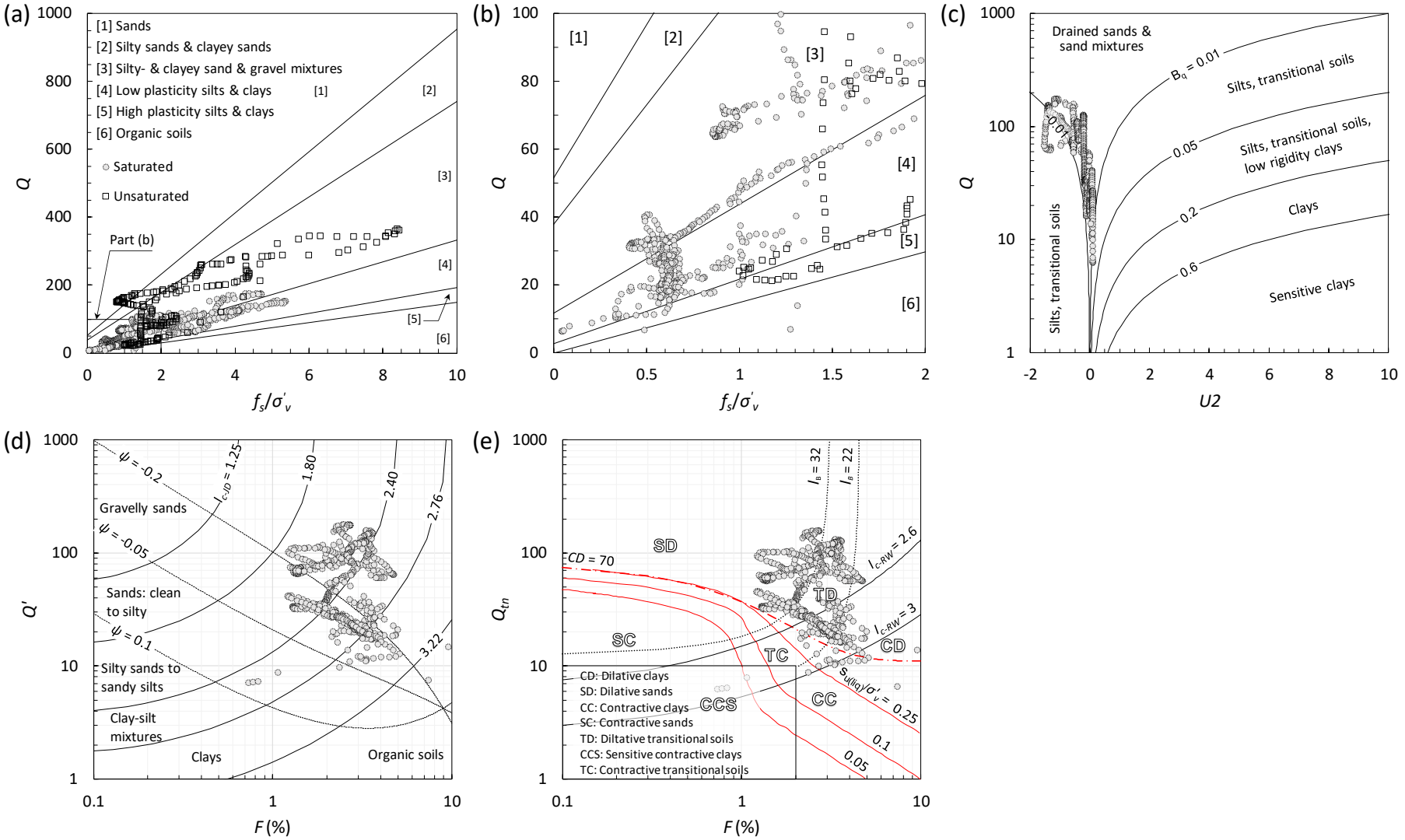

FIGURE 8 **SOIL BEHAVIOUR TYPE CHARTS FOR CPT POSITION JDFTSF02 (A) Q VS F_S/Σ'_{VO} (B) INSET FROM Q VS F_S/Σ'_{VO} (C) Q VS $U2$ (D) Q' VS F AND (E) Q_{TN} VS F.**

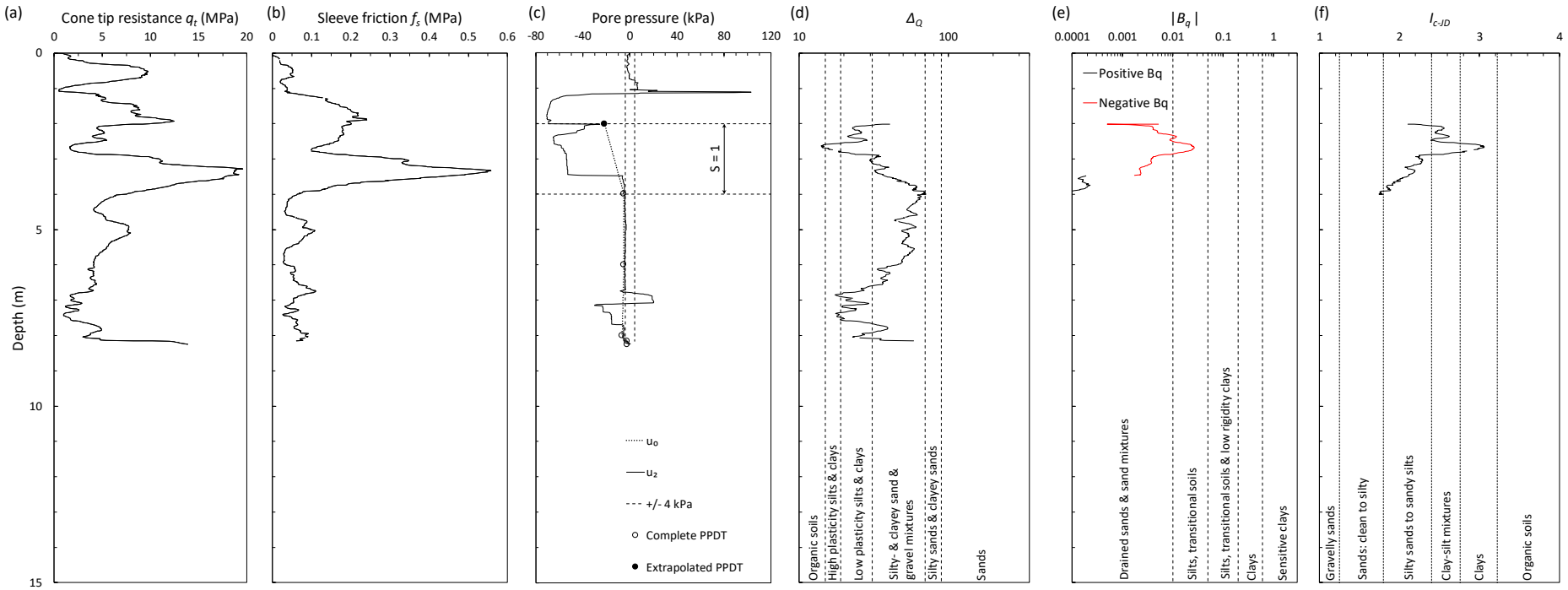

FIGURE 9 PROFILES OF THE CPTU SOUNDING JDFTSF03: (A) CONE TIP RESISTANCE Q_T (B) SLEEVE FRICTION F_S (C) DYNAMIC AND INTERPOLATED U_0 PORE PRESSURES (D) Δ_Q (E) B_Q AND (F) I_{C-JD}.

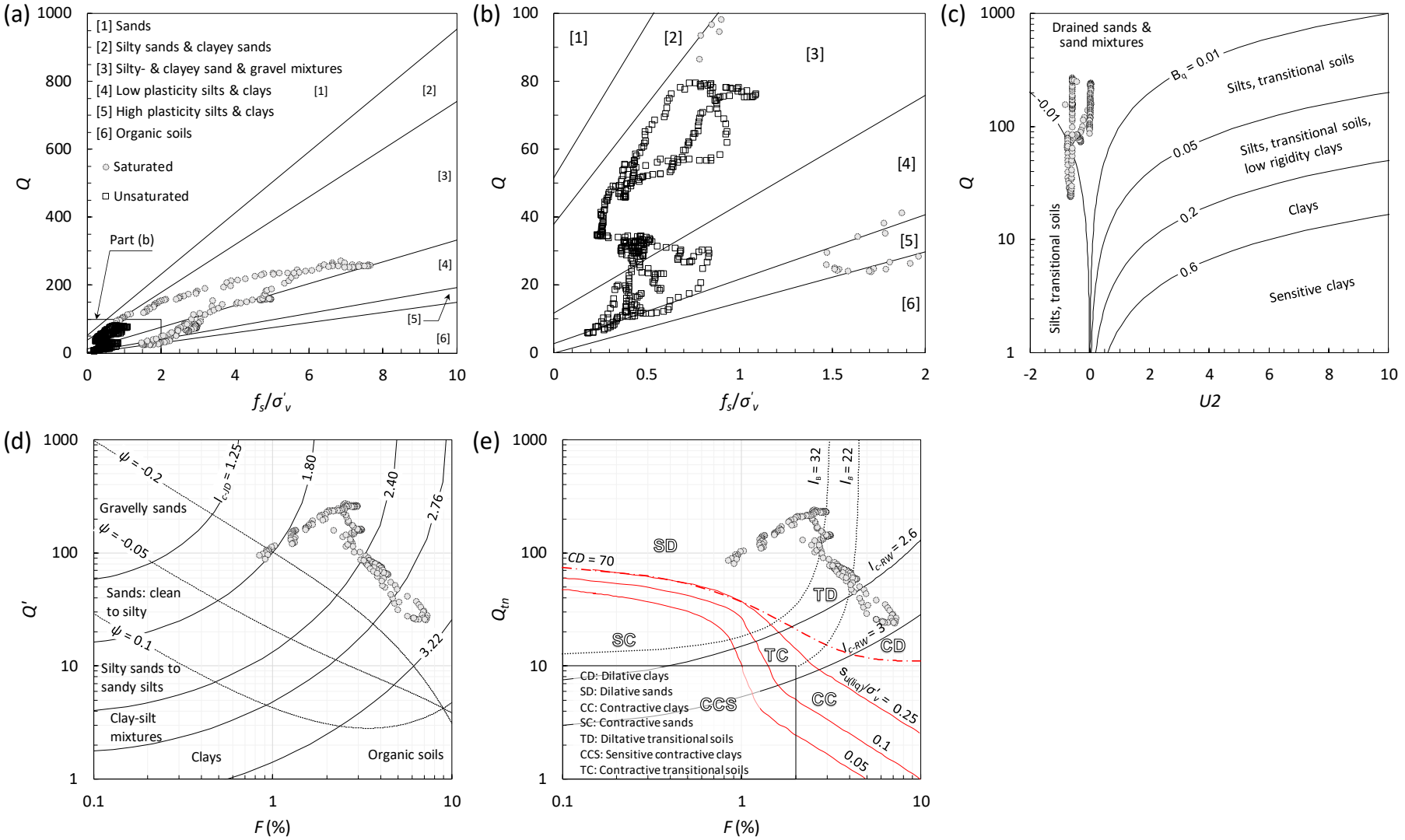

FIGURE 10 SOIL BEHAVIOUR TYPE CHARTS FOR CPT POSITION JDFTSF03 (A) *Q* VS F_S/Σ'_{VO} (B) INSET FROM *Q* VS F_S/Σ'_{VO} (C) *Q* VS *U2* (D) Q' VS *F* AND (E) Q_{TN} VS *F*.

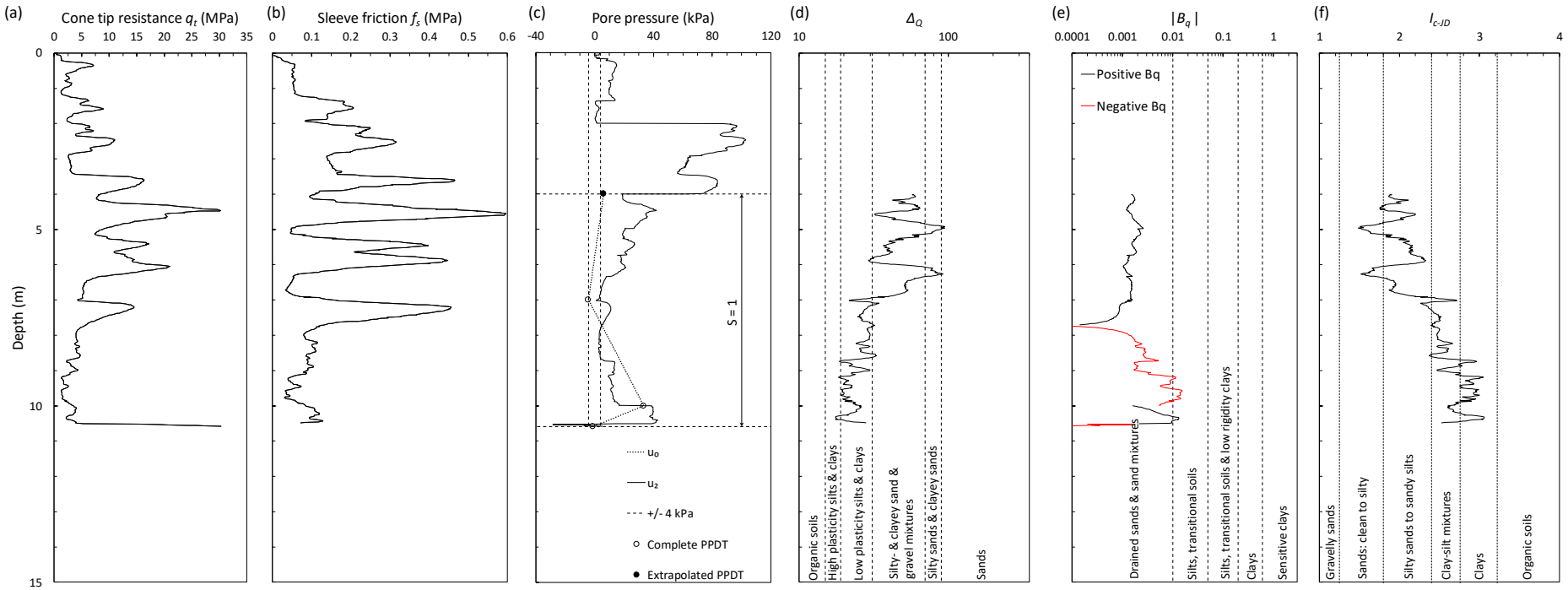

FIGURE 11 PROFILES AT CPT POSITION JDFTSF04 (A) CONE TIP RESISTANCE Q_T (B) SLEEVE FRICTION F_S (C) DYNAMIC AND INTERPOLATED U_0 PORE PRESSURES (D) Δ_Q (E) B_Q AND (F) I_{C-JD}.

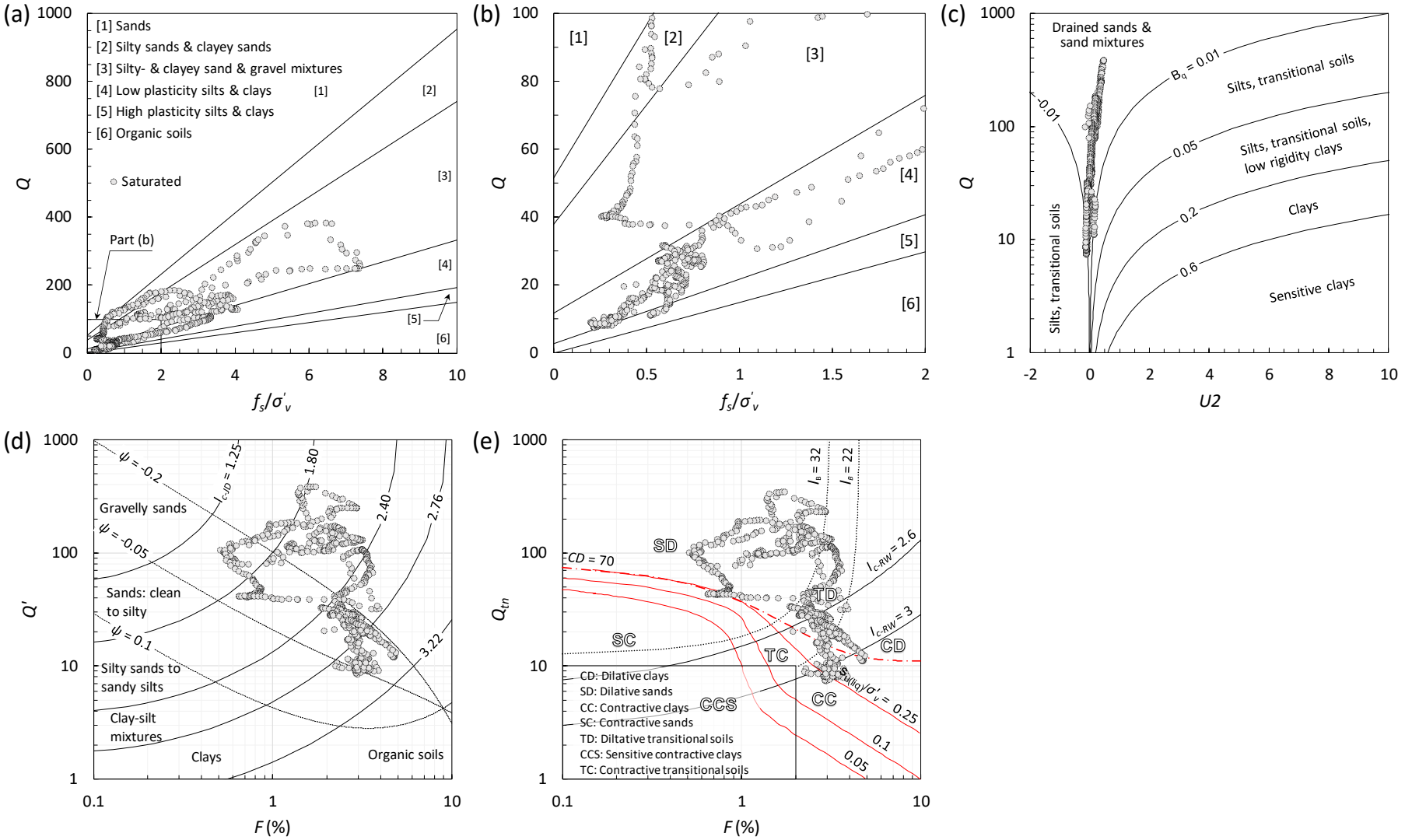

FIGURE 12 SOIL BEHAVIOUR TYPE CHARTS FOR CPT POSITION JDFTSF04 (A) Q VS F_S/Σ'_V (B) ENLARGED Q VS F_S/Σ'_V SPACE (C) Q VS $U2$ (D) Q' VS F AND (E) Q_{TN} VS F.

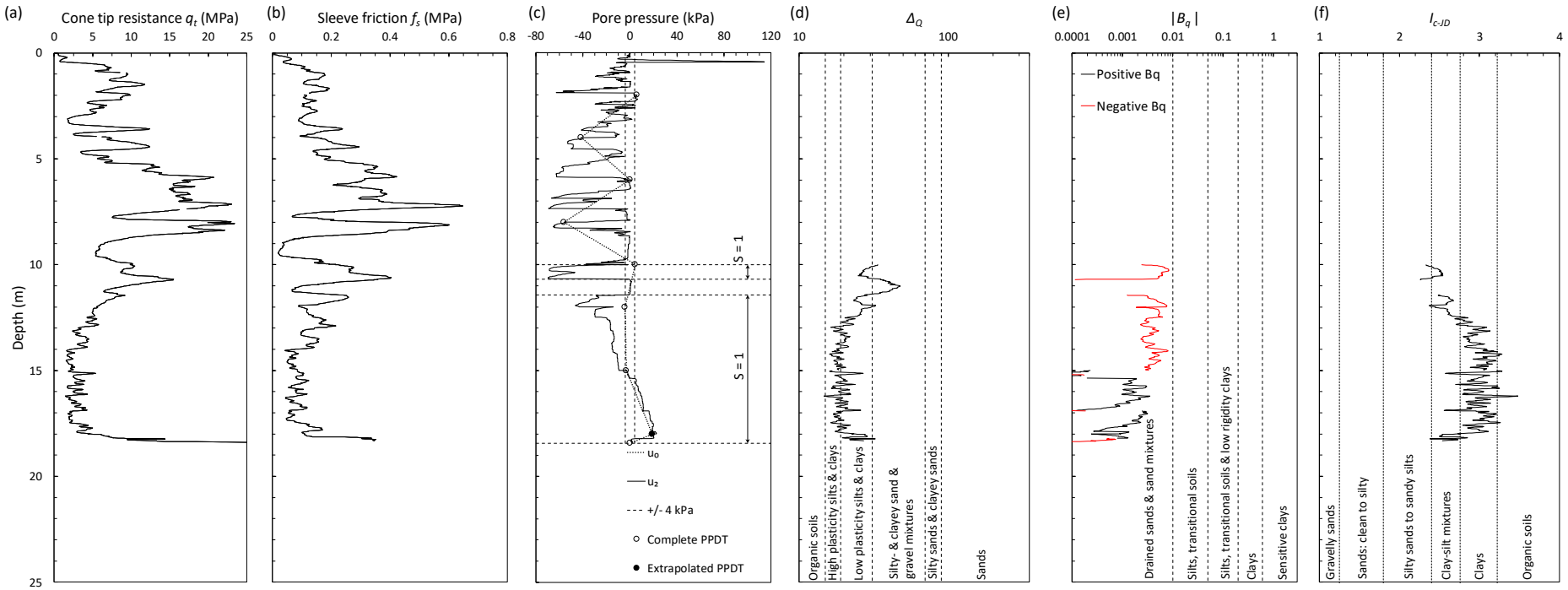

FIGURE 13 PROFILES AT CPT POSITION JDFTSF05 (A) CONE TIP RESISTANCE Q_T (B) SLEEVE FRICTION F_S (C) DYNAMIC AND INTERPOLATED U_0 PORE PRESSURES (D) Δ_Q (E) B_Q AND (F) I_{C-JD}.

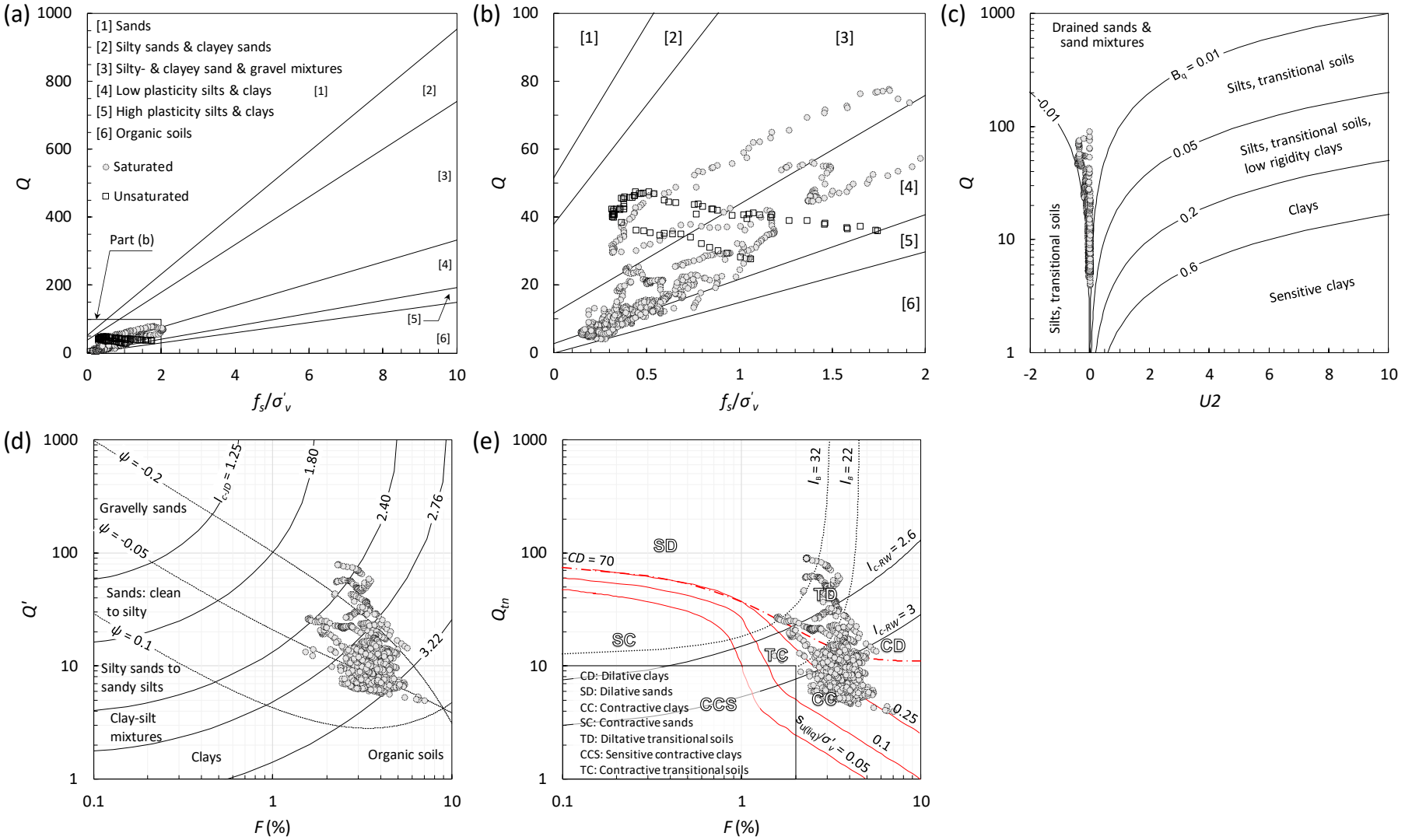

FIGURE 14 SOIL BEHAVIOUR TYPE CHARTS FOR CPT POSITION JDFTSF05 (A) *Q* VS F_S/Σ'_V (B) ENLARGED *Q* VS F_S/Σ'_V SPACE (C) *Q* VS *U2* (D) *Q'* VS *F* AND (E) Q_{TN} VS *F*.

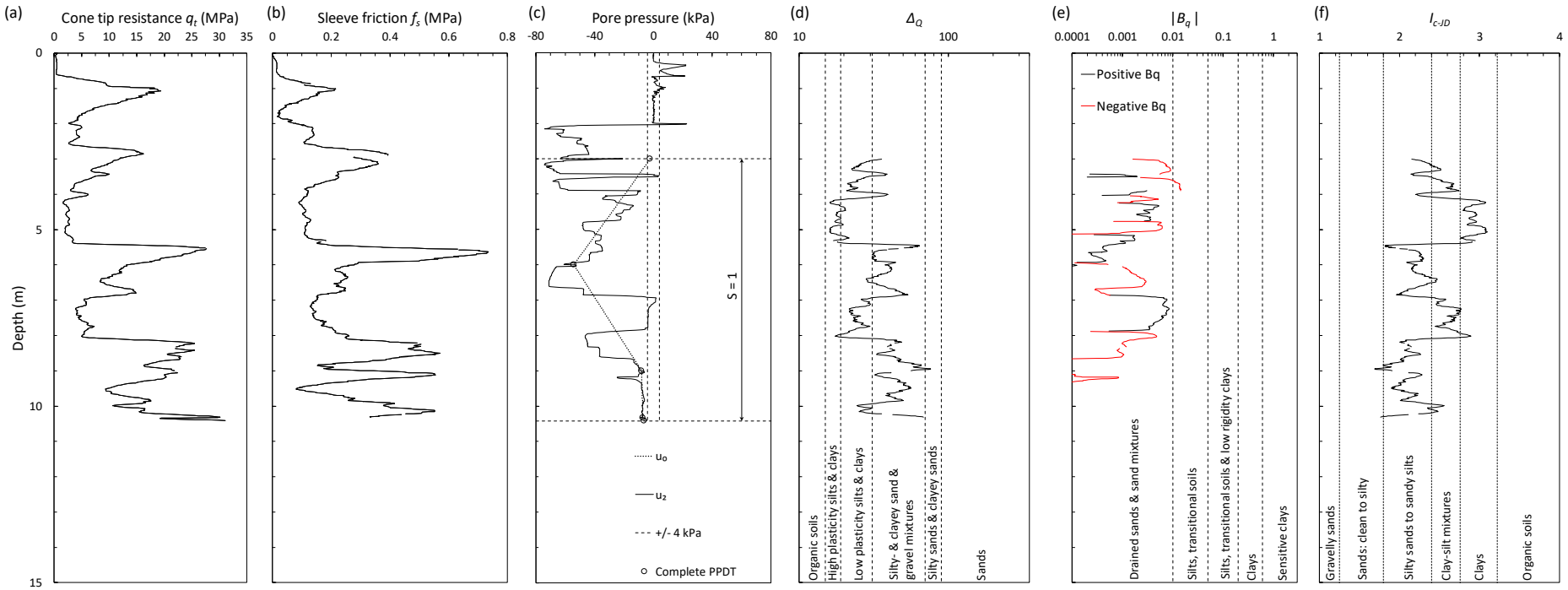

FIGURE 15 PROFILES AT CPT POSITION JDFTSF06 (A) CONE TIP RESISTANCE Q_T (B) SLEEVE FRICTION F_S (C) DYNAMIC AND INTERPOLATED U_0 PORE PRESSURES (D) Δ_Q (E) B_Q AND (F) I_{C-JD}.

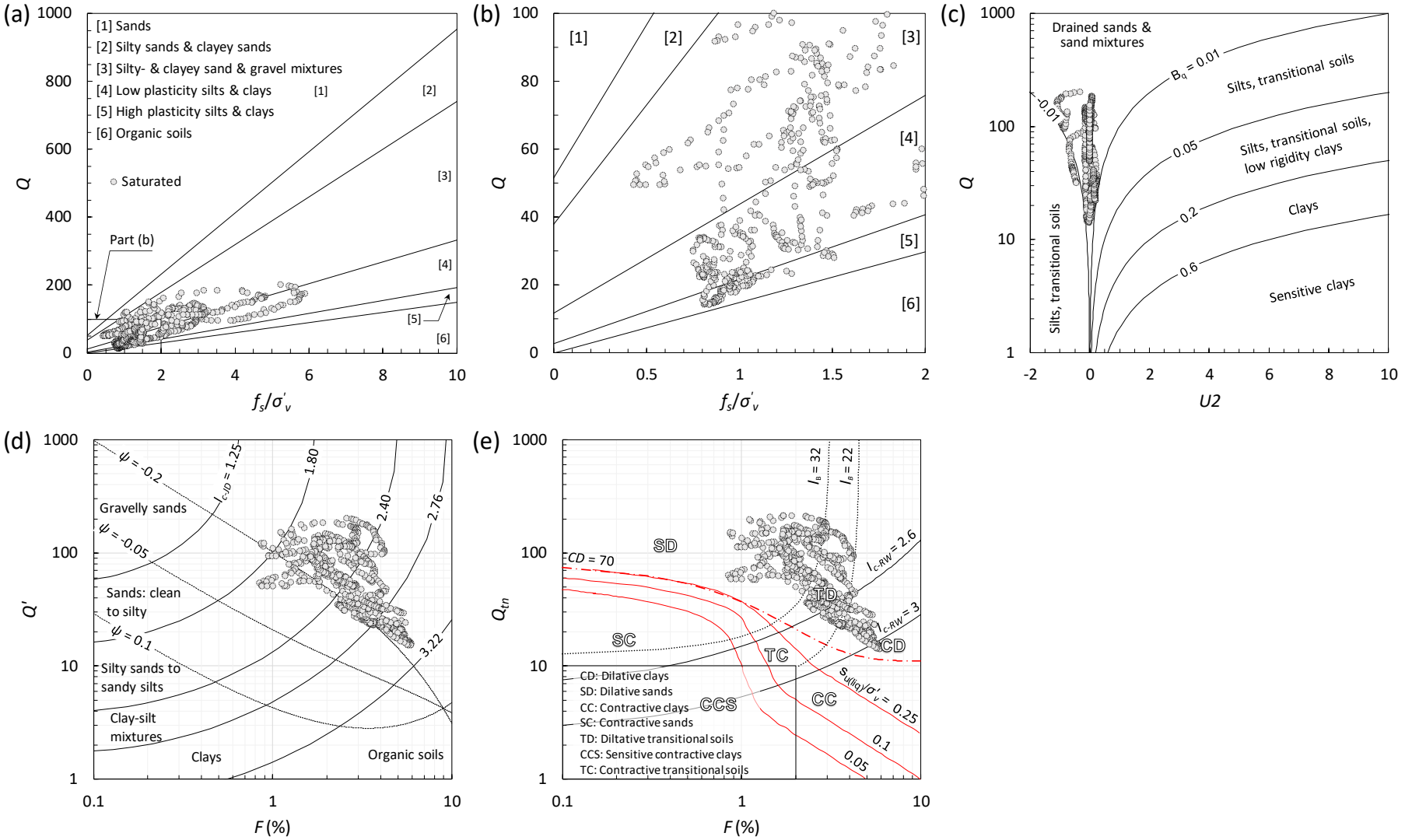

FIGURE 16 SOIL BEHAVIOUR TYPE CHARTS FOR CPT POSITION JDFTSF06 (A) *Q* VS F_S/Σ'_V (B) ENLARGED *Q* VS F_S/Σ'_V SPACE (C) *Q* VS *U2* (D) *Q'* VS *F* AND (E) Q_{TN} VS *F*.

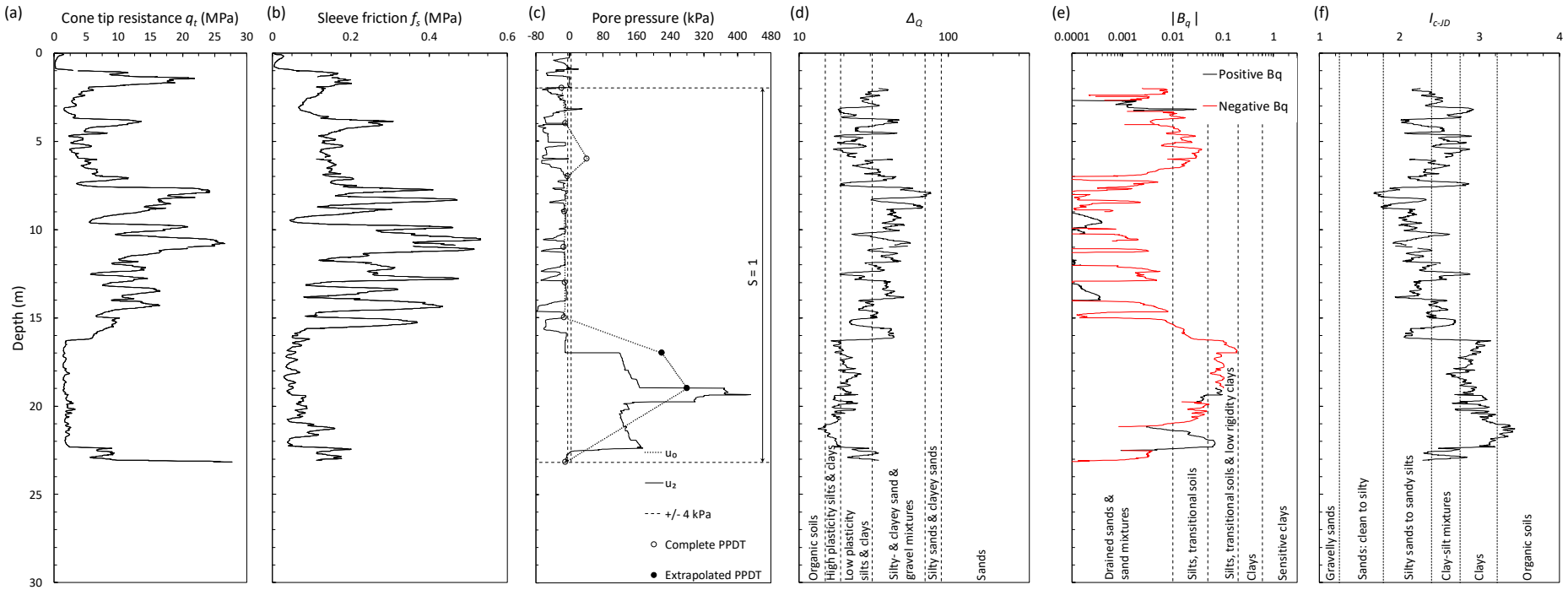

FIGURE 17 PROFILES AT CPT POSITION JDFTSF07 (A) CONE TIP RESISTANCE Q_T (B) SLEEVE FRICTION F_S (C) DYNAMIC AND INTERPOLATED U_0 PORE PRESSURES (D) Δ_Q (E) B_Q AND (F) I_{C-JD}.

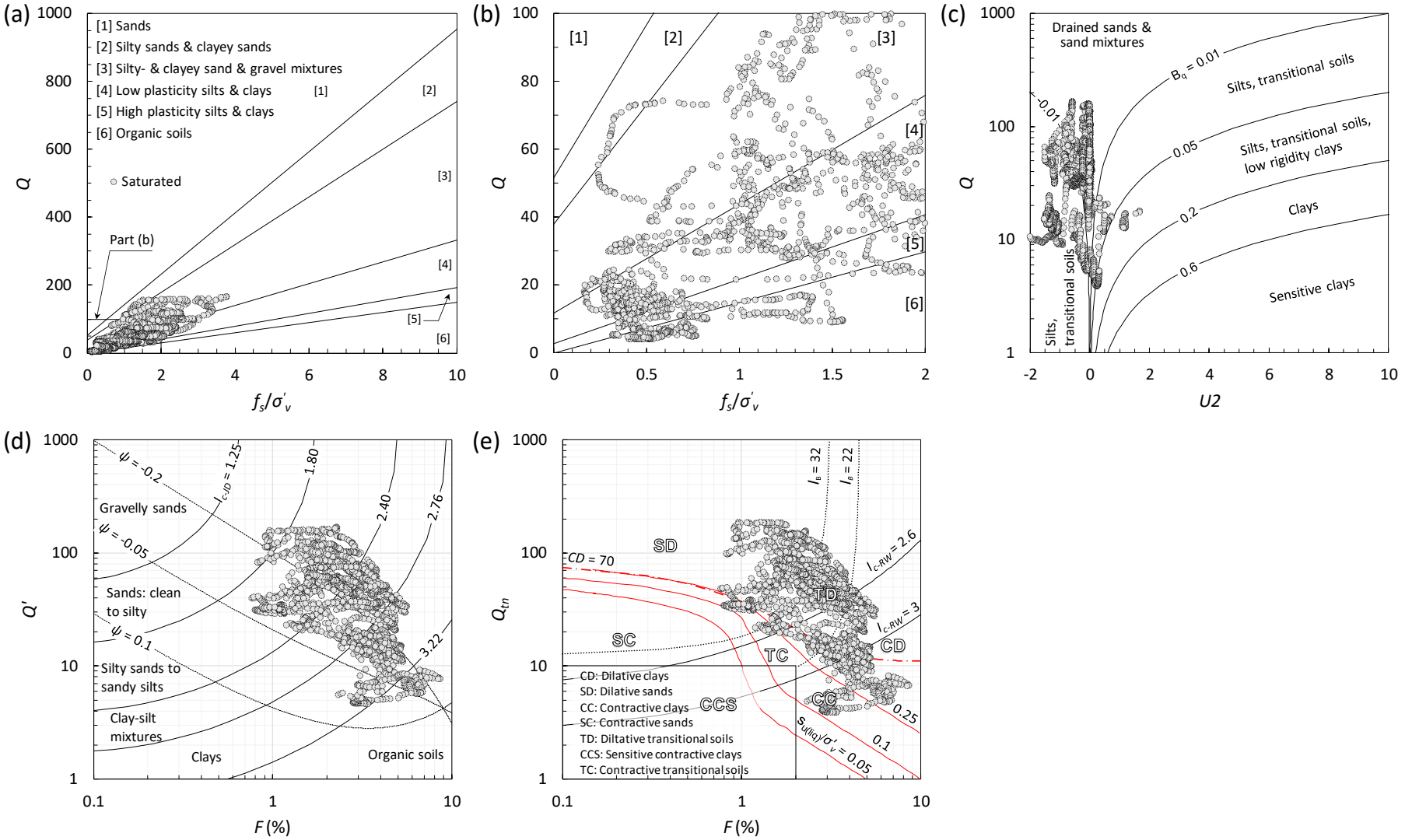

FIGURE 18 SOIL BEHAVIOUR TYPE CHARTS FOR CPT POSITION JDFTSF07 (A) *Q* VS F_S/Σ'_V (B) ENLARGED *Q* VS F_S/Σ'_V SPACE (C) *Q* VS *U2* (D) *Q'* VS *F* AND (E) Q_{TN} VS *F*.

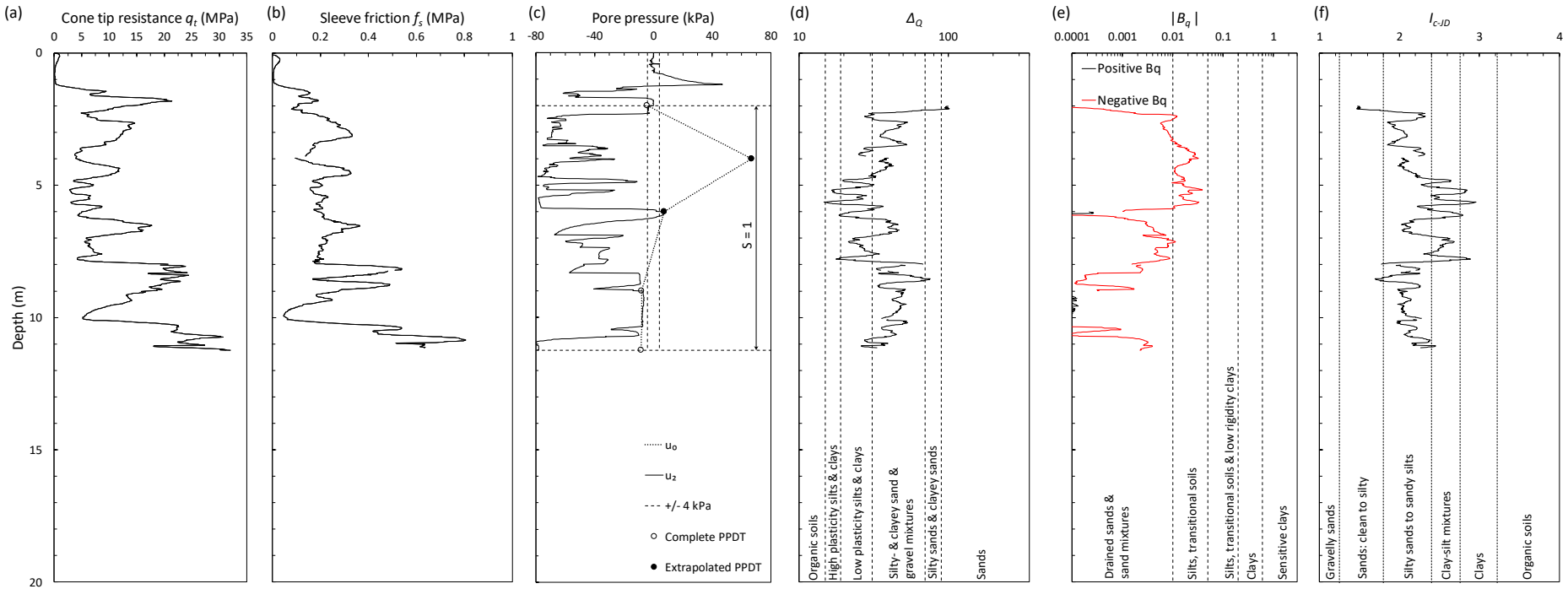

FIGURE 19 PROFILES AT CPT POSITION JDFTSF13 (A) CONE TIP RESISTANCE Q_T (B) SLEEVE FRICTION F_S (C) DYNAMIC AND INTERPOLATED U_0 PORE PRESSURES (D) Δ_Q (E) B_Q AND (F) I_{C-JD}.

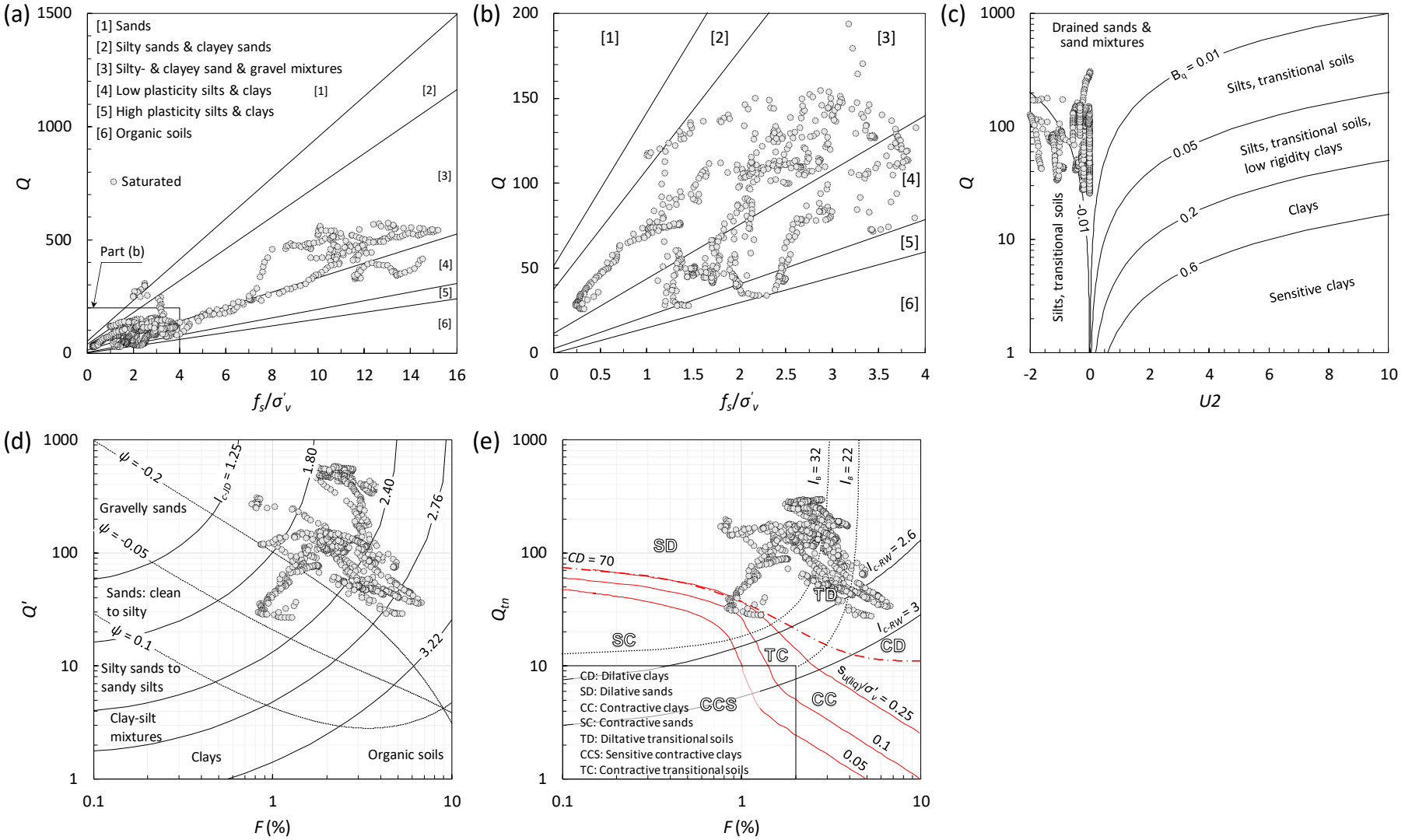

FIGURE 20 SOIL BEHAVIOUR TYPE CHARTS FOR CPT POSITION JDFTSF13 (A) Q VS F_S/Σ'_V (B) ENLARGED Q VS F_S/Σ'_V SPACE (C) Q VS $U2$ (D) Q' VS F AND (E) Q_{TN} VS F.

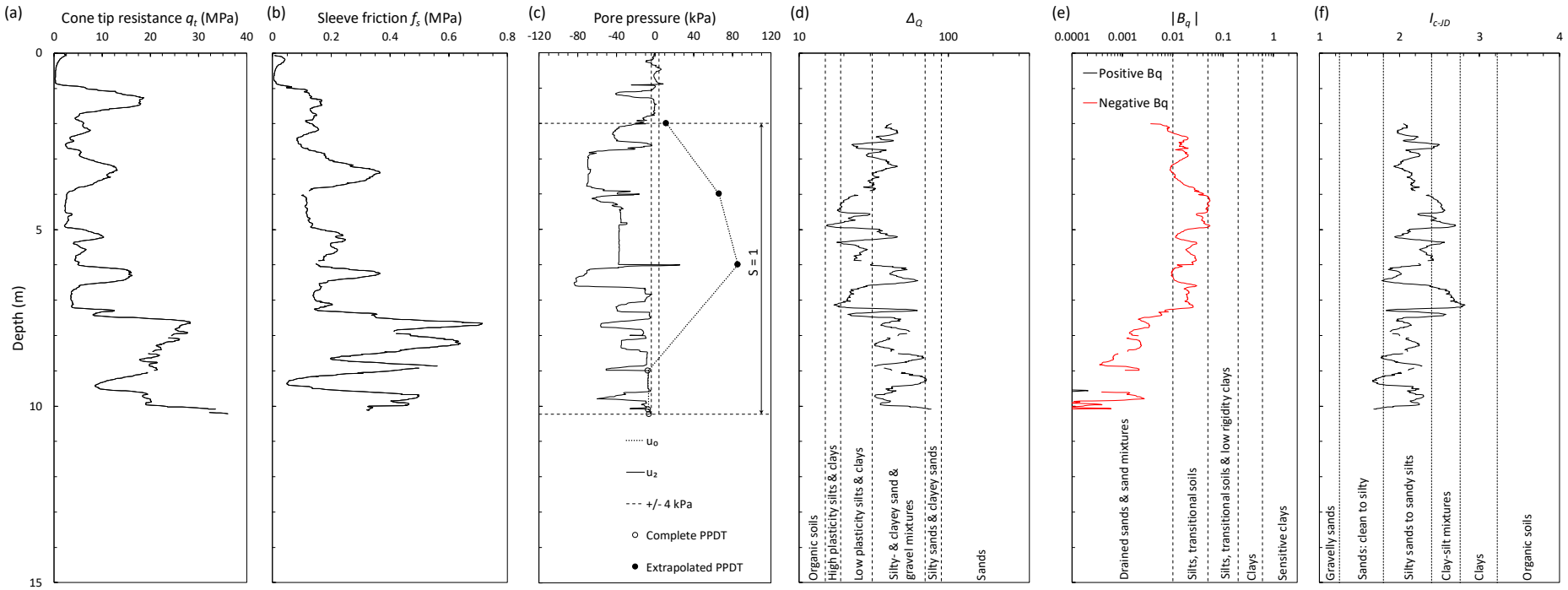

FIGURE 21 PROFILES AT CPT POSITION JDFTSF14 (A) CONE TIP RESISTANCE Q_T (B) SLEEVE FRICTION F_S (C) DYNAMIC AND INTERPOLATED U_0 PORE PRESSURES (D) Δ_Q (E) B_Q AND (F) I_{C-JD}.

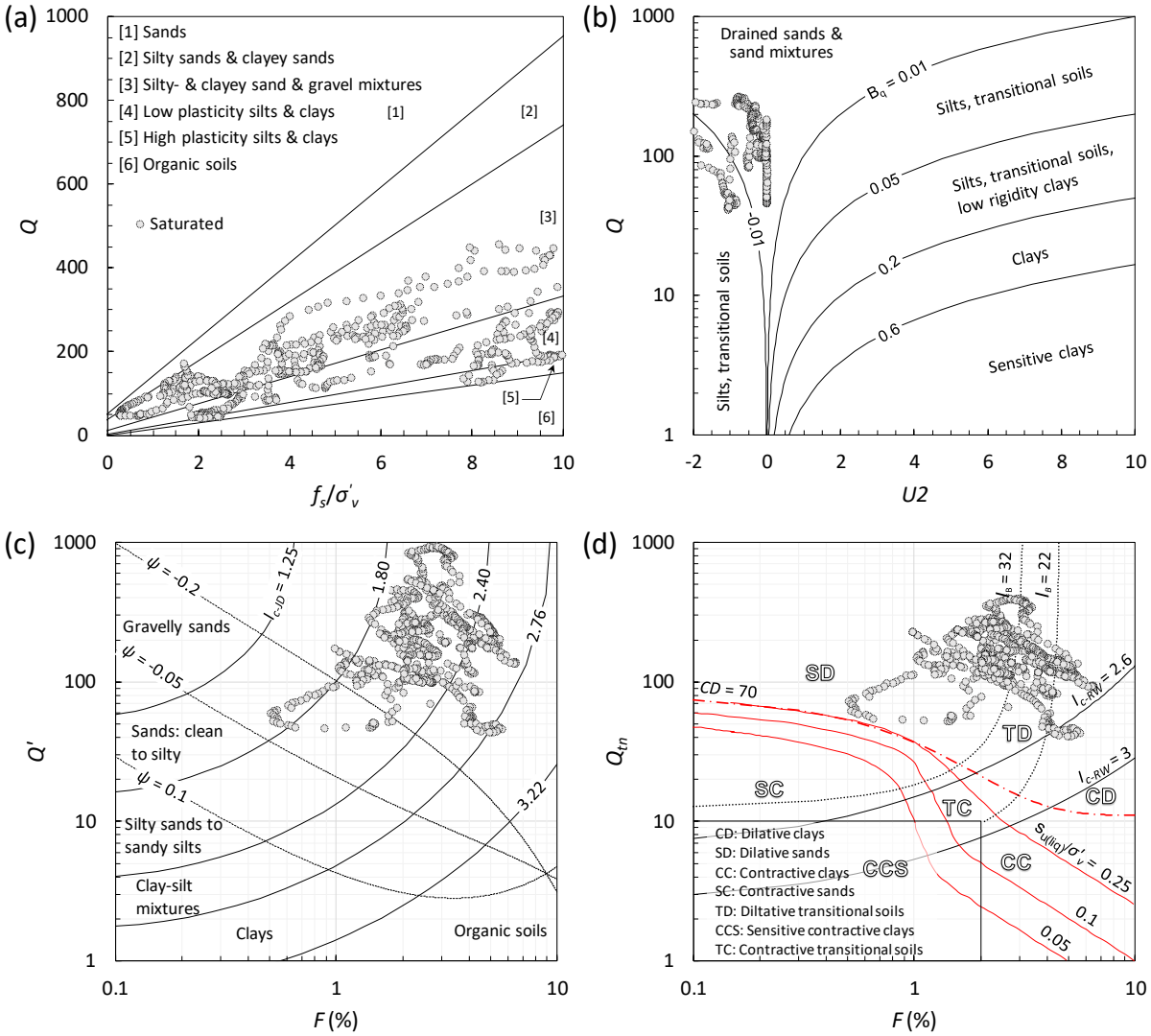

FIGURE 22 SOIL BEHAVIOUR TYPE CHARTS FOR CPT POSITION JDFTSF14 (A) Q VS F_S/Σ'_V (B) Q VS $U2$ (C) Q' VS F AND (D) Q_{TN} VS F.

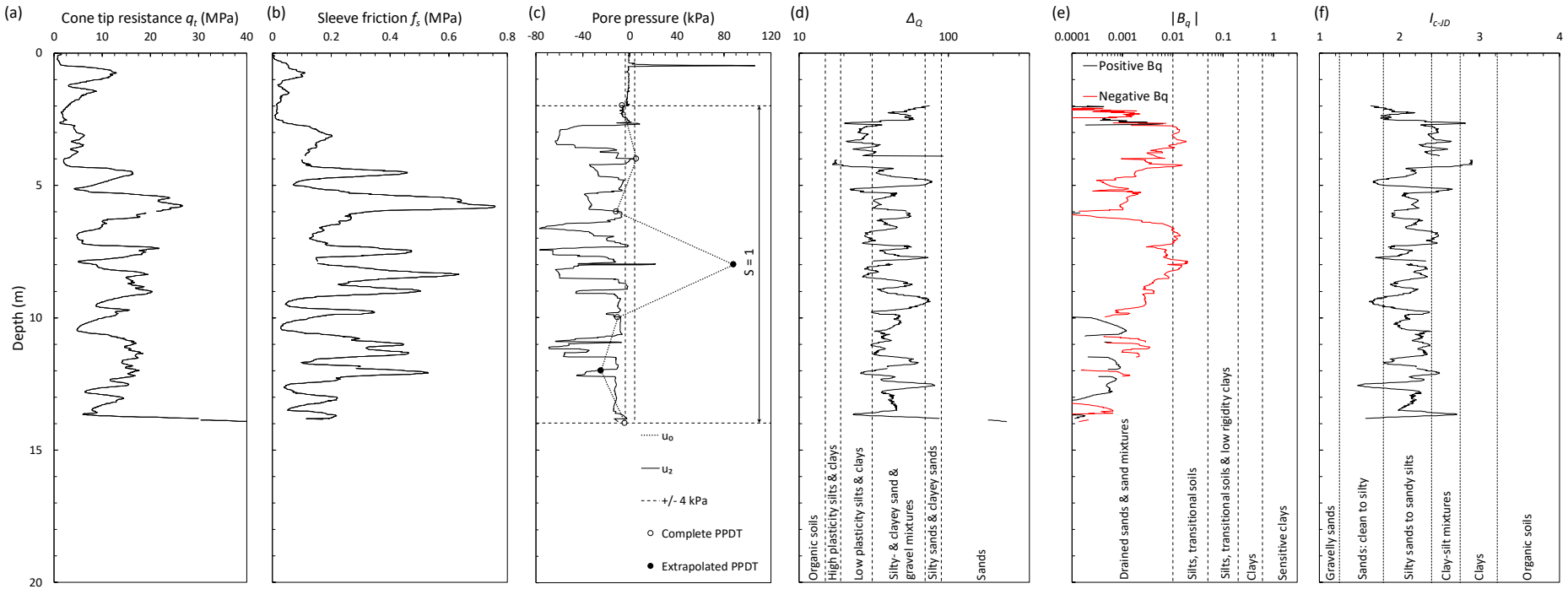

FIGURE 23 PROFILES AT CPT POSITION JDFTSF15 (A) CONE TIP RESISTANCE Q_T (B) SLEEVE FRICTION F_S (C) DYNAMIC AND INTERPOLATED U_0 PORE PRESSURES (D) Δ_Q (E) B_Q AND (F) I_{C-JD}.

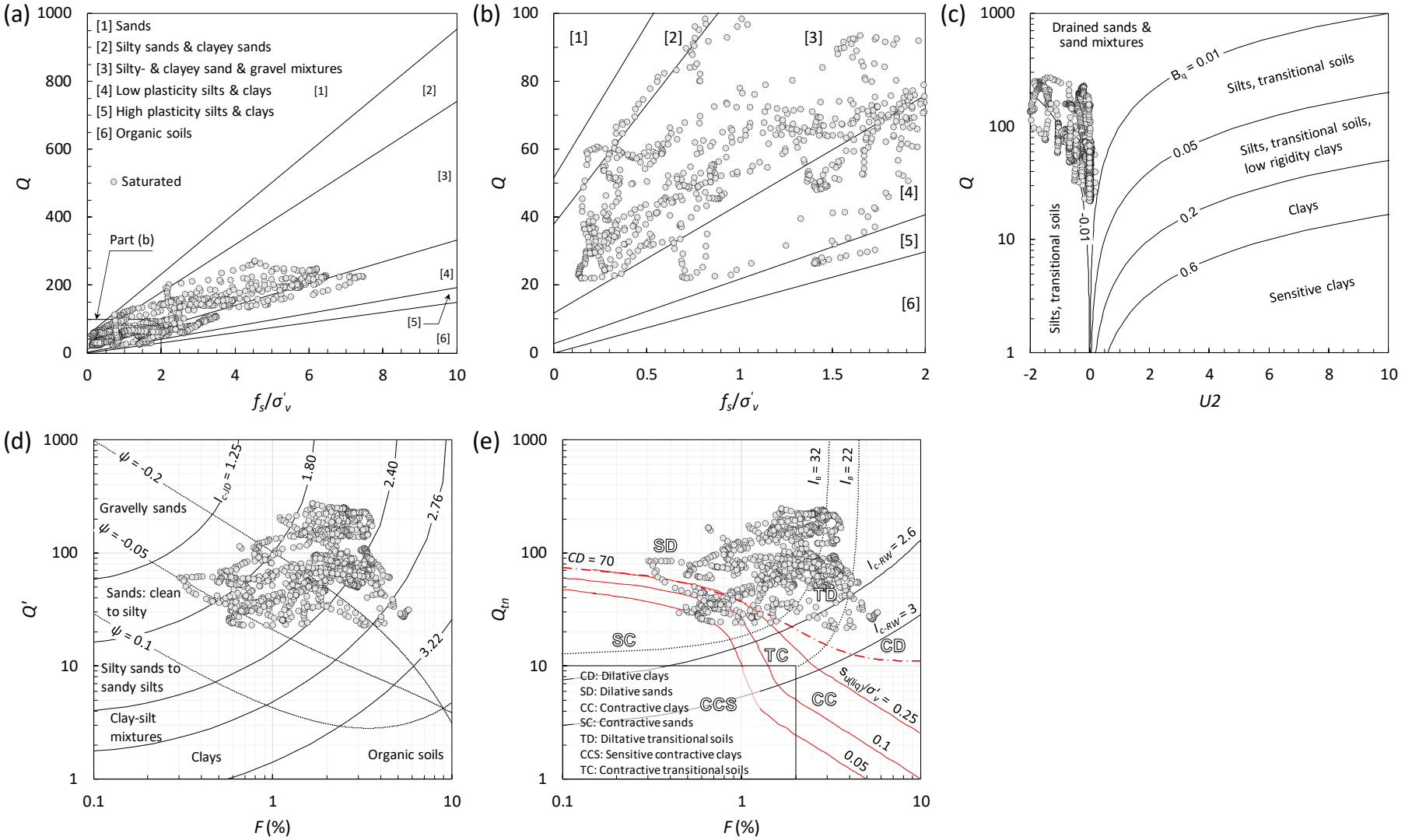

FIGURE 24 SOIL BEHAVIOUR TYPE CHARTS FOR CPT POSITION JDFTSF15 (A) Q VS F_S/Σ'_V (B) Q VS $U2$ (C) Q' VS F AND (D) Q_{TN} VS F.

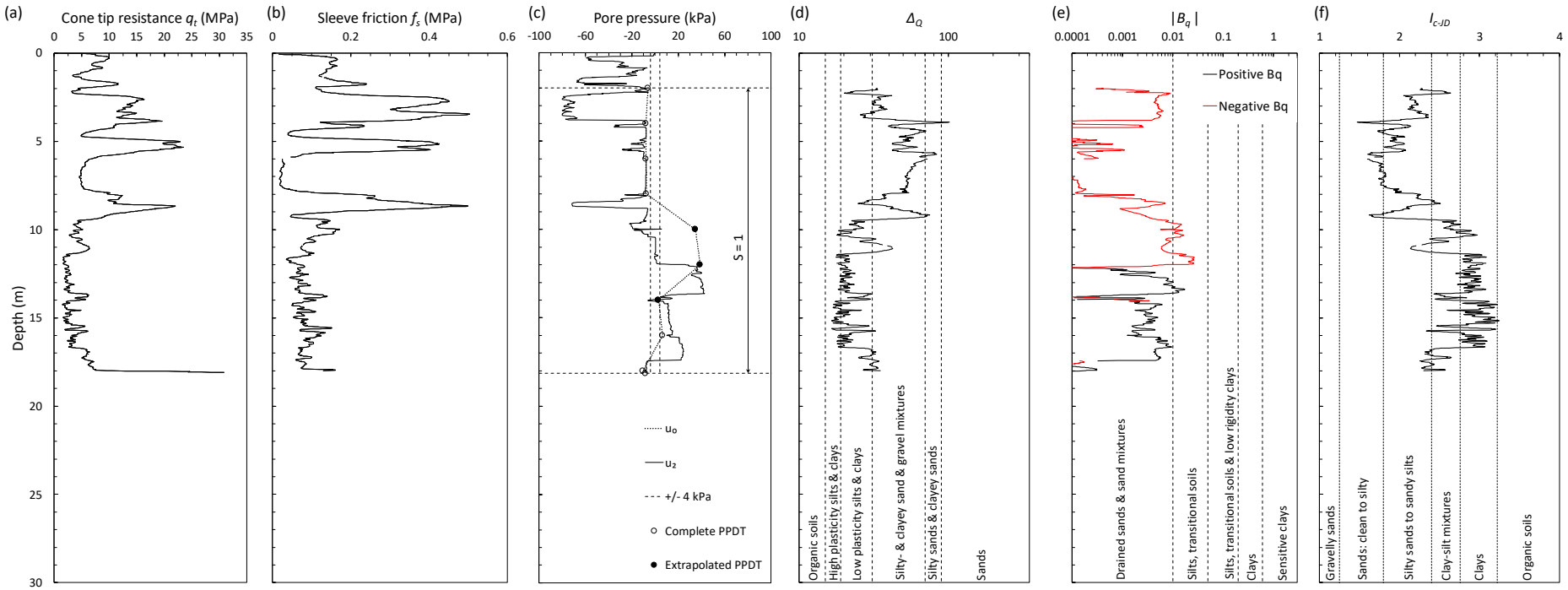

FIGURE 25 PROFILES AT CPT POSITION JDFTSF16 (A) CONE TIP RESISTANCE Q_T (B) SLEEVE FRICTION F_S (C) DYNAMIC AND INTERPOLATED U_0 PORE PRESSURES (D) Δ_Q (E) B_Q AND (F) $I_{C\text{-}JD}$.

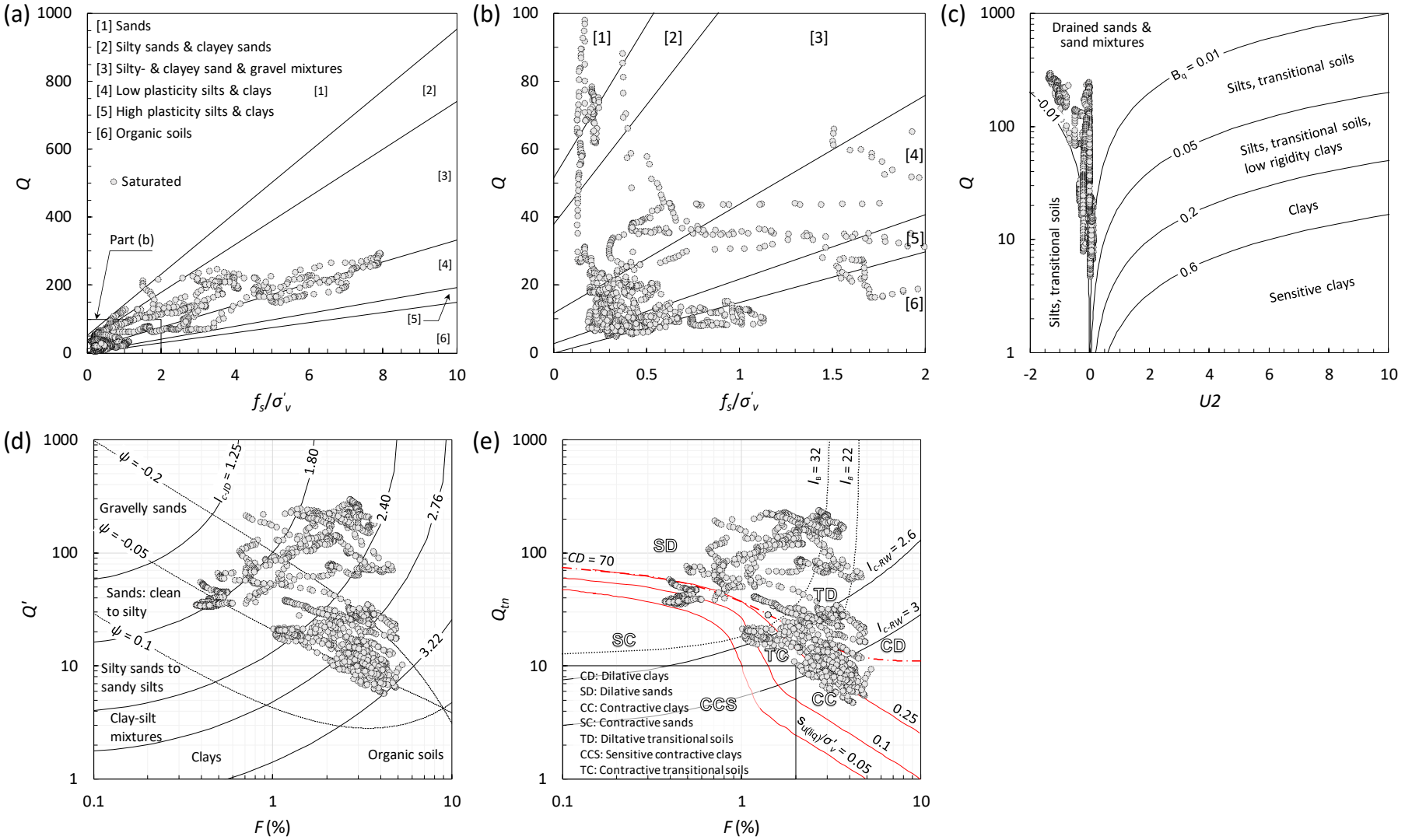

FIGURE 26 SOIL BEHAVIOUR TYPE CHARTS FOR CPT POSITION JDFTSF16 (A) Q VS F_S/Σ'_V (B) Q VS $U2$ (C) Q' VS F AND (D) Q_{TN} VS F.

4.2. Cone penetration tests performed by the investigation panel

Attachment F1 contains the results, as received from the contractor, of the CPT campaign performed by the investigation panel. Attachment F2 contains illustrations of all the PPDTs including the extrapolations performed to infer u_0 from incomplete PPDTs (Equations 2 to 5). Figures 28 to 61 contain the results of the filtering and processing of the CPT data performed by the investigation panel. From Figures 28 to 61 even numbered figures contain profiles of q_t, f_s, u_2, u_0, Δ_Q, B_q and $I_{c\text{-}JD}$; whereas odd numbered figures contain plots of Q vs f_s/σ'_v, Q vs $U2$, Q' vs F, Q_{tn} vs F and, for soundings in which V_s was measured, Q_{tn} vs I_G.

We used the soil behaviour type indices Δ_Q, B_q and $I_{c\text{-}JD}$ to assess soil type and, in particular, to identify clay-like layers at depths below the baseline level (See Chapter 6: Survey Data, in main report) which could correspond to old tailings slimes. Table 5 summarises the interpreted presence of clayey layers.

Table 5. Presence of clay-like layers as inferred from the CPT campaign (Δ_Q, B_q and $I_{c\text{-}JD}$) conducted by the investigation panel.

CPT No.	Sounding depth (m)	Baseline depth (m)	Clay at or below baseline depth?		
			Δ_Q	B_q	$I_{c\text{-}JD}$
1	8.6	-1.3	Y	N	Y
2	11.6	16.8	Baseline depth not reached		
3	17.3	28.4	Baseline depth not reached		
4	25.1	20.4	Y	N	Y
5	18.9	21.1	Baseline depth not reached		
6	21.3	18.2	Y	N	Y
7	7.6	15.3	Baseline depth not reached		
8	25.9	16.8	Y	N	Y
9	8.9	9.6	Baseline depth not reached		
10	19.6	21.2	Baseline depth not reached		
11	12.4	9.9	Y	N	Y
12	7.3	6.3	Y	Y	Y
13	24.1	20.1	Y	N	Y
14	23.7	21.1	Y	N	Y
15	26.3	25.9/20.6	Y	N	Y
16	13.3	11.2	Y	N	Y
17	7.1	7.6	Baseline depth not reached		

For sounding CPT01, the ground level was 1.3 m below the level of the baseline as inferred from the survey data. We believe this could be due to remining of the historic dumps or due to erosion that took place during failure. For seven soundings, the CPT did not extend deep enough to reach the baseline depth. For the remaining nine soundings, at least two of the

three soil behaviour type indices (Δ_Q, B_q and $I_{c\text{-}JD}$) indicate the presence of clay-like soils below the depth of the baseline level. These clay-like soils may correspond to historic dumps. This observation is consistent with our hypothesis that the failure occurred due to shearing through the legacy slimes. It is worth noting that in several soundings clay-like soils are also identified above the baseline level. We believe this reflects the fine-grained nature of the tailings generated at Jagersfontein.

Regarding the state of the probed soils, both the ψ contours in the Q' vs F plots as well as the CD contours in the Q_{tn} vs F plots suggest that the southern wall material was predominantly dilatant. This suggests that the bulk of the material in the retaining wall was not susceptible to liquefaction.

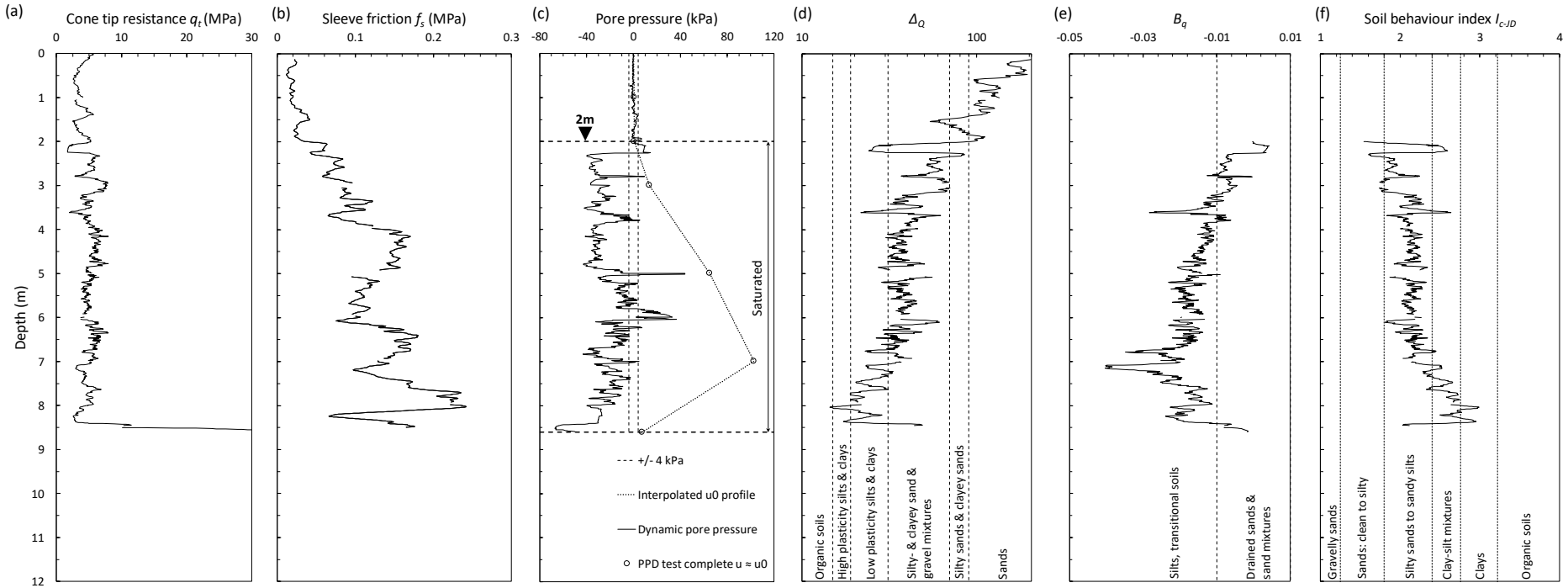

FIGURE 27 PROFILES OF CPT01: (A) CONE TIP RESISTANCE Q_T (B) SLEEVE FRICTION F_S (C) DYNAMIC AND INTERPOLATED U_0 PORE PRESSURES (D) Δ_Q (E) B_Q AND (F) SOIL BEHAVIOUR INDEX I_{C-JD}.

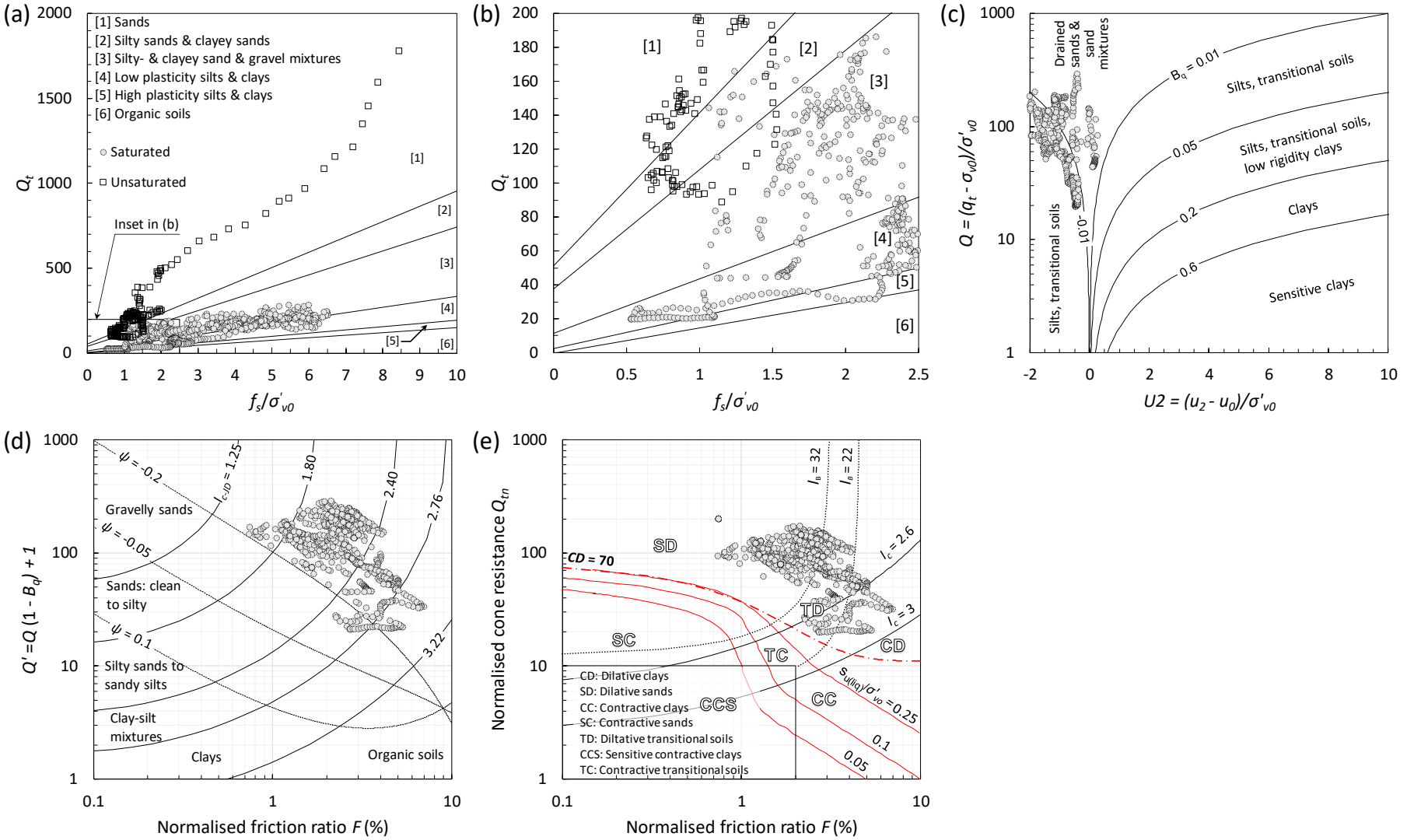

FIGURE 28 SOIL BEHAVIOUR TYPE CHARTS FOR CPT POSITION C1 (A) Q_T VS F_S/Σ'_{VO} (B) INSET FROM Q_T VS F_S/Σ'_{VO} (C) Q VS $U2$ (D) Q' VS F AND (E) Q_{TN} VS F.

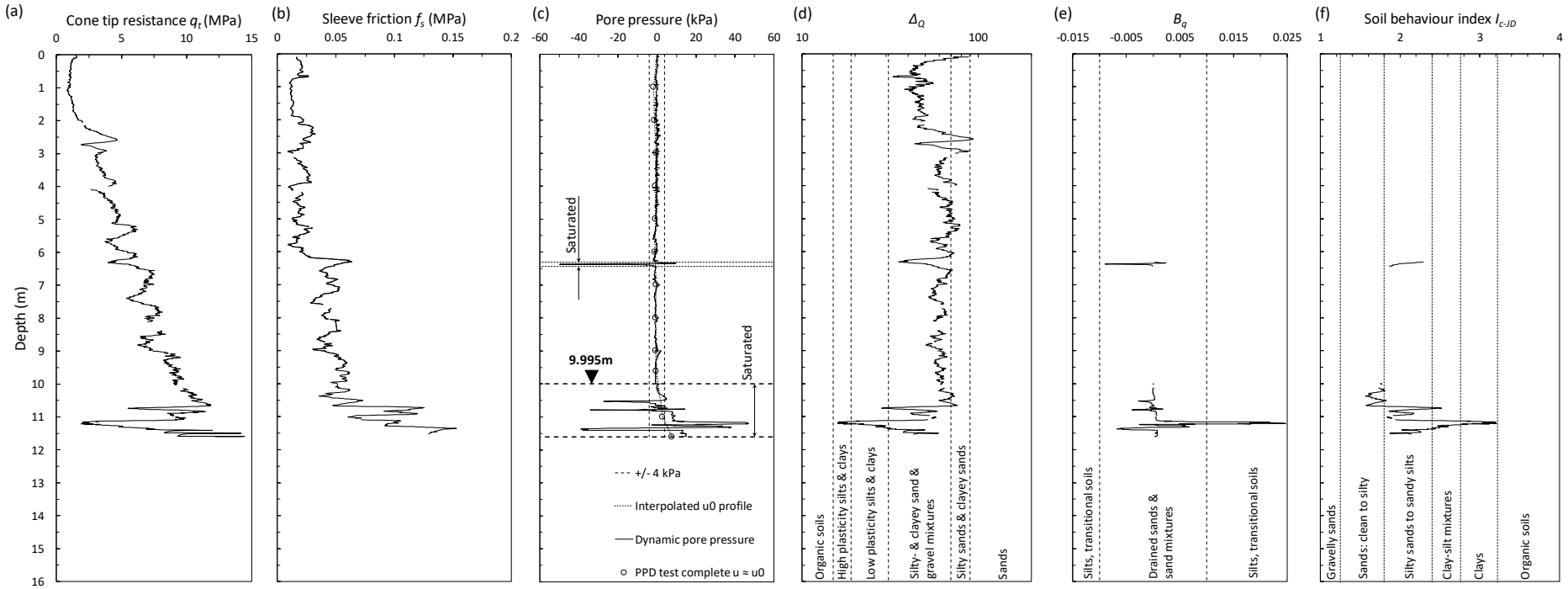

FIGURE 29 PROFILES AT CPT POSITION C2 (A) CONE TIP RESISTANCE Q_T (B) SLEEVE FRICTION F_S (C) DYNAMIC AND INTERPOLATED U_0 PORE PRESSURES (D) Δ_Q (E) B_Q AND (F) SOIL BEHAVIOUR INDEX I_{C-JD}.

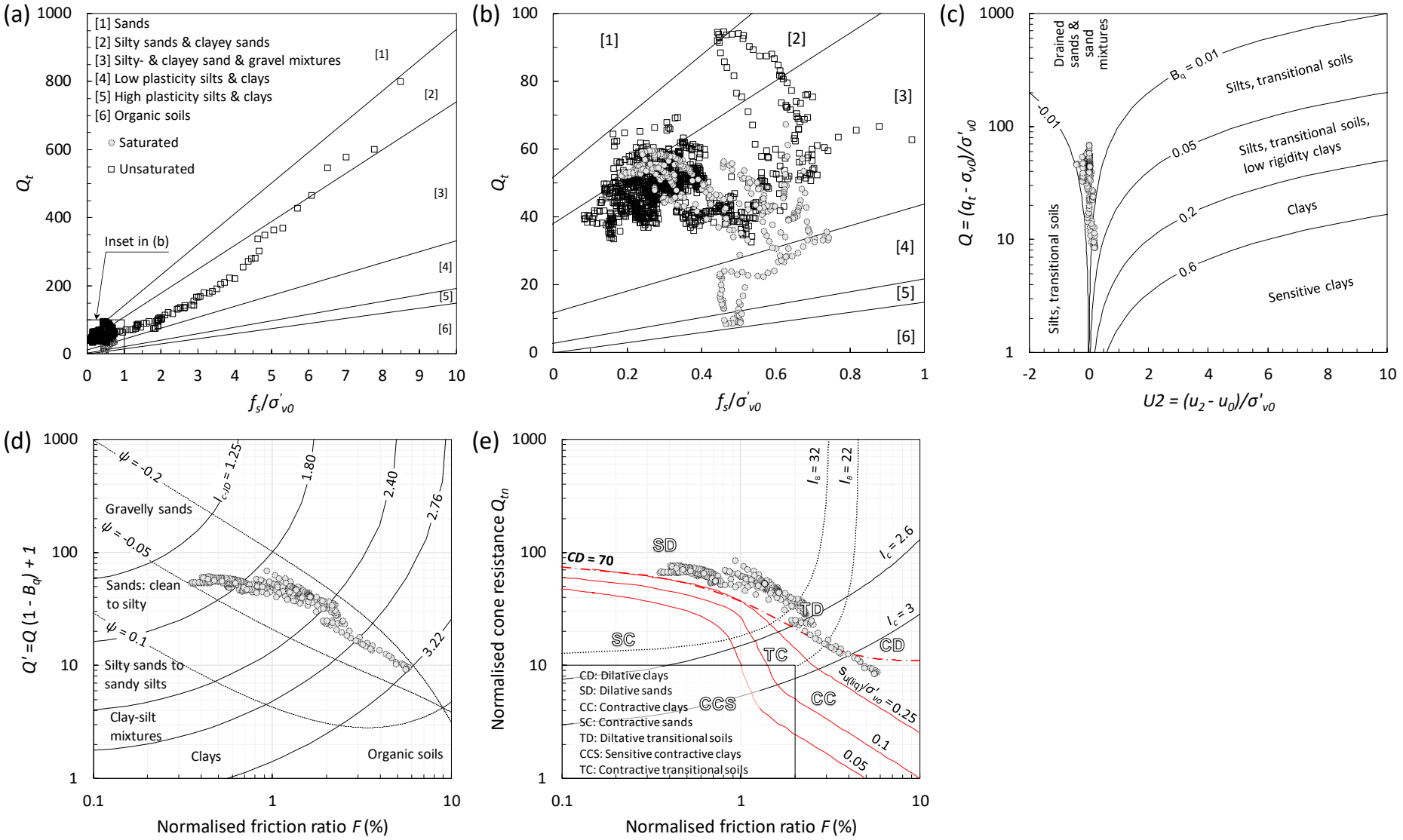

FIGURE 30 SOIL BEHAVIOUR TYPE CHARTS FOR CPT POSITION C2 (A) Q_T VS F_S/Σ'_{VO} (B) INSET FROM Q_T VS F_S/Σ'_{VO} (C) Q VS U2 (D) Q' VS F AND (E) Q_{TN} VS F.

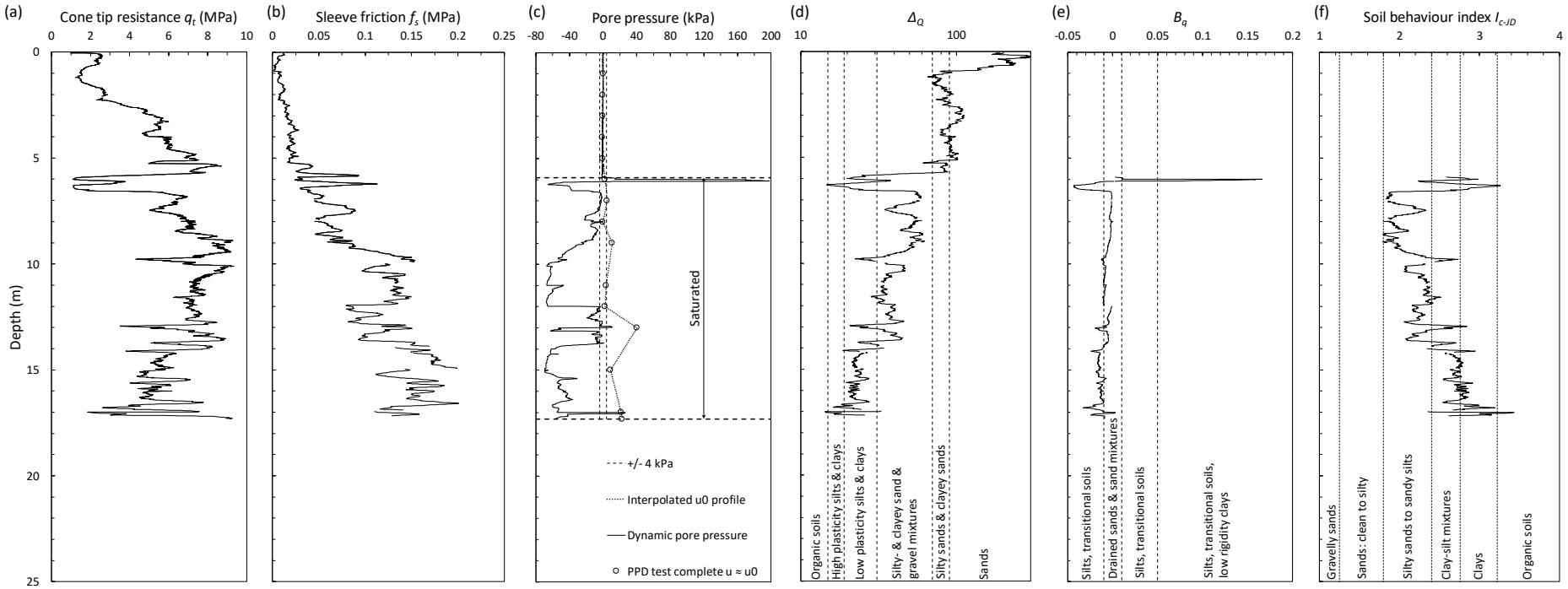

FIGURE 31 PROFILES AT CPT POSITION C3 (A) CONE TIP RESISTANCE Q_T (B) SLEEVE FRICTION F_S (C) DYNAMIC AND INTERPOLATED U_0 PORE PRESSURES (D) Δ_Q (E) B_Q AND (F) SOIL BEHAVIOUR INDEX $I_{C\text{-}JD}$.

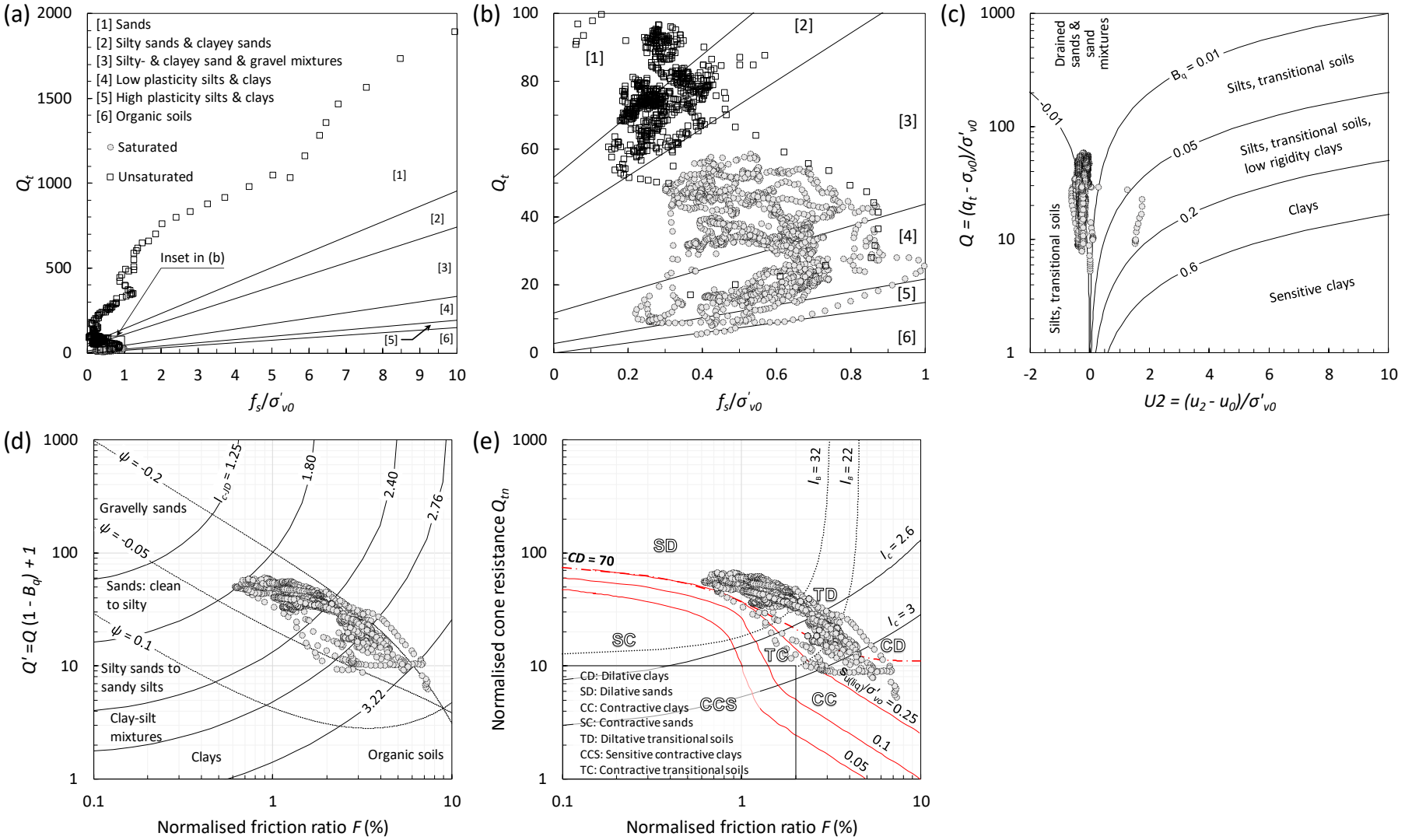

FIGURE 32 SOIL BEHAVIOUR TYPE CHARTS FOR CPT POSITION C3 (A) Q_T VS F_S/Σ'_{VO} (B) INSET FROM Q_T VS F_S/Σ'_{VO} (C) Q VS U2 (D) Q' VS F AND (E) Q_{TN} VS F.

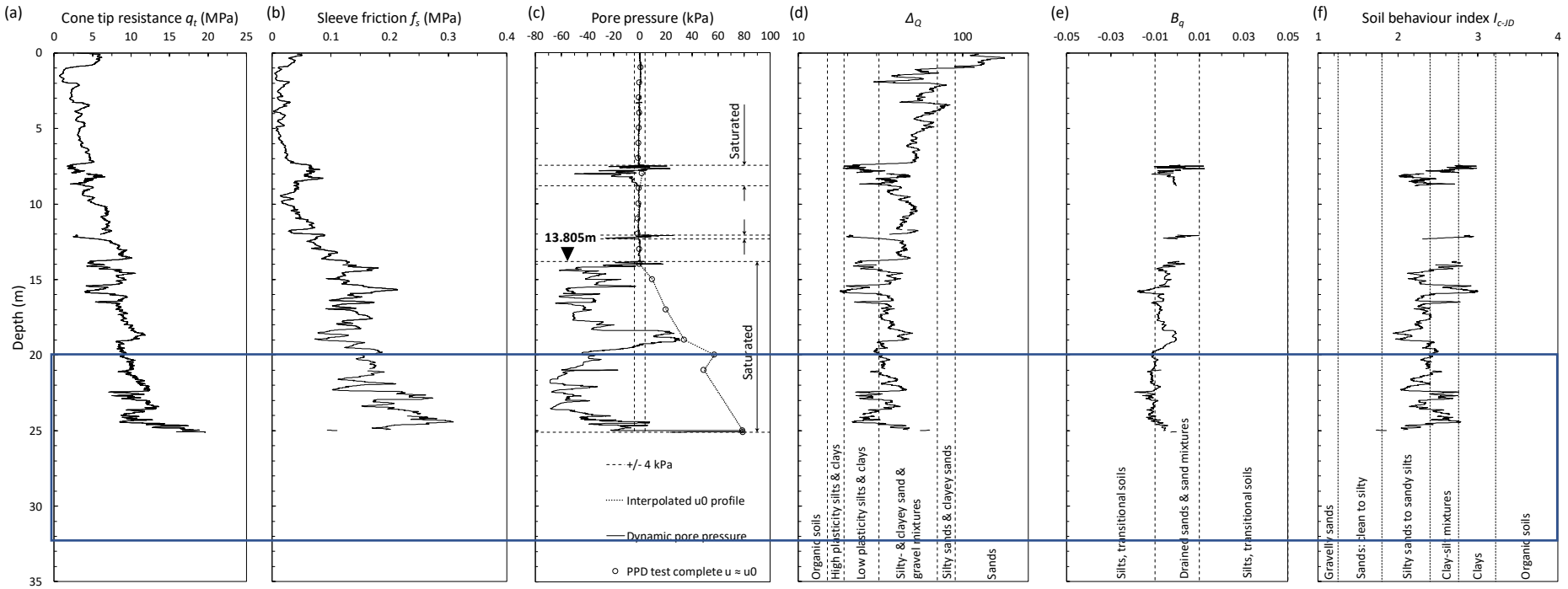

FIGURE 33 PROFILES AT CPT POSITION C4 (A) CONE TIP RESISTANCE Q_T (B) SLEEVE FRICTION F_S (C) DYNAMIC AND INTERPOLATED U_0 PORE PRESSURES (D) Δ_Q (E) B_Q AND (F) SOIL BEHAVIOUR INDEX I_{C-JD}.

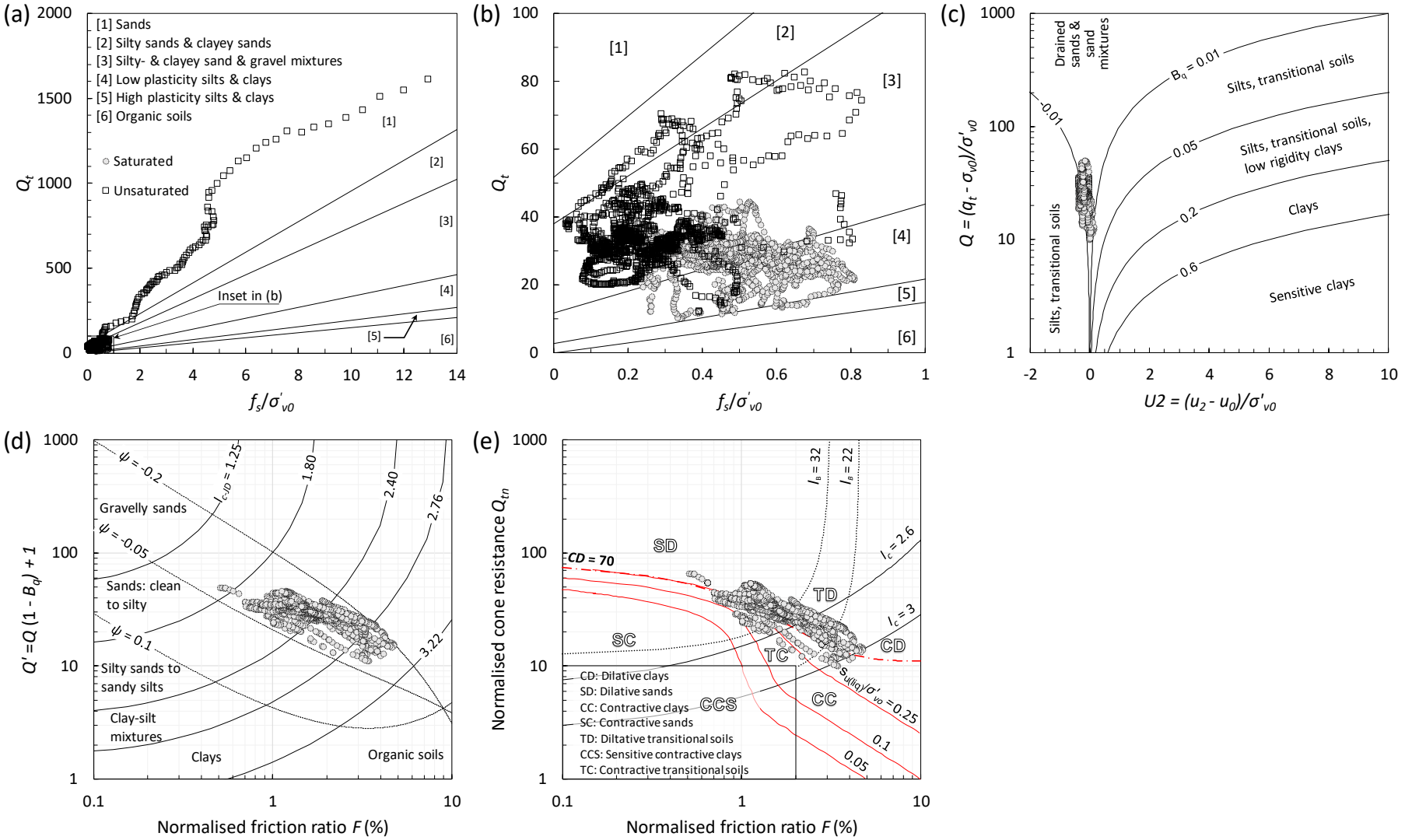

FIGURE 34 SOIL BEHAVIOUR TYPE CHARTS FOR CPT POSITION C4 (A) Q_T VS F_S/Σ'_{VO} (B) INSET FROM Q_T VS F_S/Σ'_{VO} (C) Q VS U2 (D) Q' VS F AND (E) Q_{TN} VS F.

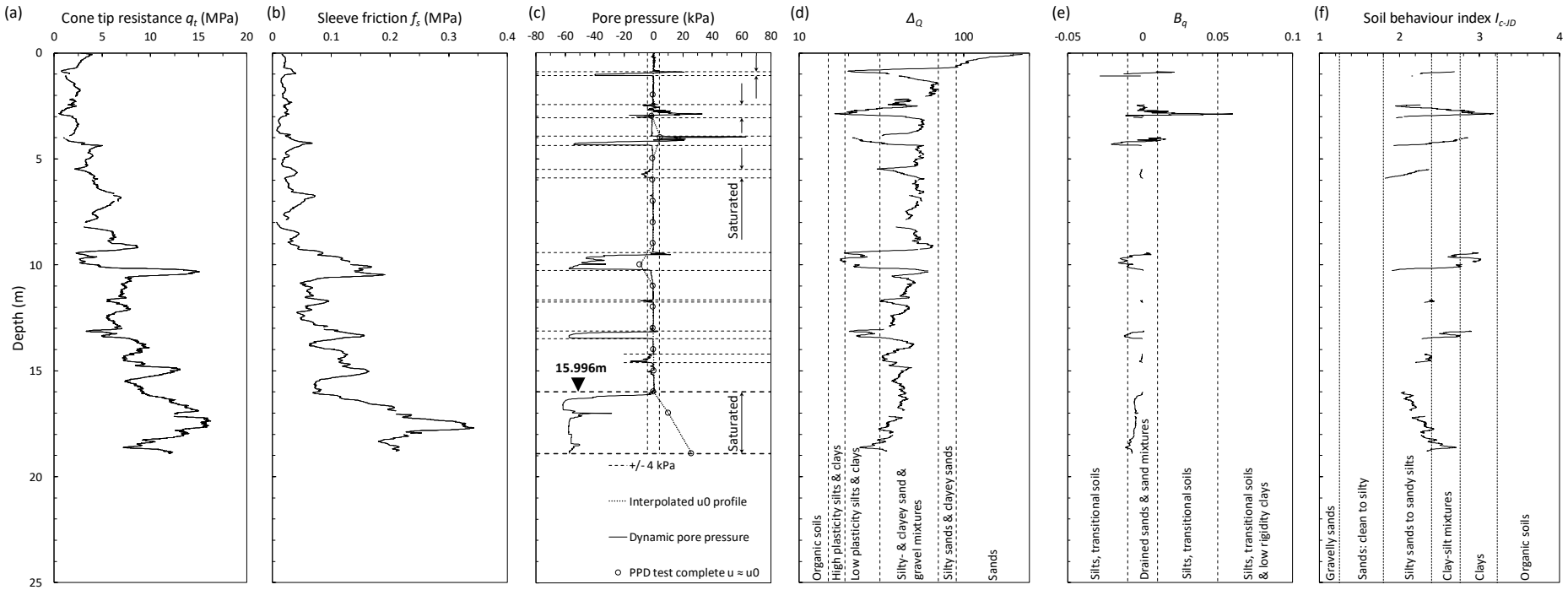

FIGURE 35 PROFILES AT CPT POSITION C5 (A) CONE TIP RESISTANCE Q_T (B) SLEEVE FRICTION F_S (C) DYNAMIC AND INTERPOLATED U_0 PORE PRESSURES (D) Δ_Q (E) B_Q AND (F) SOIL BEHAVIOUR INDEX I_{C-JD}.

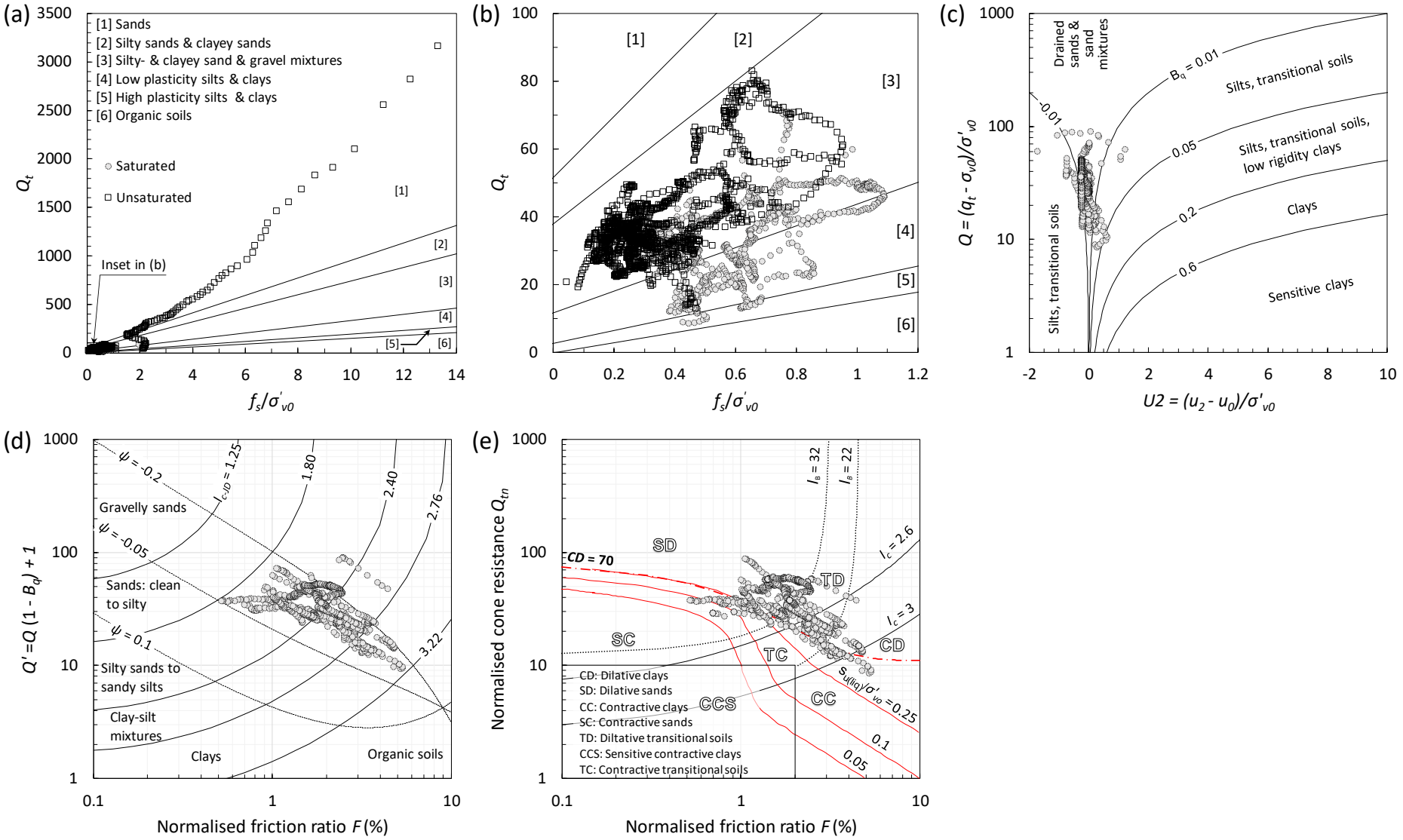

FIGURE 36 SOIL BEHAVIOUR TYPE CHARTS FOR CPT POSITION C5 (A) Q_T VS F_S/Σ'_{VO} (B) INSET FROM Q_T VS F_S/Σ'_{VO} (C) Q VS U2 (D) Q' VS F AND (E) Q_{TN} VS F.

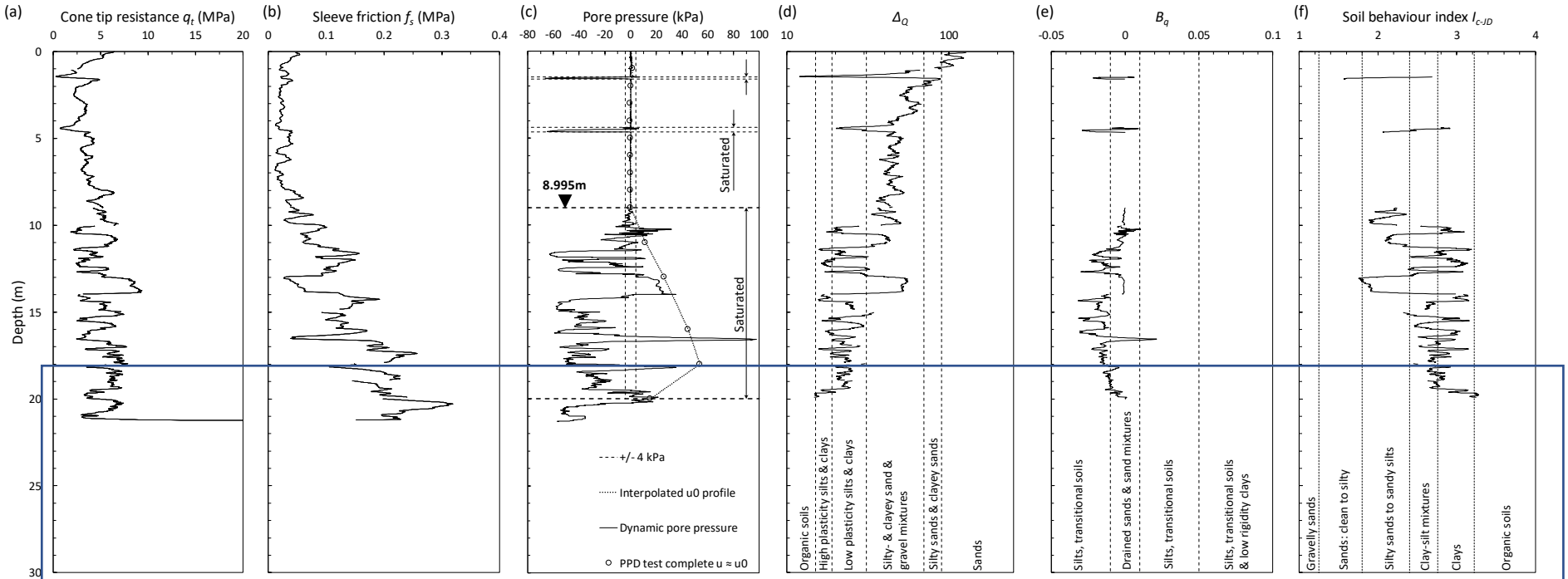

FIGURE 37 PROFILES AT CPT POSITION C6 (A) CONE TIP RESISTANCE Q_T (B) SLEEVE FRICTION F_S (C) DYNAMIC AND INTERPOLATED U_0 PORE PRESSURES (D) Δ_Q (E) B_Q AND (F) SOIL BEHAVIOUR INDEX $I_{C\text{-}JD}$.

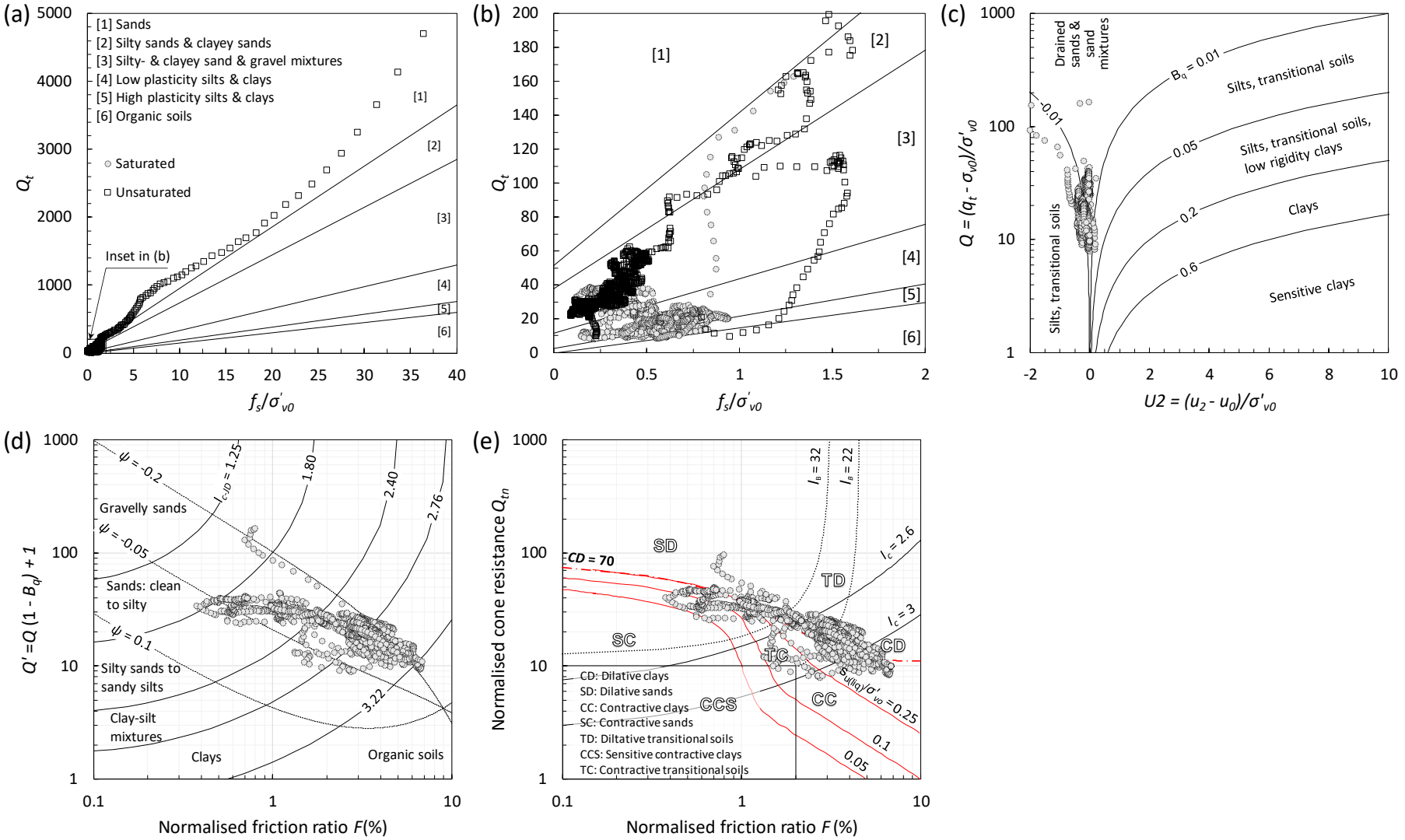

FIGURE 38 SOIL BEHAVIOUR TYPE CHARTS FOR CPT POSITION C6 (A) Q_T VS F_S/Σ'_{VO} (B) INSET FROM Q_T VS F_S/Σ'_{VO} (C) Q VS U2 (D) Q' VS F AND (E) Q_{TN} VS F.

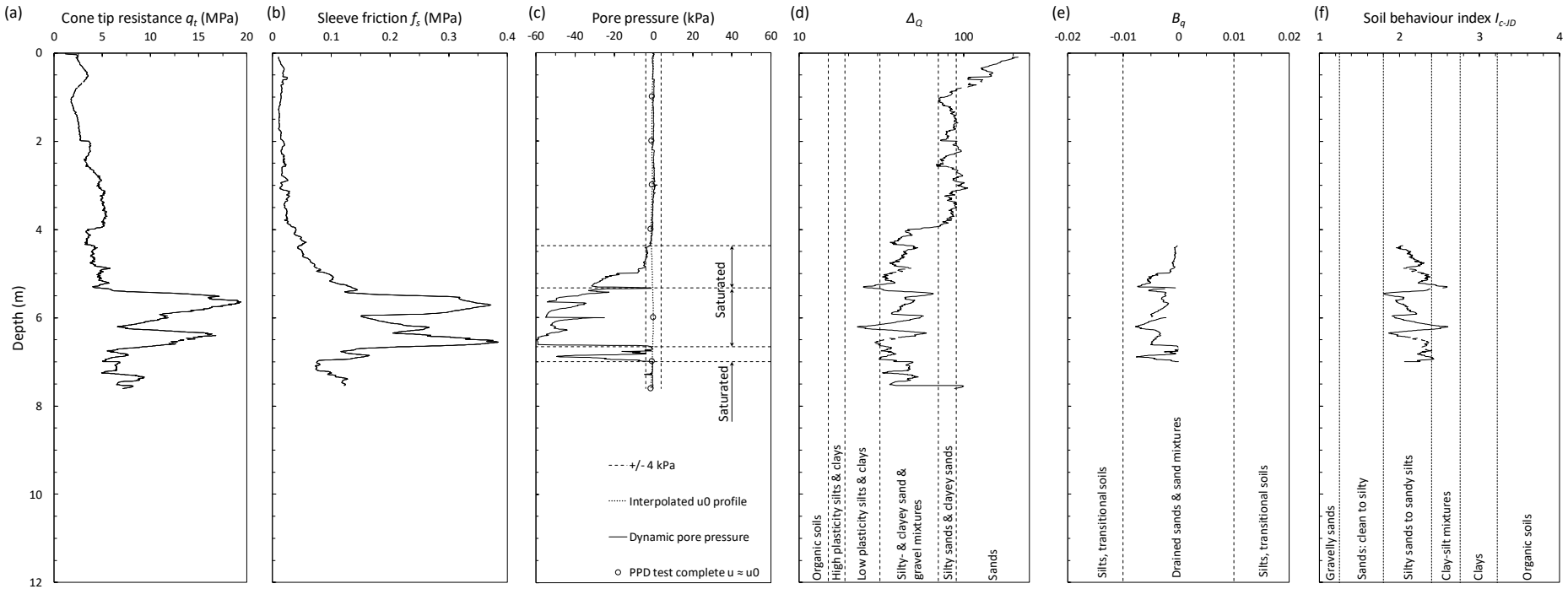

FIGURE 39 PROFILES AT CPT POSITION C7 (A) CONE TIP RESISTANCE Q_T (B) SLEEVE FRICTION F_S (C) DYNAMIC AND INTERPOLATED U_0 PORE PRESSURES (D) Δ_Q (E) B_Q AND (F) SOIL BEHAVIOUR INDEX I_{C-JD}.

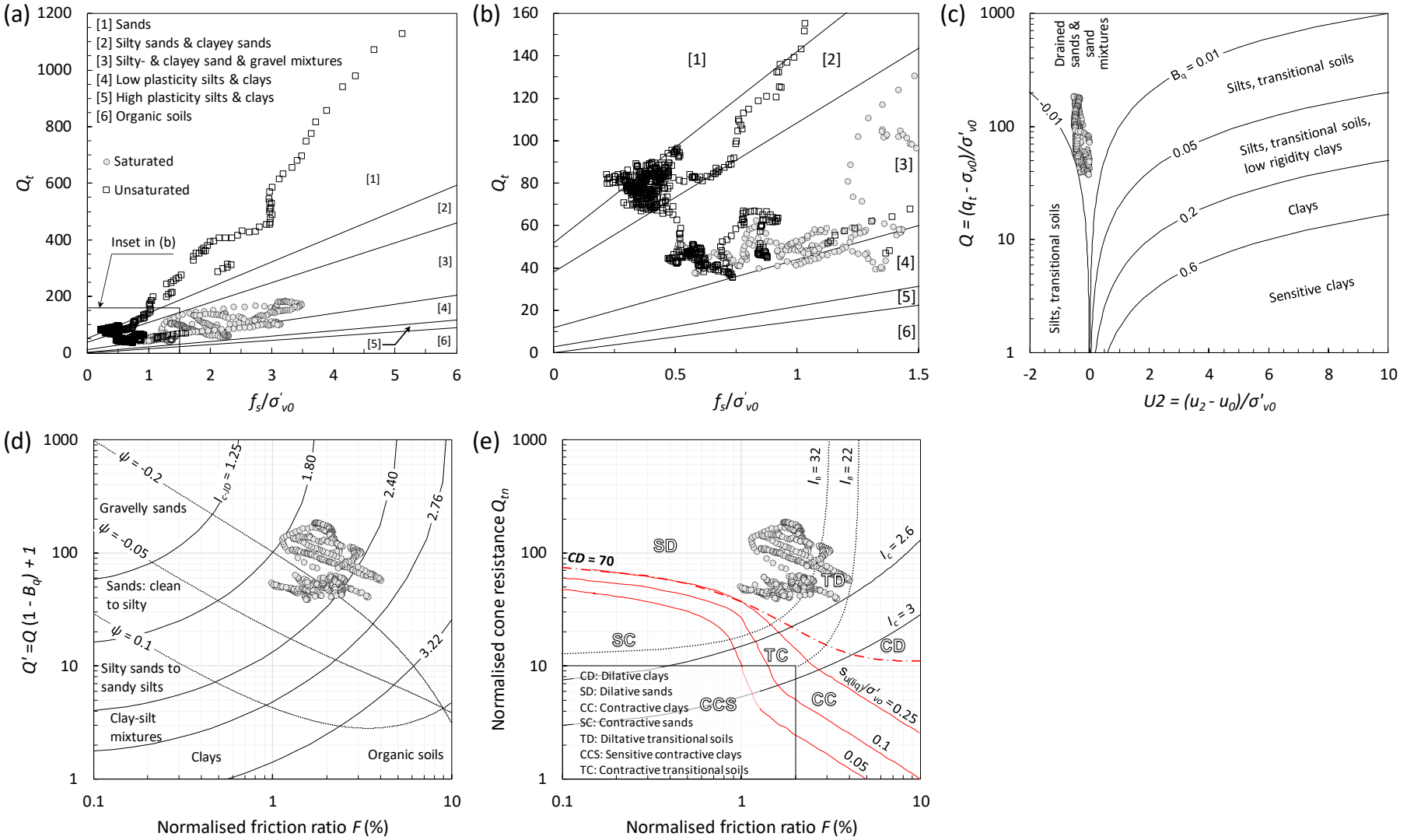

FIGURE 40 SOIL BEHAVIOUR TYPE CHARTS FOR CPT POSITION C7 (A) Q_T VS F_S/Σ'_{VO} (B) INSET FROM Q_T VS F_S/Σ'_{VO} (C) Q VS U2 (D) Q' VS F AND (E) Q_{TN} VS F.

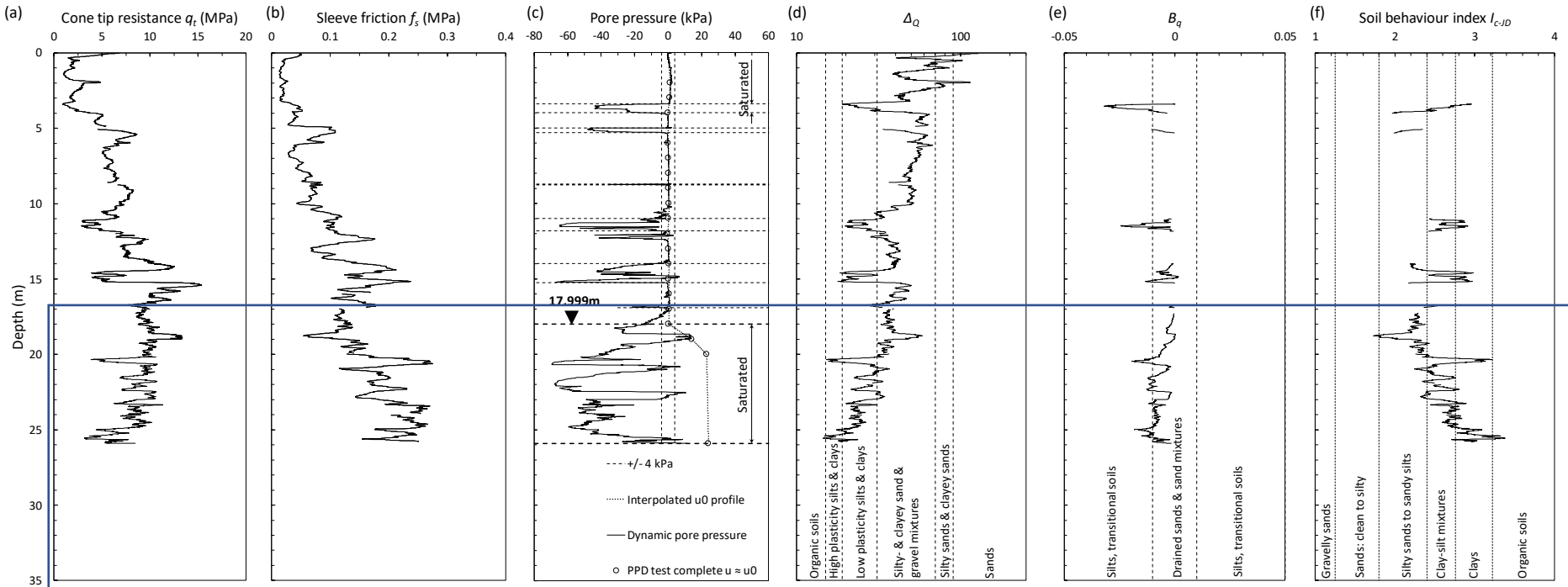

FIGURE 41 PROFILES AT CPT POSITION C8 (A) CONE TIP RESISTANCE Q_T (B) SLEEVE FRICTION F_S (C) DYNAMIC AND INTERPOLATED U_0 PORE PRESSURES (D) Δ_Q (E) B_Q AND (F) SOIL BEHAVIOUR INDEX I_{C-JD}.

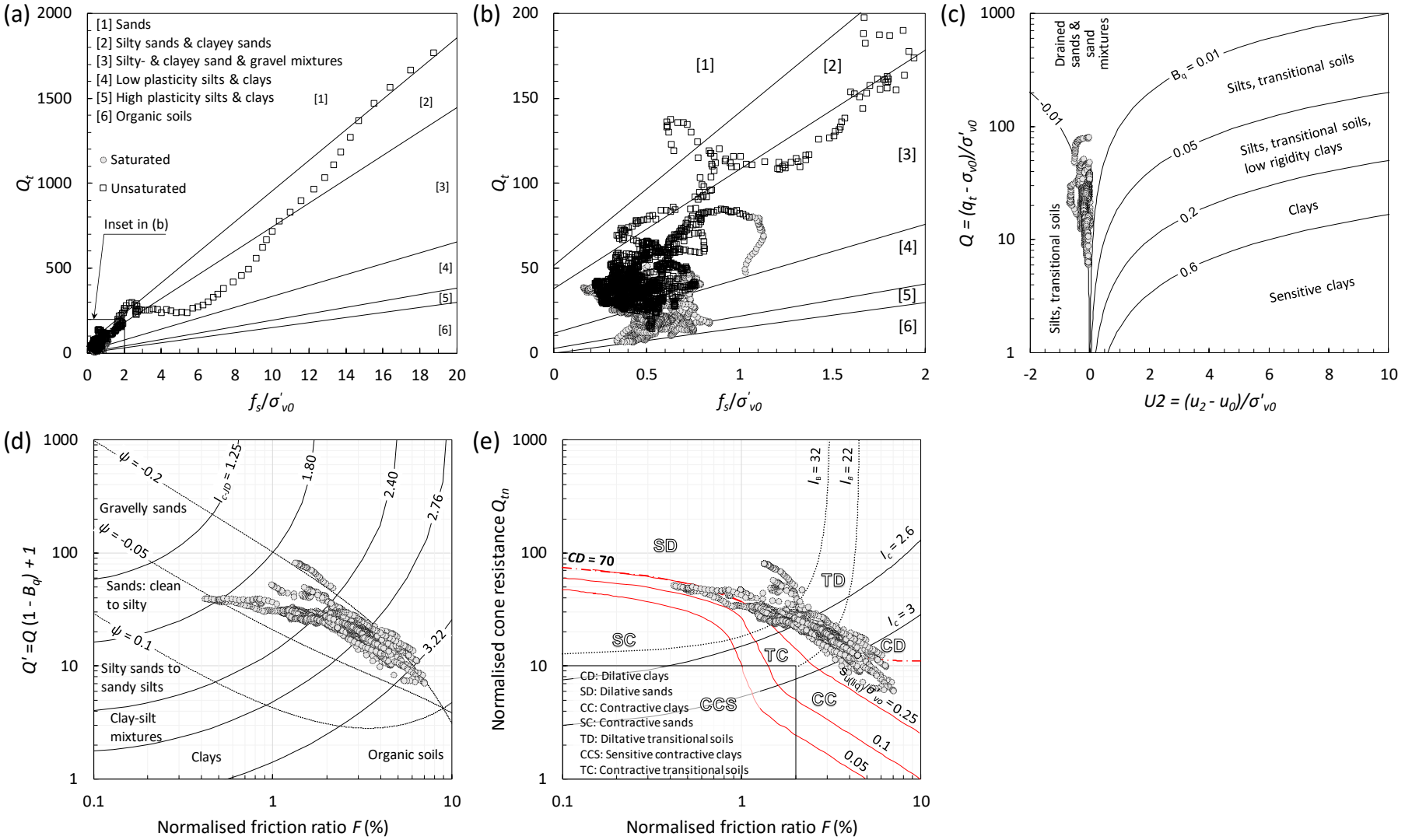

FIGURE 42 SOIL BEHAVIOUR TYPE CHARTS FOR CPT POSITION C8 (A) Q_T VS F_S/Σ'_{VO} (B) INSET FROM Q_T VS F_S/Σ'_{VO} (C) Q VS U2 (D) Q' VS F AND (E) Q_{TN} VS F.

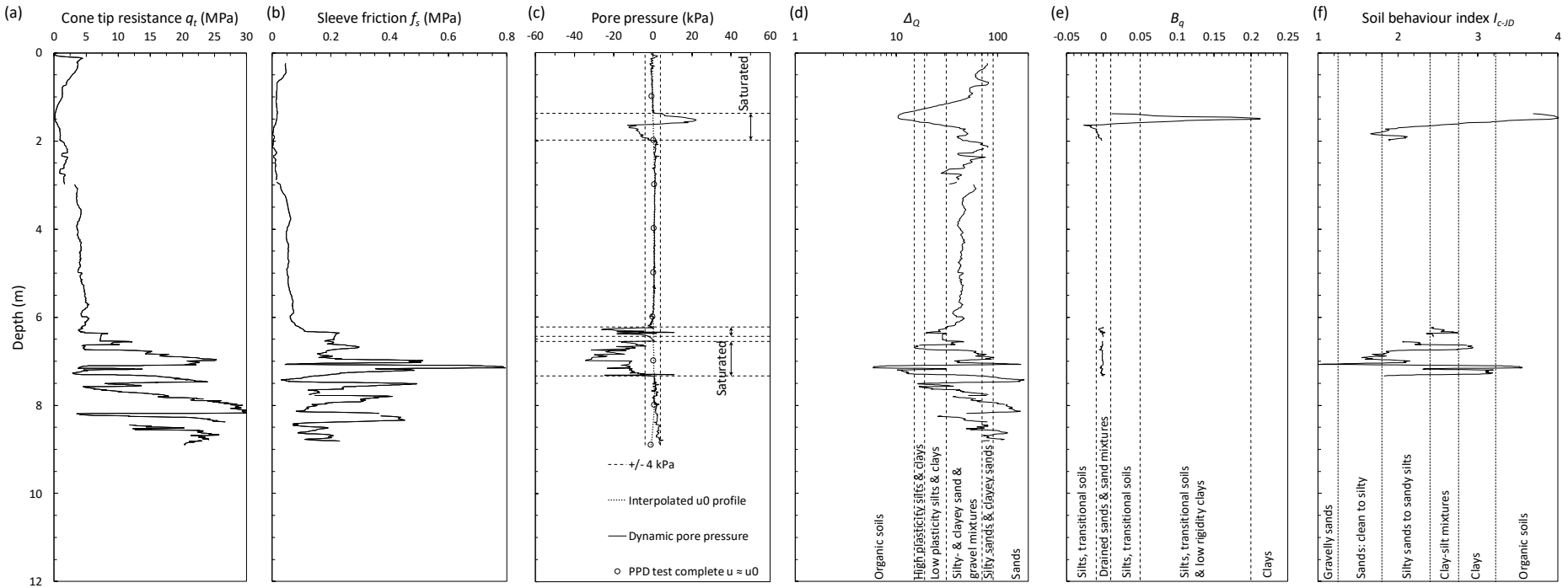

FIGURE 43 PROFILES AT CPT POSITION C9 (A) CONE TIP RESISTANCE Q_T (B) SLEEVE FRICTION F_S (C) DYNAMIC AND INTERPOLATED U_0 PORE PRESSURES (D) Δ_Q (E) B_Q AND (F) SOIL BEHAVIOUR INDEX I_{C-JD}.

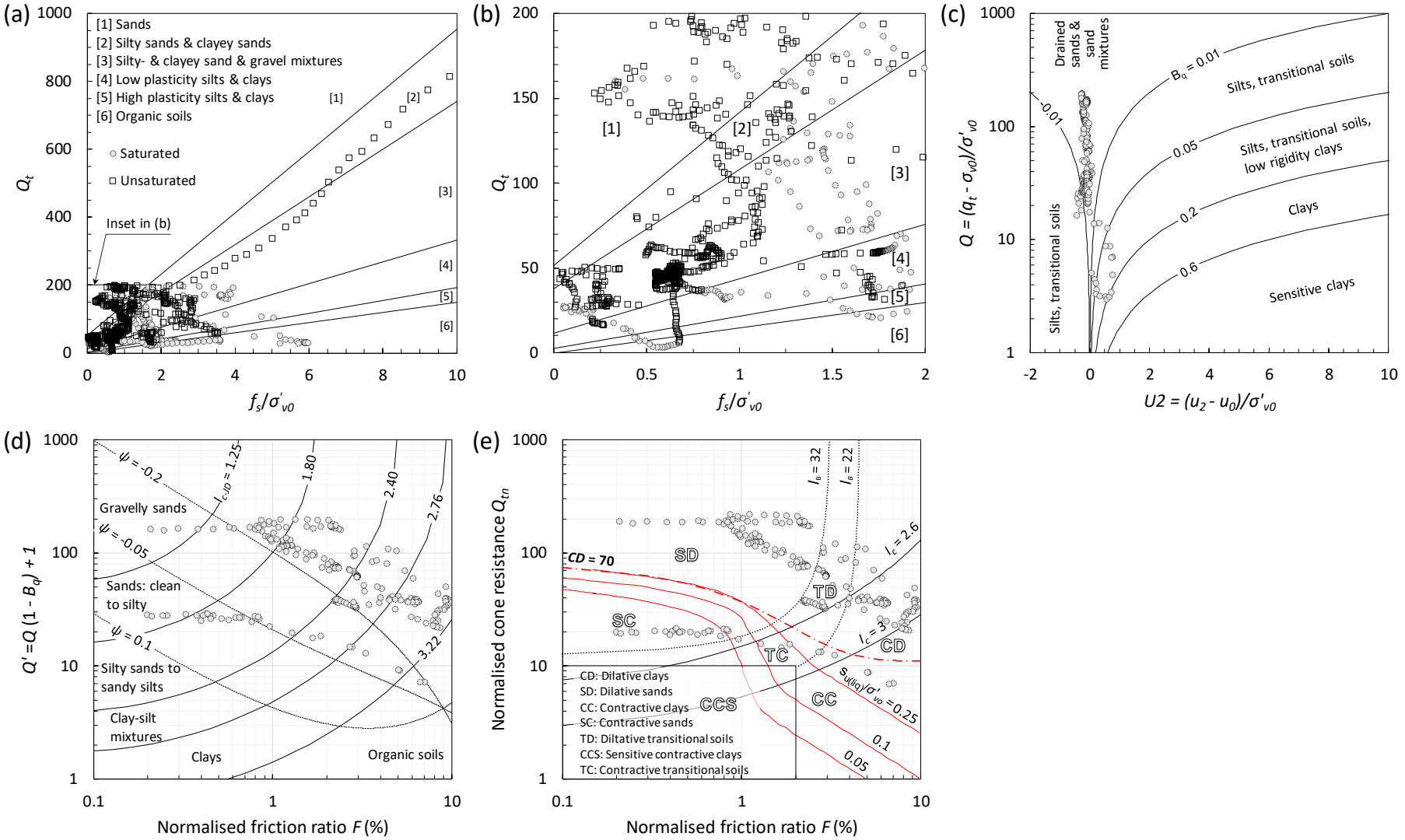

FIGURE 44 SOIL BEHAVIOUR TYPE CHARTS FOR CPT POSITION C9 (A) Q_T VS F_S/Σ'_{VO} (B) INSET FROM Q_T VS F_S/Σ'_{VO} (C) Q VS U2 (D) Q' VS F AND (E) Q_{TN} VS F.

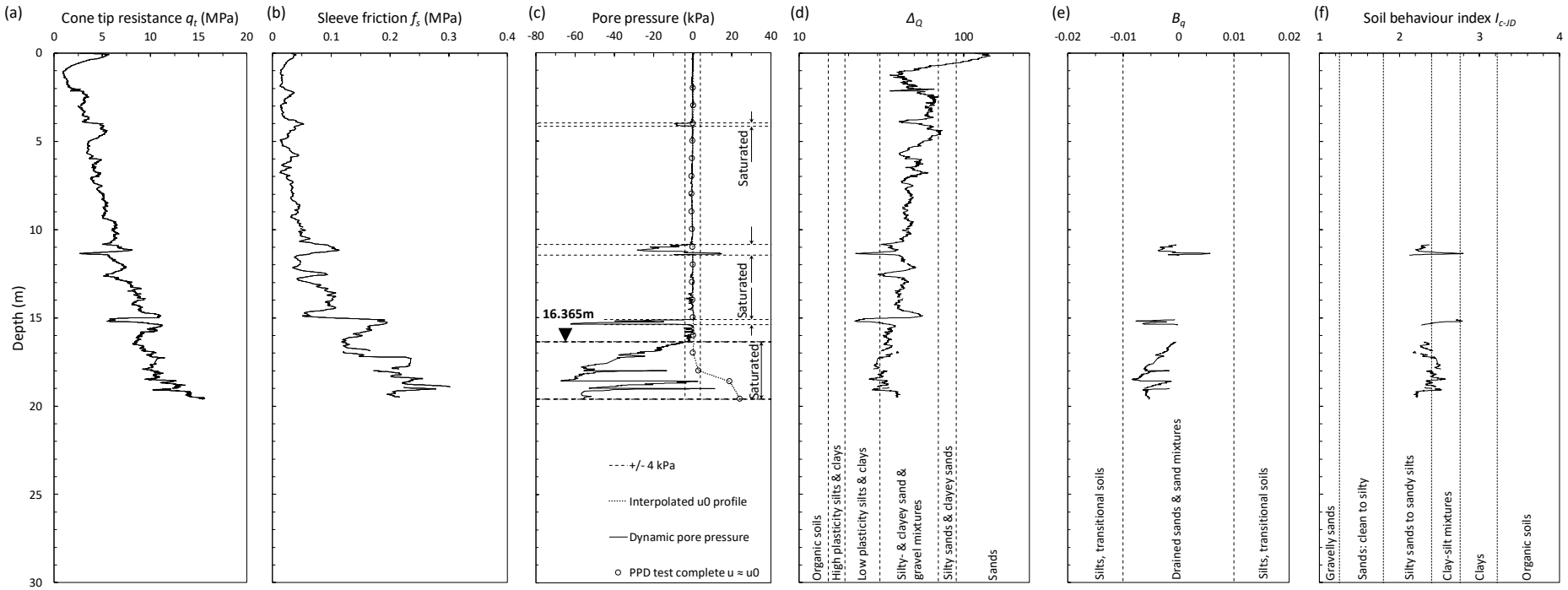

FIGURE 45 PROFILES AT CPT POSITION C10 (A) CONE TIP RESISTANCE Q_T (B) SLEEVE FRICTION F_S (C) DYNAMIC AND INTERPOLATED U_0 PORE PRESSURES (D) Δ_Q (E) B_Q AND (F) SOIL BEHAVIOUR INDEX I_{C-JD}.

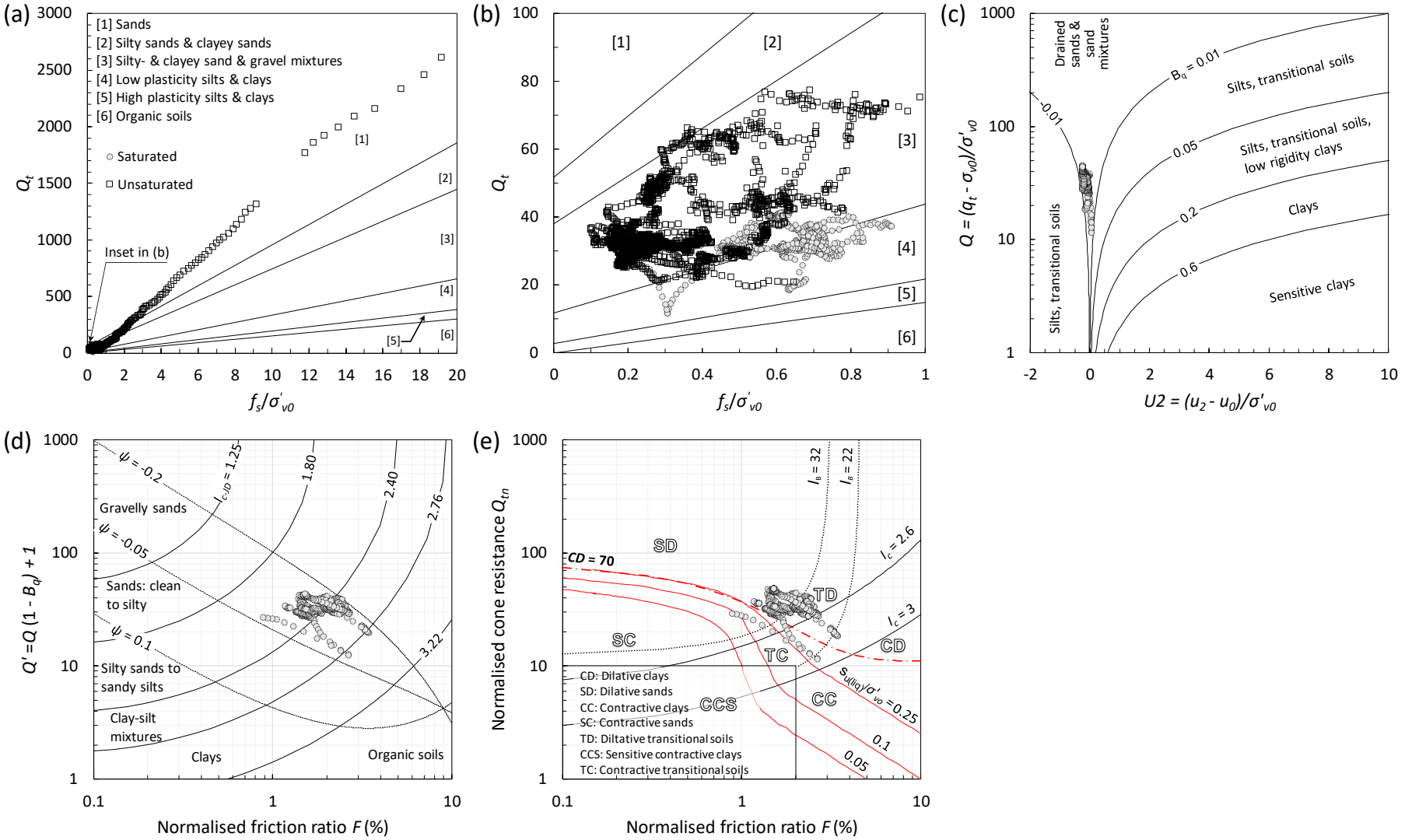

FIGURE 46 SOIL BEHAVIOUR TYPE CHARTS FOR CPT POSITION C10 (A) Q_T VS F_S/Σ'_{VO} (B) INSET FROM Q_T VS F_S/Σ'_{VO} (C) Q VS U2 (D) Q' VS F AND (E) Q_{TN} VS F.

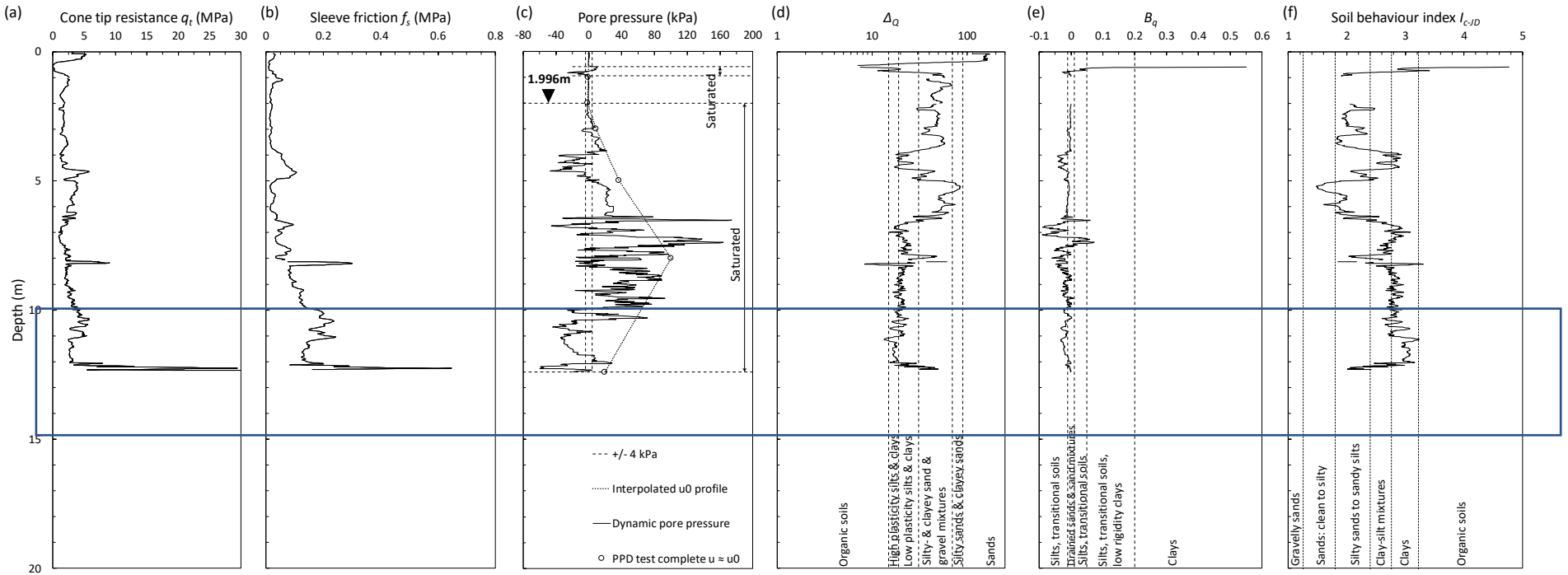

FIGURE 47 PROFILES AT CPT POSITION C11 (A) CONE TIP RESISTANCE Q_T (B) SLEEVE FRICTION F_S (C) DYNAMIC AND INTERPOLATED U_0 PORE PRESSURES (D) Δ_Q (E) B_Q AND (F) SOIL BEHAVIOUR INDEX I_{C-JD}.

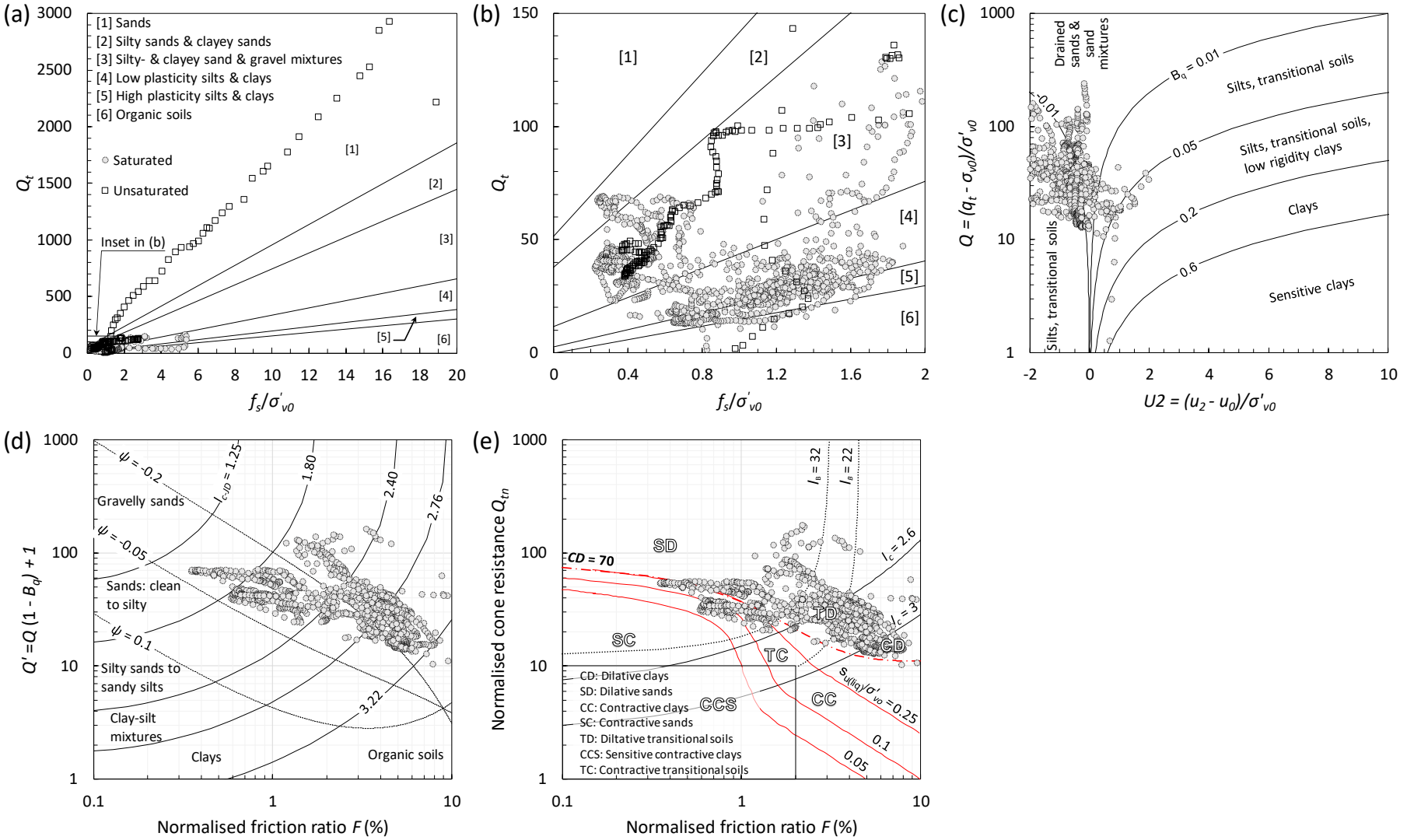

FIGURE 48 SOIL BEHAVIOUR TYPE CHARTS FOR CPT POSITION C11 (A) Q_T VS F_S/Σ'_{VO} (B) INSET FROM Q_T VS F_S/Σ'_{VO} (C) Q VS U2 (D) Q' VS F AND (E) Q_{TN} VS F.

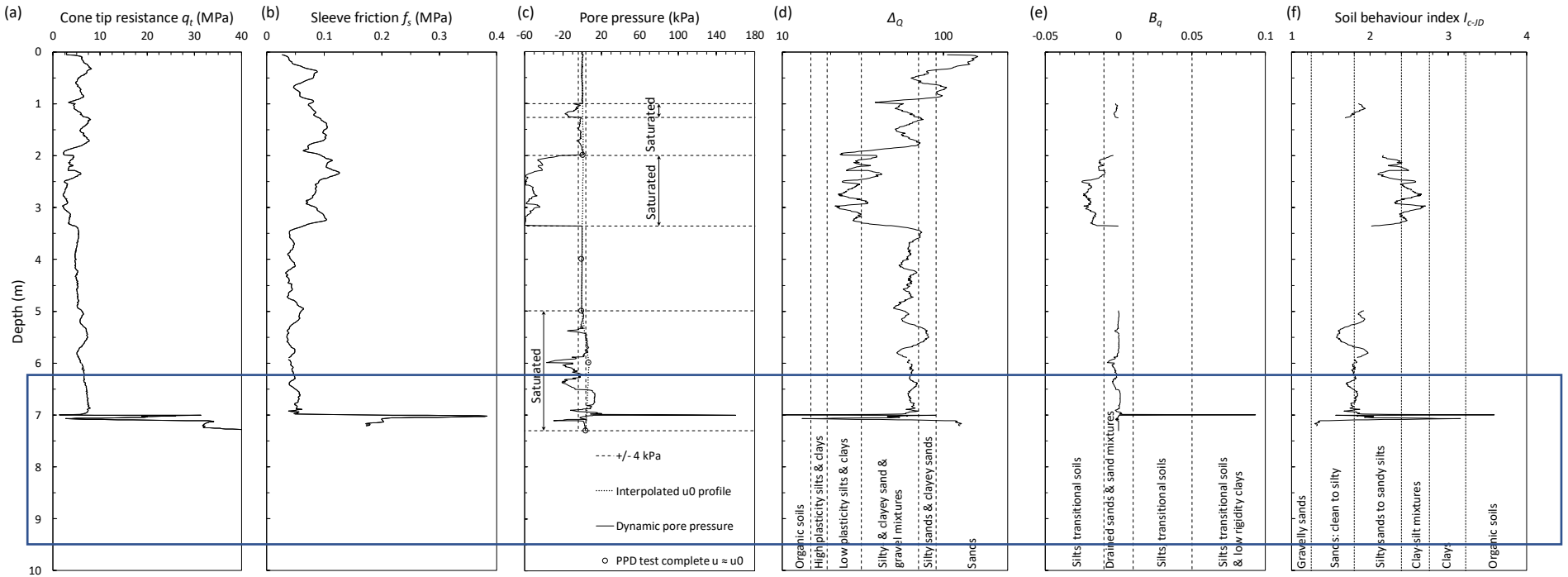

FIGURE 49 PROFILES AT CPT POSITION C12 (A) CONE TIP RESISTANCE Q_T (B) SLEEVE FRICTION F_S (C) DYNAMIC AND INTERPOLATED U_0 PORE PRESSURES (D) Δ_Q (E) B_Q AND (F) SOIL BEHAVIOUR INDEX I_{C-JD}.

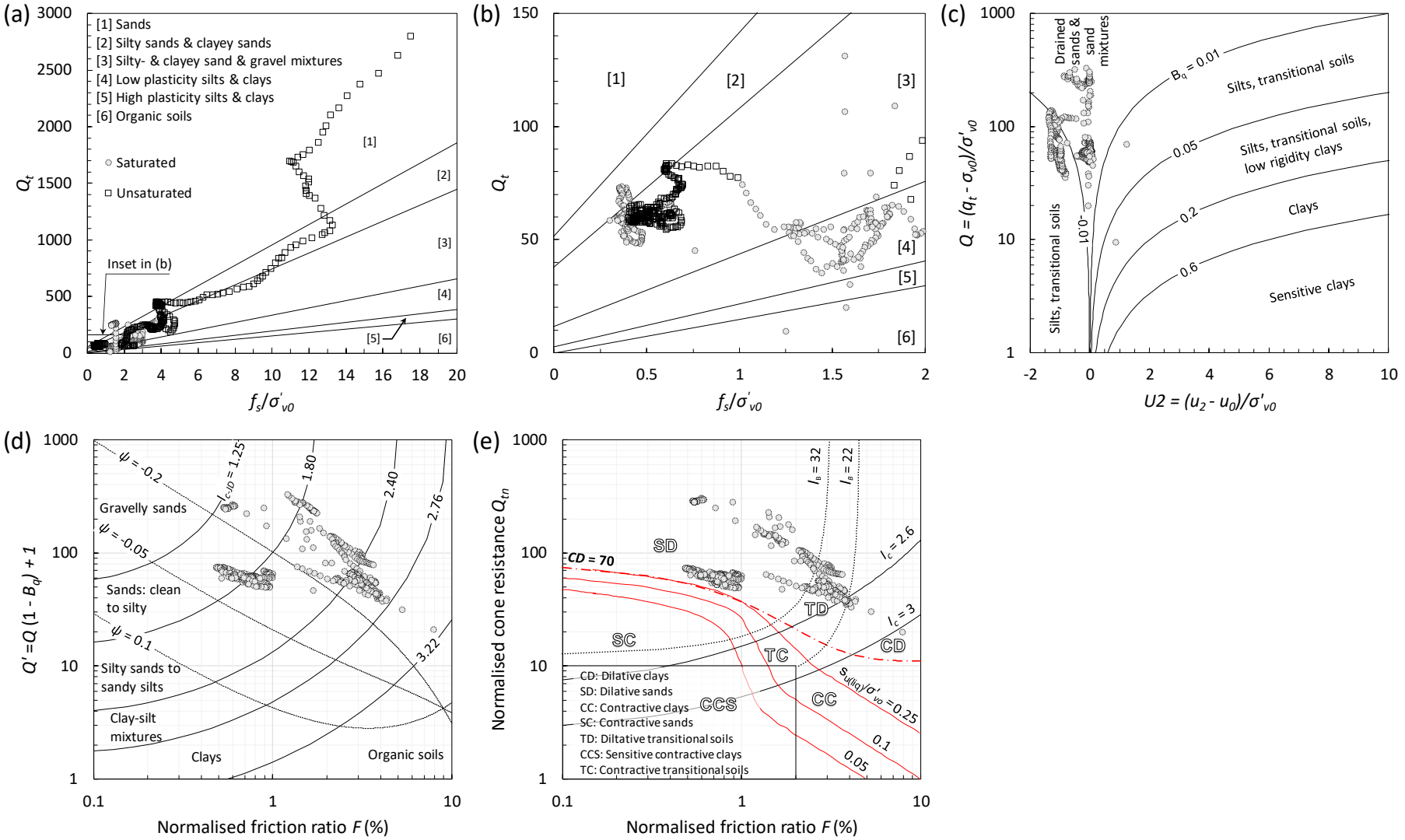

FIGURE 50 SOIL BEHAVIOUR TYPE CHARTS FOR CPT POSITION C12 (A) Q_T VS F_S/Σ'_{VO} (B) INSET FROM Q_T VS F_S/Σ'_{VO} (C) Q VS U2 (D) Q' VS F AND (E) Q_{TN} VS F.

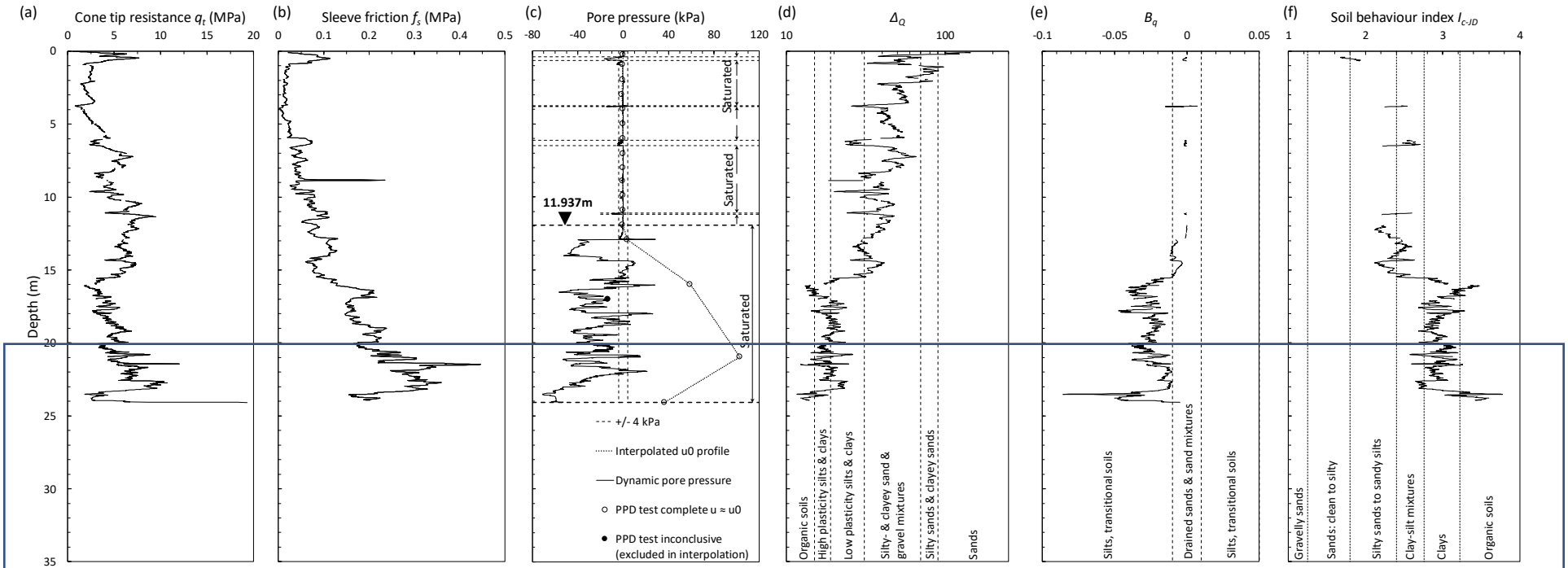

FIGURE 51 PROFILES AT CPT POSITION C13 (A) CONE TIP RESISTANCE Q_T (B) SLEEVE FRICTION F_S (C) DYNAMIC AND INTERPOLATED U_0 PORE PRESSURES (D) Δ_Q (E) B_Q AND (F) SOIL BEHAVIOUR INDEX I_{C-JD}.

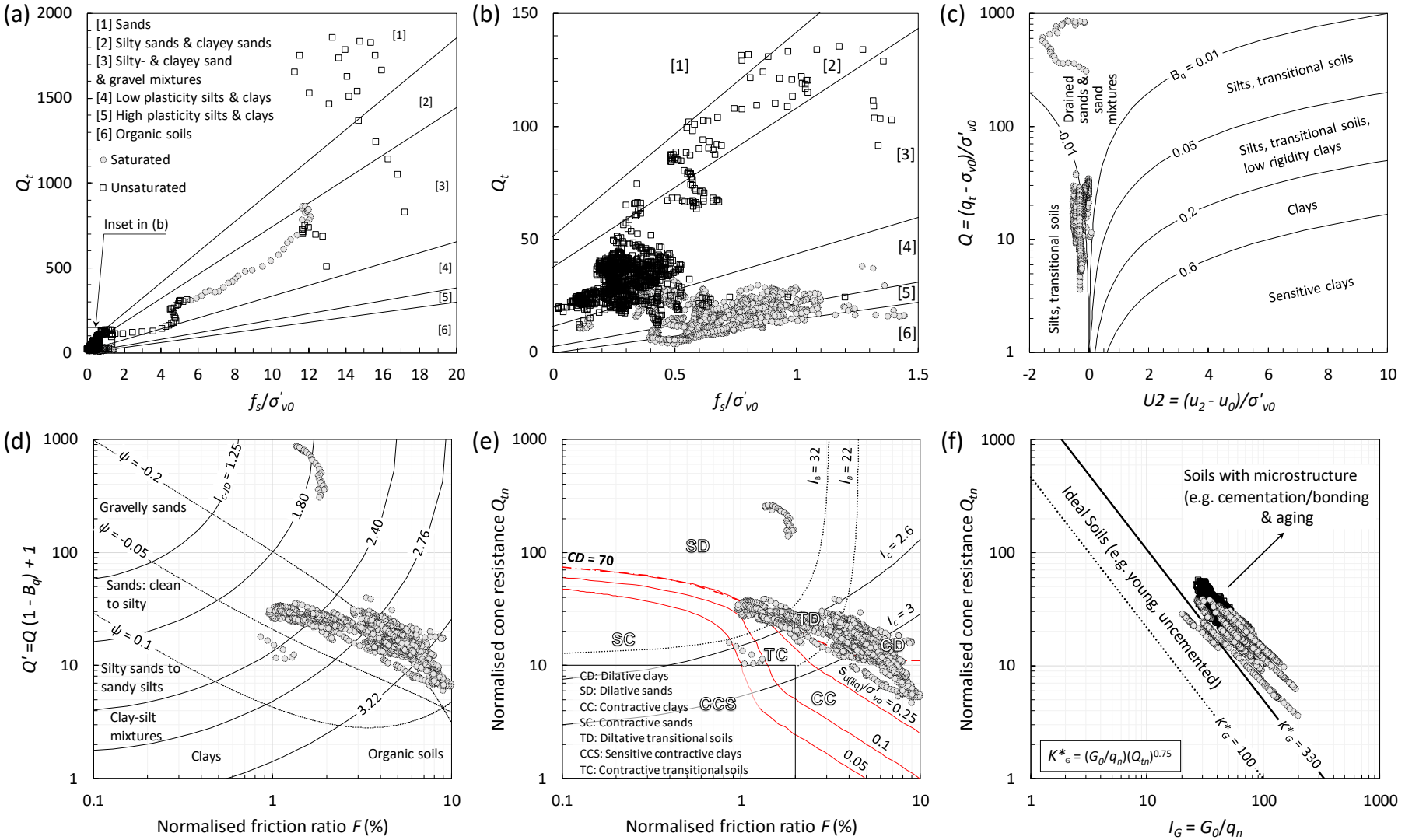

FIGURE 52 SOIL BEHAVIOUR TYPE CHARTS FOR CPT POSITION C13 (A) Q_T VS F_S/Σ'_{VO} (B) INSET FROM Q_T VS F_S/Σ'_{VO} (C) Q VS U2 (D) Q' VS F (E) Q_{TN} VS F AND (F) Q_{TN} VS I_G.

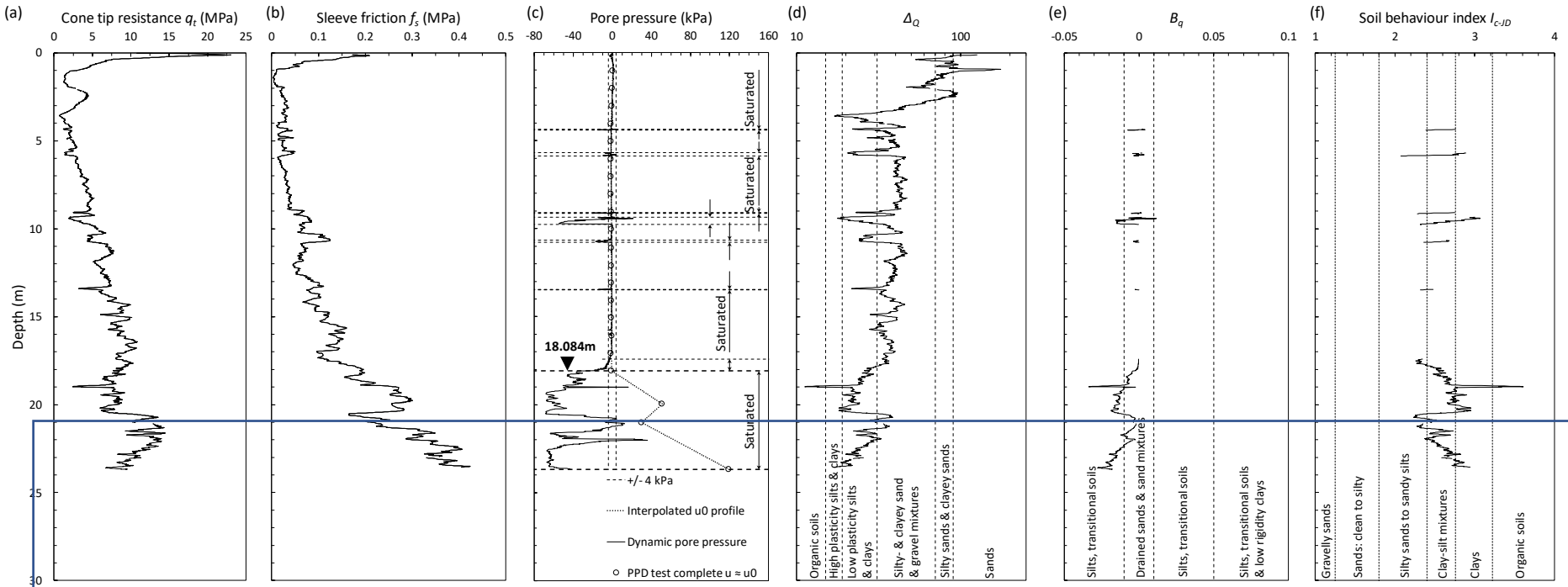

FIGURE 53 PROFILES AT CPT POSITION C14 (A) CONE TIP RESISTANCE Q_T (B) SLEEVE FRICTION F_S (C) DYNAMIC AND INTERPOLATED U_0 PORE PRESSURES (D) Δ_Q (E) B_Q AND (F) SOIL BEHAVIOUR INDEX I_{C-JD}.

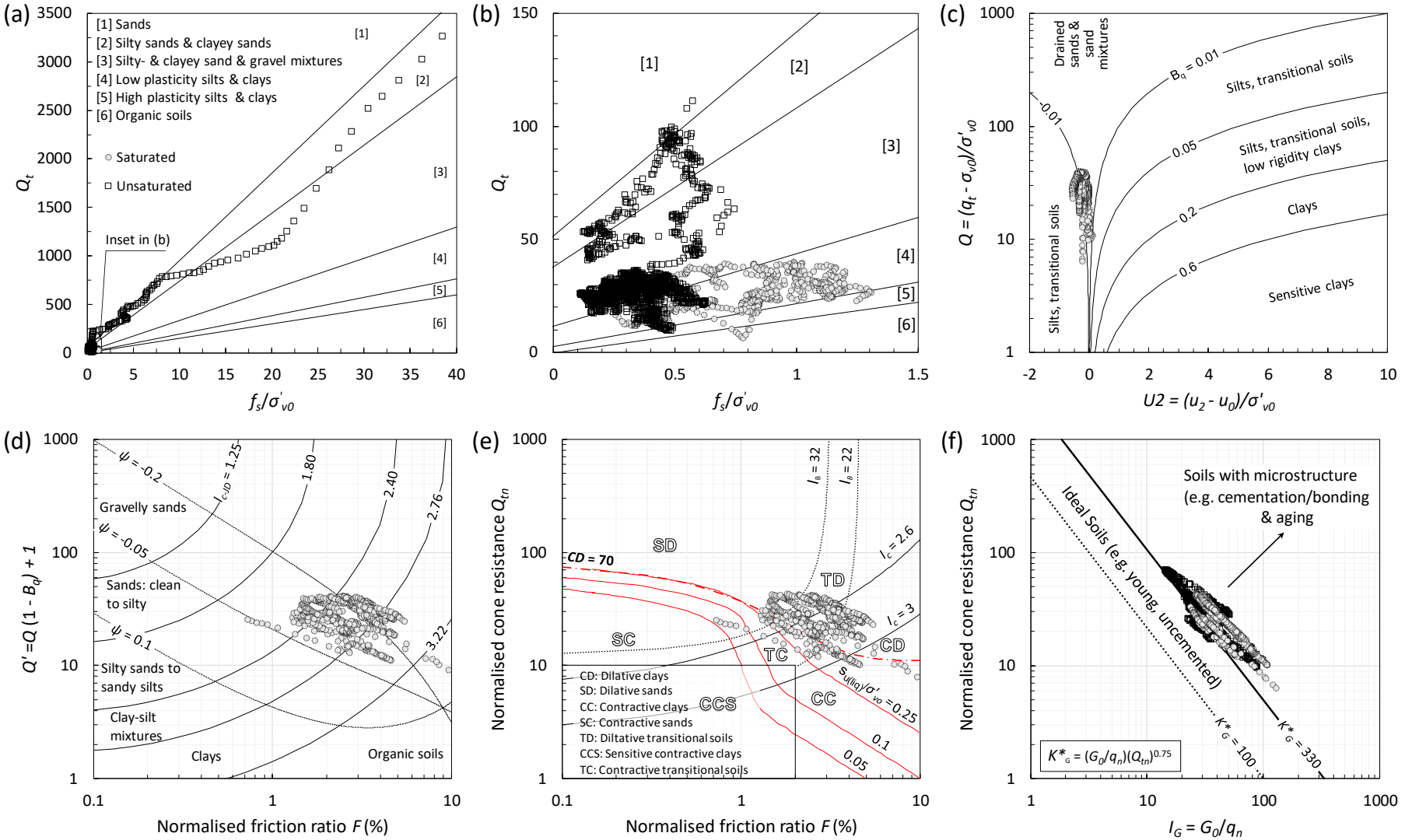

FIGURE 54 SOIL BEHAVIOUR TYPE CHARTS FOR CPT POSITION C14 (A) Q_T VS F_S/Σ'_{VO} (B) INSET FROM Q_T VS F_S/Σ'_{VO} (C) Q VS U2 (D) Q' VS F (E) Q_{TN} VS F AND (F) Q_{TN} VS I_G.

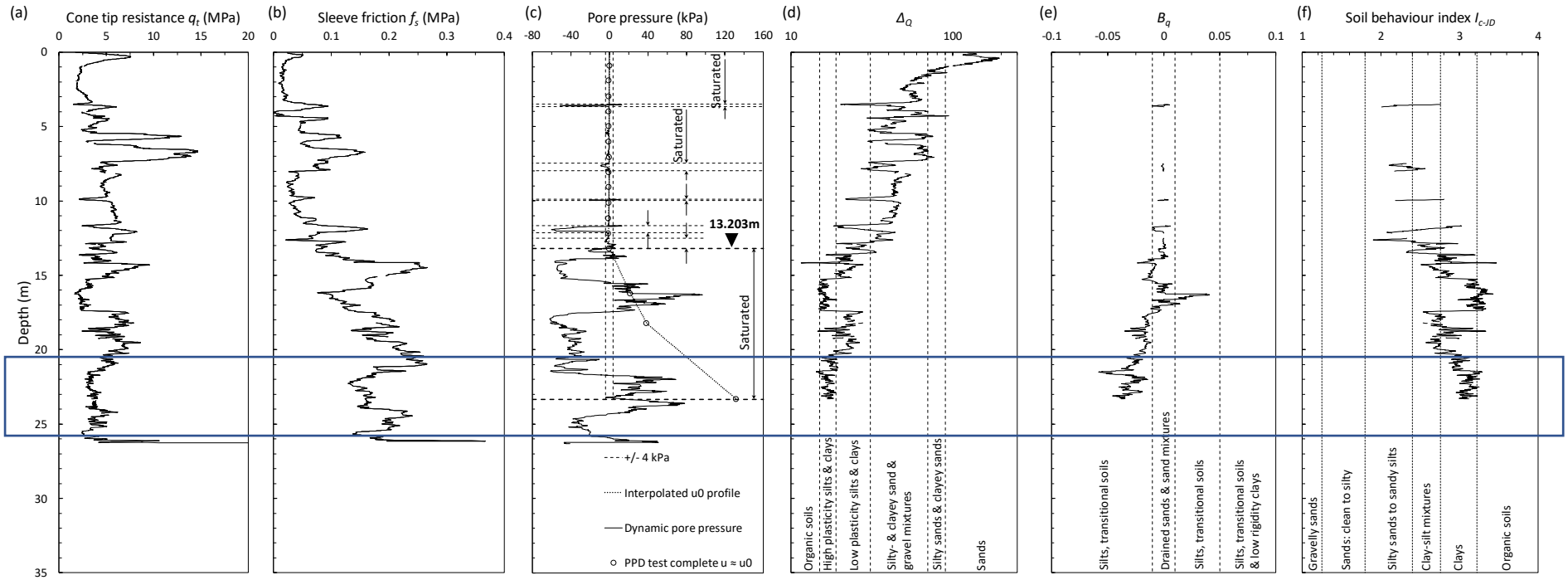

FIGURE 55 PROFILES AT CPT POSITION C15 (A) CONE TIP RESISTANCE Q_T (B) SLEEVE FRICTION F_S (C) DYNAMIC AND INTERPOLATED U_0 PORE PRESSURES (D) Δ_Q (E) B_Q AND (F) SOIL BEHAVIOUR INDEX I_{C-JD}.

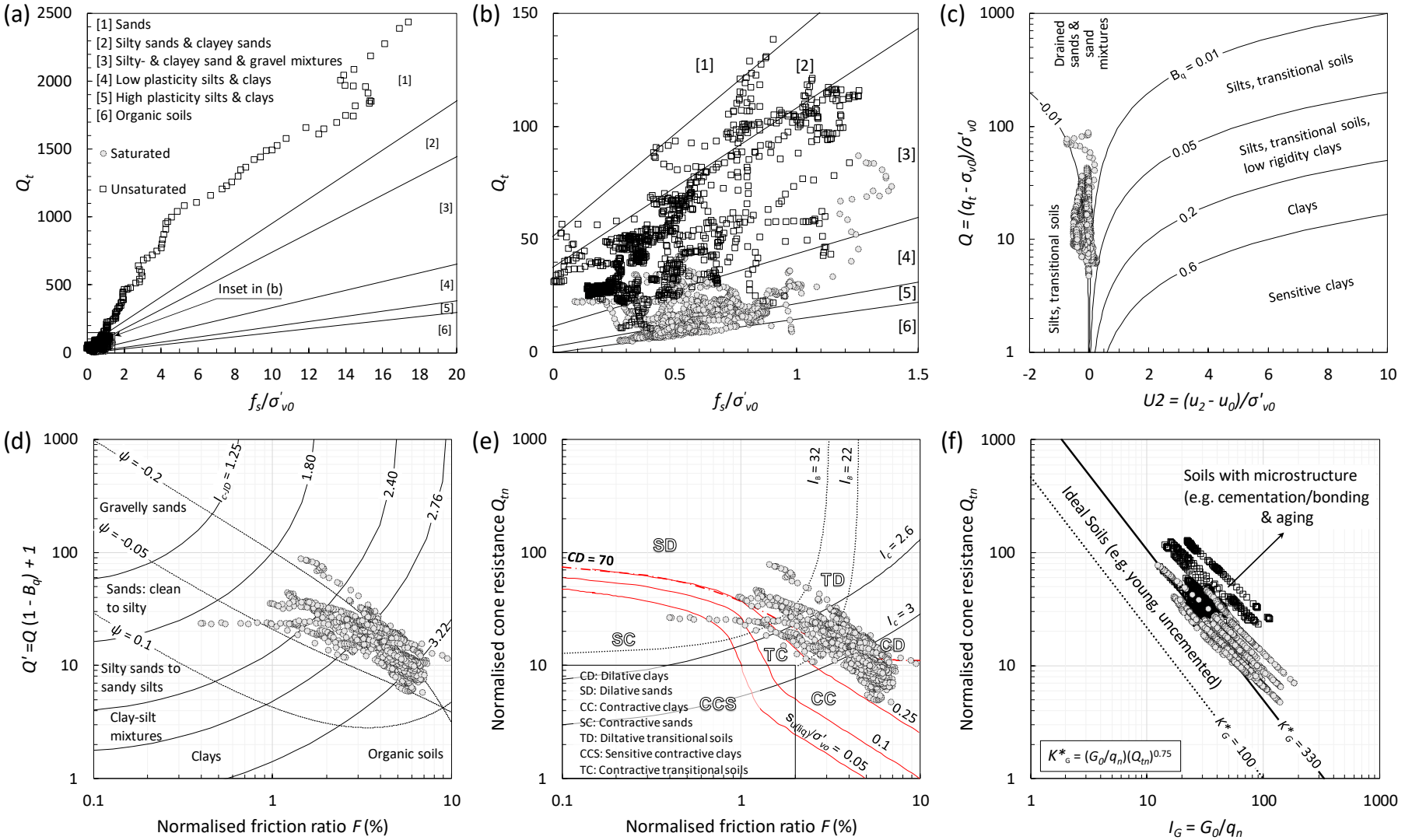

FIGURE 56 SOIL BEHAVIOUR TYPE CHARTS FOR CPT POSITION C15 (A) Q_T VS F_S/Σ'_{VO} (B) INSET FROM Q_T VS F_S/Σ'_{VO} (C) Q VS U2 (D) Q' VS F (E) Q_{TN} VS F AND (F) Q_{TN} VS I_G.

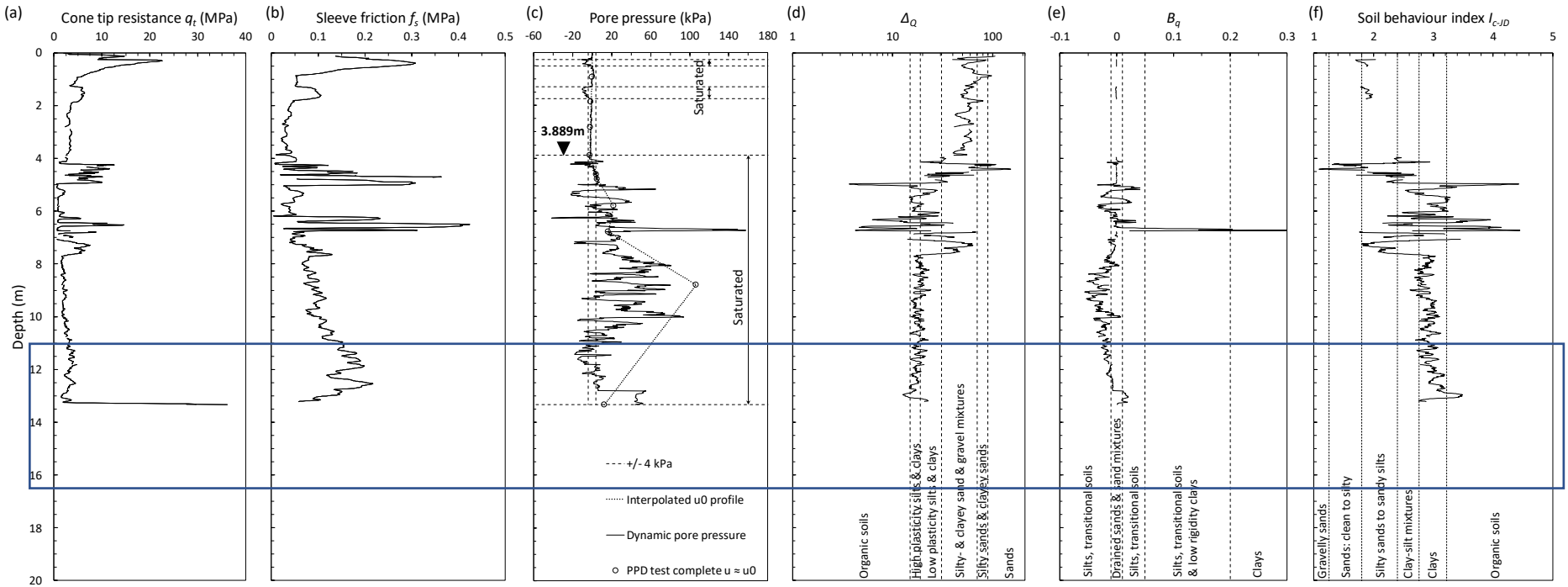

FIGURE 57 PROFILES AT CPT POSITION C16 (A) CONE TIP RESISTANCE Q_T (B) SLEEVE FRICTION F_S (C) DYNAMIC AND INTERPOLATED U_0 PORE PRESSURES (D) Δ_Q (E) B_Q AND (F) SOIL BEHAVIOUR INDEX I_{C-JD}.

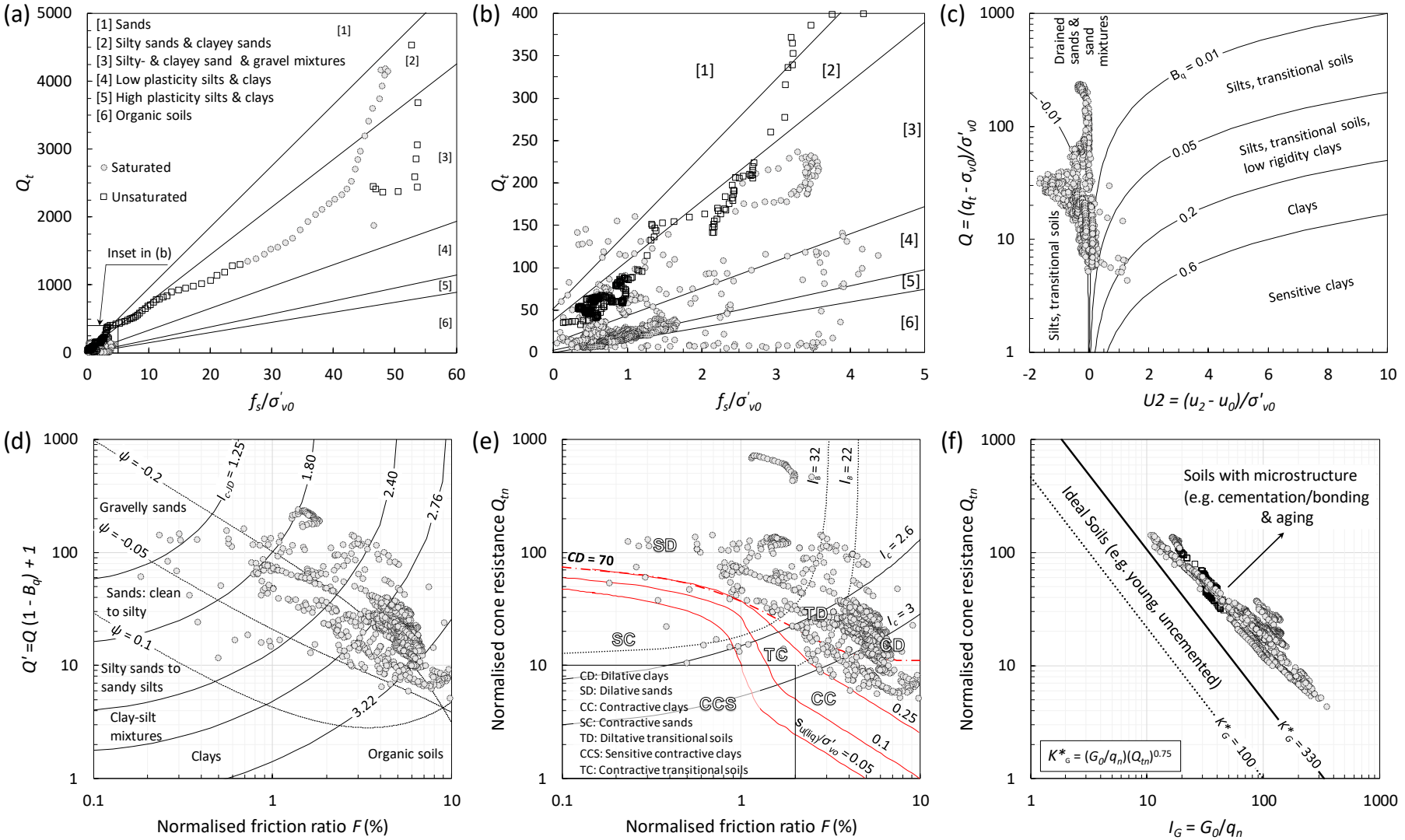

FIGURE 58 SOIL BEHAVIOUR TYPE CHARTS FOR CPT POSITION C16 (A) Q_T VS F_S/Σ'_{VO} (B) INSET FROM Q_T VS F_S/Σ'_{VO} (C) Q VS U2 (D) Q' VS F (E) Q_{TN} VS F AND (F) Q_{TN} VS I_G.

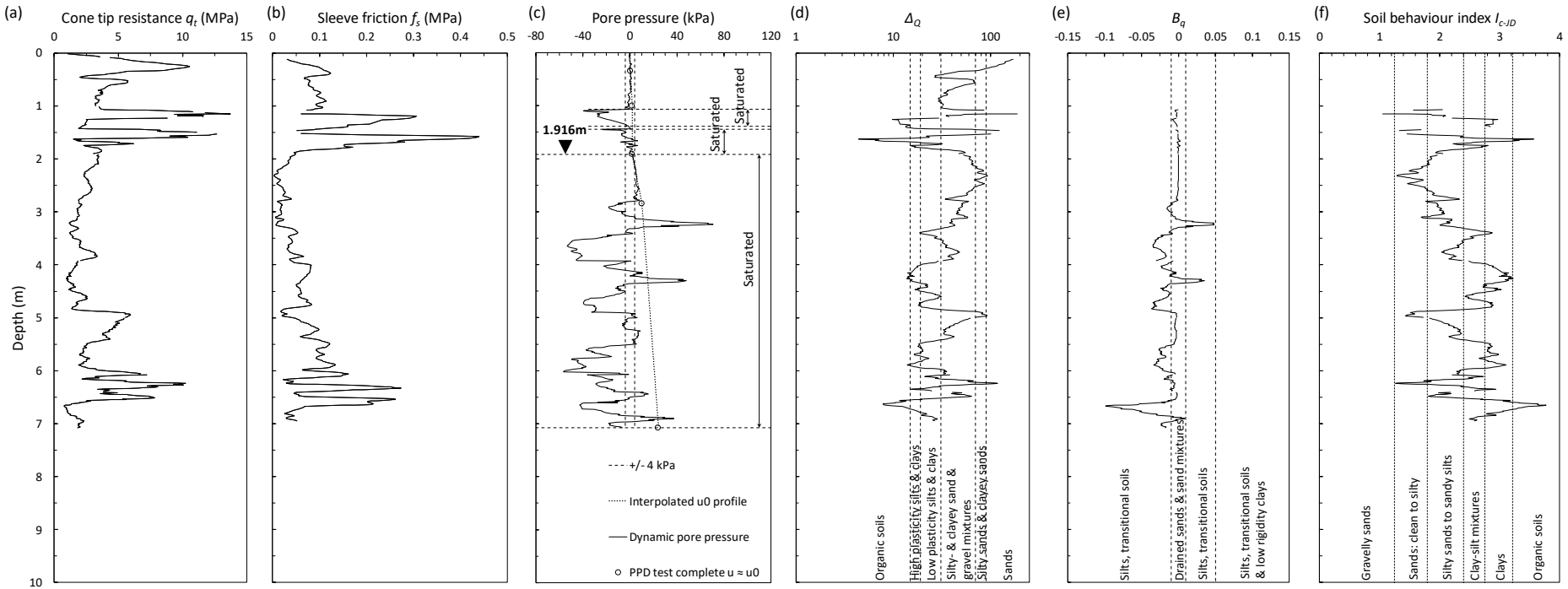

FIGURE 59 PROFILES AT CPT POSITION C17 (A) CONE TIP RESISTANCE Q_T (B) SLEEVE FRICTION F_S (C) DYNAMIC AND INTERPOLATED U_0 PORE PRESSURES (D) Δ_Q (E) B_Q AND (F) SOIL BEHAVIOUR INDEX I_{C-JD}.

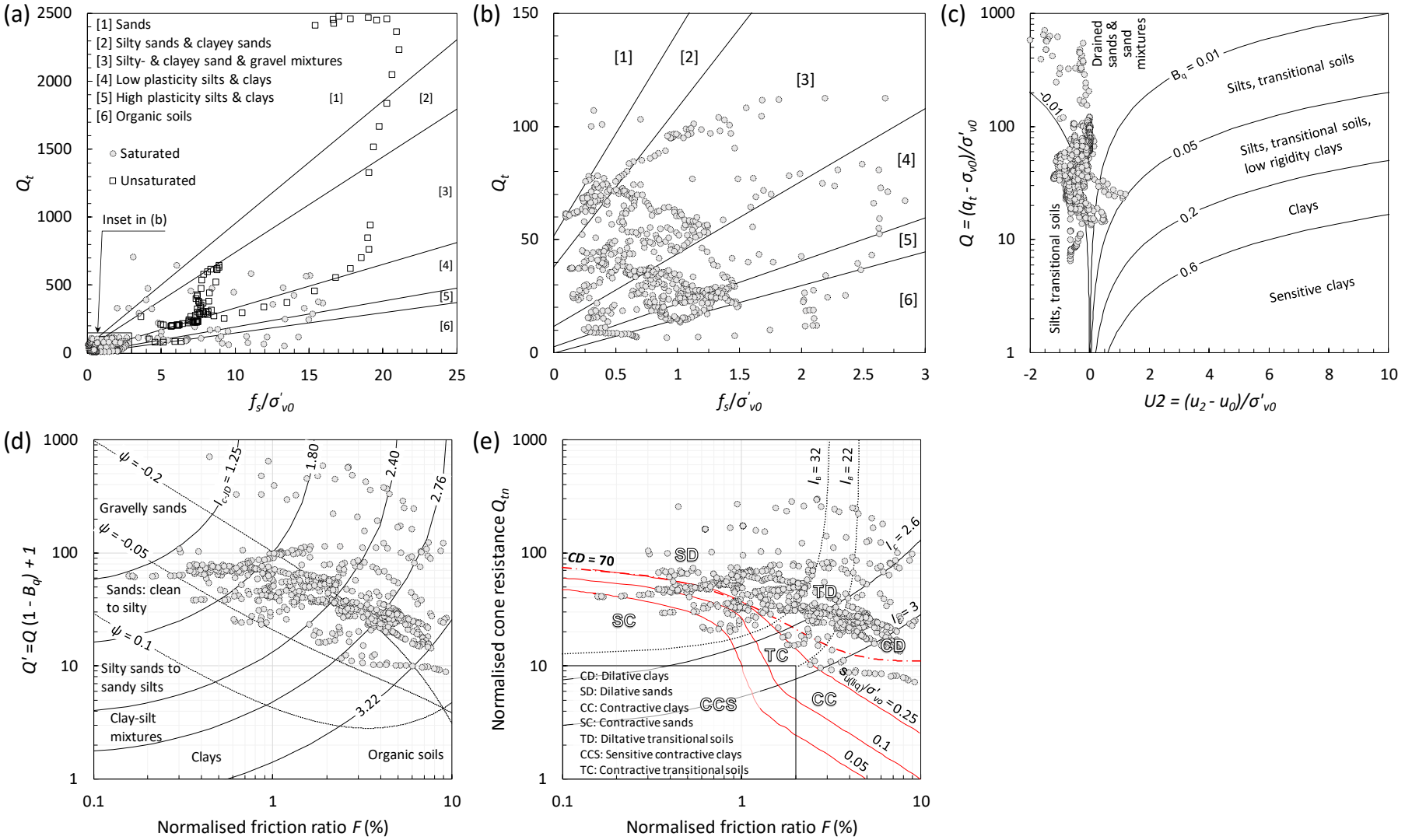

FIGURE 60 SOIL BEHAVIOUR TYPE CHARTS FOR CPT POSITION C17 (A) Q_T VS F_S/Σ'_{VO} (B) INSET FROM Q_T VS F_S/Σ'_{VO} (C) Q VS U2 (D) Q' VS F AND (E) Q_{TN} VS F.

5. Mostap samples

A number of samples were recovered during the Investigation Panel's SCPTu investigation. The results are summarised in the table below. The results of tests listed in Table 1 carried out on the samples can be found in the ground investigation report contained in Appendix E. The Investigation Panel is not confident that all the densities and void ratios presented are representative of the actual in situ densities because the sample tubes were often found not to be completely filled. Due to the high consistency of the materials generally encountered towards the bottom of the profile at the probed locations, it is believed that the sampler could have become clogged or partially clogged so that not all materials could be sampled. That said, the higher densities measured were deemed more reliable and were used to inform the unit weights used in the slope stability analyses.

TABLE 1 MOSTAP SAMPLES RECOVERED DURING INVESTIGATION BY PANEL.

Mostap Sample	Sr	w	e	Bulk density	Dry density	Tests carried out
	%	%	-	kg/m³	kg/m³	
C5/1	60.2%	13.4%	0.580	1866	1645	SG
C6/1	70.8%	14.5%	0.532	1943	1697	FI, SG, XRD
C6/2	65.7%	14.9%	0.589	1880	1636	FI, SG, XRD
C6/3	73.6%	13.1%	0.463	2010	1778	FI, SG, XRD
C6/4	88.0%	16.6%	0.491	2034	1744	SG, XRD, FI after XRD
C8/1	63.8%	13.8%	0.563	1894	1664	FI, SG
C8/2	79.5%	13.4%	0.437	2051	1810	FI, SG
C11/1	51.3%	19.4%	0.984	1565	1310	FI, SG, XRD
C11/2	49.0%	18.6%	0.989	1550	1307	FI, SG, XRD
C11/3	74.0%	21.7%	0.761	1796	1476	FI, SG, XRD
C12/1	40.1%	25.6%	1.657	1229	978	SG, XRD, FI after XRD
C12/2	19.2%	14.7%	1.990	997	870	combined with C12/1

6. Cross section profile from SCPTu results for stability analysis

A representative cross section profile through the dam embankment as informed by the CPTu investigation is presented in Figure 61. For the purposes of compiling this profile, the soil classification identification chart by Jones and Rust (1983) was used in addition to the methods referred to earlier in this appendix as, in addition to offering a soil description, this method also indicates the soil consistency. This method employs penetration resistance and dynamic pore pressure for material identification. As such, it can only be employed in the saturated zone. The method generally offers material identification at a higher resolution than methods employing sleeve friction as the latter is measured over a certain length of the probe shaft, while dynamic pore pressure is measured at a single position just above the cone shoulder.

In general, the downstream slope profile probed can be subdivided into an upper coarse and lower fine-grained zone. The coarse material represents the coarse tailings (grits) which generally classified as a sand. The consistency varies from very loose at the surface, with density increasing with depth, generally to a medium dense consistency above the underlying fine-grained material. The fine-grained material is not homogeneous. This material classified as a dense silty sand at C10 and clayey silt at C15, interbedded with layers that classified as stiff clayey silt or clay at C6, C13 and C14. The fine-grained material appeared most heterogeneous at C11 (near the embankment toe) where alternating

layers of loose silty sand, very soft clayey silt and firm clay occurred. The consistency of the fine-grained material was found to be lower closer to the toe of the dam.

The phreatic surface as inferred from the piezocone investigation occurs above the interface between the coarse- and fine-grained material, implying that the fine-grained material was saturated at the time of the piezocone investigation. It is therefore reasonable to assume that the fine-grained material was also saturated at the time of the failure in Sept 2022.

In addition to penetration resistance, sleeve friction and dynamic pore pressure, the SCPTu investigation included measurement of the shear wave velocity at locations C13 to C16 (Figure 2). Qualitative plots of shear wave velocity are included in Figure 61. A higher shear wave velocity indicates soil of greater shear stiffness. There appears to be some evidence of a somewhat reduced shear wave velocity just above the depths of refusal (C13, C15 and C16). This may be indicative of the depth where the slip surface passed through, although the shear zone cannot be located with complete certainty from the information available. The detailed seismic CPTu results are included in Attachment F3.

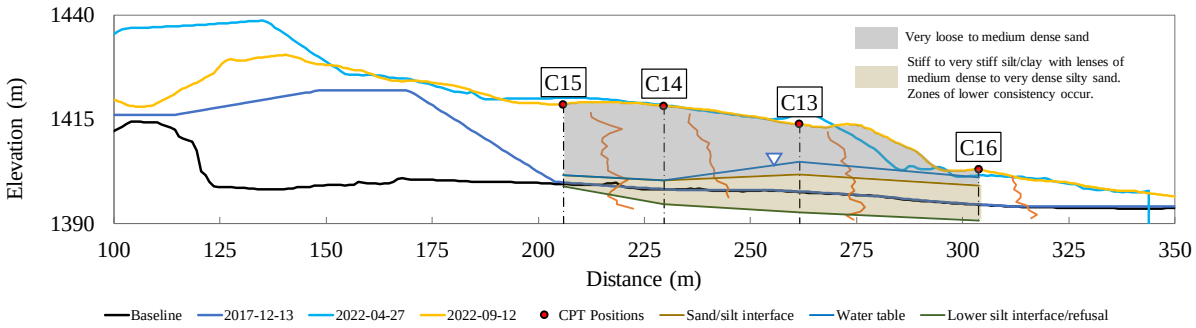

FIGURE 61 CROSS SECTION PROFILE SHOWING MATERIAL ZONES FOR STABILITY ANALYSIS.

7. Concluding remarks

The investigation panel considered two sources of in situ geotechnical data, i.e. a CPT campaign performed by SRK and a CPT campaign performed by the Investigation Panel. The results from the SRK CPT campaign were not considered to any significant extent because all the soundings were located away from the area where failure occurred. The CPT campaign performed by the Panel included soundings within the area of the failure and thus constituted the main source of in situ geotechnical data.

The CPT soundings performed by the panel indicate the presence of clay-like soils below the baseline survey level (refer to Section 6 of the main report) in several of the locations probed. This is consistent with the hypothesis that failure occurred due to the shearing of legacy slimes over which part of the failed wall was constructed. The analysis also suggests that most of the probed material in the failed wall was in a dilatant state and thus not susceptible to liquefaction.

References

Been, K., and Jefferies, M.G. 1985. *A state parameter for sands*. Géotechnique 35(2): 99-112.

Been, K., and Jefferies, M.G. 1992. Towards systematic CPT interpretation. Predictive Soil Mechanics - Proceedings of the Wroth Memorial Symposium, Thomas Telford, London, pp 121–134.

Campanella, R., and Robertson, P.K. 1988. Current status of the piezocone test. Proceedings of the First International Symposium on Penetration Testing: ISOPT-1. pp. 93-116. Balkema, Rotterdam.

Fourie, A., Verdugo, R., Bjelkevik, A., Torres-Cruz, L.A., and Znidarcic, D. 2022. Geotechnics of mine tailings: a 2022 state of the art. In Proceedings of the 20th International Conference on Soil Mechanics and Geotechnical Engineering.

Jefferies, M., and Been, K. 2015. Soil liquefaction: A critical state approach (Second edition). Taylor & Francis.

Jefferies, M.G., and Davies, M.P. 1993. Use of CPTu to Estimate Equivalent SPT N60. Geotechnical Testing Journal 16(4):458-458.

Jones, G.A. and Rust, E. 1983. Piezometer probe (CPTU) for subsoil identification. International Symposium on In-Situ Testing, Paris, Vol 2, pp 303-308.

Plewes, H., Davies, M., and Jefferies, M. 1992. CPT based screening procedure for evaluating liquefaction susceptibility. Proceedings of the 45th Canadian Geotechnical Conference. Toronto, Canada.

PMI. 2023. Jagersfontein Diamond Mine, Cone Penetration Testing & Mostap Sampling. PMI Construction Services, Field report no. 23-029 PMI RPT.

Reid, D., Rodriguez, C., Fourie, A. and Tiwari, B. 2023. Partial drainage effects during vane shear tests, with an emphasis on the measurement of remoulded strengths. Proceedings of Tailings and Mine Waste. Vancouver, Canada.

Roberston, P.K. 2022. Evaluation of flow liquefaction and liquefied strength using the cone penetration test: an update. Canadian Geotechnical Journal 59(4): 620-624.

Robertson, P. K. 2009. Interpretation of cone penetration tests—A unified approach. Canadian Geotechnical Journal 46(11): 1337–1355.

Robertson, P.K. 2016. Cone penetration test (CPT)-based soil behaviour type (SBT) classification system - an update. Canadian Geotechnical Journal 53(12): 1910-1927.

Robertson, P.K., and Wride, C.E. 1998. Evaluating cyclic liquefaction potential using the cone penetration test. Canadian Geotechnical Journal 35(3): 442-459.

Rust, E., and Rust, M. 2023. Determination of the degree of saturation above the water table from CPTu probing in tailings. Proceedings of Tailings and Mine Waste. Vancouver, Canada.

Saye, S.R., Santos, J., Olson, S.M., and Leigh, R.D. 2017. Linear trendlines to assess soil classification from cone penetration test data. J. Geotech. Geoenviron. Eng. 143(9).

Scheremeta, M.S. 2014. A practical method for extrapolating ambient pore pressures from incomplete pore pressure dissipation tests conducted in fine grained soils. Proceedings of Tailings and Mine Waste. Keystone, Colorado, USA.

Schneider, J. A., Randolph, M. F., Mayne, P. W. and Ramsey, N. R. 2008. Analysis of factors influencing soil classification using normalized piezocone tip resistance and pore pressure parameters. J. Geotech. Geoenviron. Eng. 134(11): 1569–1586.

Torres-Cruz, L.A. 2021. The Plewes Method: A Word of Caution. Mining, Metallurgy & Exploration 38(3: 1329-1338.

ATTACHMENT F1

CPTu REPORTS BY OSIMO (CPT CONTRACTOR)

PIEZOCONE PENETRATION TEST

Recorded Field Results (Cone, Pore Pressure and Static Pore Pressure from Dissipations)

HOLE: C1

PROJECT: 2024 Jagersfontein

SITE: TSF

DATE: 24/01/30 At: 07:42:13 A **DEPTH:** 8.602

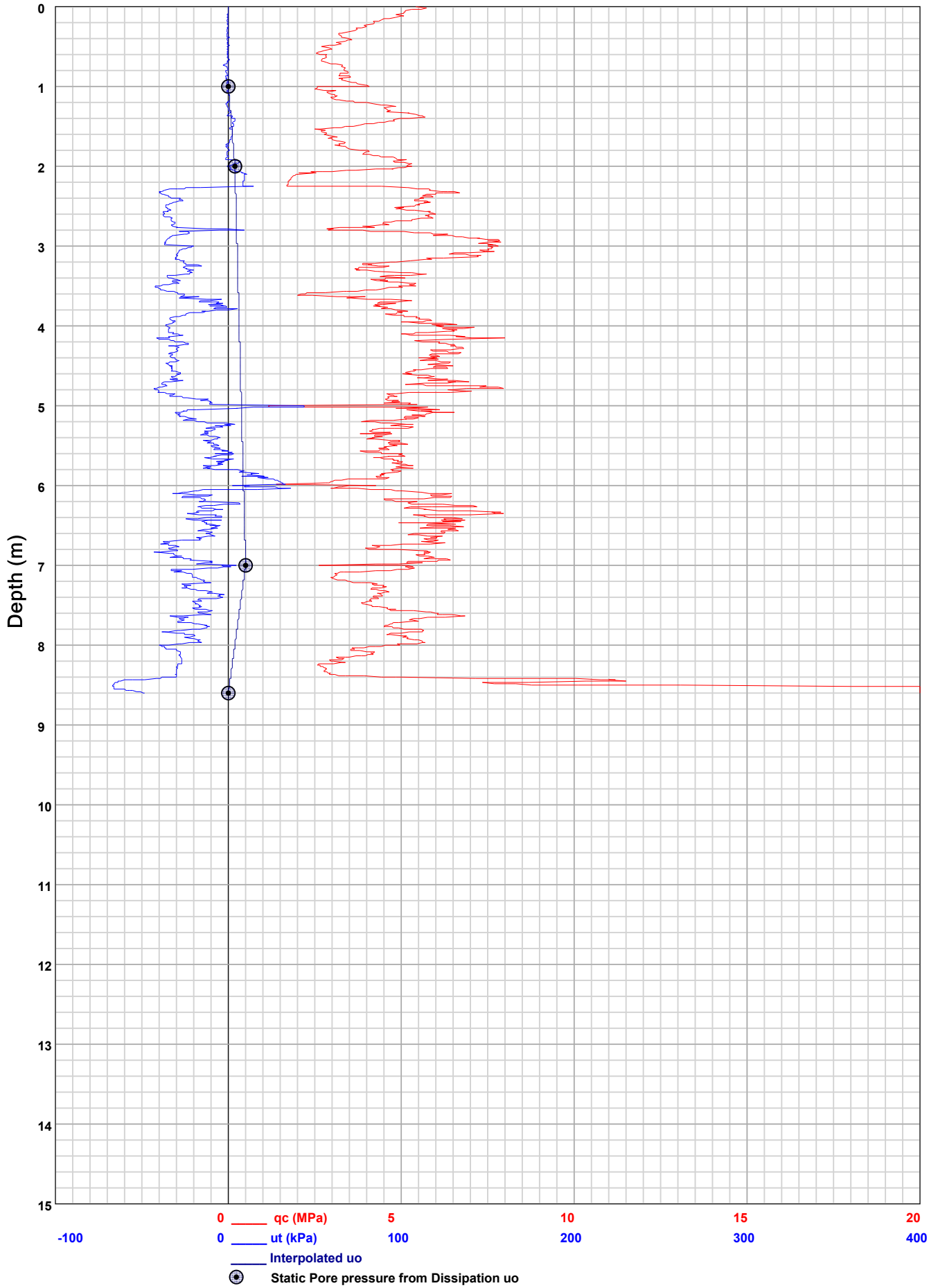

PIEZOCONE PENETRATION TEST

HOLE: C1

PROJECT: 2024 Jagersfontein

SITE: TSF

DATE: 24/01/30 At: 07:42:13 A

DEPTH: 8.602

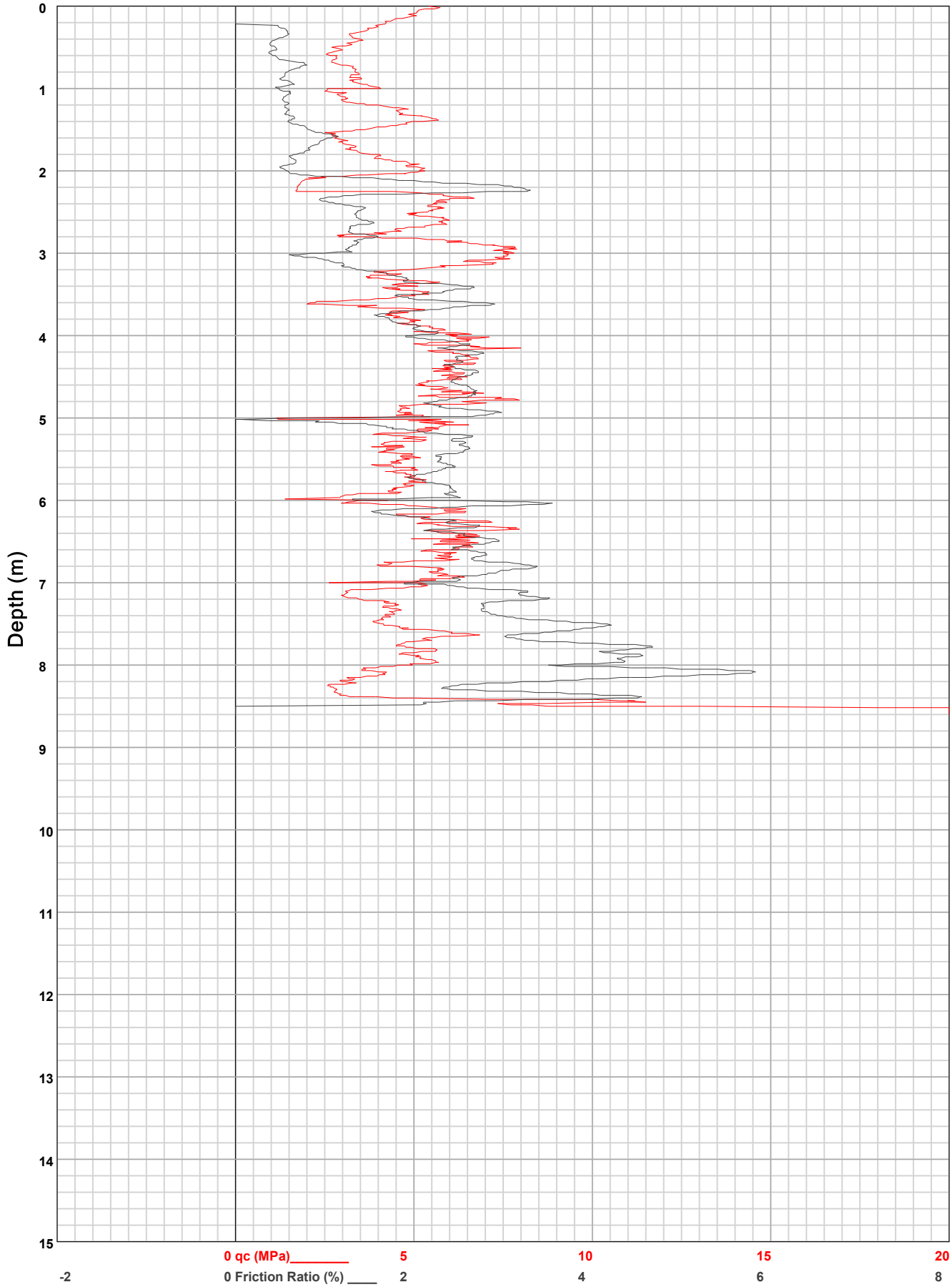

PIEZOCONE PENETRATION TEST

Dissipation Tests

HOLE: C1

PROJECT: 2024 Jagersfontein

SITE: TSF

DATE: 24/01/30 At: 07:42:13 A

DEPTH: 8.602

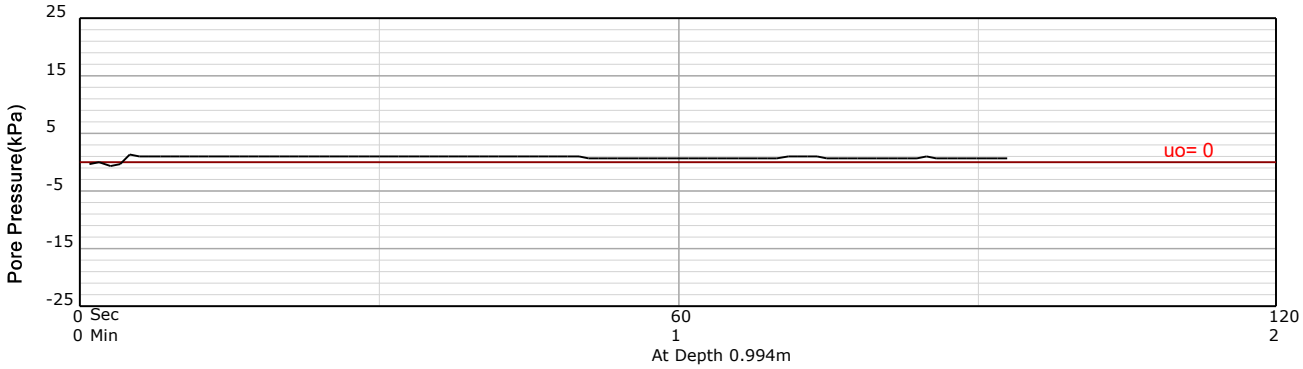

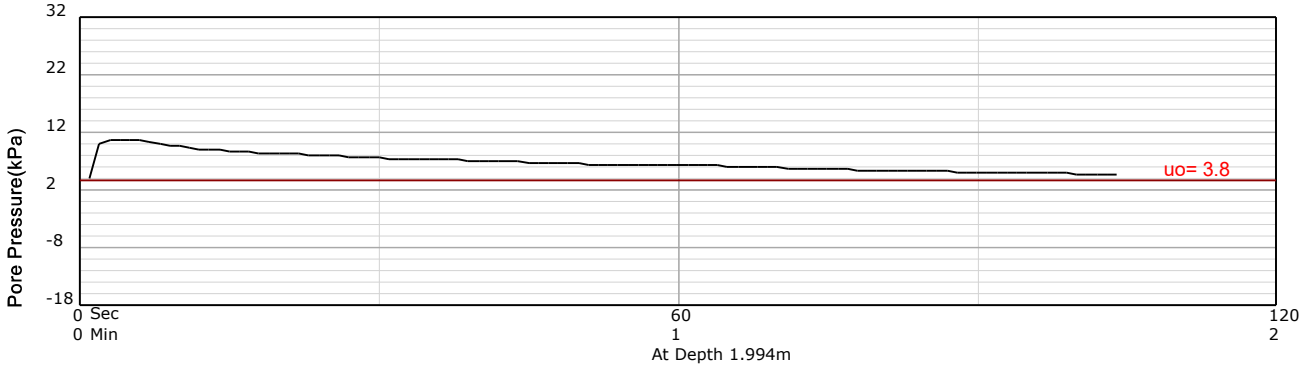

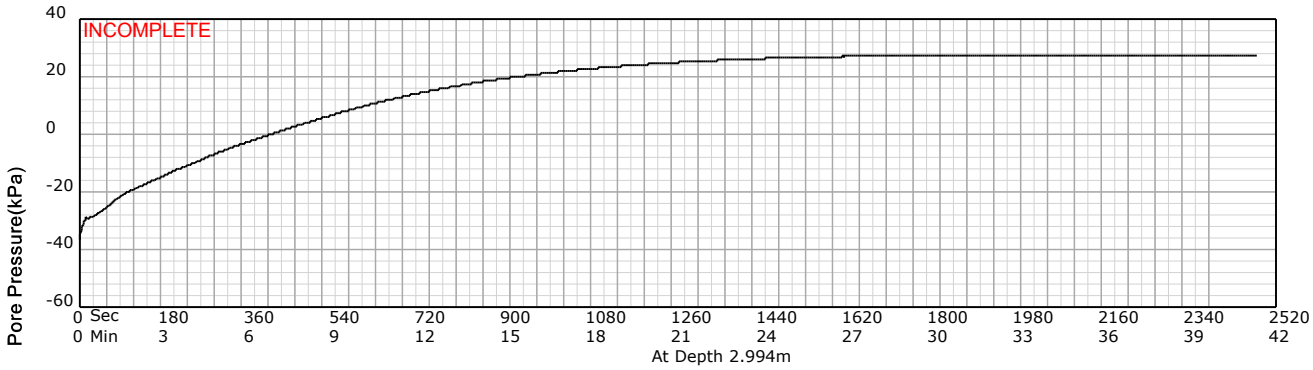

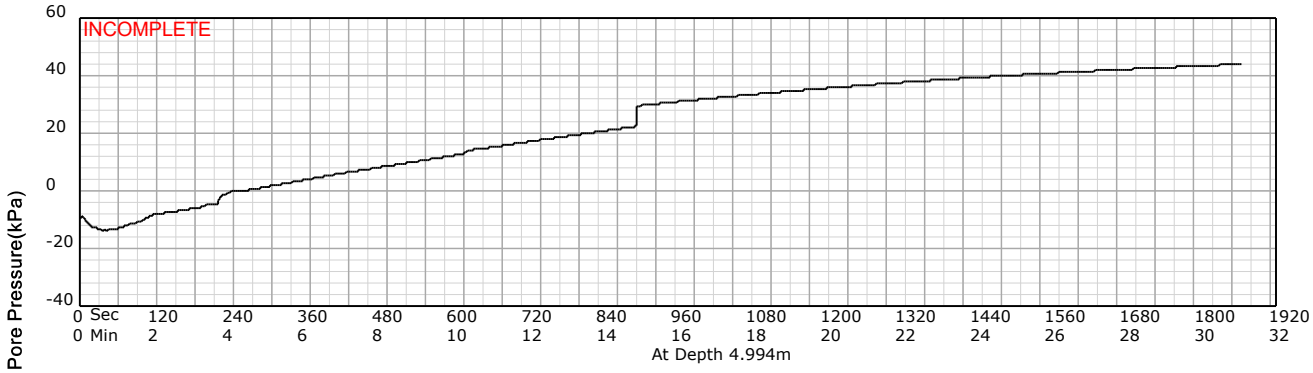

PIEZOCONE PENETRATION TEST

Dissipation Tests

HOLE: C1

PROJECT: 2024 Jagersfontein

SITE: TSF

DATE: 24/01/30 At: 07:42:13 A

DEPTH: 8.602

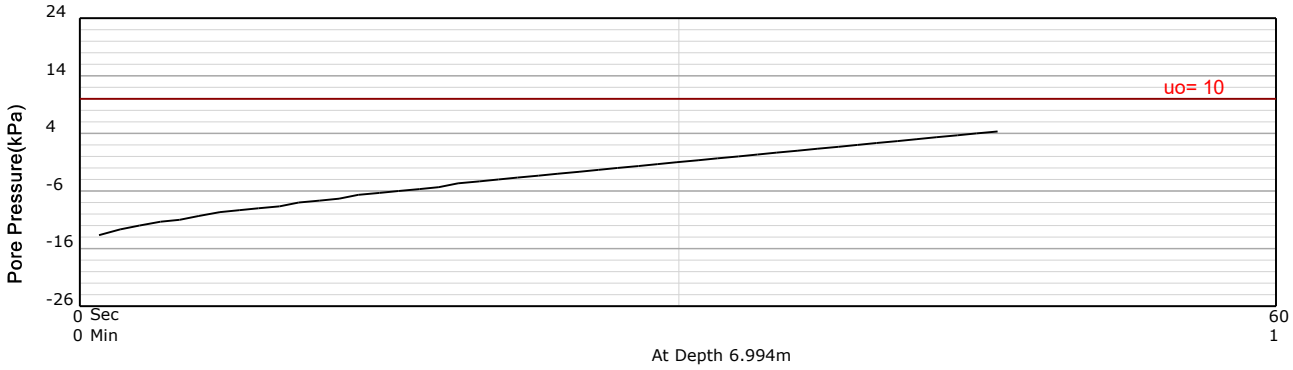

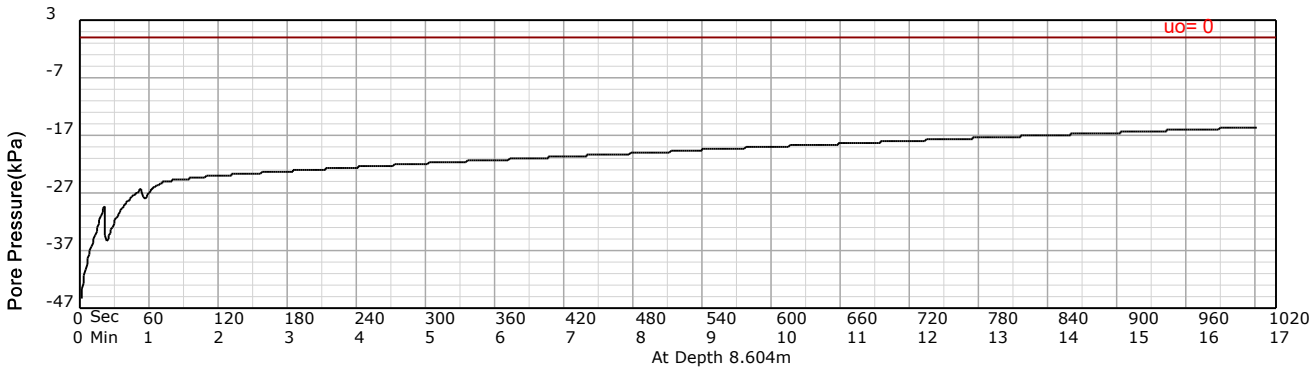

PIEZOCONE PENETRATION TEST

Equivalent Soil Behaviour Type Profile

HOLE: C1

PROJECT: 2024 Jagersfontein

SITE: TSF

DATE: 24/01/30 At: 07:42:13 A

DEPTH: 8.602

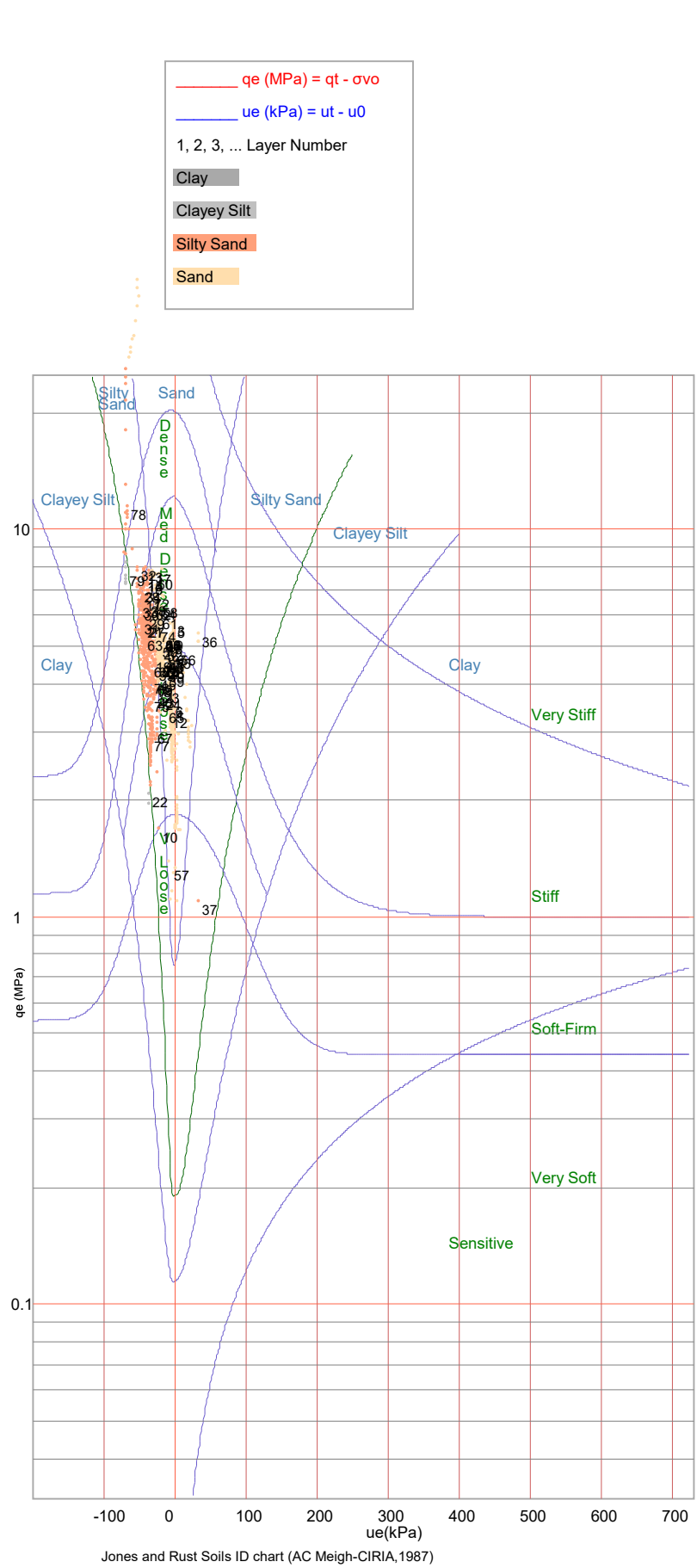

Jones and Rust Soils ID chart (AC Meigh-CIRIA,1987)

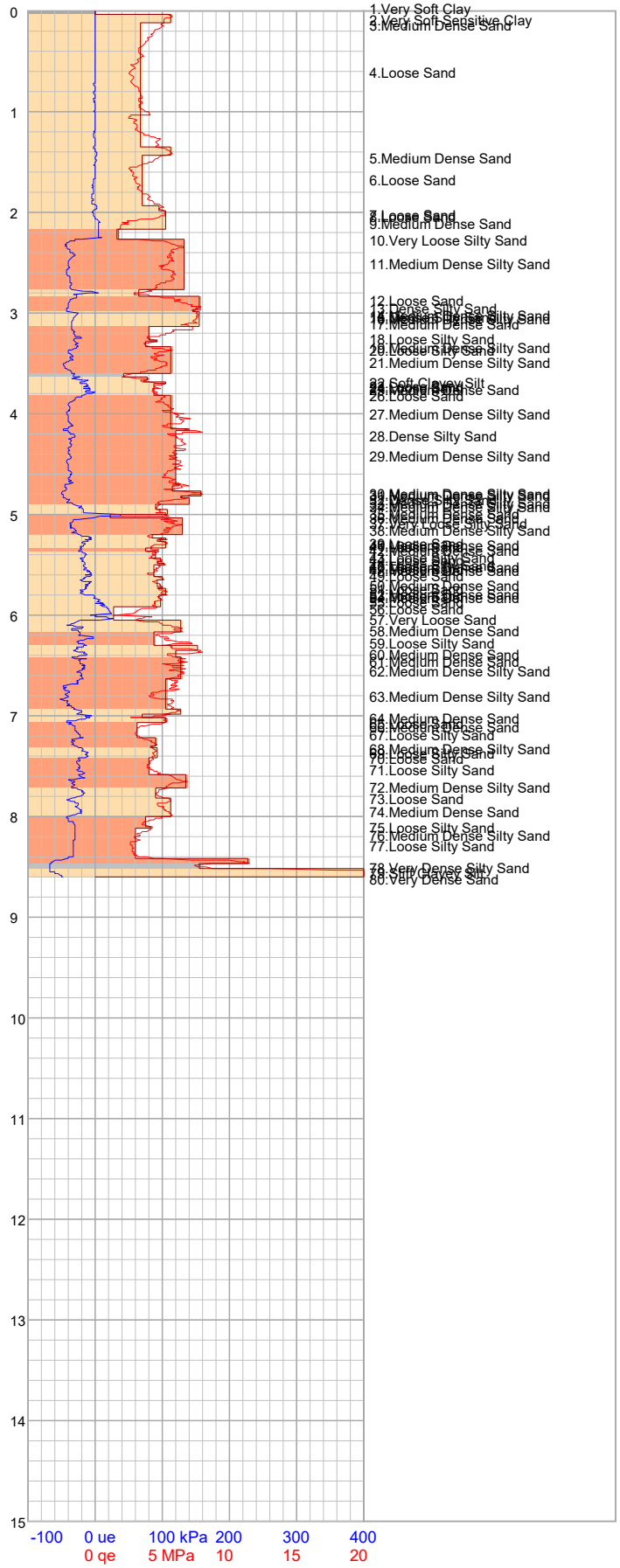

PIEZOCONE PENETRATION TEST

Recorded Field Results (Cone, Pore Pressure and Static Pore Pressure from Dissipations)

HOLE: C2

PROJECT: 2024 Jagersfontein

SITE: TSF

DATE: 24/01/30 At: 15:20:50 A **DEPTH:** 11.602

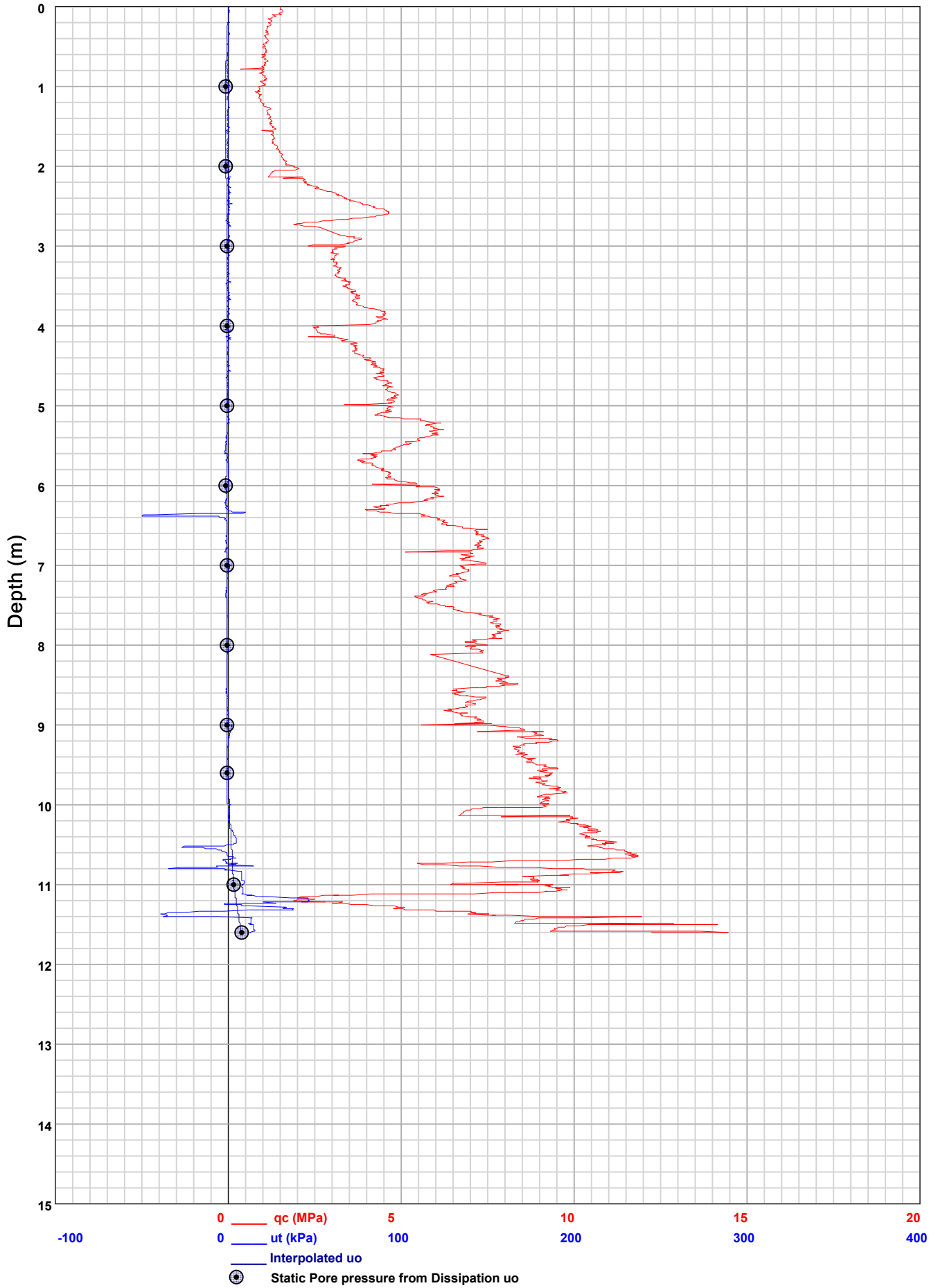

PIEZOCONE PENETRATION TEST

HOLE: C2

PROJECT: 2024 Jagersfontein

SITE: TSF

DATE: 24/01/30 At: 15:20:50 A

DEPTH: 11.602

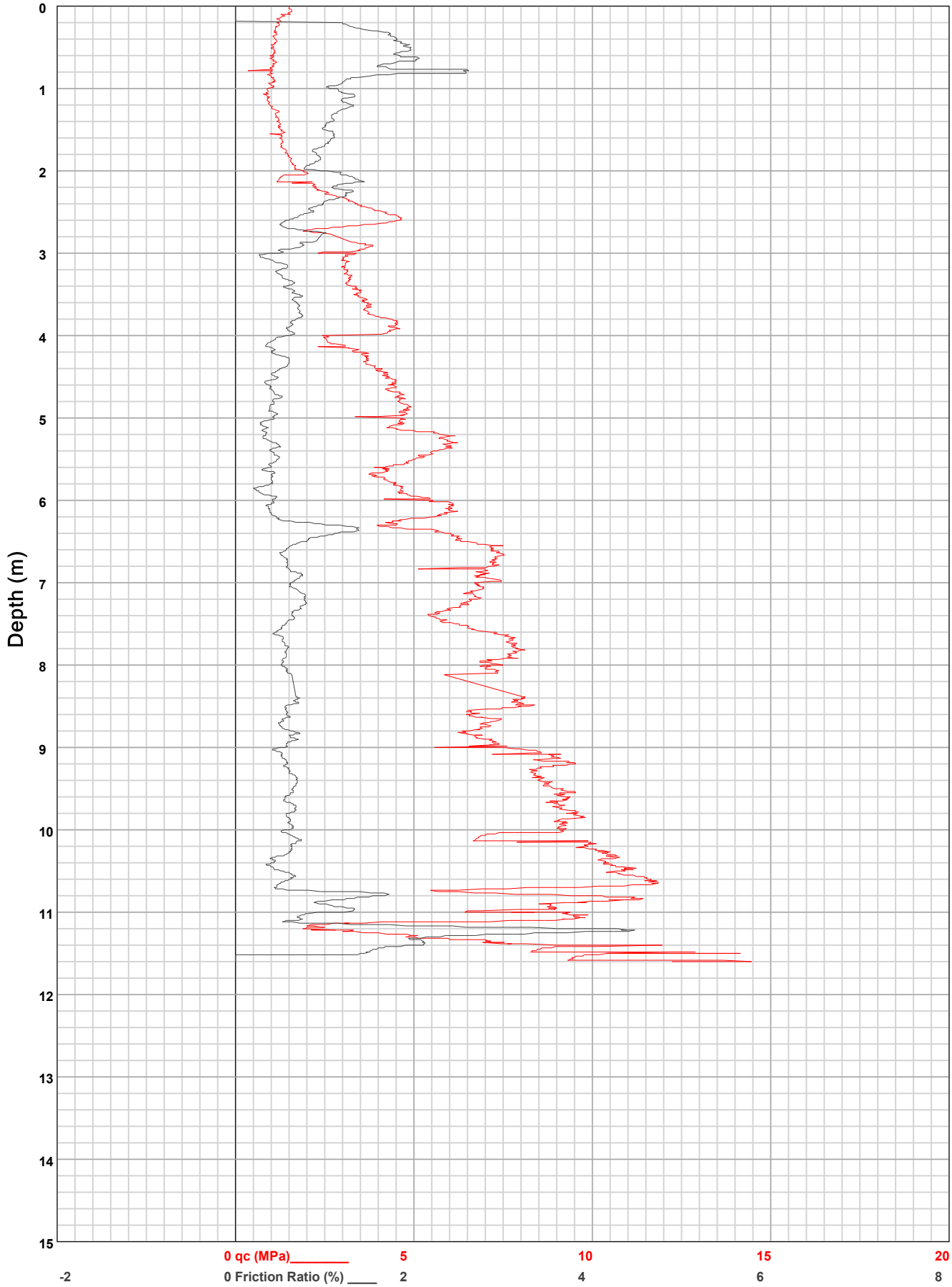

PIEZOCONE PENETRATION TEST

Dissipation Tests

HOLE: C2

PROJECT: 2024 Jagersfontein

SITE: TSF

DATE: 24/01/30 At: 15:20:50 A

DEPTH: 11.602

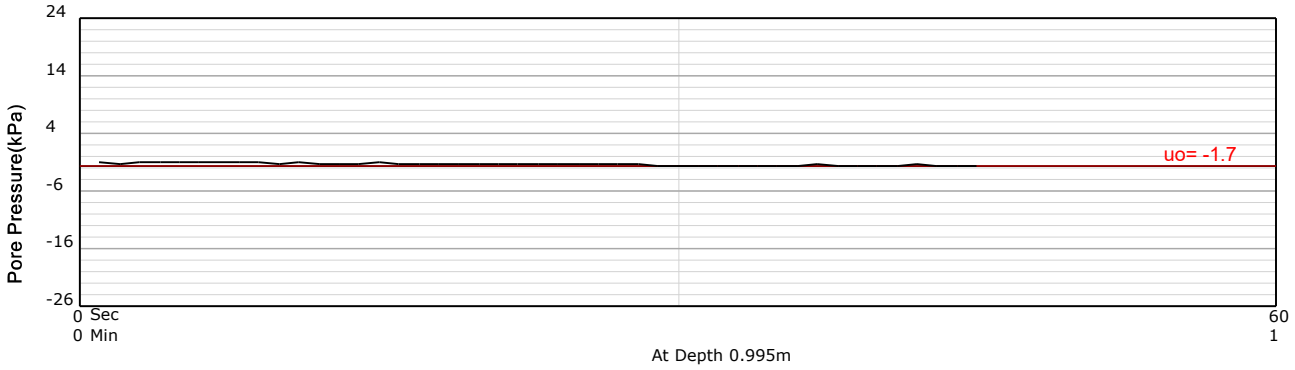

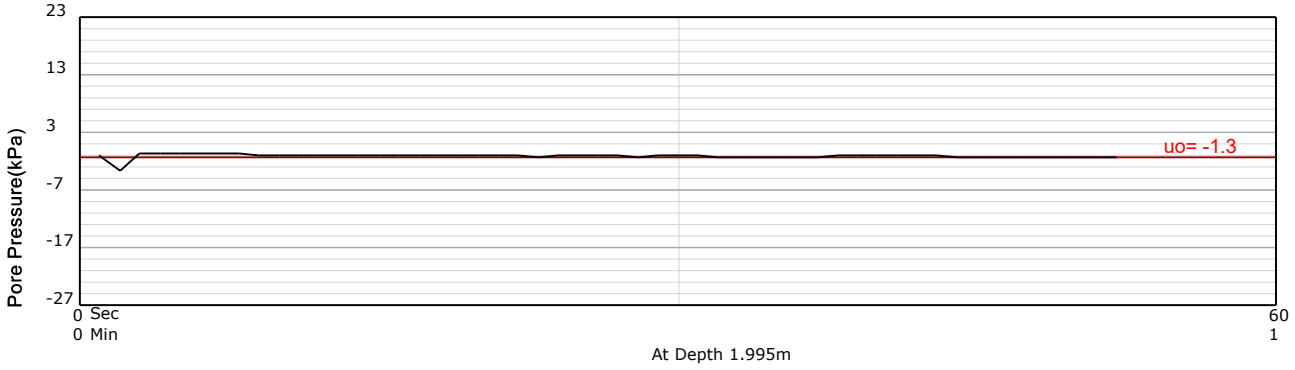

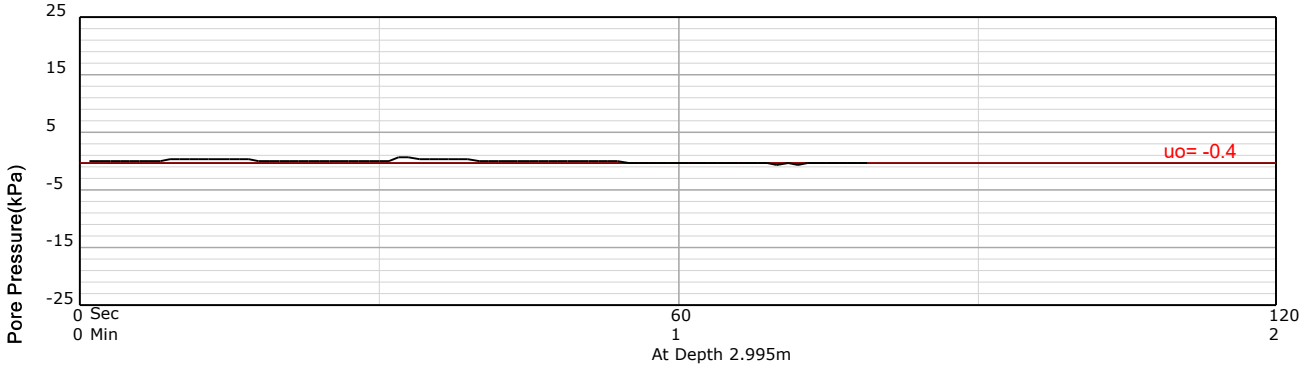

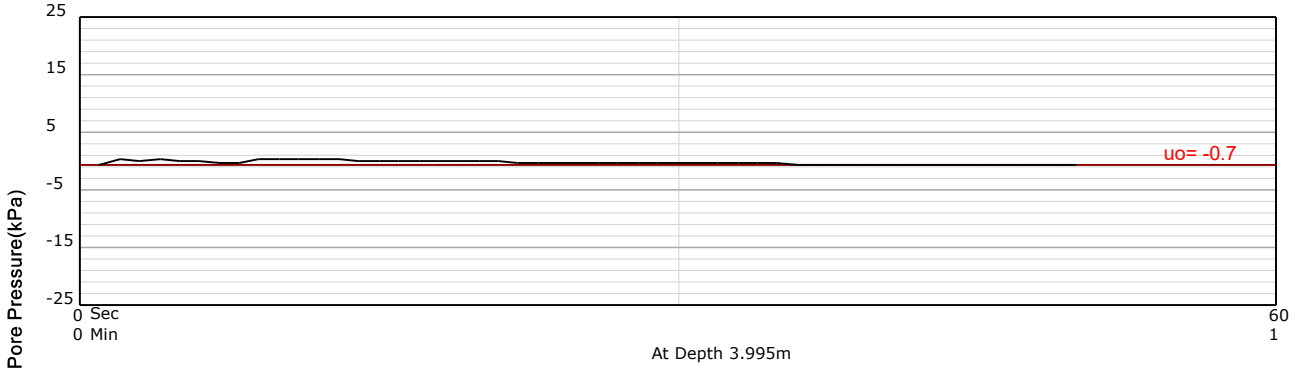

PIEZOCONE PENETRATION TEST

Dissipation Tests

HOLE: C2

PROJECT: 2024 Jagersfontein

SITE: TSF

DATE: 24/01/30 At: 15:20:50 A

DEPTH: 11.602

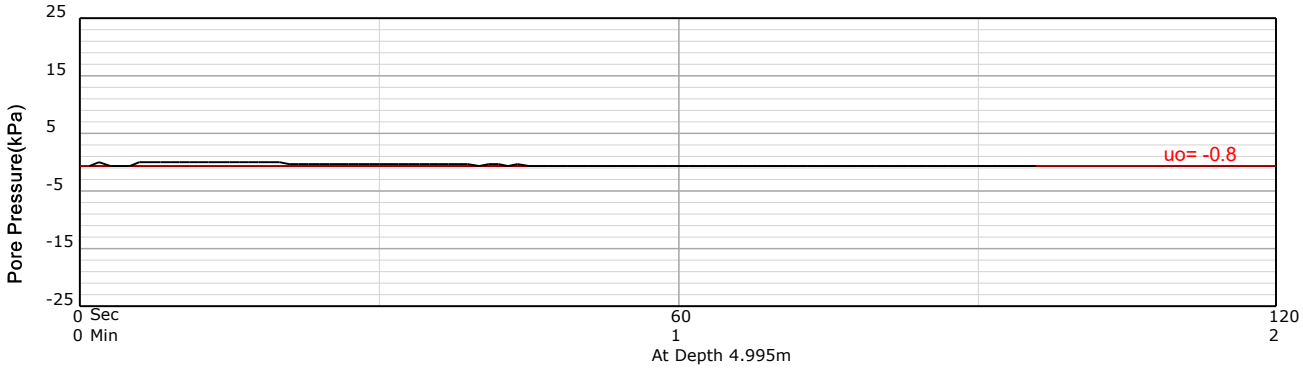

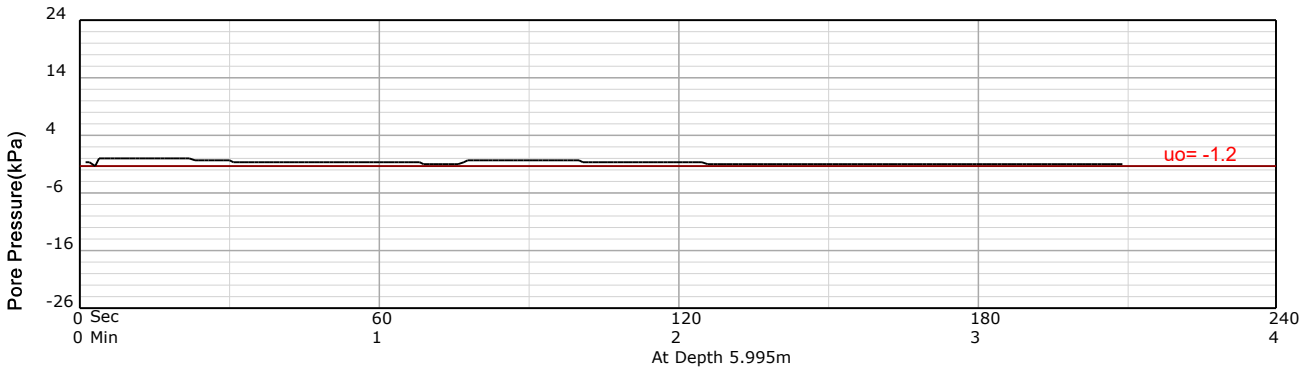

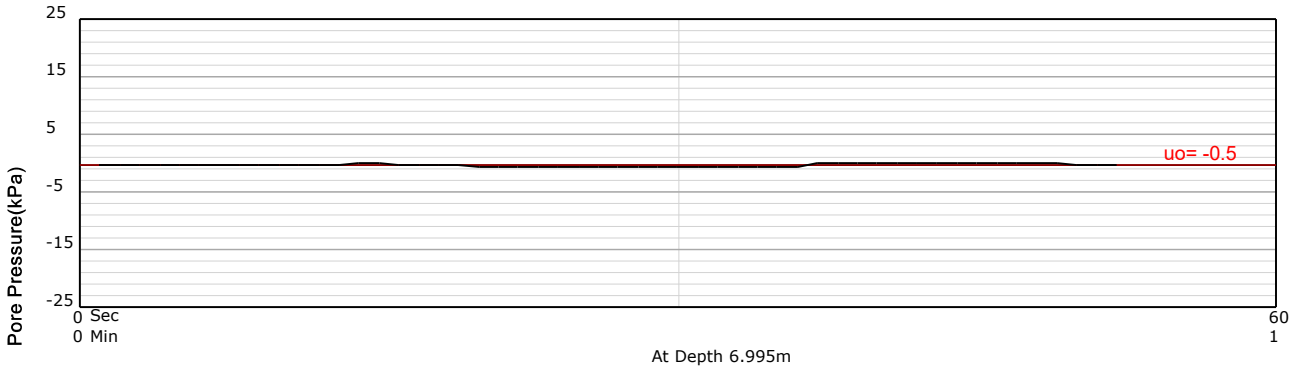

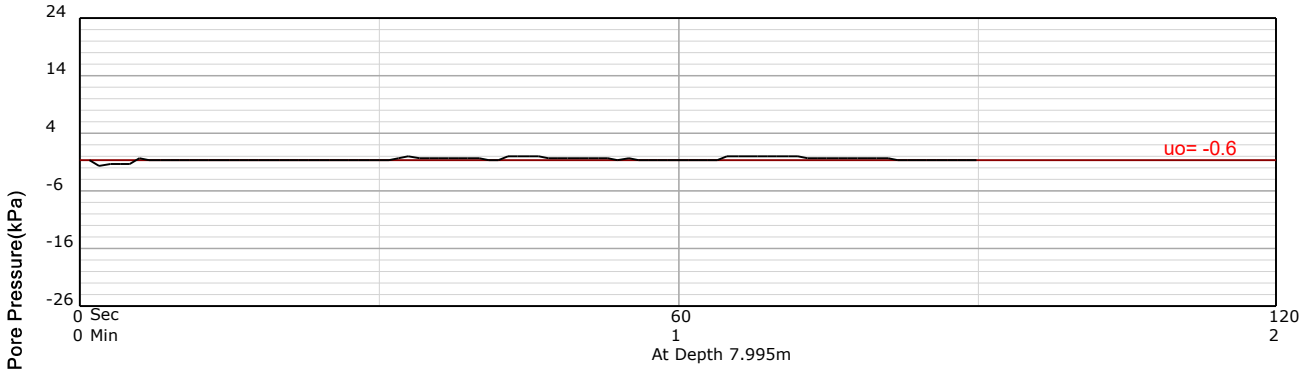

PIEZOCONE PENETRATION TEST

Dissipation Tests

HOLE: C2

PROJECT: 2024 Jagersfontein

SITE: TSF

DATE: 24/01/30 At: 15:20:50 A

DEPTH: 11.602

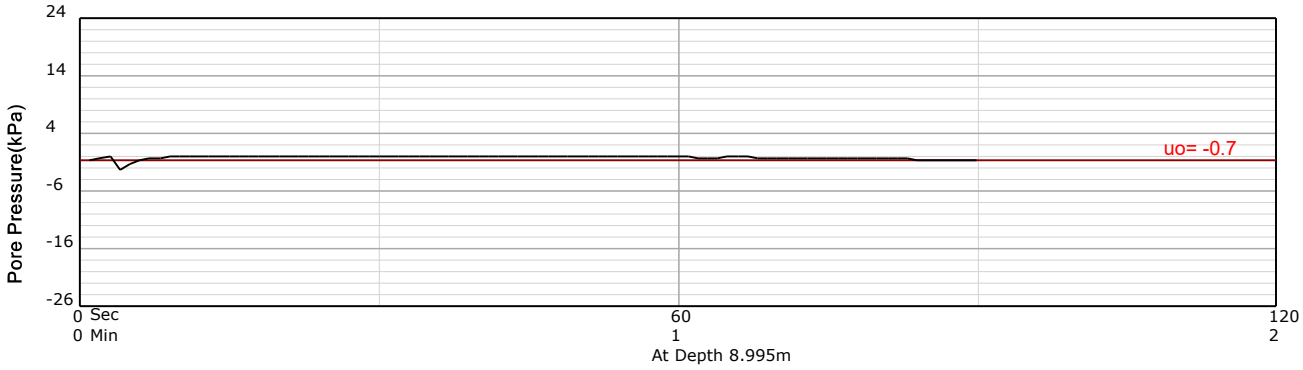

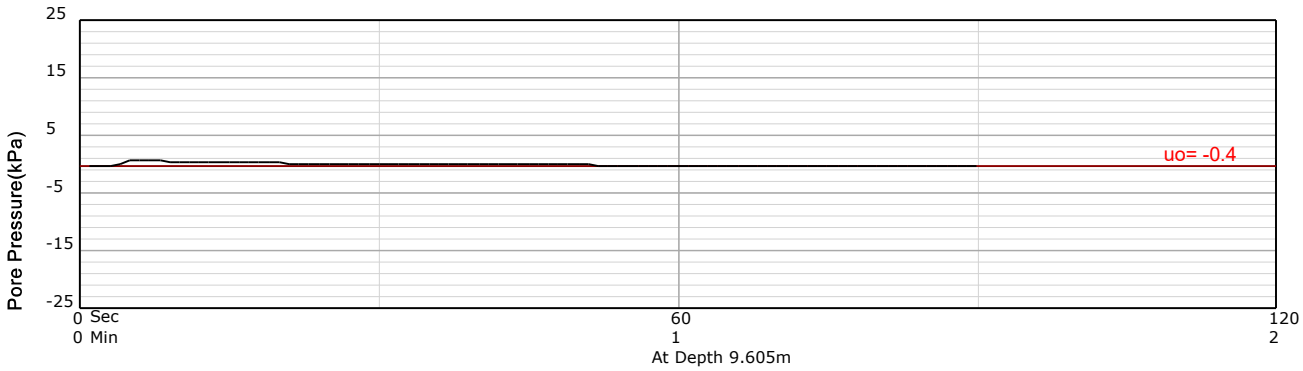

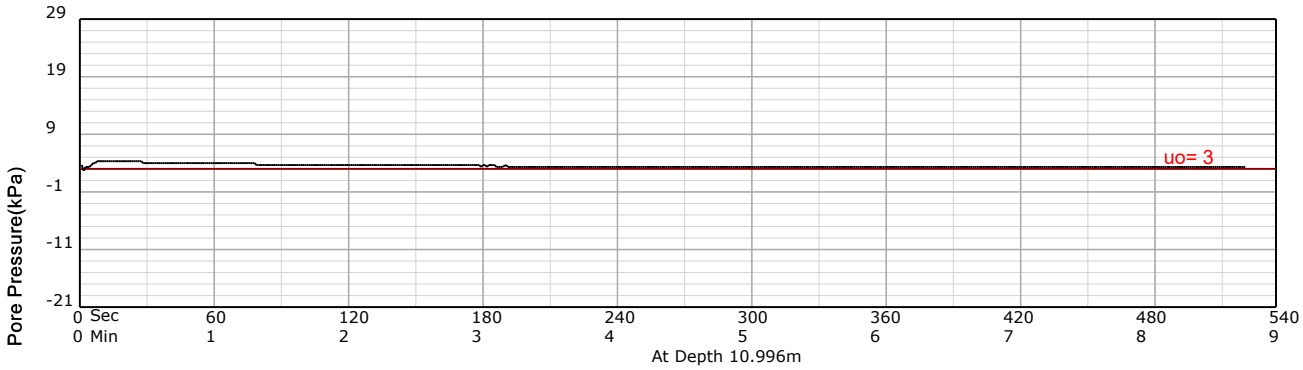

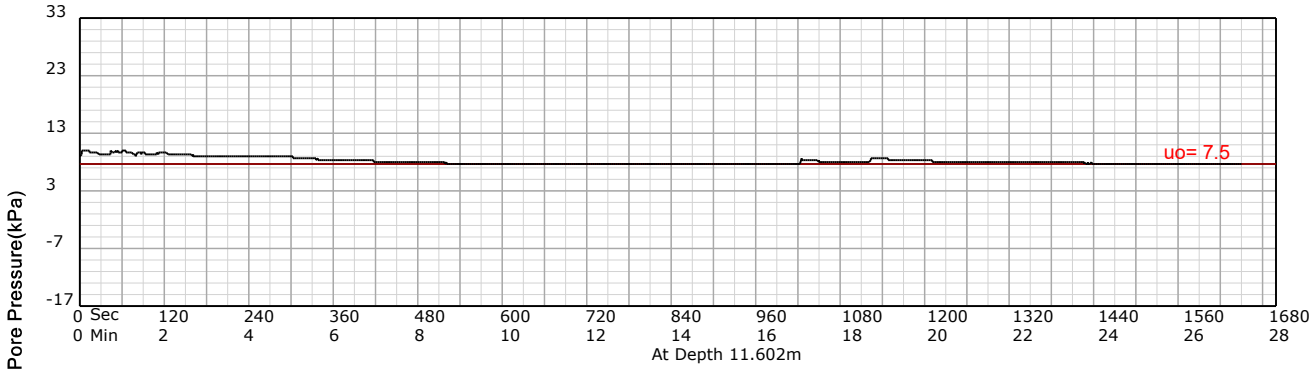

PIEZOCONE PENETRATION TEST

Equivalent Soil Behaviour Type Profile

HOLE: C2

PROJECT: 2024 Jagersfontein

SITE: TSF

DATE: 24/01/30 At: 15:20:50 A

DEPTH: 11.602

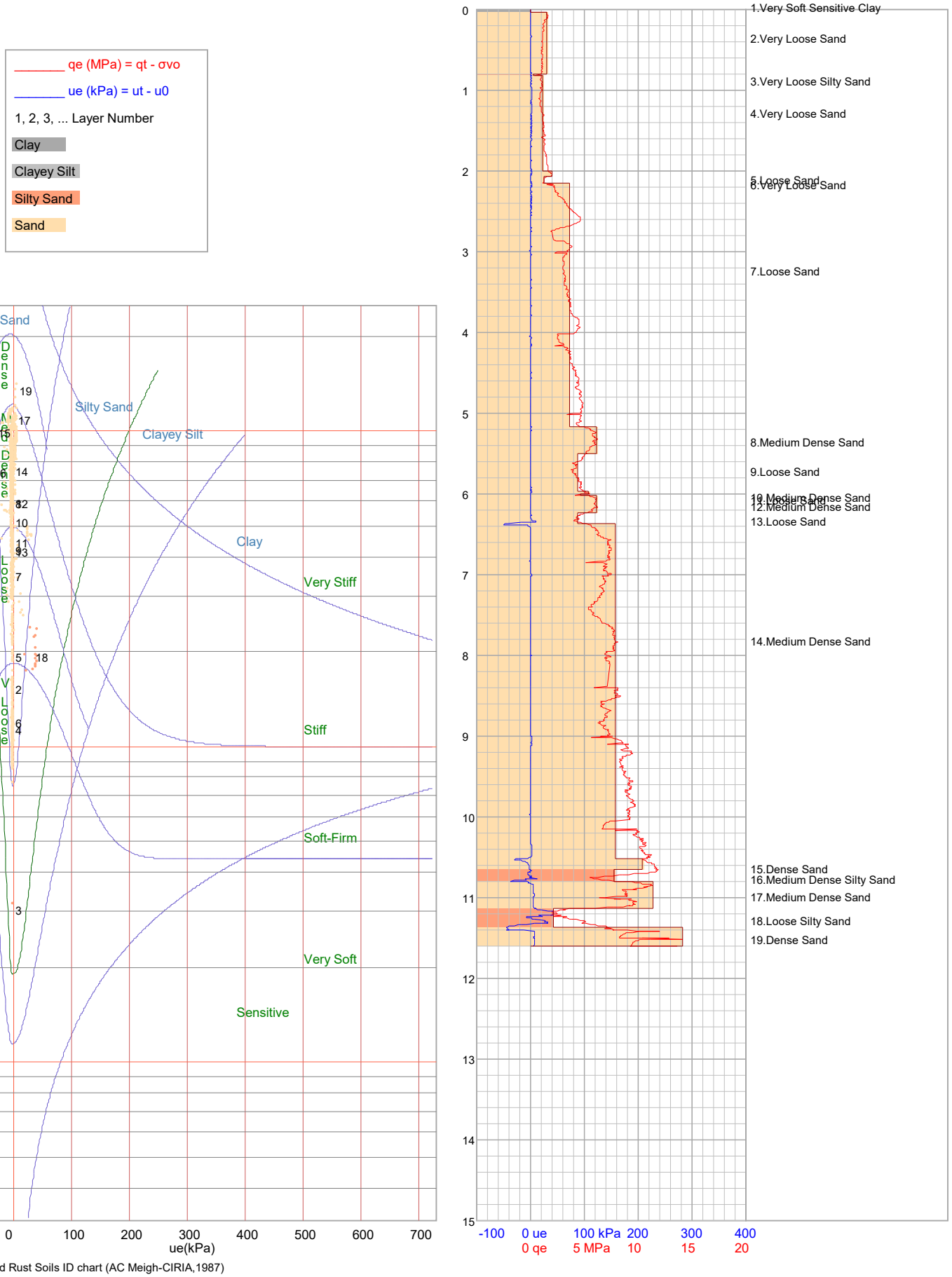

Jones and Rust Soils ID chart (AC Meigh-CIRIA,1987)

PIEZOCONE PENETRATION TEST

Recorded Field Results (Cone, Pore Pressure and Static Pore Pressure from Dissipations)

HOLE: C3

PROJECT: 2024 Jagersfontein

SITE: TSF

DATE: 24/01/31 At: 08:34:59 **DEPTH:** 17.298

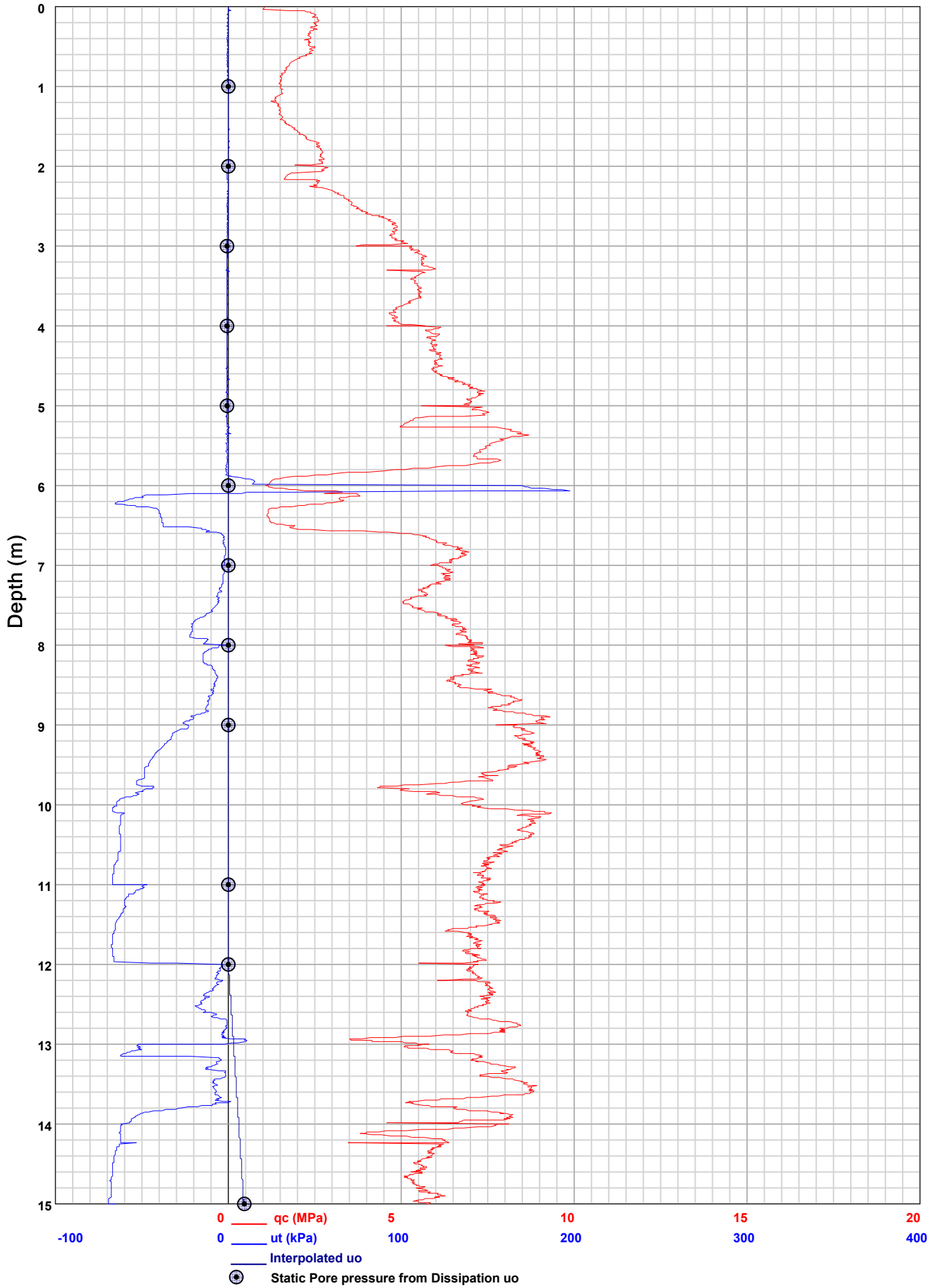

PIEZOCONE PENETRATION TEST

Recorded Field Results (Cone, Pore Pressure and Static Pore Pressure from Dissipations)

HOLE: C3

PROJECT: 2024 Jagersfontein

SITE: TSF

DATE: 24/01/31 At: 08:34:59 **DEPTH:** 17.298

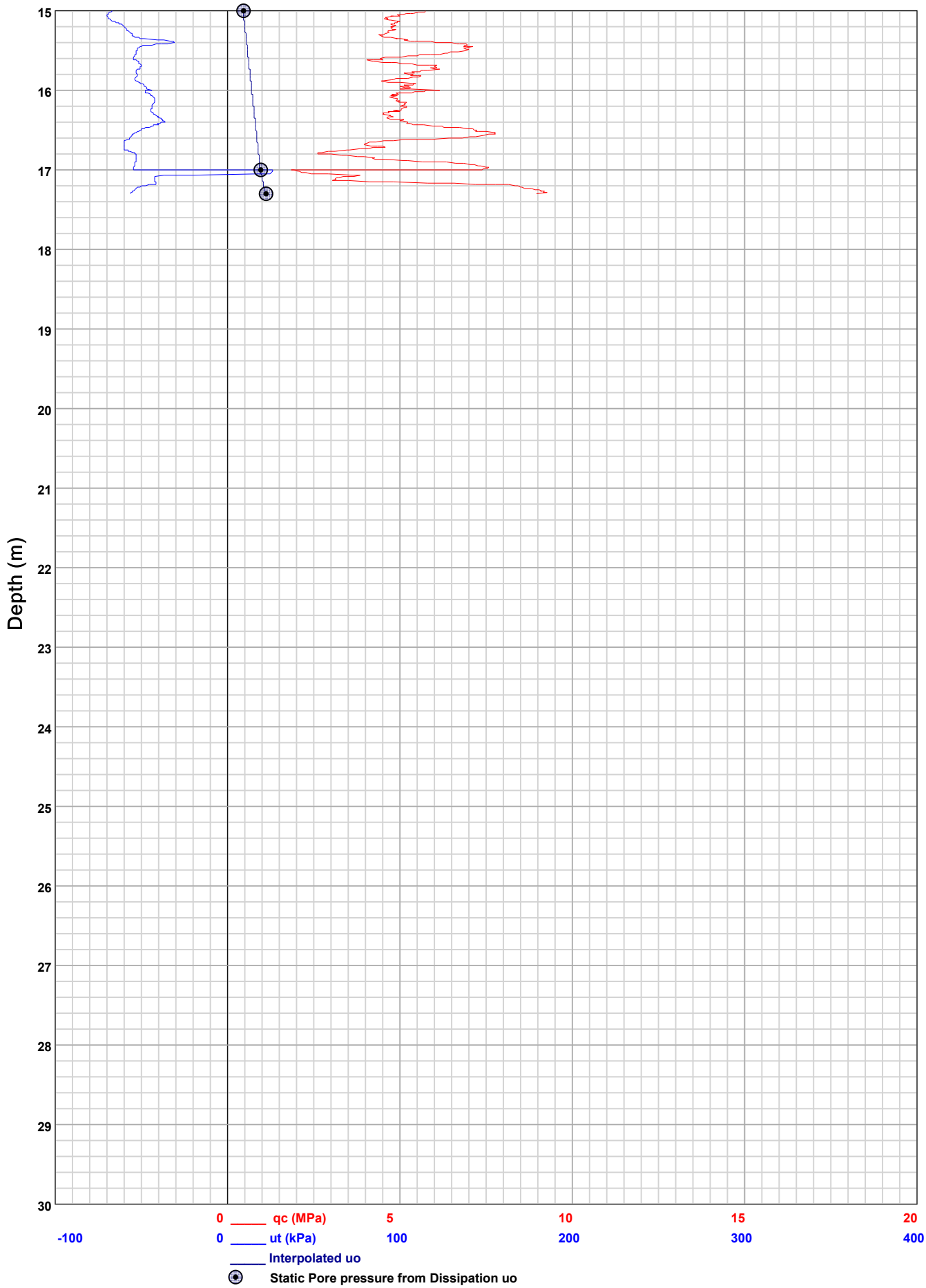

PIEZOCONE PENETRATION TEST

HOLE: C3

PROJECT: 2024 Jagersfontein

SITE: TSF

DATE: 24/01/31 At: 08:34:59

DEPTH: 17.298

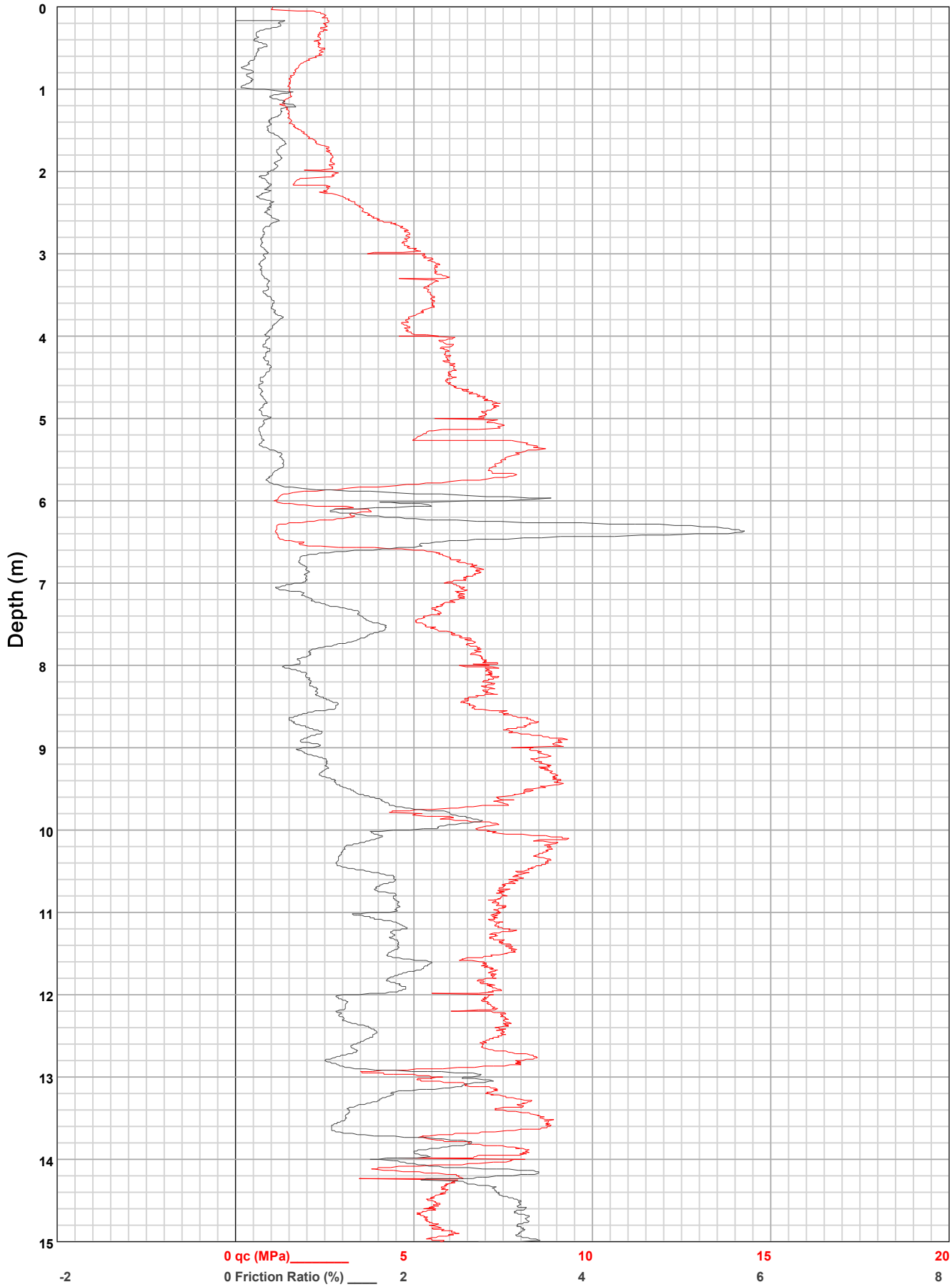

PIEZOCONE PENETRATION TEST

HOLE: C3

PROJECT: 2024 Jagersfontein

SITE: TSF

DATE: 24/01/31 At: 08:34:59 **DEPTH:** 17.298

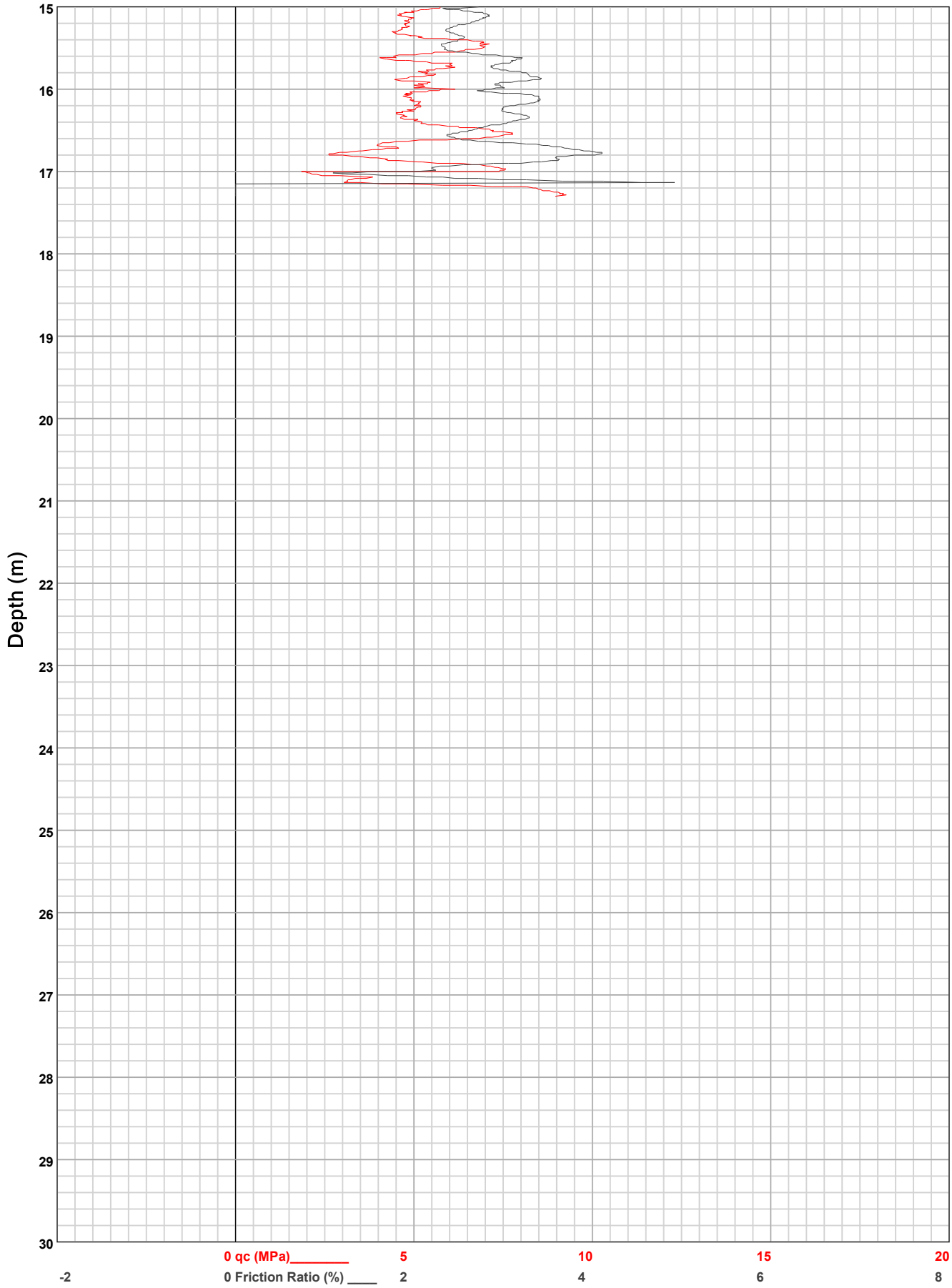

PIEZOCONE PENETRATION TEST

Dissipation Tests

HOLE: C3

PROJECT: 2024 Jagersfontein

SITE: TSF

DATE: 24/01/31 At: 08:34:59 **DEPTH:** 17.298

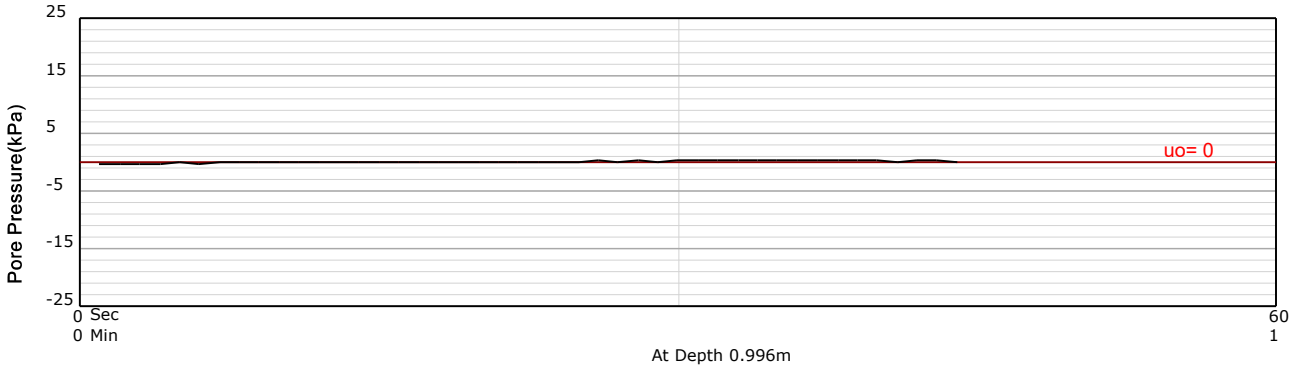

At Depth 0.996m

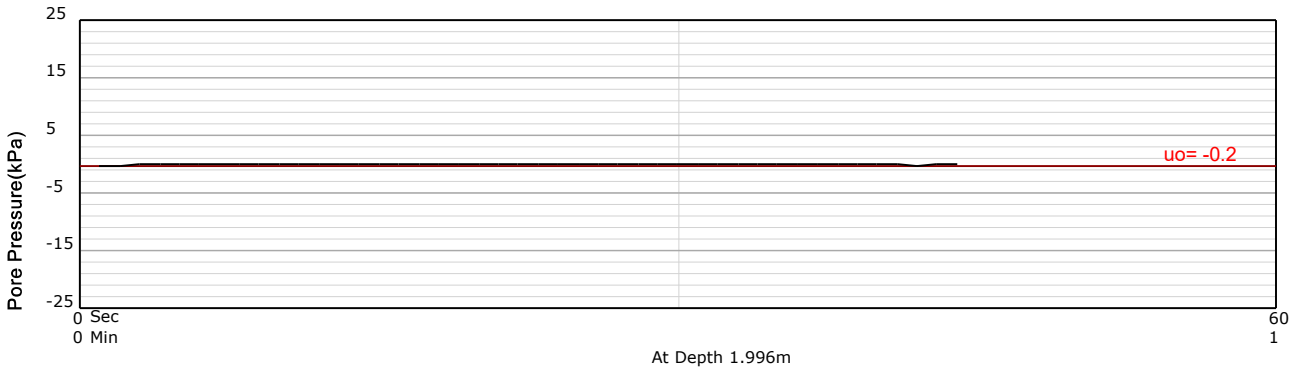

At Depth 1.996m

At Depth 2.996m

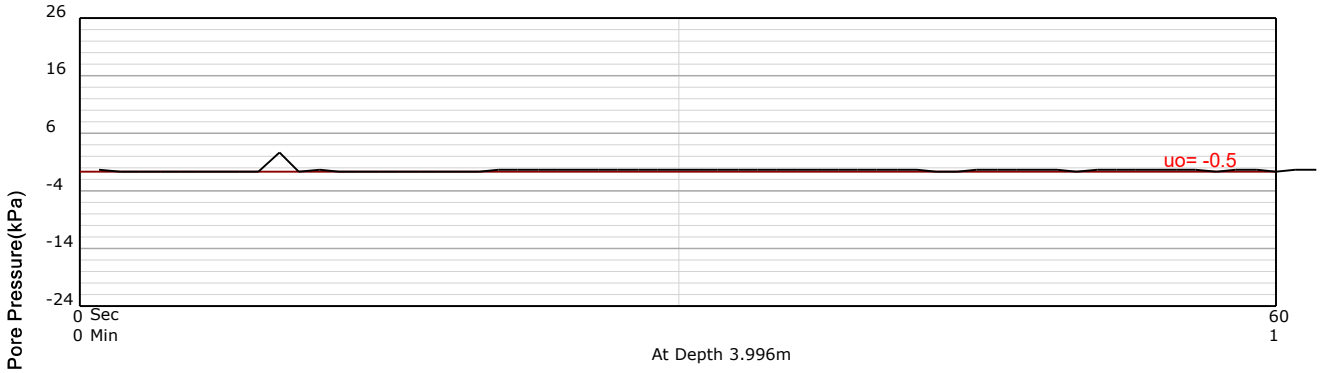

At Depth 3.996m

PIEZOCONE PENETRATION TEST

Dissipation Tests

HOLE: C3

PROJECT: 2024 Jagersfontein

SITE: TSF

DATE: 24/01/31 At: 08:34:59 **DEPTH:** 17.298

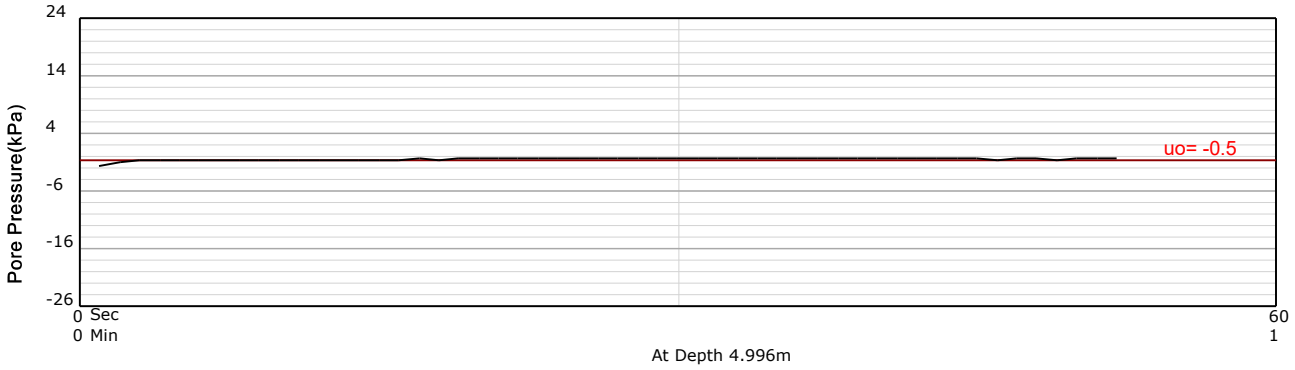

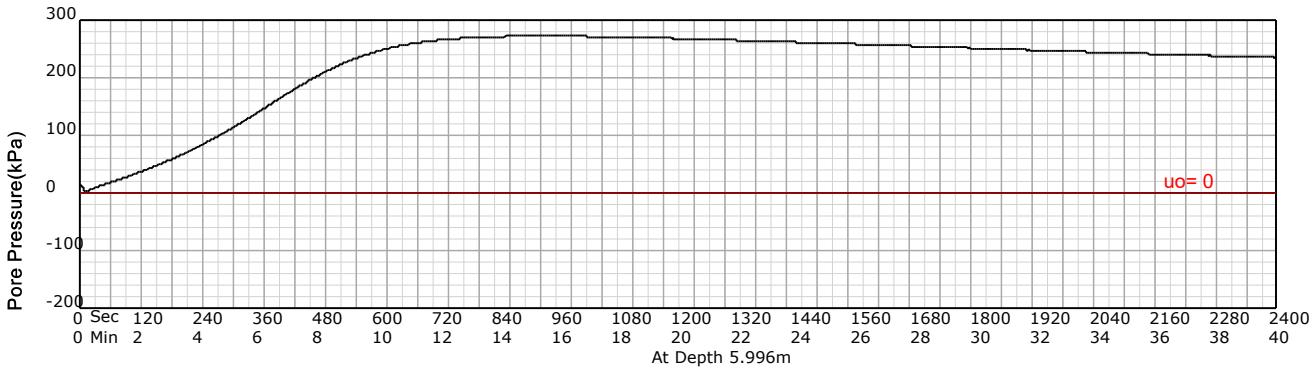

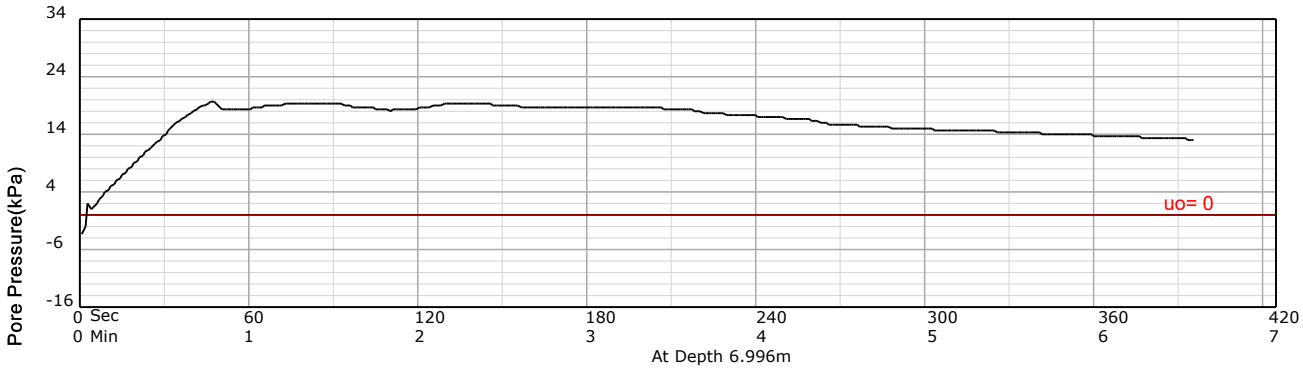

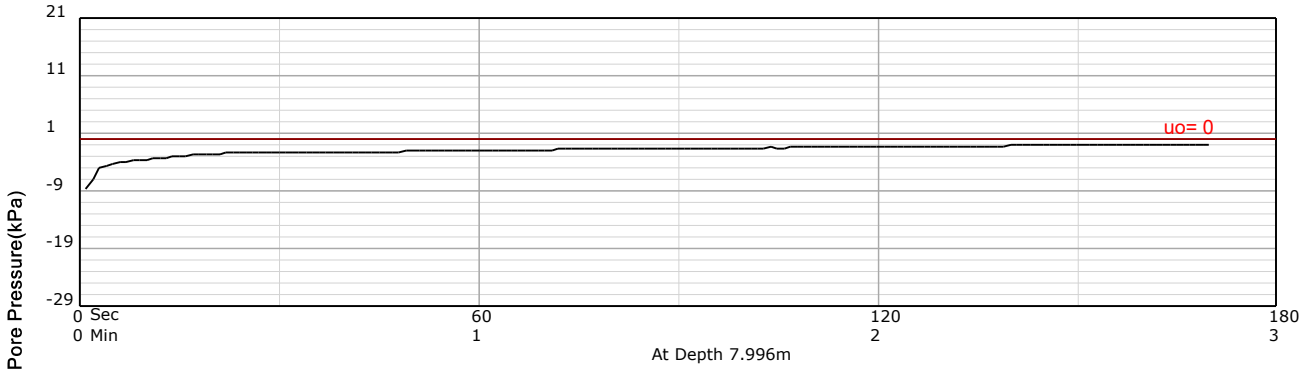

PIEZOCONE PENETRATION TEST

Dissipation Tests

HOLE: C3

PROJECT: 2024 Jagersfontein

SITE: TSF

DATE: 24/01/31 At: 08:34:59 **DEPTH:** 17.298

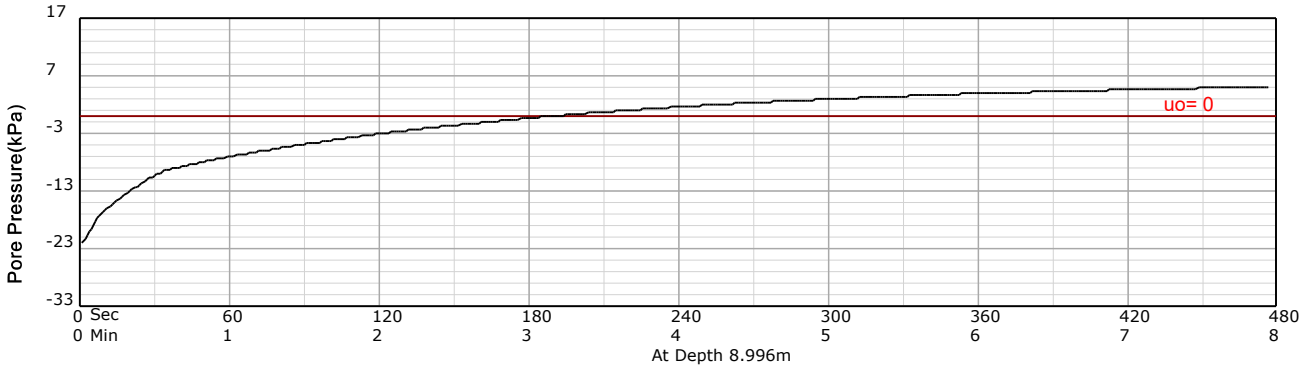

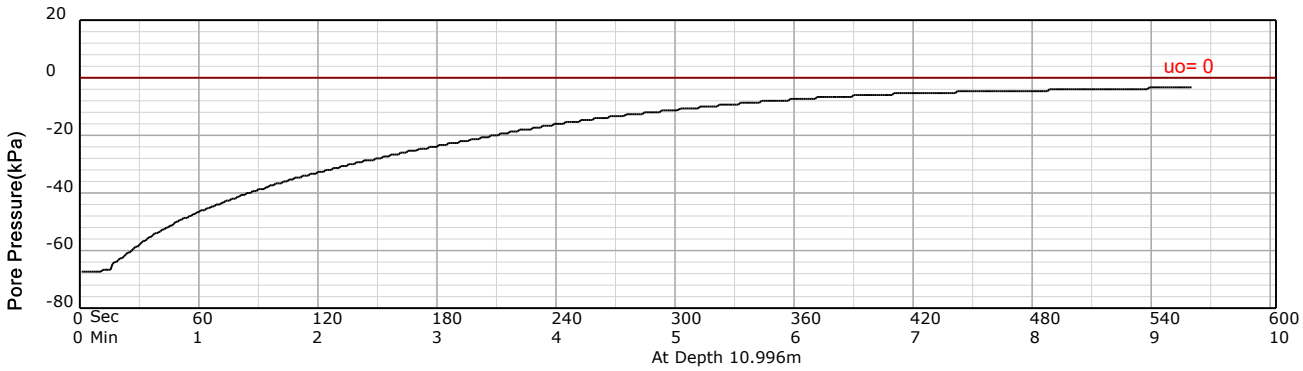

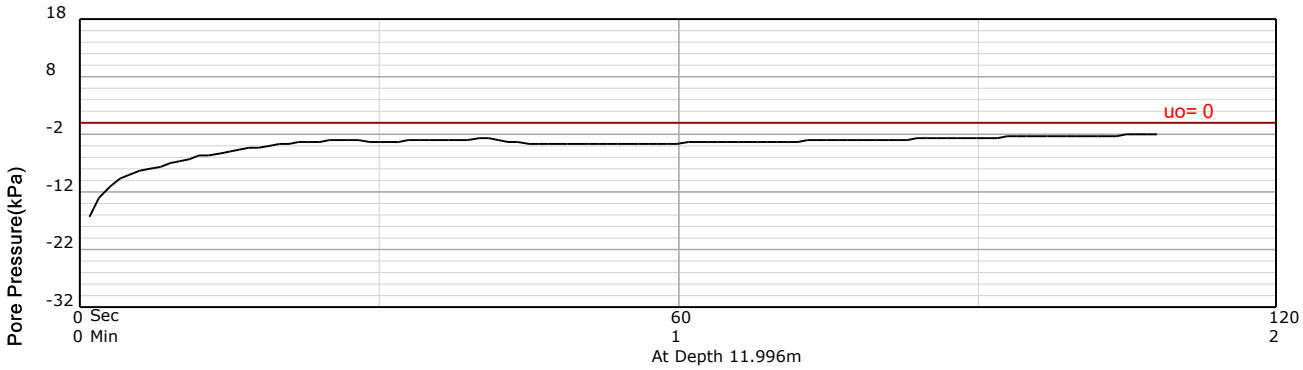

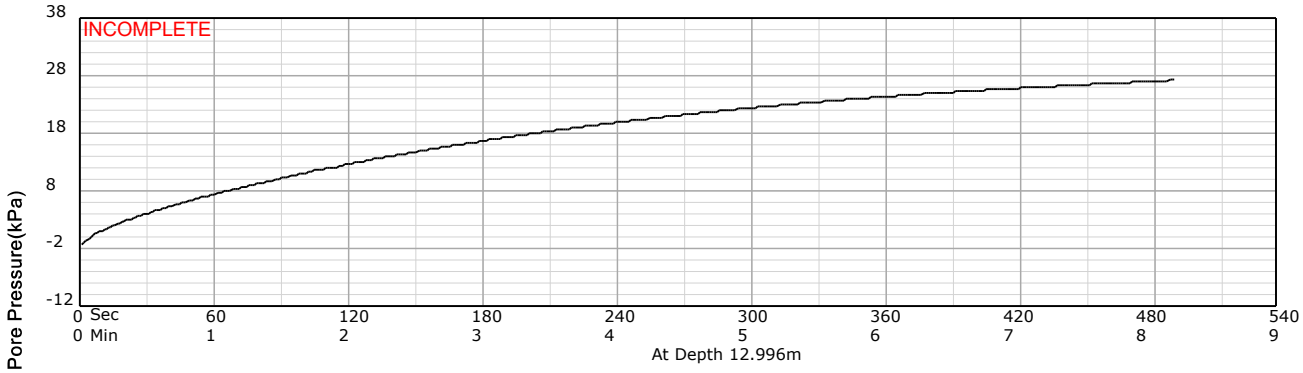

PIEZOCONE PENETRATION TEST

Dissipation Tests

HOLE: C3

PROJECT: 2024 Jagersfontein

SITE: TSF

DATE: 24/01/31 At: 08:34:59 **DEPTH:** 17.298

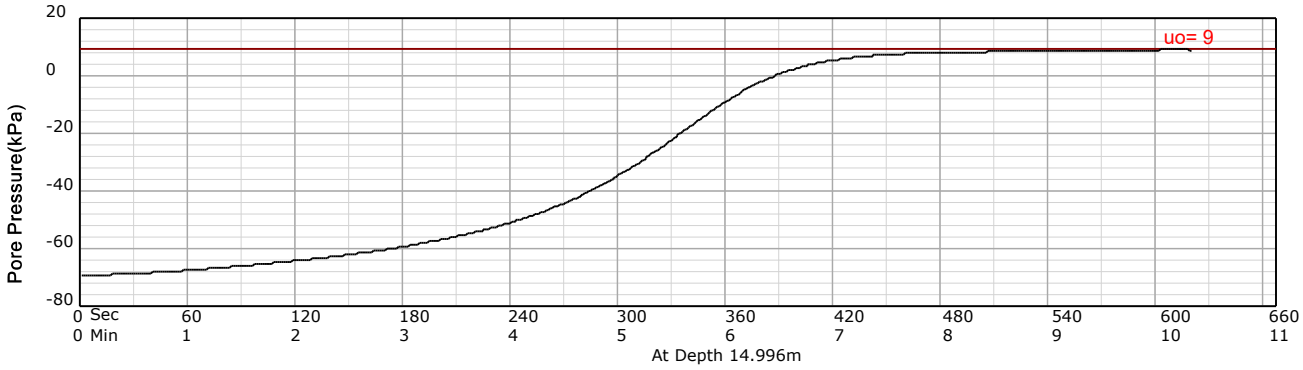

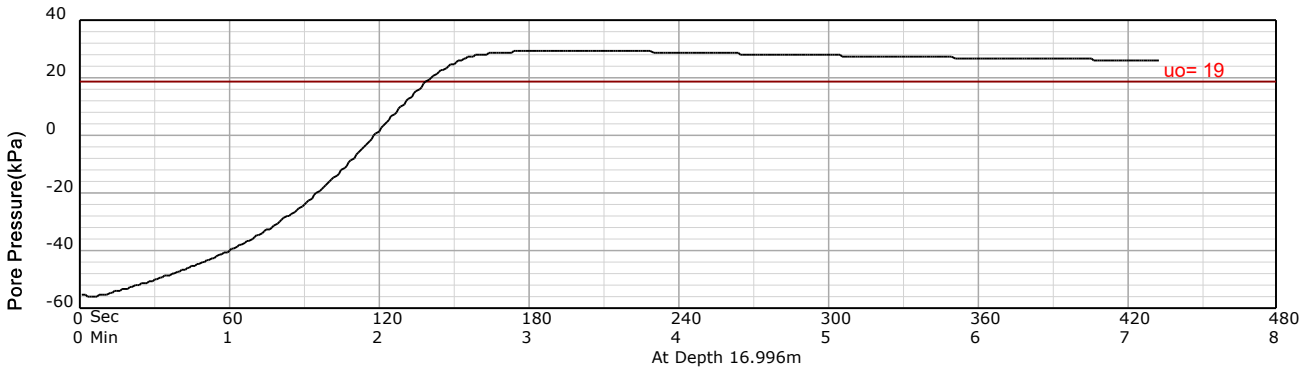

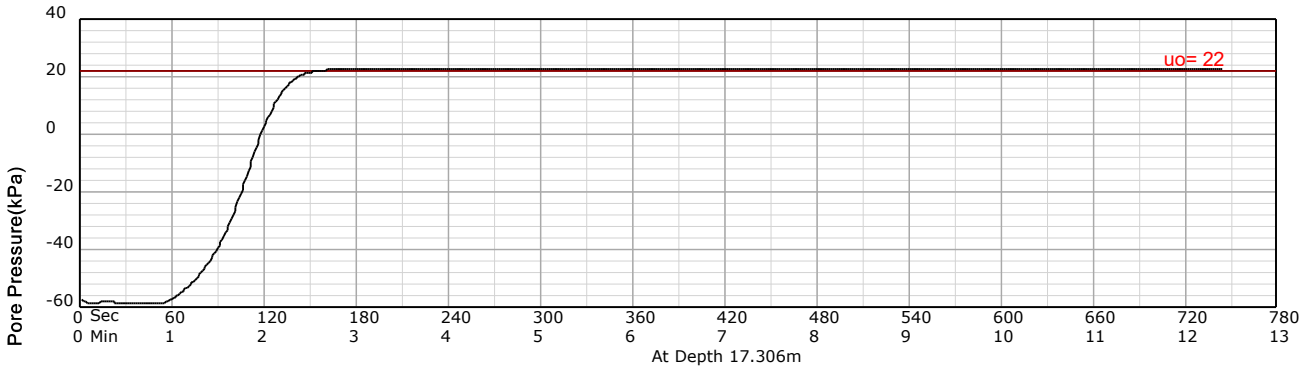

PIEZOCONE PENETRATION TEST

Equivalent Soil Behaviour Type Profile

HOLE: C3

PROJECT: 2024 Jagersfontein

SITE: TSF

DATE: 24/01/31 At: 08:34:59

DEPTH: 17.298

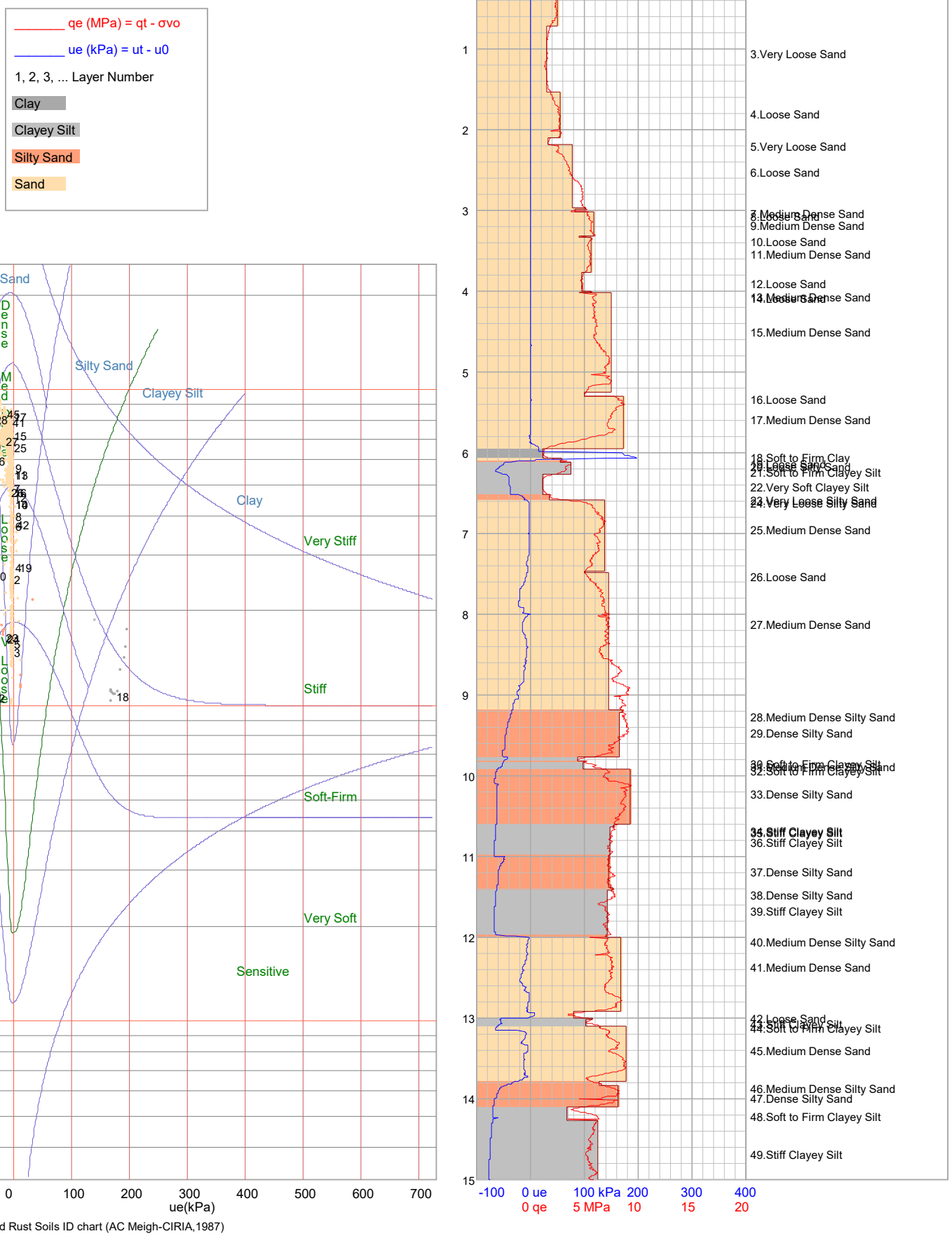

PIEZOCONE PENETRATION TEST

Equivalent Soil Behaviour Type Profile

HOLE: C3

PROJECT: 2024 Jagersfontein

SITE: TSF

DATE: 24/01/31 At: 08:34:59

DEPTH: 17.298

qe (MPa) = qt - σvo

ue (kPa) = ut - u0

1, 2, 3, ... Layer Number

Clay

Clayey Silt

Silty Sand

Sand

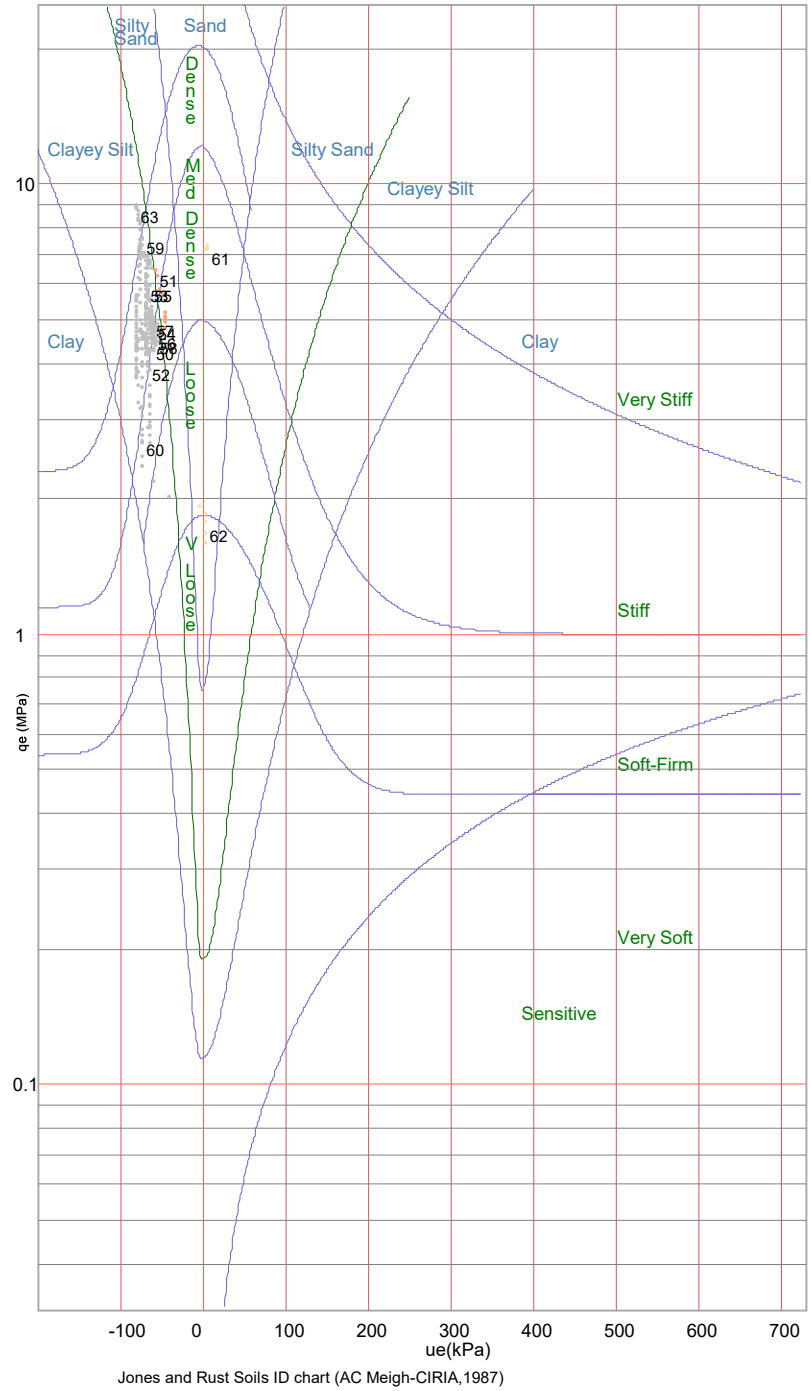

Jones and Rust Soils ID chart (AC Meigh-CIRIA,1987)

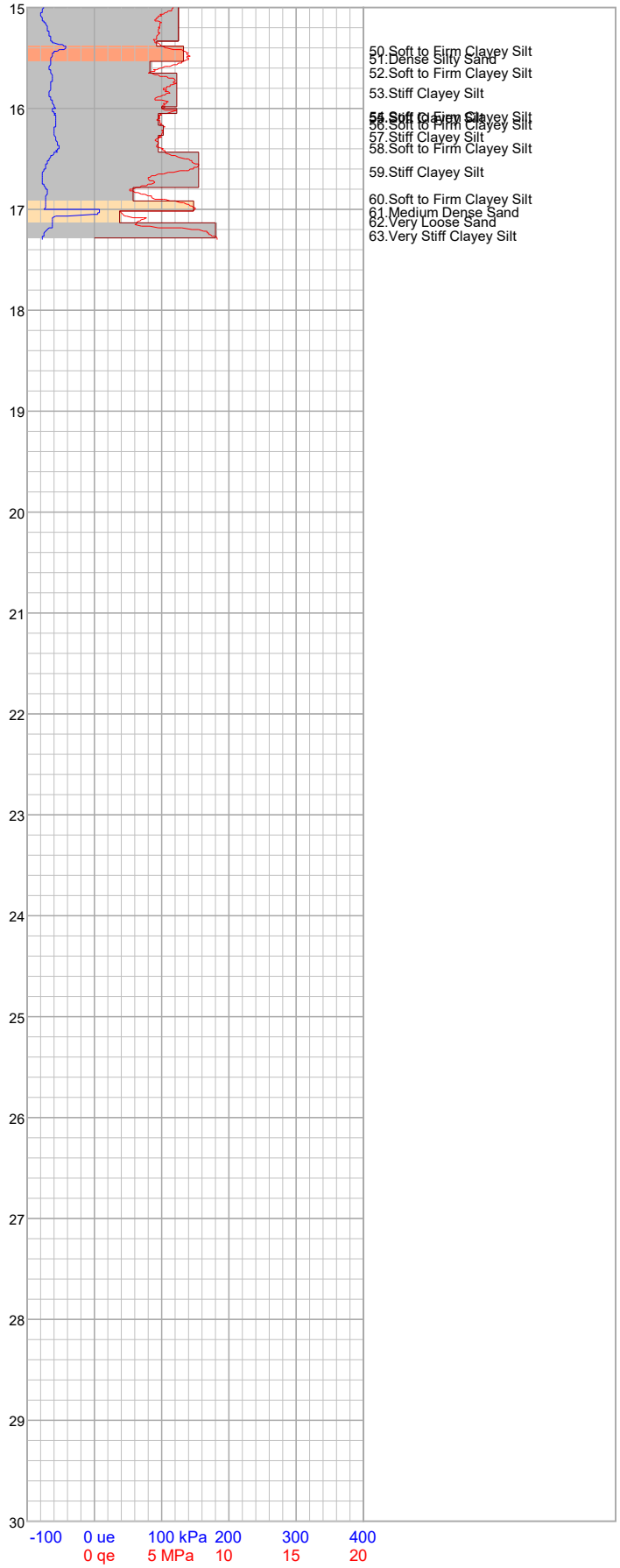

PIEZOCONE PENETRATION TEST

Recorded Field Results (Cone, Pore Pressure and Static Pore Pressure from Dissipations)

HOLE: C4

PROJECT: 2024 Jagersfontein

SITE: TSF

DATE: 24/01/31 At: 14:07:34 A **DEPTH:** 25.101

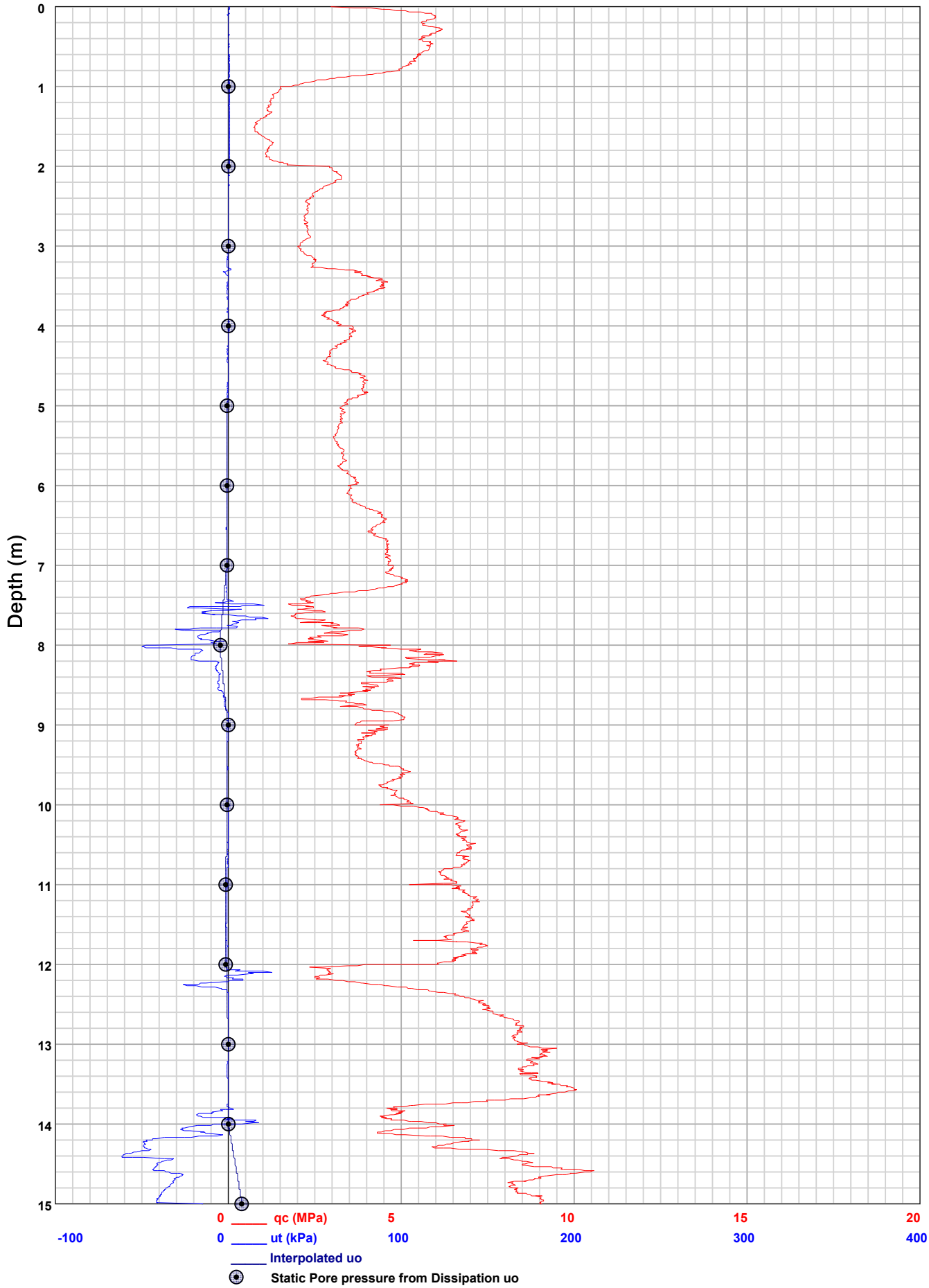

PIEZOCONE PENETRATION TEST

Recorded Field Results (Cone, Pore Pressure and Static Pore Pressure from Dissipations)

HOLE: C4

PROJECT: 2024 Jagersfontein

SITE: TSF

DATE: 24/01/31 At: 14:07:34 A **DEPTH:** 25.101

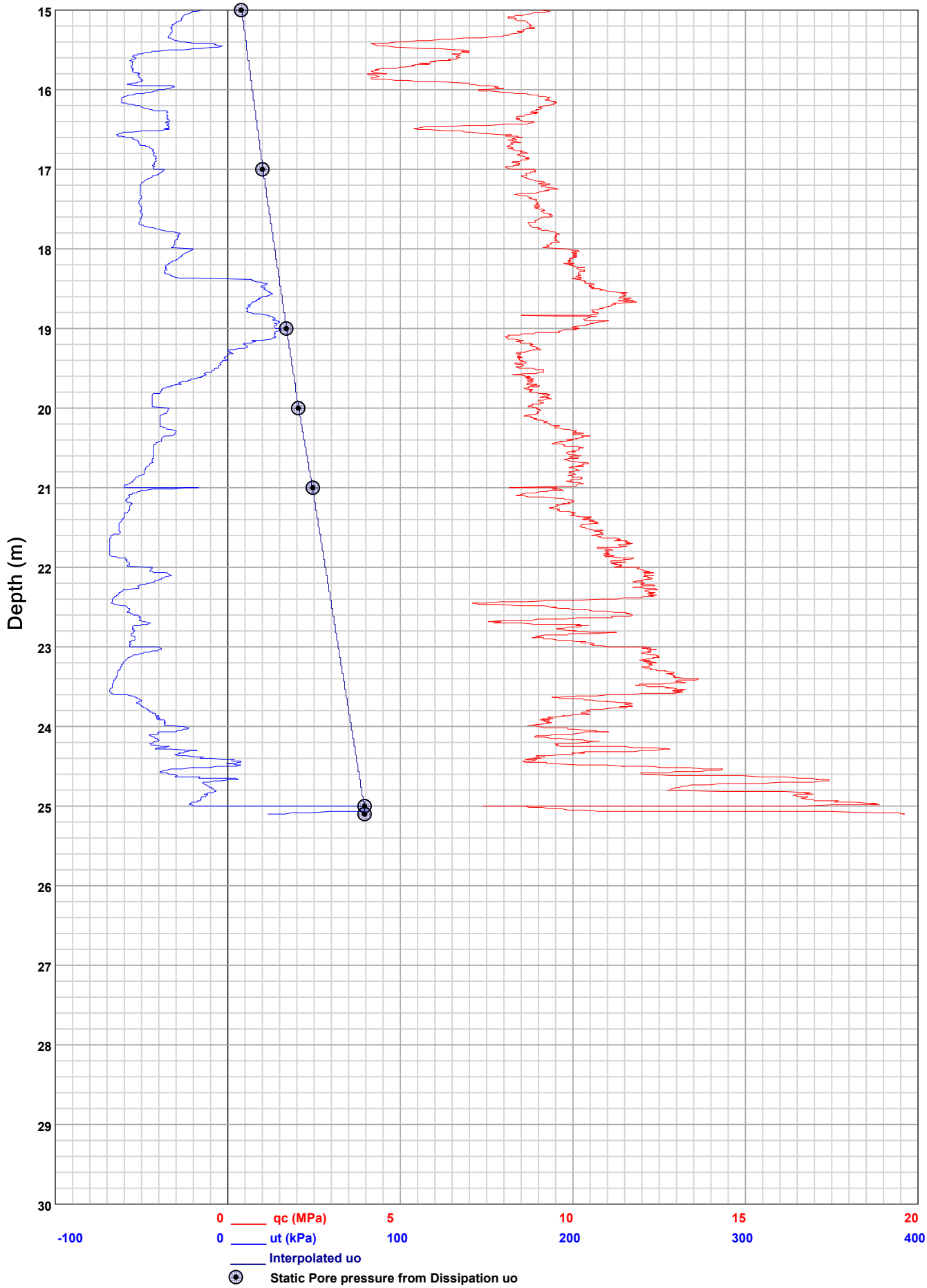

PIEZOCONE PENETRATION TEST

HOLE: C4

PROJECT: 2024 Jagersfontein

SITE: TSF

DATE: 24/01/31 At: 14:07:34 A

DEPTH: 25.101

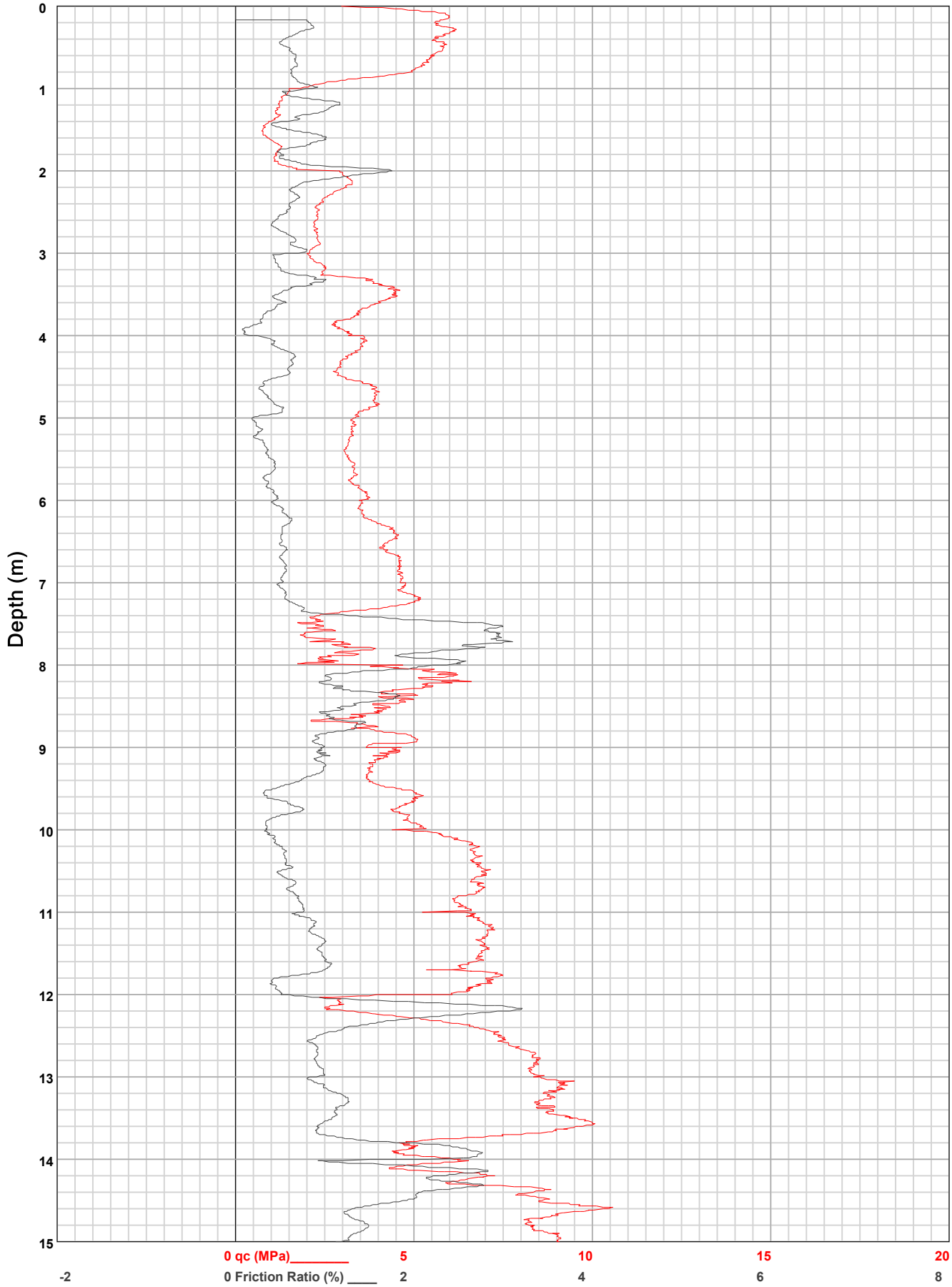

PIEZOCONE PENETRATION TEST

HOLE: C4

PROJECT: 2024 Jagersfontein

SITE: TSF

DATE: 24/01/31 At: 14:07:34 A

DEPTH: 25.101

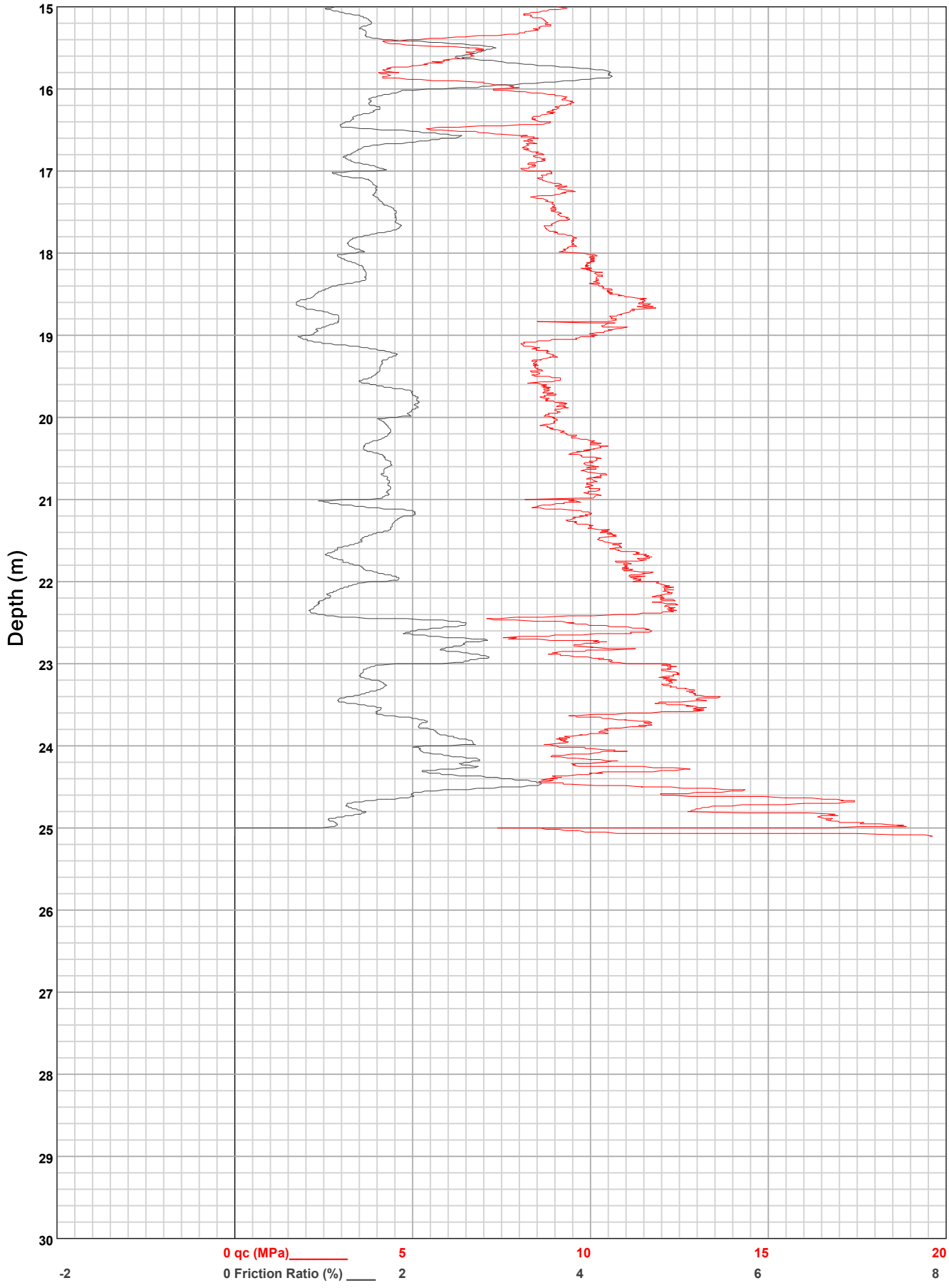

PIEZOCONE PENETRATION TEST

Dissipation Tests

HOLE: C4

PROJECT: 2024 Jagersfontein

SITE: TSF

DATE: 24/01/31 At: 14:07:34 A

DEPTH: 25.101

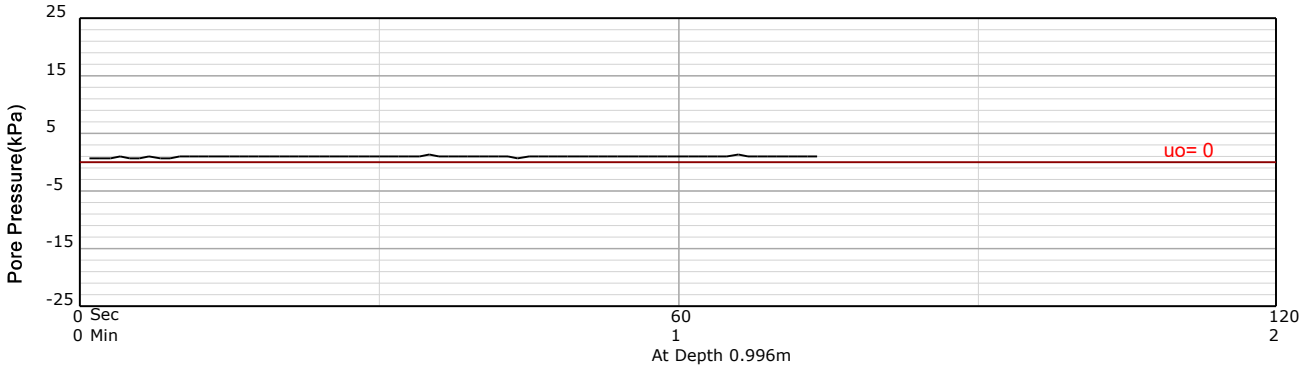

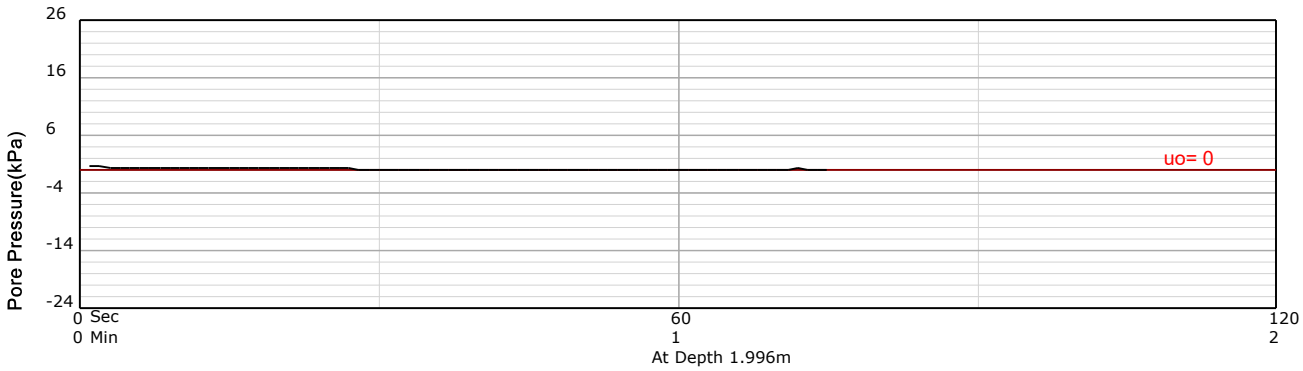

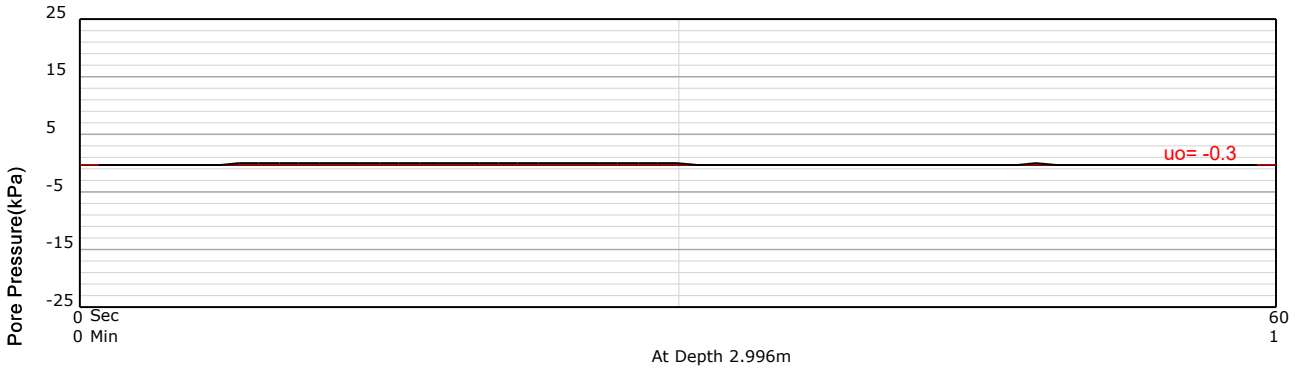

PIEZOCONE PENETRATION TEST

Dissipation Tests

HOLE: C4

PROJECT: 2024 Jagersfontein

SITE: TSF

DATE: 24/01/31 At: 14:07:34 A

DEPTH: 25.101

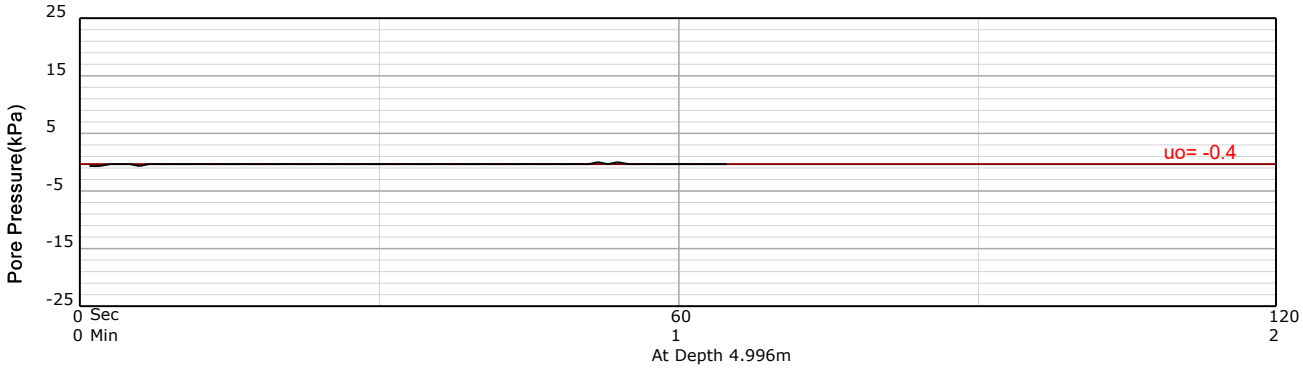

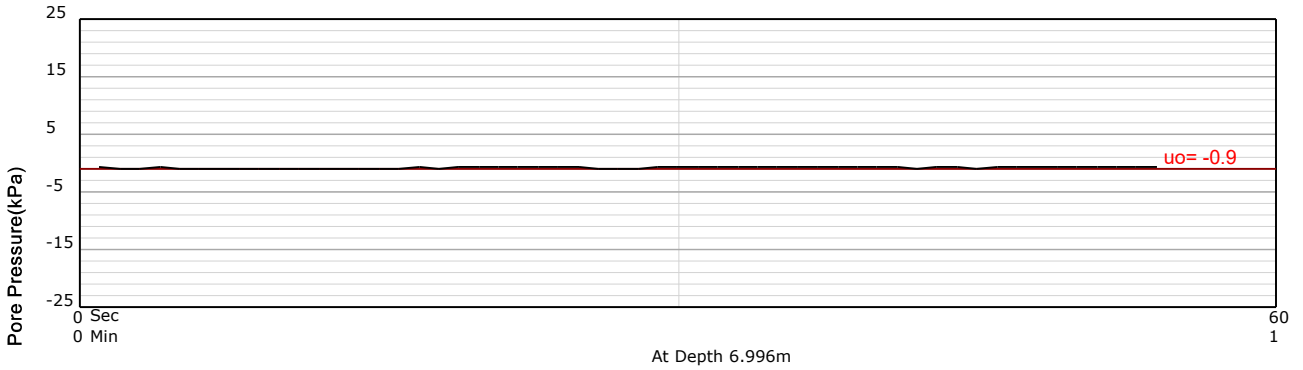

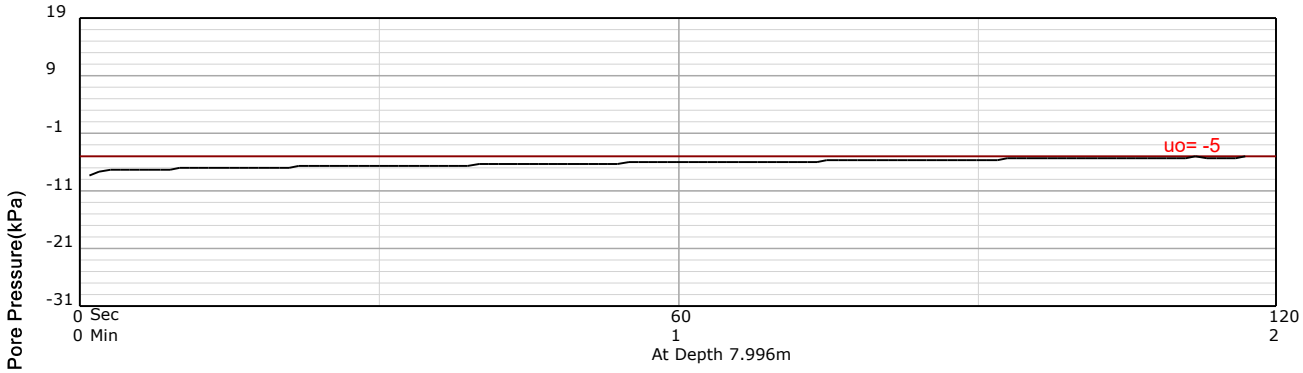

PIEZOCONE PENETRATION TEST

Dissipation Tests

HOLE: C4

PROJECT: 2024 Jagersfontein

SITE: TSF

DATE: 24/01/31 At: 14:07:34 A

DEPTH: 25.101

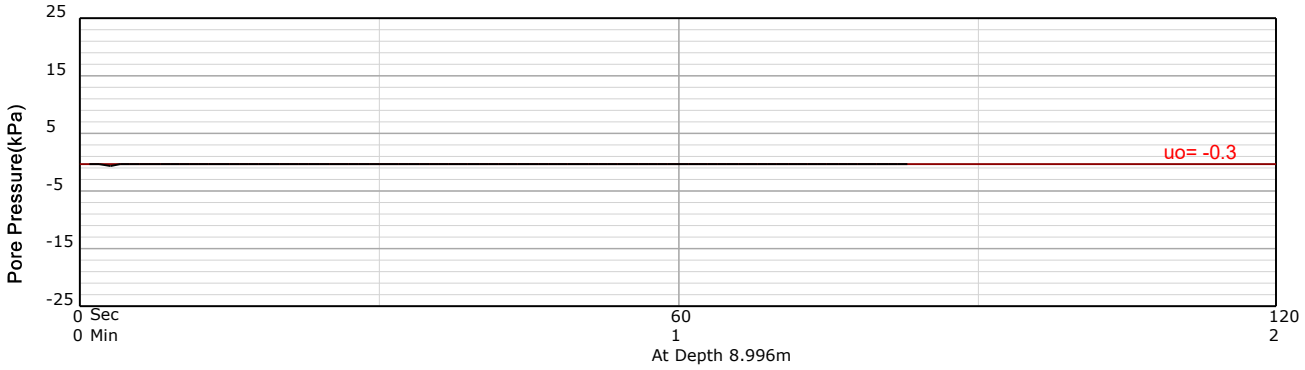

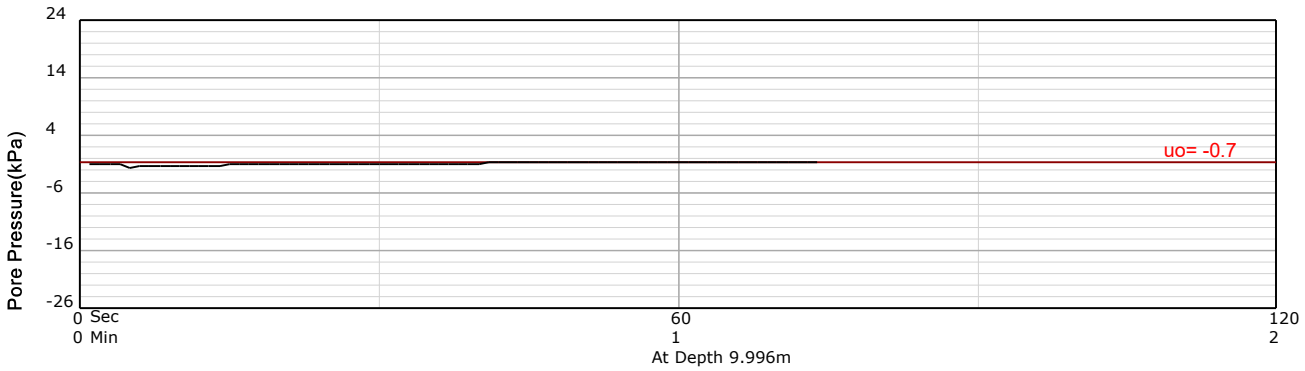

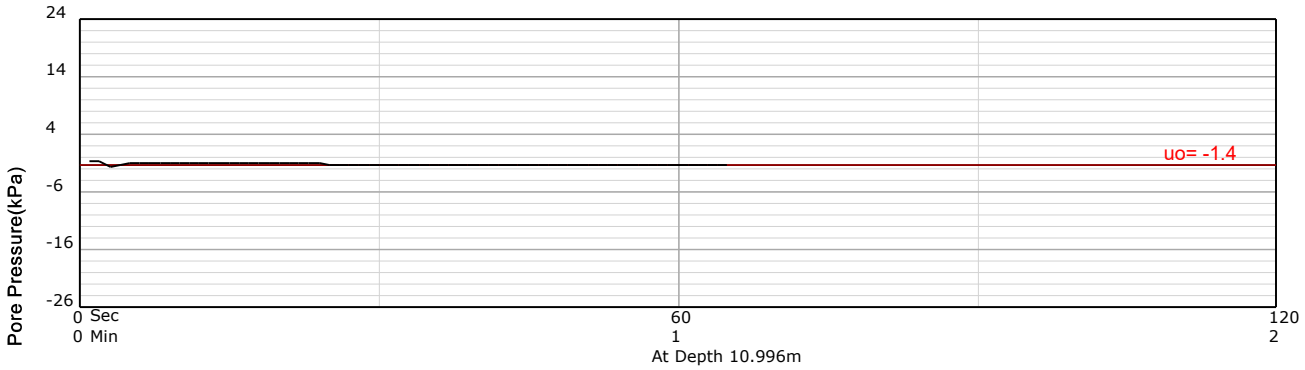

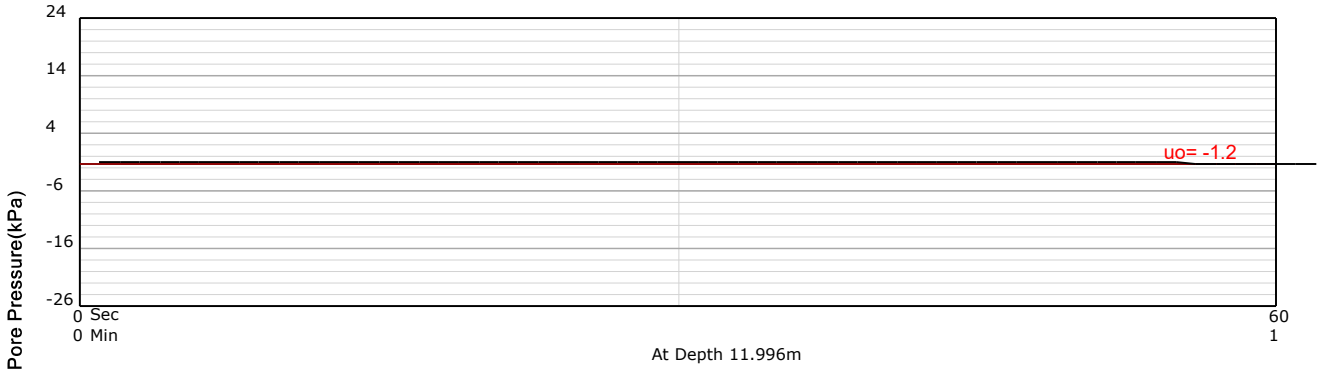

PIEZOCONE PENETRATION TEST

Dissipation Tests

HOLE: C4

PROJECT: 2024 Jagersfontein

SITE: TSF

DATE: 24/01/31 At: 14:07:34 A

DEPTH: 25.101

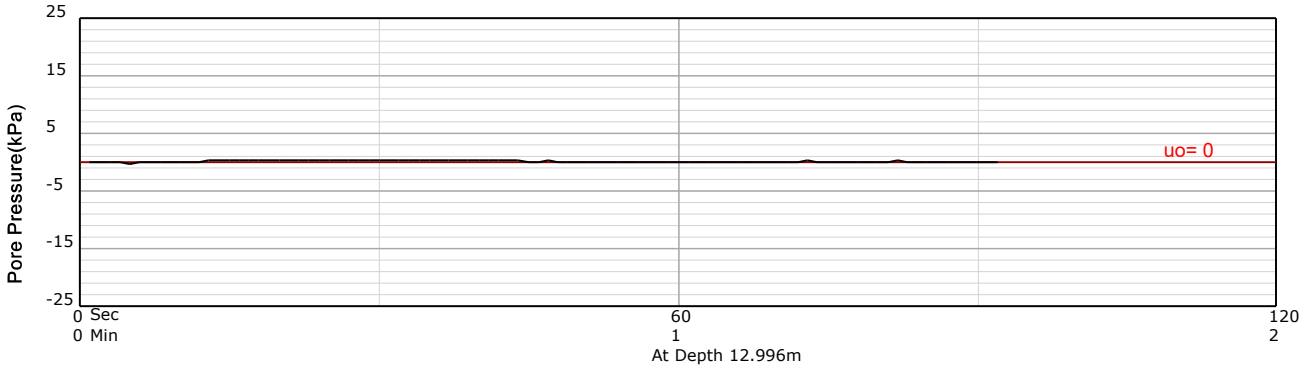

At Depth 12.996m

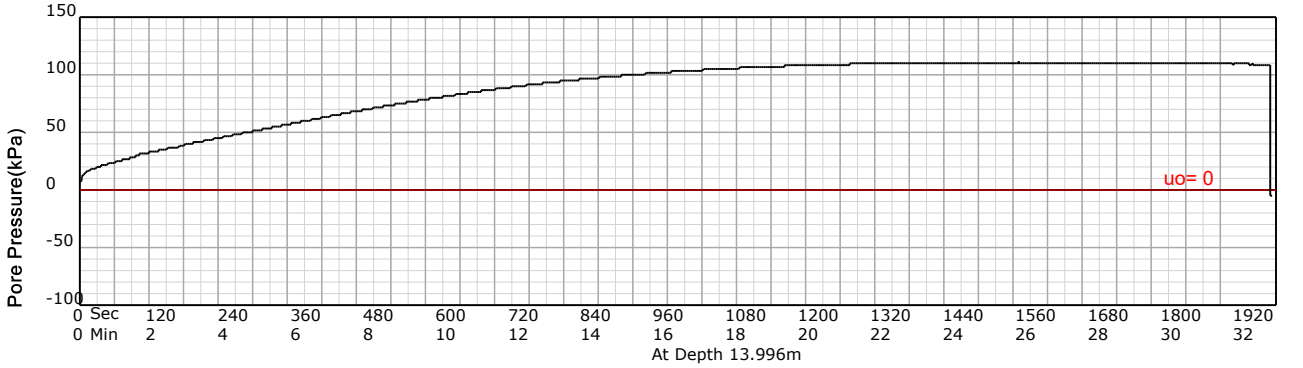

At Depth 13.996m

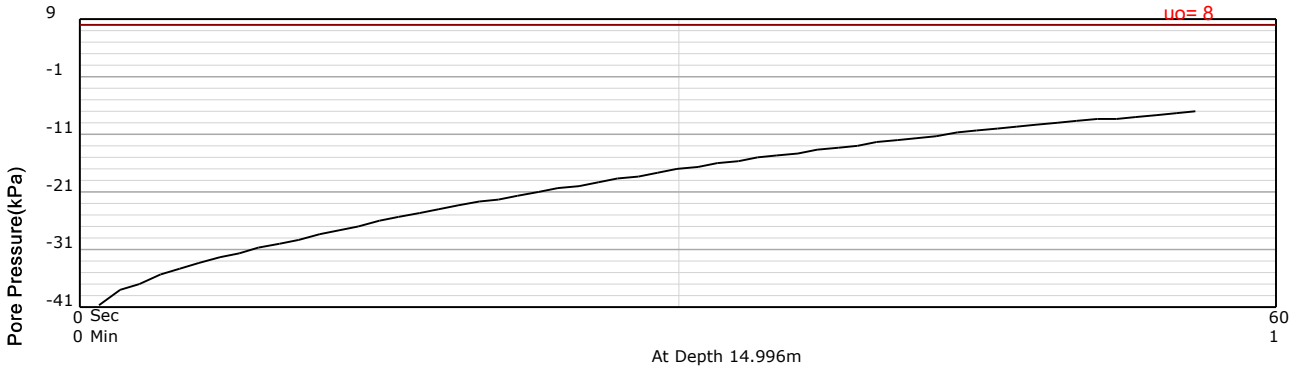

At Depth 14.996m

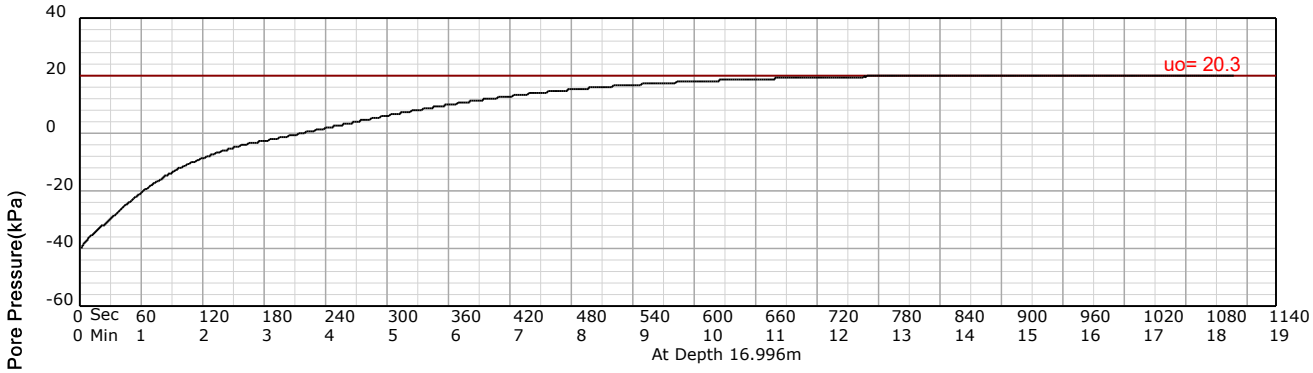

At Depth 16.996m

PIEZOCONE PENETRATION TEST

Dissipation Tests

HOLE: C4

PROJECT: 2024 Jagersfontein

SITE: TSF

DATE: 24/01/31 At: 14:07:34 A

DEPTH: 25.101

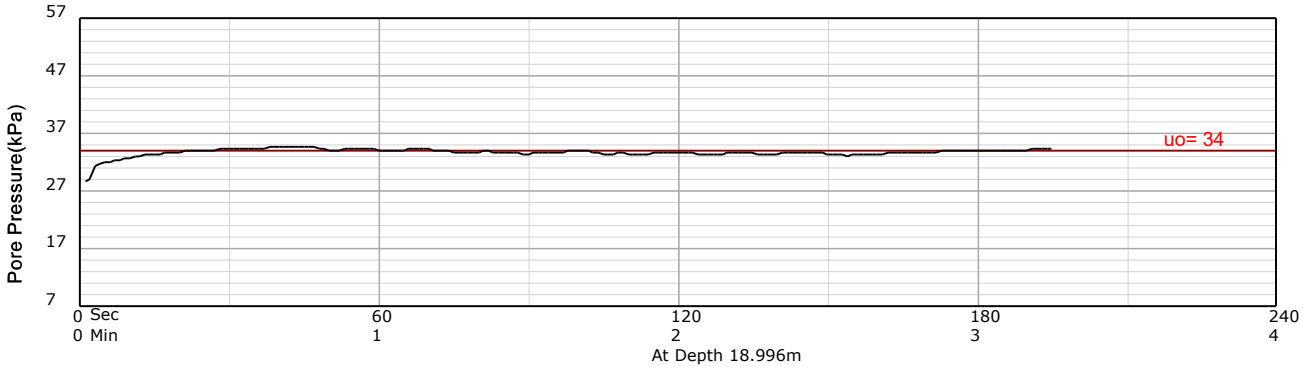

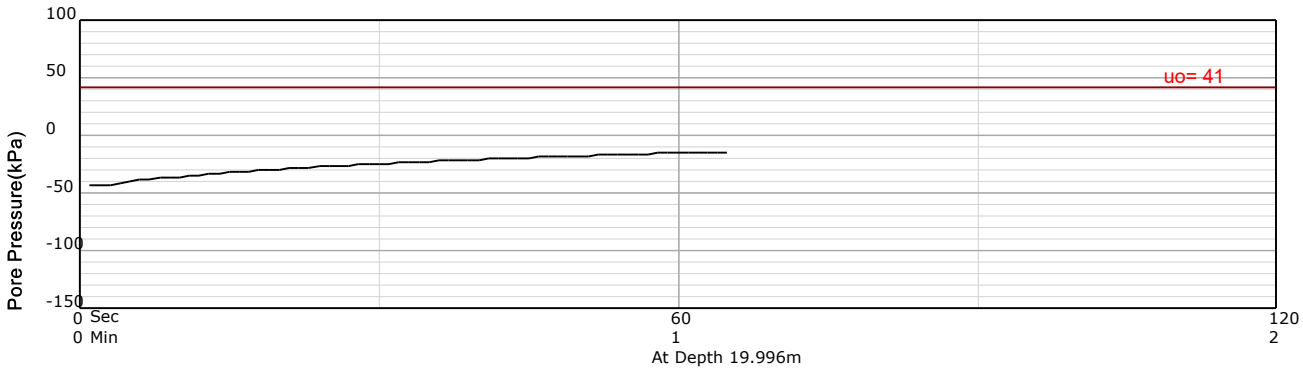

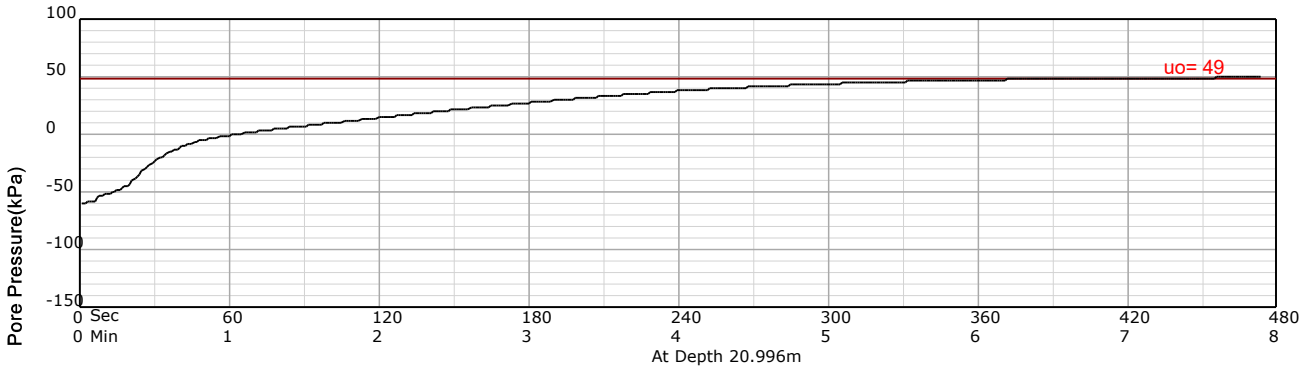

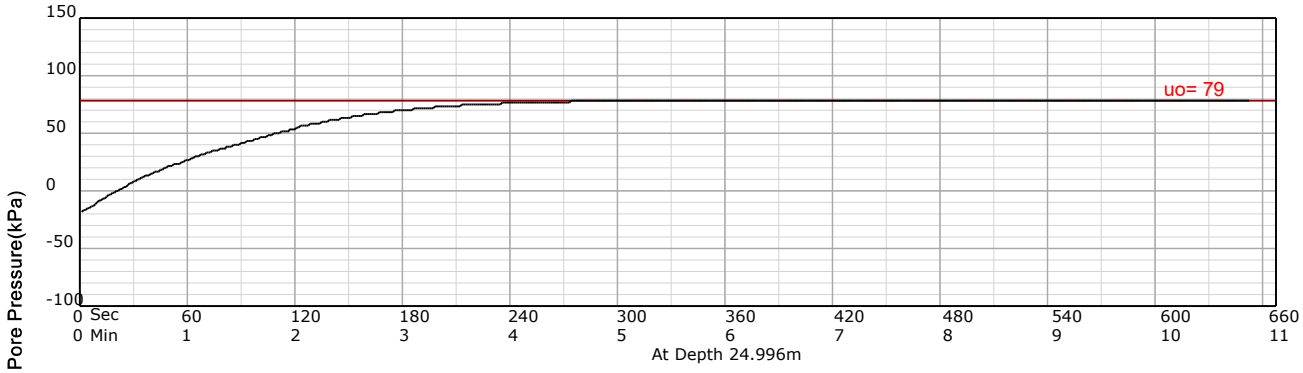

PIEZOCONE PENETRATION TEST

Dissipation Tests

HOLE: C4

PROJECT: 2024 Jagersfontein

SITE: TSF

DATE: 24/01/31 At: 14:07:34 A

DEPTH: 25.101

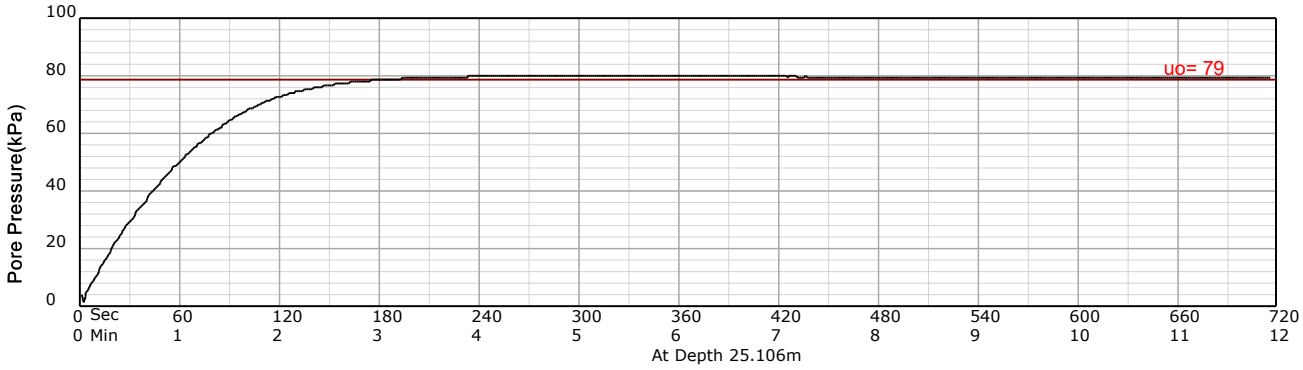

PIEZOCONE PENETRATION TEST

Equivalent Soil Behaviour Type Profile

HOLE: C4

PROJECT: 2024 Jagersfontein

SITE: TSF

DATE: 24/01/31 At: 14:07:34 A

DEPTH: 25.101

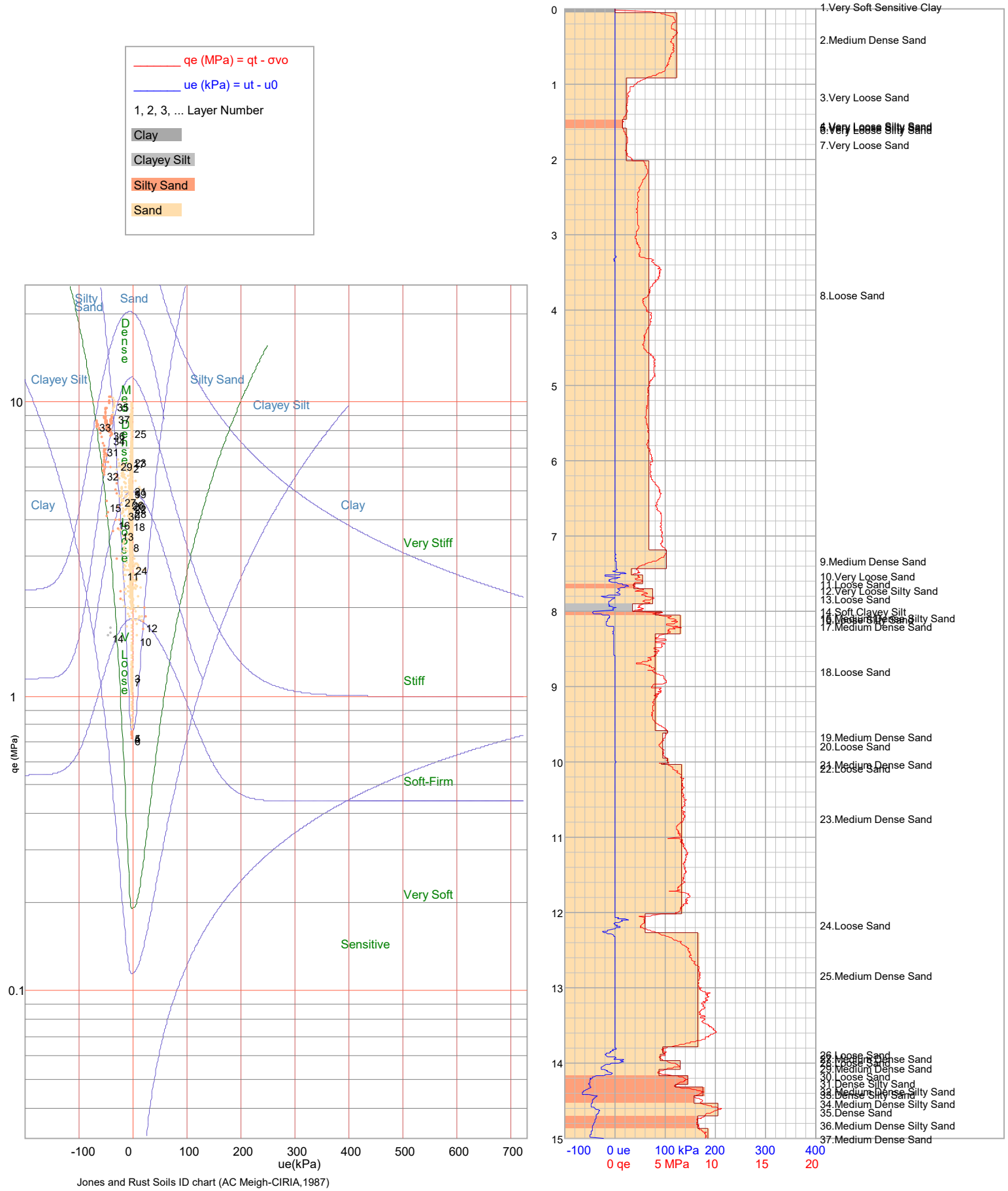

Jones and Rust Soils ID chart (AC Meigh-CIRIA,1987)

PIEZOCONE PENETRATION TEST

Equivalent Soil Behaviour Type Profile

HOLE: C4

PROJECT: 2024 Jagersfontein

SITE: TSF

DATE: 24/01/31 At: 14:07:34 A

DEPTH: 25.101

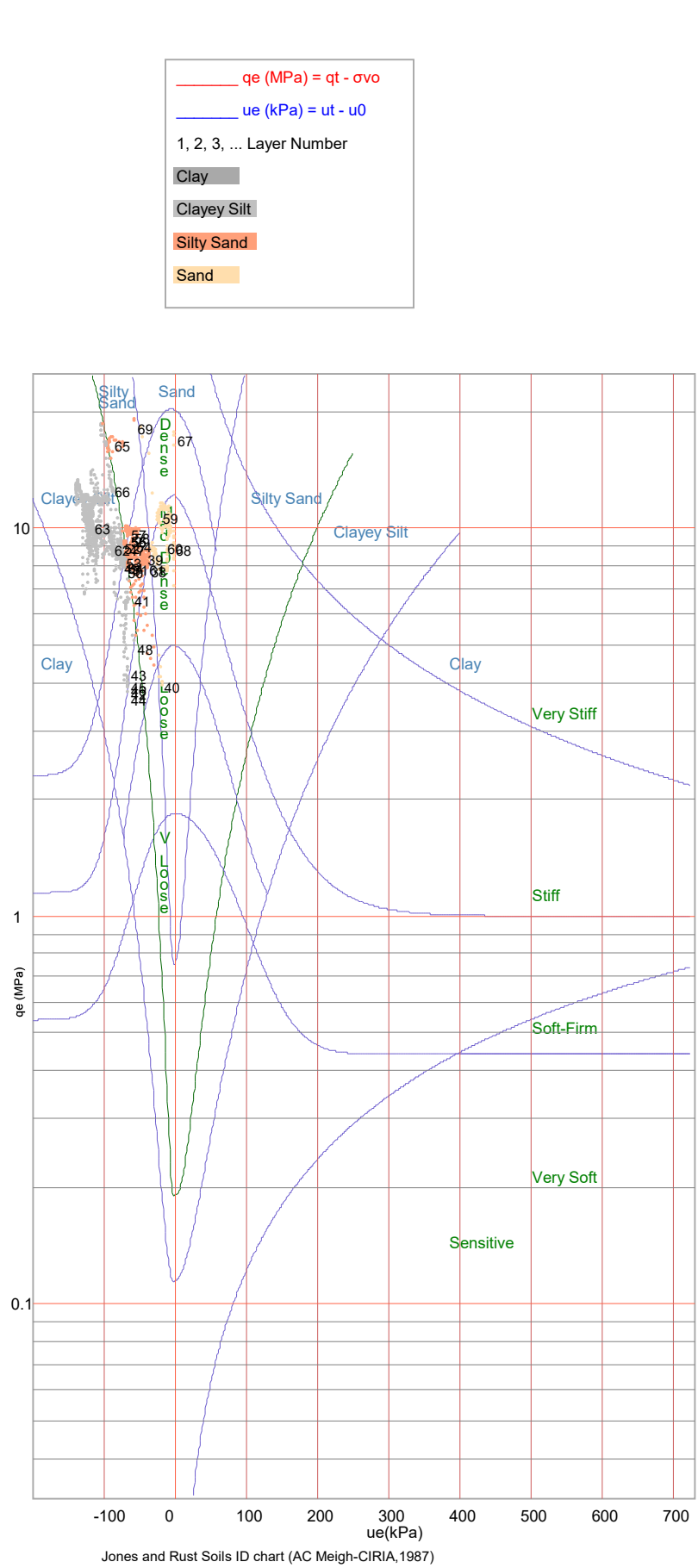

Jones and Rust Soils ID chart (AC Meigh-CIRIA,1987)

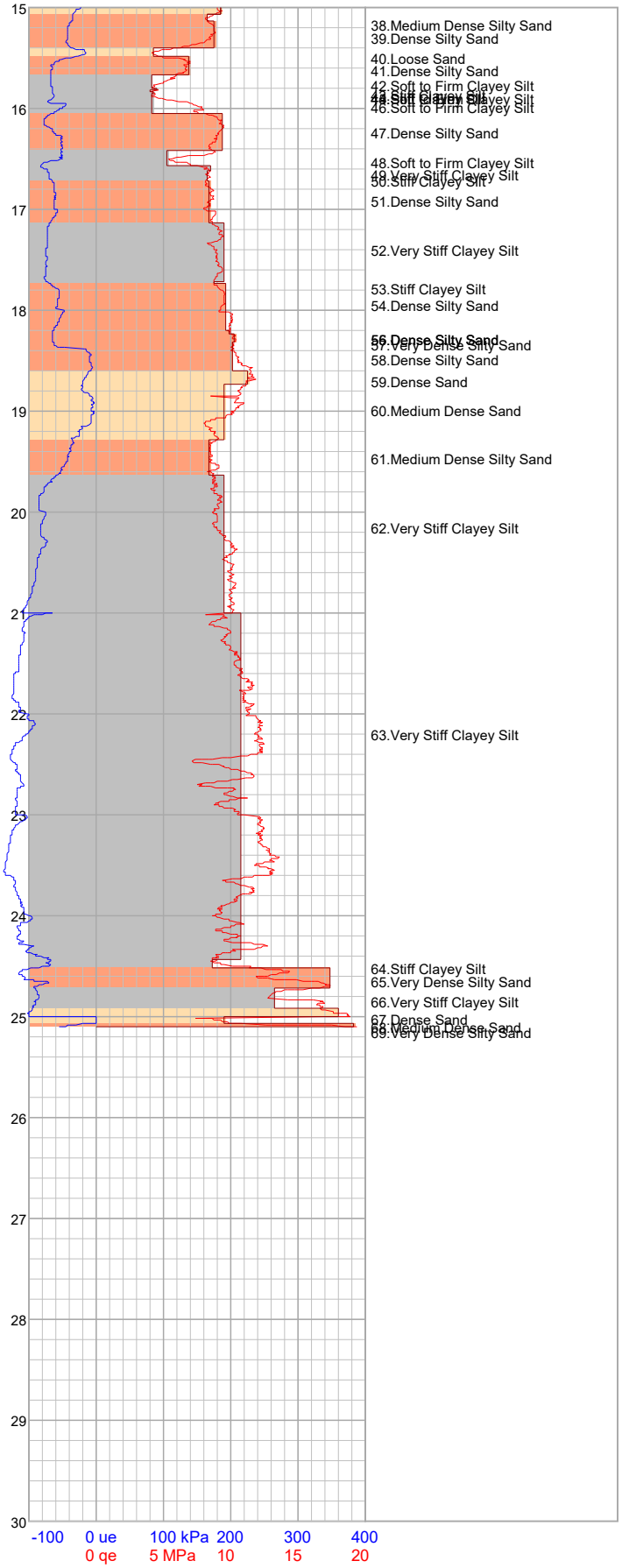

PIEZOCONE PENETRATION TEST

Recorded Field Results (Cone, Pore Pressure and Static Pore Pressure from Dissipations)

HOLE: C5

PROJECT: 2024 Jagersfontein

SITE: TSF

DATE: 24/02/01 At: 09:10:06 A

DEPTH: 18.903

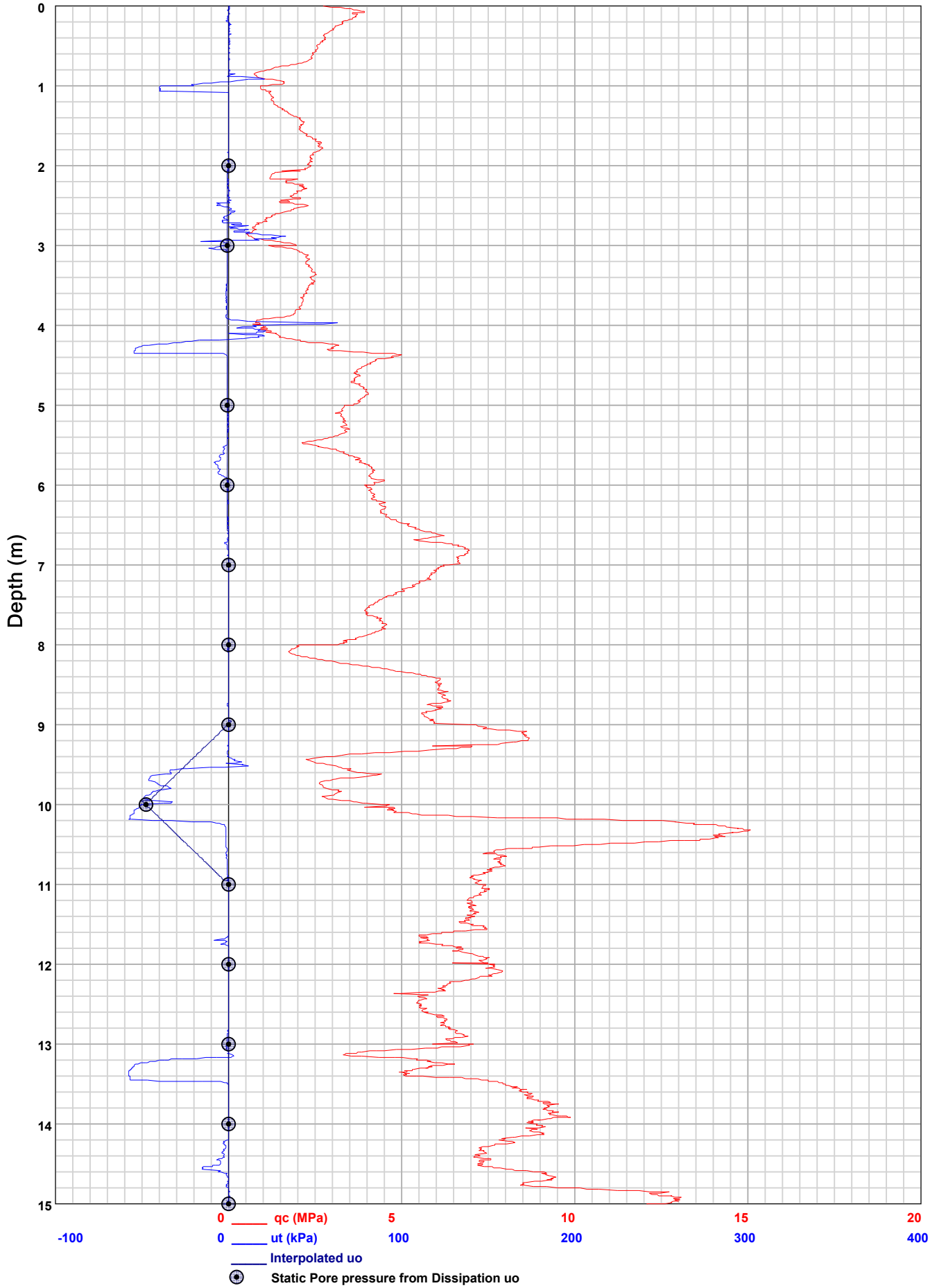

PIEZOCONE PENETRATION TEST

Recorded Field Results (Cone, Pore Pressure and Static Pore Pressure from Dissipations)

HOLE: C5

PROJECT: 2024 Jagersfontein

SITE: TSF

DATE: 24/02/01 At: 09:10:06 A **DEPTH:** 18.903

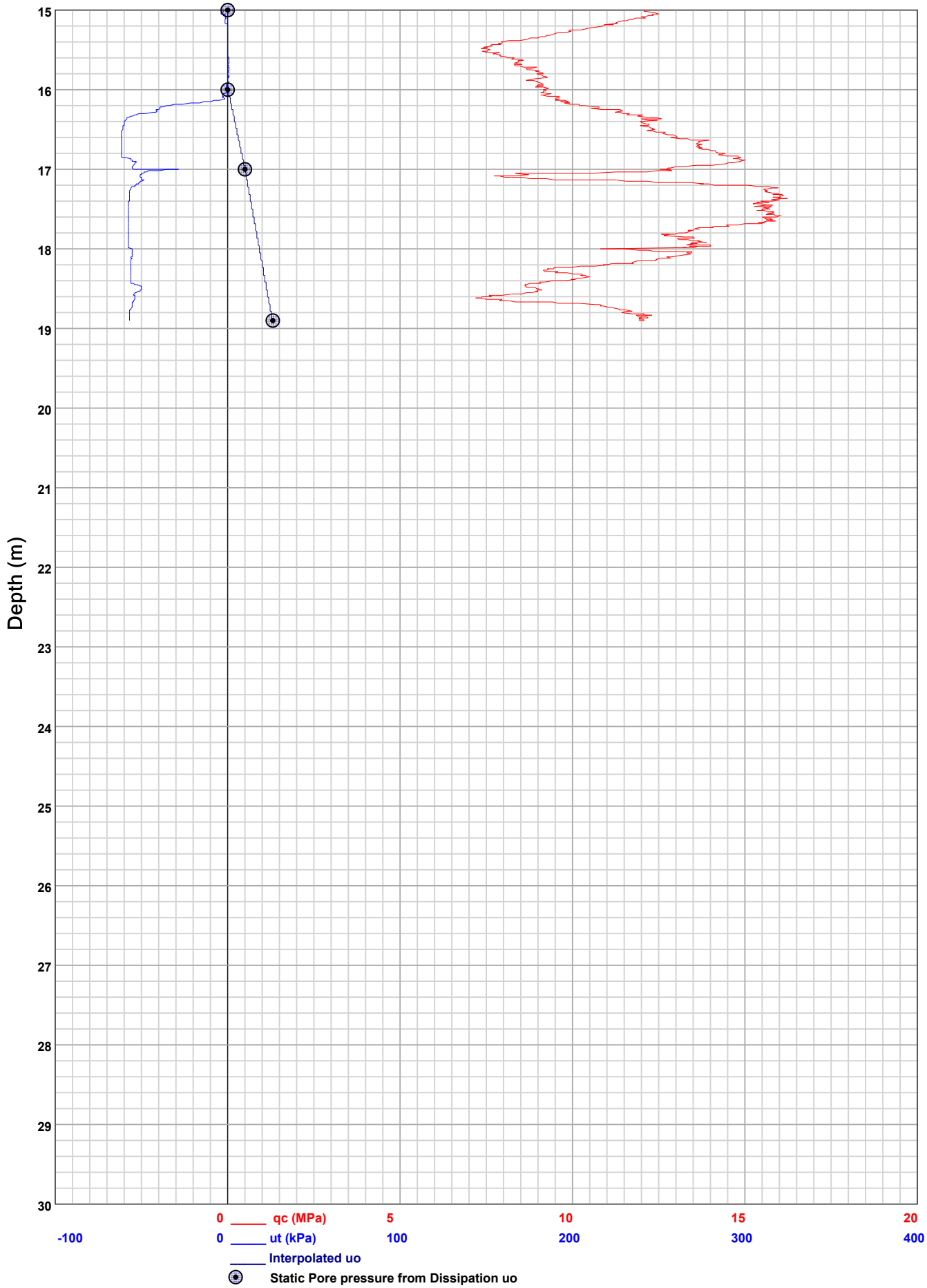

PIEZOCONE PENETRATION TEST

HOLE: C5

PROJECT: 2024 Jagersfontein

SITE: TSF

DATE: 24/02/01 At: 09:10:06 A

DEPTH: 18.903

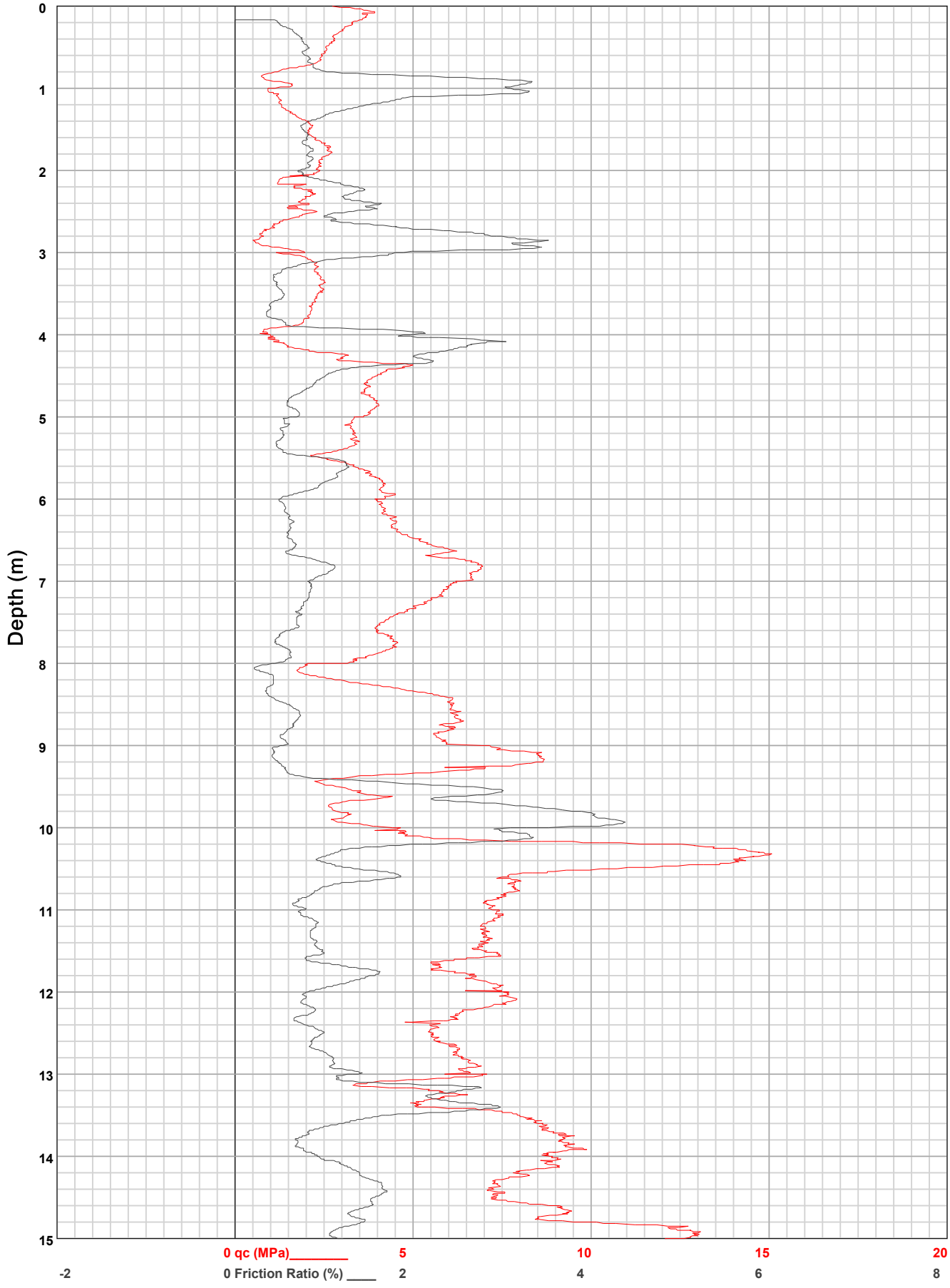

PIEZOCONE PENETRATION TEST

HOLE: C5

PROJECT: 2024 Jagersfontein

SITE: TSF

DATE: 24/02/01 At: 09:10:06 A

DEPTH: 18.903

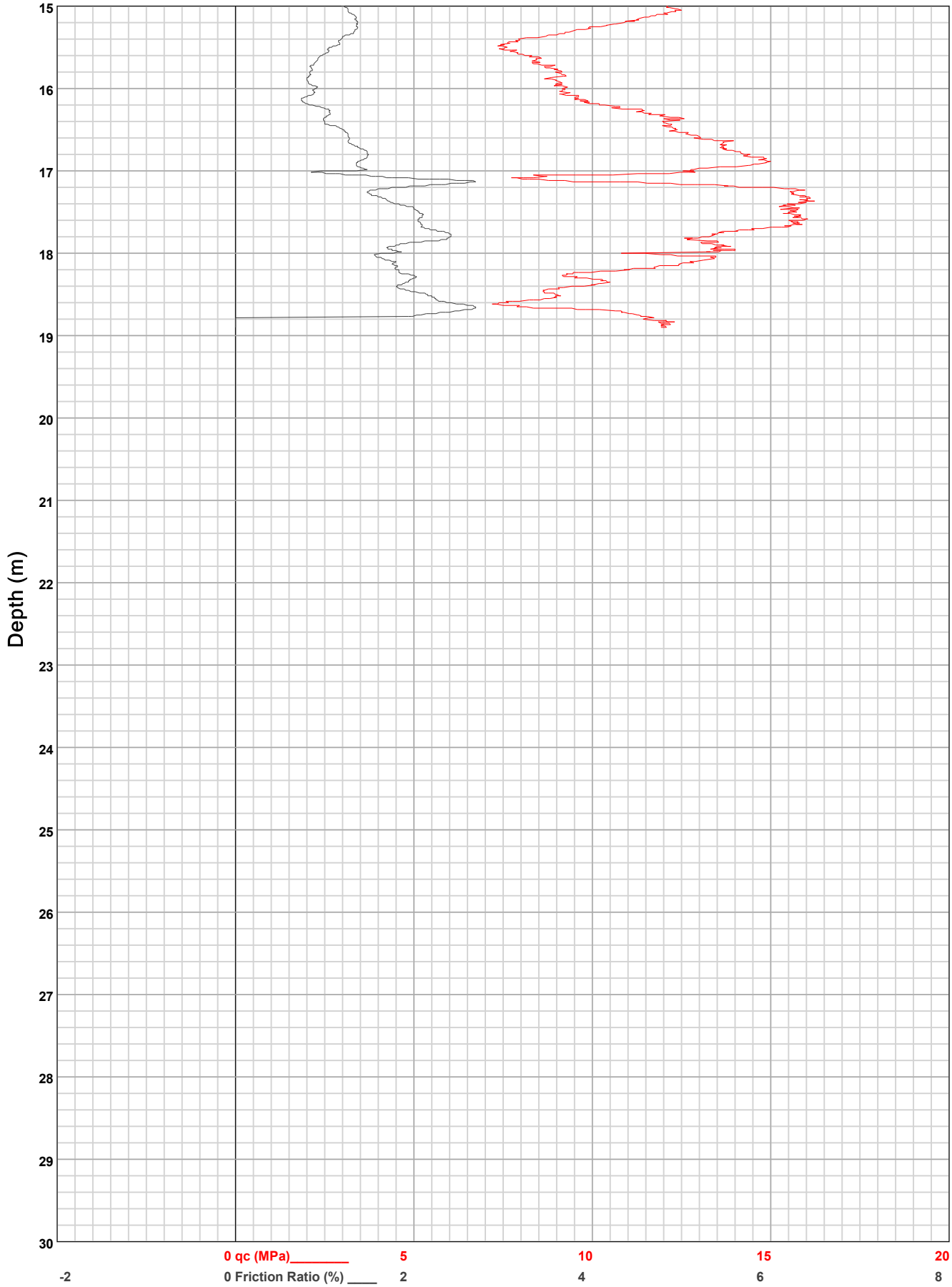

PIEZOCONE PENETRATION TEST

Dissipation Tests

HOLE: C5

PROJECT: 2024 Jagersfontein

SITE: TSF

DATE: 24/02/01 At: 09:10:06 A

DEPTH: 18.903

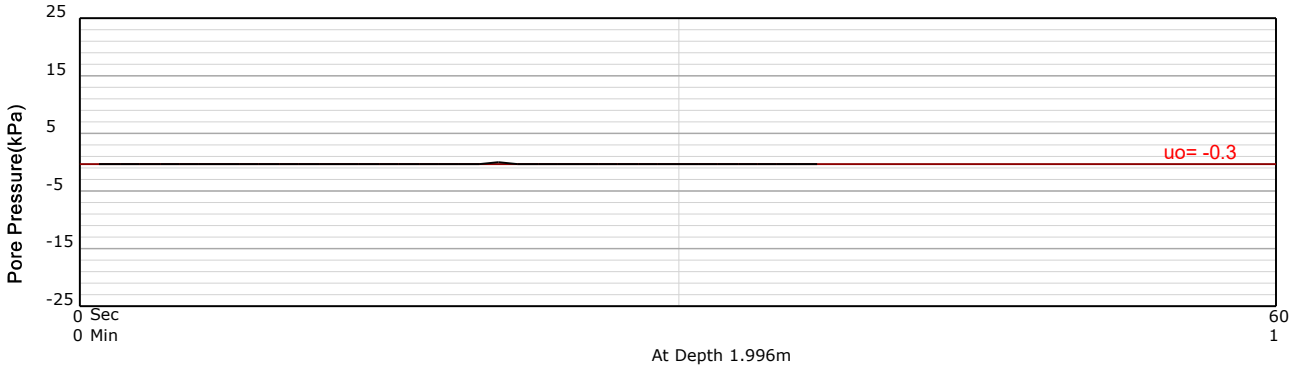

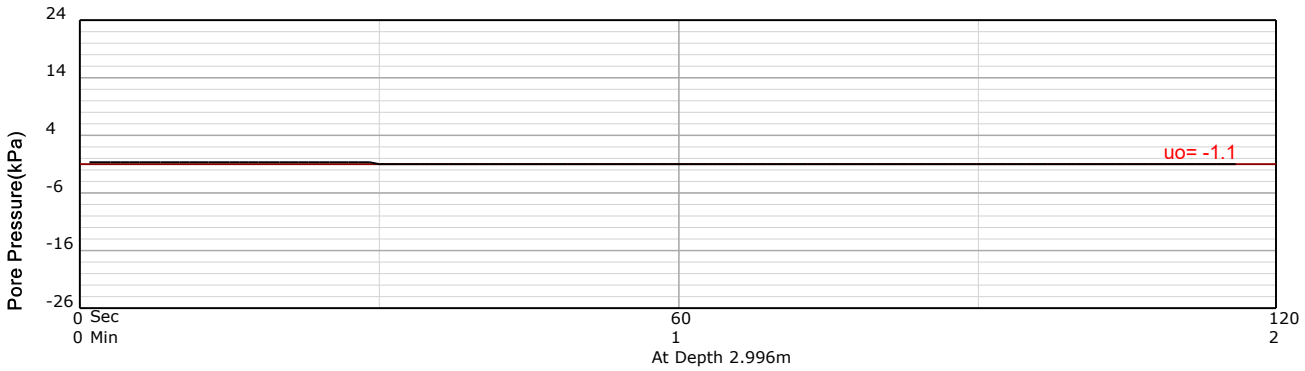

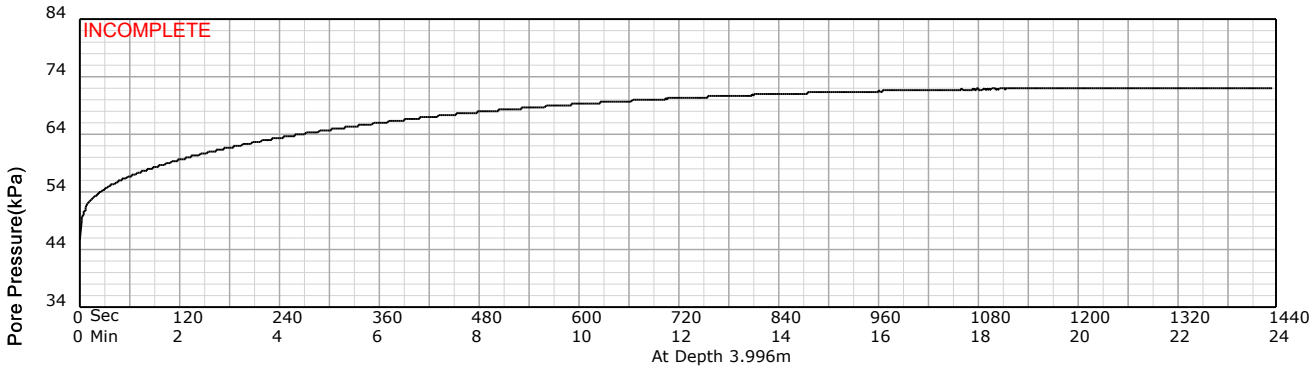

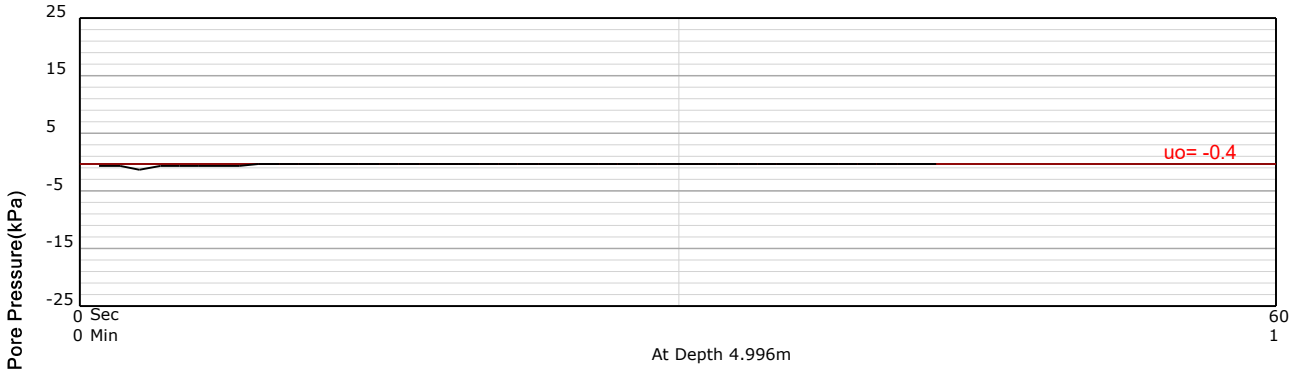

PIEZOCONE PENETRATION TEST

Dissipation Tests

HOLE: C5

PROJECT: 2024 Jagersfontein

SITE: TSF

DATE: 24/02/01 At: 09:10:06 A

DEPTH: 18.903

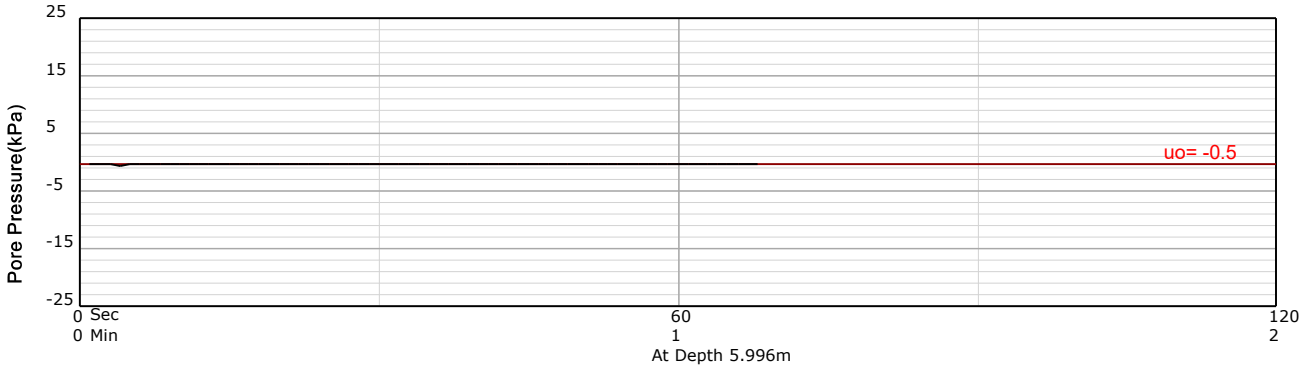

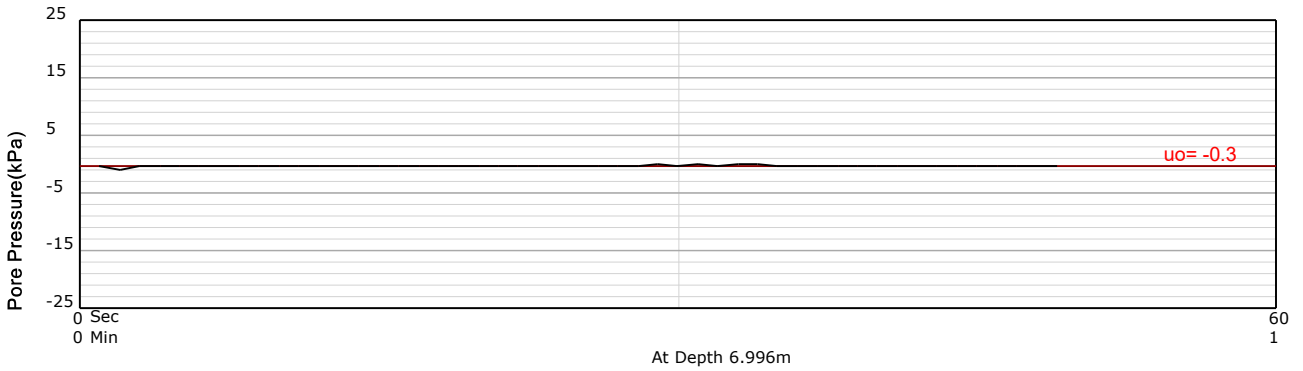

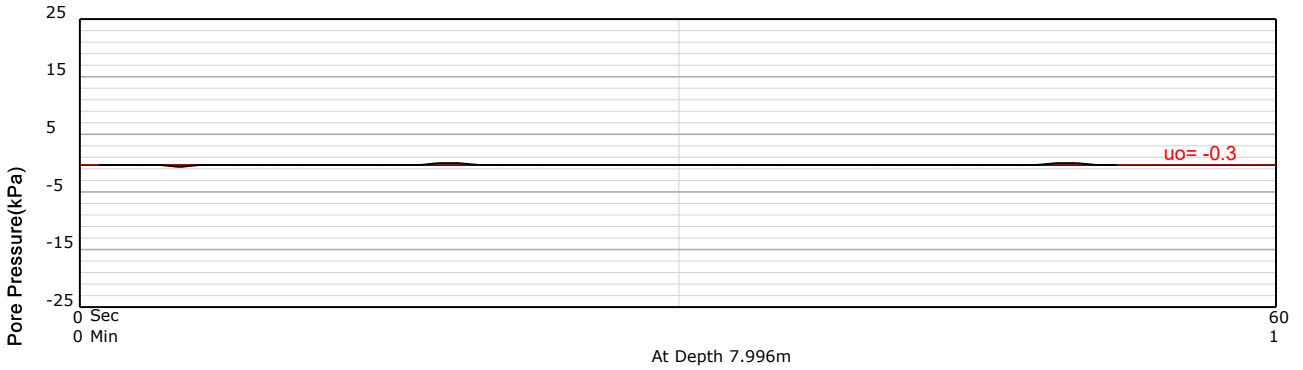

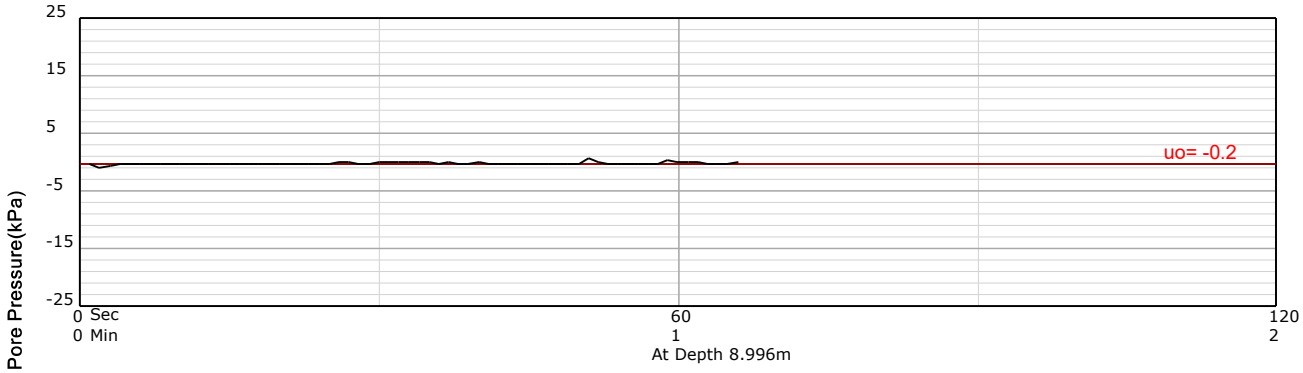

PIEZOCONE PENETRATION TEST

Dissipation Tests

HOLE: C5

PROJECT: 2024 Jagersfontein

SITE: TSF

DATE: 24/02/01 At: 09:10:06 A

DEPTH: 18.903

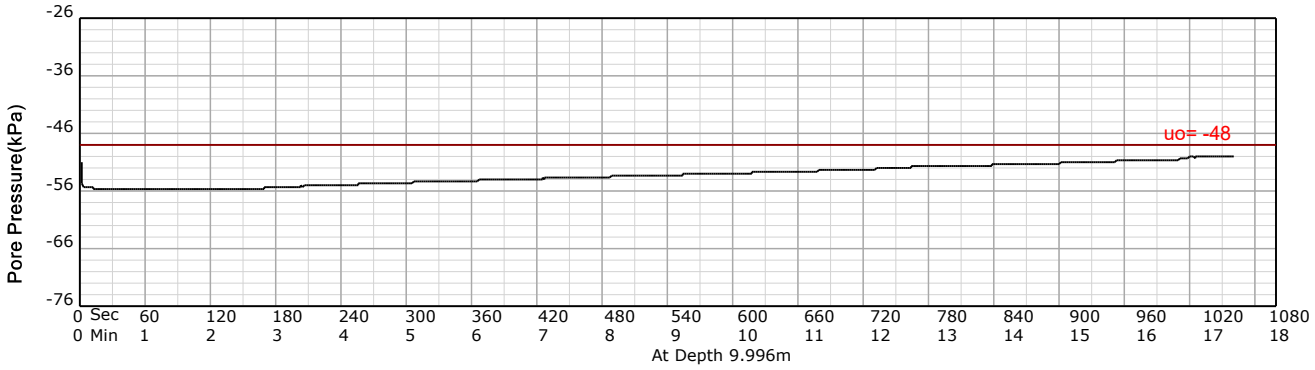

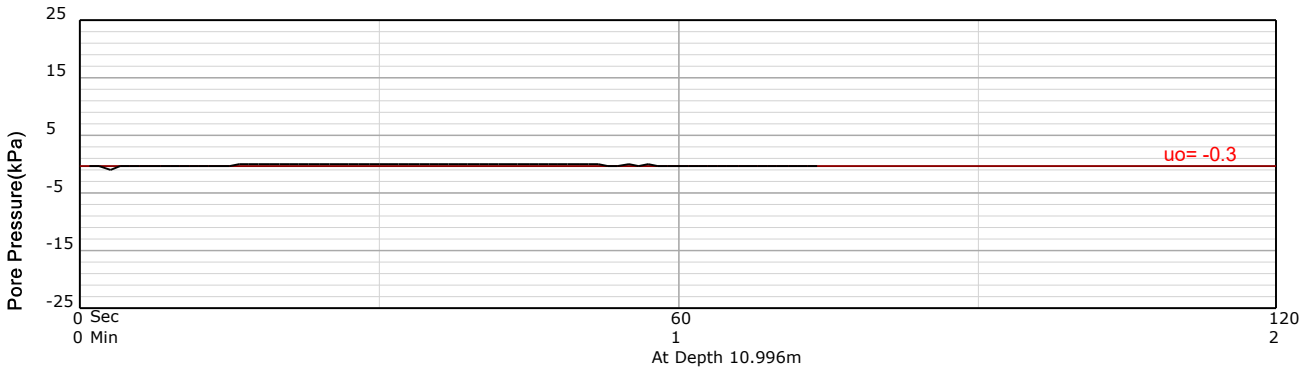

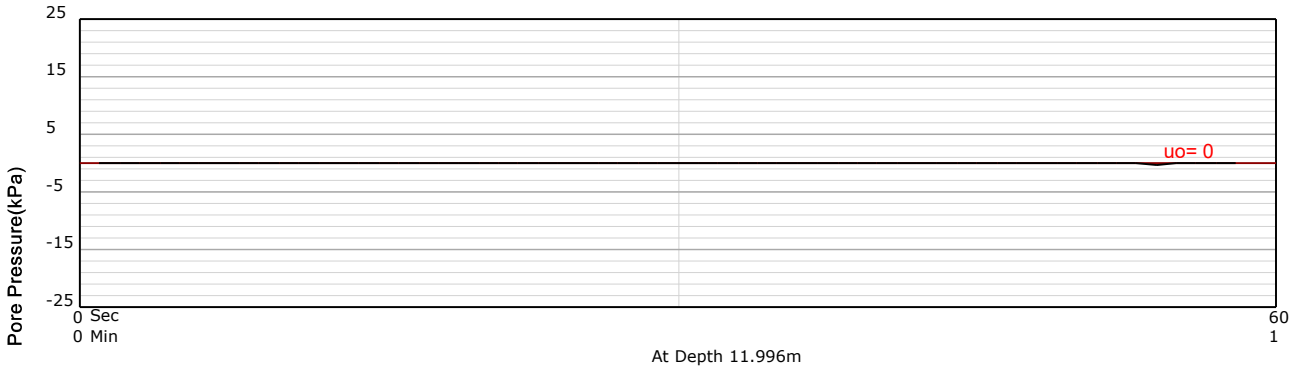

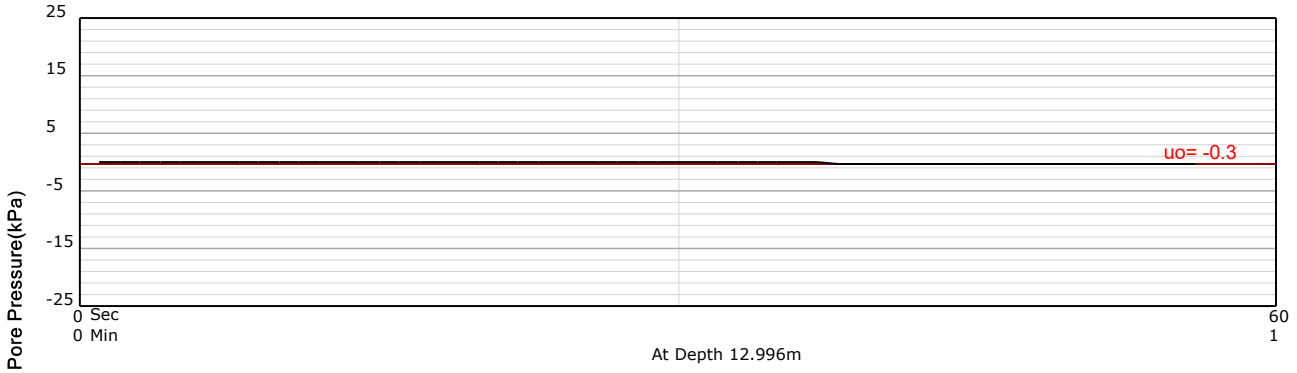

PIEZOCONE PENETRATION TEST

Dissipation Tests

HOLE: C5

PROJECT: 2024 Jagersfontein

SITE: TSF

DATE: 24/02/01 At: 09:10:06 A

DEPTH: 18.903

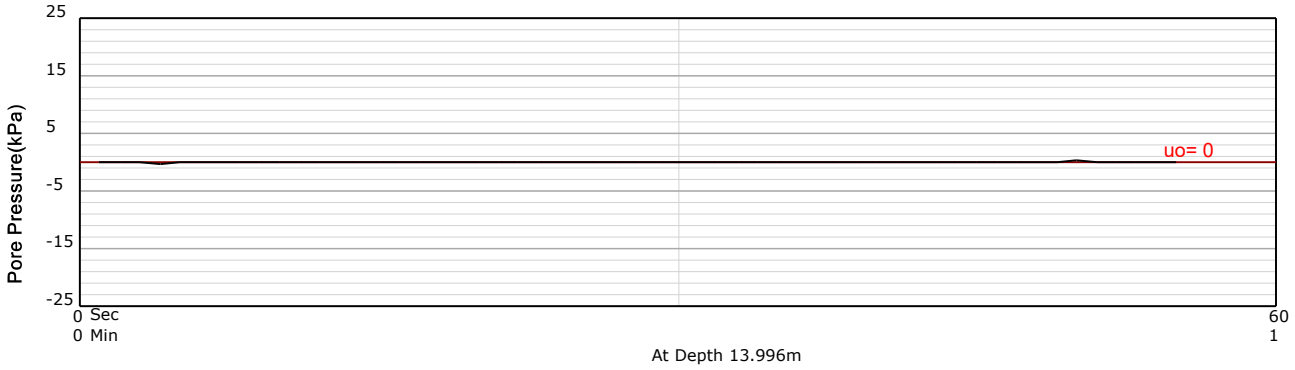

At Depth 13.996m

At Depth 14.996m

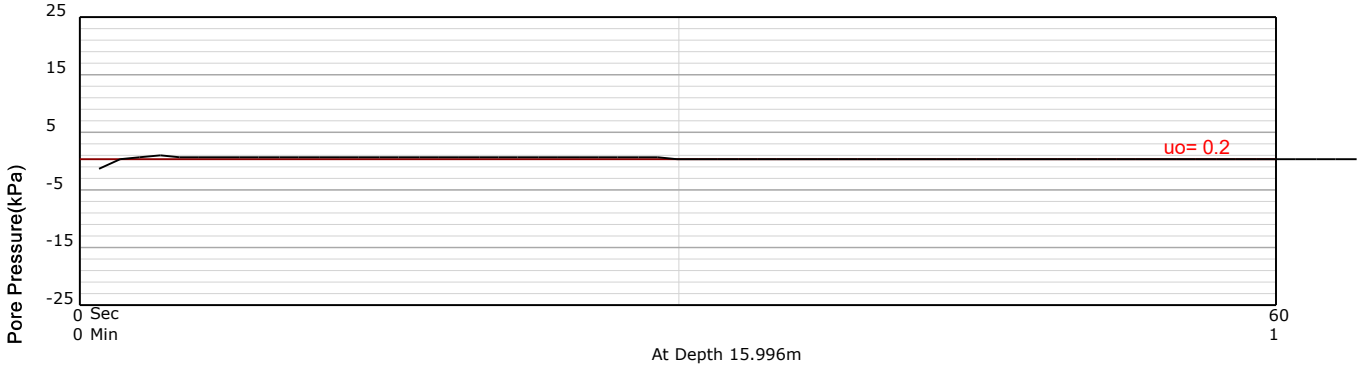

At Depth 15.996m

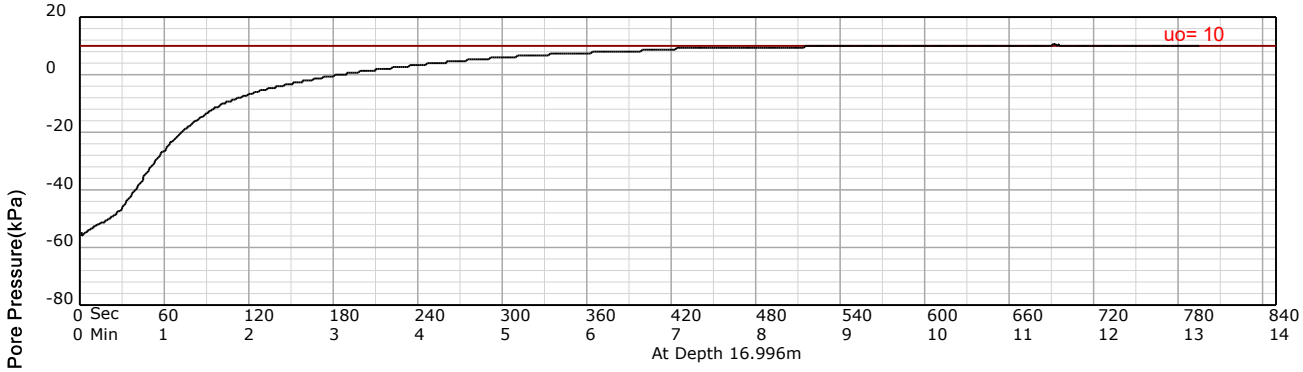

At Depth 16.996m

PIEZOCONE PENETRATION TEST

Dissipation Tests

HOLE: C5

PROJECT: 2024 Jagersfontein

SITE: TSF

DATE: 24/02/01 At: 09:10:06 A **DEPTH:** 18.903

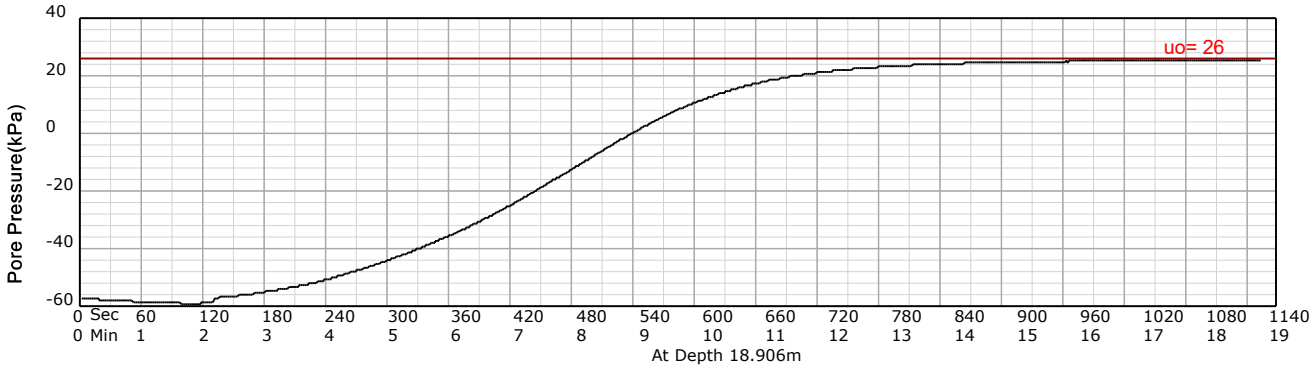

PIEZOCONE PENETRATION TEST

Equivalent Soil Behaviour Type Profile

HOLE: C5

PROJECT: 2024 Jagersfontein

SITE: TSF

DATE: 24/02/01 At: 09:10:06 A

DEPTH: 18.903

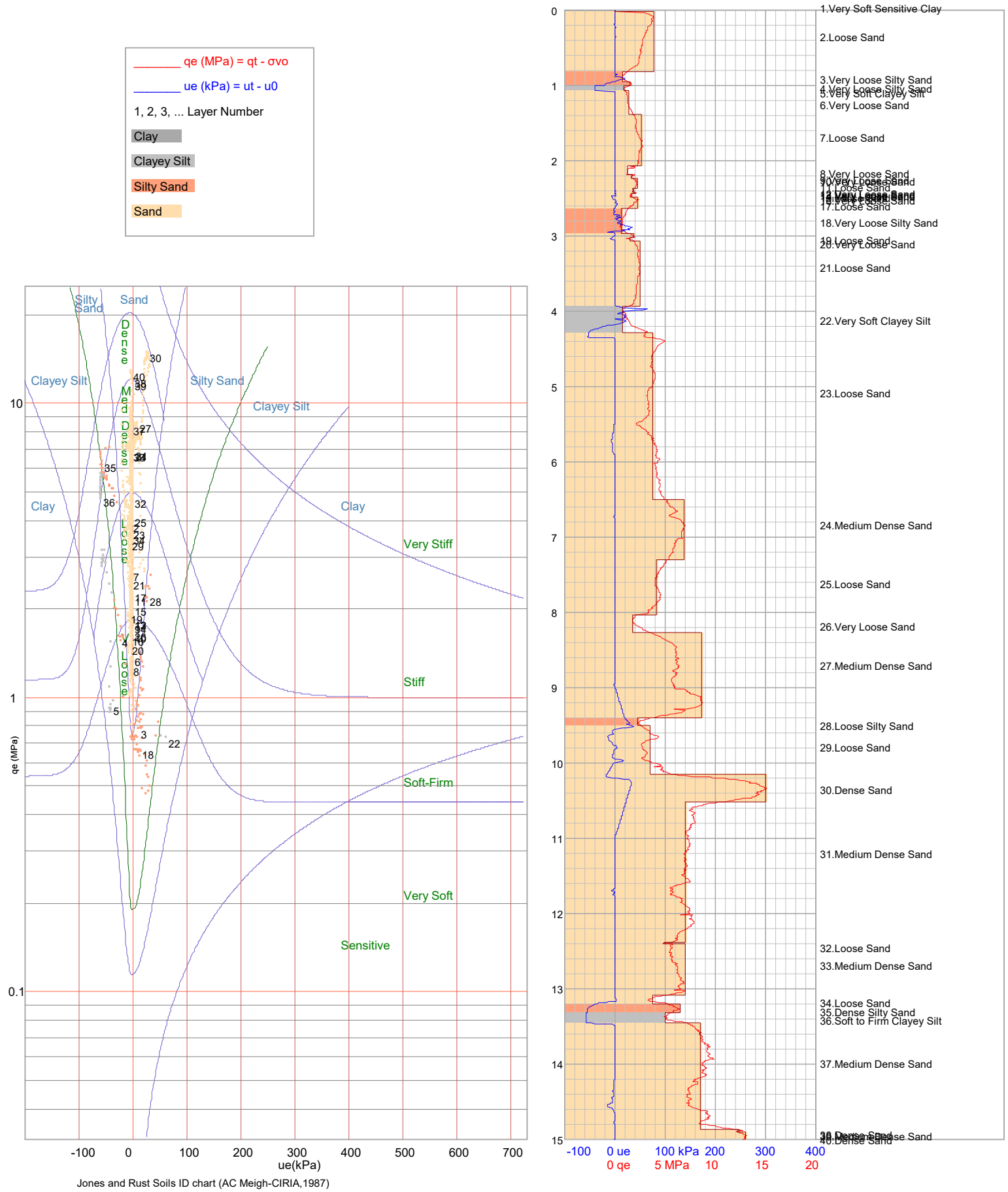

Jones and Rust Soils ID chart (AC Meigh-CIRIA,1987)

PIEZOCONE PENETRATION TEST

Equivalent Soil Behaviour Type Profile

HOLE: C5

PROJECT: 2024 Jagersfontein

SITE: TSF

DATE: 24/02/01 At: 09:10:06 A

DEPTH: 18.903

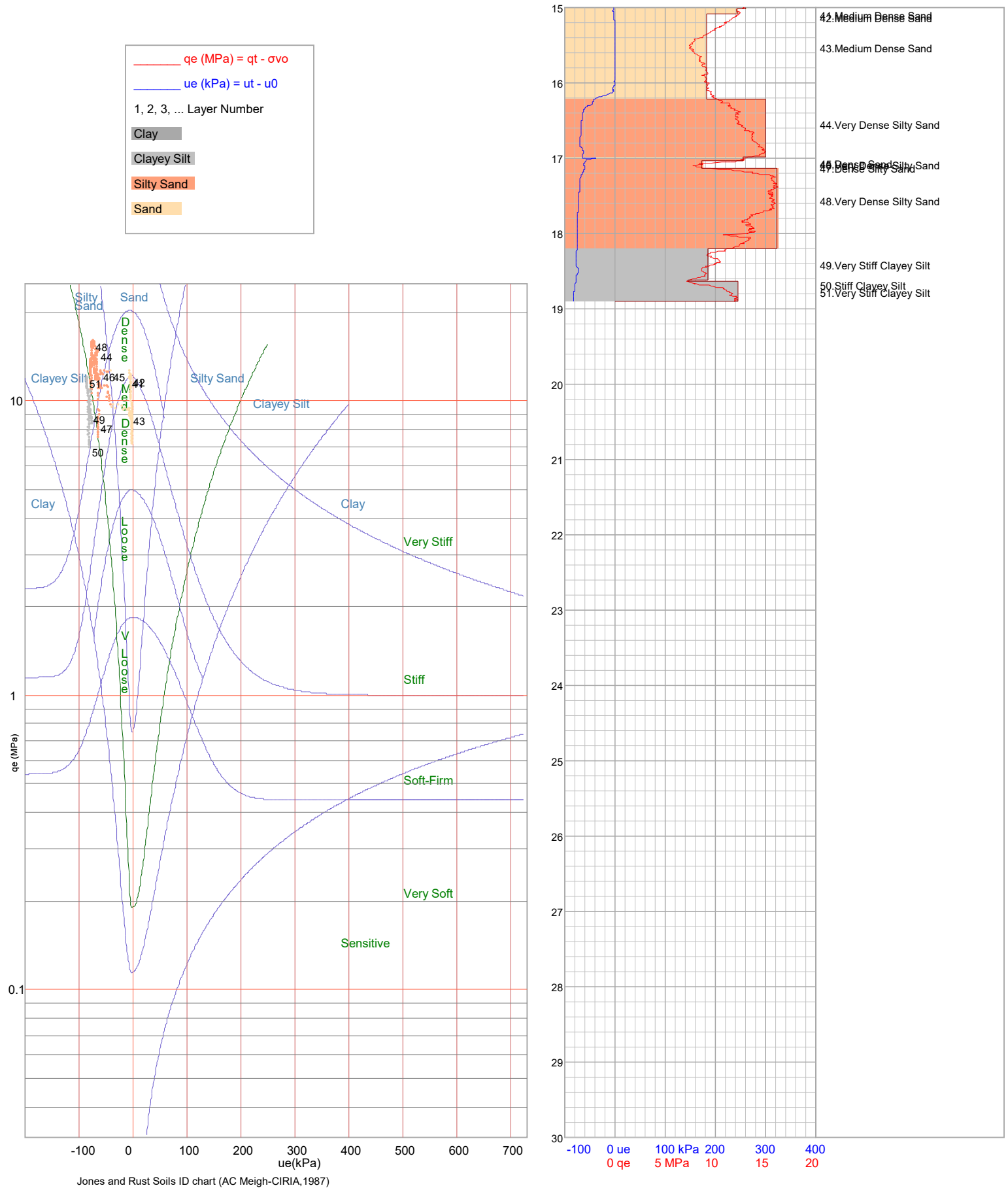

Jones and Rust Soils ID chart (AC Meigh-CIRIA,1987)

PIEZOCONE PENETRATION TEST

Recorded Field Results (Cone, Pore Pressure and Static Pore Pressure from Dissipations)

HOLE: C6

PROJECT: 2024 Jagersfontein

SITE: TSF

DATE: 24/02/03 At: 07:29:54 A **DEPTH:** 21.303

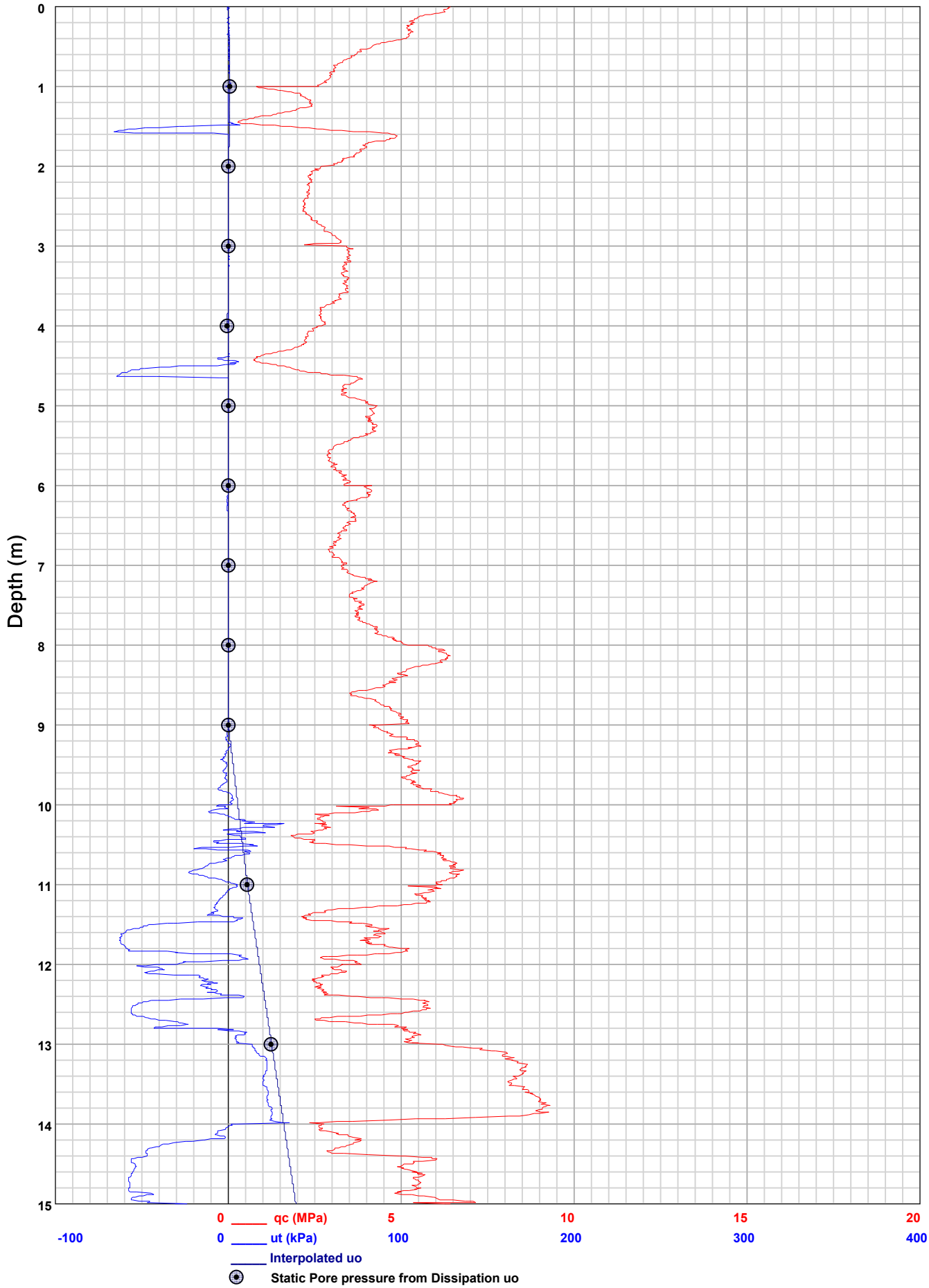

PIEZOCONE PENETRATION TEST

Recorded Field Results (Cone, Pore Pressure and Static Pore Pressure from Dissipations)

HOLE: C6

PROJECT: 2024 Jagersfontein

SITE: TSF

DATE: 24/02/03 At: 07:29:54 A **DEPTH:** 21.303

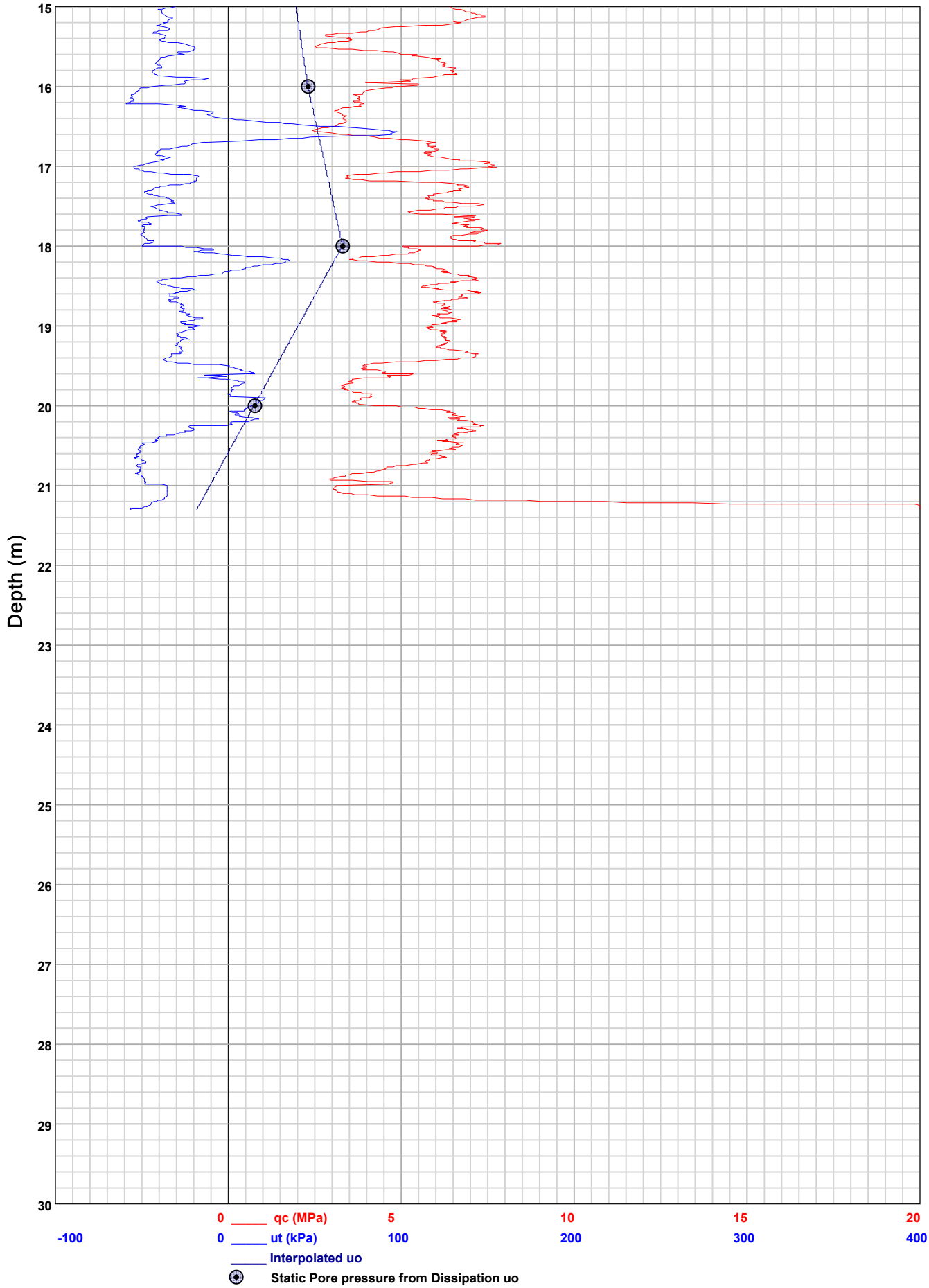

PIEZOCONE PENETRATION TEST

HOLE: C6

PROJECT: 2024 Jagersfontein

SITE: TSF

DATE: 24/02/03 At: 07:29:54 A

DEPTH: 21.303

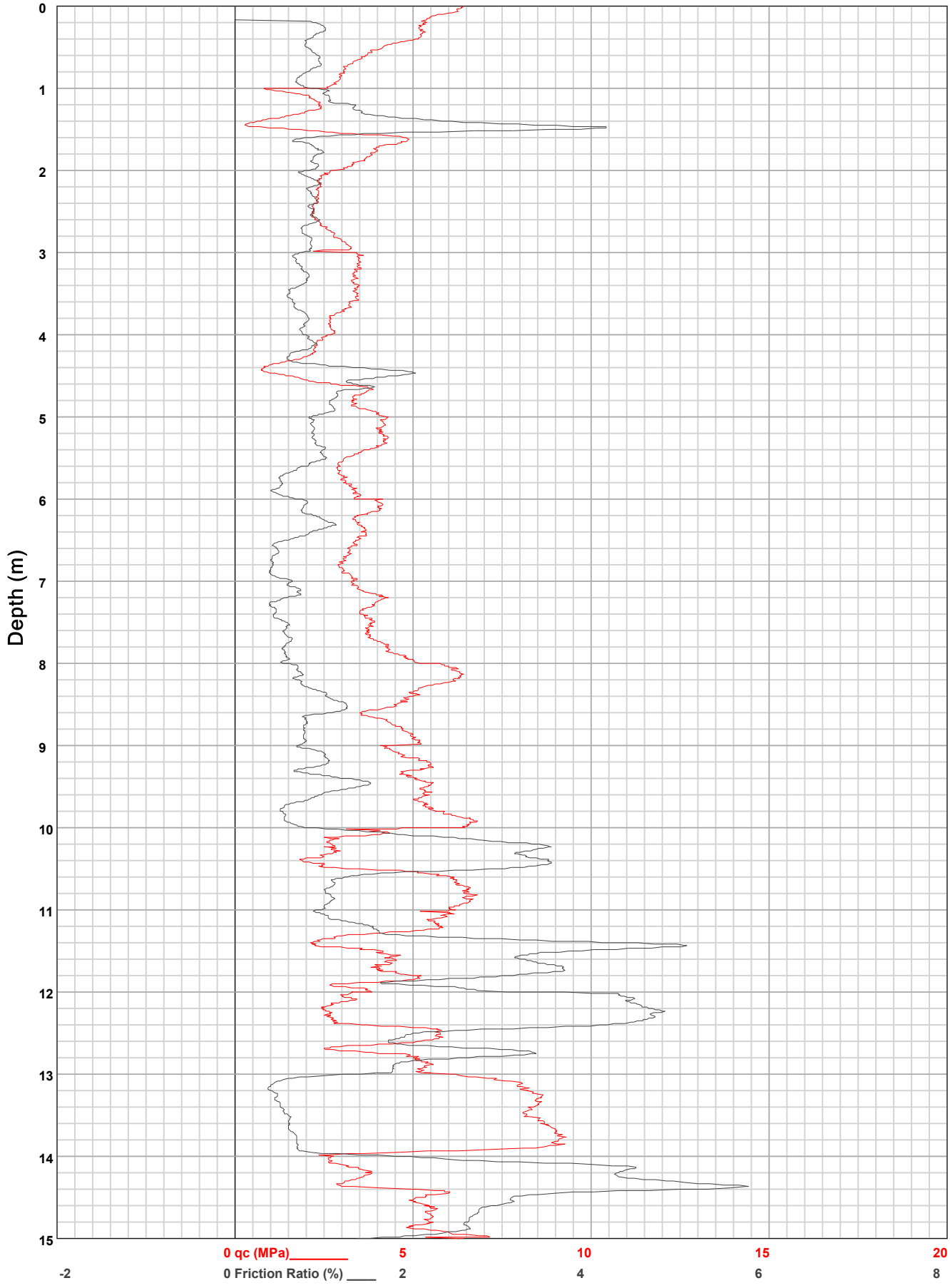

PIEZOCONE PENETRATION TEST

HOLE: C6

PROJECT: 2024 Jagersfontein

SITE: TSF

DATE: 24/02/03 At: 07:29:54 A

DEPTH: 21.303

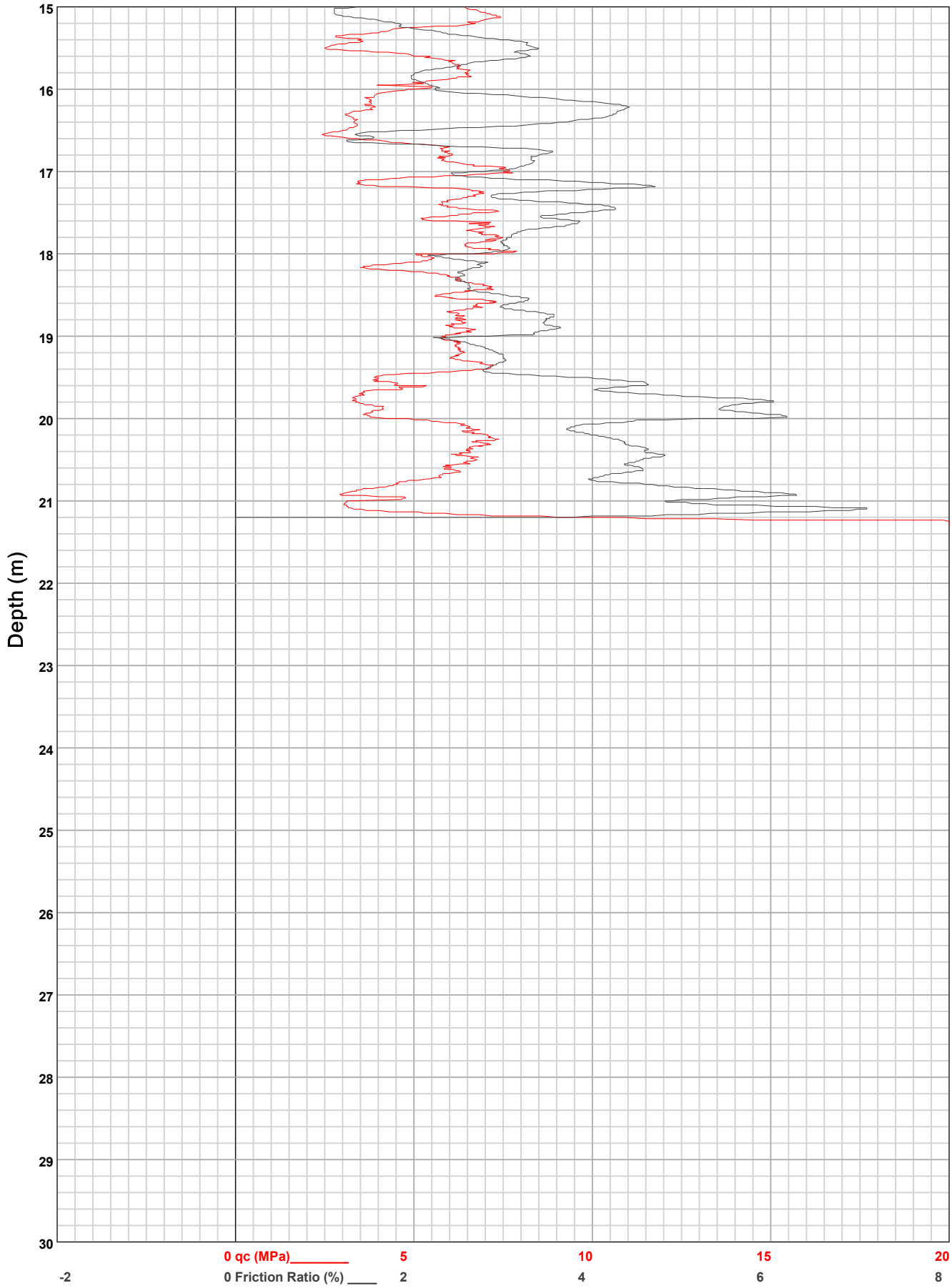

PIEZOCONE PENETRATION TEST

Dissipation Tests

HOLE: C6

PROJECT: 2024 Jagersfontein

SITE: TSF

DATE: 24/02/03 At: 07:29:54 A

DEPTH: 21.303

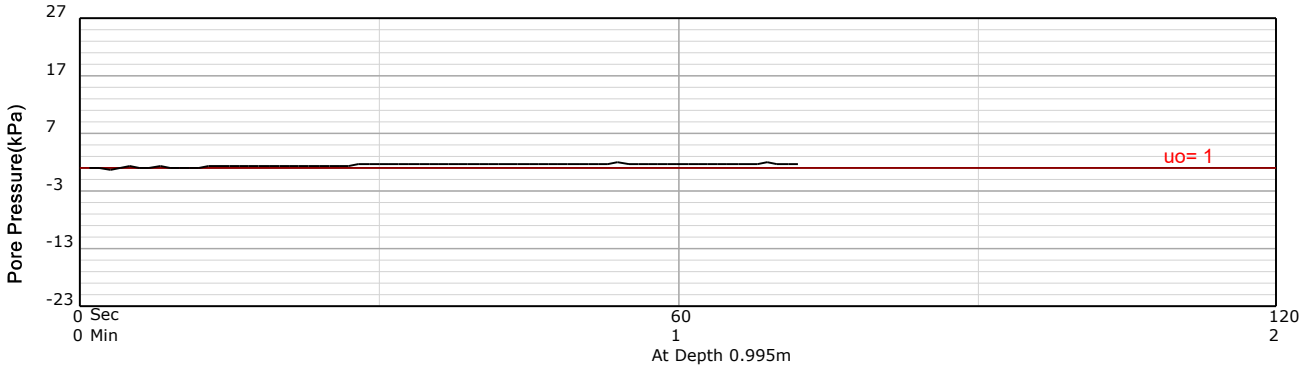

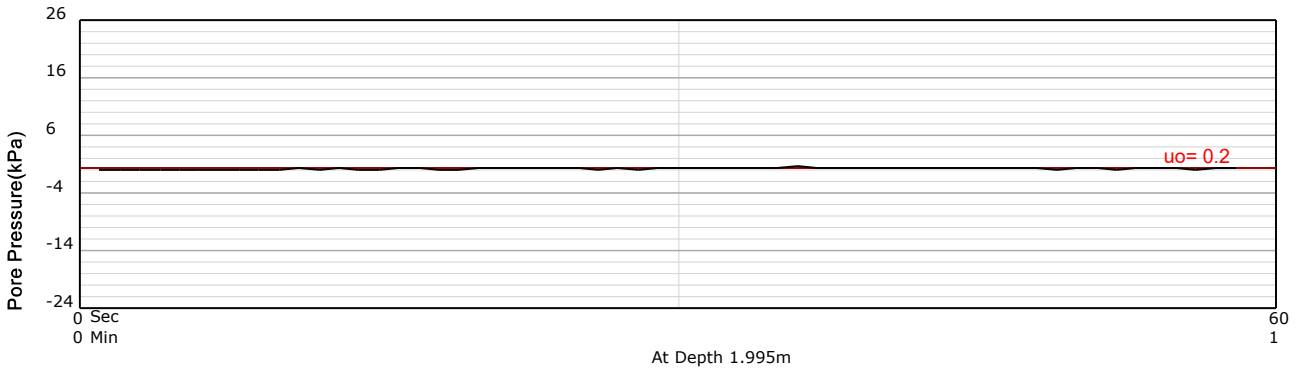

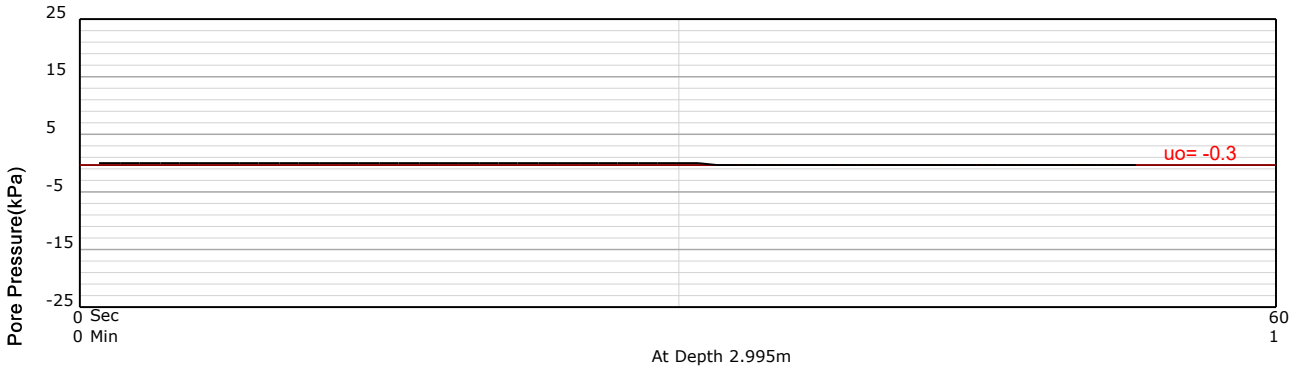

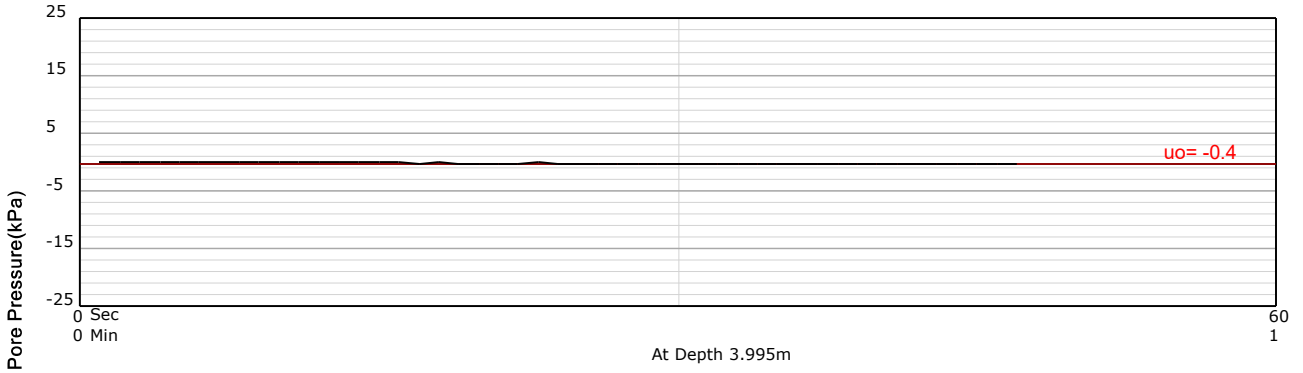

PIEZOCONE PENETRATION TEST

Dissipation Tests

HOLE: C6

PROJECT: 2024 Jagersfontein

SITE: TSF

DATE: 24/02/03 At: 07:29:54 A

DEPTH: 21.303

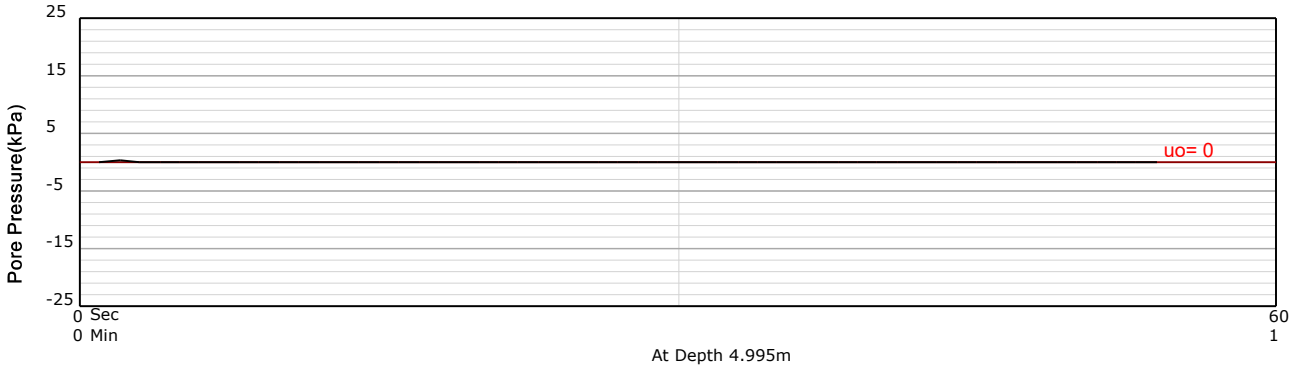

At Depth 4.995m

At Depth 5.995m

At Depth 6.995m

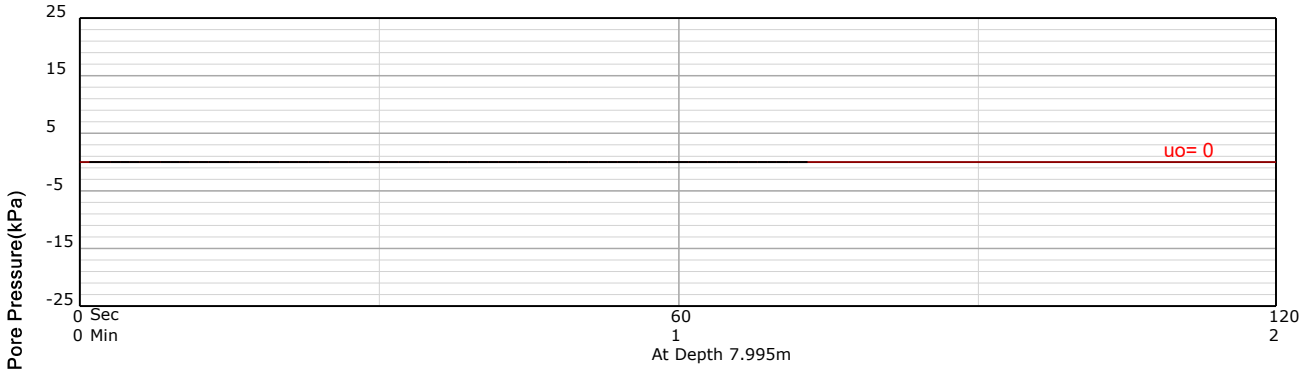

At Depth 7.995m

PIEZOCONE PENETRATION TEST

Dissipation Tests

HOLE: C6

PROJECT: 2024 Jagersfontein

SITE: TSF

DATE: 24/02/03 At: 07:29:54 A

DEPTH: 21.303

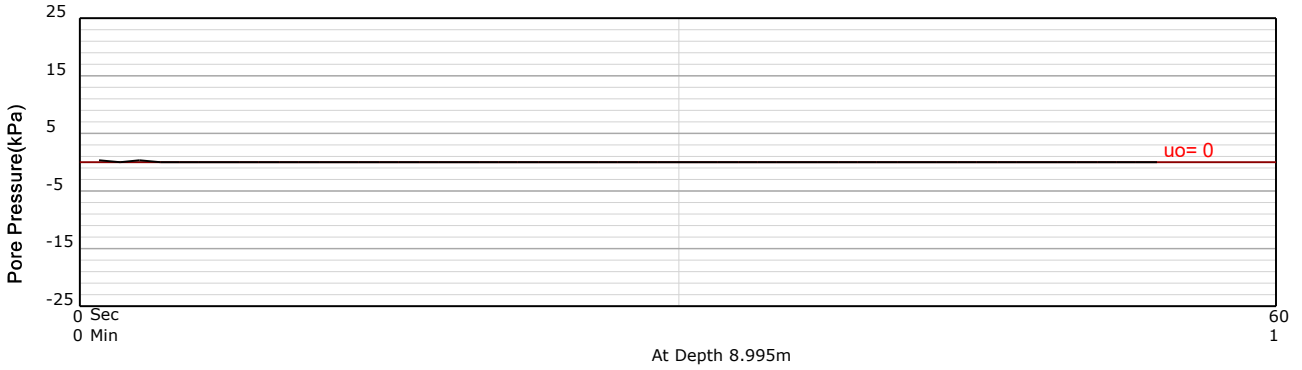

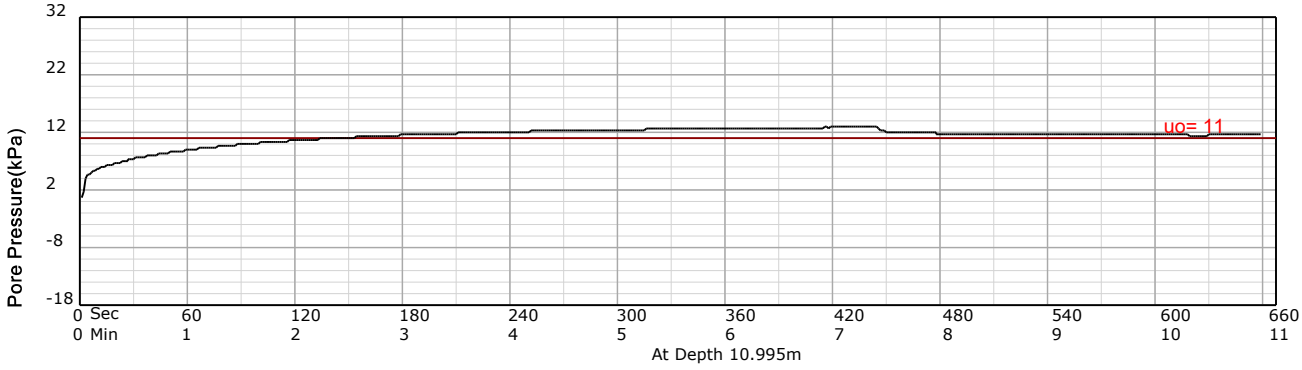

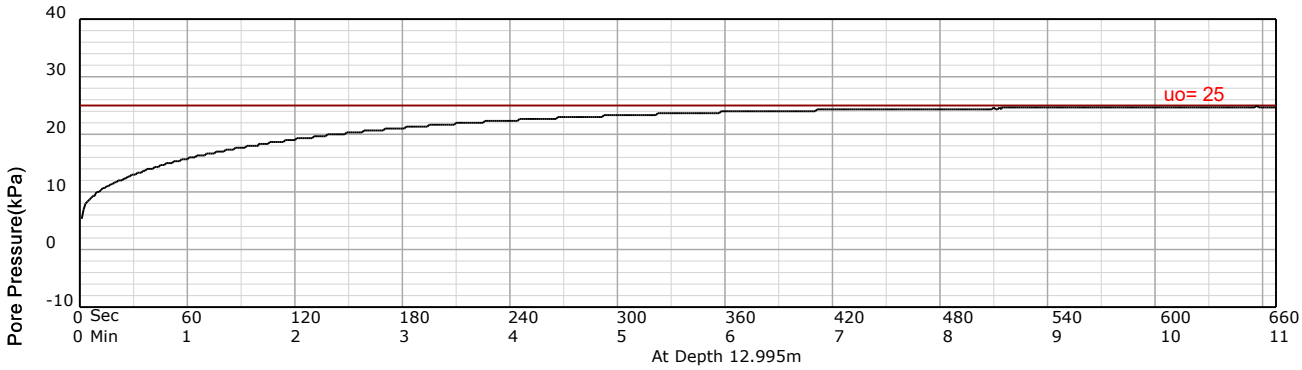

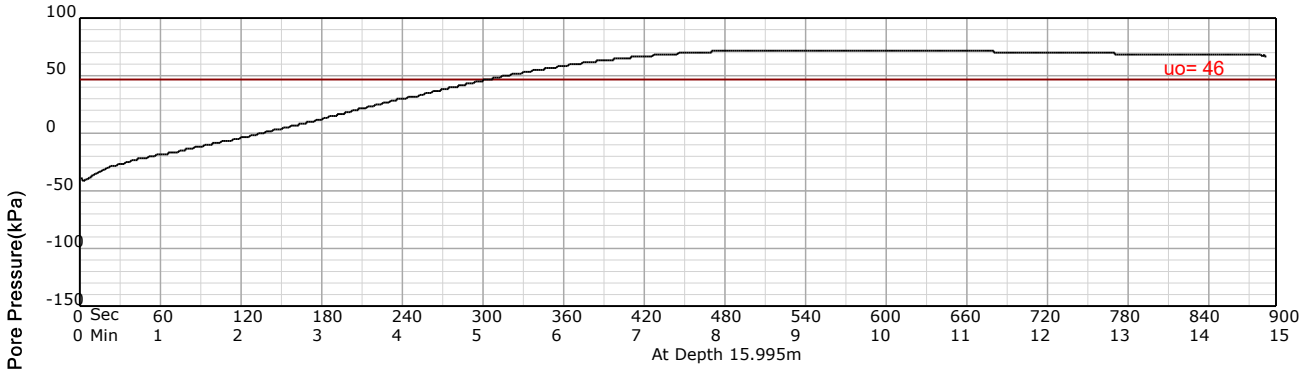

PIEZOCONE PENETRATION TEST

Dissipation Tests

HOLE: C6

PROJECT: 2024 Jagersfontein

SITE: TSF

DATE: 24/02/03 At: 07:29:54 A

DEPTH: 21.303

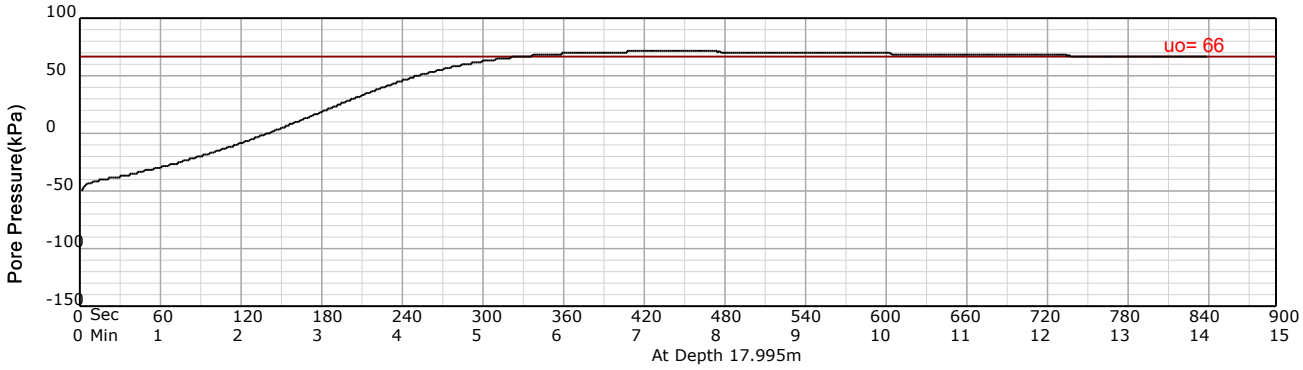

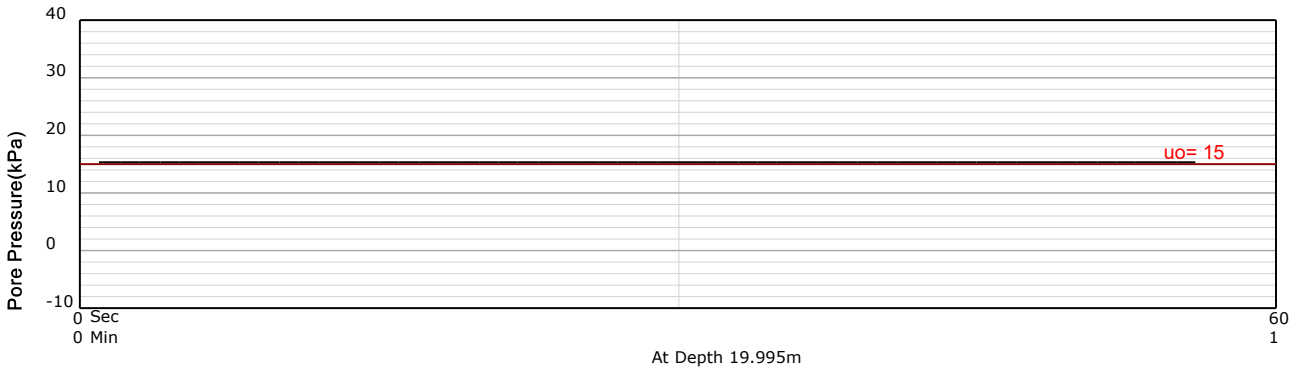

PIEZOCONE PENETRATION TEST

Equivalent Soil Behaviour Type Profile

HOLE: C6

PROJECT: 2024 Jagersfontein

SITE: TSF

DATE: 24/02/03 At: 07:29:54 A

DEPTH: 21.303

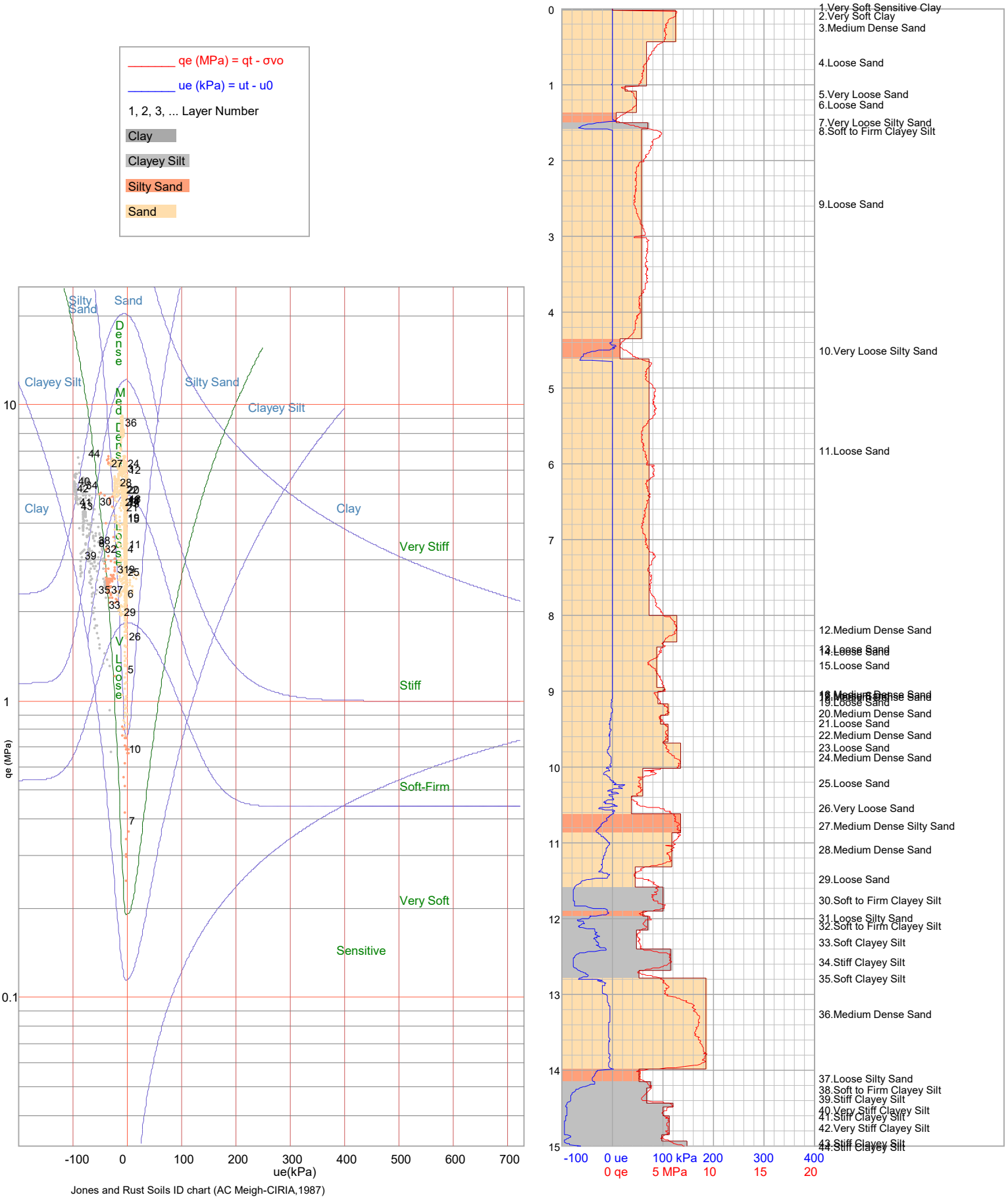

Jones and Rust Soils ID chart (AC Meigh-CIRIA,1987)

PIEZOCONE PENETRATION TEST

Equivalent Soil Behaviour Type Profile

HOLE: C6

PROJECT: 2024 Jagersfontein

SITE: TSF

DATE: 24/02/03 At: 07:29:54 A

DEPTH: 21.303

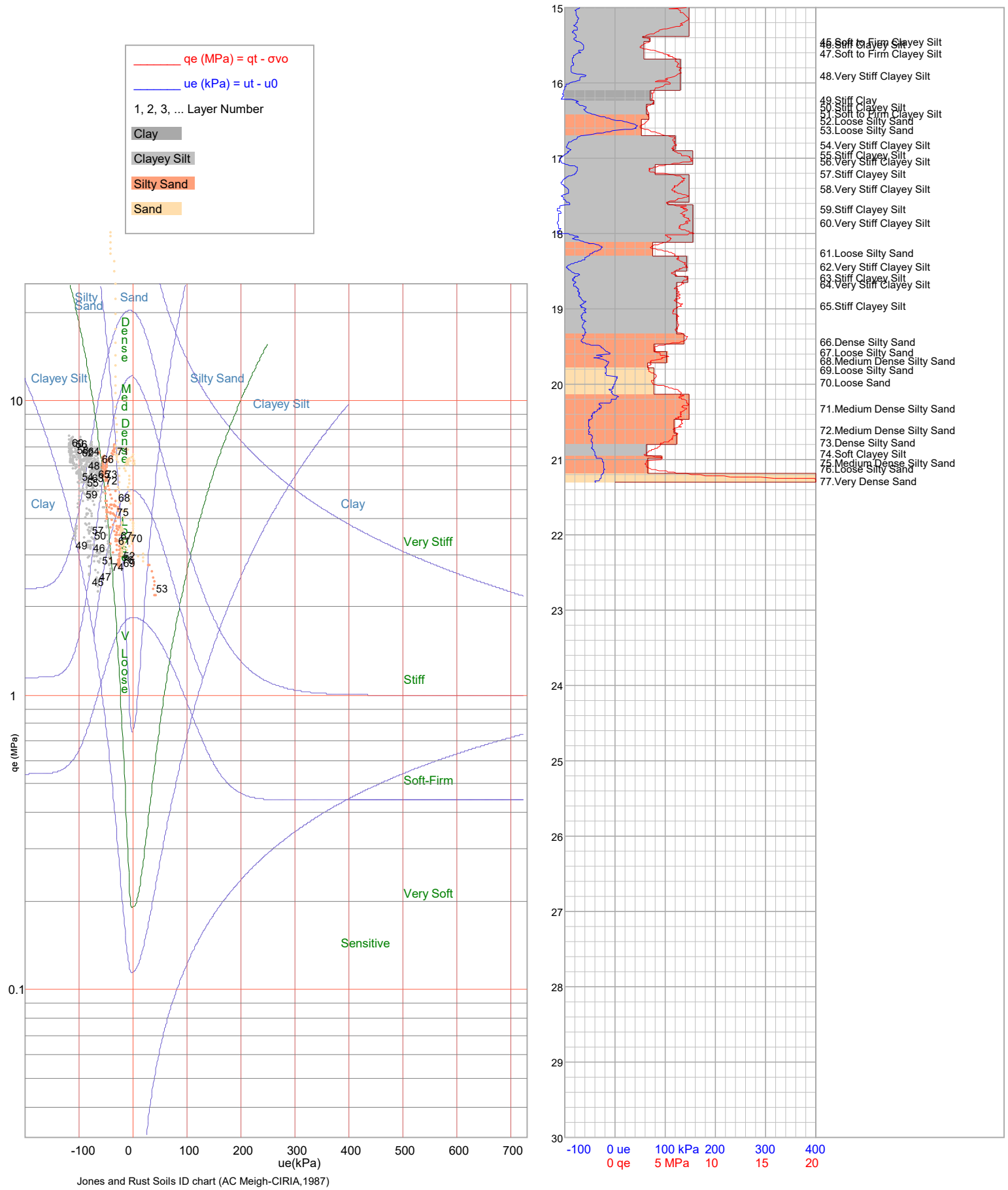

Jones and Rust Soils ID chart (AC Meigh-CIRIA,1987)

PIEZOCONE PENETRATION TEST

Recorded Field Results (Cone, Pore Pressure and Static Pore Pressure from Dissipations)

HOLE: C7

PROJECT: 2024 Jagersfontein

SITE: TSF

DATE: 24/02/01 At: 13:12:10 A **DEPTH:** 7.603

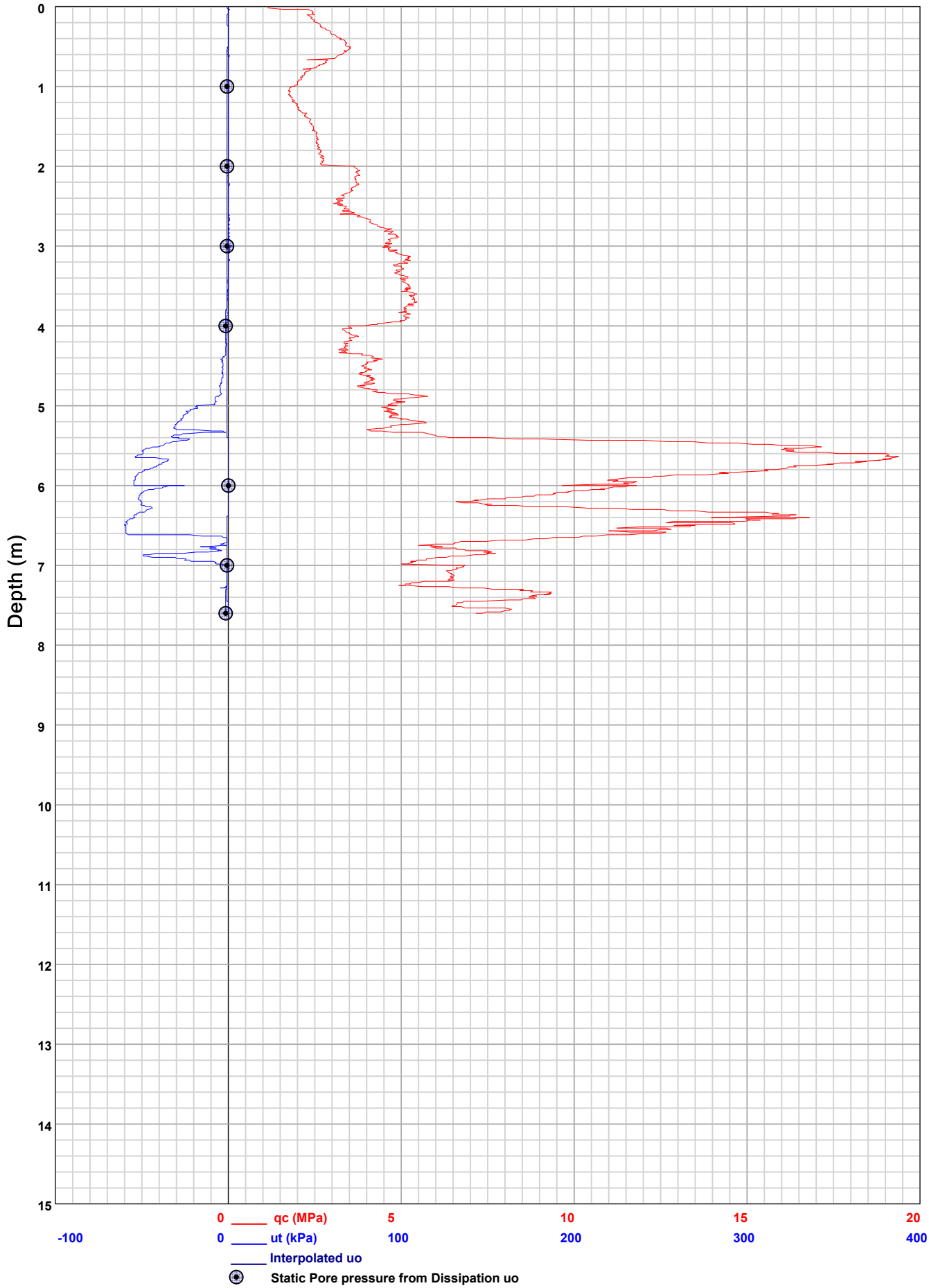

PIEZOCONE PENETRATION TEST

HOLE: C7

PROJECT: 2024 Jagersfontein

SITE: TSF

DATE: 24/02/01 At: 13:12:10 A

DEPTH: 7.603

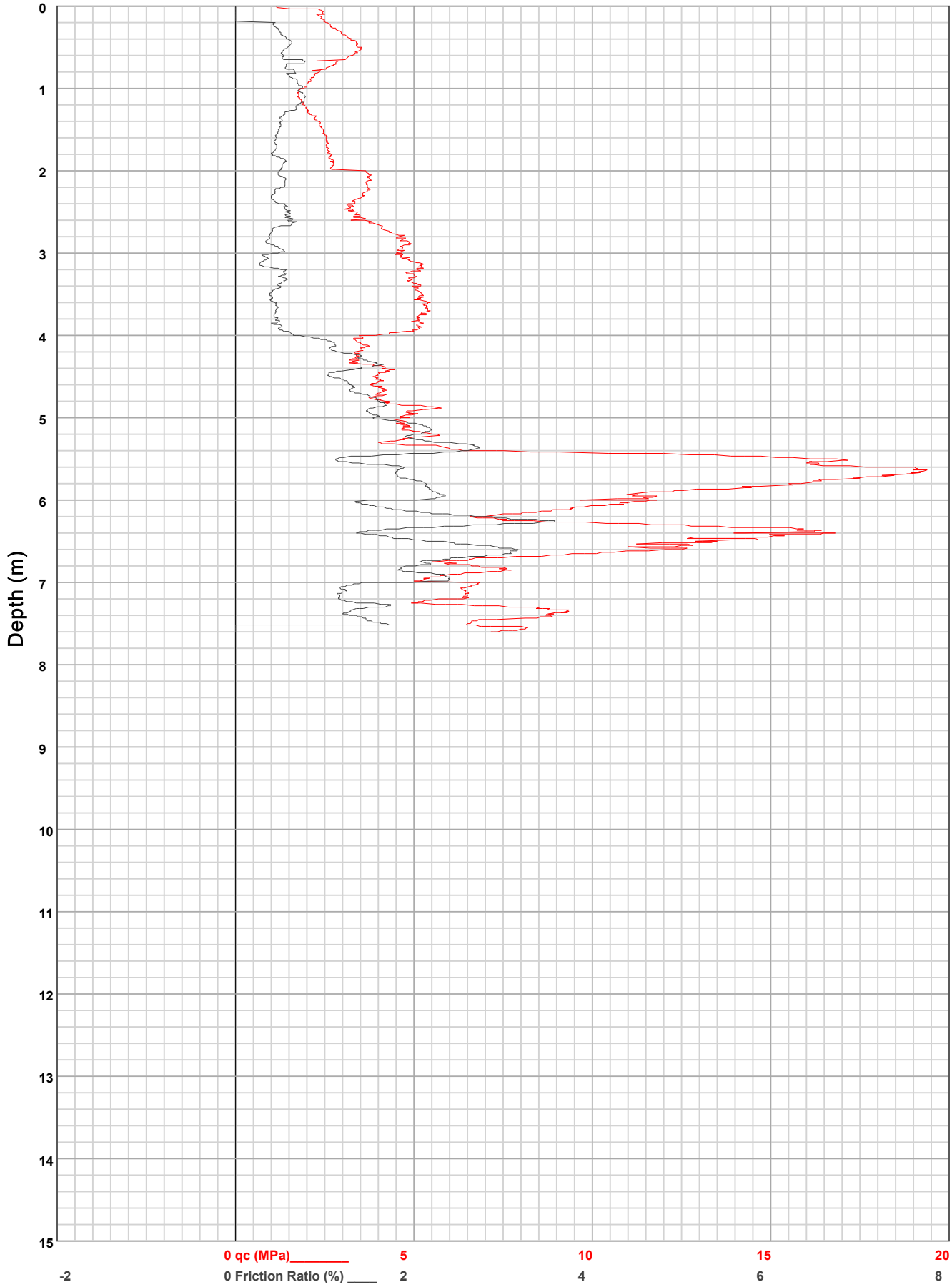

PIEZOCONE PENETRATION TEST

Dissipation Tests

HOLE: C7

PROJECT: 2024 Jagersfontein

SITE: TSF

DATE: 24/02/01 At: 13:12:10 A

DEPTH: 7.603

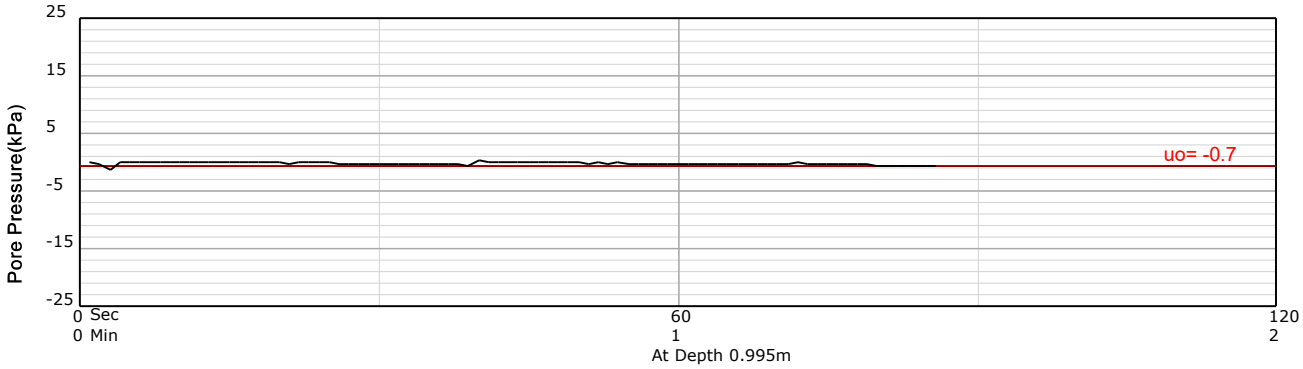

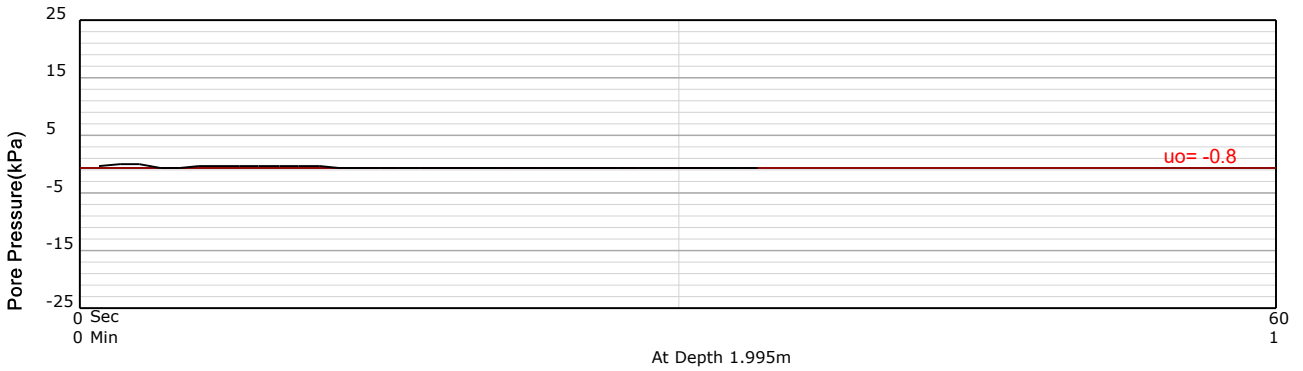

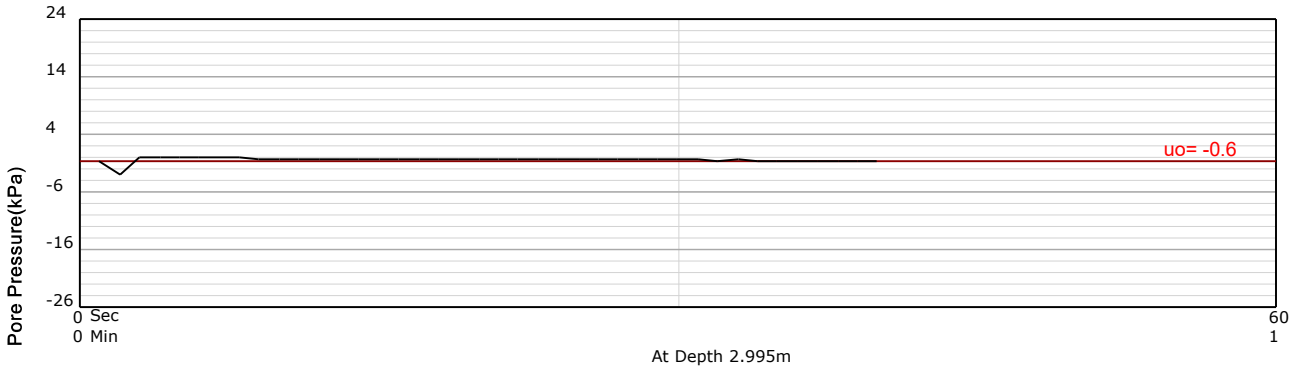

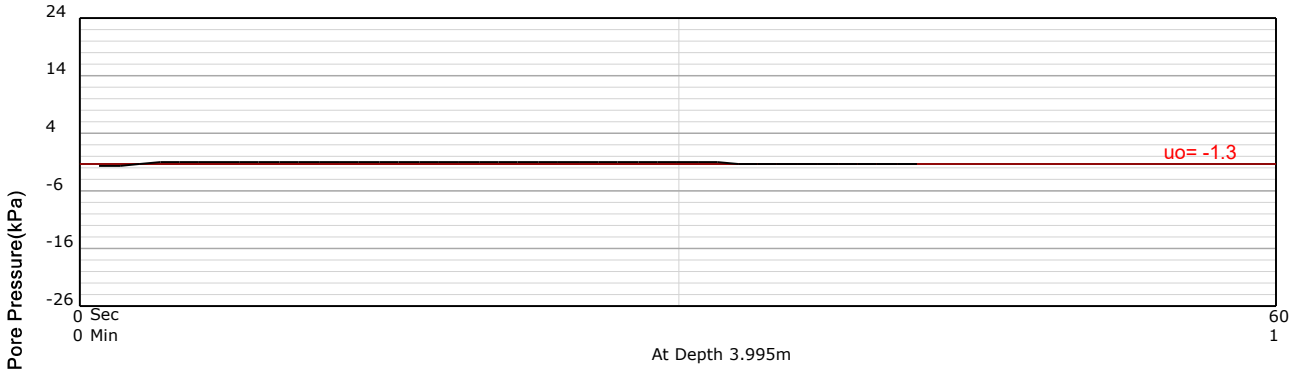

PIEZOCONE PENETRATION TEST

Dissipation Tests

HOLE: C7

PROJECT: 2024 Jagersfontein

SITE: TSF

DATE: 24/02/01 At: 13:12:10 A

DEPTH: 7.603

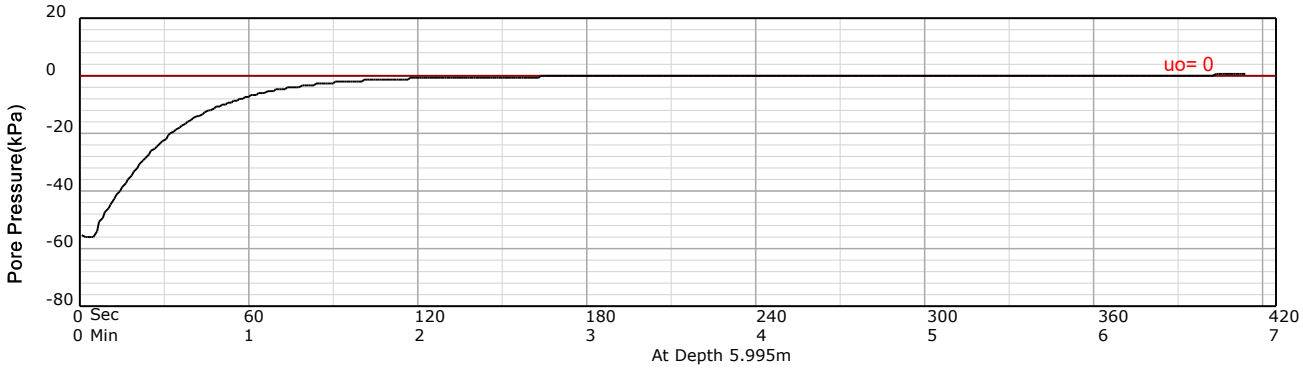

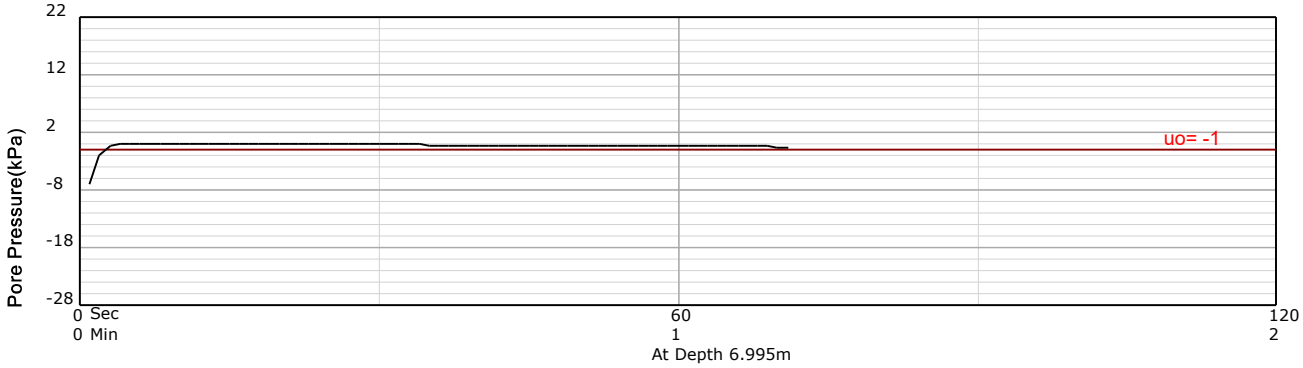

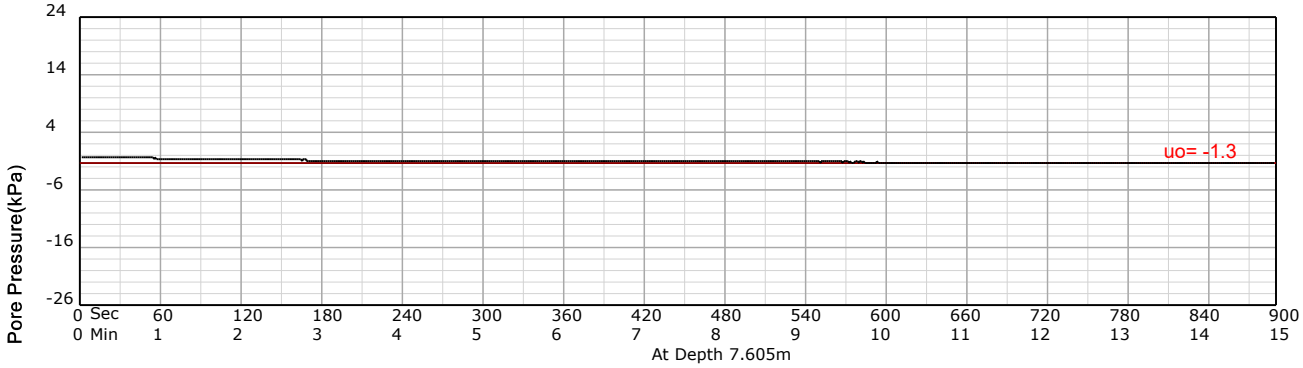

PIEZOCONE PENETRATION TEST

Equivalent Soil Behaviour Type Profile

HOLE: C7

PROJECT: 2024 Jagersfontein

SITE: TSF

DATE: 24/02/01 At: 13:12:10 A

DEPTH: 7.603

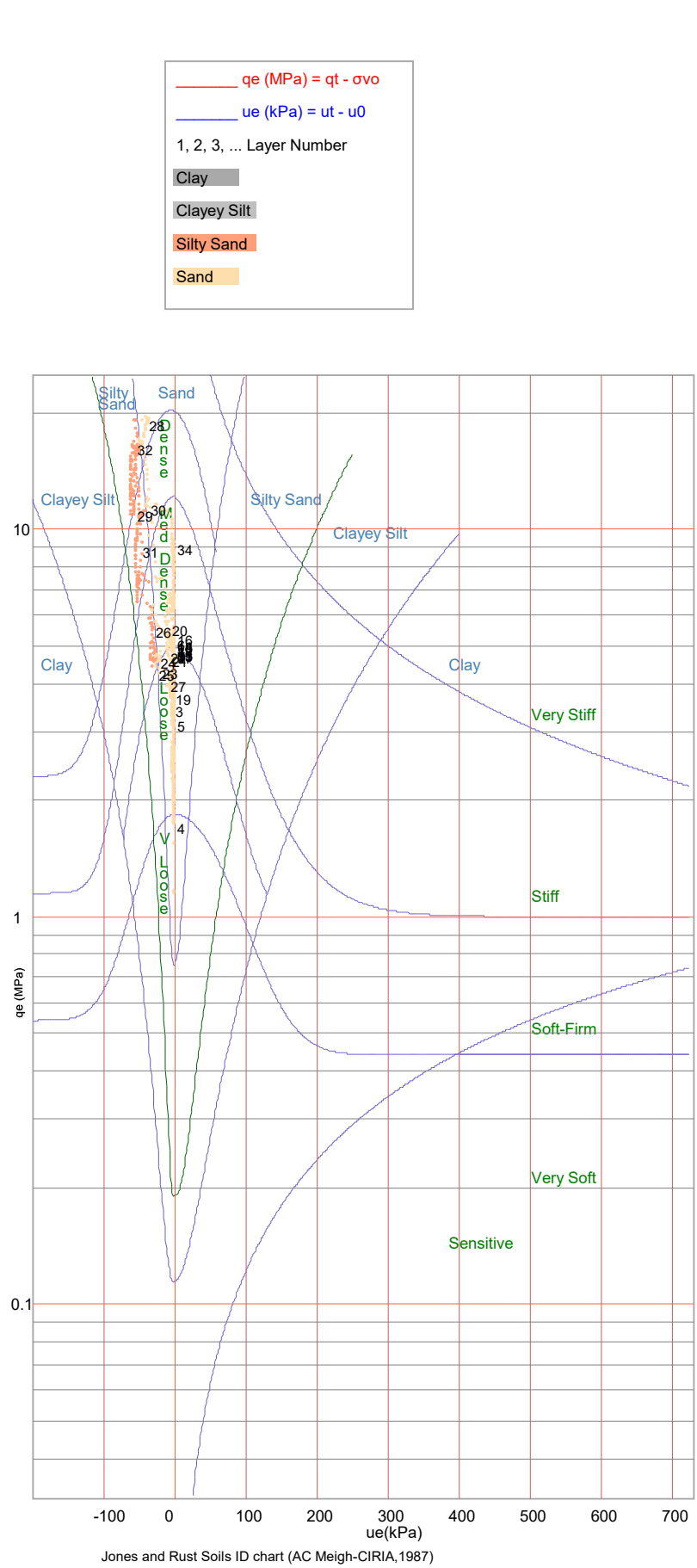

Jones and Rust Soils ID chart (AC Meigh-CIRIA,1987)

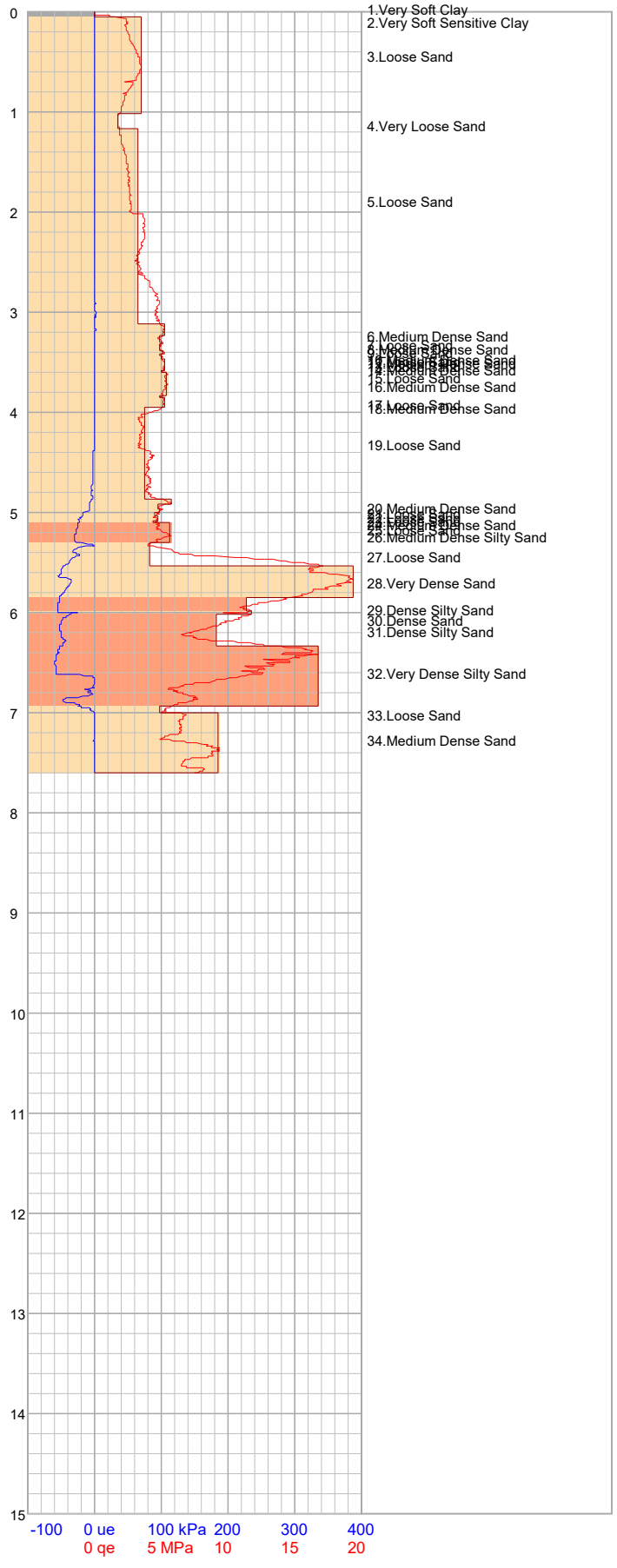

PIEZOCONE PENETRATION TEST

Recorded Field Results (Cone, Pore Pressure and Static Pore Pressure from Dissipations)

HOLE: C8

PROJECT: 2024 Jagersfontein

SITE: TSF

DATE: 24/02/02 At: 07:40:29 A **DEPTH:** 25.901

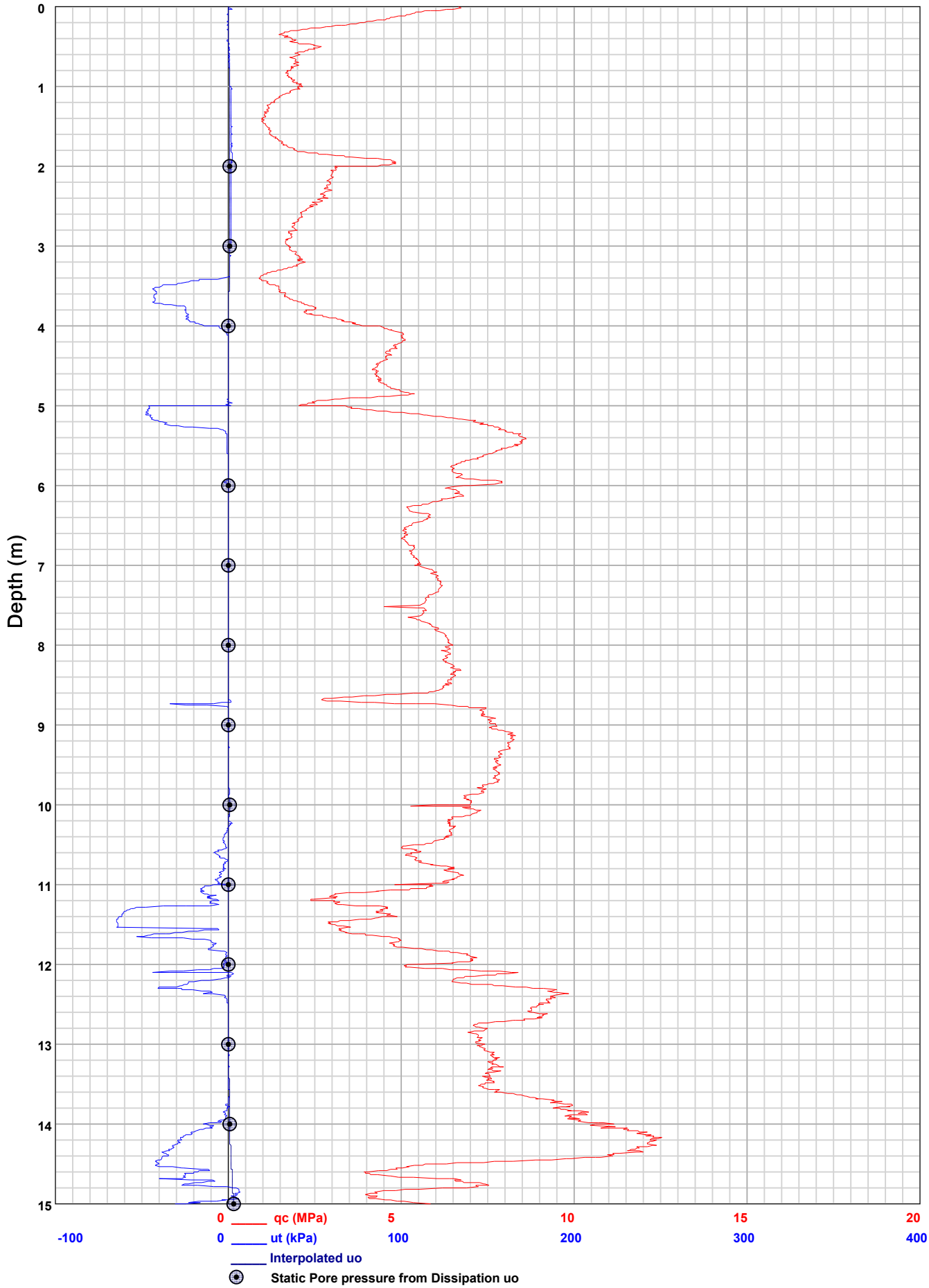

PIEZOCONE PENETRATION TEST

Recorded Field Results (Cone, Pore Pressure and Static Pore Pressure from Dissipations)

HOLE: C8

PROJECT: 2024 Jagersfontein

SITE: TSF

DATE: 24/02/02 At: 07:40:29 A **DEPTH:** 25.901

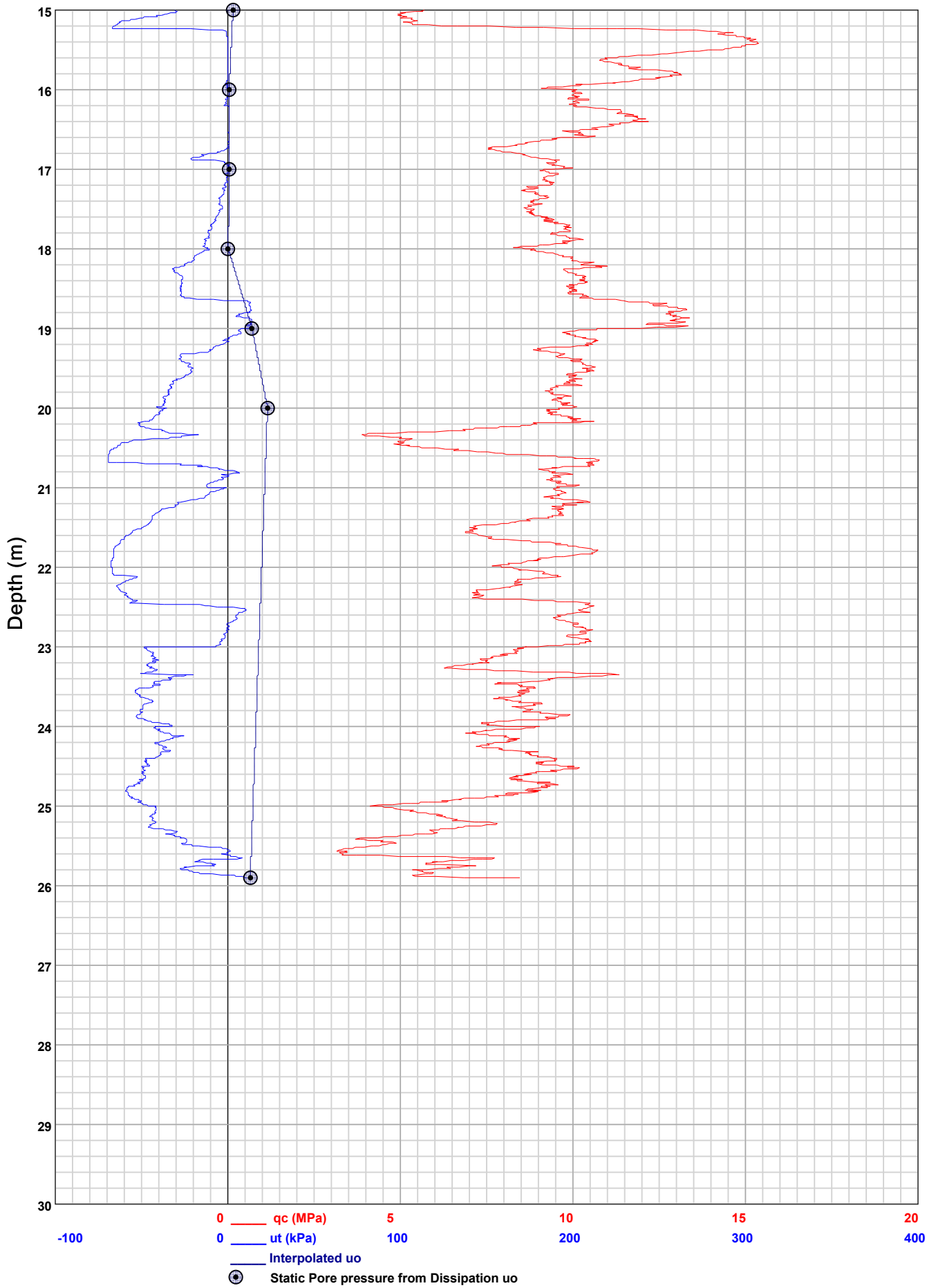

PIEZOCONE PENETRATION TEST

HOLE: C8

PROJECT: 2024 Jagersfontein

SITE: TSF

DATE: 24/02/02 At: 07:40:29 A

DEPTH: 25.901

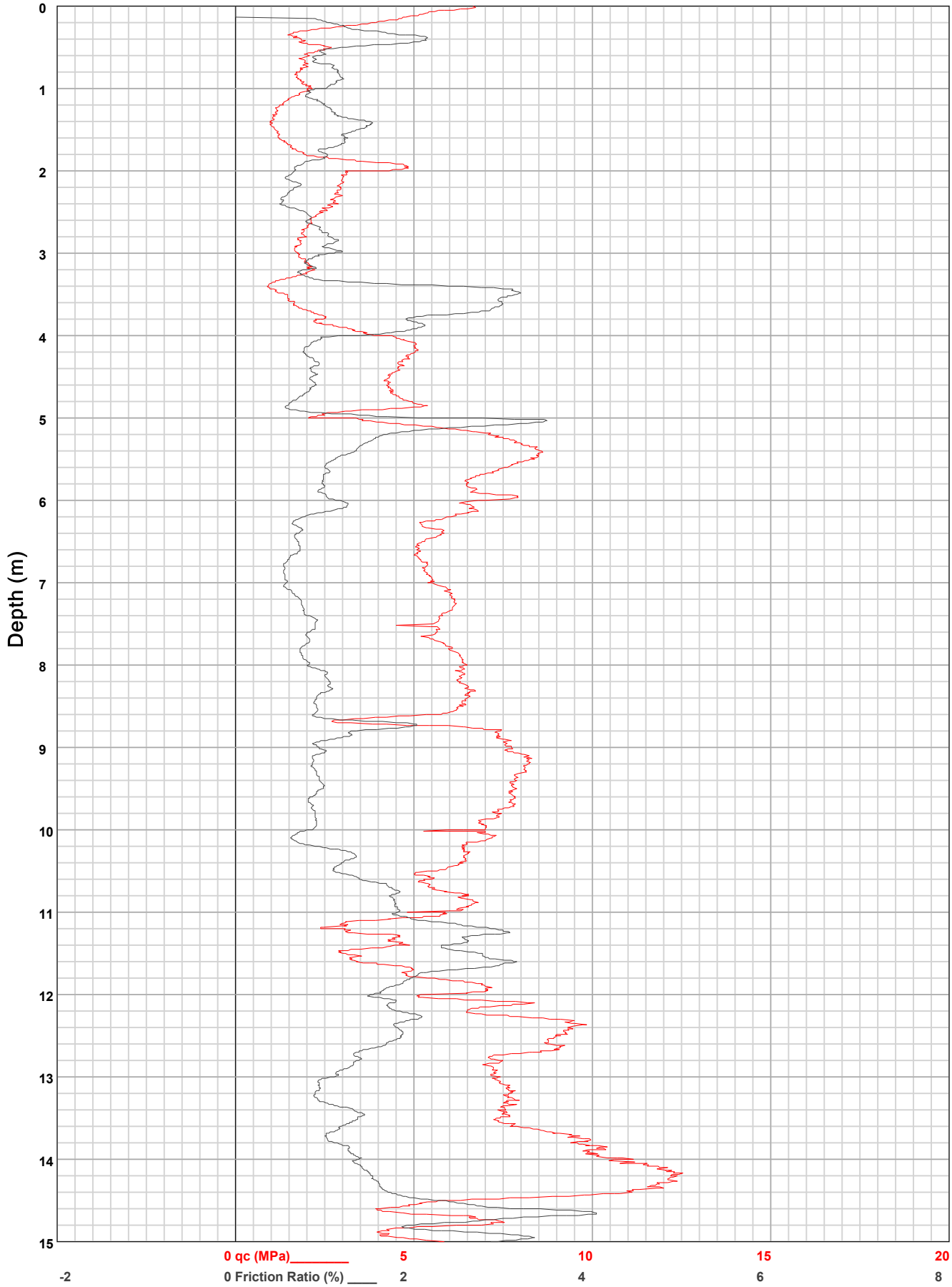

PIEZOCONE PENETRATION TEST

HOLE: C8

PROJECT: 2024 Jagersfontein

SITE: TSF

DATE: 24/02/02 At: 07:40:29 A

DEPTH: 25.901

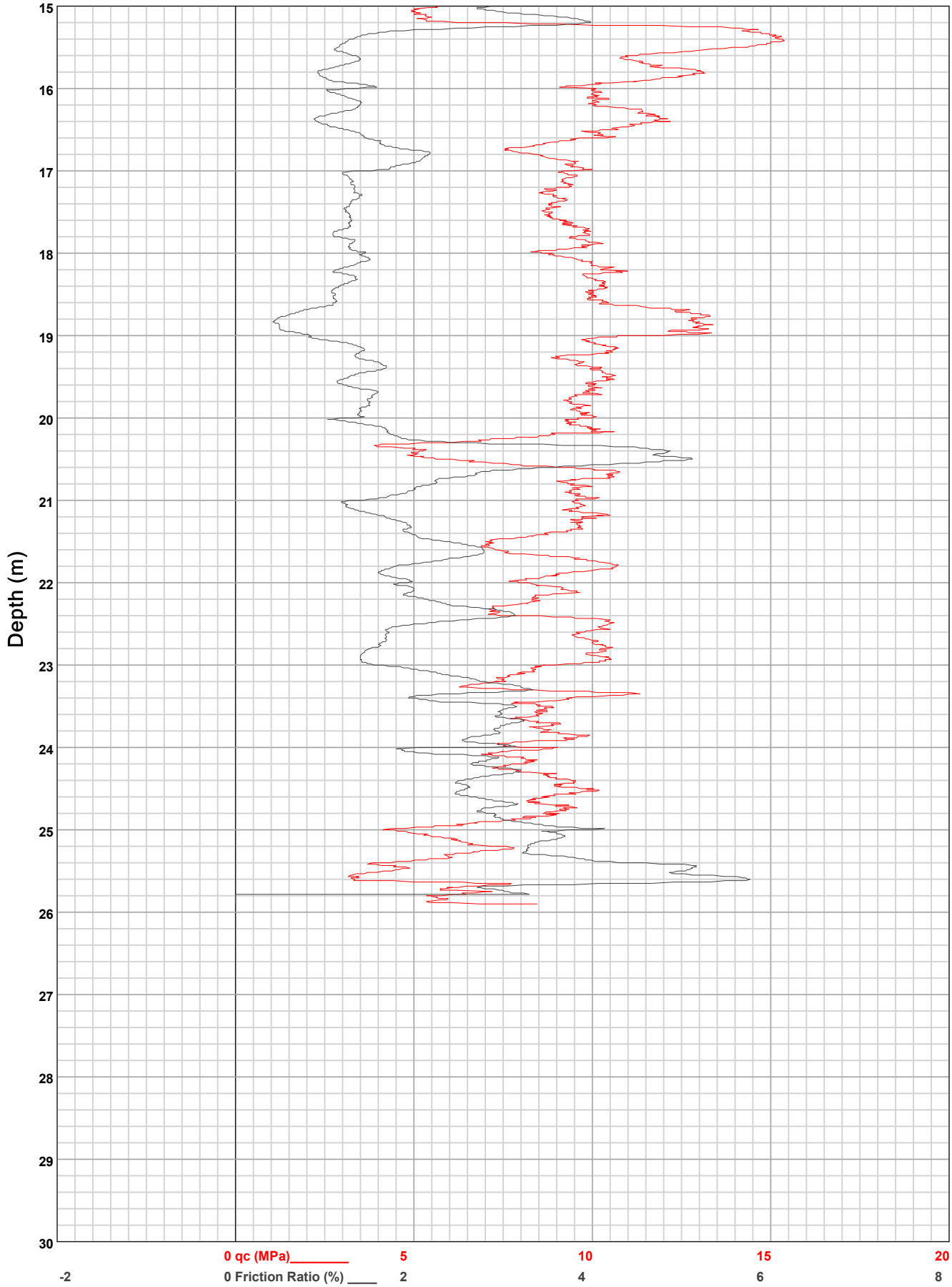

PIEZOCONE PENETRATION TEST

Dissipation Tests

HOLE: C8

PROJECT: 2024 Jagersfontein

SITE: TSF

DATE: 24/02/02 At: 07:40:29 A

DEPTH: 25.901

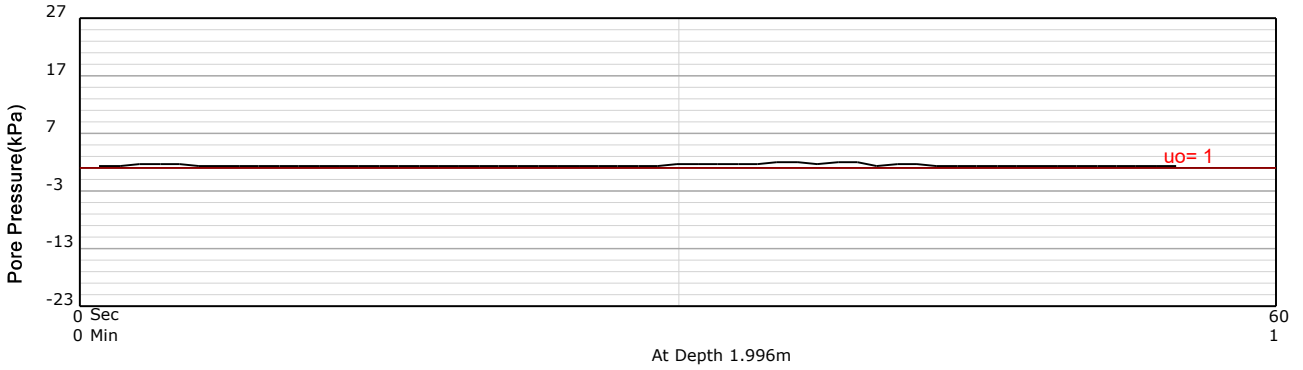

At Depth 1.996m

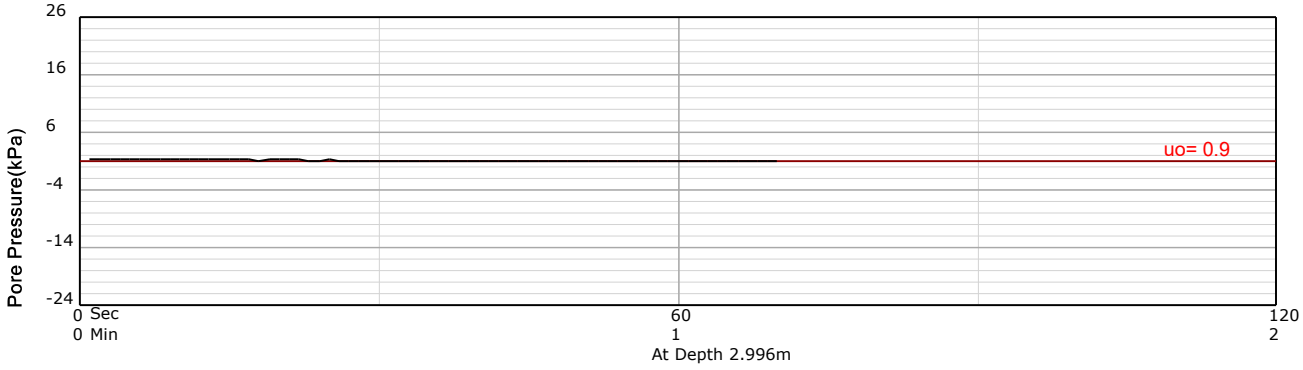

At Depth 2.996m

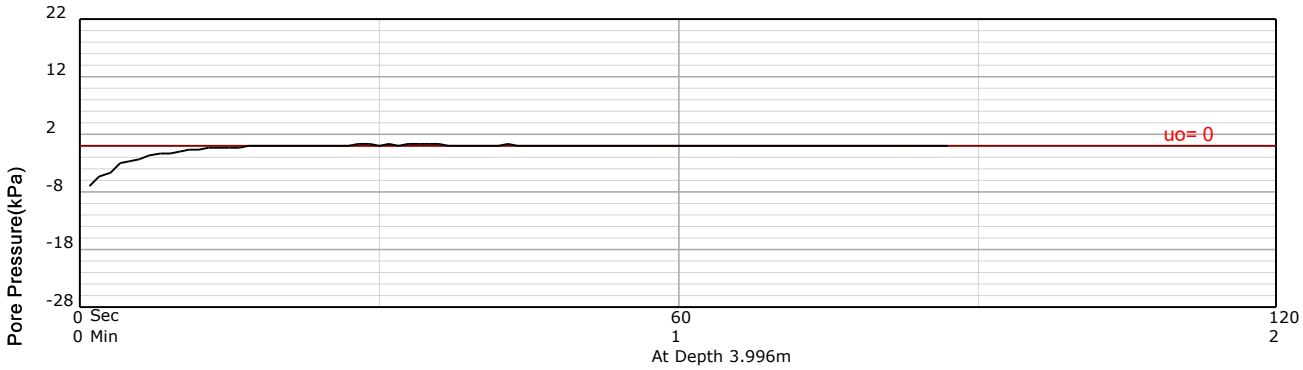

At Depth 3.996m

At Depth 5.996m

PIEZOCONE PENETRATION TEST

Dissipation Tests

HOLE: C8

PROJECT: 2024 Jagersfontein

SITE: TSF

DATE: 24/02/02 At: 07:40:29 A **DEPTH:** 25.901

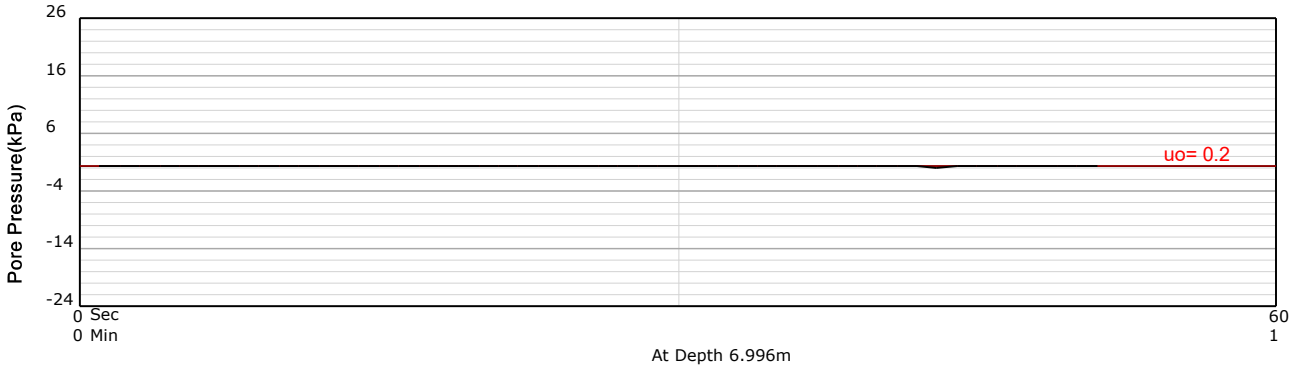

At Depth 6.996m

At Depth 7.996m

At Depth 8.996m

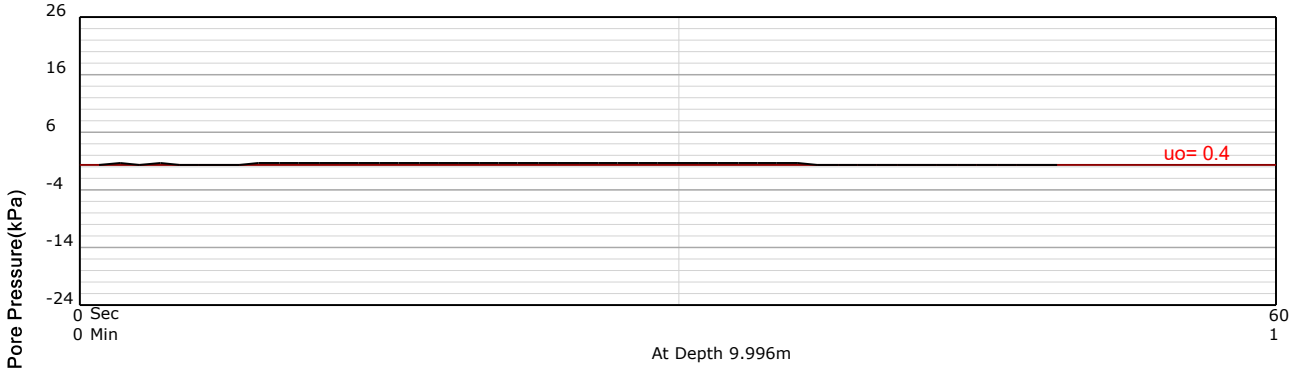

At Depth 9.996m

PIEZOCONE PENETRATION TEST

Dissipation Tests

HOLE: C8

PROJECT: 2024 Jagersfontein

SITE: TSF

DATE: 24/02/02 At: 07:40:29 A

DEPTH: 25.901

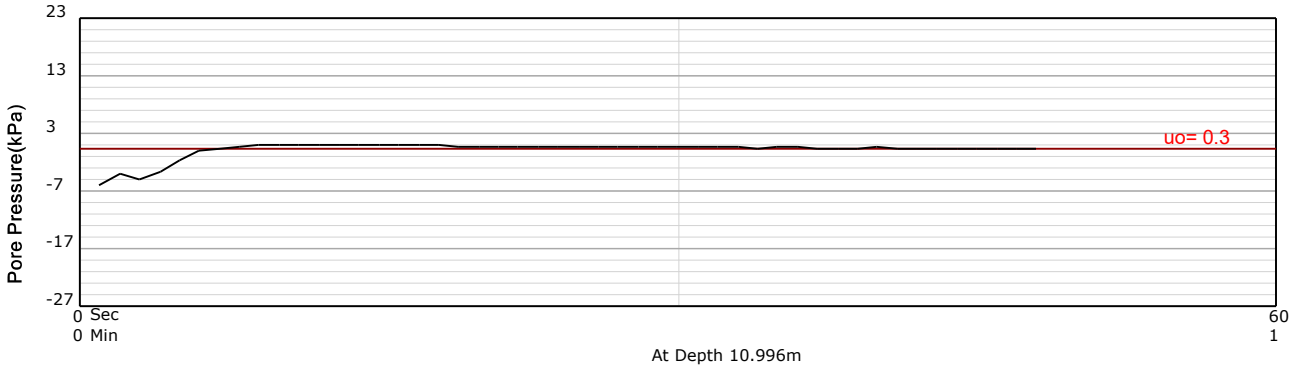

At Depth 10.996m

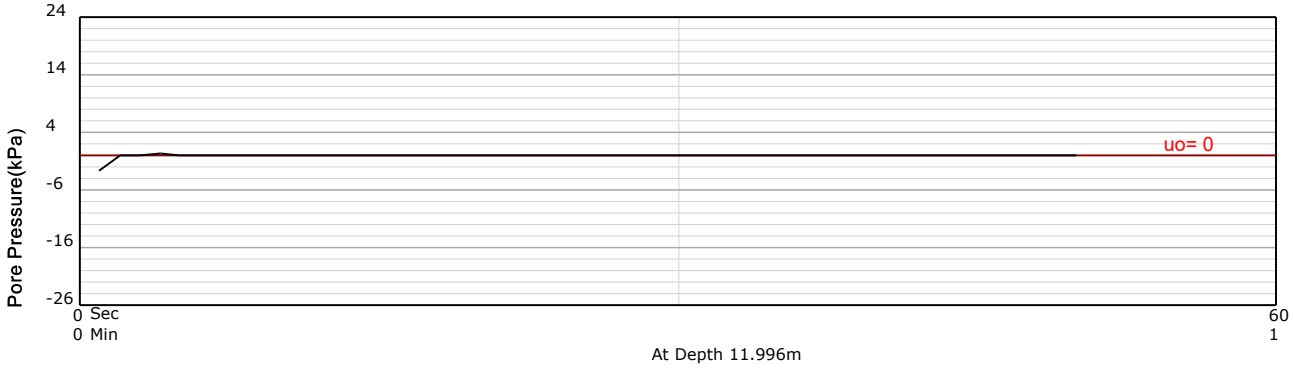

At Depth 11.996m

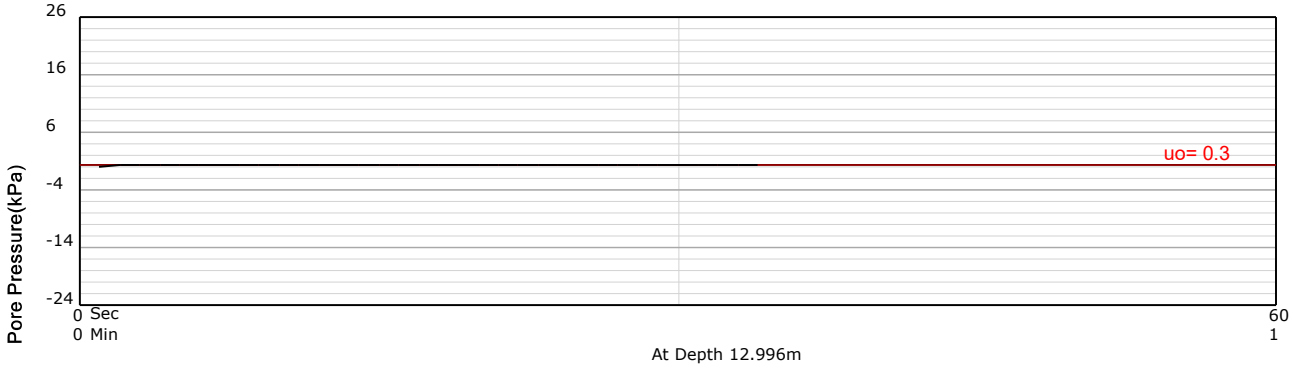

At Depth 12.996m

At Depth 13.996m

PIEZOCONE PENETRATION TEST

Dissipation Tests

HOLE: C8

PROJECT: 2024 Jagersfontein

SITE: TSF

DATE: 24/02/02 At: 07:40:29 A

DEPTH: 25.901

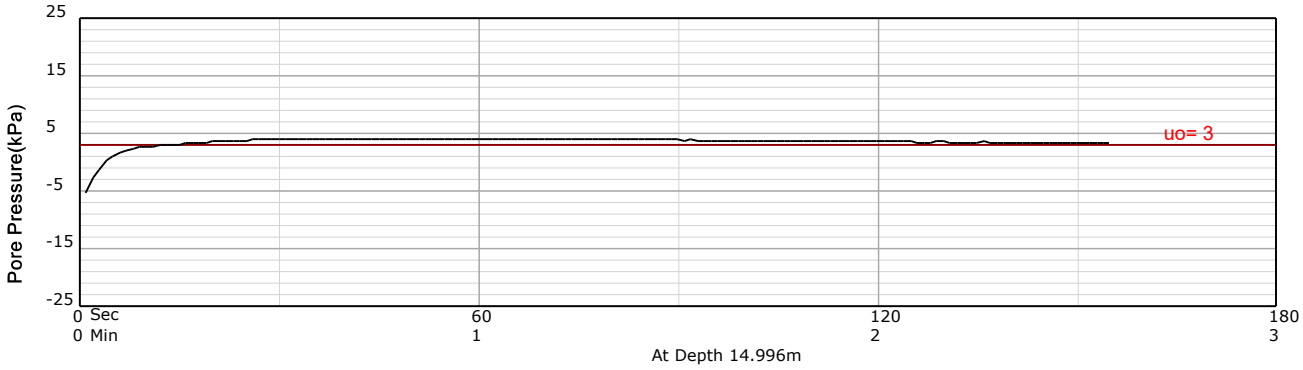

At Depth 14.996m

At Depth 15.996m

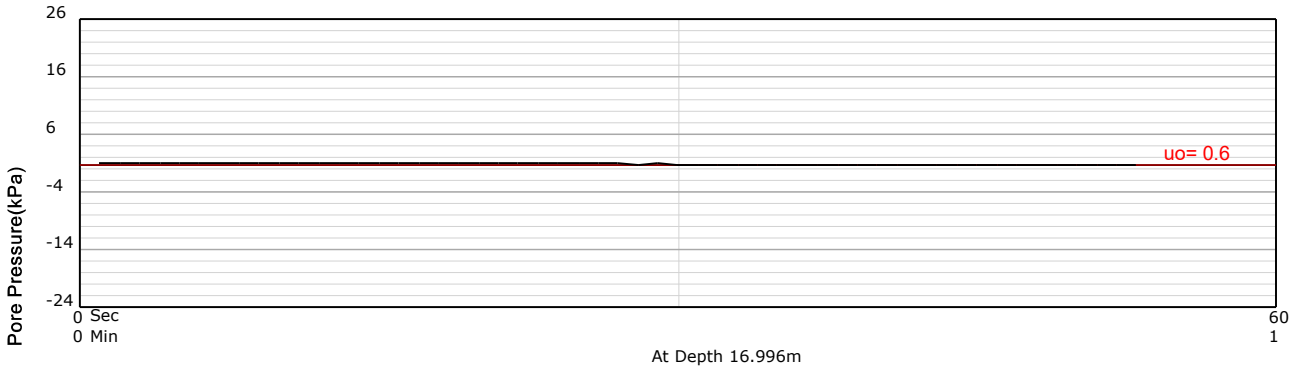

At Depth 16.996m

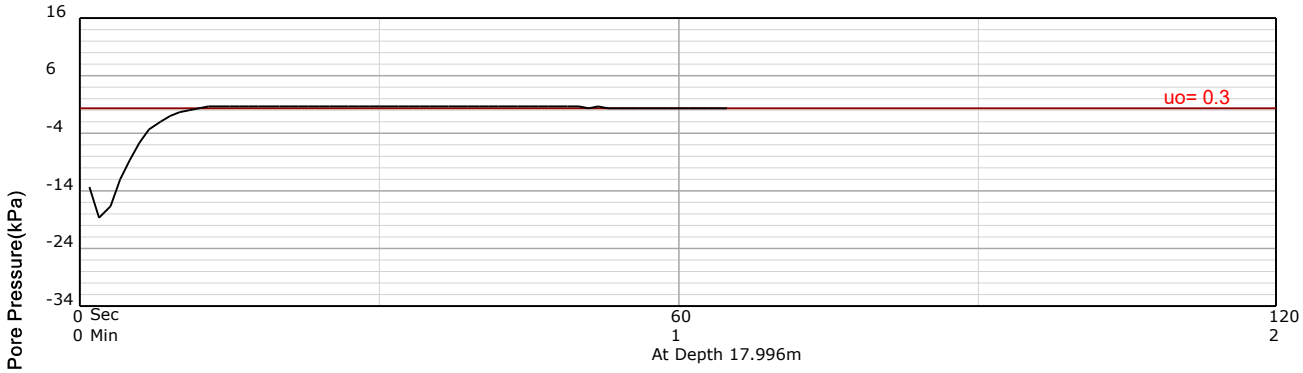

At Depth 17.996m

PIEZOCONE PENETRATION TEST

Dissipation Tests

HOLE: C8

PROJECT: 2024 Jagersfontein

SITE: TSF

DATE: 24/02/02 At: 07:40:29 A

DEPTH: 25.901

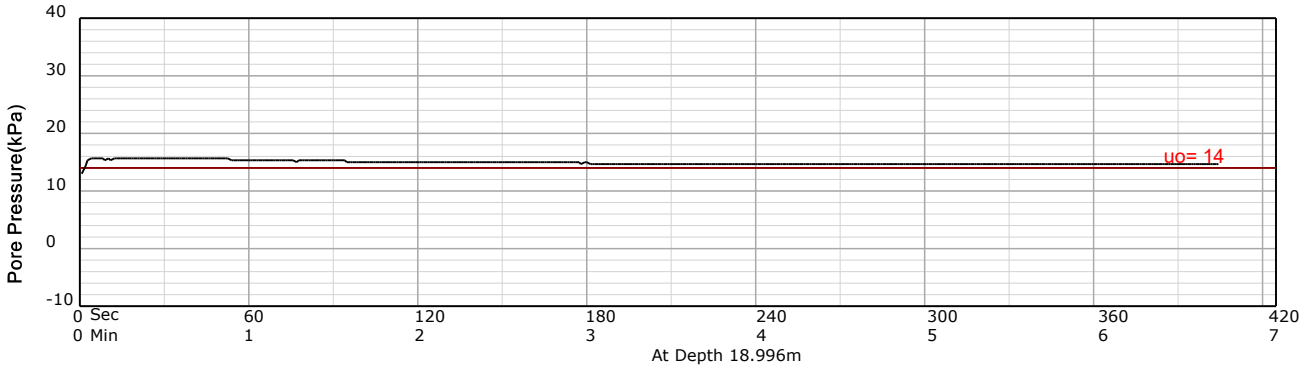

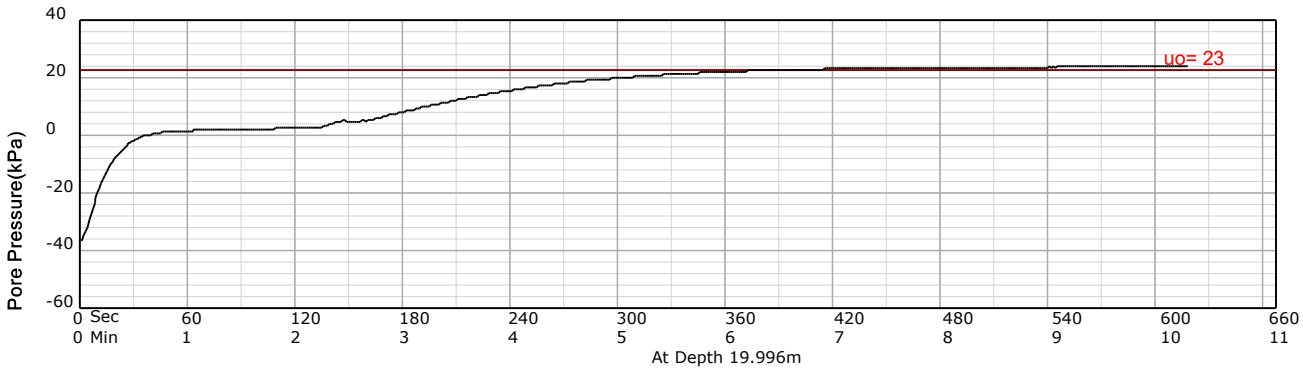

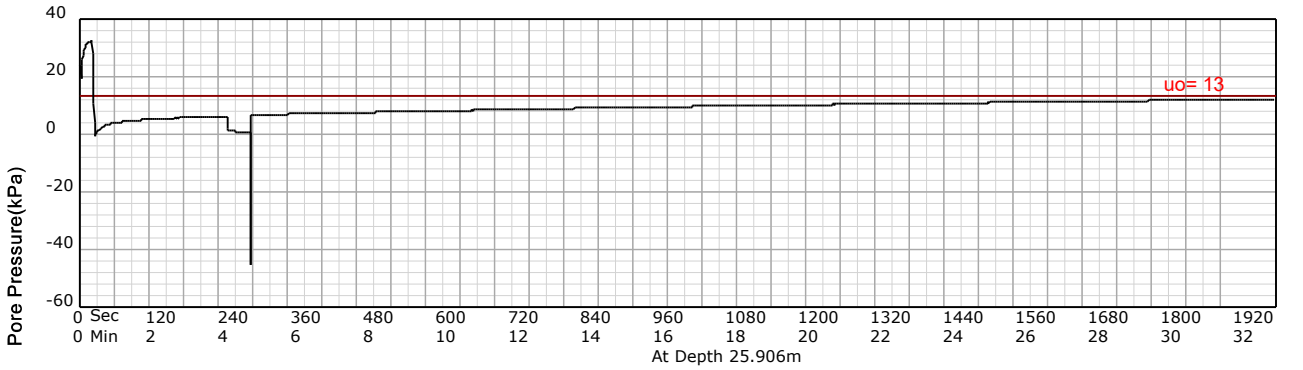

PIEZOCONE PENETRATION TEST

Equivalent Soil Behaviour Type Profile

HOLE: C8

PROJECT: 2024 Jagersfontein

SITE: TSF

DATE: 24/02/02 At: 07:40:29 A

DEPTH: 25.901

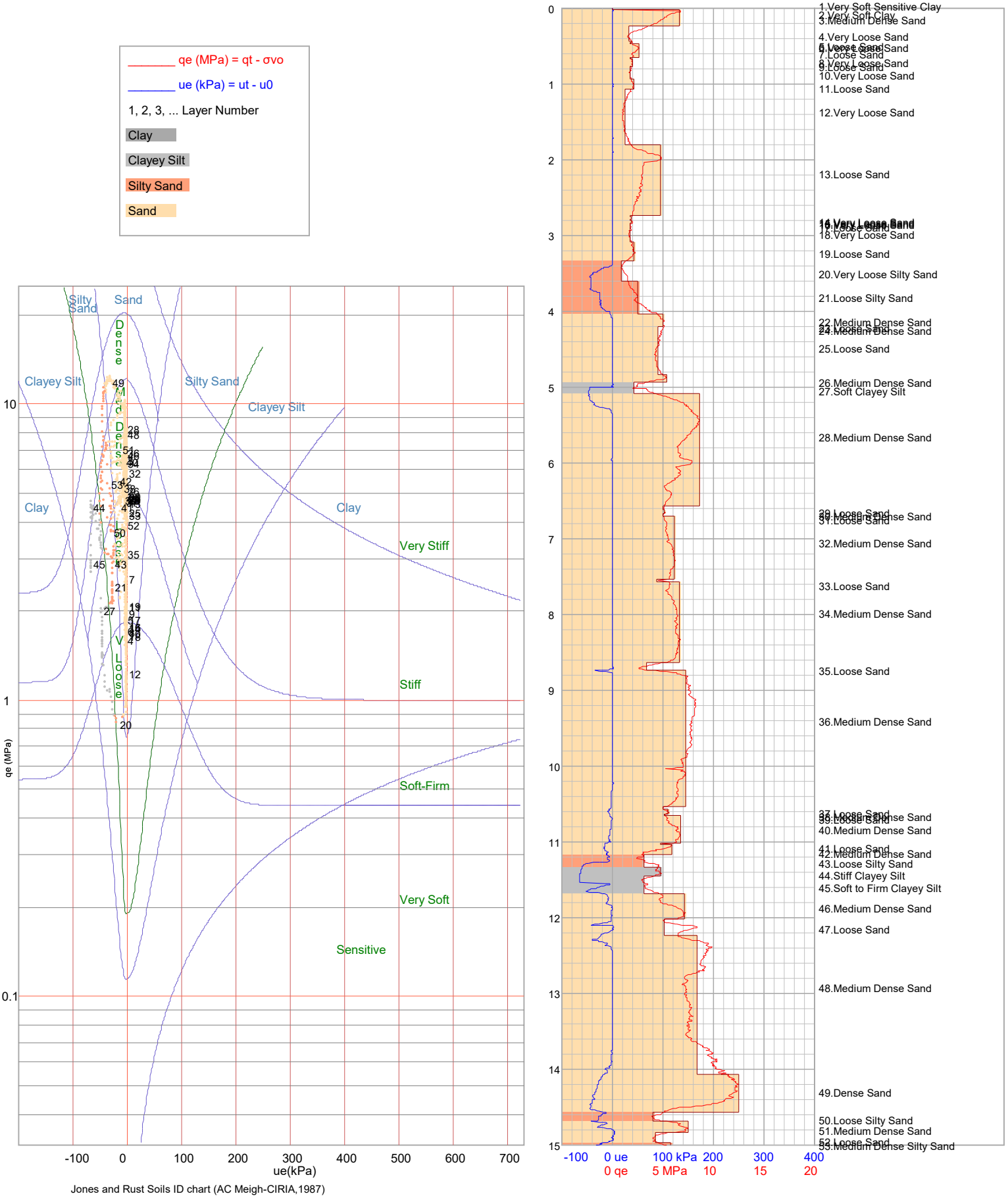

Jones and Rust Soils ID chart (AC Meigh-CIRIA,1987)

PIEZOCONE PENETRATION TEST

Equivalent Soil Behaviour Type Profile

HOLE: C8

PROJECT: 2024 Jagersfontein

SITE: TSF

DATE: 24/02/02 At: 07:40:29 A

DEPTH: 25.901

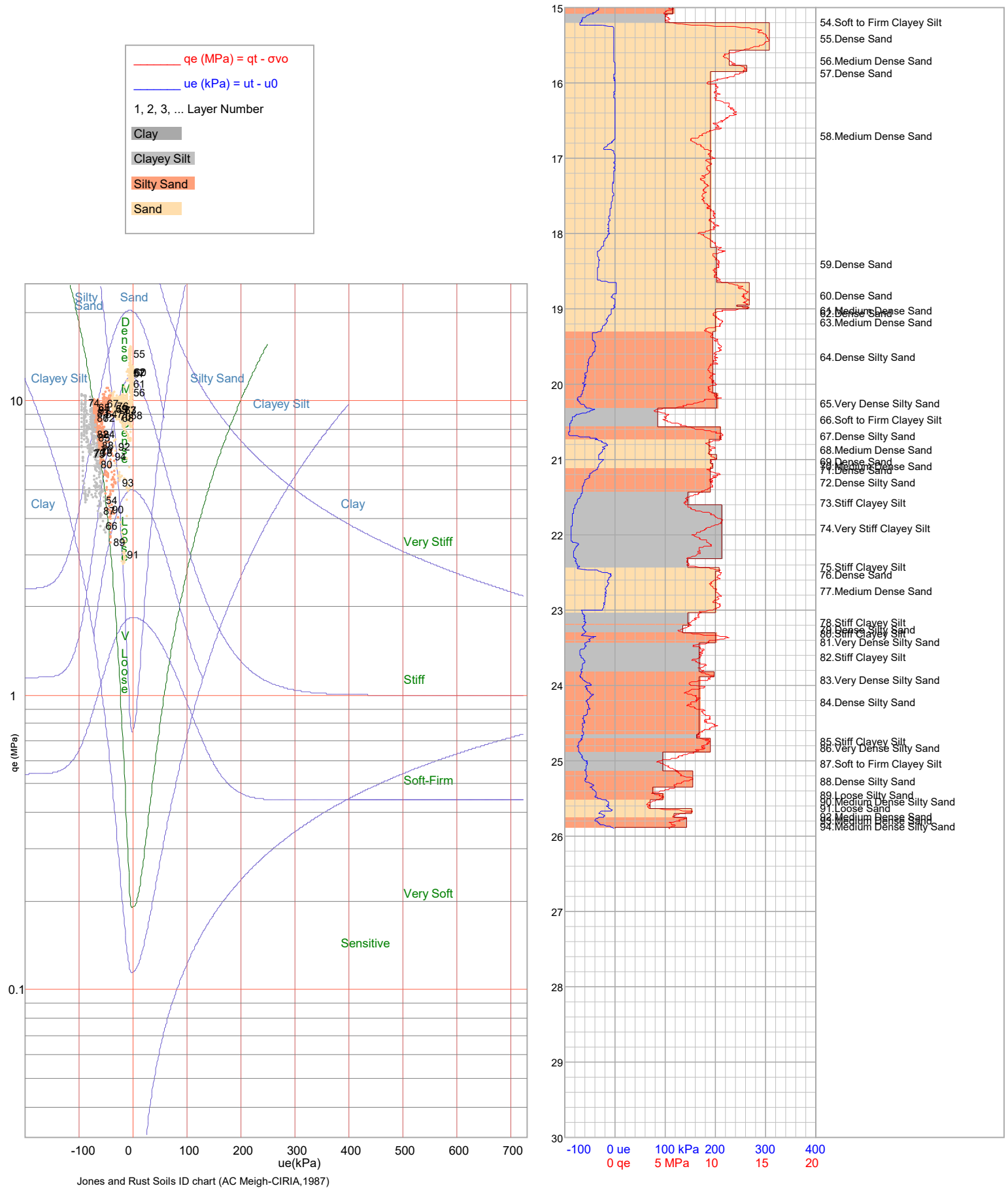

PIEZOCONE PENETRATION TEST

Recorded Field Results (Cone, Pore Pressure and Static Pore Pressure from Dissipations)

HOLE: C9

PROJECT: 2024 Jagersfontein

SITE: TSF

DATE: 24/02/04 At: 07:18:04 A **DEPTH:** 8.898

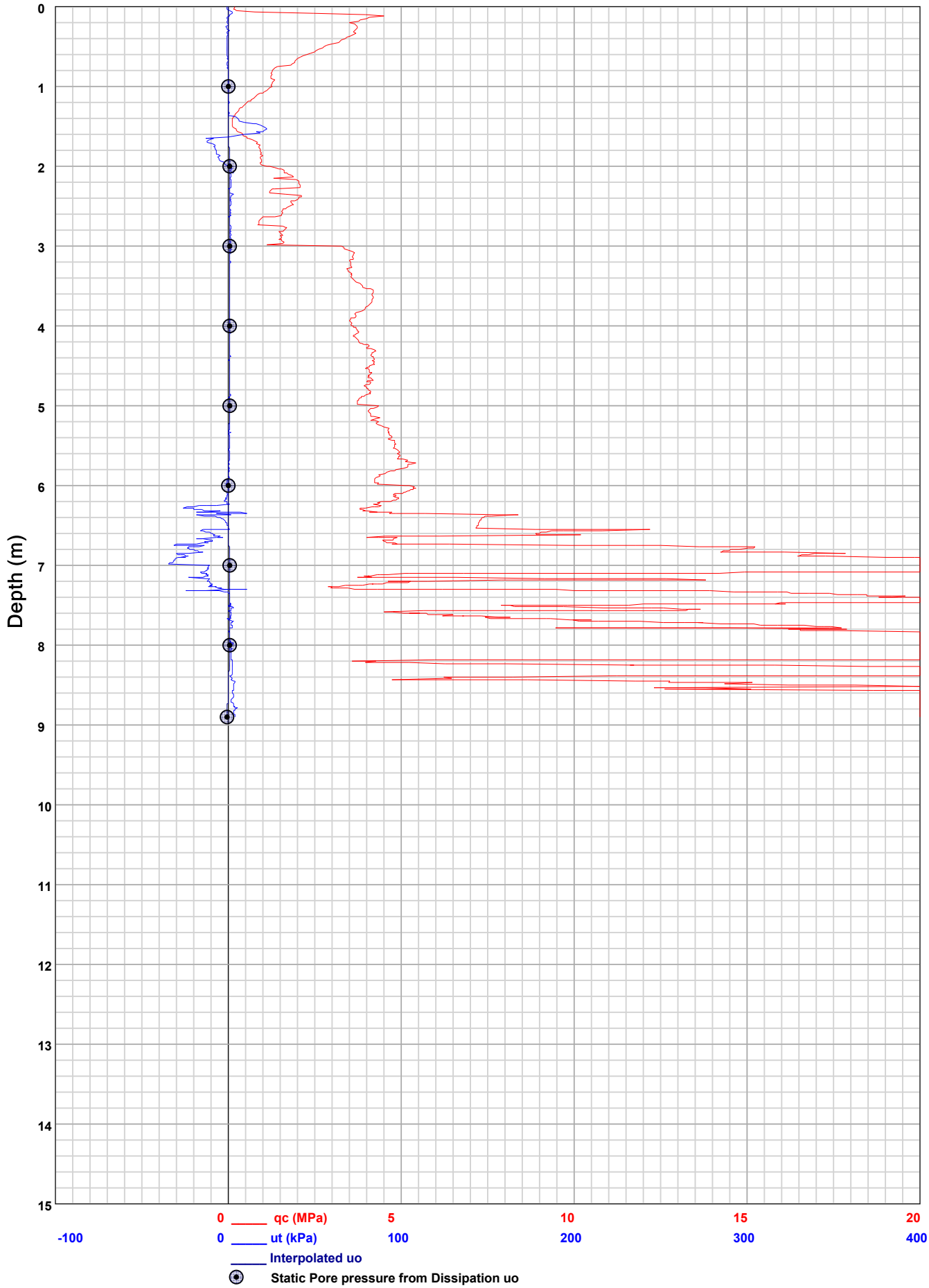

PIEZOCONE PENETRATION TEST

HOLE: C9

PROJECT: 2024 Jagersfontein

SITE: TSF

DATE: 24/02/04 At: 07:18:04 A

DEPTH: 8.898

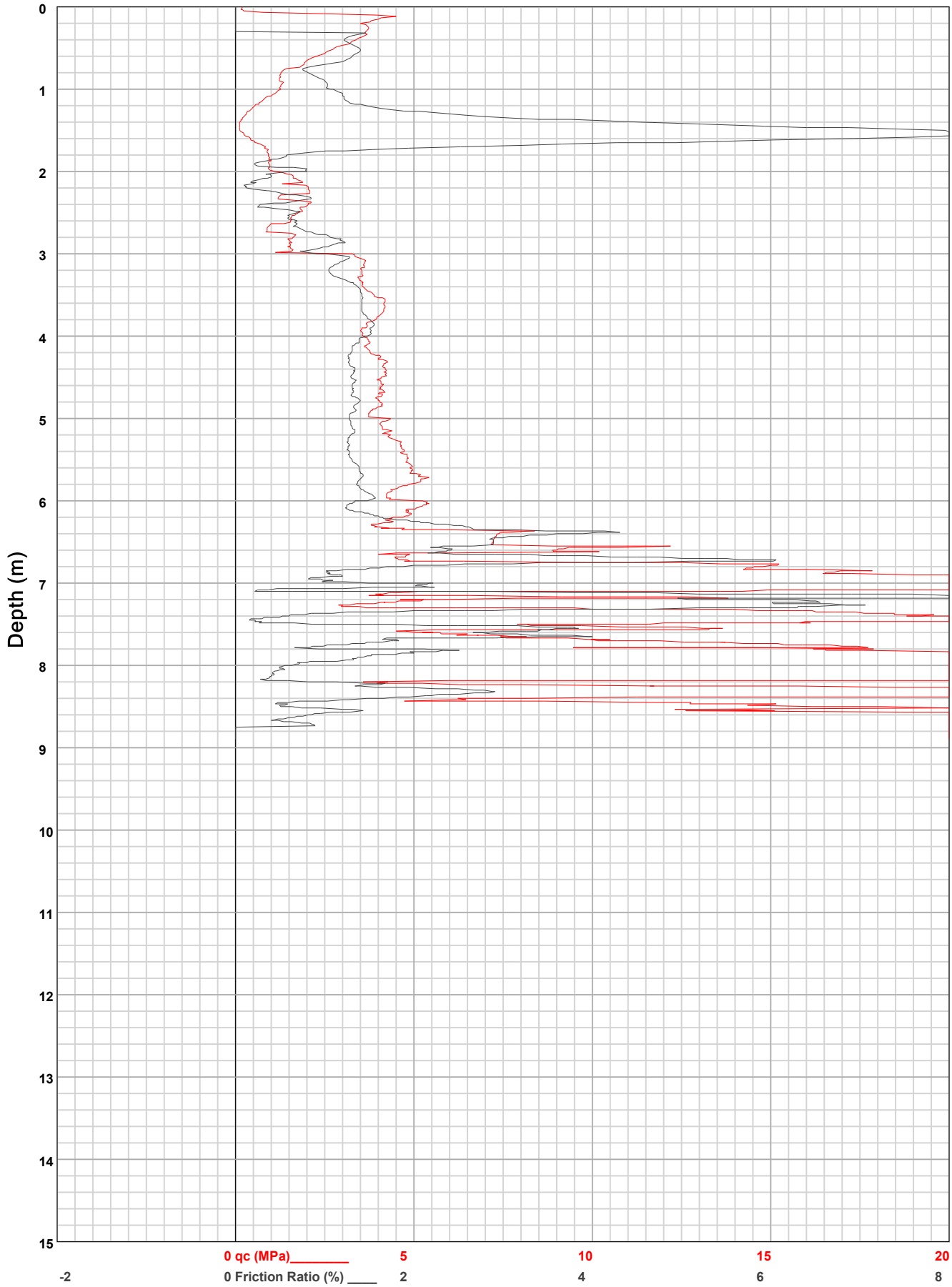

PIEZOCONE PENETRATION TEST

Dissipation Tests

HOLE: C9

PROJECT: 2024 Jagersfontein

SITE: TSF

DATE: 24/02/04 At: 07:18:04 A **DEPTH:** 8.898

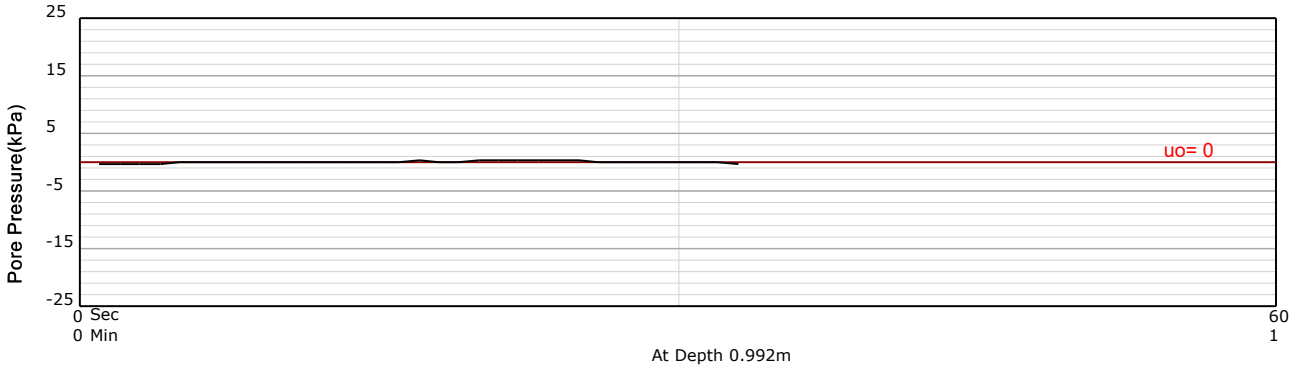

At Depth 0.992m

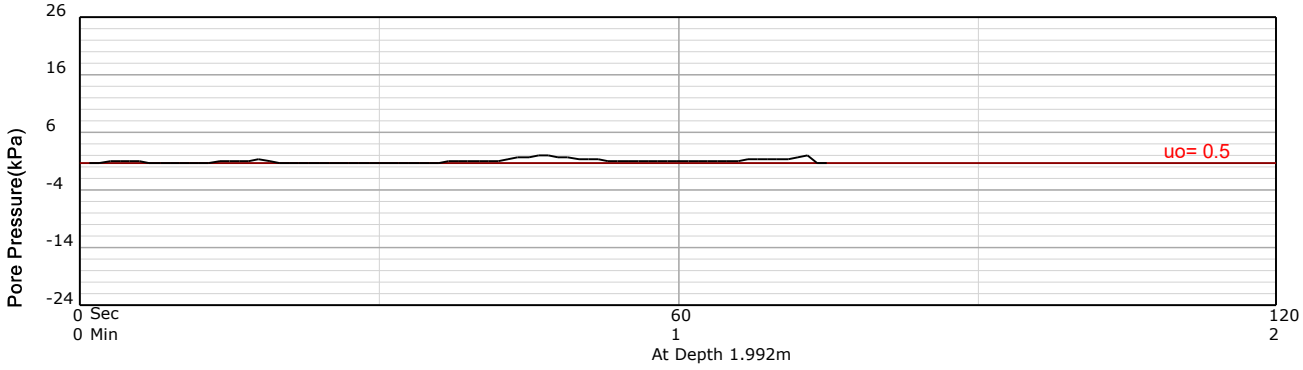

At Depth 1.992m

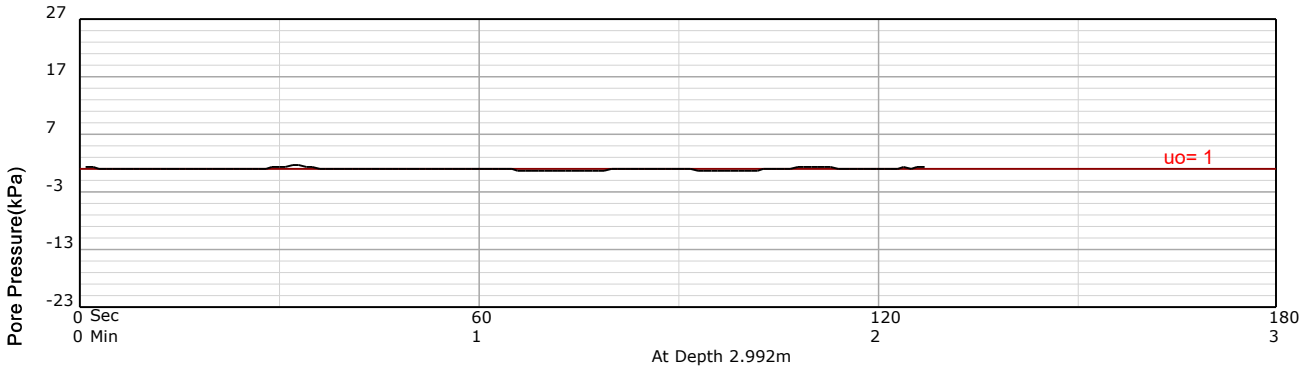

At Depth 2.992m

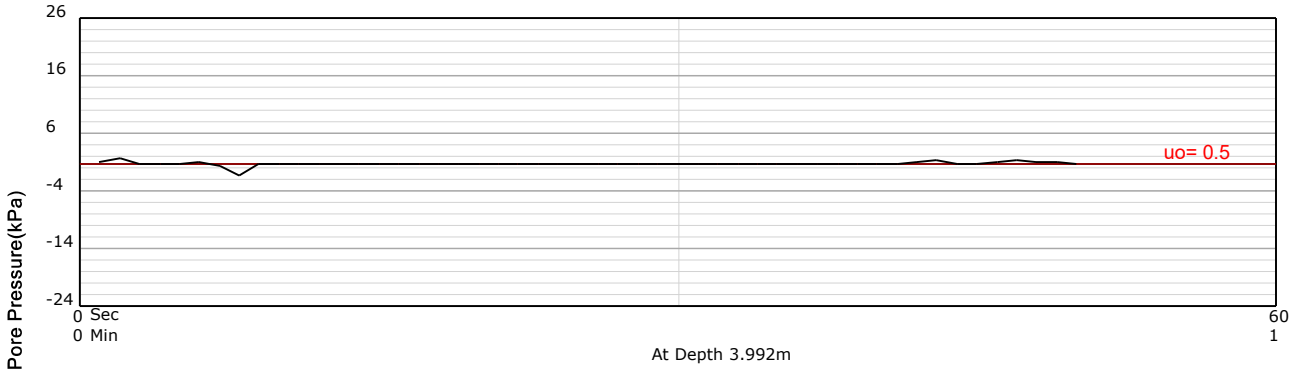

At Depth 3.992m

PIEZOCONE PENETRATION TEST

Dissipation Tests

HOLE: C9

PROJECT: 2024 Jagersfontein

SITE: TSF

DATE: 24/02/04 At: 07:18:04 A **DEPTH:** 8.898

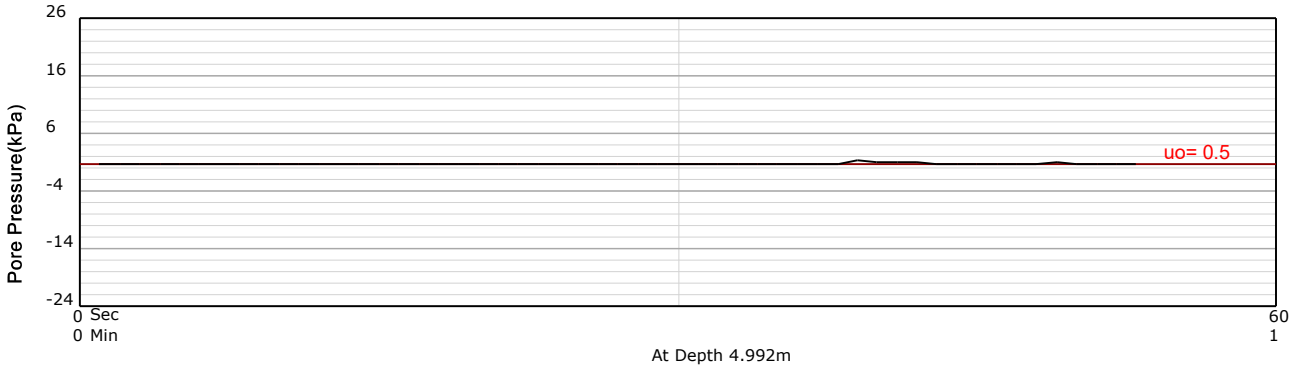

At Depth 4.992m

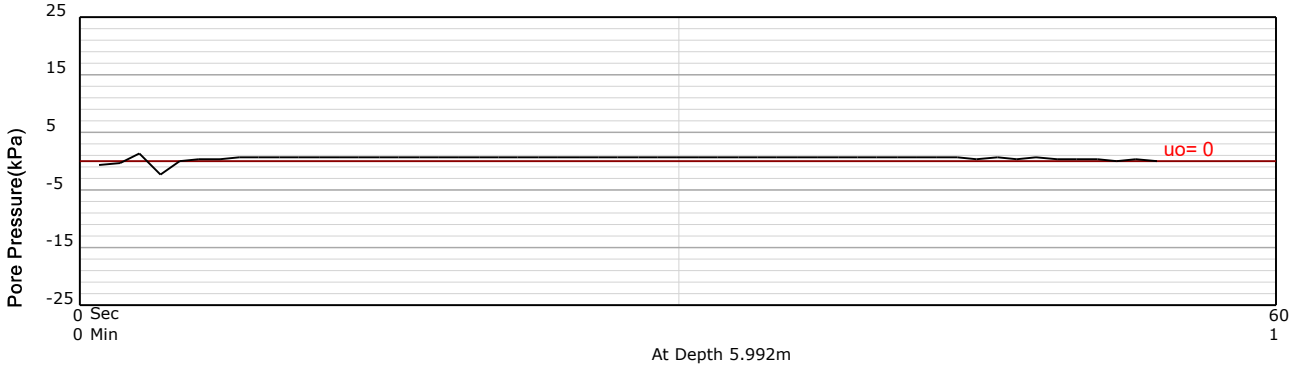

At Depth 5.992m

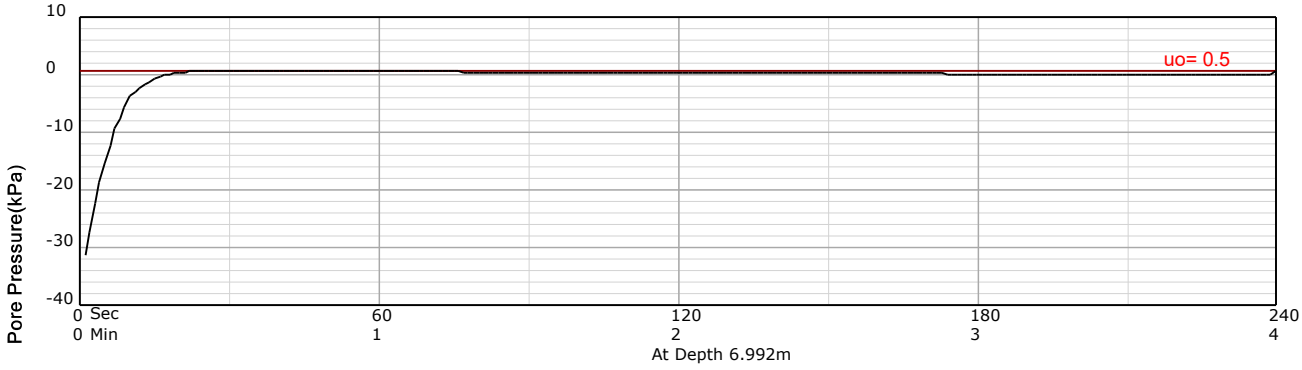

At Depth 6.992m

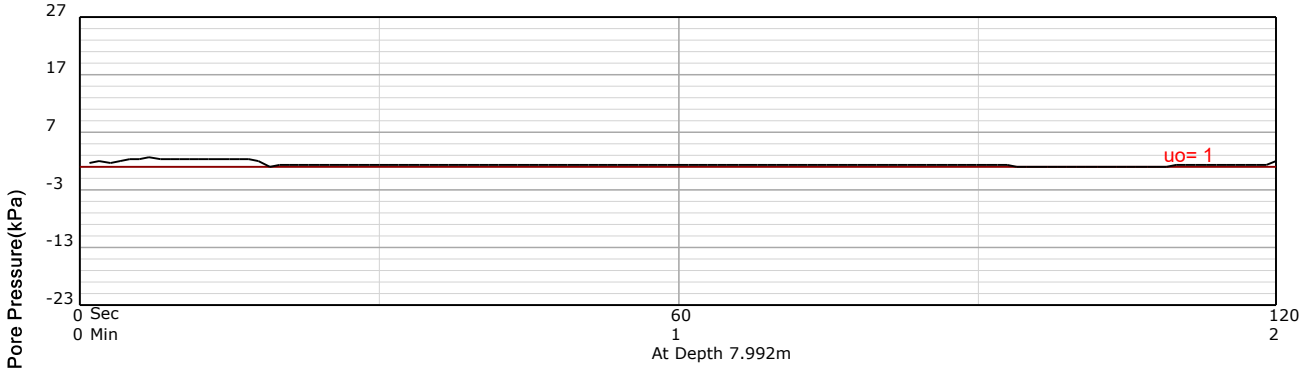

At Depth 7.992m

PIEZOCONE PENETRATION TEST

Dissipation Tests

HOLE: C9

PROJECT: 2024 Jagersfontein

SITE: TSF

DATE: 24/02/04 At: 07:18:04 A

DEPTH: 8.898

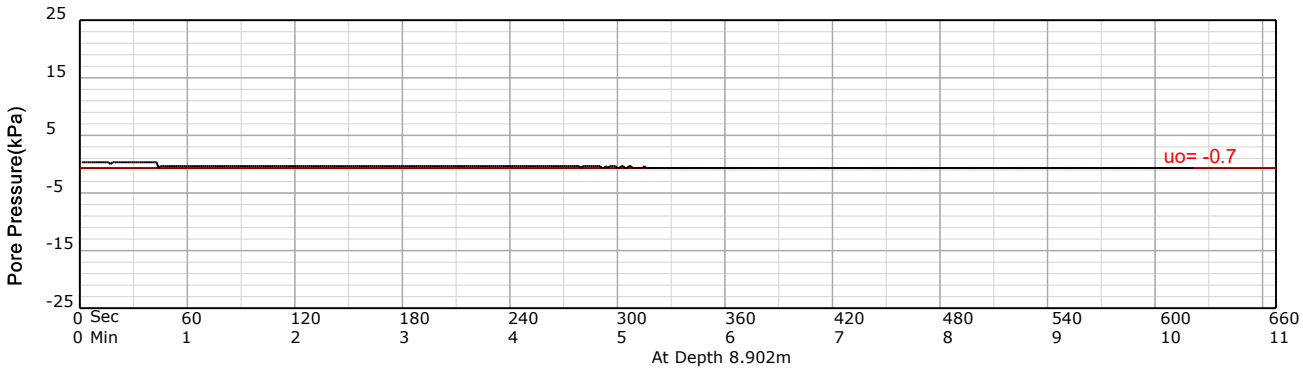

PIEZOCONE PENETRATION TEST

Equivalent Soil Behaviour Type Profile

HOLE: C9

PROJECT: 2024 Jagersfontein

SITE: TSF

DATE: 24/02/04 At: 07:18:04 A

DEPTH: 8.898

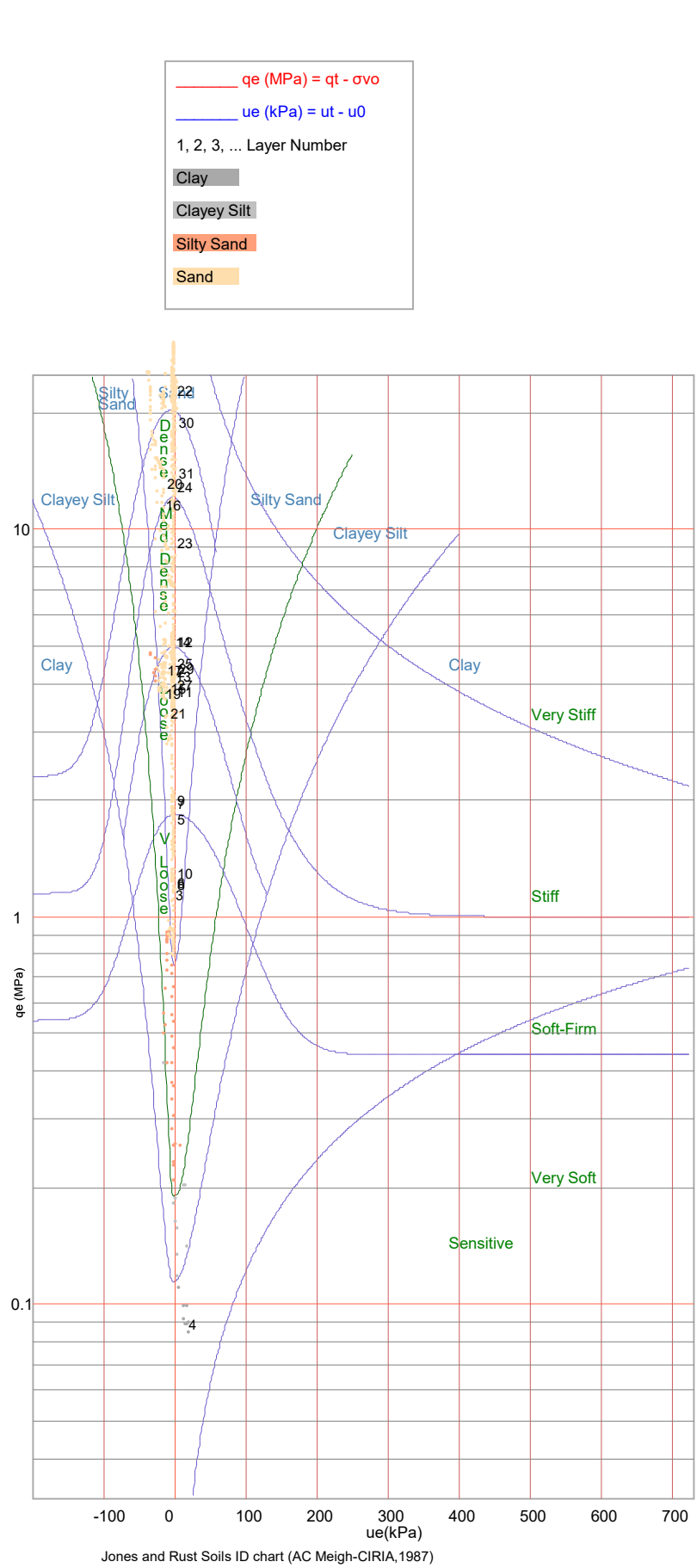

Jones and Rust Soils ID chart (AC Meigh-CIRIA,1987)

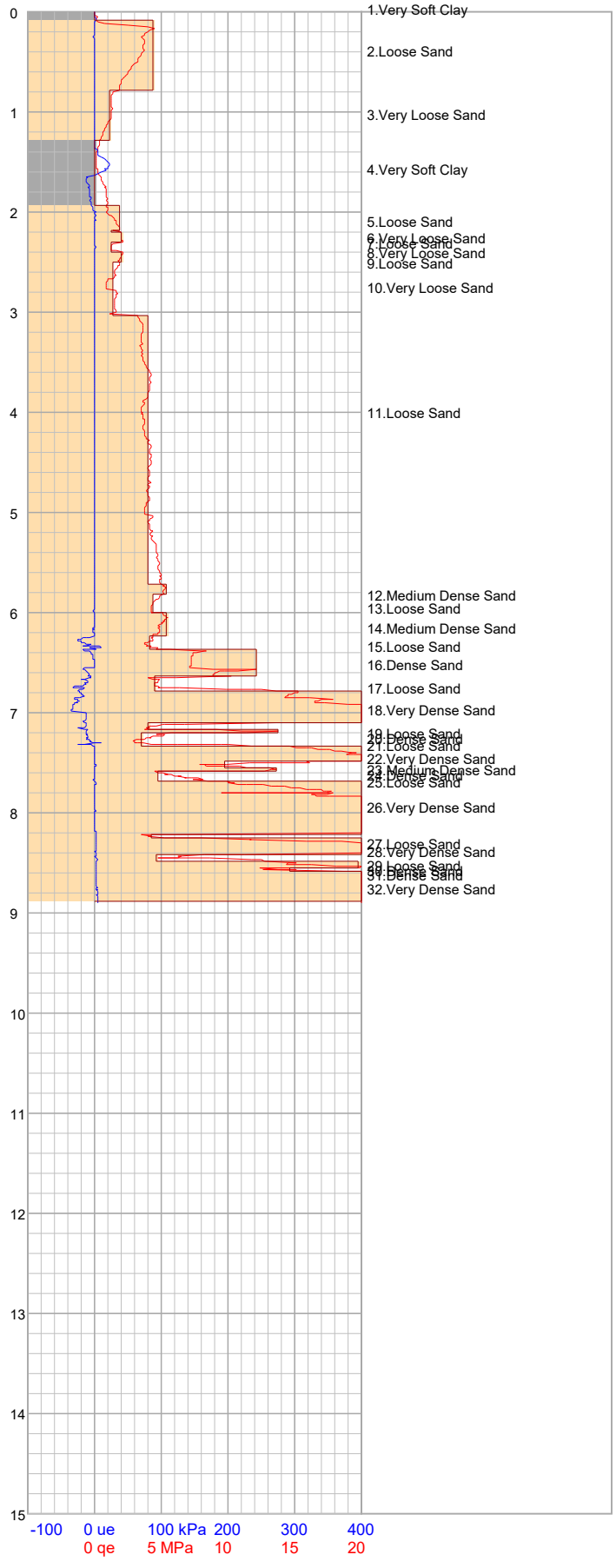

PIEZOCONE PENETRATION TEST

Recorded Field Results (Cone, Pore Pressure and Static Pore Pressure from Dissipations)

HOLE: C10

PROJECT: 2024 Jagersfontein

SITE: TSF

DATE: 24/02/02 At: 12:16:56 A **DEPTH:** 19.602

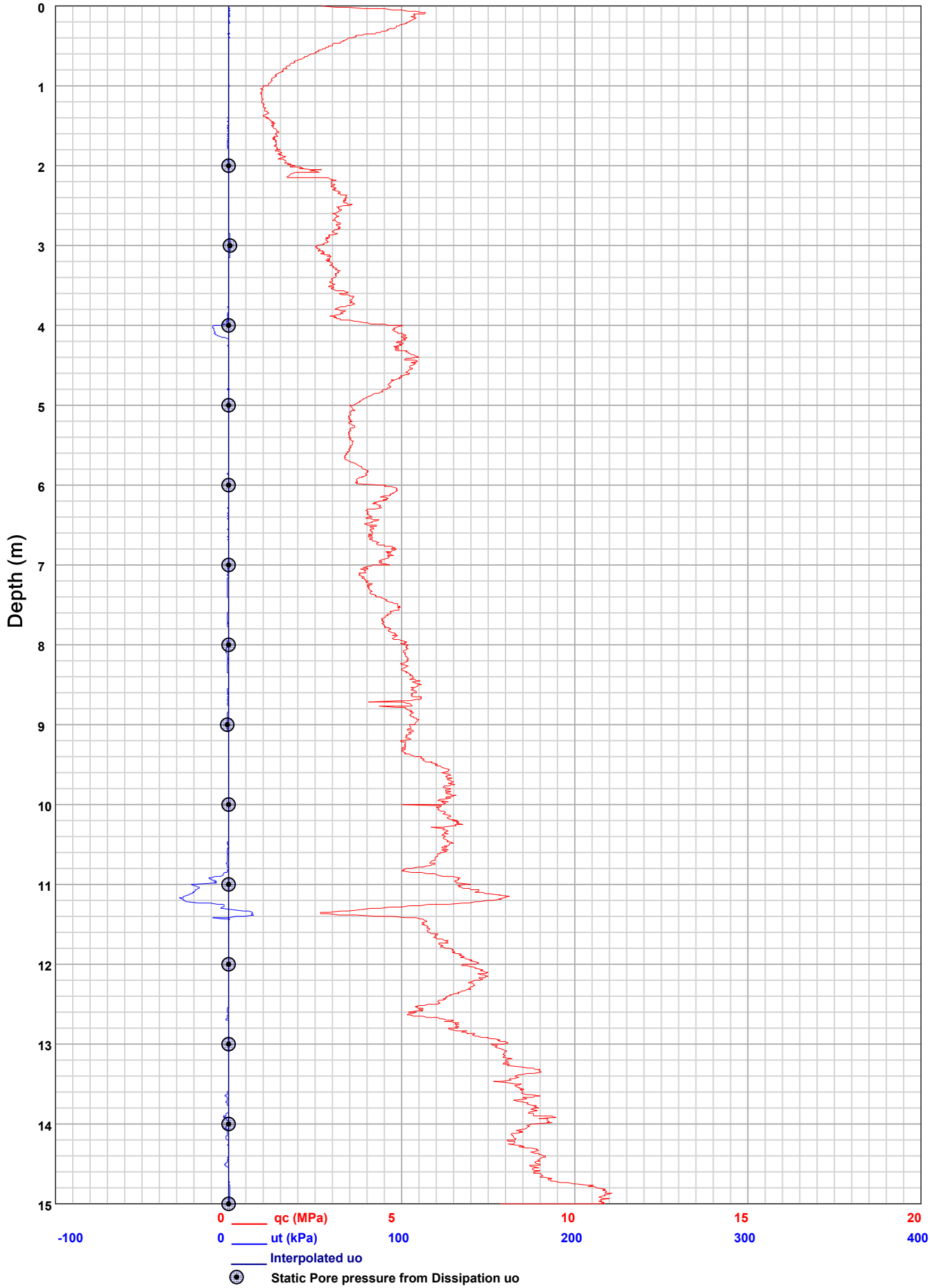

PIEZOCONE PENETRATION TEST

Recorded Field Results (Cone, Pore Pressure and Static Pore Pressure from Dissipations)

HOLE: C10

PROJECT: 2024 Jagersfontein

SITE: TSF

DATE: 24/02/02 At: 12:16:56 A **DEPTH:** 19.602

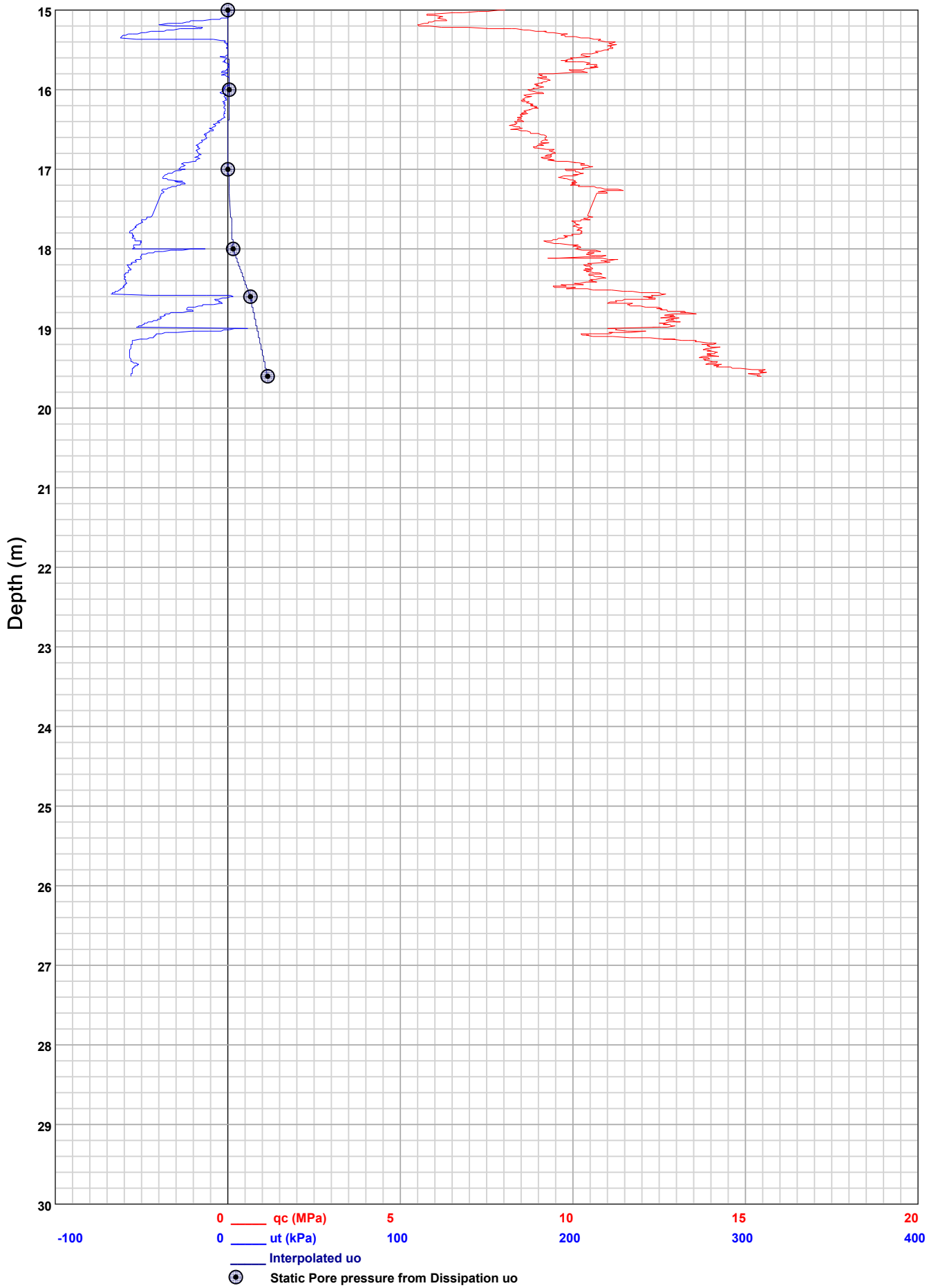

PIEZOCONE PENETRATION TEST

HOLE: C10

PROJECT: 2024 Jagersfontein

SITE: TSF

DATE: 24/02/02 At: 12:16:56 A

DEPTH: 19.602

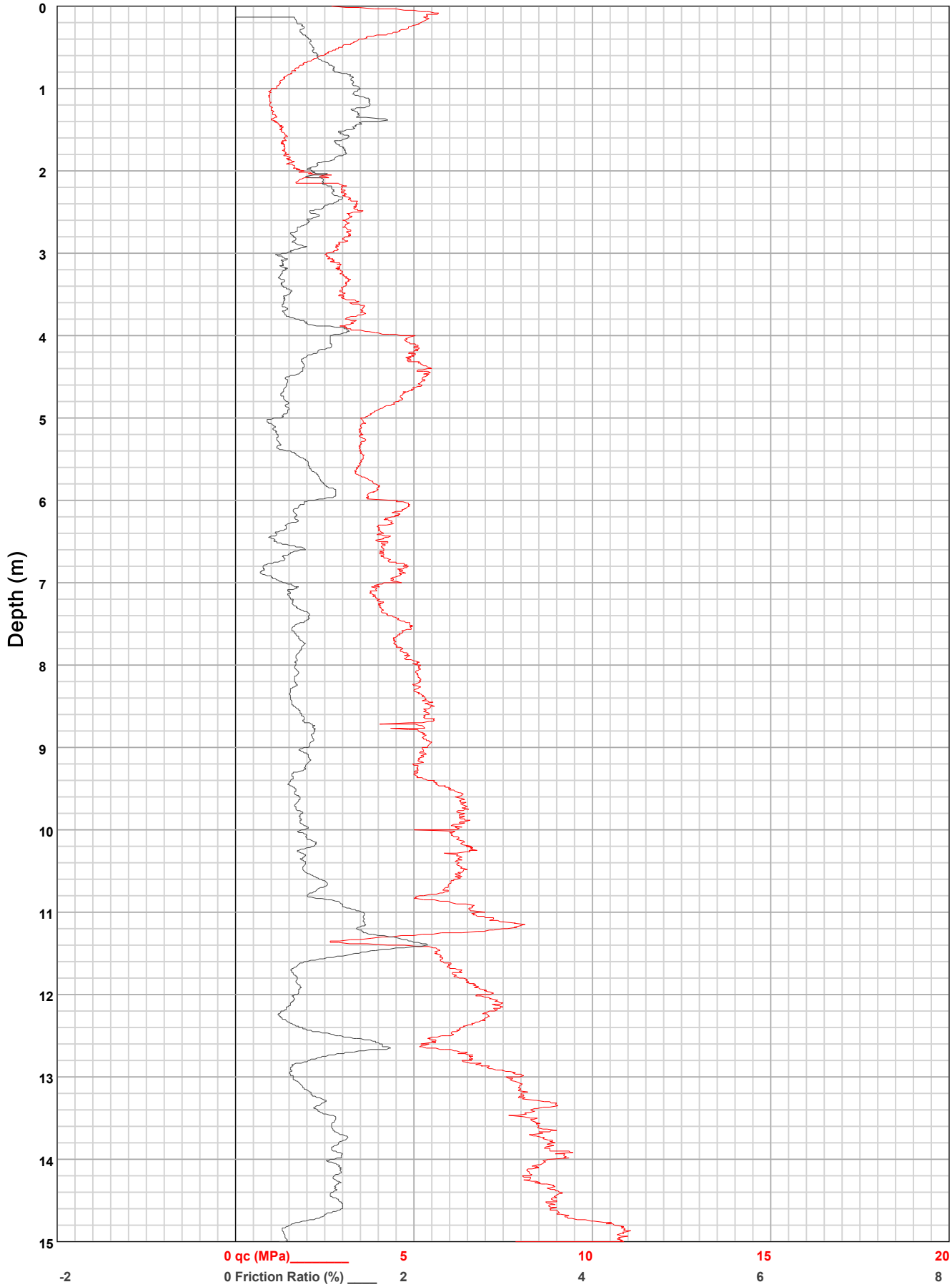

PIEZOCONE PENETRATION TEST

HOLE: C10

PROJECT: 2024 Jagersfontein

SITE: TSF

DATE: 24/02/02 At: 12:16:56 A

DEPTH: 19.602

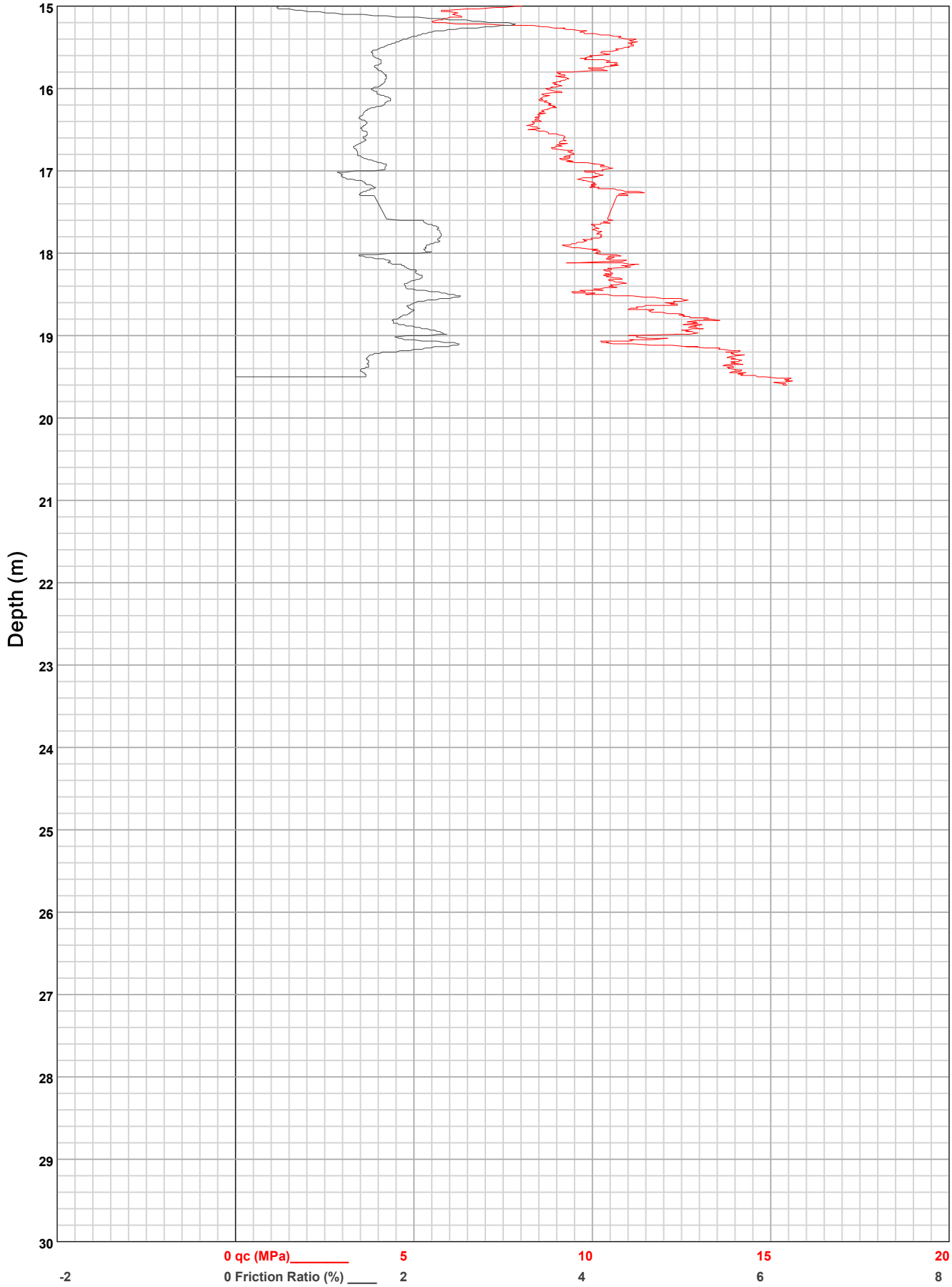

PIEZOCONE PENETRATION TEST

Dissipation Tests

HOLE: C10

PROJECT: 2024 Jagersfontein

SITE: TSF

DATE: 24/02/02 At: 12:16:56 A

DEPTH: 19.602

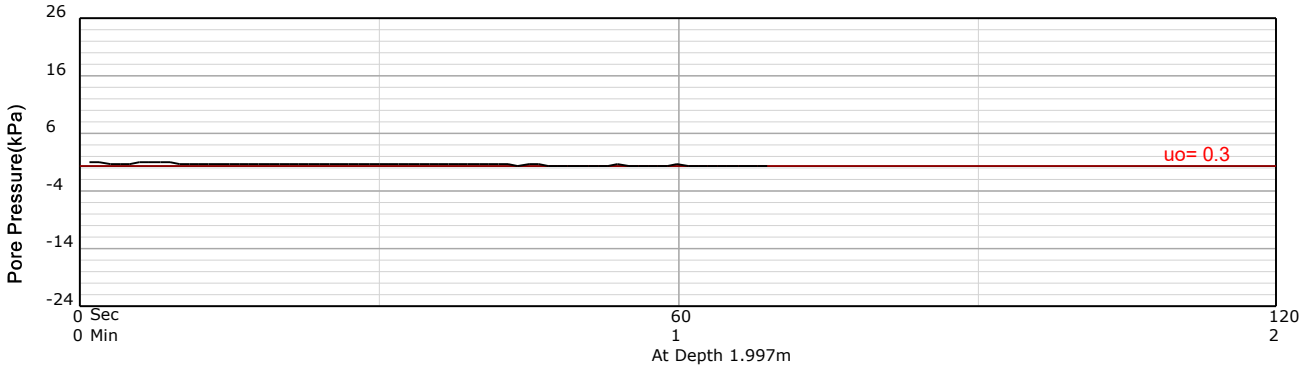

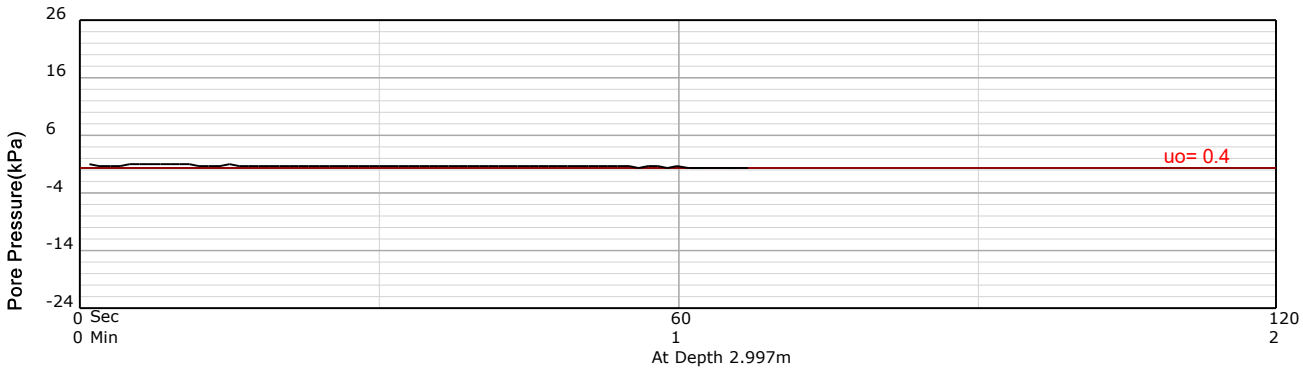

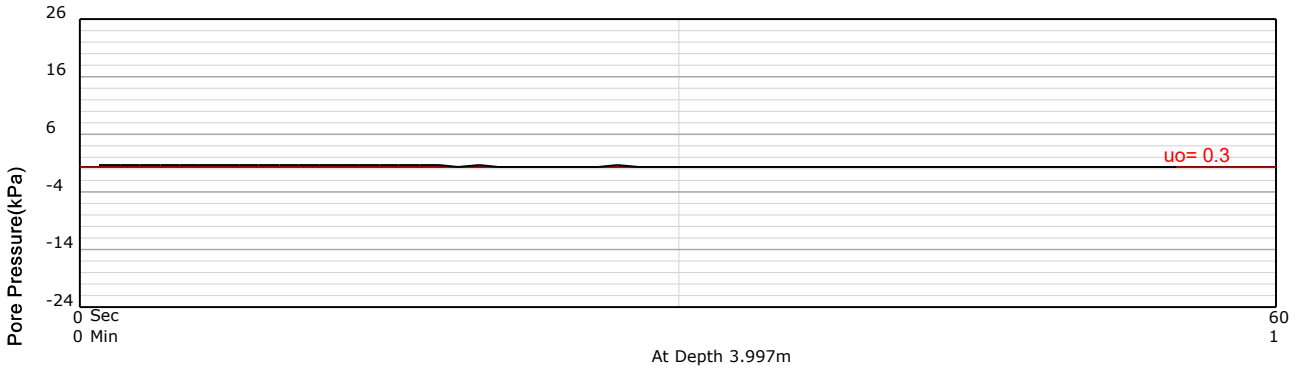

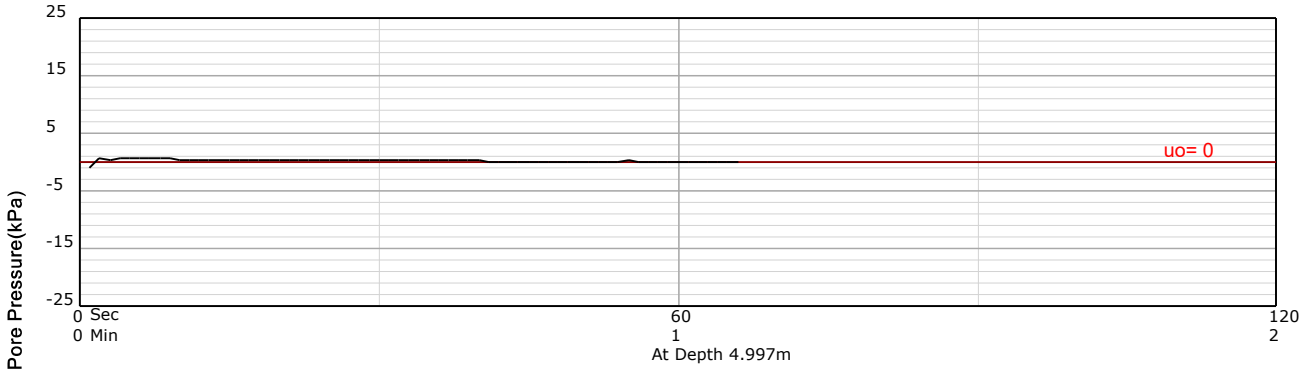

PIEZOCONE PENETRATION TEST

Dissipation Tests

HOLE: C10

PROJECT: 2024 Jagersfontein

SITE: TSF

DATE: 24/02/02 At: 12:16:56 A

DEPTH: 19.602

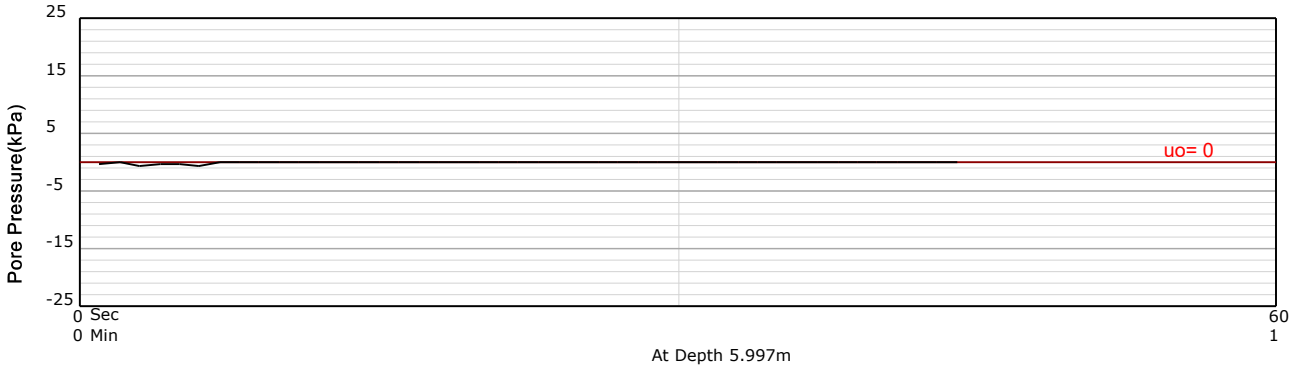

At Depth 5.997m

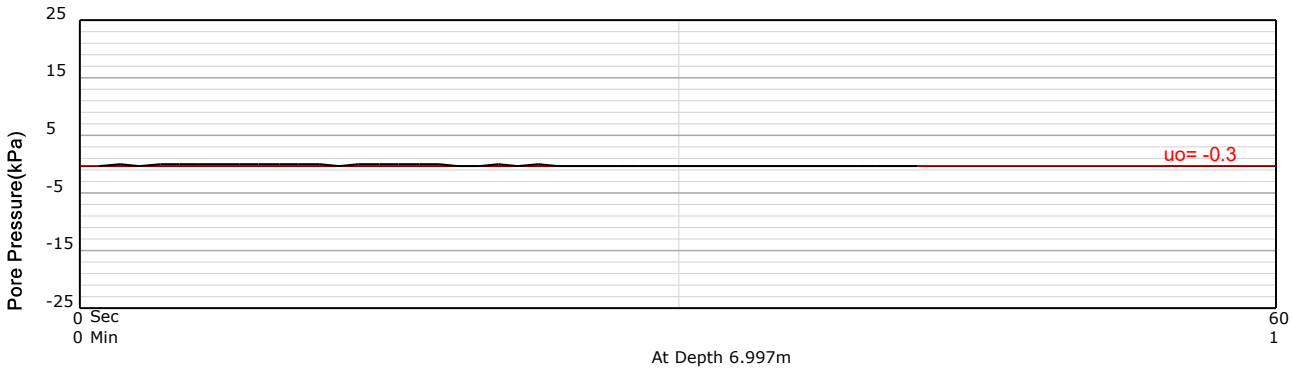

At Depth 6.997m

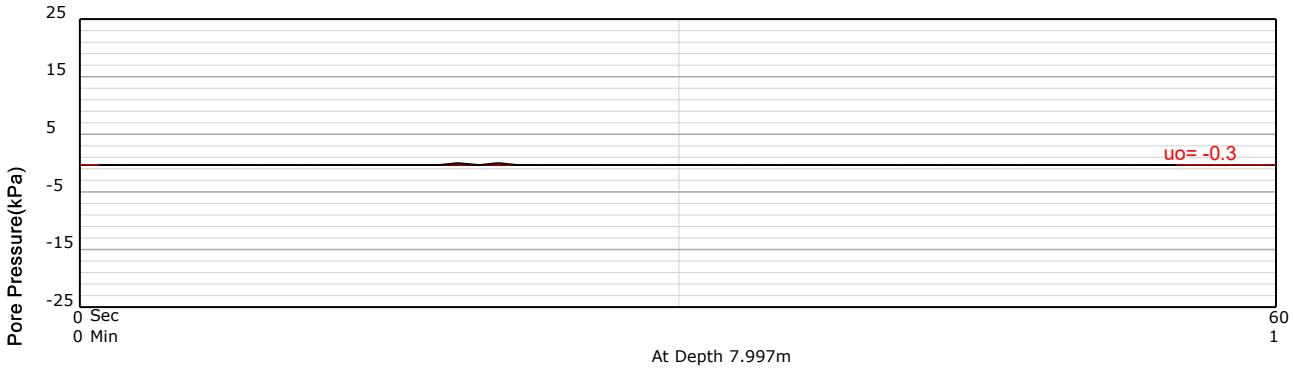

At Depth 7.997m

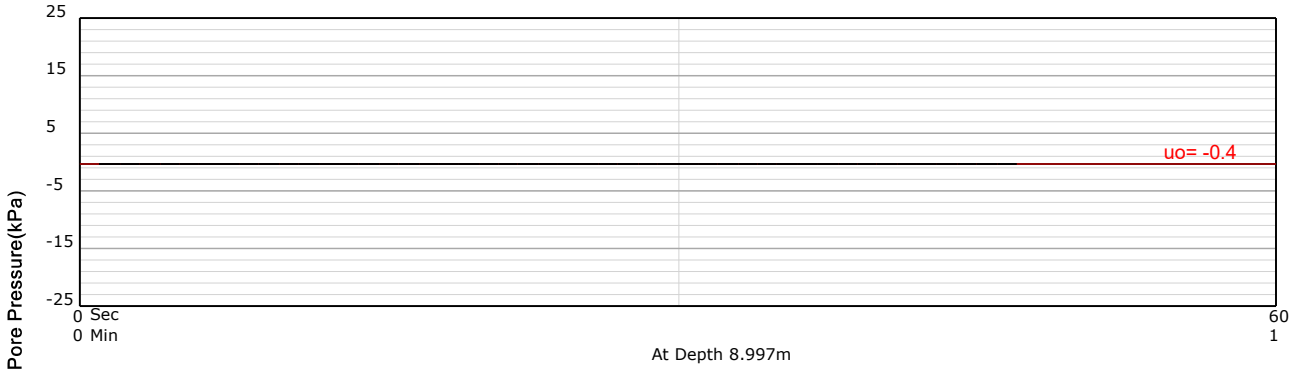

At Depth 8.997m

PIEZOCONE PENETRATION TEST

Dissipation Tests

HOLE: C10

PROJECT: 2024 Jagersfontein

SITE: TSF

DATE: 24/02/02 At: 12:16:56 A

DEPTH: 19.602

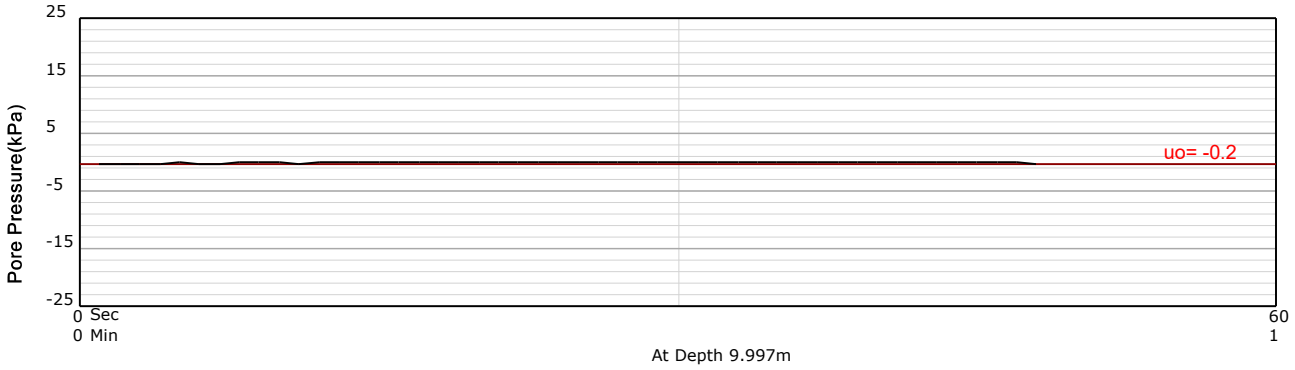

At Depth 9.997m

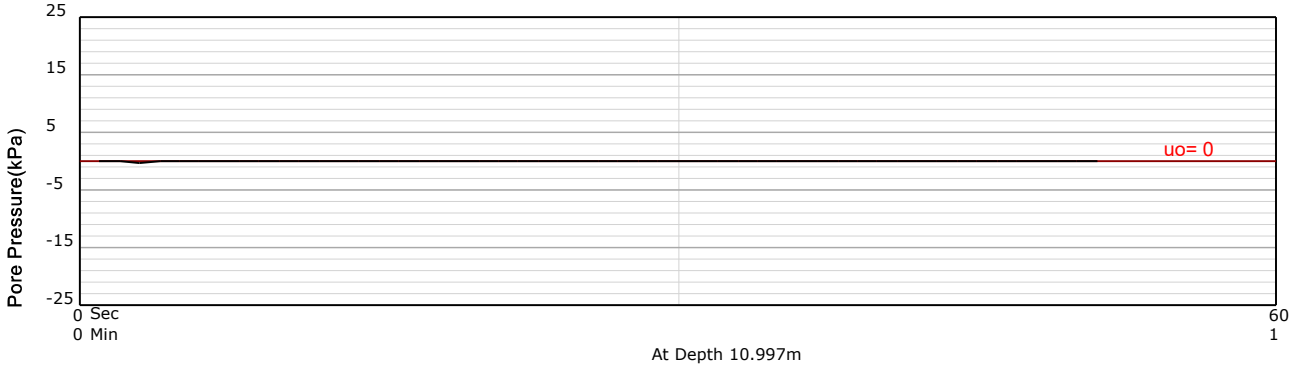

At Depth 10.997m

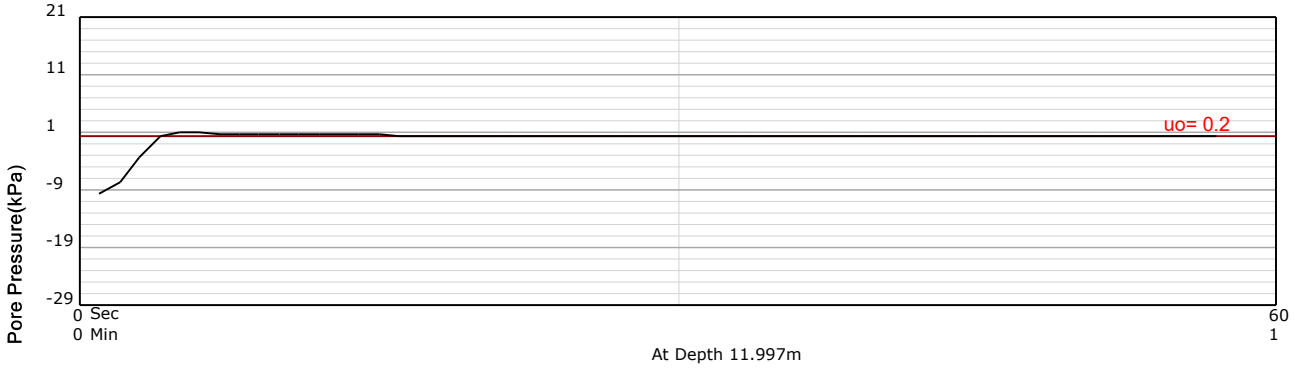

At Depth 11.997m

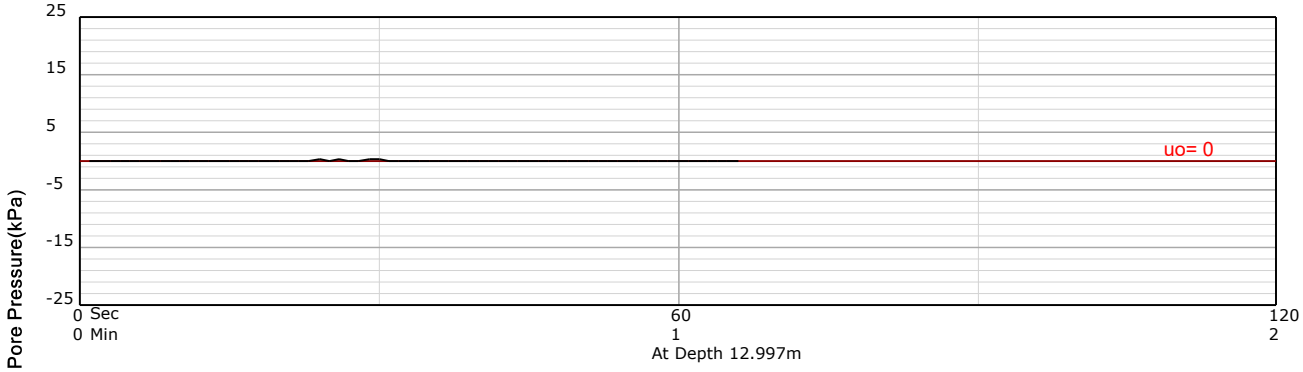

At Depth 12.997m

PIEZOCONE PENETRATION TEST

Dissipation Tests

HOLE: C10

PROJECT: 2024 Jagersfontein

SITE: TSF

DATE: 24/02/02 At: 12:16:56 A

DEPTH: 19.602

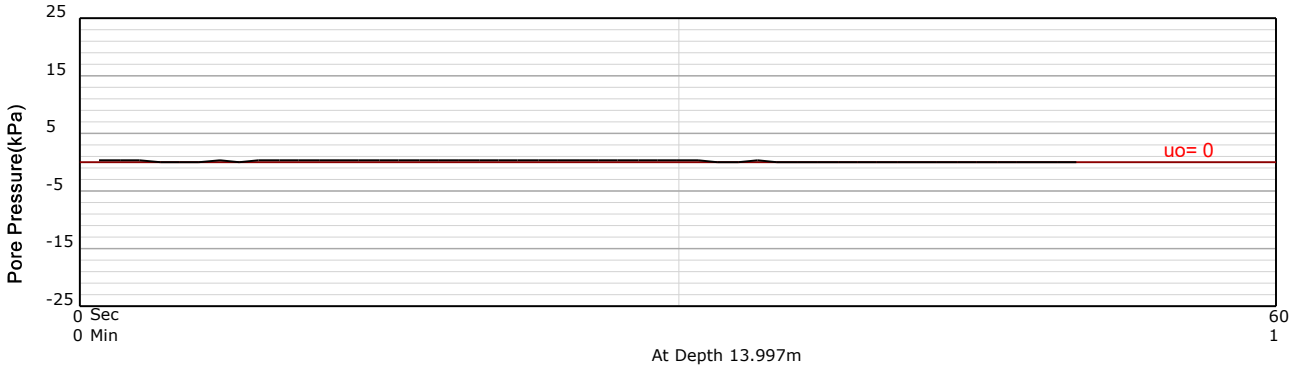

At Depth 13.997m

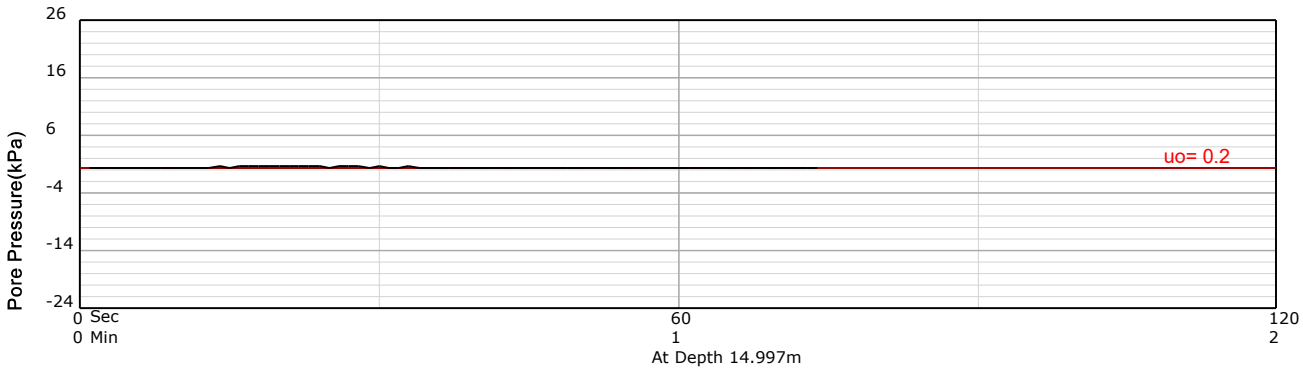

At Depth 14.997m

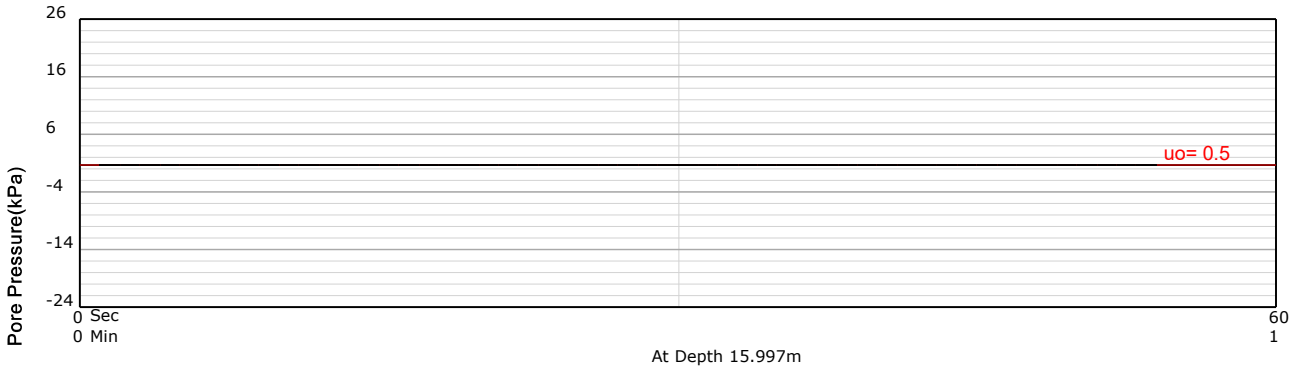

At Depth 15.997m

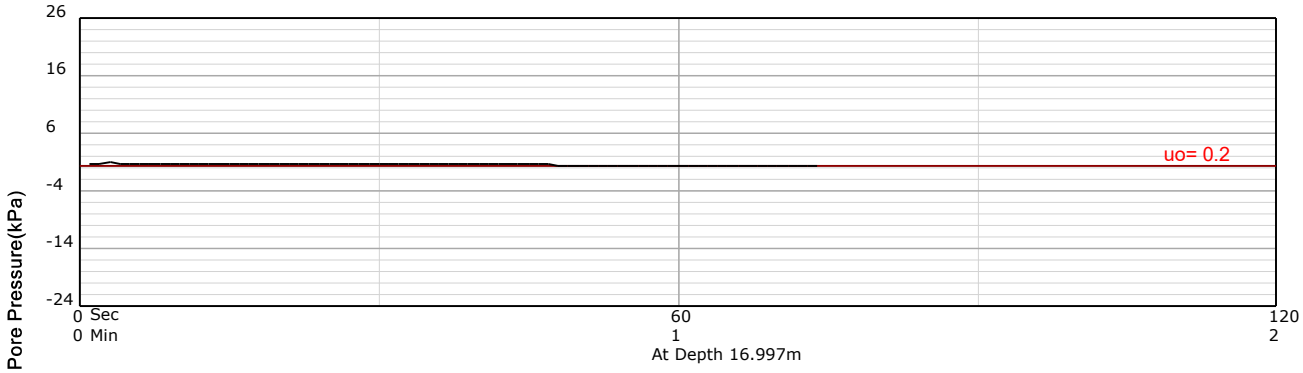

At Depth 16.997m

PIEZOCONE PENETRATION TEST

Dissipation Tests

HOLE: C10

PROJECT: 2024 Jagersfontein

SITE: TSF

DATE: 24/02/02 At: 12:16:56 A

DEPTH: 19.602

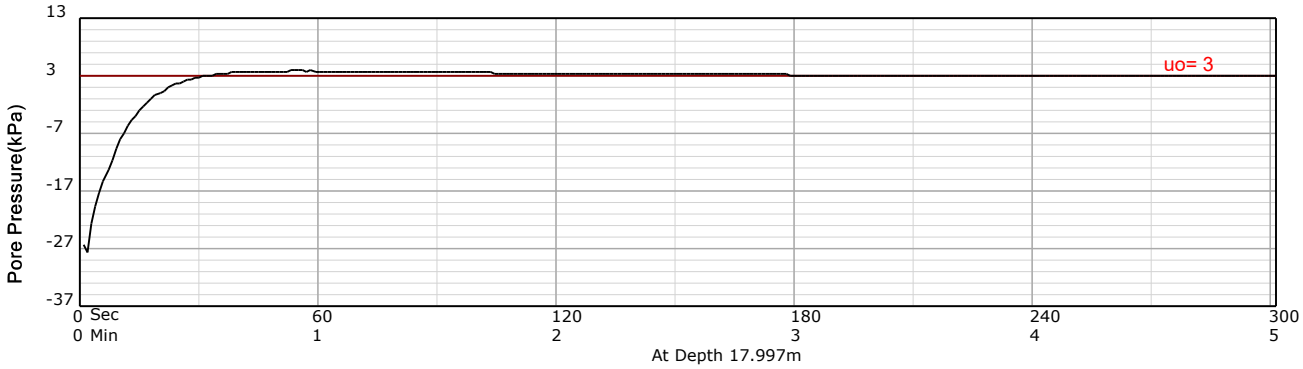

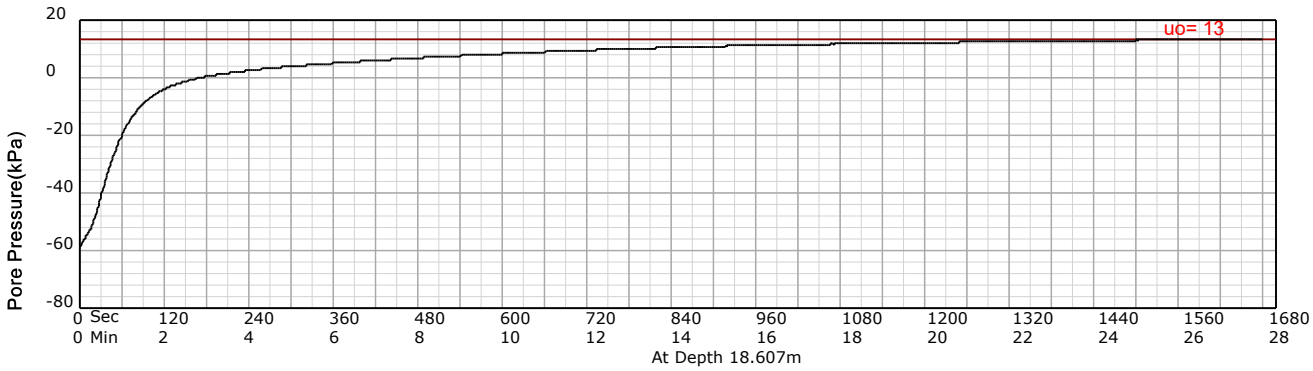

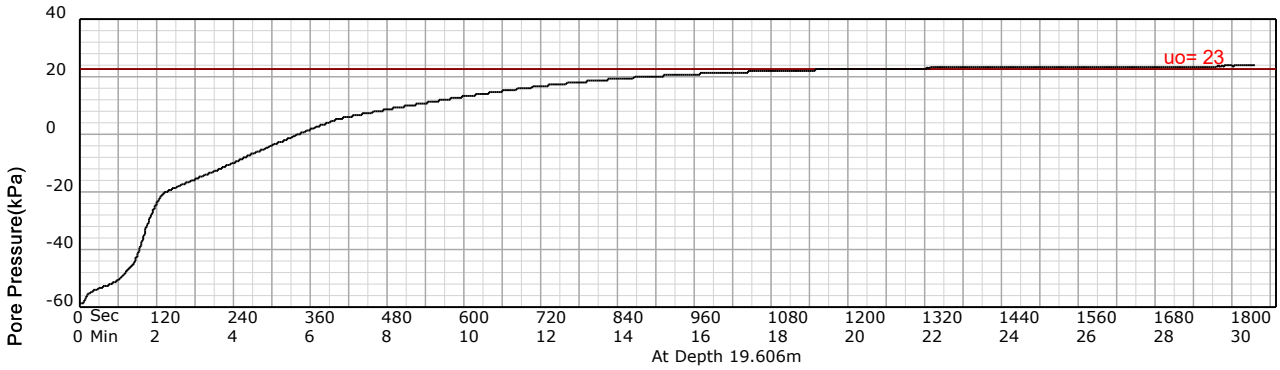

PIEZOCONE PENETRATION TEST

Equivalent Soil Behaviour Type Profile

HOLE: C10

PROJECT: 2024 Jagersfontein

SITE: TSF

DATE: 24/02/02 At: 12:16:56 A

DEPTH: 19.602

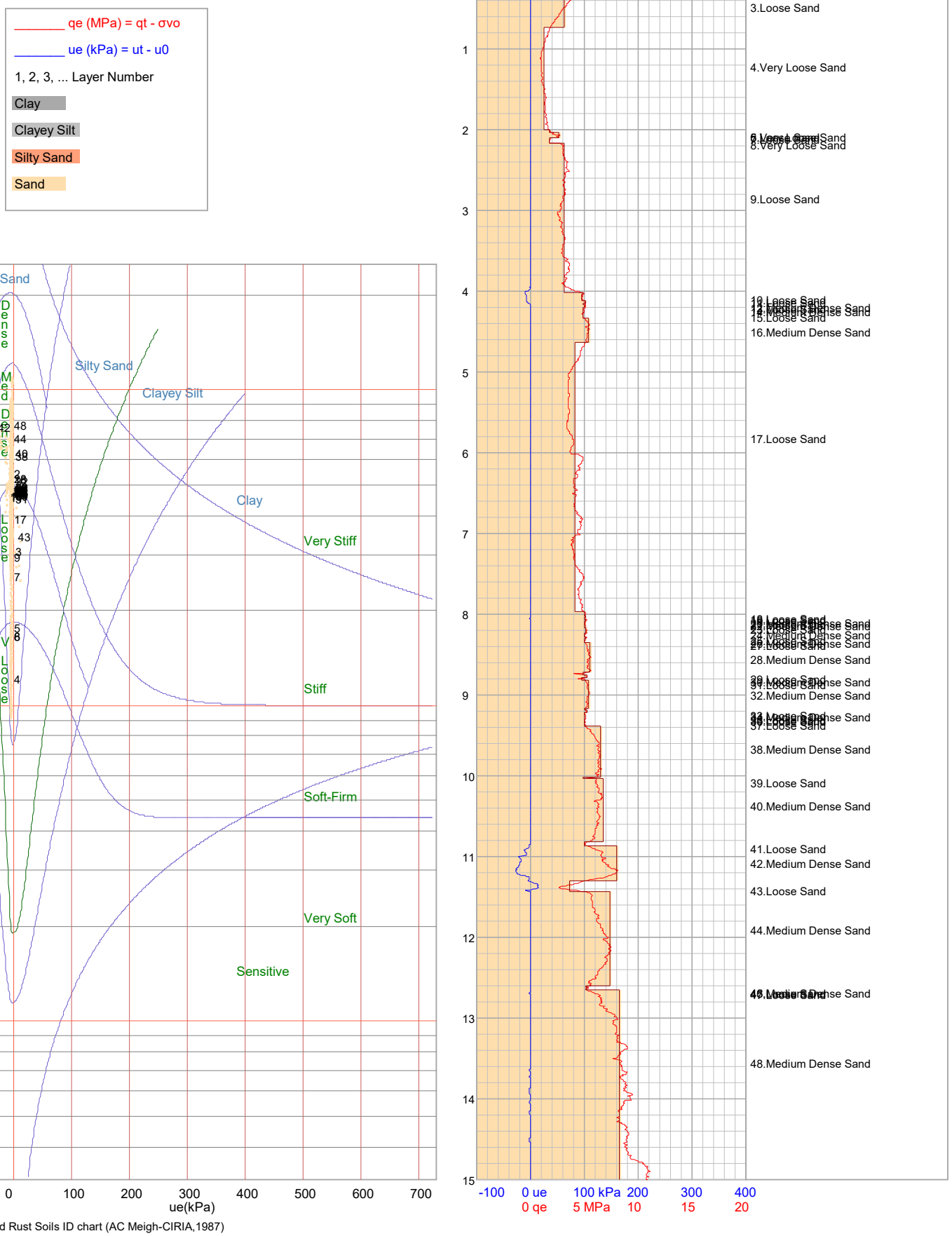

Jones and Rust Soils ID chart (AC Meigh-CIRIA,1987)

PIEZOCONE PENETRATION TEST

Equivalent Soil Behaviour Type Profile

HOLE: C10

PROJECT: 2024 Jagersfontein

SITE: TSF

DATE: 24/02/02 At: 12:16:56 A

DEPTH: 19.602

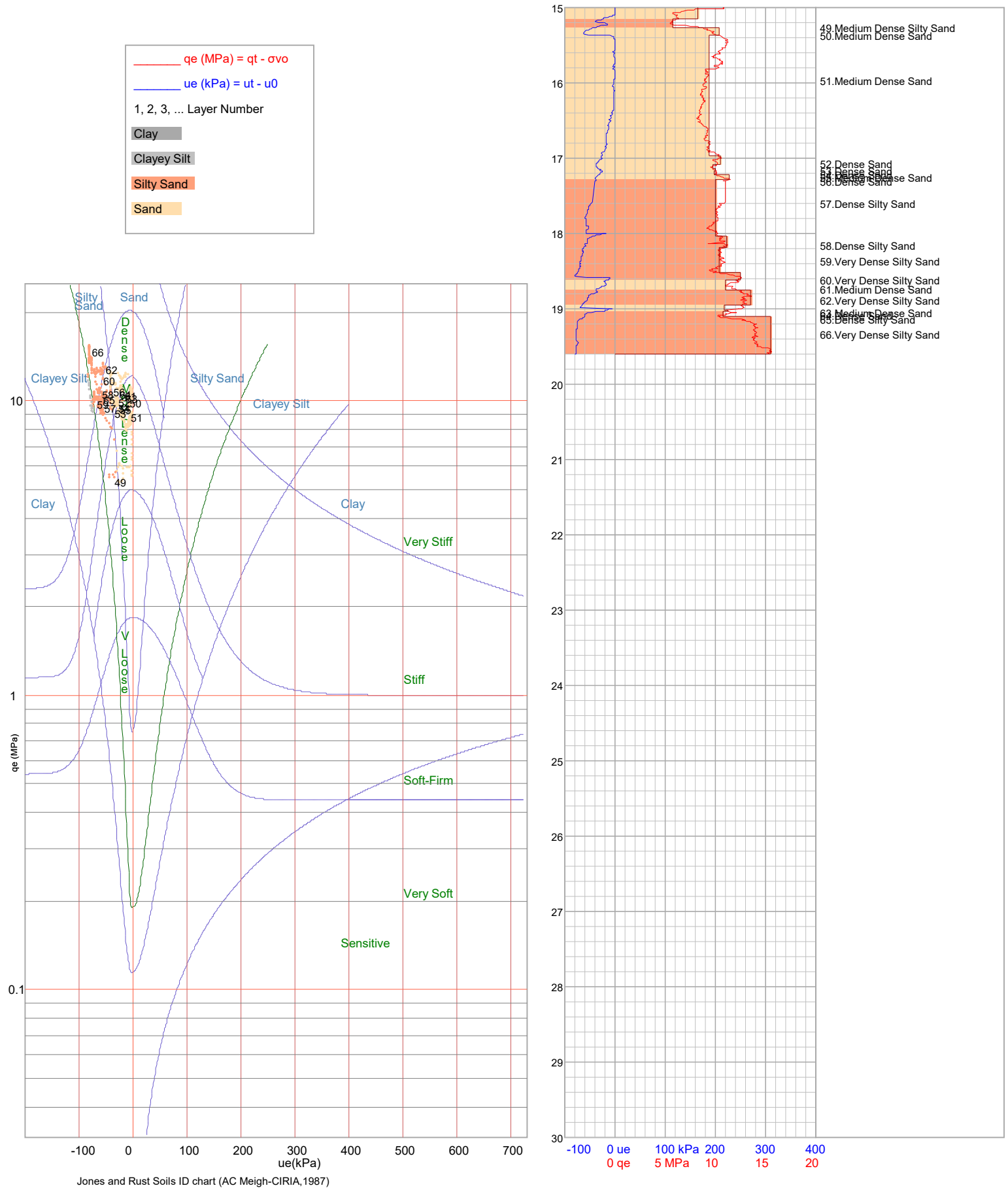

PIEZOCONE PENETRATION TEST

Recorded Field Results (Cone, Pore Pressure and Static Pore Pressure from Dissipations)

HOLE: C11

PROJECT: 2024 Jagersfontein

SITE: TSF

DATE: 24/02/03 At: 11:51:54 A **DEPTH:** 12.401

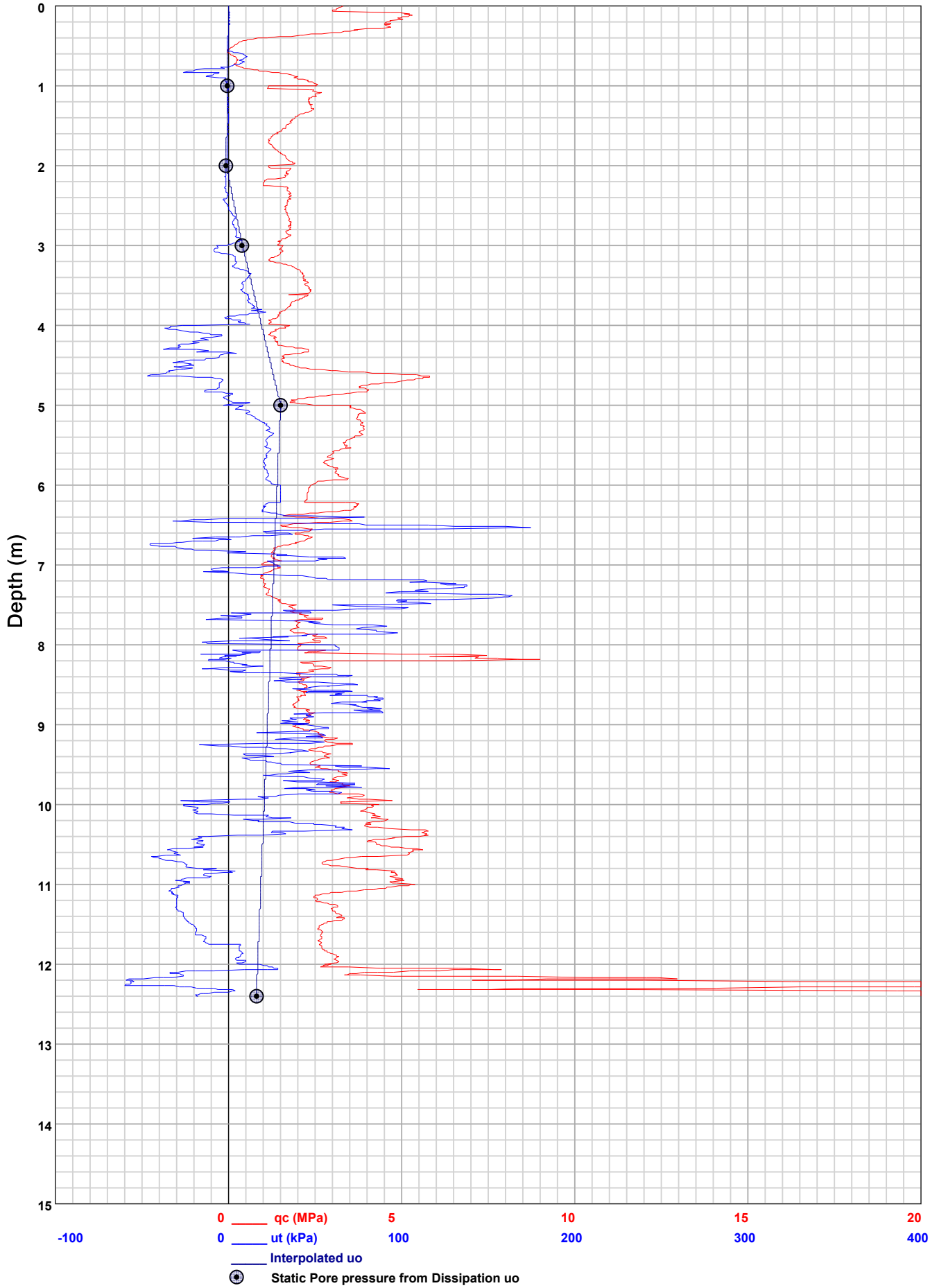

PIEZOCONE PENETRATION TEST

HOLE: C11

PROJECT: 2024 Jagersfontein

SITE: TSF

DATE: 24/02/03 At: 11:51:54 A

DEPTH: 12.401

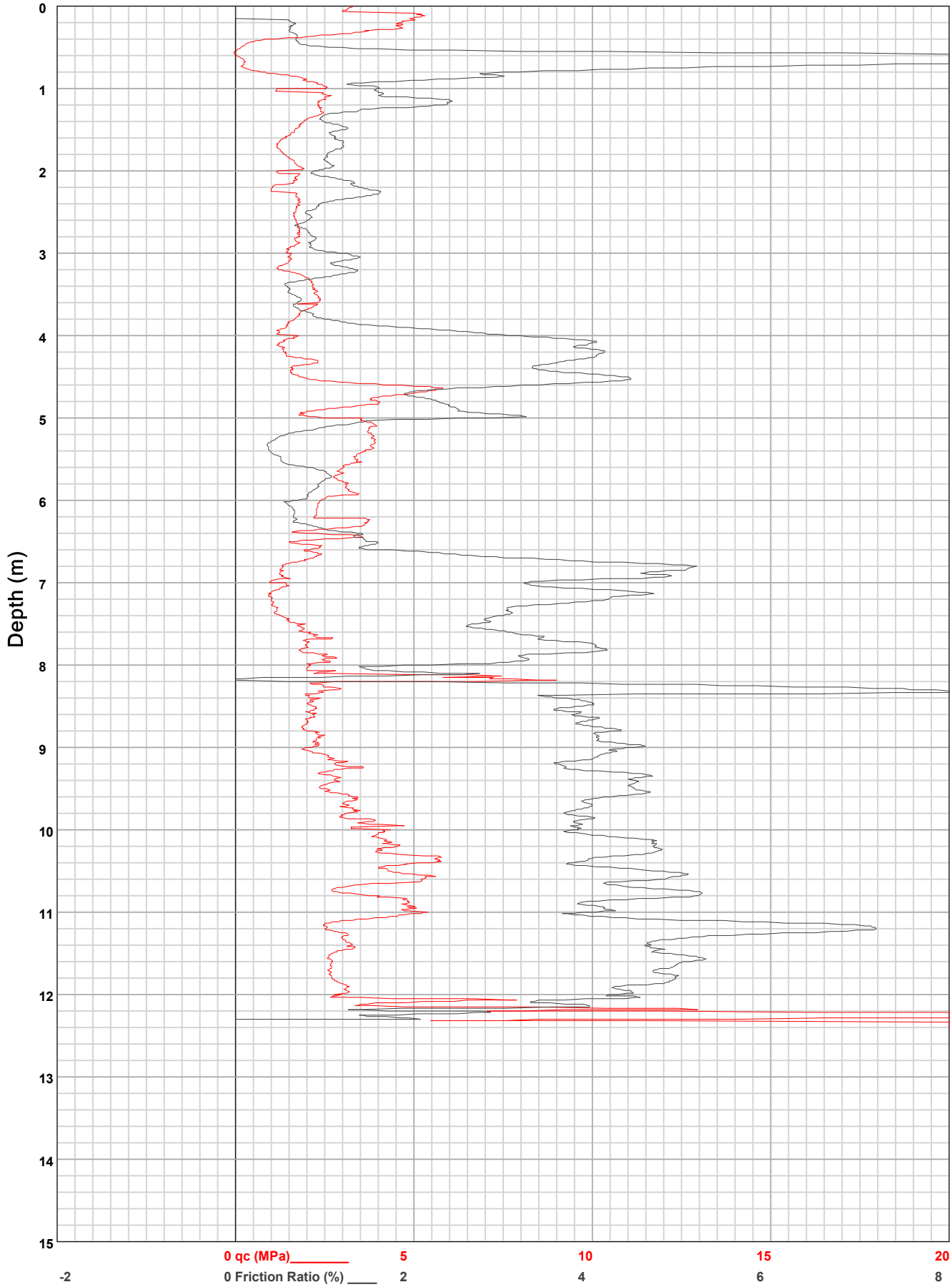

PIEZOCONE PENETRATION TEST

Dissipation Tests

HOLE: C11

PROJECT: 2024 Jagersfontein

SITE: TSF

DATE: 24/02/03 At: 11:51:54 A

DEPTH: 12.401

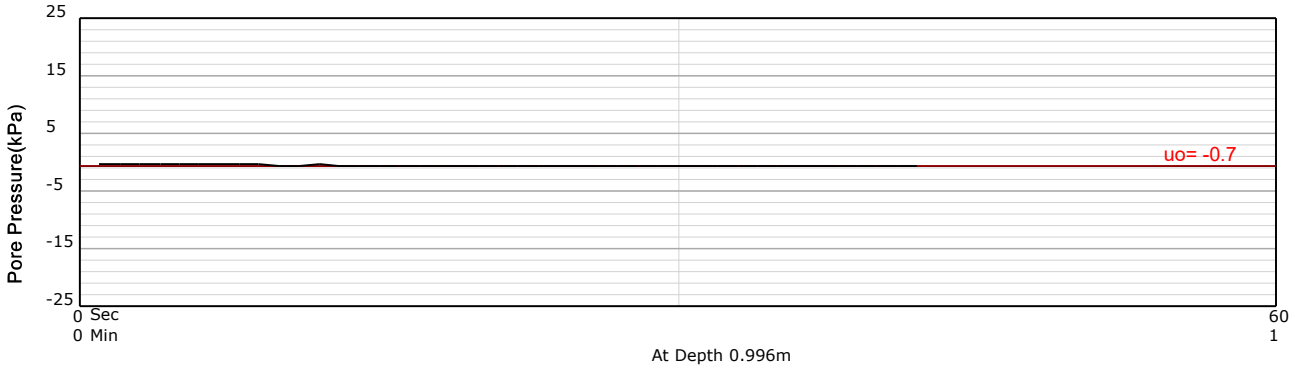

At Depth 0.996m

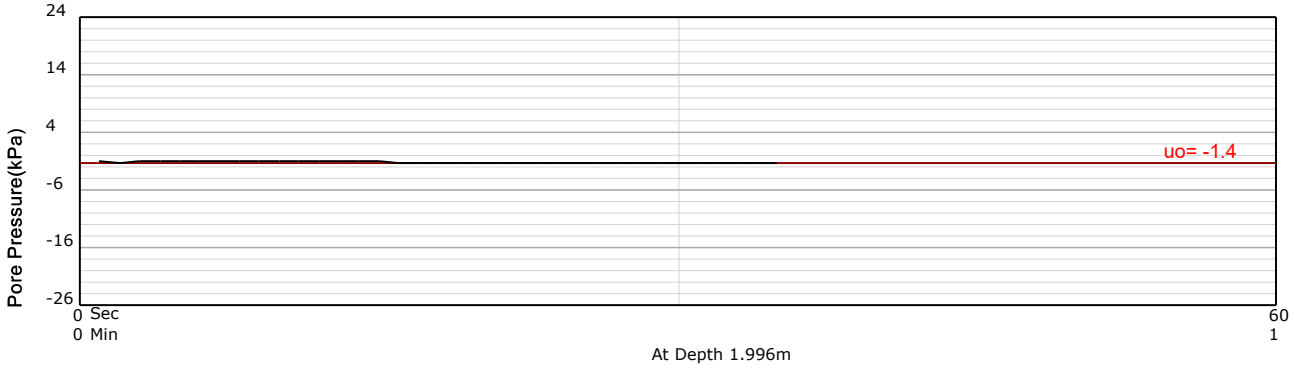

At Depth 1.996m

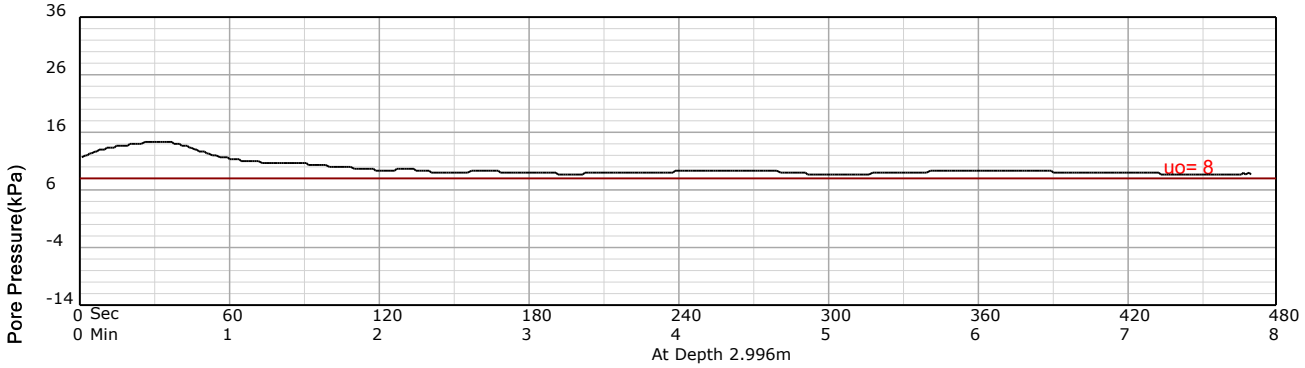

At Depth 2.996m

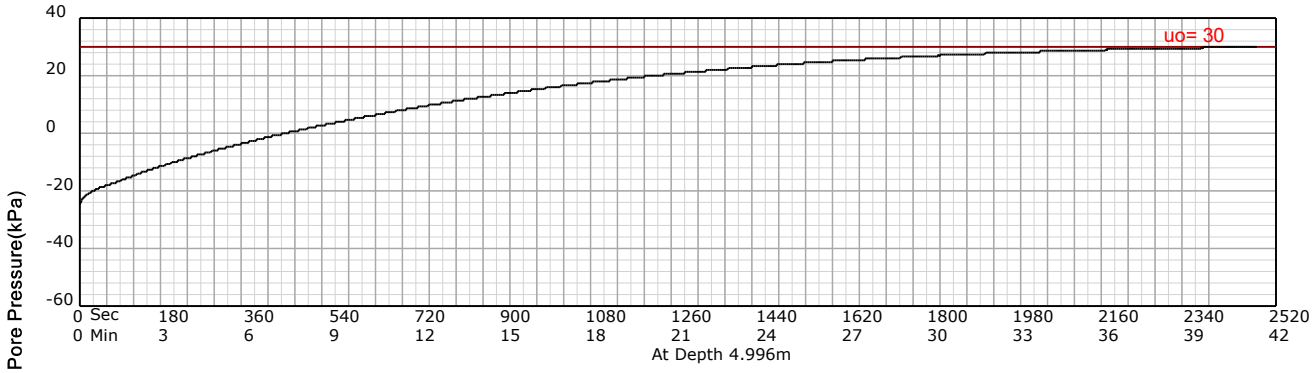

At Depth 4.996m

PIEZOCONE PENETRATION TEST

Dissipation Tests

HOLE: C11

PROJECT: 2024 Jagersfontein

SITE: TSF

DATE: 24/02/03 At: 11:51:54 A

DEPTH: 12.401

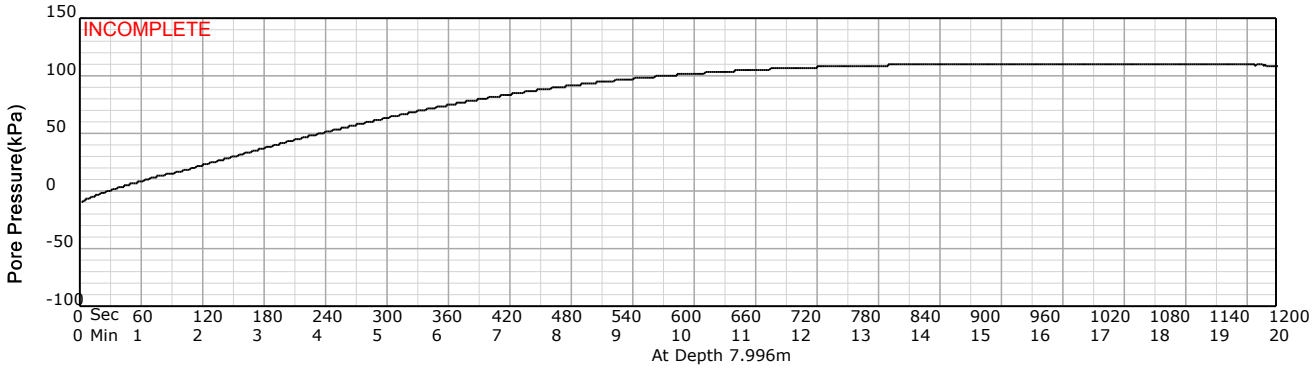

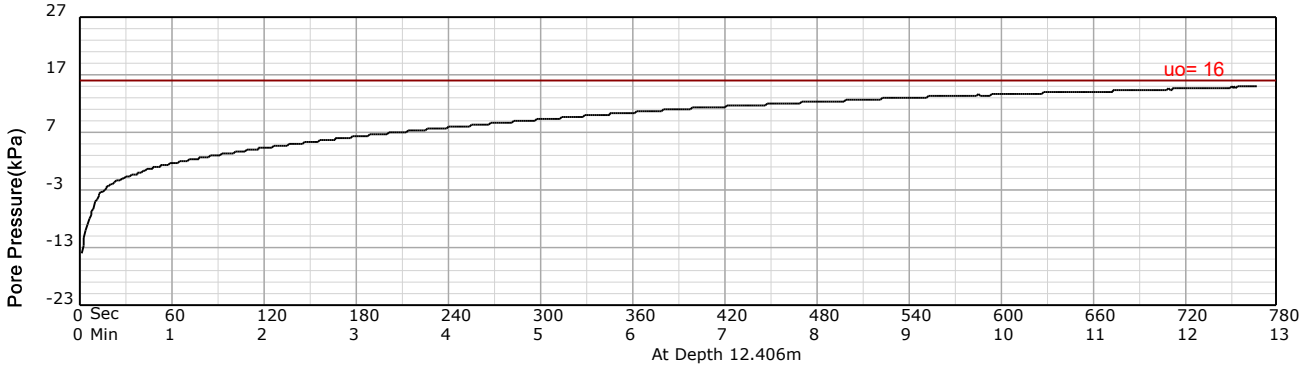

PIEZOCONE PENETRATION TEST

Equivalent Soil Behaviour Type Profile

HOLE: C11

PROJECT: 2024 Jagersfontein

SITE: TSF

DATE: 24/02/03 At: 11:51:54 A

DEPTH: 12.401

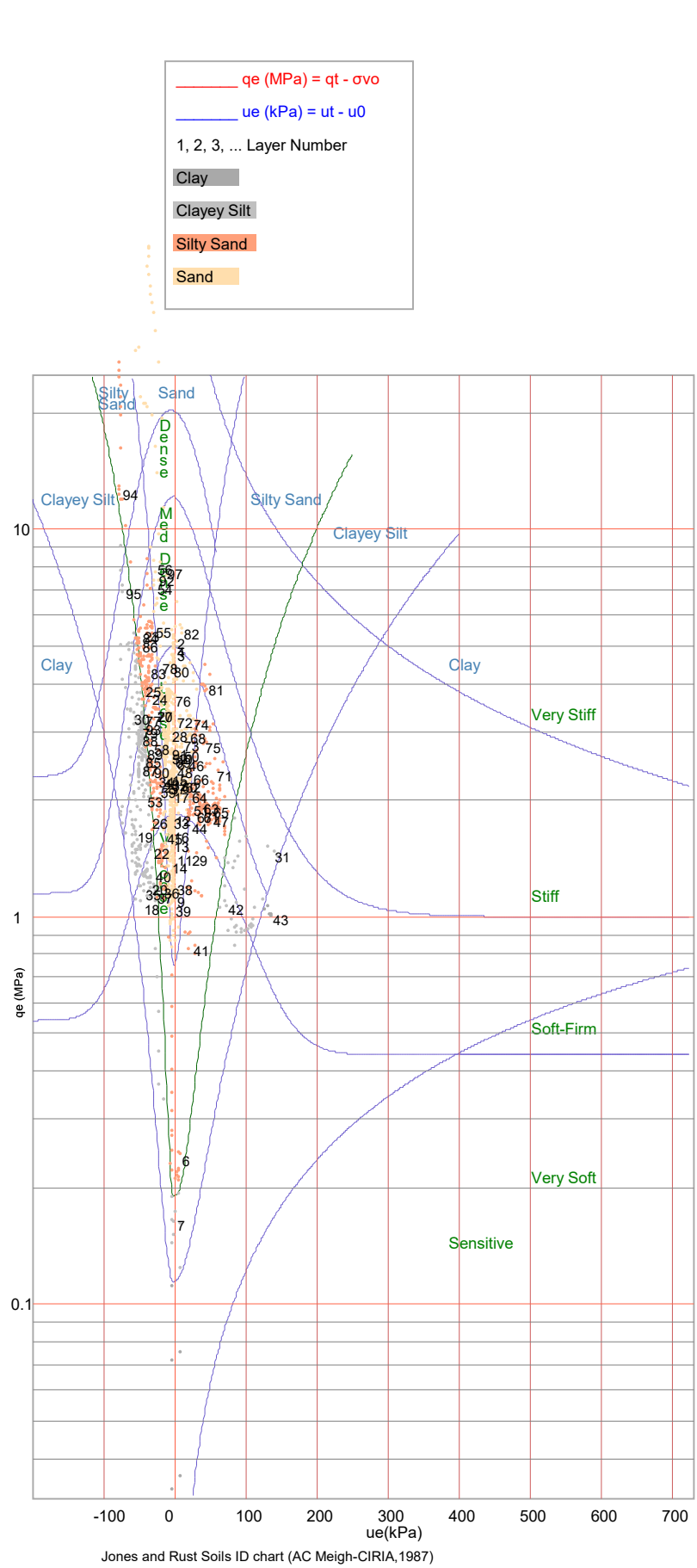

Jones and Rust Soils ID chart (AC Meigh-CIRIA,1987)

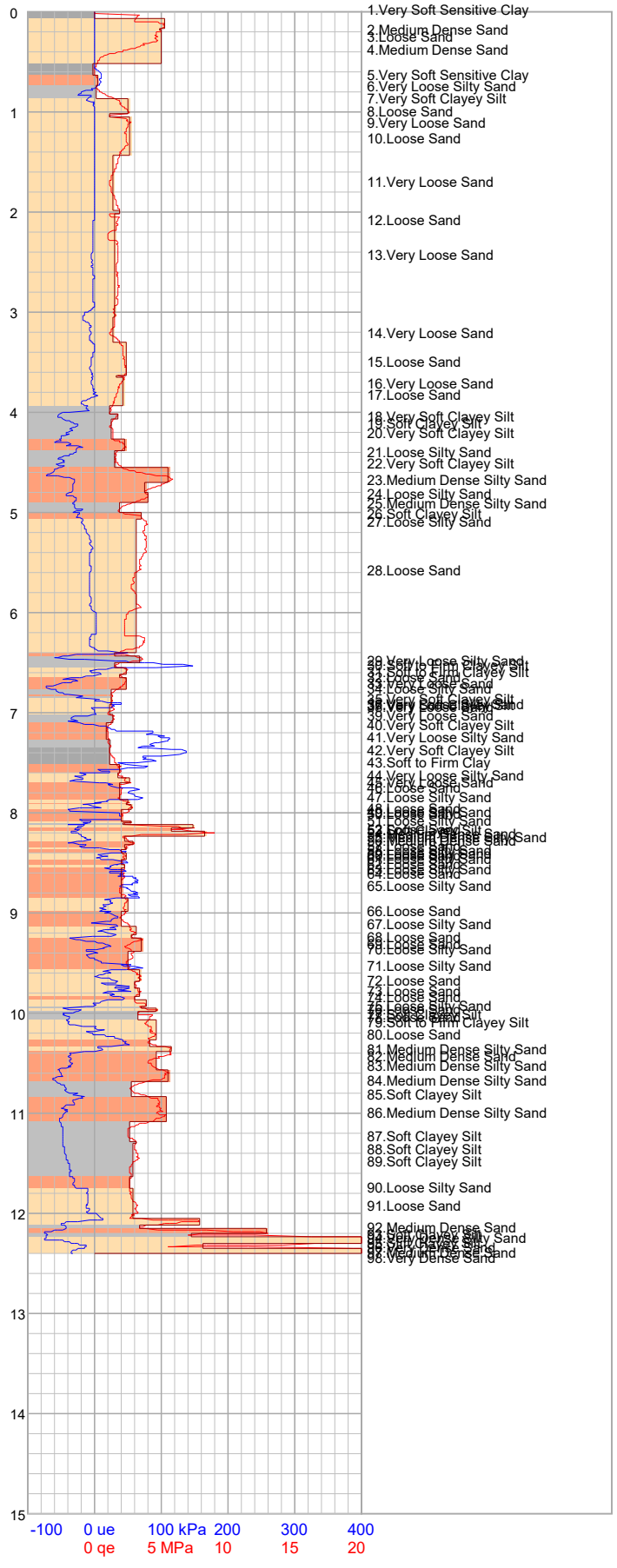

PIEZOCONE PENETRATION TEST

Recorded Field Results (Cone, Pore Pressure and Static Pore Pressure from Dissipations)

HOLE: C12

PROJECT: 2024 Jagersfontein

SITE: TSF

DATE: 24/02/04 **At:** 09:54:15 **DEPTH:** 7.303

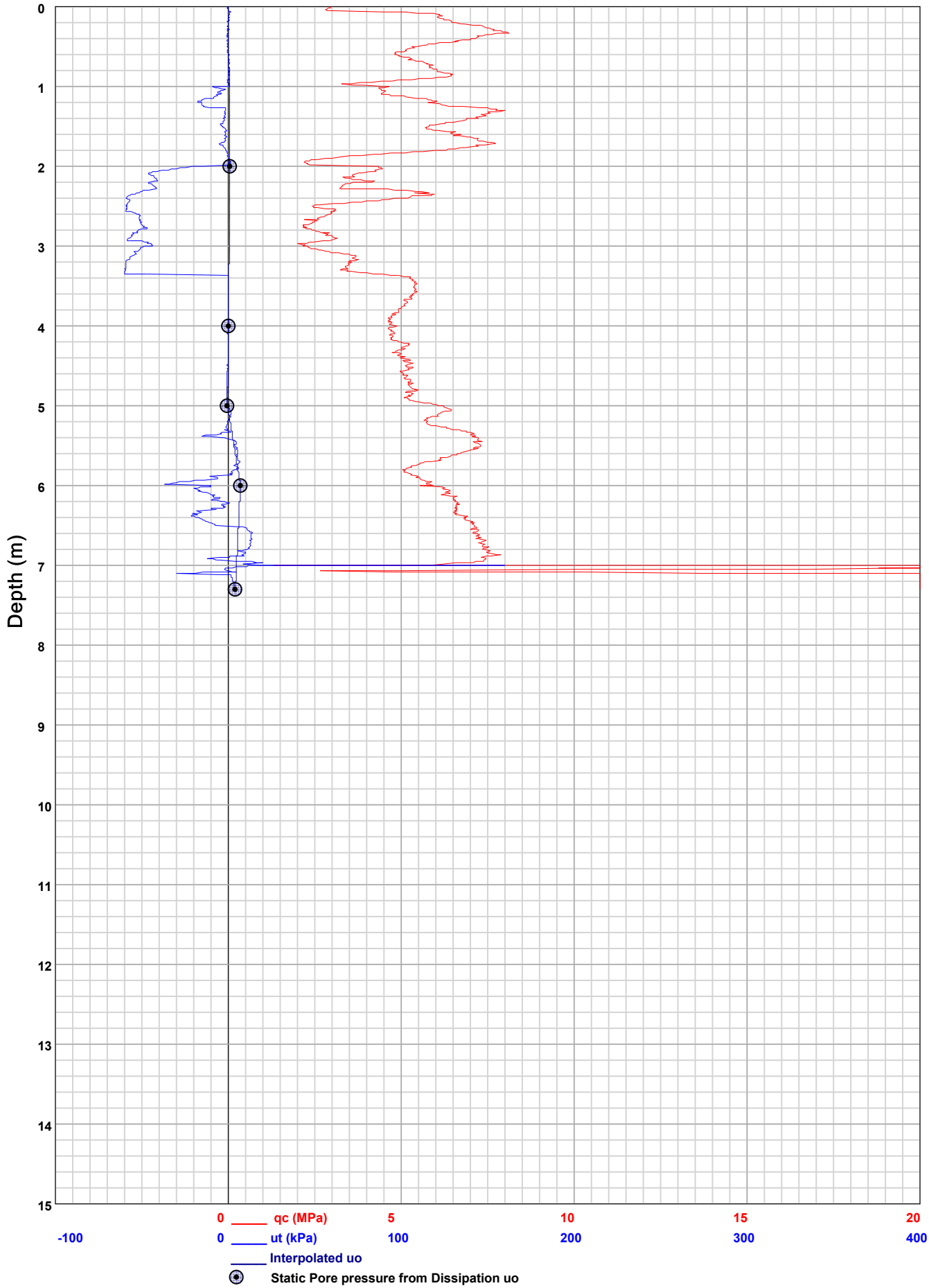

PIEZOCONE PENETRATION TEST

HOLE: C12

PROJECT: 2024 Jagersfontein

SITE: TSF

DATE: 24/02/04 At: 09:54:15 **DEPTH:** 7.303

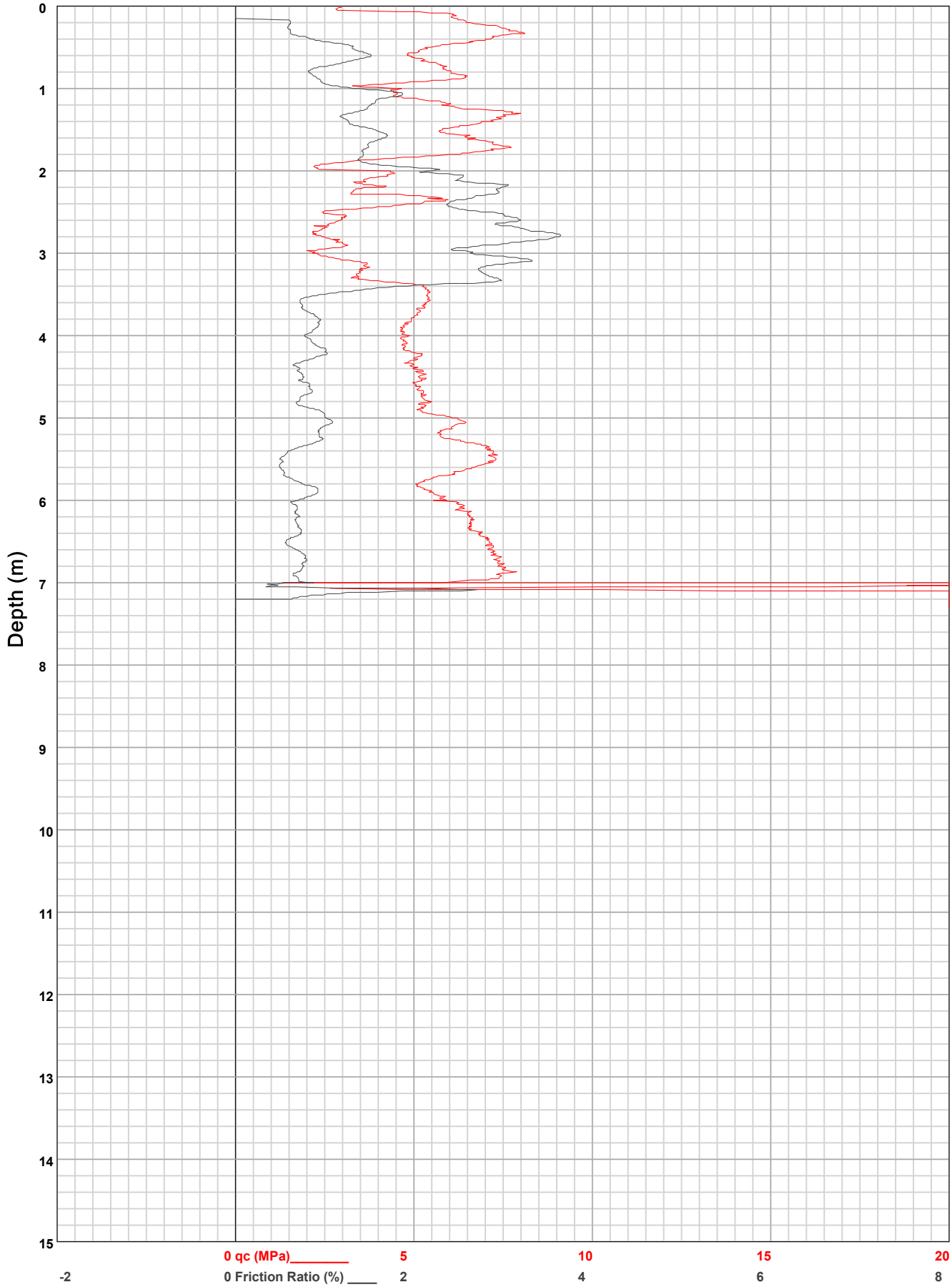

PIEZOCONE PENETRATION TEST

Dissipation Tests

HOLE: C12

PROJECT: 2024 Jagersfontein

SITE: TSF

DATE: 24/02/04 At: 09:54:15 **DEPTH:** 7.303

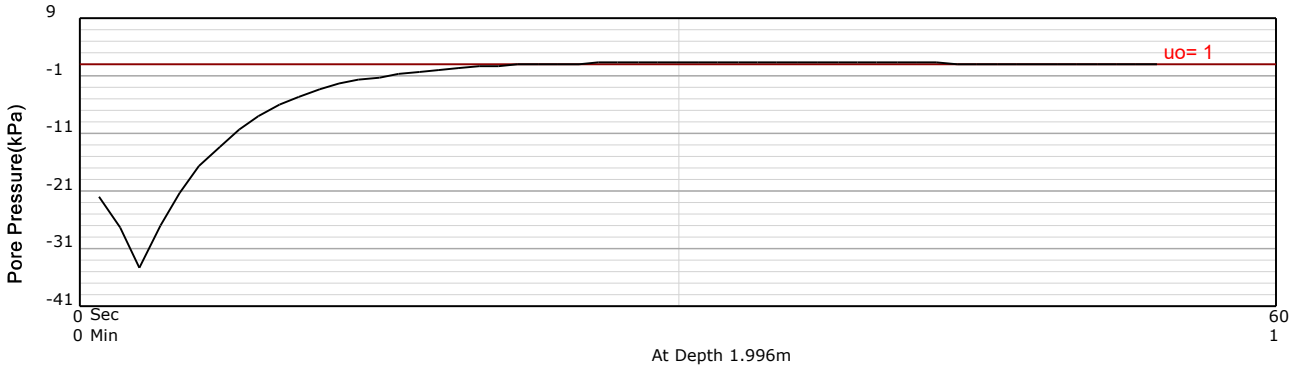

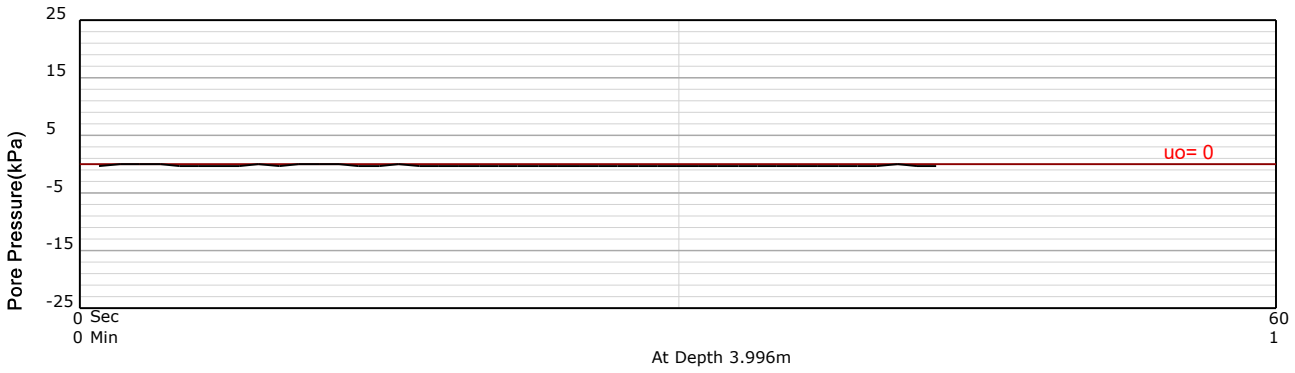

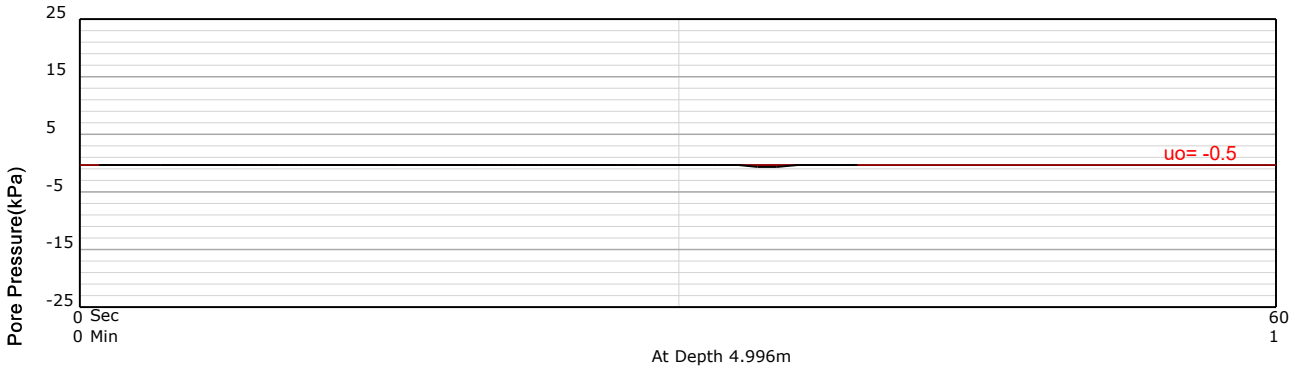

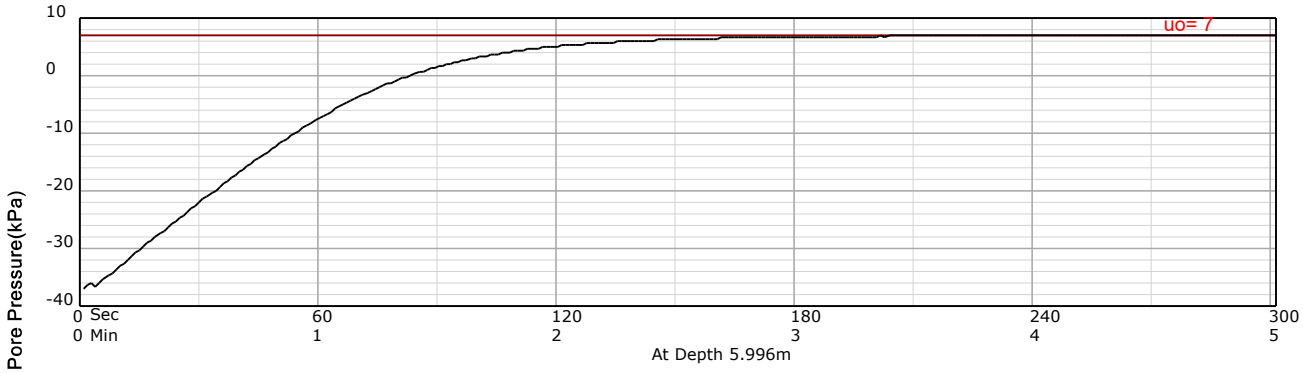

PIEZOCONE PENETRATION TEST

Dissipation Tests

HOLE: C12

PROJECT: 2024 Jagersfontein

SITE: TSF

DATE: 24/02/04 At: 09:54:15 **DEPTH:** 7.303

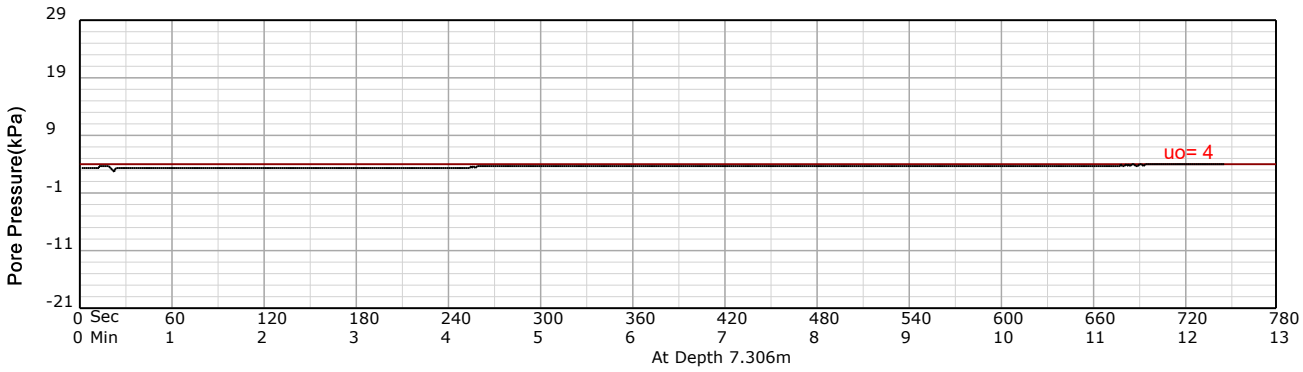

PIEZOCONE PENETRATION TEST

Equivalent Soil Behaviour Type Profile

HOLE: C12

PROJECT: 2024 Jagersfontein

SITE: TSF

DATE: 24/02/04 At: 09:54:15

DEPTH: 7.303

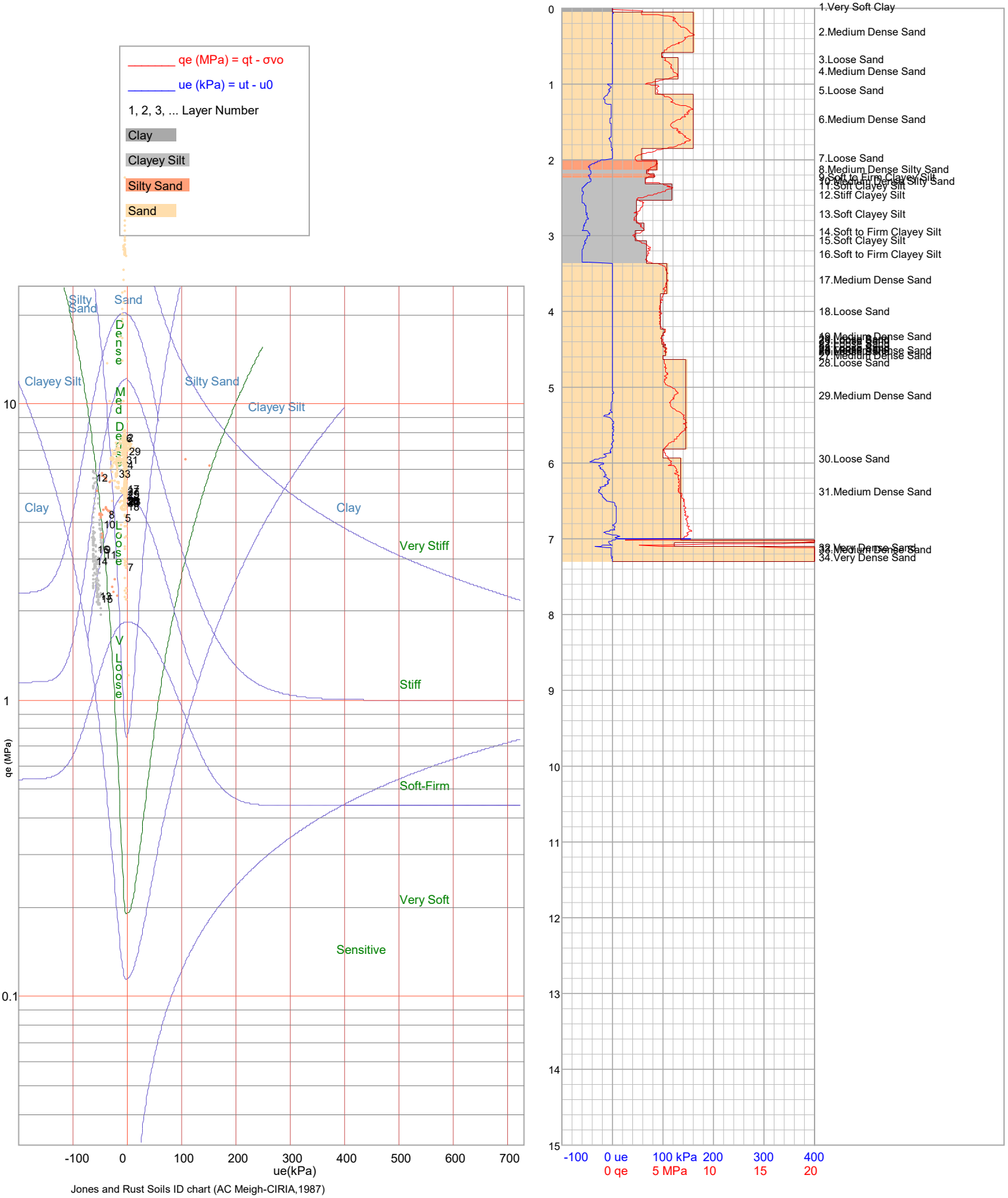

Jones and Rust Soils ID chart (AC Meigh-CIRIA,1987)

PIEZOCONE PENETRATION TEST

Recorded Field Results (Cone, Pore Pressure and Static Pore Pressure from Dissipations)

HOLE: C13

PROJECT: 2024 Jagersfontein

SITE: TSF

DATE: 24/03/01 At: 15:19:59 A **DEPTH:** 24.082

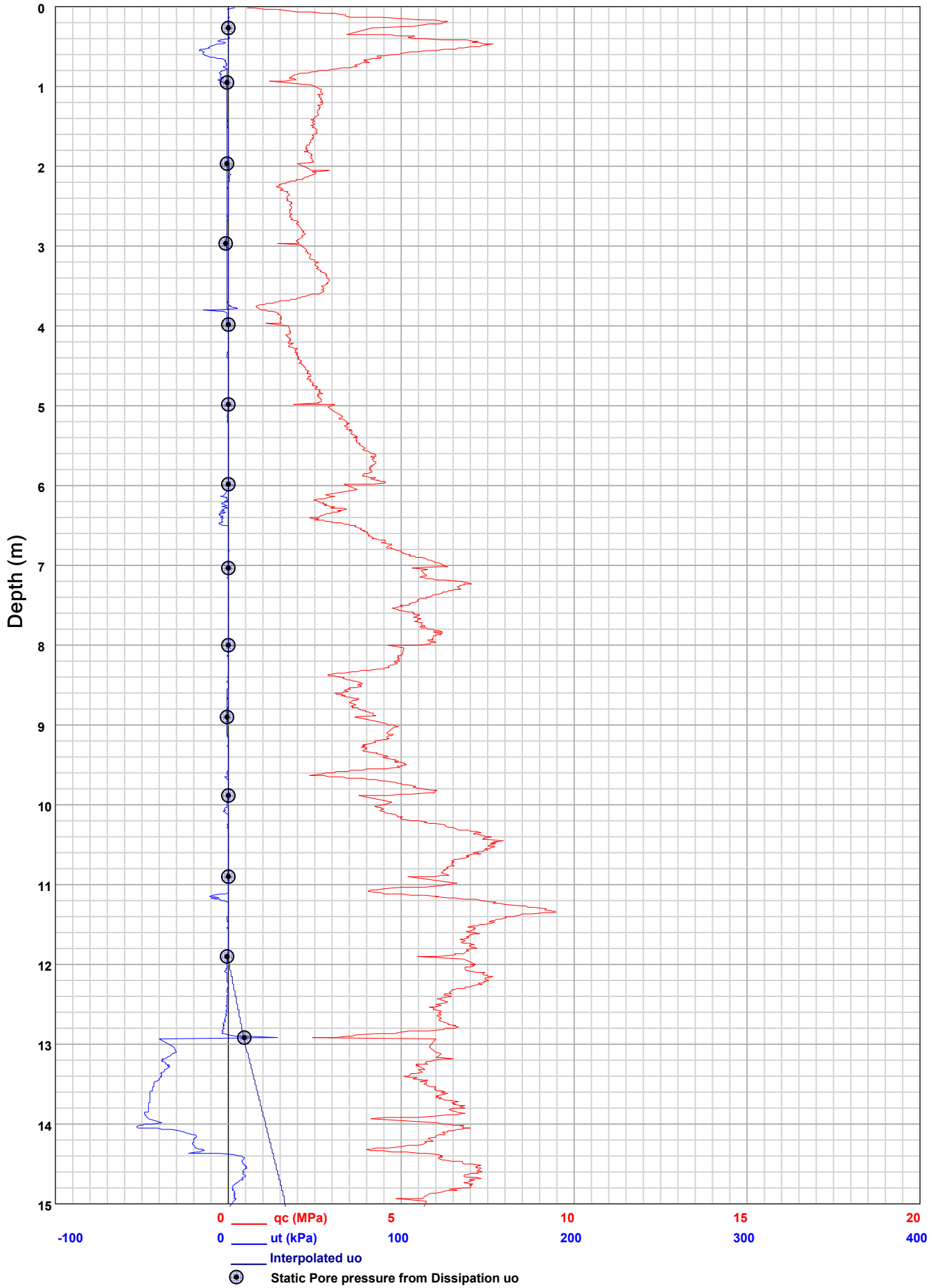

PIEZOCONE PENETRATION TEST

Recorded Field Results (Cone, Pore Pressure and Static Pore Pressure from Dissipations)

HOLE: C13

PROJECT: 2024 Jagersfontein

SITE: TSF

DATE: 24/03/01 At: 15:19:59 A **DEPTH:** 24.082

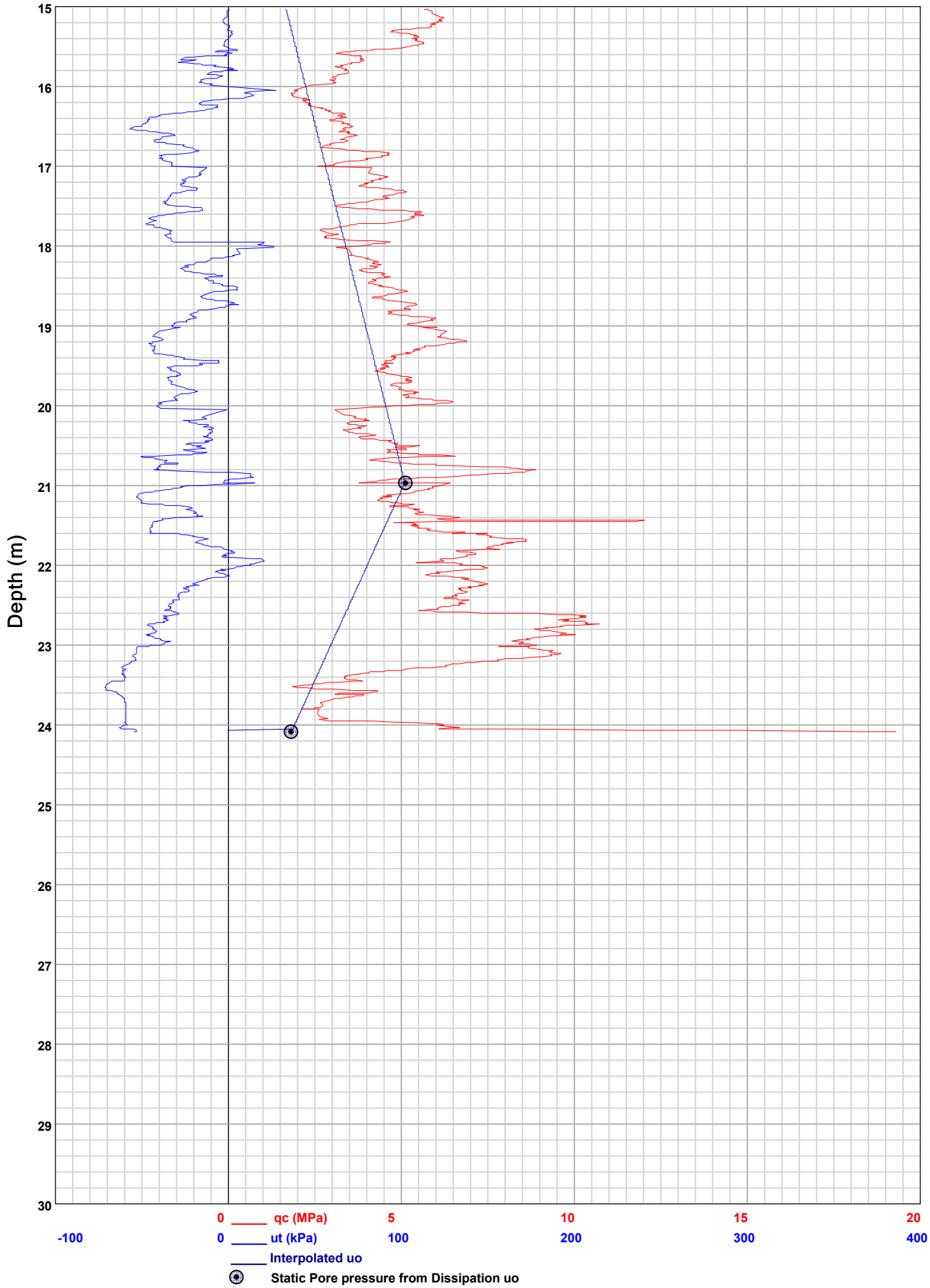

PIEZOCONE PENETRATION TEST

HOLE: C13

PROJECT: 2024 Jagersfontein

SITE: TSF

DATE: 24/03/01 At: 15:19:59 A

DEPTH: 24.082

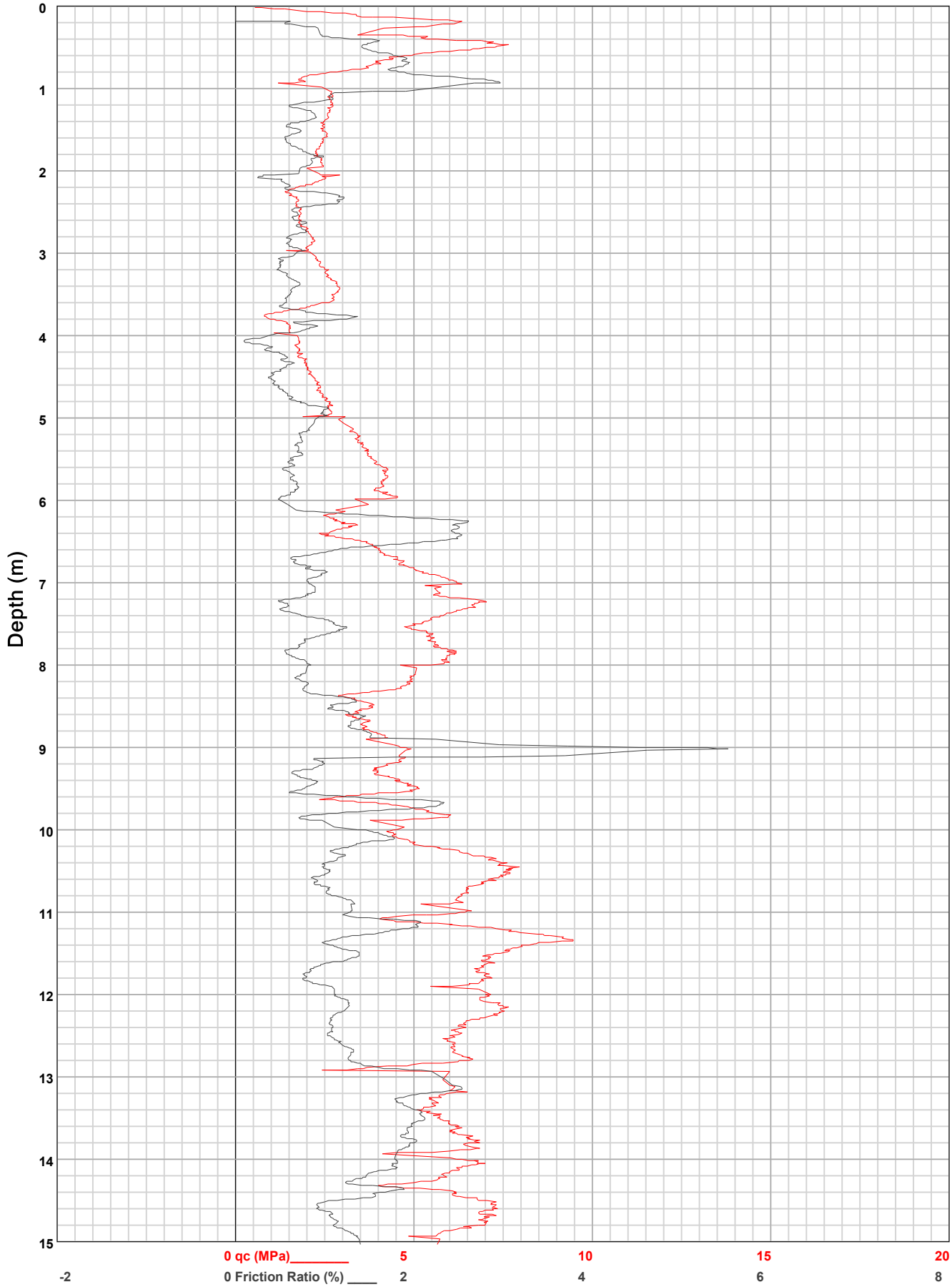

PIEZOCONE PENETRATION TEST

HOLE: C13

PROJECT: 2024 Jagersfontein

SITE: TSF

DATE: 24/03/01 At: 15:19:59 A

DEPTH: 24.082

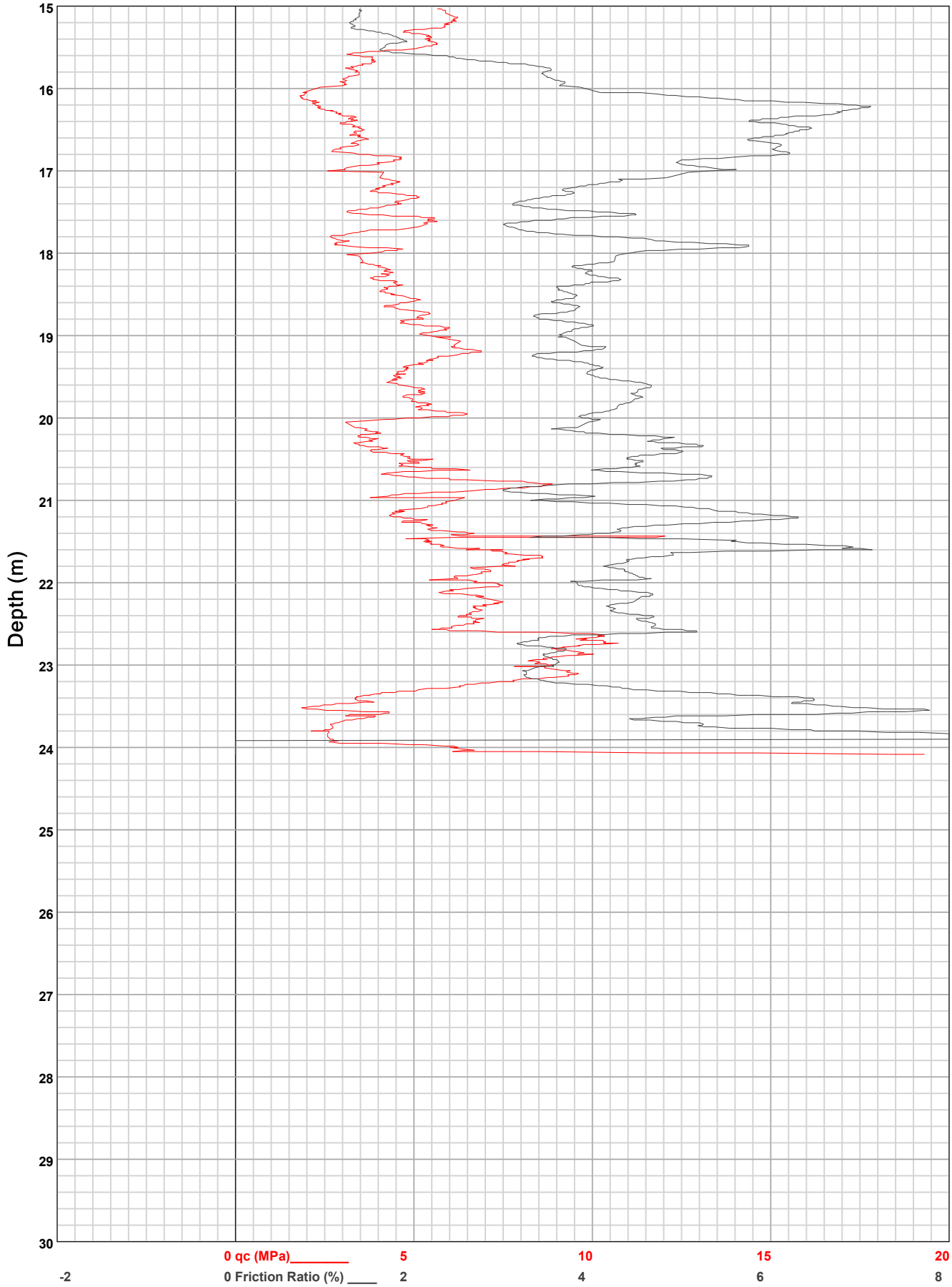

PIEZOCONE PENETRATION TEST

Dissipation Tests

HOLE: C13

PROJECT: 2024 Jagersfontein

SITE: TSF

DATE: 24/03/01 At: 15:19:59 A

DEPTH: 24.082

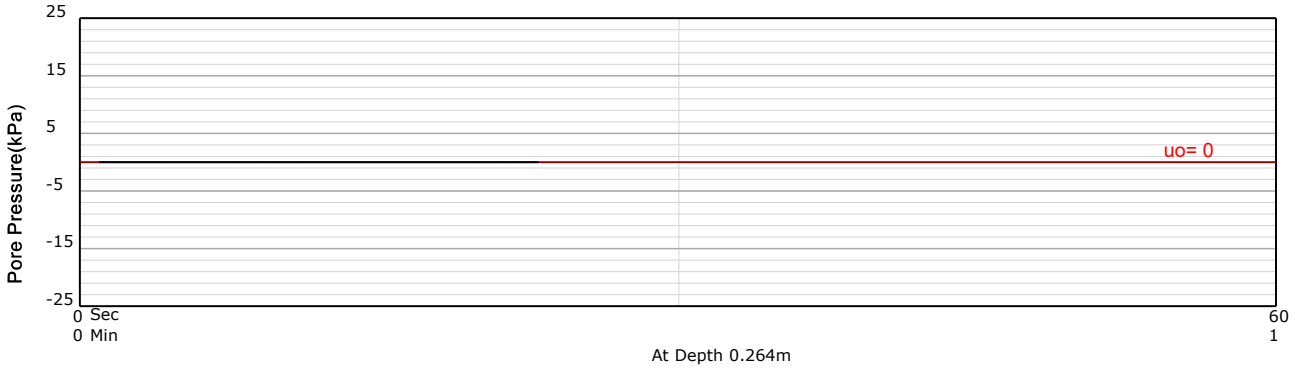

At Depth 0.264m

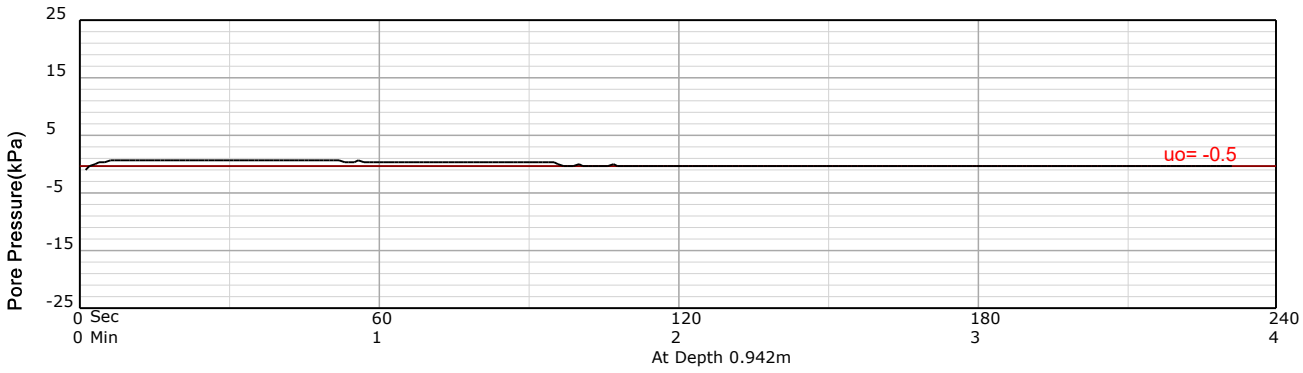

At Depth 0.942m

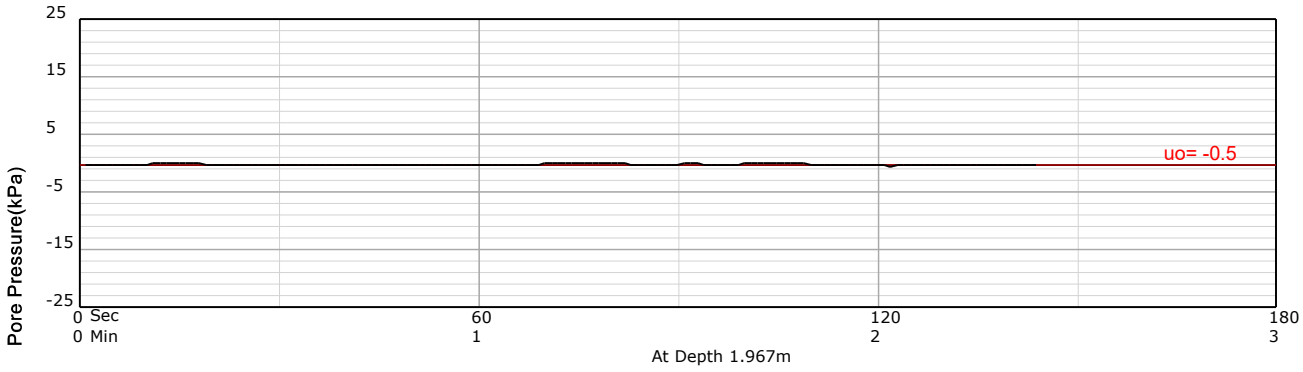

At Depth 1.967m

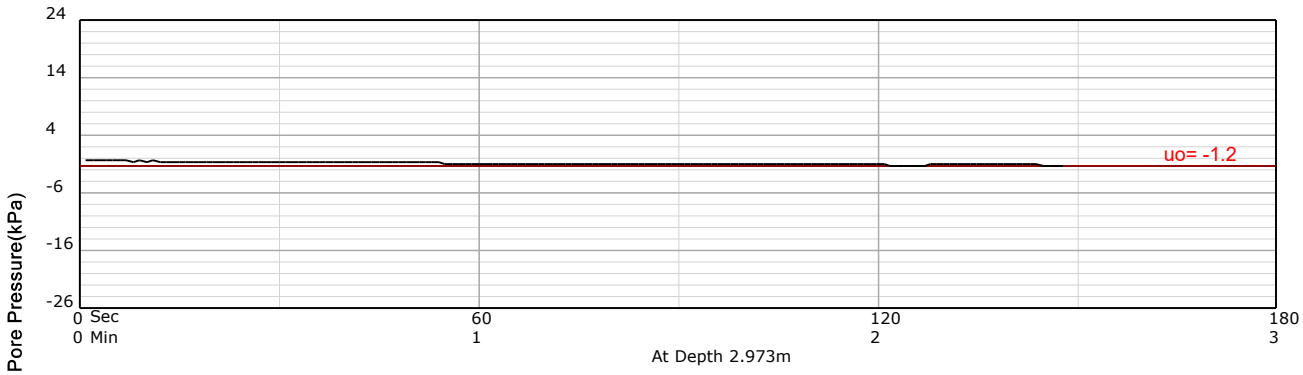

At Depth 2.973m

PIEZOCONE PENETRATION TEST

Dissipation Tests

HOLE: C13

PROJECT: 2024 Jagersfontein

SITE: TSF

DATE: 24/03/01 At: 15:19:59 A

DEPTH: 24.082

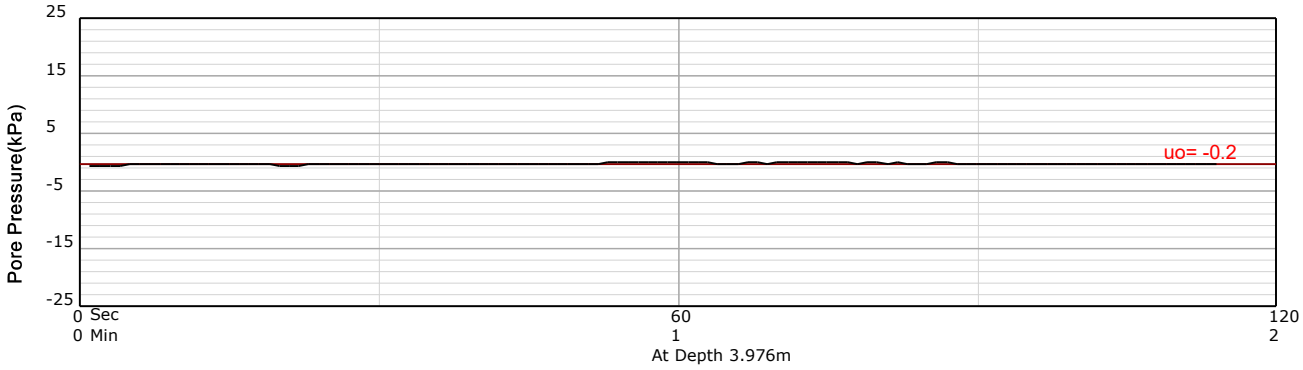

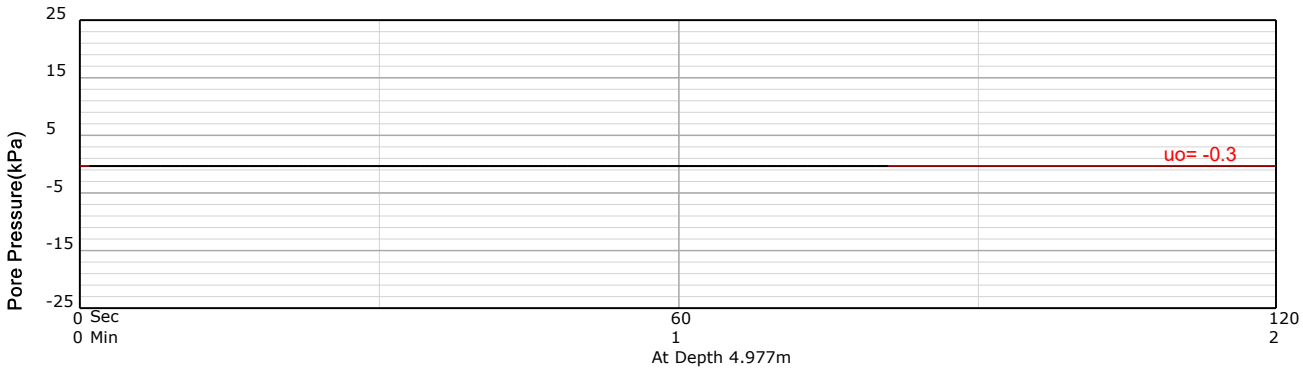

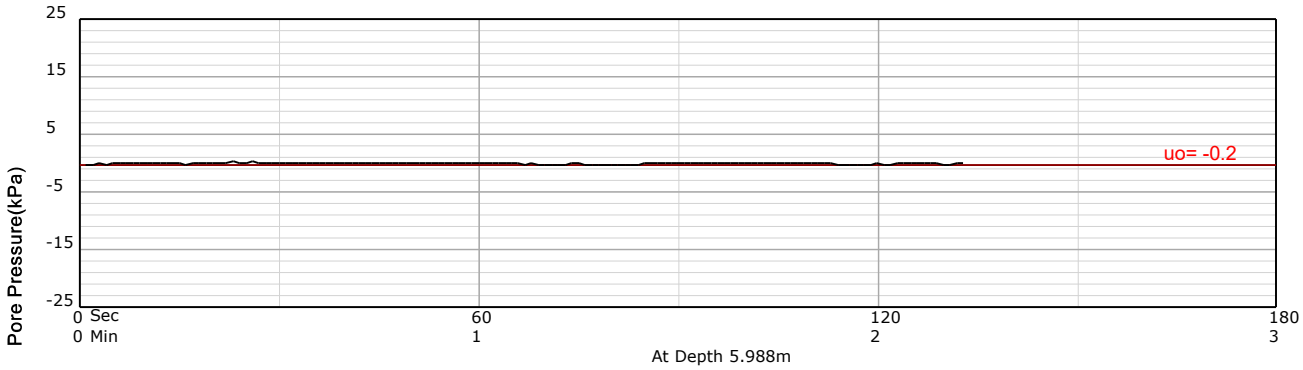

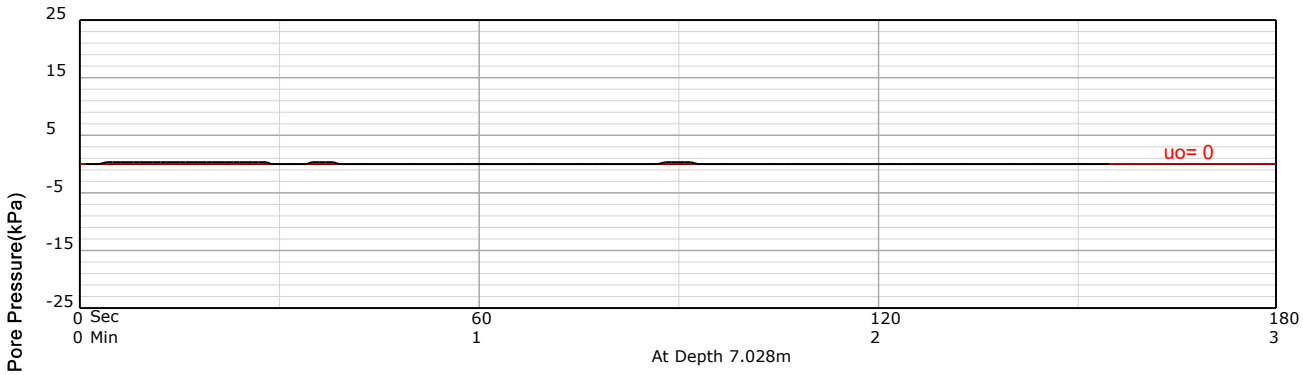

PIEZOCONE PENETRATION TEST

Dissipation Tests

HOLE: C13

PROJECT: 2024 Jagersfontein

SITE: TSF

DATE: 24/03/01 At: 15:19:59 A

DEPTH: 24.082

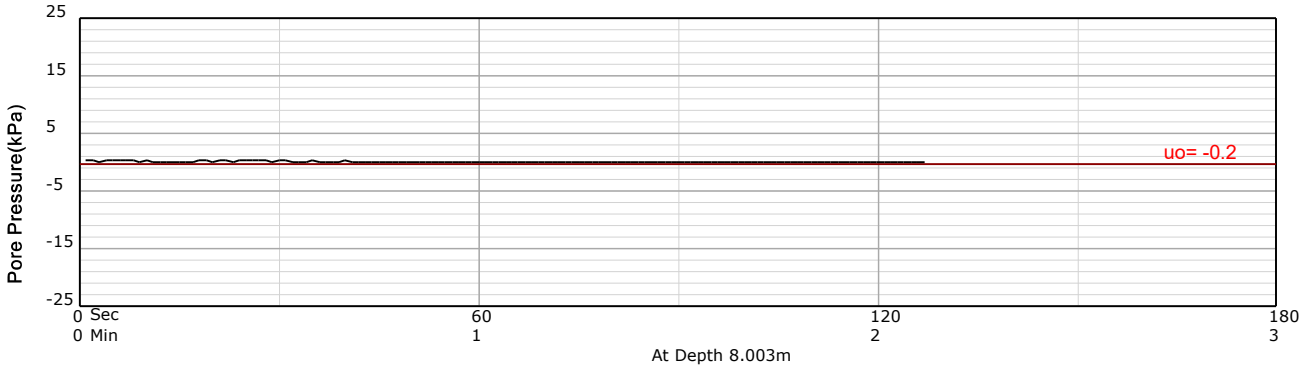

At Depth 8.003m

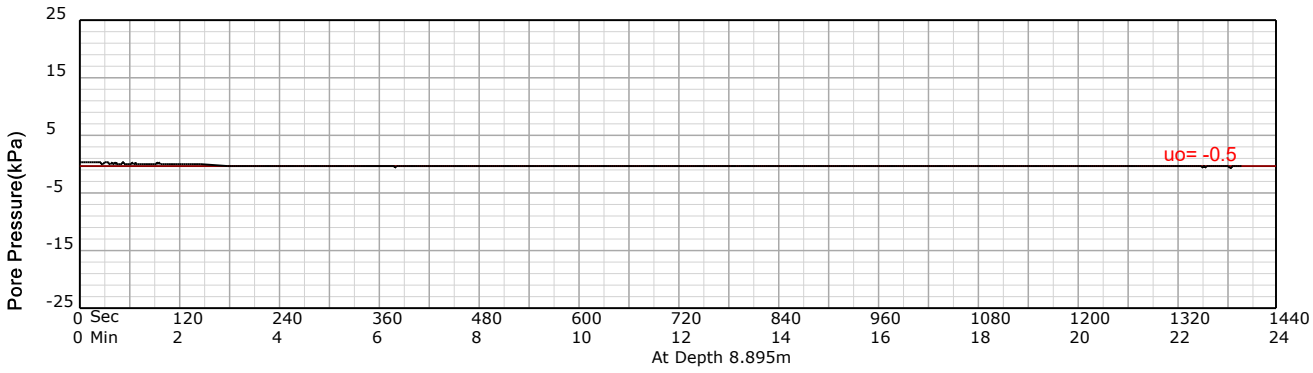

At Depth 8.895m

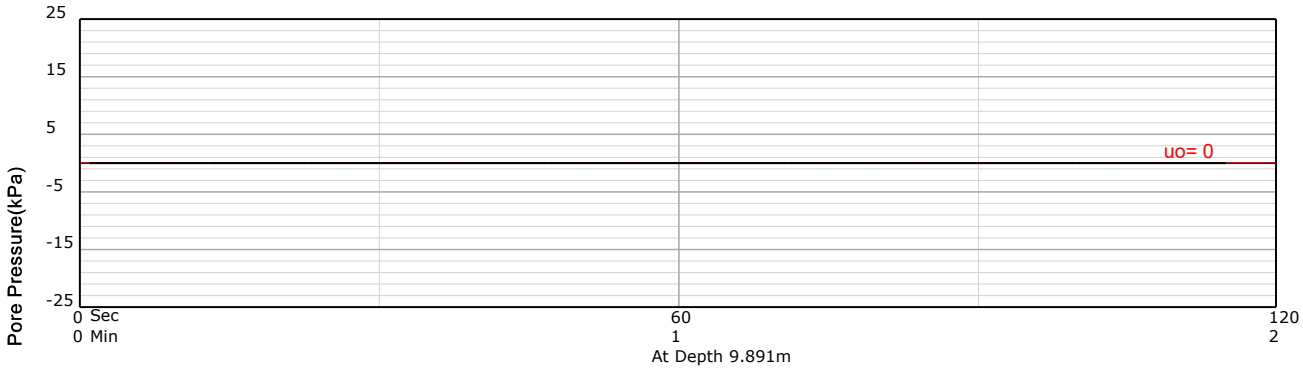

At Depth 9.891m

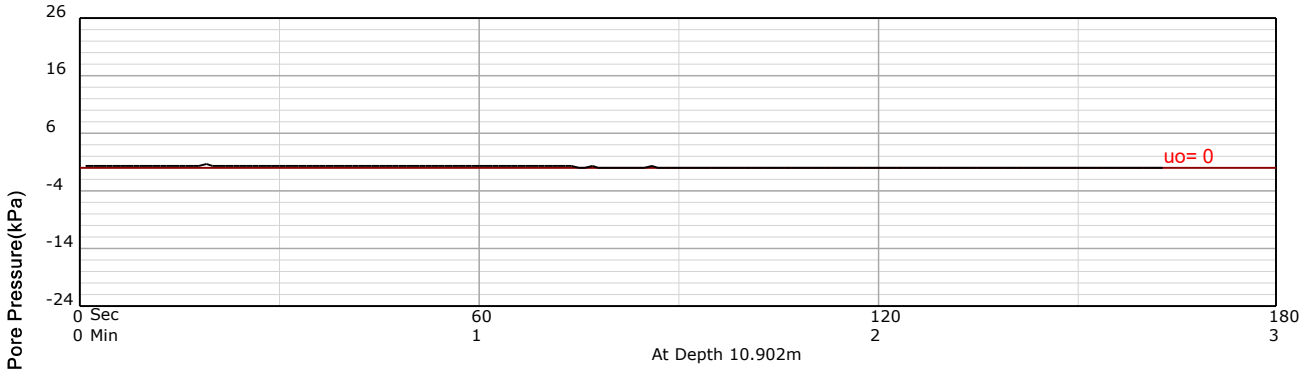

At Depth 10.902m

PIEZOCONE PENETRATION TEST

Dissipation Tests

HOLE: C13

PROJECT: 2024 Jagersfontein

SITE: TSF

DATE: 24/03/01 At: 15:19:59 A

DEPTH: 24.082

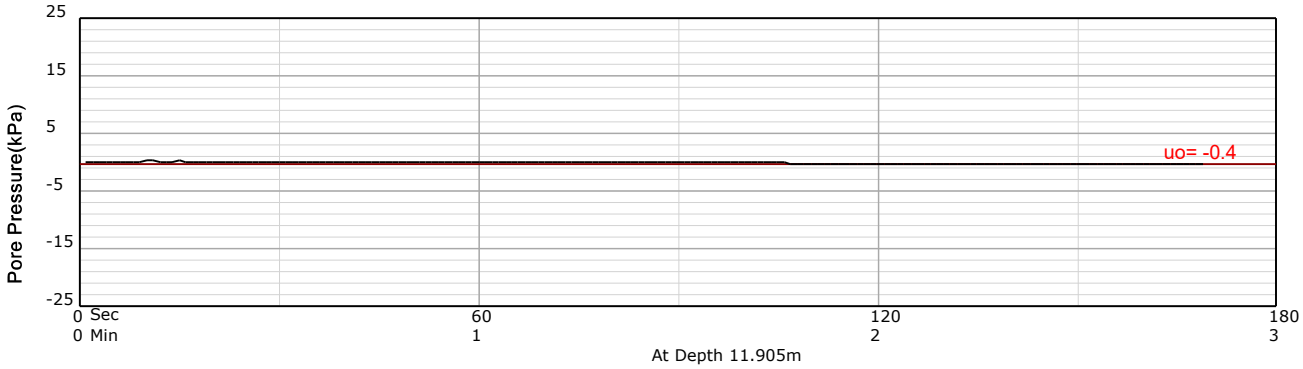

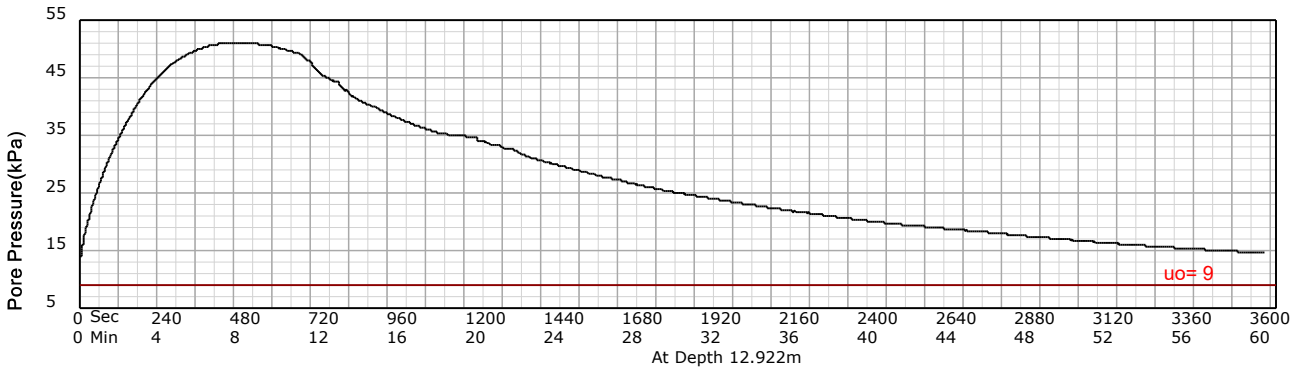

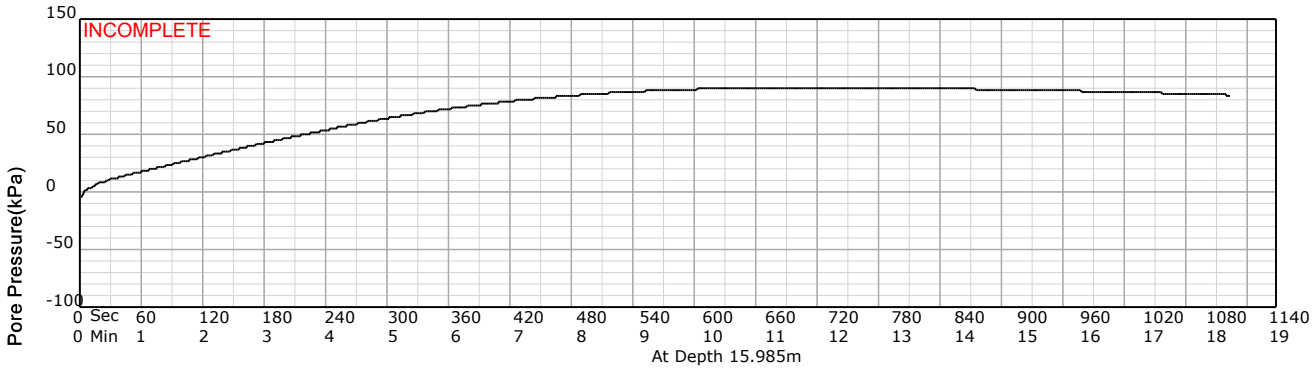

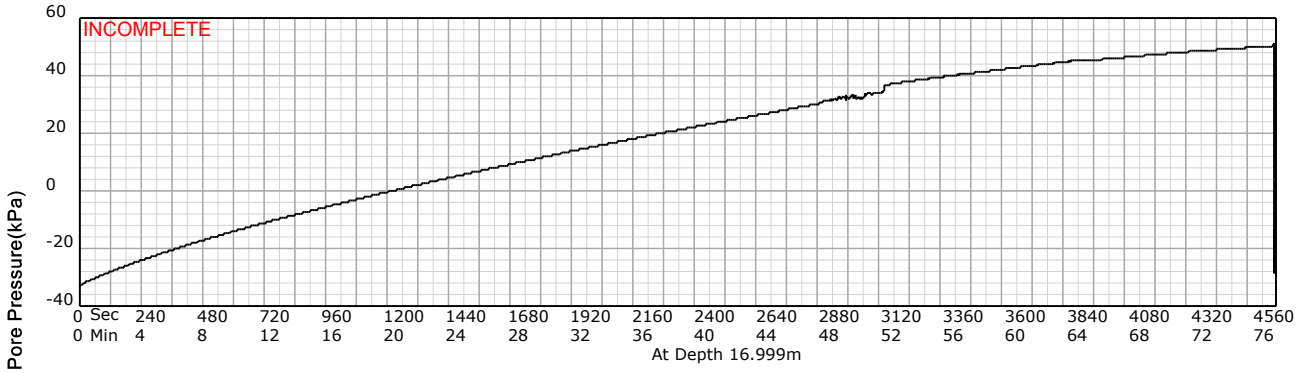

PIEZOCONE PENETRATION TEST

Dissipation Tests

HOLE: C13

PROJECT: 2024 Jagersfontein

SITE: TSF

DATE: 24/03/01 At: 15:19:59 A

DEPTH: 24.082

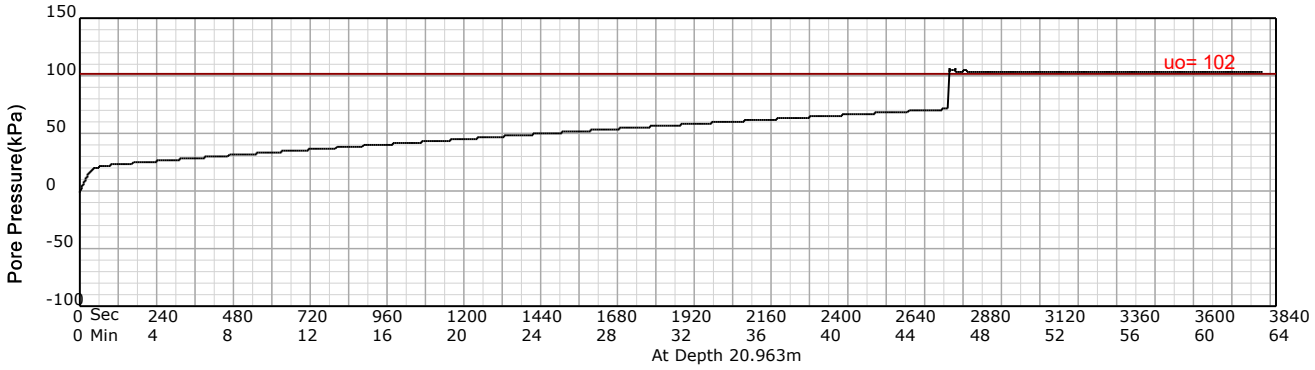

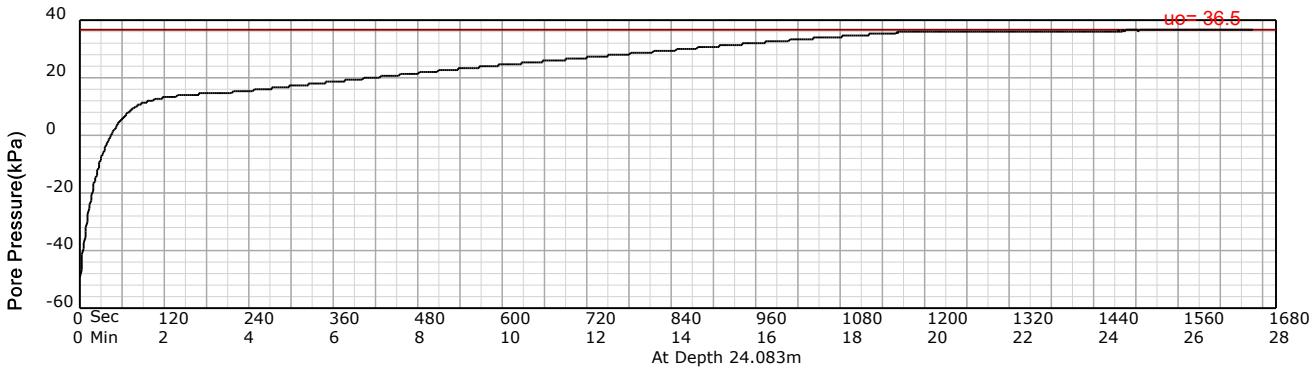

PIEZOCONE PENETRATION TEST

Equivalent Soil Behaviour Type Profile

HOLE: C13

PROJECT: 2024 Jagersfontein

SITE: TSF

DATE: 24/03/01 At: 15:19:59 A

DEPTH: 24.082

qe (MPa) = qt - σvo

ue (kPa) = ut - u0

1, 2, 3, ... Layer Number

Clay

Clayey Silt

Silty Sand

Sand

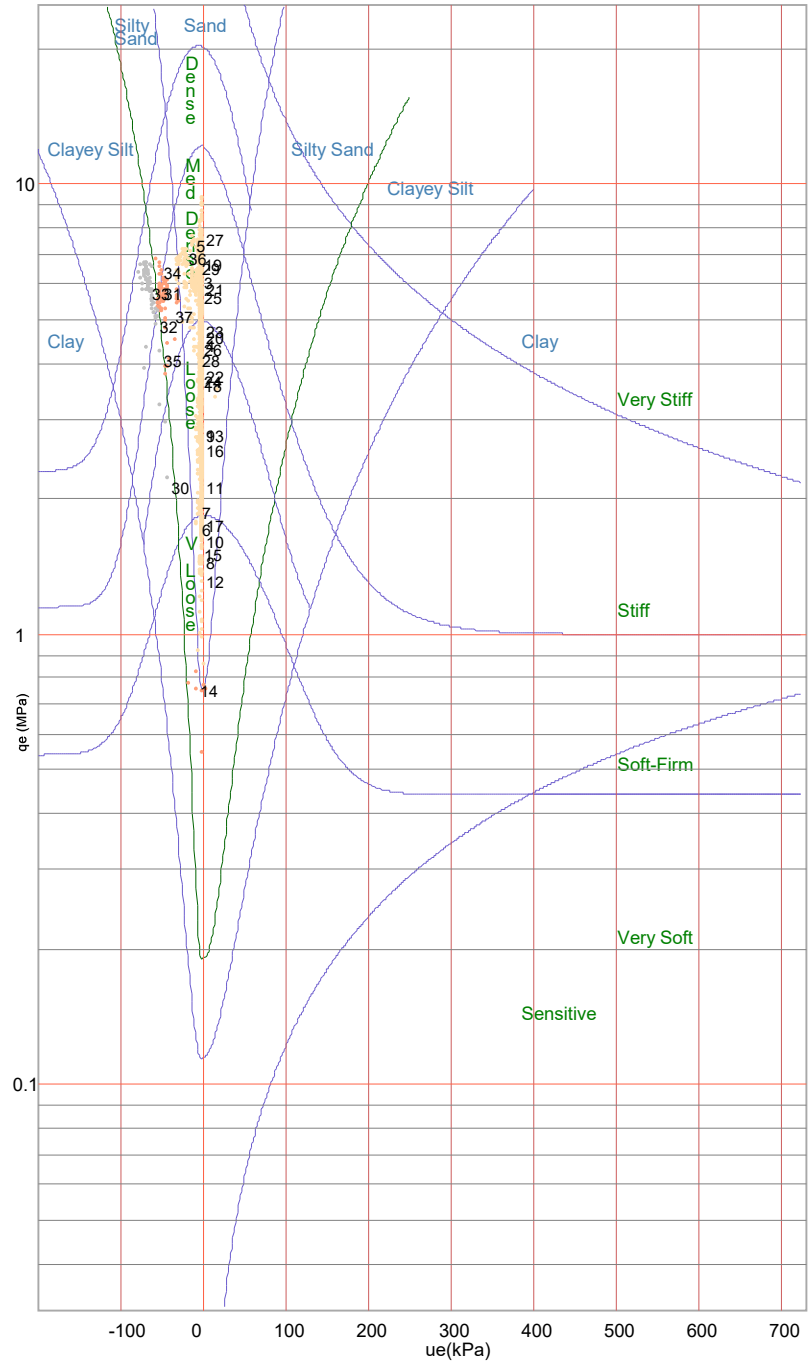

Jones and Rust Soils ID chart (AC Meigh-CIRIA,1987)

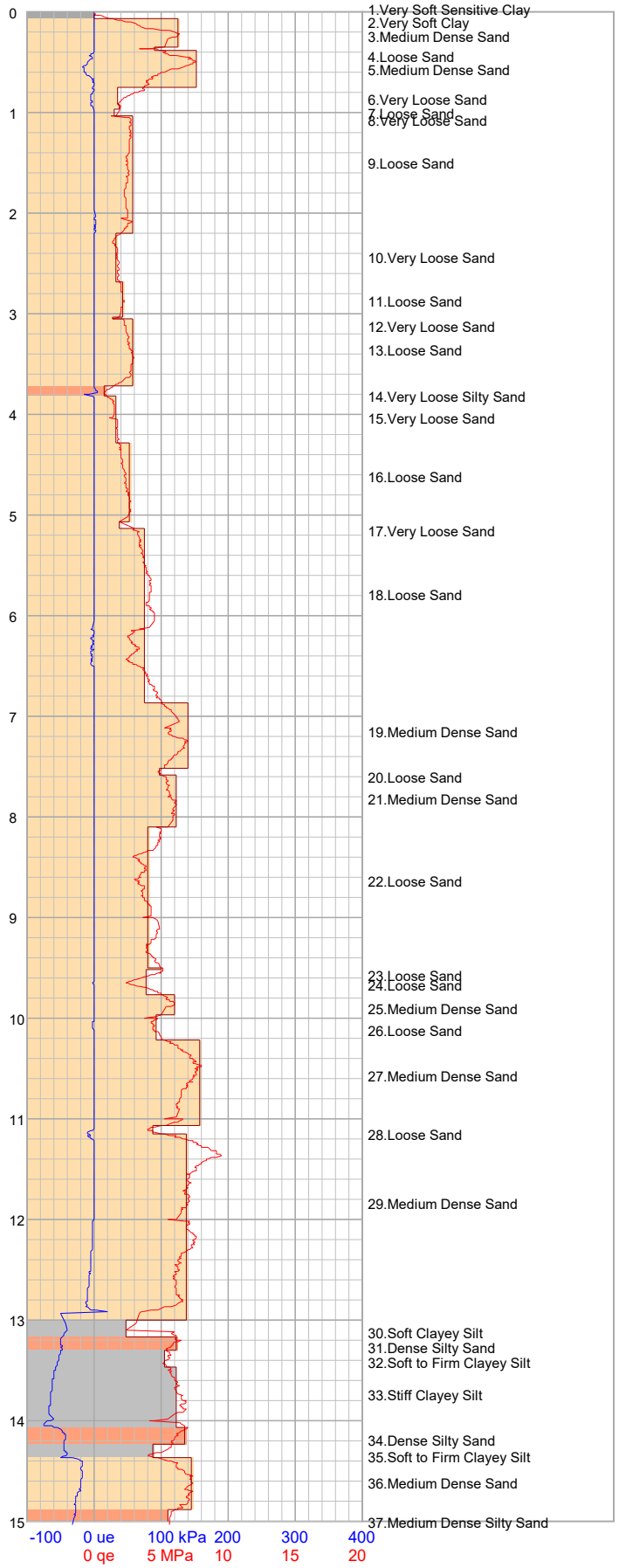

PIEZOCONE PENETRATION TEST

Equivalent Soil Behaviour Type Profile

HOLE: C13

PROJECT: 2024 Jagersfontein

SITE: TSF

DATE: 24/03/01 At: 15:19:59 A

DEPTH: 24.082

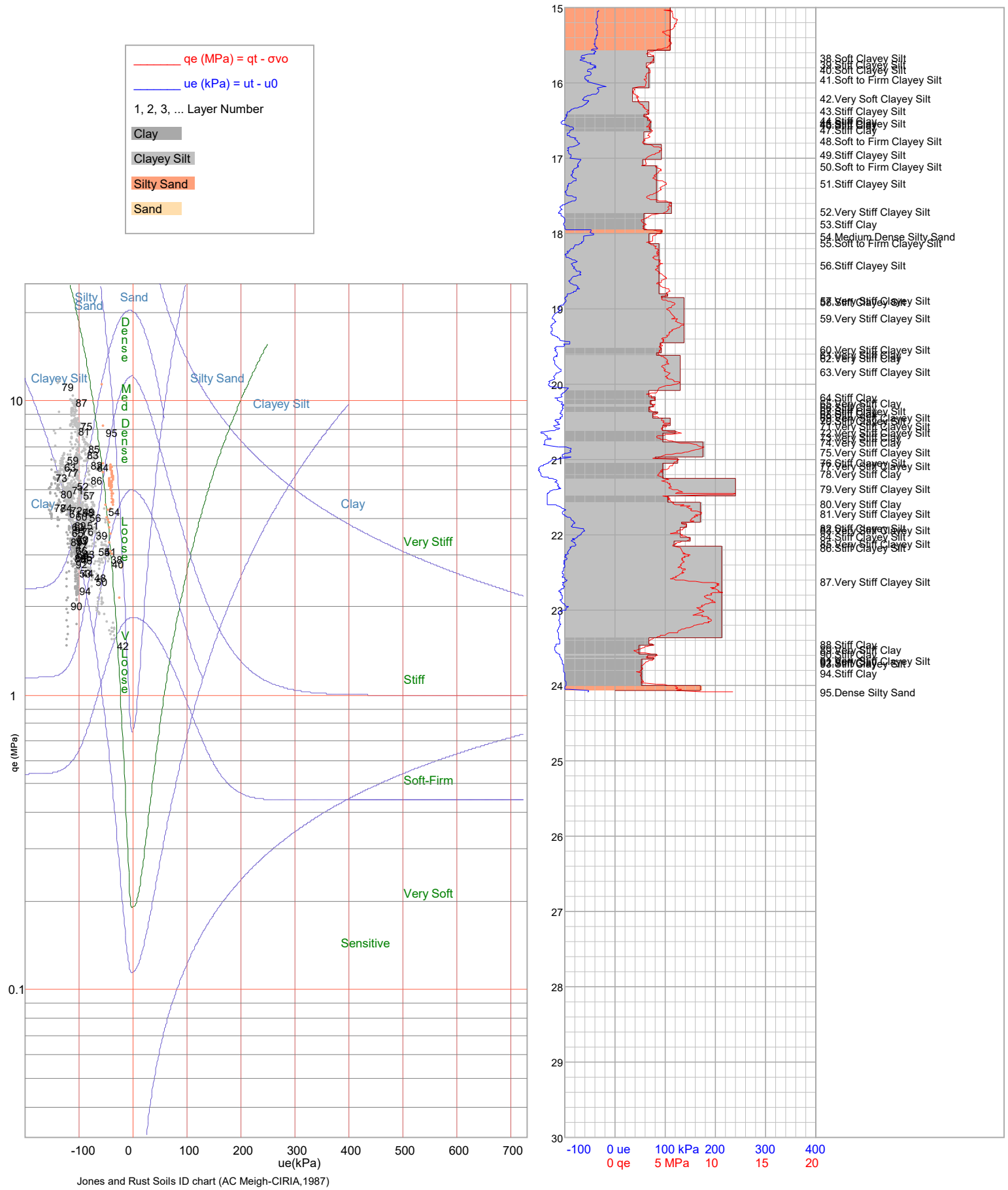

Jones and Rust Soils ID chart (AC Meigh-CIRIA,1987)

PIEZOCONE PENETRATION TEST

Recorded Field Results (Cone, Pore Pressure and Static Pore Pressure from Dissipations)

HOLE: C14

PROJECT: 2024 Jagersfontein

SITE: TSF

DATE: 24/03/02 At: 14:12:00 **DEPTH:** 23.68

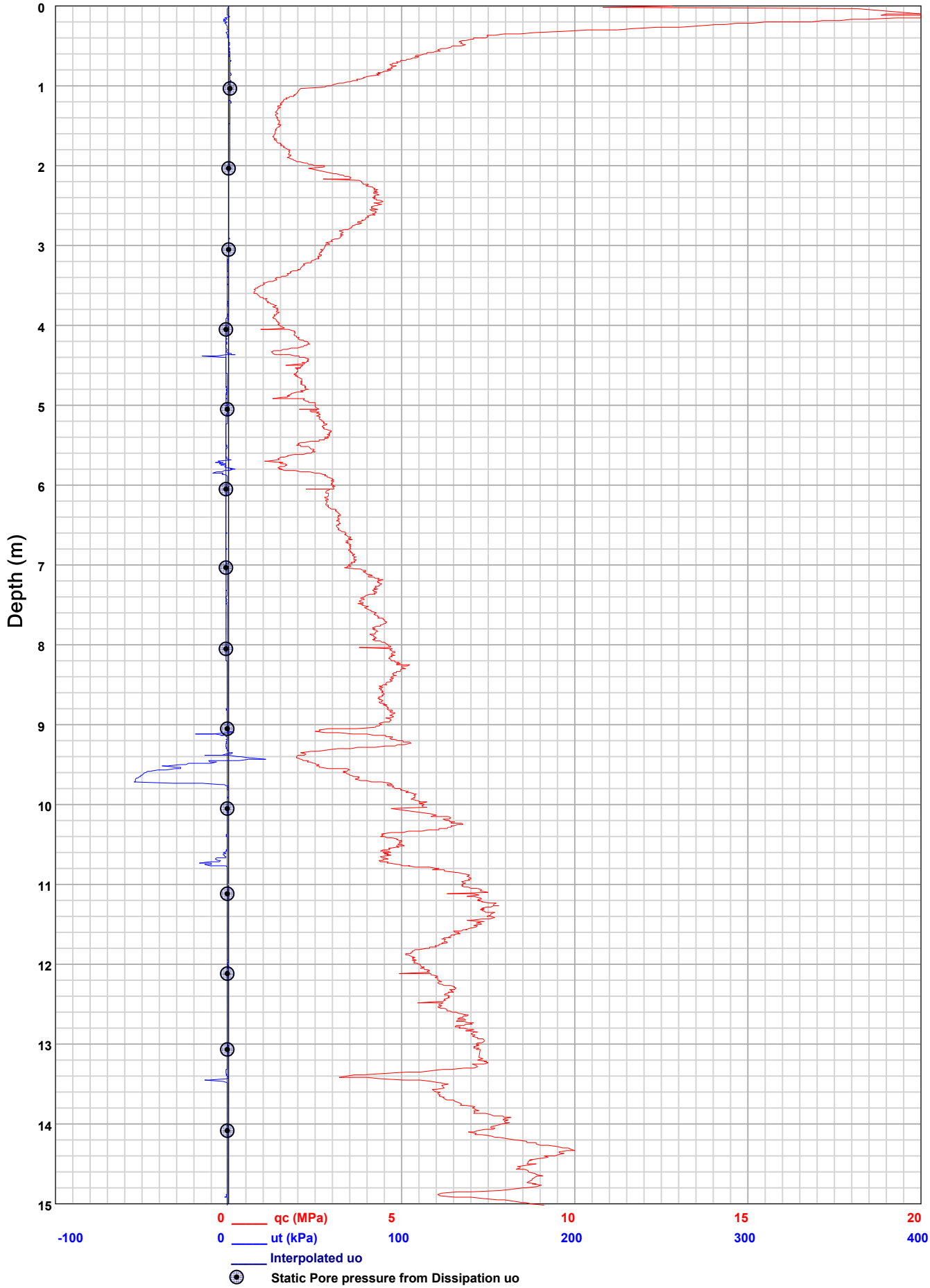

PIEZOCONE PENETRATION TEST

Recorded Field Results (Cone, Pore Pressure and Static Pore Pressure from Dissipations)

HOLE: C14

PROJECT: 2024 Jagersfontein

SITE: TSF

DATE: 24/03/02 At: 14:12:00 **DEPTH:** 23.68

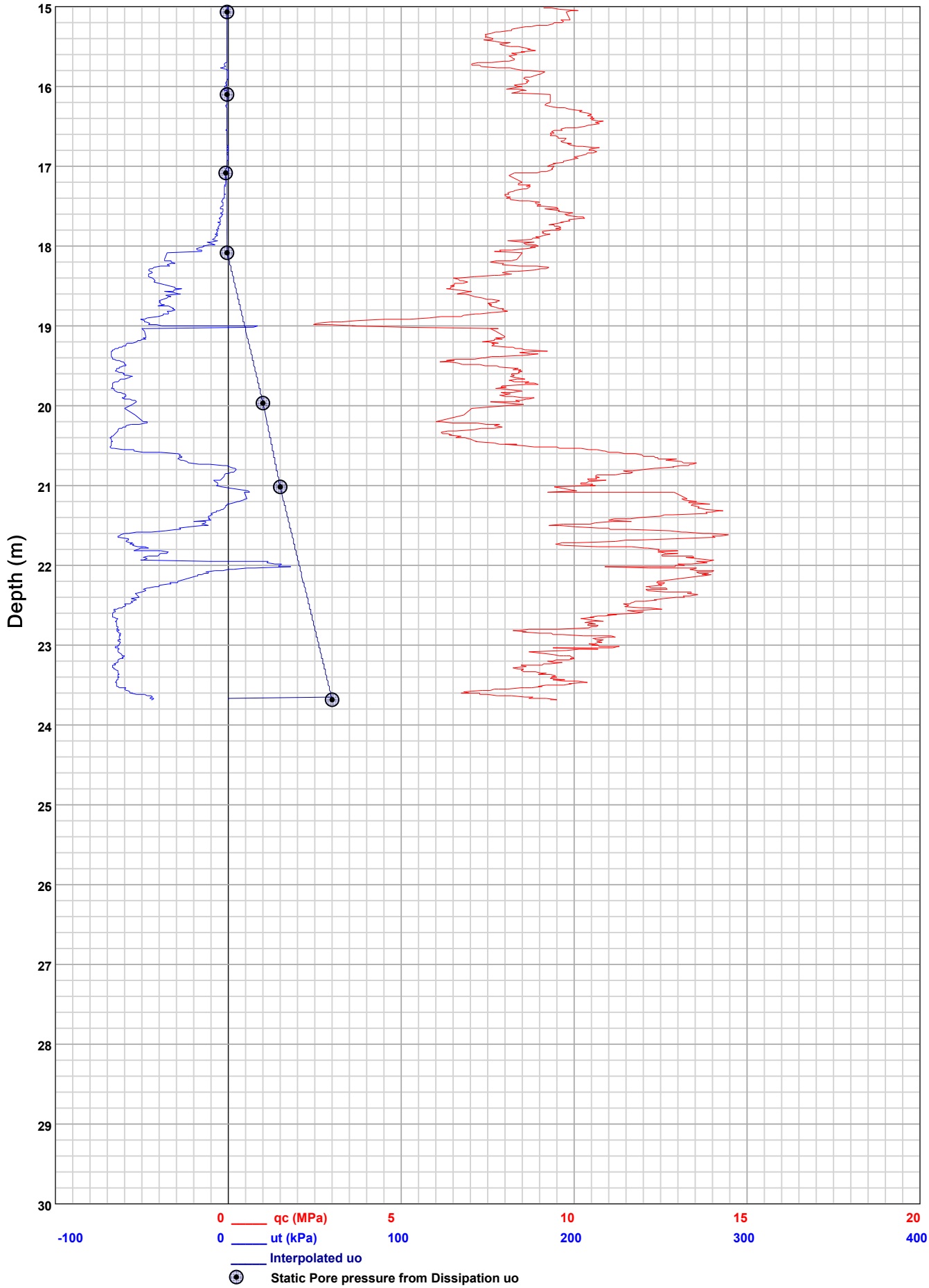

PIEZOCONE PENETRATION TEST

HOLE: C14

PROJECT: 2024 Jagersfontein

SITE: TSF

DATE: 24/03/02 At: 14:12:00 **DEPTH:** 23.68

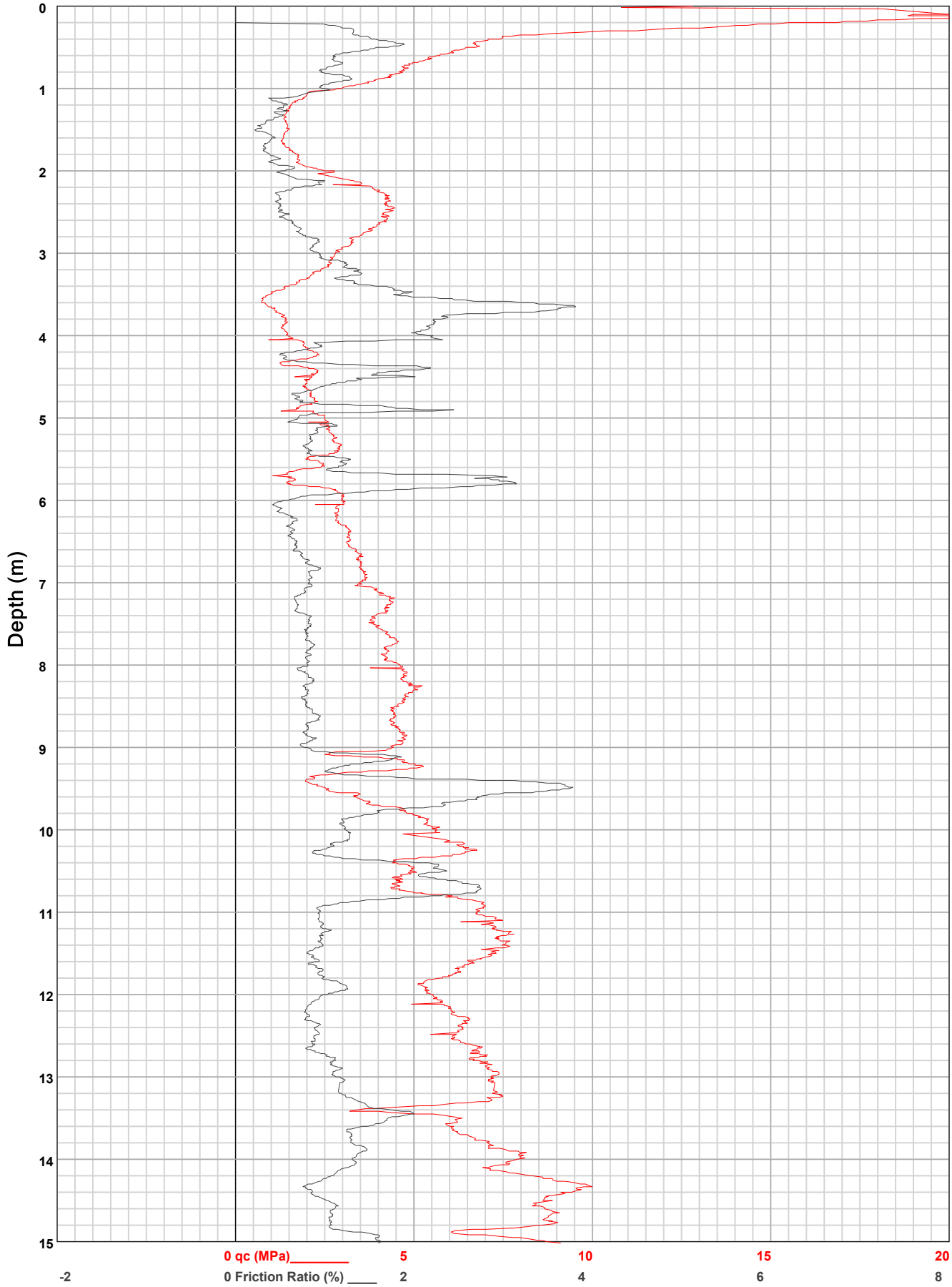

PIEZOCONE PENETRATION TEST

HOLE: C14

PROJECT: 2024 Jagersfontein

SITE: TSF

DATE: 24/03/02 At: 14:12:00 **DEPTH:** 23.68

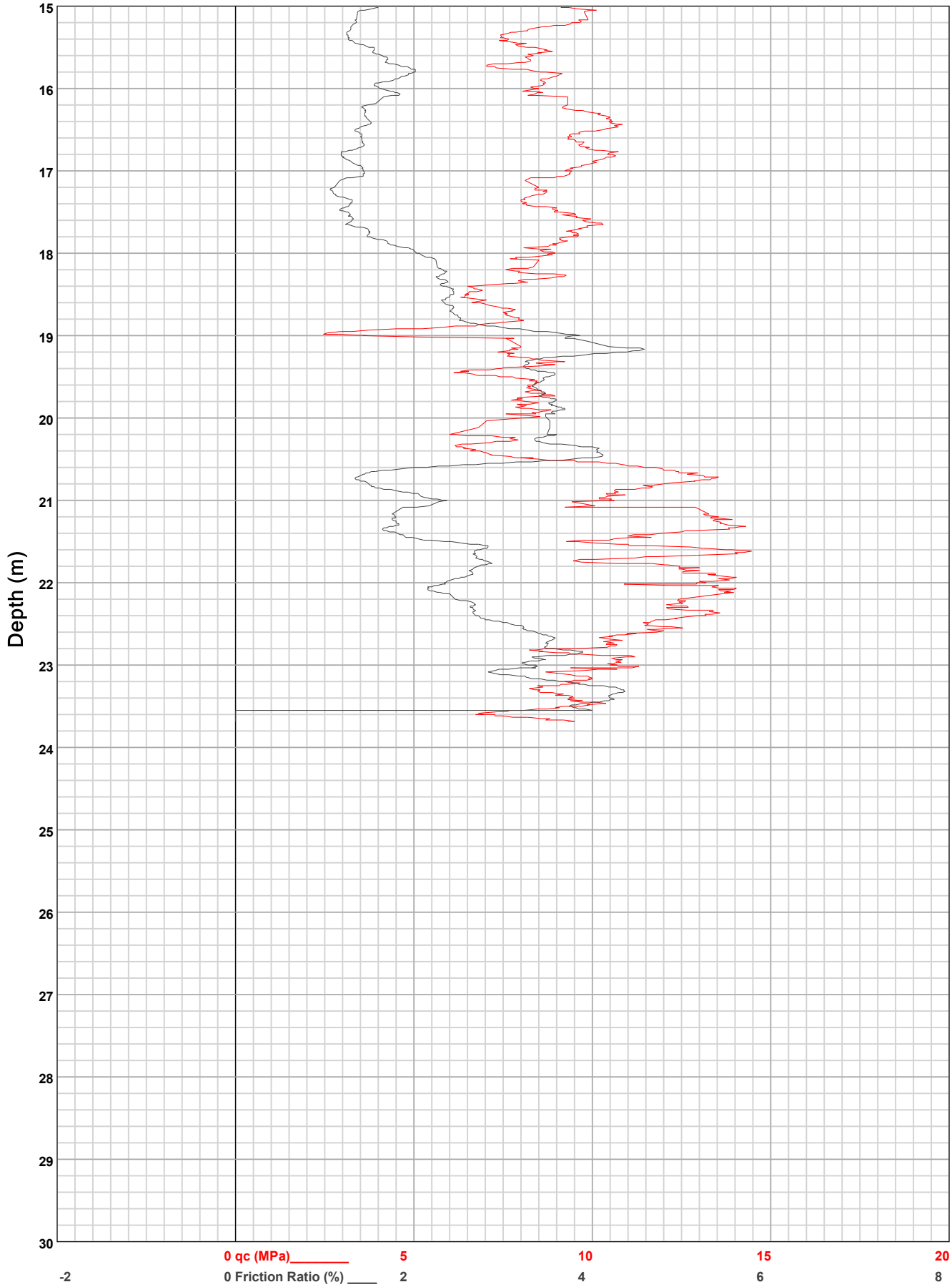

PIEZOCONE PENETRATION TEST

Dissipation Tests

HOLE: C14

PROJECT: 2024 Jagersfontein

SITE: TSF

DATE: 24/03/02 At: 14:12:00 **DEPTH:** 23.68

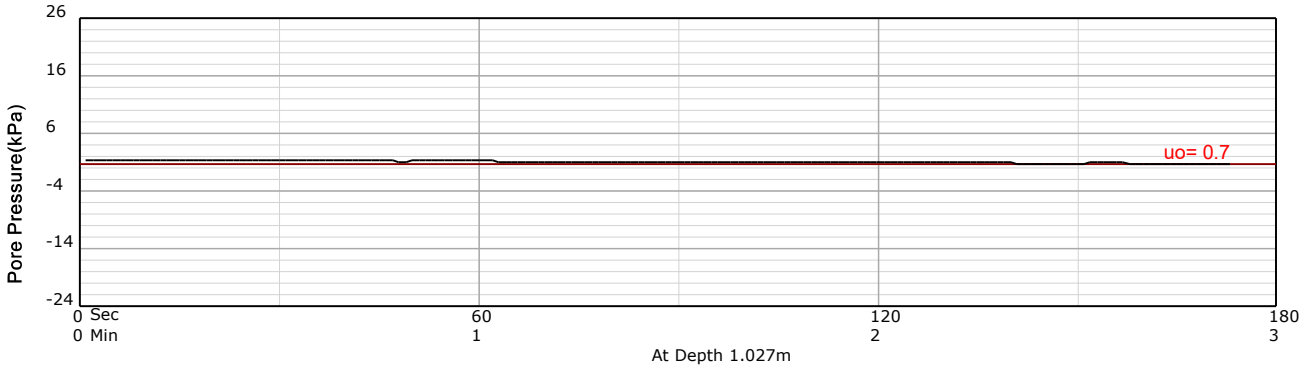

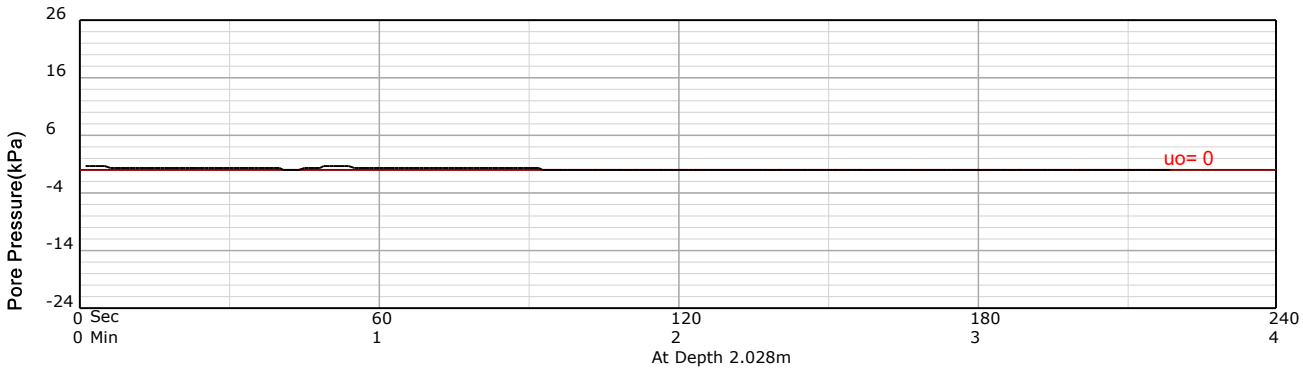

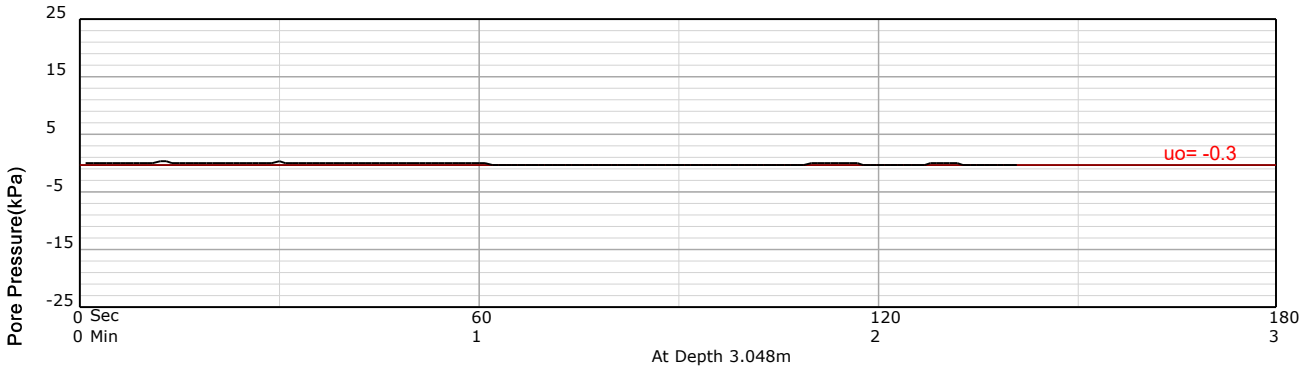

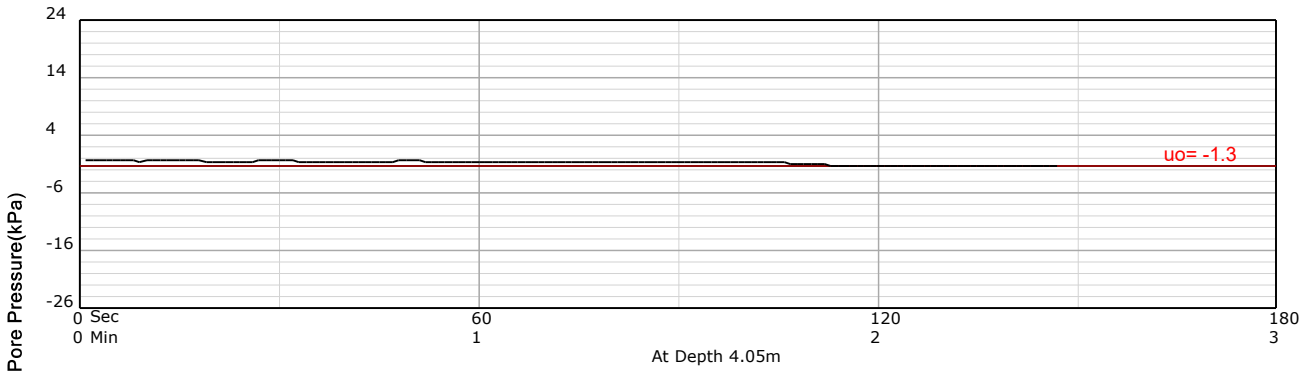

PIEZOCONE PENETRATION TEST

Dissipation Tests

HOLE: C14

PROJECT: 2024 Jagersfontein

SITE: TSF

DATE: 24/03/02 At: 14:12:00 **DEPTH:** 23.68

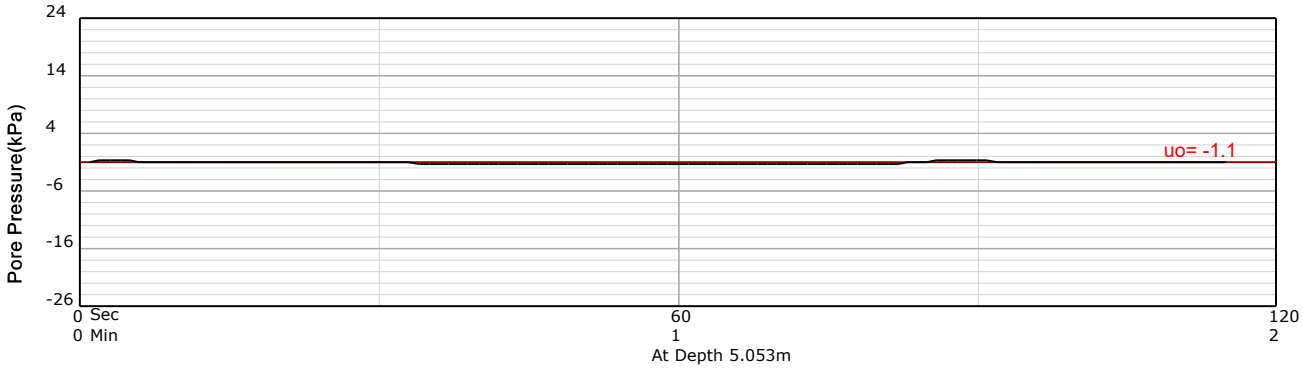

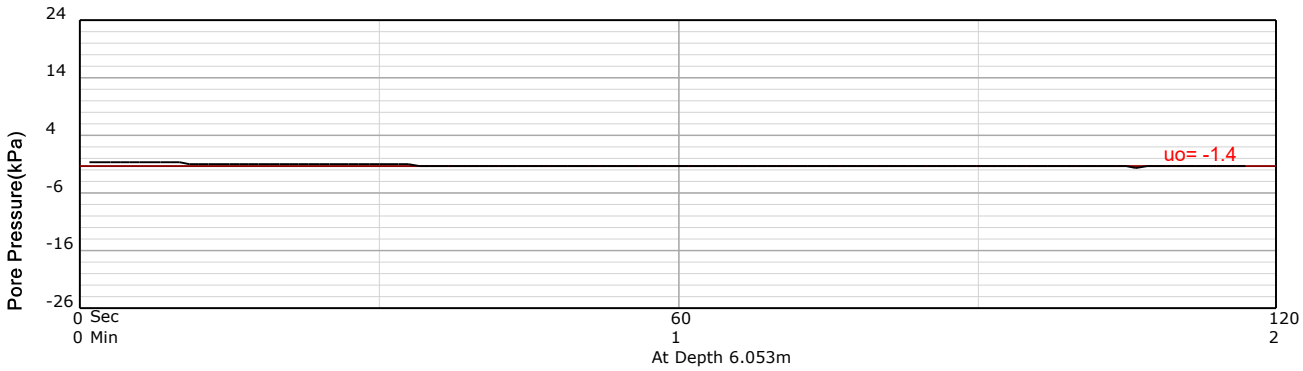

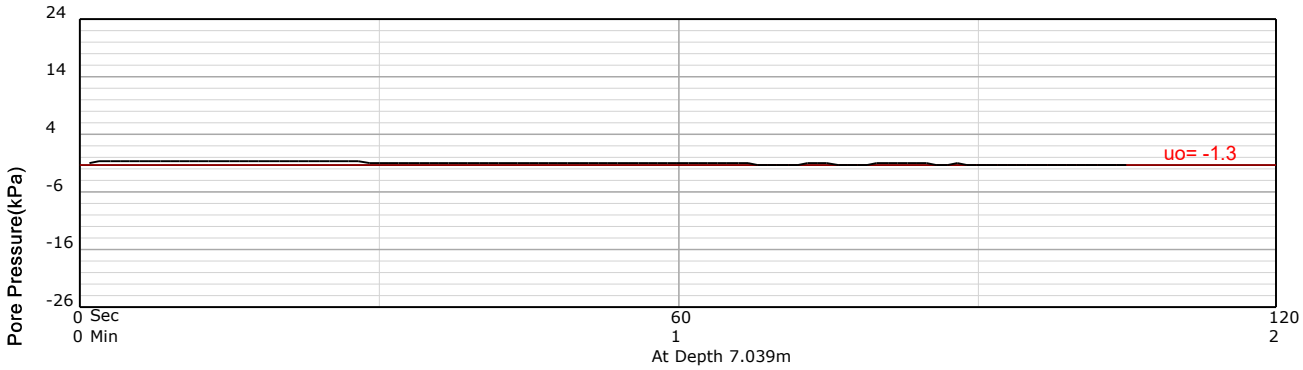

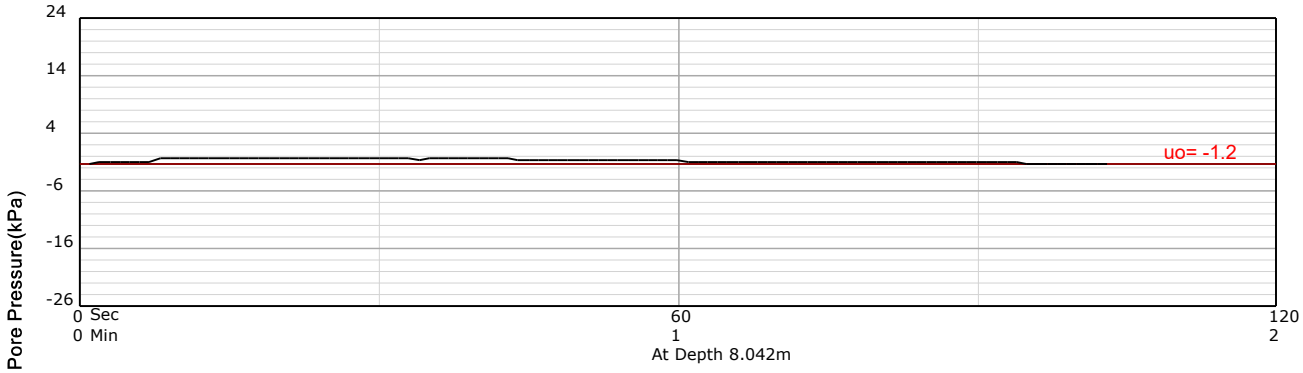

PIEZOCONE PENETRATION TEST

Dissipation Tests

HOLE: C14

PROJECT: 2024 Jagersfontein

SITE: TSF

DATE: 24/03/02 At: 14:12:00 **DEPTH:** 23.68

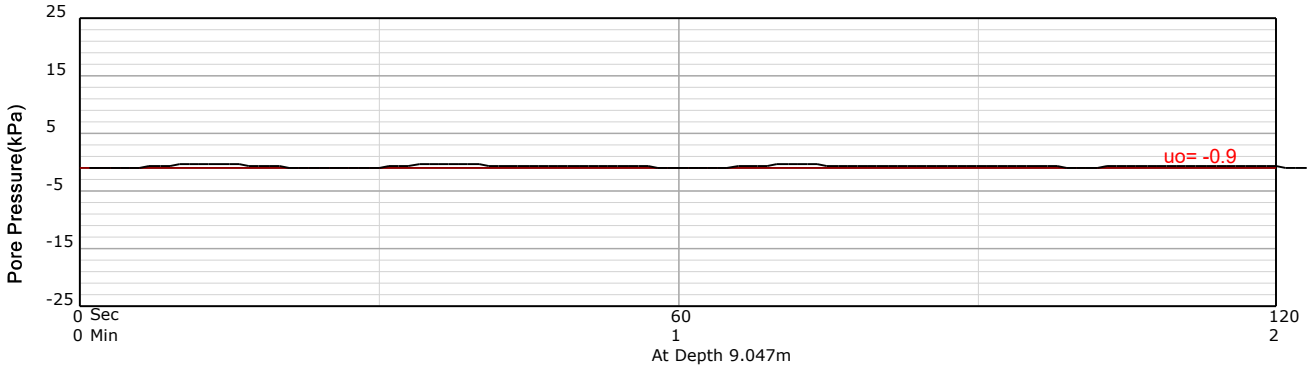

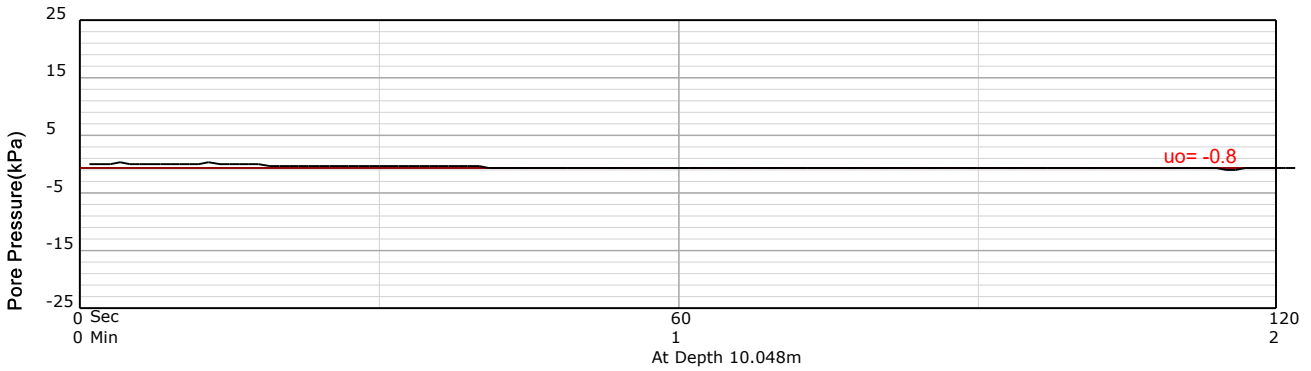

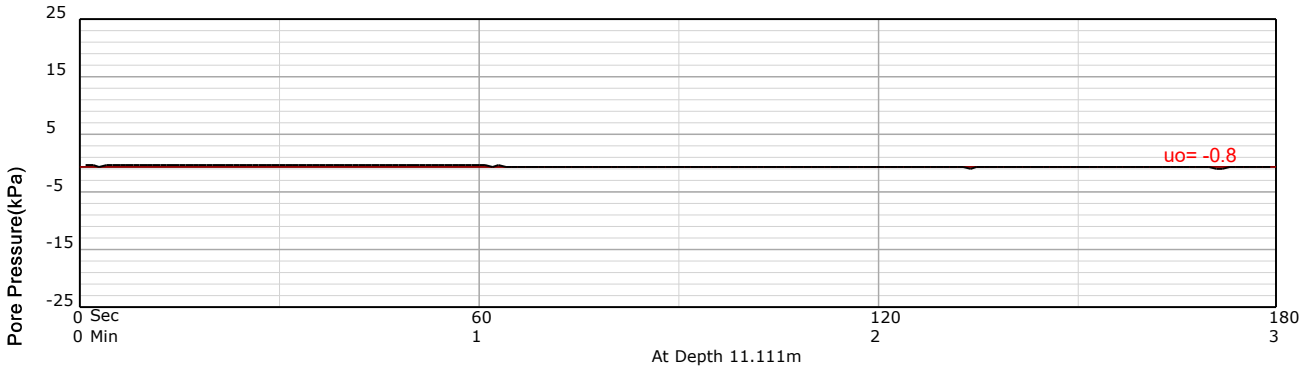

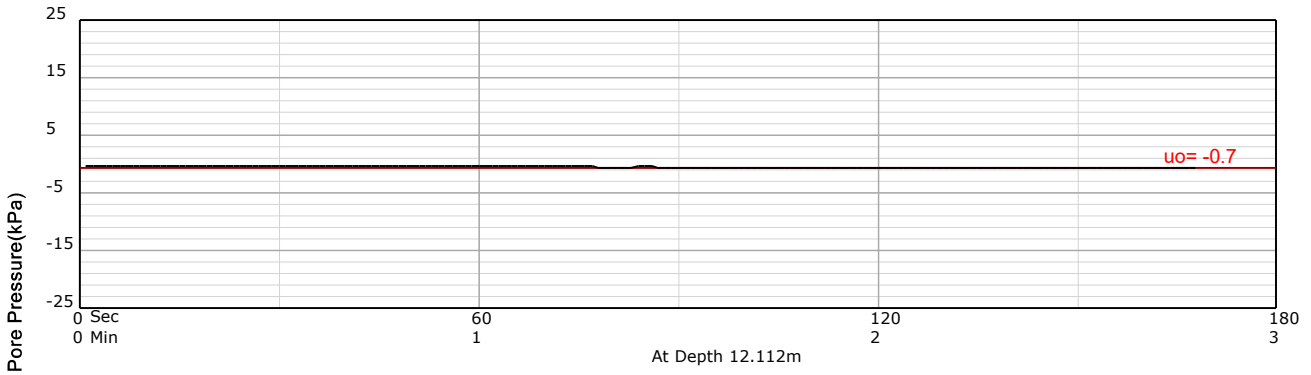

PIEZOCONE PENETRATION TEST

Dissipation Tests

HOLE: C14

PROJECT: 2024 Jagersfontein

SITE: TSF

DATE: 24/03/02 At: 14:12:00 **DEPTH:** 23.68

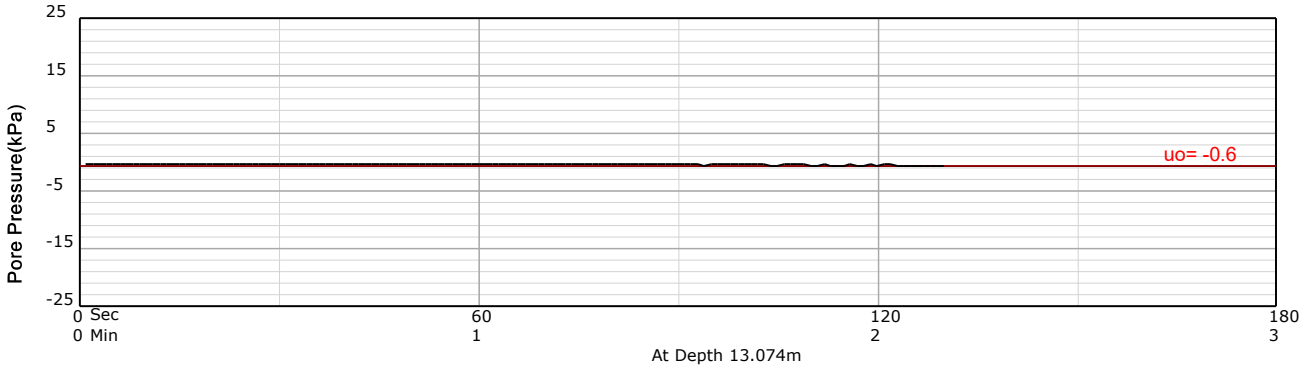

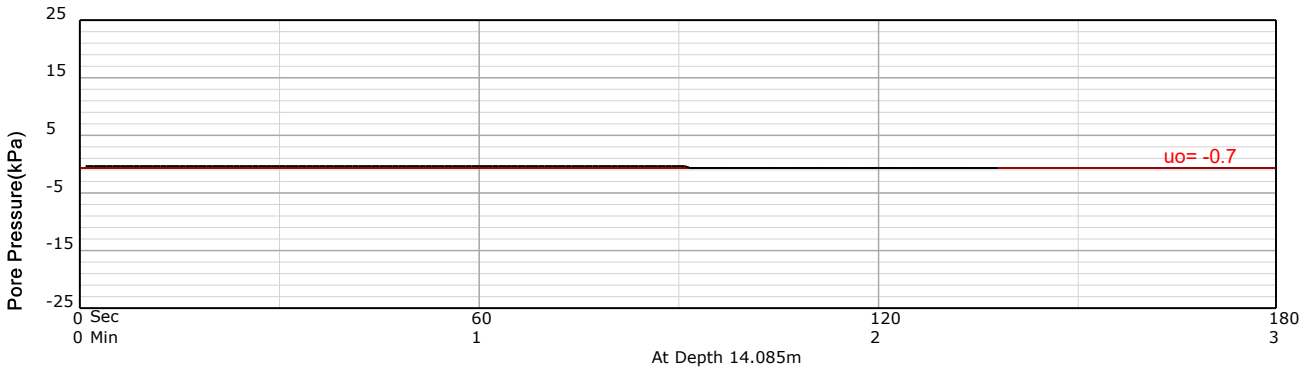

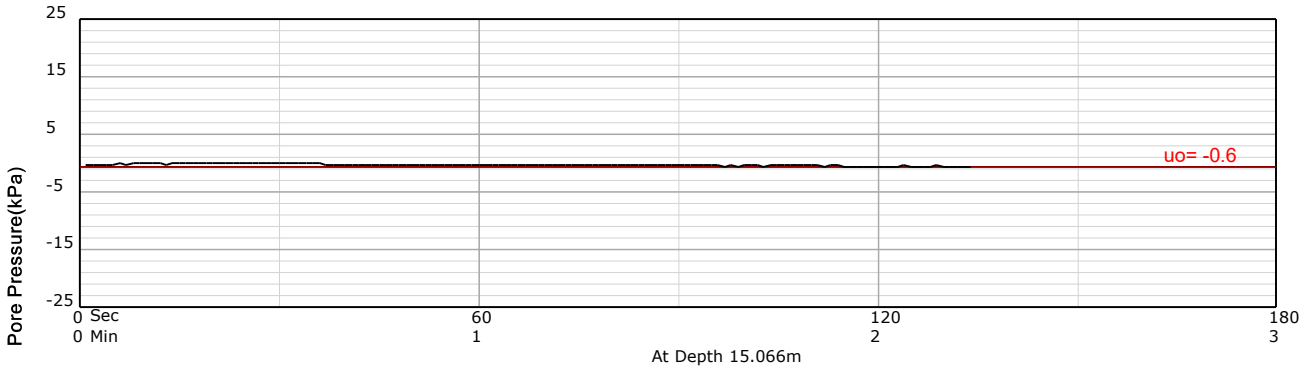

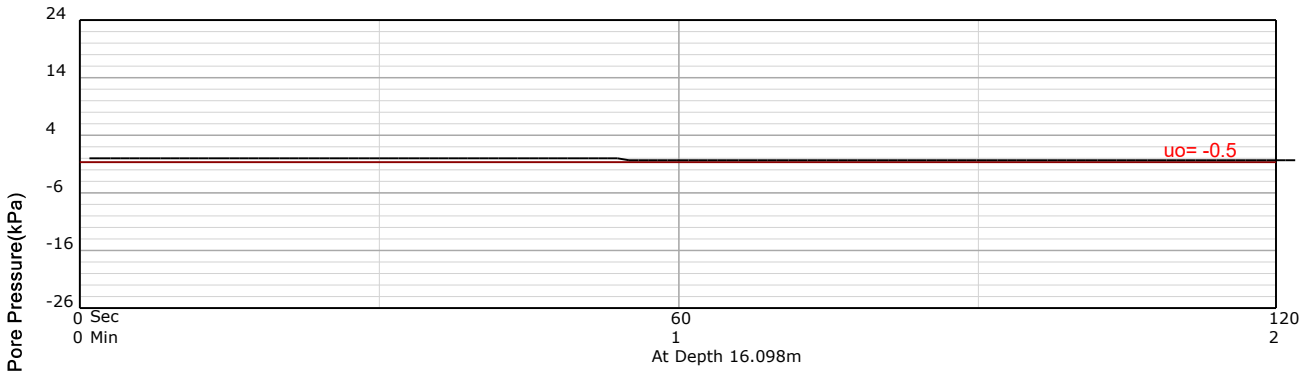

PIEZOCONE PENETRATION TEST

Dissipation Tests

HOLE: C14

PROJECT: 2024 Jagersfontein

SITE: TSF

DATE: 24/03/02 At: 14:12:00 **DEPTH:** 23.68

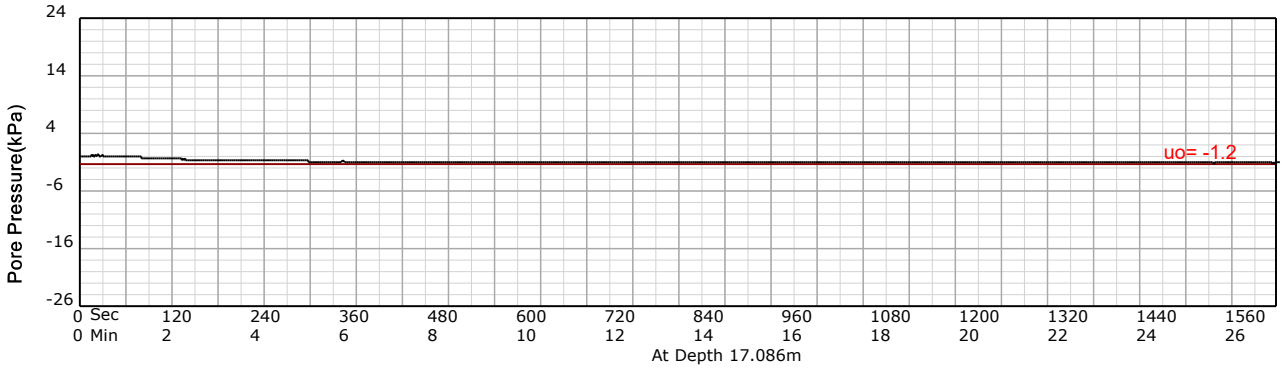

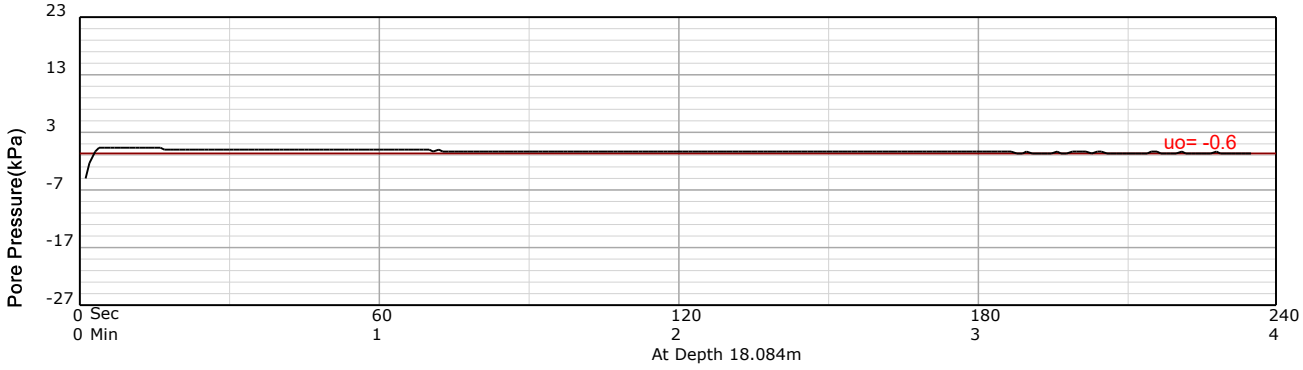

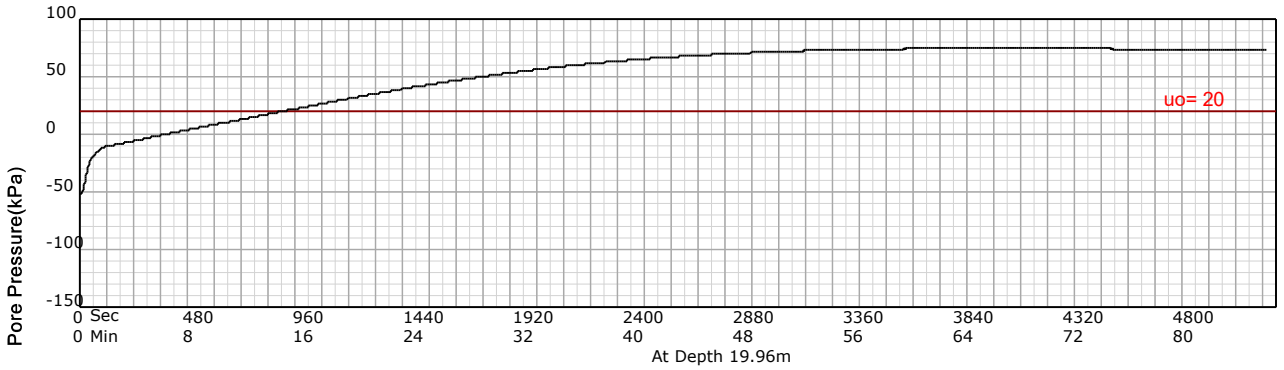

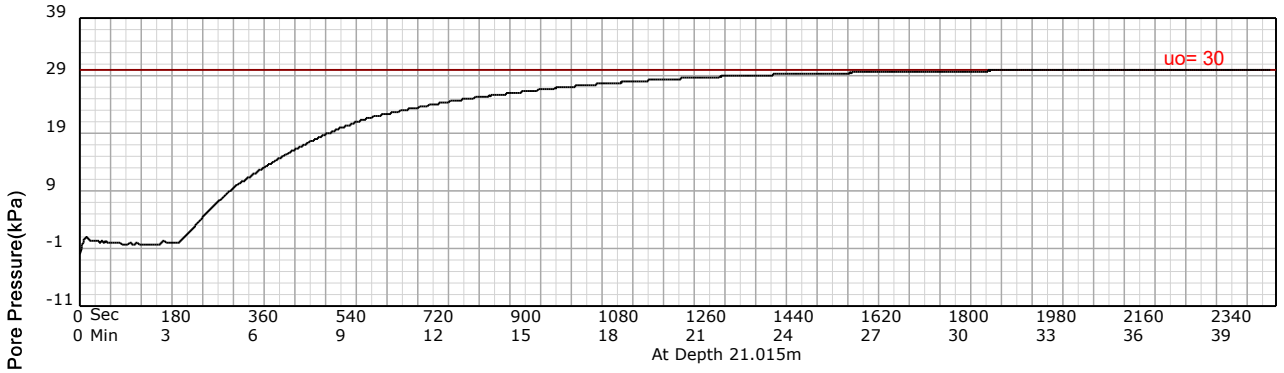

PIEZOCONE PENETRATION TEST

Dissipation Tests

HOLE: C14

PROJECT: 2024 Jagersfontein

SITE: TSF

DATE: 24/03/02 At: 14:12:00 **DEPTH:** 23.68

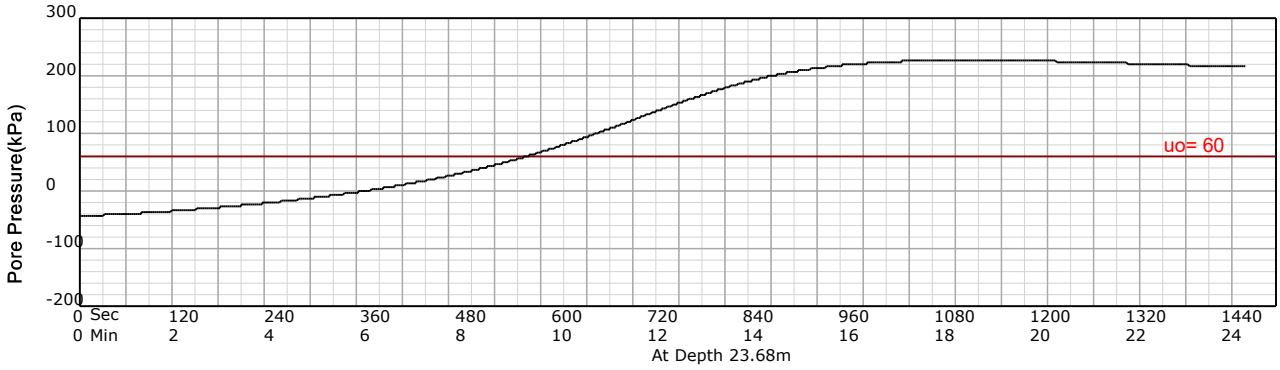

PIEZOCONE PENETRATION TEST

Equivalent Soil Behaviour Type Profile

HOLE: C14

PROJECT: 2024 Jagersfontein

SITE: TSF

DATE: 24/03/02 At: 14:12:00

DEPTH: 23.68

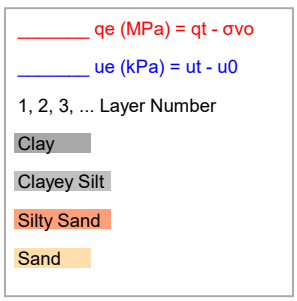

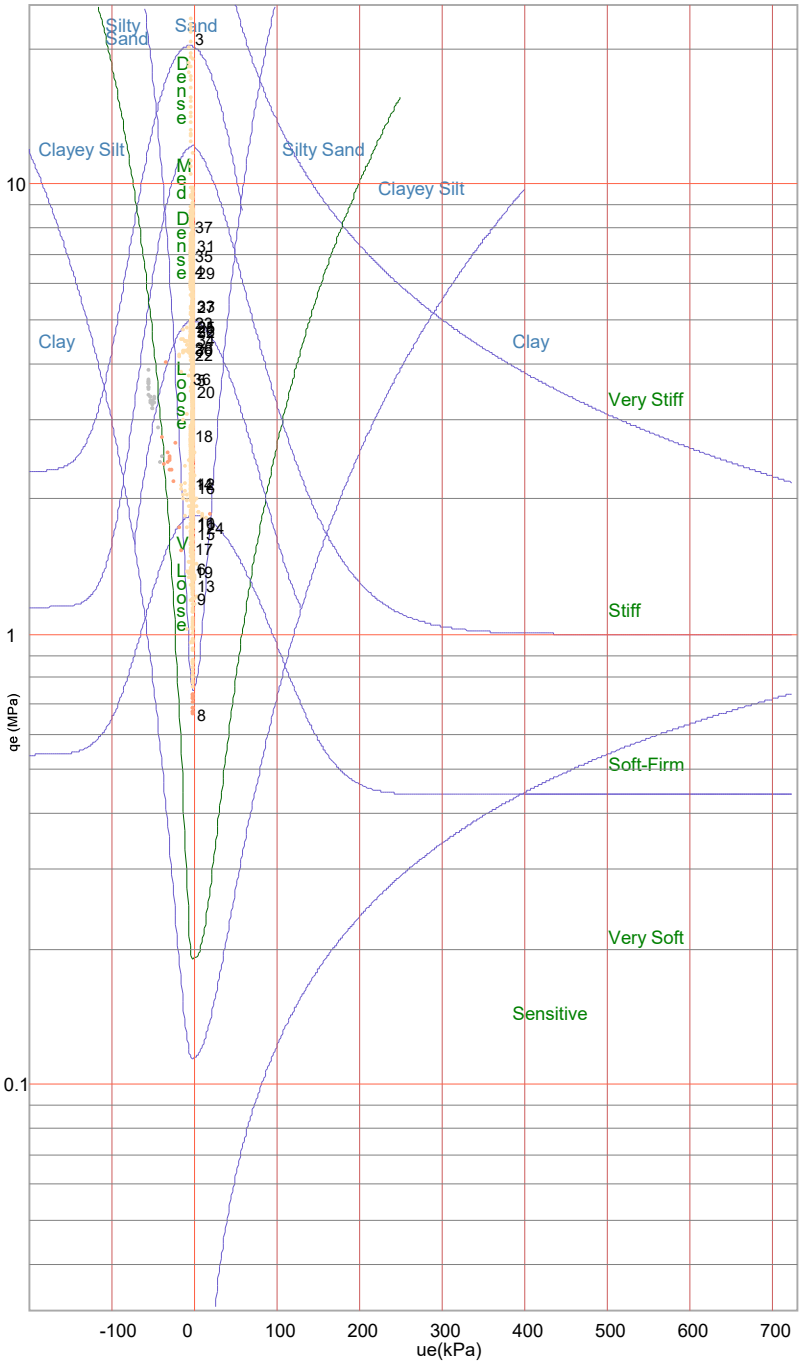

Jones and Rust Soils ID chart (AC Meigh-CIRIA,1987)

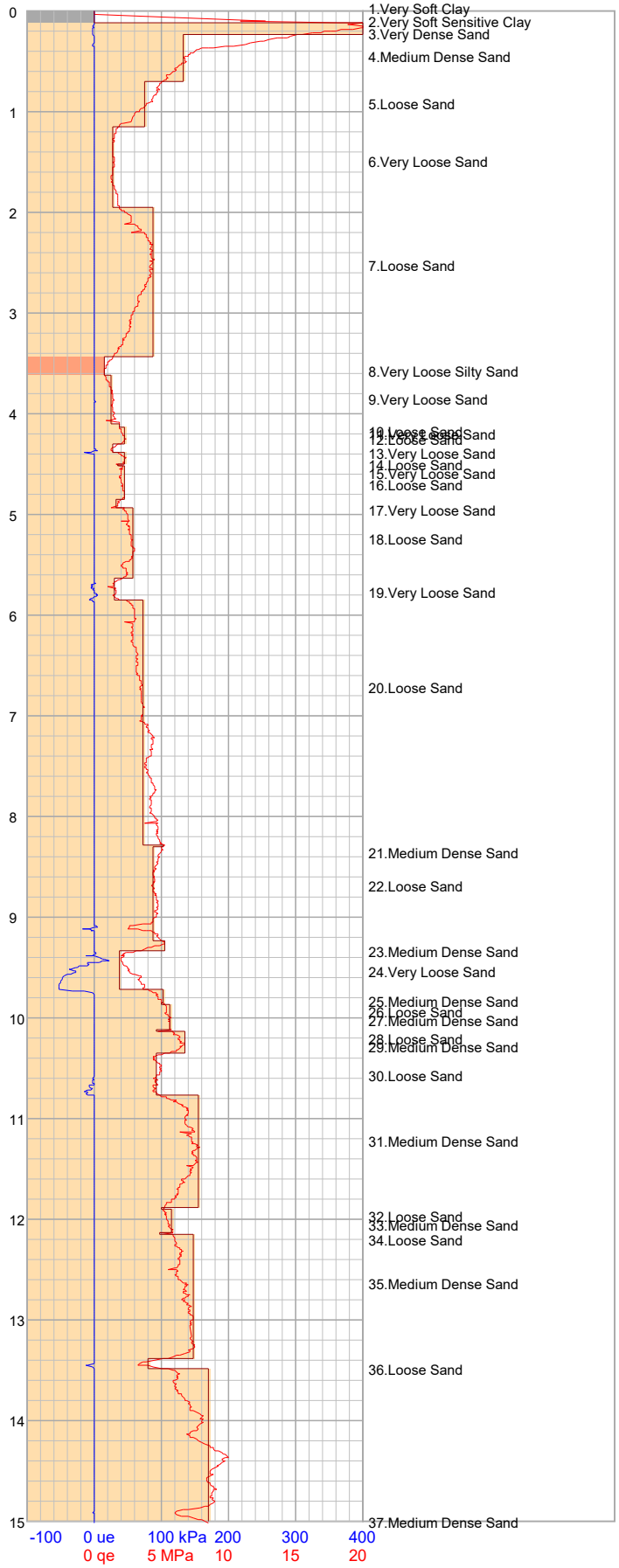

PIEZOCONE PENETRATION TEST

Equivalent Soil Behaviour Type Profile

HOLE: C14

PROJECT: 2024 Jagersfontein

SITE: TSF

DATE: 24/03/02 At: 14:12:00

DEPTH: 23.68

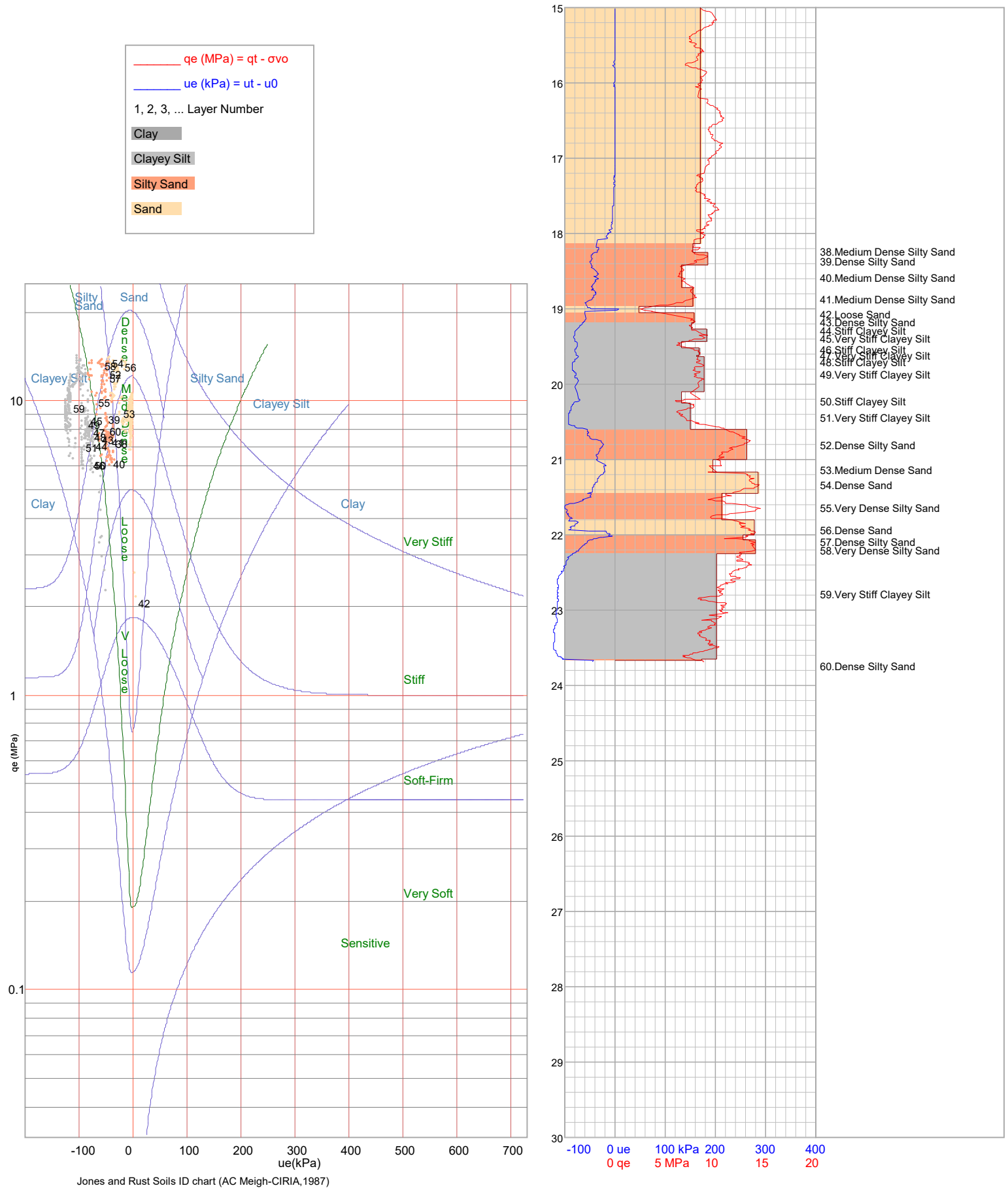

Jones and Rust Soils ID chart (AC Meigh-CIRIA,1987)

PIEZOCONE PENETRATION TEST

Recorded Field Results (Cone, Pore Pressure and Static Pore Pressure from Dissipations)

HOLE: C15

PROJECT: 2024 Jagersfontein

SITE: TSF

DATE: 24/03/11 At: 07:41:28 A **DEPTH:** 26.326

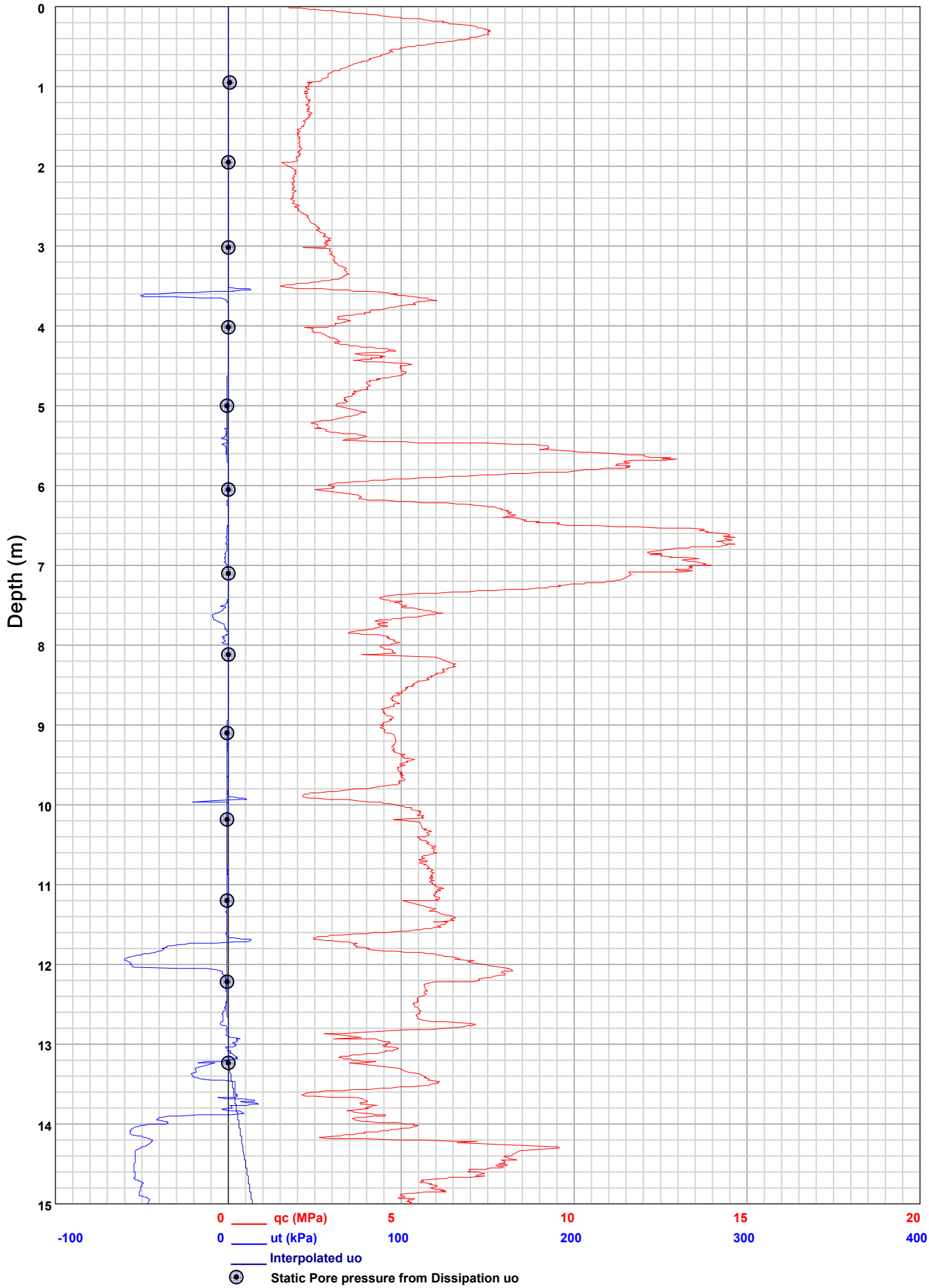

PIEZOCONE PENETRATION TEST

Recorded Field Results (Cone, Pore Pressure and Static Pore Pressure from Dissipations)

HOLE: C15

PROJECT: 2024 Jagersfontein

SITE: TSF

DATE: 24/03/11 At: 07:41:28 A **DEPTH:** 26.326

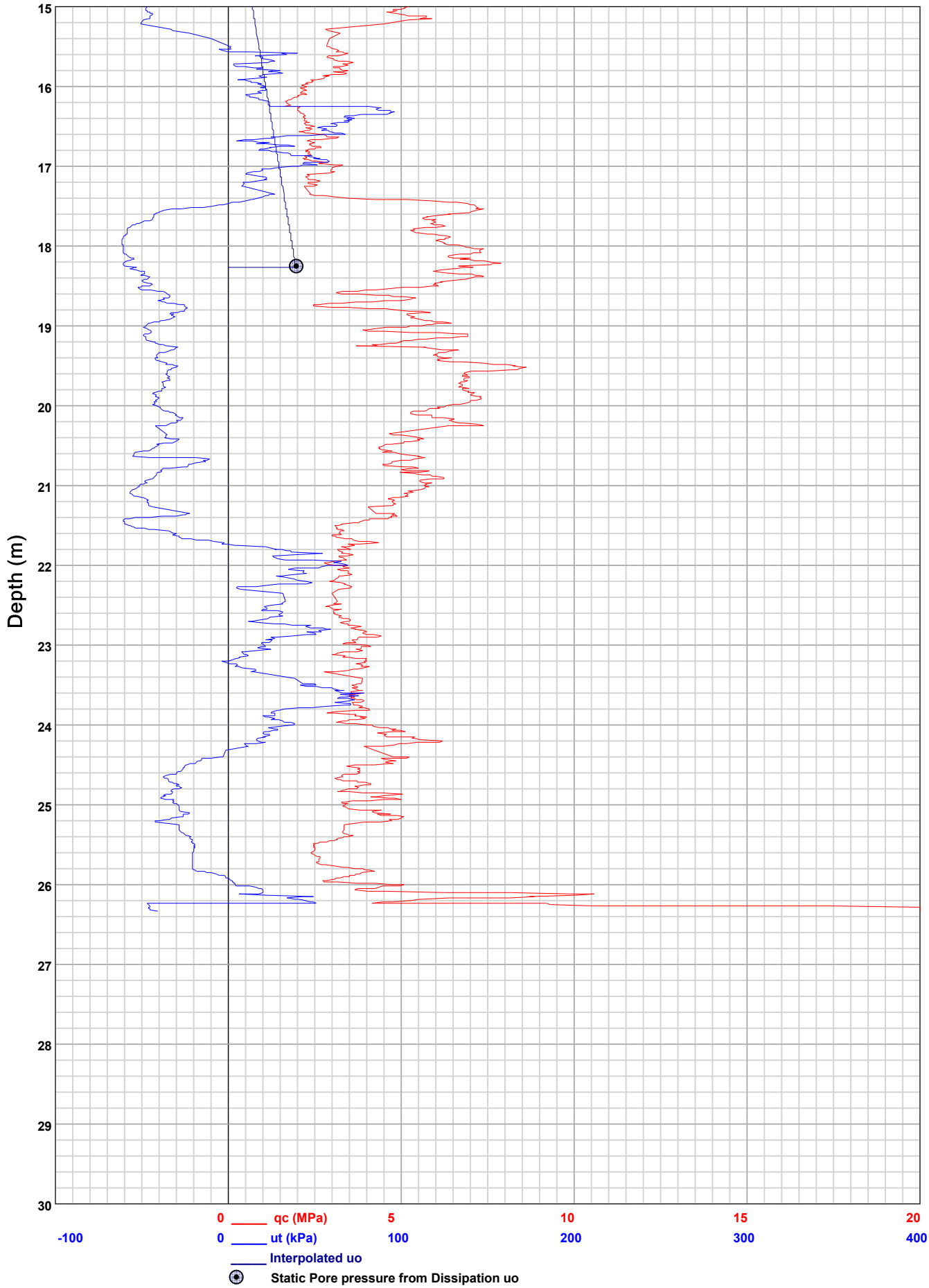

PIEZOCONE PENETRATION TEST

HOLE: C15

PROJECT: 2024 Jagersfontein

SITE: TSF

DATE: 24/03/11 At: 07:41:28 A

DEPTH: 26.326

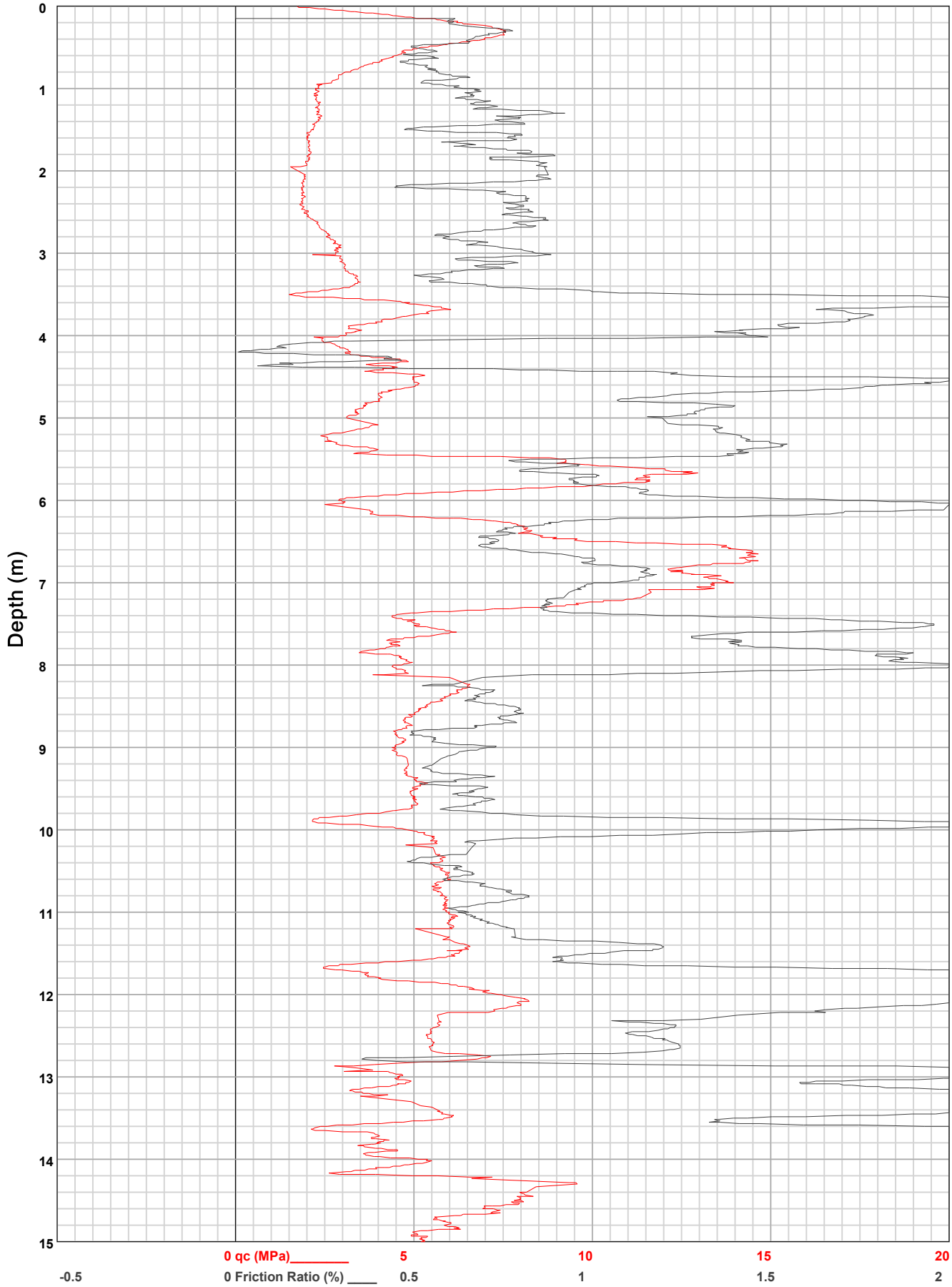

PIEZOCONE PENETRATION TEST

HOLE: C15

PROJECT: 2024 Jagersfontein

SITE: TSF

DATE: 24/03/11 At: 07:41:28 A

DEPTH: 26.326

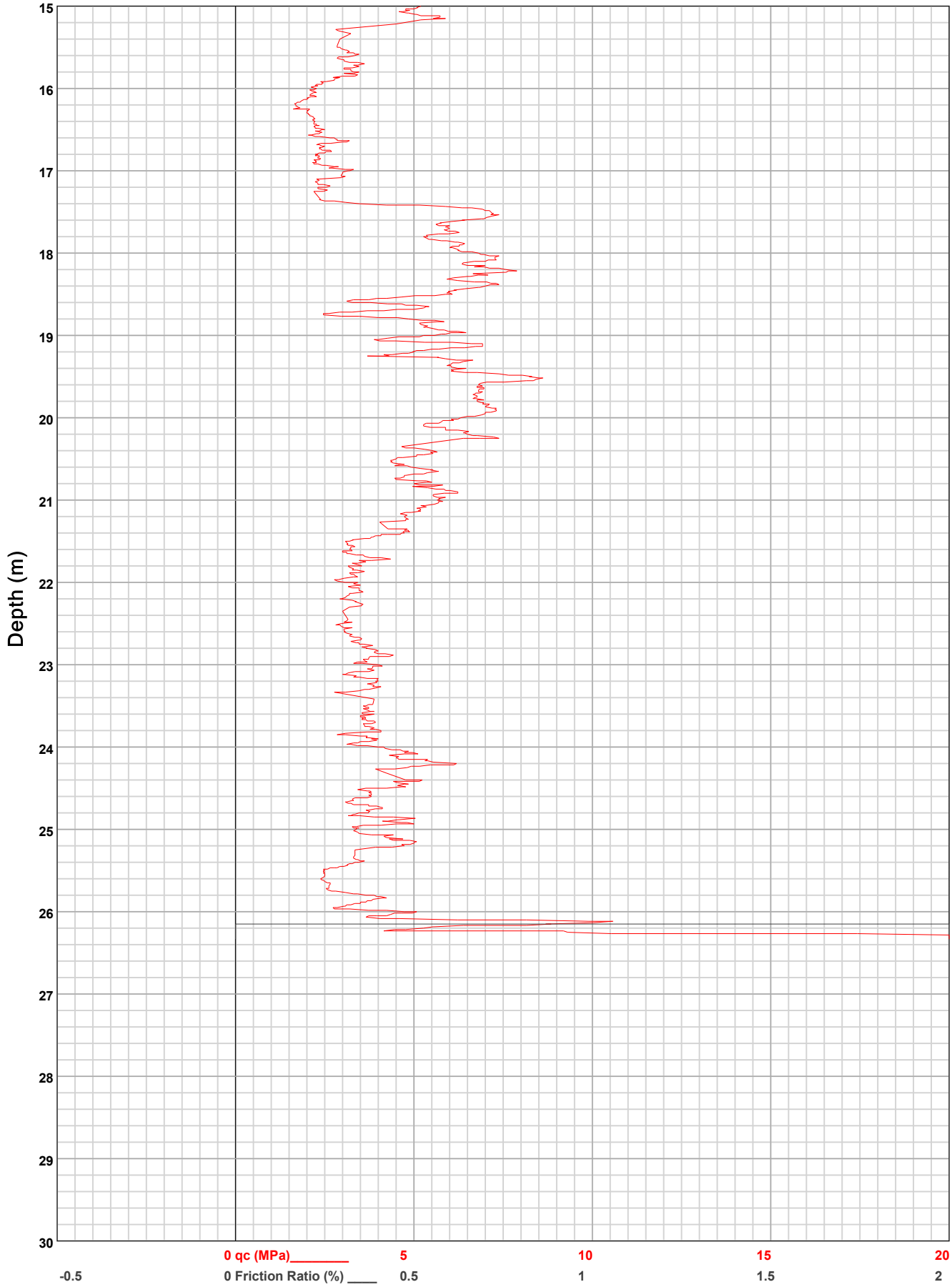

PIEZOCONE PENETRATION TEST

Dissipation Tests

HOLE: C15

PROJECT: 2024 Jagersfontein

SITE: TSF

DATE: 24/03/11 At: 07:41:28 A

DEPTH: 26.326

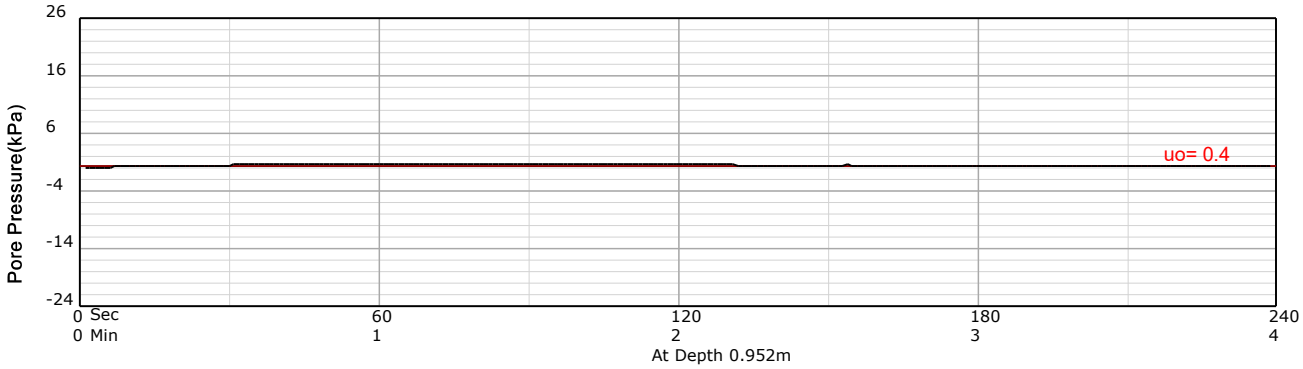

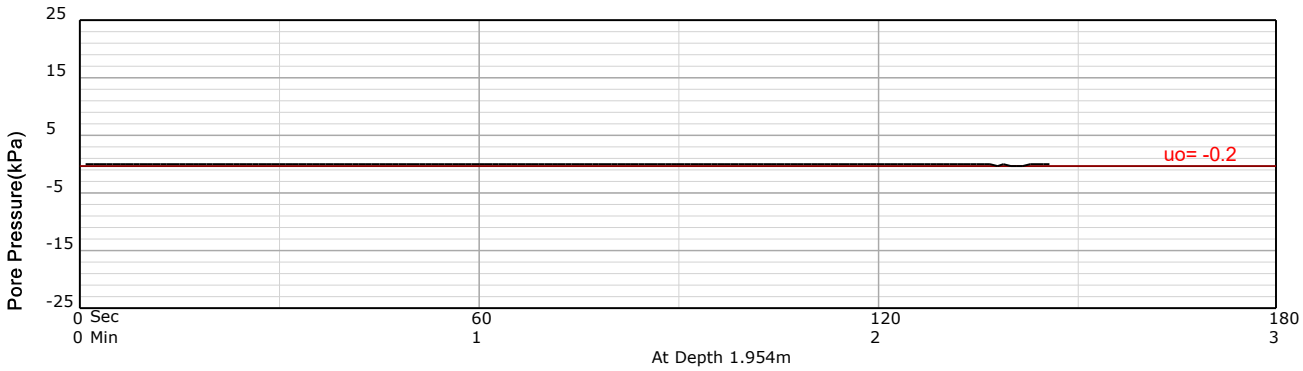

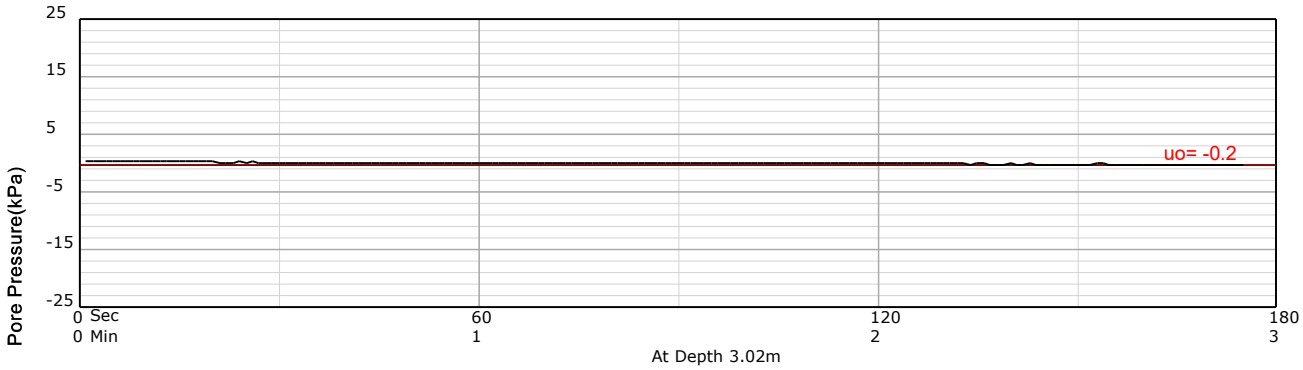

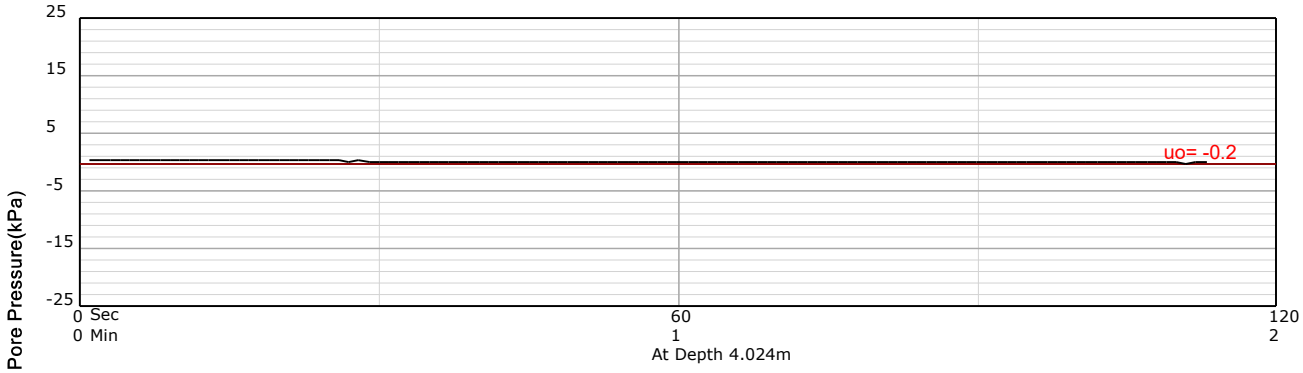

PIEZOCONE PENETRATION TEST

Dissipation Tests

HOLE: C15

PROJECT: 2024 Jagersfontein

SITE: TSF

DATE: 24/03/11 At: 07:41:28 A

DEPTH: 26.326

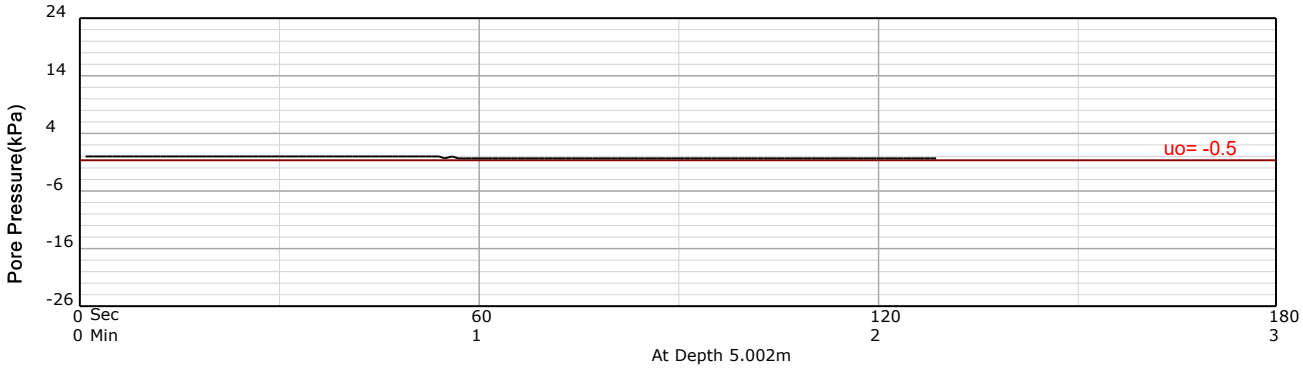

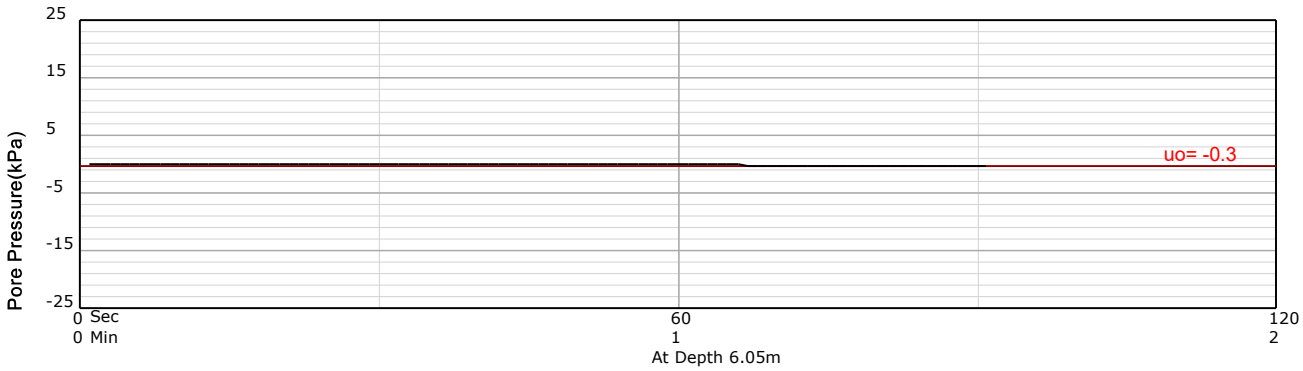

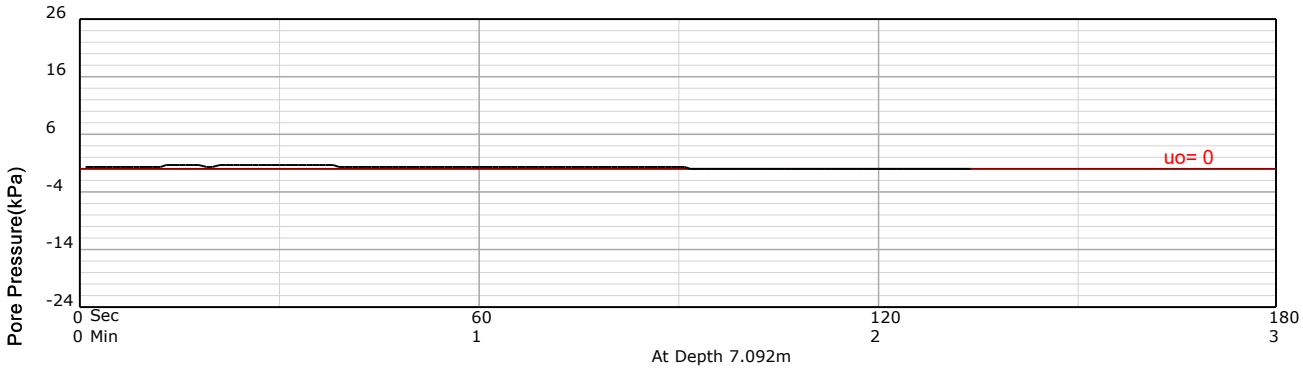

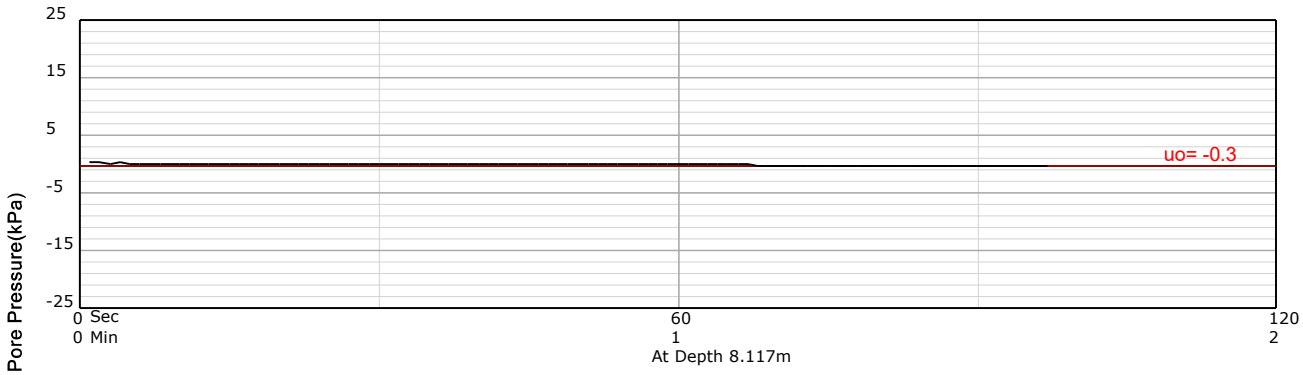

PIEZOCONE PENETRATION TEST

Dissipation Tests

HOLE: C15

PROJECT: 2024 Jagersfontein

SITE: TSF

DATE: 24/03/11 At: 07:41:28 A

DEPTH: 26.326

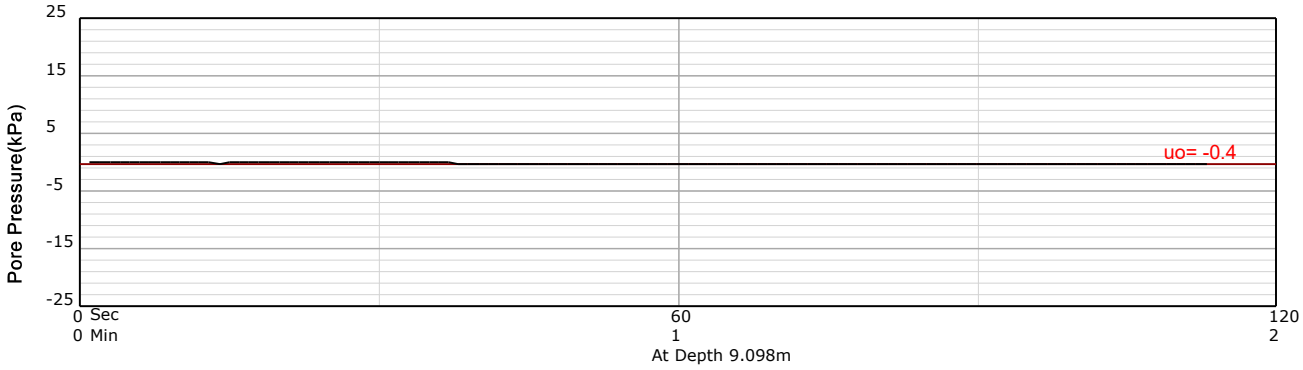

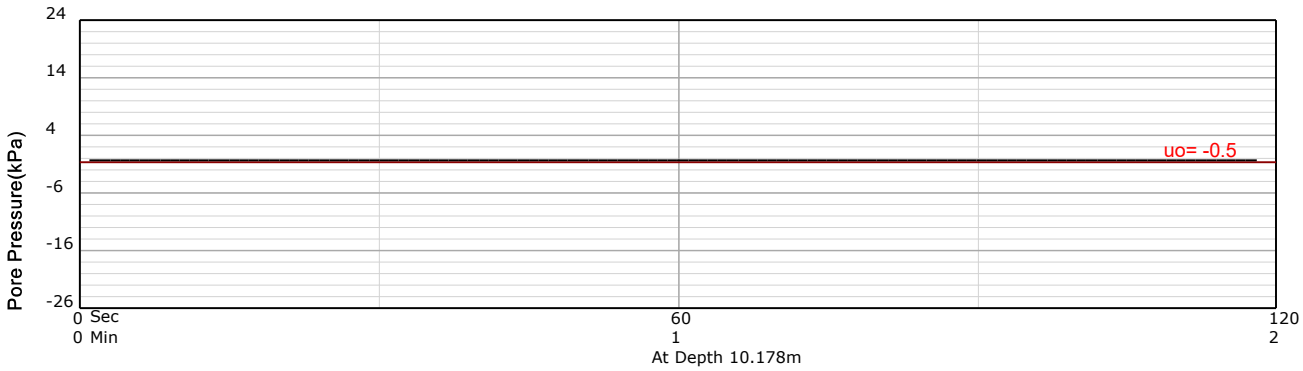

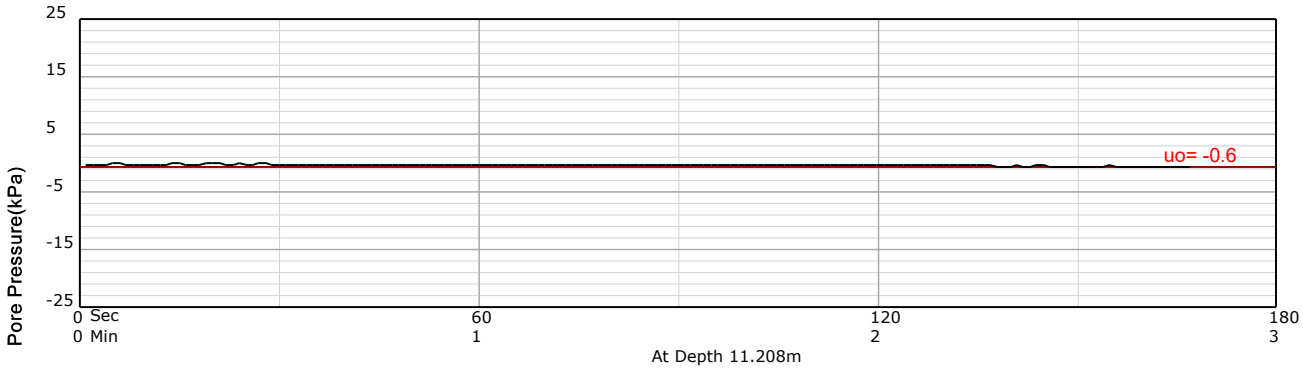

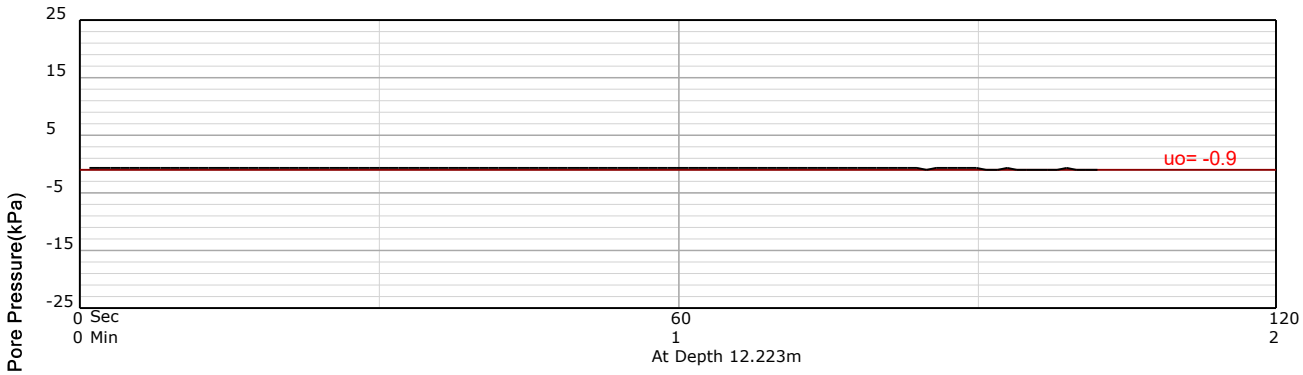

PIEZOCONE PENETRATION TEST

Dissipation Tests

HOLE: C15

PROJECT: 2024 Jagersfontein

SITE: TSF

DATE: 24/03/11 At: 07:41:28 A

DEPTH: 26.326

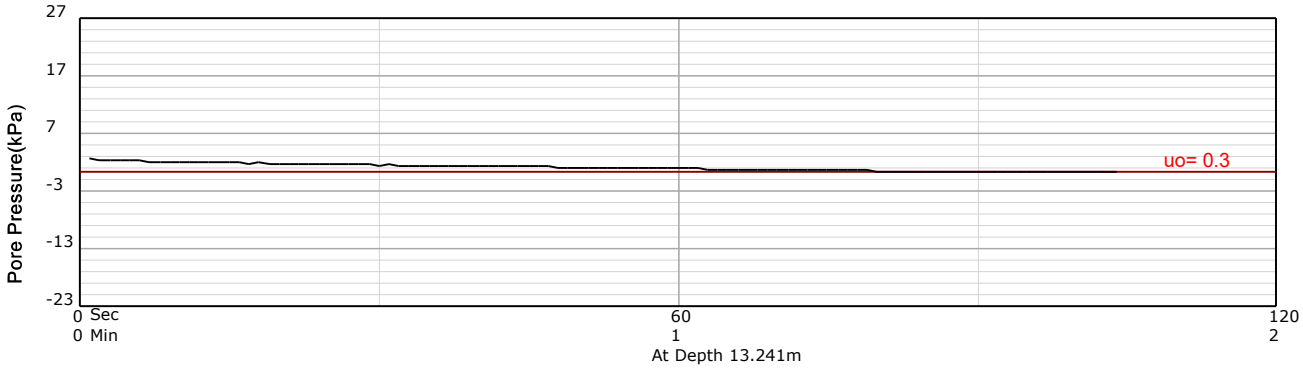

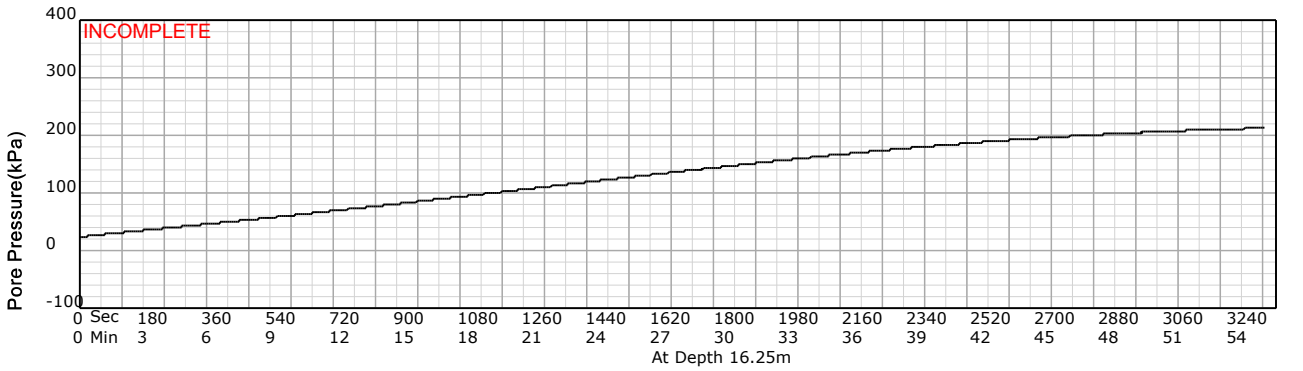

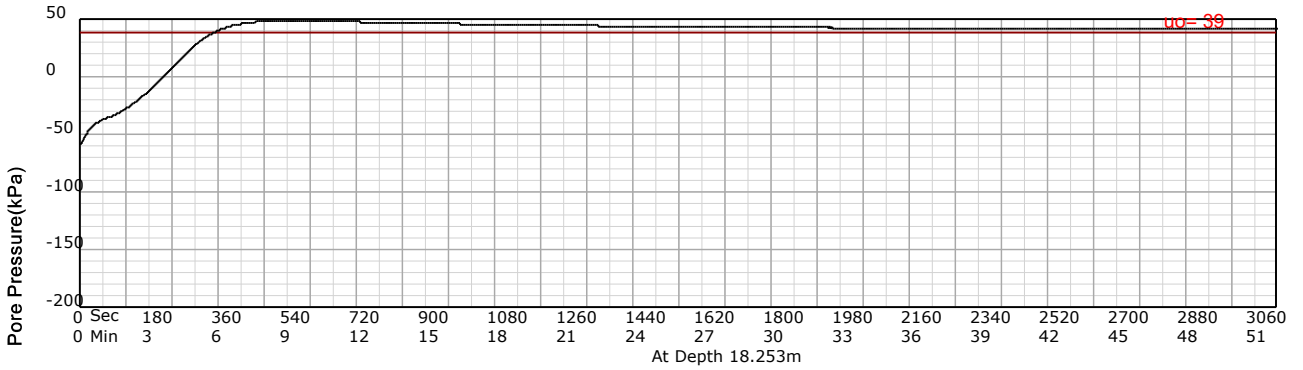

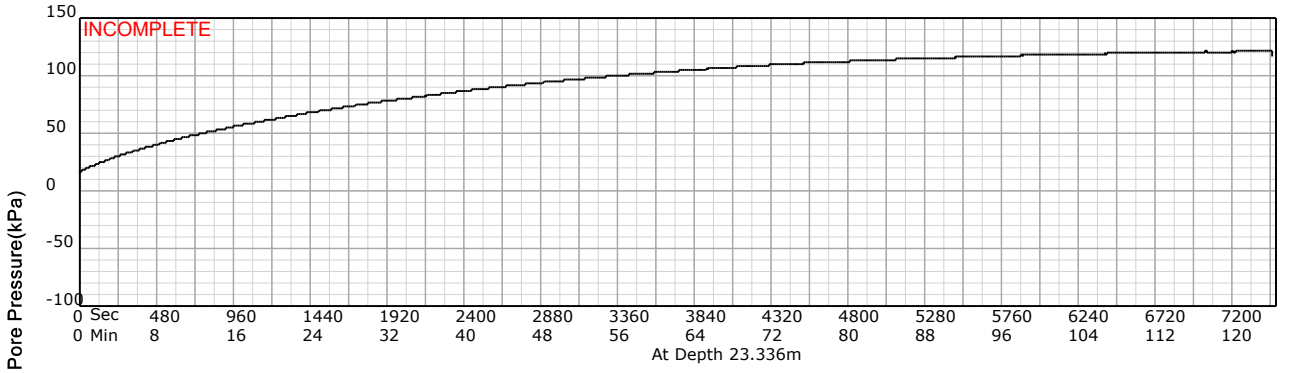

PIEZOCONE PENETRATION TEST

Equivalent Soil Behaviour Type Profile

HOLE: C15

PROJECT: 2024 Jagersfontein

SITE: TSF

DATE: 24/03/11 At: 07:41:28 A

DEPTH: 26.326

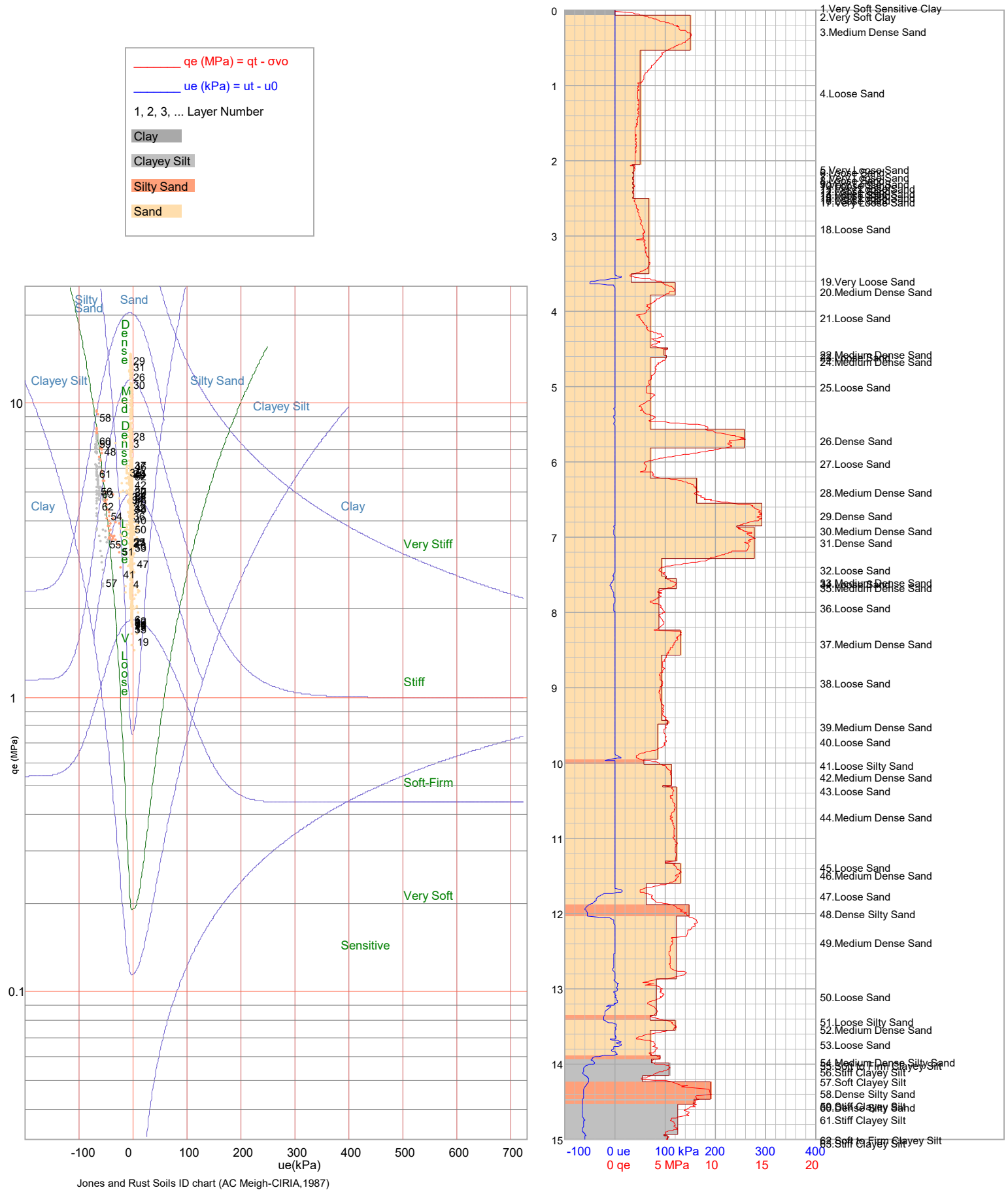

Jones and Rust Soils ID chart (AC Meigh-CIRIA,1987)

PIEZOCONE PENETRATION TEST

Equivalent Soil Behaviour Type Profile

HOLE: C15

PROJECT: 2024 Jagersfontein

SITE: TSF

DATE: 24/03/11 At: 07:41:28 A

DEPTH: 26.326

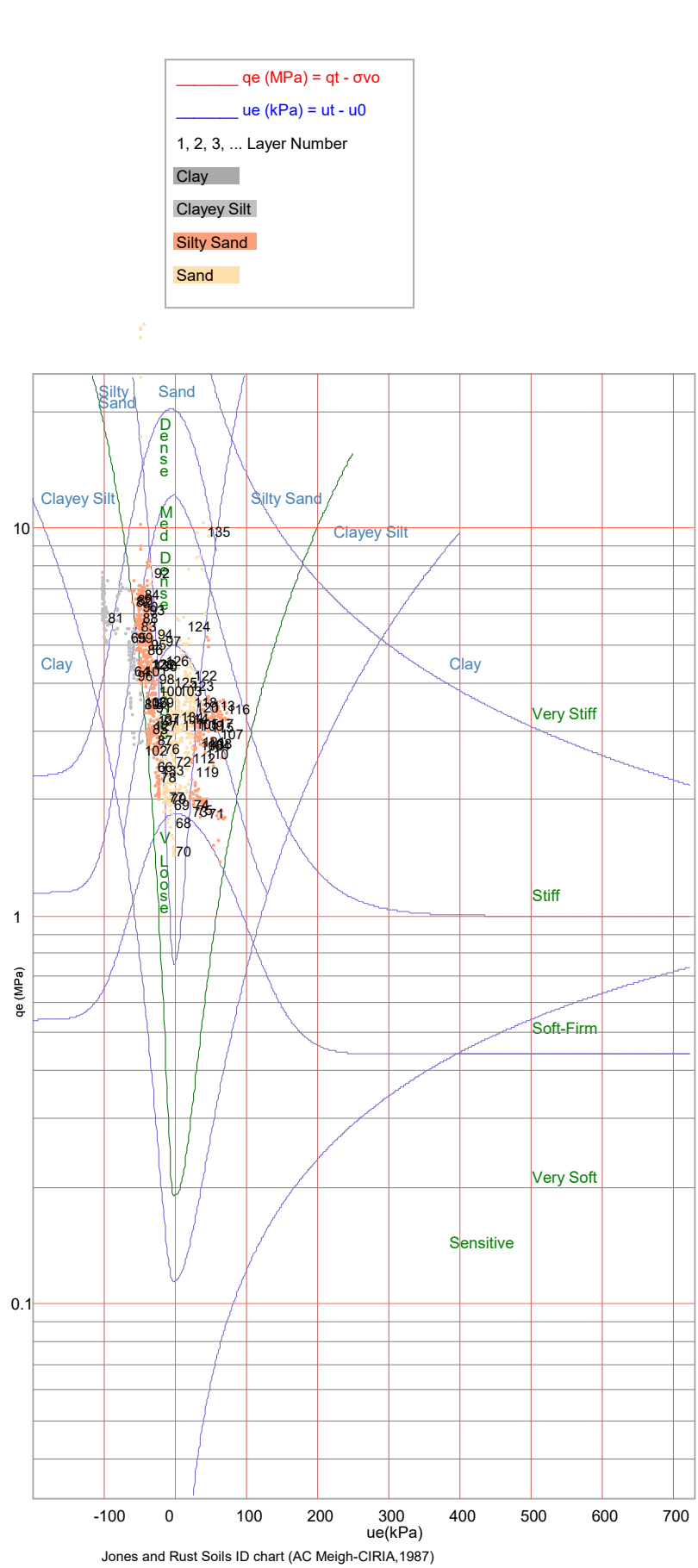

Jones and Rust Soils ID chart (AC Meigh-CIRIA,1987)

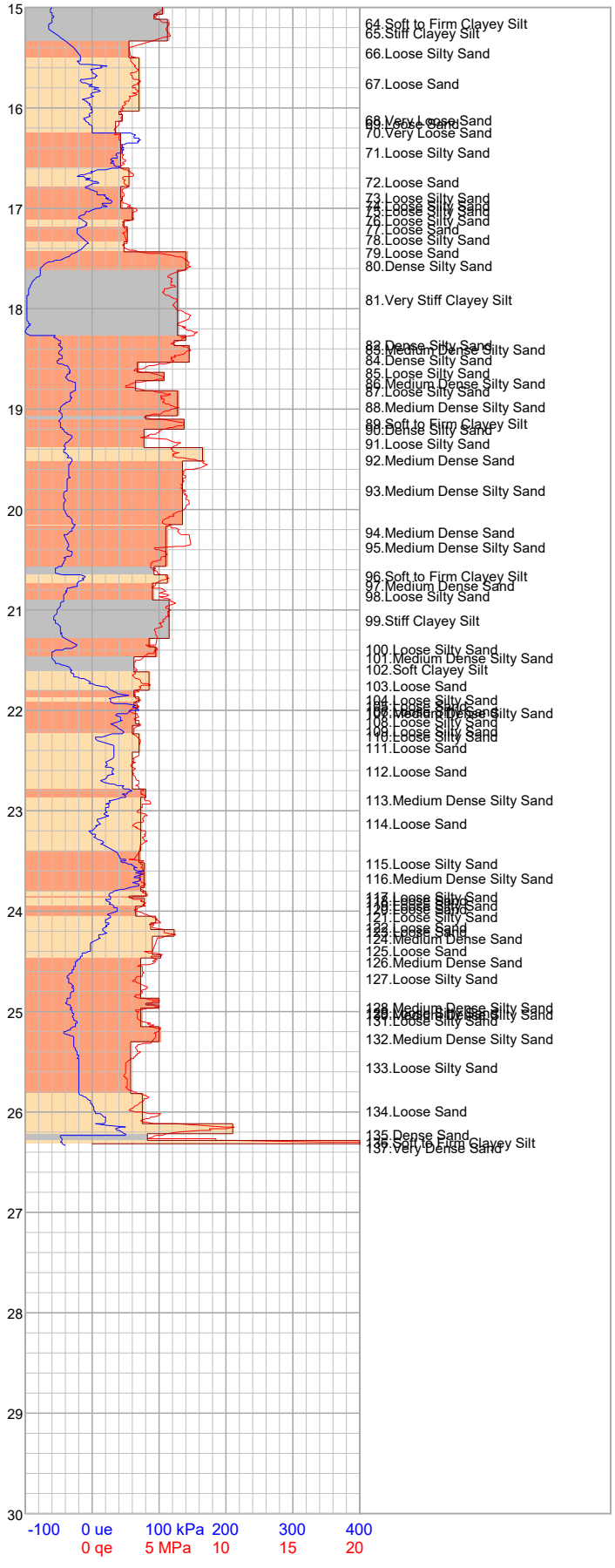

PIEZOCONE PENETRATION TEST

Recorded Field Results (Cone, Pore Pressure and Static Pore Pressure from Dissipations)

HOLE: C16

PROJECT: 2024 Jagersfontein

SITE: TSF

DATE: 24/03/11 At: 16:15:38 A **DEPTH:** 13.333

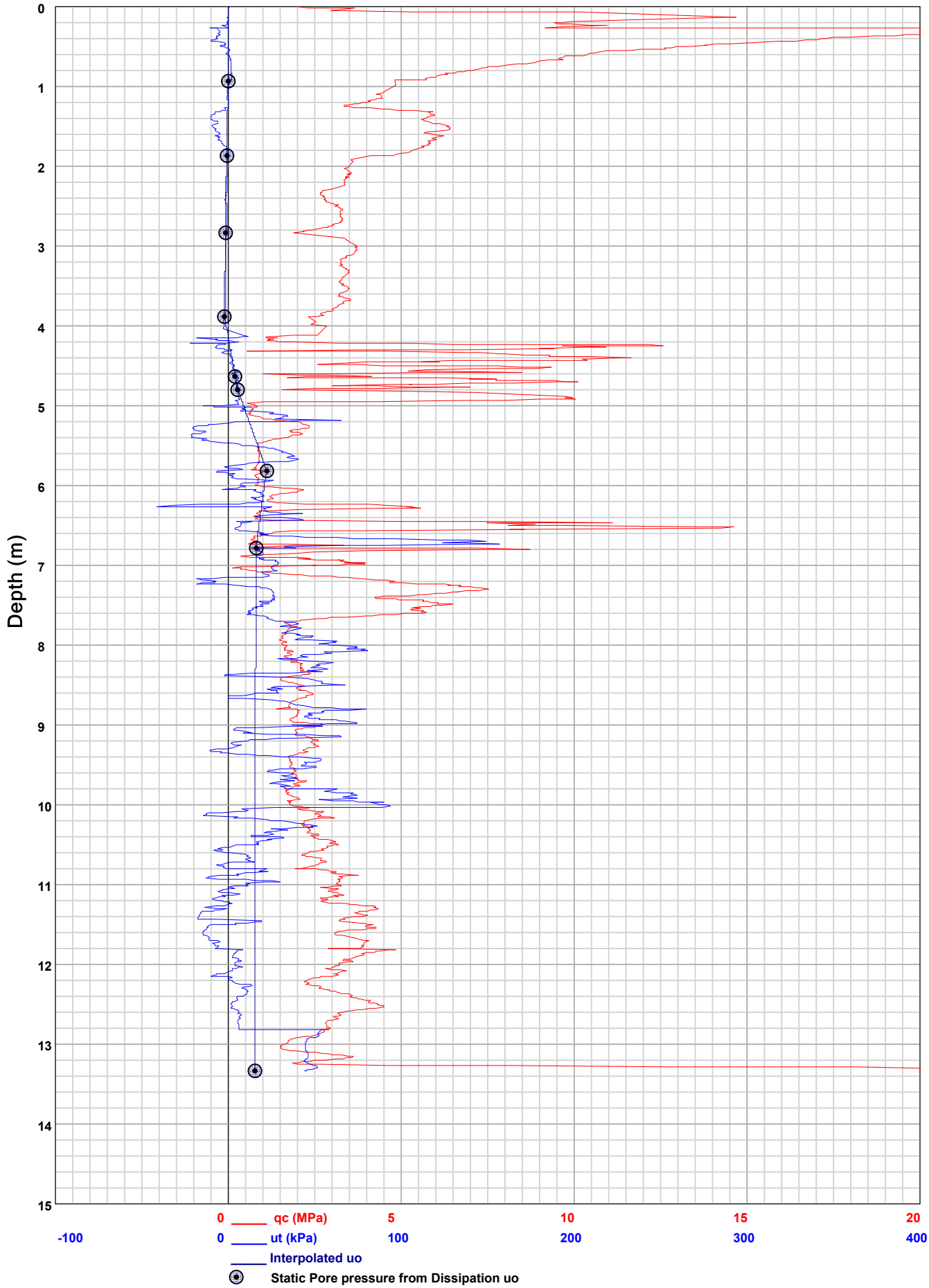

PIEZOCONE PENETRATION TEST

HOLE: C16

PROJECT: 2024 Jagersfontein

SITE: TSF

DATE: 24/03/11 At: 16:15:38 A

DEPTH: 13.333

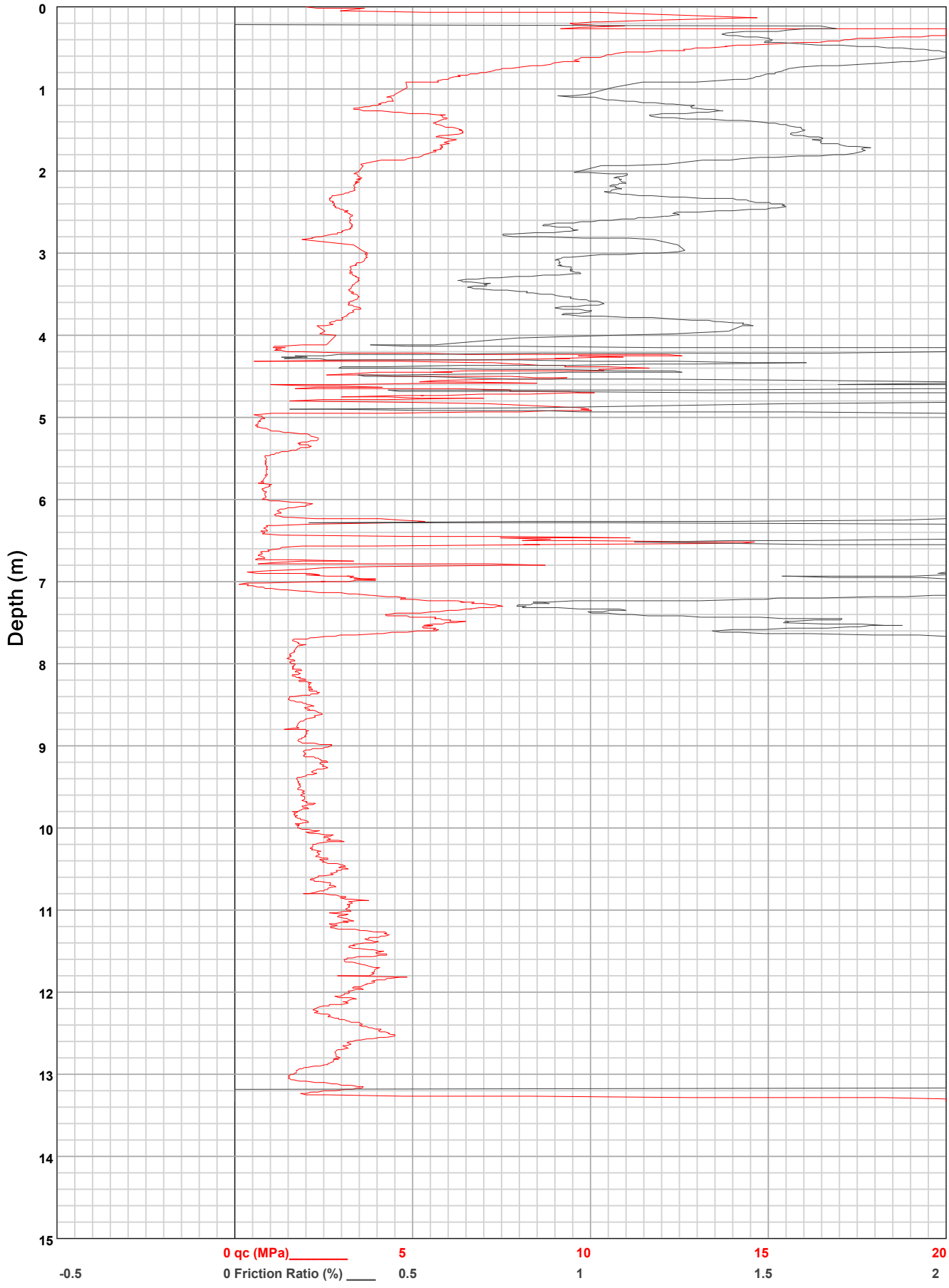

PIEZOCONE PENETRATION TEST

Dissipation Tests

HOLE: C16

PROJECT: 2024 Jagersfontein

SITE: TSF

DATE: 24/03/11 At: 16:15:38 A

DEPTH: 13.333

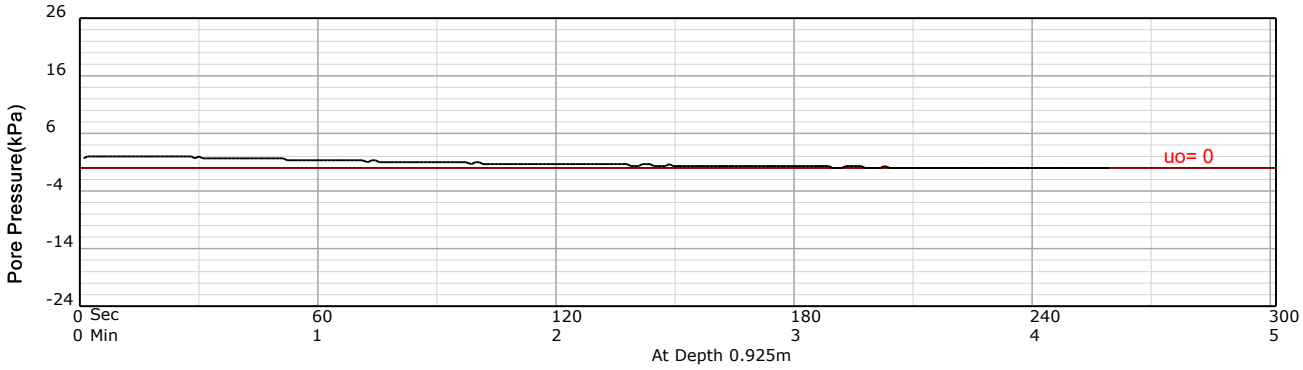

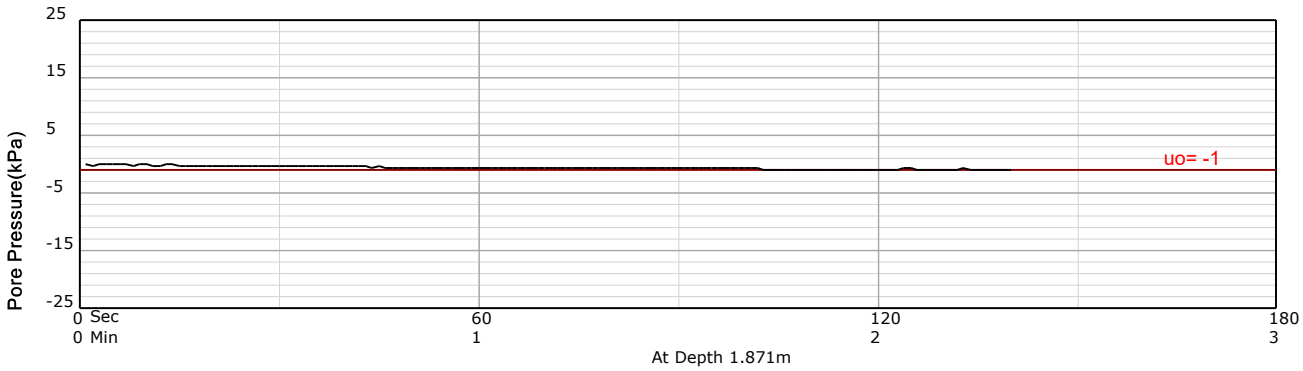

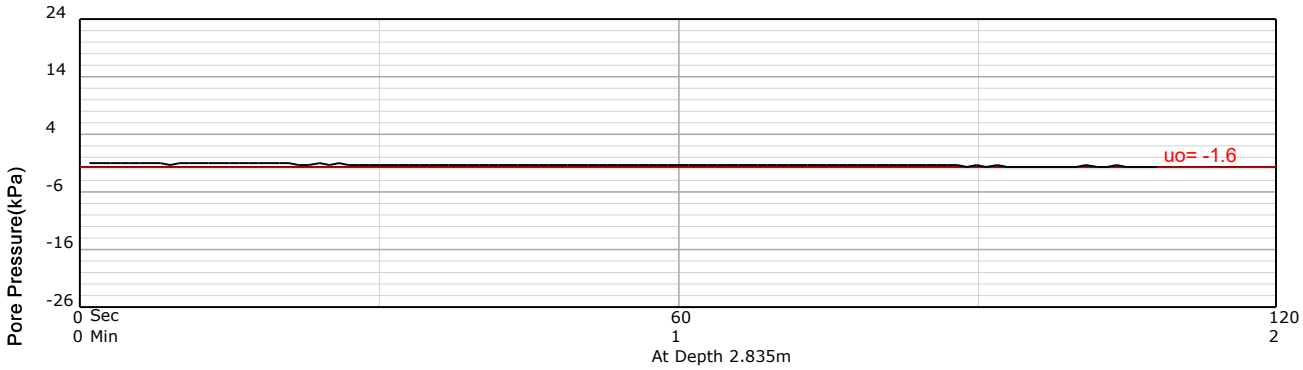

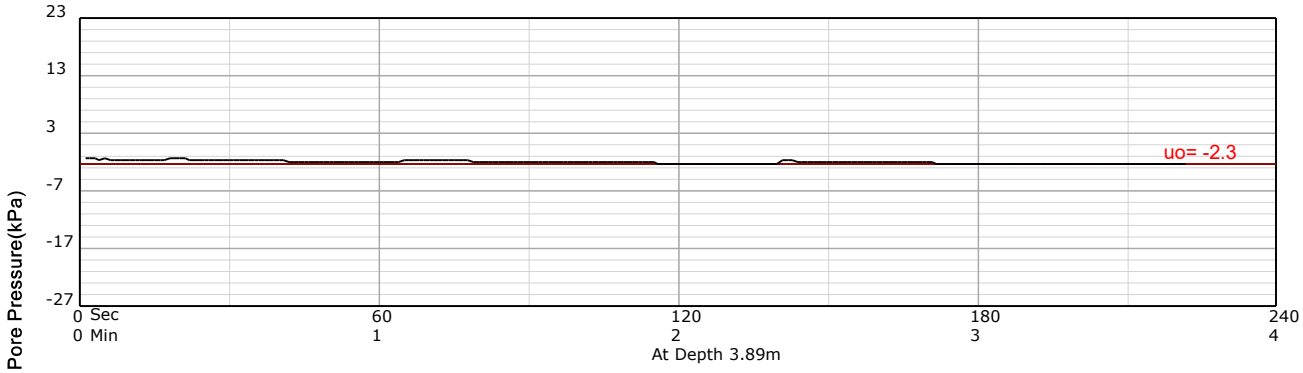

PIEZOCONE PENETRATION TEST

Dissipation Tests

HOLE: C16

PROJECT: 2024 Jagersfontein

SITE: TSF

DATE: 24/03/11 At: 16:15:38 A

DEPTH: 13.333

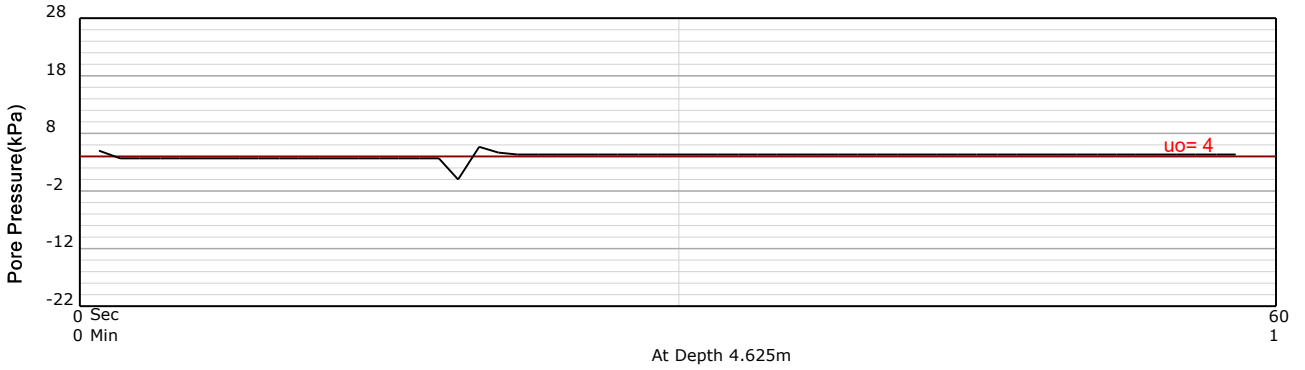

At Depth 4.625m

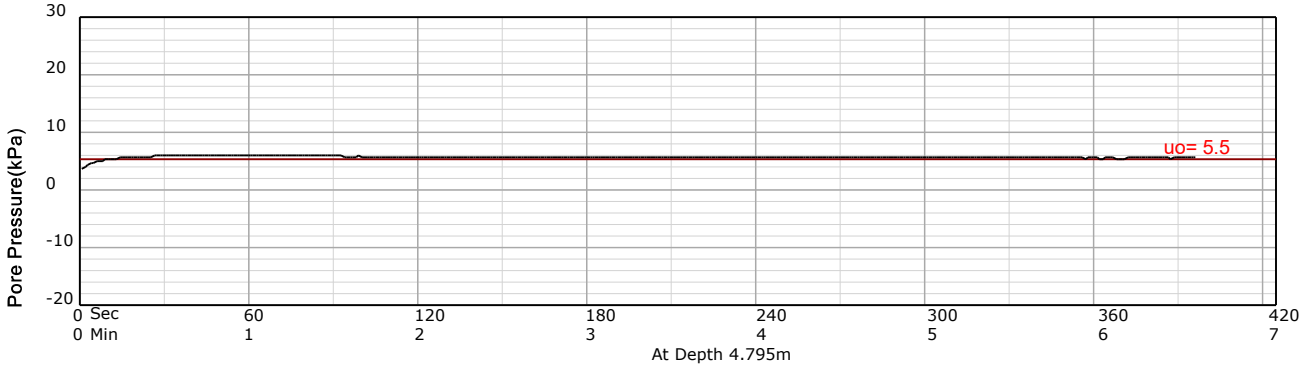

At Depth 4.795m

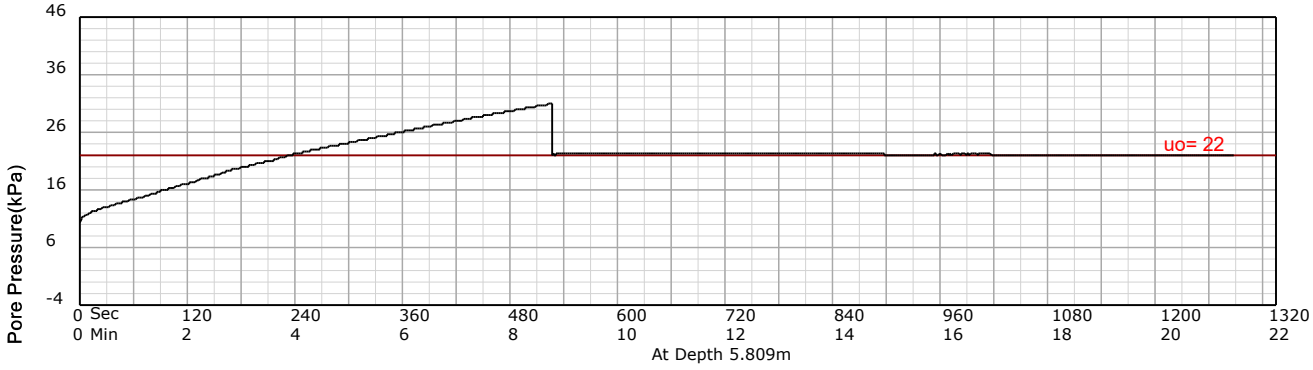

At Depth 5.809m

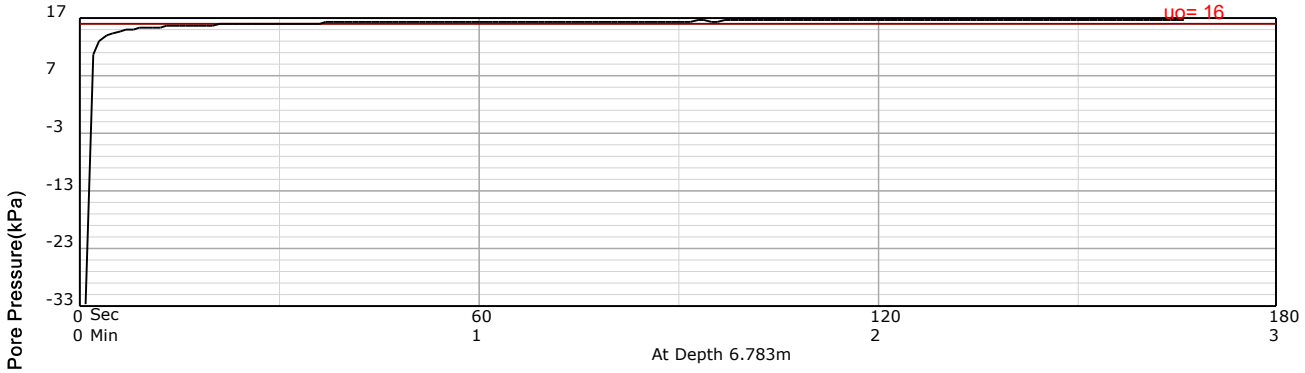

At Depth 6.783m

PIEZOCONE PENETRATION TEST

Dissipation Tests

HOLE: C16

PROJECT: 2024 Jagersfontein

SITE: TSF

DATE: 24/03/11 At: 16:15:38 A **DEPTH:** 13.333

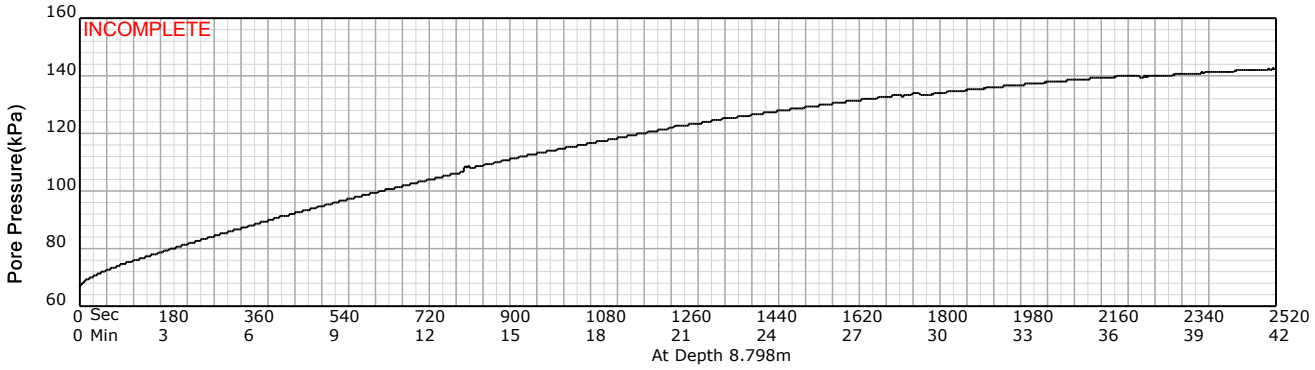

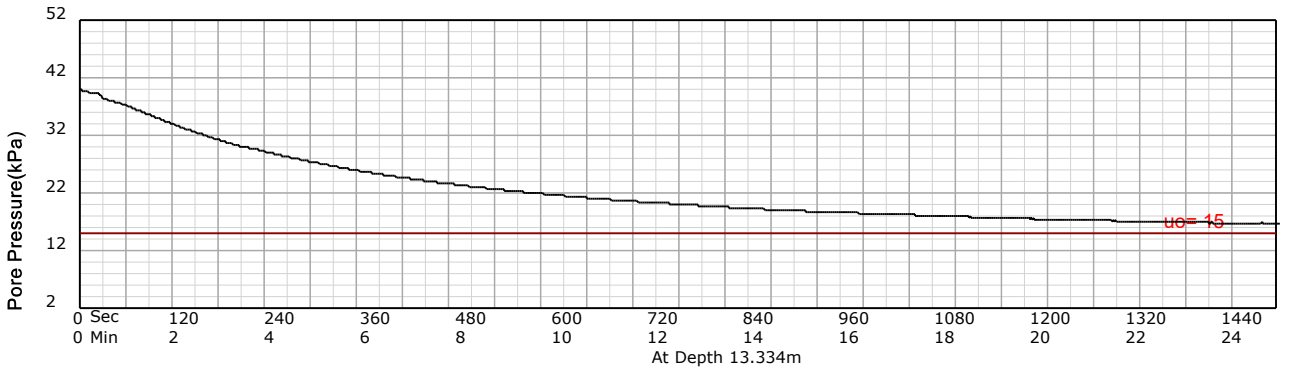

PIEZOCONE PENETRATION TEST

Equivalent Soil Behaviour Type Profile

HOLE: C16

PROJECT: 2024 Jagersfontein

SITE: TSF

DATE: 24/03/11 At: 16:15:38 A

DEPTH: 13.333

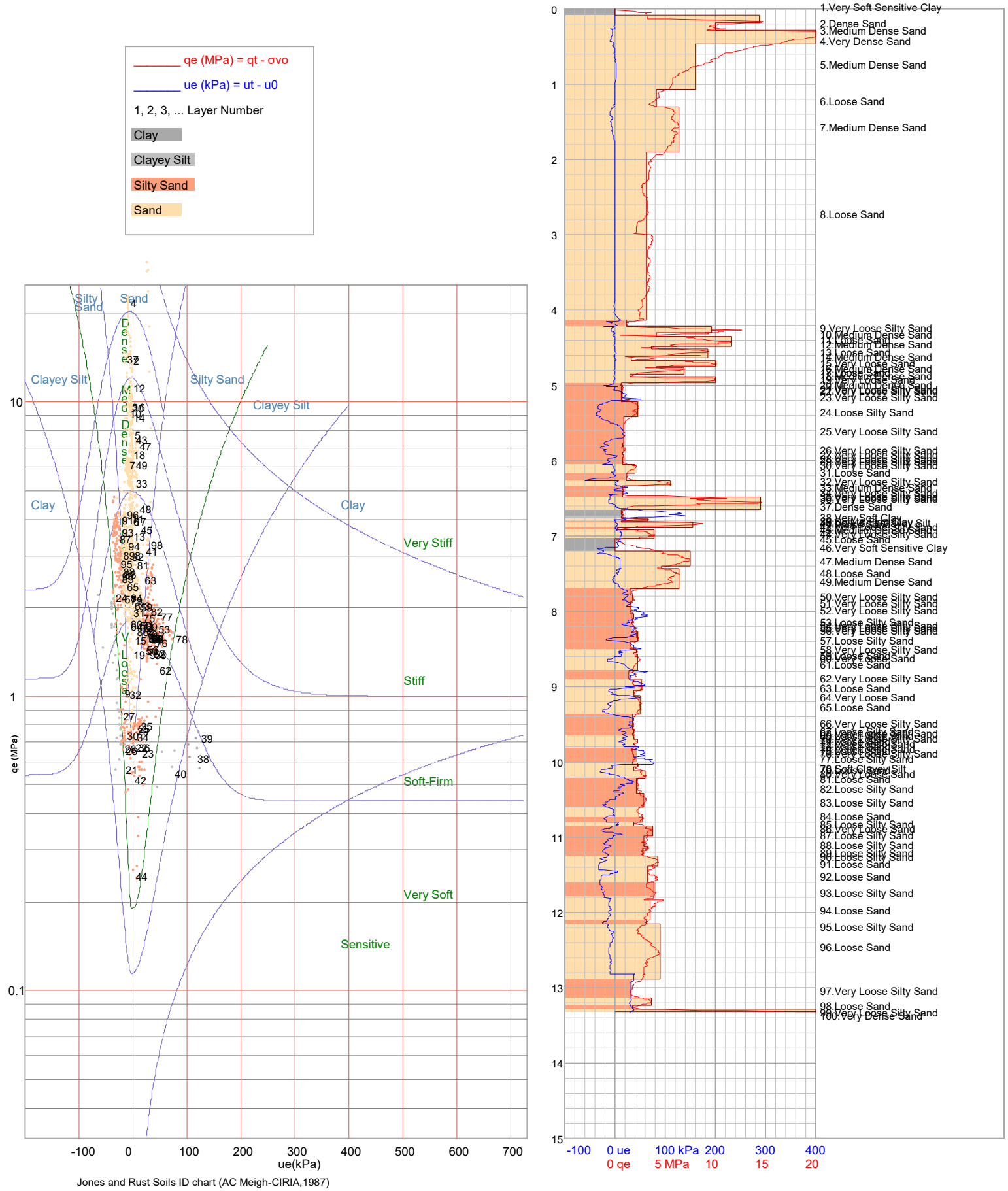

Jones and Rust Soils ID chart (AC Meigh-CIRIA,1987)

PIEZOCONE PENETRATION TEST

Recorded Field Results (Cone, Pore Pressure and Static Pore Pressure from Dissipations)

HOLE: C17

PROJECT: 2024 Jagersfontein

SITE: TSF

DATE: 24/03/14 At: 08:22:13 A **DEPTH:** 7.076

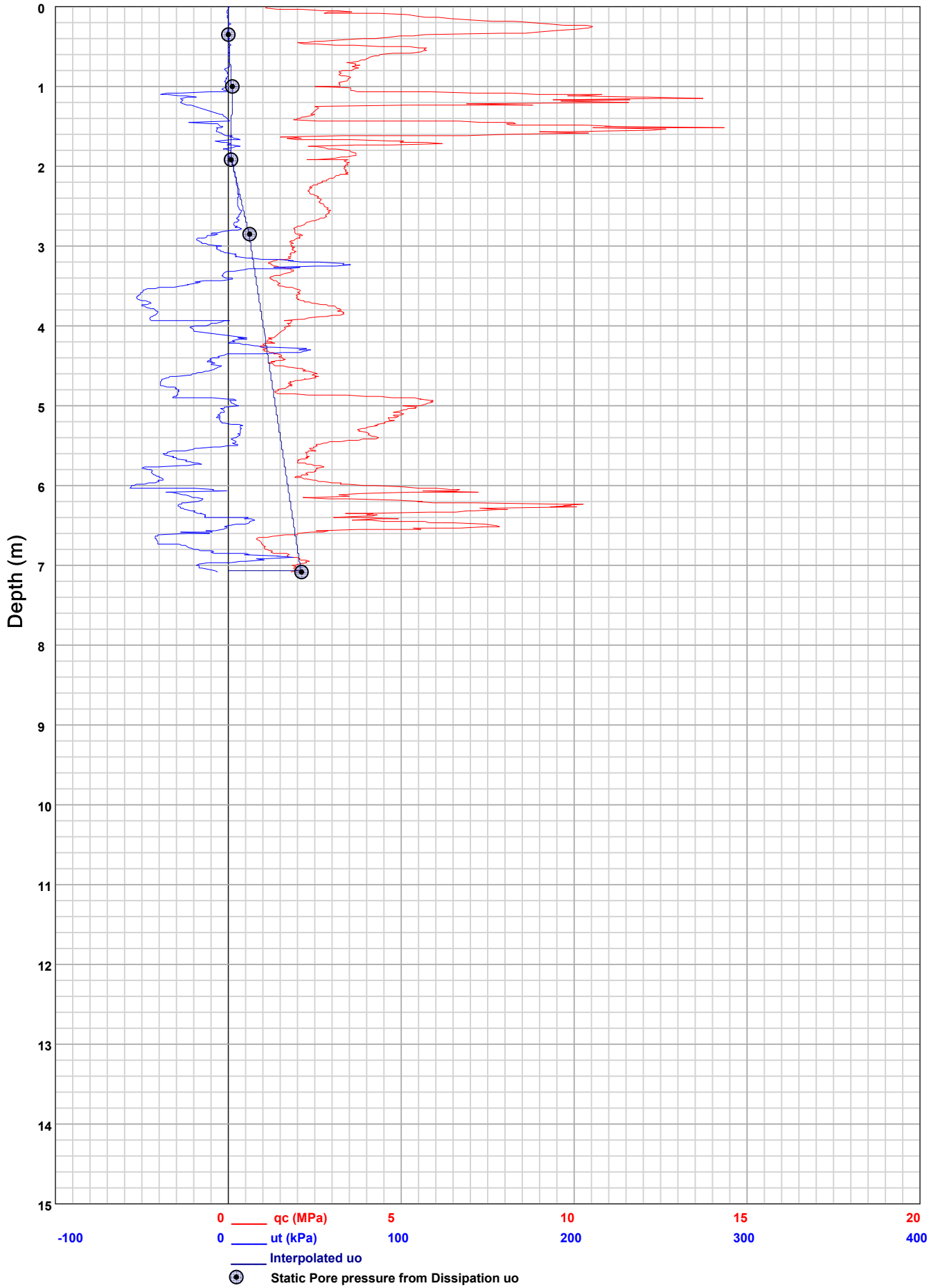

PIEZOCONE PENETRATION TEST

HOLE: C17

PROJECT: 2024 Jagersfontein

SITE: TSF

DATE: 24/03/14 At: 08:22:13 A

DEPTH: 7.076

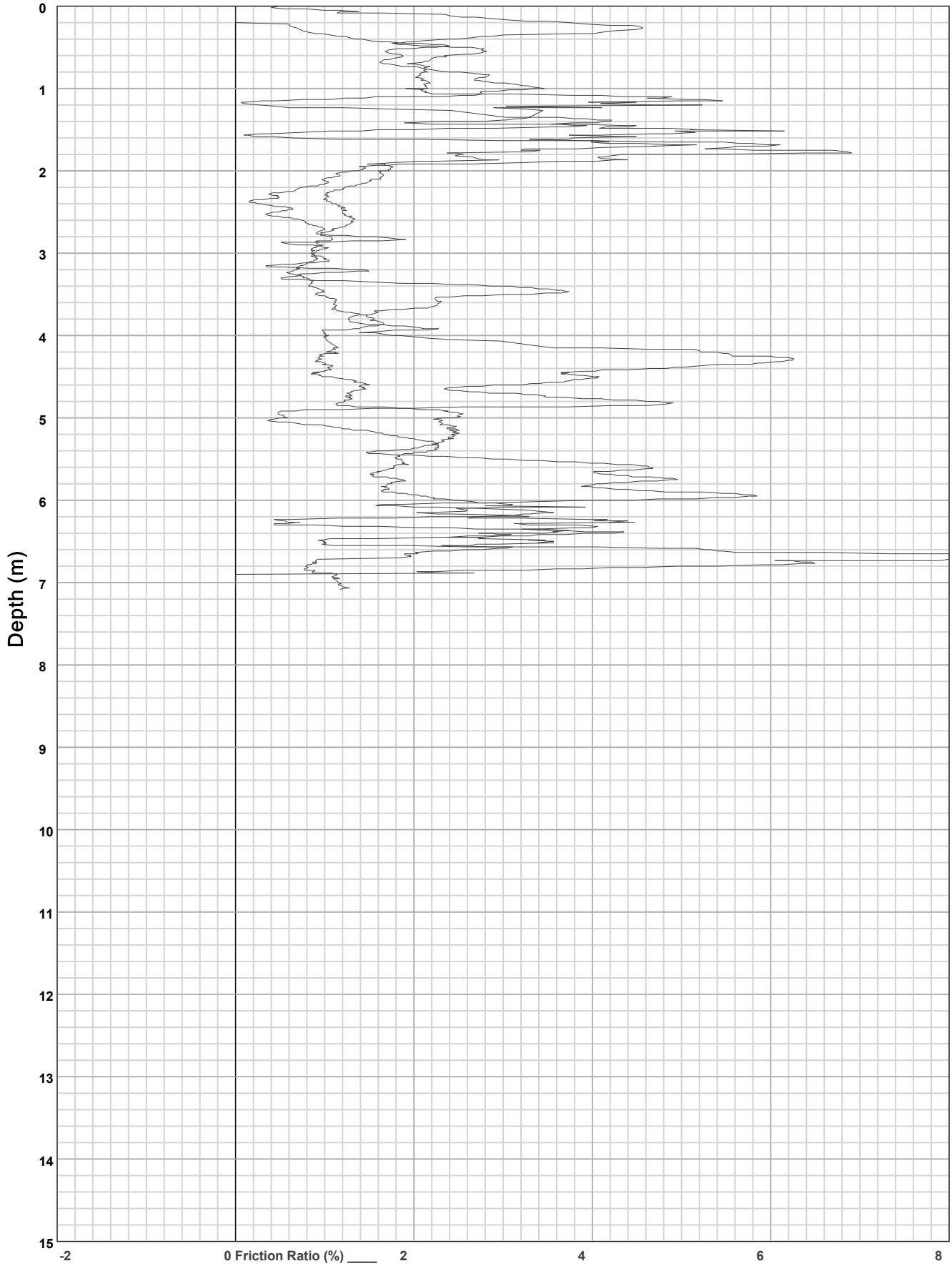

PIEZOCONE PENETRATION TEST

Dissipation Tests

HOLE: C17

PROJECT: 2024 Jagersfontein

SITE: TSF

DATE: 24/03/14 At: 08:22:13 A

DEPTH: 7.076

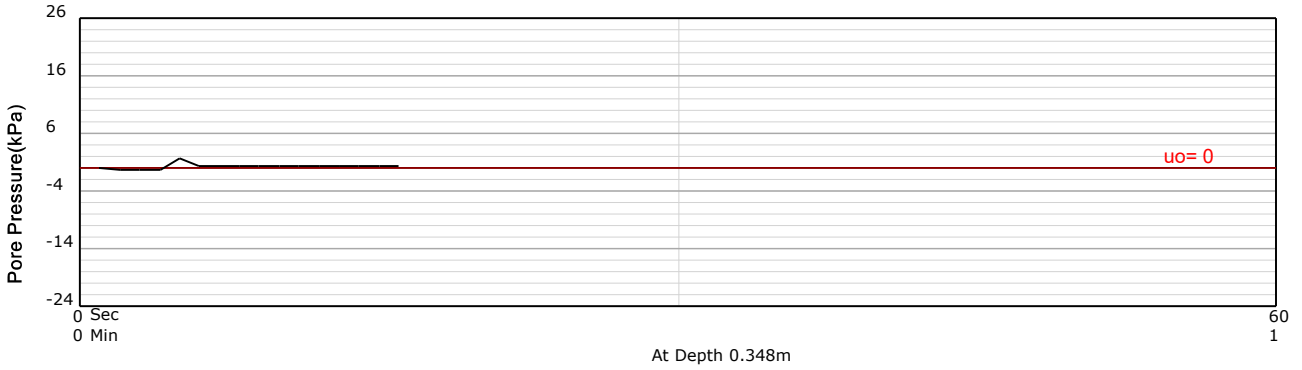

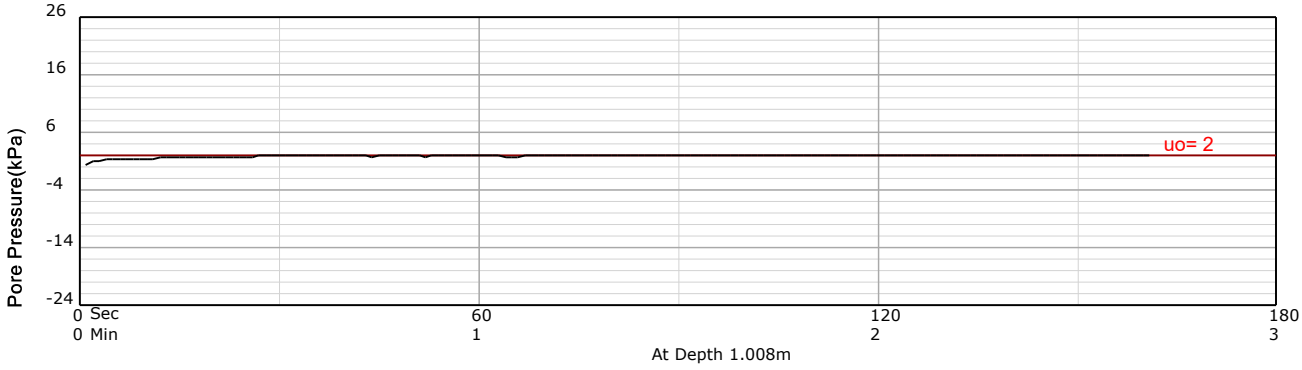

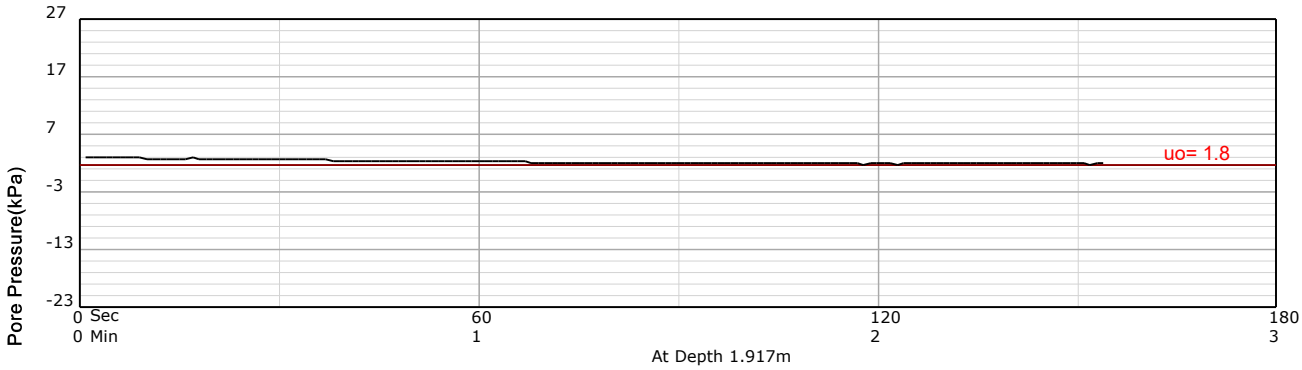

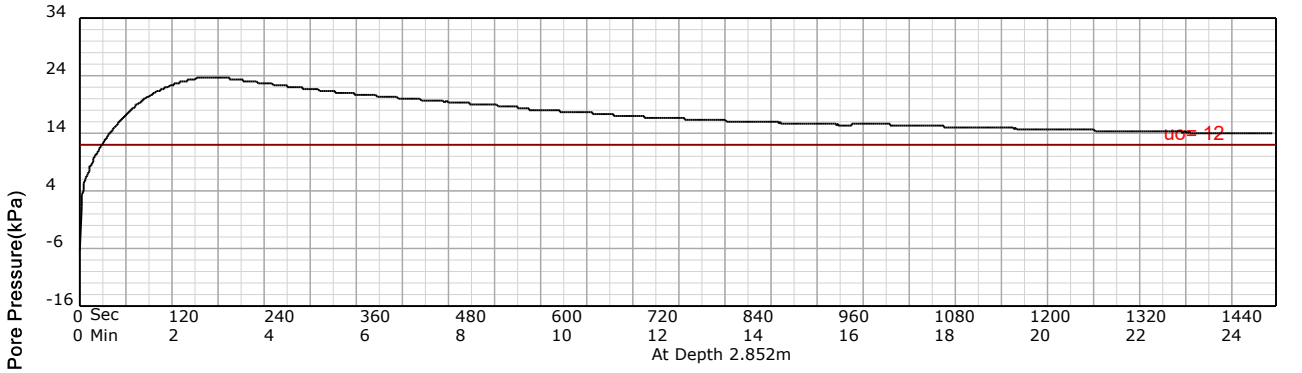

PIEZOCONE PENETRATION TEST

Dissipation Tests

HOLE: C17

PROJECT: 2024 Jagersfontein

SITE: TSF

DATE: 24/03/14 At: 08:22:13 A

DEPTH: 7.076

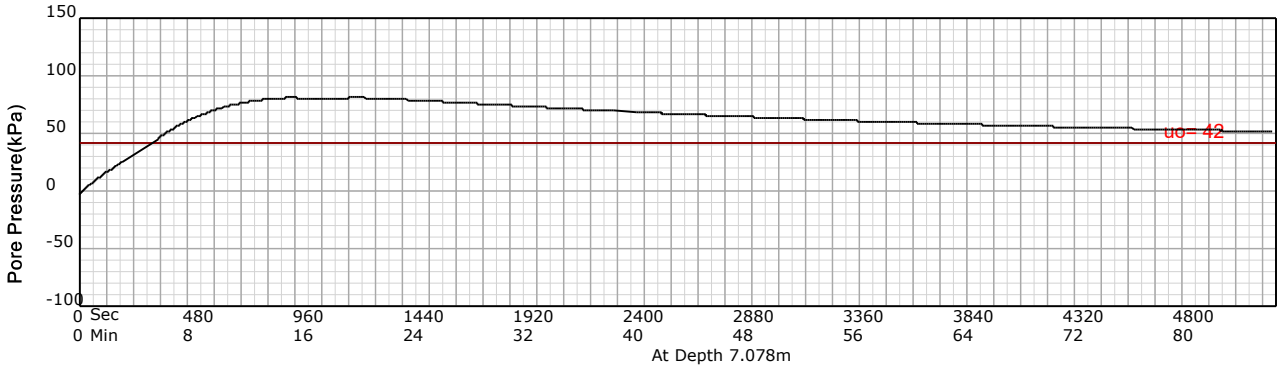

PIEZOCONE PENETRATION TEST

Equivalent Soil Behaviour Type Profile

HOLE: C17

PROJECT: 2024 Jagersfontein

SITE: TSF

DATE: 24/03/14 At: 08:22:13 A

DEPTH: 7.076

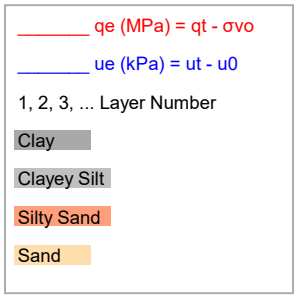

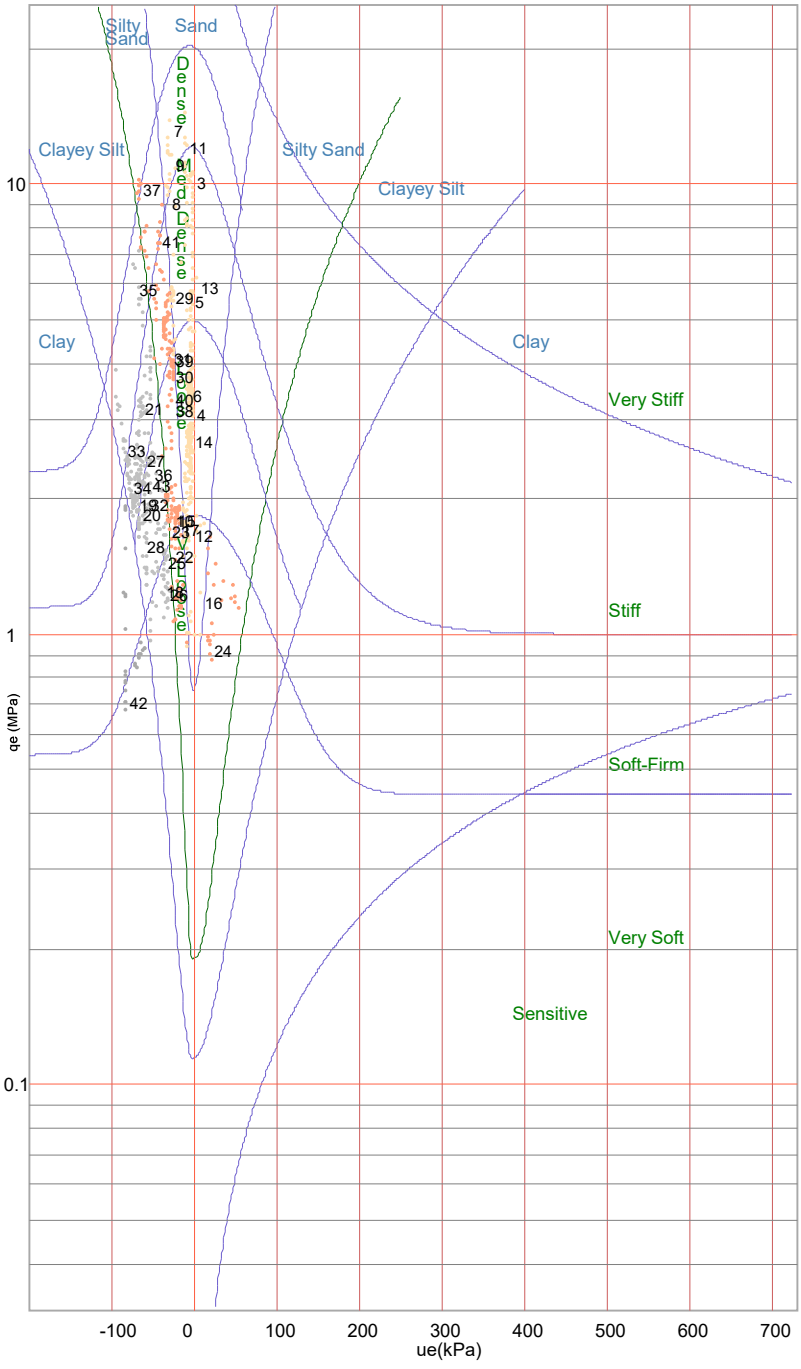

Jones and Rust Soils ID chart (AC Meigh-CIRIA,1987)

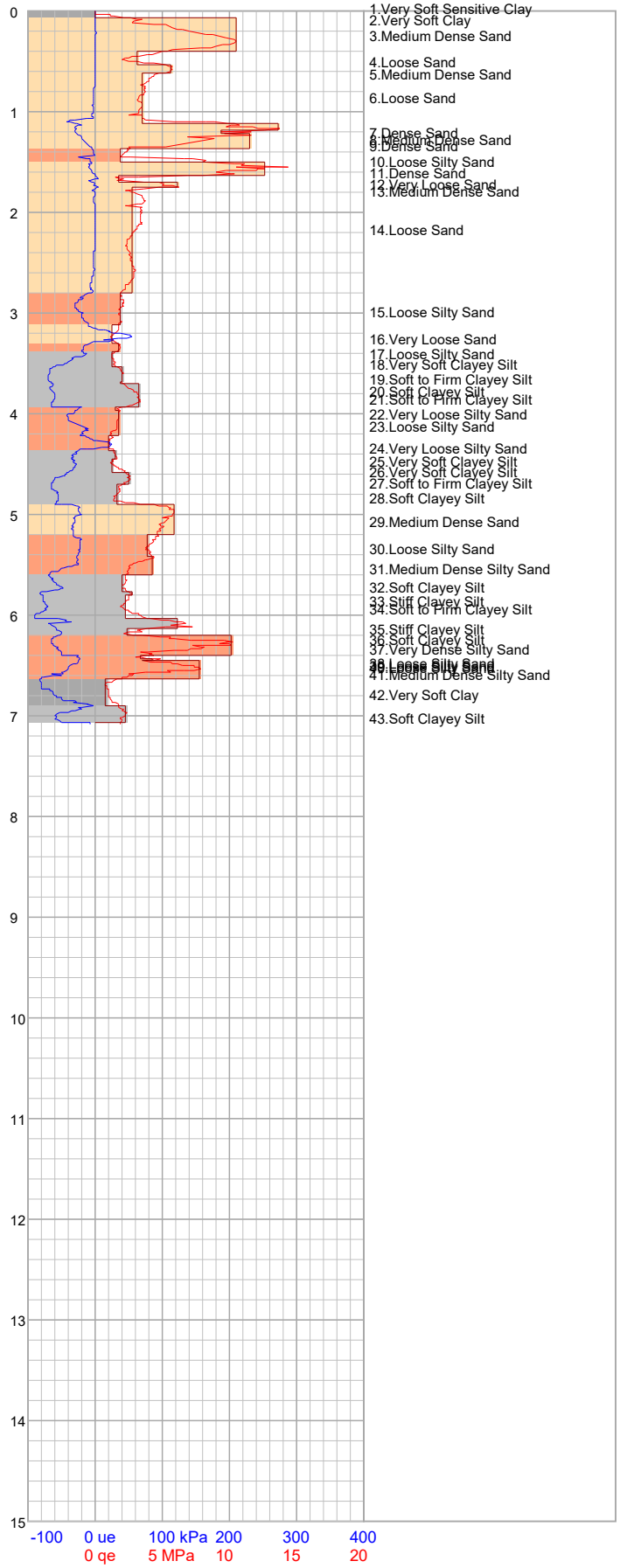

ATTACHMENT F2

CPTu PORE PRESSURE DISSIPATION RESULTS

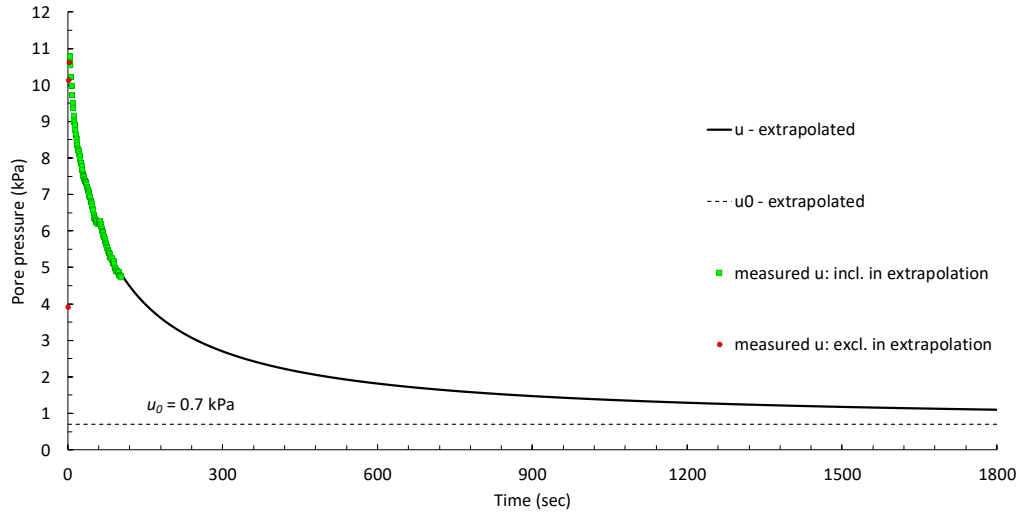

*Figure 1: Extrapolated pore pressure dissipation curve from an incomplete pore pressure dissipation test at **CPT1 – 1.994m**.*

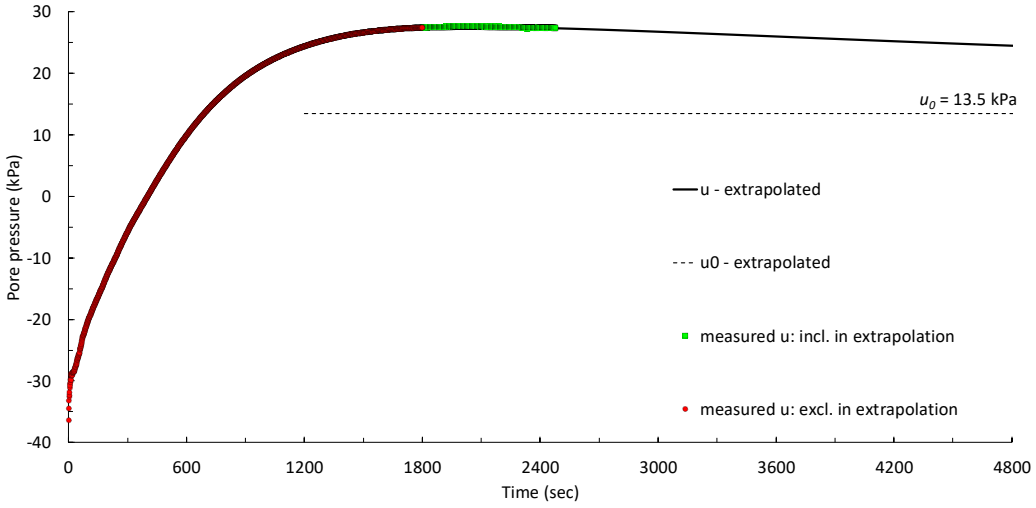

*Figure 2: Extrapolated pore pressure dissipation curve from an incomplete pore pressure dissipation test at **CPT1 – 2.994m**.*

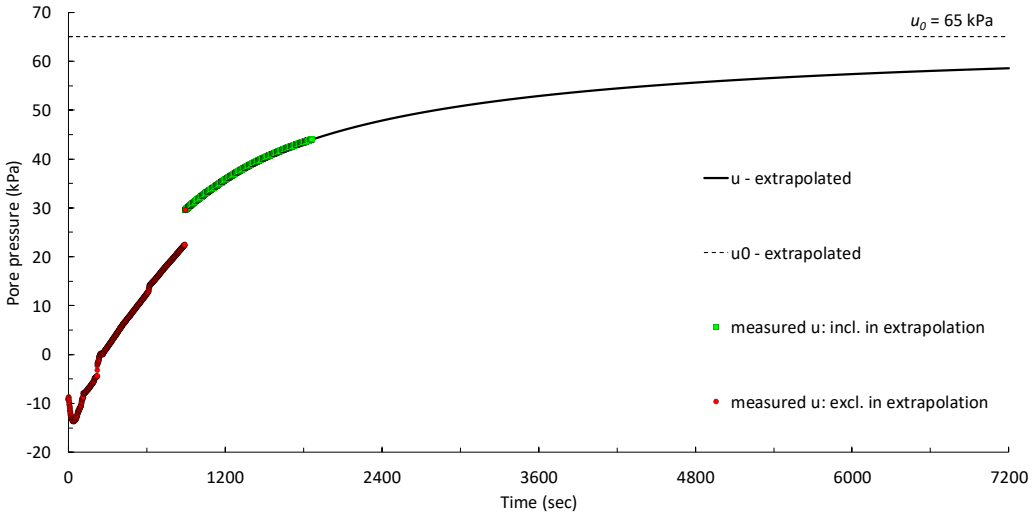

*Figure 3: Extrapolated pore pressure dissipation curve from an incomplete pore pressure dissipation test at **CPT1 – 4.994m**.*

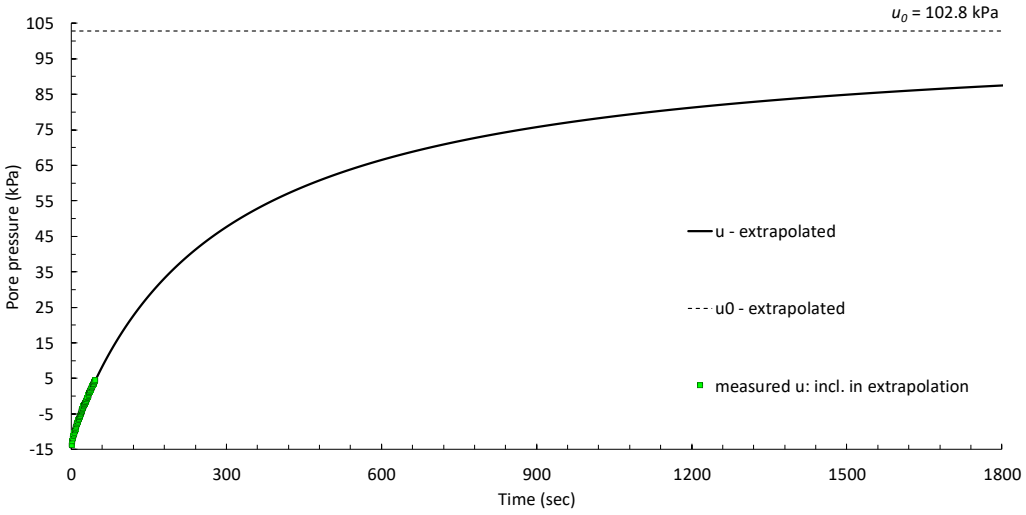

*Figure 4: Extrapolated pore pressure dissipation curve from an incomplete pore pressure dissipation test at **CPT1 – 6.994m**.*

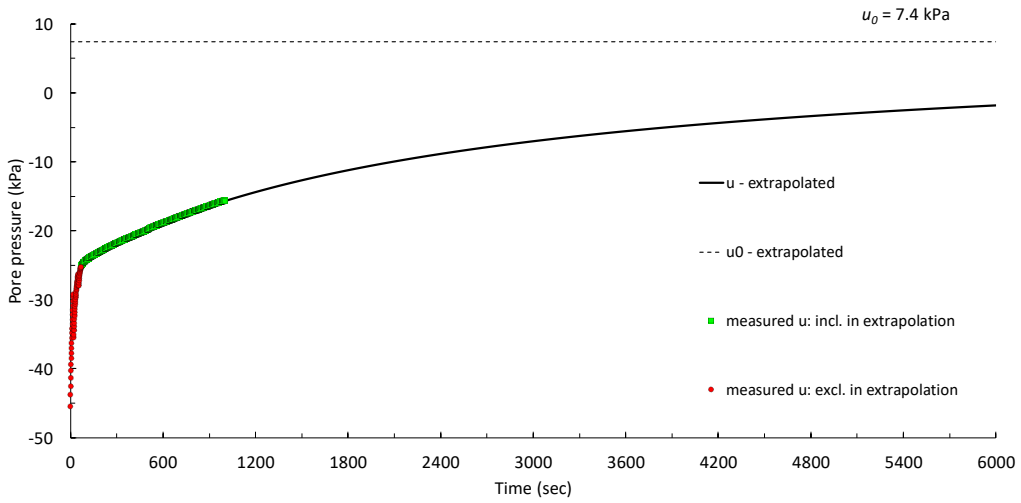

*Figure 5: Extrapolated pore pressure dissipation curve from an incomplete pore pressure dissipation test at **CPT1 – 8.604m**.*

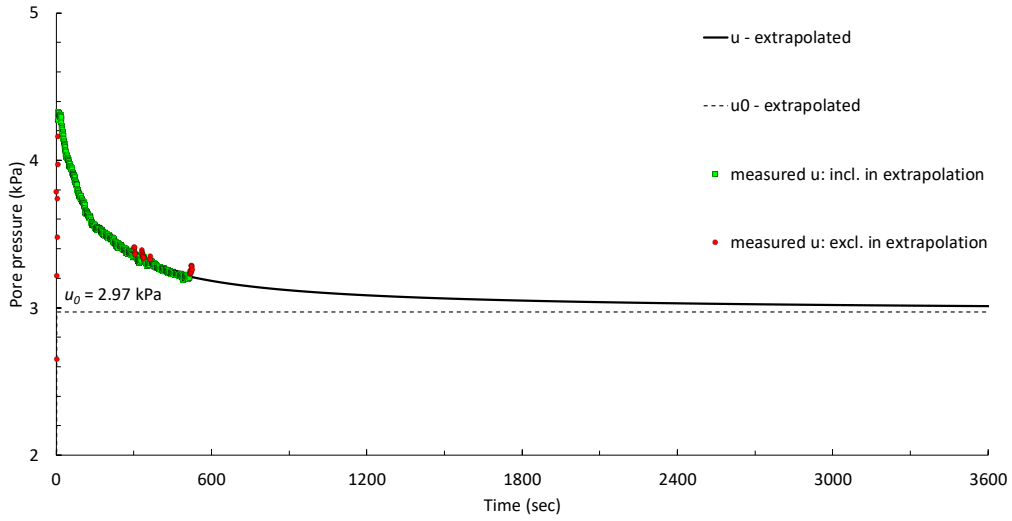

*Figure 6: Extrapolated pore pressure dissipation curve from an incomplete pore pressure dissipation test at **CPT2 – 10.996m**.*

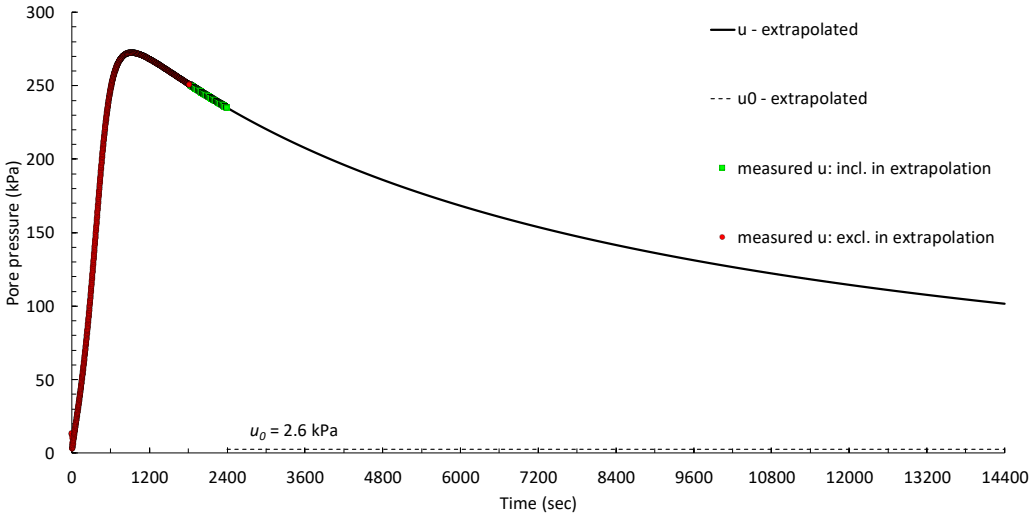

*Figure 7: Extrapolated pore pressure dissipation curve from an incomplete pore pressure dissipation test at **CPT3 – 5.996m**.*

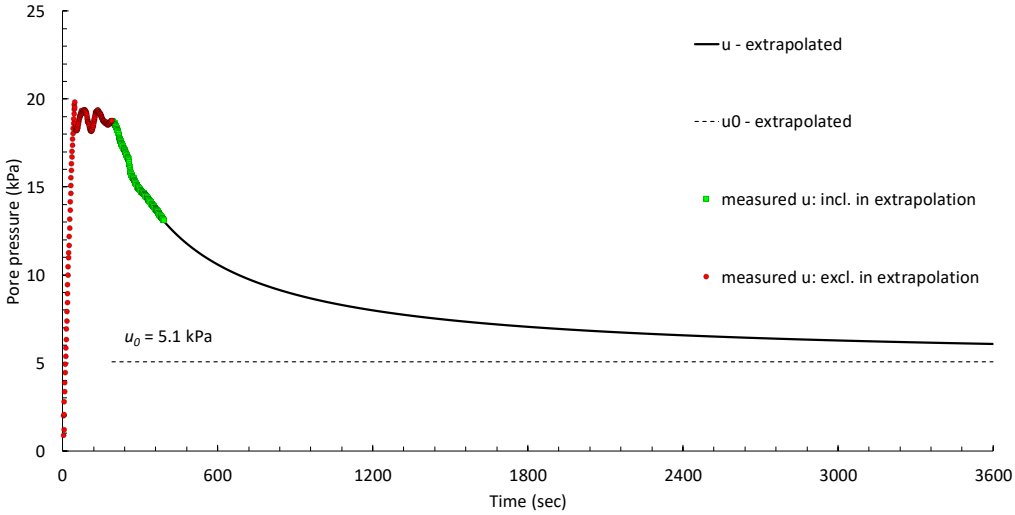

*Figure 8: Extrapolated pore pressure dissipation curve from an incomplete pore pressure dissipation test at **CPT3 – 6.996m**.*

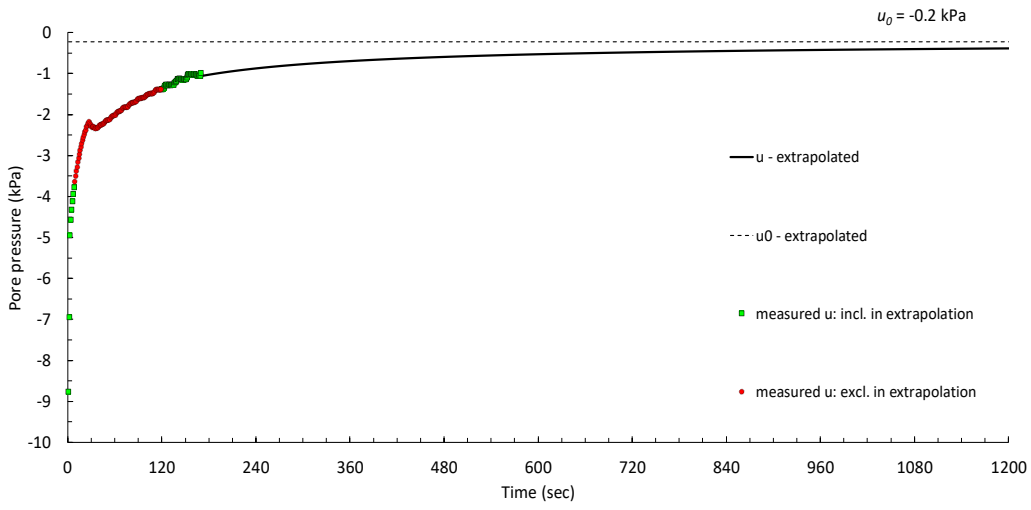

*Figure 9: Extrapolated pore pressure dissipation curve from an incomplete pore pressure dissipation test at **CPT3 – 7.996m**.*

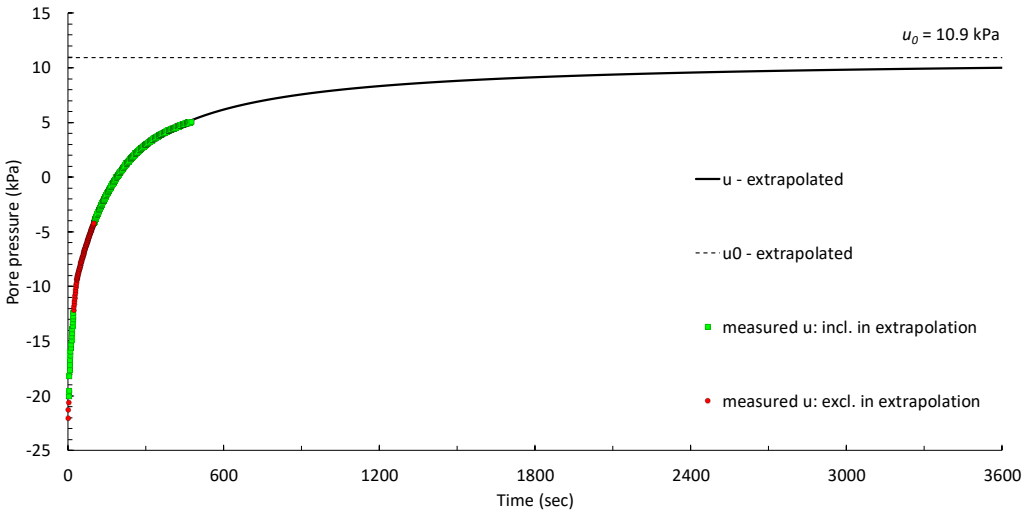

*Figure 10: Extrapolated pore pressure dissipation curve from an incomplete pore pressure dissipation test at **CPT3 – 8.996m**.*

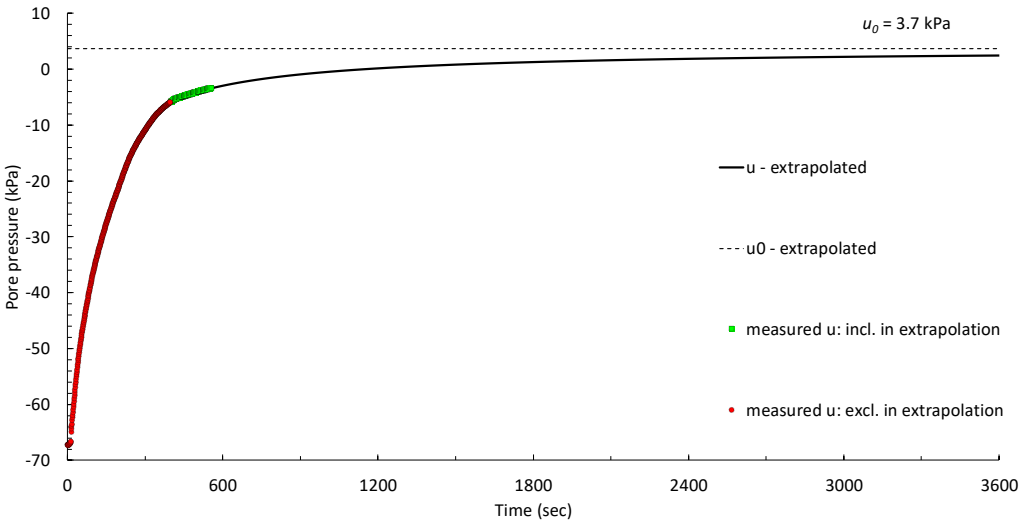

*Figure 11: Extrapolated pore pressure dissipation curve from an incomplete pore pressure dissipation test at **CPT3 – 10.996m**.*

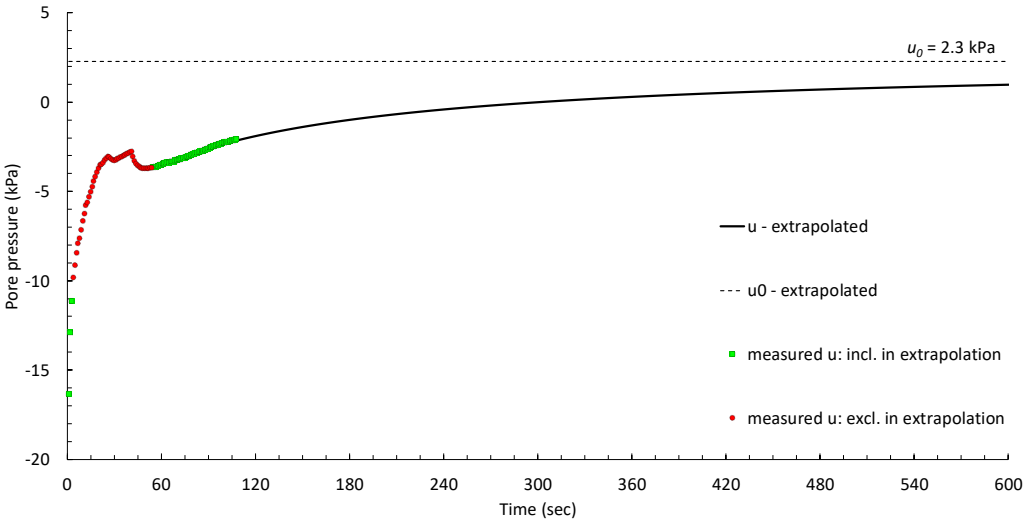

*Figure 12: Extrapolated pore pressure dissipation curve from an incomplete pore pressure dissipation test at **CPT3 – 11.996m**.*

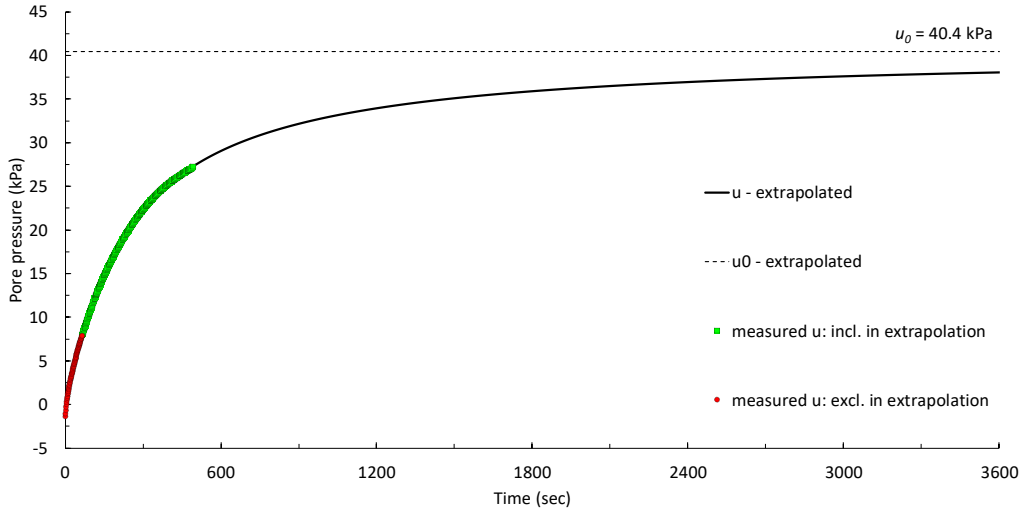

*Figure 13: Extrapolated pore pressure dissipation curve from an incomplete pore pressure dissipation test at **CPT3 – 12.996m**.*

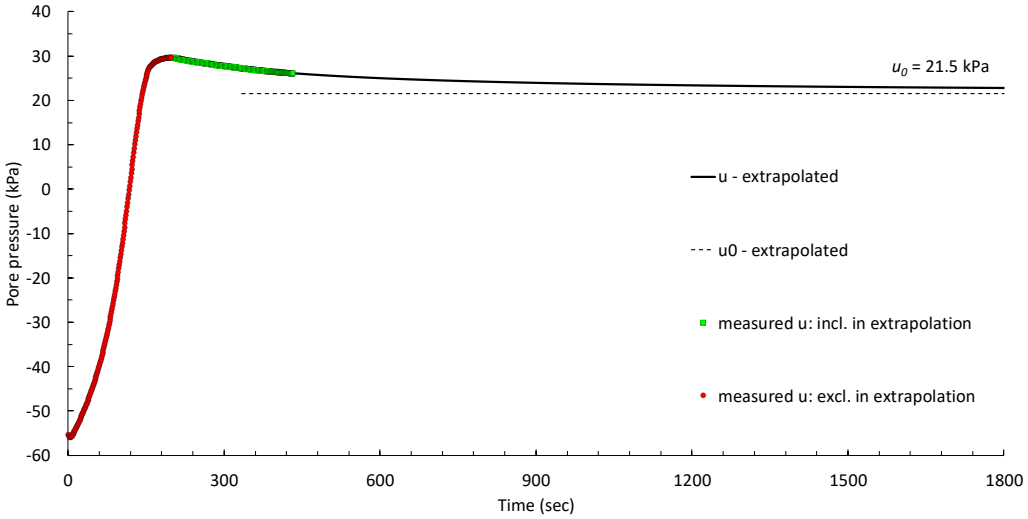

*Figure 14: Extrapolated pore pressure dissipation curve from an incomplete pore pressure dissipation test at **CPT3 – 16.996m**.*

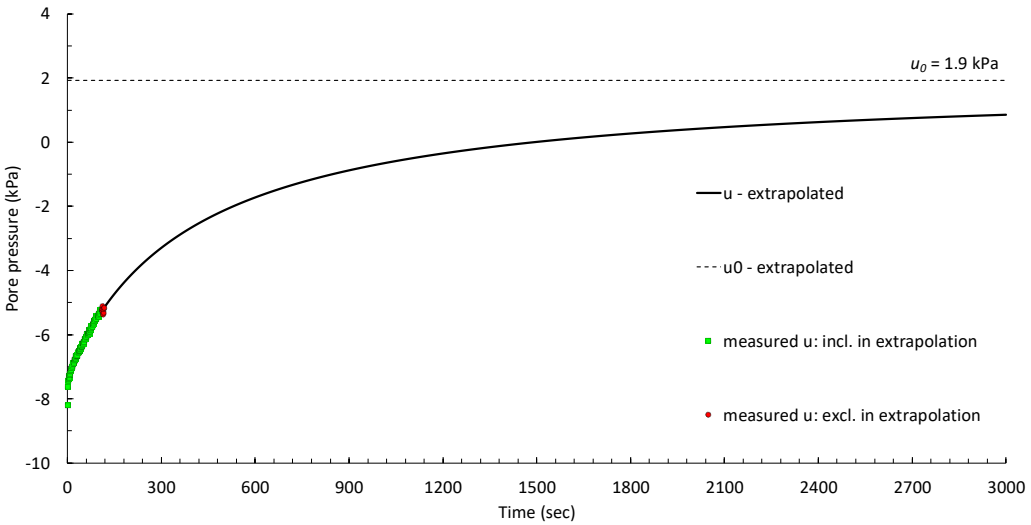

*Figure 15: Extrapolated pore pressure dissipation curve from an incomplete pore pressure dissipation test at **CPT4 – 7.996m**.*

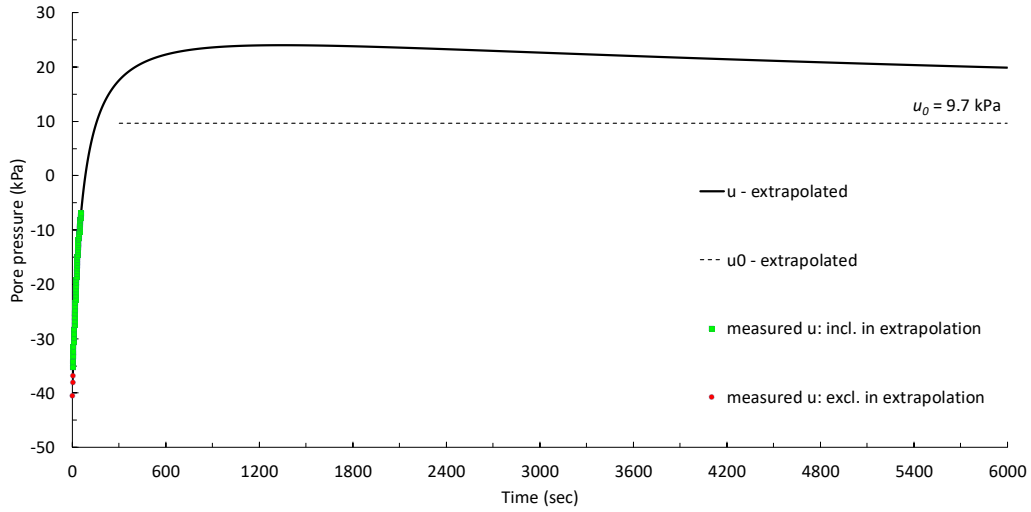

*Figure 16: Extrapolated pore pressure dissipation curve from an incomplete pore pressure dissipation test at **CPT4 – 14.996m**.*

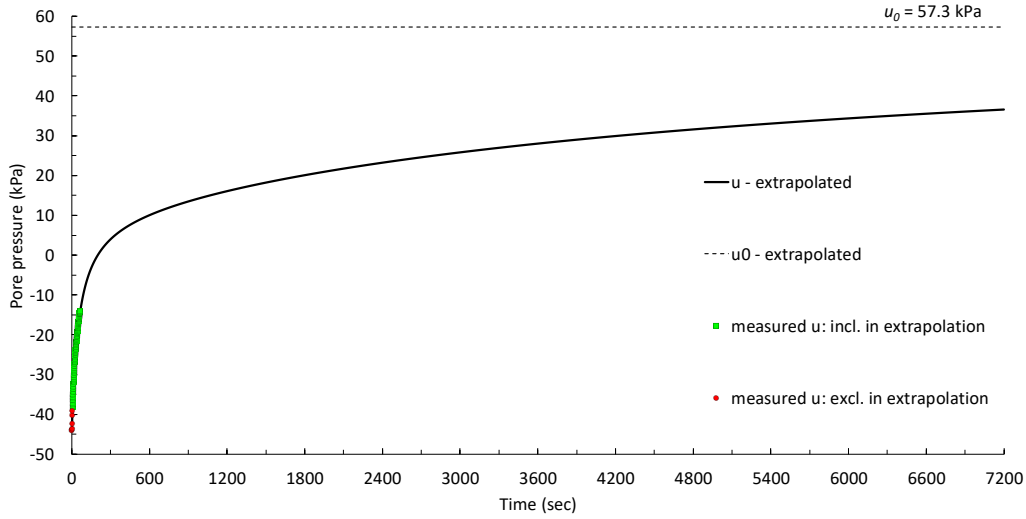

*Figure 17: Extrapolated pore pressure dissipation curve from an incomplete pore pressure dissipation test at **CPT4 – 19.996m**.*

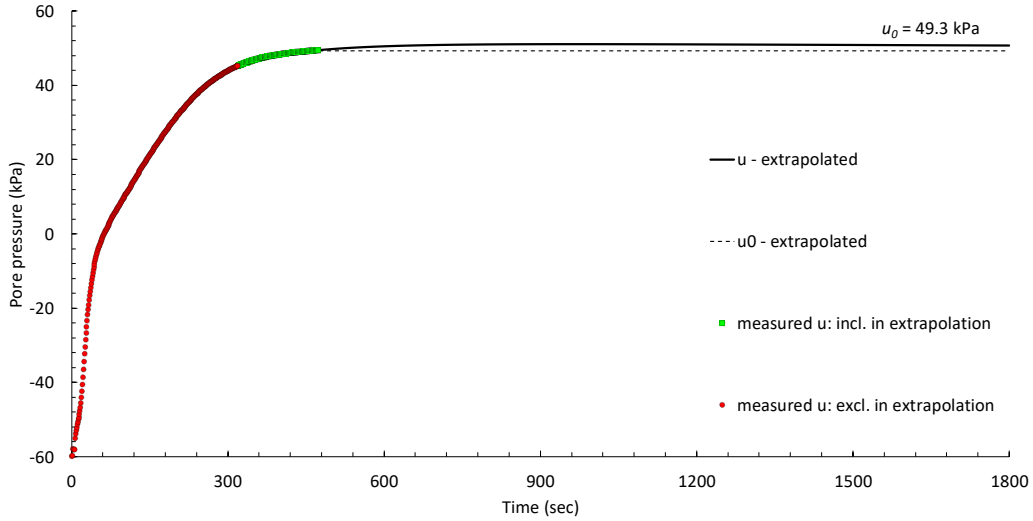

*Figure 18: Extrapolated pore pressure dissipation curve from an incomplete pore pressure dissipation test at **CPT4 – 20.996m**.*

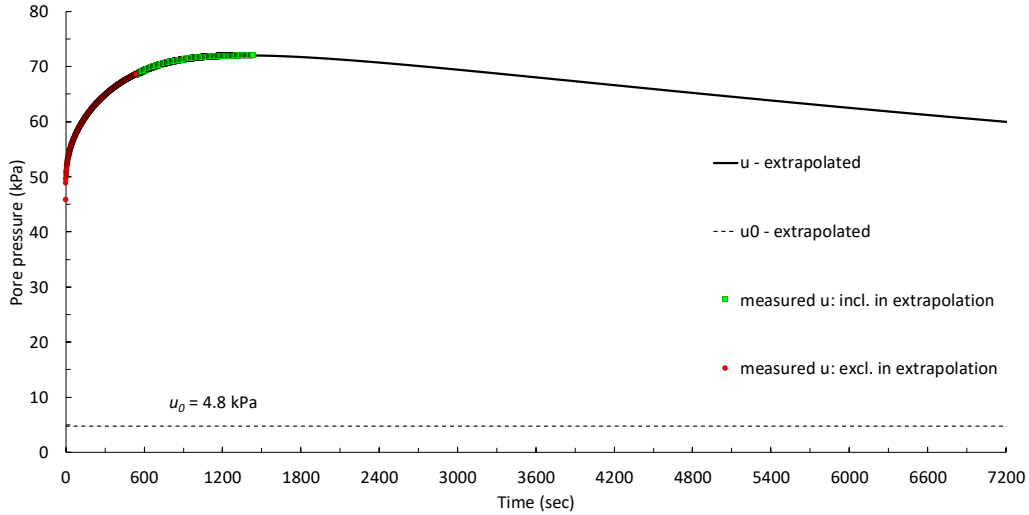

*Figure 19: Extrapolated pore pressure dissipation curve from an incomplete pore pressure dissipation test at **CPT5 – 3.996m**.*

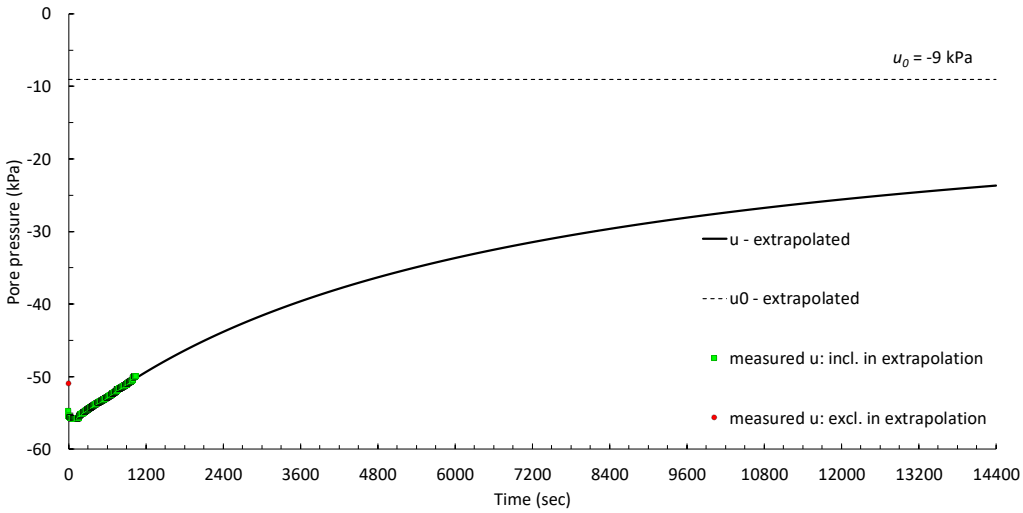

*Figure 20: Extrapolated pore pressure dissipation curve from an incomplete pore pressure dissipation test at **CPT5 – 9.996m**.*

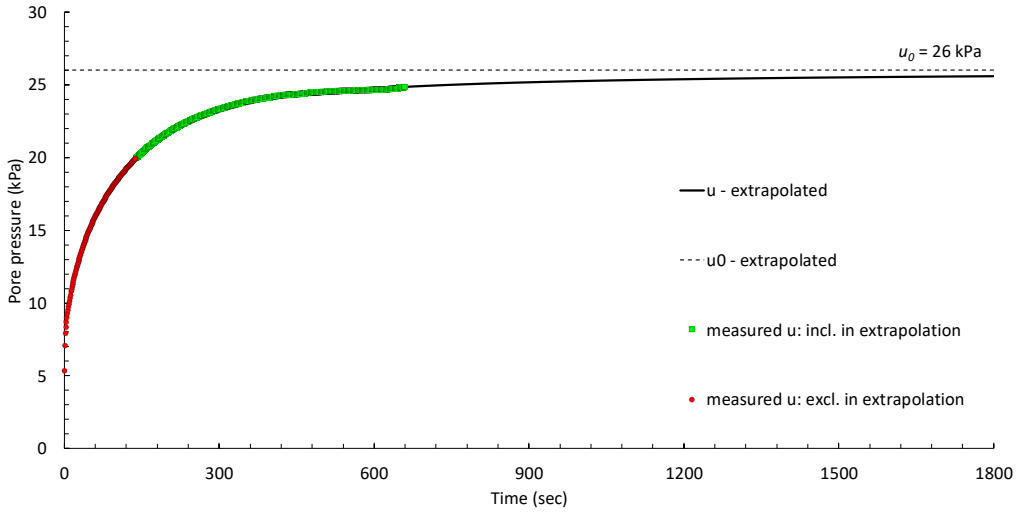

*Figure 21: Extrapolated pore pressure dissipation curve from an incomplete pore pressure dissipation test at **CPT6 – 12.995m**.*

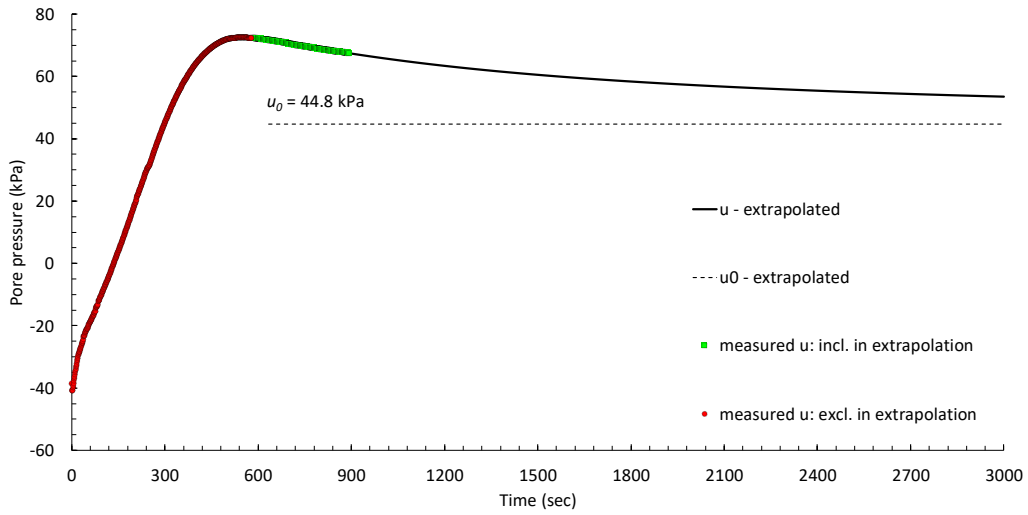

*Figure 22: Extrapolated pore pressure dissipation curve from an incomplete pore pressure dissipation test at **CPT6 – 15.995m**.*

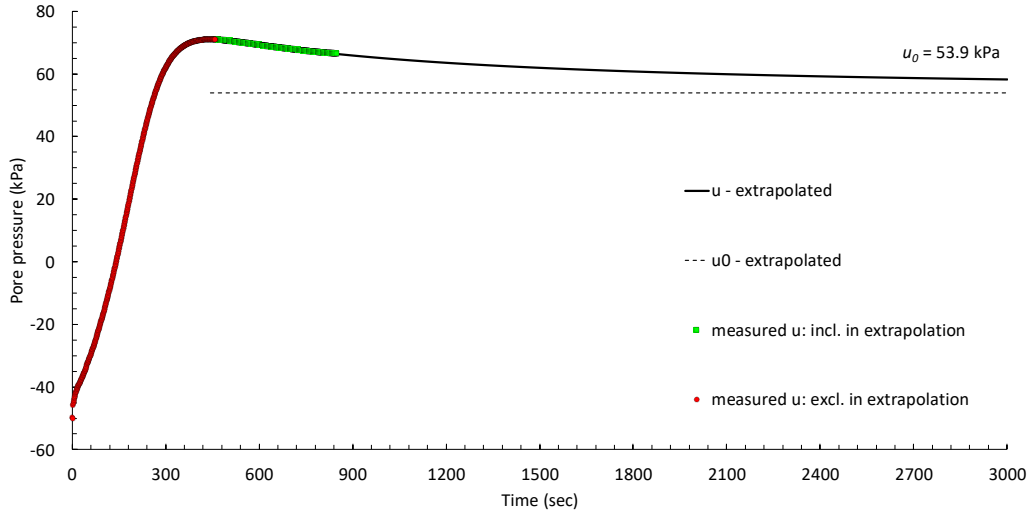

*Figure 23: Extrapolated pore pressure dissipation curve from an incomplete pore pressure dissipation test at **CPT6 – 17.995m**.*

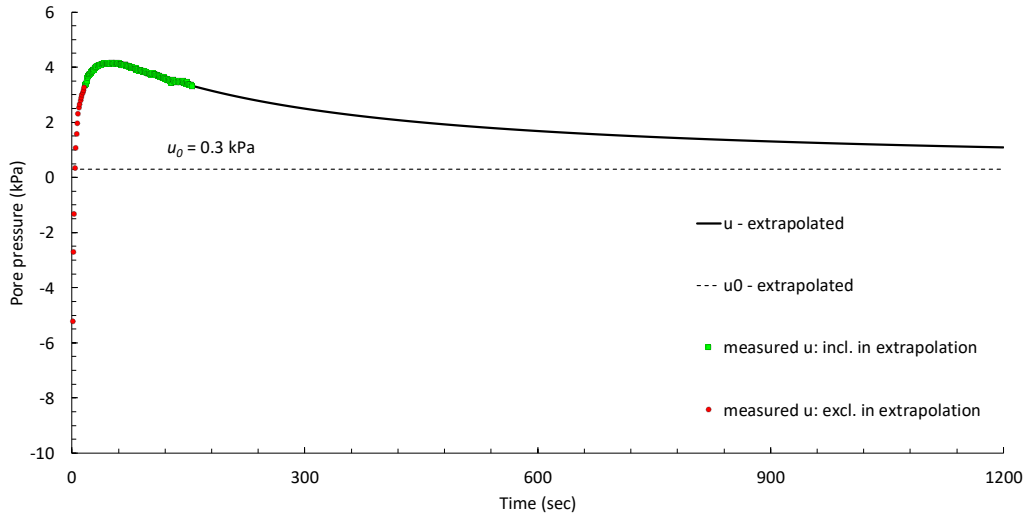

*Figure 24: Extrapolated pore pressure dissipation curve from an incomplete pore pressure dissipation test at **CPT8 – 14.996m**.*

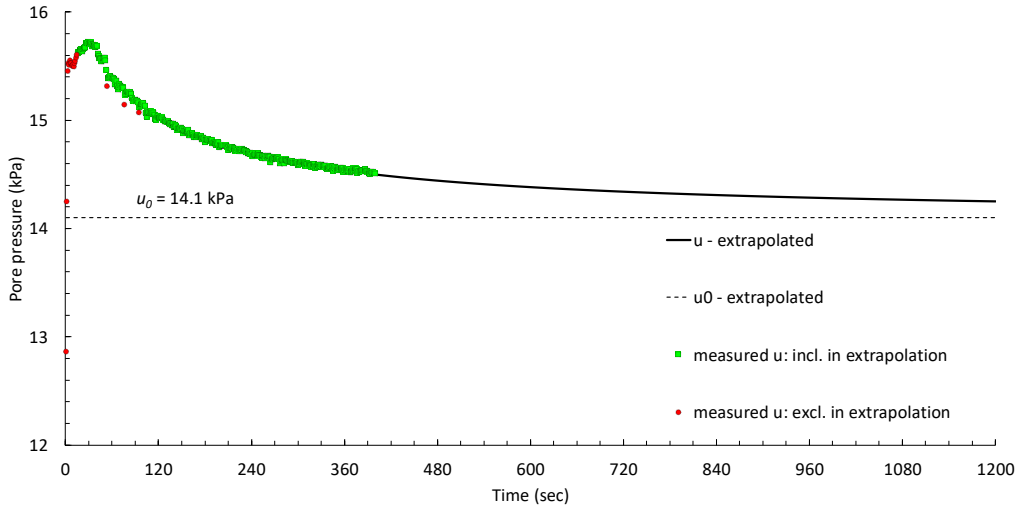

*Figure 25: Extrapolated pore pressure dissipation curve from an incomplete pore pressure dissipation test at **CPT8 – 18.996m**.*

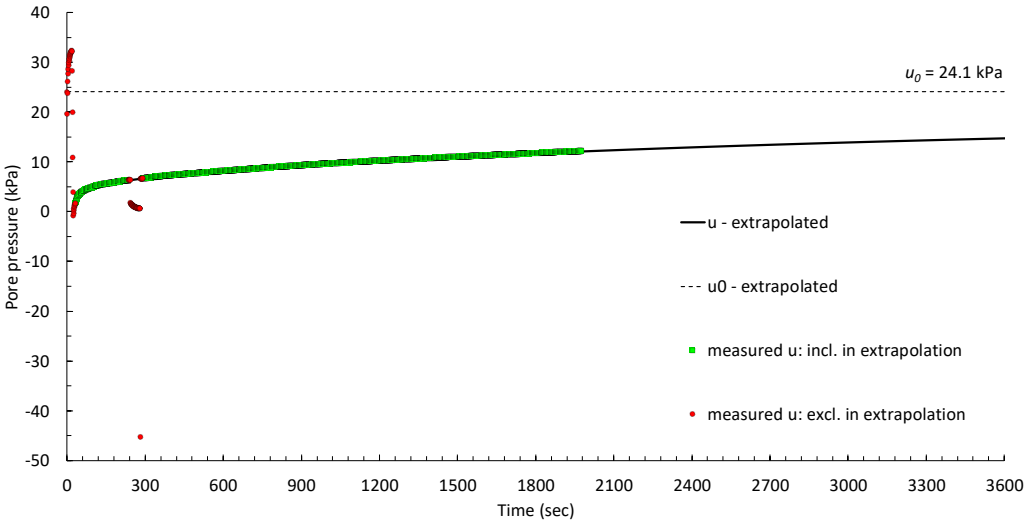

*Figure 26: Extrapolated pore pressure dissipation curve from an incomplete pore pressure dissipation test at **CPT8 – 25.906m**.*

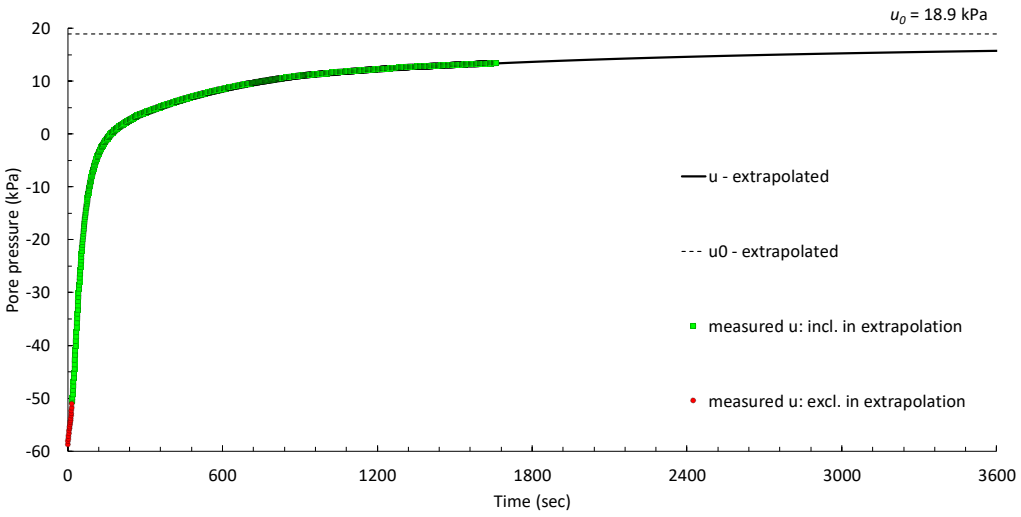

*Figure 27: Extrapolated pore pressure dissipation curve from an incomplete pore pressure dissipation test at **CPT10 – 18.607m**.*

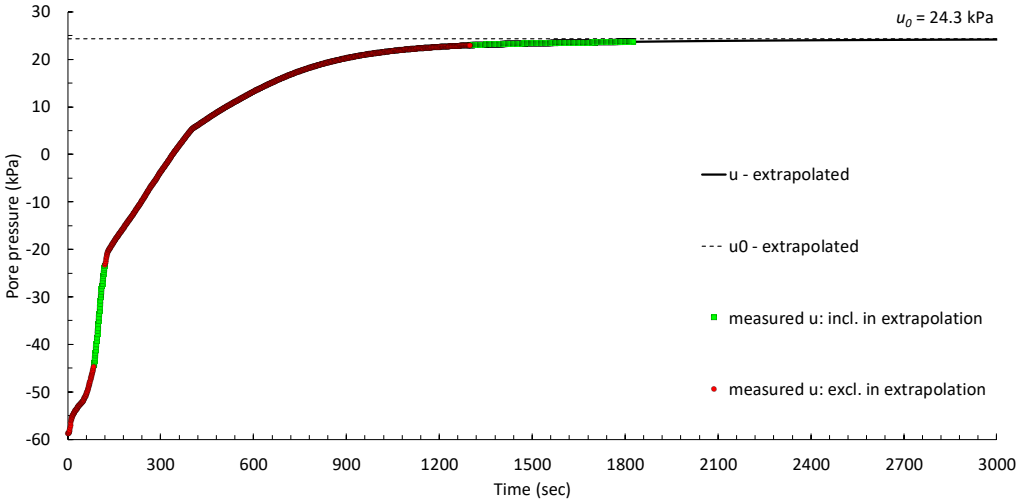

*Figure 28: Extrapolated pore pressure dissipation curve from an incomplete pore pressure dissipation test at **CPT10 – 19.610m**.*

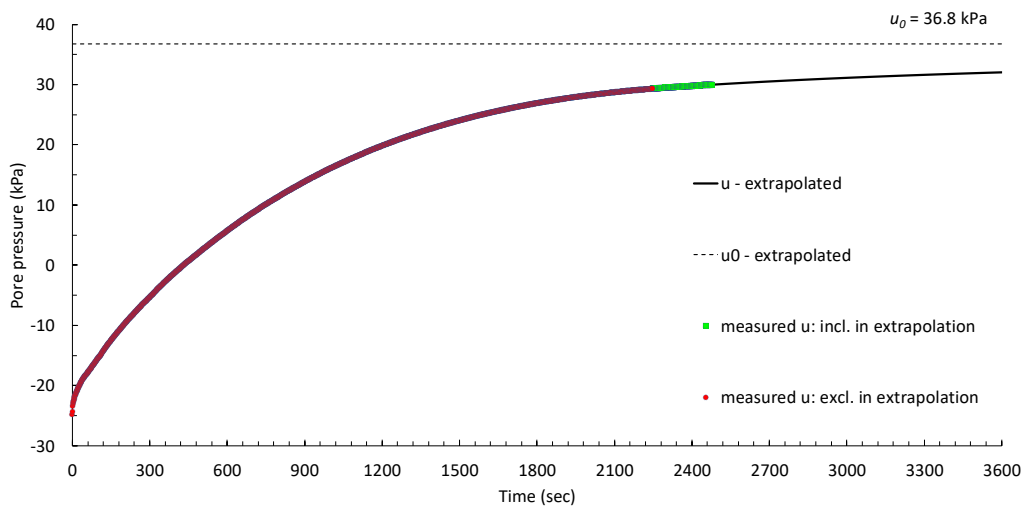

*Figure 29: Extrapolated pore pressure dissipation curve from an incomplete pore pressure dissipation test at **CPT11 – 4.996m**.*

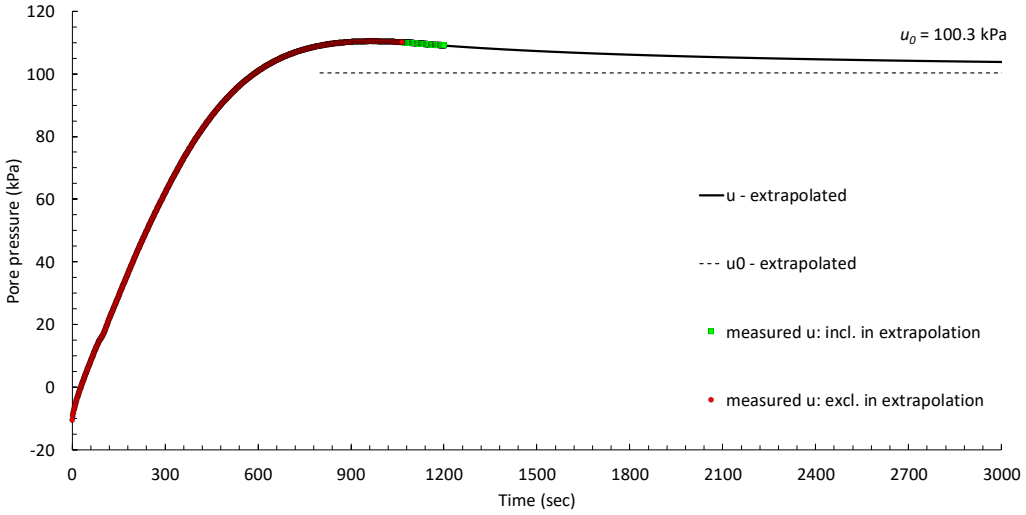

*Figure 30: Extrapolated pore pressure dissipation curve from an incomplete pore pressure dissipation test at **CPT11 – 7.996m**.*

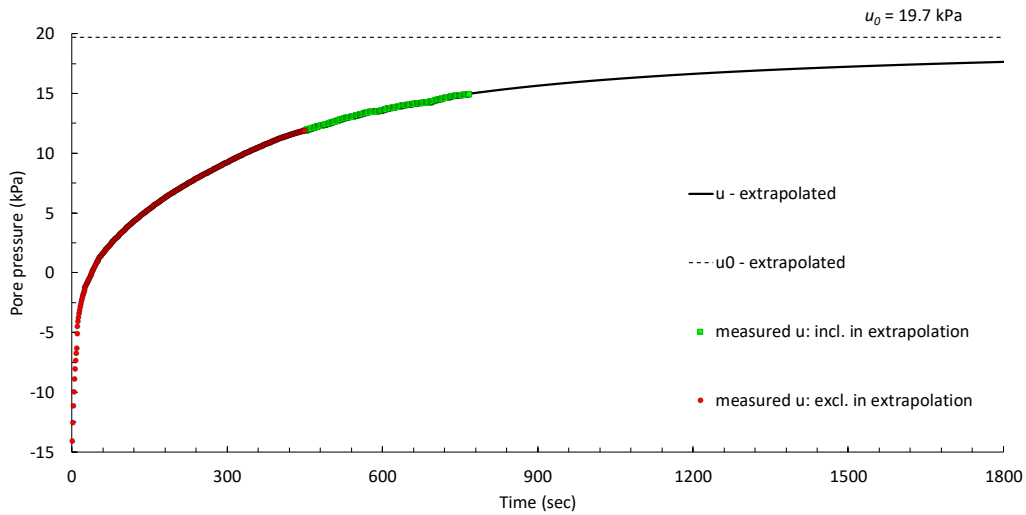

*Figure 31: Extrapolated pore pressure dissipation curve from an incomplete pore pressure dissipation test at **CPT11 – 12.406m**.*

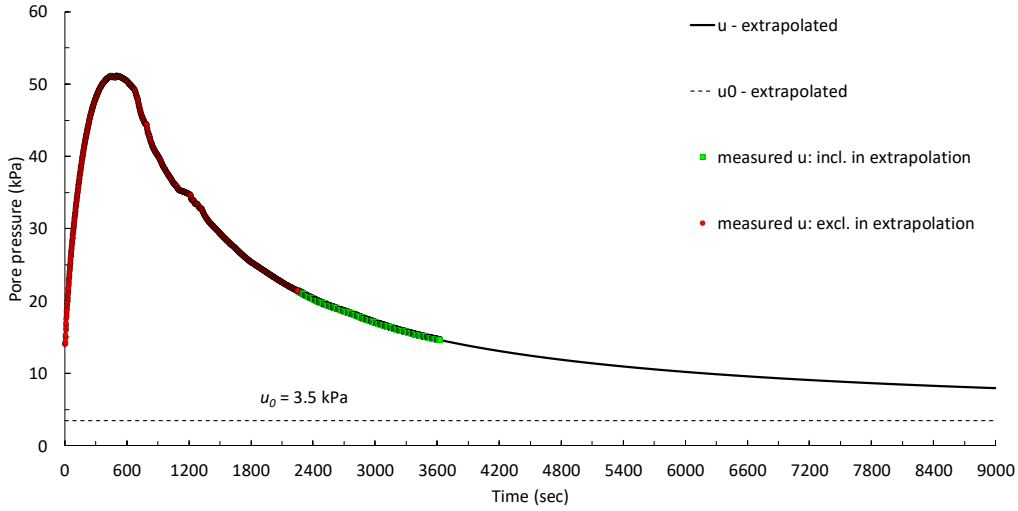

*Figure 32: Extrapolated pore pressure dissipation curve from an incomplete pore pressure dissipation test at **CPT13 – 12.922m**.*

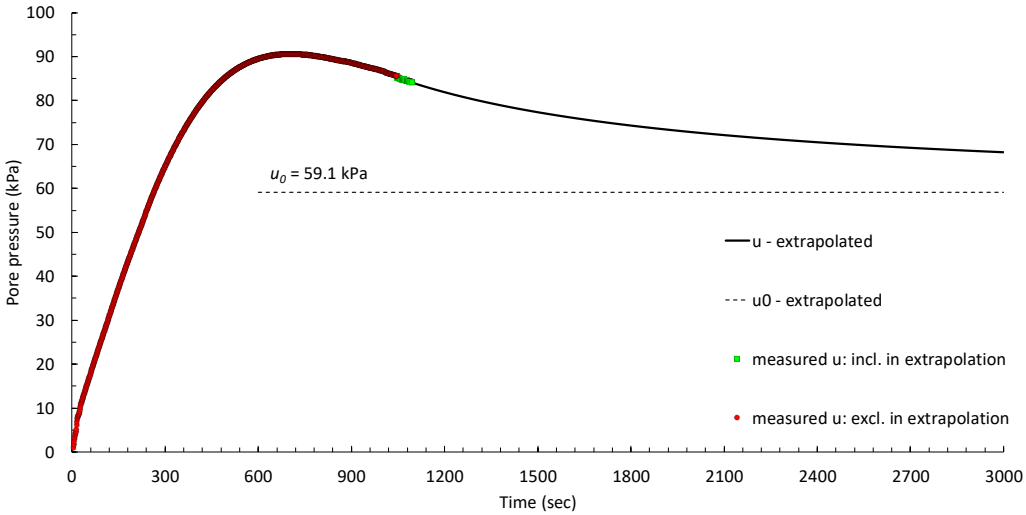

*Figure 33: Extrapolated pore pressure dissipation curve from an incomplete pore pressure dissipation test at **CPT13 – 15.985m**.*

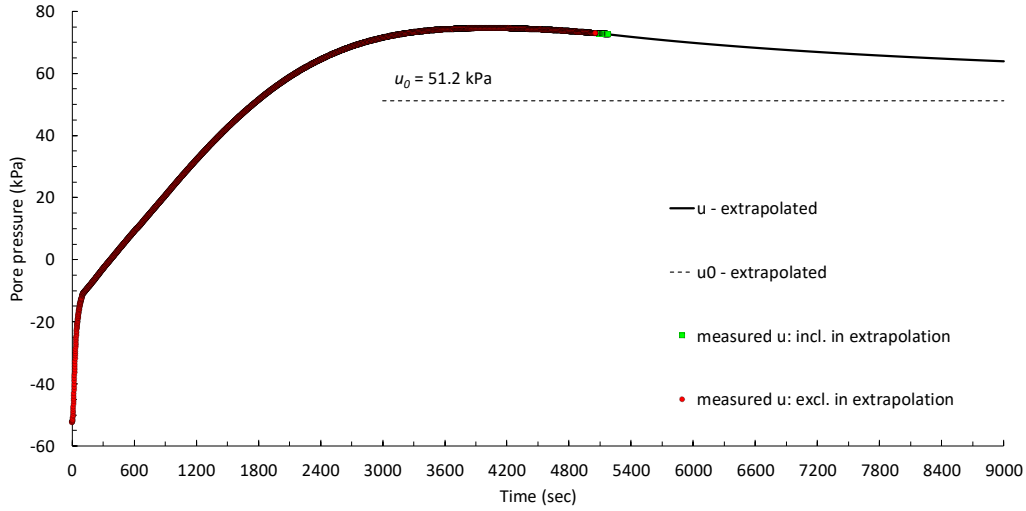

*Figure 34: Extrapolated pore pressure dissipation curve from an incomplete pore pressure dissipation test at **CPT14 – 19.96m**.*

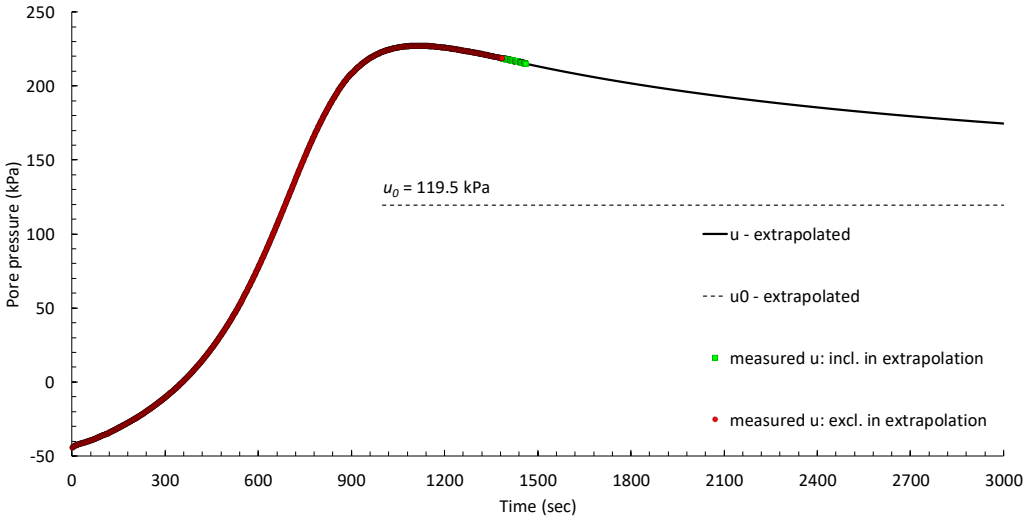

*Figure 35: Extrapolated pore pressure dissipation curve from an incomplete pore pressure dissipation test at **CPT14 – 23.68m**.*

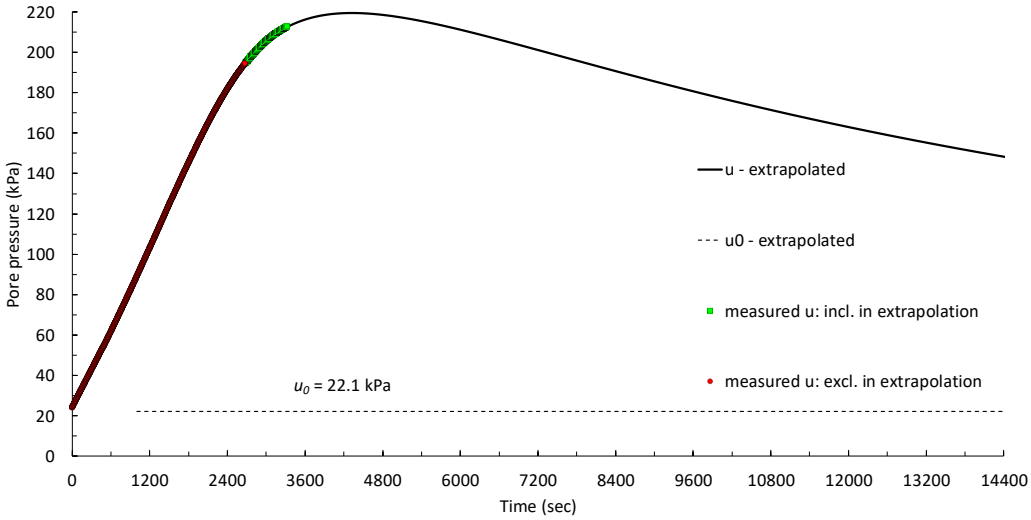

*Figure 36: Extrapolated pore pressure dissipation curve from an incomplete pore pressure dissipation test at **CPT15 – 16.25m**.*

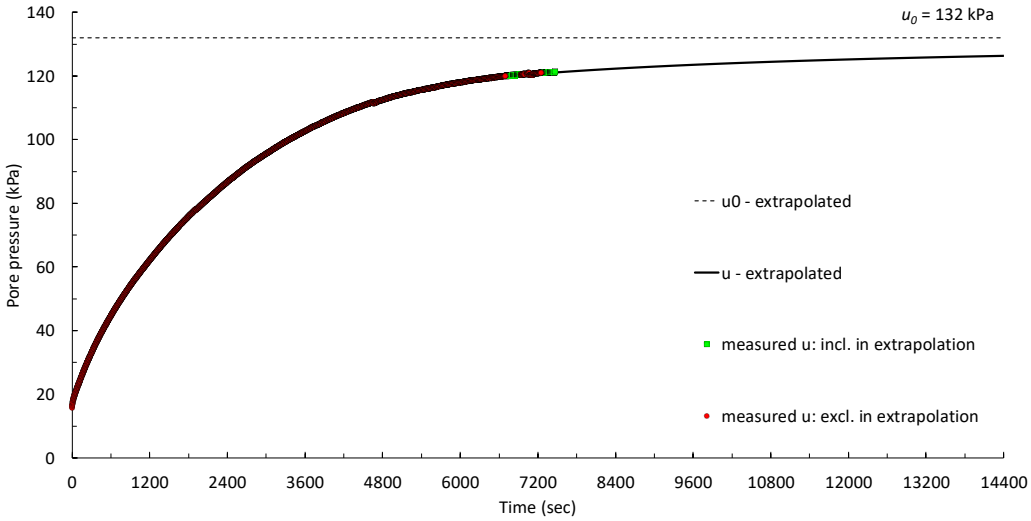

*Figure 37: Extrapolated pore pressure dissipation curve from an incomplete pore pressure dissipation test at **CPT15 – 23.336m**.*

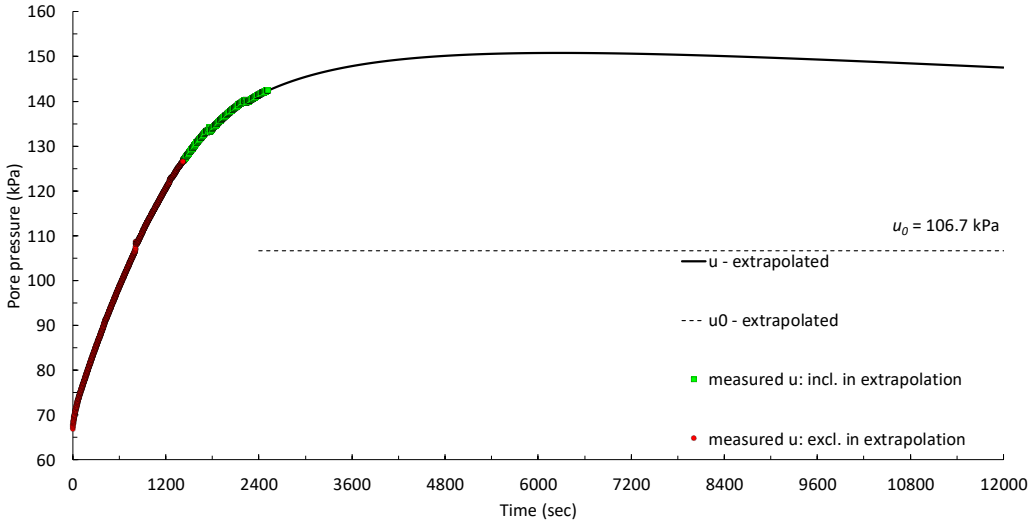

*Figure 38: Extrapolated pore pressure dissipation curve from an incomplete pore pressure dissipation test at **CPT16 –8.798m**.*

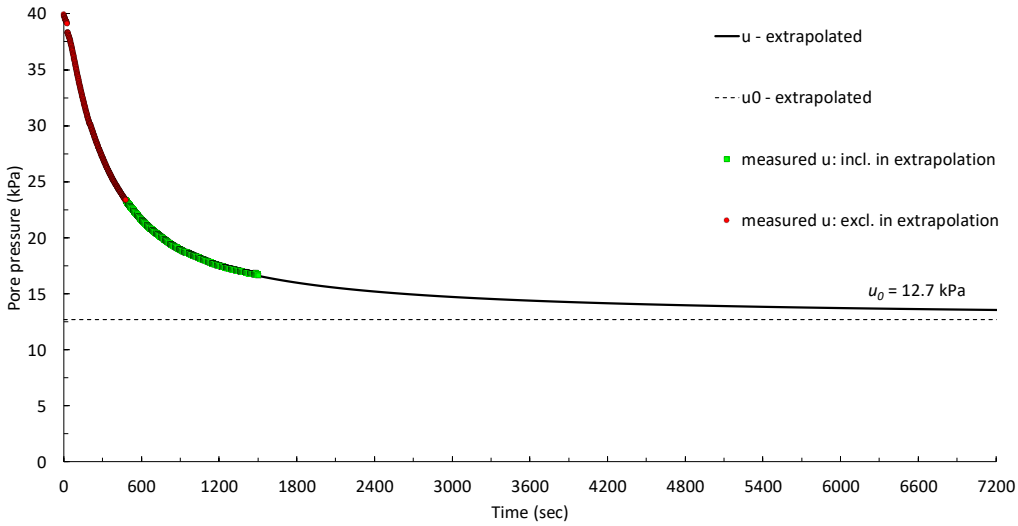

*Figure 39: Extrapolated pore pressure dissipation curve from an incomplete pore pressure dissipation test at **CPT16 – 13.334m**.*

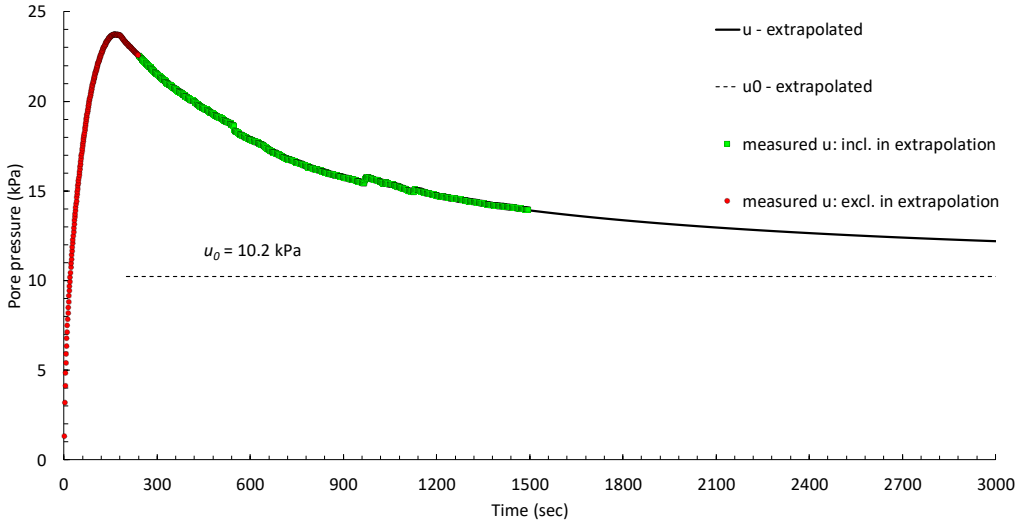

*Figure 40: Extrapolated pore pressure dissipation curve from an incomplete pore pressure dissipation test at **CPT17 – 2.852m**.*

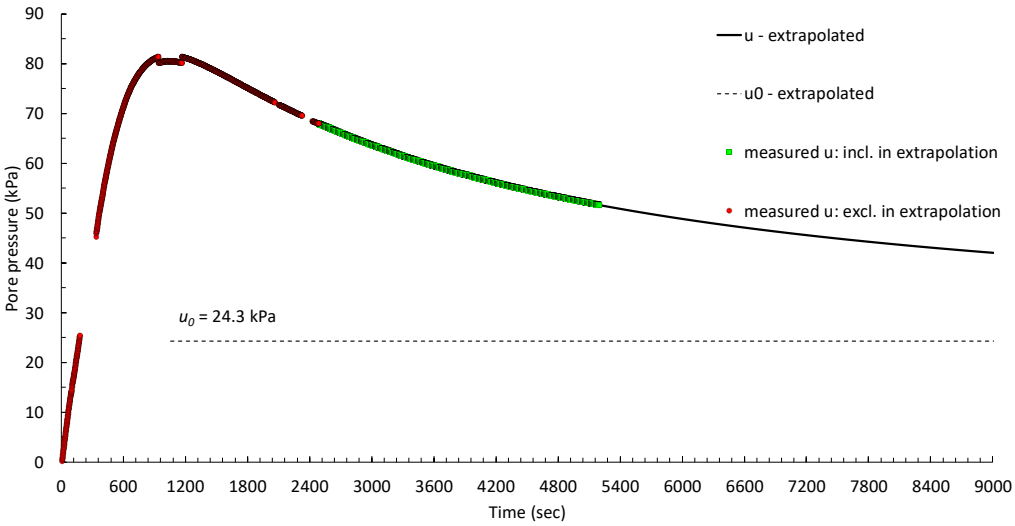

*Figure 41: Extrapolated pore pressure dissipation curve from an incomplete pore pressure dissipation test at **CPT17 – 7.078m**.*

ATTACHMENT F3

SCPTu SHEAR WAVE DATA

Project:	2024 Jagersfontein
Site:	TSF
Hole:	C13
Date:	2024/03/09

TEST DETAILS

Operator:	Osimo
Source:	sledge hammer
Anvil:	timber beam
Source horizontal offset (m):	0.5
Source vertical offset (m):	0.0
Rod length (m):	1.00
Cone depth with one rod (m):	0.94
Receivers:	omni-directional geophone
Receiver orientation:	horizontal
Recording equipment:	Pasi GEA24 seismograph

CSW Soil Engineering (Pty) Ltd
2015/450496/07
gerhard.heymann@up.ac.za
Tel: +2782 375 6666

Project:	2024 Jagersfontein
Site:	TSF
Hole:	C13
Date:	2024/03/09

Geophone depth (m)	Source slant dist. (m)	1st Arrival (s)	S-wave regression (m/s)	S-wave average (m/s)
0.94	1.06	0.00600		
1.94	2.00	0.01076	201.3	186.2
2.94	2.98	0.01552	206.7	192.1
3.94	3.97	0.02029	220.5	195.8
4.94	4.97	0.02450	274.8	202.6
5.94	5.96	0.02745	313.6	217.2
6.94	6.96	0.03085	318.2	225.6
7.94	7.96	0.03370	323.9	236.1
8.94	8.95	0.03700	293.6	242.0
9.94	9.95	0.04050	337.2	245.7
10.94	10.95	0.04285	360.7	255.6
11.94	11.95	0.04600	324.7	259.8
12.94	12.95	0.04900	378.2	264.3
13.94	13.95	0.05125	394.4	272.2
14.94	14.95	0.05405	366.5	276.6
15.94	15.95	0.05670	387.9	281.3
16.94	16.95	0.05920	345.9	286.3
17.94	17.95	0.06245	359.6	287.4
18.94	18.95	0.06470	434.6	292.8
19.94	19.95	0.06705	463.7	297.5
20.94	20.95	0.06900	431.4	303.6
21.94	21.95	0.07165	331.7	306.3
22.94	22.95	0.07500	382.1	305.9
23.94	23.95	0.07670		312.2

Project:	2024 Jagersfontein
Site:	TSF
Hole:	C13
Date:	2024/03/09

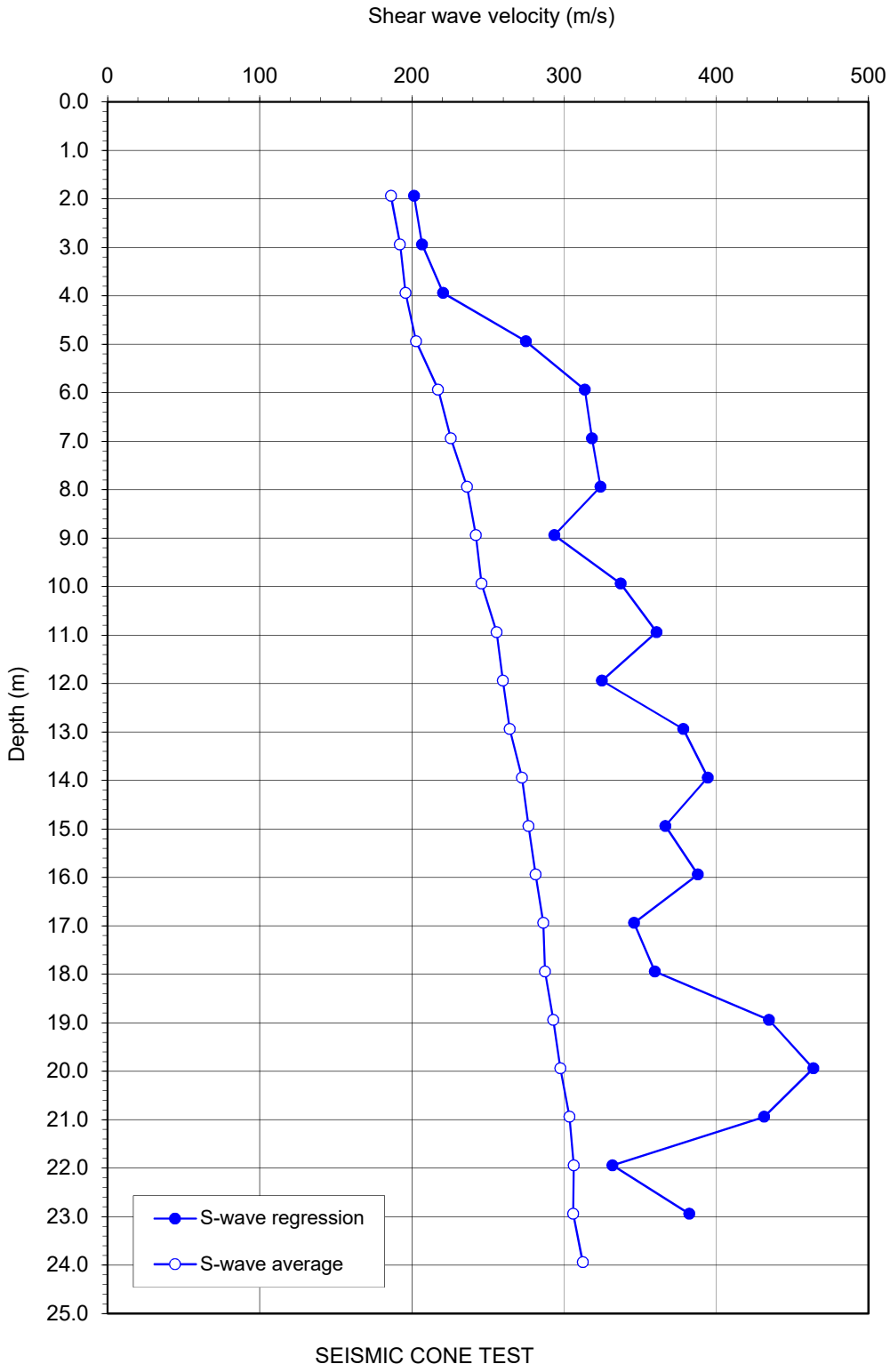

SEISMIC CONE TEST

CSW Soil Engineering (Pty) Ltd
2015/450496/07
gerhard.heymann@up.ac.za
Tel: +2782 375 6666

Project:	2024 Jagersfontein
Site:	TSF
Hole:	C13
Date:	2024/03/09

Hammer blow: Horizontal 1
Geophone orientation: Horizontal

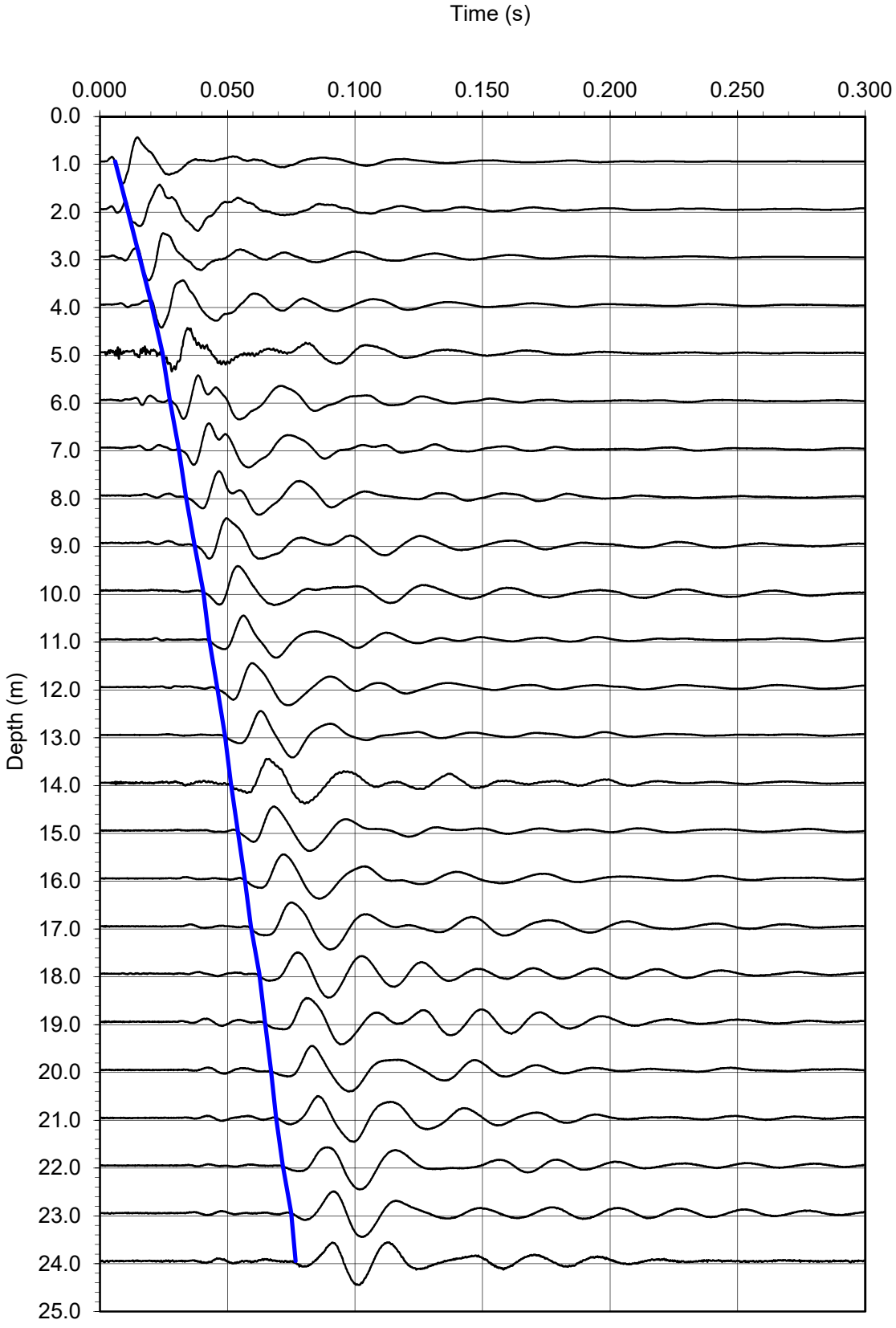

CSW Soil Engineering (Pty) Ltd
2015/450496/07
gerhard.heymann@up.ac.za
Tel: +2782 375 6666

Project:	2024 Jagersfontein
Site:	TSF
Hole:	C13
Date:	2024/03/09

Hammer blow: Horizontal 2
Geophone orientation: Horizontal

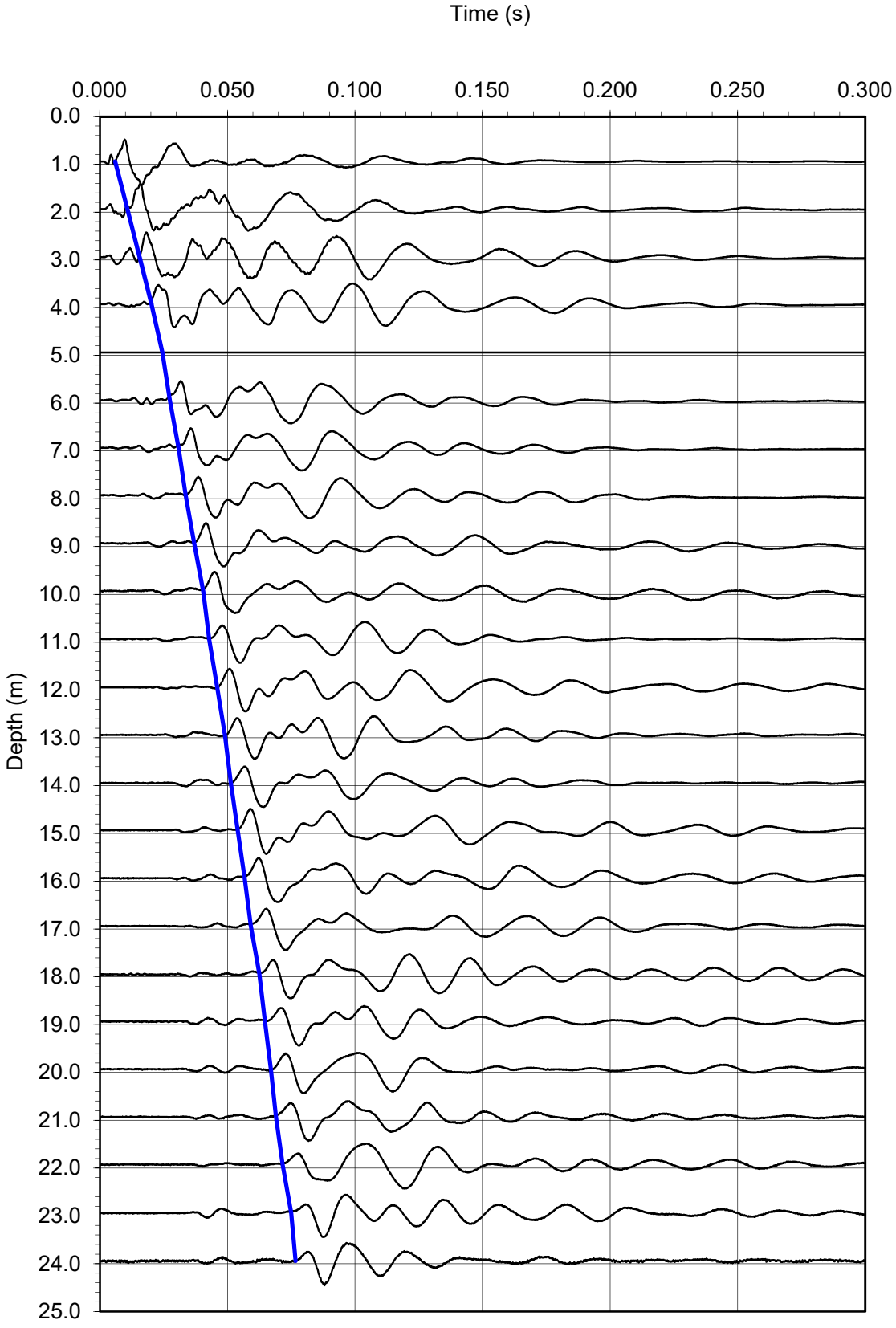

CSW Soil Engineering (Pty) Ltd
2015/450496/07
gerhard.heymann@up.ac.za
Tel: +2782 375 6666

Project:	2024 Jagersfontein
Site:	TSF
Hole:	C13
Date:	2024/03/09

Geophone orientation: Horizontal

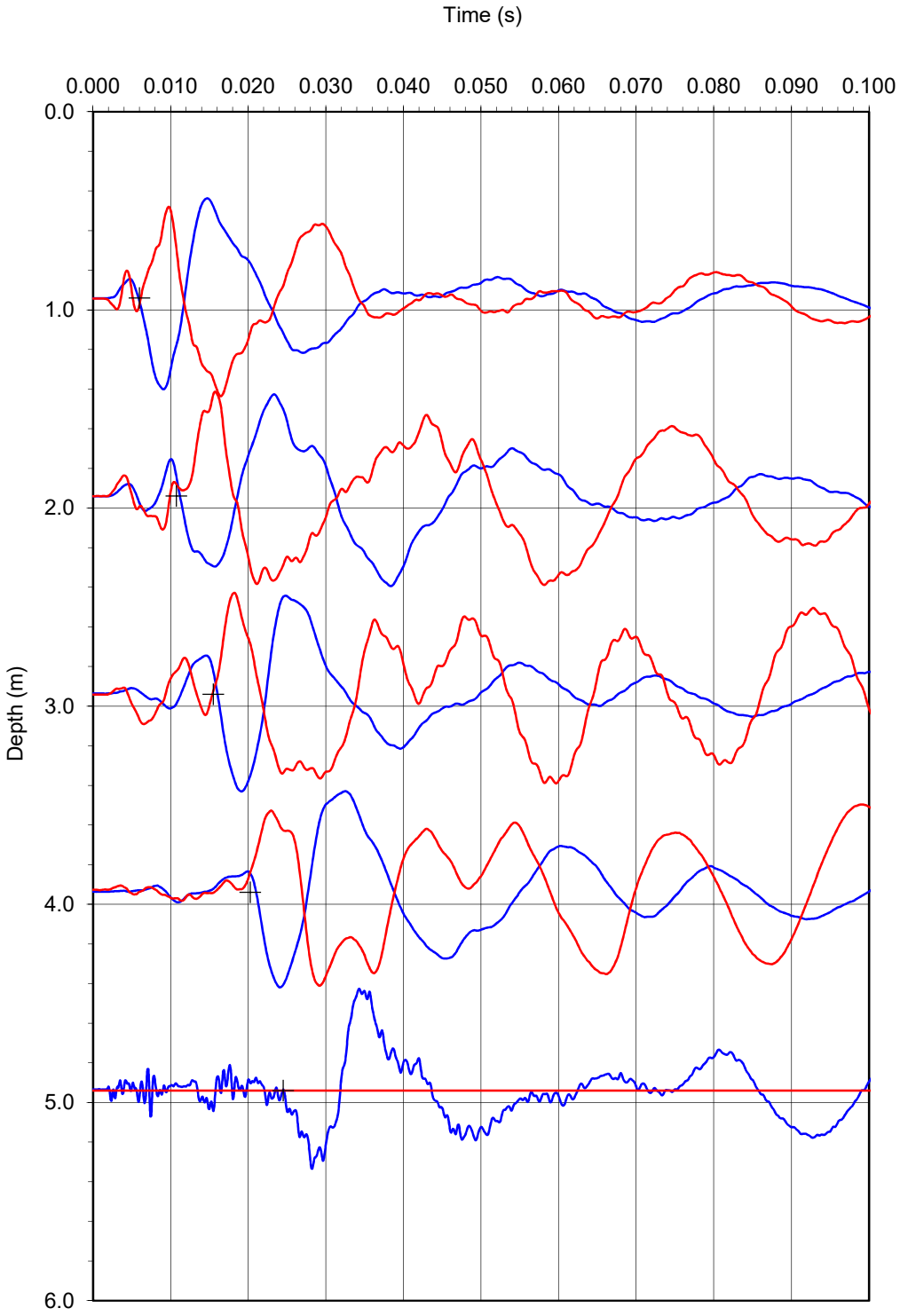

CSW Soil Engineering (Pty) Ltd
2015/450496/07
gerhard.heymann@up.ac.za
Tel: +2782 375 6666

Project:	2024 Jagersfontein
Site:	TSF
Hole:	C13
Date:	2024/03/09

Geophone orientation: Horizontal

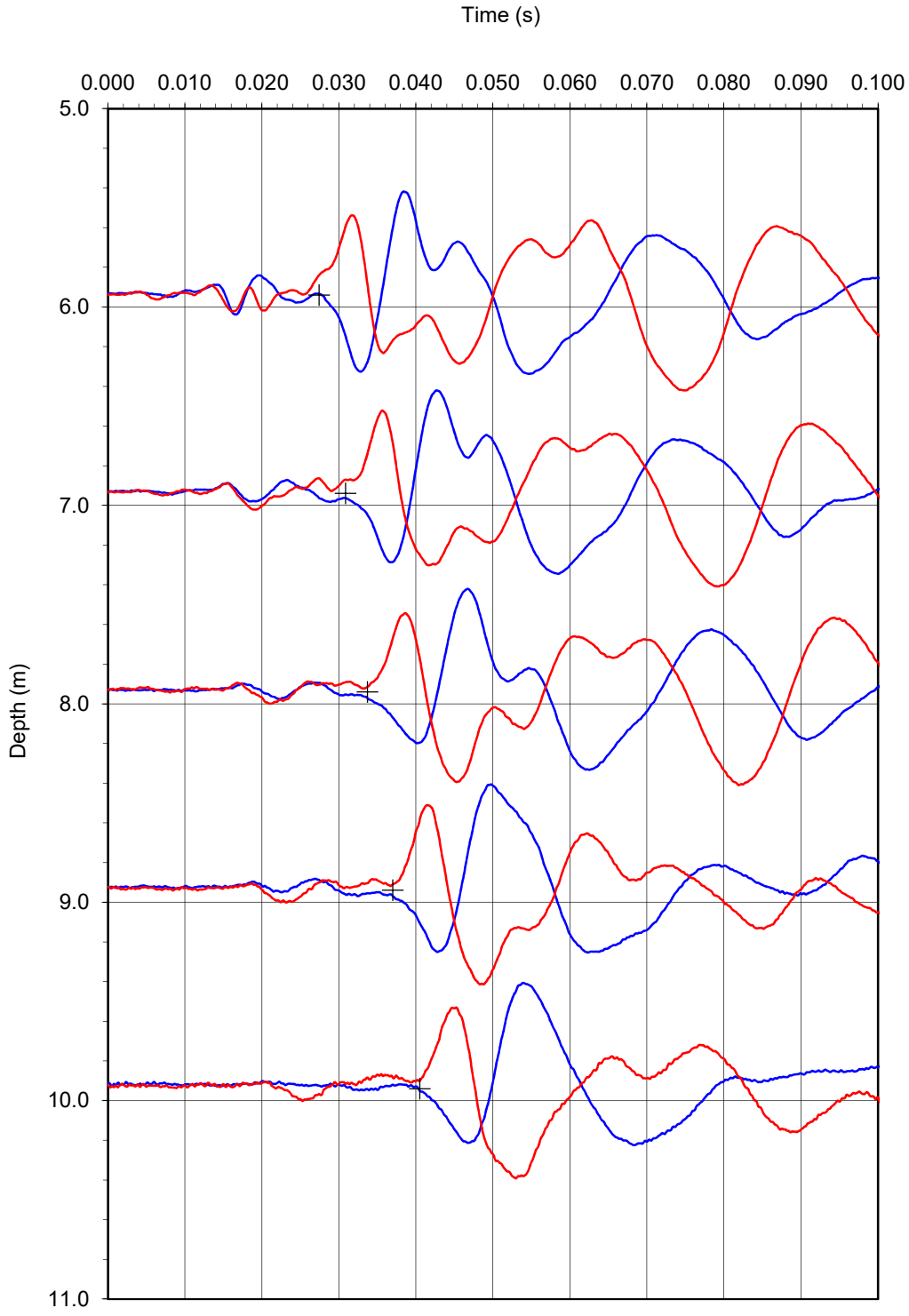

CSW Soil Engineering (Pty) Ltd
2015/450496/07
gerhard.heymann@up.ac.za
Tel: +2782 375 6666

Project:	2024 Jagersfontein
Site:	TSF
Hole:	C13
Date:	2024/03/09

Geophone orientation: Horizontal

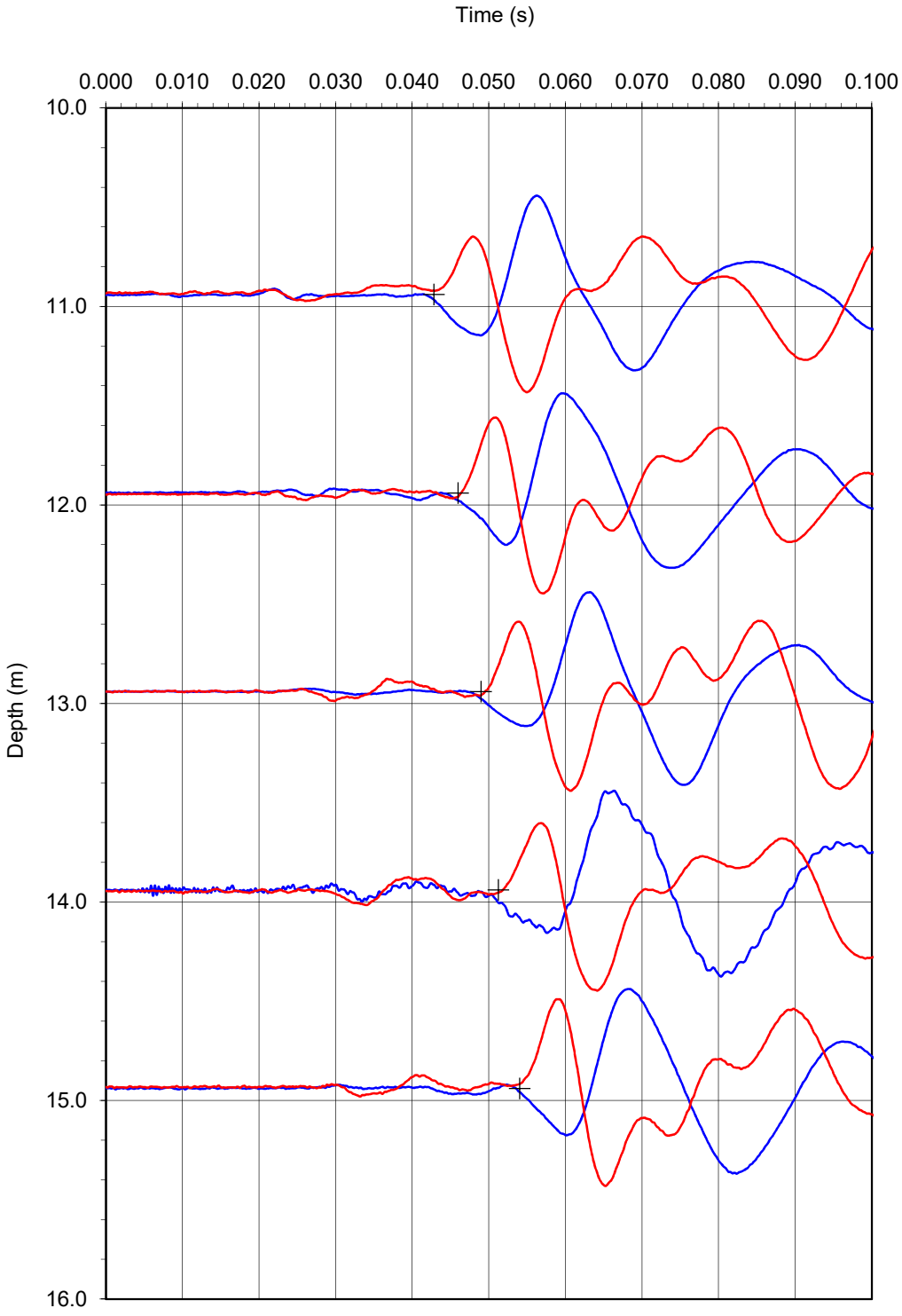

CSW Soil Engineering (Pty) Ltd
2015/450496/07
gerhard.heymann@up.ac.za
Tel: +2782 375 6666

Project:	2024 Jagersfontein
Site:	TSF
Hole:	C13
Date:	2024/03/09

Geophone orientation: Horizontal

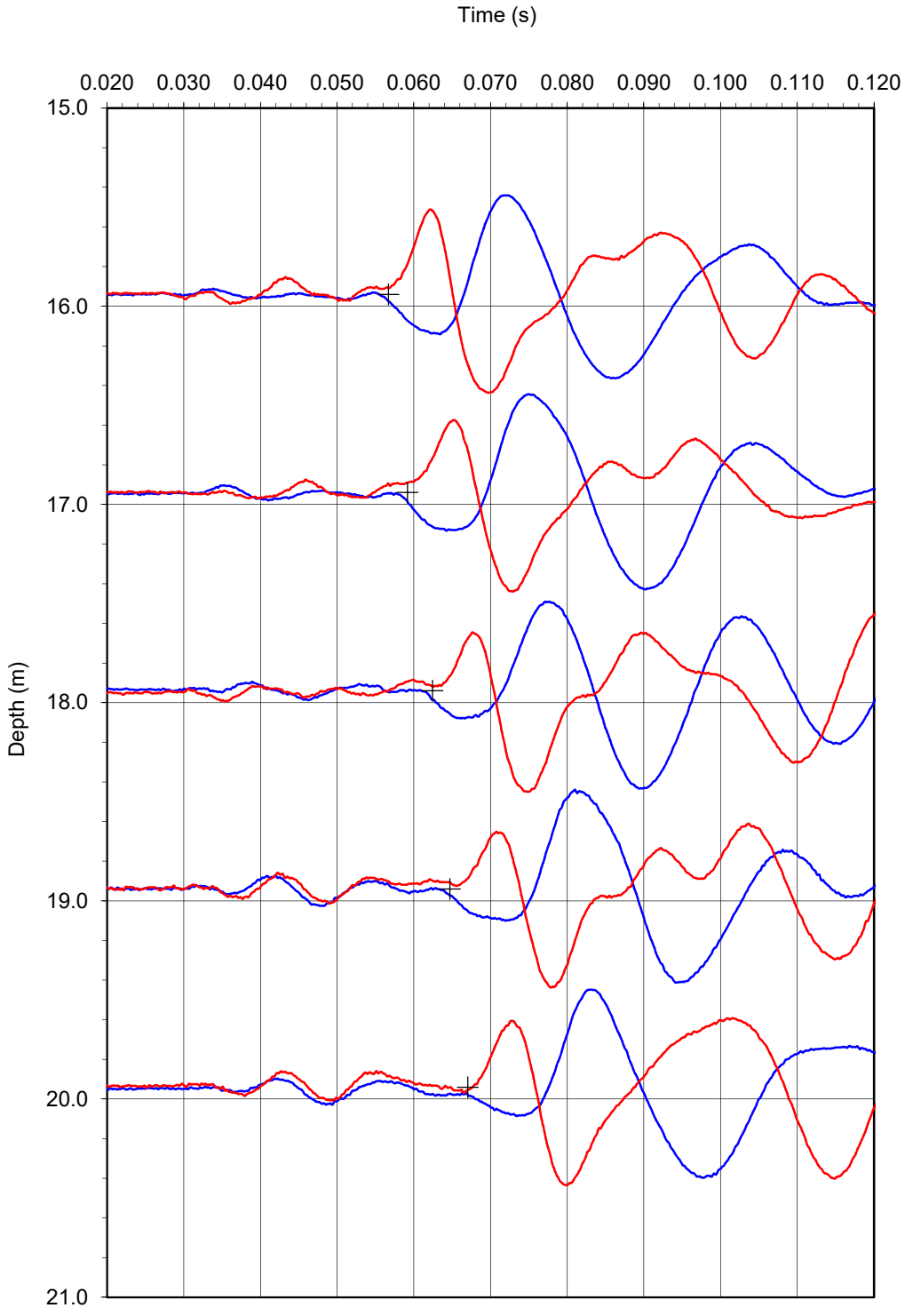

CSW Soil Engineering (Pty) Ltd
2015/450496/07
gerhard.heymann@up.ac.za
Tel: +2782 375 6666

Project:	2024 Jagersfontein
Site:	TSF
Hole:	C13
Date:	2024/03/09

Geophone orientation: Horizontal

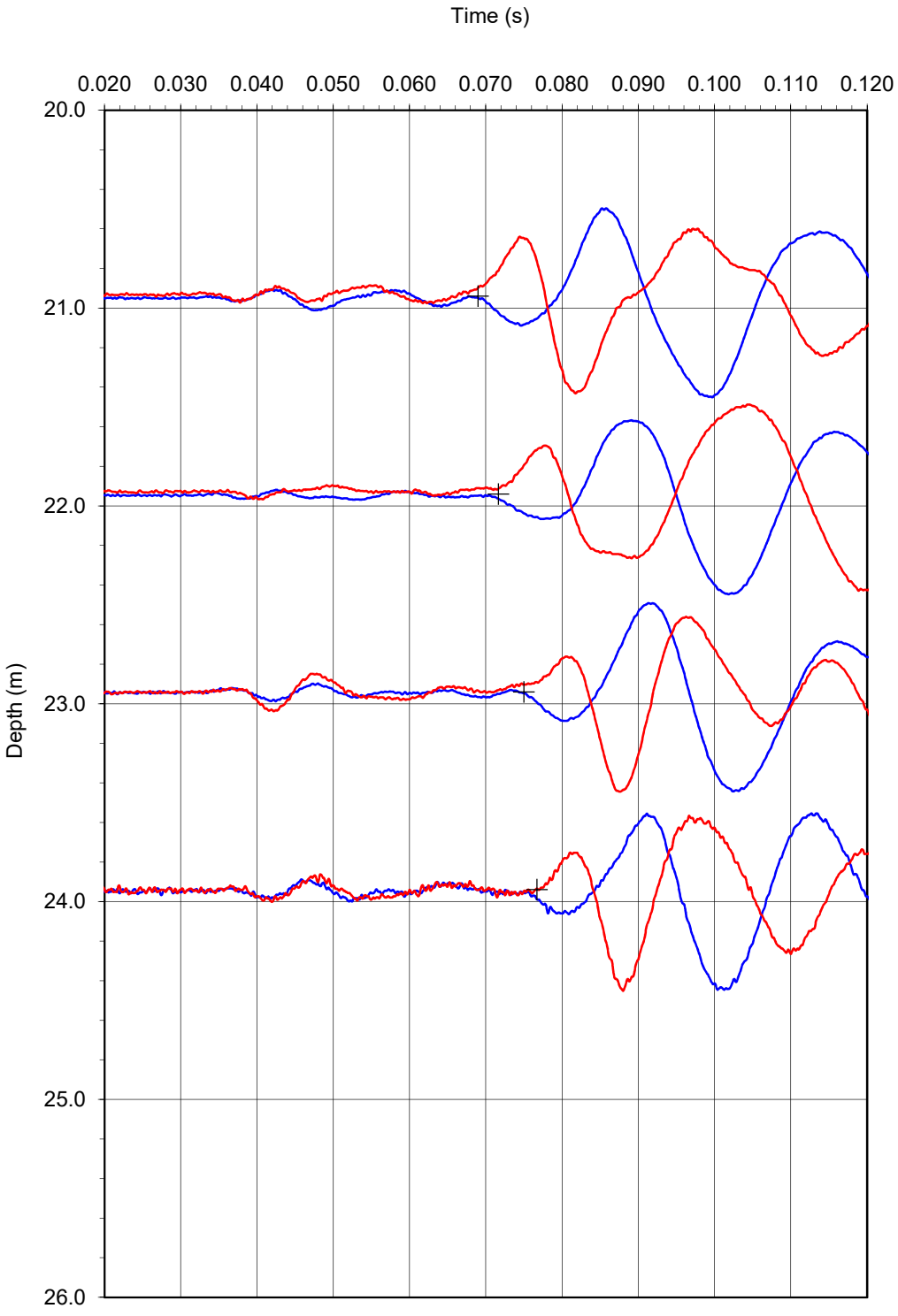

CSW Soil Engineering (Pty) Ltd
2015/450496/07
gerhard.heymann@up.ac.za
Tel: +2782 375 6666

Project:	2024 Jagersfontein
Site:	TSF
Hole:	C14
Date:	2024/03/10

TEST DETAILS

Operator:	Osimo
Source:	sledge hammer
Anvil:	timber beam
Source horizontal offset (m):	0.5
Source vertical offset (m):	0.0
Rod length (m):	1.00
Cone depth with one rod (m):	1.05
Receivers:	omni-directional geophone
Receiver orientation:	horizontal
Recording equipment:	Pasi GEA24 seismograph

CSW Soil Engineering (Pty) Ltd
2015/450496/07
gerhard.heymann@up.ac.za
Tel: +2782 375 6666

Project:	2024 Jagersfontein
Site:	TSF
Hole:	C14
Date:	2024/03/10

Geophone depth (m)	Source slant dist. (m)	1st Arrival (s)	S-wave regression (m/s)	S-wave average (m/s)
1.05	1.16	0.00400		
2.05	2.11	0.00950	183.4	222.1
3.05	3.09	0.01450	175.1	213.2
4.05	4.08	0.02071	172.8	197.0
5.05	5.07	0.02595	203.0	195.5
6.05	6.07	0.03050	232.8	199.0
7.05	7.07	0.03450	235.8	204.9
8.05	8.07	0.03895	264.5	207.1
9.05	9.06	0.04195	319.5	216.0
10.05	10.06	0.04520	305.7	222.6
11.05	11.06	0.04849	326.9	228.1
12.05	12.06	0.05130	328.8	235.1
13.05	13.06	0.05455	322.1	239.4
14.05	14.06	0.05750	329.4	244.5
15.05	15.06	0.06062	352.4	248.4
16.05	16.06	0.06315	357.2	254.3
17.05	17.06	0.06620	353.2	257.7
18.05	18.06	0.06880	377.2	262.5
19.05	19.06	0.07150	439.6	266.5
20.05	20.06	0.07329	458.3	273.7
21.05	21.06	0.07582	440.7	277.7
22.05	22.06	0.07780	455.0	283.5
23.05	23.06	0.08020		287.5

Project:	2024 Jagersfontein
Site:	TSF
Hole:	C14
Date:	2024/03/10

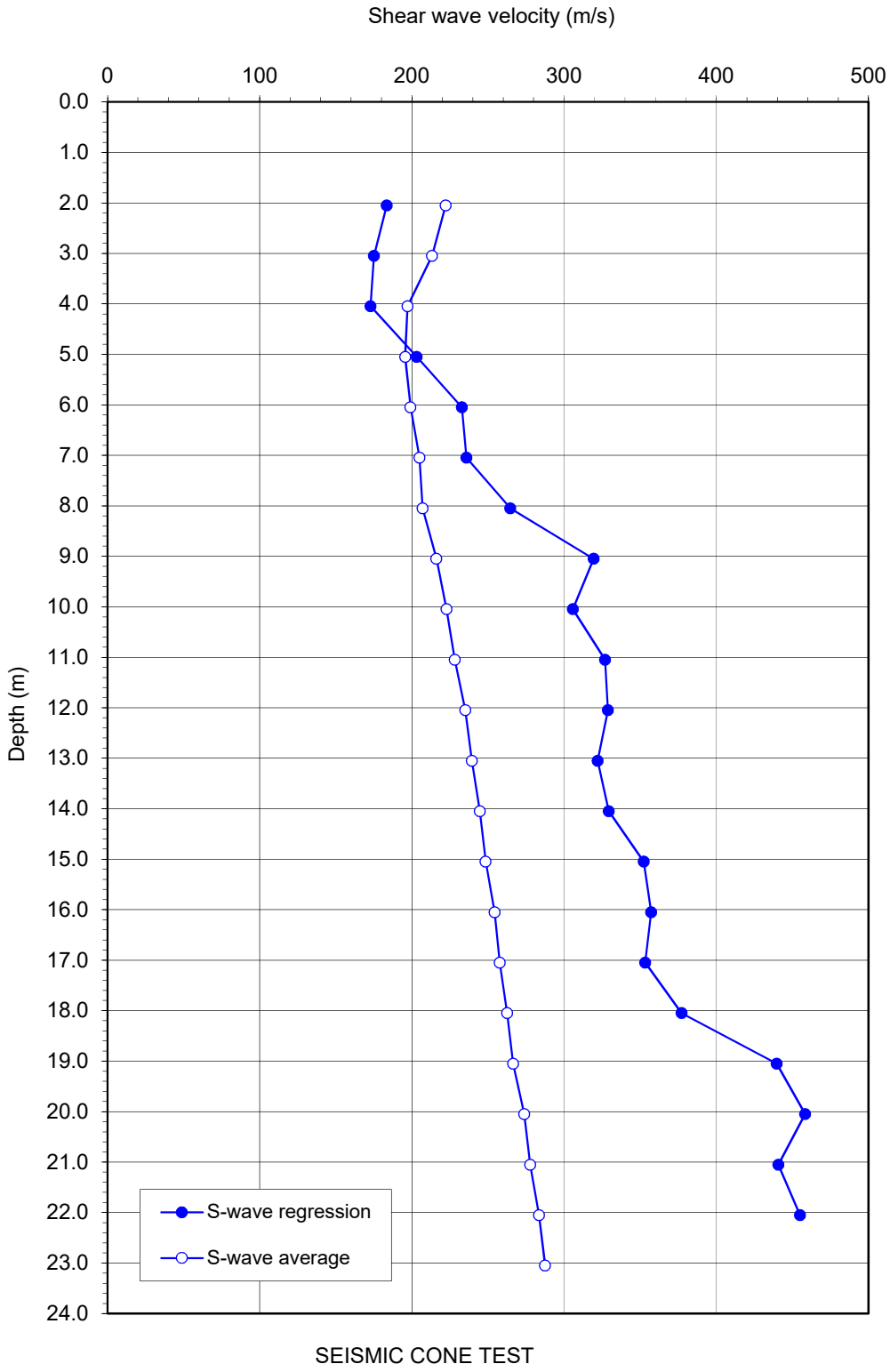

SEISMIC CONE TEST

CSW Soil Engineering (Pty) Ltd
2015/450496/07
gerhard.heymann@up.ac.za
Tel: +2782 375 6666

Project:	2024 Jagersfontein
Site:	TSF
Hole:	C14
Date:	2024/03/10

Hammer blow: Horizontal 1
Geophone orientation: Horizontal

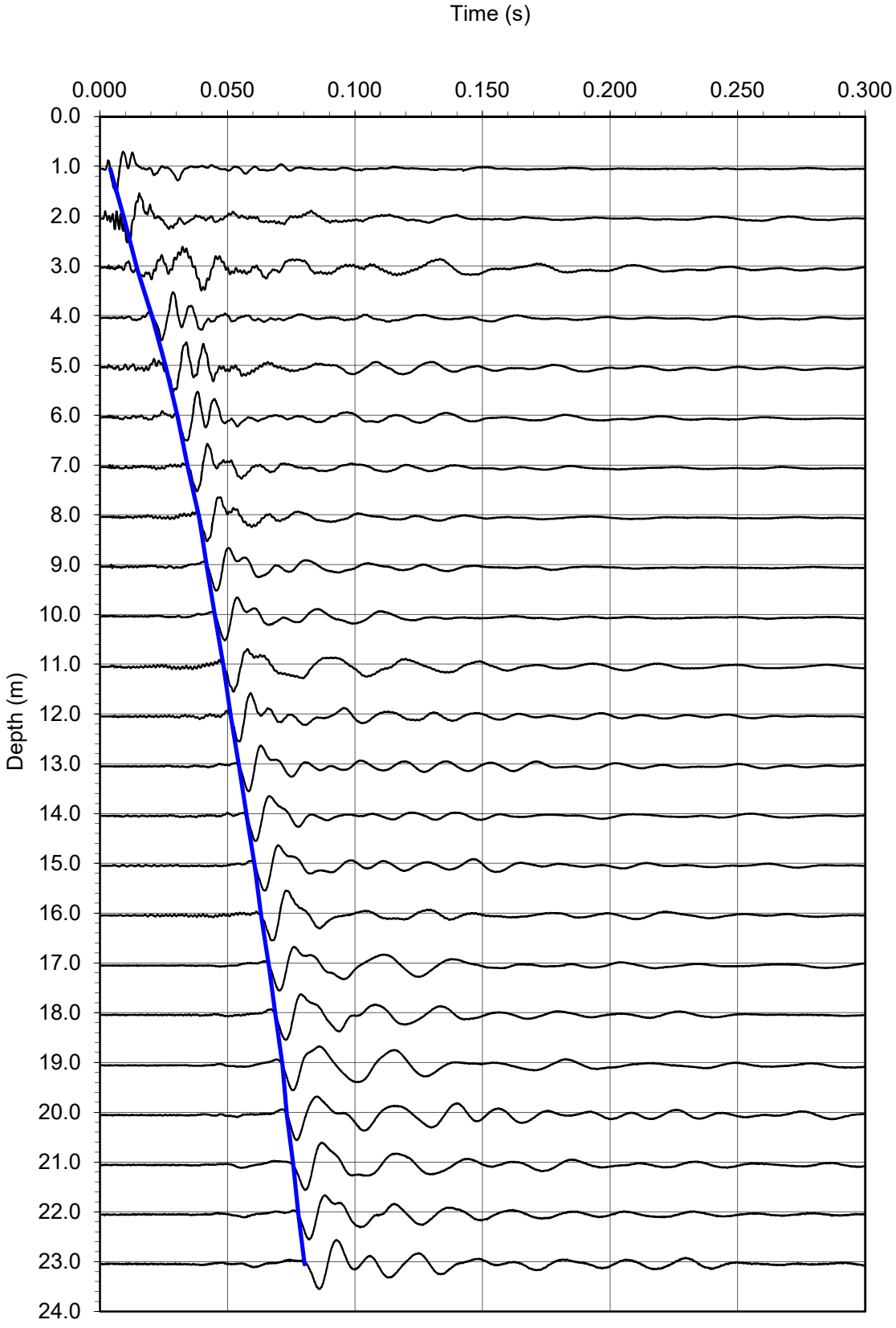

CSW Soil Engineering (Pty) Ltd
2015/450496/07
gerhard.heymann@up.ac.za
Tel: +2782 375 6666

Project:	2024 Jagersfontein
Site:	TSF
Hole:	C14
Date:	2024/03/10

Hammer blow: Horizontal 2
Geophone orientation: Horizontal

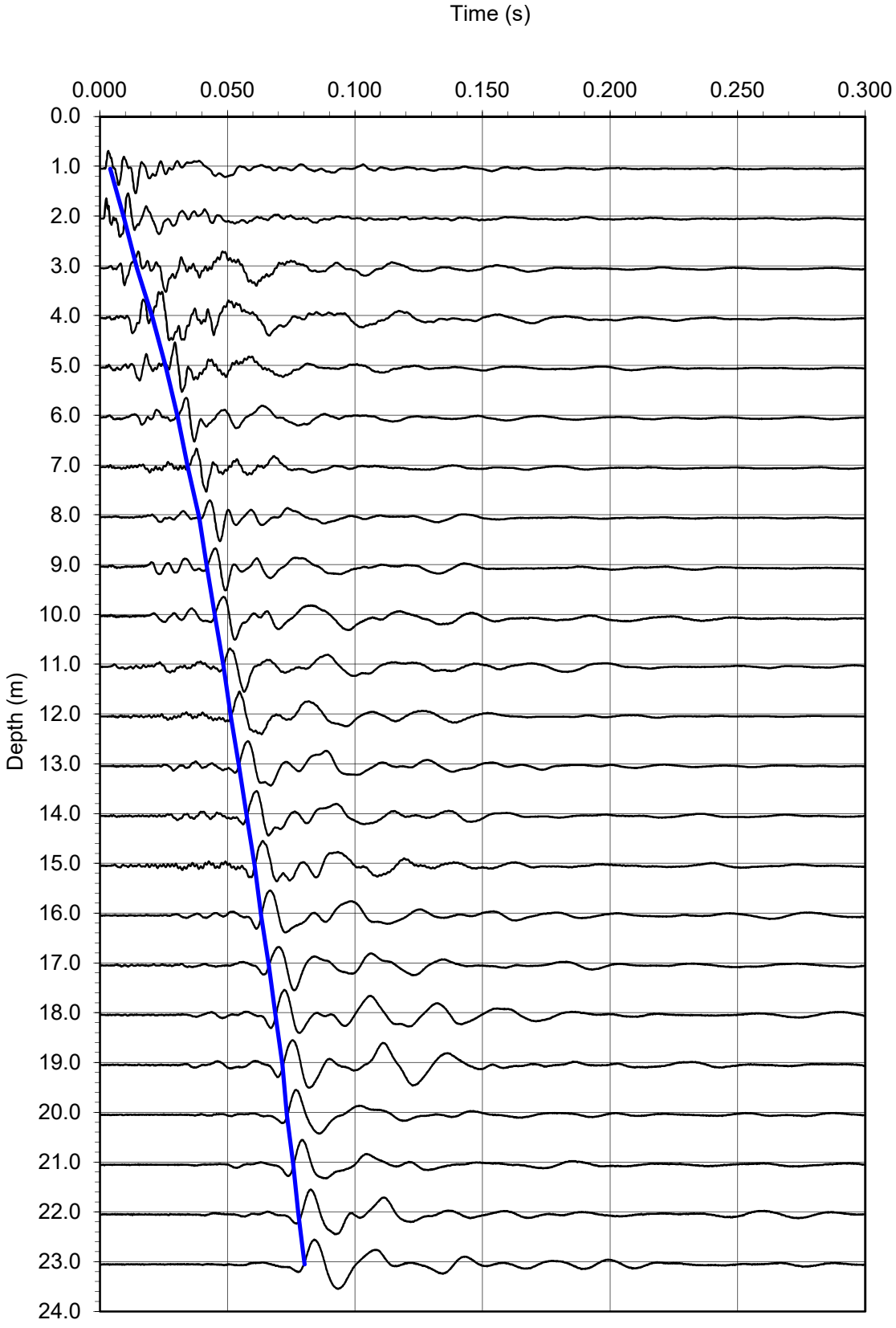

CSW Soil Engineering (Pty) Ltd
2015/450496/07
gerhard.heymann@up.ac.za
Tel: +2782 375 6666

Project:	2024 Jagersfontein
Site:	TSF
Hole:	C14
Date:	2024/03/10

Geophone orientation: Horizontal

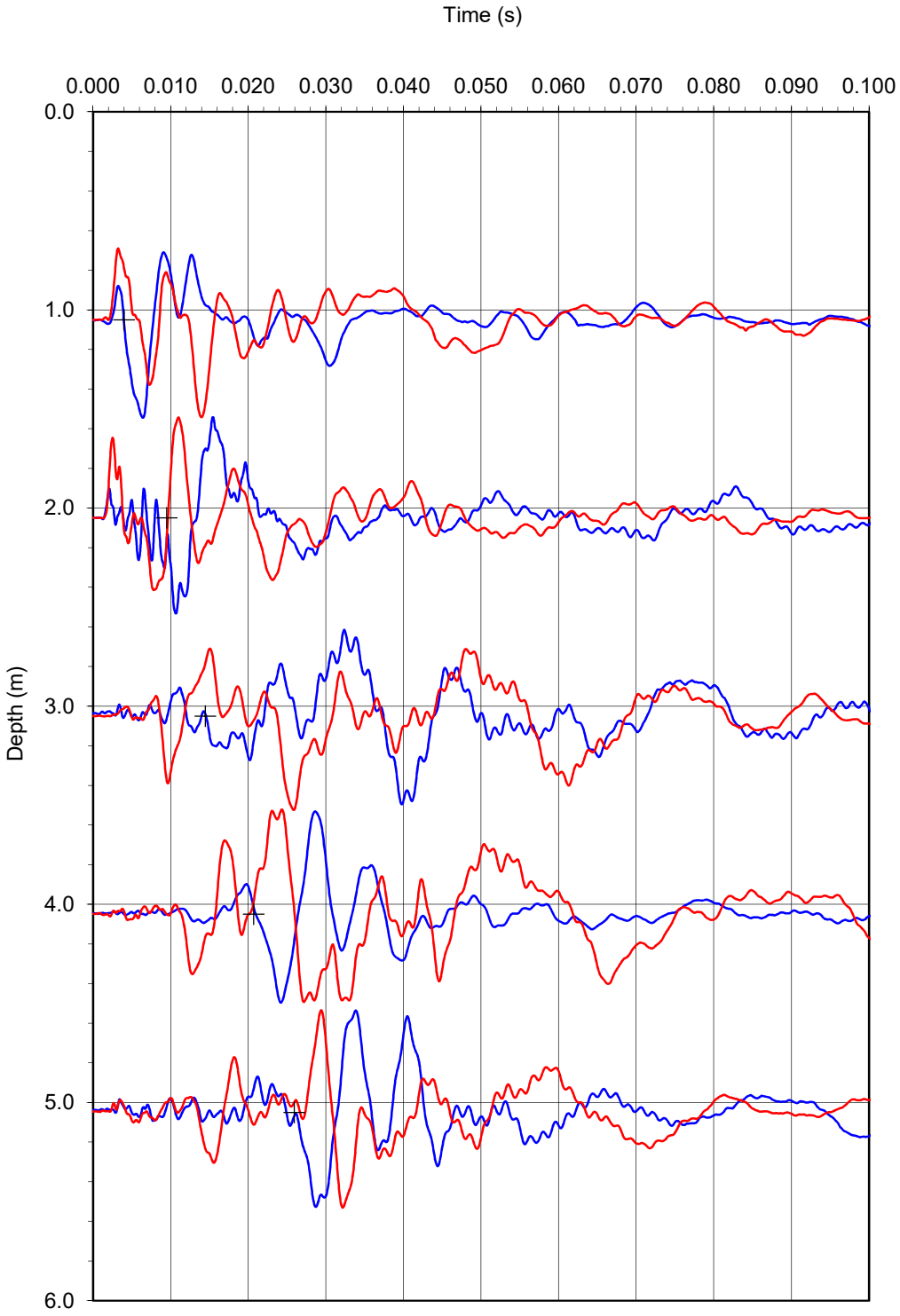

CSW Soil Engineering (Pty) Ltd
2015/450496/07
gerhard.heymann@up.ac.za
Tel: +2782 375 6666

Project:	2024 Jagersfontein
Site:	TSF
Hole:	C14
Date:	2024/03/10

Geophone orientation: Horizontal

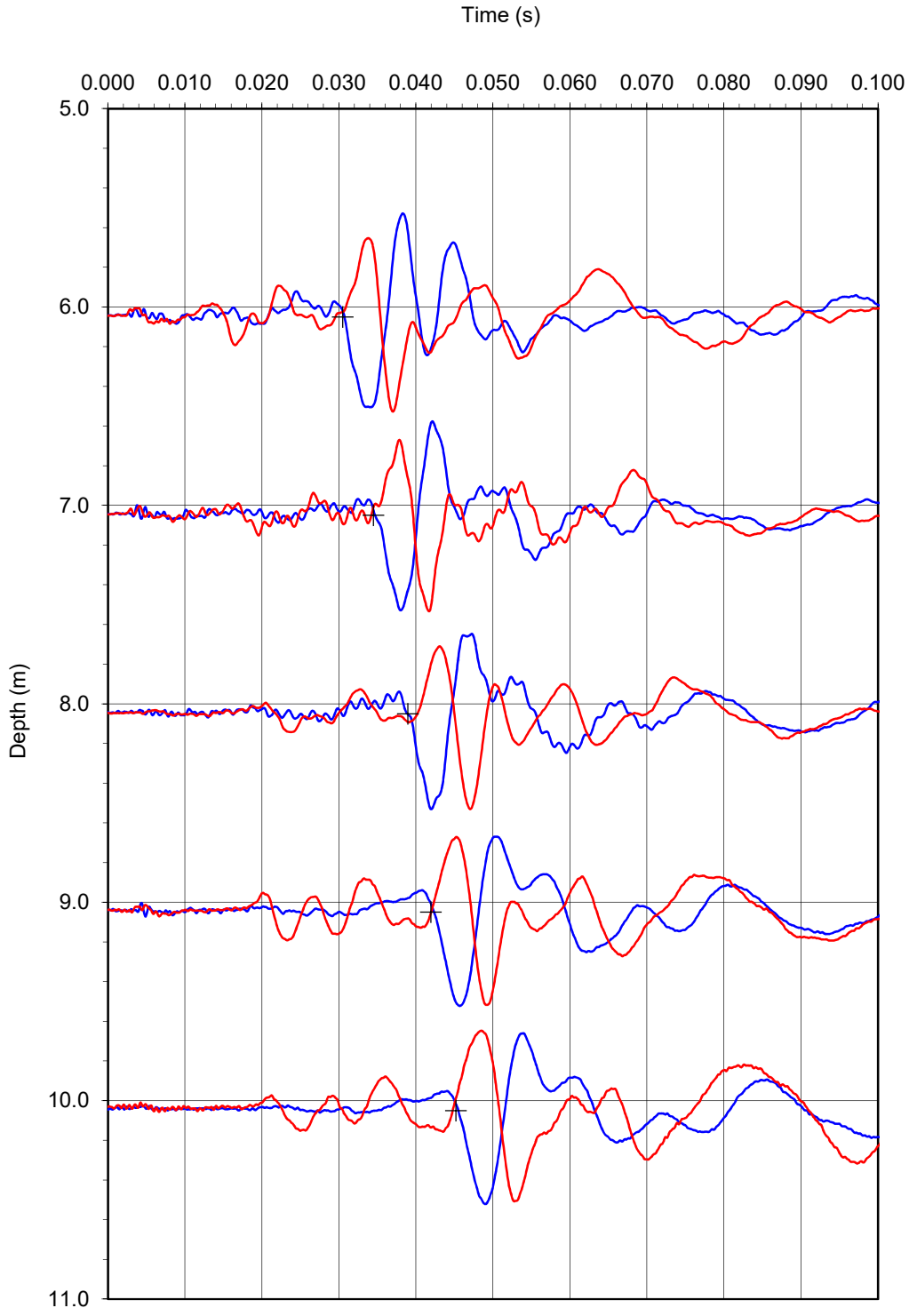

CSW Soil Engineering (Pty) Ltd
2015/450496/07
gerhard.heymann@up.ac.za
Tel: +2782 375 6666

Project:	2024 Jagersfontein
Site:	TSF
Hole:	C14
Date:	2024/03/10

Geophone orientation: Horizontal

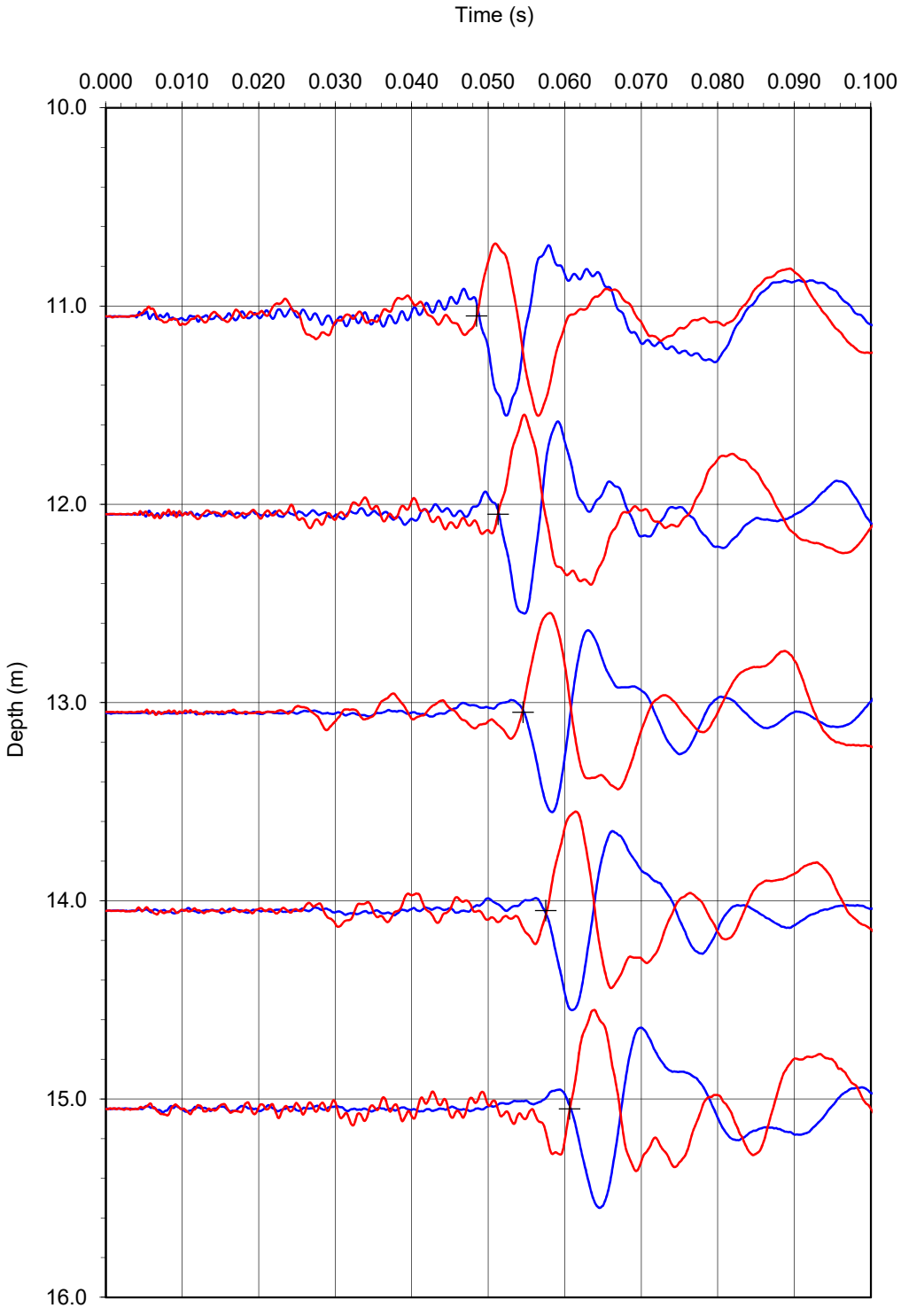

CSW Soil Engineering (Pty) Ltd
2015/450496/07
gerhard.heymann@up.ac.za
Tel: +2782 375 6666

Project:	2024 Jagersfontein
Site:	TSF
Hole:	C14
Date:	2024/03/10

Geophone orientation: Horizontal

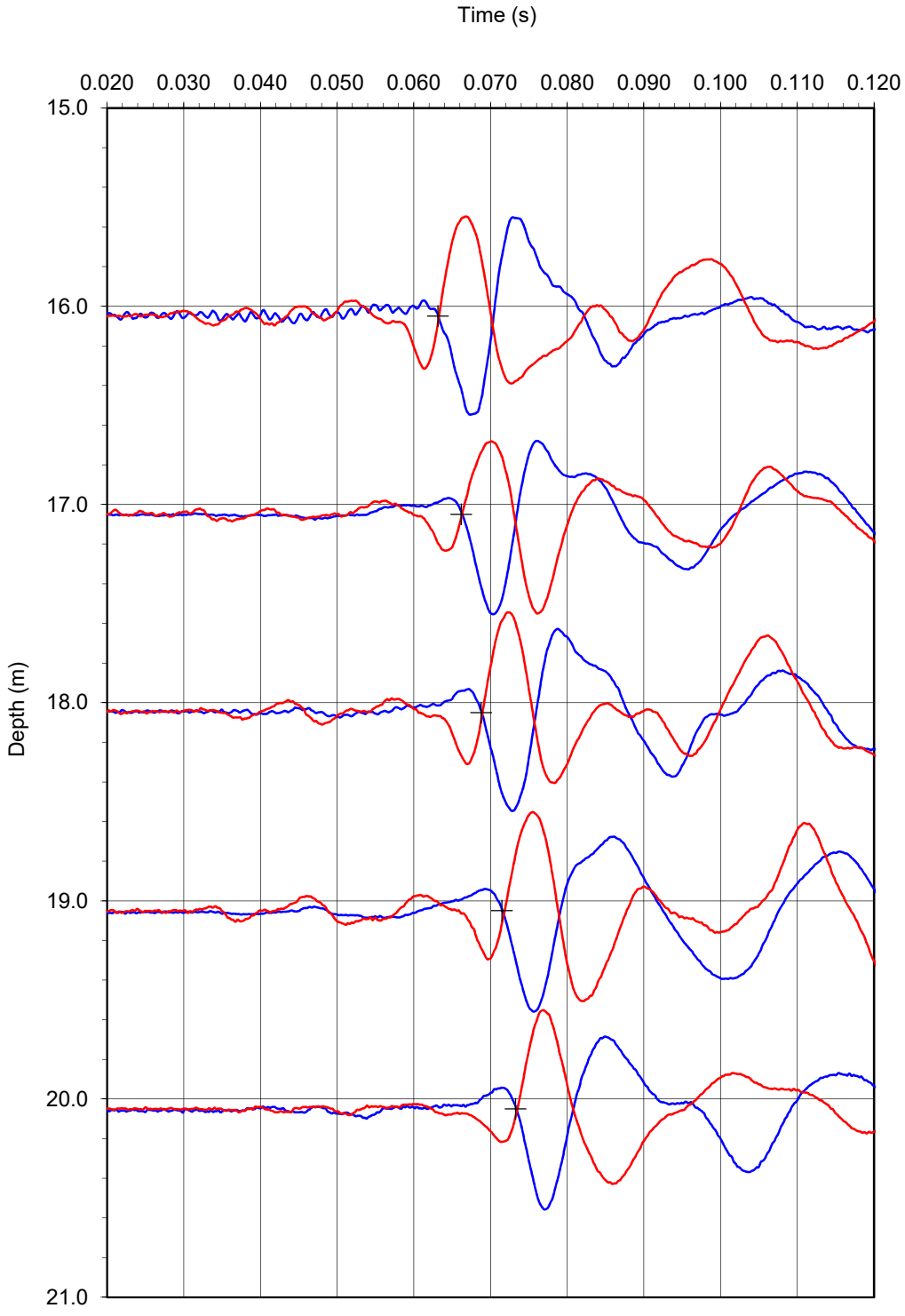

CSW Soil Engineering (Pty) Ltd
2015/450496/07
gerhard.heymann@up.ac.za
Tel: +2782 375 6666

Project:	2024 Jagersfontein
Site:	TSF
Hole:	C14
Date:	2024/03/10

Geophone orientation: Horizontal

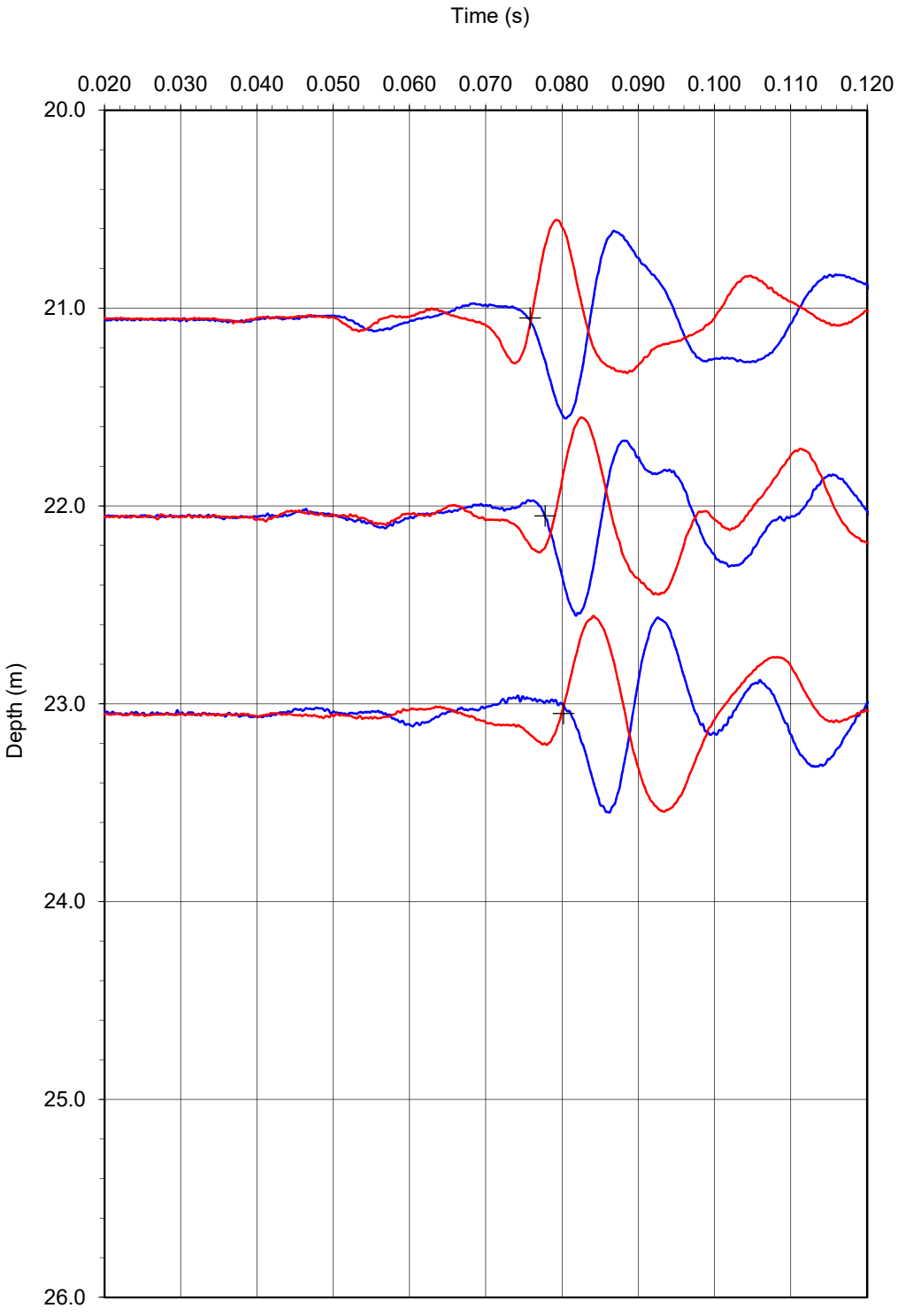

CSW Soil Engineering (Pty) Ltd
2015/450496/07
gerhard.heymann@up.ac.za
Tel: +2782 375 6666

Project:	2024 Jagersfontein
Site:	TSF
Hole:	C15
Date:	2024/03/11

TEST DETAILS

Operator:	Osimo
Source:	sledge hammer
Anvil:	timber beam
Source horizontal offset (m):	0.5
Source vertical offset (m):	0.0
Rod length (m):	1.00
Cone depth with one rod (m):	1.00
Receivers:	omni-directional geophone
Receiver orientation:	horizontal
Recording equipment:	Pasi GEA24 seismograph

CSW Soil Engineering (Pty) Ltd
2015/450496/07
gerhard.heymann@up.ac.za
Tel: +2782 375 6666

Project:	2024 Jagersfontein
Site:	TSF
Hole:	C15
Date:	2024/03/11

Geophone depth (m)	Source slant dist. (m)	1st Arrival (s)	S-wave regression (m/s)	S-wave average (m/s)
1.00	1.12	0.00550		
2.00	2.06	0.01030	192.3	200.2
3.00	3.04	0.01550	198.8	196.2
4.00	4.03	0.02020	245.4	199.6
5.00	5.02	0.02350	330.5	213.8
6.00	6.02	0.02620	413.4	229.8
7.00	7.02	0.02830	322.7	248.0
8.00	8.02	0.03220	276.6	248.9
9.00	9.01	0.03550	272.7	253.9
10.00	10.01	0.03950	310.7	253.5
11.00	11.01	0.04176	277.2	263.7
12.00	12.01	0.04643	268.6	258.7
13.00	13.01	0.04900	311.9	265.5
14.00	14.01	0.05276	307.9	265.5
15.00	15.01	0.05543	313.0	270.8
16.00	16.01	0.05910	313.0	270.9
17.00	17.01	0.06176	374.8	275.4
18.00	18.01	0.06443	453.3	279.5
19.00	19.01	0.06610	406.7	287.6
20.00	20.01	0.06920	371.5	289.1
21.00	21.01	0.07143	332.6	294.1
22.00	22.01	0.07510	313.1	293.0
23.00	23.01	0.07776	374.9	295.8
24.00	24.01	0.08043	374.9	298.5
25.00	25.00	0.08310	493.1	300.9
26.00	26.00	0.08430		308.5

Project:	2024 Jagersfontein
Site:	TSF
Hole:	C15
Date:	2024/03/11

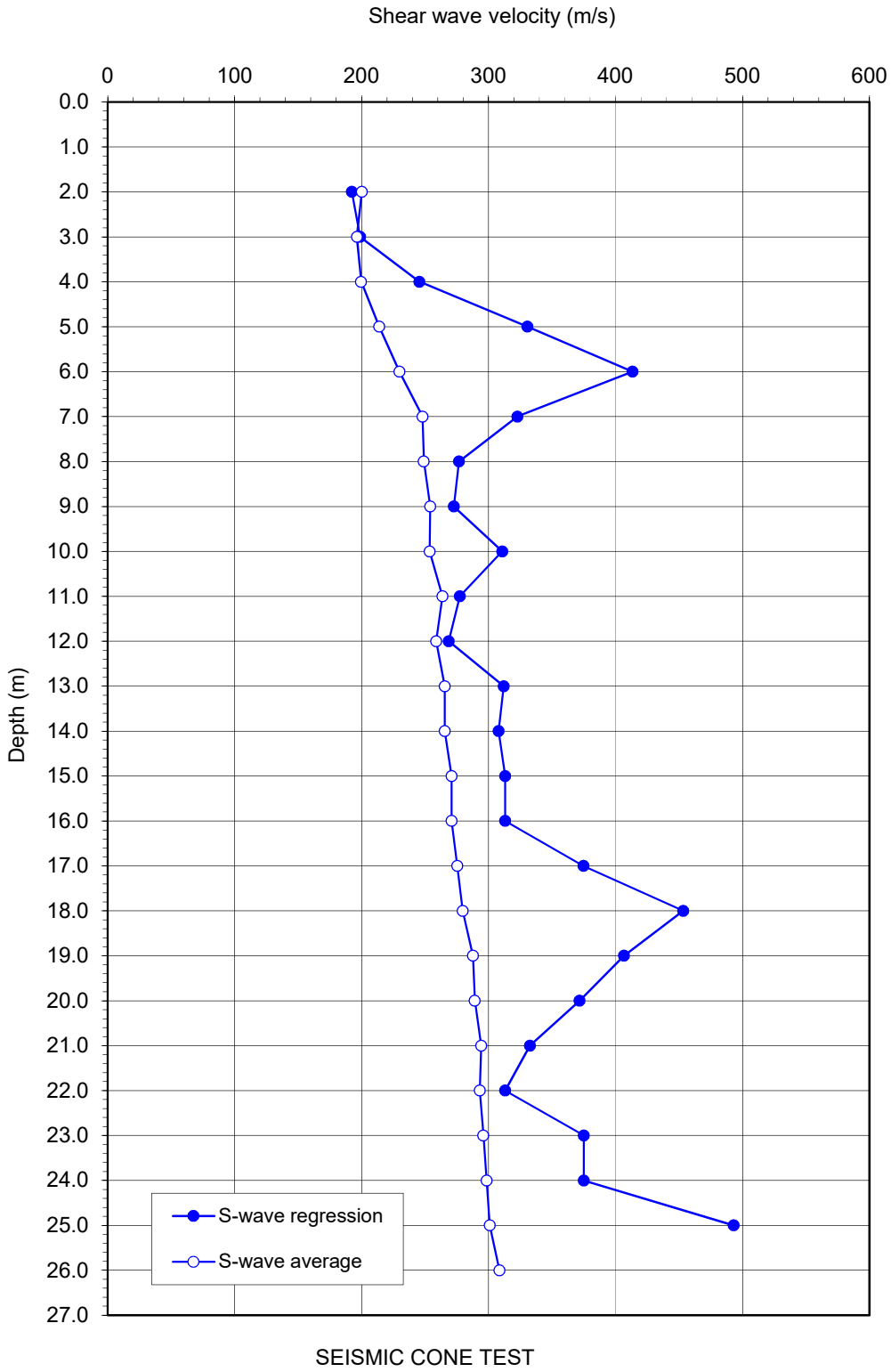

SEISMIC CONE TEST

CSW Soil Engineering (Pty) Ltd
2015/450496/07
gerhard.heymann@up.ac.za
Tel: +2782 375 6666

Project:	2024 Jagersfontein
Site:	TSF
Hole:	C15
Date:	2024/03/11

Hammer blow: Horizontal 1
Geophone orientation: Horizontal

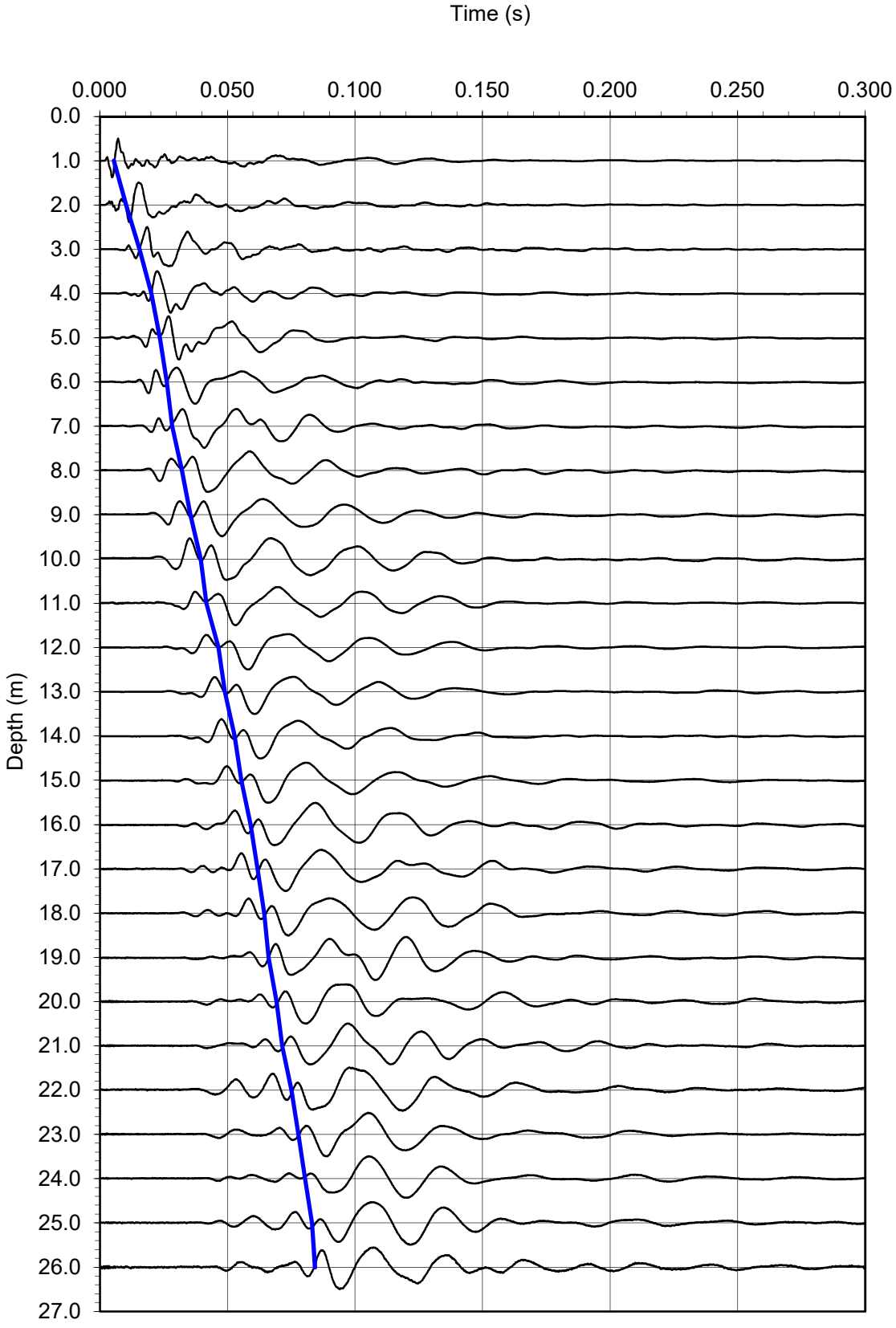

CSW Soil Engineering (Pty) Ltd
2015/450496/07
gerhard.heymann@up.ac.za
Tel: +2782 375 6666

Project:	2024 Jagersfontein
Site:	TSF
Hole:	C15
Date:	2024/03/11

Hammer blow: Horizontal 2
Geophone orientation: Horizontal

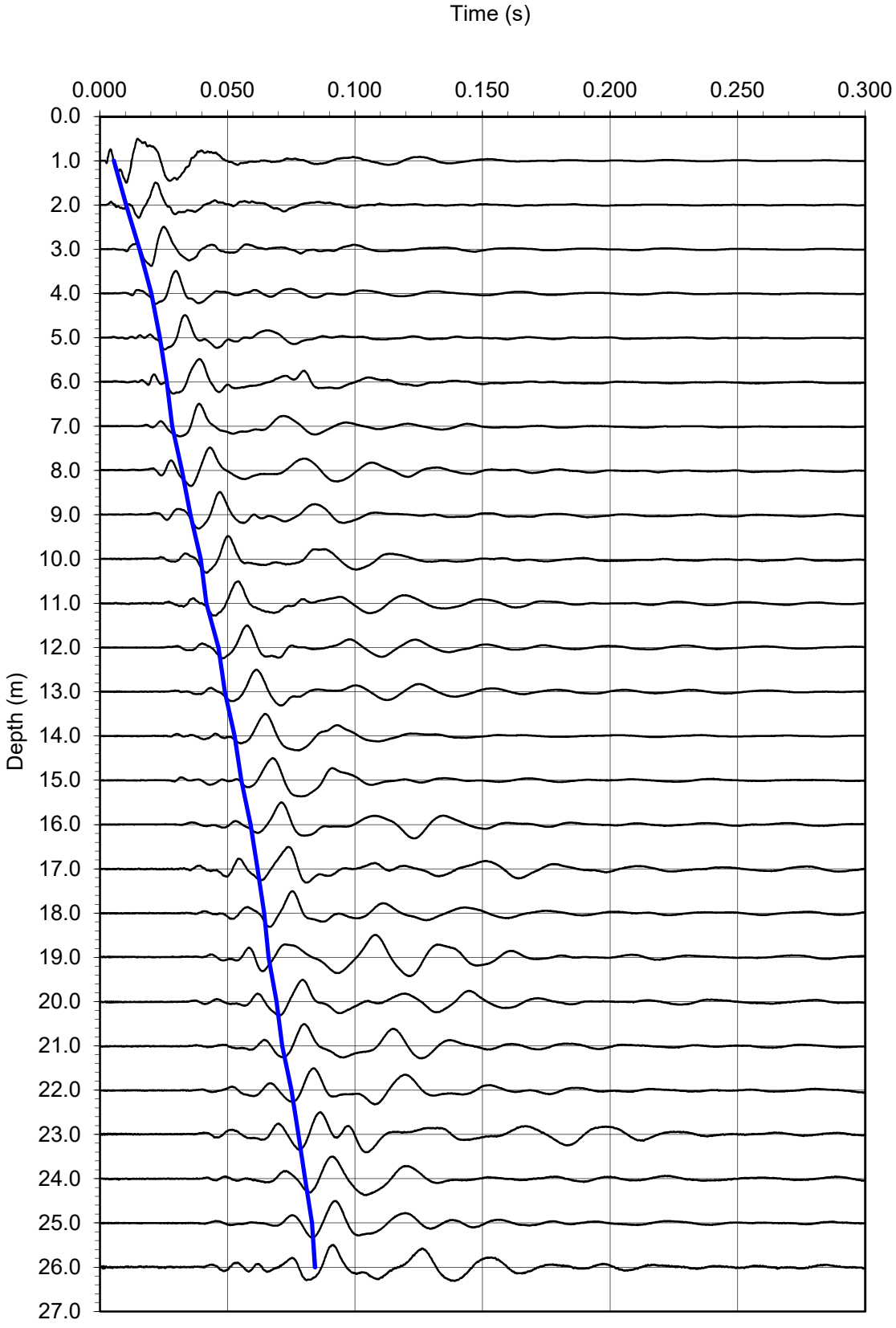

CSW Soil Engineering (Pty) Ltd
2015/450496/07
gerhard.heymann@up.ac.za
Tel: +2782 375 6666

Project:	2024 Jagersfontein
Site:	TSF
Hole:	C15
Date:	2024/03/11

Geophone orientation: Horizontal

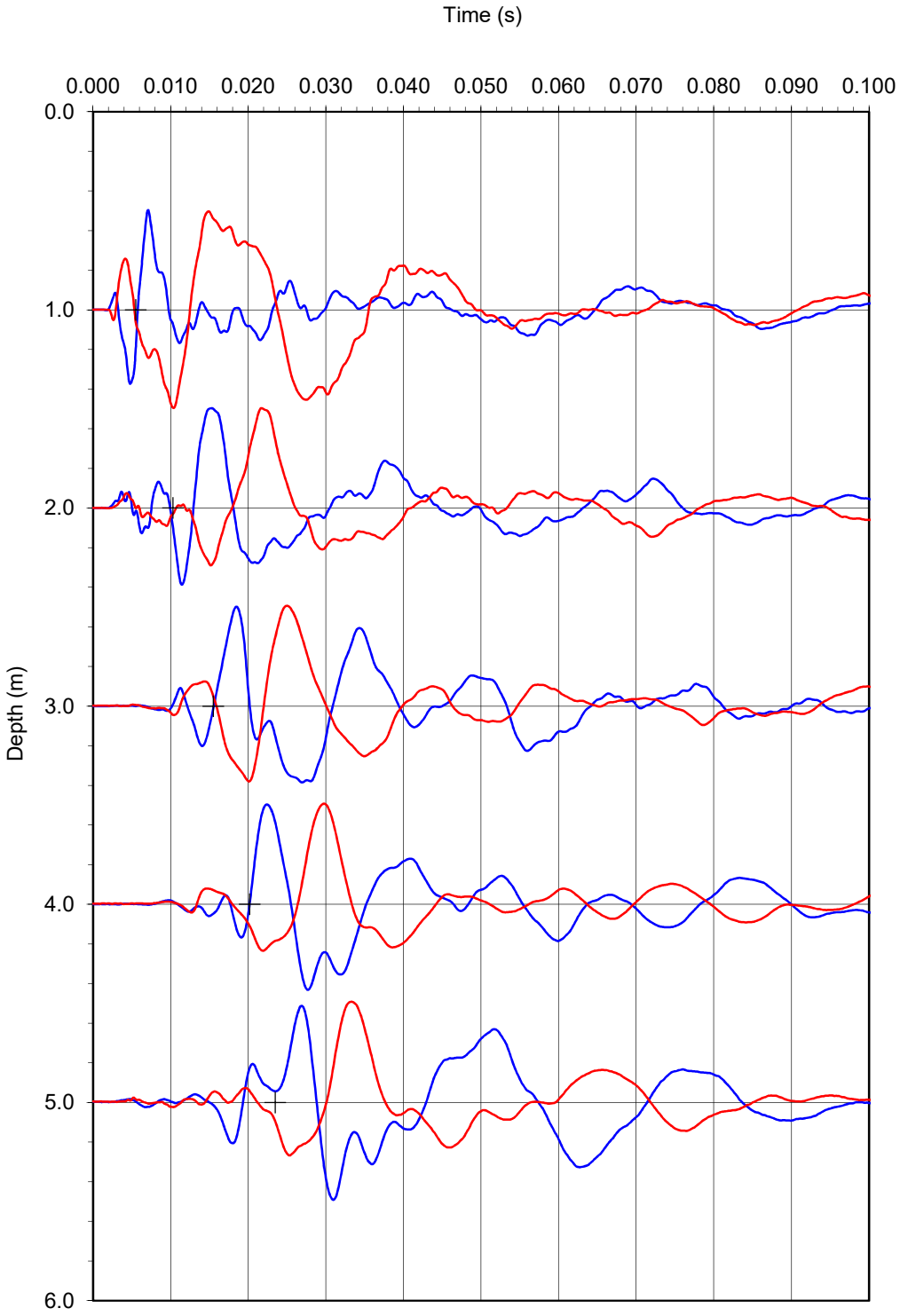

CSW Soil Engineering (Pty) Ltd
2015/450496/07
gerhard.heymann@up.ac.za
Tel: +2782 375 6666

Project:	2024 Jagersfontein
Site:	TSF
Hole:	C15
Date:	2024/03/11

Geophone orientation: Horizontal

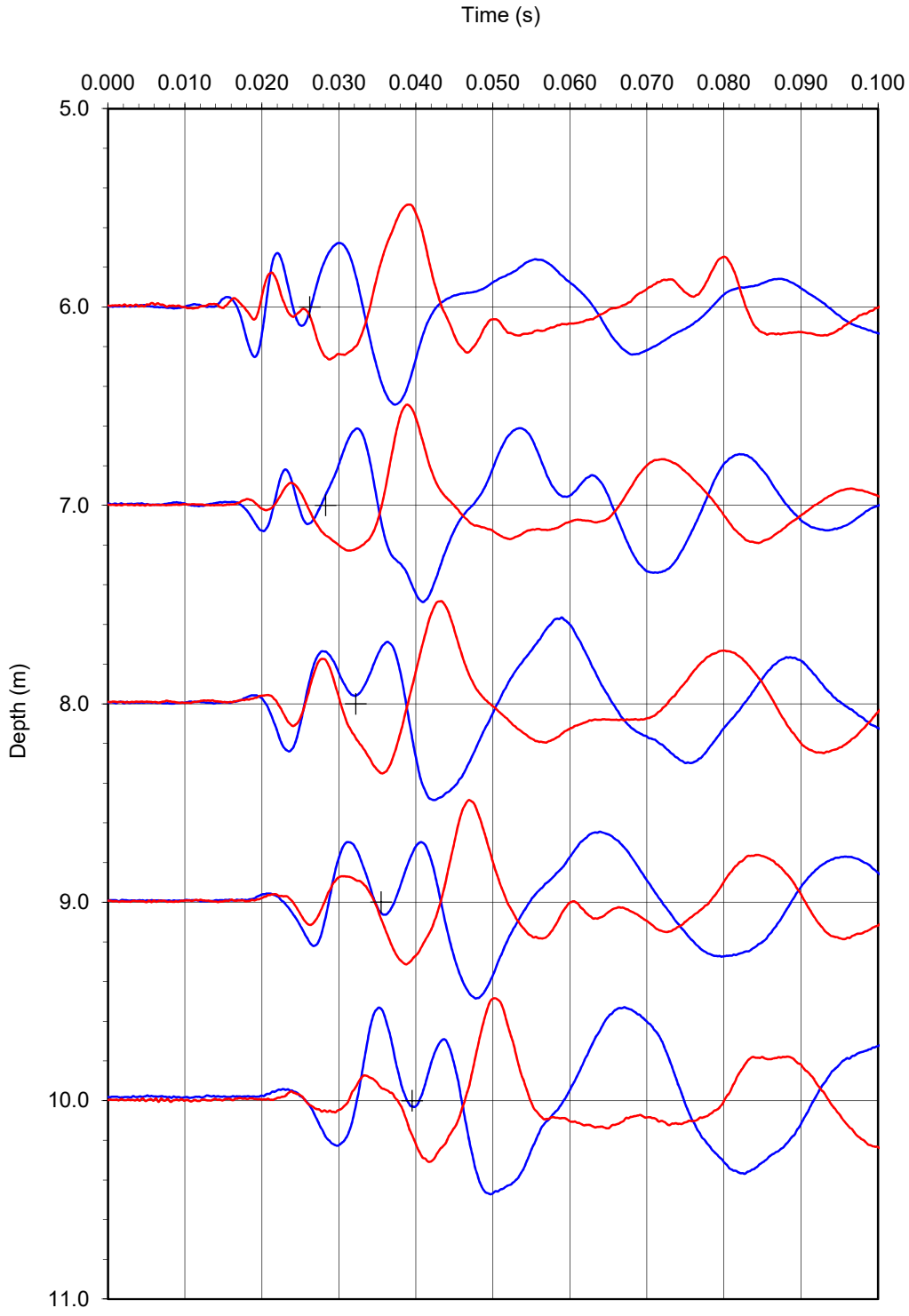

CSW Soil Engineering (Pty) Ltd
2015/450496/07
gerhard.heymann@up.ac.za
Tel: +2782 375 6666

Project:	2024 Jagersfontein
Site:	TSF
Hole:	C15
Date:	2024/03/11

Geophone orientation: Horizontal

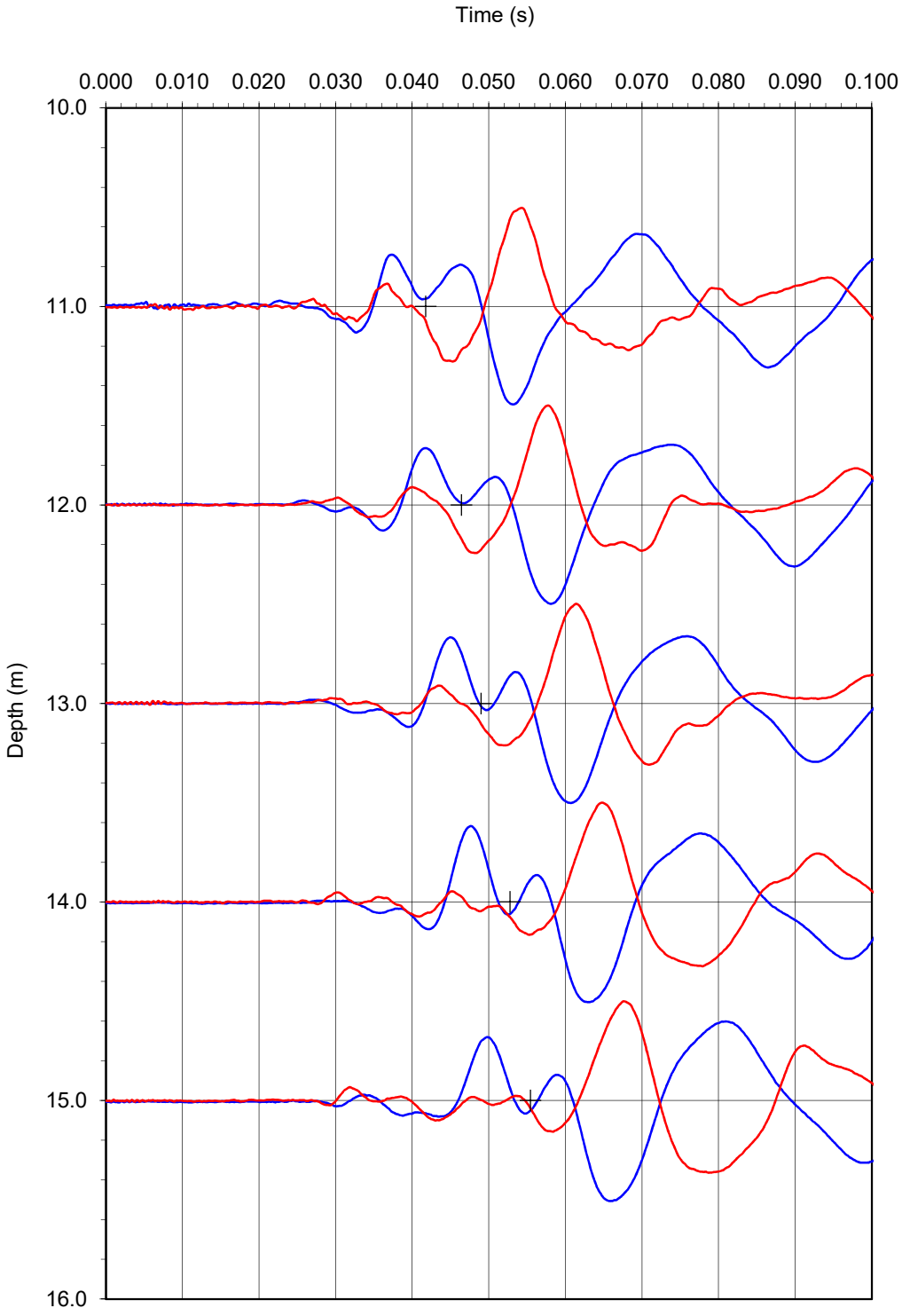

CSW Soil Engineering (Pty) Ltd
2015/450496/07
gerhard.heymann@up.ac.za
Tel: +2782 375 6666

Project:	2024 Jagersfontein
Site:	TSF
Hole:	C15
Date:	2024/03/11

Geophone orientation: Horizontal

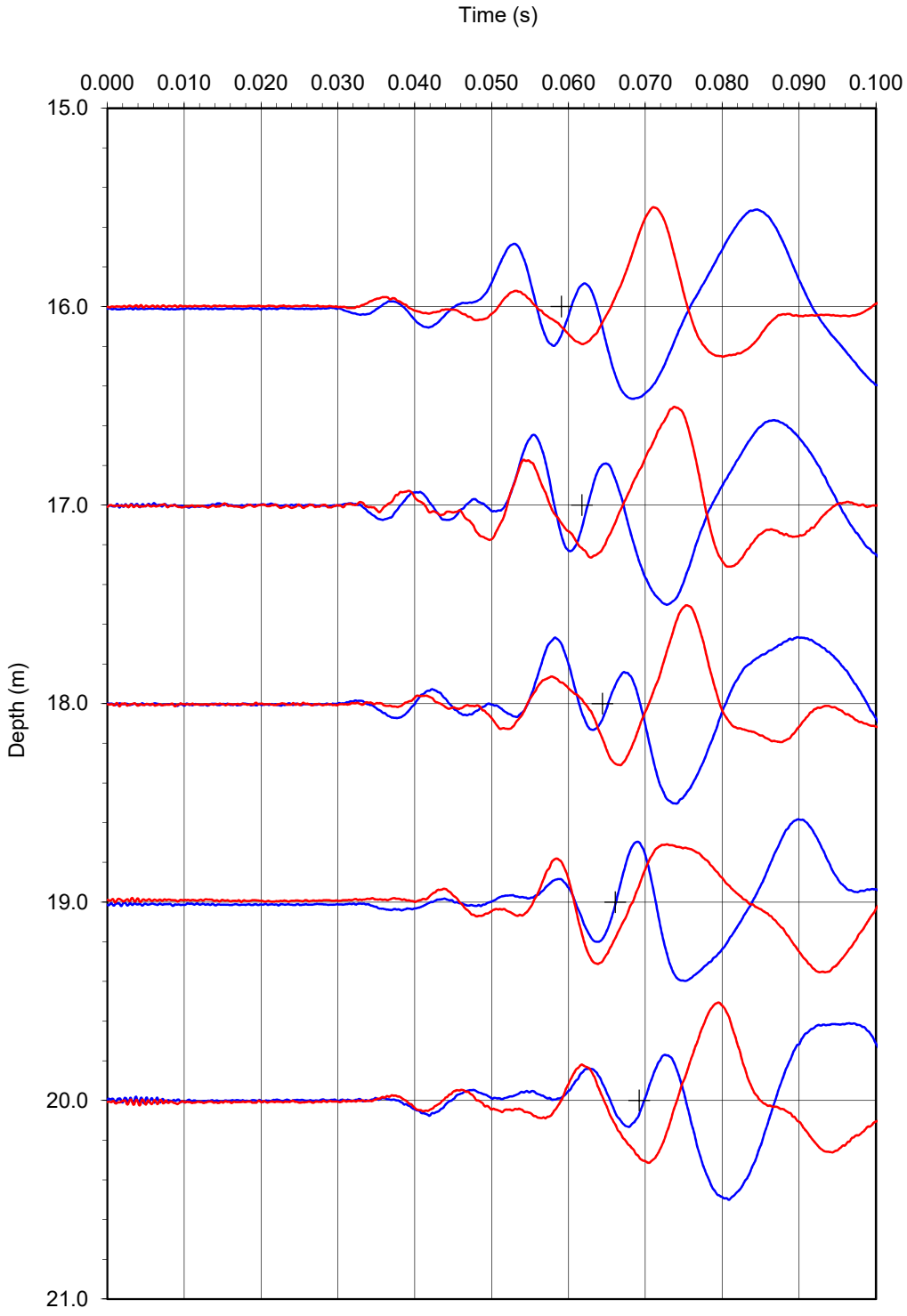

CSW Soil Engineering (Pty) Ltd
2015/450496/07
gerhard.heymann@up.ac.za
Tel: +2782 375 6666

Project:	2024 Jagersfontein
Site:	TSF
Hole:	C15
Date:	2024/03/11

Geophone orientation: Horizontal

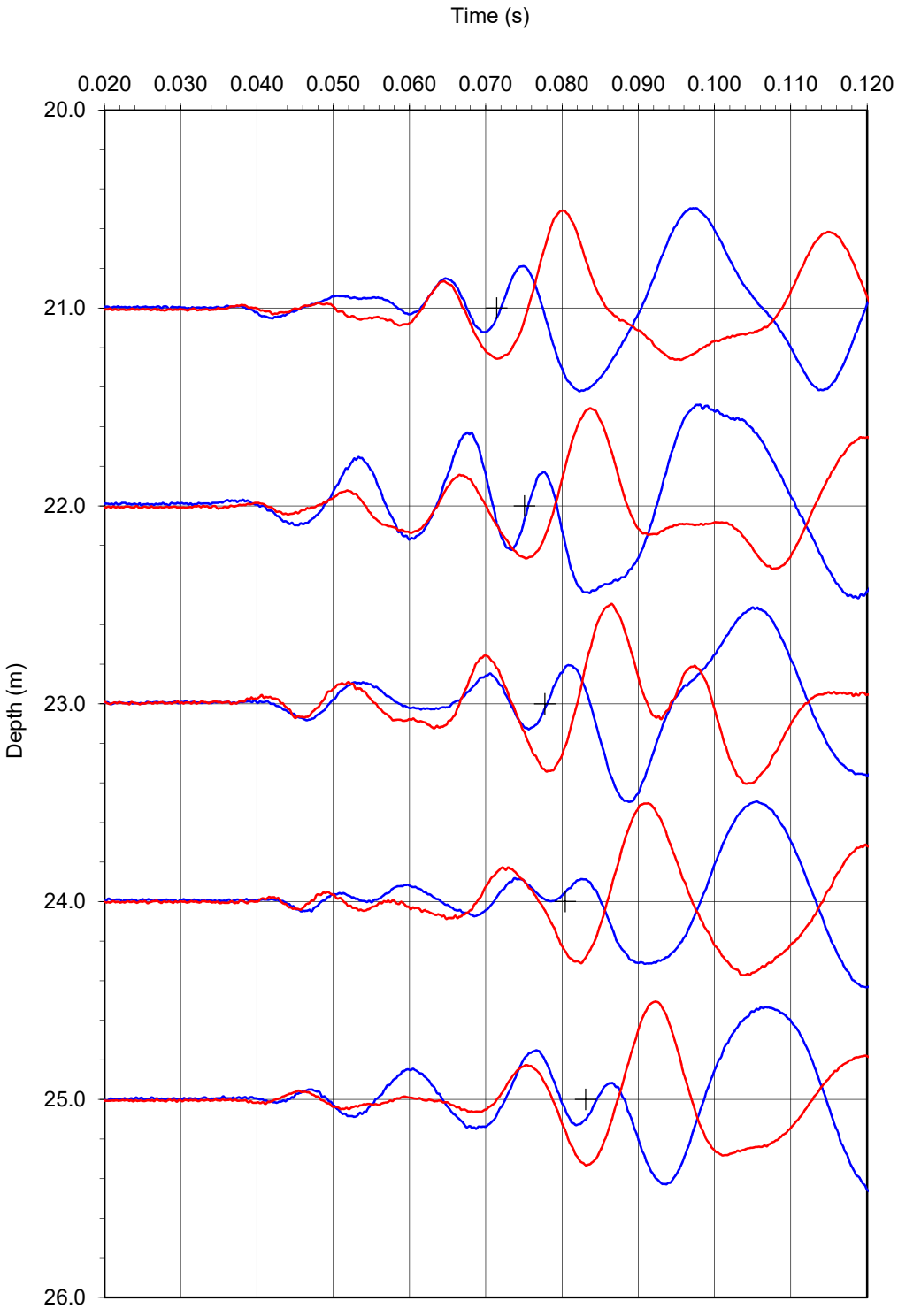

CSW Soil Engineering (Pty) Ltd
2015/450496/07
gerhard.heymann@up.ac.za
Tel: +2782 375 6666

Project:	2024 Jagersfontein
Site:	TSF
Hole:	C15
Date:	2024/03/11

Geophone orientation: Horizontal

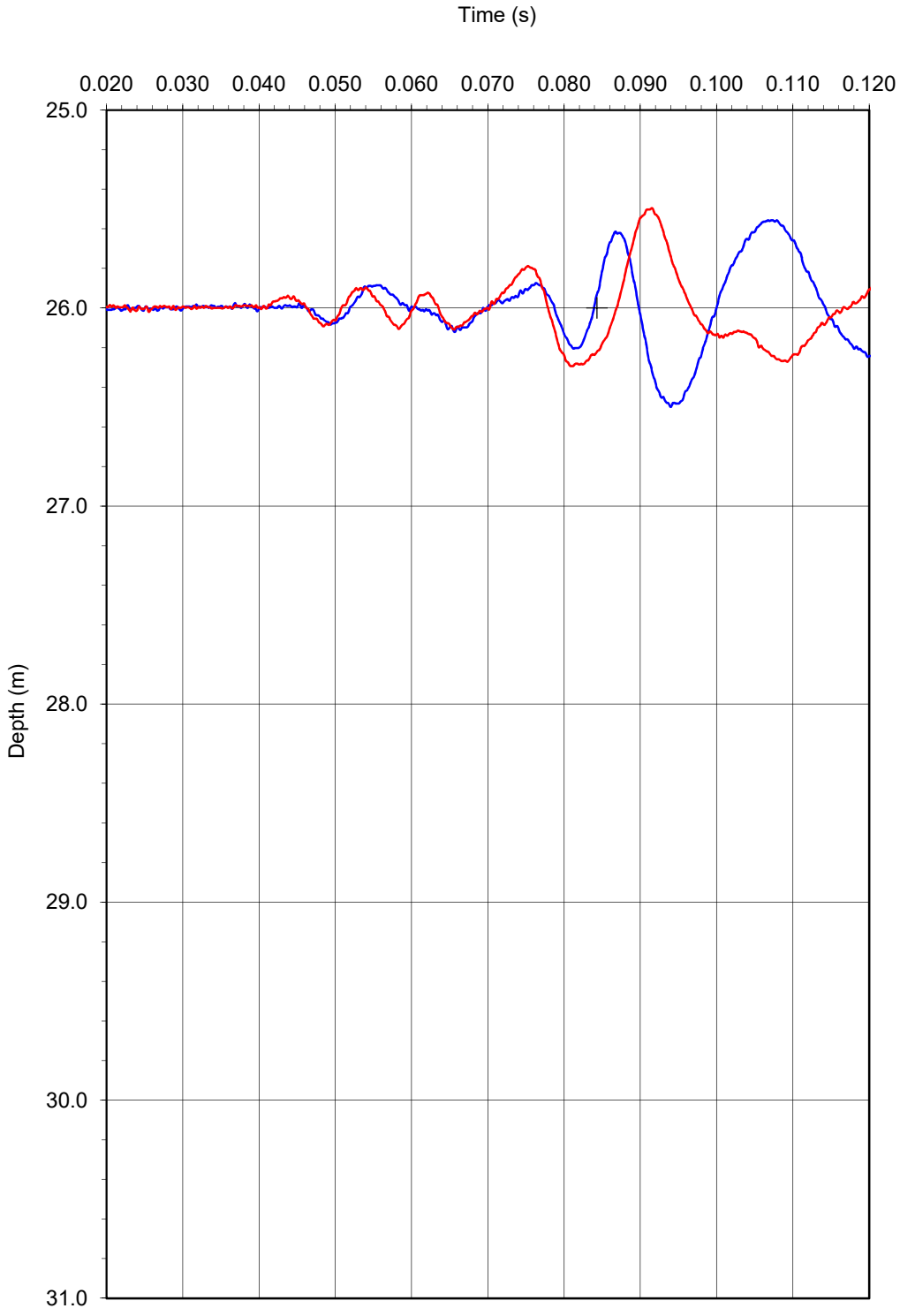

CSW Soil Engineering (Pty) Ltd
2015/450496/07
gerhard.heymann@up.ac.za
Tel: +2782 375 6666

Project:	2024 Jagersfontein
Site:	TSF
Hole:	C16
Date:	2024/03/11

TEST DETAILS

Operator:	Osimo
Source:	sledge hammer
Anvil:	timber beam
Source horizontal offset (m):	0.5
Source vertical offset (m):	0.0
Rod length (m):	1.00
Cone depth with one rod (m):	0.90
Receivers:	omni-directional geophone
Receiver orientation:	horizontal
Recording equipment:	Pasi GEA24 seismograph

CSW Soil Engineering (Pty) Ltd
2015/450496/07
gerhard.heymann@up.ac.za
Tel: +2782 375 6666

Project:	2024 Jagersfontein
Site:	TSF
Hole:	C16
Date:	2024/03/11

Geophone depth (m)	Source slant dist. (m)	1st Arrival (s)	S-wave regression (m/s)	S-wave average (m/s)
0.90	1.03	0.00400		
1.90	1.96	0.00805	236.3	244.1
2.90	2.94	0.01210	243.0	243.3
3.90	3.93	0.01614	267.0	243.6
4.90	4.93	0.01950	248.0	252.6
5.90	5.92	0.02410	295.4	245.7
6.90	6.92	0.02580	296.3	268.1
7.90	7.92	0.03039	264.6	260.5
8.90	8.91	0.03320	344.2	268.5
9.90	9.91	0.03619	352.7	273.9
10.90	10.91	0.03886	413.8	280.8
11.90	11.91	0.04100	369.9	290.5
12.90	12.91	0.04419		292.1

Project:	2024 Jagersfontein
Site:	TSF
Hole:	C16
Date:	2024/03/11

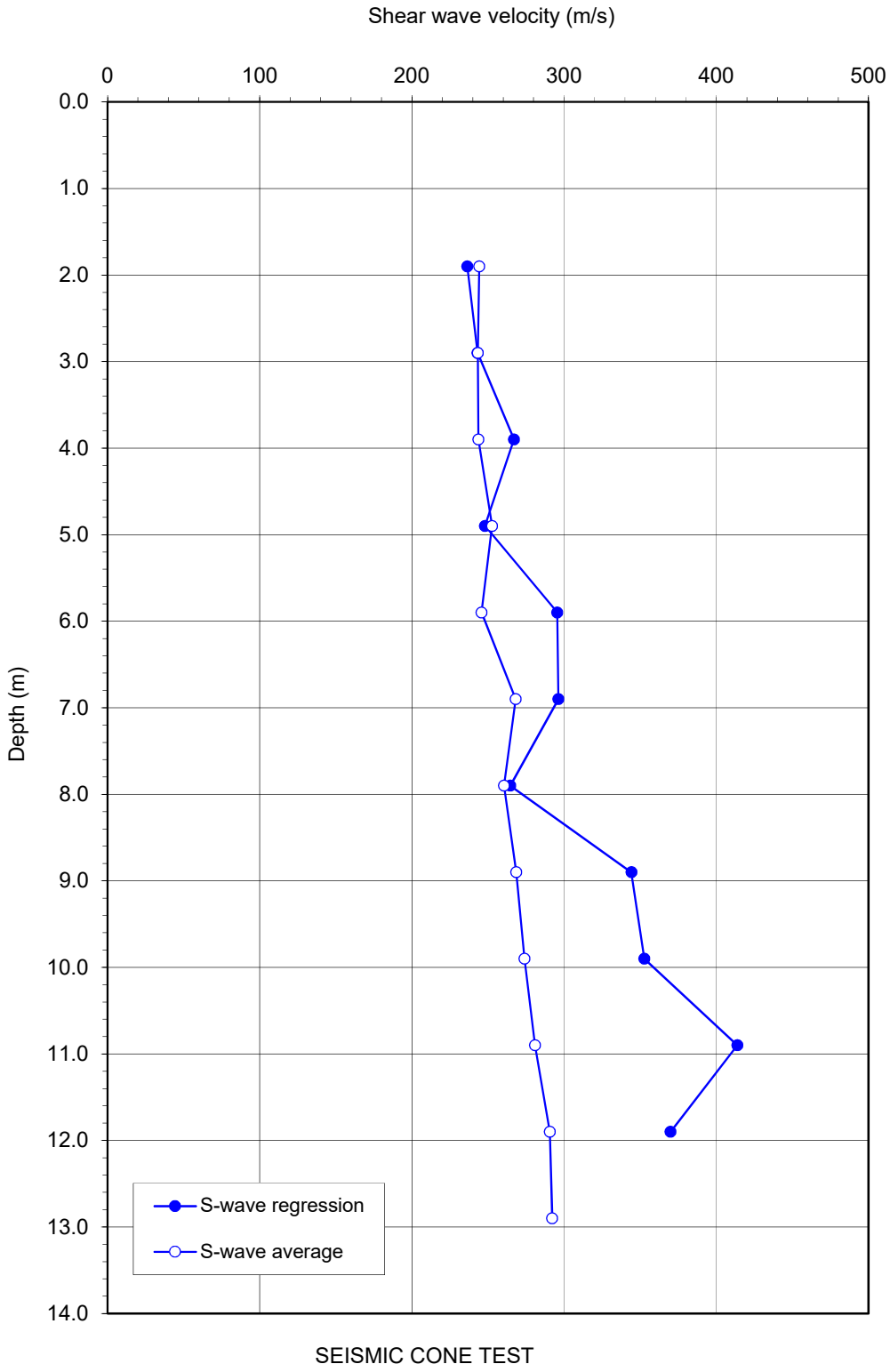

SEISMIC CONE TEST

CSW Soil Engineering (Pty) Ltd
2015/450496/07
gerhard.heymann@up.ac.za
Tel: +2782 375 6666

Project:	2024 Jagersfontein
Site:	TSF
Hole:	C16
Date:	2024/03/11

Hammer blow: Horizontal 1
Geophone orientation: Horizontal

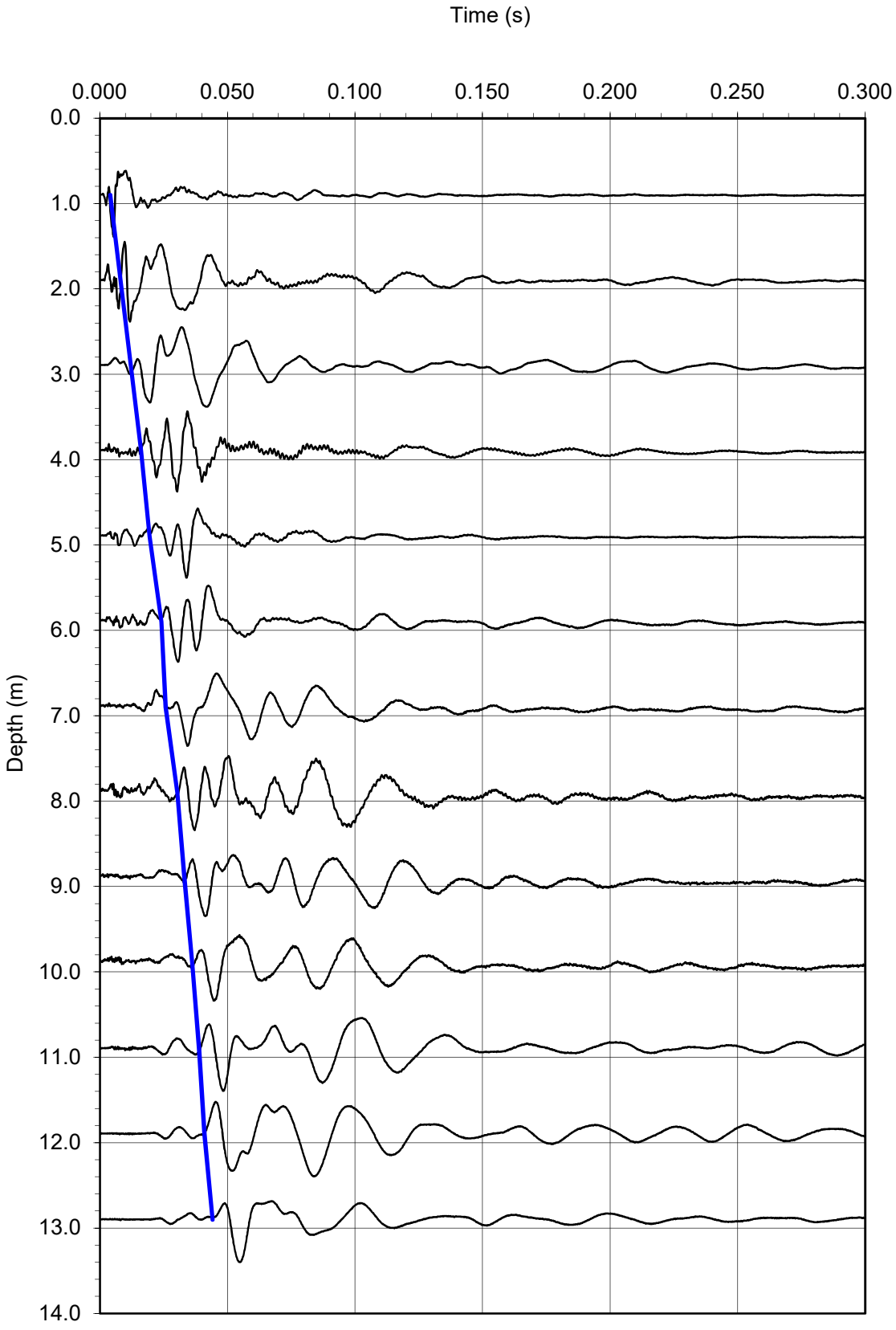

CSW Soil Engineering (Pty) Ltd
2015/450496/07
gerhard.heymann@up.ac.za
Tel: +2782 375 6666

Project:	2024 Jagersfontein
Site:	TSF
Hole:	C16
Date:	2024/03/11

Hammer blow: Horizontal 2
Geophone orientation: Horizontal

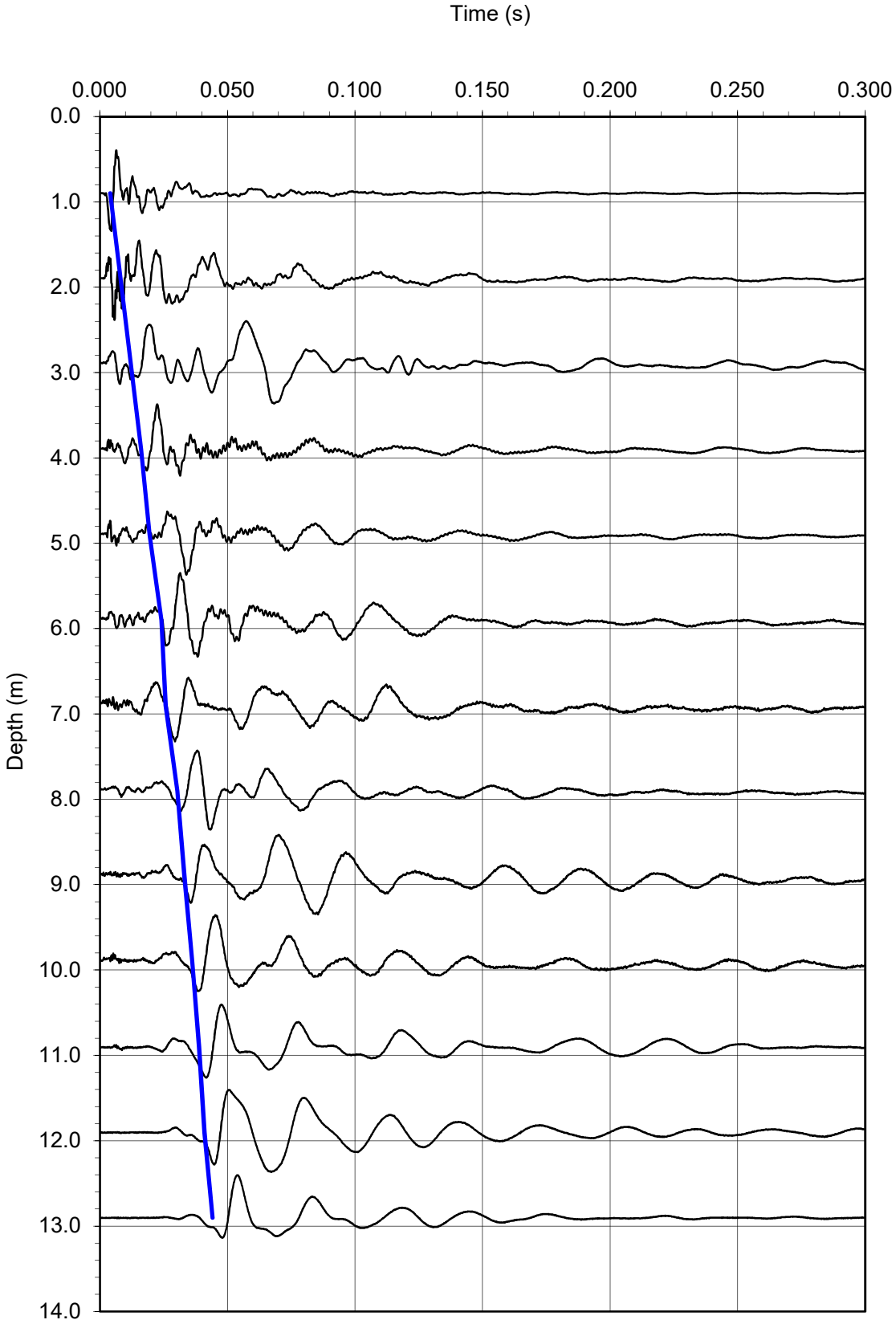

CSW Soil Engineering (Pty) Ltd
2015/450496/07
gerhard.heymann@up.ac.za
Tel: +2782 375 6666

Project:	2024 Jagersfontein
Site:	TSF
Hole:	C16
Date:	2024/03/11

Geophone orientation: Horizontal

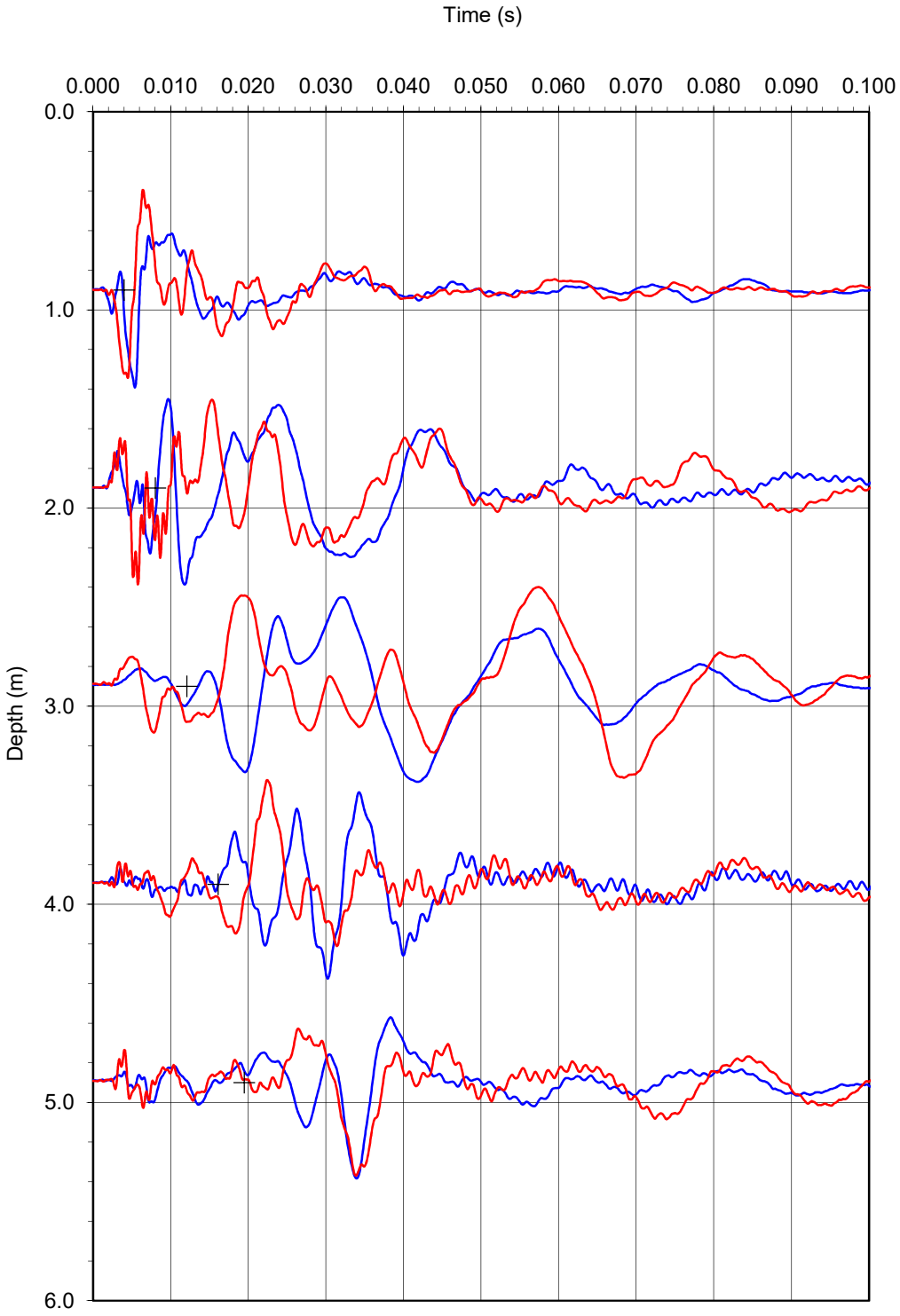

CSW Soil Engineering (Pty) Ltd
2015/450496/07
gerhard.heymann@up.ac.za
Tel: +2782 375 6666

Project:	2024 Jagersfontein
Site:	TSF
Hole:	C16
Date:	2024/03/11

Geophone orientation: Horizontal

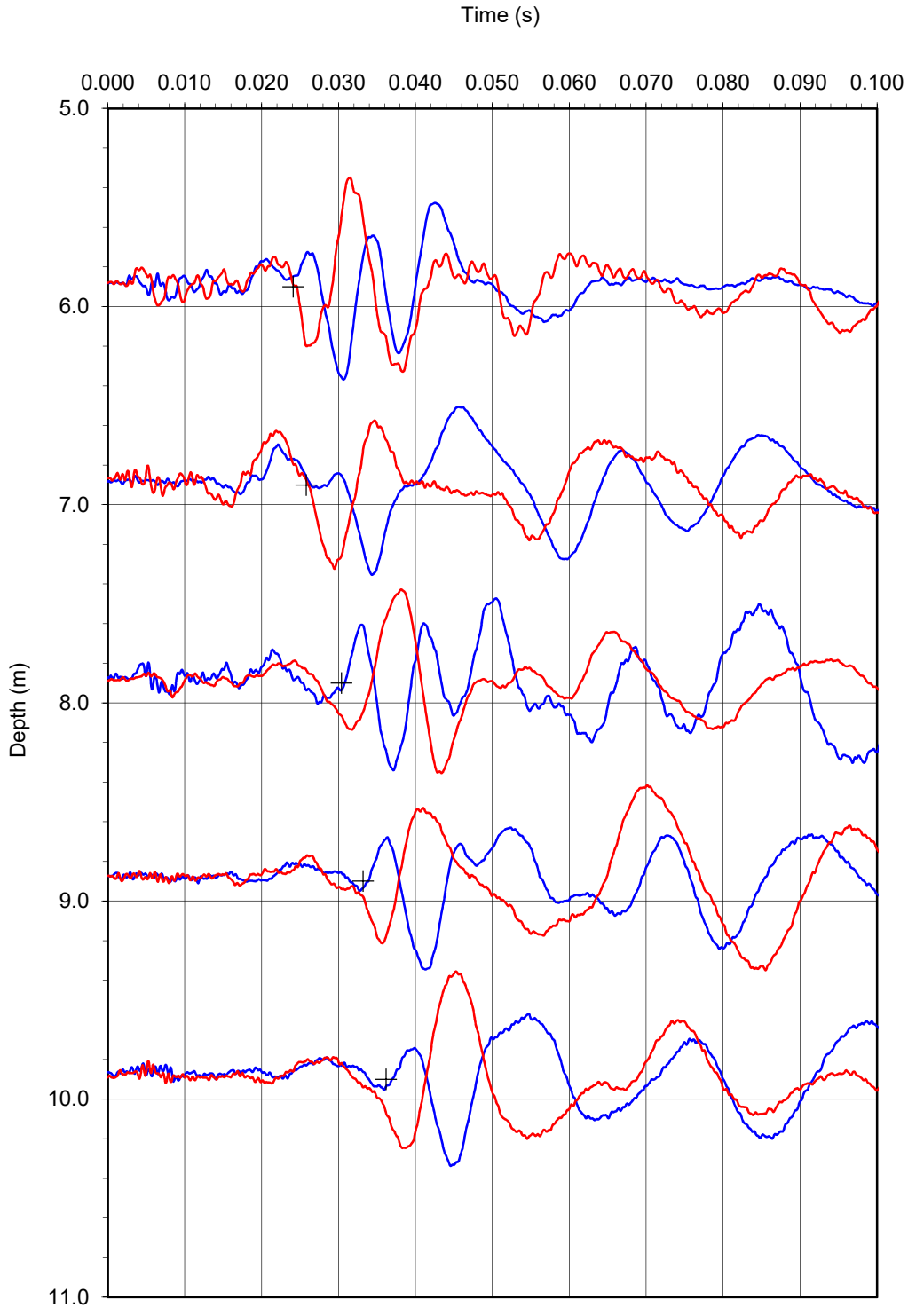

CSW Soil Engineering (Pty) Ltd
2015/450496/07
gerhard.heymann@up.ac.za
Tel: +2782 375 6666

Project:	2024 Jagersfontein
Site:	TSF
Hole:	C16
Date:	2024/03/11

Geophone orientation: Horizontal

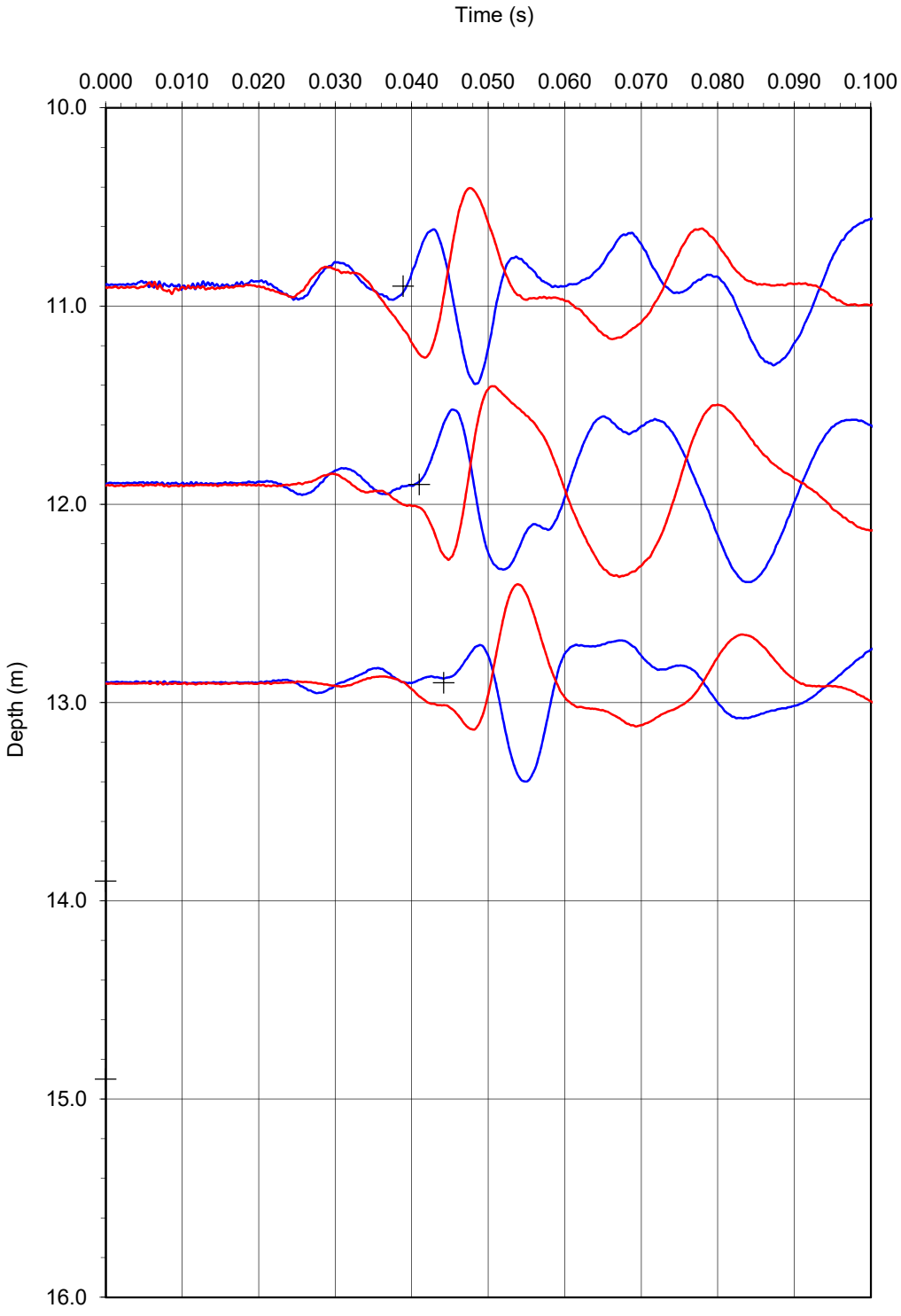

CSW Soil Engineering (Pty) Ltd
2015/450496/07
gerhard.heymann@up.ac.za
Tel: +2782 375 6666